PALEOCLIMATOLOGY

THIRD EDITION

PALEOCLIMATOLOGY

Reconstructing Climates of the Quaternary

THIRD EDITION

RAYMOND S. BRADLEY
University of Massachusetts, Amherst, Massachusetts



ELSEVIER

AMSTERDAM • BOSTON • HEIDELBERG • LONDON
NEW YORK • OXFORD • PARIS • SAN DIEGO
SAN FRANCISCO • SINGAPORE • SYDNEY • TOKYO

Academic Press is an imprint of Elsevier



Academic Press is an imprint of Elsevier
The Boulevard, Langford Lane, Kidlington, Oxford OX5 1GB, UK
Radarweg 29, PO Box 211, 1000 AE Amsterdam, The Netherlands
225 Wyman Street, Waltham, MA 02451, USA
525 B Street, Suite 1800, San Diego, CA 92101-4495, USA

Copyright © **2015** Raymond S. Bradley. Published by Elsevier Inc. All rights reserved.

First Edition: Copyright © **1985** Elsevier Inc. All rights reserved.
Second Edition: Copyright © **1999** Elsevier Inc. All rights reserved.

No part of this publication may be reproduced, stored in a retrieval system or transmitted in any form or by any means electronic, mechanical, photocopying, recording or otherwise without the prior written permission of the publisher Permissions may be sought directly from Elsevier's Science & Technology Rights Department in Oxford, UK: phone (+44) (0) 1865 843830; fax (+44) (0) 1865 853333; email: permissions@elsevier.com. Alternatively you can submit your request online by visiting the Elsevier web site at http://elsevier.com/locate/permissions, and selecting Obtaining permission to use Elsevier material.

Notice
No responsibility is assumed by the publisher for any injury and/or damage to persons or property as a matter of products liability, negligence or otherwise, or from any use or operation of any methods, products, instructions or ideas contained in the material herein. Because of rapid advances in the medical sciences, in particular, independent verification of diagnoses and drug dosages should be made.

Library of Congress Cataloging-in-Publication Data

Bradley, Raymond S., 1948-
Paleoclimatology : reconstructing climates of the Quaternary / by Raymond S. Bradley. – Third edition.
pages cm
Includes bibliographical references and index.
ISBN 978-0-12-386913-5
1. Paleoclimatology–Quaternary. 2. Geology, Stratigraphic–Quaternary. I. Title.
QC884.B614 2014
551.609'01–dc23

2013040342

British Library Cataloguing in Publication Data
A catalogue record for this book is available from the British Library

For information on all **Academic Press** publications
visit our web site at store.elsevier.com

Printed and bound in China
14 15 16 17 18 10 9 8 7 6 5 4 3 2 1

ISBN: 978-0-12-386913-5



Dedication

To Jane

Acknowledgments

As with earlier editions, I benefited greatly from discussions with colleagues who are often far more deeply immersed in a particular aspect of paleoclimatology than I am. I want to especially thank Lonnie Thompson who took the time to read many early drafts of this extensively revised edition and who gave me very useful feedback. I am also grateful to An Zhisheng, Larry Benson, Mark Besonen, Isla Castañeda, John Chappell, Francisco da Cruz, Jr., P. Thompson Davis, Scott Elias, Kristine DeLong, Donna Francis, Mark Leckie, Juerg Luterbacher, Martín Medina-Elizalde, Bill McCoy, Steve Roof, John Smol, and Mathias Vuille for their helpful comments on various draft sections, or advice on particular issues. Many thanks to Stefan Kropelin, who once again provided a great selection of photographs for the cover. Rajarshi Roychowdhury did a wonderful job assembling all the figures, which was much appreciated. Many thanks to all of you. I know the book is a lot better as a result of your efforts. If there are still errors or omissions, they are of course my responsibility (and probably indicate that I did not do what was suggested)! Nevertheless, I hope you find that the final product justified your time.

Front Cover Photograph

HOLOCENE ROCK ART FROM THE NORTHWESTERN FLANKS OF THE ENNEDI HIGHLANDS, EASTERN SAHARA, CHAD

The Ennedi highlands in the remote desert of Northeast Chad (17°22′N-21°09′E) have been called the "Garden Eden of the Sahara." The triangularly shaped sandstone plateau features spectacular cliffs and rock formations and is dissected by a labyrinth of canyons some of which include ecological niches with remnant crocodiles. Numerous rock shelters contain some of the best preserved painted rock art on Earth. An ideal sequence of superposed layers starts with engravings of archaic round-headed people roaming peacefully with herds of rhinos or giraffes, indicating a fully developed savanna landscape. They are overlain by imposing paintings of domestic cattle and detailed scenes of the village life of the later prehistoric pastoralist population. Subsequent layers include galloping horsemen which may be attributed to the Iron Age. Superposed layers show "flying" camels which were introduced only about 2000 years ago into an increasingly arid environment evidenced by plentiful snakes. The paintings hence vividly illustrate human adaption to the gradual desiccation of the "green" Sahara about 8000 years ago, to the planet's largest hyperarid desert. These changes are documented in a complete Holocene record of subannually varved deposits of proximate Lake Yoa, Ounianga Kebir.

Photograph courtesy by Stefan Kröpelin, University of Cologne.

References

Kröpelin, S., 2004. New petroglyph sites in the Southern Libyan Desert (Sudan-Chad). Sahara. 15, 111–117.

Kröpelin, S., Verschuren, D., Lézine, A.-M., Eggermont, H., Cocquyt, C., Francus, P., Cazet, J.-P., Fagot, M., Rumes, B., Russell, J.M., Darius, F., Conley, D.J., Schuster, M., Suchodoletz, H.v., Engstrom, D.R., 2008. Climate-driven ecosystem succession in the Sahara: The past 6000 years. Science. 320, 765–768.

Foreword

Earth is a constantly changing dynamic entity, composed of multiple complex physical, chemical, and biological systems that interact on a spectrum of time and spatial scales. To comprehend the Earth System as a whole, we must understand the nature of these complex subsystems, both now and in the past, and identify the important linkages among them. Earth is now experiencing many changes, some large and more rapid than others. To attempt predictions of how the Earth System may change in the future requires an assessment of the conditions that preceded the present, a perspective that can only be gained from the records of past climate. Studies of the past also reveal just how quickly some components of the Earth Systems have responded to specific external (e.g., solar) and internal (e.g., atmospheric chemistry) forcing factors. Knowledge of these changes and understanding their key drivers are critical to efforts to anticipate and plan for future environmental changes.

We are very fortunate that today we have a rich body of knowledge and numerous diverse natural systems that record many types of climatic and environmental information across a spectrum of temporal scales. Additionally, we now have rich array of technologies that allow us to tap information at ever smaller concentrations and from both common and rare archives. However, to reconstruct the nature, magnitude, and timing of these changes, paleoclimatologists must also understand the biological and physical processes that govern the formation of these diverse proxy records. As importantly, the strengths and limitations of each proxy indicator must be known and considered for robust interpretations. The field of paleoclimatology is continually becoming more interdisciplinary as practitioners strive to understand and incorporate an ever increasing number of highly specialized proxy climate and environmental indicators.

In concert with these developments in the field, the first two editions of Professor Raymond Bradley's book, *Paleoclimatology*, have proven to be an indispensable resource for earth scientists at all stages of their careers, from undergraduate students to seasoned professionals. The second edition is not only required reading in my graduate paleoclimatology course but it also occupies a prominent and easily accessible place in my research library. For almost the last three decades, *Paleoclimatology* has provided readers with a broad perspective on the development and interpretation of a wide variety of climate records, including explanations of both established and state-of-the-art techniques used to reconstruct Quaternary climates. The text, which is accompanied by numerous illustrations, is sufficiently concise and instructive for established researchers and educators but is also easy for scientific novices to comprehend.

The third edition, *Paleoclimatology: Reconstructing Climates of the Quaternary*, has been extensively updated, but maintains its mission of broad appeal across the various subdisciplines of earth science. One can quickly appreciate the comprehensive nature of this book by browsing through the bibliography, which contains almost 2500 references. Speaking as a long-practicing paleoclimatologist, I often become immersed in the details

of my specialty area and lose track of the extremely important work of colleagues in other fields that are equally essential to understand the larger scale processes that constitute our climate system. As with other scientific fields, climatologists cannot use a "silver bullet" approach when working on and presenting their research. They must understand and reference literature and data from other areas. The beauty of Professor Bradley's book is that it compiles and organizes masses of both interconnected and disparate information (silver buckshot) in a holistic way that helps us understand the complexities and interdependencies in the climate system.

This third edition is one of the best written reference books in the field, using prose that is easy to understand and explanations of difficult concepts that are presented as only an experienced lecturer and teacher of Professor Bradley's caliber can do. The text is logically arranged, beginning with an overall review of the reconstruction of paleoclimate records and a discussion of the climate system and forcing mechanisms. This is followed by a considerably detailed overview of dating techniques, which is critical since the key to understanding any climatic or environmental record lies in robust time control. Professor Bradley provides an excellent up-to-date overview of the strengths and weaknesses of the various techniques, ranging from classical and widely used methods such as radiocarbon dating to more specialized and less "publicly" familiar methods such as luminescence, dating, amino-acid, lichenometry, and dendrochronology.

The majority of the book provides overviews of the various archives used for climatic and environmental reconstruction. For each of the archives, the author summarizes the various parameters recorded by and extracted from each type of proxy, as well as how the time control is established, and what calibration techniques are used. Abundant examples of records derived from these archives are provided from around the world.

In addition to revising and updating the chapters in the second edition, he expands the discussions of proxy records that were previously grouped together. Specifically, discussions on loess, speleothems, and lake sediments, which were previously grouped in a chapter called "Non-Marine Geological Evidence," now appear in separate chapters in the third edition.

In the chapter on ice cores, which is my specialty, Professor Bradley provides a coherent and understandable primer on stable isotopes in precipitation that includes information on their calibration for paleotemperature reconstruction. The discussion of the records is more comprehensive than many other treatments of the subject, as it includes records from both high and low latitudes and deals with a multitude of ice core parameters. The longest chapter is devoted to marine sediment records. This is appropriate given the huge amount of diverse literature. Other chapters cover tree rings, corals, insects and biological evidence, and pollen. The final chapter covers the information available from historical documentation.

I first met Professor Raymond Bradley in 1983 at a NATO/NSF Workshop on Abrupt Climatic Change in Biviers, France. For 30 years, our paths have crossed many times at professional meetings, seminars, and workshops. I have also had the pleasure of working with him on manuscripts and book projects. His interests include climatology, paleoclimatology, global change, and the Arctic environment. Professor Bradley is a member of the Real Climate blog and has made sustained and significant contributions to discussions on global warming. He has a true passion for the paleoclimate community and has worked diligently and

effectively on programs (such as PAGES) which strive to bring together the paleoclimate and the modeling communities to forge a more robust understanding of global climate variability in the present, past, and future.

We are just beginning to realize how climate change has emerged as a powerful causal agent in the evolution of civilizations, including those that exist today. One of the major challenges to predicting future climate is to determine the specific causes of both past and present changes. In light of the general conclusion of the latest Intergovernmental Panel on Climate Change that "it is extremely likely that human interference has been the dominant cause of the observed warming since the mid-20th century," we urgently need to understand the natural factors that forced climate variability in the past. This body of knowledge provides the critical baseline and corpus of knowledge that will underpin more robust predictions of the future impact of human activities. Professor Raymond Bradley has provided the field of paleoclimatology an excellent spatial and temporal summary of where we are along the continuum to a deeper understanding of Earth's past and present climate.

Lonnie G. Thompson
Byrd Polar Research Center
The Ohio State University
Columbus

Preface to the Third Edition

The first edition of *Quaternary Paleoclimatology* was published in 1985 when the field of paleoclimatology was still in its infancy and there was a reasonable chance that you could read most of the relevant papers. The field grew rapidly over the next decade, and so I wrote a much more extensive and updated version, *Paleoclimatology*: *Reconstructing Climates of the Quaternary*, which was published in 1999. Over the last decade, the field has grown even faster so that it is now almost impossible to keep track of every aspect of the subject. As just one example, more than 3500 papers with the keywords "ice cores" have been published since 1999—a number greater than the entire field of paleoclimatology in the early 1980s. Inevitably, this means that research is becoming ever more specialized so that it is increasingly difficult to gain a broad perspective on the field, and to appreciate the pros and cons of particular proxies being used in paleoclimatic reconstruction. Consequently, I think a book like this can serve an even more useful purpose than the first and second editions, for all those interested in understanding past climates. My goal from the beginning has been to enable nonspecialists in any one subfield of paleoclimatology to learn enough of the basics in other subfields to allow them to read and appreciate the literature they might not otherwise understand. Hopefully, this will promote better communication of ideas within the community of paleoclimatologists and beyond. As I noted in the Preface of the previous edition, I believe there are advantages in having one lens through which this rapidly evolving field is viewed, rather than a spectrum of perspectives that an edited volume of specialists might present. I hope that those who turn to their particular areas of expertise will do so with the overall objectives of the book in mind; it was simply not possible to provide a comprehensive review of every subfield and still try to maintain an up-to-date overview of the rest of paleoclimatology. The final product is thus a compromise between completeness, expediency, and (eventually) exhaustion. Nevertheless, I hope I have done justice to most topics, and that the new references I have included will enable interested readers to quickly access the important literature. There is no substitute for reading the original scientific papers.

My goal in writing this edition was to provide a comprehensive overview of the field of paleoclimatology and the record of climatic changes during the Quaternary. New records are being obtained all the time, and new analytical techniques are being developed and applied, giving us new and exciting insights into how climates have changed over time. I have tried to capture some of these developments in the book. All sections have been comprehensively revised and updated, but in particular, the book includes new material on dating (including updates on calibration of the radiocarbon timescale and surface exposure dating) extensively revised chapters on ice cores and marine sediments and ocean circulation in the past, new chapters on loess, speleothems, lake sediments, and corals and greatly revised chapters on insects, pollen analysis, tree rings, and historical records. To keep the task somewhat manageable, I decided not to include a separate chapter on paleoclimate models, but to keep the

focus on proxies used in paleoclimatic reconstruction. Over 1200 new references have been added, almost all of them published within the last decade, and there are ~200 new figures, all with detailed explanatory captions. I have learned a lot in writing this book, and so I hope that those who read it will find it equally informative in their own studies.

Ray Bradley
Leverett, MA, November 2013

CHAPTER

1

Paleoclimatic Reconstruction

OUTLINE

1.1 Introduction 1
1.2 Sources of Paleoclimatic Information 4
1.3 Levels of Paleoclimatic Analysis 9
1.4 Modeling in Paleoclimatic Research 10

1.1 INTRODUCTION

Paleoclimatology is the study of climate prior to the period of instrumental measurements. Instrumental records span only a tiny fraction ($<10^{-7}$) of the Earth's climatic history and so provide a totally inadequate perspective on climatic variation and the evolution of climate today. A longer perspective on climatic variability can be obtained by the study of natural phenomena, which are climate-dependent and which incorporate into their structure a measure of this dependency. Such phenomena provide a proxy record of climate and it is the study of proxy data from natural archives that is the foundation of paleoclimatology. As a more detailed and reliable record of past climatic fluctuations is built up, the possibility of identifying causes and mechanisms of climatic variation is increased. Indeed, many natural archives also provide a record of past forcing (factors that may have caused the climate to change). Thus, paleoclimatic data provide the basis for reconstructing climates of the past and for testing hypotheses about the causes of climatic change. When the causes of past climatic fluctuations are understood, forecasts of climatic variations in the future will be on firmer ground (Bradley and Eddy, 1991; Alverson et al., 1999, 2003; Bradley, 2008).

Studies of past climates must begin with an understanding of the types of proxy data available and the methods used in their analysis. One must be aware of the difficulties associated with each method used and of the assumptions each entails. With such a background, it may then be possible to synthesize different lines of evidence into a comprehensive picture of former climatic fluctuations and to test hypotheses about the causes of climatic change. This

Copyright © 2015 Raymond S. Bradley.
Published by Elsevier Inc. All rights reserved.

book deals with the different types of proxy data and how these have been used in paleoclimatic reconstructions. The organization is methodological, but through the discussion of examples, selected from major contributions in each field, an overview of the climatic record during the Quaternary period (the last 2.6 Ma) is also provided. The climate of earlier periods can be studied by some of the methods discussed here (particularly those in Chapters 6, 7, and 9) but the further back in time one goes, the greater are the problems of dating, preservation, disturbance, and hence interpretation. For a thorough discussion of climate over a much longer period, the reader is referred to Frakes et al. (1992), Huber et al. (2000), Cronin (2009), and Bender (2013).

The Quaternary was a period of major environmental changes, possibly greater than at any other time in the last 60 million years (Figure 1.1). Oxygen isotope records from carbonate-rich deep-sea sediments provide a long-term perspective on global climate because $\delta^{18}O$ is primarily an indicator of deepwater temperature and global ice volume (see Chapter 6, Section 6.3). Prior to ~34 Ma ago, there was no significant ice on the continents so the $\delta^{18}O$ record reflects deep-sea temperatures, which varied from ~12 °C (in the Paleocene-Eocene thermal maximum, PETM) to ~4 °C in the Late Eocene. Ice sheets first developed (in Antarctica) around 34 Ma ago, and thereafter, the $\delta^{18}O$ signal is dominated by changing ice volume effects. Ice sheet growth was greatest in the Pleistocene when there were extensive continental ice sheets in both hemispheres. All of these changes reflect a combination of factors: long-term changes in continental position (affecting, *inter alia*, varying patterns of continental heating and precipitation, and of ocean circulation); mountain-building episodes (affecting atmospheric circulation, atmospheric composition through weathering processes, and providing upland areas for snow accumulation); changes in the Earth's orbital position relative to the Sun (affecting the seasonal and geographical distribution of solar radiation; see Chapter 2, Section 2.6); and changes in atmospheric chemistry, in particular the concentration of the greenhouse gas carbon dioxide (Zachos et al., 2001, 2008; Pagani et al., 2005; DeConto et al., 2008). The marine sedimentary record thus provides a fascinating glimpse of how the Earth's climate has evolved over very long periods of time. In this book, the focus is on the latest part of this record, the last ~2.6 Ma that comprises the Quaternary period (Head et al., 2008). It is in this period that well-dated, undisturbed records are available from both marine and continental archives, providing a rich source of material to use in documenting the evolution of the Earth's climate and in understanding the forcing factors and feedbacks involved. An understanding of climatic variation and change during the Quaternary period is necessary not only to appreciate many features of the contemporary natural environment but also to fully comprehend present climate. Today, anthropogenic effects on the atmosphere, on the biosphere, and on continental hydrology have developed to the point that they constitute a force comparable to the natural geologic forces that shaped the Earth's history in the past, leading to the suggestion that we have now entered a new and uncertain era, the Anthropocene (Crutzen, 2002; Crutzen and Steffen, 2003; Ruddiman, 2003, 2007). Disentangling the underlying natural factors involved in climate change from anthropogenic effects is a critical requirement as we seek to understand how climate may change in the future.

Different components of the climate system change and respond to external factors at different rates (see Section 2.2); in order to understand the role such components play in the evolution of climate, it is necessary to have a record considerably longer than the time it takes for

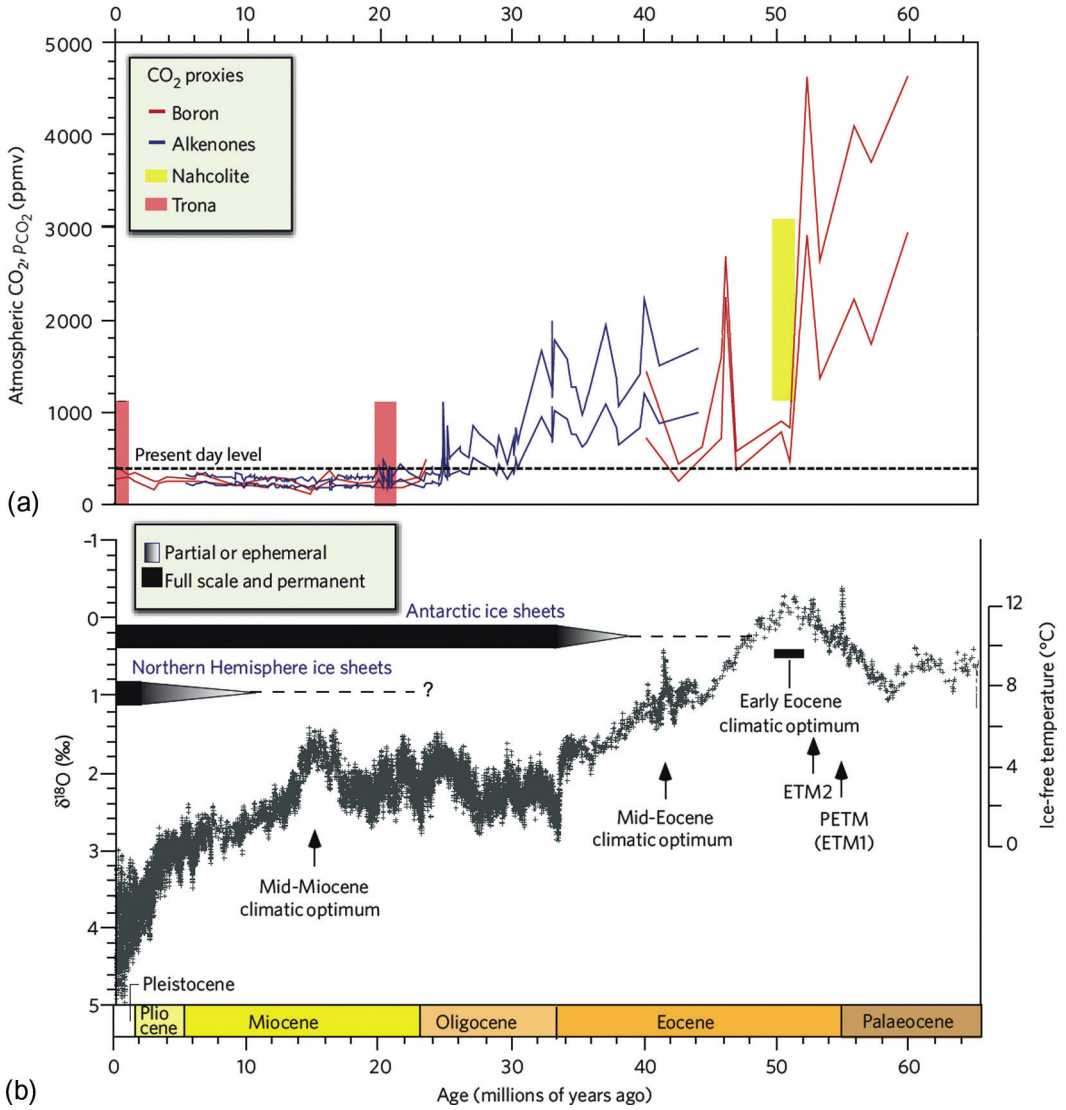


FIGURE 1.1 Evolution of atmospheric CO_2 levels and global climate over the past 65 million years. (a) Cenozoic pCO_2 based on a compilation of marine and lacustrine proxy records. The upper and lower colored lines show the range of uncertainty for the alkenone and boron proxies. The current CO_2 level of 400 ppmv is shown. (b) The climate for the same period, represented by a stacked deep-sea benthic foraminiferal oxygen isotope curve, smoothed by a five-point running mean. The $\delta^{18}O$ temperature scale, on the right axis, assumes an ice-free ocean and so only applies to the time preceding the onset of large-scale glaciation on Antarctica (about 35 million years ago). The figure clearly shows the 2-million-year-long Early Eocene climatic optimum and the more transient Mid-Eocene climatic optimum and the very short-lived Early Eocene hyperthermals such as the PETM (also known as Eocene thermal maximum 1, ETM1) and Eocene thermal maximum 2 (ETM2; also known as ELMO). *From Zachos et al. (2008).*

them to undergo significant changes. For example, the growth and decay of continental ice sheets may take tens of thousands of years; to understand the factors leading up to such changes (and the effects the surface changes subsequently have on global climate), it is necessary to have a record considerably longer than the cryospheric (snow and ice) changes that have taken place. Furthermore, since major periods of global ice buildup and decay appear to have occurred on a quasiperiodic basis during at least the Late Quaternary, a much longer record than the mean duration of this period ($\sim 10^5$ years) is necessary to determine the causative factors and to appreciate how those factors play a role in climate today. A detailed paleoclimatic record, spanning at least the Late Quaternary period, is therefore fundamental to comprehension of modern climate and the causes of climatic variation and change (Kutzbach, 1976; Wunsch, 2003; Huybers and Curry, 2006). Furthermore, unless the natural variability of climate is understood, it will constrain our ability to isolate anthropogenic effects on climate. Computer models can be used to estimate the spatial and temporal pattern of climate change as greenhouse gas concentrations increase in the atmosphere. This provides a "target" of expected change against which contemporary observations can be compared. If the climate system evolves toward such a target, it can then be argued that anthropogenic effects have been detected on a global scale (Santer et al., 1996). But natural variability, unless fully represented in model simulations, may confound such detection efforts. Whatever anthropogenic effects there are on climate, they will be superimposed on, and interact with, the underlying background of "natural" climate variability that may be varying on all timescales in response to different forcing factors. Paleoclimatic research provides the essential understanding of climate system variability, its relationship to forcing mechanisms and to feedbacks that may amplify or reduce the direct consequences of particular forcings. It is abundantly clear from the paleoclimate record that abrupt changes have occurred in the global climate system at certain times in the past (National Research Council, 2002; Alley et al., 2003). Apparently, nonlinear responses have occurred as critical thresholds were passed. Our knowledge of what these thresholds are is completely inadequate; we cannot be certain that anthropogenic changes in the climate system will not lead us inexorably across such a threshold, beyond which may lie a dramatically different future climate state (Broecker, 1987, 1997). Only by careful attention to such episodes in the past can we hope to fully comprehend the potential danger of future global changes due to human-induced effects on the climate system.

1.2 SOURCES OF PALEOCLIMATIC INFORMATION

Evidence of past climatic conditions is commonly preserved in natural archives—marine and lacustrine sediments, loess, ice, cave deposits (speleothems), and subfossil biological material—and in geomorphological features (glacial deposits, erosional features, paleosols, and periglacial phenomena). These provide materials that are indirect indicators, or proxies, of past climatic conditions. By definition, such proxy records of climate all contain a climatic signal, but that signal may be relatively weak, embedded in a great deal of extraneous "noise" arising from the effects of other (nonclimatic) influences. The proxy material has acted as a filter, transforming climatic conditions at a point in time, or over a period, into a more or less

permanent record, but the record is complex and incorporates other signals that may be irrelevant to the paleoclimatologist.

To extract the paleoclimatic signal from proxy data, the record must first be interpreted or calibrated. Calibration involves using modern climatic records and proxy materials to understand how and to what extent proxy materials are climate-dependent. It is assumed that the modern relationships observed have operated, unchanged, throughout the period of interest (the principle of uniformitarianism). All paleoclimatic research, therefore, must build on studies of climate dependency in natural phenomena today. Dendroclimatic studies, for example, have benefited from a wealth of research into climate-tree growth relationships, which have enabled dendroclimatic models to be based on sound ecological principles (Chapter 13). Significant advances have also been made in palynological research by improvements in our understanding of the relationships between modern climate and modern pollen rain (Chapter 12). It is apparent, therefore, that an adequate modern database and an understanding of contemporary processes in the climate system and in the proxies themselves are important prerequisites for reliable paleoclimatic reconstructions (Evans et al., 2013). However, not all environmental conditions in the past are represented in the period of modern experience. Situations existed during glacial and early postglacial times, which defy characterization by modern analogs. One must therefore be aware of the possibility that erroneous paleoclimatic reconstructions may result from the use of modern climate-proxy data relationships when past conditions have no analog in the modern world (Sachs et al., 1977; Jackson and Williams, 2004; Williams and Jackson, 2007). By the use of more than one calibration equation, it may be possible to detect such periods and avoid the associated errors (Hutson, 1977; Bartlein and Whitlock, 1993; see also Chapter 6, Section 6.4).

Major types of proxy climatic data available are listed in Table 1.1. Each line of evidence differs according to its spatial coverage, the period to which it pertains, and its ability to resolve events accurately in time. For example, ocean sediment cores are potentially available from 70% of the Earth's surface and may provide continuous proxy records of climate spanning many millions of years. However, these records are often difficult to date accurately; commonly, there is a dating uncertainty of $\pm 1\%$ of a sample's true age (the absolute magnitude of the uncertainty thus increasing with sample age). Mixing of sediments by marine organisms (bioturbation) and generally low sedimentation rates also make it difficult to obtain samples from the open ocean, which represent less than 200-year intervals (depending on depth in the core). This large minimum sampling interval means that the value of most marine sediment studies lies in low-frequency (long-term) paleoclimatic information (on the order of 5×10^2-10^4 years; see Chapter 6). However, areas with high sedimentation rates (that can provide higher resolution data) have been the focus of major coring efforts in recent years (Kemp, 1996; Lückge et al., 2001). Sediments from such areas can document changes on the decadal to 100-year timescale (e.g., Keigwin, 1996) or even at the subdecadal scale in exceptional circumstances (e.g., Hughen et al., 1996; Risebrobakken et al., 2003). By contrast, tree rings from much of the (extratropical) continental land mass can be accurately dated to an individual year and may provide continuous records of more than a thousand years in duration (e.g., Naurzbaev and Vaganov, 2000; Salzer and Hughes, 2007). With a minimum sampling interval of 1 year, they provide primarily high-frequency (short-term) paleoclimatic information (Chapter 13). Table 1.2 documents the main characteristics of these and other sources of paleoclimatic data. The value of proxy data to paleoclimatic reconstructions is very

TABLE 1.1 Principal Sources of Proxy Data for Paleoclimatic Reconstructions

Geologic
Marine (ocean sediment cores)
Biogenic sediments (planktonic and benthic fossils)
Oxygen isotopic composition
Faunal and floral abundance
Trace elements (e.g., Mg/Ca)
Organic biomarkers (e.g., alkenones and Tex_{86})
Inorganic sediments
Terrestrial (Aeolian) dust and ice-rafted debris; grain size
Elemental ratios (e.g., Pa/Th)
Terrestrial
Speleothems (stable isotope and trace element composition)
Glacial deposits and features of glacial erosion
Lacustrine sediments and erosional features (shorelines)
Aeolian deposits (mainly loess; also relict sand dunes)
Periglacial features
Shorelines (eustatic and glacioeustatic features)
Pedological features (relict soils)
Glaciological (ice cores)
Geochemistry (major ions; isotopes of oxygen and hydrogen)
Gas composition and air pressure in air bubbles
Microparticle concentration and elemental composition
Physical properties (e.g., ice fabric, borehole temperatures)
Biological
Tree rings (width, density, and stable isotope composition)
Pollen (type, relative abundance, and/or absolute concentration)
Diatoms, ostracods, and other biota in lake sediments (assemblages, abundance, and geochemistry, including organic biomarkers)
Insects (assemblage characteristics)
Corals (geochemistry, fluorescence, and growth rates)
Plant macrofossils (age and distribution)
Modern population distribution (refugia and relict populations of plants and animals)
Historical
Written records of environmental indicators (parameteorological phenomena)
Phenological records

TABLE 1.2 Characteristics of Natural Archives

Archive	Minimum Sampling Interval	Temporal Range (Order: Year)	Potential Information Derived
Historical records	Day/h	$\sim 10^3$	*T*, *P*, *B*, *V*, *L*, *S*
Tree rings	Year/season	$\sim 10^4$	*T*, *P*, *B*, *V*, *S*
Lake sediments	Year (varves) to 20 years	$\sim 10^4$-10^6	*T*, *B*, *M*, *P*, *V*, C_w
Corals	Year	$\sim 10^4$	C_w, *L*, *T*, *P*
Ice cores	Year/season	$\sim 10^6$	*T*, *P*, C_a, *B*, *V*, *M*, *S*
Pollen	20 years	$\sim 10^6$	*T*, *P*, *B*
Speleothems	Year	$\sim 5 \times 10^5$	C_w, *T*, *P*, *V*, *B*
Paleosols	100 years	$\sim 10^6$	*T*, *P*, *B*
Loess	100 years	$\sim 10^6$	*P*, *B*, *M*
Geomorphic features	100 years	$\sim 10^6$	*T*, *P*, *V*, *L*, *P*
Marine sediments	100 years[a]	$\sim 10^7$	*T*, C_w, *B*, *M*, *L*, *P*, *S*

T, temperature; *P*, precipitation, humidity, or water balance (*P*-*E*); *C*, chemical composition of air (C_a) or water (C_w); *B*, information on biomass or vegetation patterns; *V*, volcanic eruptions; *M*, geomagnetic field variations; *L*, sea level; *S*, solar activity.
[a]*In rare circumstances (varved sediments) ≤10 years.*
After Bradley and Eddy (1991).

dependent on the minimum sampling interval and dating resolution, since it is these that primarily determine the degree of detail available from each record. At the present time, annual and even seasonal resolution of climatic fluctuations in the timescale 10^1-10^3 years is provided by ice-core, coral, varved sediments, tree-ring studies, and some speleothems (Chapters 5, 8, 9, 13 and 14). Detailed analyses of pollen in varves may provide annual data, but it is likely that the pollen itself is an integrated measure of the pollen rain over a number of prior years (Jacobson and Bradshaw, 1981). On the longer timescale ($>10^6$ years) loess and ocean cores provide the best records at present, though resolution probably decreases to plus or minus a few thousand years in the Early Quaternary. Historical records have the potential of providing annual (or intra-annual) data for up to a thousand years in some areas, but this potential has been realized only for the last few centuries in a few areas (Chapter 15).

Commonly, there is a frequency dependence that precludes reconstruction of past climates over part of the spectrum, because of inherent attributes of the archive itself. Marine sediments typically have a strong red noise spectrum with most of the variance at low frequencies due to low sedimentation rates and bioturbation. Tree rings, on the other hand, rarely provide information at very low frequencies (i.e., greater than a few hundred years); removal of the biological growth function (a necessary prerequisite to paleoclimatic analysis) essentially filters out such low-frequency components from the raw data. All paleorecords have some frequency-dependent bias that must be understood to make sensible use of the data.

Not all paleoclimatic records are sensitive indicators of abrupt changes in climate; the climate-dependent phenomenon may lag behind the climatic perturbation so that abrupt

changes appear as gradual transitions in the paleoclimatic record. Different proxy systems have different levels of inertia with respect to climate, such that some systems vary essentially in phase with climatic variations whereas others lag behind by as much as several centuries. This is not simply a question of dating accuracy but a fundamental attribute of the proxy system in question. For example, glaciers in some regions may advance or retreat many decades after climatic conditions have changed, whereas an ice-core record from the same ice mass may register the change (in oxygen isotopes or glaciochemistry) almost immediately. Pollen (from vegetation) has been used as an indicator of past changes in climate, but not all plant species respond to abrupt climate change at the same rate, making it sometimes difficult to assess the rapidity of a change in climate from pollen indicators. Some species might take up to a few hundred years to adjust to an abrupt change in climate, whereas vegetation changes in other regions respond quickly to abrupt climate changes (cf. Williams et al., 2002; Birks and Birks, 2008). Fossil insect remains (in lake sediments and peat deposits) can provide valuable supporting evidence because insect populations are often highly mobile and sensitive to temperature fluctuations (see Chapter 11, Section 11.2). However, even if there is a rapid biological response to abrupt climate change, bioturbation in lacustrine and marine sediments may smooth the record, disguising the abrupt nature of a climate-related change.

In terms of the resolution provided by proxy data, it is also worth noting that not all data sources provide a continuous record. Certain phenomena provide discontinuous or episodic information; glacier advances, for example, may leave geomorphological evidence of their former extent (moraines, trimlines, etc.), but these represent discrete events in time, resulting from the integration of climatic conditions prior to the ice advance (Chapter 10, Section 10.3). Such deposits say nothing about times of ice recession. Furthermore, major ice advances may obliterate evidence of previous, smaller advances, so the geomorphological record is likely to be not only discontinuous but also incomplete. Studies of *continuous* paleoclimatic records can help to place such episodic information in perspective, and for this reason, the continuous marine sedimentary records are commonly used as a chronological and paleoclimatic frame of reference for long-term climatic fluctuations recorded on land (e.g., Kukla, 1977). This does not mean that the growth and decay of ice sheets in different areas were globally synchronous; indeed, there is much evidence that this was not the case.

So far, the focus has been on paleorecords of past climatic change (i.e., the response of the climate system to some external or internal forcing). However, paleorecords can also provide critical information on the nature of past forcing factors. Ice cores, for example, register the occurrence of major explosive eruptions in the record of non sea-salt sulfate, resulting from acidic fallout after such events. ^{10}Be in ice also provides insight into past solar variability and the dust content of ice records past atmospheric turbidity. Changes in radiatively important greenhouse gases (CO_2, CH_4, and N_2O) are also recorded in air bubbles in the ice. Such records are extremely valuable in understanding what factors may have been important in bringing about changes in past climate and in defining the significance of future environmental changes.

In all paleorecords, accurate dating is of critical importance. Without accurate dating, it is impossible to determine if events occurred synchronously or if certain events led or lagged others. This is a fundamental requirement if we are to understand the nature of global changes of the past (Chapters 3 and 4). Accurate dating is required in any assessment of

the rate at which past environmental changes occurred, particularly when considering high-frequency, short-term changes in climate. Indeed, the duration of such events may be shorter than the normal error associated with many dating methods.

1.3 LEVELS OF PALEOCLIMATIC ANALYSIS

Paleoclimatic reconstruction may be considered to proceed through a number of stages or levels of analysis. The first stage is that of data collection, generally involving fieldwork, followed by initial laboratory analyses and measurements. This results in primary or level 1 data (cf. Hecht et al., 1979, Peterson et al., 1979). Measurements of tree-ring widths or the isotopic content of marine foraminifera from an ocean core are examples of primary data. At the next stage, the level 1 data are calibrated and converted to estimates of paleoclimate. The calibration may be entirely qualitative, involving a subjective assessment of what the primary data represent (e.g., "warmer," "wetter," and "cooler" conditions), or may involve an explicit, reproducible procedure that provides quantitative estimates of paleoclimate. These derived or level 2 data provide a record of climatic variation through time at a particular location. For example, tree-ring widths from a site near the alpine or arctic tree line may be transformed into a paleotemperature record for that location, using a calibration equation derived from the relationship between modern climatic data and modern tree-ring widths (see Chapter 13). Different calibration procedures may result in different paleoclimatic reconstructions, so a critical evaluation of the calibration procedure and its associated uncertainties is quite appropriate.

Data may also be mapped to provide a regional synthesis of paleoclimate at a particular time, the synthesis providing greater insight into former circulation patterns than any of the individual level 1 or 2 data sets could provide alone (e.g., Mann et al., 2009). In some cases, three-dimensional arrays of level 2 data (i.e., spatial patterns of paleoclimatic estimates through time) have been transformed into objectively derived statistical summaries. For example, spatial patterns of drought in the eastern United States over the last 300 years (based on level 1 tree-ring data) have been converted into a small number of principal components (eigenvectors), which account for most of the variance in the level 2 data set (Cook et al., 1992a). The eigenvectors show that there are a small number of modes or patterns of drought that characterize the data. The statistics derived from such analyses constitute a third level of paleoclimatic analysis (level 3 data).

Most paleoclimatic research involves level 1 and level 2 data at individual sites, though regional syntheses are becoming more common (see, e.g., individual chapters in Wright et al., 1993). At the larger, hemispheric or global scale, there are a few important studies of the spatial patterns of climate at particular periods in the past, notably the CLIMAP and COHMAP reconstructions of marine and continental conditions at the last glacial maximum (LGM) and at 3000-year intervals from 18,000 years BP to the present (CLIMAP, 1976; COHMAP, 1988; Webb et al., 1993a). These were followed by other large-scale syntheses and model simulations of selected time periods since the LGM (PMIP; Prentice et al., 2000) and further studies of surface conditions at the LGM (e.g., EPILOG, GLAMAP, and MARGO) (Mix et al., 2001; Pflaumann et al., 2003; Kucera et al., 2005a,b). Such syntheses enable rigorous tests to be made of the ability of general circulation models to simulate climate under different

boundary conditions and different forcing mechanisms. There have also been efforts to reconstruct large-scale patterns of climate over more recent time intervals (e.g., Mann et al., 2009) in order to understand conditions leading up to the period when anthropogenic greenhouse gases began to overwhelm natural forcing mechanisms.

1.4 MODELING IN PALEOCLIMATIC RESEARCH

Although the primary focus of this book is the study of natural archives, it is important to note that paleoclimatic research also involves the use of numerical models of the climate system. These models are based on simulations of the modern environment but are applied to those periods in the past when boundary conditions were different from today. Much of the impetus for developing models of the climate system has come from concerns over the increase in trace (greenhouse) gases in the atmosphere, due to human activity, and the consequences such increases will have for society. Commonly, general circulation models (GCMs) are first run with preindustrial levels of CO_2 and then again with higher CO_2 levels to examine the projected changes (equilibrium simulations). Alternatively, models are run sequentially, with CO_2 levels slowly increasing until $2\times$ CO_2 levels are reached (transient simulations). Such experiments, performed by many different modeling research groups, have formed the basis of the Intergovernmental Project on Climatic Change (IPCC) estimates of the probable consequences of anthropogenic increases in greenhouse gases (e.g., Meehl et al., 2007). But how reliable are such models? They may be able to simulate modern climatic conditions quite well, but how do we know that they can reliably simulate a future climate state different from today (Trenberth, 1997)? One approach that has been widely adopted to allay such concerns is to use the same models to simulate climates of the past (Braconnot et al., 2012). If models can reproduce climatic conditions, which are *known* to have occurred (i.e., reconstructed from paleodata), then confidence in their ability to simulate future (*unknown*) climates will be enhanced. This line of reasoning has driven paleoclimate modeling over the last decade or so, but the resulting experiments have had many collateral benefits (Schmidt, 2010). Models have provided considerable insight into the sensitivity of the climate system to different forcing factors that have influenced the climate system in the past (e.g., Shindell et al., 2001; Chiang et al., 2003; Vettoretti and Peltier, 2004; Ammann et al., 2007; LeGrande and Schmidt, 2008; Otto-Bliesner et al., 2009). They have also helped to elucidate the interactions between different subsystems of the climate system (atmosphere, biosphere, ice sheets, surface, and deep ocean), through positive or negative feedbacks at different times (Bonfils et al., 2004; Braconnot et al., 2007). Furthermore, complex simulations involving terrestrial and ocean biogeochemistry are becoming more commonplace so that some of the same parameters that are examined in paleoarchives can be directly obtained from the simulations. For example, in some GCMs, at each change of phase in the water cycle, appropriate fractionation factors are employed to calculate the mass of the isotopes in each reservoir (water vapor, precipitation, ice, surface, and groundwater) (Jouzel et al., 1991, 1994; Joussaume and Jouzel, 1993). This "forward-modeling" approach enables direct comparisons to be made between model simulations and isotopes in "pseudoproxies"—ice, sediments, biological materials, speleothems, etc.—in order to compare them with measured values in the natural archives. Model simulations suggest that the modern spatial relationship between

temperature and oxygen isotopes has not remained constant over time, and changes in the trajectory of water vapor transport and its attendant isotopic fractionation may have pronounced effects on the isotopic composition of precipitation incorporated into paleoclimate archives (LeGrande and Schmidt, 2009; Lewis et al., 2010; Sturm et al., 2010). For example, Charles et al. (1994) used a GCM to examine how source regions of precipitation reaching Greenland may have changed from the LGM to the present. The modern (control) simulation showed that 26% of Greenland precipitation was derived from the North Atlantic (30-50°N), 18% from the Norwegian-Greenland Sea, and 13% from the North Pacific. At the LGM, these values changed to 38%, 11%, and 15%, respectively. However, northern Greenland received distinctly more moisture at the LGM from the North Pacific, due to displacement of storm tracks around the Laurentide Ice Sheet. Southern Greenland received most of its snowfall from North Atlantic moisture sources. Because of the much longer (and colder) trajectory of the Pacific air masses, snow deposited on Greenland from those sources was much more depleted in $\delta^{18}O$ than snow from North Atlantic sources ($\sim$15‰ lower). Charles et al. (1994) point out that if there was no change in temperature in Greenland, but only a shift in source region from purely North Atlantic moisture to a 50:50 mix of North Atlantic and North Pacific moisture, changes in $\delta^{18}O$ of snowfall could change by $\sim$7‰, equivalent to the large amplitude oscillations seen during late glacial time in the GISP2/GRIP ice cores. This raises the interesting possibility that abrupt changes in $\delta^{18}O$ seen in the ice cores from Greenland may be partly related to changes in storm tracks rather than large-scale (hemispheric) shifts in temperature.

Studies such as these have the dual benefits of broadening our appreciation of the range and complexity of climatic conditions in the past while improving the reliability of GCMs to simulate future climate. This is not an irrelevant academic exercise. Changes in atmospheric CO_2 and CH_4 levels recorded in ice cores were of the same magnitude, from glacial to interglacial periods, as the changes that have already been wrought by human activities over the last century (though anthropogenic changes have been much more rapid). Together, paleoenvironmental data and modeling can help us to evaluate known changes in the past and to comprehend the feedbacks and system responses that are of direct relevance to understanding the future impact of greenhouse gases (Bradley et al., 2003a; Raynaud et al., 2003).

CHAPTER

2

Climate and Climatic Variation

OUTLINE

2.1 The Nature of Climate and Climatic Variation 13
2.2 The Climate System 16
2.3 Feedback Mechanisms 24
2.4 Energy Balance of the Earth and Its Atmosphere 27
2.5 Timescales of Climatic Variation 33
2.6 Variations of the Earth's Orbital Parameters 36
2.7 Solar Forcing 46
2.8 Volcanic Forcing 50

2.1 THE NATURE OF CLIMATE AND CLIMATIC VARIATION

Climate is the statistical expression of daily weather events; more simply, climate is the expected weather. Naturally, for a particular location, certain weather events will be common (or highly probable); these will lie close to the central tendency or mean of the distribution of weather events. Other types of weather will be more extreme and less frequent; the more extreme the event, the lower the probability of recurrence. Such events would appear at the margins of a distribution of weather events characterizing a particular climate. The overall distribution of climatic parameters defines the climatic variability of the place. If we were to measure temperature in the same location for a finite period of time, the statistical distribution of measured values would reflect the geographical situation of the site (in relation to solar radiation receipts, degree of continentality, and elevation) as well as the relative frequency of synoptic weather patterns and the associated airflow over the region. Given a long enough period of observations, it would be possible to characterize the temperature of the site in terms of mean and variance. Similarly, observations of other meteorological parameters, such as precipitation, relative humidity, solar radiation, cloudiness, wind speed, and direction,

Copyright © 2015 Raymond S. Bradley.
Published by Elsevier Inc. All rights reserved.

would enable a more comprehensive understanding of the climate of the site to be obtained. However, implicit in such statistics is the element of time. For how long should observations be taken to obtain a reliable picture of the climate at a particular place? The World Meteorological Organization has recommended the adoption of standardized 30-year periods to characterize climate (World Meteorological Organisation, 2007; Arguez and Vose, 2011). Adoption of a standard reference period is necessary because the statistics that define climate in one area may vary over time so that climate, strictly speaking, should always be defined with reference to the period used in its calculation. Recent studies of global warming express global temperature changes relative to the 1951-1980 or 1961-1990 mean (e.g., Hansen et al., 2012), but many paleoclimate studies reference climatic data from earlier decades. This becomes important when attempting to compare the fairly subtle climatic variations of the recent past (or general circulation model simulations) with the climate of "today," as in most areas the last 30 years has been significantly warmer than in previous decades; in fact, on a global scale, 1981-2010 was the warmest 30-year period of the last millennium (Mann et al., 1999). The problem is even more difficult in dealing with precipitation, where one 30-year climatic average may be quite different from another (Bradley, 1991). There is no simple solution, so changes in climate should always be expressed relative to some defined time interval, to allow different reconstructions to be appropriately compared.

Climate may vary in different ways. Some examples of climatic variation are shown in Figure 2.1. Variations may be periodic (and hence predictable), quasiperiodic (predictable only in the very broadest terms), or nonperiodic. Central tendencies (mean values) may remain more or less constant or exhibit trends or impulsive changes from one mean to another (Hare, 1979). Such occurrences may appear to be random in a time series, but this does not necessarily mean they are not predictable. For example, a number of studies have shown that abrupt changes in climate generally result from large explosive volcanic eruptions (e.g., Bradley, 1988). Consequently, the climatic effects of similar eruptions can be anticipated. Hansen et al. (1996), for example, used a general circulation model to estimate the changes in temperature expected from the 1991 eruption of Mount Pinatubo (Philippines). Their estimates tracked very closely observed temperature changes in the years following the eruption. Such studies indicate that in some circumstances, reliable climate predictions can be made, even though the eruptions themselves are nonperiodic.

A very important aspect of variability in the climate system involves nonlinear feedbacks, in which drastic changes may occur if some critical threshold is exceeded. One example of this is the oceanic thermohaline circulation that may cease to operate if the salinity-density balance in near-surface waters of the North Atlantic Ocean is disturbed beyond a certain point. The circulation would then cease, until salinity increased to the level where density-induced overturning of the water column could resume (see Chapter 6, Section 6.8).

Finally, climatic variation may be characterized by an increase in variability without a change in central tendency, though commonly a change in variability accompanies a change in overall mean. Climatic variability is an extremely important characteristic of climate in our increasingly overstressed world. Every year, unexpected weather events (extremes in the climate spectrum) result in hundreds of thousands of deaths and untold economic and social hardships. If climatic variability increases, the unexpected becomes more probable, and the strain on social and political systems increases. High-resolution paleoclimatic data can shed light on this important aspect of climatic variation.

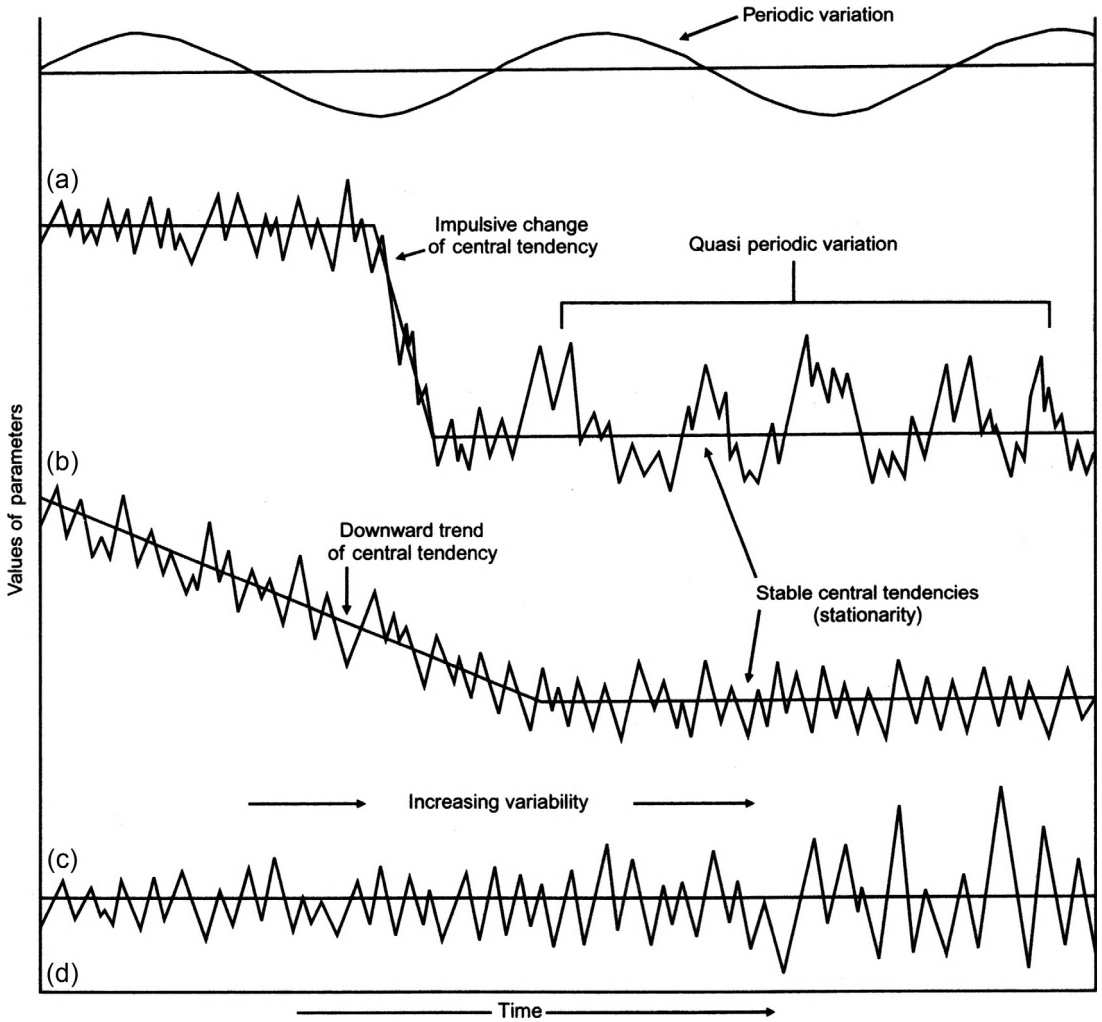


FIGURE 2.1 Examples of climatic variation and variability. *From Hare (1979).*

In the light of these discussions, it is appropriate to consider the term *climatic change*. Clearly, climates may change on different scales of time and in different ways. In paleoclimatic studies, climatic changes are characterized by significant differences in the mean condition between one time period and another. Given enough detail and chronological control, the significance of the change may be calculated from statistics describing the time periods in question. Markedly different climatic conditions between two time periods imply an intervening period of climate characterized by an upward or downward trend or by an impulsive change in central tendency (Figure 2.1). Many paleoclimatic records appear to provide evidence for there being distinct modes of climate, within which short-term variations are essentially stochastic (random). Brief periods of rapid, steplike,

climatic change appear to separate these seemingly stable interludes (Alley et al., 1997c). Analysis of several thousand ^{14}C dates on stratigraphic discontinuities (primarily in pollen records from western Europe but including data from elsewhere) lends some support to this idea (Wendland and Bryson, 1974). Certain periods stand out as having been times of environmental change on a worldwide scale[1] (Figure 2.2). Such widespread discontinuities imply abrupt, globally synchronous climatic changes, presumably brought about by some large-scale forcing. In particular, the period 2760-2510 years BP (the beginning of sub-Atlantic time) stands out in both palynological and archaeological data as a period of major environmental and cultural change, the cause of which is not known (though solar forcing is commonly cited). There is also mounting evidence for a change in the climate of many regions around 4200 years ago, which had significant societal impacts (Dalfes et al., 1997; Weiss and Bradley, 2001). Understanding the causes of such changes is increasingly important as world population continues to grow, increasing by a billion people every ~15 years, placing severe pressure on all environmental systems (Rockström et al., 2009). Abrupt disturbances of the climate system in the future will have major social, economic, and political consequences (Parry et al., 2007).

2.2 THE CLIMATE SYSTEM

Although it is common to consider climate as simply a function of the atmospheric circulation over a period of time, to do so overlooks the complexity of factors that determine the climate of a particular region. Climate is the end product of a multitude of interactions between several different subsystems—the atmosphere, oceans, biosphere, land surface, and cryosphere—which collectively make up the climate system. Each subsystem is coupled in some way to the others (Figure 2.3) such that changes in one subsystem may give rise to changes elsewhere (Section 2.3). Of the five principal subsystems, the atmosphere is the most variable; it has a relatively low heat capacity (low specific heat) and responds most rapidly to external influences (on the order of 1 month or less). It is coupled to other components of the climate system through energy exchanges at the surface (the atmospheric boundary layer) as well as through chemical interactions that may affect atmospheric composition (Overpeck et al., 2003; Pedersen et al., 2003; Raynaud et al., 2003). Only recently has it been possible to assess variations in atmospheric composition and turbidity over long periods of time, through studies of ice cores from pristine environments (Lambert et al., 2008; Loulergue et al., 2008; Lüthi et al., 2008; Bigler et al., 2009; Wolff et al., 2010b; Abbott and Davies, 2012). Such variations are of particular importance since they may be a fundamental cause of climatic changes in the past.

The oceans are a much more sluggish component of the climate system than the atmosphere. Surface layers of the ocean respond to external influences on a timescale of months to years, whereas changes in the deep oceans are much slower; it may take centuries for significant changes to occur at depth. Because water has a much higher heat capacity than air, the

[1] As discussed in Chapter 3, changes in the ^{14}C content of the atmosphere may result in periods of apparently rapid change, because events that were in reality separate in time appear near synchronous when ^{14}C dated. This effect may have influenced the pattern of change noted Wendland and Bryson (1974).

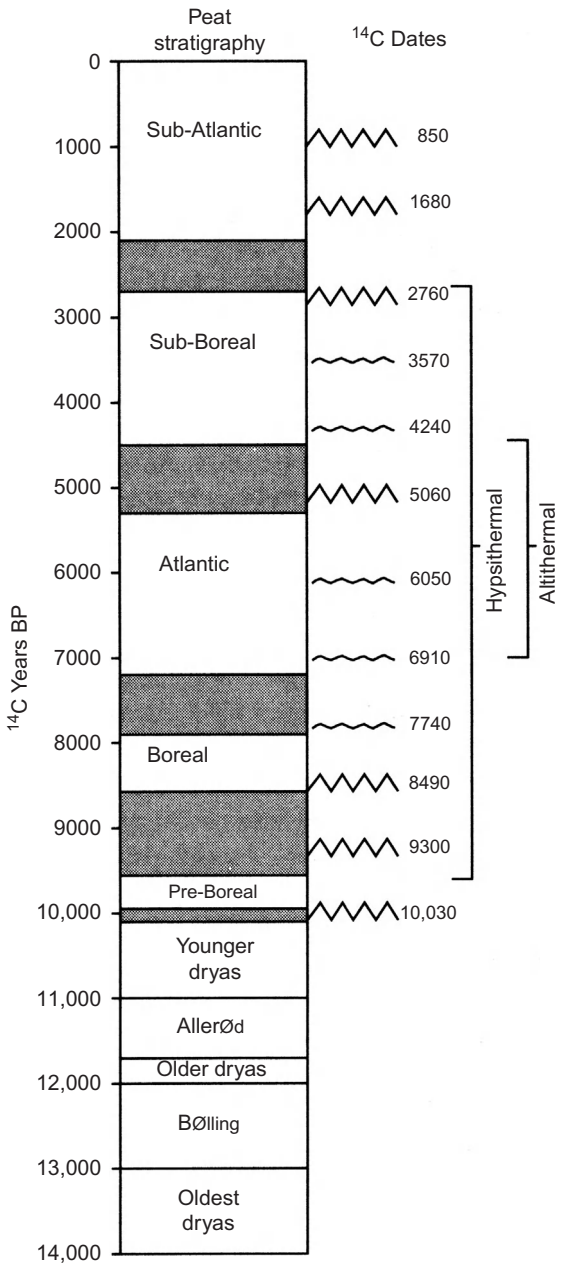


FIGURE 2.2 "Climatic discontinuities" revealed by analysis of over 800 ^{14}C dates on stratigraphic discontinuities in paleoenvironmental (primarily botanical) records (based on data in Wendland and Bryson, 1974). Major and minor discontinuities are shown by large and small jagged lines, respectively. Time limits of the hypsithermal and the altithermal are from Deevey and Flint (1957). The Blytt-Sernander scheme of European peat stratigraphy was developed before ^{14}C dating techniques were available. It is based on changes in peat growth that were considered to be climate-related. Radiocarbon dates now indicate that the boundaries are not precise but vary over the ranges indicated (based on summaries by Godwin, 1956; Deevey and Flint, 1957). Objective analyses of peat stratigraphy indicate that the "classic" stages of peat stratigraphy may not be of regional significance after all (except for the subboreal/sub-Atlantic transition at about 2500 years BP) (Birks and Birks, 1981). Nevertheless, the descriptors (Atlantic, sub-Atlantic, etc.) are still commonly used to refer to a particular time period, albeit vaguely defined, both climatically and chronologically. Late Glacial/Early Holocene chronozones are from Mangerud et al. (1974).

oceans store very large quantities of energy and act as a buffer against large seasonal changes of temperature. On a large scale, this is reflected in the differences between seasonal temperature ranges of the Northern and Southern Hemispheres (Table 2.1). On a smaller scale, proximity to the ocean is a major factor affecting the climate of a region. Indeed, it is probably the single most important factor, after latitude and elevation.

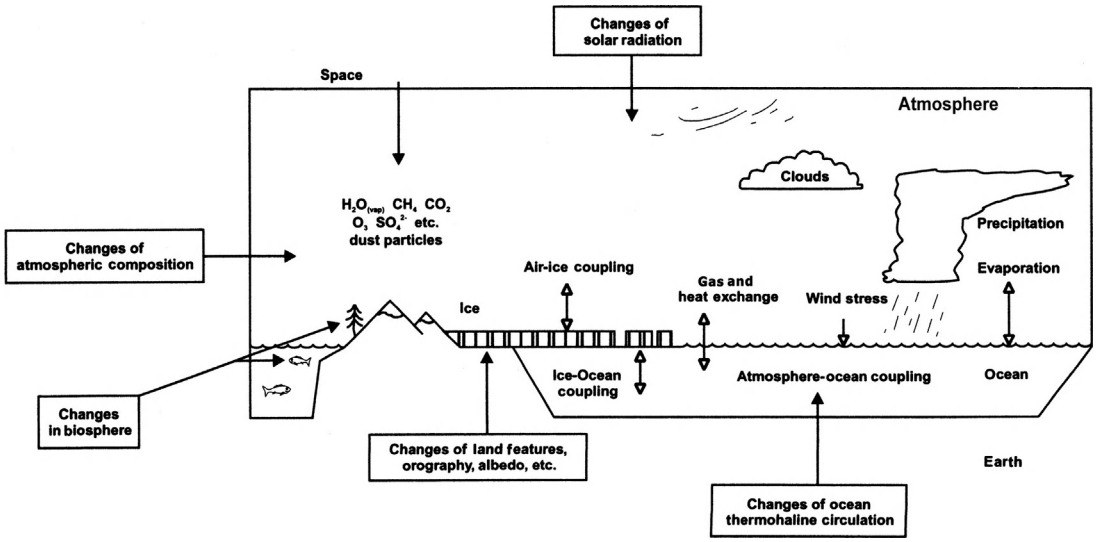


FIGURE 2.3 Schematic diagram of major components of the climatic system. Feedbacks between various components play an important role in climate variations.

TABLE 2.1 Mean Temperatures (°C) and Temperature Differences

	Extreme Months		Years
(a) Surface			
Northern Hemisphere	8.0 (January)	21.6 (July)	15.0
Southern Hemisphere	10.6 (July)	16.5 (January)	13.4
Entire globe	12.3 (January)	16.1 (July)	14.2
(b) Middle troposphere (300-700 mb layer)			
Mean temperatures			
Equator	−8.6	−8.6	−8.6
North Pole	−41.5 (January)	−25.9 (July)	−35.9
South Pole	−52.7 (July)	−38.3 (January)	−47.7
Temperature differences			
Equator-North Pole	32.9 (January)	17.3 (July)	27.3
Equator-South Pole	29.7 (January)	44.1 (July)	39.1

After Flohn (1978) and Van Loon et al. (1972).

At the present time, the oceans cover 71% (361×10^6 km^2) of the Earth's surface and hence play an enormously important role in the energy balance of the Earth (Section 2.4). The oceans are most extensive in the Southern Hemisphere, between 30 and 70°S, and least extensive in the zone 50-70°N and poleward of 70°S (Figure 2.4). This distribution of land and sea is of great significance; it is largely responsible for the differences in atmospheric circulation

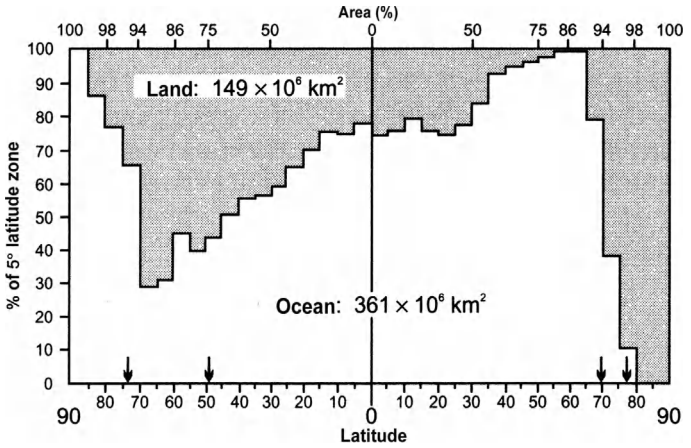


FIGURE 2.4 Percentage distribution of land and ocean by 5° latitude band. Land area shaded. Upper figures give percentage of hemispheric surface area equatorward of latitudes shown. Arrows indicate mean latitudinal ranges of seasonal snow cover (cf. Table 2.3).

between the two hemispheres and has important implications for glaciation of the Earth (Flohn, 1978). On a global scale, the relative proportions of land and sea have changed little during the Quaternary, in spite of sea-level changes due to the growth and decay of continental ice sheets. When sea level was 120-130 m below its present level, ocean area decreased by only 3% (though this is equivalent to a 10% increase in land-surface area). Such changes undoubtedly had regional significance; in particular, sea-level changes may have had important effects on oceanic circulation and certainly must have influenced the degree of continentality of some areas (e.g., Nix and Kalma, 1972; Kurek et al., 2009).

The oceans play a critical role in the chemical balance of the atmospheric system, particularly with respect to atmospheric carbon dioxide levels. Because the oceans contain very large quantities of CO_2 in solution, even a small change in the oceanic CO_2 balance may have profound consequences for the radiation balance of the atmosphere and, hence, climate (Sundquist, 1985, 1993). The role of the oceans in global CO_2 exchanges is of particular importance, not only for an understanding of past climatic variations but also for insight into future CO_2 trends in the atmosphere (Sabine et al., 2004; Le Quéré et al., 2009). Changes in the ventilation rate of the oceans at certain times in the past (due to variations in the thermohaline circulation) have also affected the amount of radiocarbon in the atmosphere, leading to plateaus in the radiocarbon timescale (e.g., Muscheler et al., 2008; Skinner et al., 2010).

The land surface of the Earth interacts with other components of the climate system on all timescales. Over very long periods of time, continental plate movements (in relation to the Earth's rotational axis) have had major effects on world climate (Tarling, 1978; Frakes et al., 1992). It is no coincidence that the frequency of continental glaciation increased as the plates moved to increasingly polar positions. Similarly, mountain-building episodes (orogenies) have had major effects on world climate. Apart from the dynamic effects on atmospheric circulation (Yoshino, 1981; Ruddiman and Kutzbach, 1989; Liu and Yin, 2011), the presence of elevated surfaces at relatively high latitudes, where snow can persist throughout the year, may be a prerequisite for the development of continental ice sheets (Ives et al., 1975).

The latitudinal distribution of land and sea is of fundamental significance for both regional and global climate. In particular, the presence of highly reflective snow- and ice-covered regions at high latitudes strongly affects equator-pole temperature gradients (Table 2.1b). In the Southern Hemisphere, the presence of the high-elevation Antarctic plateau south of

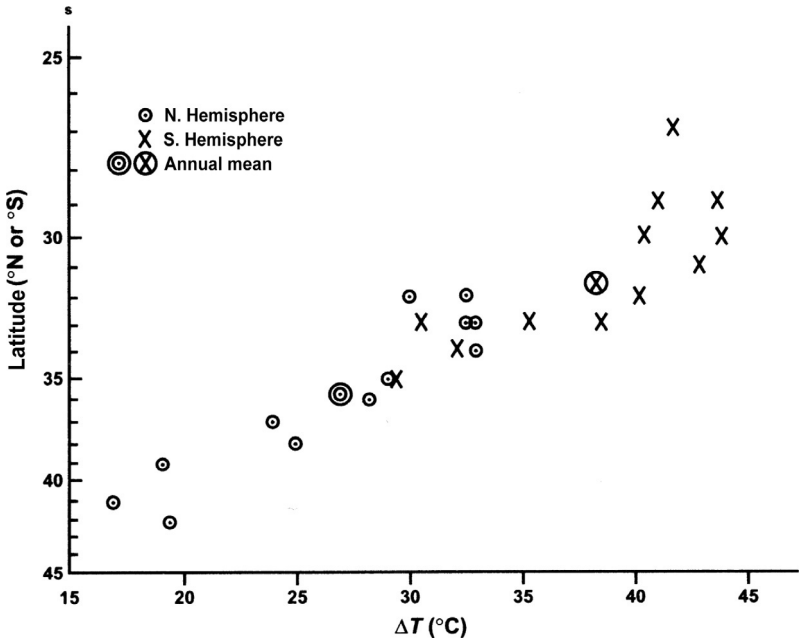


FIGURE 2.5 Relationship between latitude of main axis of subtropical anticyclones and hemispheric (pole-equator) temperature gradient in preceding month. *After Korff and Flohn (1969).*

~75°S (Figure 2.4) causes there to be a much stronger equator-pole temperature gradient than in the Northern Hemisphere. As a result, an intense westerly circulation pattern develops above the surface layers (60% stronger, on average, than westerlies in the Northern Hemisphere; Peixoto and Oort, 1992). The stronger temperature gradient also results in the subtropical high-pressure belt of the Southern Hemisphere being located closer to the equator than in the Northern Hemisphere (29-35°S as compared with 33-41°N; Figure 2.5). This difference, stemming primarily from the polar location of Antarctica and its associated low temperatures, gives rise to a basic asymmetry in the position of climatic zones in both hemispheres (Korff and Flohn, 1969; Flohn, 1978).

The cryosphere consists of mountain glaciers and continental ice sheets, seasonal snow and ice cover on land, and sea ice. Its importance in the climate system stems from the high albedo of snow- and ice-covered regions, which greatly affects global energy receipts (Kukla, 1978). At present, about 8% of the Earth's surface is permanently covered by snow and ice (Table 2.2), but seasonal expansion of the cryosphere causes this figure to double (Table 2.3). The hemispheric differences are particularly profound. In the Northern Hemisphere, 4% of the total area is permanently ice-covered (mainly the Arctic Ocean (~3%) and Greenland). In winter months, sea-ice formation and snowfall on the continents result in a six-fold increase in snow and ice cover. By midwinter, 24% of the Northern Hemisphere is generally covered by snow and ice. In the Southern Hemisphere, most of the permanent ice cover is land-based, on the Antarctic continent, and seasonal changes are almost entirely due to an increase in sea-ice formation (Figure 2.6). By midwinter, 13% of the Southern Hemisphere is

TABLE 2.2 Present Extent of Permanent Snow and Ice (Glaciers, Ice Caps, and Sea Ice)

	Area ($\times 10^6$ km^2)	Volume ($\times 10^6$ km^3)	Sea-Level Equivalent (m)
Northern Hemisphere			
Greenland	1.73	3.0	7.5
Other locations	0.5	0.12	0.3
Total land-based snow and ice	2.23		
Sea ice	8.87		
Total for Northern Hemisphere	11.0		
Southern Hemisphere			
Antarctica	13.0	29.4	73.5
Other locations	0.032	<0.01	<0.02
Total land-based snow and ice	13.032		
Sea ice	4.2		
Total for Southern Hemisphere	17.23		
Entire globe			
Total land-based snow and ice	~15.3		
Sea ice	~13.0		
Total for entire globe	~28.3		

Compiled from Kukla (1978), Hollin and Schilling (1981), and Hughes et al. (1981).

TABLE 2.3 Seasonal Changes in Snow and Ice Cover Area ($\times 10^6$ km^2); Snow and Ice Extent Based on the Period 1967-1974 (Kukla, 1978)

	Maximum Extent			Minimum Extent		
	Month	Area	(%)	Month	Area	(%)
Northern Hemisphere	February	60.1	24[a]	August	11.0	4[a]
Southern Hemisphere	October	34.0	13[a]	February	17.2	7[a]
Entire globe	December	79.1	16[b]	August	42.3	8[b]

[a] *Percentage of area of hemisphere.*
[b] *Percentage of area of entire globe.*

generally covered by snow and ice. It is of particular interest that the cryosphere, considered on a global scale, doubles in area over a relatively short period, from August to December, on average. Given the variability in seasonal timing of snow- and ice-cover changes in both hemispheres, it is quite probable that very large area increases may occur over an even shorter period, and this has important implications for theories of climatic change (Kukla, 1975a).

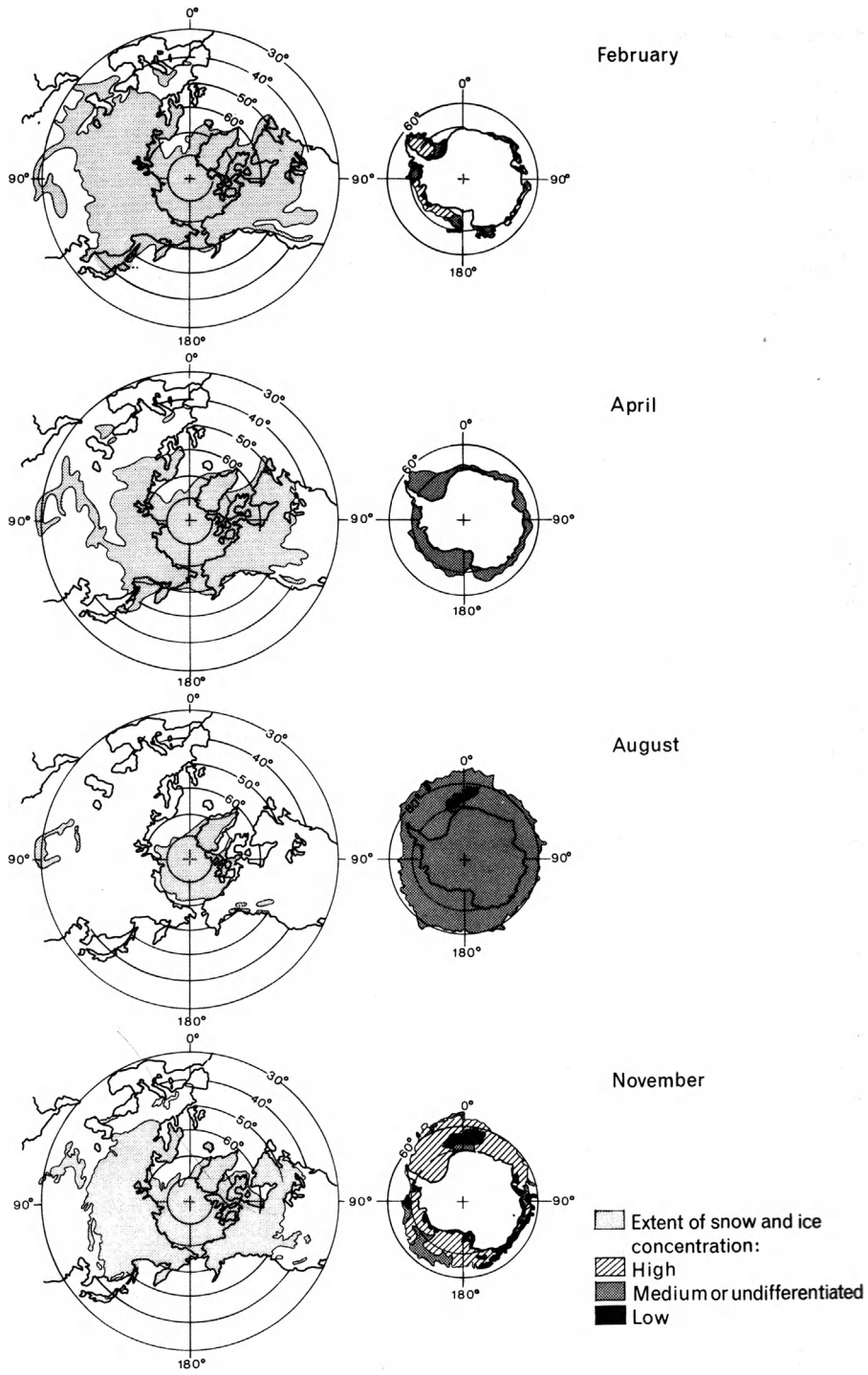


FIGURE 2.6 Extent of snow and ice at four intervals during the year. Note that the maximum global ice extent is in November/December and the minimum is in August (cf. Table 2.3). *From Kukla (1978).*

Clearly, part of the cryosphere undergoes extremely large seasonal variations and hence has a very short response time. Glaciers and ice sheets, on the other hand, respond very slowly to external changes, on the timescale of decades to centuries; for large ice sheets, adjustment times may be measured in millennia. Simulations of the climate system over long periods of time indicate that the growth and decay of ice sheets at high latitudes are critically dependent on the orbital configuration of the Earth and the level of CO_2 in the atmosphere. When CO_2 is $<$280 ppmv. and the Earth is in a "cold orbit" (i.e., high eccentricity, low obliquity, and perihelion occurring in the Northern Hemisphere winter—see Section2.6), conditions are more favorable situation for ice sheets to develop at high northern latitudes (DeConto et al., 2008). For Antarctica, the onset of glaciation began at much higher CO_2 levels, two to four times preindustrial values (Pollard and DeConto, 2005).

The final component of the climate system is the biosphere, consisting of the plant and animal worlds, though vegetation cover and type are mainly of significance for climate. As vegetation has changed over time, there have been important biogeochemical and biophysical feedbacks with the atmosphere (Claussen, 2009). Vegetation not only affects the albedo, roughness, and evapotranspiration characteristics of a surface but also influences atmospheric composition through the removal of carbon dioxide and the production of aerosols and oxygen (Claussen, 2009; Carslaw et al., 2010). Absence of vegetation may result in significant increases in particulate loading of the atmosphere, at least locally, and this may of itself be a significant factor in altering climate (Overpeck et al., 1996). Model simulations show that loss of vegetation cover in semiarid areas of North Africa causes changes in surface hydrology such that the sensible heat flux to the atmosphere increases and the latent heat flux declines, which leads to an increase in atmospheric subsidence. Such a change tends to suppress convective rainfall so that a loss in vegetation may lead to a reduction in rainfall through positive feedbacks in the atmosphere, which would likely amplify the initial decline in vegetation (Charney et al., 1975; Xue, 1997). At high latitudes, strong feedbacks are associated with albedo changes when forests replace snow-covered tundra, or vice versa. Vegetation has thus played an important role in the dynamics of Quaternary climate change (Overpeck et al., 2003).

Vegetation type varies greatly from one region to another (Table 2.4). Forests and woodlands cover ~34% of the continents and play a major role in the removal of atmospheric CO_2 (Woodwell et al., 1978; Bonan, 2008). Deserts and desert scrublands occupy ~13% of the continents and are the major sources of wind-blown dust (though cultivated lands are increasingly susceptible to wind erosion also). The response time of the biosphere varies widely, on the order of years for individual elements of the biosphere to centuries for entire vegetation communities. Carbon sequestration in terrestrial ecosystems has varied over glacial-interglacial cycles because of large-scale changes in the area of different ecosystem types. Thus, the area of forests during the last glacial maximum (LGM) was reduced to less than a third of the forest cover today, with a corresponding reduction in carbon storage in forest ecosystems (Van Campo et al., 1993). Overall, carbon storage on land was ~30% lower than today in the LGM.

Human beings are, of course, part of the biosphere, and human activities play an increasingly important role in the climate system. Increases in atmospheric CO_2 concentration, changes in natural vegetation, increases in particulate loading of the lower troposphere, and reductions in atmospheric ozone concentrations in the stratosphere are a consequence of man's worldwide activities (Forster et al., 2007). The rate of such changes is rapid, and the extent to which the climate system can adjust to them without drastic changes in climate

TABLE 2.4 Areas of Major Ecosystems of the World and Their Estimated Carbon Content and Albedo, Today, and at the Last Glacial Maximum

Ecosystem	Modern Area (10^6 km^2)	Modern Carbon Storage (Pg)	Albedo[a] (%)	LGM Area (10^6 km^2)	LGM Carbon Storage (Pg)
Boreal forest	11.8	310.2	7-15	2.3	63.5
Temperate forest	13.0	343.9	13-17	3.9	109.2
Tropical forest	14.3	399.9	7-15	6.1	159.4
Xerophytic woodlands	11.3	147.0	15-20	19.0	249.2
All forests and woodlands	*50.4*	*1201.0*		*31.3*	*581.3*
Arctic and alpine tundra	10.7	204.4	10-15	14.7	281.9
Steppes and mountain shrublands	30.8	337.9	15-20	41	444.7
All steppes and tundras	*41.5*	*542.3*		*55.7*	*726.6*
Cool and polar deserts	4.0	27.4	10-20	15.8	64.0
Hot deserts	14.5	21.8	25-44	19.7	29.6
All deserts	*18.5*	*49.2*		*35.5*	*93.6*
Cultivated lands	*14.1*	*195.0*	8-20		
Bogs	*0.7*	*128.1*			
Total	125.2	2115.6		122.5	1401.5

[a]*From Lieth (1975)*
From Van Campo et al. (1993).

or climatic variability remains uncertain. The only certainty is that mankind has become exceedingly vulnerable to any unexpected perturbations of climate. Common sense argues for action to limit those activities that may contribute to global-scale climatic disturbances (Metz et al., 2007).

2.3 FEEDBACK MECHANISMS

Interactions within the climate system often involve complex, nonlinear relationships. All components of the climate system are intimately linked or coupled with all other components such that changes in one subsystem may involve compensatory changes throughout the entire climate system. These changes may amplify the initial disturbance (anomaly) or dampen it. Interactions that tend to amplify the disturbance are termed positive feedback mechanisms or processes; they operate in such a way that the system is increasingly destabilized. Interactions that tend to dampen the initial disturbance are termed negative feedback mechanisms or processes; they provide a stabilizing influence on the system, tending to preserve the status quo (National Research Council, 2003).

Growth of continental ice sheets provides an example of positive feedback mechanisms. Whatever the initial perturbation of the climate system that led to continental ice-sheet

growth in the past (see Section 2.6) once snow and ice persisted year round, the higher continental albedo would have resulted in lower global radiation receipts, hence lower temperature, and a more favorable environment for ice-sheet growth. Clearly, at some point, other factors (such as precipitation starvation, bedrock depression, and mass losses through calving) must have come into play as the ice sheet grew in size to reverse this trend toward increasing glacierization of the planet (MacAyeal, 1993; Clark et al., 1999).

Changes in atmospheric CO_2 concentration also may induce positive feedbacks. As CO_2 levels increase, there will be an increase in the absorption of longwave (infrared) terrestrial radiation by CO_2; concomitantly, there will be an increase in longwave absorption by water vapor, resulting from enhanced Earth surface and atmospheric infrared emissions. Lower tropospheric temperatures will thus increase (the "greenhouse effect"), though the magnitude of this increase remains difficult to assess, mainly due to the complexities of feedback effects. As atmospheric temperatures increase, the temperature of the upper layers of the ocean will also increase, causing CO_2 in solution to be released to the atmosphere, thereby reinforcing the trend toward higher temperatures. This (rather simplistic) example of a physical-biochemical feedback is sometimes referred to as a "runaway greenhouse effect." However, the prospect that such an eventuality will occur due to the anthropogenic production of excess CO_2 from fossil fuel combustion is unlikely. As temperatures increase, there would be more evaporation from the oceans, increased cloudiness (higher global albedo), and hence a decrease in solar energy to the system. In addition, higher temperatures at high latitudes, associated with increased poleward advection of moisture, might be accompanied by more snowfall, resulting in higher continental albedo (and/or a shorter snow-free period) and hence lower overall global energy receipts. Such mechanisms are examples of negative feedbacks, whereby the system tends to become stabilized after an initial perturbation. Determining the relative importance of positive and negative feedbacks is critical, in order to quantify the role of forcing factors in past (and future) climate changes.

Interactions between different parts of the climate system that are brought about by a process within the system are considered *internal* mechanisms of climatic variation. They involve initiation by a factor within the climate system, such as the upwelling of cool deep-ocean water or an unusually persistent snow cover over an extensive area of the land surface, which may be amplified by other components of the climate system and eventually lead to an adjustment in the atmospheric circulation. These adjustments within the climate system may in turn alter, and perhaps eliminate, the original factor that initiated the climatic variation. Generally, such mechanisms are stochastic in nature, so that the climatic consequences are not predictable over timescales much longer than the timescale of the initiating process. By contrast, there are factors *external* to the climate system that may bring about (force) adjustments in climate, but those changes have no influence on the initiating factor (Mitchell, 1976). Changes in solar output and/or spectral characteristics, changes in the Earth's orbital parameters, and changes in atmospheric turbidity due to explosive volcanic eruptions are examples of external factors that may cause changes in the climate system but that are not affected by those changes (Robock, 1978). Some of these mechanisms of climate variation are deterministic (predictable) since they vary in a known way. This is particularly the case with the Earth's orbital variations, which have been calculated accurately both for periods back in time and into the future (Berger and Loutre, 1991; Berger et al., 1991). There is therefore an element of predictability in the consequent climatic changes, though these may, in turn, depend on the particular internal

conditions of the climate system prevailing at the time of the external forcing. Orbital, solar, and volcanic forcing is considered further in Sections 2.6–2.8.

An important concept that occupies much discussion about future climate changes due to anthropogenic greenhouse gases is the notion of climate sensitivity, *S*. In this context, climate sensitivity is defined as the global mean temperature response to a doubling of CO_2. If climate sensitivity is low, temperatures will not rise very much as CO_2 levels increase; on the other hand, a high sensitivity implies more temperature drastic changes ahead (Knutti and Hegerl, 2008). Different models, used to estimate future temperature changes due to rising levels of greenhouse gases, have different climate sensitivities (due to feedback differences within models), which leads to uncertainty about future temperature changes. In the current generation of models being used in the 5th IPCC assessment, *S* ranges from ~2.0 to 4.4 °C. More generally, climate sensitivity can be considered as the equilibrium temperature response to any change in radiative forcing, taking into account all of the feedbacks that may be involved. Several studies have tried to assess the value of *S* using paleoclimatic estimates of global temperature in the past, together with estimates of past changes in radiative forcing (e.g., Köhler et al., 2010; Rohling et al., 2012; Schmittner et al., 2011; PALAEOSENS Project Members, 2012). Paleoclimate studies implicitly take into account phenomena that take a long time to come into equilibrium, such as changes in ice-sheet volume or deep-ocean temperatures (slow feedbacks that take far longer to come into equilibrium than the timescale of the initial forcing), as well as phenomena that respond more rapidly (fast feedbacks) (Figure 2.7). Particular attention has been paid to estimating climate sensitivity by using paleoclimate data for the last glacial maximum, when CO_2 levels were ~180 ppmv, versus 280 ppmv in preindustrial

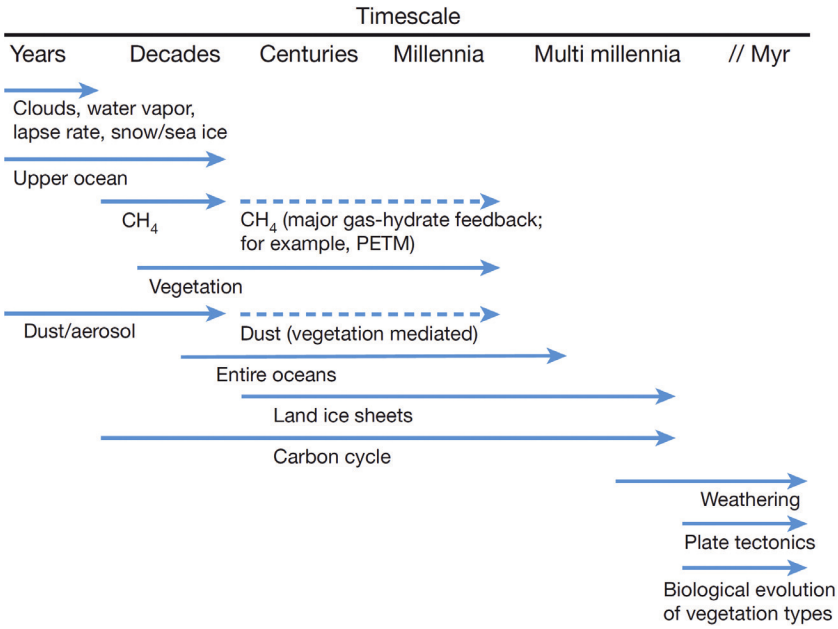


FIGURE 2.7 Timescales of different feedbacks that are relevant to estimating equilibrium climate sensitivity. *From PALAEOSENS (2013).*

times, and ~400 ppmv in 2014. However, there is much uncertainty about just how much colder globally averaged temperatures were at the LGM, since paleotemperature estimates are limited geographically. Furthermore, the feedbacks in the system depend to some extent on the "climate state"—and LGM conditions, with extensive terrestrial ice sheets, much more sea ice, large amounts of aerosols in the atmosphere, etc., were far from similar to modern climate boundary conditions (Crucifix, 2006; Yoshimori et al., 2011). Nevertheless, most estimates of climate sensitivity based on paleodata fall within the IPCC range, generally around 2-3 °C, and they tend to rule out the possibility of much larger sensitivity values, which would have resulted in much greater changes in past climate than were observed.

2.4 ENERGY BALANCE OF THE EARTH AND ITS ATMOSPHERE

As the Earth sweeps through space on its annual revolution around the Sun, it intercepts a minute fraction of the energy emitted by this all-important star. Because the Earth is (approximately) spherical and rotates on an axis inclined (at present) 23.4° to the plane across which it moves around the Sun (the ecliptic), energy receipts vary greatly from one part of the globe to another. Furthermore, the pattern of energy receipts is constantly changing. These differential energy receipts are the fundamental driving force of the atmospheric circulation. If solar output is assumed to be invariant, the spatial and temporal patterns of energy receipts impinging on the outer atmosphere can be calculated (Figure 2.8; Newell and Chiu, 1981). However, for conditions near the surface of the Earth, the role of the atmosphere must be considered, since the atmosphere greatly diminishes potential solar radiation receipts. Estimating how the energy received then cascades through the atmosphere is complex and requires both surface-based and satellite-based observational data, as well as model simulations. The best current estimates are given in Figure 2.9, but each component has some uncertainty, as the diagram indicates (Wild et al., 2012). Nevertheless, the broad picture is not in dispute, and this provides some insight into the potentially important factors involved in climatic variations and variability. For the system as a whole, energy receipts at the outer limits of the atmosphere during the course of a year are 340 W m^{-2} (Kopp and Lean, 2011). As radiation penetrates the atmosphere, as a global average, 76 W m^{-2} (22%) is either reflected from cloud tops or scattered upward by molecules and particulate matter in the air. Because the Earth's surface is also reflective, another ~24 W m^{-2} (7%) of incoming solar radiation is returned to space, without heating the atmosphere or the Earth's surface. The overall planetary albedo (reflectivity) is thus ~29% (100 W m^{-2}). A further 79 W m^{-2} (23%) is absorbed by ozone, by water vapor and water droplets in clouds, and by particulates, thereby raising the temperature of the atmosphere. Thus, only ~47% (161 W m^{-2}) of the energy impinging on the outer atmosphere reaches the surface, where it is absorbed, increasing the surface temperature. Energy is reradiated from the Earth's surface at longer wavelengths (terrestrial radiation), much of which is absorbed by water vapor, carbon dioxide, and other trace gases in the atmosphere (the greenhouse effect). The atmosphere is thus warmed further (adding to the shortwave energy it has absorbed) and so emits longwave radiation (both upward and downward). Overall, however, there is a net loss of longwave radiation from the Earth to space via the atmosphere; ~34% of energy absorbed by the Earth's surface (55 W m^{-2}) is lost

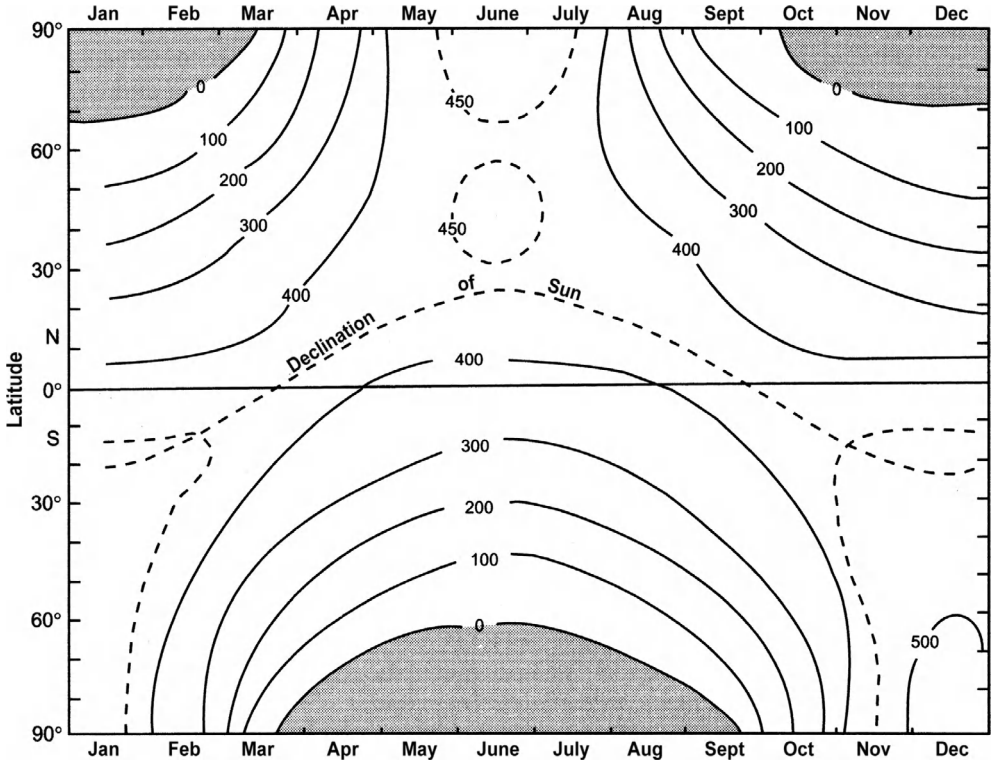


FIGURE 2.8 Distribution of solar radiation at top of atmosphere (in W m^{-2}). Apparent position of Sun overhead at noon (declination) is shown by dotted line.

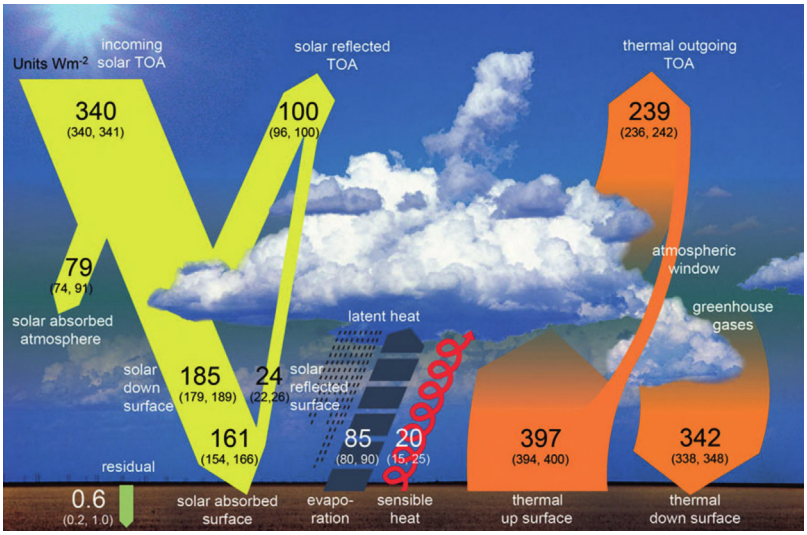


FIGURE 2.9 Schematic diagram of the global average energy balance of the Earth, in W m^{-2}. Uncertainties are given in parentheses. Note that the latest estimate for total solar irradiance during the minimum of the last solar cycle is 1360 W m^{-2}; this value is divided by 4 to obtain the energy distributed across the Earth's (circular) cross-sectional area (i.e., 340 W m^{-2}, as shown here). *From Wild et al. (2012).*

by radiative emissions in this way. The remaining energy at the surface, or net radiation, is transferred to the atmosphere via sensible and latent heat transfers. Sensible heat flux (H) involves the transfer of heat directly from the surface to layers of air immediately adjacent to it by the processes of conduction and convection. Latent heat flux (LE) involves the transfer of heat from the surface via the evaporation of water; as water evaporates from the surface, latent heat is extracted, only to be released to the atmosphere later when the water condenses. This is the most important mechanism by which energy is transferred from the Earth to the atmosphere, accounting for ~80% (85 W m^{-2}) of the net radiation at the Earth's surface (Figure 2.9). The relative importance of sensible and latent heat mechanisms in the transfer of heat from the Earth's surface is sometimes characterized by the Bowen ratio (H/LE); high values (≥ 10) are typical of desert areas where values of latent heat flux are very low, whereas low Bowen ratios (≤ 1) are typical of oceanic areas where most energy is transferred through the evaporation of water.

The global mean values for the energy balance provide a basis for appreciating the importance of a number of parameters in the climate system. Consider, for example, the role of cloudiness in global energy receipts. On a global scale, ~22% of all energy entering the atmosphere is reflected by cloud tops, because of their extremely high albedo. Clouds also absorb longwave energy emitted from the Earth's surface. Small variations in global cloud cover, or even of cloud type, may thus have very large consequences for the global energy balance, yet in the paleoclimatic record, we have few clues as to how cloudiness may have varied through time on a global scale (Bradley et al., 1993). At the Earth's surface, albedo is of particular significance, though this is more apparent when zonal (latitude band) averages are considered (Figure 2.10). The

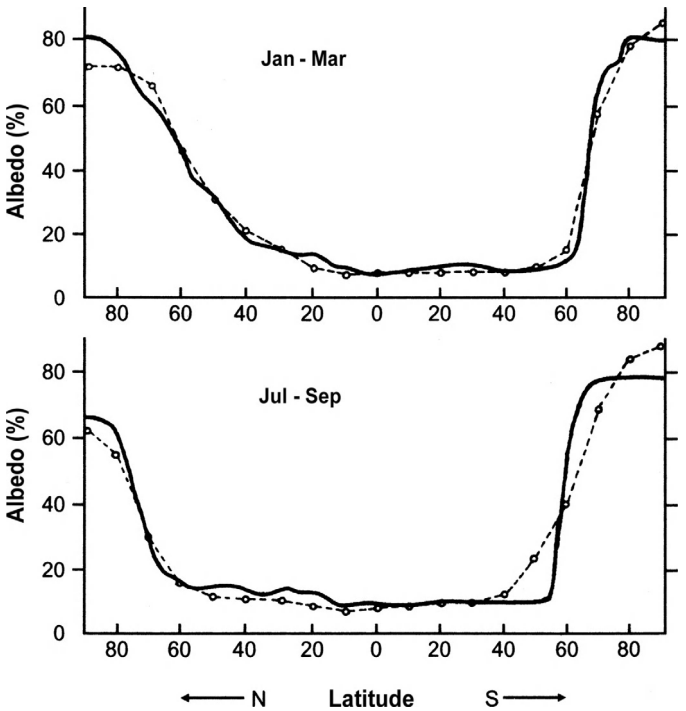


FIGURE 2.10 Latitudinal distribution of seasonal average surface albedo (averaging around latitude bands, i.e., zonally). ———, estimates by Kukla and Robinson (1980); -----, estimates by Hummel and Reck (1979). *After Kukla and Robinson (1980).*

distribution of snow and ice dominates this pattern (cf. Figure 2.6) and is largely responsible for the large energy deficits at high latitudes (i.e., higher radiative losses than gains, accommodated by energy transfers from low latitudes). It is only during the last 35 years that satellites have provided a global perspective on snow- and ice-cover variations, both seasonally and interannually. Although the records are quite short, it is clear that variations in snow and ice extent from year to year can alter area-weighted hemispheric surface albedo by 3-4%, which may influence atmospheric circulation in subsequent seasons, providing a positive feedback to the system (Groisman et al., 1994a,b). Over longer time periods, changes in surface albedo have been very large, and their effects on albedo must have been profound. Not only did continental ice sheets and more extensive sea ice (Table 2.5) increase global albedo, but also the more extensive deserts and savanna grasslands at the time of glacial maxima would have accentuated this effect.

The significance of atmospheric CO_2 and water vapor is also apparent from Figure 2.9; these gases play a vital role in the global energy balance because of their relative opacity to terrestrial radiation. An increase in CO_2 would reinforce this energy exchange, increasing atmospheric temperatures. However, many other interactions and consequences would also ensue, and it is this complexity that makes forecasts of the climatic impact of CO_2 increases so difficult (Meehl et al., 2007).

This thumbnail sketch of the radiation balance of the Earth-atmosphere system is very much a simplification of reality. Most importantly, there are large regional differences in values of net radiation and of latent and sensible heat flux due to the geography of the Earth (distribution of continents and oceans, surface relief, vegetation, and snow cover) and the basic climatic differences from one region to another (principally variations in cloud cover and type) (Budyko, 1978). This is readily apparent from a consideration of annual energy balance components for the Earth's surface, shown as zonal averages in Table 2.6 and mapped in Figures 2.11–2.13. Net radiation varies from $\sim$30 W m^{-2} at high latitudes to $\sim$170 W m^{-2} over parts of the tropical and equatorial oceans (Figure 2.11). On the continents, net radiation is lower than the zonal average due to higher albedo of the surface (e.g., in desert regions) or because of higher cloud amounts that reduce surface radiation receipts (Table 2.6). For the Earth as a whole (Table 2.6, bottom line), 84% of net radiation is accounted for by latent

TABLE 2.5 Maximum Extent of Land-Based Ice Sheets During the Pleistocene

	Area ($\times 10^6$ km^2)
North America	16.22
Greenland	2.30
Europe	7.21
Asia	3.95
South America	0.87
Australasia	0.03
Antarctica	13.81

Note that not all areas experienced maximum ice cover at the same time during the Pleistocene. It is therefore not appropriate to total these values. Also seasonal snow cover and sea-ice extent are not included, so these figures represent minimum changes in the area of the overall cryosphere (cf. Tables 2.3 and 2.4).
After Flint (1971) and Hollin and Schilling (1981).

TABLE 2.6 Mean Latitudinal Values of the Heat Balance Components of the Earth's Surface (W m^{-2})

Latitude	Land			Ocean				Earth			
	R	LE	P	R	LE	P	F_0	R	LE	P	F_0
70-60°N	29	21	8	30	41	29	−40	29	27	15	−12
60-50°N	42	30	12	57	62	25	−31	49	44	17	−12
50-40°N	60	33	27	85	89	21	−25	72	60	24	−12
40-30°N	77	31	46	119	127	19	−27	101	86	31	−16
30-20°N	85	25	60	147	145	9	−7	125	100	28	−3
20-10°N	98	42	56	161	155	97	−4	145	126	21	−3
10-0°N	105	76	29	165	138	9	17	151	123	13	15
0-10°S	105	81	24	169	131	8	29	154	119	12	23
10-20°S	100	60	40	162	150	12	0	149	130	19	0
20-30°S	94	37	57	145	141	15	−11	133	117	24	−8
30-40°S	82	38	44	122	109	15	−1	117	101	19	−3
40-50°S	58	29	29	96	68	8	20	94	66	9	19
50-60°S	46	29	17	61	46	12	3	61	46	12	3
Entire Earth	66	36	30	121	109	12	0	105	88	17	0

R is the radiative flux of heat (radiation balance of the Earth's surface) equal to the difference of absorbed shortwave radiation and the net longwave radiation outgoing from the Earth's surface; *LE* is the heat expenditure for evaporation (*L* is the latent heat of vaporization and *E* is the rate of evaporation); *P* is the turbulent flux of heat between the Earth's surface and the atmosphere; F_0 is the heat income resulting from heat exchange through the sides of the vertical column of a unit section going through the Earth's surface with the ambient layers. Values for the Earth as a whole are slightly different from the most recent estimates of Wild et al. (2012) shown in Figure 2.8, which give values for *R* of 106 W m^{-2} and for *LE* of 85 W m^{-2}, but the values here are well within the uncertainties provided by Wild et al. (2012). Estimates for smaller geographical regions are more difficult, but the values in this table are likely to be correct within ±10%.
From Budyko (1978).

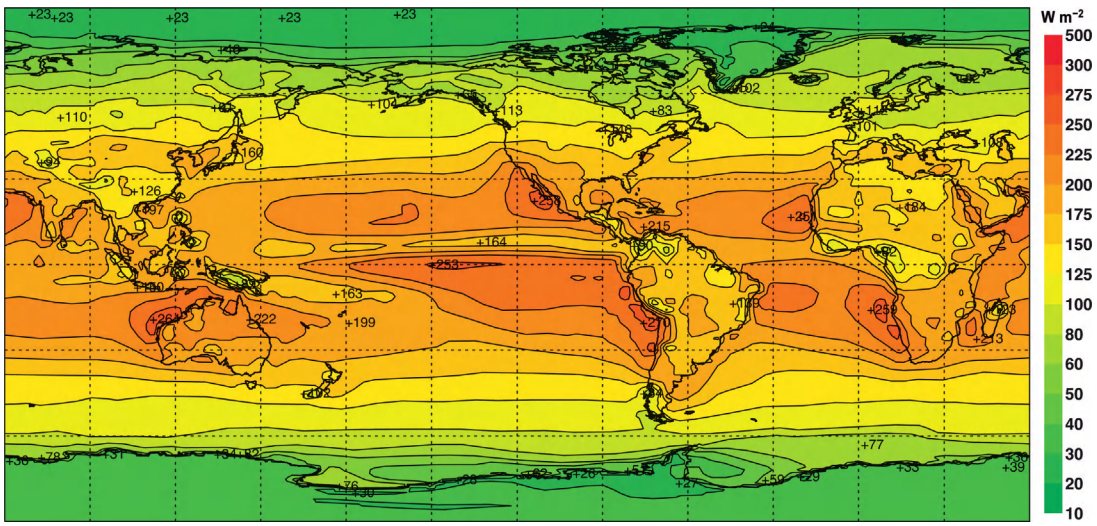


FIGURE 2.11 Global distribution of annual net shortwave radiation (R_n) at the Earth's surface. Values generally increase from the polar regions to the equatorial zone, but cloudy regions (such as the intertropical convergence zone and the Amazon Basin) have lower values. *From the European Centre for Medium Range Weather Forecasting, ERA-40 Atlas.*

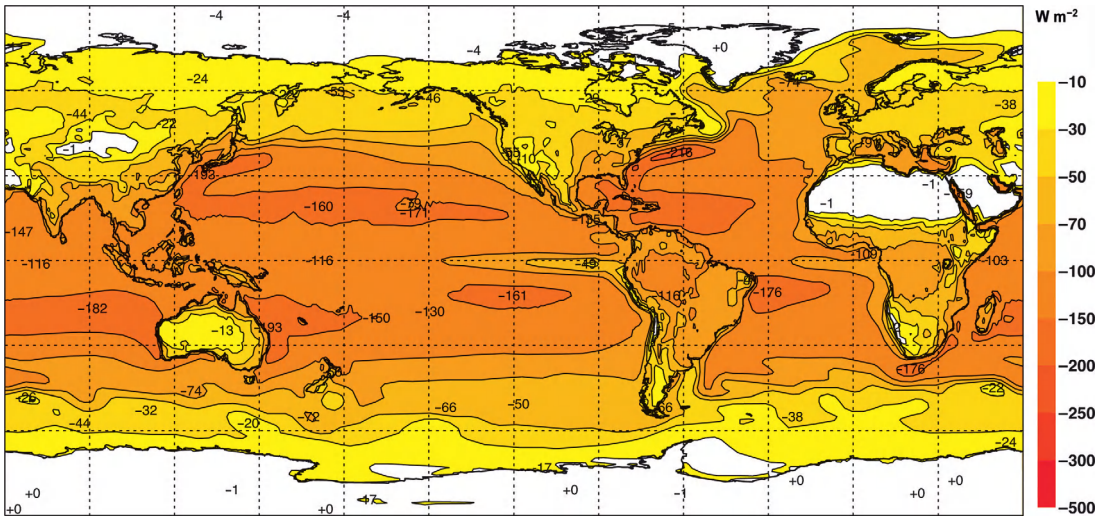


FIGURE 2.12 Global annual distribution of latent heat flux at the Earth's surface (W m^{-2}). Negative values indicate that the flux of energy is from the surface to the atmosphere. The maximum latent heat flux (greatest negative values) is in oceanic regions of the subtropics. *From the European Centre for Medium Range Weather Forecasting, ERA-40 Atlas.*

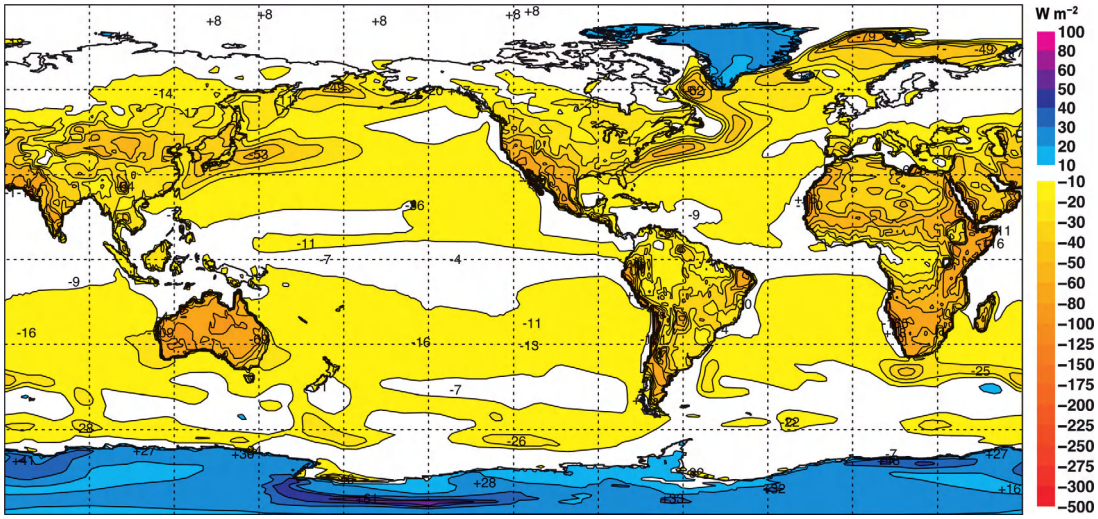


FIGURE 2.13 Global annual distribution of sensible heat flux at the Earth's surface (W m^{-2}). Negative values indicate that the flux of energy is from the surface to the atmosphere. The maximum sensible heat flux from the Earth to the atmosphere (greatest negative values) is associated with the major desert regions. Positive values indicate that heat is transferred from the atmosphere to the Earth's surface (principally in the Arctic and Antarctic). *From the European Centre for Medium Range Weather Forecasting, ERA-40 Atlas.*

TABLE 2.7 Energy Balance for Different Surfaces (W m^{-2})

	R	L	H	a	H/L
Tropical rainforest	110	85	25	13	0.3
Savanna	65	40	25	33	0.6
Desert	70	8	62	46	8.0

After Baumgartner (1979).

heat expenditures (88 of 105 W m^{-2}) (or 80% according to the revised estimates of Wild et al., 2012, discussed earlier). However, if we just consider the oceans, 90% of net radiation (109 of 121 W m^{-2}) is utilized in evaporation compared to only 55% on the continents. In fact, in extremely arid areas, latent heat transfer may account for <20% of the net radiation (cf. Figures 2.11 and 2.12). In those areas, sensible heat flux is of primary importance (Figure 2.13). For the continents as a whole, 45% of net radiation is utilized in sensible heat transfers. Over the oceans, sensible heat flux is only important at high northern latitudes where northward-flowing currents bring warm water into contact with cold polar air masses (Figure 2.13). Ocean currents themselves play a very important role in energy transport, as is clear from column 8 in Table 2.6. "Excess" heat is transferred from equatorial and tropical regions to higher latitudes where the energy thereby made available may even exceed net radiation at the surface (e.g., 60-70°N; cf. Figures 2.11 and 2.13).

From this overview of the energy balance of different regions, it is only a short step to consider how components of the energy balance of some areas may have varied in the past and how human activities may affect the energy balance of some areas in the future. Of course, it will only be possible to do this in a crude way since the energy balance of any one site is a function of a great many variables, including parts of the climate system far from the site in question. Nevertheless, some general points can be made. Consider, for example, the vast Saharan Desert region. At the present time, net radiation in this area averages ~70 W m^{-2} with a Bowen ratio of ~8 (Table 2.7; Baumgartner, 1979). During the early to mid-Holocene, the area was wetter and supported a sparse grassland vegetation cover, increasing to savanna along the Sahelian margin to the south (Hoelzmann et al., 2004; Lézine et al., 2011); if modern analogues are any guide, the area would have had a lower albedo, higher net radiation, and much lower Bowen ratio. Other desert regions also experienced similar changes in vegetation and hence in energy balance (though changes elsewhere were commonly greatest at the last glacial maximum). As deserts and semideserts today occupy more than 10% of the continental area, such changes had major consequences for the energy balance of the world as a whole. It also seems likely that overgrazing and desertification of marginal environments today, as well as the destruction of tropical forest ecosystems, will bring about marked changes in the energy balance of low latitudes, with possible global consequences.

2.5 TIMESCALES OF CLIMATIC VARIATION

Climate varies on all timescales and space scales, from interannual climatic variability to very long-period variations related to the evolution of the atmosphere and changes in the lithosphere. Examples of known climatic fluctuations are shown in Figure 2.14. In this diagram,

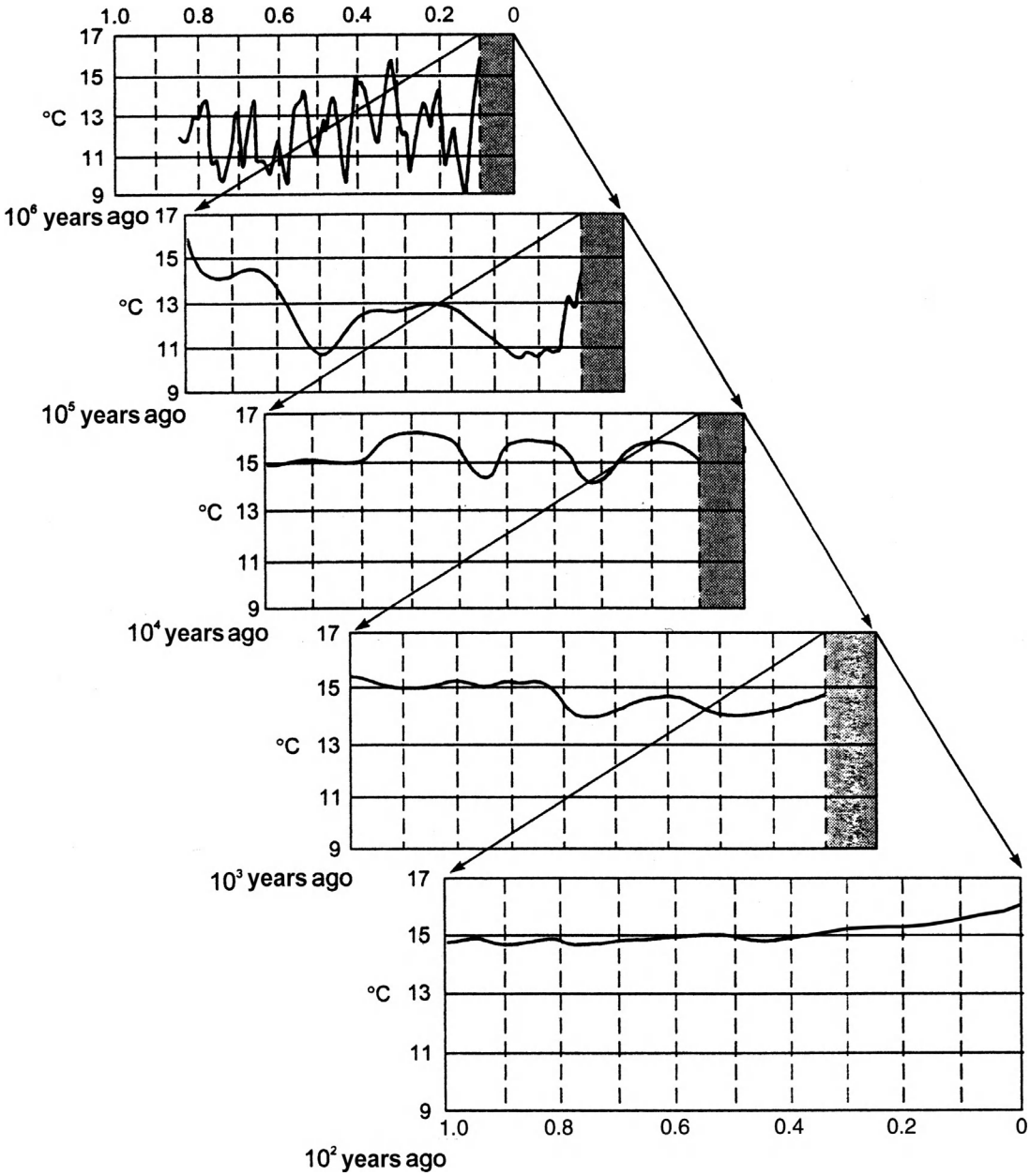


FIGURE 2.14 Schematic diagram illustrating climatic fluctuations at timescales ranging from decadal (the last 100 years, lowest panel) to centennial (the last 1000 years, second panel) to millennial (the last 10,000 years), to the last million years (top panel). Each successive panel, from the back to the front, is an expanded version (expanded by a factor of 10) of one-tenth of the previous column. Thus, higher-frequency climatic variations are "nested" within lower-frequency changes. Note that the temperature scale (representing global mean annual temperature) is the same on all panels. This demonstrates that temperature changes over the last 100 years (lower panel) have been minor compared to changes over long periods of time. Such changes have occurred throughout history, but they are lost in the noise of the longer-term climatic record; only the larger amplitude changes are detectable as we look far back in time.

each row represents an expansion, by a factor of 10, of each interval on the row above it. Thus, one can envisage short-term (high-frequency) variations nested within long-term (lower-frequency) variations (Webb, 1991). However, in the paleoclimatic record, as we delve further and further back in time, it is increasingly difficult to resolve the higher-frequency variations, though in some circumstances, brief snapshots of conditions in the past may be revealed at high resolution (e.g., Tudhope et al., 2001). As climatic variations on the timescale of years to decades are of the utmost importance to modern society, increasing attention must be focused on paleoclimatic data pertinent to this problem (Bradley and Jones, 1992a).

Climatic fluctuations on different timescales may be brought about by internal or external mechanisms, which operate at different frequencies (Figure 2.15). Changes in the Earth's orbital parameters, for example, are likely candidates for climatic variations on the timescale of glacials and interglacials during the late Quaternary but cannot account for the multidecadal climatic variations that have occurred over the last thousand years. For fluctuations on that timescale, other factors such as volcanic dust loading of the atmosphere, solar variability, or internal adjustments between different subsystems in the climate system are more likely to be involved (Jones et al., 1996). Of course, different forcing factors may have operated together causing climatic fluctuations of varying magnitude at different times in the past, though individual factors may account for the variance of climate at a particular frequency. Mitchell (1976) pointed out that much of the variance of the climate record results from stochastic processes internal to the climate system. This includes short-period atmospheric processes (e.g., turbulence) with time constants on the scale of minutes or hours, to slower-acting processes or feedback mechanisms

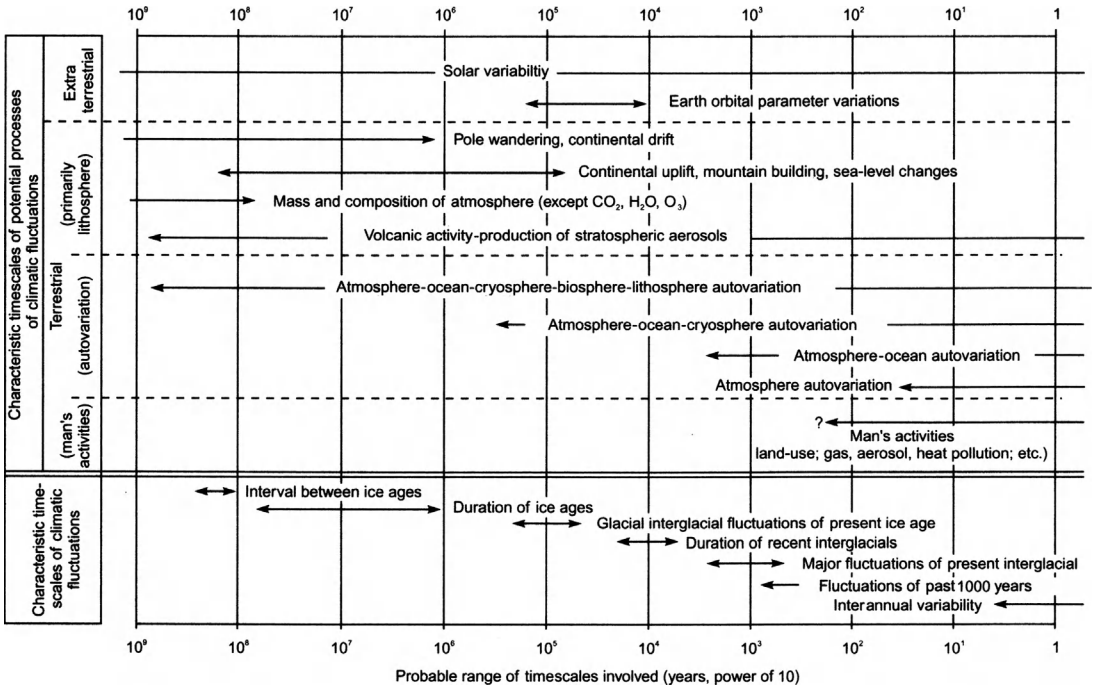


FIGURE 2.15 Examples of potential processes involved in climatic fluctuations and their characteristic timescales (Kutzbach, 1974).

that add to climatic variance over longer timescales. However, these factors only contribute white noise to the climate spectrum on timescales longer than the timescale of the process in question (i.e., they contribute to the variance of climate in a random, unpredictable manner, with no effects concentrated at a particular frequency). Superimposed on this background noise are certain peaks in the variance spectrum of climate that correspond to external forcing mechanisms operating over a restricted time domain (i.e., they are periodic or quasiperiodic phenomena). Such temporal variability may be associated with characteristic *spatial* variability (Mann et al., 1996). For example, ENSO (El Niño-Southern Oscillation) events recur on timescales of 3-7 years and have distinct spatial anomaly patterns (Diaz and Kiladis, 1992).

Deterministic forcing mechanisms are only known to operate at a few relatively narrow frequencies, and although very important to climatic variance at those frequencies, their contribution to overall climatic variation is minor compared to the role of stochastic processes. This presents problems for both climatic predictability and the interpretation of past climatic changes (as seen in the paleoclimatic record) in terms of particular causative factors (Mitchell, 1976). Nevertheless, certain external forcing mechanisms have often been called upon to account for features of the paleoclimatic record. The most important of these for climatic fluctuations in the Quaternary period are variations in the Earth's orbital parameters that are the underlying cause of glacial-interglacial cycles over at least the last million years (Berger and Loutre, 1991). This is discussed further in the next section and in Chapter 6, Section 6.3.3.

2.6 VARIATIONS OF THE EARTH'S ORBITAL PARAMETERS

Although it has been known for over 2000 years that the position and orientation of the Earth relative to the Sun have not been constant, it was not until the mid-nineteenth century that the significance of such variations for the Earth's climate was really appreciated. At that time, James Croll, a Scottish natural historian, developed a hypothesis in which the ultimate cause of glaciations in the past was considered to be changes in the Earth's orbital parameters (orbital forcing) (Croll, 1867a,b, 1875). The hypothesis was elaborated upon by Milankovitch (1941) and later by Berger (1977a, 1978, 1979, 1988) and Laskar et al. (1993). An excellent account of the way in which this hypothesis developed into a crucial theory in paleoclimatology (the astronomical or Milankovitch theory) is given by Imbrie and Imbrie (1979).

The basic elements of the Earth's orbital motion around the Sun today are as follows: The Earth moves in a slightly elliptical path during its annual revolution around the Sun; because of the elliptical path, the Earth is closest to the Sun (perihelion) around January 3, and around July 5, it is farthest away from the Sun (aphelion). As a result, at perihelion, the Earth receives ~3.5% more solar radiation than the annual mean (outside the atmosphere) and ~3.5% less at aphelion. The Earth is also tilted on its rotational axis 23.4° from a plane perpendicular to the plane of the ecliptic (the apparent surface over which it moves during its revolution around the Sun). None of these factors have remained constant through time due to gravitational effects of the Sun, Moon, and the other planets on the Earth. Variations have occurred in the degree of orbital eccentricity around the Sun, in the axial tilt (obliquity) of the Earth from the plane of the ecliptic, and in the timing of the perihelion with respect to seasons on the Earth (precession of the equinoxes) (Figure 2.16).

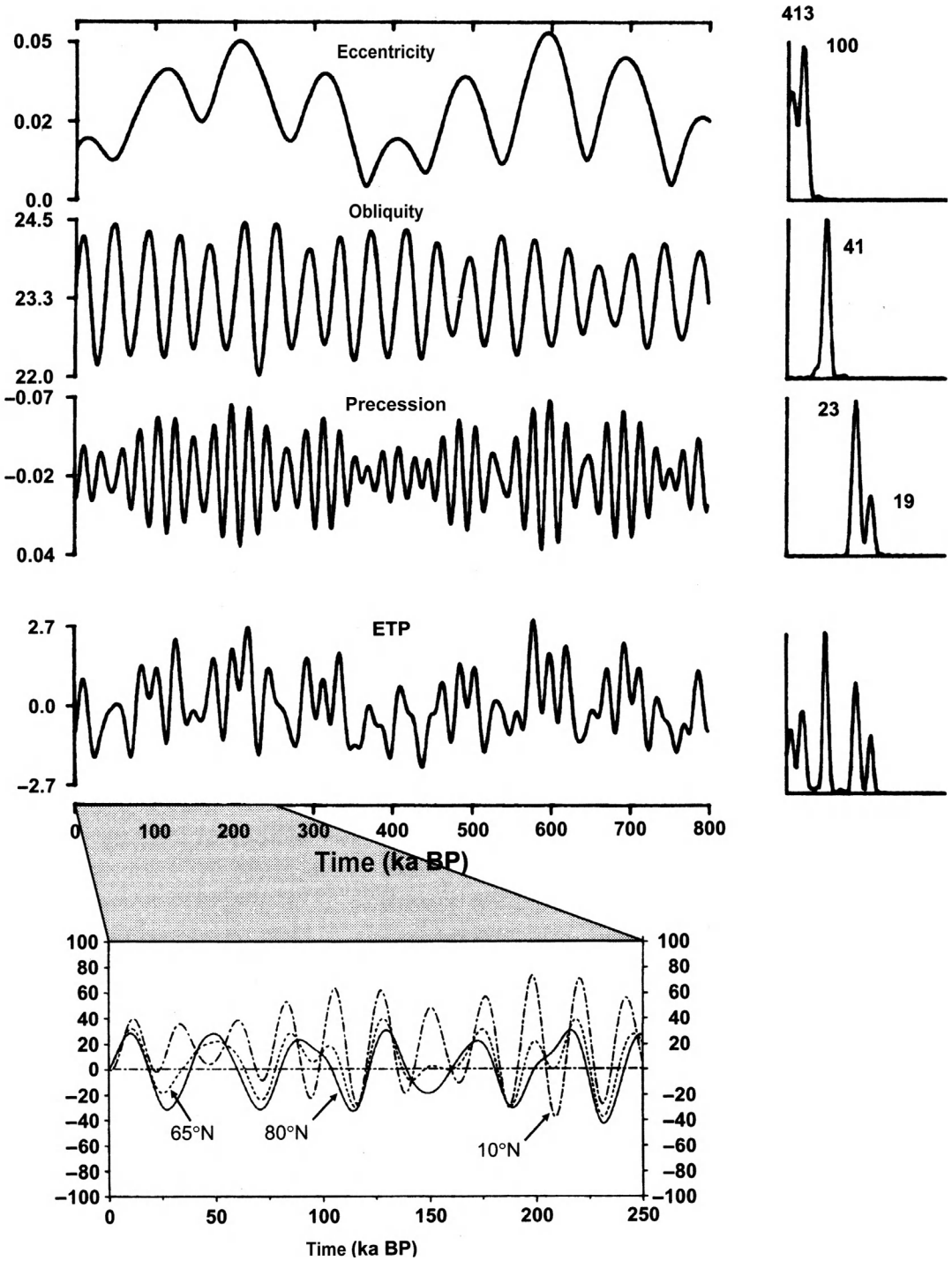


FIGURE 2.16 Variations of eccentricity, tilt (obliquity), precession, and the combination of all three factors (ETP) over the last 800,000 years with their principal periodic characteristics indicated by the power spectrum to the right of each time series (upper diagram). Below is the time series of July solar radiation anomalies at 10, 65, and 80°N (expressed as departures from 1950 AD values). Note that the insolation anomaly signal at high latitudes is dominated by the 41,000-year obliquity cycle, whereas at lower latitudes, the 23,000 precessional cycle is more significant. *After Imbrie et al. (1993a); lower diagram: data from Berger and Loutre (1991).*

Variations in orbital eccentricity are quasiperiodic with an average period length of ~95,800 years over the past 5 million years. The orbit has varied from almost circular (thus, essentially no difference between perihelion and aphelion) to maximum eccentricity when solar radiation receipts (outside the atmosphere) varied by ~30% between aphelion and perihelion (e.g., at ~210,000 years BP; Figure 2.16). Eccentricity variations thus affect the relative intensities of the seasons, which implies an opposite effect in each hemisphere.

Changes in axial tilt are periodic with a mean period of 41,000 years. The angle of inclination has varied from 21.8° to 24.4° with the most recent maximum occurring about 100,000 years ago (Figure 2.16). The angle defines the latitudes of the polar circles (Arctic and Antarctic) and the Tropics of Cancer and Capricorn, which in turn delimit the area of day-long polar night in winter and the maximum latitudes reached by the zenith Sun in midsummer in each hemisphere. Changes in obliquity have relatively little effect on radiation receipts at low latitudes, but the effect increases toward the poles. As obliquity increases, summer radiation receipts at high latitudes increase significantly, while winter radiation totals at midlatitudes decline (Figure 2.17). Thus, summer radiation variations over the last 250,000 years for 65° and 80°N (Figure 2.16) mainly vary with the periodic changes in axial tilt. Since the tilt is the same in both hemispheres, changes in obliquity affect radiation receipts in the Southern and Northern Hemispheres equally.

Changes in the seasonal timing of perihelion and aphelion result from a slight wobble in the Earth's axis of rotation as it moves around the Sun (Figure 2.18a). The effect of the wobble (which is independent of variations in axial tilt) is to systematically change the timing of the solstices and equinoxes relative to the extreme positions the Earth occupies on its elliptical path around the Sun (known as *precession of the equinoxes*) (Figure 2.18b). Thus, 11,000 years ago, perihelion occurred when the Northern Hemisphere was tilted toward the Sun

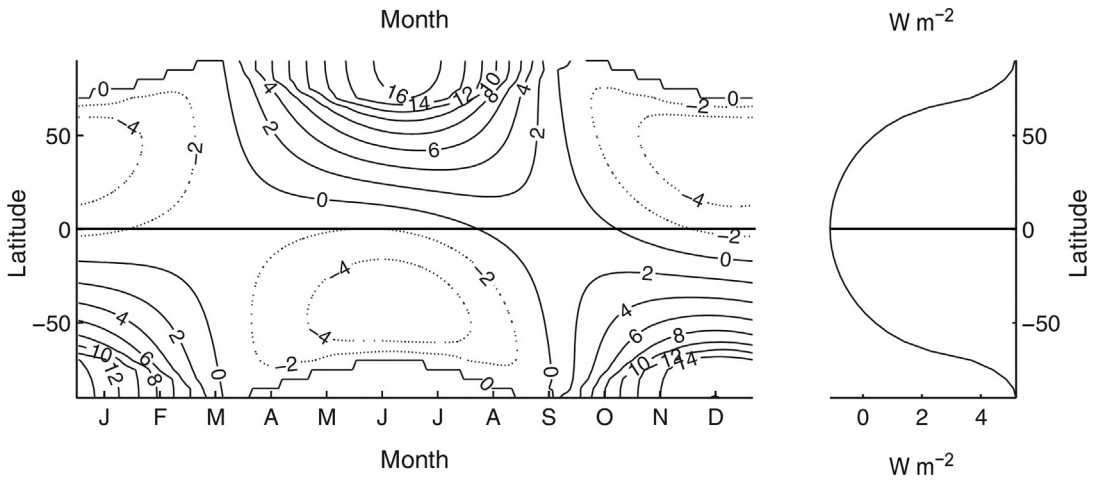


FIGURE 2.17 Insolation averaged during each maxima of obliquity during the last 2 Ma and contoured as an anomaly from average conditions, along with the anomaly in the annual average (right). Negative insolation anomalies are indicated by dotted contours. *From Huybers (2007).*

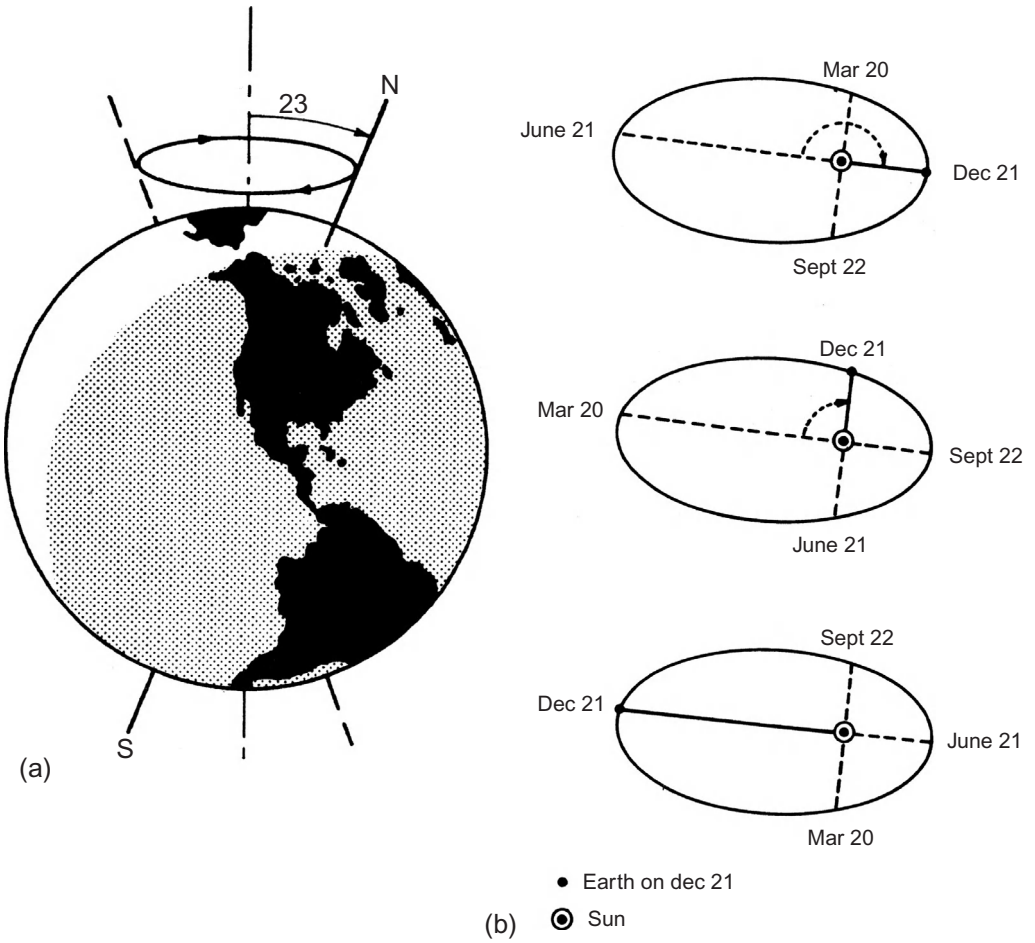


FIGURE 2.18 (a) The Earth wobbles slightly on its axis (due to the gravitational pull of the Sun and Moon on the equatorial bulge of the Earth). In effect, the axis moves slowly around a circular path and completes one revolution every 23,000 years. This results in precession of the equinoxes. This effect is independent of changes in the angle of tilt (obliquity) of the Earth, which changes with a period of ~41,000 years. (b) As a result of the wobble in the Earth's axis, the position of the equinox (March 20 and September 22) and solstice (June 21 and December 21) changes slowly around the Earth's elliptical orbit, with a period of ~23,000 years. Thus, 11,000 years ago, the Earth was at perihelion at the time of the summer solstice, whereas today, the summer solstice coincides with aphelion. *From Imbrie and Imbrie (1979).*

(mid-June) rather than in the Northern Hemisphere's midwinter, as is the case today. Precessional effects are opposite in the Northern and Southern Hemispheres, and the change in precession occurs with a mean period of ~21,700 years (Figure 2.16).

Clearly, the effects of precession of the equinoxes on radiation receipts will be modulated by the variations in eccentricity; when the orbit is near circular, the seasonal timing of perihelion is inconsequential. However, at maximum eccentricity, when differences in solar radiation may amount to 30%, seasonal timing is crucial. The solar radiation receipts of low latitudes are mainly affected by variations in eccentricity and precession of the equinoxes,

whereas higher latitudes are mainly affected by variations in obliquity. Since the eccentricity and precessional effects in each hemisphere are opposite but the obliquity effects are not, there is an asymmetry between the two hemispheres, in terms of the combined orbital effects, which becomes minimal poleward of ~70°. It is also worth emphasizing that the orbital variations do not cause any significant overall (annual) change in solar radiation receipts; they simply result in a seasonal redistribution such that a low summer radiation total is compensated for by a high winter total, and vice versa (Berger, 1980).

It is important to note that the periods mentioned for each orbital parameter (41,000, 95,800, and 21,700 years for obliquity, eccentricity, and precession, respectively) are averages of the principal periodic terms in the equations used to calculate the long-term changes in orbital parameters. For the precessional parameter, for example, the most important terms in the series expansion of the equation correspond to periods of ~23,700 and ~22,400 years; the next three terms are close to ~19,000 years (Berger, 1977b). When the most important terms are averaged, the mean period is 21,700 years, but some paleoclimatic records may be capable of resolving the principal ~19,000- and ~23,000-year periods separately (cf. Hays et al., 1976). Similarly, the mean period of changes in eccentricity is 95,800 years, but it may be possible to detect separate periods of ~95,000 and ~123,000 years in long high-resolution ocean core records corresponding to important terms (or "beats" produced by interactions of important terms) in the equation (cf. Wigley, 1976). Eccentricity also has a longer-term periodicity of 412 ka that has been identified in some marine sedimentary records (Imbrie et al., 1993a). Furthermore, the relative importance of all these periods may have changed over time. For example, the 19 ka precessional and 100 ka eccentricity cycles were more significant prior to ~600 ka BP (Imbrie et al., 1993a). This is one of the enigmas of the paleoclimatic spectrum; during the last 1 million years, the 100 ka period in geological records increased in amplitude, yet over the same interval of time, the main period associated with eccentricity shifted to lower frequencies (~412 ka).

Orbital variations may also have significance for climatic variations on much shorter timescales. Loutre et al. (1992) calculated insolation changes over the last few thousand years, resulting from changes in precession, obliquity, and eccentricity. They found statistically significant periodicities in insolation (at 65°N in July) of 2.67, 3.98, 8.1, 18.6, 29.5, and 40.2 years (cf. Borisenkov et al., 1983, 1985). At other seasons and locations, periodicities of 61, 245, and 830-900 years are significant. These higher-frequency variations are very small in amplitude compared to the orbital changes discussed earlier, but they may nevertheless play some role in modulating climatic variability on the decadal to millennial timescale. Interestingly, some of the periodicities in incoming insolation due to orbital effects are similar to those identified in sunspot data (which may relate to solar irradiance changes) so the cumulative effects may be significant for short-term climate variability. This matter has received relatively little attention so far.

Considered together, the superimposition of variations in eccentricity, obliquity, and precession produces a complex, ever-varying pattern of solar radiation receipts at the outer edge of the Earth's atmosphere. To appreciate the magnitude of these variations and their spatial and temporal patterns, it is common to express the radiation receipts for a particular place and moment in time as a departure (or anomaly) from corresponding seasonal or monthly values in 1950. An example is shown in Figure 2.19 for the month of July at all latitudes (90°N-90°S) from 0 to 200 ka BP (Berger, 1979). Of particular interest are the radiation anomalies at high northern latitudes (60-70°N), which Milankovitch (1941) considered to be critical

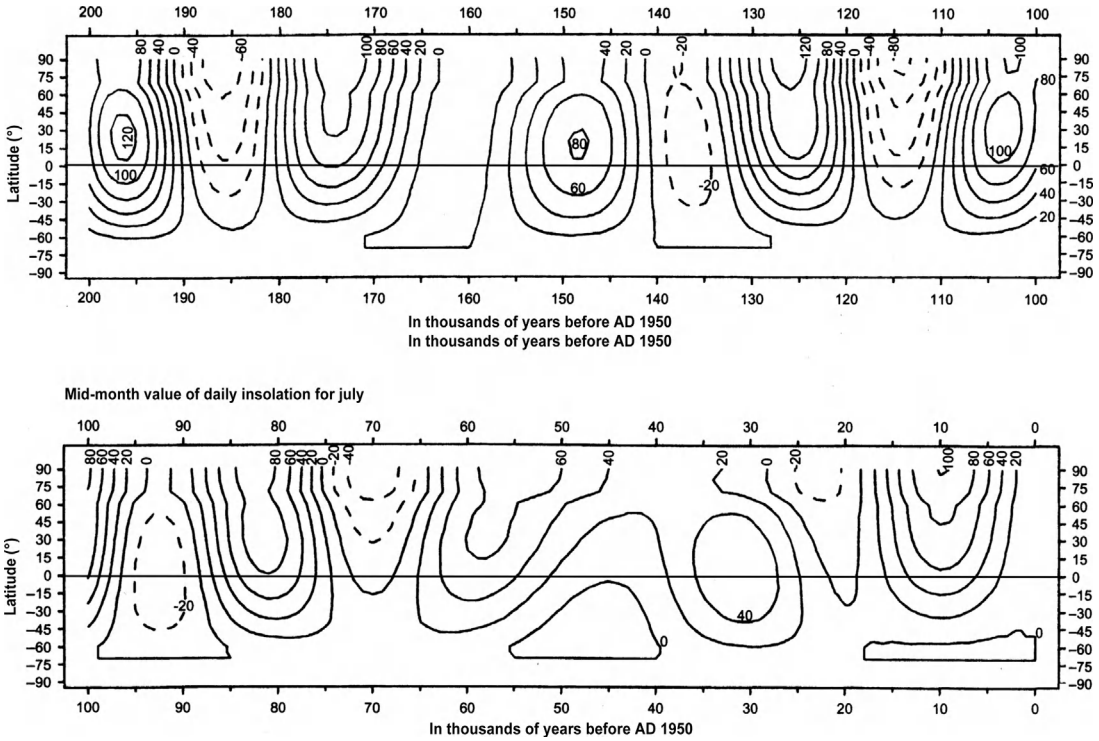


FIGURE 2.19 Long-term deviations of solar radiation from their AD 1950 values. Values were calculated at 10° latitude intervals from 100,000 years BP to the present day (lower diagram) and from 200,000 years BP to 100,000 years BP (upper diagram). Negative departures are shown by dotted lines. Values are given in calories per square centimeter per day. Shaded area denotes areas (south of the Antarctic Circle) that receive no direct solar radiation in July. *After Berger (1979).*

for the growth of continental ice sheets. In this zone, periods of lower summer radiation receipts would have favored the persistence of winter snow into summer months, eventually leading to the persistence of snow cover throughout the year. Such conditions may have occurred at 185, 115, and 70 ka BP (Figure 2.19). At these times, there was the combination of conditions that Milankovitch suggested were most conducive to glaciation—minimum obliquity, relatively high eccentricity, and the Northern Hemisphere summer coinciding with aphelion, the combination of which is sometimes referred to as a "cold orbit" (cf. Figure 2.18b). At the same time, warmer winters (i.e., Northern Hemisphere winters coinciding with perihelion) would have favored increased evaporation from the subtropical oceans, thereby providing abundant moisture for precipitation (snowfall) at higher latitudes. Stronger equator-pole temperature gradients in summer and winter would have resulted in an intensified general circulation and more moisture transported to high latitudes to fuel the growing ice sheets. It is of great interest, therefore, that the analysis of ocean cores points to these periods as being important times of ice growth on the continents (see Chapter 6, Section 6.3.3).

Most of Milankovitch's attention focused on the radiation anomalies in summer and winter months, but it is noteworthy that transitional months appear to be most sensitive to changes in solar radiation receipts and to snow-cover expansion. In particular, autumn months appear to

be especially critical for the buildup of snow in continental interiors (Kukla, 1975a,b). To examine the monthly pattern of solar radiation change through time, Berger (1979) computed month by month values of solar radiation departures from long-term means at 60°N, for the last 500,000 years (e.g., Figure 2.20). From these calculations, it is clear that not only do the monthly departures vary greatly in amplitude but also the seasonal timing of the anomalies may shift very rapidly from one part of the year to another. For example, a large positive anomaly of solar radiation in June and July at ~125 ka BP was replaced by a large negative anomaly in the same month by 120 ka BP. Such features of the record have been termed insolation signatures (Berger, 1979) and are considered to be characteristic of a change from a relatively warm climate phase to a cooler one. During the last 500,000 years, such signatures are observed centered at 486, 465, 410, 335, 315, 290, 243, 220, 199, 127, 105, and 84 ka BP, all periods that coincide remarkably well with geological evidence of rapidly deteriorating climatic conditions.

It is important to recognize that although the zone centered on 65°N may be of great importance in the actual mechanism of continental ice growth, a more fundamental control on glaciation is the atmospheric circulation that is largely a function of the equator-pole temperature gradients at different times of the year (stronger radiation gradients produce stronger temperature gradients). When radiation gradients are strong, a more vigorous atmospheric circulation can be expected; subtropical high-pressure systems would tend to be displaced to lower latitudes (cf. Figure 2.5), and a more intense circumpolar westerly flow would develop, leading to increased moisture flux to high latitudes. Weaker radiation gradients imply that the major axis of subtropical high-pressure cells would be displaced poleward, and a more sluggish westerly circulation would lead to a reduction in moisture flux to the continents at high latitudes. It is of interest, therefore, that the stronger summer and winter radiation gradients (resulting mainly from anomalously low radiation receipts at high latitudes) occurred during periods of major ice growth (e.g., 72,000 and 115,000 years BP). By contrast, periods of deglaciation or interglacials correspond to weaker latitudinal radiation gradients, mainly resulting from higher radiation receipts, particularly at high latitudes (Figure 2.21). Thus, the resulting circulation intensities amplify the overall anomaly, be it positive or negative (Young and Bradley, 1984). It is also noteworthy that the insolation gradient varies with a 41 ka periodicity, which is the dominant periodicity from ~3 to 0.8 Ma BP (Raymo and Nisancioglu, 2003).

Finally, it must be recognized that the insolation changes calculated by Berger and others are for solar radiation *entering* the atmosphere (often stated as radiation at the top, or outside, the atmosphere). However, radiation passing through the atmosphere is reflected and absorbed differently from one region to another (depending to a large extent on the type and amount of cloud cover). Furthermore, surface albedo conditions also determine how much of the radiation reaching the surface will be absorbed (cf. Figure 2.9). Such factors can minimize the significance of certain orbital frequencies. For example, Figure 2.22 shows that the radiation gradient from 30 to 70°N in mid-July over the last 200 ka had a strong ~40 ka periodicity in extraterrestrial radiation (cf. Raymo and Nisancioglu, 2003). However, because of differential effects on radiation attenuation in the atmosphere and latitudinal differences in surface albedo, the high-latitude obliquity signal is reduced, leading to a dominant ~23 ka period in the latitudinal gradient of *absorbed* radiation (Berger, 1988; Tricot and Berger, 1988).

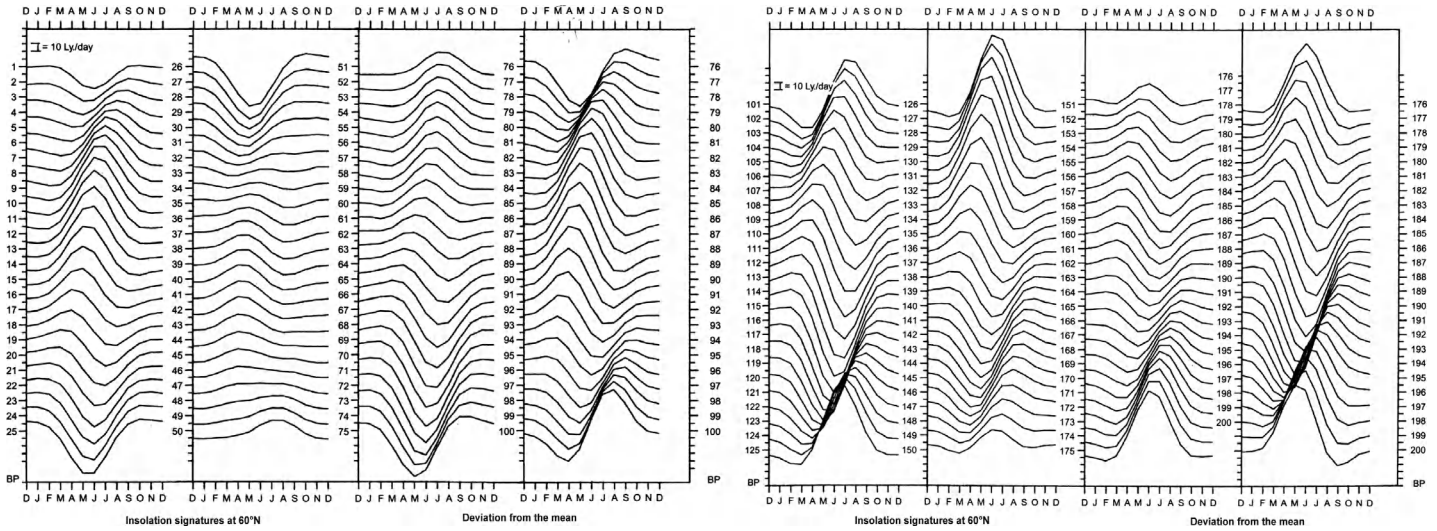


FIGURE 2.20 "Insolation signatures" at 60°N from 200,000 years BP (bottom right) to the present (top left). Each line shows the annual cycle of deviations from mean midmonthly insolation for the last 500,000 years. Vertical scale in upper left corner (langleys (calories cm^2) per day). Periods when large positive summer solar radiation anomalies change to large negative anomalies (insolation signatures) correspond to times when the climate changed from warm to cool. *From Berger (1979).*

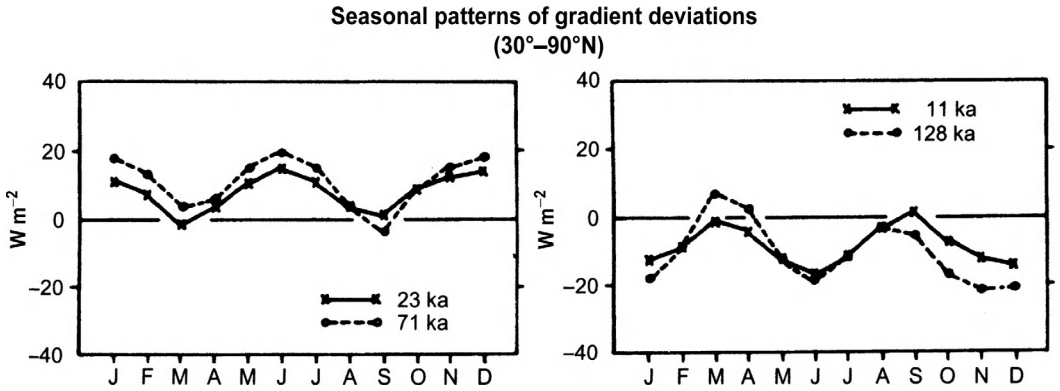


FIGURE 2.21 Variations in insolation gradients (monthly) expressed as departures from the last 150,000 years' averages for selected time periods. Periods of maximum ice growth (e.g., at 71,000 and 23,000 years BP) correspond to periods of stronger than average insolation gradients in all months (left-hand diagram). Times of rapid ice decay (e.g., 128,000 and 11,000 years BP) correspond to generally weaker than average gradients (right-hand diagram). Gradients calculated for Northern Hemisphere (30-90°N). *After Young and Bradley (1984).*

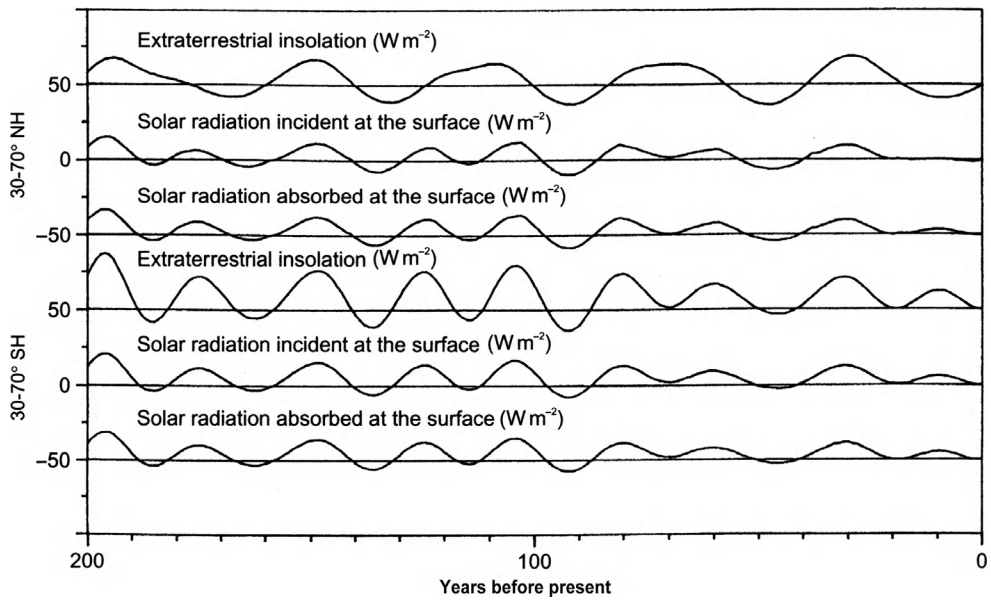


FIGURE 2.22 The gradient (from 30 to 70°N) of incoming solar radiation in mid-July over the last 200 ka (top) compared to the modeled gradient of radiation reaching the surface (middle) and of the gradient of radiation absorbed at the surface (bottom). Because of differential absorption and reflection with latitude, the dominant periodicity of radiation absorbed at the surface shifts from that of obliquity to that of precession, which is more characteristic of a lower latitude influence on the gradient. *From Tricot and Berger (1988).*

The Milankovitch theory of climatic change has tremendous implications for Quaternary paleoclimatology, but there was little reliably dated field evidence to support or refute the idea until the mid-1970s when Hays et al. (1976) identified the main frequencies of orbital forcing in a sediment core from the Indian Ocean. Since then, many studies have demonstrated that variations in the Earth's orbital parameters are indeed fundamental factors in glacial-interglacial cycles and the growth and decay of continental ice sheets (e.g., Broecker et al., 1968; Mesolella et al. 1969; Imbrie et al., 1992, 1993a,b; Petit et al., 1999; Pollard and DeConto, 2005; Ruddiman, 2006; Jouzel et al., 2007b; DeConto et al., 2008). This evidence is discussed in more detail in Chapter 6, Section 6.3.3, but the major issues are summarized here in Figure 2.23. Variations of incoming June solar radiation at 65°N are broken down into their component parts

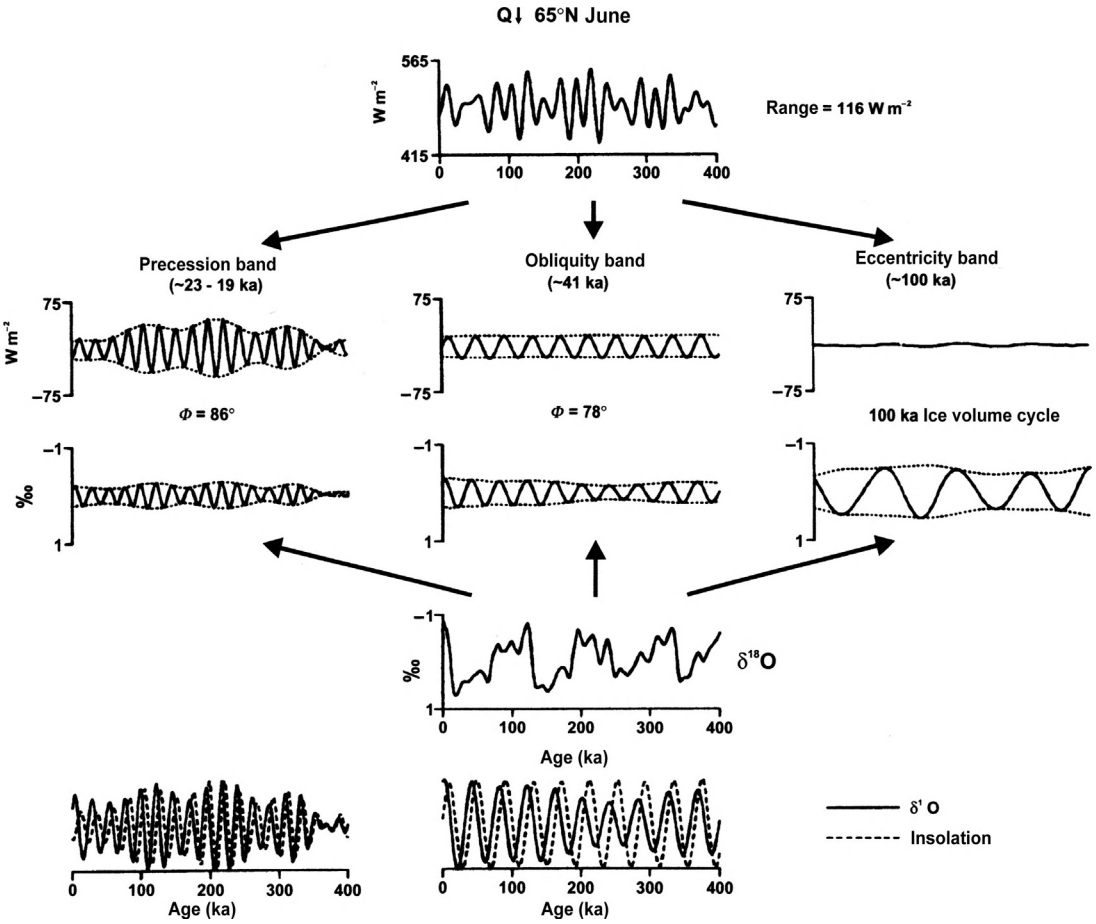


FIGURE 2.23 Incoming radiation over the last 400 ka at 65°N, broken down (band-pass-filtered) into its principal orbital components (top) compared to the record of continental ice volume (recorded by $\delta^{18}O$ in marine sediments) and its principal components at the same frequencies (below). The lower panel shows the normalized precessional and obliquity bands in insolation and $\delta^{18}O$ superimposed to show the strong coherence between the radiation forcing and the continental ice volume response. The strong direct relationship between insolation changes related to obliquity and precession contrasts strongly with the apparent lack of correspondence between the eccentricity forcing and the climate system response. *From Imbrie et al. (1993b).*

(precession, obliquity, and eccentricity) and compared to the same band-pass-filtered components of the marine $\delta^{18}O$ record of the last 400 ka (representing changes in continental ice volume). Clearly, the frequency bands associated with precession and obliquity are similar with (and coherent with) the $\delta^{18}O$ ice volume signal, but the 100 ka radiation signal is completely inadequate to explain the strong 100 ka cycle in ice volume. Several possible reasons for this discrepancy have been proposed. For example, there may be a nonlinear response within the climate system, perhaps involving some internal feedback mechanism, which sets up the observed 100 ka periodicity, or there may be oscillations within the climate system that in some way interact with precessional and obliquity changes to generate a cycle of 100 ka, in phase with eccentricity (Ruddiman, 2006). Whichever mechanism is correct, it must also explain the shift toward much larger amplitude cycles in the climate system in the last ~800 ka (as recorded by ice volume changes, loess deposition, pollen records, etc.) at a time when eccentricity forcing at the 100 ka period was declining in significance.

In summary, orbital forcing has been an important factor in driving Quaternary climatic fluctuations, and hence, the periodicities associated with orbital variations are prominent signals in many paleoclimate records (Berger et al., 1992a). However, the precise mechanism of how such forcing is translated into a climate response remains the subject of much debate (e.g., Ruddiman, 2006; Schulz and Zeebe, 2006; Raymo and Huybers, 2008). Computer modeling studies have provided a great deal of insight in bridging the gap between paleoclimatic theory and field data (e.g., Berger, 1990; Crucifix et al., 2006; Kutzbach et al., 2008; Yin and Berger, 2012). This topic is discussed further in Chapter 6, Section 6.3.3.

2.7 SOLAR FORCING

Orbital forcing involves the redistribution of incoming solar energy, both latitudinally and seasonally. Thus, there are differential effects on the climate system that can lead to circulation changes, and there may be different responses to the forcing in the Northern and Southern Hemispheres. Changes in solar irradiance (energy emitted by the Sun) might be expected to affect all parts of the Earth equally. However, this is not so, because the response to solar irradiance forcing is amplified regionally, as a result of feedbacks and interactions within the atmosphere (Rind, 2002; Haigh, 2005).

For many years, it was assumed (based on measurements in dry, high-altitude locations) that total irradiance did not vary, at least not on interannual to decadal scales—hence the term "solar constant" was coined to describe the energy that is intercepted by the atmosphere when the Sun is overhead (Hoyt and Schatten, 1997; Kopp and Lean, 2011). Satellite measurements over the last ~25 years tell a different story—total solar irradiance, TSI (incoming radiation integrated over all wavelengths) varies by ~0.08% over a Schwabe solar cycle (average length of ~11 years), with maximum values at times of maximum solar activity (when there are many sunspots and bright solar faculae) (Lean, 2010). Sunspots reduce solar irradiance and faculae increase it, so the overall changes during a solar cycle reflect the net effect of these two phenomena, with faculae outweighing sunspots during solar maxima (Figure 2.24). Furthermore, irradiance changes at very short (ultraviolet) wavelengths and vary even more over a solar cycle (Lean, 2000). Such changes have significance because an increase in UV radiation causes more ozone (O_3) to be produced in the upper stratosphere. Ozone absorbs

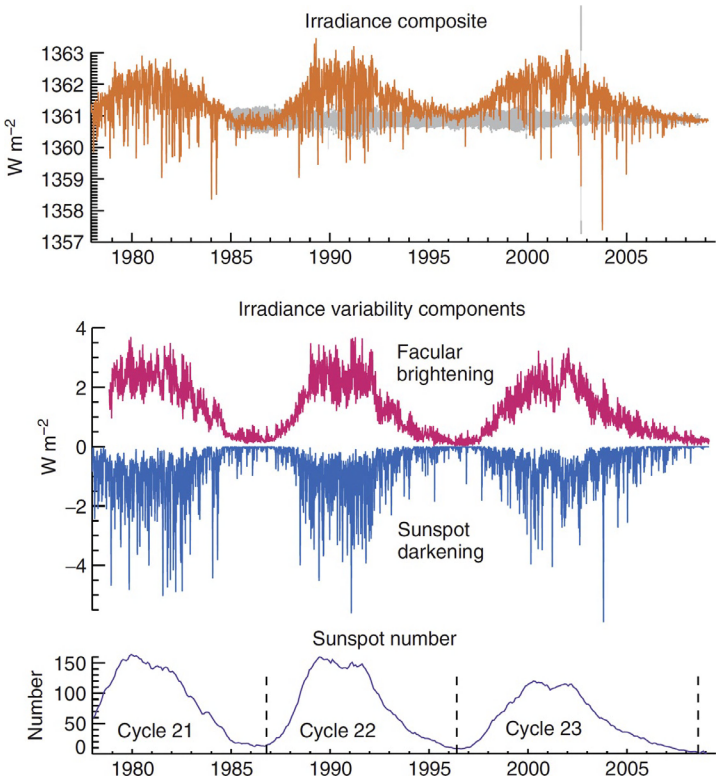


FIGURE 2.24 Satellite measurements of solar faculae and sunspots for the last three solar activity cycles. The faculae increase energy emissions from the Sun, while sunspots reduce them. The net result is a 0.1% increase in total solar irradiance between the minimum and maximum of the solar cycles (top). Unfortunately, longer measurements of these phenomena do not exist, and so, there is considerable uncertainty about how irradiance changed in the past. *From Lean (2010).*

radiation (at UV wavelengths of 200-340 nm) so heating rates in the upper atmosphere are increased during times of enhanced solar activity. This then affects stratospheric winds (strengthening stratospheric easterlies), which can in turn influence surface climate via dynamical linkages between the stratosphere and the troposphere (Shindell et al., 1999; Baldwin and Dunkerton, 2001; Haigh, 2005; Ineson et al., 2011). Model simulations of these effects indicate that there is a poleward shift of the tropospheric westerly jet and a poleward extension of the Hadley circulation, by ~70 km from solar minimum to solar maximum, in the summer hemisphere (Haigh, 1996; Larkin et al., 2000). Although such changes are small, if irradiance changes in the past were larger and more persistent than solar cycle variability, the effects may have been quite significant.

How much has irradiance changed over longer timescales? Satellite measurements are too short to shed light on longer-term irradiance changes, so these must be inferred from other lines of evidence. Sunspot observations began in the early seventeenth century, but observations of solar faculae are much shorter, so the difficulty is how to estimate changes in total irradiance when the only long-term data are from sunspot numbers (Figure 2.25). Of particular interest is the period from ~1645 to 1715 (the Maunder Minimum) when virtually no sunspots were seen (Eddy, 1976). Many studies have tried to reconstruct the overall change in TSI since the Maunder Minimum, with estimates varying from <0.1% to 0.24% (Figure 2.25), with presumably larger changes in UV radiation. Numerous GCM simulations have used these

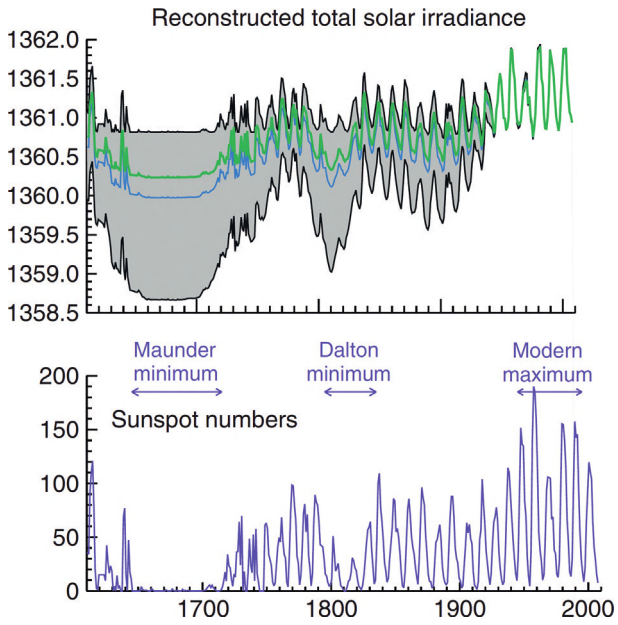


FIGURE 2.25 Sunspot numbers recorded since the early 1600s, showing the strong 11-year Schwabe cycle and longer-term variations, from near zero during the Maunder Minimum to over 150 in recent decades. In the upper diagram, estimates of the changes in total solar irradiance (TSI) are given, based on different models of solar activity. The latest estimate for solar minimum during the last solar cycle is 1360 W m^{-2} (Kopp and Lean, 2011) (cf. Figure 2.24). *From Lean (2000, 2010), Wang et al. (2005a,b), and Tapping et al. (2007).*

estimates to examine how solar irradiance may have affected temperatures over recent centuries. Notwithstanding the uncertainties in estimating the magnitude of solar forcing, these studies generally conclude that much of the low-frequency variability in Northern Hemisphere temperatures over the last millennium (prior to the onset of global anthropogenic effects) can be explained in terms of solar and volcanic forcing, though internal climate system variability may mask the overall (large-scale) warming and cooling effects at the regional scale (e.g., Rind et al., 1999; Crowley, 2000; Goosse et al., 2005). In fact, distinct patterns of regional temperature change may be associated with solar forcing, as seen in both empirical and modeling studies, due to complex interactions between the circulation in the stratosphere and the troposphere, and feedbacks between the atmosphere and the ocean circulation (Waple et al., 2001; Swingedouw et al., 2011). By varying solar irradiance forcing in a GCM, Shindell et al. (2001) simulated cooler winter temperatures over eastern North America and western Europe (by 1-2 °C), compared to a century later when solar irradiance was higher, changes that are consistent with the paleoclimatic evidence for the late Maunder Minimum (Pfister et al., 1999; Luterbacher et al., 2001) (Figure 2.26). Such a pattern is characteristic of a shift in the North Atlantic Oscillation (NAO) toward lower index conditions, in which the pressure gradient between Iceland and the Azores is reduced, leading to less advection of warm, moist air from the Atlantic into western Europe and cooler temperatures over Eurasia (cf. Ineson et al., 2011).

If solar irradiance changed by ~0.1-0.24% over the last 350 years, how much change occurred over longer periods of time? It may be possible to estimate long-term changes in solar activity from changes in cosmogenic isotopes preserved in natural archives. Cosmic rays intercepted by the upper atmosphere produce cosmogenic isotopes—such as ^{10}Be and ^{14}C—which eventually enter the terrestrial environment at the Earth's surface. During times of high

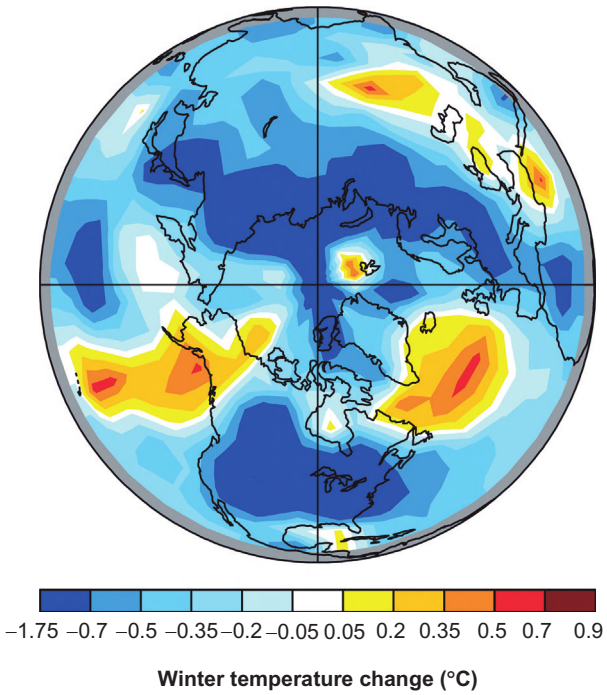


FIGURE 2.26 The change in winter surface air temperature between 1680 and 1780 (1680–1780), based on a GCM simulation in which solar irradiance was increased by 0.32 W m^{-2} (~0.1%) between those times. The GCM had an interactive stratospheric chemistry component so that UV effects on ozone could be included. The pattern of change is similar to that associated with a negative phase of the North Atlantic Oscillation. *From Shindell et al. (2001).*

solar activity, the flux of cosmic rays to the atmosphere is reduced, leading to a reduction in the production rate of these isotopes. Thus, variations in cosmogenic isotopes are inversely related to solar activity. If we make the assumption that solar activity is correlated with TSI changes (a fairly big assumption, though it is supported by observations in the recent instrumental period—see Beer et al., 1996; Steinhilber et al., 2009), long-term changes in ^{14}C (seen as departures from expected age, in tree rings) or ^{10}Be (in ice cores) could be used as an index of solar irradiance changes over time. However, there are questions about the role of atmospheric processes in transferring ^{10}Be from its production in the stratosphere to deposition sites at the Earth's surface and about the rate at which radiocarbon was sequestered in the deep ocean (due, for example, to thermohaline circulation changes) that may also have affected atmospheric concentrations in radiocarbon over time. Furthermore, other factors have also affected the production rate of cosmogenic isotopes over the Holocene, and these must be accounted for in order to isolate the effects of solar variability. In particular, geomagnetic field variations have had a large impact on production rates (a weaker field being associated with higher production levels), and variations of the Earth's magnetic field are not well understood (see Chapter 4, Section 4.1.5). To examine some of these questions, Bard et al. (2000) used a box model of ocean carbon variations driven by ^{10}Be variations measured in an ice core to assess whether ^{14}C variations over the last 1000 years had been affected by ocean circulation changes. On this time scale, such effects appear to have been minimal, suggesting that ^{14}C can be used to assess solar variability over the millennium and perhaps longer. A similar result was found by Beer et al. (1996) for the last 4000 years. Thus, many studies have compared paleoclimatic reconstructions with ^{14}C anomalies, as an implicit proxy for solar

variability. In this way, precipitation variability across the tropics, in northern South America and Yucatan (Black et al., 1999; Haug et al., 2001; Hodell et al., 2001), in east Africa and the Arabian Peninsula (Verschuren et al., 2001; Neff et al., 2001), and in China (Wang et al., 2005b), has been correlated with solar activity variations, represented by ^{14}C anomalies (though the total amount of variance accounted for is quite small). Solar variability has also been linked to midcontinental drought frequency on both short and long timescales (Cook et al., 1996; Yu and Ito, 1999; Dean et al., 2002), and other studies have identified potential links between solar activity variations and climate changes in the Holocene (Magny, 1993; van Geel et al., 2000; Eichler et al., 2009). Bond et al. (2001) argued that the abundance of ice-rafted debris in North Atlantic sediments varied with the same frequency (~1450-1500 years) as ^{14}C anomalies, and Stuiver et al. (1991) also noted the similarity between a ~1470-year periodicity in ^{14}C data and a similar periodicity in oxygen isotopic data from GISP2. It remains to be seen how robust these relationships are and what plausible mechanisms might link very small solar activity/irradiance variations with climate in such diverse parts of the globe. One possibility (seen in some model simulations) involves solar variations influencing the tropical Hadley circulation, which leads to changes in the distribution of clouds and precipitation anomalies, with further teleconnections to extratropical regions (e.g., Meehl et al., 2009).

A more physically based reconstruction of total solar irradiance changes over the Holocene has been produced by Steinhilber et al. (2009, 2012), based on a calibration of ^{10}Be from ice cores and observed variations in the open magnetic field of the Sun. After considering estimates of how the Earth's magnetic field has changed over the Holocene (as estimated by Knudsen et al., 2008), their reconstructed irradiance reveals a large number of anomalies that were comparable to the Maunder Minimum (as well as episodes of enhanced solar activity) (Figure 2.27). Note, however, that a different estimate of geomagnetic field effects could shift those values. Nevertheless, their estimates indicate that TSI generally varied by less than $\pm 0.1\%$ from modern levels during the Holocene, which means that solar effects on surface climate are probably brought about by strong feedbacks within the climate system. Longer-term variations have not yet been estimated (Bard and Frank, 2006).

2.8 VOLCANIC FORCING

It is well known, from studies of instrumental records, that explosive volcanic eruptions can have short-term cooling effects on overall hemispheric or global mean temperatures (Bradley, 1988; Robock, 2000). Volcanic aerosols have a direct climatic impact by reducing energy receipts at the surface (Figure 2.28), but there may also be associated changes in atmospheric circulation (often involving an amplification of the upper Rossby wave pattern), which can lead to large temperature anomalies in some regions. For example, major eruptions during the twentieth century were often associated with positive winter temperature anomalies in northern Scandinavia and northern Russia due to a northward displacement of the westerlies (a positive phase of the North Atlantic Oscillation) (Groisman, 1992; Robock and Mao, 1995). There is also evidence that major eruptions in the tropics can bring about the development of an El Niño event, due to differential radiative effects in the cloudy versus cloud-free sectors of the Walker circulation (Adams et al., 2003; Mann et al., 2005; Emile-Geay et al., 2007).

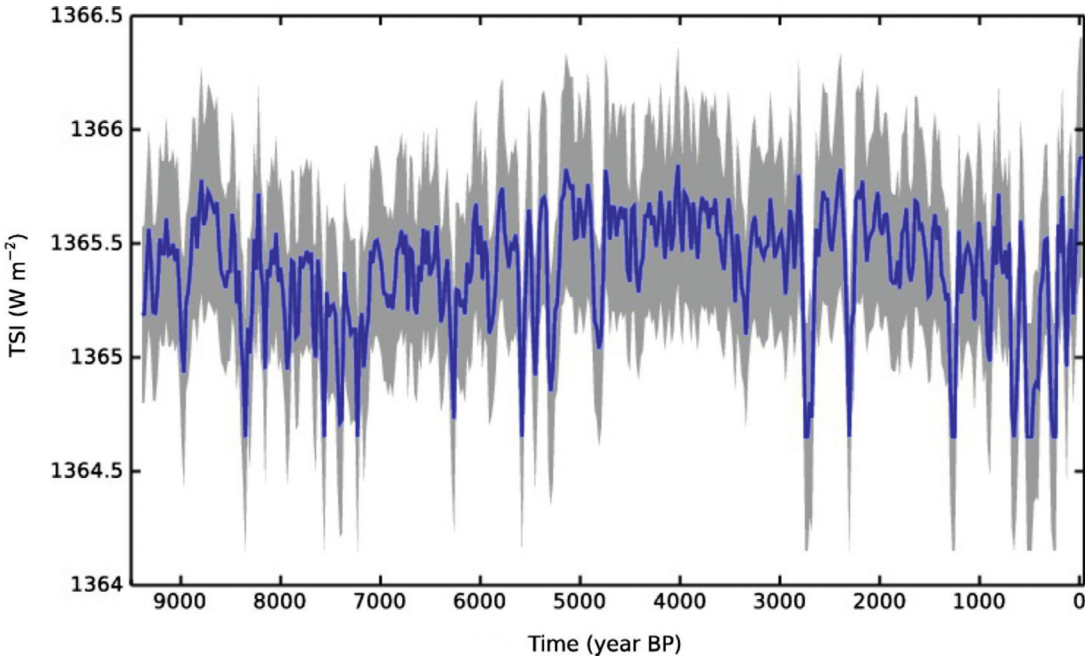


FIGURE 2.27 A reconstruction of total solar irradiance for the last 9300 years based on the relationship between the Sun's open magnetic field (which modulates galactic cosmic rays reaching the Earth) and ^{10}Be measured in ice cores, after taking into account changes in the Earth's magnetic field. The shaded band is the 1σ uncertainty considering the uncertainties of the calibration and of the reconstruction of the Sun's open magnetic field record. *From Steinhilber et al. (2012).*

Most temperature effects are not detectable after a few years, so individual explosive eruptions only contribute short-term variability to the spectrum of Holocene climate. However, if eruptions were more frequent in the past or if they happened to occur in clusters of events, it is possible that the cumulative effect of eruptions could have persisted for longer, resulting in decadal to multidecadal scale impacts. Such effects would be enhanced if the initial cooling led to feedbacks within the climate system, such as more persistent snow and sea-ice cover, which would raise the surface albedo and possibly alter the atmospheric circulation. For example, Miller et al. (2012) found that plateau ice caps expanded across a wide area of Baffin Island, Arctic Canada, following major explosive eruptions in AD 1258 and 1452. They argue that the larger ice caps remained long after the volcanic dust had settled out of the atmosphere, due to feedbacks associated with Arctic sea ice. Model simulations indicate that the cooler conditions led to more extensive sea ice, which in turn reduced air temperatures further. Collectively, the increase in continental glacierization and the greater amount of sea ice led to persistence of the initial perturbation. This persistence lasted long enough for other less dramatic eruptions to occur, further prolonging the changes that were triggered by the initial major volcanic events.

A study of volcanic deposits (tephra) in Pacific marine sediment cores over the last million years found a statistically significant relationship between episodes of explosive volcanism

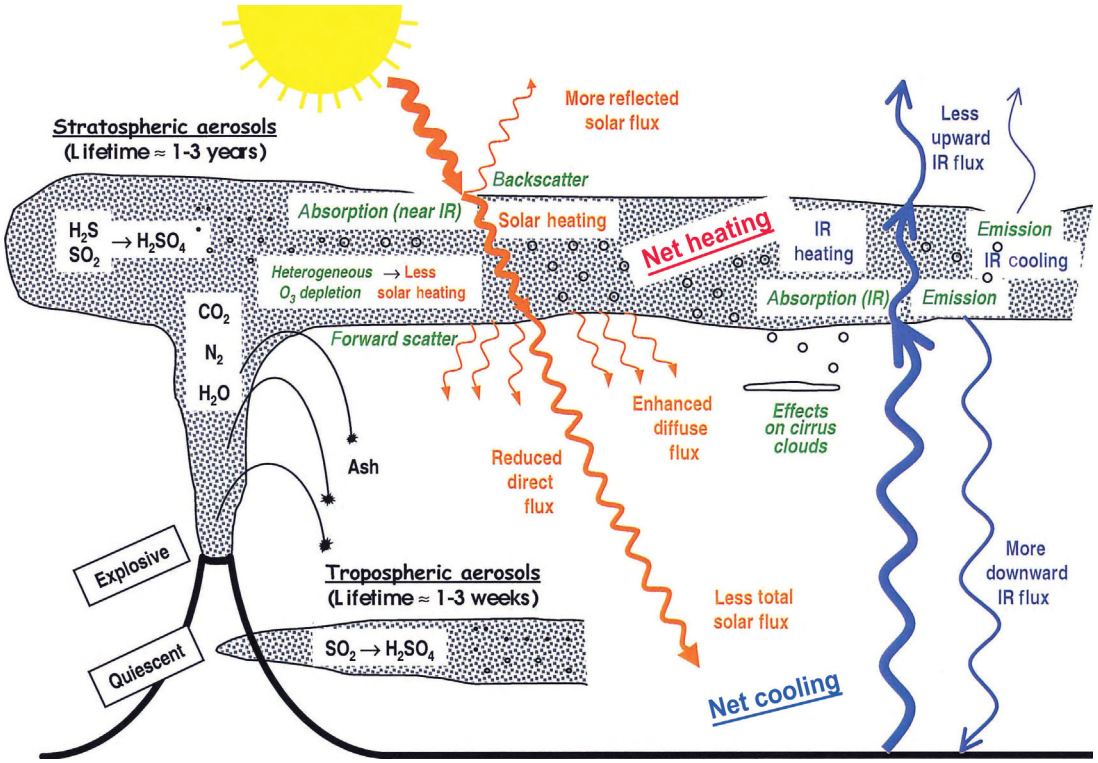


FIGURE 2.28 Schematic diagram showing the many effects of explosive volcanic eruptions that eject particulate matter, water vapor, and gases into the stratosphere, where they intercept incoming solar radiation. *From Robock (2000).*

and orbital forcing, particularly at the 41,000 (obliquity) frequency (Kutterolf et al., 2012). This was thought to be related to changes in crustal stress on the Earth's crust due to the growth and decay of ice sheets and associated changes in sea level. Sulfate levels in ice cores from Greenland and Antarctica also provide a record of explosive volcanism (Castellano et al., 2005; Gao et al., 2007, 2008), and the GISP2 sulfate record indicates that there were periods of more frequent explosive eruptions from 9500 to11,500 calendar years BP, perhaps also related to postglacial crustal unloading around Iceland (Zielinski et al., 1994). There were many large sulfate peaks during this period, often greater than the signal from Tambora (in 1815), which was the largest eruption in recent centuries (Figure 2.29). Of course, a larger sulfate signal is not indicative of the source of the eruption—it might simply mean that the eruption was close to the ice core site (Coulter et al., 2012). To address this issue, detailed analysis of ice cores from Greenland has led to tephra shards being extracted from the ice, so they can be geochemically fingerprinted to identify their source. This indicates that there were many tephras deposited on the Greenland ice sheet, mainly from Iceland, but there were even a few from explosive North American eruptions (Abbott and Davies, 2012). These tephras provide a chronology of major eruptions that may have had significant climatic effects (cf. Chapter 4, Section 4.3). However, to resolve these effects, what is really needed is a record

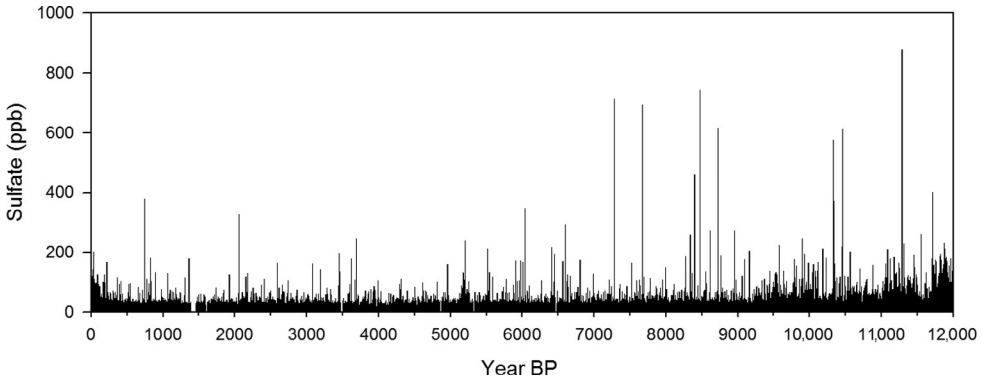


FIGURE 2.29 The Holocene record of volcanic sulfate (anomalies from background variations) recorded in the GISP2 ice core from Summit, Greenland. *From Zielinski et al. (1994).*

of how the volcanic dust affected atmospheric optical depth, both latitudinally and seasonally. This is extremely challenging, and so far, it has only been attempted for recent centuries (Robertson et al., 2001; Ammann et al., 2003). Using such data, energy balance and general circulation models indicate that explosive volcanism has strongly contributed to the natural variability of hemispheric and global mean temperatures over the last millennium (Crowley and Kim, 1999; Free and Robock, 1999; Crowley, 2000).

Many paleoclimatic studies that cite a relationship to particular forcing mechanisms do so via simple correlations either in the time domain (curve matching) or in the frequency domain (finding a spectral peak that corresponds to something similar in a particular forcing factor) (e.g., Black et al., 1999; Bond et al., 2001). There has generally been little interaction between those working at the frontiers of understanding how forcings affect the climate system, in a mechanistic or dynamic sense, and those reconstructing the paleoclimatic record. Modeling provides a link between these two approaches, particularly when simulations involve fully coupled ocean-atmosphere GCMs, with realistic stratospheric chemistry, vegetation, and land-surface (hydrological) feedbacks and a sea-ice component. With such tools, it may be possible to comprehend the complex interactions that are driven by what often appears to be a simple forcing function. Importantly, models can provide insight into the spatial climatic response to particular forcing factors, and perhaps, thresholds and feedbacks within the system can also be identified to help explain the observed Quaternary paleoclimatic record.

It must be recognized that there are also internal modes of climate system variability that can give rise to large regional-scale climate anomalies (e.g., El Niño-Southern Oscillation, the Atlantic Multidecadal Oscillation, and Pacific Decadal Oscillation). These modes vary on both long and short timescales (though we know relatively little about their long-term behavior). Some of this variability may be modulated by external forcing factors, but it may also result from random interactions with other parts of the climate system. Stochastic resonance in the climate system—in which a weak quasiperiodic forcing signal may be amplified into a nonlinear, bistable climate signal—could have brought about relatively abrupt changes in the past by pushing the system across critical thresholds (Lawrence and Ruzmaikin, 1998; Ruzmaikin, 1999; Rahmstorf and Alley, 2002).

Finally, not all paleoclimatic variability seen in the Holocene can be ascribed to specific external forcings (orbital, solar, or volcanic). Perhaps the best example of this is the ~8200 calendar year BP "event," which resulted from the catastrophic drainage of a huge proglacial lake at the margins of the Laurentide Ice Sheet (Alley et al., 1997c; Barber et al., 1999; Cheng et al., 2009). This was unrelated to any external forcing and led to rapid flooding of the North Atlantic with freshwater, thereby reducing the Atlantic meridional overturning circulation (AMOC), which affected the climate of many places around the world (Rohling and Pälike, 2005). Other widespread climate anomalies are more enigmatic, with (as yet) no obvious causative factor, such as the 4200-year BP episode that is seen in many records, from the Middle East (Weiss et al., 1993; Weiss, 2012), India (Berkelhammer et al., 2012), Alaska (Fisher et al., 2008), and the midwestern United States (Booth et al., 2005).

CHAPTER

3

Dating Methods I

OUTLINE

3.1 Introduction and Overview 55

3.2 Radioisotopic Methods 57

3.2.1 *Radiocarbon Dating* 59

3.2.1.1 Principles of ^{14}C Dating 60

3.2.1.2 Measurement Procedures, Materials, and Problems 62

3.2.1.3 Accuracy of Radiocarbon Dates 63

3.2.1.4 Sources of Error in ^{14}C Dating 64

3.2.1.5 Long-Term Changes in Atmospheric ^{14}C Content 72

3.2.1.6 Causes of Temporal Radiocarbon Variations 81

3.2.1.7 Radiocarbon Variations and Climate 82

3.2.2 *Potassium-Argon Dating ($^{40}K/^{40}Ar$)* 83

3.2.2.1 Problems of $^{40}K/^{40}Ar$ Dating 84

3.2.2.2 $^{40}Ar/^{39}Ar$ Dating 84

3.2.3 *Uranium-Series Dating* 85

3.2.3.1 Problems of U-Series Dating 91

3.2.4 *Luminescence Dating: Principles and Applications* 91

3.2.4.1 Thermoluminescence (TL) Dating 93

3.2.4.2 Problems of Thermoluminescence Dating 95

3.2.4.3 Optically and Infrared-Stimulated Luminescence (OSL and IRSL) Dating 95

3.2.5 *Surface Exposure Dating* 98

3.2.6 *Fission-Track Dating* 100

3.1 INTRODUCTION AND OVERVIEW

Accurate dating is of fundamental importance to paleoclimatic studies. Without reliable estimates on the age of events in the past, it is impossible to investigate if they occurred synchronously or if certain events led or lagged others; neither is it possible to assess accurately

Copyright © 2015 Raymond S. Bradley.
Published by Elsevier Inc. All rights reserved.

the rate at which past environmental changes occurred. Strenuous efforts must therefore be made to date all proxy materials, to avoid sample contamination, and to ensure that the stratigraphic context of the sample is clearly understood. It is equally important that the assumptions and limitations of the dating procedure used are understood so that a realistic interpretation of the date obtained can be made. It is often just as important to know the margins of error associated with a date as to know the date itself. In this chapter, we discuss the main dating methods widely used in Quaternary studies today. Further details can be found in Geyh and Schleicher (1990), Noller et al. (2000), and Walker (2005).

Dating methods fall into four basic categories (Figure 3.1): (a) radioisotopic methods, which are based on the rate of atomic disintegration in a sample or its surrounding environment; (b) paleomagnetic (correlation) methods,[1] which rely on past reversals of the Earth's magnetic field and their effects on a sample; (c) organic and inorganic chemical methods, which are based on time-dependent chemical changes in the sample or chemical characteristics of a sample; and (d) biological methods, which are based on the growth of an organism to date the substrate on which it is found. Depending on the time period of interest, different dating methods will be more suitable than others (Figure 3.2).

Not all dating methods provide a reliable numerical age, but may give an indication of the *relative* age of different samples. In these cases, it may be possible to calibrate the "relative age" technique by numerical (e.g., radioisotopic) methods, as discussed, for example, in Chapter 4, Section 4.2.1.3. Thus, there is a spectrum of approaches to dating: numerical age methods, calibrated age methods, relative age methods, and methods involving

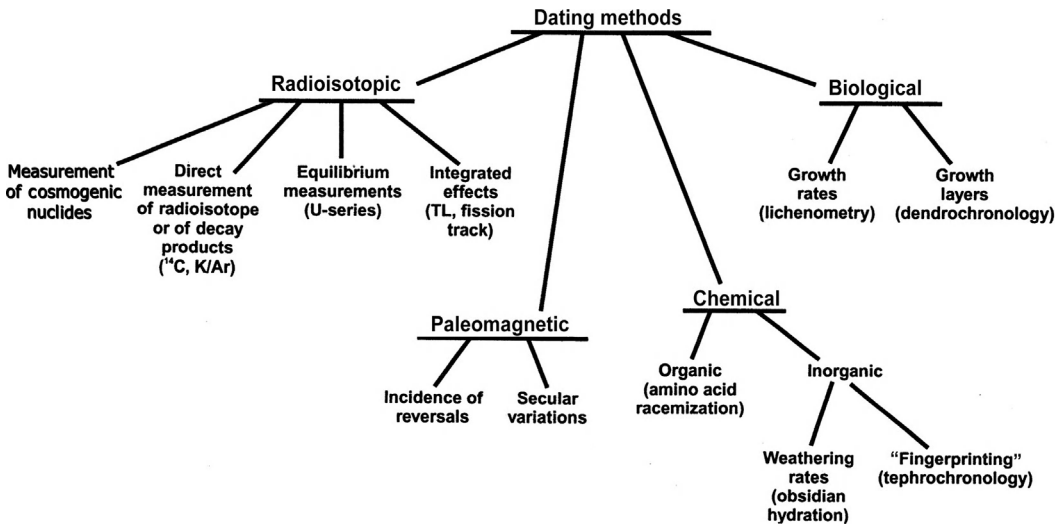


FIGURE 3.1 Principal dating methods used in paleoclimatic research.

[1] One could argue that paleomagnetic changes do not constitute a method of dating but rather a method of stratigraphic correlation. Nevertheless, the development of a reliable timescale for paleomagnetic changes (Section 4.1.3) has meant that paleomagnetic changes are often used, *de facto*, as dated reference horizons.

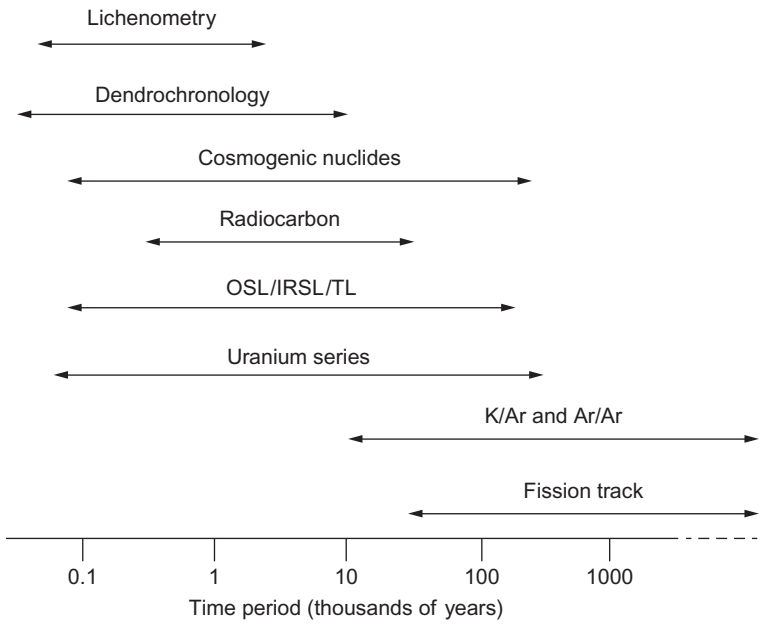


FIGURE 3.2 Schematic diagram showing the age ranges for which different dating methods are suitable.

stratigraphic correlation (Colman et al., 1987). In this and the following chapter, all of these approaches are discussed, beginning with numerical age methods.

3.2 RADIOISOTOPIC METHODS

Atoms are made up of neutrons, protons, and electrons. For any one element, the number of protons (the atomic number) is invariant, but the number of neutrons may vary, resulting in different isotopes of the same element. Carbon, for example, exists in the form of three isotopes; it always has six protons but may have six, seven, or eight neutrons, giving atomic mass numbers (the total number of protons and neutrons) of 12, 13, and 14, designated ^{12}C, ^{13}C, and ^{14}C. Generally each element has one or more stable isotopes that account for the bulk of its occurrence on Earth. For example, in the case of carbon, ^{12}C and ^{13}C are the stable isotopes; ^{12}C is by far the most abundant form. It is estimated that the carbon exchange reservoir (atmosphere, biosphere, and the oceans) contains 42×10^{12} tons of ^{12}C, 47×10^{10} tons of ^{13}C, and only 62 tons of ^{14}C. Unstable atoms undergo spontaneous radioactive decay by the loss of nuclear particles (α- or β-particles), and, as a result, they may transmute into a new element.[2] For example, radiocarbon (^{14}C) decays to ^{14}N, and ^{40}K decays to ^{40}Ar and ^{40}Ca. Furthermore, the decay rate is invariant so that a given quantity of the radioactive isotope will decay to its

[2] An α-particle is made up of two protons and two neutrons (i.e., a helium nucleus), and a β-particle is an electron. Neutrons may decay to produce a β-particle and a proton, thereby causing a transmutation of the element itself.

TABLE 3.1 Half-Lives of Radioisotopes Used in Dating

^{14}C	5.730×10^3 years
^{238}U	4.468×10^9 years
^{235}U	0.704×10^9 years
^{40}K	1.310×10^9 years

Although the half-life of ^{14}C is calculated to be 5730 ± 40 years, by convention the "Libby half-life" of 5568 ± 30 years is used.

daughter product in a known interval of time; this is the basis of radioisotopic dating methods. Providing that the radioisotope "clock" is started close to the stratigraphically relevant date, measurement of the isotope concentration today will indicate the amount of time that has elapsed since the sample was emplaced. The amount of time that it takes for a radioactive material to decay to half its original amount is termed its half-life. Table 3.1 lists the half-lives of some radioisotopes that have been used in the context of dating. In the case of ^{14}C, the half-life is 5730 ± 30 years. This means that a plant that died 5730 years ago has only half its original ^{14}C content remaining in it today. After a further 5730 years from today, it will have only half as much again, i.e., 25% of its original ^{14}C content, and so on (Figure 3.3). When Libby expounded the principles of radiocarbon dating (Libby, 1955), he actually calculated a half-life for ^{14}C of 5568 years. This was the average of a number of wide-ranging estimates up to that time and was adopted by all radiocarbon-dating laboratories. By the early 1960s, further work had demonstrated that the original estimate was in error by 3% and the half-life was closer to 5730 years (Godwin, 1962). To avoid confusion, it was decided to continue using the "Libby half-life" (rounded to 5570 years), and this practice has continued; all dates are still reported using the Libby half-life. However, when comparing "radiocarbon years" with calendar years (historical, archeological, and/or astronomical events) and dates obtained by other techniques, adjustments are necessary (see Section 3.2.1.5). Recently, questions have been raised about the true half-life of ^{14}C and if it is really greater (around 6000 years), which could explain at least part of the long-term differences between radiocarbon and calendar year ages (Chiu et al., 2007). However, there is no compelling evidence for this adjustment, and it would probably create more problems than it would solve (Hughen et al., 2006; Broecker and Barker, 2007).

For a radioactive isotope to be directly useful for dating, it must possess several attributes: (a) the isotope itself, or its daughter products, must occur in measurable quantities and be capable of being distinguished from other isotopes, or its rate of decay must be measurable; (b) its half-life must be of a length appropriate to the period being dated; (c) the initial concentration level of the isotope must be known; and (d) there must be some connection between the event being dated and the start of the radioactive decay process (the "clock"). The relevance of these factors will be made clear in the ensuing sections.

In general terms, radioisotopic dating methods can be considered in three groups (Figure 3.1), those which measure (a) the quantity of a radioisotope as a fraction of a presumed initial level (e.g., ^{14}C dating) or the reciprocal buildup of a stable daughter product (e.g., potassium-argon and argon-argon dating); (b) the degree to which members of a chain of radioactive

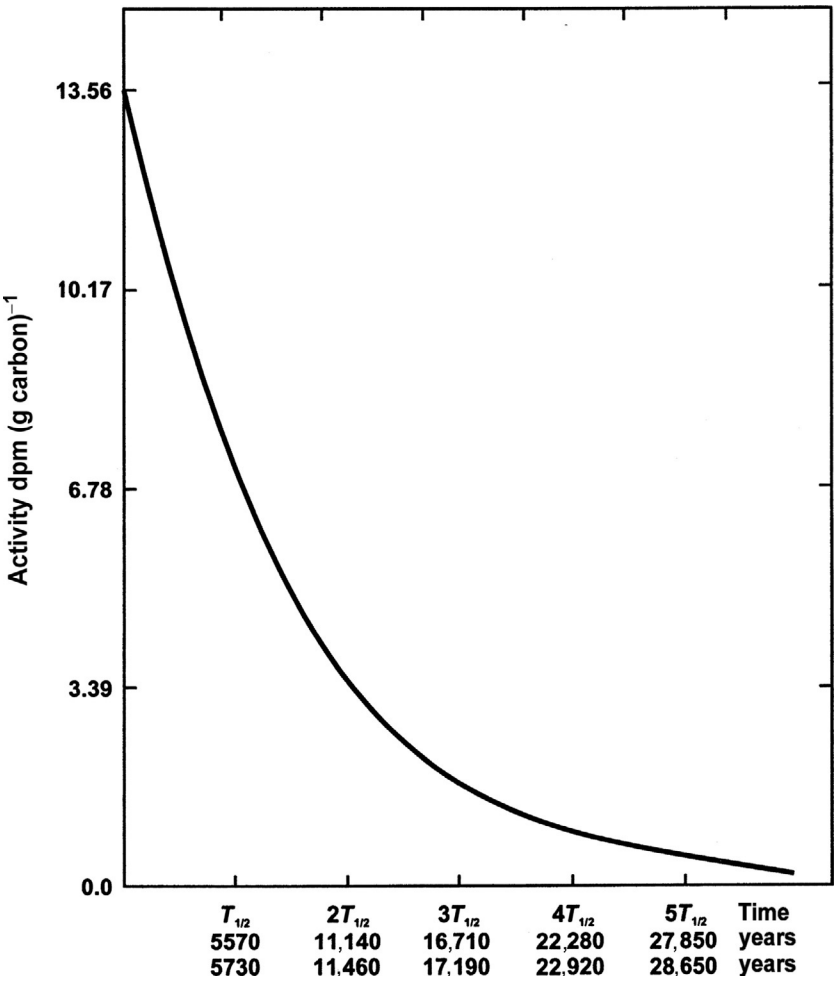


FIGURE 3.3 The decay of radiocarbon with time. Both the Libby and revised half-lives ($T_{1/2}$) are shown on the abscissa. The ordinate scale is in disintegrations per minute per gram of carbon. *After Olsson (1968).*

decay are restored to equilibrium following some initial external perturbation (uranium-series dating); and (c) the integrated effect of some local radioactive process on the sample materials, compared to the value of the local (environmental) flux (fission-track and thermoluminescence dating). Each of these methods will be considered separately.

3.2.1 Radiocarbon Dating

For studies of Late Quaternary climatic fluctuations, ^{14}C or radiocarbon dating has proved to be by far the most useful. Because of the ubiquitous distribution of ^{14}C, the technique can be used throughout the world and has been used to date samples of peat, wood, bone, shell,

paleosols, "old" seawater, marine and lacustrine sediments, and carbonaceous particles trapped in glacier ice. Furthermore, the useful time frame for radiocarbon dating spans a period of major, global environmental change that would be virtually impossible to decipher in any detail without accurate dating control. Radiocarbon dating is also ideal for dating mankind's development from paleolithic time to the recent historical past, and it has therefore proved invaluable in archeological studies. In addition, variations in the ^{14}C content of the atmosphere are of interest in themselves because of the implications these have for solar and/or geomagnetic variations through time, or for changes in the ocean circulation, and hence for climatic fluctuations.

3.2.1.1 *Principles of ^{14}C Dating*

Radiocarbon ($^{14}_{6}C$) is produced in the upper atmosphere by neutron bombardment of atmospheric nitrogen atoms:

$$^{14}_{7}N + {}^{1}_{0}n \rightarrow {}^{14}_{6}C + {}^{1}_{1}H \tag{3.1}$$

The neutrons have a maximum concentration at around 15 km and are produced by cosmic radiation entering the upper atmosphere. Although cosmic rays are influenced by the Earth's magnetic field and tend to become concentrated near the geomagnetic poles (thus causing a similar distribution of neutrons and hence ^{14}C), rapid diffusion of ^{14}C atoms in the lower atmosphere obliterates any influence of this geographical variation in production. ^{14}C atoms are rapidly oxidized to $^{14}CO_2$, which diffuses downward and mixes with the rest of atmospheric carbon dioxide and hence enters into all pathways of the biosphere (Figure 3.4). As Libby (1955) stated, "Since plants live off the carbon dioxide, all plants will be radioactive; since the animals on earth live off the plants, all animals will be radioactive. Thus . . . all living things will be rendered radioactive by the cosmic radiation."

During the course of geologic time, an equilibrium has been achieved between the rate of new ^{14}C production in the upper atmosphere and the rate of decay of ^{14}C in the global carbon reservoir. This means that the 7.5 kg of new ^{14}C that is estimated to be produced each year in the upper atmosphere is approximately equal to the weight of ^{14}C lost throughout the world by the radioactive decay of ^{14}C to nitrogen, with the release of a β-particle (an electron):

$$^{14}_{6}C \rightarrow {}^{14}_{7}N + \beta + \text{neutrino} \tag{3.2}$$

The total weight of global ^{14}C thus remains constant.[3] This assumption of an essentially steady concentration of radiocarbon during the period useful for dating is fundamental to the method though, in detail, this assumption is invalid (see Section 3.2.1.5).

Plants and animals assimilate a certain amount of ^{14}C into their tissues through photosynthesis and respiration; the ^{14}C content of these tissues is in equilibrium with that of the atmosphere because there is a constant exchange of new ^{14}C as old cells die and are replaced. However, as soon as an organism dies, this exchange and replacement of ^{14}C ceases. From

[3] Prior to atomic bomb explosions in the atmosphere, the equilibrium quantity of ^{14}C was estimated to be ~62 metric tons. Since the 1950s, the amount of artificially produced ^{14}C has increased by perhaps ~4%, though most of this has, as yet, remained in the atmosphere; consequently, ^{14}C levels there have almost doubled (Aitken, 1974).

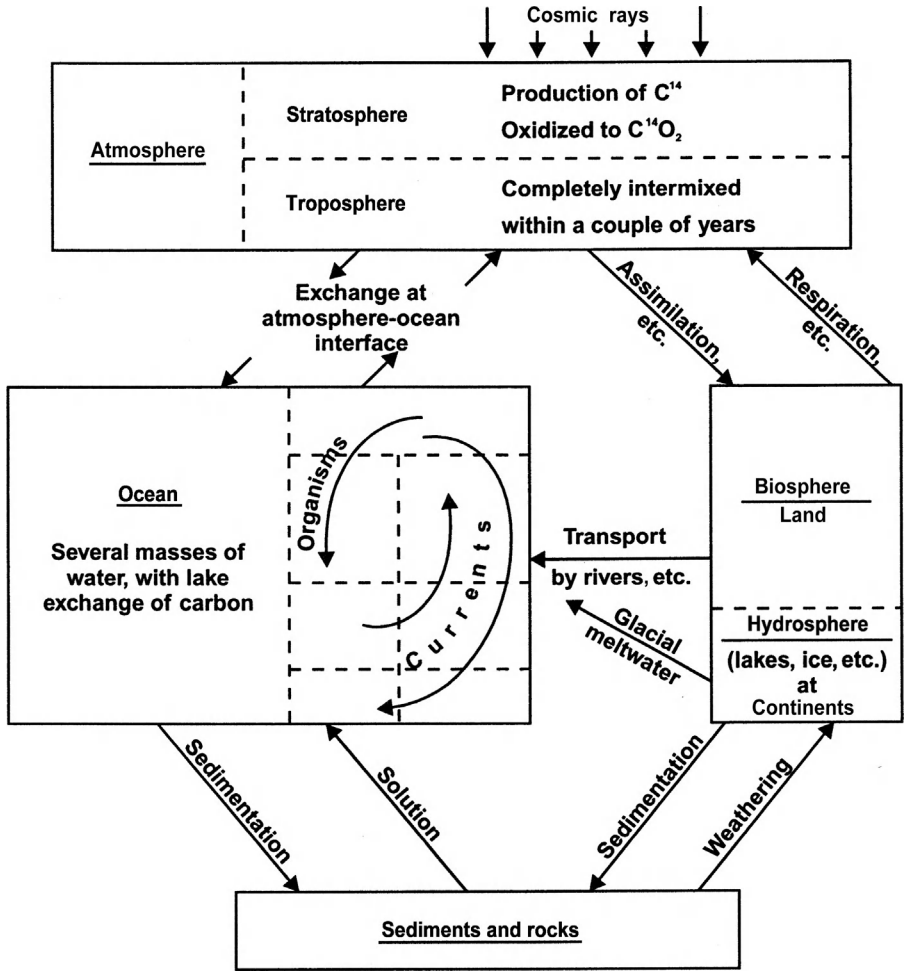


FIGURE 3.4 Schematic diagram of carbon circulation in nature. *After Mangerud (1972).*

that moment on, the ^{14}C content of the organism declines as the ^{14}C decays to nitrogen, and the ^{14}C content is henceforth purely a function of time; the radioactive "clock" has been activated. Because the ^{14}C content declines at a negative exponential rate (Figure 3.3) by the time that ten half-lives have elapsed (57,300 years), the sample contains less than 0.01% of the original ^{14}C content of the organism when it was alive. To put this in a more practical way, in a 1 g sample of carbon with a ^{14}C content equivalent to modern levels, decay of the radiocarbon atoms in the sample will produce about 15 β-particles per minute, a rate which is relatively easy to count by conventional dating methods. By contrast, 57,300 years after an organism has died, 1 g of its carbon will produce only about 21 β-particles per day (Aitken, 1974). It is this ever-decreasing quantity of ^{14}C with increasing sample age that makes conventional

radiocarbon dating so difficult; it simply becomes impossible to separate disintegrations of the sample from the extraneous background radiation (typically ~132 β-particles per day in a modern counter) as the signal-to-noise ratio becomes too small.

3.2.1.2 *Measurement Procedures, Materials, and Problems*

Until the early 1980s, nearly all radiocarbon-dating laboratories used proportional gas counters or liquid scintillation techniques (Povinec et al., 2009). In the former method, carbon is converted into a gas (methane, carbon dioxide, or acetylene), which is then put into a "proportional counter" capable of detecting β-particles (variations in output voltage pulses being proportional to the rate of β-particle emission). In liquid scintillation procedures, the carbon is converted into benzene or some other organic liquid and placed in an instrument that detects scintillations (flashes of light) produced by the interaction of β-particles and a phosphor added to the organic liquid. In both methods, stringent measures are necessary to shield the sample counters from extraneous radioactivity in the instrument components, laboratory materials, and surrounding environment, including cosmic rays penetrating the Earth's atmosphere from outer space. Few labs use these methods nowadays as they are slow and require several grams of carbon per sample.

Radiocarbon dating underwent a technological revolution in the late 1970s and early 1980s when a method for dating very small organic samples was developed, using an accelerator coupled to a mass spectrometer (AMS dating) (Muller, 1977; Nelson et al., 1977; Litherland and Beukens, 1995). Instead of measuring the quantity of ^{14}C in a sample indirectly, by counting β-particle emissions, the concentrations of individual ions (^{12}C, ^{13}C, and ^{14}C) are measured. Ions are accelerated in a tandem electrostatic accelerator to extremely high velocities; they then pass through a magnetic field that separates the different ions, enabling them to be distinguished (Stuiver, 1978a; Elmore and Phillips, 1987). Sample sizes used in this technique are much smaller than in conventional ^{14}C dating (only ~1 mg of carbon is required, and samples with as little as 30 μg have been dated) so that dates on small samples of foraminifera, pollen grains isolated from their surrounding matrix, or even individual seeds can be dated (Brown et al., 1992; Regnell, 1992). For example, typically 700-2000 tests of the planktonic foram *Globigerina bulloides* will provide 1 mg of carbon for dating. There are now many accelerators designed specifically for ^{14}C dating applications, and several labs can produce results within days of receiving a sample.

Another important development is radiocarbon dating of specific compounds extracted from a sedimentary matrix (Ingalls and Pearson, 2005). Often, organic samples contain a mixture of material that may have different sources and different ages, and thus, even small bulk organic samples may not provide an accurate date for a particular stratigraphic level (e.g., Mollenhauer et al., 2005). By extracting organic compounds such as lipids from cell membranes, produced by specific organisms (*biomarkers*; Gaines et al., 2009), a clearer connection can be made to the stratigraphy (Figure 3.5; Eglinton et al., 1996, 1997). For example, Smittenberg et al. (2004) extracted crenarchaeol (a biomarker produced by single-celled planktonic Archaea, Crenarchaeota) to date the varved sediments of Saanich Inlet, British Columbia. By comparing compound-specific ages with the varve chronology, they were able to assess changes in marine reservoir ages over time at this location. Compound-specific dating is also valuable in dating organic compounds (such as glycerol dibiphytanyl glycerol tetraethers (GDGTs) or alkenones) that are used as paleotemperature indicators in marine

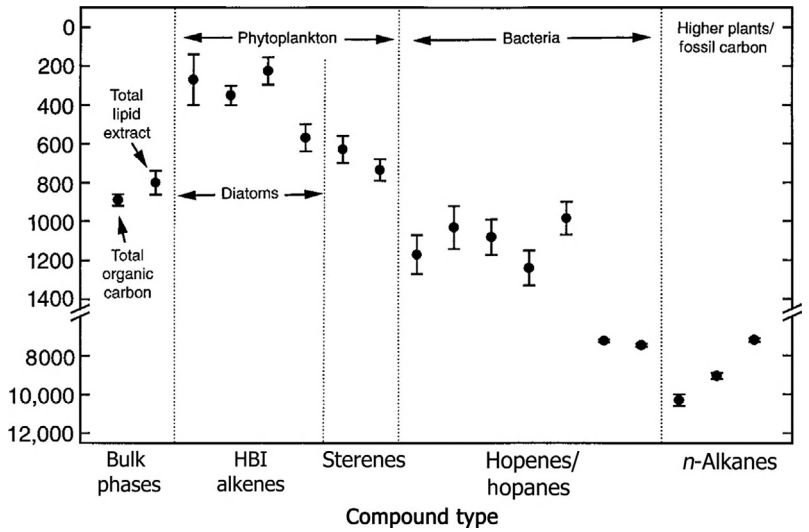


FIGURE 3.5 Radiocarbon ages (determined by AMS) for individual hydrocarbons and bulk fractions for the upper 2-4 cm of a sediment core from the Arabian Sea, showing that material settling to the ocean floor can be of quite different ages. Note break in *y*-axis. Error bars represent uncertainty associated with statistics of the AMS $\delta^{14}C$ measurement (overall error is <5%). *From Eglinton et al. (1997).*

sediments. By dating the specific molecules used as temperature proxies, the chronology of the reconstruction is likely to be more secure, and the paleotemperature itself may be more meaningfully understood. For example, Ohkouchi et al. (2002) found that alkenones from a core in the Sargasso Sea were much older than the surrounding sedimentary matrix; the organic molecules had been reworked from older sediments and carried southward from colder waters to the north. Thus, the paleotemperature reconstruction from alkenones (see Chapter 6, Section 6.5.1) was much colder and unrepresentative of the Sargasso Sea location. Furthermore, the input of older material appears to have varied over time, due to changes in current strength. Understanding that would have been impossible without the ability to isolate and date just the alkenones alone (cf. Shah et al., 2008). Technological developments in AMS dating may offer the prospect of dating carbon samples as small as ~1 μg from single compounds in the near future (Povinec et al., 2009).

3.2.1.3 *Accuracy of Radiocarbon Dates*

It is tempting to accept a radiocarbon date as the gospel truth, particularly if it confirms a preconceived notion of what the sample age should be! Radiocarbon dates are, however, statements of probability (as are all radiometric measurements). Radioactive disintegration varies randomly about a mean value; it is not possible to predict when a particular ^{14}C atom will decay, but for a sample containing 10^{10}-10^{12} atoms of ^{14}C, a certain number of disintegrations will occur, on average, in a certain length of time. This statistical uncertainty in the sample radioactivity (together with similar uncertainty in the radioactive decay of calibration samples and "noise" due to background radiation) is inherent in all ^{14}C dates. A single "absolute" (i.e., numerical) age can therefore never be assigned to a sample. Rather, dates are

reported as the midpoint of a Poisson probability distribution; together with its standard deviation, the date thus defines a known level of probability. A date of 5000 ± 100 years BP, for example, indicates a 68% probability that the true (radiocarbon) age is between 4900 and 5100 years BP, a 95% probability that it lies between 4800 and 5200 years BP, and a 99% probability of it being between 4700 and 5300 years BP. In conventional dating, the use of large samples, extended periods of counting, and the reduction of laboratory background noise will all improve the precision of the age determination. However, even rigorous ^{14}C analysis cannot account for all sources of error, and these must be evaluated before putting a great deal of confidence in the date obtained. A sample age may be precisely determined (analytically), but it may not be an *accurate* reflection of the true age if the sample is contaminated or if appropriate corrections are not made, as discussed in the following sections. It is worth bearing in mind that if an infinitely old sample has even 0.1% contamination by modern carbon, it will yield a finite date of ~55,500 years BP, illustrating the inherent dangers of interpreting extremely old ^{14}C dates. In practice, ^{14}C dates of >45,000 should be viewed with caution.

3.2.1.4 Sources of Error in ^{14}C Dating

3.2.1.4.1 PROBLEMS OF SAMPLE SELECTION AND CONTAMINATION

It is self-evident that a contaminated sample will give an erroneous date, but it is frequently very difficult to ascertain the extent to which a sample has been contaminated. Some forms of contamination are relatively straightforward: Modern rootlets, for example, may penetrate deep into a peat section, and without careful inspection of a sample and removal of such material, gross errors may occur. More abstruse problems arise when dating materials containing carbonates (e.g., shell, coral, and bone). These materials are particularly susceptible to contamination by modern carbon because they readily participate in chemical reactions with rainwater and/or groundwater. Most mollusks, for example, are primarily composed of calcium carbonate in the metastable crystal form, aragonite. This aragonite may dissolve and be redeposited in the stable crystal form of calcite. During the process of solution and recrystallization, exchange of modern carbon takes place and the sample is thereby contaminated (Grant-Taylor, 1972). This problem also exists in corals that are all aragonite. Commonly, X-ray diffraction is used to identify different carbonate mineral species, and materials with a high degree of recrystallization are discarded. However, Chappell and Polach (1972) have noted that recrystallization can occur in two different modes: one open system and therefore susceptible to modern ^{14}C contamination and one closed system that is internal and involves no contamination. The former process tends to be concentrated around the sample margins, as one might expect, and so a common strategy is to dissolve away the surface 10-20% of the sample with hydrochloric acid and to date the remaining material. For shells thought to be very old, in which recrystallization may have affected a deep layer, the remaining inner fraction should ideally be dated in two fractions (an "outer inner" and an "inner inner" fraction) to test for consistency of results. However, even repeated leaching with hydrochloric acid may not produce a reliable result in cases where recrystallization has permeated the entire sample as very small amounts of modern carbon can lead to gross errors. A possible remedy to this problem of dating old shells is to isolate a protein, conchiolin, present in very small quantities in shells (1-2%) and to date this, rather than the carbonate (Berger et al., 1964).

Carbon in conchiolin does not undergo exchange with carbon in the surrounding environment and hence is far less likely to be contaminated. Unfortunately, to isolate enough conchiolin, very large samples (>2 kg) are needed, and these are often not available.

Similar problems are encountered in dating bone; because of exchange reactions with modern carbon, dates on total inorganic carbon or on apatite carbonate are unreliable (Olsson et al., 1974). As in the case of shells, a more reliable approach is to isolate and date carbon in specific amino acids that are extracted from the bone. For example, Nelson (1990) dated bone samples using the specific amino acid ninhydrin (2,2-dihydroxy-1,3 indandione). As noted earlier, this approach of isolating compound-specific material is now widely used to provide a clear connection to a specific organism being dated.

Another form of error concerns the "apparent age" or "hard-water effect" (Shotton, 1972). This problem arises when the materials to be dated, such as freshwater mollusks or aquatic plants, take up carbon from water containing bicarbonate derived from old, inert sources. This is a particularly difficult problem in areas where limestone and other calcareous rocks occur. In such regions, surface and groundwater may have much lower $^{14}C/^{12}C$ ratios than that of the atmosphere due to solution of the essentially ^{14}C-free bedrock. Plants and animals existing in these environments will assimilate carbon in equilibrium with their surrounding milieu rather than the atmosphere; hence, they will appear older than they are in reality, sometimes by as much as several thousand years. This problem was well illustrated by Shotton (1972) who studied a late glacial stratigraphic section in North Jutland, Denmark. Dates on contemporaneous twigs and a fine-grained vegetable residue, thought to be primarily algal, fell neatly into two groups, with the algal material consistently 1700 years older than the terrestrial material. The difference was considered to be the result of a hard-water effect, the aquatic plants assimilating carbon in equilibrium with water containing bicarbonate from old, inert sources.

Other studies have demonstrated further complexities in that the degree of "old carbon" contamination may change over time. For example, Karrow and Anderson (1975) suggested that some lake sediments in southwestern New Brunswick, Canada, studied by Mott (1975) were contaminated with old carbon shortly after deglaciation. Initial sedimentation was mainly marl derived from carbonate-rich till and carbonate bedrock, but as the area became vegetated and soil development took place, the sediments became more organic and less contaminated by "old carbon." Dates on the deepest lake sediments are thus anomalously old and would appear to give a date of deglaciation inconsistent with the regional stratigraphy. This points to the more general observation that the geochemical balance of lakes may have changed through time and that the modern water chemistry may not reflect former conditions. This is particularly likely in formerly glaciated areas where the local environment immediately following deglaciation would have been quite different from that of today. One should thus interpret basal dates on lake sediments or peat bogs with caution. Equally, dates on aquatic flora and fauna, in closed lake basins that have undergone great size changes, must also be viewed in the light of possible changes in the aqueous geochemistry of the site.

It is important to recognize that not all types of contamination are equally significant; contamination by modern carbon is far more important than that by old carbon because of its much higher activity (Olsson, 1974). Figures 3.6 and 3.7 show the errors associated with different percentage levels of contamination by modern and old material, respectively. It will be seen that a 5000-year-old sample, 20% contaminated with 15,000-year-old carbon (unlikely as

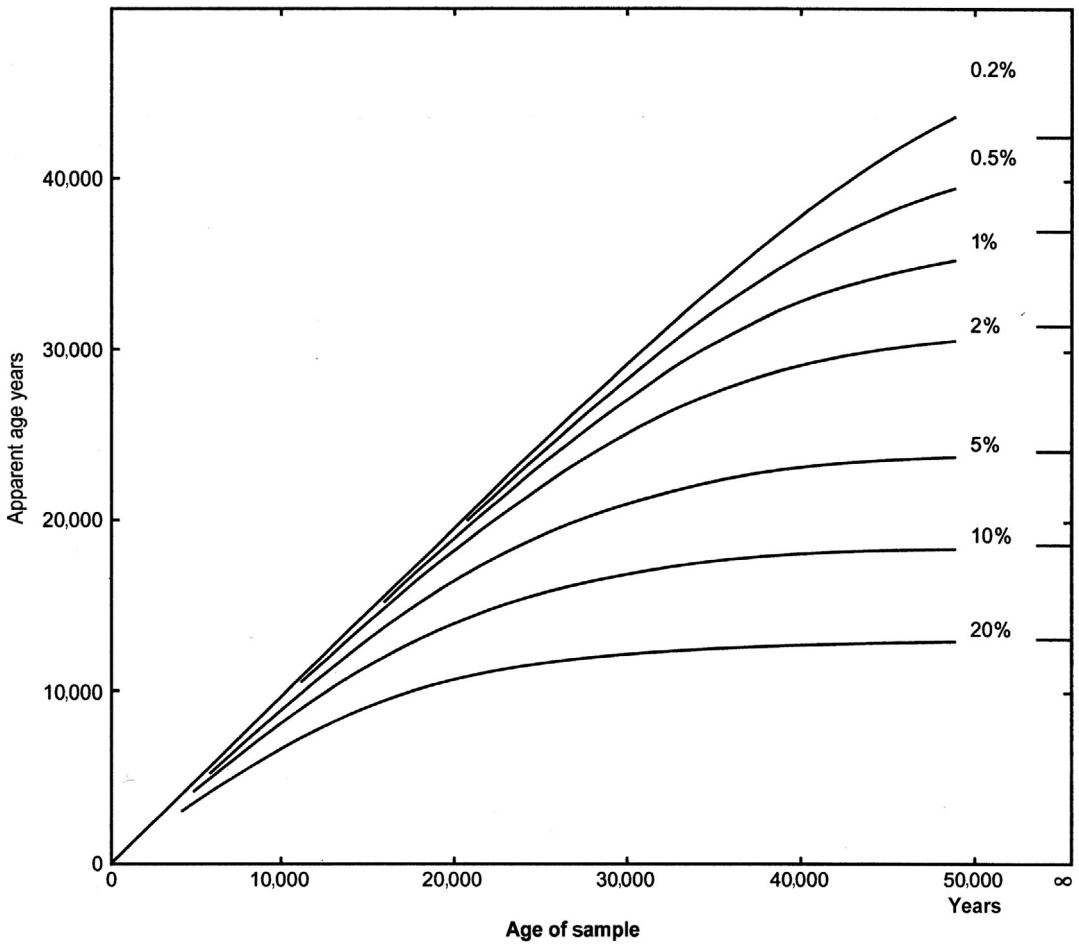


FIGURE 3.6 Apparent ages as a function of sample age if there are different levels of contamination by modern material in the sample. Thus, a 20,000-year-old sample contaminated with 10% of modern material would appear to be ~15,000 years old. *From Olsson and Eriksson (1972).*

that might be!), would give a date in error by only ~1250 years. By contrast, a 15,000-year-old sample contaminated with only 3% of modern carbon would result in a dating error of about the same magnitude. Very careful sample selection is therefore needed; dating errors are most commonly the result of inadequate sampling.

3.2.1.4.2 VARIATIONS IN ^{14}C CONTENT OF THE OCEANIC RESERVOIR AND VENTILATION OF THE DEEP OCEAN BASINS

In Section 3.2.1.4.1, the problem that some freshwater aquatic plants or mollusks may be contaminated by water containing low levels of ^{14}C was discussed. In the case of marine organisms, the problem is much more universal. First, when carbon dioxide is absorbed into the oceans, a fractionation takes place which leads to an enrichment of 15‰ (equivalent

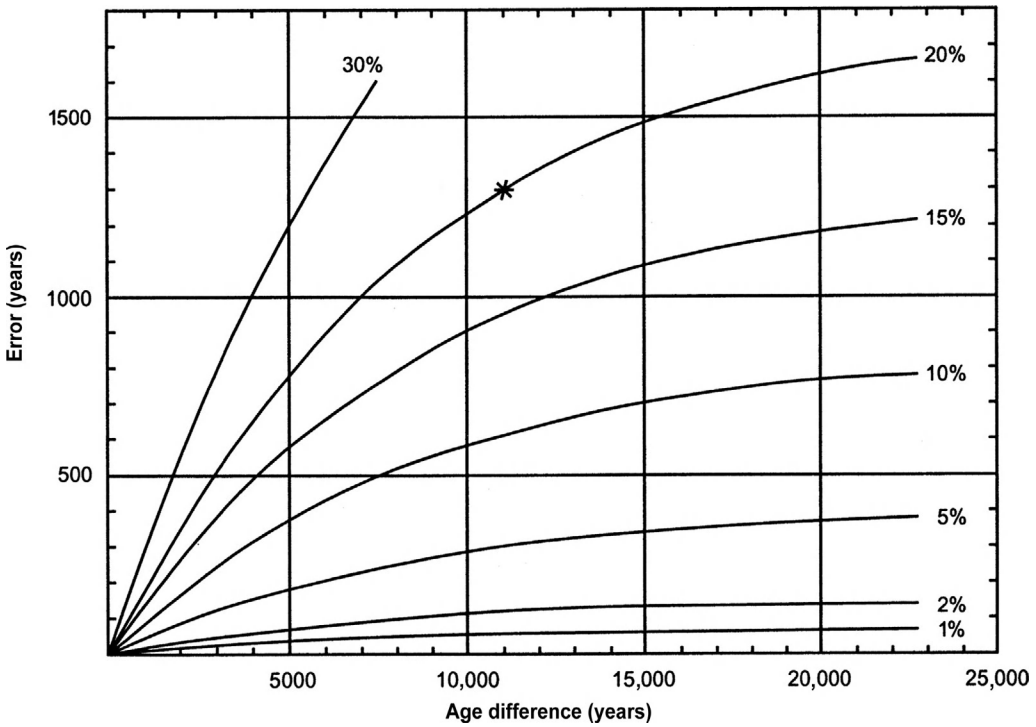


FIGURE 3.7 The error in a radiocarbon date if a certain fraction of the sample (indicated by each curve) is contaminated by *older* material (having a lower ^{14}C activity). Errors expressed as age differences (abscissa) between the sample and contaminant. For example, a 5000-year-old sample with 20% contamination by 16,000-year-old material (i.e., material 11,000 years older than the true age—see star on figure) will yield a date in error (too old) by 1300 years. *From Olsson (1974).*

to ~120 years) in the ^{14}C activity of oceanic bicarbonate relative to that of the atmosphere. However, ocean surface waters are not in isotopic equilibrium with the atmosphere because oceanic circulation brings ^{14}C-depleted water to the surface to mix with "modern" water. Consequently, the ^{14}C age of the surface water (the apparent age, or reservoir age) varies geographically (Figure 3.8; Bard, 1988). In the lower latitudes of all oceans, the mean reservoir age of surface waters is ~400 years, which means that 400 years must be *subtracted* from a ^{14}C date on marine organic material from the mixed layer, in order to compare it with terrestrial material. At higher latitudes, this correction can be much larger due to upwelling of older water and the effect of sea ice that limits the ocean-atmosphere exchange of CO_2. As Figure 3.8 illustrates, the modern North Atlantic is different from other high-latitude regions because of advection of warmer waters (relatively enriched in ^{14}C) from lower latitudes and strong convection (deepwater formation), which limits any upwelling of ^{14}C-depleted water.

The extent to which such ^{14}C gradients have been constant over time is of great significance for dating older events in the marine environment and comparing them with terrestrial records, as well as for understanding changes in ocean circulation (Okazaki et al., 2010). For example, if North Atlantic Deep Water (NADW) formation ceased during the Last Glacial

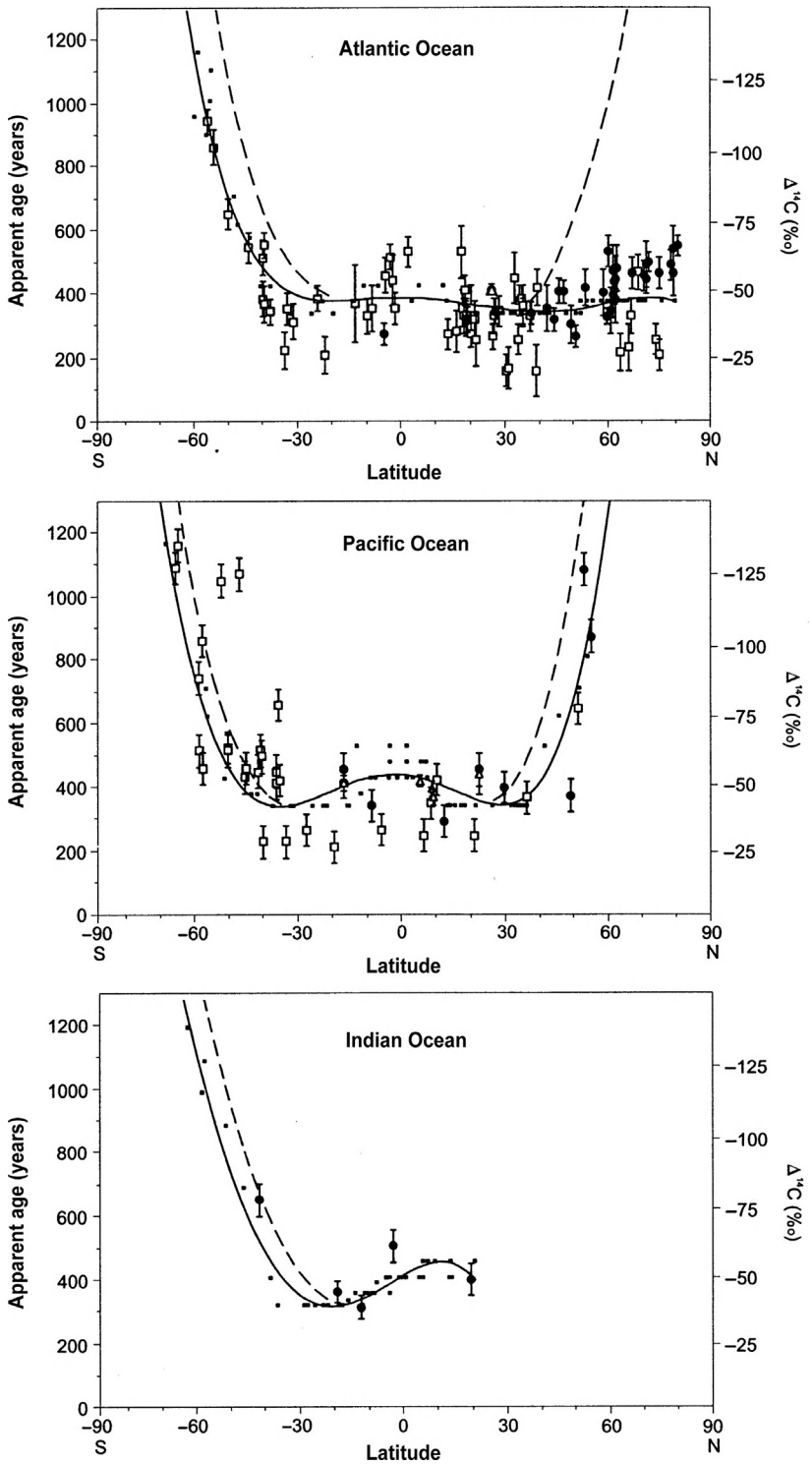


FIGURE 3.8 Apparent age of the surface waters of the major oceans, averaged by latitude, based on measurements of corals (open triangles) mollusks (closed circles) and seawater ΣCO_2 samples (open squares); closed squares are reconstructions of prebomb $\Delta^{14}C$ levels (Broecker et al., 1985a). The solid lines are least-squares polynomials fitted to the data; the dashed line represents a hypothetical profile for the last glacial maximum, assuming there was no North Atlantic Deep Water forming at that time. *From Bard (1988).*

(see Chapter 6, Section 6.8), then the surface water reservoir age would be similar to other high-latitude areas, as depicted by the dashed line in Figure 3.8 (upper panel). Hence, late Glacial planktonic samples from this area might require an age adjustment of as much as 1000 years, and if deepwater switched on and off rapidly, age corrections would be equally volatile, possibly even leading to age inversions in otherwise stratigraphically undisturbed sediments (Voelker et al., 1998). The matter was addressed by Bard et al. (1994) and Austin et al. (1995) who compared marine and terrestrial ^{14}C-dated samples associated with the Vedde volcanic ash. This ash layer originated from an explosive Icelandic eruption and was widely distributed across the North Atlantic and adjacent land areas around 10,300 ^{14}C years BP, according to AMS dates on terrestrial samples from the time of ash deposition. However, all planktonic samples associated with the ash layer dated ~11,000 ^{14}C years BP, indicating that the surface reservoir effect then was ~700 years, versus ~400 years today, probably as a result of reduced North Atlantic Deep Water (NADW) formation (thus, less advection of southern waters) and/or increased sea-ice cover at that time. Similarly, Sikes et al. (2000) obtained a surface reservoir age off the coast of New Zealand of ~800 years at 11,900 ^{14}C years BP, increasing to ~2000 years at the LGM.

So far, we have focused primarily on surface water, but the same issues arise in deepwater changes. North Atlantic Deep Water and the Antarctic Bottom Water may remain out of contact with the atmosphere for centuries because of the overlying warmer water in mid- and low latitudes. During this time, the ^{14}C content of the deepwater decreases so that deepwater samples commonly give ^{14}C ages more than 1000 years older than surface water (Figure 3.9). Indeed, the change in ^{14}C activity of oceanic water has been used to assess the former "ventilation rate" of

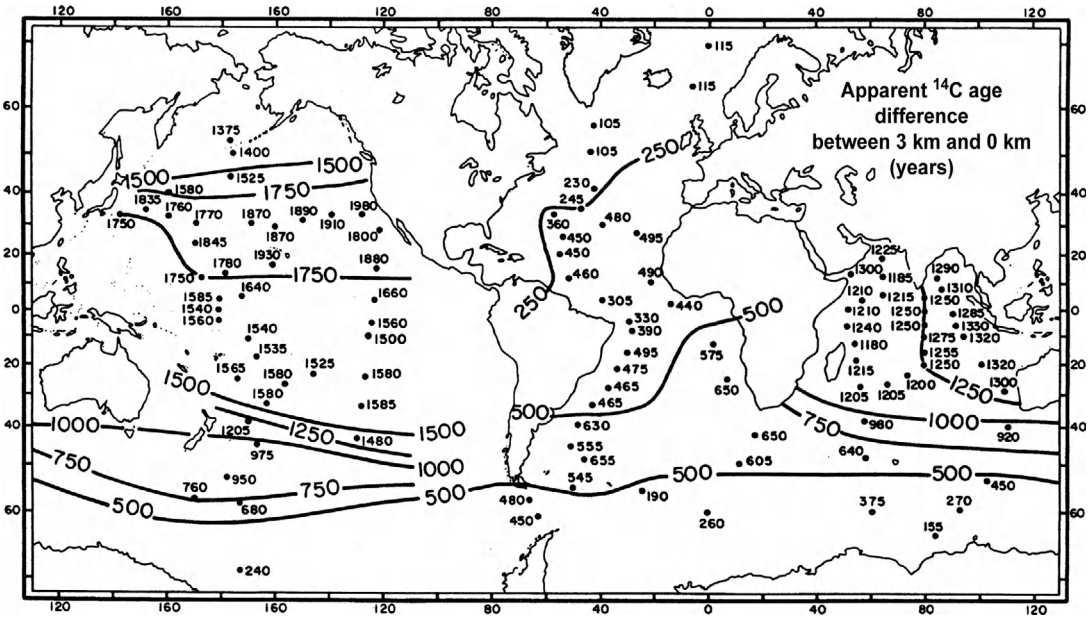


FIGURE 3.9 Present-day radiocarbon age differences between surface waters and waters at 3 km depth. *From Broecker et al. (1988).*

the ocean, by comparing the age of ^{14}C-dated planktonic and benthic foraminifera, or cold-water corals (surface- and deep-dwelling organisms, respectively) in marine sediments from the same site (Broecker et al., 1988, 2004a; Robinson et al., 2005; Cao et al., 2007). Then, by comparing modern (core-top) samples with those from earlier periods, a record of changes in ventilation rate and ocean circulation can be established (cf. Chapter 6, Section 6.8.1).

A change in ventilation rate, resulting from a reduction or cessation in deepwater formation, has significant implications for poleward heat transport, with implications for all aspects of the climate system. Furthermore, changes in oceanic ventilation will influence the atmospheric radiocarbon content (by venting "old carbon" into the atmosphere) and also influence the CO_2 concentration of the atmosphere (since the ocean has a much larger reservoir of CO_2) (Skinner et al., 2010). Ventilation rates therefore provide lots of insights into the workings of the climate system, and consequently, they have received a great deal of attention (e.g., Keigwin and Schlegel, 2002; Broecker et al., 2004a,b; Skinner and Shackleton, 2004; Okazaki et al., 2010; Sigman et al., 2010). For example, studies that compare radiocarbon-dated material with calendar year chronologies show that during the LGM, there was a relatively high concentration of ^{14}C in the atmosphere because oceanic processes that previously (and subsequently) carried surface waters to great depths in the oceans were greatly reduced (see Chapter 6, Section 6.8). Because of this (relative) enrichment, radiocarbon dates on material of LGM age must be adjusted (upward) to account for the higher "starting" concentration of ^{14}C in the samples. This is important for geochronology, but the underlying reasons are even more significant because they point to major changes in ocean circulation and associated heat transfer within the entire climate system. Studies of ventilation ages changes can illuminate these changes. Thus, Skinner et al. (2010) examined radiocarbon dates on pairs of benthic and planktonic foraminifera in a core from the South Atlantic (adjusting the difference for changes in atmospheric ^{14}C concentration—see Adkins and Boyle (1997) and Chapter 6, Section 6.8.1) to calculate changes in deepwater ventilation rates of the deep Southern Ocean. Ventilation rate declined through the LGM, reaching ~4000 years (relative to the modern atmosphere) around 19,000 cal. years BP, and then decreased to ~1500 years at the start of the Bolling-Allerød interstadial (Figure 3.10). This change was accompanied by a rise in atmospheric CO_2 levels from ~180 to ~235 ppmv, indicating that upwelling of old, carbon-rich water from the deep ocean occurred during this time period. These results are similar to the record from a core in the Tropical Eastern Pacific that registered changes in the ventilation age of intermediate waters, which closely parallel shifts in atmospheric CO_2 (Marchitto et al., 2007). Both results point to the formation and isolation of deep, salty waters in the Southern Ocean during the LGM, as sea ice expanded and brine was ejected. During deglaciation of the Southern Hemisphere, sea ice retreated and the ^{14}C-depleted waters began to circulate and mix, shifting the ^{14}C content of deep and intermediate waters in regions far beyond the Southern Ocean and releasing CO_2 to the atmosphere. Marchitto et al. (2007) argue that this process was in fact initiated by changes in deepwater production in the North Atlantic, triggered by meltwater from the waning northern continental ice sheets, which reduced the formation of NADW; this led to a compensating shift in upwelling of Southern Ocean deepwater (dubbed a "bipolar seesaw" by Broecker, 1998). Tracking changes in intermediate and deepwater, with their associated radiocarbon anomalies, is proving to be complex, with geographical and temporal variations, as well as differences that are apparent at different depths in the ocean (cf. Broecker et al., 2004b, 2008; Stott et al., 2009; Okazaki et al., 2010). Understanding these

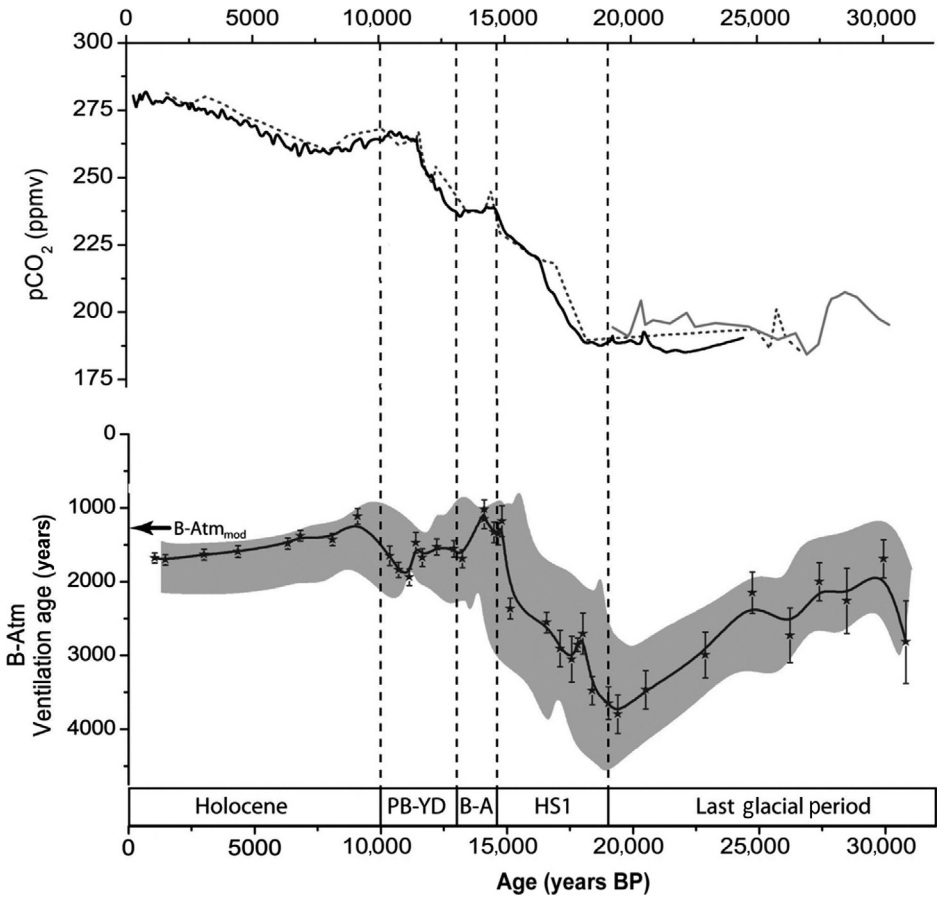


FIGURE 3.10 Above: Atmospheric CO_2 from the EPICA Dome C, Taylor Dome, and Byrd (Antarctica) ice cores, shown by solid dark gray, dashed, and light gray lines, respectively, and placed on the age scale of Lemieux-Dudon et al. (2010). Below: Apparent deepwater ventilation in core MD07-3076 from the Atlantic sector of the Southern Ocean. Black line and stars indicate the best estimate ventilation history and associated chronology. Vertical error ranges show the magnitude of combined planktonic/benthic ^{14}C date uncertainties (1σ). The shaded area shows the range of ventilation histories (smoothed) that could be supported by alternative surface reservoir age scenarios. Labels at the base indicate approximate timing of North Atlantic event-stratigraphy chronozones. *From Skinner et al. (2010).*

changes is critical for deciphering the links between ocean circulation, the terrestrial biosphere and atmospheric CO_2, and associated climate shifts and their causes in both the Southern and Northern Hemispheres (Broecker, 2009; Yu et al., 2010). The record of radiocarbon anomalies has a central role in resolving these issues.

3.2.1.4.3 FRACTIONATION EFFECTS

Basic to the principle of ^{14}C dating is the assumption that plants assimilate radiocarbon and other carbon isotopes in the same proportion as they exist in the atmosphere (i.e., the $^{14}C/^{12}C$ ratio of plant tissue is the same as that in the atmosphere). However, during photosynthesis,

when CO_2 is converted to carbohydrates in plant cells, an isotopic fractionation occurs such that ^{12}C is more readily "fixed" than ^{14}C, resulting in a lower ^{14}C content in plants than that of the atmosphere (Olsson, 1974). ^{14}C "depletion" may be as much as 5% below atmospheric levels, but this is not consistent among all organisms. The magnitude of the fractionation effect varies from one plant species to another by a factor of 2-3 and depends on the particular biochemical pathways evolved by the plant for photosynthesis (Lerman, 1972). This is discussed in further detail in Appendix A. Fortunately, some assessment of the ^{14}C fractionation effect can be made relatively easily by measuring the ^{13}C content of a sample. ^{14}C fractionation is very close to twice that of ^{13}C (Craig, 1953), a stable isotope that occurs in far greater quantities than ^{14}C and can hence be routinely measured by a mass spectrometer. ^{13}C content is generally expressed as a departure from a Cretaceous limestone standard (PeeDee Belemnite; see Appendix A):

$$\delta^{14}C = 2\delta^{13}C = \frac{\left(^{13}C/^{12}C\right)_{\text{sample}} - \left(^{13}C/^{12}C\right)_{\text{PDB}}}{\left(^{13}C/^{12}C\right)_{\text{PDB}}} \times 10^3‰ \tag{3.3}$$

A change in $\delta^{14}C$ of only 1‰ (i.e., a change in $\delta^{13}C$ of 0.5‰) corresponds to an age difference of ~8 years. Consequently, if two contemporaneous samples differed in $\delta^{13}C$ by 25‰, they would appear to have an age difference of ~400 years (Olsson and Osadebe, 1974). To avoid such confusion, the ^{13}C value of all samples is normalized to −25‰, the average value for wood. By adopting this reference value, comparability of dates is possible. This is particularly important in the case of marine shell samples, which characteristically have $\delta^{13}C$ values in the range +3 to −2‰. Standardization to $\delta^{13}C = -25‰$ thus involves an age adjustment of as much as 450 years (to be *added* to the uncorrected date).

This is further complicated because of the low ^{14}C content of the oceans that gives modern seawater an "apparent age" of 400-2500 years (see Section 3.2.1.4.2) and results in a correction (a value to be *subtracted* from the uncorrected age) in the opposite direction from the correction for fractionation effects. For the North Atlantic region, the apparent age of seawater is ~400 years (Stuiver et al., 1986), so the fractionation and oceanic effect more or less cancel out. In other areas, particularly at high latitudes, the oceanic adjustment is >450 years, so the adjusted date will be lower (younger) than the original estimate, before correction for fractionation effects. Of course, for comparison of dates on similar materials within one area, these adjustments are irrelevant. However, if one wishes to compare, for example, dates on terrestrial peat with dates on marine shells or to compare a shell date from high latitudes with one from another area, care must be taken to ascertain what corrections, if any, have been applied. Details of reservoir corrections for Holocene samples from different locations can be found in Stuiver et al. (1986).

3.2.1.5 *Long-Term Changes in Atmospheric ^{14}C Content*

Fundamental to the principles of radiocarbon dating is the assumption that atmospheric ^{14}C levels have remained constant during the period useful for ^{14}C dating. However, even in the early days of radiocarbon dating, comparisons between archeologically established Egyptian chronologies and ^{14}C dates suggested that the assumption of temporal constancy in ^{14}C levels might not be correct. It is now abundantly clear that ^{14}C levels have varied over

TABLE 3.2 Possible Causes of Radiocarbon Fluctuations

I. Variations in the rate of radiocarbon production in the atmosphere

1. Variations in the cosmic-ray flux throughout the solar system
a. Cosmic-ray bursts from supernovas and other stellar phenomena
b. Interstellar modulation of the cosmic-ray flux
2. Modulation of the cosmic-ray flux by solar activity
3. Modulation of the cosmic-ray flux by changes in the geomagnetic field
4. Production by antimatter meteorite collisions with the Earth
5. Production by nuclear weapons testing and nuclear technology

II. Variations in the rate of exchange of radiocarbon between various geochemical reservoirs and changes in the relative carbon dioxide content of the reservoirs

1. Control of CO_2 solubility and dissolution as well as residence times by temperature variations
2. Effect of sea-level variations on ocean circulation and capacity
3. Assimilation of CO_2 by the terrestrial biosphere in proportion to biomass and CO_2 concentration, and dependence of CO_2 on temperature, humidity, and human activity
4. Dependence of CO_2 assimilation by the marine biosphere upon ocean temperature and salinity, availability of nutrients, upwelling of CO_2-rich deepwater, and turbidity of the mixed layer of the ocean

III. Variations in the total amount of carbon dioxide in the atmosphere, biosphere, and hydrosphere

1. Changes in the rate of introduction of CO_2 into the atmosphere by volcanism and other processes that result in CO_2 degassing of the lithosphere
2. The various sedimentary reservoirs serving as a sink of CO_2 and ^{14}C. Tendency for changes in the rate of sedimentation to cause changes in the total CO_2 content of the atmosphere
3. Combustion of fossil fuels by human industrial and domestic activity

From Damon et al. (1978).

time, though fortunately the magnitude of these variations can be assessed. Variations in atmospheric ^{14}C concentration may result from a wide variety of factors, as indicated in Table 3.2, and it is worth noting that many of these factors may themselves be important influences on climate. It is a sobering thought that fluctuations in the concentration of radiocarbon may help to explain the very paleoclimatic events to which radiocarbon dating has been applied for so many years; there could be no better illustration of the essential unity of science (Damon, 1970).

Early work on carefully dated tree rings indicated that ^{14}C estimates showed systematic, time-dependent variations (de Vries, 1958). Both European and North American tree-ring samples spanning the last 400 years showed departures from the average of up to 2%, with ^{14}C maxima around AD 1500 and 1700 (Figure 3.11). These secular ^{14}C variations are closely related to variations in solar activity, as discussed further in Section 3.2.1.6 (Suess, 1980). Also seen in Figure 3.11 is the marked decline in ^{14}C activity during the last 100 years. This resulted primarily from the combustion of fossil fuel during the period (Suess, 1965), causing a rapid increase in the abundance of "old" (essentially ^{14}C-free) carbon in the atmosphere (the so-called Suess effect).

These studies generated further interest in testing the assumptions of radiocarbon dating and led to thousands of checks being made between ^{14}C dates and corresponding wood samples, each carefully dated according to dendrochronological principles (Chapter 10). The

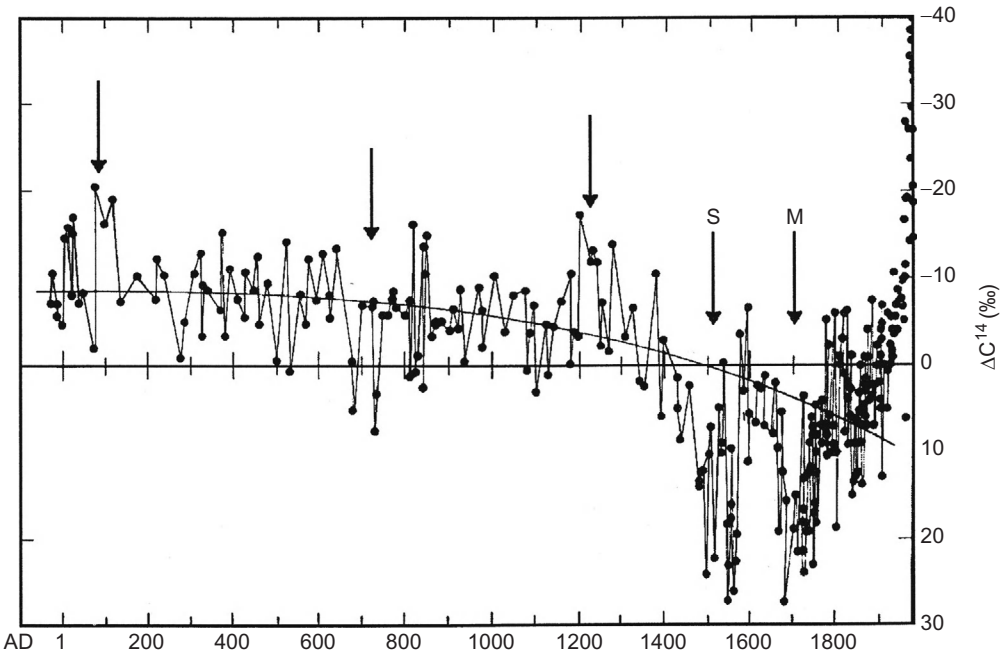


FIGURE 3.11 Radiocarbon variations over the last 2000 years expressed as departures from the long-term average. Trend due to geomagnetic field variation shown by curved line. Positive ^{14}C anomalies around AD 1500 and 1700 correspond to periods of reduced solar activity (the Spörer and Maunder minima, S and M, respectively). At these times, the increased cosmic-ray flux produces more ^{14}C in the upper atmosphere. Combustion of fossil fuel has contaminated the atmosphere with ^{14}C-free CO_2, hence the large negative departures shown since 1850. Note that the ordinate is plotted with positive departures lowermost, corresponding to periods of *reduced* solar activity. *From Eddy (1977).*

longest tree-ring calibration set is the German oak and pine chronology of ~12,400 years, made up of more than 5000 different overlapping tree-ring sections from living trees, medieval housing timbers, and subfossil wood excavated from river gravels (Becker, 1993; Friedrich et al., 2004). Similar chronologies have been constructed from Irish oaks (to 5289 BC) and from Douglas fir and bristlecone pine in the US Pacific Northwest and California (to >6000 BC). Other "floating chronologies," derived from radiocarbon-dated subfossil wood, have now been accurately fixed in time by matching de Vries-type ^{14}C variations in the chronology with those observed in the well-dated continuous tree-ring records (e.g., Kuniholm et al., 1996). By being able to precisely match such "wiggles," recorded in wood from places thousands of kilometers apart, it is clear that the high-frequency variations have real geophysical significance and are not simply the result of noise in the radiocarbon chronology (de Jong et al., 1980).

By radiocarbon dating wood of known age from different regions of the world, a very consistent picture of the relationship between ^{14}C age and calendar year age has been built up for the last ~12,556 years (Kromer and Becker, 1993; Pearson and Stuiver, 1993; Pearson et al., 1993; Stuiver and Pearson, 1993; Friedrich et al., 2004; Schaub et al., 2008a). This calibration

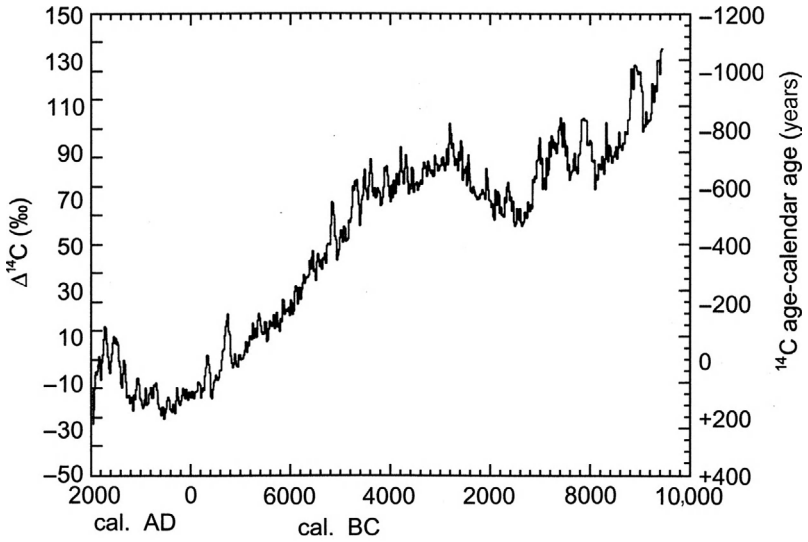


FIGURE 3.12 Bidecadal anomalies of $\Delta^{14}C$ (‰) (left axis) in relation to the calendar year age of the wood samples analyzed. An anomaly of +1‰ corresponds to the radiocarbon age underestimating the dendrochronological age by 8 years (right axis). *From Stuiver and Reimer (1993).*

is based on bidecadal and decadal wood samples for most of the period, but for the last ~500 years, year-by-year analysis of wood has provided a very detailed comparison of calendar year and ^{14}C ages (Stuiver, 1993). The ^{14}C age is very close to the dendrochronological age (±100 years) for the last ~2500 years, but before that, there was a systematic difference (^{14}C underestimating true age) increasing to ~1000 years by ~10,000 cal. years BP (Figure 3.12).

For the period before reliable dendrochronologically dated wood samples are available, other types of material must be used to calibrate the radiocarbon record. These include annually laminated (varved) lake sediments, corals, stalagmites, and marine sediments calibrated to stalagmite oxygen isotope variations. By applying stringent criteria for acceptance of such samples, a composite calibration of the radiocarbon timescale, in calendar years, has been obtained for the last 50,000 years (Figure 3.13; Reimer et al., 2009). To incorporate varved sediments into the calibration, a robust annual chronology must be obtained, based on multiple sediment records and repeated lamination counts (e.g., Wohlfarth et al., 1995; Bronk Ramsey et al., 2012). These can then be compared to radiocarbon dates on material extracted from the sediments, assuming it has the same age as the enclosing varve (which is regrettably not always the case). For corals, uranium-series ($^{230}Th/^{234}U/^{238}U$) dates obtained by thermal ionization mass spectrometry (TIMS) on carefully selected pristine samples (chosen to avoid postdepositional contamination) can be compared with radiocarbon dates on the same samples, adjusted for the marine reservoir effect in surface waters (assuming this has not changed over time) (Chiu et al., 2005; Fairbanks et al., 2005). Very important additional records for calibration are marine sediments from the Cariaco Basin, off the coast of Venezuela. This anoxic basin contains sediments that are varved for more than 5000 years, but the varve section does not extend to the surface, leaving the chronology "floating" in time. The floating varve

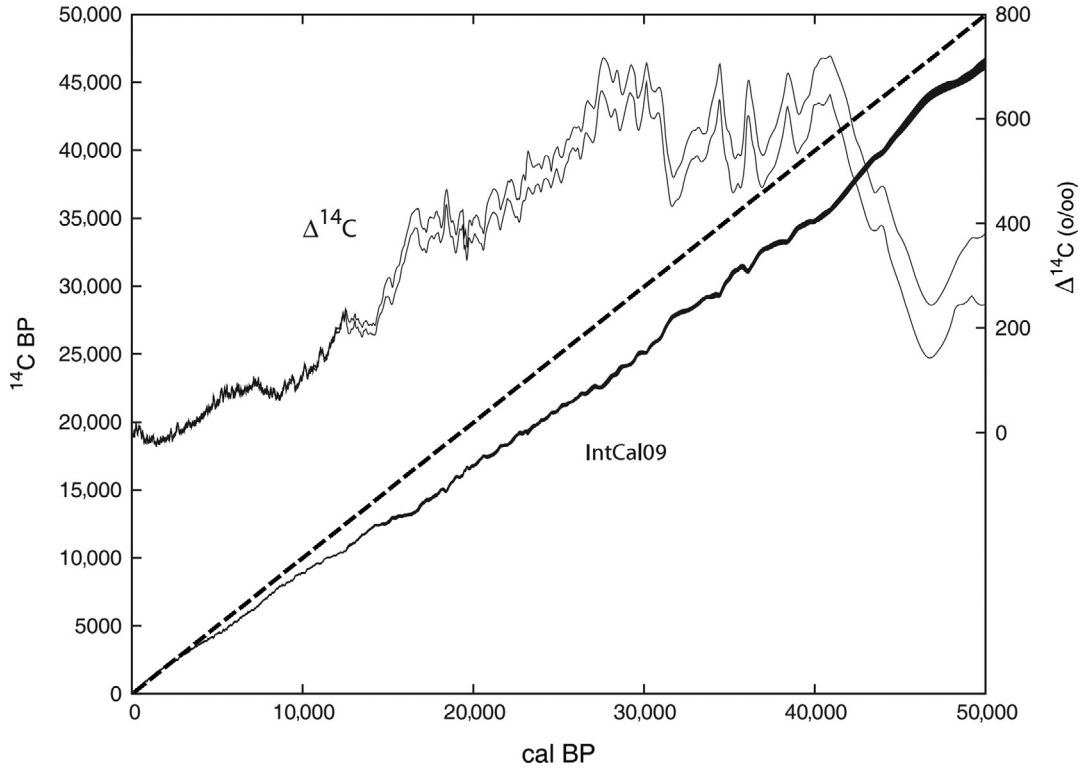


FIGURE 3.13 IntCal09 calibration curve and age-corrected Δ^{14}C (‰) with 1-standard deviation envelopes. Dashed lines show the 1:1 correspondence, if ^{14}C ages and calendar years were identical. *From Reimer et al. (2009).*

chronology was first nailed down by finding the best fit between "wiggles" in the radiocarbon versus calendar year age record of the German oak/pine chronology and a comparable record of AMS-dated forams in the annually laminated sediments from the Cariaco Basin (Hughen et al., 2000). Once this section of the varved record was firmly anchored to the tree-ring series, the older varves could be assigned individual calendar ages, extending the annual record back to 14,700 cal. years BP (Hughen et al., 1996, 1998). Unfortunately, the older Cariaco Basin sediments are not continuously varved, but changes in characteristics of the sediments can be directly linked to other records where the chronology is known, thereby providing an opportunity to extend the radiocarbon-dated Cariaco Basin record even further back in time. This comes about because the Cariaco Basin sediments are sensitive to changes in upwelling (which vary with the strength of trade winds blowing across the basin) and to changes in the position of the intertropical convergence zone (ITCZ) and associated rainfall. When the ITCZ is displaced to the south, it leads to more precipitation on the adjacent continent, which increases runoff and sediment flux, which in turn affects productivity in the basin. These changes can be seen in the color of the sediments, measured at different wavelengths or simply in visible light (grayscale). The ITCZ position and the trade wind strength are directly linked to the temperature gradient between the equator and pole, such that cooling at high latitudes increases this gradient, causing the ITCZ to shift southward and for trade wind

strength to increase. Thus, the Cariaco Basin sediment color changes reflect very large-scale features of the climate system and so are strongly correlated with other records, from as far away as Greenland and China (Hughen et al., 2004, 2006). Taking advantage of this, Hughen et al. (2006) were able to directly link the $\delta^{18}O$ record in stalagmites from Hulu Cave (eastern China), which had been extremely well dated by ^{230}Th (back to ~75,000 cal. years BP) to the radiocarbon-dated Cariaco Basin sediments in order to calibrate the ^{14}C timescale far beyond both the available tree-ring record and the Cariaco varved sediment record (Figure 3.14). However, uncertainties remain, not least because of the assumption made in the case of

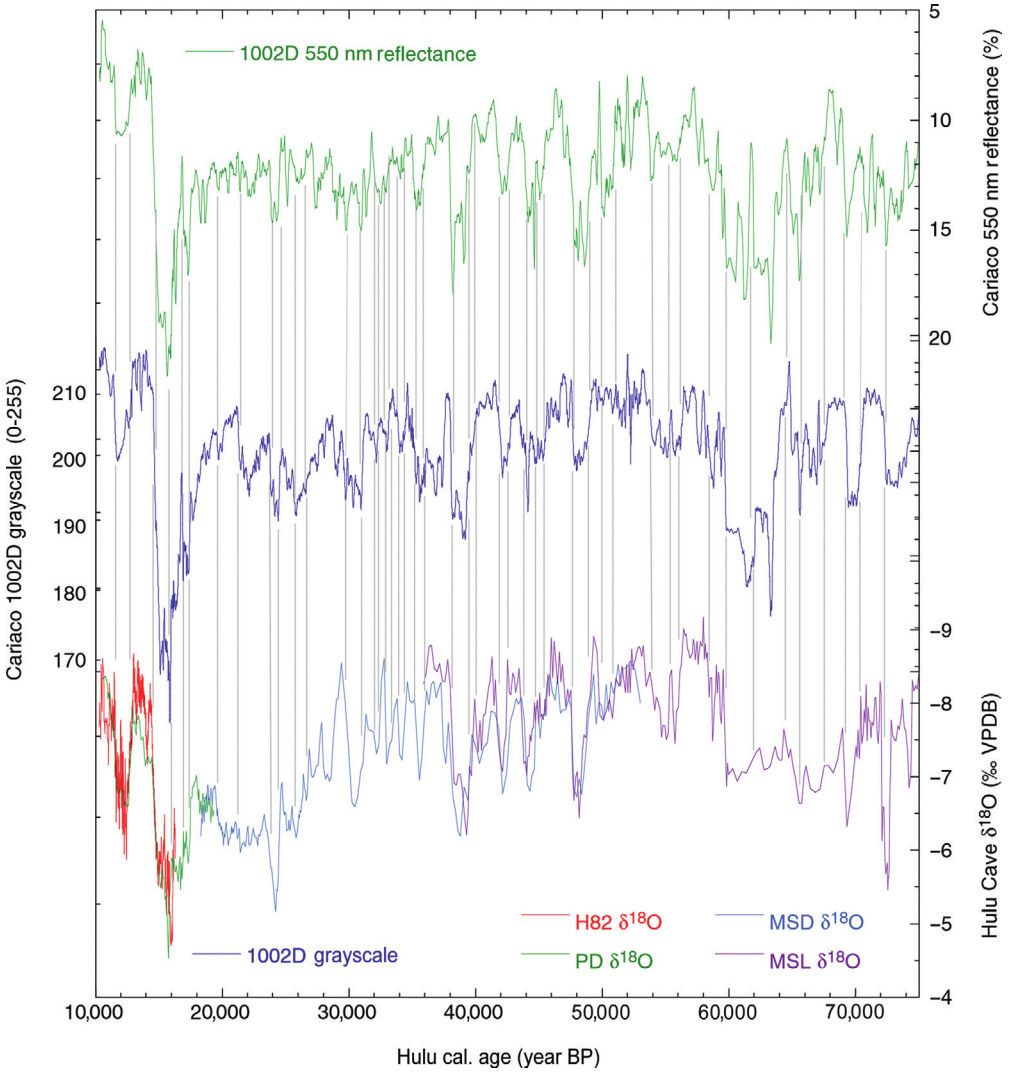


FIGURE 3.14 High-resolution paleoclimate time series for Cariaco Basin sediment 550 nm and grayscale reflectance (top, middle) and Hulu Cave speleothems $\delta^{18}O$ (bottom), plotted against Hulu ^{230}Th calendar age. Tie lines used for correlating and aligning the Cariaco records to Hulu calendar age are shown in gray. The different samples used to construct the Hulu Cave isotopic record are shown by the colors in the bottom right of the figure. *From Hughen et al. (2006).*

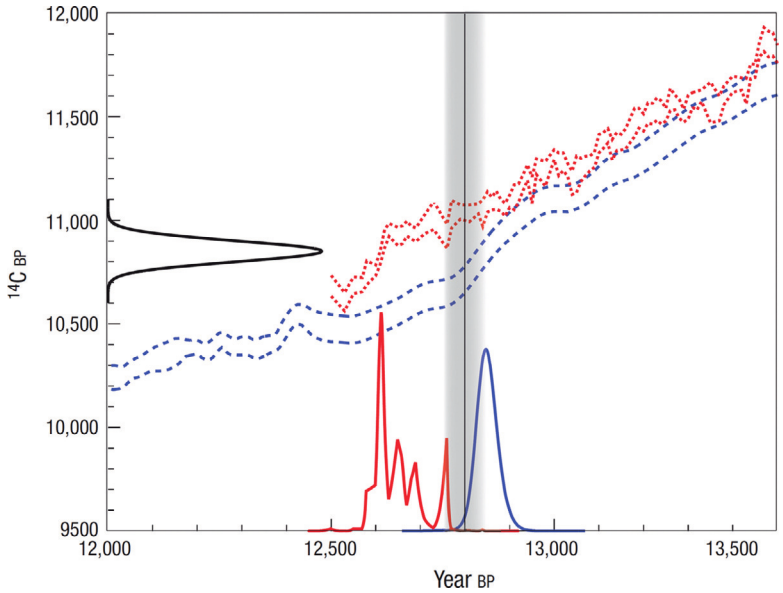


FIGURE 3.15 Comparison of two calibrations of a hypothetical radiocarbon-dated event. The radiocarbon chronologies based on a floating tree-ring record (red dashed lines) and the internationally accepted IntCal045 combined record (blue dashed lines) are shown at the top of the figure. Both curves are plotted as uncertainty envelopes (2σ). A hypothetical event with a measured radiocarbon age of $10{,}850 \pm 50$ ^{14}C BP (black) is calibrated using the respective calibrations. The potential dates that would be given by the tree-ring time series (red) and IntCal04 (blue) calibrations are shown by the probability distribution functions on the bottom calendar axis. A calendar-dated event (thick black line) that could be obtained from, for example, a U/Th-dated speleothem is shown at $12{,}800 \pm 25$ BP with gray shading representing the uncertainty (2σ). Depending on which calibration curve is used, the radiocarbon-dated event could be interpreted as either leading or lagging the U/Th-dated event. *From Reimer and Hughen (2008).*

the Cariaco Basin radiocarbon dates that there has been no significant change in the marine reservoir age correction (assumed to be ~420 years) throughout the record. Cross-checking with other, independent data from the overall calibration curve suggests that this may be the case for most of the period, but there is evidence that it may not have been so during periods when there were rapid changes of ^{14}C in the atmosphere (Muscheler et al., 2008). Ironically, these are periods when obtaining accurate dates is essential, as slight differences in the ^{14}C-calendar year calibration can lead to quite different interpretations of events (Figure 3.15; Reimer and Hughen, 2008).

No doubt further refinements will be made to the overall calibration of radiocarbon dates, as new data and ideas for correlating well-dated records emerge (e.g., Muscheler et al., 2008; Schaub et al., 2008b), but for now, the IntCal09 calibration curve provides a widely accepted reference curve for which software is available to compute calendar year probability functions for radiocarbon dates and their associated errors (see www.calib.org). If the calibration curve was, in fact, a straight line, this would be quite straightforward, but because of the many minor variations (wiggles) in the calibration curve, it is almost never possible to derive a unique calendar age for a radiocarbon date. In fact, since the radiocarbon date expresses the midpoint of a probability function, there will always be a distribution of probability in

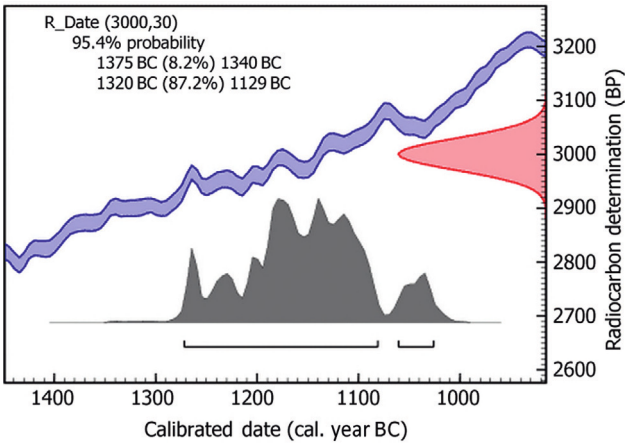


FIGURE 3.16 Calibration of a radiocarbon measurement of 3000 ± 30 years BP. The right-hand axis shows radiocarbon age expressed in years before present (1950), and the bottom axis shows calendar years (derived from tree-ring data). The blue lines show the radiocarbon measurements on the tree rings (±1 standard deviation), and the red curve on the right indicates the radiocarbon concentration in the sample. The gray histogram shows possible ages for the sample (the higher the value in the histogram, the more likely that age is). There is a 95% probability that the sample comes from between 1375 and 1129 cal. years BC. *Constructed using data from OxCal: http://c14.arch.ox.ac.uk.*

calendar years too, and this is made more complicated by the wiggles in the calibration curve. Consider, for example, Figure 3.16, which shows the calibration of a sample that has been radiocarbon-dated at 3000 ± 30 years BP. The histogram on the *x*-axis shows how the ^{14}C probability function is transformed by the "wiggles" in the calibration curve, so there is a wider range of possible ages than the initial date might have suggested. The problem is magnified at certain intervals (such as the last 450 years) when there might be several discrete sets of age, all of equal probability, due to wiggles in the calibration curve. This raises significant problems for studies attempting to resolve short-term environmental changes (such as glacier fluctuations; Porter, 1981a) and has important implications for the interpretation of radiocarbon dates at certain other times in the Holocene (McCormac and Baillie, 1993).

A very significant feature of the radiocarbon-calendar year calibration is the presence of prolonged ^{14}C age plateaus, for example, those centered at ~11.7, 11.4, 10.3, and 9.6 ^{14}C ka BP (and to a lesser extent at ~8750 and ~8250 ^{14}C years BP) (Becker et al., 1991; Lotter, 1991; Kromer and Becker, 1993; Hughen et al., 1998) (Figure 3.17). These ^{14}C age plateaus document periods of time when atmospheric ^{14}C concentrations temporarily increased, so that organisms acquired higher levels of ^{14}C at those times. Consequently, they now appear to be the same age as organisms that are, in fact, several hundred years younger. In effect, this means that two samples with ^{14}C ages of 10,000 and 9600 years BP, for example, could in reality be as much as 860 years different in age or as little as 90 years different. The changes in atmospheric ^{14}C beginning at ~10.6 ka (radiocarbon) BP (+40-70‰ in <300 years) correspond to the onset of the Younger Dryas cold episode (Goslar et al., 1995). A sudden reduction in North Atlantic Deep Water formation at that time (or more probably a shift from deepwater transport to intermediate water) would have changed the equilibrium atmospheric ^{14}C concentration (maintaining relatively high levels of atmospheric ^{14}C) by reducing the ventilation rate of the deep ocean (Hughen et al., 1996, 1998, 2006; Muscheler et al., 2008).

Another consequence of the nonlinear calendar year-^{14}C age relationship is that a series of equally probable calendar dates may produce a histogram of strongly clustered ^{14}C dates (Figure 3.18). Similarly, at certain times in the past, a histogram of ^{14}C dates showing two

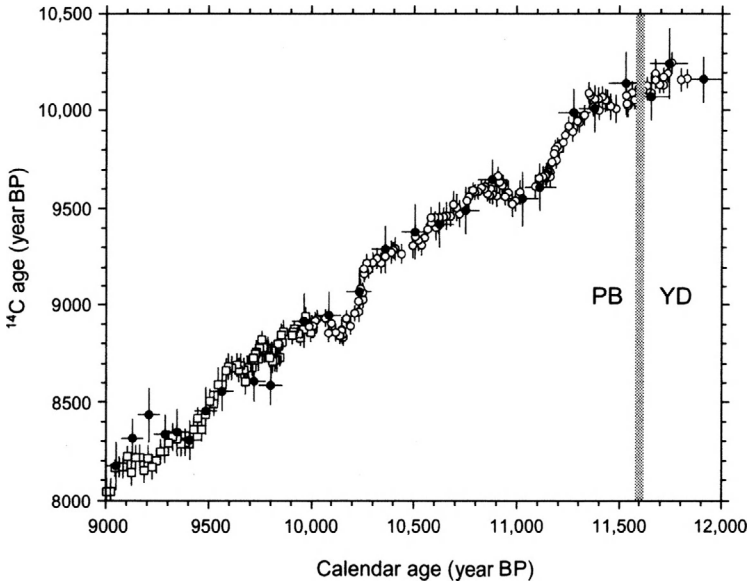


FIGURE 3.17 The very detailed radiocarbon chronology of tree rings from German oaks (squares) and pines (open circles) has been used to place the "floating" chronology of annually laminated (varved) sediments from the Cariaco Basin, north of Venezuela (solid circles) into a firm chronological framework ($r = 0.99$). By finding the optimum fit between both records, through matching the "wiggles" in the tree-ring record with those of the varve record, the varve sequence (which extends 3000 years further back in time) has been fixed in time. Since the varves can be counted, giving calendar year ages, and they also have been AMS dated (using forams in the sediments), they can be used to further extend the calibration of the radiocarbon timescale. Timing of the Younger Dryas-Preboreal transition (recognized in the varves) is shown by the vertical shaded line. *From Hughen et al. (1998).*

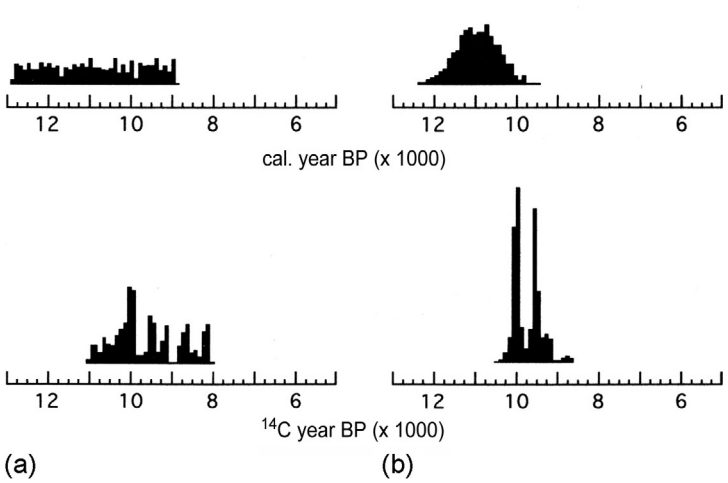


FIGURE 3.18 Simulations of the effect of differences between radiocarbon age and calendar year age. The top diagram shows a set of calendar years, and below are the equivalent ^{14}C ages, derived from the CALIB (ver. 3.03) program of Stuiver and Reimer (1993). In case A, the set of uniformly distributed calendar years leads to a set of clustered radiocarbon ages. In B, a cluster of dates around a mean of 11,000 calendar years (and a standard deviation of 500 years) is compared to the equivalent radiocarbon distribution. A bimodal distribution is apparent in the ^{14}C data, which does not reflect reality. *From Bartlein et al. (1995).*

pronounced "events" may, in fact, correspond to a normal distribution around a single event (Bartlein et al., 1995). This is not the case for the entire period calibrated so far, because there are times when there is less (local) variability around the ^{14}C-calendar year relationship, but certain key intervals (such as the Younger Dryas-Preboreal transition) require very careful interpretation of radiocarbon dates to avoid misinterpretation of the true sequence of events. Similar caution is appropriate in dealing with estimates of rates of change during the Late Glacial and Early Holocene (Lotter et al., 1992).

3.2.1.6 *Causes of Temporal Radiocarbon Variations*

The calibration curve shown in Figure 3.13 reveals much more of interest than the nominal transfer of radiocarbon years to calendar ages. The long-term drift between ^{14}C and calendar year ages, with differences of up to ~700‰ in Δ^{14}C (~5500 years) from ~40,000 to 27,000 cal. years BP, reveals a great deal about Earth system processes. There are three main candidates to explain this pattern of differences (Table 3.2): a change in the ^{14}C production rate in the upper atmosphere (by cosmic rays) due to changes in the Earth's magnetic field or to variations in solar energy (the solar wind). Both factors modulate the production of cosmogenic isotopes (such as ^{14}C and ^{10}Be). A third possibility is that there may also have been changes in the ocean-atmosphere carbon cycle, isolating radiocarbon in the deep ocean for long periods of time (thousands of years).

Geologic records reveal that there were two geomagnetic excursions (see Chapter 4, Section 4.14) ~41,000 years ago (Laschamp) and ~33,000 years ago (Mono Lake) when the Earth's magnetic field was reduced to low levels (for a few thousand and a few hundred years, respectively). This resulted in a high production rate of ^{14}C and ^{10}Be, which accounts for at least part of the high levels of Δ^{14}C in the early part of the record. However, the Earth's magnetic field (dipole moment) also underwent changes in strength over time and was relatively weak from ~25 to 15 ka cal. BP. Thus, the combination of reduced field strength and geomagnetic excursions accounts for the large anomalies in the early part of the record. Subsequently, as the magnetic field strengthened, Δ^{14}C anomalies declined toward the present. That said, realistic estimates of the magnitude of these effects cannot account for the persistently high anomalies from ~28 to 17 ka cal. BP, and the most likely explanation is that there was significant isolation (sequestration) of carbon in the deep ocean during this period (Lal and Charles, 2007).

Variations in solar activity have also influenced ^{14}C concentrations, and these effects may account for short-term Δ^{14}C anomalies on the order of ±20‰. Solar magnetic (heliomagnetic) activity is reduced during periods of low sunspot number (reduced solar wind), and this allows an increase in the intensity of galactic cosmic rays incident on the Earth's outer atmosphere, thereby increasing ^{14}C and ^{10}Be production. Thus, during the three most recent periods of minimum solar activity (AD 1654-1714, 1416-1534, and ~1280-1350, known as the Maunder, Spörer, and Wolf Minima, respectively), ^{14}C concentrations were at their maximum levels for the past thousand years (Eddy, 1976; Stuiver and Quay, 1980). Assuming that the effect of long-term geomagnetic field variations could be removed, it would then be possible to produce a long record of solar wind (and perhaps solar irradiance) variations over time. This problem is discussed further in Chapter 2, Section 2.7.

3.2.1.7 *Radiocarbon Variations and Climate*

A number of authors have observed that periods of low solar activity, such as the Maunder minimum, correspond to cooler periods in the past (e.g., Eddy, 1977; Lean et al., 1995). As minor variations in radiocarbon production seem to be related to solar activity, it has also been argued that ^{14}C variations are inversely related to worldwide temperature fluctuations (Wigley and Kelly, 1990). This implies that solar activity, radiocarbon variations, and surface temperature are all related, perhaps through fundamental variations in the solar constant (i.e., low solar activity = high ^{14}C production rate = low temperature). If so, then the ^{14}C record itself, as a proxy of solar activity, would provide important information on the causes of climatic change, and indeed, many investigations have simply used the record of ^{14}C or ^{10}Be variations as a proxy for solar irradiance (e.g., Magny, 1993; Bond et al., 2001; Hodell et al., 2001; Neff et al., 2001). However, it is not at all clear that changes in the solar wind, which give rise to the variations in cosmogenic isotope production, are linearly related to changes in irradiance (total irradiance either across all wavelengths or over just part of the spectrum) (Beer et al., 2001; Bard and Frank, 2006). Simple comparisons of proxy climate records with radiocarbon anomalies may thus be of limited value (e.g., Williams, L.D. et al., 1981a,b). Furthermore, observational data show that total irradiance changes are only ~0.1% over an ~11 year solar cycle (as measured outside the atmosphere), and it is unlikely that the changes associated with an anomaly like the Maunder minimum were much larger (Wang, Y-M. et al., 2005a,b). Given the small amplitude of these variations, the large atmospheric effects on the transmission of solar energy to the Earth's surface, and the huge inertia of the oceans, it is difficult to imagine how such small changes could have much of an influence on global climate. However, there is some evidence from modeling experiments that there might be regional effects due to feedbacks within the climate system, which amplify or modulate irradiance changes. For example, changes in ultraviolet radiation are larger (~2-3%) than changes in total irradiance over a solar cycle. Such changes have significance because an increase in UV radiation causes more ozone (O_3) to be produced in the upper stratosphere; ozone absorbs radiation (at UV wavelengths of 200-340 nm), so heating rates in the upper atmosphere are increased during times of enhanced solar activity. This then affects stratospheric winds (strengthening stratospheric easterlies), which can in turn influence surface climate via dynamical linkages between the stratosphere and the troposphere (Shindell et al., 1999; Baldwin and Dunkerton, 2001). Model simulations of these effects indicate that there is a poleward shift of the tropospheric westerly jet and a poleward extension of the Hadley circulation, by ~70 km from solar minimum to solar maximum, in the summer hemisphere (Haigh, 1996; Larkin et al., 2000). Although such changes are small, if irradiance changes in the past were larger and more persistent than this solar cycle variability, the effects may have been quite significant (Bradley, 2003). In fact, both empirical and modeling studies indicate that distinct patterns of regional temperature change may be associated with solar forcing (Waple et al., 2001). Prolonged periods of reduced solar activity, like the Maunder minimum, are associated with pronounced cooling over mid- to high-latitude continental interiors and warmer temperatures over mid- to high latitudes of the Atlantic. Such a pattern is characteristic of a shift in the North Atlantic Oscillation (NAO) toward lower index conditions, whereby the pressure gradient between Iceland and the Azores is reduced, leading to less advection of warm, moist air from the Atlantic into western Europe and cooler temperatures over Eurasia (cf. Figure 2.26; Shindell et al., 2001).

Other models indicate that changes in irradiance are amplified by the differential distribution of cloudiness in the Pacific, associated with the east-west Walker circulation. Thus, when the western equatorial Pacific is dry and cloud-free (which is commonly the case during El Niño episodes), an increase in irradiance would have a relatively stronger influence on that region than in the more cloud-covered areas of the eastern equatorial Pacific. In this way, irradiance changes could have strong regional effects, amplifying the ENSO effects across the Pacific and via teleconnections to regions elsewhere (Mann et al., 2005; Meehl et al., 2009). Solar forcing is discussed further in Chapter 2, Section 2.7.

3.2.2 Potassium-Argon Dating ($^{40}K/^{40}Ar$)

Compared to radiocarbon dating, potassium-argon dating is used far less in Quaternary paleoclimatic studies. However, potassium-argon and argon-argon dating have indirectly made major contributions to Quaternary studies (Walker, 2005). The techniques have proved to be invaluable in dating seafloor basalts and enabling the geomagnetic polarity timescale to be accurately dated and correlated on a worldwide basis (Harland et al., 1990; Renne, 2000; see also Chapter 4, Section 4.1.3). Potassium-argon dating has also been used to date lava flows and volcanic tuff, which in some areas of the world may be juxtaposed with glacial deposits or be stratigraphically related to early hominid fossils. In this way, limiting dates on the age of the glacial event or fossil occurrence may be assigned (e.g., Loffler, 1976; Porter, 1979; McDougall and Brown, 2006).

Potassium-argon dating is based on the decay of the radioisotope ^{40}K to a daughter isotope ^{40}Ar. Potassium is a very common component of minerals and occurs in the form of three isotopes, ^{39}K and ^{41}K, both stable, and ^{40}K, which is unstable. ^{40}K occurs in small amounts (0.012% of all potassium atoms) and decays to either ^{40}Ca or ^{40}Ar, with a half-life of 1.31×10^9 years. Although the decay to ^{40}Ca is more common, the relative abundance of ^{40}Ca in rocks precludes the use of this isotope for dating purposes, as the incremental production of ^{40}Ca from the decay of ^{40}K would be miniscule. Instead, the abundance of argon is measured and sample age is a function of the $^{40}K/^{40}Ar$ ratio. Argon is a gas that can be driven out of a sample by heating. Thus, the method is used for dating volcanic rocks that contain no argon after the molten lava has cooled, thereby setting the isotopic "clock" to zero. With the passage of time, ^{40}Ar is produced and retained within the mineral crystals, until driven off by heating in the laboratory during the dating process (Dalrymple and Lanphere, 1969). Unlike conventional ^{14}C dating, $^{40}K/^{40}Ar$ dating relies on measurements of the decay product, ^{40}Ar. As the abundance ratios of the isotopes of potassium are known, the ^{40}K content can be derived from a measurement of total potassium content or by measurement of another isotope, ^{39}K. Because of the relatively long half-life of ^{40}K, the production of argon is extremely slow. Hence, there are large analytical uncertainties in samples younger than ~100,000 years, and its primary use has been in dating volcanic rocks formed over the last 30 million years (though, theoretically, rocks as old as 10^9 years could be dated by this method). Dating is usually carried out on minerals such as sanidine, plagioclase, biotite, hornblende, and olivine in volcanic lavas and tuffs. It may also be useful in dating authigenic minerals (i.e., those formed at the time of deposition) such as glauconite, feldspar, and sylvite in sedimentary rocks (Dalrymple and Lanphere, 1969).

3.2.2.1 Problems of $^{40}K/^{40}Ar$ Dating

The fundamental assumptions in potassium-argon dating are that (a) no argon was left in the volcanic material after formation and (b) the system has remained closed since the material was produced, so that no argon has either entered or left the sample since formation. The former assumption may be invalid in the case of some deep-sea basalts, which retain previously formed argon during formation under high hydrostatic pressure. Similarly, certain rocks may have incorporated older "argon-rich" material during formation. Such factors result in the sample age being overestimated (Fitch, 1972). Similar errors result from modern argon being absorbed on to the surface and interior of the sample, thereby invalidating the second assumption. Fortunately, atmospheric argon contamination can be assessed by measurement of the different isotopes of argon present. Atmospheric argon occurs as three isotopes, ^{36}Ar, ^{38}Ar, and ^{40}Ar. As the ratio of $^{40}Ar/^{36}Ar$ in the atmosphere is known, the specific concentrations of ^{36}Ar and ^{40}Ar in a sample can be used as a measure of the degree of atmospheric contamination, and the apparent sample age appropriately adjusted (Miller, 1972).

A more common problem in $^{40}K/^{40}Ar$ dating is the (unknown) degree to which argon has been lost from the system since the time of the geologic event to be dated. This may result from a number of factors, including diffusion, recrystallization, solution, and chemical reactions as the rock weathers (Fitch, 1972). Obviously, any argon loss will give a minimum age estimate only. Fortunately, some assessment of these problems and their effect on dating may be possible.

3.2.2.2 $^{40}Ar/^{39}Ar$ Dating

One important disadvantage of the conventional $^{40}K/^{40}Ar$ dating technique is that potassium and argon measurements have to be made on different parts of the same sample; if the sample is not completely homogeneous, an erroneous age may be assigned. This problem can be circumvented by $^{40}Ar/^{39}Ar$ dating, in which measurements are made simultaneously, not only on the same sample but also on the same precise location within the crystal lattice where the ^{40}Ar is trapped. Instead of measuring ^{40}K directly, it is measured indirectly by irradiating the sample with neutrons in a nuclear reactor. This causes the stable isotope ^{39}K to transmute into ^{39}Ar; by collecting both the ^{40}Ar and ^{39}Ar, and knowing the ratio of ^{40}K to ^{39}K (which is a constant), the sample age can be calculated. Further details are given by Richards and Smart (1991), McDougall (1995), and McDougall and Harrison (1999).

Actually, $^{40}Ar/^{39}Ar$ dating has no advantages over conventional $^{40}K/^{40}Ar$ dating for samples, which have not been weathered, which have not been subjected to heating or metamorphism of any kind since formation, or which are free of inherited or extraneous argon. In such cases, dates from $^{40}K/^{40}Ar$ methods would be identical to those from $^{40}Ar/^{39}Ar$ methods. In practice, however, there is no way of knowing the extent to which a sample has been modified or contaminated; hence, the $^{40}Ar/^{39}Ar$ method has significant advantages over $^{40}K/^{40}Ar$ because it is often possible to identify the degree to which a sample has been altered or contaminated and thus may increase confidence in the date assigned. Furthermore, several dates can be obtained from one sample and the results treated statistically to yield a date of high precision (Curtis, 1975). The advantages stem from the fact that the ^{40}K, which yields the ^{40}Ar by decay, occupies the same position in the crystal lattice of the mineral as the much more abundant ^{39}K, which produces the ^{39}Ar on irradiation. Heating of the sample thus drives off the argon isotopes simultaneously. Any atmospheric argon contaminating the

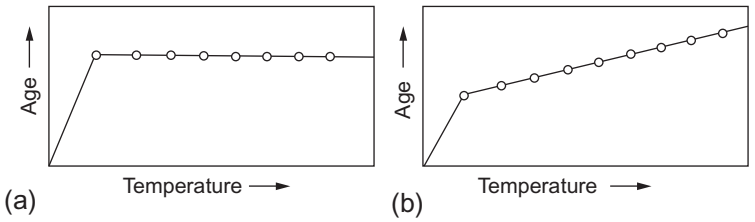


FIGURE 3.19 Schematic plots of $^{40}Ar/^{39}Ar$ data. Each point in (a) and (b) indicates the aged obtained for that increment of argon released as the temperature in increased in steps from 0 °C to the fusion point (1000 °C). In (a), the data show uniform ages for all increments, the plateau indicating a precise age determination. In (b), the ages appear to be progressively older as the temperature rises, indicating loss of argon after original crystallization of the sample so that a precise age cannot be determined; even the oldest age obtained is probably too young. *After Curtis (1975).*

sample occurs close to the surface of the mineral grains, so it is liberated at low temperatures. Similarly, loss of radiogenic argon by weathering would mainly be confined to the outer surface of a mineral. In such cases, the $^{40}Ar/^{39}Ar$ ratios on the initial gas samples would indicate an age that is too young (Figure 3.19b). At higher temperatures, the deeper-seated argon from the unweathered, uncontaminated interiors of the crystals will be driven off and can be measured repeatedly as the temperature rises to fusion levels. If such gas increments indicate a stable and consistent age, considerable confidence can be placed in the result. By contrast, conventional $^{40}K/^{40}Ar$ dating on a sample such as that shown in Figure 3.19b would yield a meaningless age, resulting from a mixture of the gases from different levels.

Plots of "apparent age" calculated from the ratios of ^{40}Ar to ^{39}Ar at different temperatures can indicate much information about the past history of the sample, including whether the sample has lost argon since formation or whether the rock was contaminated by excess radiogenic argon at the time of formation. Such interpretations are discussed further by Curtis (1975) and by Miller (1972). $^{40}Ar/^{39}Ar$ dating thus possesses considerable advantages over conventional $^{40}K/^{40}Ar$ dating methods, by providing more confidence in the resulting dates.

$^{40}Ar/^{39}Ar$ dating has been used to assess the age of the major geomagnetic polarity reversal in the Quaternary-the Brunhes/Matuyama (B/M) boundary. Early $^{40}K/^{40}Ar$ studies had placed the age at ~730 ka BP, but this was questioned by Johnson (1982) and Shackleton et al. (1990) who found that a consequence of tuning the marine oxygen isotope record to maximize coherence with Milankovitch orbital frequencies was to push the B/M boundary back to ~780 ka BP. They therefore, rather boldly, argued that the hitherto accepted age of 730 ka was probably incorrect. Several subsequent studies deriving $^{40}Ar/^{39}Ar$ dates from lava flows have supported this assertion (e.g., Baksi et al., 1992; Spell and McDougall, 1992; Izett and Obradovich, 1994) or at least demonstrated that the uncertainties in both approaches span the interval 730-780 ka BP, making the two estimates statistically indistinguishable (Tauxe et al., 1992, 1996).

3.2.3 Uranium-Series Dating

Uranium-series dating is a term that encompasses a range of dating methods, all based on various decay products of ^{238}U or ^{235}U (Ku, 2000; van Calsteren and Thomas, 2006). Figure 3.20

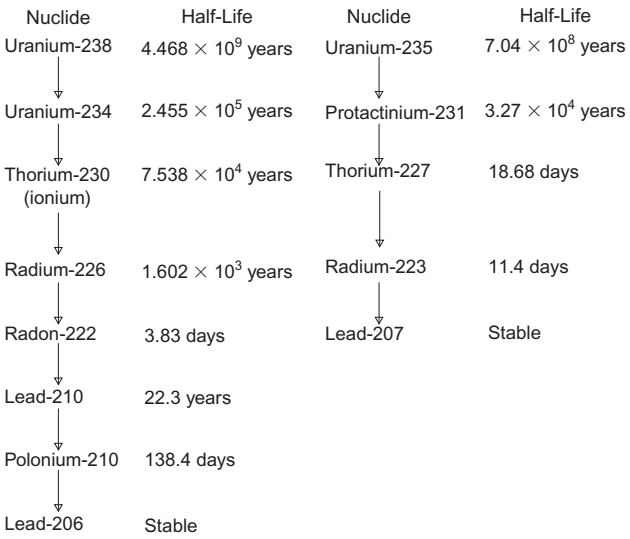


FIGURE 3.20 Decay series of uranium-238 and uranium-235.

illustrates the principal decay series nuclides and their respective half-lives; some intermediate products with very short half-lives (in the order of seconds or minutes) have been omitted. The main isotopes of significance for dating are ^{238}U and ^{235}U, ^{230}Th (also known as ionium), and ^{231}Pa. The ultimate product of the uranium decay series is stable lead (^{206}Pb or ^{207}Pb).

In a system containing uranium, which is undisturbed for a long period of time ($\sim 10^6$ years), a dynamic equilibrium will prevail in which each daughter product will be present in such an amount that it is decaying at the same rate as it is formed by its parent isotope (Broecker and Bender, 1972). The ratio of one isotope to another will be essentially constant. However, if the system is disturbed, this balance of production and loss will no longer prevail, and the relative proportions of different isotopes will be in disequilibrium. By measuring the degree to which a disturbed system of decay products has returned to a new equilibrium, an assessment of the amount of time elapsed since disturbance can be made (Ivanovich and Harmon, 1982). Isotopic decay is expressed in terms of the activity ratios[4] of different isotopes, such as ^{230}Th/^{238}U and ^{231}Pa/^{235}U; for the former, the useful dating range is from a few years to ~450,000 BP, and for the latter 5000-250,000 BP, though dating uncertainties may be large at the upper end of the age range as equilibrium values are approached (Figures 3.21 and 3.22). Thermal ionization mass spectrometry (TIMS) revolutionized uranium-series dating in the mid-1980s, making very precise analyses of small samples routine. Subsequent developments, such as the use of multicollector, inductively coupled plasma ionization mass spectrometers (MC-ICP-MS), have made possible analyses that are even more precise, enabling corals of last interglacial age to be dated to within ±1 ka (2σ error) (Edwards et al., 1987b, 1993; Gallup et al., 1994; McCulloch and Mortimer, 2008). Furthermore, in view of the inconstancy of atmospheric (and oceanic) radiocarbon content, ^{230}Th dating of corals can

[4] Concentrations of radioactive isotopes are reported in units of decays per minute per gram of sample. In U-series dating, these rates are considered relative to each other and are referred to as activity ratios.

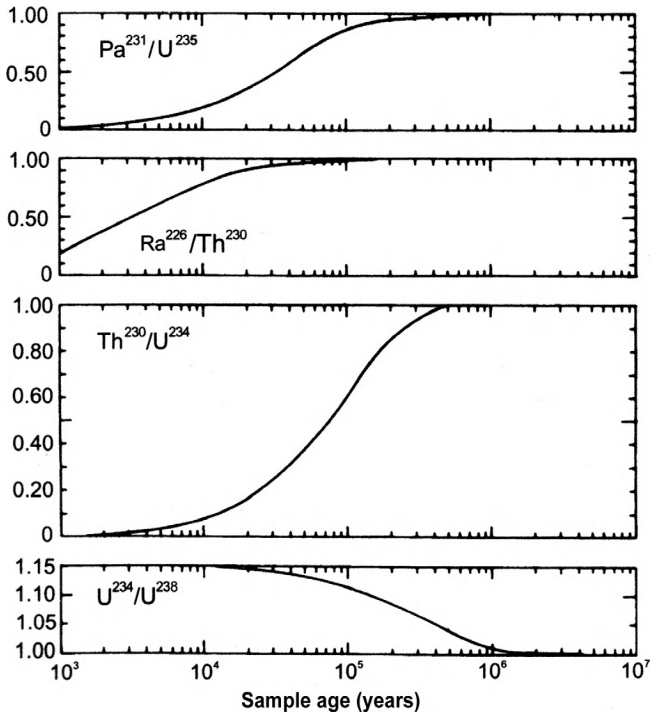


FIGURE 3.21 Temporal changes in activity ratios of $^{231}Pa/^{235}U$, $^{226}Ra/^{230}Th$, $^{230}Th/^{234}U$, and $^{234}U/^{238}U$. *After Broecker and Bender (1972).*

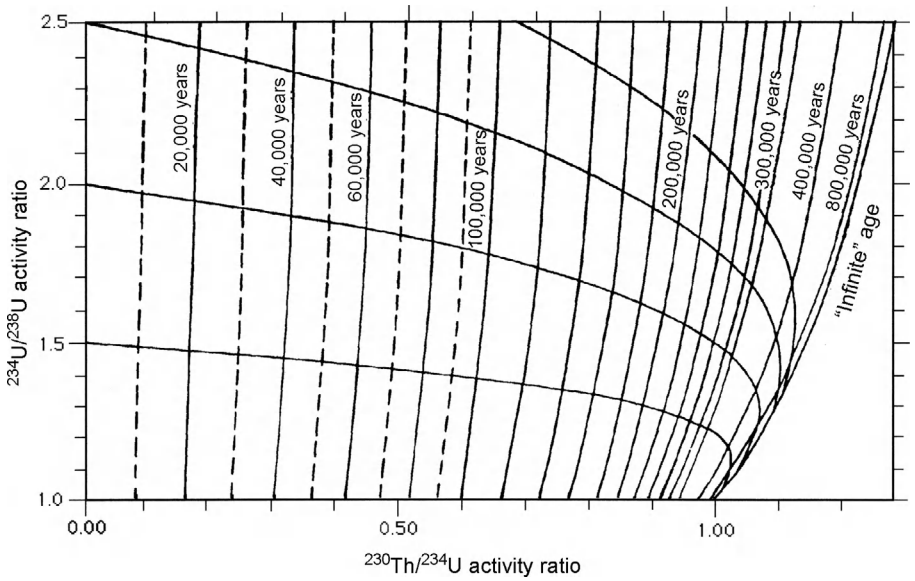


FIGURE 3.22 Variation of $^{234}U/^{238}U$ and $^{230Th}/^{234}U$ activity ratios with time in a closed system with no initial ^{230}Th. The near-vertical lines are isochrones (lines of constant age). The near-horizontal lines are "growth curves" showing change in nuclide activity ratios as age increases for different initial $^{234}U/^{238}U$ activity ratios as indicated. *From Ku (2000).*

provide results that exceed the accuracy of ^{14}C dates and for recent decades have comparable accuracy to the counting of annual growth bands (Edwards et al., 1987a).

In natural systems, disturbance of the decay series is common, because of the different physical properties of the intermediate decay series products. Most important of these is the fact that ^{230}Th and ^{231}Pa are virtually insoluble in water. In natural waters, these isotopes are precipitated from solution as the uranium decays and collect in sedimentary deposits. As the isotope is buried beneath subsequent sedimentary accumulations, it decays at a known rate, "unsupported" by further decay of the parent isotopes (^{234}U and ^{235}U, respectively) from which it has been separated. This is known as the *daughter excess* or unsupported dating method (Blackwell and Schwarcz, 1995). In sediment which has been deposited at a uniform rate, the ^{230}Th and ^{231}Pa concentrations decrease exponentially with depth. Providing that this initial concentration of the isotopes is known, the extent to which they have decayed in sediment beneath the surface can be related to the amount of time elapsed since the sediment was first deposited (Figure 3.23).

This procedure is an example of dating based on the physical separation of the parent and daughter isotopes, with age calculated as a function of the decay rate of the unsupported daughter isotope (Ku, 1976; Walker, 2005). Another method relies on the growth of an isotope that is initially absent, toward equilibrium with its parent isotope; this is known as *daughter deficiency* dating (Blackwell and Schwarcz, 1995) and is most commonly applied to carbonate materials (corals, mollusks, and speleothems). It is based on the fact that uranium is coprecipitated with calcite or aragonite from natural waters that are essentially free of thorium and protactinium. Initial values of ^{230}Th and ^{231}Pa in the carbonates are thus negligible. Providing that the carbonate remains a closed system, the amounts of ^{230}Th and ^{231}Pa produced as the ^{234}U and ^{235}U decay will be a function of time and of the initial uranium content of the sample. In the growth of corals, for example, uranium is coprecipitated from seawater to form part of the coral structure, but thorium concentrations are essentially zero. Since the $^{234}U/^{238}U$ ratio in ocean water is constant at $\sim$1.145 (and studies show it has been almost constant over long periods of time), the buildup of ^{230}Th in the coral as the uranium isotopes decay thus provides chronometric control on the time since the coral formed. Providing the coral has not undergone recrystallization (thereby incorporating anew more uranium), this approach can provide useful dating control from a few years to $\sim$350,000 years BP with extremely high precision (Edwards et al., 1987b). New Guinea (Huon Peninsula) coral samples demonstrate 2σ errors of only 30-80 years on Late Glacial/Early Holocene materials, considerably smaller than the errors associated with AMS ^{14}C dates on the same samples (Edwards et al., 1993). The method has been widely used to date raised coral terraces and hence to provide a chronologically accurate assessment of glacioeustatic changes of sea level, with broad implications for paleoclimatology (e.g., Bard et al., 1990; Edwards et al., 1993; Gallup et al., 1994; Stirling and Anderson, 2009).

Attempts have also been made to date mollusks in the same way as coral, but the results are generally inconsistent (see, however, Szabo, 1979a). The main problem is that mollusks appear to freely exchange uranium postdepositionally (i.e., they do not constitute a closed system) with the result that fossil mollusks commonly have higher uranium concentrations than their modern counterparts. Hence, the resulting thorium and protactinium concentrations are not simply a function of age (Kaufman et al., 1971). However, U-series dates on Arctic marine mollusks can provide valuable minimum age estimates when considered in

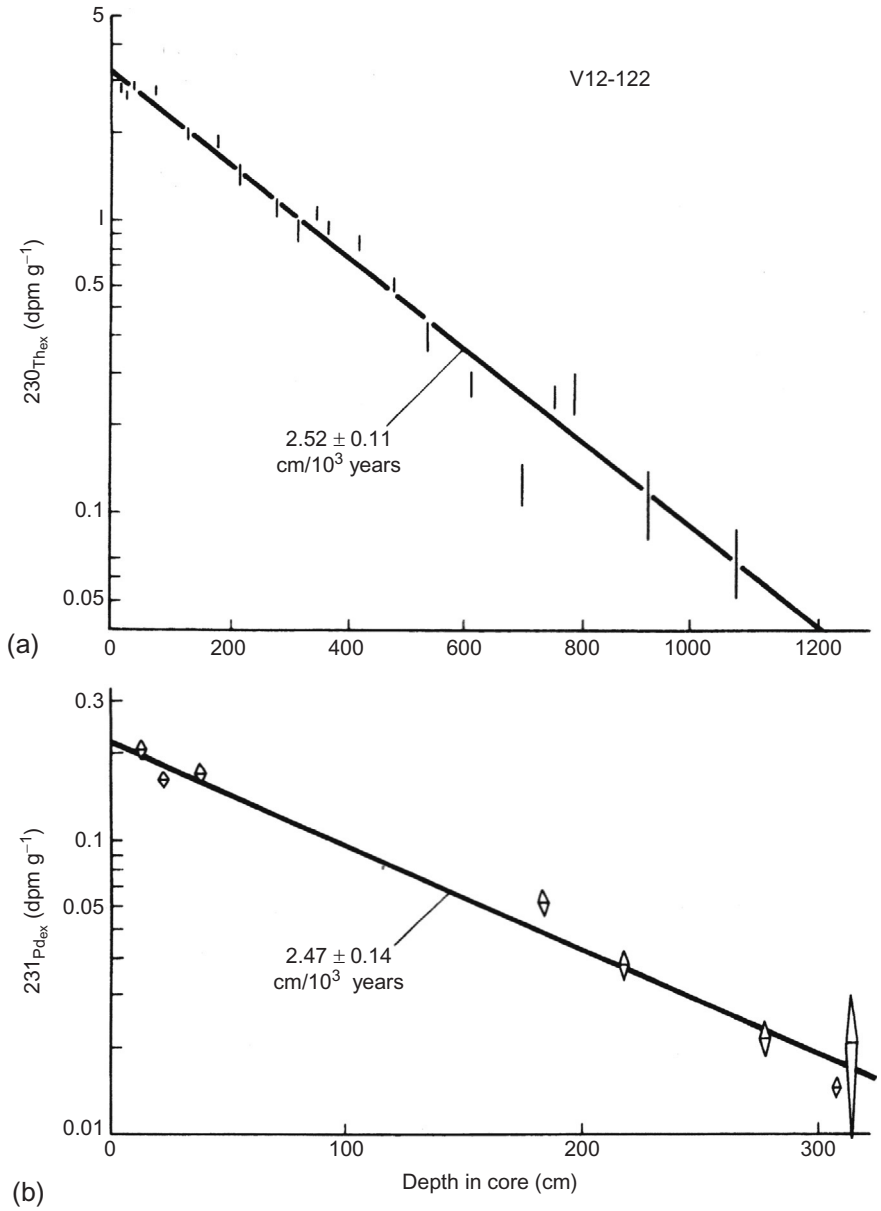


FIGURE 3.23 (a) Excess ^{230}Th concentrations and (b) excess ^{231}Pa concentrations versus depth in Caribbean core V12-122. As the original amounts of ^{230}Th and ^{231}Pa in freshly deposited sediment can be estimated, the extent to which they have been reduced with depth gives a measure of time since the sediment was deposited. Sedimentation rates are obtained from slopes of the best-fitting regression lines and a knowledge of the decay rate of each isotope. *After Ku (1976).*

relation to amino acid data on the same samples (Szabo et al., 1981). $^{230}Th/^{234}U$ dates on bone have also been attempted (Szabo and Collins, 1975), but similar problems have been encountered. Repeated checks with different dating methods suggest that accurate dates have been obtained on only 50% of shell and bone samples to which $^{230}Th/^{234}U$ and $^{231}Pa/^{234}U$ dating methods have been applied (Ku, 1976). "Open system" models have been developed to compensate for postdepositional exchange problems (e.g., Thompson et al., 2003; Villemant and Feuillet, 2003; Stirling and Anderson, 2009), but many assumptions are required that reduce confidence in the resultant dates.

Much more confidence can be placed in uranium-series dates obtained on carbonate samples from speleothems (stalactites and stalagmites). Such deposits are dense and not subject to postdepositional leaching. Because ^{230}Th is so insoluble, the water from which the speleothem carbonate is precipitated can be considered to be essentially thorium-free. Hence, providing that the initial uranium concentration is sufficient, measurement of the $^{230}Th/^{234}U$ ratio will indicate the buildup of ^{230}Th with the passage of time (Harmon et al., 1975). The main problem is to determine reliably the initial $^{234}U/^{238}U$ ratio and to ensure that detrital ^{230}Th has not contaminated the sample, thereby negating the assumption that the initial thorium content is zero (see Chapter 8, Section 8.1). In high-quality samples, remarkably high precision can be achieved (on the order of $\pm 0.2\%$) (e.g., Zhang et al., 2008). Indeed, U-series dating has been used to calibrate the radiocarbon timescale back to >50 ka BP (Hughen et al., 2006; see Section 3.2.1.5).

On a much shorter timescale, unsupported ^{210}Pb may also be used as a chronological aid. ^{210}Pb is derived from the decay of ^{222}Rn following the decay of ^{226}Ra from ^{230}Th (Figure 3.20). Both ^{226}Ra and ^{222}Rn escape from the Earth's surface and enter the atmosphere, where the ^{210}Pb is eventually produced. ^{210}Pb is then washed out of the atmosphere by precipitation or settles out as dry fallout, where it accumulates in sedimentary deposits and decays (with a half-life of 22 years) to stable ^{206}Pb (Figure 3.24). Assuming that the atmospheric flux of ^{210}Pb is constant, the decay rate of ^{210}Pb to ^{206}Pb with depth can be used to date sediment

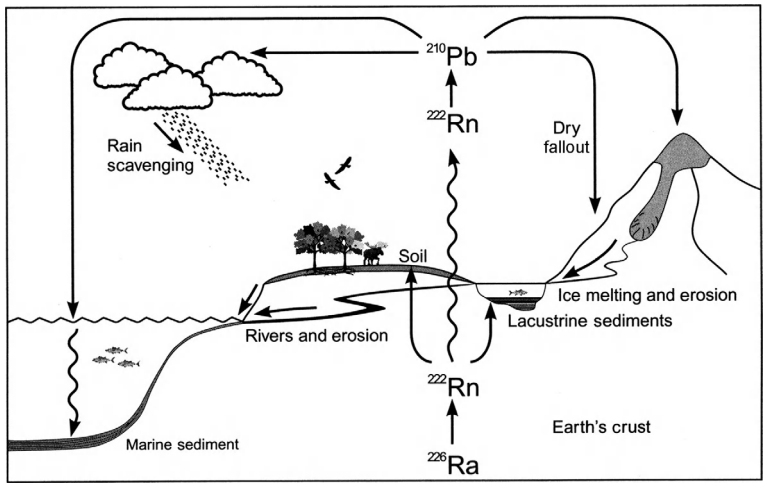


FIGURE 3.24 Schematic diagram of the ^{210}Pb global cycle, illustrating the source, transport, deposition, and postdepositional redistribution processes. *From Preiss et al. (1996).*

accumulation rates (Appleby and Oldfield, 1978, 1983; Appleby, 2001). It is of value only in dating sediments over the last ~150 years, but this may be of particular value in confirming that laminated sediments are true varves (i.e., annual) or in confirming that core tops are undisturbed, enabling floral and faunal contents to be calibrated with instrumental climatic data to derive accurate transfer functions for paleoclimatic reconstructions (Wolfe et al., 2004).

3.2.3.1 *Problems of U-Series Dating*

The major problems in U-series dating have already been alluded to briefly. First, an assumption must be made as to the initial $^{230}Th/^{234}U$, $^{234}U/^{238}U$, and/or $^{231}Pa/^{235}U$ ratios in the sample. In the deep oceans, this may not be a significant problem, as modern oceanic ratios are known to have been relatively constant over long periods of time (though see discussion by Stirling and Anderson, 2009), but in terrestrial environments such as closed inland lakes, this assumption is far less robust. The second problem concerns the extent to which the sample to be dated has remained a closed system through time. Assessing the extent of recrystallization of aragonitic carbonate to calcite may provide some guidance, but as discussed in Section 3.2.1.4, this is not always reliable. Reliability can be checked by obtaining activity ratios for different isotopes from the same sample. If the sample has remained "closed," the dates should all cross-check and be internally consistent (Figure 3.21). In speleothems, the principal problem is whether there is detrital thorium in the sample, as this will confound efforts to use $^{230}Th/^{234}U$ for dating.

3.2.4 Luminescence Dating: Principles and Applications

Luminescence is the light emitted from a mineral crystal (mainly quartz and feldspars) when subjected to heating or when exposed to light. Light emitted in response to heating is referred to as thermoluminescence or TL; light emitted in response to radiation in the visible or infrared parts of the spectrum is termed optically stimulated luminescence (OSL) or infrared-stimulated luminescence (IRSL), respectively (Aitken, 1998). In each case, the quantity of light emitted is related to the amount of ionizing radiation (from U-series radionuclides and ^{40}K) that the sample has been exposed to over time, from surrounding sediments. The decay of radioisotopes in the surrounding matrix produces free electrons in the mineral grains that become trapped at defects in the crystal lattice; the longer the mineral has been exposed to radiation, the higher will be its trapped electron population and the greater the resulting luminescence signal. Luminescence is thus a measure of the accumulated dose of ionizing radiation (expressed in units of grays, Gy), which is a function of sample exposure age. Age is determined by exposing subsets of the sample to known doses of radiation and measuring the resulting luminescence signal when the sample is heated or exposed to light. The amount of radiation needed to produce the same luminescence signal as that from the original sample is called the equivalent dose or D_e (sometimes known as the paleodose; Duller, 1996). If the amount of radiation a sample is exposed to each year (the dose rate) is known (by direct measurement of the radioactive properties of the surrounding matrix), the sample age can be calculated as

$$\text{Age(a)} = \frac{\text{Equivalent dose}(D_e)\,(\text{Gy})}{\text{Dose rate}\,(\text{Gy a}^{-1})}$$

The key constraint is that either the sample to be dated must have no residual luminescence signal from the period before the event being dated or any residual signal must be quantifiable. Since luminescence is released by either heating or optical bleaching of the sample, the event to be dated must have involved one of these processes which effectively set the "luminescence clock" to zero. Thus, TL dating has been widely used in archeology to date pottery or baked clay samples as well as baked flints from fire hearths attributable to early man (Wintle and Aitken, 1977). TL has also been used to date sediment baked by contact with molten lava (Fattahi and Stokes, 2003). By controlled heating experiments in the laboratory, measurements of TL can indicate the amount of time that has elapsed since the sample was last heated.

The same principles apply to wind-blown and fluvially transported sediments, where exposure to sunlight can also dislodge trapped electrons, resetting the luminescence clock (Figure 3.25). It is this attribute that makes OSL and IRSL of particular importance in Quaternary geochronology (Wallinga, 2002; Duller, 2004; Lian and Roberts, 2006). When aeolian sediments are transported in full sunlight, bleaching of acquired luminescence can occur within minutes, resetting the chronometer to zero so that, in their new location (e.g., in a sand dune, for example), the quartz and feldspar grains can once again slowly accumulate electrons as a function of the environmental dose rate at their new location (Wintle, 1990, 1993). The measured OSL (or IRSL) signal will thus indicate the amount of time that has elapsed since the grains were transported to their depositional site (Huntley et al., 1985; Duller, 1996; Prescott and Robertson, 2008). In principle, the same bleaching can occur when sediments are transported in streams, but light transmission in turbid waters may be dramatically reduced, making removal of previously acquired luminescence more problematical. Consequently, luminescence dating of fluvial sediments (and sediments transported via rivers and streams to lakes) must contend with the likelihood that not all of the electron traps were emptied, leading to overestimation of sample age (e.g., Forman et al., 1994). Various approaches have been developed to assess the magnitude of this problem and correct for it (Wallinga, 2002).

The range of time over which luminescence dating is useful is constrained by saturation of the electron-trapping sites in a crystal. Samples with high quantities of potassium feldspars are potentially useful for dating older deposits, because such minerals are less easily

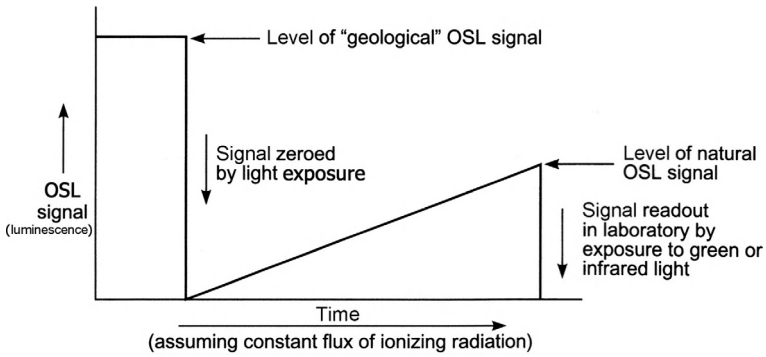


FIGURE 3.25 Schematic illustration of changes in optically stimulated luminescence (OSL) signals with time. The same pattern would apply to TL, with the zeroing resulting from a past heating event, and the cumulative signal revealed by laboratory heating. *From Rendell (1995).*

saturated; ages of up to 1 Ma BP have been reported from areas where dose rates are extremely low and saturation levels are potentially high (discussed in Lian and Roberts, 2006). Accuracy of luminescence dates may approach ±10% of the sample age, though comparison with $^{40}Ar/^{39}Ar$ dates suggest that TL dates on older samples are commonly 5-15% too young, perhaps due to saturation of the electron traps (see Section 3.2.4.2). OSL dating of quartz grains is generally useful for younger samples, ranging from a few decades in age to ~150 ka BP, with the upper limit again imposed by saturation of traps.

3.2.4.1 *Thermoluminescence (TL) Dating*

The thermoluminescence of a sample is a function of age. The older the sample, the greater will be the TL intensity. This is assessed by means of a glow curve, a plot of TL intensity versus temperature as the sample is heated (Figure 3.26). TL emission at lower temperatures is not a reliable age indicator; such emissions correspond to shallow traps in the sample where

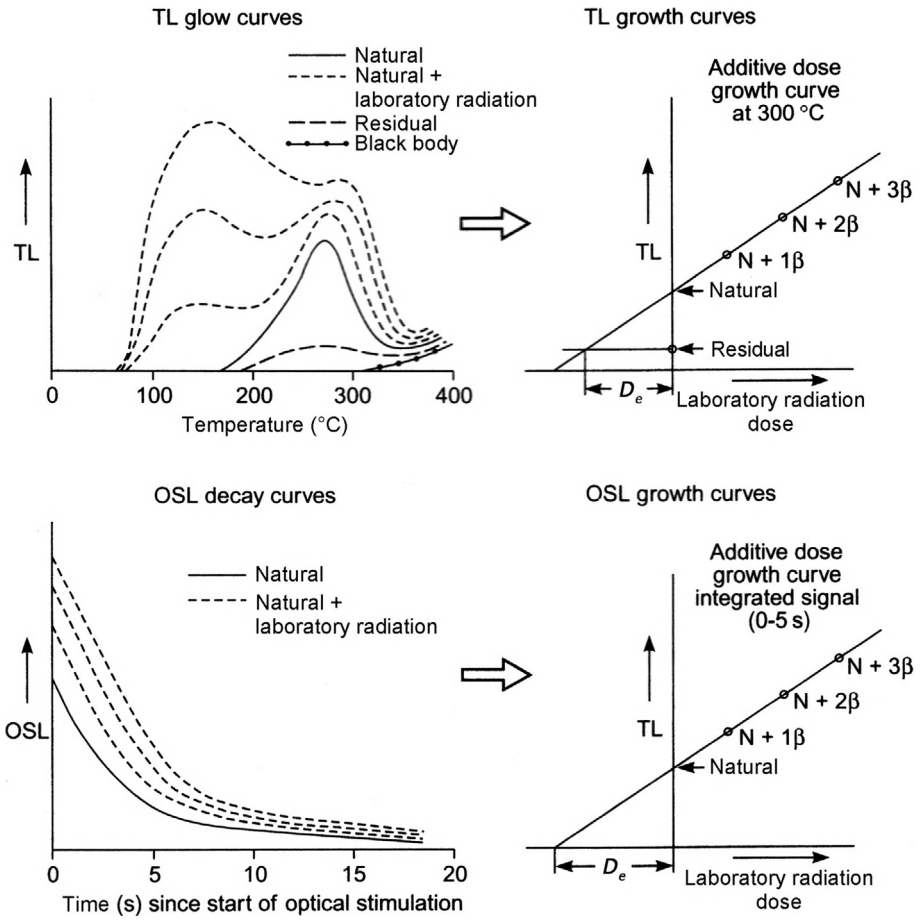


FIGURE 3.26 (a–d) Schematic representation of equivalent dose (ED) determination by the additive dose method for TL and OSL. OSL is measured after the removal of an unstable component of the signal by preheating or long-term storage of the samples. *From Rendell (1995).*

electrons are not stable. The precise temperature necessary to dislodge the deeper "stable" electrons will depend on individual sample characteristics and is assessed by finding the point at which the ratio of natural TL to artificially induced TL becomes approximately constant. Generally this is in the range 300-450 °C, so TL intensity at these temperatures is used for age assessment.

To determine the age of a sample, it is necessary first to know how much TL results from a given radiation dose, as not all materials produce the same amount of TL from such a dose. In one approach (the *additive dose* method), subsets of the sample are exposed to known quantities of radiation that are added to whatever the sample has been exposed to (Figure 3.27). TL is then measured in each of the irradiated samples; the initial paleodose can then be determined by extrapolation to a laboratory-determined residual level. Another approach (the *regenerative* method) involves first bleaching subsamples of all their TL and then exposing them to different levels of radiation, followed by measurement of the TL emitted, corresponding to different levels of radiation exposure (Figure 3.27). The TL in the original sample (taken from a separate subset, or aliquot) is then measured and compared with the artificially radiated samples to assess the corresponding paleodose (ED) as accurately as possible. Sample age can then be calculated simply by dividing the paleodose by the measured dose rate at the sample site. The dose rate is assessed by measuring the quantity of radioactive uranium, thorium, and potassium in the sample itself and in the surrounding matrix, using a portable gamma ray spectrometer. Alternatively, radiation-sensitive phosphors (such as calcium

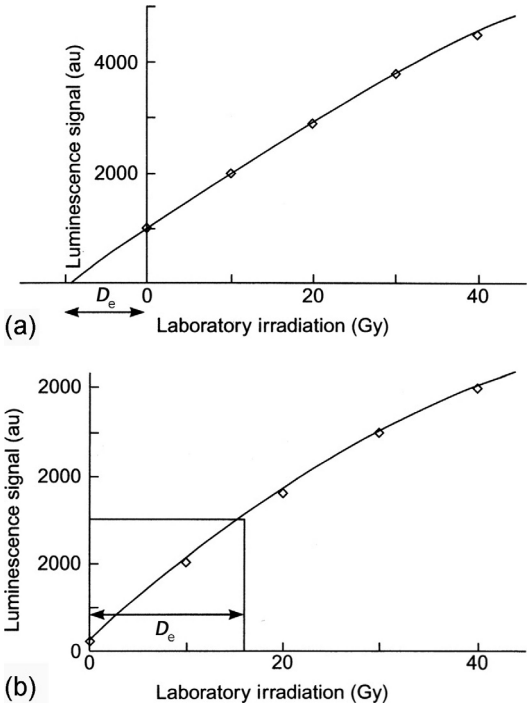


FIGURE 3.27 Examples of (a) the additive dose and (b) the regenerative methods of estimating paleodose in thermoluminescence dating. In the additive dose method, the samples are exposed to increasing levels of radiation, and the associated TL is measured. Extrapolation back to zero reveals the paleodose of the sample before it was exposed to further radiation exposure. In the regenerative method, subsamples are first bleached then exposed to radiation, and the TL is measured for each exposure level. The radiation exposure corresponding to TL measured in the original sample is then readily obtained. *After Duller (1996).*

fluoride) may be buried at the sample site for a year or more to measure directly the environmental radiation dosage, including that from cosmic radiation (Aitken, 1998).

3.2.4.2 *Problems of Thermoluminescence Dating*

In the age equation, in the preceding text, it is assumed that there is a linear relationship between radiation dose and the resulting TL. It is known, however, that this is not always the case at extremely low radiation dose levels or at extremely high dose levels. The former problem (supralinearity) is most significant for relatively young samples (<5000 years old) as the rate at which a sample acquires TL is reduced at relatively low radiation dose levels (or perhaps is nonexistent until a certain radiation threshold is exceeded). Furthermore, there is commonly a residual, light-insensitive TL signal that remains in sediments after deposition, which has to be estimated in order to obtain accurate age estimates. These factors limit the use of TL in dating sediments less than 1000 or 2000 years old. At the other end of the scale, very long exposures to radiation (high doses) may result in saturation of the available electron traps so that further exposure will not appreciably increase the sample TL. When this is likely to occur depends on sample age and mineral composition, but in general, very old ages indicated by TL dating (greater than several hundred thousand years) are likely to be only minimum estimates.

A further difficulty in assessing the relationship between TL and radiation dose occurs when irradiated samples "lose" TL after very short periods of time, perhaps only a few weeks. This phenomenon is called anomalous fading (Wintle, 1973) and is common among certain minerals, particularly feldspars of volcanic origin. Unless corrected for, anomalous fading will result in underestimation of a sample age, but different techniques have been developed to address this problem (Duller, 2004). Because of these and other complicating factors, most applications in paleoclimatology now use OSL applied to quartz grains (Lian and Roberts, 2006).

3.2.4.3 *Optically and Infrared-Stimulated Luminescence (OSL and IRSL) Dating*

The first samples dated by measurement of an optically stimulated luminescence (OSL) signal were carried out by Huntley et al. (1985). The OSL signal was shown to be zero for modern sediments, thus opening up the possibility of dating sediments as young as a few decades in age. Subsequently, Godfrey-Smith et al. (1988) measured the OSL (stimulated with green light from a laser) from a number of quartz and feldspar samples extracted from sediments. They showed that not only was there a negligible residual OSL signal after a prolonged sunlight bleach but also the initial rate of luminescence signal loss was several orders of magnitude faster than that for the TL signal from the same samples (Figure 3.28). Thus, there is a much greater probability that the optical luminescence signal will be zeroed out as sediment is transported to a depositional site, compared to the thermoluminescence signal. Hütt et al. (1988) discovered that they were able to stimulate trapped electrons from feldspars (but not quartz) using near-infrared radiation (around 850-880 nm). This resulted in infra-red stimulated luminescence (IRSL) signals that could be observed in a wider wavelength range (blue and green) since an optical filter could be chosen to reject the stimulation wavelength region (Figure 3.28).

The OSL signal is derived from electrons displaced from electron traps in the crystal by photons, from a light source of a particular wavelength or range of wavelengths rather than by heat, as in TL. With careful selection of the light source (generally in the blue (~470 nm) or

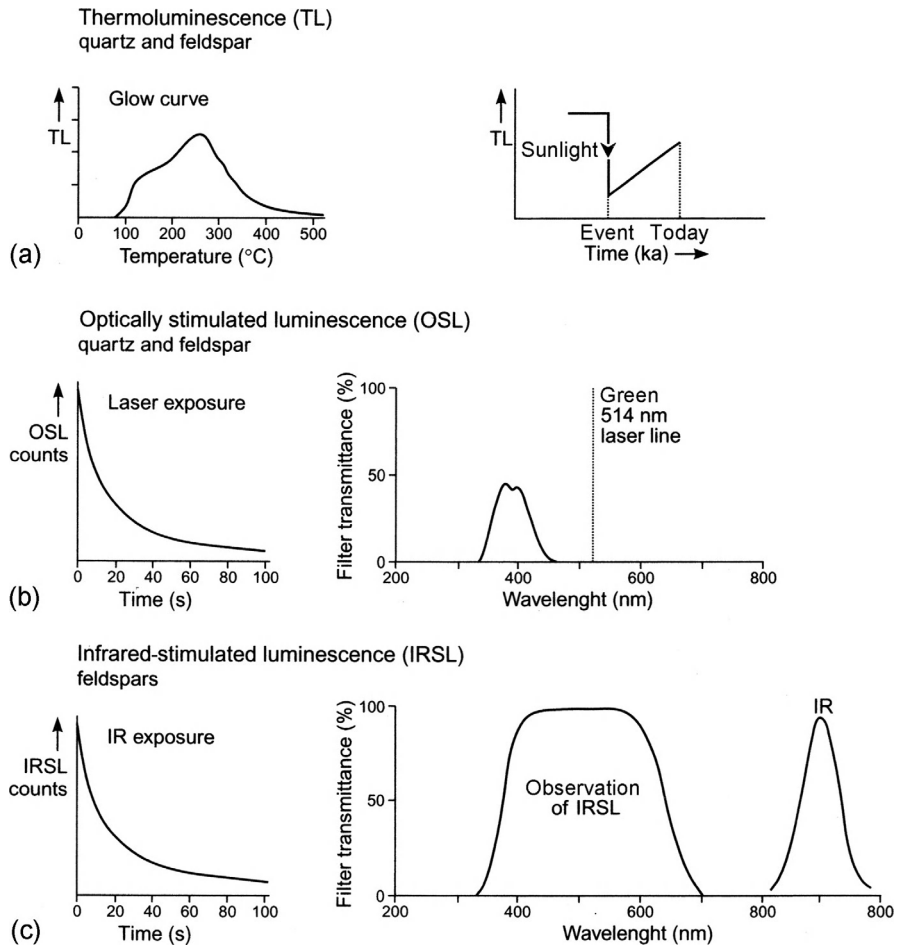


FIGURE 3.28 (a–c) Schematic representation of the principles of luminescence dating techniques. *From Wintle et al. (1993).*

green (~530 nm) part of the spectrum), only the most light-sensitive electron traps are affected, so that the resulting luminescence signal relates just to the most recent episode of bleaching. In this way, the "contaminating" influence of older, more stable electron traps, which might not have been completely emptied during the most recent episode of sediment transport, will be reduced. Furthermore, new procedures allow luminescence measurements to be made on individual quartz grains that have each been exposed to a green laser (532 nm), so that a very large number of independent age estimates can be obtained (by the *single-aliquot* (sample) *regenerative dose* technique, SAR), rather than acquiring an average signal from a large composite sample. D_e is obtained by extrapolation, as for TL (Figure 3.27). This means that a luminescence-based age distribution can be obtained from each location sampled, which allows the analyst to distinguish between samples that did not get zeroed, from those that did, providing much more insight into the actual age of the depositional site (Murray and

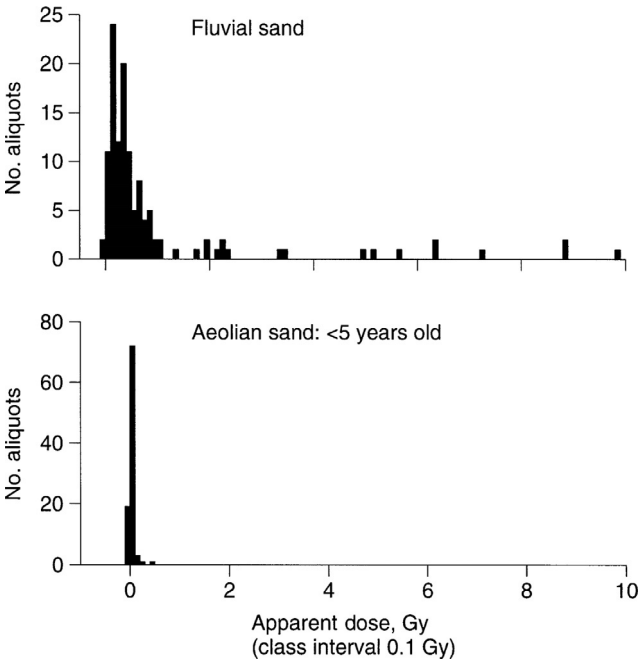


FIGURE 3.29 Measurements of the equivalent dose in aliquots of individual quartz grains from (a) fluvial sediments (Murrumbidgee River, Queensland, Australia) and (b) aeolian sediments (Cooloola, Queensland). Both are modern samples and so should have an equivalent dose (D_e) of zero Gy. D_e was determined for ~100 single aliquots, of 60-100 grains each. The Murrumbidgee samples contain grains that were not completely bleached, so a bulk sample would have given an erroneous date. By contrast, the aeolian grains were almost entirely bleached. *From Olley et al. (1998).*

Wintle, 2000; Duller, 2004). This is illustrated in Figure 3.29, in which single grain aliquots were analyzed from modern samples of fluvial and aeolian sediments. Their true age is thus zero, which is seen in the distribution of luminescence (D_e) from the aeolian quartz grains, indicating the sediment was thoroughly bleached during transportation to the site. However, the fluvial sediments clearly contain quartz grains that were not completely bleached. If a bulk sample had been analyzed (effectively averaging luminescence from all the individual grains), an erroneous age would have been assigned to the sample.

The principal advantage of OSL and IRSL is that the laser-stimulated electron traps are very sensitive to light, so that a relatively brief exposure to sunlight (on the order of a few tens of seconds to a few minutes) is likely to have reduced the sample luminescence to near zero (Figure 3.30). Such brief exposures would certainly not zero the luminescence signal measured in TL studies; thus, OSL and IRSL open up the prospect of dating a wider variety of material, particularly quite young aeolian sands and silts (loess) as well as fluvial and lacustrine sediments where exposure to sunlight may have been brief (Wintle, 1993). For example, recent studies have dated aeolian sands deposited only a few decades to a few centuries ago, using IRSL techniques (Wintle et al., 1994; Clarke et al., 1996). OSL dating of quartz grains is most useful for the time interval extending back to the last interglacial (~125,000 years BP).

Apart from the technical issues involved in measuring luminescence and obtaining accurate estimates of D_e, the most significant problem is obtaining the environmental dose rate or, more particularly, understanding how that might have varied over time. Of particular importance is the mean water content of the sample and surrounding matrix during sample emplacement. Water greatly attenuates radiation, so a saturated sample will receive considerably less radiation in a given time period than a similar sample in a dry site; as a result, the

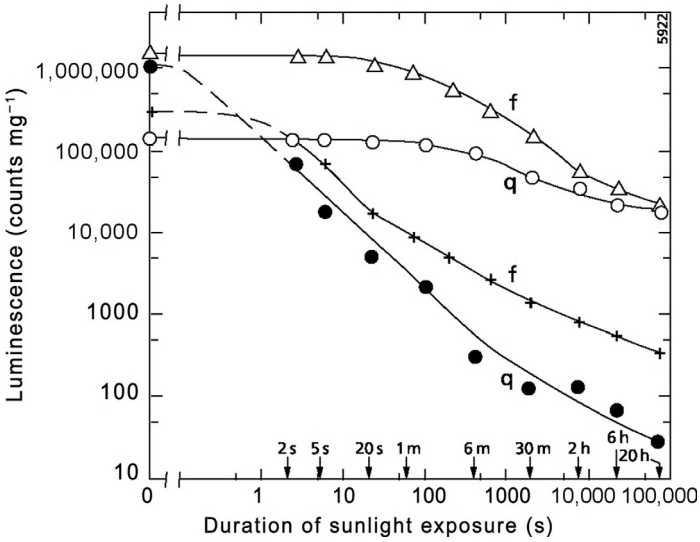


FIGURE 3.30 Sunlight bleaching of natural TL and of natural OSL in quartz grains (q) and K-feldspar grains (f). The unbleached luminescence levels are shown on the *y*-axis. OSL of the minerals (• and +) is reset more readily than the TL (O and Δ), and the quartz OSL is reset more quickly than the feldspar OSL. *After Wallinga (2002); from Godfrey-Smith et al. (1988).*

luminescence intensity will be much lower, giving an incorrect age indication. Wallinga (2002) equates a 1% error in water content with a 1% error in the resulting age estimate. However, if the water content of the site can be assessed, this problem can be taken into account in the age calculation. Better still, if a radiation-sensitive dosimeter can be placed in the environmental setting of the sample for a period of time, the effect of groundwater on the radiation dose may be assessed directly. However, there is always the problem of knowing how groundwater content has varied in the past, and this uncertainty can be a limitation to obtaining more accurate luminescence dates. Groundwater may also leach away radioactive decay products, so long-term changes in groundwater content may further complicate the luminescence-dose relationship. Fortunately, these issues are of minimal significance in dating samples from arid environments such as dune fields; not surprisingly then, luminescence dating has commonly been applied to dating loess (Singhvi et al., 2001) and aeolian sediments (Prescott and Robertson, 2008).

3.2.5 Surface Exposure Dating

Surface exposure (or cosmogenic nuclide) dating relies on the fact that the Earth is constantly being bombarded by cosmic rays that penetrate exposed rock surfaces. These energetic particles impact the nucleus of certain elements causing in quartz (fragmentation) and the creation of new nuclides (isotopes) within the rock. For example, ^{10}Be is produced by spallation of the atoms of oxygen and silica in quartz; over time, ^{10}Be will accumulate in the rock as a measure of the time that the surface has been exposed to cosmic-ray bombardment. Other elements that are commonly measured to assess exposure ages are ^{36}Cl, ^{26}Al, ^{14}C, and the noble gases ^{3}He and ^{21}Ne.

Although it is reasonable to assume a constant rate of cosmic-ray bombardment at the outer edge of the atmosphere, two important factors influence the number of cosmic particles reaching the Earth's surface. First, the atmosphere itself reduces the cosmic-ray flux so that at sea level, the surface may be exposed to only ~50% of the cosmic-ray exposure at 4000 m

(Lal, 1991; Dunai, 2000; Stone, 2000). Second, cosmic rays are modulated by the Earth's magnetic field, such that more cosmic rays reach the Earth's surface at high latitudes than at low latitudes, resulting in cosmogenic isotope production rates in polar regions that are two to three times those at the equator (Lal, 1991). Furthermore, there have been changes in the Earth's magnetic dipole field strength over time (cf. Figure 4.5), which have modulated the cosmic-ray flux accordingly, and these effects must also be considered (Masarik et al., 2001). Because of these factors, the actual surface exposure to cosmic rays at any one location must be appropriately scaled to be comparable with exposures at other sites. Much effort has gone into refining these scaling factors, but there is not yet a universally accepted set of adjustment factors that can be applied in order to reduce uncertainties in the interpretation of exposure ages (Dunai, 2010; Balco, 2011). Consequently, a locally derived, independently dated scaling scheme offers the best calibration of cosmogenic isotopes in any one region. This might be provided, for example, by radiocarbon dates related to the emplacement of moraines or to exposed surfaces resulting from landslides of known age.

Conditions that may have affected the cumulative cosmic-ray exposure of a rock surface also influence the accuracy of exposure age dating. If a rock surface has been shielded from cosmic rays by a cover of surficial material for long periods of time, this would compromise the exposure age. For example, if a rock surface had only recently emerged from under a persistent snow cover or if surficial material such as till or dune sands had formerly covered what is now an exposed rock surface, this could lead to an underestimation of the true age of the surface (Zreda and Phillips, 2000). Also, the production and accumulation of cosmogenic nuclides in rocks declines rapidly with depth, so if an exposed surface has been eroded over time, the cosmogenic isotopes present in the rock will be less than in a similar-aged surface that was not eroded. In granitic rocks, for example, spallation decreases by a factor of 2 every 40 cm of depth, which means that the rate of erosion of the rock surface is a critical factor when interpreting exposure ages. This can be an important factor when dating rocks that predate the LGM, but may not be so critical for surfaces of Holocene (Figure 3.31). On the other

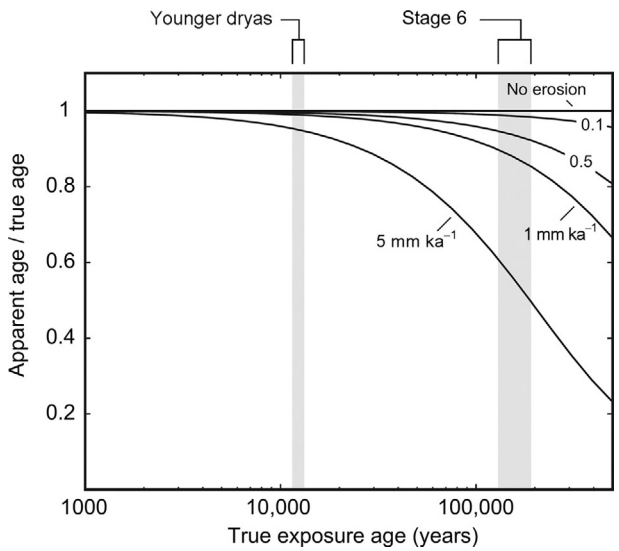


FIGURE 3.31 The effect of surface erosion on age estimation using cosmogenic isotopes in rocks for dating. Typical erosion rates are in the range of 2-3 mm ka^{-1}, so on samples of Holocene or Younger Dryas age, the effect of erosion would be minimal (around 5%), but for older samples, it could result in significant underestimation of the actual surface's age (by perhaps 20-30%). *From Balco (2011).*

hand, if the objective is to date a surface that was unearthed following a glacial episode, the ideal situation would be one in which the surface had been eroded by ice, so that the surface was "wiped clean" of older cosmogenic nuclides, allowing the freshly exposed surface to be reset and accumulate isotopes that pertain to the most recent glacier recession. If any cosmogenic isotopes remain present from previous episodes of subaerial exposure, the sample will have "inherited" cosmogenic isotope that will result in an anomalously old age for the sample. Thus, the technique is most commonly applied to glacially plucked rock surfaces or to erratic boulders that are assumed to have been well weathered during their transportation to the sampling site (Balco, 2011). All of these factors lead to inherent uncertainties in surface exposure dates that may average on the order of 10-15%, so that the technique is not useful to resolve high-frequency changes that may have occurred. On the other hand, it often provides the only useful dating technique in Alpine and Arctic environments where other approaches to dating are simply unavailable. Consequently, exposure age dating has been of revolutionary benefit to geomorphological studies, with many implications for paleoclimatology, particularly in studies of glacier fluctuations (e.g., Rood et al., 2011).

3.2.6 Fission-Track Dating

As already discussed in Section 3.2.3, uranium isotopes decay slowly through a complex decay series, ultimately resulting in stable atoms of lead. In addition to this slow decay, via the emission of α- and β-particles, a small number of uranium atoms also undergo spontaneous fission, in which the nucleus splits into two fragments. The amount of energy released in this process is large, causing the two nuclear fragments to be ejected into the surrounding material. The resulting damage paths are called fission tracks, generally 10-20 μm in length. The number of fission tracks is simply a function of the uranium content of the sample and time (Naeser and Naeser, 1988). Rates of spontaneous fission are very low (for ^{238}U, 10^{-16} a^{-1}) but if there is enough uranium in a rock sample a statistically significant number of tracks may occur over periods useful for paleoclimatic research (Fleischer, 1975).

The value of fission-track counting as a dating technique stems from the fact that certain crystalline or glassy materials may lose their fission-track records when heated, through the process of annealing. Thus, igneous rocks and adjacent metamorphosed sediments contain fission tracks produced since the rock last cooled down. Similarly, archeological sites may yield rocks which were heated in a fire hearth, thereby annealing the samples and resetting the "geologic" record of fission tracks to zero. In this respect, the environmental requirements of the sample are similar to those necessary for $^{40}K/^{40}Ar$ dating. Because different minerals anneal at different temperatures, careful selection is necessary; minerals with a low annealing temperature threshold, such as apatite, will be the most sensitive indicator of past thermal effects (Faul and Wagner, 1971).

Fission tracks can be counted under an optical microscope after polishing the sample and etching the surface with a suitable solvent; the damaged areas are preferentially attacked by solvents, revealing the fission tracks quite clearly (Fleischer and Hart, 1972). After these have been counted, the sample is heated to remove the "fossil" fission tracks and then irradiated by a slow neutron beam, which produces a new set of fission tracks as a result of the fission of ^{235}U. The number of induced fission tracks is proportional to the uranium content and this

enables the ^{238}U content of the sample to be calculated. Sample age is then obtained from a knowledge of the spontaneous fission rate of ^{238}U. For a much more detailed discussion of the technique, and the problems of calibrating fission-track dates, see Hurford and Green (1982) and Dumitru (2000).

Fission-track dating may be undertaken on a wide variety of minerals in different rock types, though it has been most commonly carried out on apatites, micas, sphenes, and zircons in volcanic ashes, basalts, granites, tuffs, and carbonatites. It has also been widely used in dating amorphous (glassy) materials such as obsidian and is therefore useful in tephrochronological studies (see Section 4.2.3; Westgate and Naeser, 1995). Its useful age range is large, from 10^4 to 10^8 years, but it has occasionally been applied to date younger samples. Error margins are generally large; Dumitru (2000) gives typical (2σ) error ranges of $\pm 10\%$ for zircon or glass samples >800 ka in age, $\pm 50\%$ for samples >30 ka, and $\pm 200\%$ for samples >2 ka. Microvariations in crystal uranium content may lead to large variations in the fission-track count on different sections of the same sample (Fleming, 1976). This potential source of error may be reduced by repeated measurements, but for samples that are old and/or contain little uranium, the labor involved in counting precludes such checks being made. Tracks may also "fade" under the influence of mechanical deformation or in particular chemical environments and thus lead to underestimation of age (Fleischer, 1975). Fission-track dating is rarely used in paleoclimatology, but its use in archeology and in tephrochronology is more common (e.g., Meyer et al., 1991). In most cases where fission-track dating is used, $^{40}Ar/^{39}Ar$ dating would be preferable, but may not always be feasible.

CHAPTER

4

Dating Methods II

OUTLINE

4.1 Paleomagnetism 103
- 4.1.1 *The Earth's Magnetic Field* 104
- 4.1.2 *Magnetization of Rocks and Sediments* 105
- 4.1.3 *The Paleomagnetic Timescale* 107
- 4.1.4 *Geomagnetic Excursions* 108
- 4.1.5 *Relative Paleointensity Variations* 110
- 4.1.6 *Secular Variations of the Earth's Magnetic Field* 111

4.2 Dating Methods Involving Chemical Changes 111
- 4.2.1 *Amino Acid Dating* 113
  - 4.2.1.1 Principles of Amino Acid Dating 113
  - 4.2.1.2 Numerical Age Estimates Based on Amino Acid Ratios 119
  - 4.2.1.3 Relative Age Estimates Based on Amino Acid Ratios 121
  - 4.2.1.4 Paleotemperature Estimates from Amino Acid Racemization and Epimerization 122
- 4.2.2 *Obsidian Hydration Dating* 124

4.3 Tephrochronology 125

4.4 Biological Dating Methods 129
- 4.4.1 *Lichenometry* 129
  - 4.4.1.1 Principles of Lichenometry 130
  - 4.4.1.2 Problems of Lichenometry 132
- 4.4.2 *Dendrochronology* 135

4.1 PALEOMAGNETISM

Variations in the Earth's magnetic field, as recorded by magnetic particles in rocks and sediments, may be used as a means of stratigraphic correlation. Major reversals of the Earth's magnetic field are now well known and have been independently dated in many localities throughout the world. Consequently, the record of these reversals in sediments can be used

Copyright © 2015 Raymond S. Bradley.
Published by Elsevier Inc. All rights reserved.

as time markers or chronostratigraphic horizons. In effect, the reversal is used to date the material by correlation with reversals dated independently elsewhere. However, as all episodes of "normal polarity" have the same magnetic signal and all episodes of "reversed polarity" are similarly indistinguishable from just the polarity signal, it is necessary to know approximately the age of the material under study to avoid miscorrelations.

In addition to aperiodic global-scale geomagnetic reversals, changes in the intensity of the Earth's magnetic field have occurred on the 10^3-10^4 timescale. There have also been secular (century to millennial-scale) variations in the nondipole field that were regional in scale (over distances of 1000-3000 km), and these can be used to construct well-dated "master chronologies" for comparison with undated records exhibiting similar paleomagnetic variations.

4.1.1 The Earth's Magnetic Field

The magnetic field of the Earth is generated by electric currents within the Earth's molten core. The exact mechanism of its formation is not agreed upon, but for our purposes, it is sufficient to consider the field as if it were produced by a bar magnet at the center of the Earth, inclined at $\sim 11^\circ$ to the axis of rotation (Figure 4.1a). At the Earth's surface, we are familiar with this global field through magnetic compass variations. If a magnetized needle is allowed to swing freely, it will not only rotate laterally to point toward the magnetic pole but also

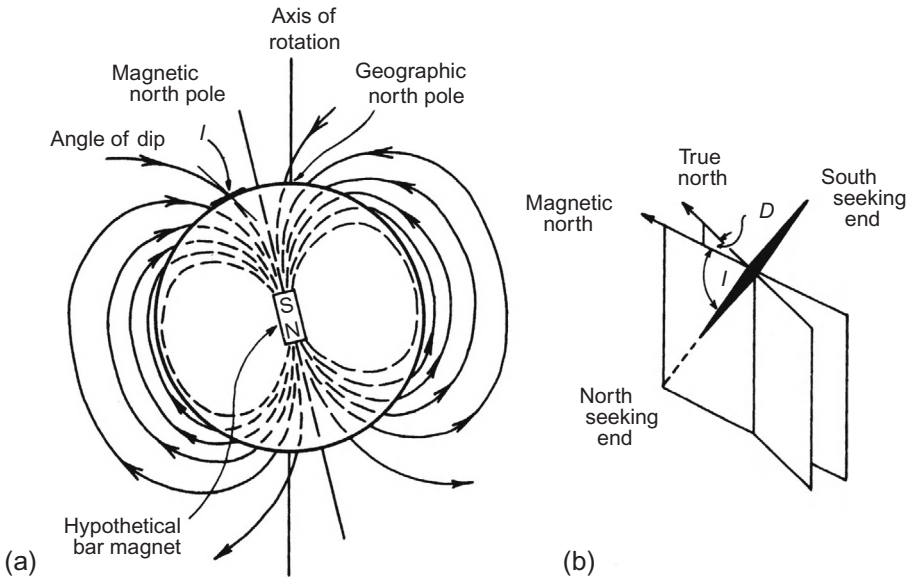


FIGURE 4.1 (a) The Earth's magnetic field. The main part of the Earth's magnetic field (the dipole field) can be thought of hypothetically as a bar magnet centered at the Earth's core. The lines of force represent, at any point, the direction in which a small magnetized needle tries to point. The concentration of these lines is a measure of the magnetic field strength. (b) Declination and inclination. Declination is a measure of the horizontal departure of the field from true north; inclination is a measure of dip from the horizontal. The resultant force is a vector representing declination, inclination, and field strength.

become inclined vertically from the horizontal plane. The angle the needle makes with the horizontal is called the inclination (Figure 4.1b). The inclination varies greatly, from near 0° at the equator to 90° at the magnetic poles. If the needle is weighted, to maintain it in a horizontal plane, it will remain pointing toward magnetic north, and the angle it makes with true (geographic) north is called the declination (Figure 4.1b).

The Earth's magnetic field is considered to be made up of two components—a primary and fairly stable component (the dipole field), which is represented by the bar magnet model, and a much smaller residual or secondary component (the nondipole field), which is less stable and geographically more variable (McElhinny and McFadden, 2000). Major changes in the Earth's magnetic field are the result of changes in the dipole field, but minor variations may be due to nondipole factors (see Section 4.1.5).

Because of the nature of the (dipole) field and the way in which it is generated, any change in its characteristics will affect all parts of the world. Records of significant magnetic field variations in a stratigraphic column (magnetostratigraphy) can thus be used directly to correlate sedimentary sequences in widely dispersed locations, regardless of whether they have common fossils or even similar facies. The broader significance of the magnetic characteristics of sediments, in a wide range of paleoenvironmental applications, is well documented by Thompson and Oldfield (1986), Maher and Thompson (1999), and Evans and Heller (2003).

4.1.2 Magnetization of Rocks and Sediments

So far, we have referred to paleomagnetic variations and their usefulness without considering how such variations are recorded. It has been known for over 50 years that molten lava will acquire a magnetization parallel to the Earth's magnetic field at the time of its cooling. This is known as thermoremanent magnetization (TRM). The same phenomenon has been observed in baked clays from archeological sites; iron oxides in the clay, when heated above a certain temperature (the Curie point), realign their magnetic fields to that at the time the clay was baked. In this way, archeological sites of different ages have preserved a unique record of geomagnetic field variations over the last several thousand years (Aitken, 1974; Tarling, 1975).

Igneous rocks are not the only recorders of paleomagnetic field information; lake and ocean sediments may also register variations through the acquisition of detrital or depositional remanent magnetization (DRM). Magnetic particles become aligned in the direction of the ambient magnetic field as they settle through a water column. Providing that the sediment is not disturbed by currents or slumping or bioturbation, the magnetic particles will provide a record of the magnetic field of the Earth at the time of deposition. Verosub (1977) noted that the acquisition of magnetization by sediments may occur after deposition due to the mobility of magnetic carriers within fluid-filled voids in the sediment. Once the water content of the sediment drops below a critical level (depending on the sediment characteristics), the magnetic particles can no longer rotate and magnetization becomes "locked in" to the sediment. This postdepositional DRM provides a more accurate record of the ambient magnetic field than simple depositional DRM, but in some circumstances, it may lead to distinct regional differences because some sediments became realigned postdepositionally, while others, perhaps more densely packed, did not (e.g., Coe and Liddicoat, 1994).

Unlike thermoremanent magnetization, detrital remanent magnetization is not an "instantaneous" event. Once the molten lava has cooled, perhaps in a matter of minutes, the ambient field becomes a permanent fixed record. In sediments, the record is subject to disturbance (e.g., by burrowing organisms) that may raise the water content of the sediment enough for magnetic particles to rotate again, changing the magnetization until the sediment is sufficiently dewatered to fix the record once more. Thus, the sedimentary record of the Earth's magnetic field, although continuous, should be considered as a smoothed or average record, unlikely to record short-term variations except in unusual circumstances where sedimentation rates are sufficiently high. Furthermore, it has been demonstrated by Verosub (1975) that sediment disturbance may result in apparent reversals, which would be hard, if not impossible, to detect in cores of nonlaminated sediments (Figure 4.2). This may have contributed to erroneous reports of short-term variations of the Earth's magnetic field (excursions; see Section 4.1.4).

Finally, it is now also recognized that iron minerals in some sediments undergo postdepositional chemical changes, which result in a magnetization characteristic of the Earth's magnetic field long after initial deposition. This is known as chemical remanent magnetization (CRM); identification of the minerals typically affected in a sample can provide a warning that errors may be expected.

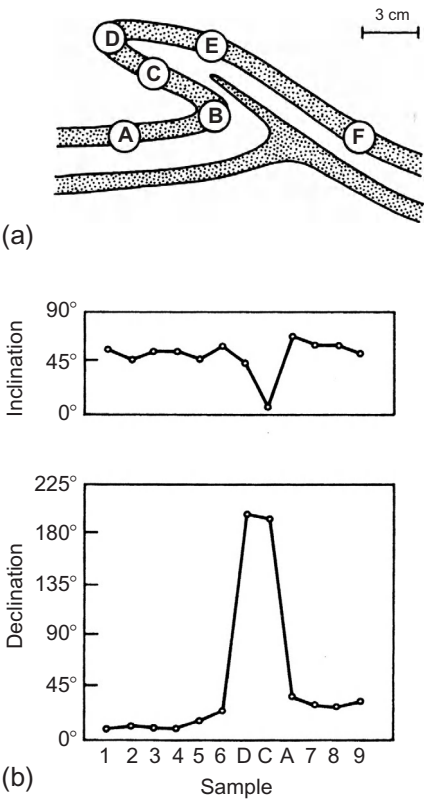


FIGURE 4.2 Problems of paleomagnetic stratigraphy illustrated by a varved sedimentary record. (a) A folded varved sediment sequence; shaded layers represent winter (clay) sediments; and the unshaded layer the summer (silt) deposits. (b) Paleomagnetic record obtained on a hypothetical core through the fold shown in (a), intersecting points A, C, and D. Because of sediment deformation an apparent paleomagnetic excursion is recorded. In uniform, fine-grained sediments such deformation would probably not be visible, so that the presence of an excursion might be erroneously reported. *After Verosub (1975).*

4.1.3 The Paleomagnetic Timescale

Most of the early work on establishing a chronology or timescale of paleomagnetic events was carried out on lava flows. It was demonstrated that at times in the past the Earth's magnetic field has been the reverse of today's and that these periods of reversal (chrons) lasted hundreds of thousands of years. Potassium-argon dating methods enabled dates to be assigned to periods of "reversed" and "normal" fields so that eventually, a complete chronology spanning several million years was constructed (Cox, 1969). Indeed, the development of this chronology went hand in hand with the theory of plate tectonics since new lavas, produced at the centers of spreading (e.g., the Mid-Atlantic Ridge), were found to record identical paleomagnetic sequences on either side of the ridge (Opdyke and Channell, 1996). Careful study of lava flows and seafloor paleomagnetic anomaly patterns has so far enabled a fairly accurate chronology of reversals to be constructed for the Cenozoic (Cande and Kent, 1992, 1995) and less certain chronologies have been constructed for even longer periods of time (Harland et al., 1990). Major periods of normal or reversed polarity are termed polarity chrons or epochs, the most recent of which are named after early workers in the field. Thus, we are currently in the Brunhes chron of "normal" polarity that began ~780,000 year BP. Prior to that, the Earth experienced a period of reversed polarity, the Matuyama chron, which began in late Pliocene times (Figure 4.3).

In addition to major polarity epochs in which reversals persist for periods of $\sim 10^6$ years or more, the igneous record has also shown that reversals have occurred more frequently, but less persistently, for periods known as *polarity events* (or subchrons). These are intervals of a

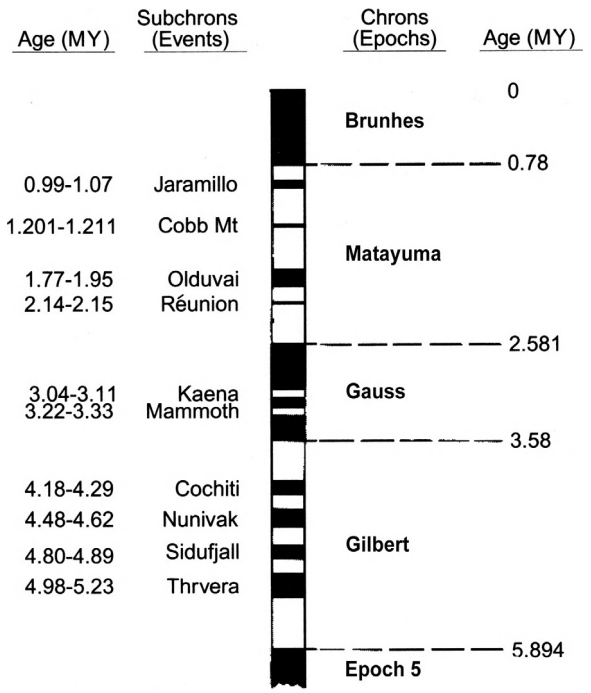


FIGURE 4.3 Paleomagnetic polarity timescale for the last 6 million years. Normal polarity periods in black. Dates are based on K/Ar dates on lava flows. *After Cande and Kent (1995) and Berggren et al. (1995).*

single geomagnetic polarity generally lasting 10^4-10^5 years within a polarity chron. During the last 2 million years, several such events are thought to have occurred, all within the Matuyama reversed-polarity chron. Thus, the Jaramillo (0.99-1.07 Ma BP) and the Olduvai (1.77-1.95 Ma BP) subchrons are periods of normal polarity, named after the locality of the lava samples studied. The dating of these relatively brief events is subject to change as new analyses are carried out (particularly by more accurate $^{40}Ar/^{39}Ar$ dating of samples). Figure 4.3 gives the current status of the polarity timescale.

All of the preceding discussion has referred to studies of polarity changes observed in lavas, but the widest application of paleomagnetism to paleoclimatic studies has been in the identification of reversals in sedimentary deposits, notably in marine sediments and in loess deposits (e.g., Rutter et al., 1990; Hilgen, 1991). Studies of detrital remanent magnetization in ocean sediments may, in favorable circumstances, give a paleomagnetic record comparable in detail with the terrestrial volcanic record (Opdyke, 1972). The Quaternary record of $\delta^{18}O$ in marine sediments and its relationship to orbital forcing is now so well established that it has been used to refine age estimates on the timing of paleomagnetic reversals (Shackleton et al., 1990; Bassinot et al., 1994; Tauxe et al., 1996). Indeed, astrochronological estimates for the ages of magnetic reversals are now considered by some to provide the best framework for the late Quaternary geomagnetic timescale (Renne et al., 1994; Berggren et al., 1995; Cande and Kent, 1995).

4.1.4 Geomagnetic Excursions

In addition to polarity epochs and events (chrons and subchrons), there have been many reports of short-term geomagnetic fluctuations known as polarity excursions (Laj and Channell, 2007; Roberts, 2008). Excursions are considered to last for a few thousand years (at most) and are associated with paleointensity minima. Cosmogenic isotopes, such as ^{36}Cl and ^{10}Be (the production of which is increased during times of low geomagnetic field intensity), provide some insight into the duration of recent excursions. ^{36}Cl in Greenland ice cores increased for ~2500 years during the Laschamp excursion and ~1200 years during the Mono Lake excursion (Wagner et al., 2000). They differ from geomagnetic events in that a fully reversed field does seem to have occurred; current theory suggests that they result from reversals of polarity in the Earth's liquid outer core, but not in the solid inner core, at times when the magnetic field intensity fell to low values. Because of their short duration, they are only likely to be recorded in areas with high sedimentation rates and/or very frequent lava flows. Hence, it is often the case that an excursion apparently found in one location may not be registered nearby, where sedimentation rates at the critical time may not have been sufficient to record it. Such occurrences are common and lead to skepticism about the reality and significance of reported excursions (e.g., Verosub and Banerjee, 1977; Lund and Banderjee, 1979). For an excursion to warrant recognition, it should be based on observations of synchronous changes in both declination and inclination in several geographically separate cores, and the analysis should be restricted to fine-grained, homogeneous sediment.

In a recent review, Roberts (2008) concluded that there were ~14 times in the Quaternary when there is credible evidence for excursions, and (at least) another 6 for which the evidence

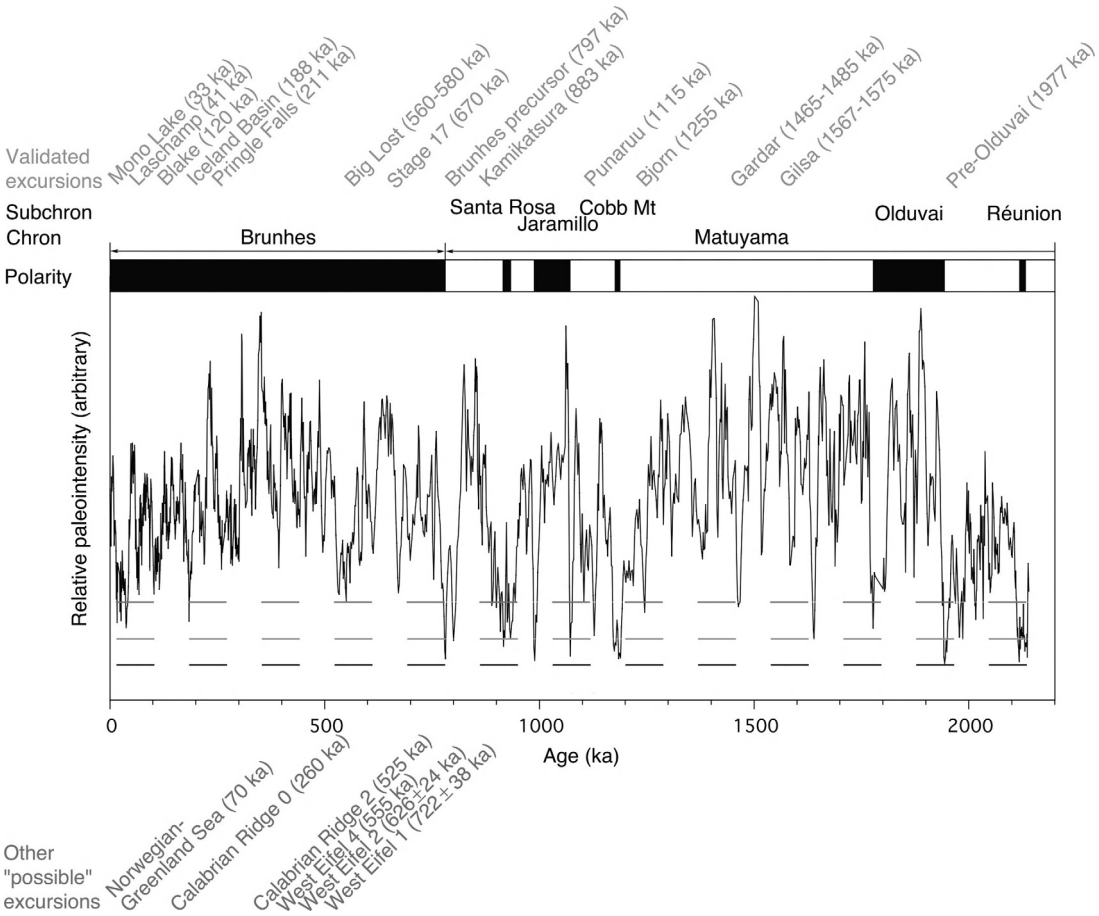


FIGURE 4.4 Geomagnetic reversals and relative paleointensity variations (in a sediment core from the western Philippines Sea) for the last 2.14 Ma. The succession of polarity intervals is depicted by the black bars for normal (and white for reversed) polarity at the top of the panel. Validated and "possible" excursions are shown; all coincide with paleointensity minima. *From Roberts (2008).*

is equivocal (Figure 4.4). Each one is named after the region where the record was first recognized; the most recent were Mono Lake (33 ka BP), Laschamp (41 ka BP), Blake (120 ka BP), Pringle Falls (211 ka BP), and Big Lost (~560-580 ka BP). The Blake excursion has been widely recorded, having been recognized in Chinese loess, as well as in marine sediments from the Caribbean, Atlantic, and Mediterranean. The Laschamp excursion has been recorded in many locations, most notably in sediments from the Bermuda Rise and the Black Sea and in lava flows from Iceland and the Massif Central, France, where it was originally identified (Condomes et al., 1982; Levi et al., 1990; Channell et al., 2012; Nowaczyk et al., 2012). The other excursions are all from the western United States where they have been seen in some (but not all) lake sediments.

4.1.5 Relative Paleointensity Variations

It is now recognized that there have been globally coherent changes in the intensity of the Earth's magnetic field, and so normalized records of paleointensity (*relative paleointensity*, RPI) can provide a stratigraphic tool for correlation of widely separated records. This is a developing field and many records are noisy, requiring the stacking or averaging of data to produce a clear signal from the assembled records (Guyodo and Valet, 1999; Valet et al., 2005). Stacking tends to smooth out high-frequency changes ($<10^4$ years) but retains the lower-frequency characteristics of the record (Stoner and St-Onge, 2007) (Figure 4.5). From these data, it is clear that large changes in relative paleointensity have occurred in the past, the main features of which can be useful in establishing a chronology. More detailed composites are also becoming available, where sets of high-resolution records can be combined (Figure 4.6). In this period of record, the minimum intensity around 41 ka BP is related to the Laschamp excursion. Even higher resolution paleointensity records are available for the Holocene, in part due to magnetic intensity data from archeological material (potsherds)

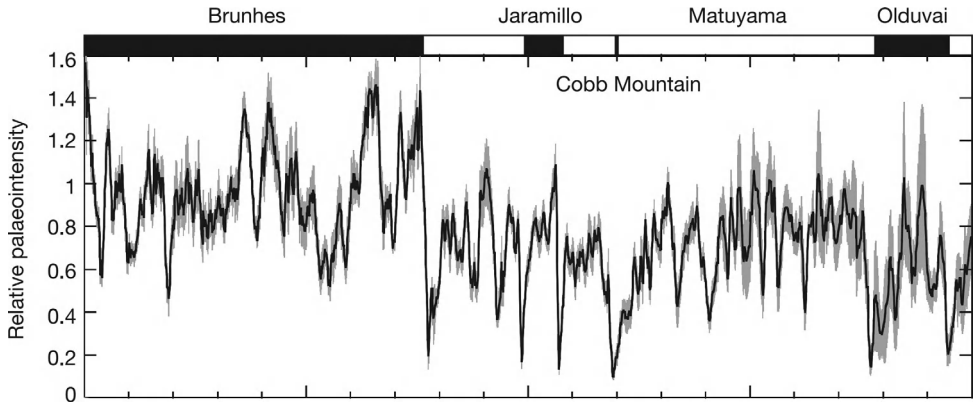


FIGURE 4.5 Composite record depicting the evolution of the Earth's magnetic field intensity during the past 2 Ma (Sint-2000) obtained after stacking a set of individual records, shown with the 95% confidence interval in gray. The succession of polarity intervals is depicted by the black bars for normal (and white for reversed) polarity at the top of the panel. Compare this record with that for a single site in Figure 4.4. *From Valet et al. (2005).*

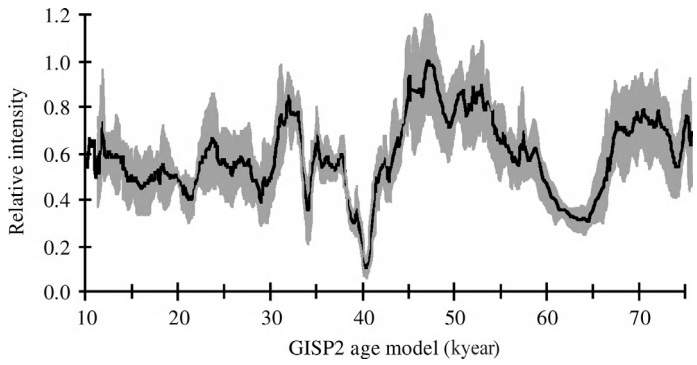


FIGURE 4.6 Stacked relative paleointensity record obtained from six north Atlantic sediment cores for the last 75,000 years (NAPIS-75). The shaded area indicates uncertainty associated with the stacking procedure. *From Laj et al. (2000).*

that were fired in prehistoric time and retain a measure of field strength at that time (Hagstrum and Blinman, 2010; Korte et al., 2011). Paleointensity data are extremely important for our understanding of the radiocarbon record, as a strong geomagnetic field protects the Earth from galactic cosmic rays, which produce cosmogenic isotopes in the outer atmosphere. Thus, ^{14}C and ^{10}Be vary inversely with the intensity of the Earth's magnetic field, as can be seen in the discrepancy between calendar year ages and radiocarbon ages of wood (see Chapter 3, Section 3.2.1.5). Furthermore, in order to use ^{10}Be or ^{14}C anomaly as index of solar activity (see Chapter 2, Section 2.7), it is first necessary to remove the effects of the geomagnetic field intensity changes, which have varied by a factor of ~1.5 over the course of the Holocene (being weakest from ~9 to 5 ka BP) (cf. Snowball and Muscheler, 2007).

4.1.6 Secular Variations of the Earth's Magnetic Field

A number of studies of well-dated lake sediments from different parts of the world indicate that quasi-periodic changes in declination (and to a lesser extent inclination) have occurred during the Holocene (Mackereth, 1971; Verosub, 1988; Snowball et al., 2007). These paleomagnetic secular variations (PSV) are of a smaller magnitude than those described as excursions and appear to be regional in extent (over distances of 1000-3000 km) presumably because they result from changes in the nondipole component of the Earth's magnetic field.

If the changes observed can be accurately dated in one or more cores, a "master chronology" can be constructed, which enables peaks and troughs in the record to then be used as a chronostratigraphic template. Such templates are valuable in estimating the age of highly inorganic sediments, which do not yield enough carbon for conventional ^{14}C dating, but which do contain a clear record of declination and inclination variations (providing they have approximately the same sedimentation rate as the master record). However, it is first necessary to establish a reliable, well-dated magnetostratigraphic record for a "type section" and to determine over what area this record can be considered to provide a master chronology. So far, this has been demonstrated in both lake and marine sediments from a number of locations (see Stoner and St-Onge, 2007; Barletta et al., 2010 for summaries). Figure 4.7 shows a set of Holocene paleomagnetic records extending from western North America to western Europe, which have many features in common. Providing correlations between a master record and an undated target record are statistically significant and changes in both inclination and declination support the match, it should be possible to use these regional PSV records to establish chronologies in many areas.

4.2 DATING METHODS INVOLVING CHEMICAL CHANGES

Two general categories of dating methods are based on chemical changes within the samples being studied since they were emplaced. The first involves amino acid analysis of organic samples, generally used to assess the age of associated inorganic deposits. The method may also be used to estimate paleotemperatures from organic samples of known age. The second category encompasses a number of methods, which assess the amount of weathering that an inorganic sample has experienced. They are primarily used to assess the relative age of freshly

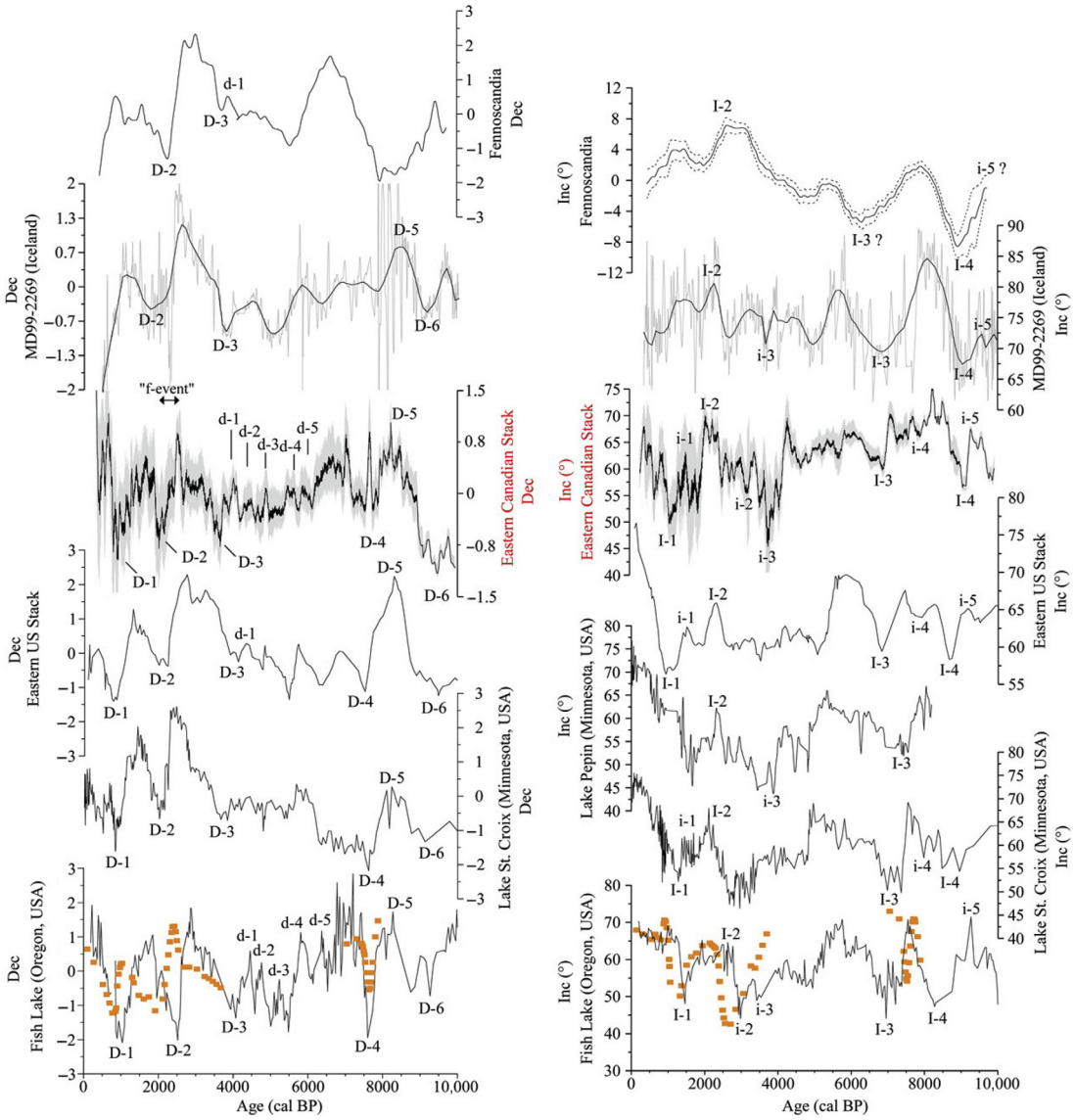


FIGURE 4.7 Holocene paleomagnetic secular variations from Northern Hemisphere sites, showing changes in declination (left) and inclination (right). Profiles are stacked records from (top to bottom): Fennoscandia, Iceland, eastern Canada, and the eastern United States. The lowermost records are from Lake St. Croix, Minnesota, Lake Pepin, Minnesota (inclination only), and Fish Lake, Oregon. Dots on lower panel are secular variations recorded in lava flows from the western United States. Correlative declination and inclination features are indicated by the letters assigned to peaks and troughs. The prominent magnetic declination swing at ~2500 calendar years BP is labeled as the "f-event." All the declination data were standardized to allow a direct comparison; note that the inclination scales are not identical. *From Barletta et al. (2010), who provide details about all the sources and the processing of each record.*

exposed rock surfaces in episodic deposits such as moraines or till sheets. There are a number of possible approaches (see Colman and Dethier, 1986) but they must be calibrated by independent dating methods to convert the relative age to a numerical age estimate. Nevertheless, even without such calibration, weathering studies have proven to be useful in distinguishing and correlating glacial deposits in many alpine areas (e.g., Rodbell, 1993). One of the most widespread and well-tested methods is obsidian hydration dating (Section 4.2.2), an example of the general group of methods that involve measurements of weathering rinds (e.g., Chinn, 1981; Colman and Pierce, 1981).

Another method involves the chemical "fingerprinting" of volcanic ashes that often blanket wide areas after a major eruption (Section 4.3). Chemical analyses of tephra deposits have proved to be successful in identifying unique geochemical signatures in ashes of different ages. Where the age of a tephra layer has been independently determined, the ash may be used as a chronostratigraphic marker to date the associated deposits and to correlate events over wide areas.

4.2.1 Amino Acid Dating

As all living organisms contain amino acids, a dating method based on amino acids offers a tremendous range of possible applications. Since the first use of amino acids in estimating the age of fossil mollusk shells (Hare and Mitterer, 1968), significant advances in the use of amino acids as a geochronological tool have been made. Relative ages are generally obtained, but where an independent age calibration is possible and the thermal history of the sample can be estimated, more quantitative age estimates can be made. The method can be applied to material ranging in age from a few thousand to a few million years old and is therefore useful in dating organic material well beyond the range of radiocarbon dating.

Amino acid analyses use very small samples (e.g., <2 mg in the case of mollusks and foraminifera). However, for reliable results, multiple analyses on a suite of samples are recommended (Miller and Brigham-Grette, 1989). The application of amino acid dating is thus of particular significance in dating fragmentary hominid remains, where, in many cases, a conventional radiocarbon analysis would require destruction of the entire fossil to obtain a date (Bada, 1985). Analyses have also been carried out on samples of wood, speleothems, coral, foraminifera, and marine, freshwater, and terrestrial mollusks (Schroeder and Bada, 1976; Lauritzen et al., 1994). Because amino acid changes are both temperature- and time-dependent, it is often difficult to be definitive in assigning an age to a sample. More often, the method enables relative chronologies to be established and stratigraphic sequences to be checked (Miller et al., 1979; Oches and McCoy, 1995a). It is perhaps in this application (aminostratigraphy) that amino acid analysis offers the greatest potential (Miller and Hare, 1980).

4.2.1.1 Principles of Amino Acid Dating

Amino acids are so-called because they contain in their molecular structure an amino group (—NH_2) and a carboxylic acid group (—COOH). These are attached to a central carbon atom, which is also linked to a hydrogen atom (—H) and a hydrocarbon group (—R) (Figure 4.8a). If all atoms or groups of atoms attached to the central carbon atom are different, the molecule is said to be chiral or asymmetric. The significance of this is that chiral molecules can exist in two

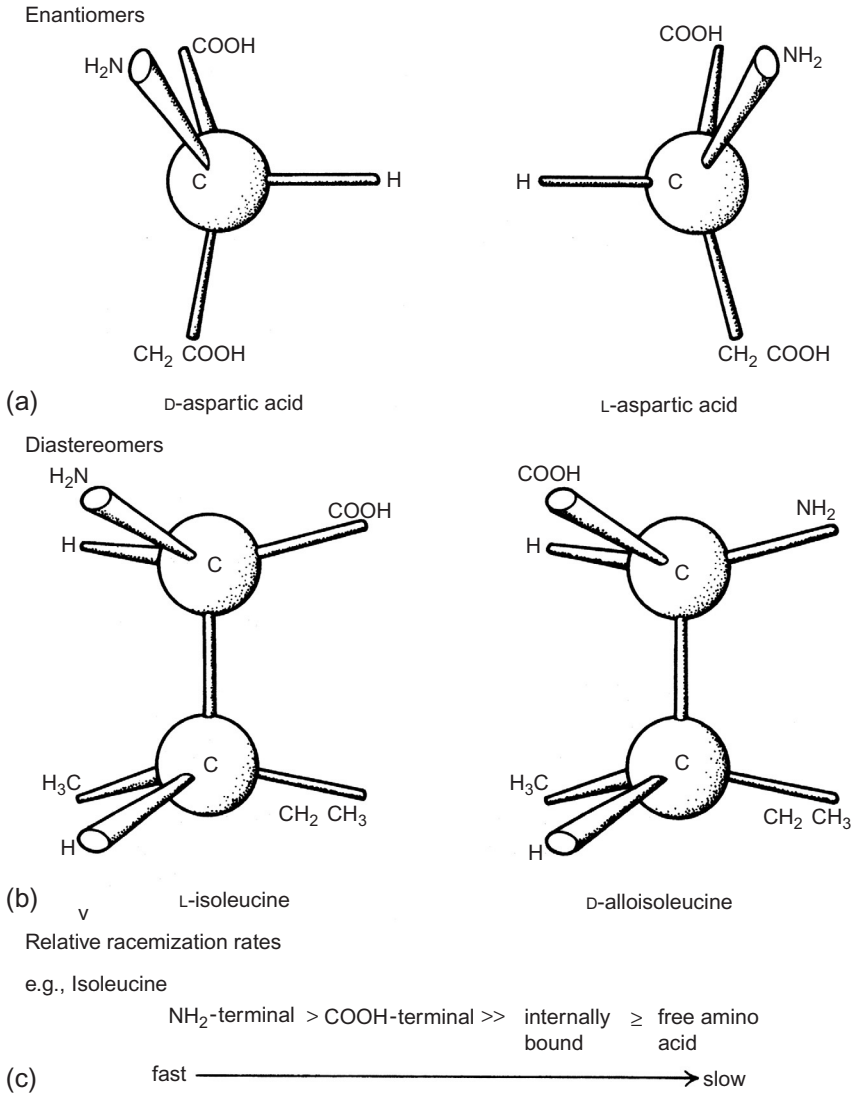


FIGURE 4.8 (a) An example of enantiomers (D-aspartic acid and L-aspartic acid). (b) An example of diastereomers (L-isoleucine and D-alloisoleucine). (c) Relative rates of racemization depending on whether the amino acid is internally bound, terminally bound, or free.

optically different forms (stereoisomers), each being the mirror image of the other (Figure 4.8b). These optical isomers or enantiomers have the same physical properties and differ only in the way in which they rotate plane-polarized light. The relative configuration of enantiomers is designated, by convention, D or L *(dextro* or *levo)* and virtually all chiral amino acids in living organisms occur in the L configuration. Conversion to the D configuration takes place by a process known as racemization. The extent of the racemization (expressed by the enantiomeric

ratio, D/L) increases with time after the death of the organism. This can be measured by gas or liquid chromatographic methods.

Not all amino acids have only one chiral carbon atom. Some amino acids (e.g., isoleucine) contain two chiral carbon atoms, which means that they can exist as four stereoisomers—a set of mirror image isomers (enantiomers) and a set of nonmirror image isomers (diastereomers) (Figure 4.8b). Interconversion of L-isoleucine could thus theoretically produce all four stereoisomers. However, in diagenetic processes, only one of the two chiral atoms undergoes interconversion, thereby producing only one other isomer (D-alloisoleucine, a diastereomer) by a process known as epimerization[1] (Schroeder and Bada, 1976; Rutter and Blackwell, 1995). The ratio of D-alloisoleucine to L-isoleucine (abbreviated as aIle/Ile, or D/L) increases on the death of an organism from near zero to ~1.3 at equilibrium. The time it takes to reach equilibrium varies with temperature (as discussed below) and may range from 150 to 300 ka in the tropics, to ~2 Ma at midlatitudes to >10 Ma in polar regions (Miller and Brigham-Grette, 1989). Diastereomers have physical properties that are sufficiently different that they can be separated by ion-exchange chromatography. Several different amino acids have been used to assess the age of a sample, particularly aspartic acid, leucine, and isoleucine. Epimerization of L-isoleucine to D-alloisoleucine is an order of magnitude slower than aspartic acid racemization, so it is potentially of more value in dating older samples or those from warmer climates where epimerization and/or racemization rates are faster. Conversely, aspartic acid can be used in resolving differences between Arctic mollusks from the last glacial cycle, the temperature history of which is too low for them to have undergone significant isoleucine epimerization (Goodfriend et al., 1996). Aspartic acid racemization has also provided excellent results in dating recent fossils, such as banded corals (Figure 4.9) and land snails of Holocene age (Goodfriend, 1991, 1992; Goodfriend et al., 1992).

Unlike radionuclide decay rates, racemization and epimerization rates are sensitive to a number of environmental factors, particularly temperature. In addition, racemization and epimerization rates vary depending on the type of matrix in which the amino acids are found (shell, wood, bone, etc.). In carbonate fossils, rates vary from one genus to another (Figure 4.10) so it is important to compare amino acid ratios derived from analyses on similar genera (Miller and Hare, 1975; King and Neville, 1977). Racemization rates also depend on how amino acids are bound to each other or if they are free (unbound). When an amino

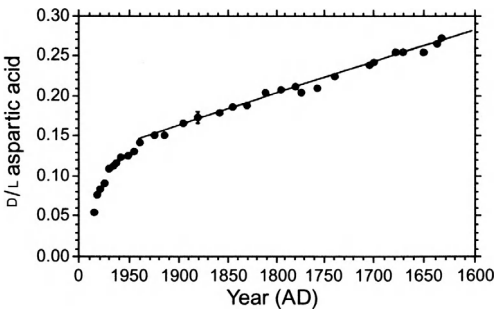


FIGURE 4.9 Racemization (D/L) values of total aspartic acid (hydrolyzed samples) in relation to the counted age of annual bands in the coral *Porites australiensis*, from the Great Barrier Reef, Australia. The linear regression for the period 1632-1985 is shown (Goodfriend et al., 1992).

[1] For our purposes, racemization and epimerization of amino acids can be considered as essentially equivalent processes.

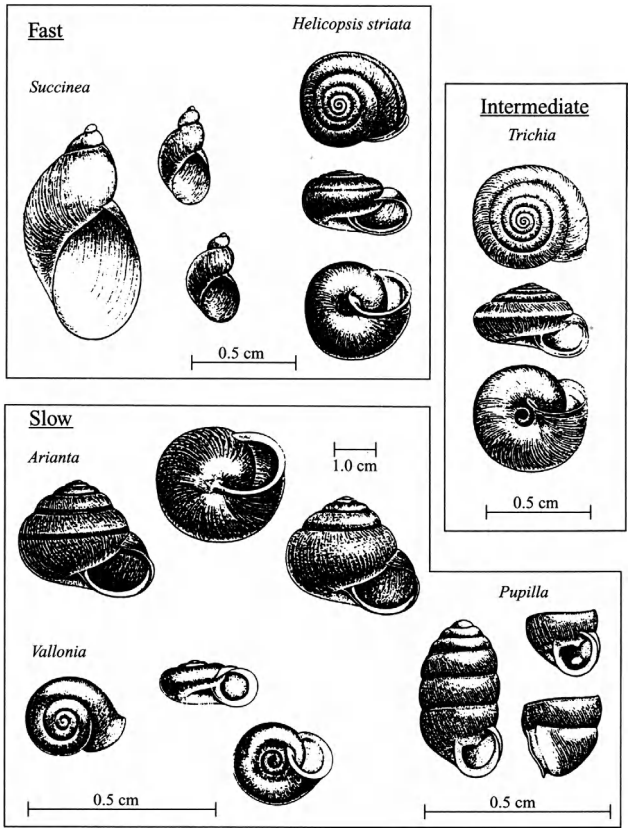


FIGURE 4.10 Some fossil gastropods commonly found in European loess deposits, grouped according to the relative racemization rates of isoleucine in the shell matrix. Note the variable scale. *From Oches and McCoy (1995b).*

acid is bound together with others, its position in the molecule may be internal or terminal (Figure 4.8c). If it is terminally bound, it may be attached to other amino acids by a carbon atom or a nitrogen atom. Racemization rates are fastest when the amino acid is terminally bound and slowest when the individual amino acid is free, having been separated from the rest of the molecule by hydrolysis. Racemization rates of internally bound amino acids are intermediate between rates of terminally bound and free amino acids (Figure 4.8c). What this means is that as the peptide is hydrolyzed, at some point, each amino acid will become terminally bound before being eventually split off (free). In the terminally bound position, racemization rates are greatest, so the probability is relatively high that the free amino acid, when released, will already be in the D-form. Consequently, the D/L ratios in the free fraction are higher than in the bound fraction. It is thus important to note whether analyses reported in the literature are based on free fraction or the total acid hydrolysate (free and bound) since the resulting ratios can vary by an order of magnitude (Table 4.1). Commonly, the D/L ratios from the free fraction and the total acid hydrolysate will be plotted against each other to help differentiate units of different age (Figure 4.11). Recent studies have involved isolating the high molecular weight (HMW) polypeptides in a sample, which are considered to be less contaminated (by postdepositional bacterial degradation of the amino acids) (Kaufman and Sejrup,

TABLE 4.1 Temperature Sensitivity of Amino Acid Reactions in Dated Early Postglacial Mollusk Samples (Miller and Hare, 1980)

Location	^{14}C Age (years)	MAT (°C)[a]	Species[b]	Allo:Iso[c]	
				Total	Free
Washington	13,010	+10	*H.a.*	0.078	0.27
Denmark	13,000	+7.7	*H.a.*	0.053	0.21
Maine	12,230	+7	*H.a.*	0.050	0.21
New Brunswick	12,500	+5	*H.a.*	0.043	0.18
Southeastern Alaska	10,640		*H.a.*	0.040	0.15
Anchorage	14,160	+2.1	*M.t.*	0.034	0.16
Southern Greenland	13,380	−1	*H.a.*	0.027	<0.09
Southern Baffin Island	10,740	−7	*M.t.*	0.024	<0.1
Spitzbergen	11,000	−8	*M.t.*	0.022	<0.1
Northern Baffin Island	10,095	−12	*H.a.*	0.020	ND
Somerset Island	9000	−16	*H.a.*	0.018	ND
Modern	0		*H.a.*	0.018	ND

[a]*Mean annual temperature of the past one to five decades based on records of the nearest representative weather station.*
[b]H.a., Hiatella arctica; M.t., Mya truncata. *Hydrolysis rates in* Mya *are not directly comparable with those in* Hiatella. *For most localities, three or more separate values were analyzed; ratios given here are mean values.*
[c]*Ratio of* D*-alloisoleucine to* L*-isoleucine; ND, no detectable alloisoleucine.*

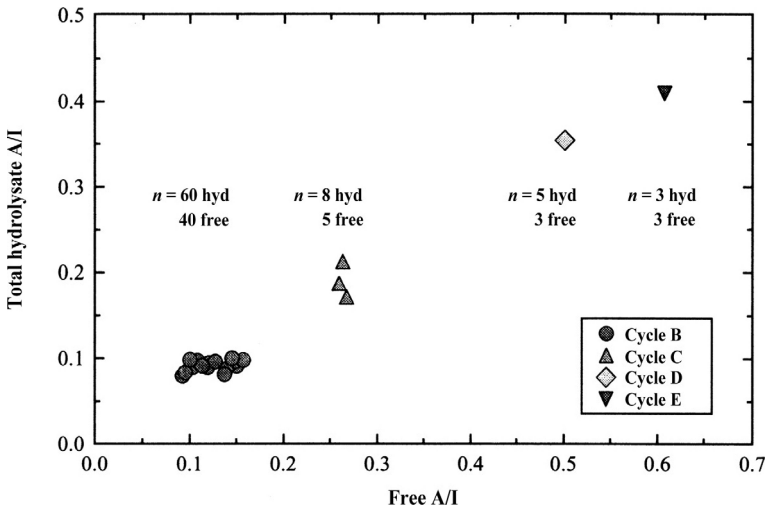


FIGURE 4.11 Total vs. free aIle/Ile for *Succinea* snails in loess units from central Europe. The sample means (shown by different symbols) fall into distinct clusters that correspond to loess units of different age. A number of subsample preparations are indicated. *From Oches and McCoy (1995b).*

1995). Analysis of the HMW fraction produces more consistent results (i.e., a lower standard deviation) and a much slower rate of racemization because of the presence of fewer terminally bound amino acids. This approach could extend the potential range of dating, which would be useful in some situations, though problematic in resolving age differences between samples from colder regions.

By far, the most significant factor affecting the rate of racemization is temperature, specifically the effective diagenetic temperature (EDT), which is an integrated temperature of the sample since deposition (Table 4.1). Racemization rates more or less double for a 4-5 °C increase in temperature, so the thermal history of a sample becomes of critical importance to the apparent age. An uncertainty of only ±2 °C is equivalent to an age uncertainty of ±50%, so this is clearly a major source of error in assessing the numerical age of a sample (McCoy, 1987a). Thermal histories are rarely known to within ±2 °C, even in isolated environments, such as in caves or in the deep oceans. However, the temperature dependence of racemization rates may be put to advantage if the sample age is known independently (e.g., by ^{14}C dating). In such cases, the relative amount of racemization can indicate the EDT of the sample since deposition (Bada et al., 1973) or the extent of a step change in temperature (Schroeder and Bada, 1973; see Section 4.2.1.4). It is important to note that because racemization rates increase exponentially with temperature, the amount of time a sample experiences high temperatures is much more significant than the time spent at low temperatures (Figure 4.12). EDT is thus not simply the long-term mean temperature of the site and will always be higher than the actual long-term mean. This means that at mid- to high-latitude sites, samples from the beginning or end of the last glacial period may be indistinguishable in terms of their D/L ratios, but they would be distinctly different from samples of the last interglacial or preceding glacial period (which had passed through the last interglacial). This strong temperature influence on racemization also imposes strict sampling criteria, as samples which have been close to the surface for a prolonged period (either the modern surface or a paleosurface) may give erroneous results because they were exposed to high temperatures, significantly raising their effective diagenetic temperature. Experiments suggest that samples should be deeply buried (>2 m) to avoid such problems (Miller and Brigham-Grette, 1989).

There are basically three approaches used in amino acid geochronological work. Two of these aim at producing an estimate of numerical age and the third uses enantiomeric ratios as simply a stratigraphic tool, to establish the relative age of two or more samples.

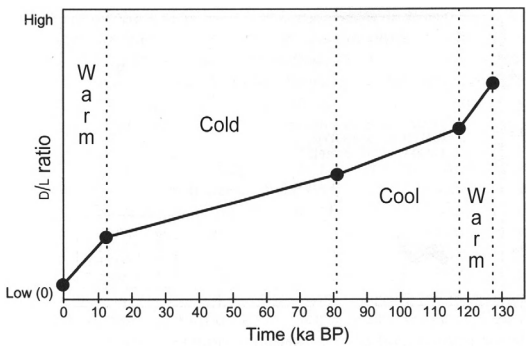


FIGURE 4.12 Schematic diagram illustrating the increase in D/L ratio in a fossil mollusk over the course of the last glacial-interglacial cycle. Most of the change in D/L values occurs during the warm interglacial episodes. *From Miller and Mangerud (1985).*

4.2.1.2 *Numerical Age Estimates Based on Amino Acid Ratios*

Numerical sample ages are estimated by either calibrated or uncalibrated methods (Williams and Smith, 1977). The *uncalibrated method* is based on high-temperature laboratory experiments, which attempt to simulate in a short period of time, the much slower processes that occur in samples at the lower temperatures typical in nature. The general amino acid racemization reaction is as follows:

$$\text{L} - \text{amino acid} \;\; k_1/k_2 \;\; \text{D} - \text{amino acid}$$

where k_1 and k_2 are rate constants for the forward and reverse reactions. In the high-temperature studies, racemization rates are determined by sealing in a tube a sample of the same species as the fossil under investigation and heating it for known lengths of time in a constant temperature bath. Providing the initial ratio of the sample is known, genus-specific rate constants for the amino acid in question can be determined in this way, at different (elevated) temperatures. These are then plotted on an Arrhenius plot in which the log of the rate constant forms the ordinate and the reciprocal of the absolute temperature forms the abscissa (Figure 4.13). If the calculated rate constants fall on a straight line, extrapolation is made (beyond the experimental results) to obtain the rate constants applicable at lower temperatures (e.g., Miller and Hare, 1980). Providing that the EDT of the sample since its deposition is known

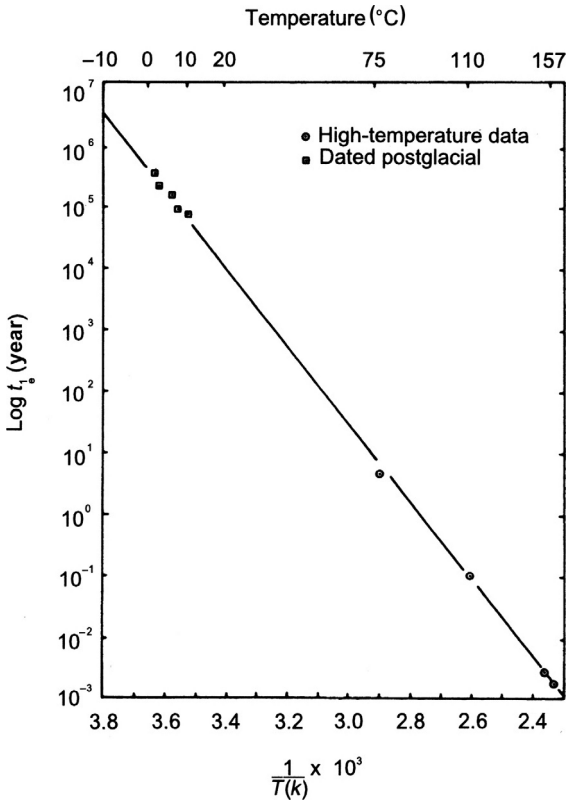


FIGURE 4.13 Arrhenius plot of isoleucine epimerization in *Hiatella arctica* derived from heating experiments at 75, 110, 152, and 157 °C and ^{14}C-dated early postglacial samples. *After Miller and Hare (1980).*

(or can be closely estimated), racemization rate constants can be obtained for that temperature from the Arrhenius plot; sample age can then be calculated from the measured D/L ratio (for the appropriate equations, see Williams and Smith, 1977, p. 102). One might question whether such high-temperature, short-term laboratory kinetic studies accurately reflect the low-temperature, long-term diagenetic changes, which occur in fossils. However, there is an increasing body of evidence that this is not a problem and that the high-temperature results can be extrapolated to real-life situations (e.g., Figure 4.10; Goodfriend and Meyer, 1991). The real difficulty concerns the problem of knowing accurately the thermal history of the sample, since slight errors in this parameter lead to large errors in numerical age estimates (McCoy, 1987a). As a result, the ages derived by means of this uncalibrated method are considered to be the least reliable.

A more fruitful approach, though not entirely free of the problems discussed earlier, is to derive rate constants empirically by the measurement of D/L ratios *in situ*, in fossil samples of known age (the *calibrated method).* Other samples at the same site can then be dated, if it is assumed that they have experienced essentially the same EDT as the fossil used for calibration (Bada and Schroeder, 1975). A Holocene fossil calibration sample is thus not suitable for assessing the age of older "glacial age" samples since their thermal histories will be quite different. Because of the reduction in racemization rate with sample age and the sensitivity of the process to temperature, resolution of age becomes increasingly more uncertain in very old samples (Wehmiller, 1993). Miller and Brigham-Grette (1989) suggest that age estimates that are independently calibrated and are within the early "linear" stage of sample racemization ($D/L < 0.3$) should be reliable to ±15-20%, but this is likely to increase to ±30-40% for older samples. However, further cross-checks with independent age estimates can reduce such uncertainties.

Figure 4.14 illustrates the calibrated approach to estimating sample age. The three lines are calculated aIle/Ile ratios (based on a kinetic model, from heating experiments) for EDTs of 8,

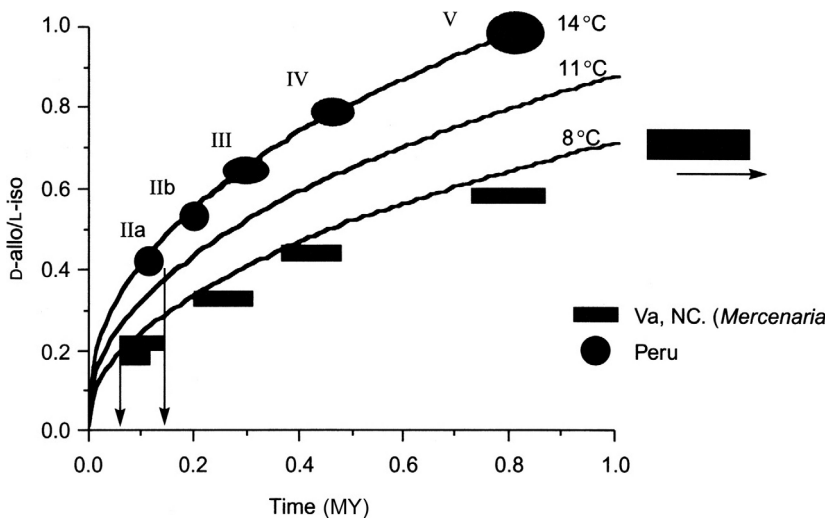


FIGURE 4.14 Isoleucine epimerization model curves for different EDTs, in relation to mean aIle/Ile ratios for samples from Peru (ovals) and from the US Atlantic Coastal Plain (rectangles). The last interglacial samples used for calibration are shown by arrows. *Adapted from Wehmiller (1993).*

11, and 14 °C (Wehmiller, 1993). The Peruvian samples are from a series of uplifted coastal terraces; sample IIa was independently dated at 100-130 ka BP (i.e., last interglacial, *sensu lato*) and thus provides an age calibration point. Assuming a long-term EDT of 14 °C for this area, the age of the older samples (IIb-V) can be estimated. A similar approach is also shown for samples of *Mercenaria* from the North Carolina and Virginia coastal plain, again using samples from the last interglacial as the single age calibration point. Greater confidence in the ages of older samples would be achieved by having more than one calibration point. Note that the estimation of EDT is critical for obtaining a "correct" age and that its importance increases with sample age. For example, an aIle/Ile value of 0.6 could indicate a sample age of 0.4 Ma with an EDT of 11 °C or 0.8 Ma with an EDT of 8 °C. Fortunately, since for most of the last million years, the Earth was in a glacial mode, the EDT is primarily controlled by the temperature during relatively brief interglacial episodes; the long-term EDT is therefore assumed to be similar to that experienced by a sample since the time of the last interglacial. Such an assumption could be drastically in error if, for example, a sample that had been submerged below sea level for a significant amount of time was compared to a sample that has been subjected to air temperature changes. Table 4.2 illustrates this point; it shows aIle/Ile ratios on marine mollusks (*Hiatella arctica*) from Svalbard, Norway. Shells of the same ^{14}C age had significantly different values, depending on whether they had been continuously submerged for the entire Holocene or exposed to much lower air temperatures (therefore reducing the racemization rate). Table 4.2 also shows that shells that dated >61 ka BP from the same area gave aIle/Ile ratios identical to the continuously submerged early Holocene samples, illustrating the potential for misinterpretation if the thermal history of a sample is not understood.

4.2.1.3 *Relative Age Estimates Based on Amino Acid Ratios*

In view of the numerous difficulties surrounding the assignment of numerical ages to fossil samples, many investigators have found it prudent to use amino acid ratios as relative age criteria only. By establishing a standard aminostratigraphic framework for deposits in a region (where it is reasonable to assume a similar EDT history), other units can then be fitted into that relative age chronology (Wehmiller, 1993). For example, Oches and McCoy (1995a) showed that the conventional interpretation of loess stratigraphy in Hungary was incorrect, based on D/L ratios in fossil gastropods shells (snails) associated with each deposit. In some sections, units of quite different age had been assumed to be correlative, but they were clearly diachronous according to the aminostratigraphy. This approach has provided an independent means of testing the veracity of TL dates on loess across a wide swath of central Europe,

TABLE 4.2 The Effect of Contrasting Thermal Histories on ^{14}C-Dated *Hiatella arctica* from Western Spitsbergen, Svalbard, Norway (Miller and Brigham-Grette, 1989)

Thermal History	Current MAT (°C)	D/L Ratio	^{14}C Age
Continuously submerged	+2.2	0.031	9900
Emerged shortly after deposition	−6.0	0.018	9940
Emerged shortly after deposition	−6.0	0.031	>61,000

from Germany to the Ukraine (Zöller et al., 1994; Oches and McCoy, 1995b). Furthermore, by correlating the revised loess-paleosol sequences with marine isotope stages, as first suggested by Kukla (1977), it is possible to assign approximate ages to the D/L ratios in the snails of each loess unit (Figure 4.15). A similar approach was taken by Miller and Mangerud (1985) who used aIle/Ile ratios in shallow water marine mollusks from European interglacial deposits to correlate deposits of similar age and thermal history and to distinguish units of last interglacial age from older deposits. The results were helpful in resolving previous uncertainties in the age of many isolated and fragmentary stratigraphic sections. Bowen et al. (1989) also found that aminostratigraphic studies of nonmarine mollusks were extremely useful in reassessing the chronology of Pleistocene depositional units in Great Britain; the revised stratigraphy could then be correlated with the SPECMAP standard marine chronostratigraphy. These are all relatively simple applications, using racemization of a single amino acid to solve a stratigraphic problem. More rigorous differentiation seems possible using several enantiomeric ratios and multivariate statistical techniques such as discriminant analysis.

At the present time, using amino acid racemization and epimerization processes for establishing relative age seems to be the most practical application of the method. There may still be problems of contamination, leaching, and possibly thermal differences among sites, but these are relatively minor problems compared to those associated with numerical age determinations.

4.2.1.4 Paleotemperature Estimates from Amino Acid Racemization and Epimerization

Although amino acid analyses are being increasingly used in stratigraphic studies, perhaps the most significant application of amino acid ratios is in paleotemperature reconstruction. As noted earlier, a major barrier to accurate age estimates from amino acid ratios is a knowledge of the integrated thermal history of the sample. However, the "age equation" (which includes the important thermal term) can be solved for temperature if the sample age is known. In the resulting "temperature equation," the time value is of relatively minor significance; as a result, for samples of known age, quite accurate estimates of the integrated thermal history of the depositional site can be achieved. Typically, for well-dated late Wisconsin or Holocene age samples, an uncertainty of ~3 °C (~1% of the absolute temperature of the site) can be expected in the paleotemperature estimates. However, if paleotemperatures are calculated from two samples of differing age, the temperature *difference* between the two periods can be estimated with considerably more accuracy (typically to within ±1 °C). This is because many of the factors that cause the initial uncertainty in an individual paleotemperature estimate cancel out when temperature differences are computed (McCoy, 1987a). Using this approach, McCoy (1987b) cast new light on the controversy of "cooler or wetter" conditions in the Great Basin during the late Wisconsin. Mean annual temperatures from 16,000 to 11,000 years BP were estimated to have been 9 °C or more below the post-11,000 year BP averages. If correct, no increase in regional precipitation would be required to explain the high levels of Lake Bonneville during the late glacial, with the maximum lake-level phase occurring during a relatively cold, dry climate compared to the present (cf. Section 8.2.3). In another interesting application, Oches et al. (1996) used aIle/Ile ratios in gastropods from Mississippi Valley Peoria Loess (dating from the last glacial maximum) to estimate effective diagenetic temperature gradients from the Gulf of Mexico (30°N) to inland sites at 43°N. Today, the gradient is

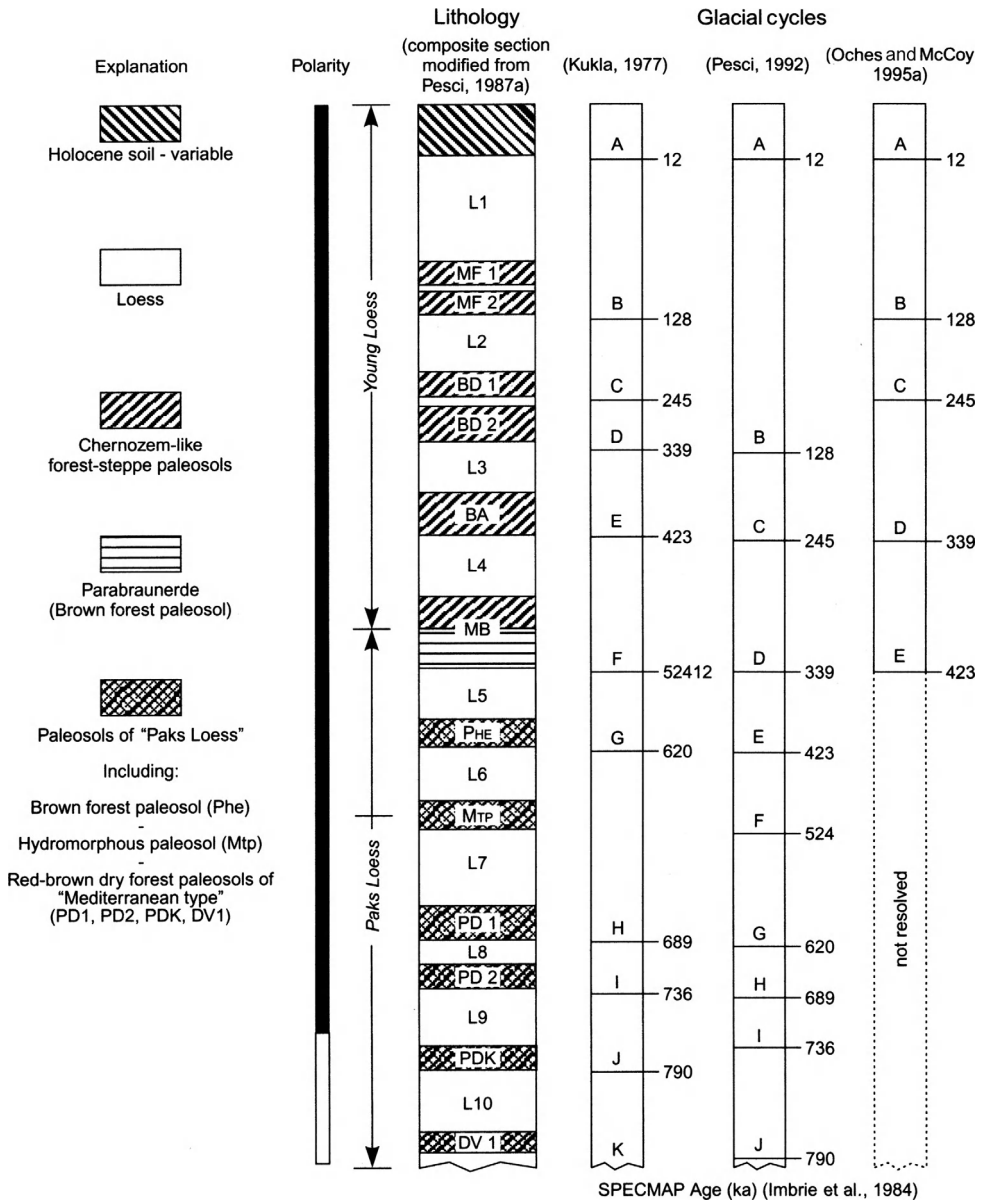


FIGURE 4.15 The composite loess-paleosol stratigraphy characteristic of sites in Hungary is shown schematically in the center column (generally the sections are incomplete in any one area). Columns to the right show previous interpretations of the stratigraphy, subdivided into the main interglacial-glacial cycles (designated A to K), according to Kukla (1977) and Pécsi (1992). Their proposed correlations with the marine isotope stages are indicated by the age of glacial stage terminations (based on SPECMAP dated records of Imbrie et al., 1984). Amino acid relative age dating on snails in the loess suggests that the "correct" interpretation is that shown in the right-hand column. *Derived from Oches and McCoy (1995a) and Zöller et al. (1994).*

0.9 °C/degree of latitude, whereas the amino acid data point to gradients of only 0.3-0.6 °C/degree of latitude and overall temperatures at least 7-13 °C lower than today. This suggests that SSTs in the Gulf of Mexico were significantly lower than today; otherwise, the temperature depression would have been less in the lower Mississippi Valley, and the overall temperature gradient would probably have been stronger, not weaker.

4.2.2 Obsidian Hydration Dating

Obsidian is one of the glassy products of volcanic activity, formed by the rapid cooling of silica-rich lava. Although its precise chemical composition varies from one extrusion to another, it always contains >70% silica by weight. Obsidian hydration dating is based on the fact that a fresh surface of obsidian will react with water from the air or surrounding soil, forming a hydration rind. The thickness of the hydration rind can be identified in thin sections cut normal to the surface; a distinct diffusion front can be recognized by an abrupt change in refractive index at the inner edge of the hydration rind. Hydration begins after any event that exposes a fresh surface (e.g., cracking of the lava flow on cooling, manufacture of an obsidian artifact, or glacial abrasion of an obsidian pebble); thus, providing one can identify the type of surface or crack in the rock, it is possible to date the event in question.

As one might expect, hydration rind thickness is a (nonlinear) function of time; hydration rate is primarily a function of temperature, though chemical composition of the sample is also an important factor. For this reason, it is necessary to calibrate the samples within a limited geographic area against a sample of known age and similar chemical composition. These are difficult criteria to meet in a paleoclimatic context but are somewhat easier in archeological studies, where obsidian hydration dating has been most widely applied (Michels and Bebrich, 1971). Obsidian was widely traded in prehistoric time and often the precise source of the material can be identified and its diffusion throughout a geographic area can be traced. If samples can be found in a ^{14}C-dated stratigraphic sequence, hydration rinds can be calibrated, providing an empirically derived hydration scale for the site. This can then be used to clarify stratigraphy elsewhere, where radiocarbon-dated samples are unavailable. Alternatively, the hydration rate can be calibrated in the laboratory by heating experiments; if the effective hydration temperature of the sample can be estimated (i.e., its integrated temperature history), age can then be calculated (see Lynch and Stevenson, 1992). In general, age is proportional to the square of hydration rind thickness (Pierce and Friedman, 2000).

Obsidian hydration may also be used to date glacial events if obsidian has been fortuitously incorporated into the glacial deposits. Glacial abrasion of obsidian fragments creates radial pressure cracks normal to the surface and shear cracks subparallel to the surface. The formation of such "fresh" cracks allows new hydration surfaces to develop, and these effectively "date" the time of glacial activity. Hydration rinds resulting from glacial abrasion can then be compared with rinds, which have developed on microfractures produced when the lava cooled initially. This event can be dated by potassium-argon isotopic methods (Section 3.2.2), providing independent calibration for the primary hydration rind thicknesses. Pierce et al. (1976), for example, analyzed obsidian pebbles in two major moraine systems in the mountains of western Montana. Dates on two nearby lava flows indicated ages of $114{,}500 \pm 7300$ and $179{,}000 \pm 3000$ years BP. Hydration rinds on cracks produced during the initial cooling of these flows averaged 12 and 16 μm, respectively. These points enabled

a graph of hydration thickness versus age to be plotted. It was then possible to estimate, by interpolation, the age of hydration rinds produced on glacially abraded cracks in the moraine samples. Two distinct clusters of hydration rind thicknesses enabled glacial events to be distinguished, at 35,000-20,000 and 155,000-130,000 years BP. Although the dates are by no means precise, they do at least indicate the important fact that the earlier glacial event predated the Sangamon interglacial (~125,000 years BP), a point of some controversy in the glacial history of the western United States.

Obsidian hydration dating methods are limited by the problems of independent (radioisotopic) calibration and of variations in sample composition and temperature over time. Temperature effects are particularly difficult to evaluate. It is really necessary to produce a calibration curve for each area being studied, and this is not always possible. Nevertheless, where the right combination of conditions is found, obsidian hydration methods can provide a useful time frame for events, which might otherwise be impossible to date.

4.3 TEPHROCHRONOLOGY

Tephra is a general term for airborne pyroclastic material ejected during the course of a volcanic eruption (Thorarinsson, 1981). Extremely explosive eruptions may produce a blanket of tephra covering vast areas, in a period which can be considered as instantaneous on a geological timescale. Tephra layers thus form regional isochronous stratigraphic markers. Tephras themselves may be dated directly, by potassium-argon or fission-track methods, or indirectly, by closely bracketing radiocarbon dates on organic material above and below the tephra layer (e.g., Naeser et al., 1981). In favorable circumstances, organic material incorporated within the tephra may provide quite precise time control on the eruption event (e.g., Lerbemko et al., 1975; Blinman et al., 1979). Providing that the dated tephra layer can be uniquely identified in different areas, it can be used as a chronostratigraphic marker horizon to provide limiting dates on the sediments with which it is associated. For example, a tephra layer of known age provides a *minimum* date on the material over which it lies and a *maximum* date on material superimposed on the tephra. If a deposit is sandwiched between two identifiable tephra layers of known age, they provide bracketing dates for the intervening deposit (Figure 4.16). A prerequisite for such tephrochronological

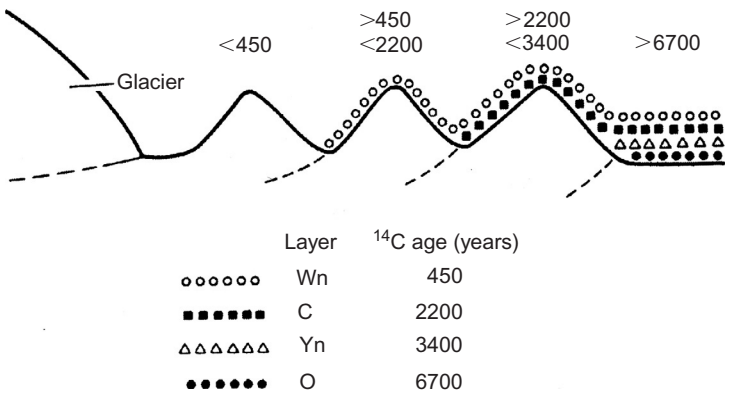


FIGURE 4.16 The use of tephra to date glacial deposits. If tephra age is known and tephra can be uniquely identified, ages can be used to "bracket" the timing of glacial advances. *After Porter (1981a).*

applications is that each tephra layer be precisely identified. This has been the subject of much study both in the field and in the laboratory. In the field, stratigraphic position, thickness, color, degree of weathering, and grain size are important distinguishing characteristics. In the laboratory, a combination of petrographic studies, electron microprobe or laser ablation inductively coupled mass spectrometry (ICP-MS) analyses, is generally used to identify a unique tephra signature (e.g., Kittleman, 1979; Westgate and Gorton, 1981; Hunt and Hill, 1993; Pearce et al., 2007). Multivariate analysis may be employed on the various parameters measured to provide optimum discrimination (or correlation) between the tephras being studied (e.g., Beget et al., 1996; Shane and Froggatt, 1994).

In many volcanic regions of the world, tephrochronology is a very important tool in paleoclimatic studies. In northwestern North America, explosive eruptions have produced dozens of widely distributed tephra layers (Table 4.3). Some, such as the Pearlette "O" ash, covered almost the entire western United States and probably had a significant impact on hemispheric albedo (Bray, 1979). Others were more local in extent; around Mt. Rainier, for example, at least 10 tephra layers have been identified spanning the interval from 8000 to 2000 years BP (Mullineaux, 1974). Because of the eruption frequency and widespread distribution of tephra in this area, tephrochronological studies have proved to be invaluable in understanding its glacial history (e.g., Porter, 1979).

TABLE 4.3 Some Important Tephra Layers in North America

Tephra Layer	Source	Approximate Age
Katmai	Mt. Katmai, Alaska	AD 1912
Mt. St. Helens, Set T	Mt. St. Helens, Washington	AD 1800
Mt. St. Helens, Set W	Mt. St. Helens, Washington	450*
White River East	Mt. Bona, Southeastern Alaska	1250*
White River North	Mt. Bona, Southeastern Alaska	1890*
Bridge River	Plinth-Meager Mt, British Columbia	2600*
Mt. St. Helens, Set Y	Mt. St. Helens, Washington	3400*
Mazama	Crater Lake, Oregon	6600*
Glacier Peak B	Glacier Peak, Washington	11,200*
Glacier Peak G	Glacier Peak, Washington	12,750 – 12,000*
Pearlette O	Yellowstone National Park	600,000 ± 100,000
Bishop	Long Valley, California	700,000 ± 100,000
Pearlette S	Yellowstone National Park	1,200,000 ± 40,000
Pearlette B	Yellowstone National Park	2,000,000 ± 100,000

An asterisk in column 3 indicates that an age is given in radiocarbon years.
After Porter (1981b) and Westgate and Naeser (1995).

Tephrochronology has provided valuable time control in many paleoclimatic studies. For example, in the North Atlantic, the Icelandic Vedde ash has been identified in both lake and marine sediments across much of western Europe and the North Atlantic (e.g., Mangerud et al., 1984) and in ice cores from Greenland (Grönvald et al., 1995). It is thus a very important chronostratigraphic marker (10,320 ± 50 ^{14}C years BP or 12,171 ± 60 [ice-core counted] calendar years BP) at a critical time for correlating the rapid environmental changes that were then taking place (Turney et al., 2004). Other important ash layers found in both marine sediments and ice cores are the Saksunarvatn ash (~9000 ^{14}C years BP or ~10,347 ± 45 calendar years [ice cores]) (Birks et al., 1996; Zielinski et al., 1997; Rasmussen et al., 2006) and the Z2 ash zone, which derives from Tindfjallajökull in eastern Iceland, with an ^{40}Ar/^{39}Ar date of 57,000 years BP (Figure 4.17). A comparison of dates on time-synchronous tephras in marine and terrestrial settings can provide invaluable insights into marine reservoir corrections for radiocarbon dates (Mangerud et al., 1984). Tephras have also been isolated from many Holocene peat deposits (e.g., Pilcher et al., 1995) offering widespread applications of tephrochronology in paleoclimatic studies.

Not all tephras are clearly visible in peat or sedimentary records; many deposits contain finely dispersed cryptotephra (hidden tephra), which were often dispersed over a much greater area than the tephras that blanketed the landscape and now make up more visible layers. However, finding cryptotephras is not easy, requiring careful sieving and heavy liquid separation to isolate the tephra shards prior to microprobe analysis (Gehrels et al., 2008). Cryptotephra in peat can be more easily isolated by burning or chemically removing the peat matrix to reveal the residual eolian material in each sample (e.g., Pilcher et al., 2005), but even then, isolating unaltered shards for analysis is a time-consuming and difficult task. Recent discoveries of Icelandic cryptotephra in Greenland ice cores may enable diverse archives (ice, peat, lake, and marine sediments) to be tied together chronologically, with a near absolute chronology provided by annual layer counting of the ice-core glaciochemical stratigraphy (Figure 4.18) (Mortensen et al., 2005; Davies et al., 2010; Abbott and Davies, 2012). Even when tephras are not present, electrical conductivity and geochemical signals in ice cores (principally excess sulfate washed out of the atmosphere following major explosive eruptions) are important geochronological markers for dating ice at depth and hence for correlating different records (Vinther et al., 2006) (see Chapter 5, Section 5.3.2). However, not all sulfate or ECM peaks in ice cores are associated with the presence of tephra and some major volcanic eruptions that had global climatic effects (e.g., Tambora, in 1815) are not as prominent in the sulfate and ECM data as other more local (Icelandic) eruptions (Coulter et al., 2012).

Expanding our understanding of the frequency and extent of explosive eruptions in the past is extremely important (Beget et al., 1996). There is abundant evidence to demonstrate that such eruptions lead to lower temperatures, at least for a limited time period (Bradley, 1988; Robock, 2000). Whether periods with a high frequency of explosive eruptions in the past experienced a persistent temperature depression (possibly reinforced by additional positive feedbacks in the climate system, due to persistence of high albedo snow cover, or more extensive sea ice) remains controversial (see Chapter 2, Section 2.8). However, there is persuasive circumstantial evidence that episodes of explosive volcanism have been associated with periods of glacier advance in the past, including the most recent neoglacial

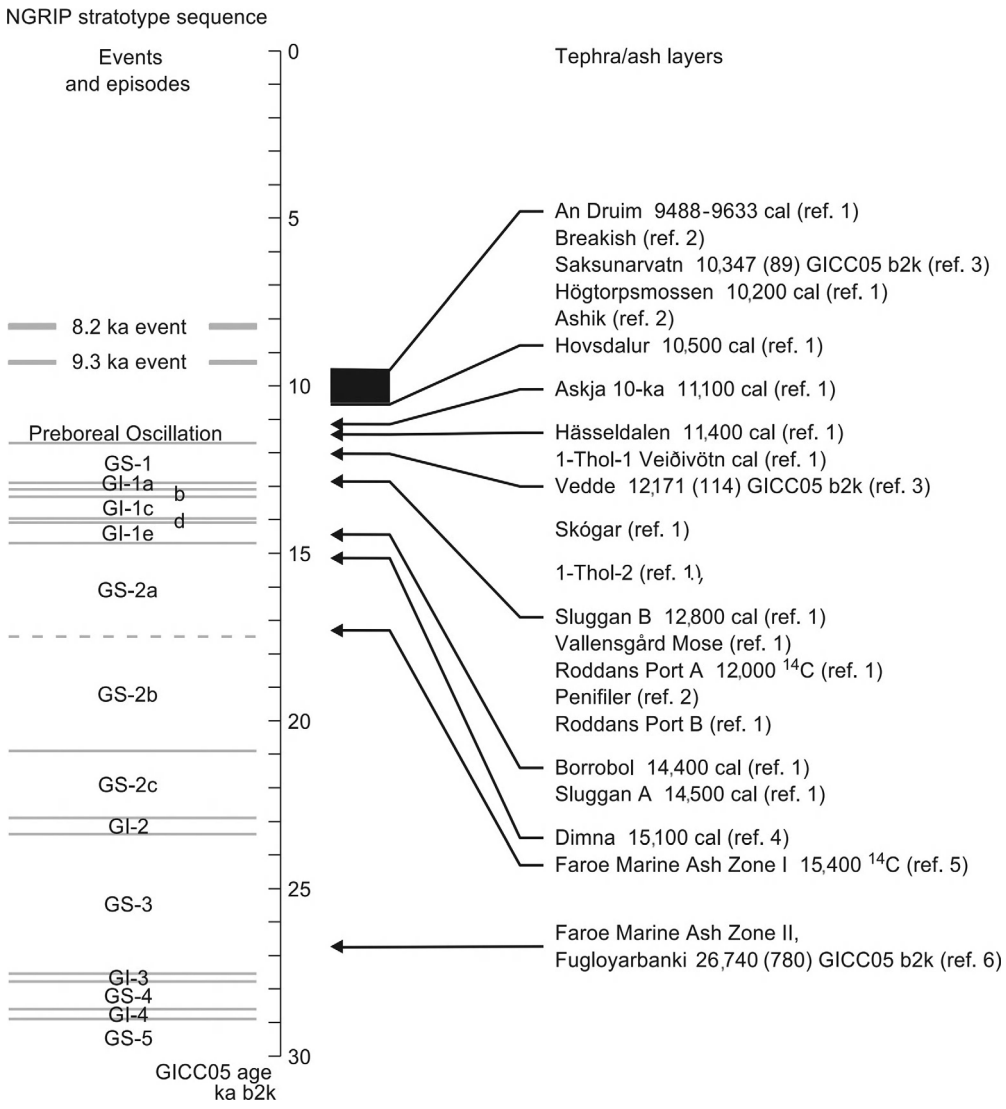


FIGURE 4.17 The sequence of (mostly) nonvisible distal volcanic ash layers of Icelandic origin in marine and terrestrial records from the North Atlantic region. The most recent age estimate published for each tephra layer is provided, with preference given to the age obtained from the annually counted Greenland Ice Sheet chronology (GICC05) (maximum counting errors given in brackets) where known. Radiocarbon-based ages are expressed in radiocarbon (^{14}C) or calibrated radiocarbon (cal) ages according to published data. *From Lowe et al. (2008), where the specific references are provided.*

episode, the "Little Ice Age" (Bray, 1974; Porter, 1986; Grove, 1988; Miller et al. 2012). Numerous other examples of the importance of tephrochronological studies in paleoclimatic research are found in the two volumes edited by Sheets and Grayson (1979) and by Self and Sparks (1981) and in dedicated issues of *Quaternary Science Reviews* (2008, vol. 25) and *Quaternary International* (2008, vol. 178x).

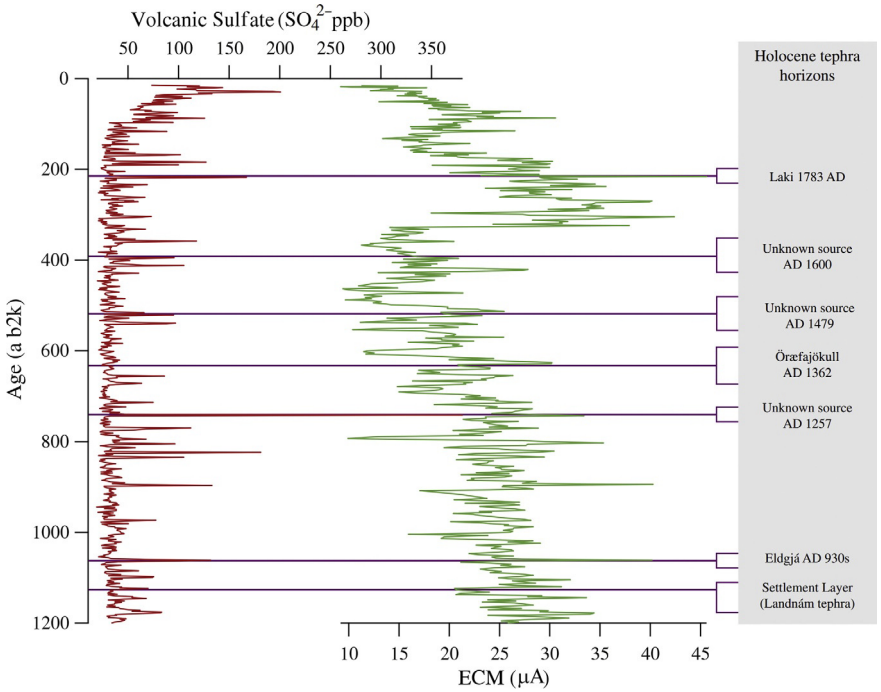


FIGURE 4.18 Stratigraphic position of Late Holocene tephra layers identified within the GISP2 and GRIP ice-core records (right column) compared to sulfate and electrical conductivity measurements (ECM). Note that not all sulfate or ECM peaks are associated with the presence of tephra. Also, some major volcanic eruptions that had global climatic effects (e.g., Tambora, in 1815) are not as prominent in the sulfate and ECM data as other more local (Icelandic) eruptions. The timescale is from Meese et al. (1997) and corrected to the b2k (before AD 2000) reference point. Volcanic sulfate and ECM records from the GISP2 core, from Zielinski et al. (1996) and Taylor et al. (1997), respectively. *From Abbott and Davies (2012).*

4.4 BIOLOGICAL DATING METHODS

Biological dating methods generally use the size of an individual species of plant as an index of the age of the substrate on which it is growing. They may be used to provide minimum-age estimates only, since there is inevitably a delay between the time a substrate is exposed and the time it is colonized by plants, particularly if the surface is unstable (as, for example, in an ice-cored moraine). Fortunately, this delay may be short and not significant, particularly if the objective is simply establishing a relative age.

4.4.1 Lichenometry

Lichens are made up of algal and fungal communities living together symbiotically. The algae provide carbohydrates via photosynthesis and the fungi provide a protective environment in which the algal cells can function. Morphologically, lichens range from those with small bush-like thalli (foliose lichens) to flat disklike forms, which grow so close to a rock

surface as to be inseparable from it. These crustose lichens commonly increase in size radially as they grow and this is the basis of lichenometry, the use of lichen size as an indicator of substrate age (Locke et al., 1979). Lichenometry has been most widely used in dating glacial deposits in tundra environments where lichens often form the major vegetation cover and other types of dating methods are inapplicable (Beschel, 1961; Benedict, 1967). The technique may also be used to date lake-level (and perhaps even sea-level) changes, glacial outwash, and trimlines, rockfalls, talus stabilization, and the former extent of permanent or very persistent snow cover.

4.4.1.1 Principles of Lichenometry

Lichenometry is based on the assumption that the largest lichen growing on a rock substrate is the oldest individual. If the growth rate of the particular species is known, the maximum lichen size will give a minimum age for the substrate, since all other thalli must be either late colonizers or slower-growing individuals (i.e., those growing in less than optimum conditions). Lichen size dates the time at which the freshly deposited rocks became stable, since an unstable substrate will prevent uninterrupted lichen growth. Growth rates can be obtained by measuring maximum lichen sizes on substrates of known age, such as gravestones, historic or prehistoric rock buildings, or moraines of known age (perhaps dated independently by historical records or radiocarbon). It is also possible to measure growth directly by photographing or tracing lichens of varying sizes every few years on identifiable rock surfaces (Miller and Andrews, 1973; Ten Brink, 1973). Generally, the maximum diameter of the lichen thallus is measured on individuals that have shown fairly uniform radial growth.

Growth rates vary from one region to another so it is necessary to calibrate the technique for each study site (e.g. Roof and Werner, 2011), but the general form of the growth curve is now fairly well established. After initial colonization of the rock surface, growth is quite rapid (known as the great period); growth then slows to a more or less constant rate (Figure 4.19; Beschel, 1961). Different lichens grow at different rates and indeed some species may approach senescence, while other species are still in their great period of growth. The black foliose lichen *Alectoria minuscula*, for example, rarely exceeds 160 mm in diameter on rock surfaces in Baffin Island; lichens of this size represent a substrate age of ~500-600 years BP. By contrast, *Rhizocarpon geographicum* has only just entered its period of linear growth by this time (at ~30 mm diameter) and will continue to grow at a nearly constant rate for thousands of years after that. In fact, it has been estimated that a 280 mm thallus of *Rh. geographicum* on eastern Baffin Island dates its substrate at $\sim 9500 \pm 1500$ years BP (Miller and Andrews, 1973). Similarly, a 480 mm *Rhizocarpon alpicola* thallus in the Sarek Mountains of Swedish Lapland is thought to have begun its growth following deglaciation of the region ~9000 years BP (Denton and Karlén, 1973b). Different lichens may thus be selected to provide optimum dating resolution over different timescales. However, in view of its ubiquity, ease of recognition, and useful size variation over the last several thousand years, the lichen *Rh. geographicum* has been most commonly used in lichenometric studies (Figure 4.20; Locke et al., 1979). Once a growth curve for the species in question has been established, measurements of maximum lichen sizes on moraines and other geomorphological features can be used to estimate substrate age (Figure 4.21).

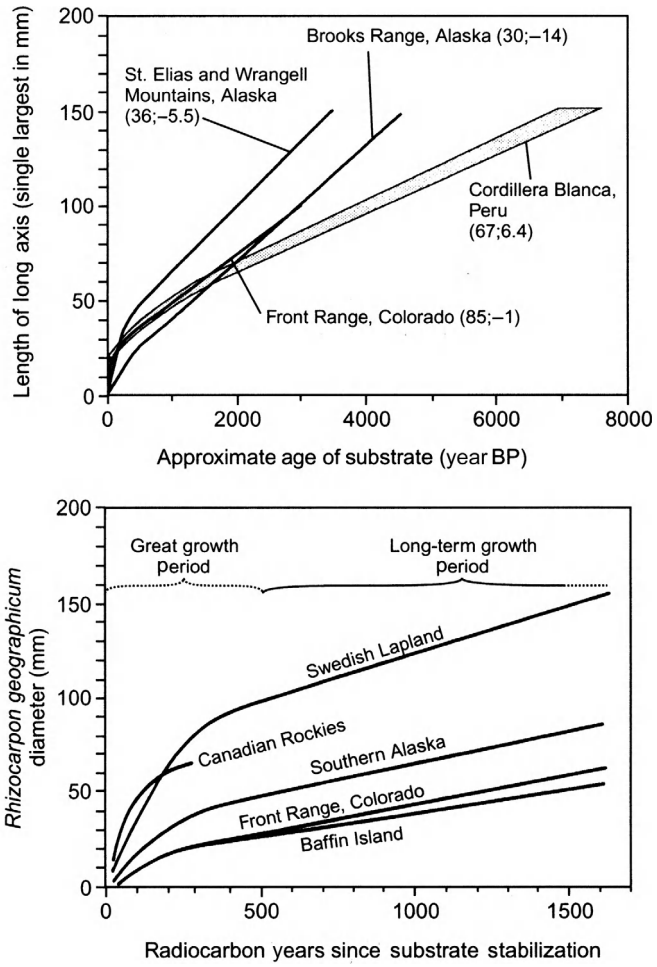


FIGURE 4.19 Growth rates of *Rhizocarpon geographicum* in different areas of the world for the Holocene and for the last 1600 years. Numbers in parentheses on the upper diagram show mean annual precipitation (mm) and mean annual temperature (°C) in each region. Error bars on each curve are probably ±15-20%. *Left: from Rodbell (1992). Right: after Calkin and Ellis (1980).*

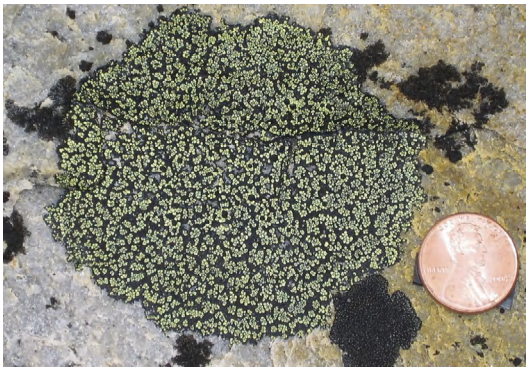


FIGURE 4.20 *Rhizocarpon geographicum*, a lichen that grows radially, enabling substrates to be dated if the growth rate of the lichen is known. The coin is 19 mm in diameter. *Photograph kindly provided by Steve Roof, Hampshire College.*

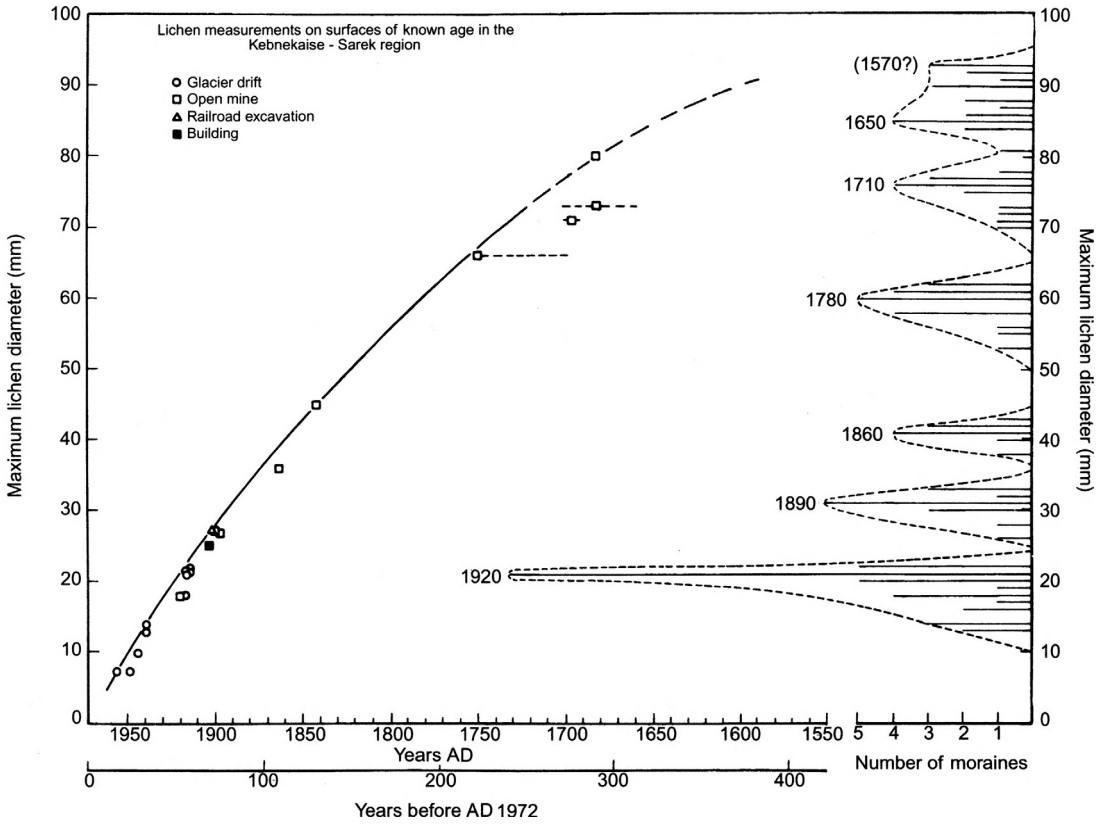


FIGURE 4.21 Growth curve of *Rhizocarpon geographicum* and *Rh. alpicola* for the last four centuries based on measurements in the Sarek and Kebnekaise Mountains, Swedish Lapland. Bar graph at right shows the frequency of moraines, as characterized by the appropriate maximum thallus diameters. Several discrete moraine groups are evident. *After Denton and Karlén (1973b).*

4.4.1.2 Problems of Lichenometry

There are three general areas of uncertainty in lichenometry, relating to biological, environmental, and sampling factors (Jochimsen, 1973).

4.4.1.2.1 BIOLOGICAL FACTORS

Lichens are exceedingly difficult to identify to species level in the field and most users of lichenometry have no training in lichen taxonomy. Indeed, lichen taxonomy is itself a contentious subject, which compounds the users' difficulties. *Rh. geographicum* is exceedingly similar to *Rhizocarpon superficiale* and *Rh. alpicola* (King and Lehmann, 1973) and doubtless many investigations have been based on a mixture of observations (Denton and Karlén, 1973b). This presents no problem, of course, providing that the different species grow at similar rates, but generally, such factors are not well known. What evidence there is suggests that growth rates may vary between species (e.g., Calkin and Ellis, 1980; Innes, 1982). Lichen dispersal and propagation rates are also inadequately understood. Many lichens propagate their algal

and fungal cells independently so that it may take some time for two individuals to find each other and form a new symbiotic union. In other cases, lichens are propagated when part of the parent breaks off the rock substrate and is blown or washed away to a new site. In either case, there may be a significant delay between the exposure of a fresh rock surface and colonization by lichens. Furthermore, even when lichen cells become established, decades may elapse before the thallus becomes visible to the naked eye. As time passes, rock surfaces may become virtually covered in lichens, and inevitably, this results in competition between individuals; indeed, some lichens appear to secrete a chemical, which inhibits growth in their immediate vicinity (Ten Brink, 1973). Such factors seem likely to reduce growth rates as rocks become heavily lichen-covered and this may give the erroneous impression of a relatively young age for the substrate.

Finally, as lichens become very old, growth rates may decline. Little information is available on senescence in lichens and unfortunately this corresponds to the part of the growth curve where there is the least dating control. Often, growth rates beyond a certain age (i.e., the final dated control point) are assumed to continue at a constant rate, whereas in all probability, the rate declines with increasing lichen age. This will lead to (possibly large) underestimates of substrate age; such errors can be avoided if extrapolation of growth rates is not attempted.

4.4.1.2.2 ENVIRONMENTAL FACTORS

Lichen growth is dependent on substrate type (particularly surface texture) and chemical composition (e.g., Porter, 1981c). Rocks that weather easily or are friable may not remain stable long enough for a slow-growing lichen to reach maturity. Conversely, extremely smooth rock surfaces may preclude lichen colonization for centuries and possibly many never support lichens. Extremely calcareous rocks may also inhibit growth of certain lichens. Measurements should thus be restricted to lichens growing on similar lithologies whenever possible.

Climate is a major factor affecting lichen growth rates; the comparison of growth rates from different areas suggests that slower growth rates are found in areas of low temperature, short-growing seasons, and low precipitation (Figure 4.21). However, both macro- and microclimatic factors are of significance. In particular, lichens require moisture for growth and the frequency of small precipitation amounts, even from fog and dew, may be of more significance than annual precipitation totals. Radiation receipts are also important because they largely determine rock temperatures. Generally, it is impossible to equate such factors on those rocks used to calibrate the lichen growth curve with rocks that are eventually to be dated. Commonly, calibration will be carried out on buildings or gravestones in a valley bottom, whereas the features to be dated are hundreds of meters higher than the calibration site. Similar problems may be encountered along extensive fiord systems where conditions at the fiord mouth are less continental than at the fiord head. Lichen growth is far slower in the more continental locations, even over distances as short as 50 km, probably due to the lower frequency of coastal fogs and generally drier climates inland. Increasing elevation also appears to be significant in reducing growth rates, even though moisture availability might be expected to increase (Miller, 1973; Porter, 1981c). Presumably, this is offset by longer-lying snow and a reduced growing season due to lower temperatures (Flock, 1978). All these factors may complicate the construction of a simple growth curve for a limited geographic area. Further problems arise due to the possible influence of long-term climatic fluctuations. Apart

from the general effect of lower temperatures in the past, it is quite probable that in the high-elevation and/or high-latitude sites where lichenometry is most widely used, periods of cooler climate resulted in the persistence of snow banks, which would have reduced lichen growth rates (Koerner, 1980; Benedict, 1993). Growth curves may thus not be linear, but rather made up of periods of reduced growth separated by periods of more rapid growth (cf. Curry, 1969). Lack of resolution in calibration curves may obliterate such variations, but this could account for apparent "scatter" in some attempts at calibration. There is evidence that such factors have been of significance in some regions; on upland areas of Baffin Island, for example, persistence of snow cover during the Little Ice Age is thought to have resulted in "lichen-free zones," where lichen growth was either prevented altogether or severely reduced (Locke and Locke, 1977; R.K. Anderson et al., 2008; Miller et al., 2012). These zones can be recognized today, even on satellite photographs, by the reduced lichen cover of the rocky substrate compared to lower elevations where snow cover was only seasonal (Andrews et al., 1976). Similarly, attempts to date moraines that have periodically been covered by snow for long intervals would give erroneously young ages for the deposits (Karlén, 1979).

4.4.1.2.3 SAMPLING FACTORS

It is of fundamental importance in lichenometric studies that the investigator locates the largest lichen on the substrate in question, but this is not always something one can be certain of doing (Locke et al., 1979). Furthermore, very large lichens are often not circular and may sometimes be mistaken for two individuals that have grown together into one seemingly large and old thallus. It is also possible that a newly formed moraine may incorporate debris from rockfalls or from older glacial deposits; if such debris already supports lichens and if they survive the disturbance, the deposit would appear to be older than it actually was (Jochimsen, 1973). A number of innovative methods to improve the reliability of lichenometry have been proposed (e.g., McCarroll, 1994) and these generally provide a firmer statistical basis for the sampling procedure.

Finally, in establishing a calibrated growth curve for lichens, reference points at the "older" end of the scale are often obtained from a radiocarbon date on organic material overridden by a moraine. This date is then equated with the maximum-sized lichen growing on the moraine today. Such an approach can lead to considerable uncertainty in the growth curve. First, dates on organic material in soils overridden by ice may be very difficult to interpret (e.g., Matthews, 1980). Second, there may be a gap of several hundred years between the time organic material is overridden by a glacial advance and the time the morainic debris becomes sufficiently stable for lichen growth to take place. This would lead to overestimation of lichen age in a calibration curve. Third, ^{14}C dates must be converted to calendar years, which often results in very large margins of error, especially for the most recent Little Ice Age period, because of the nonlinearity between ^{14}C and calendar ages in this interval. This only amplifies the uncertainties associated with lichen growth curves such as those shown in Figure 4.19. In reality, each curve should probably have an error bar of around 15-20%, perhaps even more for growth curves that are extrapolated beyond a dated control point (Bickerton and Matthews, 1992; Beget, 1994).

A consideration of all these factors indicates that caution is needed in using lichenometry as a dating method, even for establishing relative age. Nevertheless, if consideration is given to the possible pitfalls, it can provide useful age estimates. Most problems would result in

only minimum-age estimates on substrate stability, but in some cases, overestimation of age could result. Although it is worth being aware of the potential difficulties of the method, it is unreasonable to expect that all of the problems, discussed earlier, would subvert the basic assumptions of the method all of the time, and often, the potential errors can be eliminated in various ways. Lichenometry is thus likely to continue to play a role in dating rocky deposits in arctic and alpine areas and hence make an important contribution to paleoclimatic studies in these regions.

4.4.2 Dendrochronology

Although not a widely used dating technique in paleoclimatology, the use of tree rings for dating environmental changes has proved useful in some cases (e.g., Luckman, 1994). The concepts and methods used in dendrochronological studies are discussed in more detail in Chapter 13 and need not be repeated here. Basically, dendrochronological studies are used in three ways: (a) to provide a minimum date for the substrate on which the tree is growing (e.g., an avalanche track or deglaciated surface), (b) to date an event that disrupted tree growth but did not terminate it, and (c) to date the time of tree growth that was terminated by a glacier advance or a climatic deterioration associated with a glacier advance (e.g., Luckman, 1988, 1995).

The first application is straightforward but to obtain a *close* minimum date assumes that the "new" surface is colonized very rapidly. This is highly probable in the case of avalanche zones (indeed, young saplings may survive the event), but in deglaciated areas, surface instability due to subsurface ice melting and inadequate soil structure may delay colonization for several decades. Different approaches toward estimating the time delay before colonization of recently deglacierized terrain are described by Sigafoos and Hendricks (1961) and McCarthy and Luckman (1993). Unlike lichens, which may live for thousands of years, trees found on moraines are rarely more than a few hundred years old. Even when very old trees are located and dated, it cannot be assumed that they represent first-generation growth. For example, Burbank (1981) found that a moraine on which the oldest tree was ~750 years old (dated by dendrochronological methods) was in fact older than 2500 years BP according to the local tephrochronology.

A more widespread application of dendrochronology involves the study of growth disturbance in trees. When trees are tilted during their development, they respond by producing compression or reaction wood on the lower side of the tree in order to restore their natural stance. This causes rings to form eccentrically after the event that tilted the tree; the event can be accurately dated by identifying the year when growth changes from concentric to eccentric (Burrows and Burrows, 1976). Such techniques have been used in dating the former occurrence of avalanches (Potter, 1969; Carrara, 1979) and hurricanes (Pillow, 1931) and the timing of glacier recession (Lawrence, 1950). They have also been successfully applied in more strictly geomorphological applications, in studying stream erosion rates and soil movements on permafrost (Shroder, 1980).

Valuable insights into the history of glacier advances in the Canadian Rockies have been obtained by Luckman (1996) using tree snags (partially eroded or damaged trees) or tree stumps, from areas exposed by receding glaciers. By cross-dating these samples, evidence of formerly more extensive forest in areas only recently deglacierized have been documented, and the timing of climatic deterioration and glacier advance has been clearly revealed (Figure 4.22).

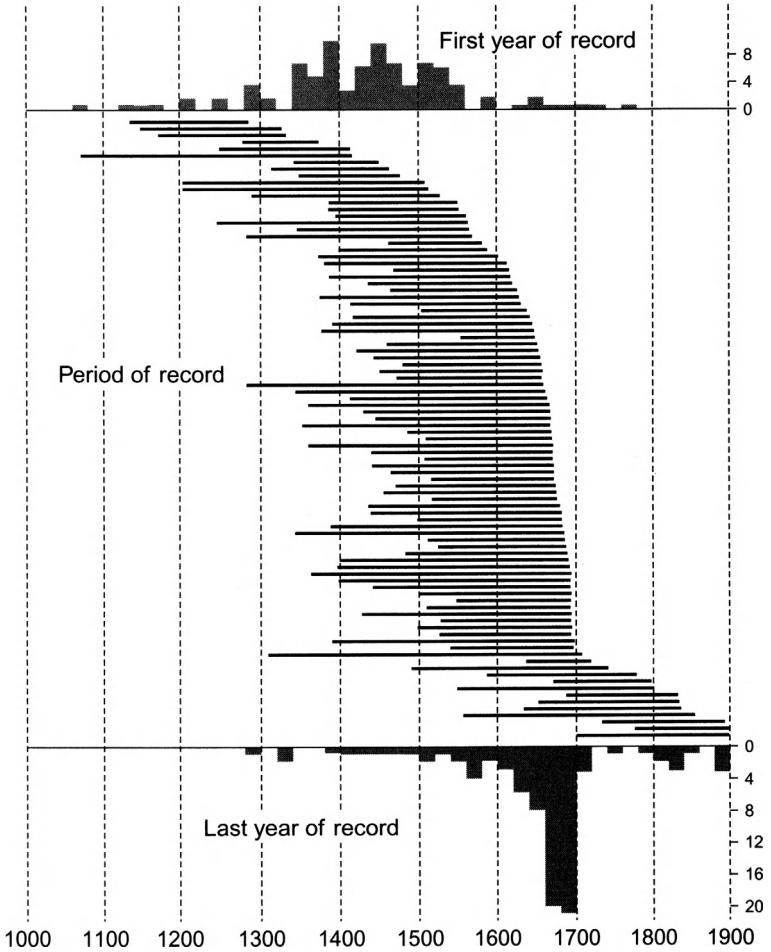


FIGURE 4.22 Length of record of calendar-dated tree pieces (snags) recovered from the Athabasca Glacier area. Each piece was cross-dated relative to other samples to place them in historical position. Because the snags found are eroded and may not contain the full growth period, the length of record shown for each sample may only be a minimum estimate of the life of the tree. Nevertheless, there is clearly a relationship between termination of growth in many samples and an important Little Ice Age glacier advance around AD 1714, as shown by the lower histogram. *From Luckman (1994).*

CHAPTER

5

Ice Cores

OUTLINE

5.1 Introduction 137

5.2 Stable Isotope Analysis 141
- 5.2.1 *Stable Isotopes in Water: Measurement and Standardization* 143
- 5.2.2 *Oxygen-18 Concentration in Atmospheric Precipitation* 144
- 5.2.3 *Factors Affecting the Stable Isotope Record in Ice Cores* 145
- 5.2.4 *Deuterium Excess* 151

5.3 Dating Ice Cores 154
- 5.3.1 *Radioisotopic Methods* 155
- 5.3.2 *Seasonal Variations and Episodic Events* 155
  - 5.3.2.1 Visual Stratigraphy 156
  - 5.3.2.2 $\delta^{18}O$ 158
  - 5.3.2.3 Glaciochemistry 159
  - 5.3.2.4 Electrical Conductivity Measurements (ECM) 160
  - 5.3.2.5 Radioactive Fallout 161
  - 5.3.2.6 Volcanic Sulfate and Tephra 161
- 5.3.3 *Theoretical Models* 165
- 5.3.4 *Chronostratigraphic Correlations* 167

5.4 Paleoclimatic Reconstruction from Ice Cores 167
- 5.4.1 *Ice-Core Records from Greenland* 167
- 5.4.2 *Ice-Core Records from Antarctica* 175
- 5.4.3 *Past Atmospheric Composition from Polar Ice Cores* 180
- 5.4.4 *Greenhouse Gas Records in Ice Cores* 184
- 5.4.5 *Ice-Core Records from Low Latitudes* 189

5.1 INTRODUCTION

The accumulation of past snowfall in the polar ice caps and ice sheets of the world provides an extraordinarily valuable record of paleoclimatic and paleoenvironmental conditions. These conditions are studied by detailed physical and chemical analyses of ice and firn (snow

Copyright © 2015 Raymond S. Bradley.
Published by Elsevier Inc. All rights reserved.

that has survived the summer ablation season) in cores recovered from very high elevations on the ice surface. The metamorphism of snow crystals to firn, and eventually to ice, occurs as the weight of overlying material causes crystals to settle, deform, and recrystallize, leading to an overall increase in unit density. When firn is buried beneath subsequent snow accumulations, density increases as the air spaces between snow crystals are reduced by mechanical packing and plastic deformation until, at a unit density of about 0.83 kg m^{-3}, interconnected air passages between grains are sealed off into individual air bubbles (Herron and Langway, 1980). At this point, the resulting material is considered to be ice. The depth of this transition varies considerably from one ice body to another, depending on surface temperature and accumulation rate; for example, it does not occur until about 77 m depth at Summit Camp, Greenland, and ~95 m at Dome C, Antarctica (approximating ages of ~230 and 2500 years before present, respectively). Thus, "ice cores" *sensu stricto* are actually firn cores near the surface (cf. Table 2.2 in Cuffey and Paterson, 2010). This distinction is not very important except in the reconstruction of past atmospheric composition (see Section 5.4.3), and the term ice core will henceforth be used to refer to both ice and firn core sections.

In the dry snow zone of polar ice sheets (Benson, 1961), snowmelt and sublimation are extremely low so that snow accumulation has been continuous, in some areas for over a million years (Jouzel and Masson-Delmotte, 2010). The snowfall provides a unique record, not only of precipitation amounts per se but also of air temperature, atmospheric composition (including gaseous composition and soluble and insoluble particulates), the occurrence of explosive volcanic eruptions, and even past variations in solar activity (Table 5.1). At present, several dozen cores spanning more than the past 10,000 years have been recovered from ice sheets, ice shelves, and glaciers in both hemispheres (Figures 5.1 and 5.2). A number of these

TABLE 5.1 Principal Sources of Paleoclimatic Information from Ice Cores

Parameter	Analysis
Temperature	
Summer	Melt layers
Annual	δD, $\delta^{18}O$ (ice), Ar, N_2 (diffusion)
Source region temperature/humidity	Deuterium excess (d)
Accumulation (net)	Seasonal signals
Volcanic activity	Conductivity, non-sea salt (nss.) SO_4^{2-}, glaciochemistry
Tropospheric turbidity	ECM, microparticle content, trace elements
Wind speed	Particle size, concentration
Atmospheric composition	Trace gases (CO_2, CH_4, and N_2O)
Sea ice extent	Glaciochemistry (Br^-, I^-, and Na^+)
Atmospheric circulation	Glaciochemistry (major ions)
Solar activity and geomagnetic field changes	^{10}Be
Forest fire history	Levoglucosan and other biomarkers

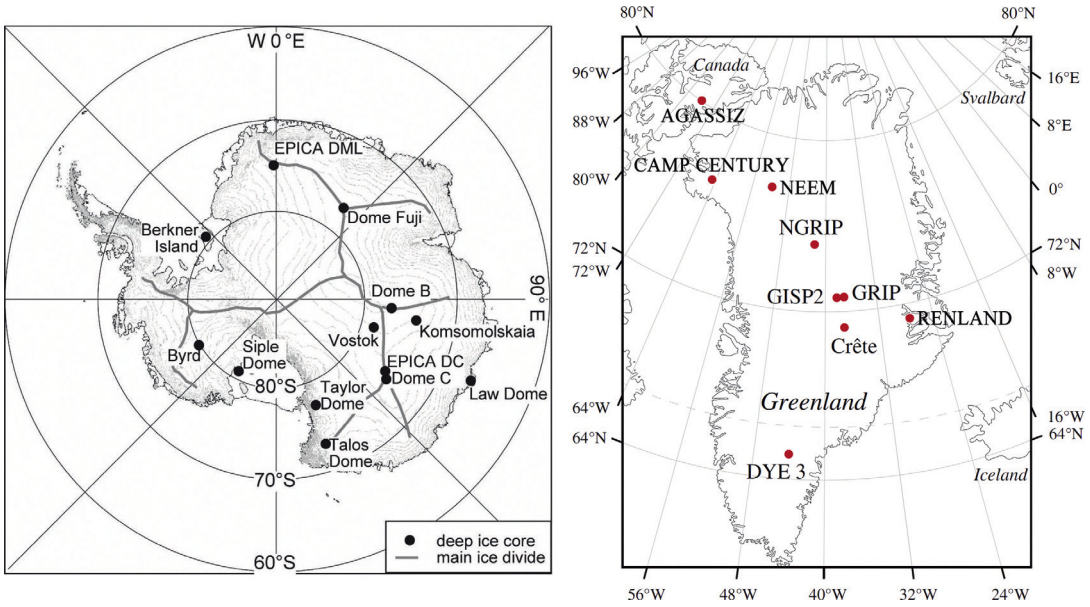


FIGURE 5.1 (a) Locations of the principal ice coring sites in Antarctica, shown with the main ice divides. (b) Locations of the principal deep ice coring sites in Greenland and the Canadian Arctic. *From Masson-Delmotte et al. (2008).*

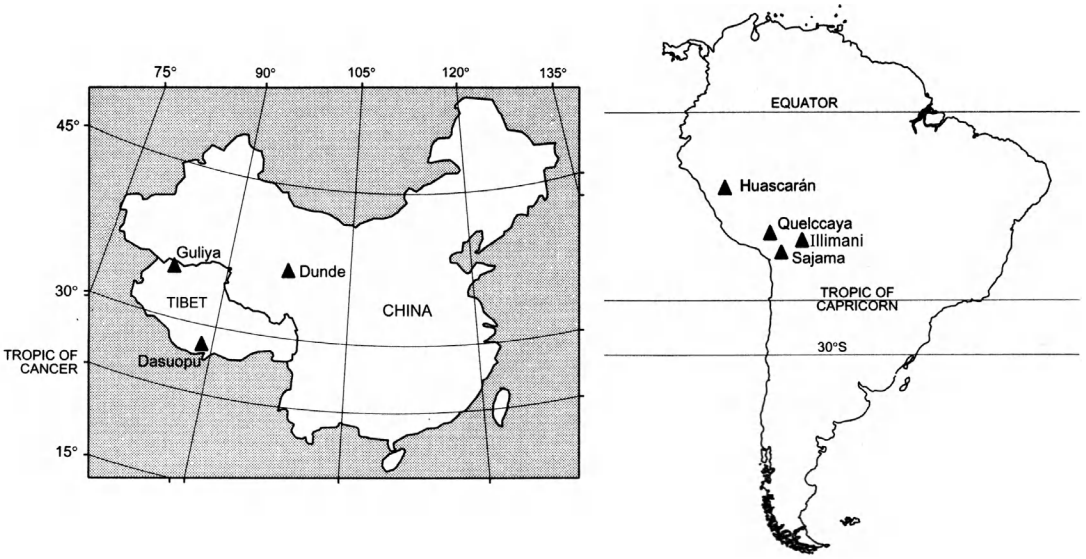


FIGURE 5.2 Location of principal ice coring sites in low latitudes.

cores extend to bedrock and contain debris from the ice/sub-ice interface (e.g., Gow et al., 1979, 1997; Herron and Langway, 1979; Koerner and Fisher, 1979; Willerslev et al., 2007). About 30 cores extend back into the last glaciation (Table 5.2) and several of these reach even earlier glacial periods, providing extremely important insights into the long-term variability

TABLE 5.2 Locations of Ice Cores with Records Going Back to the Last Glaciation or Earlier[a]

Drill site	Location[b]		Elevation
Greenland			
NEEM	77.45°N	51.06°W	2484
Camp Century	77.17°N	61.13°W	1885
NGRIP	75.10°N	42.32°W	2917
GISP2	72.58°N	38.48°W	3214
GRIP	72.58°N	37.64°W	3238
Renland	71°03°N	26.72°W	2340
Dye-3	65.18°N	43.82°W	2477
Canadian Arctic			
Agassiz	80.75°N	73.1°W	1730
Devon Island	75.47°N	82.5°W	1800
Penny	67.25°N	65.77°W	1860
Alaska			
Mount Logan	60.59°N	140.50°W	5340
Antarctica			
Siple Dome	81.65°S	148.81°W	621
Byrd	80.00°S	119.50°W	1530
Berkner Island	79.55°S	45.67°W	890
WAIS Divide	79.28°S	112.06°W	1807
Taylor Dome	77.67°S	158.00°W	2440
Dome Fuji	77.50°S	37.5°E	3810
EPICA Dome C	75.10°S	123.33°E	3233
EPICA DML	75.00°S	0.01°E	2892
Talos Dome	72.82°S	159.18°E	2315
Vostok	72.47°S	106.80°E	3500
Law Dome	66.77°S	112.81°E	1370
China			
Dundee	38.10°N	96.40°E	5325
Guliya	35.28°N	81.48°E	6710
Dasuopu	28.00°N	85.00°E	6900
Huascarán (Peru)	9.11°S	77.62°W	6048
Illimani (Bolivia)	16.62°S	67.76°W	6350
Sajama (Bolivia)	18.00°S	68.00°W	6548

[a]*Other short cores (<100 m) and surface samples from ice-sheet margins in Greenland and Antarctica have also recovered ice from the last glacial period.*
[b]*See Figures 5.1 and 5.2 for locations.*

of the climate system and unique perspectives on contemporary changes in climate and greenhouse gases. Four very readable books on the contributions that ice-core research in Greenland and Antarctica have made to our understanding of Earth's history are provided by Alley (2002), Mayewski and White (2002), Dansgaard (2004), and Jouzel et al. (2013).

Paleoclimatic information has been obtained from ice cores by four main approaches. These involve the analysis of (a) stable isotopes of water and of atmospheric O_2, (b) other gases from air bubbles in the ice, (c) dissolved and particulate matter in firn and ice, and (d) the physical characteristics of the firn and ice (Oeschger and Langway, 1989; Lorius, 1991; Delmas, 1992; Raynaud et al., 1993). Each approach has also provided a means of estimating the age of ice at depth in ice cores (Section 5.3).

5.2 STABLE ISOTOPE ANALYSIS

Water is the most abundant compound on Earth. It is the primary compound in all forms of life; is perhaps the most important agent in weathering, erosion, and geologic recycling of materials, and, of course, plays a crucial role in the global energy balance. The study of "fossil water," either directly in the form of firn and ice or indirectly through materials deposited from solution in "fossil water" (e.g., speleothems), thus has important implications in many aspects of paleoenvironmental reconstruction (Leng, 2006). The study of the stable isotopes of water (primarily deuterium and ^{18}O) is a major focus of paleoclimatic research, not only in ice cores but also in marine and lake sediments, corals, speleothems, tree rings, and peat (Swart et al., 1993). In this section, a brief introduction to the theory behind stable isotope work is provided and applications to ice-core analysis are discussed. The importance of stable isotopes in other branches of paleoclimatic research is dealt with in Chapters 6, 8, 9, 11, 13, and 14.

In common with most other naturally occurring elements, the constituents of water, oxygen, and hydrogen, may exist in the form of different isotopes. Isotopes result from variations in mass of the atom in each element. Every atomic nucleus is made up of protons and neutrons. The number of protons in the nucleus of an element (the atomic number) is always the same, but the number of neutrons may vary, resulting in different isotopes of the same element. Thus, oxygen atoms (which always have eight protons) may have 8, 9, or 10 neutrons, resulting in three isotopes with atomic mass numbers of 16, 17, and 18, respectively (^{16}O, ^{17}O, and ^{18}O). In nature, these three stable isotopes occur in relative proportions of 99.76% (^{16}O), 0.04% (^{17}O), and 0.2% (^{18}O). Hydrogen has two stable isotopes, ^{1}H and ^{2}H (deuterium), with relative proportions of 99.984% and 0.016%, respectively. Consequently, water molecules may exist as any one of nine possible isotopic combinations with mass numbers ranging from 18 ($^{1}H_2^{16}O$) to 22 ($^{2}H_2^{18}O$). However, as water with more than one "heavy" isotope is very rare, generally, only four major isotopic combinations are common, and only two are important in paleoclimatic research ($^{1}H^{2}H^{16}O$, generally written as HDO, and $^{1}H_2^{18}O$).

The basis for paleoclimatic interpretations of variations in the stable isotope content of water molecules is that the vapor pressure of $H_2^{16}O$ is higher than that of $HD^{16}O$ and $H_2^{18}O$ (10% higher than HDO and 1% higher than $H_2^{18}O$). Evaporation from a water body thus results in a vapor that is poorer in deuterium and ^{18}O than the initial water;

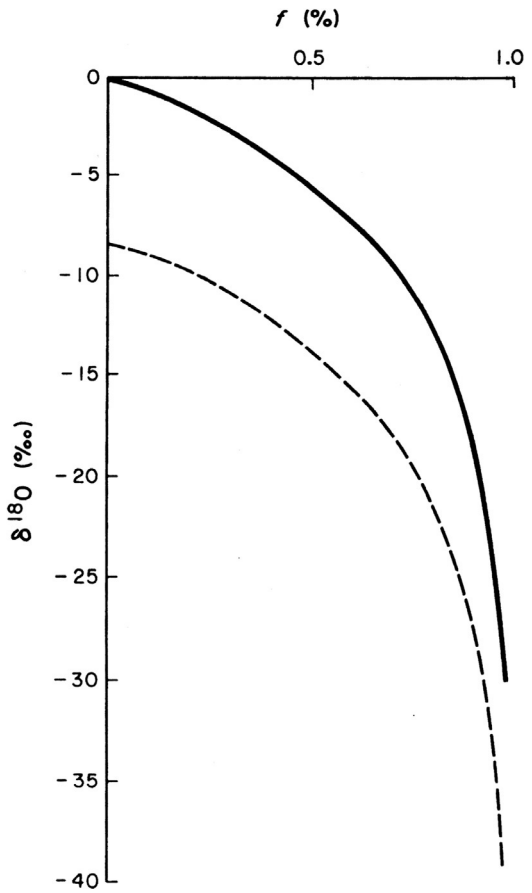


FIGURE 5.3 Diagrammatic plot of the $^{18}O/^{16}O$ ratio ($\delta^{18}O$) in a water (liquid-vapor) system in which the liquid is removed as it is formed by progressive condensation. Isotopic equilibrium between vapor and liquid is assumed (i.e., an equilibrium Rayleigh condensation process). ----, δ vapor; ——, δ liquid. *f*, percentage of the original water vapor condensed. *From Epstein and Sharp, (1959).*

conversely, the remaining water is (relatively speaking) *enriched* in deuterium and ^{18}O. At equilibrium, for example, atmospheric water vapor contains 10‰ (parts per thousand or per mil) less ^{18}O and 100‰ less deuterium than mean ocean water. When condensation occurs, the lower vapor pressure of HDO and $H_2^{18}O$ results in these two compounds passing from the vapor to the liquid state more readily than water made up of lighter isotopes. Hence, *compared to the vapor*, the condensation will be enriched in the heavy isotopes (Dansgaard, 1961). Further condensation of the vapor will continue this preferential removal of the heavier isotopes, leaving the vapor more and more depleted in HDO and $H_2^{18}O$ (Figure 5.3). As a result, continued cooling will give rise to condensate with increasingly lower HDO and $H_2^{18}O$ concentrations than when the condensation process first began. The greater the fall in temperature, the more condensation will occur and the lower will be the heavy isotope concentration, relative to the original water source (Figure 5.4). Isotopic concentration in the condensate can thus be considered as a primary function of the temperature at which condensation occurs (subject to certain reservations noted in Section 5.2.2).

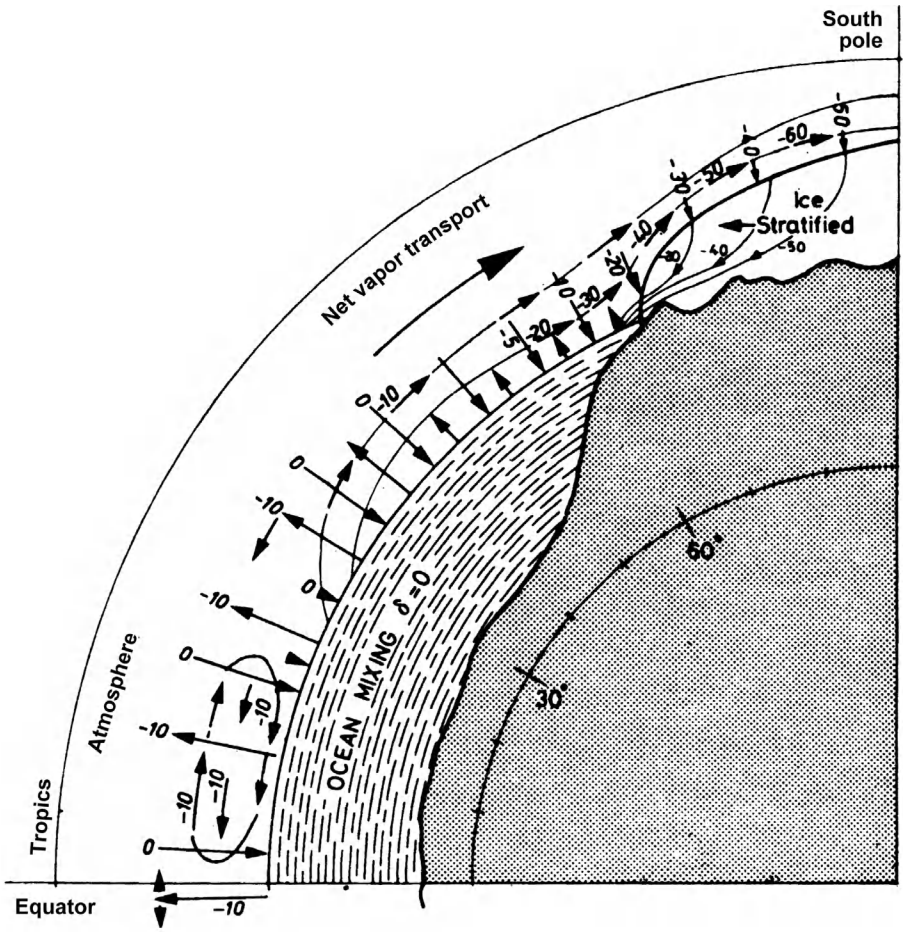


FIGURE 5.4 Schematic diagram to illustrate isotopic depletion of water vapor en route to the Antarctic Ice Sheet. As air mass cools, the precipitation produced is preferentially enriched in ^{18}O, leaving the remaining vapor relatively depleted. Consequently, with further condensation, the precipitation contains less and less ^{18}O (i.e., lower $\delta^{18}O$ values). This isobaric effect is accentuated by uplift (adiabatic) effects over the ice sheet itself, so that lowest delta ^{18}O values are found in the ice-sheet interior. *After Dansgaard et al. (1971) and Robin (1977).*

5.2.1 Stable Isotopes in Water: Measurement and Standardization

In the majority of paleoclimatic studies using stable isotopes, oxygen is generally the element of primary interest, though deuterium is important in ice-core research. In oxygen isotope work, the water sample is isotopically exchanged with carbon dioxide of known isotopic composition:

$$^{1}H_2{}^{18}O + {}^{12}C{}^{16}O_2 \rightleftharpoons {}^{1}H_2{}^{16}O + {}^{12}C{}^{16}O{}^{18}O$$

The relative proportions of ^{16}O and ^{18}O in carbon dioxide from the sample are then compared with the isotopic composition of a water standard (Standard Mean Ocean Water or SMOW[1]) and the results expressed as a departure ($\delta^{18}O$) from this standard; thus,

$$^{18}O = \frac{\left(^{18}O/^{16}O\right)_{\text{sample}} - \left(^{18}O/^{16}O\right)_{\text{SMOW}}}{\left(^{18}O/^{16}O\right)_{\text{SMOW}}} \times 10^3‰$$

All measurements are made using a mass spectrometer, and reproducibility of the results within ±0.1‰ is generally possible. A $\delta^{18}O$ value of −10 therefore indicates a sample with an $^{18}O/^{16}O$ ratio of 1% or 10‰ less than SMOW. Under our present climate, the lowest $\delta^{18}O$ value recorded in natural waters is ~−58‰ (−454‰ in δD) in snow from the highest and most remote parts of Antarctica (Qin et al., 1994).

5.2.2 Oxygen-18 Concentration in Atmospheric Precipitation[2]

In Section 5.2.1 and Figure 5.3, the isotopic composition of water in equilibrium with water vapor was considered. In reality, we cannot consider the process to be always at equilibrium between vapor and condensate, nor can the process be considered to occur in isolation. Exchanges between atmospheric water vapor, water droplets in the air, and water at the surface (which may be isotopically "light") do occur continuously, so this complicates any simple temperature-isotope effect that we might expect to find (Darling et al., 2006). There are also kinetic effects on fractionation that occur during evaporation and condensation, and the latter can be especially important at very low temperatures (see Section 5.2.4). Overall, the ^{18}O content of precipitation depends on (a) the ^{18}O content of the water vapor at the start of condensation (this could be very low if evaporation occurred over an inland lake or ice body where ^{18}O concentrations are less than mean ocean water), (b) the amount of moisture in the air compared to its initial moisture content, (c) the degree to which water droplets undergo evaporation en route to the ground and whether any of this reevaporated vapor reenters the precipitating air mass (Ambach et al., 1968), (d) the temperature at which the evaporation and condensation processes take place, and (e) the extent to which clouds become supersaturated, with respect to ice, at very low temperatures. In spite of these complications, empirical studies have demonstrated that geographic and temporal variations in isotopes do occur,

[1] In order that isotopic analyses in different laboratories be comparable, a universally accepted standard is used, known as SMOW (Standard Mean Ocean Water; Craig, 1961b). This is not an actual oceanic water sample, but is based on a US National Bureau of Standards distilled water sample (NBS-1). However, the zero point on the SMOW scale has been adjusted so that it is more or less equivalent (−0.1‰) to the isotopic composition of real ocean water (measured in samples from depths of 200–500 m in the Atlantic, Pacific, and Indian Oceans; Epstein and Mayeda, 1953). Isotopic studies based on carbonate fossils use as a standard a Cretaceous belemnite from the Peedee Formation of North Carolina (PDB-1). Carbon dioxide released from PDB-1 ≈ +0.2‰ relative to CO_2 equilibrated with SMOW (Craig, 1961b). Recent updates to international reference standards are described by Coplen (1996).

[2] In this section, $\delta^{18}O$ is generally referred to, but the same principles apply to variations in δD, which has been the primary isotope used in Antarctic ice-core studies.

reflecting temperature effects due to changing latitude, altitude, distance from moisture source, season, and long-term climatic fluctuations (Dansgaard et al., 1973; Koerner and Russell, 1979; Petit et al., 1991). As any interpretation of ice-core isotopic records is rooted in an evaluation of these factors, it is important to consider them in more detail.

5.2.3 Factors Affecting the Stable Isotope Record in Ice Cores

For the last 50 years or so, precipitation samples from many locations throughout the world have been analyzed for their $\delta^{18}O$ content (Rozanski et al., 1992, 1993). Figure 5.5 shows that $\delta^{18}O$ values of January and July precipitation generally reflect the distribution of temperature, decreasing at higher latitudes and at higher elevations (for example, in the high interior parts of Greenland and in the Andes). The influence of the Gulf Stream is also apparent on the January map (Lawrence and White, 1991). Changes in temperature from winter to summer are also reflected in $\delta^{18}O$, and this leads to an annual cycle in $\delta^{18}O$ of snowfall that can be used to count annual accumulation layers in ice cores (see Section 5.3.2). Significant departures from the overall pattern may be expected in certain circumstances. For example, if precipitation occurs in an area where very stable (i.e., inversion) conditions are common, surface temperatures will be lower than that in the atmosphere where precipitation develops. If local precipitation is derived from water, which was reevaporated from a source with an already low $\delta^{18}O$ content (e.g., a freshwater lake or snow cover), the mean annual $\delta^{18}O$ value will be anomalously low, perhaps by as much as 10‰ for complete reevaporation of precipitated water (cf. Koerner and Russell, 1979).

Figure 5.5 indicates that there is a strong latitudinal influence on $\delta^{18}O$. Lower $\delta^{18}O$ values are found at higher latitudes as a result of the loss of heavy isotopes in water condensed en route to those regions. This is sometimes referred to as an isobaric effect, implying a systematic change brought about by overall cooling at a particular level in the atmosphere rather than cooling brought about by a change in elevation (adiabatic cooling). With increasing elevation, adiabatic cooling of the precipitating air mass leads to precipitation that is more and more depleted in ^{18}O due to preferential removal of the heavier isotope in the condensation process. For example, the Quelccaya Ice Cap in Peru receives moisture that has undergone adiabatic cooling as the air rises over the Andes from the Amazon Basin. This uplift reduces $\delta^{18}O$ in precipitation by ~11‰ (Grootes et al., 1989). On large ice sheets, the adiabatic effect is superimposed on a "distance from moisture source" factor, which results in lower $\delta^{18}O$ concentrations as the distance from oceanic moisture sources increases (e.g., Koerner, 1979; Masson-Delmotte et al., 2008). Hence, at high elevations in central Antarctica, thousands of kilometers from the southern oceans, atmospheric precipitation has the lowest heavy isotope concentrations of any natural water occurring today ($\delta^{18}O = -58.4$‰ in snow, south of Vostok, Antarctica) (Morgan, 1982; Qin et al., 1994).

These different influences on $\delta^{18}O$ in precipitation lead to the geographic patterns seen in Figure 5.5. At low latitudes (generally equatorward of ~30°, where mean annual temperatures are >15 °C), $\delta^{18}O$ is unrelated to temperature and is principally a function of precipitation amount (Dansgaard, 1964; Rozanski et al., 1993; Schmidt et al., 2007). However, in extratropical regions, there is a very strong correspondence between temperature and $\delta^{18}O$ (Figure 5.6). For all locations in the extratropics (regions with mean annual temperatures

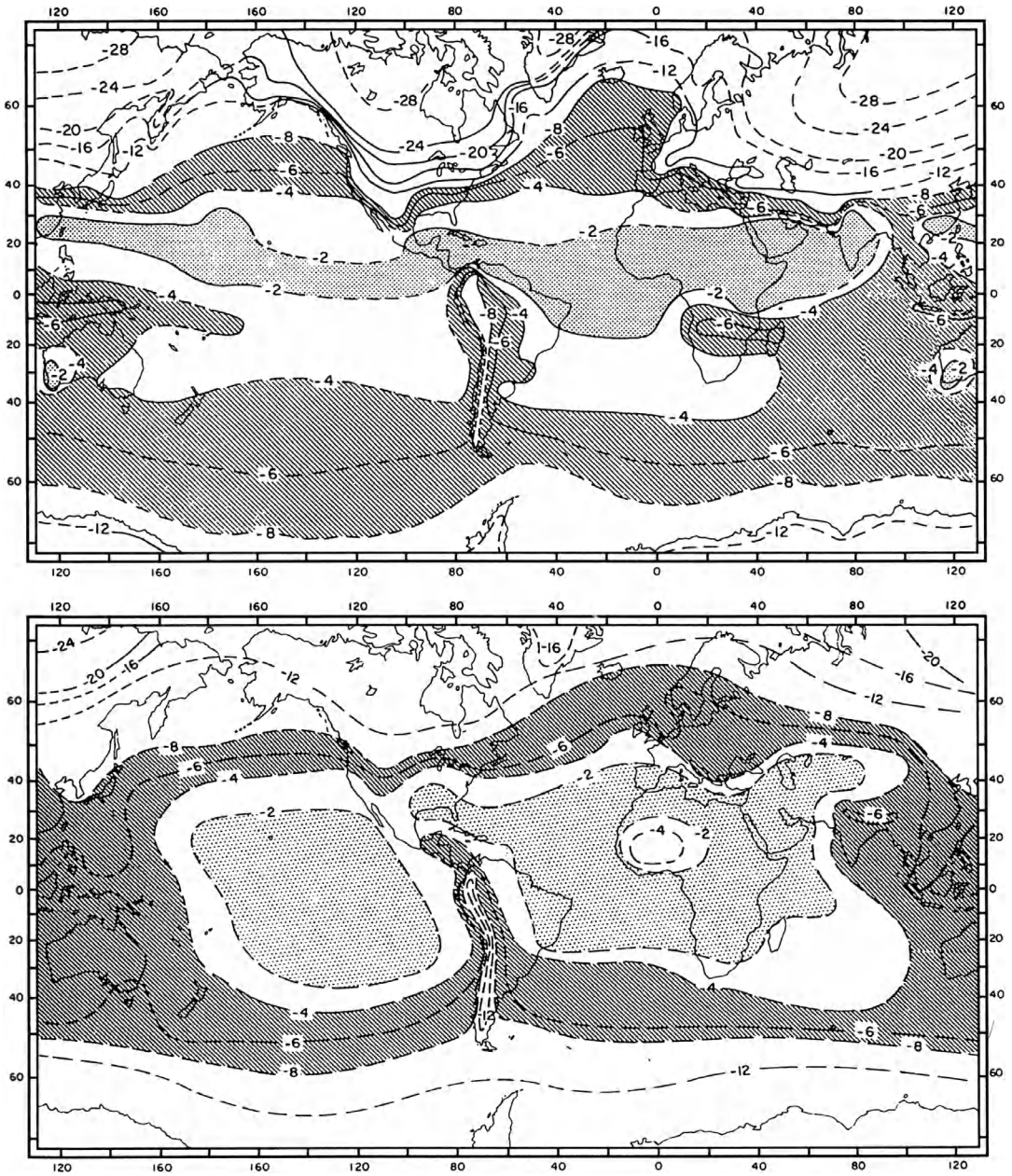


FIGURE 5.5 Mean $\delta^{18}O$ in January (upper figure) and July precipitations (lower figure) collected at precipitation stations throughout the world, based on analyses by the International Atomic Energy Authority over the last few decades. *From Lawrence and White (1991).*

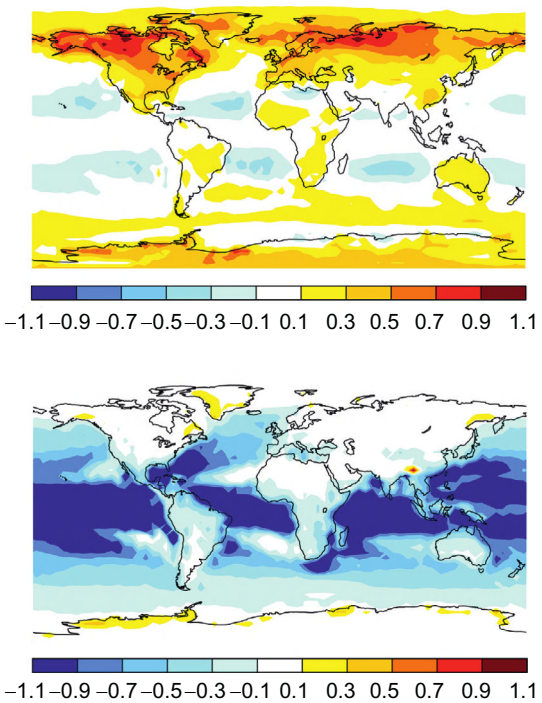


FIGURE 5.6 Slope of the relationship between $\delta^{18}O$ and temperature (above) and $\delta^{18}O$ and precipitation (below) as simulated by a coupled ocean-atmosphere GCM (GISS ModelE). There is a positive relationship between temperature and $\delta^{18}O$ over most extratropical regions (averaging 0.59‰ °C^{-1}), but in the intertropical zone, $\delta^{18}O$ is inversely related to precipitation amount. The model results are supported by observations. *From Schmidt et al. (2007).*

<15 °C), the slope of the regression line for $\delta^{18}O$ and temperature is 0.59‰ °C^{-1} ($r^2 = 0.74$) but this varies geographically (Jouzel, 1991). For the Greenland Ice Sheet, based on snow samples, $\delta^{18}O = 0.67T - 13.7$ ($r^2 = 0.88$) (Johnsen et al., 2001), and for Antarctica, $\delta^{18}O = 0.80T - 8.11$ ($r^2 = 0.92$), where T = mean annual temperature (Masson-Delmotte et al., 2008). In both cases, these relationships are highly statistically significant, which suggests that they might be applied to the paleoisotopic record from ice cores. Indeed, this strategy of using the observed spatial slope to interpret the temporally varying record was used in much of the early ice-core interpretations from Greenland, giving estimated LGM temperatures of ~7-8 °C below modern values. However, this assumed that the source regions and trajectories for moisture flux to the ice sheet had not varied and most importantly that the seasonality of precipitation had not changed. These are very large assumptions, which are in fact unsupportable (Alley and Cuffey, 2001). This became quite apparent when temperature histories were obtained from boreholes in the ice. Cuffey et al. (1994, 1995) obtained a downhole temperature profile at GISP2, which represents the thermal history of the site that was, in a sense, buried with the accumulating snow. By developing a model that optimized the fit between the down-core $\delta^{18}O$ record and the borehole temperature history, Cuffey et al. were able to show that the long-term relationship between $\delta^{18}O$ and temperature, over the past 600 years, was $\delta^{18}O = 0.53T - 18.2‰$. Considering even longer-term changes (over the last glacial-interglacial cycle), using a deeper borehole record produced a solution of $\delta^{18}O = 0.33T - 24.8‰$. On this basis, Cuffey et al. (1995) interpreted the *overall* glacial to interglacial temperature change at GISP2 as +14-16 °C, considerably greater than previous estimates that had relied on

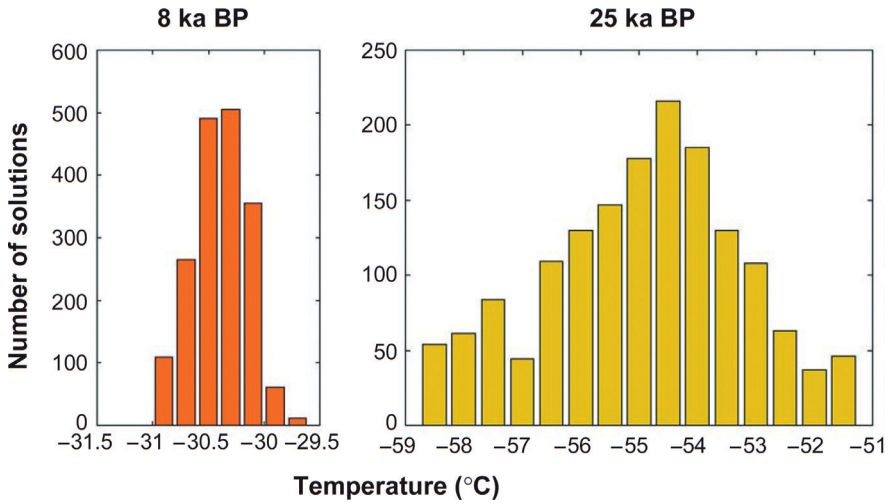


FIGURE 5.7 Probability distributions of Greenland Summit mean annual temperatures at 8 and 25 ka BP based on 2000 Monte Carlo simulations of a combined ice flow and geothermal heat flux model, with varying inputs about geothermal heat flux and surface temperature histories, aimed at finding the optimum fit to the observed borehole temperature profile. The most likely values (highest probabilities) indicate that temperatures were ~24 °C lower at 25 ka BP compared to the Early Holocene warm period maximum (8 ka BP). By comparison, the estimated temperature in 1970 was ~1 °C warmer than in the Early Holocene. *From Dahl-Jensen et al. (1998).*

$\delta^{18}O \approx 0.67T$. Further analysis of borehole temperature profiles obtained even larger estimates of the LGM-Holocene temperature difference, ~25 °C lower than today (Figure 5.7) (Dahl-Jensen et al., 1998).

Another approach to paleotemperature estimation and calibration of the oxygen isotope record is based on the thermal diffusion of gases in the firn at the time of rapid isotopic transitions (Severinghaus et al., 1998; Severinghaus and Brook, 1999). In porous firn, gases are in contact with the atmosphere, but gravitational settling causes the heavier isotopes of atmospheric gases such as argon and nitrogen to accumulate toward the base of the firn profile. When a strong temperature gradient occurs (between a suddenly warmer atmosphere and colder firn), a further separation of the isotopes occurs, such that the heavier isotopes remain at depth in the firn, while lighter isotopes diffuse towards the surface. This thermally driven diffusion occurs about ten times more rapidly than the time it takes for the firn to warm up, and the resulting isotopic gradient eventually becomes "locked in" as the firn is converted to ice. The magnitude of this gradient is thus mainly a function of the rapid temperature change that brought it about. Several studies have now used this effect to estimate temperature changes associated with changes in $\delta^{18}O$ (Table 5.3) (Landais et al., 2004, 2006; Huber et al., 2006; Capron et al., 2010). These studies all point to a time-varying relationship between oxygen isotopes and temperature, ranging from 0.29 to 0.55‰ $°C^{-1}$, considerably less than the modern observed spatial relationship of 0.67‰ $°C^{-1}$ (which would underestimate the actual temperature changes at those times) (Table 5.3) (Masson-Delmotte et al., 2005). Similar conclusions were found in a model simulation of several paleo-scenarios (Schmidt et al., 2007). These differences probably reflect changes in the seasonality of precipitation and/or moisture source regions, most likely as a consequence of rapid changes in the extent of sea-ice extent in

TABLE 5.3 Estimated Maximum Counting Errors (MCE) in the GICC05 Chronology, Estimated Temperature Changes at the Main Isotopic Transitions, and Inferred Slope of the Temperature-Isotope Relationship at those Times

Top Age (Years)	Bottom Age (Years)	Duration (Years)	MCE (%)	Absolute (Years)
21	3845	3825	0.25	10
3846	6905	3060	0.50	15
6906	7902	997	2.00	20
7903	10,276	2374	2.00	47
10,277	11703[a]	1427	0.67	10
Subtotal	11,683	0.87	102	
From Vinther et al. (2006)				
11,704	12,897	1194	3.3	39
12,898	14,076	1178	2.6	31
14,077	14,695	618	2.7	17
14,696	14,780	84	~4.0	4
Subtotal	3074	2.96	91	
From Rasmussen et al. (2006)				

		Temperature Increase (°C) (Uncertainty)	$\Delta\delta^{18}O$ (‰ °C^{-1})
Onset GI-1e	14,692 ± 93[b]		
Onset GI-2	23,340 ± 298		
Onset GI-3	27,780 ± 416		
Onset GI-4	28,900 ± 449		
Onset GI-5	32,500 ± 566		
Onset GI-6	33,740 ± 606		
Onset GI-7	35,480 ± 661		
Onset GI-8	38,220 ± 725	11 (+3, −6)	0.43
Onset GI-9	40,160 ± 790	9 (+3, −6)	0.29
Onset GI-10	41,460 ± 817	11.5 (+3, −6)	0.35
Onset GI-11	43,340 ± 868	15 (+3, −6)	0.33
Onset GI-12	46,860 ± 956	12.5 (+3, −6)	0.45
Onset GI-13	49,280 ± 1015	8 (+3, −6)	0.36
Onset GI-14	54,220 ± 1150	12 ± 2.5	0.41
Onset GI-15	55,800 ± 1196	10 (+3, −6)	0.40
Onset GI-16	58,280 ± 1256	9 (+3, −6)	0.43

Continued

TABLE 5.3 Estimated Maximum Counting Errors (MCE) in the GICC05 Chronology, Estimated Temperature Changes at the Main Isotopic Transitions, and Inferred Slope of the Temperature-Isotope Relationship at those Times—cont'd

		Temperature Increase (°C) (Uncertainty)	$\Delta\delta^{18}O$ (‰ °C^{-1})
Onset GI-17	59,440 ± 1287	12 (+3, −6)	0.33
From Svensson et al. (2008)			
Onset GI-18	~66,383	11 ± 2.5	0.41
Onset GI-19	~72,330	16 ± 2.5	0.42
Onset GI-20	~76,450	11 ± 2.5	0.55
Onset GI-21	~83,685	12 ± 2.5	0.35
Onset GI-22	~89,510	5 ± 2.5	0.40
Onset GI-23	~101,981	10 ± 2.5	0.33
Onset GI-24	~106,978	16 ± 2.5	0.31
Onset GI-25	~112,470	3	

[a] *Start of the Holocene.*
[b] *~2σ maximum counting error.*
Estimated ages of GI-18 and GI-19 based on ss09sea flow model; GI-20 to GI-25 based on correlation with EDC3 timescale.
Temperature estimates from Huber et al. (2006), Landais et al. (2004, 2006), and Capron et al. (2010).

the North Atlantic. Mean temperatures over the Greenland Ice Sheet change in the spring and fall by several degrees Celsius *per week*; a shift in the timing of major precipitation events by only a few weeks could result in large changes in $\delta^{18}O$ (cf. Steig et al., 1994). Similarly, changes in air mass trajectories could also account for the abrupt isotopic shifts (Charles et al., 1994; Kapsner et al., 1995). Indeed, the rapid changes seen in Greenland ice cores during the last glaciation are associated with changes in other parameters (e.g., dust and Ca^{2+} levels), which suggests that the precipitation source regions did vary.

The problems of using oxygen isotopes as a simple proxy of temperature over Greenland are now well documented, but the situation for Antarctica seems less problematic. Compared to the widely varying temperatures of the North Atlantic and the growth and decay of major ice sheets and sea ice affecting storm tracks around Greenland, conditions around the Antarctic continent have not changed very significantly, even over glacial-interglacial timescales. Indeed, over much of the very cold interior of East Antarctica, where many of the longest ice cores have been recovered, precipitation is extremely low (<2 cm water equivalent per year) and much of that is derived from high-level moisture flux, resulting in diamond dust (ice crystals precipitated in clear air conditions). Hence, inland precipitation is less affected by changes in low-level moisture flux (though this is not true of more coastal locations). However, strong surface-based temperature inversions essentially decouple the surface from the atmospheric circulation above the ice cap; temperatures are often much lower at the surface (Φ_g) than at the top of the inversion (Φ_i), and on average, $\Phi_i = 0.67\Phi_g - 1.2$ (Jouzel and Merlivat, 1984). Hence, there is a much stronger relationship between Φ_i (or cloud temperatures above the inversion) and $\delta^{18}O$ than between surface temperature and the

isotopic content of snowfall (Picciotto et al., 1960; Aldaz and Deutsch, 1967; Jouzel et al., 1983). Model simulations also show that surface temperatures are lower than temperatures at the level where condensation takes place in the atmosphere over Antarctica, increasingly so in the cold interior regions (Helsen et al., 2007; Masson-Delmotte et al., 2008).

Many other factors affecting $\delta^{18}O$ at a location today have not been constant over time. During glacial periods, ice thicknesses gradually increased on many ice sheets, resulting in lower $\delta^{18}O$ values at the surface because of the increase in elevation. More extensive sea ice during glacial periods would effectively have increased distance to moisture sources, leading to lower $\delta^{18}O$ values in isolated continental interiors (cf. Kato, 1978; Bromwich and Weaver, 1983). Furthermore, during glacial periods, the isotopic composition of ocean water itself changed (a $\delta^{18}O$ value of $\sim$1.1‰ higher than today) due to the storage of water that was depleted in ^{18}O in large ice sheets (Labeyrie et al., 1987; Shackleton, 1987). Finally, as temperatures fell to very low levels in some regions, $\delta^{18}O$ would have decreased more rapidly for a given drop in temperature, because of the curvilinear nature of the $\delta^{18}O$-temperature relationship. Any interpretation of isotopic values in ice cores must consider all these factors, which undoubtedly have had an effect on the isotopic composition of high-latitude precipitation over time. Understanding how these various factors have interacted to influence the isotopic content of precipitation in the past is facilitated by the use of general circulation models (GCMs) with isotopic tracers in the hydrologic cycle (e.g., Joussaume et al., 1984; Vuille et al., 2003; Schmidt et al., 2007; Sturm et al., 2010). Results from simulations with modern boundary conditions compare very well with observations (Jouzel et al., 1987b, 1991). Running the models with glacial age boundary conditions suggests that there was little change in $\delta^{18}O$ equatorward of 40°N or 50°S at the last glacial maximum (LGM) but that there were large decreases in $\delta^{18}O$ at higher latitudes (Joussaume and Jouzel, 1993; Charles et al., 1994; Jouzel et al., 1994).

5.2.4 Deuterium Excess

On a global scale, fractionation of oxygen and hydrogen during evaporation and precipitation processes approximates a well-defined relationship, whereby $\delta D = 8\delta^{18}O + 10$. This defines what is termed the meteoric water line (Craig, 1961c) that in effect characterizes the "normal" equilibrium conditions, which exist between $\delta^{18}O$ and δD. The offset value (10 in this case) is termed the deuterium excess (d, where $d = \delta D - 8\delta^{18}O$). However, deuterium excess varies under nonequilibrium conditions, providing information not available from $\delta^{18}O$ and δD alone.

Values of d vary because of kinetic effects occurring at both the evaporation and condensation stages of the water cycle (Jouzel et al., 2007a). During evaporation, higher rates of diffusion to the water surface of molecules containing light isotopes lead to an increase in the light isotope content of water vapor, relative to the water source. This effect is in addition to the fractionation effect caused by the lower vapor pressure of water containing heavier isotopes (discussed earlier). However, because of the different masses of HDO and $H_2^{18}O$, the kinetic effect is slightly greater for $H_2^{18}O$ than for HDO, resulting in changes of d when conditions deviate from equilibrium. Thus, when there is strong mixing of the surface waters (by higher wind speeds) or when relative humidities increase (reducing evaporation rates) or when water temperatures decrease (also reducing evaporation rates), the kinetic effect is reduced and values of d in precipitation will be lower. Thus, Jouzel et al. (1982) interpreted

low values of deuterium excess ($d = 4‰$) in the pre-Holocene section of an ice core from Dome C, Antarctica, as indicative of higher relative humidities and/or higher wind speeds in the water vapor source regions than during the Holocene (when $d = 8‰$). Increased levels of Na^+ (from sea salt) and aeolian dust confirmed that wind speeds and humidities were probably higher in glacial time than in the Holocene.

A model of the isotopic fractionation of precipitation, based on the Rayleigh distillation process described earlier, works well at temperatures above $\sim -10\ ^\circ C$, but under the colder conditions common in Greenland and Antarctica, the simple model cannot explain the observed δD-$\delta^{18}O$ relationship or the isotope-temperature gradients. At such low temperatures, clouds become supersaturated with respect to ice, and the transition from water vapor in clouds directly to ice crystals is the principal mode of precipitation formation. However, the lower molecular diffusivity of water molecules containing heavier isotopes (HDO and $H_2^{18}O$) leads to the preferential condensation of isotopically light water molecules on the ice crystals. This is analogous to the kinetic fractionation effect that occurs at the ocean surface during the process of evaporation. By taking this additional kinetic effect into account, a much better fit between modeled and observed deuterium excess values and a realistic isotope-temperature relationship is obtained for snow forming at very low temperatures (Jouzel and Merlivat, 1984). Unfortunately, snowfall deposited on polar ice sheets has generally undergone a complex history; the transition temperature at which clouds become primarily made up of ice crystals rather than water vapor is not well known, yet this significantly influences the value of d (Fisher, 1991, 1992).

Models of isotopic fractionation taking into account kinetic effects during evaporation and snow formation can be used to constrain the uncertainties inherent in these processes, providing good simulations of observed variations (Jouzel and Merlivat, 1984; Petit et al., 1991; Fisher, 1992). Petit et al. (1991), for example, showed that the observed relationship between d and δD in East Antarctica could only be accounted for if the initial sea surface temperature at the air mass source region was between 15 and 22 °C, corresponding to latitudes 30-40°S (Figure 5.8). Changes in humidity in the source region are of secondary importance but are of more significance at higher values of δD (warmer, lower elevation sites in Antarctica). Of course, it is unrealistic to expect that the moisture source for Antarctic snow is confined to only one latitudinal band, and this factor has also been modeled. Simulations in which moisture was added to the air mass as it passed from 30 to 40°S to Antarctica give results, which are consistent with observations, suggesting that up to 30% of moisture originates from areas with SSTs $<10\ ^\circ C$ (Petit et al., 1991). This model thus provides strong support that midlatitudes are the primary moisture source for at least the interior of Antarctica, with smaller contributions from regions at higher latitudes. On the other hand, the experiments with the NASA/GISS general circulation model incorporating calculations of deuterium excess (which could be traced back to each ocean basin) suggest that the average source region SST for Antarctic midwinter precipitation is considerably lower, in the range of 9-14 °C (Koster et al., 1992). Whatever the solution is, small seasonal variations in d ($\pm 5‰$) in snowfall at the South Pole seem to indicate that the process of delivering snow to this location involves fairly consistent pathways from the moisture source, year round. Similar conclusions were reached by Johnsen et al. (1989) for the higher elevations of Greenland, though Fisher (1992) found that the isotopic content of snow at the summit region of the ice sheet (Crête) was not compatible with a single moisture source and that a mixture of moisture from

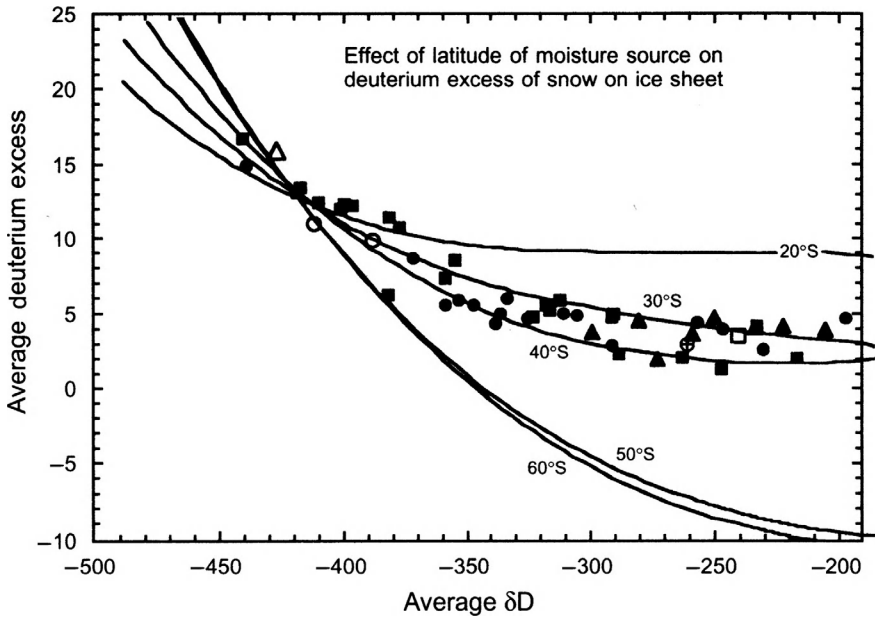


FIGURE 5.8 Model-derived estimates of how the latitude of the oceanic moisture source region influences the average δD and *d* values in Antarctic precipitation (solid lines) compared to the observed δD-*d* relationship in Antarctica (symbols—based on surface snow samples across a wide geographic region). Each model line uses a different supersaturation function (relating the supersaturation of water vapor (with respect to ice) to the snow surface temperature) optimized to produce the best fit with observed data. The latitudes 30-40 °C correspond to SSTs of ~15-21 °C. *From Petit et al. (1991).*

the east (2/3) and west (1/3) seemed probable. This conclusion is similar to that reached by Charles et al. (1994) using a GCM with isotopic tracers in the model's hydrologic cycle. When glacial age boundary conditions were imposed on the model, source regions changed; the southern part of the ice sheet was dominated by North Atlantic moisture sources, and the northern part by North Pacific moisture. With the incorporation of isotopic tracers into regional and general circulation models, further insights into fractionation processes occurring today and in the past will no doubt be obtained, providing greater confidence in the interpretation of the changes observed in ice cores (e.g., Jouzel et al., 1993; Sturm et al., 2010).

Variations in deuterium excess in relation to $\delta^{18}O$ also shed light on the abrupt changes observed in Greenland ice cores over the last glacial-interglacial cycle. These changes occur in both the $\delta^{18}O$ and *d* records, but when there were abrupt shifts to warmer conditions (higher values of $\delta^{18}O$), *d* was lower (Figure 5.9) (Masson-Delmotte et al., 2005). Temperatures in the moisture source region must therefore have been *lower* in the milder episodes (humidity and wind speed may also have been higher). Johnsen et al. (1989) explained this counterintuitive conclusion by suggesting that the milder periods of the LGM were associated with an abrupt shift in oceanic conditions in which the sea-ice boundary rapidly retreated northward, revealing colder waters, which acted as a local moisture source near to the ice sheet. During colder episodes, when there was more extensive sea ice around Greenland, the moisture

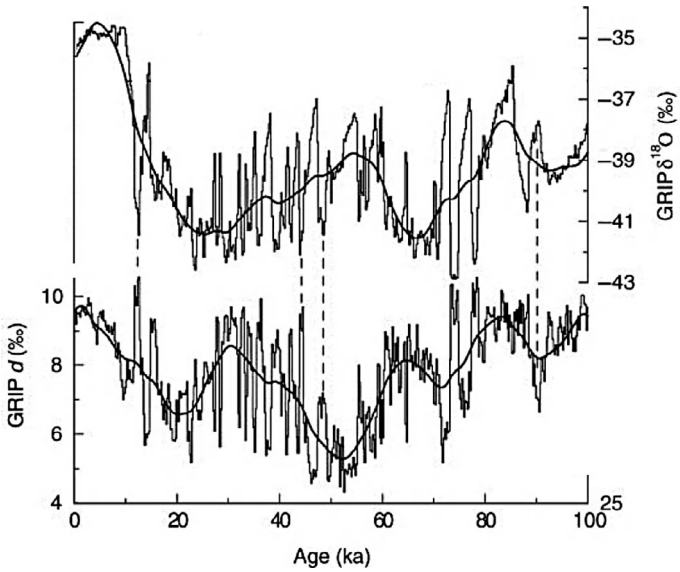


FIGURE 5.9 $\delta^{18}O$ and deuterium excess (d) over the last 100 ka at the GRIP site (Summit, Greenland). Higher values of d correspond to isotopic minima in $\delta^{18}O$, because at those times, a northward shift in the position of the polar front resulted in evaporation of water from cooler areas of the Atlantic Ocean. During times when $\delta^{18}O$ was at a minimum, the source region for precipitation reaching Greenland was Atlantic subtropical waters. *From Masson-Delmotte et al. (2005).*

source for precipitation over Greenland was further south, in subtropical waters, resulting in higher values of deuterium excess (cf. Landais et al., 2004).

5.3 DATING ICE CORES

A fundamental requirement of any ice-core study is determining the age-depth relationship. With new continuous-flow analytic techniques, annual layers can be recognized in many cores where accumulation rates are high enough, resulting in very accurate timescales—back to 60,000 years, so far, in cores from Greenland (Andersen et al., 2006a; Rasmussen et al., 2006; Vinther et al., 2006; Svensson et al., 2008). Before 60,000 years, flow models have been used to produce a chronological framework for each record. Volcanic marker horizons provide cross-checks between cores, and common isotopic features observed in independently dated stalagmites have been used to provide additional checks on absolute ages. The alignment of chronologies in ice cores from Greenland and Antarctica has been achieved by using the trace gas content in each record, as these gases are rapidly mixed in the atmosphere and so the gas record can be considered essentially synchronous across both hemispheres. All of the approaches to dating have limitations, and there are many papers devoted to the discussion of the difficulties and assumptions made in constructing ice-core chronologies and apparent inconsistencies in their chronologies vis-a-vis other dated records (e.g., Skinner, 2008). Nevertheless, great progress in this area has been made over the last decade, and ice-core chronologies now provide a remarkably accurate chronological yardstick to compare with other paleoclimatic records, enabling questions about how changes in the climate system develop (temporally and geographically) to be explored in some detail, at least over the last glacial-interglacial cycle. Before discussing that work, some of the principal methods used to date ice cores are reviewed.

5.3.1 Radioisotopic Methods

Several different radioactive isotopes have been analyzed in ice cores in an attempt to provide quantitative chronological methods for dating ice. These include ^{10}Be, ^{14}C, ^{36}Cl, ^{39}Ar, ^{81}Kr, and ^{210}Pb (Stauffer, 1989). At present, however, radioisotopic dating of ice and firn is not a routine operation, and other stratigraphic techniques are preferred.

^{210}Pb (half-life: 22.3 years) is washed out from the atmosphere as a decay product of ^{222}Rn (Figure 3.24). It has been used in a few studies of snow accumulation over the last 100-200 years, providing a useful perspective on the very short accumulation records available in remote parts of Antarctica and Greenland (e.g., Crozaz et al., 1964; Dibb and Clausen, 1997). New methods to obtain AMS ^{14}C dates from the water-insoluble organic carbon fraction of carbonaceous aerosols in ice have enabled ice samples from mid- and low-latitude ice cores with as little as 5 mg of carbon to be dated (Jenk et al., 2009). However, it is unlikely that this approach will be useful in dating ice cores from high latitudes, as the concentration of dateable material in polar ice is insufficient.

The cosmogenic isotope ^{10}Be is produced in the upper atmosphere by galactic cosmic rays. The ^{10}Be is transferred to Earth's surface by scavenging particles in the atmosphere and precipitation and thereby enters many natural archives (e.g., ice and sediments such as loess). ^{10}Be is modulated by variations in the solar wind (commonly observed as sunspot cycles), and these ~11-year (Schwabe) cycles have been detected as changes in the concentration of ^{10}Be in some polar ice cores (Beer et al., 1996, 2001; Berggren et al., 2009). However, because ^{10}Be production is not precisely cyclical and many other meteorologic and glaciological factors can affect the concentration of ^{10}Be in ice, ^{10}Be variations alone do not provide an ideal chronometer, and a temporal framework provided by other methods is required to examine down-core changes (cf. Berggren et al., 2009). Perhaps, more important are the rare but large increases in ^{10}Be concentration found in ice as a result of geomagnetic excursions in the past. These led to short-term but very high cosmogenic isotope production rates when the strength of Earth's magnetic shield was temporarily reduced. The resulting spikes in ^{10}Be (and other cosmogenic isotopes) are particularly clear in ice cores and provide important chronostratigraphic markers for many other terrestrial archives (e.g., Aldahan and Possnert, 1998; Baumgartner et al., 1998; Zhou et al., 2007). Thus, the Laschamp geomagnetic excursion has been dated (by annual layer counting) at 41,250 ± 814 b2k in the Greenland ice-core chronology (GICC05), and the Antarctic EPICA Dome C ice core has thereby been aligned chronologically with the northern hemisphere record (Raisbeck et al., 2007; Svensson et al., 2008). Raisbeck et al. (2006) had also identified a peak in ^{10}Be in the EPICA ice core associated with the Brunhes-Matuyama geomagnetic reversal ~780,000 years ago, providing another important chronostratigraphic marker, which can be identified in many natural archives.

5.3.2 Seasonal Variations and Episodic Events

Certain components of ice cores show distinct seasonal variations that enable annual layers to be detected. These can then be counted to provide an extremely accurate timescale for as far back in time as these layers can be detected. Where uncertainties exist in one seasonal chronology, a comparison with other parameters enables accurate cross-checking to

be accomplished, thereby reinforcing confidence in the timescale produced (e.g., Rasmussen et al., 2006). In this way, annual layer counts (back to 60,000 years ago) have been carried out on ice cores from Greenland, using a combination of, inter alia, visual stratigraphy, electrical conductivity measurements (ECM), laser light scattering (from dust), oxygen isotopes, and chemical variations in the ice (Figure 5.10) (Andersen et al., 2006a; Rasmussen et al., 2006; Vinther et al., 2006; Svensson et al., 2008). Several earlier efforts had been made to produce a reliable chronology (e.g., Alley et al., 1997a; Meese et al., 1997), but the current standard is known as GICC05 (Greenland Ice Core Chronology, 2005). Data from the three main drilling sites have been used (NGRIP, GRIP, and Dye 3) in order to take advantage of the best-quality records in each location, when sections of a particular ice core are problematic (Figure 5.11). Distinct ECM markers or identifiable tephras (such as that from the AD 79 Vesuvius eruption) were used to ensure proper alignment of the ice-core records at key intervals. In this way, an annually counted chronology has been established for Greenland, extending back to 60,000 b2k (before AD 2000) corresponding to a depth of 2420 m in the NGRIP ice core. For the period before that, an ice flow model (ss09sea) has been used, providing an estimate on the total NGRIP chronology of ~123,000 years (Johnsen et al., 2001; North Greenland Project Members, 2004). Table 5.3 shows estimates of the "maximum counting errors" for different sections of the GICC05 record. These are based on uncertainties in identifying annual layers in some parts of the record; additional uncertainties could result from an imperfect understanding of the seasonality of parameters being used for dating, though this seems unlikely. However, if the seasonality of the glaciochemical indicators has changed over time, for example, due to an alteration in the seasonal distribution of snowfall during times of rapid climate transitions, this would confound the "counting model" being used and affect the resulting layer counts. Nevertheless, the overall chronological uncertainties appear to be quite small (±70 years for the start of the Holocene), though in some sections, the potential errors are larger than in others, due to unresolved annual layer recognition despite the multiple parameters being considered. Comparisons with other independently dated paleoclimate records (such as stalagmites) show remarkable fidelity with the isotopic variations recorded in Greenland, lending credibility to the chronologies established and highlighting the global significance of the environmental changes recorded (Svensson et al., 2008).

In the following sections, the different types of information used in layer counting are discussed in more detail.

5.3.2.1 Visual Stratigraphy

Changes in crystal structure and the presence of dust layers provide the basis for recognizing annual layers in many ice cores. In the GISP2 ice cores, a distinctive coarse-grained depth hoar layer, which is formed each summer in the dry firn zone of the ice sheet, can be identified when ice cores are placed on a well-illuminated light table. Cloudy bands, due to dust, are also diagnostic of annual layers, particularly in the glacial sections of Greenland cores, and together, these features have been used to count annual layers back 50,000 years (Alley et al., 1997a). In cores from the Quelccaya Ice Cap (Peru) and many other low-latitude sites, a pronounced dust layer, which is diagnostic of each dry season, also permits the counting of annual layers (Thompson et al., 1985).

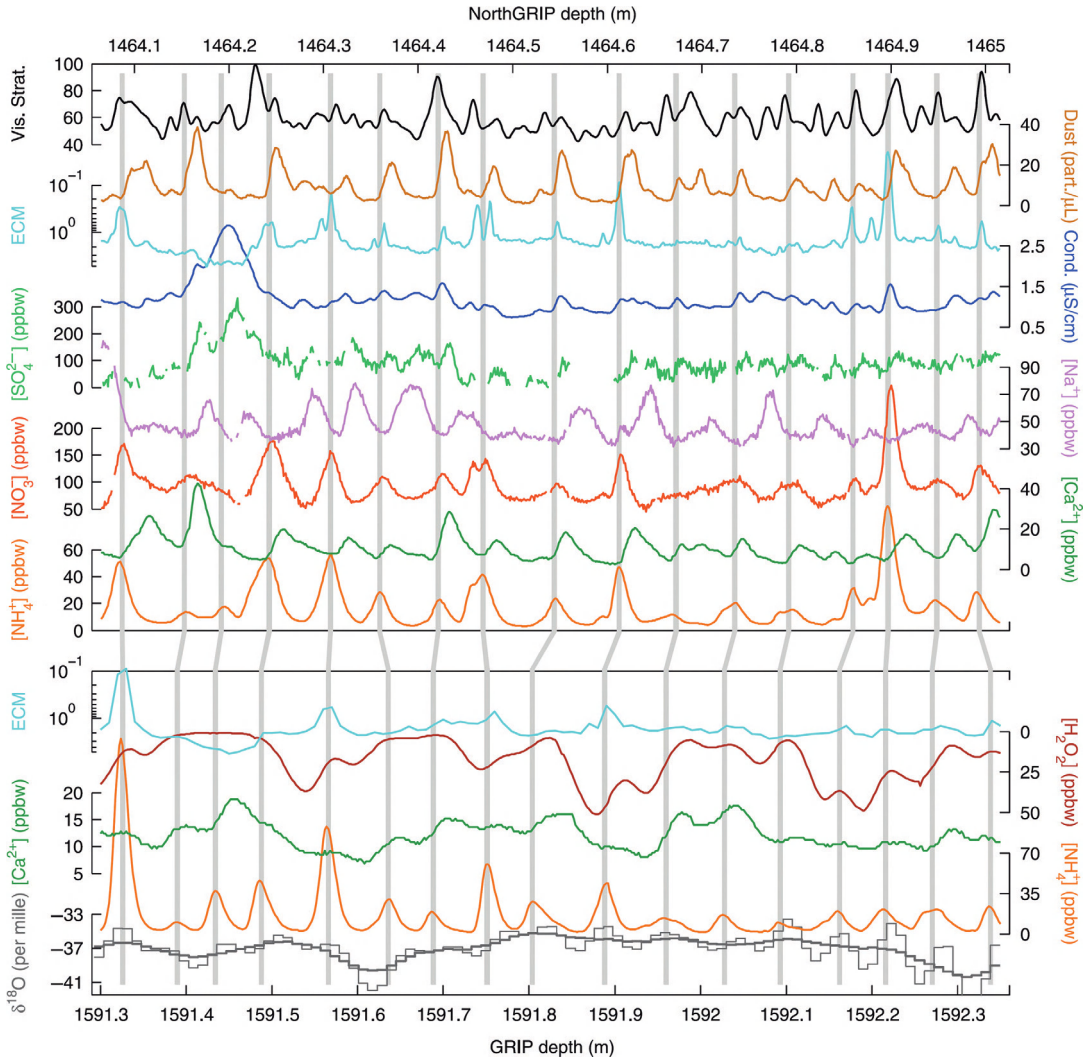


FIGURE 5.10 An example of data and annual layer markings (gray vertical bars) from the Early Holocene. The upper nine panels show a 0.95 m long section of NGRIP data, and the lower five panels show the corresponding 1.05 m section in the GRIP data set. The annual layers are marked at the summer peaks, which are defined by high $[NH_4^+]$ and $[NO_3]$. The spring is characterized by high dust mass, leading to peaks in $[Ca^{2+}]$ and dips in the $[H_2O_2]$ profile, while the $[Na^+]$ peaks in late winter. The visual stratigraphy profile does not contain clear annual layers but contains peaks corresponding to almost every dust peak. The ECM (note the reverse logarithmic scale) is strongly anticorrelated with the largest peaks in $[NH_4^+]$ but is not reliable enough to identify annual layers. The lower four panels show the same time interval in the GRIP core. The similarity of the $[NH_4^+]$ records (and consequently also to some degree the ECM records) from NGRIP and GRIP allows a close stratigraphic matching of the two cores. The annual layer identification has been based on impurity data only but is supported by comparison with high-resolution $\delta^{18}O$ data that are available for a few short sections in the Holocene. The $\delta^{18}O$ data were corrected for diffusion (raw data, thick line, and diffusion corrected data, thin line). *From Rasmussen et al. (2006).*

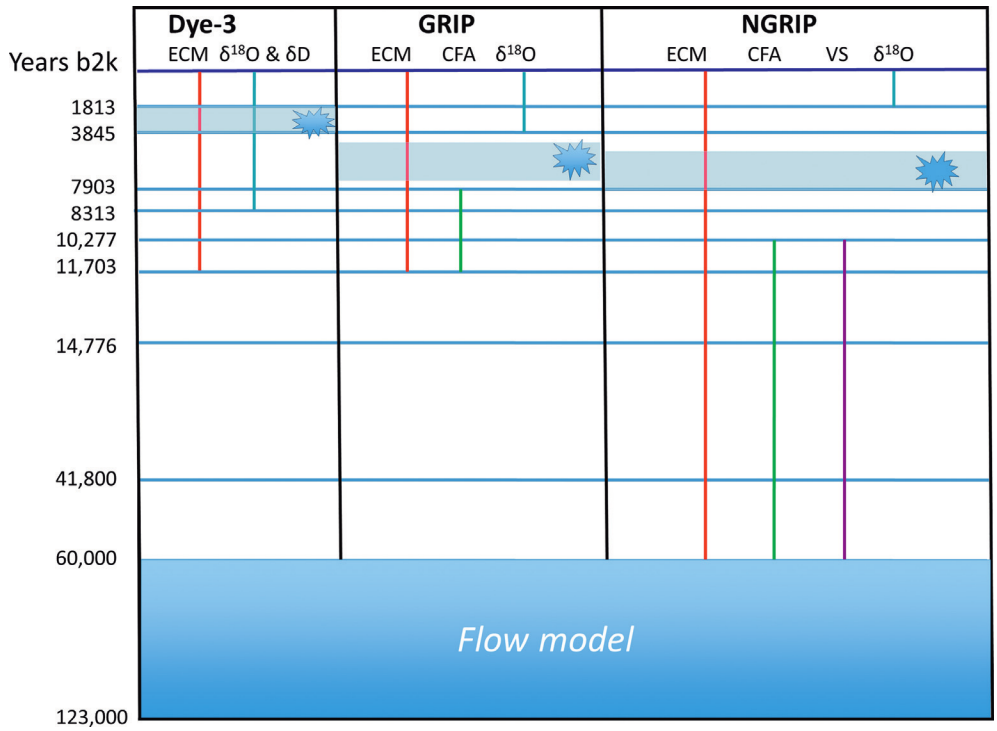


FIGURE 5.11 Schematic diagram to illustrate the parameters used in constructing the GICC05 chronology for Greenland ice cores: electrical conductivity measurements (ECM), glaciochemistry from continuous-flow analysis (CFA), visual stratigraphy (VS), or from the isotopes of oxygen or hydrogen ($\delta^{18}O$ or δD). Distinct reference horizons (principally tephra or conductivity maxima related to major explosive volcanic eruptions) were also used to cross date and align the cores. Uncertainties due to brittle ice above 1300 m in the GRIP core and above 1400 m in NGRIP (shaded zones) were resolved by using the higher-accumulation-rate Dye-3 core for dating those sections. *Based on information in Vinther et al. (2006), Rasmussen et al. (2006), Andersen et al. (2006a), and Svensson et al. (2008).*

5.3.2.2 $\delta^{18}O$

Because of the greater cooling, which occurs in winter months, much lower $\delta^{18}O$ concentrations are found in winter snow than in summer snow. This results in a very strong seasonal signal, which can be used as a chronological tool, providing accumulation rates are reasonably high (>25 cm water equivalent per year), wind scouring of snow is not severe, and no melting and refreezing of snow and firn have occurred. In effect, the annual layer thickness can be identified by counting each couplet of high and low $\delta^{18}O$ values from the top of the core downward (Figure 5.10). To provide a common reference point for such annual layer counting, dates are referred to as "b2k" (i.e., before AD 2000). Unfortunately, at increasing depths in polar ice sheets, the amplitude of the seasonal signal is reduced until it is eventually obliterated. In the upper layers, where density is <0.55 g cm^{-3}, this results from isotopic exchange between water vapor and firn. In lower, denser layers, where air channels are closed off, obliteration results from diffusion of water molecules within the ice. This process is accelerated due to thinning by plastic deformation as the annual layers approach bedrock; thinning

increases isotopic gradients in the ice, making molecular diffusion more effective in obliterating the seasonal variations, though in some cases, the record can be deconvoluted to reconstruct the seasonality of the isotopic record (Johnsen, 1977; Johnsen et al., 2001). In the North GRIP ice core, basal melting greatly reduced the thinning of annual layers (albeit, eliminating the oldest ice) with the result that seasonal isotopic variations can be recognized to great depths, enabling annual layer counts to be made back to ~60,000 years (Svensson et al., 2008).

In cores where seasonal isotopic differences are still preserved down to dense firn and ice layers, further smoothing due to molecular diffusion is so slow that the signal may then be preserved for thousands of years. This does not occur in most of Antarctica though, because of low accumulation rates that result in the seasonal signal being "lost" at relatively shallow depths. In many cases, removal of seasonal (or indeed annual) accumulation by wind scouring may occur, destroying any seasonal signal entirely. On temperate glaciers and ice caps, where snowmelt and percolation of meltwater take place, it is also often impossible to detect a reliable seasonal isotopic signal. In these conditions, seasonal differences in both δD and $\delta^{18}O$ are rapidly smoothed out (within a few meters of the surface) due to isotopic exchange as the ice recrystallizes (Amason, 1969).

5.3.2.3 *Glaciochemistry*

The development of continuous-flow analysis (CFA) has enabled seasonal changes in many parameters to be detected at high temporal resolution in ice cores from Antarctica and Greenland (Röthlisberger et al., 2000). CFA is particularly beneficial for deeper sections of ice cores, where the annual layers are more compressed, but in sections where the accumulation rate was low (such as the Younger Dryas interval, and earlier stadials), even multiparameter data from CFA are difficult to interpret and more reliance has to be placed on visual stratigraphy and ECM variations.

In constructing the GICC05 chronology, variations in NH_4^+, Na^+, Ca^{2+}, NO_3^-, SO_4^{2-}, and H_2O_2 were all used to resolve the annual cycles with depth. Typically, Na^+ (from sea salt) reaches a maximum in late winter, whereas NH_4^+ and NO_3^- peak in the summer. Ca^{2+} tends to be highest, and H_2O_2 lowest, in the spring (Figure 5.10). In this way, a careful evaluation of all variations down core provides confidence in the chronology, and peaks in ECM allow cross-checks between different ice cores at frequent intervals, to ensure that the layer count in between is not seriously in error. Seasonal changes in microparticles are also important seasonal indicators in many ice cores, especially those from low latitudes where prolonged dry seasons can result in very pronounced seasonal cycles of dust. In polar ice cores, microparticles increase to a maximum in late winter-early spring, as a result of a more vigorous atmospheric circulation at this time of year; conversely, microparticle frequency minima are generally observed in autumn (Ram and Illing, 1995).

Compared to the diffusion rate of water molecules, which leads to the obliteration of the seasonal $\delta^{18}O$ record at depth, diffusion of microparticles and metallic ions is essentially zero. This is useful in areas where accumulation rates are so low that seasonal isotopic differences are rapidly lost at depth. For example, in parts of Antarctica, the concentration of sodium ions (Na^+) varies markedly, due to pronounced seasonal changes in the influx of marine aerosols (Herron and Langway, 1979; Warburton and Young, 1981). At Vostok, in eastern Antarctica, Na^+ concentrations reach a maximum in summer layers, due to sublimation of snow, leaving higher residual ionic concentrations (Wilson and Hendy, 1981). These variations are visible

far below the level at which seasonal $\delta^{18}O$ variations become obliterated and can even be detected at ~950 m depth in the Vostok ice core.

5.3.2.4 *Electrical Conductivity Measurements (ECM)*

ECM provides a continuous record of ice acidity by recording the ability of ice (or meltwater) to conduct an electrical current. A current with a large potential difference is passed between two electrodes in contact with the surface of the ice core (1250v was used on the GRIP and 2100v on the GISP2 ice cores). When the ice contains strong acids from volcanic eruptions, ECM is high; layers containing alkaline continental dust or ammonia (e.g., from biomass burning) have low ECM (Taylor et al., 1993a,b). Changes in deposition of $CaCO_3$ dust are associated with large changes in ECM, reflecting changes in the source region and/or transport and deposition processes. Pronounced changes in ECM characterize the transitions from cold, glacial periods to warmer interstadials in the GISP2 ice core (Figures 5.12). In addition, peaks in the ECM record, which are seen in cores from sites far apart on the Greenland Ice Sheet, can identify volcanic marker horizons, enabling a composite chronology to be constructed from different cores (Rasmussen et al., 2008).

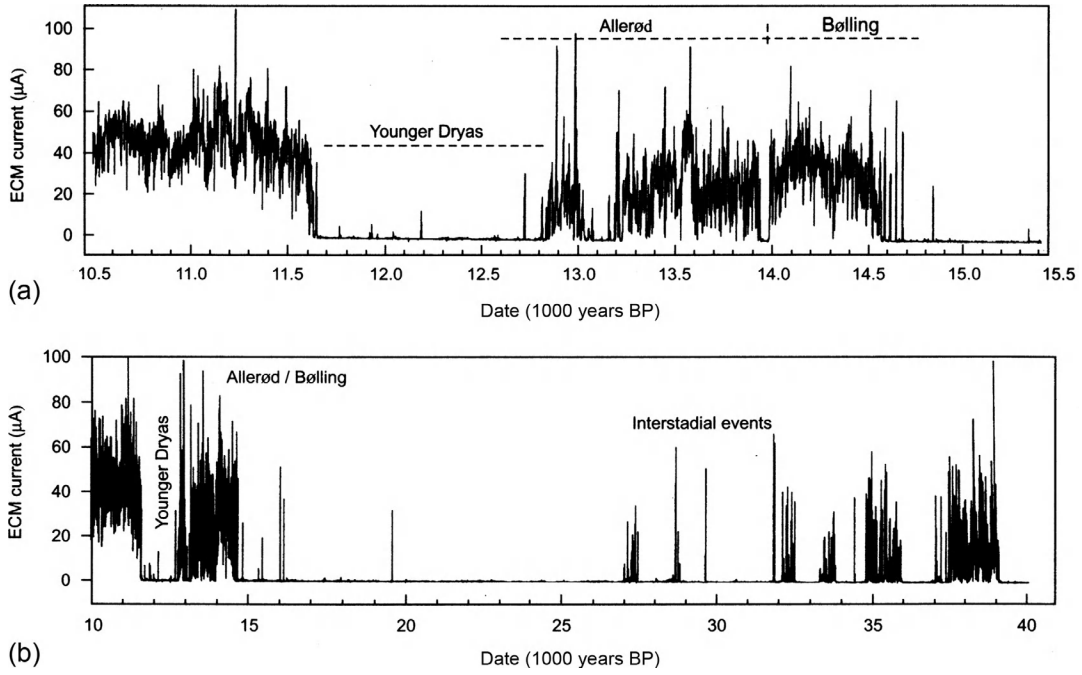


FIGURE 5.12 Electrical conductivity (ECM) in the GRIP Summit ice core (Greenland) between (a) 15,500 and 10,500 and (b) 10,000-40,000 cal. years BP. Cold episodes such as the Younger Dryas are characterized by low ECM values, and warmer episodes by higher values reflecting the relative change in atmospheric dust loading. *From Taylor et al. (1993b).*

5.3.2.5 *Radioactive Fallout*

Where characteristic layers of known age can be detected, these provide valuable chronostratigraphic markers against which other dating methods can be checked. On the short timescale, radioactive fallout from atmospheric nuclear bomb tests in the 1950s and 1960s can be detected in firn by measuring the tritium content (or gross β activity) or ^{36}Cl. As the timing of the first occurrence of these layers is fairly well known (1953 spring in Greenland and February 1955 over much of Antarctica, reaching maximum levels in 1963), they can be used as marker horizons for snow accumulation studies, facilitating regional surveys of net balance over the last few decades (Crozaz et al., 1966; Picciotto et al., 1971; Koerner and Taniguchi, 1976; Koide and Goldberg, 1985).

5.3.2.6 *Volcanic Sulfate and Tephra*

Violent eruptions may inject large quantities of dust and gases (most importantly hydrogen sulfide and sulfur dioxide) into the stratosphere where they are rapidly dispersed around the hemisphere (Devine et al., 1984; Rampino and Self, 1984; Robock, 2000). The gases are oxidized photochemically and dissolve in water droplets to form sulfuric acid, which is eventually washed out in precipitation. Hence, after major explosive volcanic eruptions, the acidity of snowfall increases to levels significantly above background values (Hammer, 1977). By identifying highly acidic layers resulting from eruptions of known age, an excellent means of checking seasonally based chronologies is available. Detailed geochemical analysis from CFA allows very detailed time series of volcanically derived sulfate (and other elements, such as Br) to be traced back in time, even on a seasonal basis. For example, Sigl et al. (2013) made a high-resolution analysis of ice cores from the West Antarctic Ice Sheet Divide and the NEEM site in northwestern Greenland (Figure 5.13). Volcanic events stand out against the low-level background sulfate variations from sea salt and marine biogenic sulfur (and the industrial era rises in sulfate in the northern hemisphere). This reveals more than 130 significant volcanic events in each hemisphere, 50 of which were common to both locations, indicating that the eruption occurred near the equator, and material was distributed via the stratosphere to both hemispheres. Often, the exact location of these historical eruptions is unknown, but the major eruption of Huaynaputina (Peru) in February 1600 provides a diagnostic reference horizon that has also been found in conductivity data from the Quelccaya and Huascarán (Peru) ice cores. The largest explosive eruption of the last millennium, in AD 1458/1459, was attributed to Kuwae, in Vanuatu (southwestern Pacific), which followed another large tropical eruption, in AD 1452. Over the same period, the largest volcanic signals in the northern hemisphere were in AD 1259 ± 1 and 1783 ± 1. The former event also left a strong signal in many Antarctic ice cores, indicating that it was also a low-latitude eruption, now thought to be from the Rinjani volcanic complex on Lombok Island, Indonesia (Palais et al., 1992; Lavigne et al. 2013). The AD 1783 event was the fissure eruption of Grimsvötn (Laki) in Iceland. It is difficult to assess the overall eruption size from measurements in individual ice cores that may be relatively close to the volcanic source. Ice cores from Greenland, for example, are likely to record Icelandic and Alaskan eruptions as larger than equivalent-sized eruptions at lower latitudes, simply because of their proximity to Greenland (Hammer, 1984). However, even deposition from nearby eruptions will not be dispersed uniformly over the ice sheets, so estimates based on

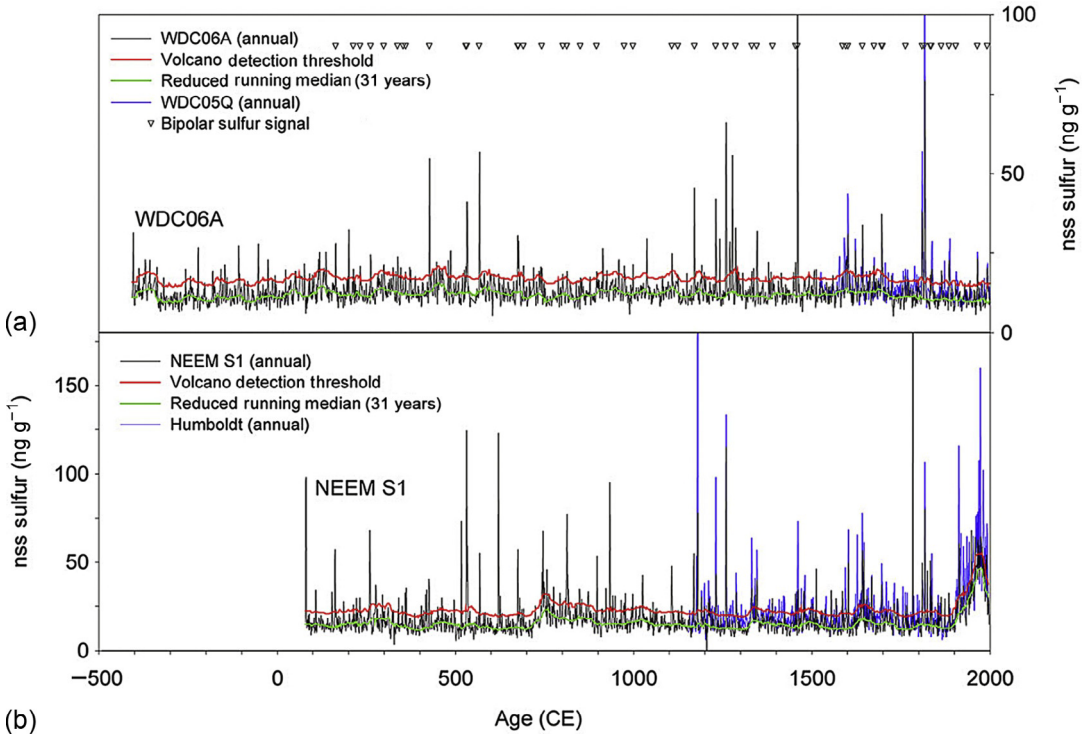


FIGURE 5.13 The high-resolution non-sea salt sulfur record from the West Antarctic Ice Divide ice core (a) and the NEEM ice core in northwest Greenland (b). The peaks in volcanic sulfate stand out above the background levels. Fifty eruptions that appear to be common in both polar regions are indicated by triangles in the upper panel. *From Sigl et al. (2013).*

single (~10-15 cm diameter!) ice-core samples may be misleading (Clausen and Hammer, 1988). Indeed, a number of major eruptions were not registered at all in some ice cores (Delmas et al., 1985). Ideally, a suite of cores extending longitudinally along the major mountain ranges of the world would be needed to get a more global picture of volcanic aerosol dispersal. However, in many high-altitude and low-latitude ice cores, the deposition of alkaline aerosols neutralizes the volcanic acids and hence masks the eruption signal (also a problem during glacial times, when atmospheric dust levels were much higher than in the Holocene). Nevertheless, the collection of many short cores from a wide area of the larger ice sheets and along polar/alpine transects (e.g., from the South Pole, via the Antarctic Peninsula and Patagonian ice fields, to Ecuador) may eventually enable a better assessment of the spatial pattern of acid deposition to be made, leading to a more reliable record of past explosive volcanism in both the northern and southern hemispheres (cf. Mulvaney and Peel, 1987; Clausen and Hammer, 1988).

One approach, which can be used to "scale" the ice-core sulfate (or acidity) record to compensate for long-distance dispersal of volcanic aerosols, is to use the concentration of atomic bomb fallout on the Greenland Ice Sheet (from both high- and low-latitude sources) as a guide to how aerosols, dispersed via the stratosphere, are depleted en route from the source area

(Clausen and Hammer, 1988). Using this idea, Zielinski (1995) estimated atmospheric optical depth changes resulting from major explosive eruptions of the last 2100 years. His analysis indicates that the overall impact of volcanic eruptions on atmospheric turbidity was significantly greater in the last 500 years than in the preceding 1500 years. In particular, multiple large eruptions in the interval AD 1588-1646 and 1784-1835 probably had a significant cumulative impact on atmospheric optical depth, leading to cooler conditions at those times (cf. Bradley and Jones, 1995).

The longest record of SO_4^{2-} concentration in an ice core comes from the GISP2 site in Greenland and spans the last ~110,000 years (Zielinski et al., 1996). This provides a unique record of the volcanic aerosol that is of most importance climatically. Temporal resolution of the analyses is ~2 years for the last 11,700 years but then declines back in time (3- to 5-year samples back to ~14,800, 8-10 to ~18,200, 10-15 to ~50,000, and up to 50 years per sample toward the oldest section of the core). This makes it difficult to directly compare these short-lived events since a single acidity spike readily seen in the Holocene would be effectively diluted over the longer periods represented by deeper samples. Nevertheless, there are many episodes when SO_4^{2-} concentrations exceeded those levels observed after recent major eruptions, suggesting that SO_4^{2-} levels may have been extraordinarily high at times in the past and/or maintained for up to several decades at climatically significant levels. Thus, the SO_4^{2-} record from GISP2 provides a very important perspective on volcanic events on a decade to millennial timescale (Zielinski et al., 1996). Several periods stand out as having been particularly active, especially 8-15 and 22-35 ka BP. It is interesting that these times correspond to the times of major ice growth and decay. This suggests that the greater frequency of eruptions may be a direct consequence of increased crustal stresses associated with glacial loading and unloading and/or changes in water loading of ocean basins, especially in areas with a thin lithosphere (such as the volcanically active island arcs of the Pacific Rim) (Zielinski et al., 1996). Thus, there may be a direct feedback between continental ice growth and explosive volcanism, with orbitally driven ice volume changes driving shorter-term climatic changes associated with the eruptions.

Volcanic dust (tephra) from large eruptions may also provide chronostratigraphic horizons if the chemical "fingerprint" of the volcanic glass shards can be correlated between different sites. In the GISP2 (Greenland) ice core, for example, volcanic particles from an Icelandic eruption dated at $55{,}380 \pm 1184$ b2k (Svensson et al., 2008) can be matched with the Z2 tephra found in many marine sediment records from the North Atlantic (Ruddiman and Glover, 1972; Kvamme et al., 1989; Zielinski et al., 1997). Similarly, volcanic particles in the Younger Dryas section of the Dye-3 and GISP2 ice cores have the same geochemical signature as the Vedde tephra, which is widely distributed in northwest Europe and the North Atlantic (dated at $12{,}171 \pm 57$ b2k in the GICC05 chronology) (Mangerud et al., 1984; Birks et al., 1996; Zielinski et al., 1997; Mortensen et al., 2005). Many other important tephras that have been identified in Greenland ice cores are discussed by Abbot and Davies (2012) (cf. Figures 5.14, 5.18, and 4.18). It is also possible to align ice-core records from both polar regions when diagnostic geochemical signatures from explosive low-latitude eruptions can be matched. Thus, Svensson et al. (2012) were able to identify the signal of Toba, one of the largest eruptions of the Quaternary, in cores from both Greenland (NGRIP) and Antarctica (EDML), at ~74 ka BP, thereby establishing an important chronostratigraphic marker horizon for both polar regions.

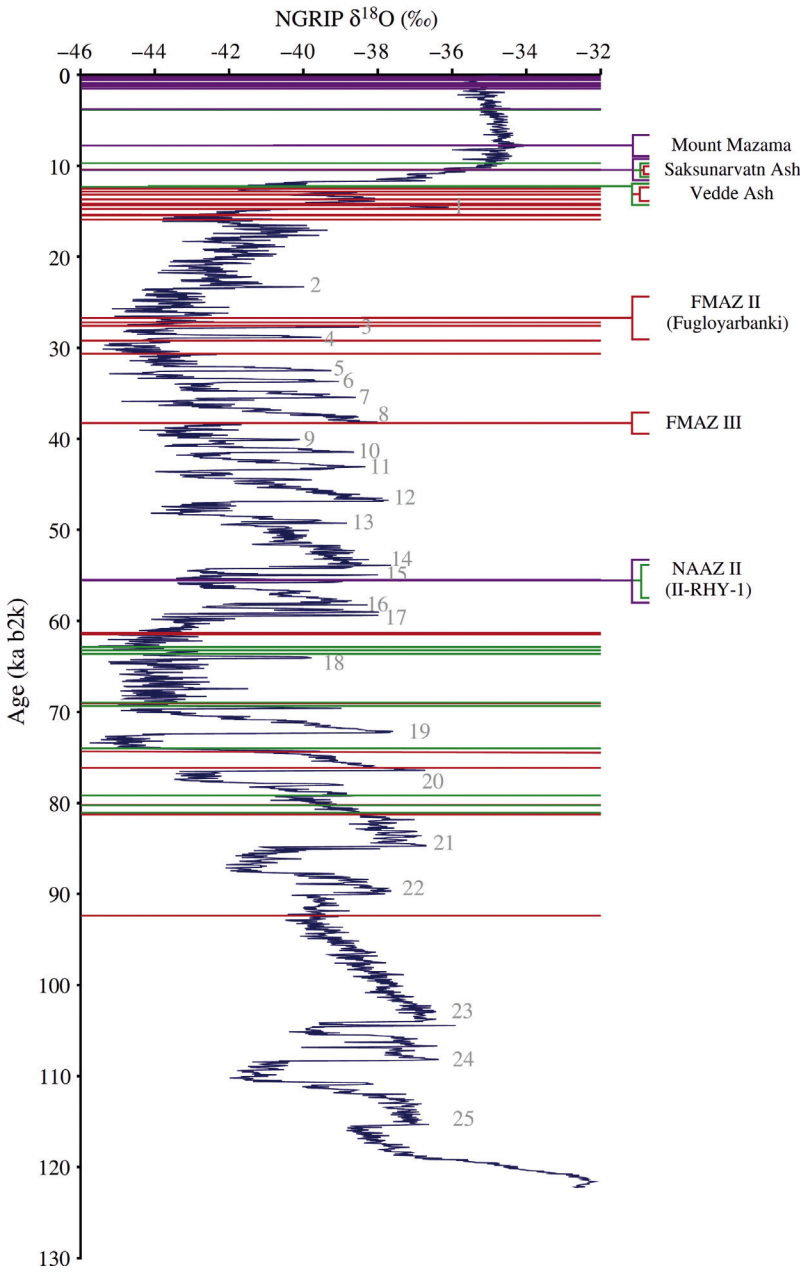


FIGURE 5.14 Major tephra horizons identified in Greenland ice cores, plotted with the NGRIP oxygen isotope record. Tephra horizons present in NGRIP (red), GRIP (green), and GISP2 (purple) are shown. Dansgaard-Oeschger (D-O) events are numbered. *From Abbott and Davies (2012).*

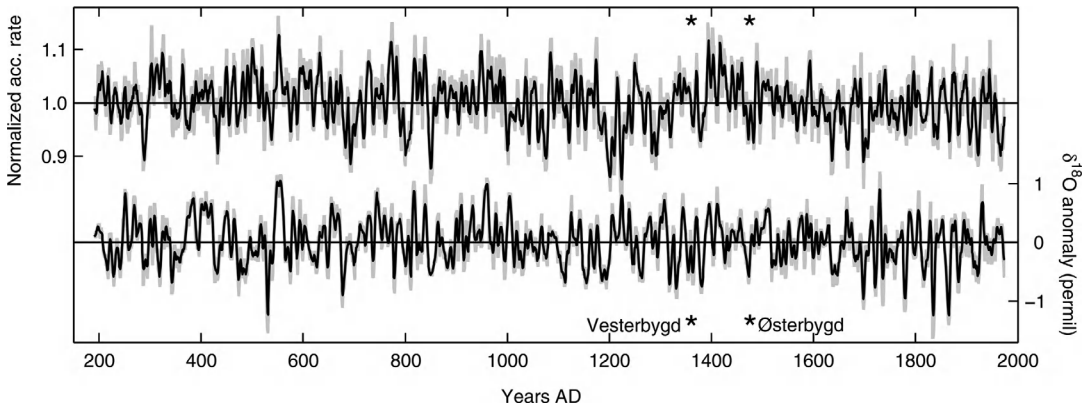


FIGURE 5.15 Accumulation at Summit, Greenland (l00-year running mean). Following an increase in accumulation from the LGM to the Early Holocene, conditions became relatively stable averaging 0.24 m ± 5% on this timescale for the last ~9000 years. *From Meese et al. (1994).*

Once an annual chronology has been established by these various approaches, it is then possible to calculate accumulation rate changes over time, given certain assumptions about vertical strain since deposition and density variations down core (Meese et al., 1994). However, precipitation is generally far more variable spatially than temperature, and so, to maximize the signal to noise ratio, there are benefits from averaging several cores to obtain a regional picture of change. To that end, Andersen et al. (2006b) averaged the accumulation data from three well-dated Greenland cores (Dye-3, GRIP, and NGRIP) for the last ~2000 years (Figure 5.15). The composite record shows no long-term trends, but there were periods of persistently low accumulation, particularly in the thirteenth and fourteenth centuries. They suggest that this may have placed added stress on the Norse farming communities in southern Greenland who were already living at the margins for agriculture (perhaps demonstrated by the fact that they built irrigation systems from upland lakes to water their lowland pastures).

5.3.3 Theoretical Models

Dating ice at great depth poses severe problems that cannot be easily resolved by the methods described earlier. At present, the method most widely used to date pre-Holocene ice is to calculate ice age at depth by means of a theoretical ice-flow model (Dansgaard and Johnsen, 1969; Reeh, 1989; Johnsen and Dansgaard, 1992). Such models describe mathematically the processes by which ice migrates through an ice sheet. Snow accumulating on an ice sheet is slowly transformed into ice during densification of the firn. As more snow accumulates, the ice is subjected to vertical compressive strain in which each layer is forced to thin and is advected laterally toward the margins of the ice sheet (Figure 5.16). Hence, a core from any site, apart from the ice divide, will contain ice deposited up slope, with the oldest and deepest ice originating at the summit. Because summit temperatures are cooler, if the core is not recovered from the highest part of the ice sheet, $\delta^{18}O$ values at depth must be corrected for this altitude effect, which will be present regardless of whether any long-term climatic

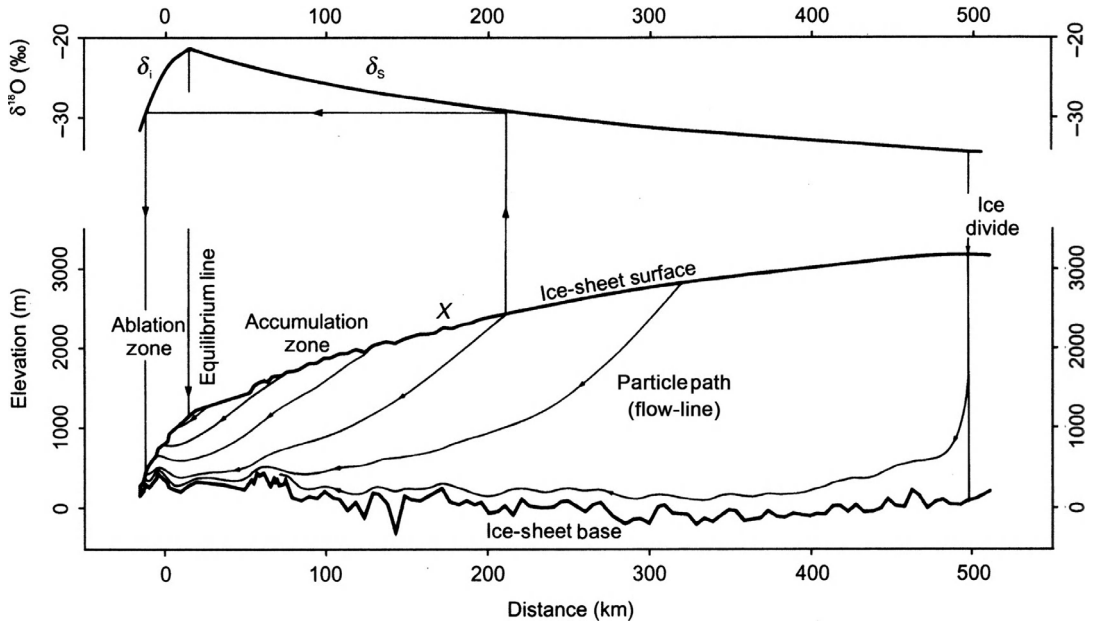


FIGURE 5.16 Schematic cross section to show flow in an ice sheet. The snow deposited on the surface is transformed to ice and follows the flow lines indicated. Ice thins by plastic deformation under compression by the overlying ice. Hence, an ice core from site X will contain a record of ice originating upstream, requiring adjustment for the colder conditions in that region. An ice core from the summit will have fewer problems, providing that the ice divide has not varied over time. Samples recovered at the surface in ice-sheet margins may represent the same paleoenvironmental record as that from an ice core through the ice sheet. *Modified from Reeh (1991).*

fluctuation has occurred. Because of the nature of ice flow and deformation, most of the time period recorded in an ice core is found in the lowest 5-10% of the record. This means that even small differences in an age-depth model can result in large discrepancies in age estimates for the lowest part of deep ice cores (see, for example, revisions made in the Dye-3 chronology by Dansgaard et al., 1982 and the discussion of age uncertainties in Reeh, 1991).

Simple models can provide a rough estimate of ice age at depth, but for more accurate age estimates, some knowledge of past changes in ice thickness and temperature, accumulation rates, flow patterns, and ice rheology (which changes with dust content) is required (Cuffey and Paterson, 2010). Many of these problems are minimized in the case of ice cores from ice divides (e.g., the GRIP core at Summit, Greenland) or in cores that penetrate very thick ice sheets to depths well above the bed (e.g., Vostok, Antarctica). Nevertheless, even in these cases, uncertainties related to past ice-sheet dimensions and the stability of ice divides, changes in ice-sheet thickness and especially changes in accumulation rate, can change age-depth relationships very significantly in the deepest sections of a core. On the other hand, if ice can be dated independently by some other means (see earlier discussion), flow models can then be constrained and used to estimate changes in those parameters, such as accumulation rate, which would otherwise be problematic (e.g., Dahl-Jensen et al., 1993). In this way, iterative changes in models, using best estimates of various parameters and how they might

realistically have varied in the past, together with the ages of certain fixed points (such as tephras of known age or the ~41,250 years b2k ^{10}Be anomaly) can be used to refine and improve an ice-core chronology. The latest version of the Greenland ice-core chronology, based on a flow model for the section of the record older than 60,000 years (Figure 5.11), is referred to as "ss09sea" (Johnsen et al., 2001).

5.3.4 Chronostratigraphic Correlations

In addition to the methods described earlier, attempts have been made to correlate certain stratigraphic features in ice cores with other proxy paleoclimatic records that may have better chronological control. For example, there are common isotopic features in ice cores from Greenland, in marine sediments from the Cariaco Basin, and in speleothems from China (e.g., Deplazes et al., 2013). As the speleothems are independently dated by U-series methods, this offers the opportunity to date (or check) the chronology of ice cores (Wang et al., 2001). One danger in this approach is that certain "events" (for example, the abrupt change to isotopically heavier snowfall in Greenland that characterizes the start of Dansgaard-Oeschger events) may be used to align records from different regions, but the timing of those transitions may not be synchronous and overly simplistic correlations may obscure potentially important leads and lags in the climate system. Other approaches to stratigraphic correlations between ice cores in Antarctica and Greenland, using the record of well-mixed trace gases, and between ice cores and other paleoclimate archives are discussed in Section 5.4.3.

5.4 PALEOCLIMATIC RECONSTRUCTION FROM ICE CORES

Ice cores have revolutionized our understanding of Quaternary paleoclimatology by providing high-resolution records of many different parameters, recorded simultaneously at each ice-core location. In the following sections, some of the main results from the northern and southern hemispheres are presented, together with a discussion of how they are related to each other and to orbital forcing.

5.4.1 Ice-Core Records from Greenland

Six ice cores to bedrock have been recovered from the Greenland Ice Sheet: Camp Century, Dye-3, two from Summit—the GISP2 (Greenland Ice Sheet Project 2) and GRIP (Greenland Ice Core Project) cores—and two from northern Greenland, the North GRIP and NEEM (North Greenland Eemian) ice cores (Figure 5.1, Table 5.2). In addition, a core from a small ice cap on the eastern edge of the ice sheet (Renland) also reached bedrock (Johnsen et al., 2001), and three other long records have been obtained by "horizontal sampling" along the ice-sheet margin (Reeh et al., 1987, 1991, 1993; Johnsen and Dansgaard, 1992). These cores have provided an enormous amount of information about the climatic history of Greenland and of processes that must have operated over a large area of the North Atlantic region, with effects of hemispheric or even global significance. Furthermore, the cores contain records (such as biomarkers, dust, and CH_4) that reflect environmental changes that occurred far from the polar regions.

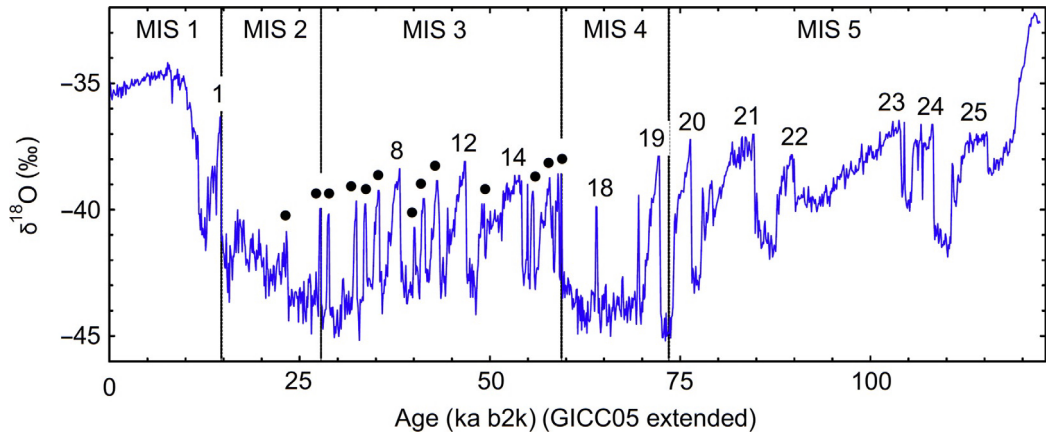


FIGURE 5.17 Oxygen isotope record ($\delta^{18}O$) from the NGRIP site on Greenland, back to ~123,000 b2k, showing the sequence of abrupt changes known as Dansgaard-Oeschger (D-O) events (numbers and black dots) from 1 to 25. These have also been formally designated Greenland interstadials and numbered GI-1 to GI-25 (cf. Figure 5.19). Chronology is based on annual layer counts across multiple ice cores (Figure 5.11) back to 60,000 b2k and by a flow model, designated ss09sea, below that (adjusted by −705 years to match the layer counting at 60,000 b2k). Corresponding marine isotope stages (MIS) are shown. *From Wolff et al. (2010b).*

Figure 5.17 shows the $\delta^{18}O$ record from the NGRIP ice core, plotted on the GICC05 timescale back to 60,000 b2k and on the ss09sea-modeled timescale below that; these chronologies constitute the best estimates of Greenland ice age with depth at the present time. The GRIP and GISP2 records are highly correlated with NGRIP back to around 95,000 b2k, with NGRIP $\delta^{18}O$ values generally lower than at the Summit core sites, as would be expected from its more northerly location. However, this difference is not constant and increases during the coldest periods suggesting a more northern trajectory of air masses delivering moisture to NGRIP at those times (North Greenland Ice Core Project members, 2004).

All Greenland ice cores show that the Late Pleistocene was characterized by abrupt, large amplitude changes in $\delta^{18}O$, unlike anything recorded in the Holocene. Between the last (Eemian) interglacial period and the beginning of the Holocene, there were 25 periods when snow accumulating on the Greenland Ice Sheet was relatively enriched in $\delta^{18}O$ (by 4-7‰) and the accumulation rate doubled, compared to the colder stadial periods, which separate them (Andersen et al., 2006a; Svensson et al., 2008). These isotopically enriched periods are termed Greenland interstadials (GI-1, ~11,700-14,680 b2k, to GI-24, ~105,000 b2k) or Dansgaard-Oeschger (D-O) events 1-24 (named after two ice-core pioneers, Willi Dansgaard and Hans Oeschger) (Johnsen et al., 1992; Dansgaard et al., 1993; Lowe et al., 2008). Intervening cold periods are Greenland stadials (GS) and are numbered accordingly. All of these abrupt changes can be correlated between cores as far apart as Dye-3 (southern Greenland), Camp Century (northwest Greenland), and Renland (east-central Greenland), so, whatever their cause, the changes were geographically extensive. Attempts have been made to use the more detailed isotopic variations as an "event stratigraphy" or chronological template that would be applicable to marine and terrestrial records from around the North Atlantic (Figure 5.18, Table 5.3) with subevents designated by letters (GI-1a-1e, GS-2a-2c, etc.) (Björck et al., 1998; Walker et al., 1999; Blockley et al., 2012). However, as Lowe et al. (2008) noted: "Defining the

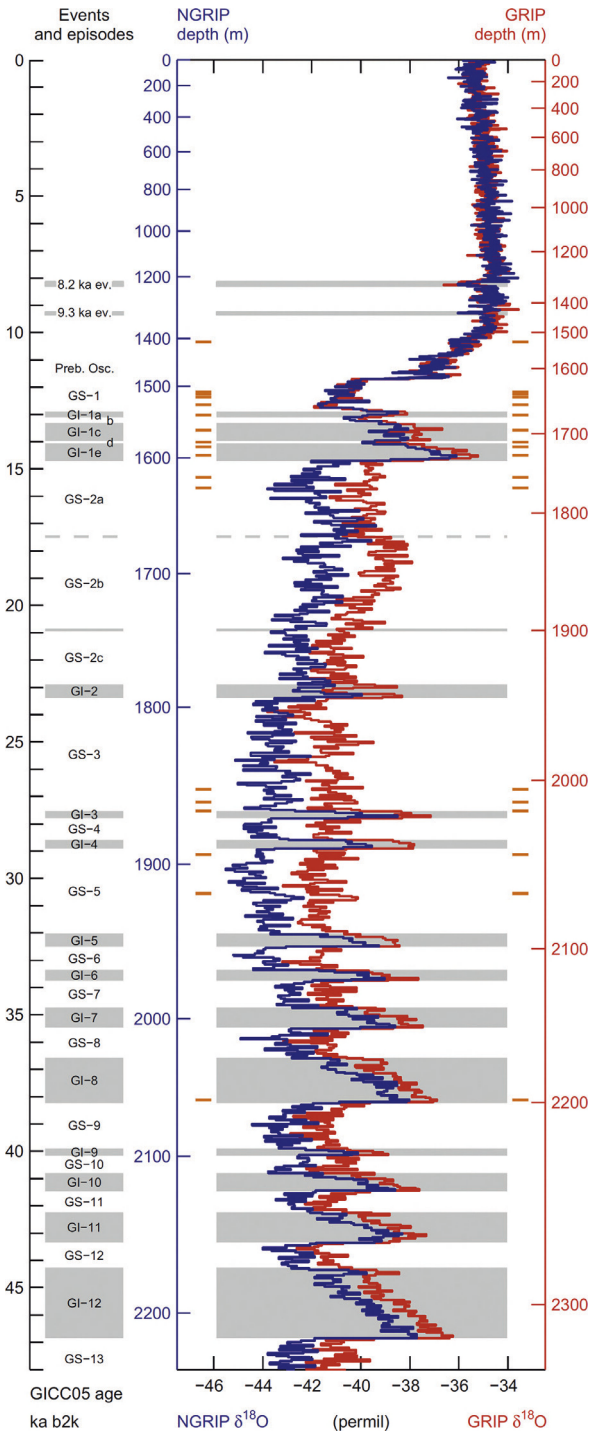


FIGURE 5.18 Event stratigraphy for the period for the last 48 ka (left axis), based on identifiable features in the ice-core isotopic records (as shown here by the $\delta^{18}O$ records from NGRIP (blue) and GRIP (red)). GS refers to Greenland stadial "events," and GI refers to Greenland interstadial "events" (shaded). Subevents (1a, 1b, 1c, etc.) are similarly identified. Tephras found in the two ice cores are indicated by orange bars. *From Blockley et al. (2012).*

onset and termination of climatic events can be an ambiguous task—the higher the temporal resolution at which this is attempted, the more difficult it becomes. In the NGRIP record, for example, the onset and termination of events GI-1e and GS-1 are defined in Rasmussen et al. (2006) using deuterium excess data, because the deuterium excess is the clearest indicator of climate change. . .The transitions denoted by deuterium excess signals most likely precede changes in temperature and vegetation recorded in other archives." This issue was examined in detail by Steffensen et al. (2008) who showed that warming at the start of the Bølling (~14.6 ka b2k) and at the end of the Younger Dryas (~11.7 ka b2k) was extremely abrupt, as recorded by a number of parameters. For example, at the NGRIP site, a change in $\delta^{18}O$ and d (deuterium excess) occurred within just a few years. Deuterium excess is a particularly sensitive indicator of the transition to warmer conditions, reflecting a rapid change in the source region of water vapor due to a reorganization of the atmospheric circulation at that time. At the onset of the Younger Dryas episode, the change in d was also very abrupt, changing within a few years (at 12,896 b2k) but other parameters ($\delta^{18}O$, dust, accumulation) adjusted more slowly, over a century or more. Steffensen et al. thus argued that the critical indicator of the timing of abrupt change should be d, not $\delta^{18}O$ nor the other parameters that changed more slowly, and on that basis, the Younger Dryas lasted 1192 ± 3 years, from 12,896 to 11,704 years b2k.

The frequent changes from stadial to interstadial values (D-O events) are the most significant features of the Greenland isotopic records, and consequently, they have received a great deal of attention. Mayewski et al. (1997) examined an extensive suite of chemical components in the GISP2 ice core and recognized two major components, which they ascribed to different circulation regimes that prevailed during the last glacial-interglacial cycle: a polar/high-latitude air mass (with higher levels of continental dust and marine-derived ions) and a mid-/low-latitude air mass (with high levels of biogenic nitrate and ammonium ions). Figure 5.19 shows that the abrupt changes in $\delta^{18}O$ during D-O events were associated with pronounced changes in these circulation regimes, as one might expect. During cold events (low $\delta^{18}O$), a polar/high-latitude circulation prevailed, whereas during the Holocene and mild interstadials, the mid-/low-latitude circulation pattern was more prevalent (Mayewski et al., 1994). The changes in dominance of circulation regimes seen so prominently during MIS 2-4 are also identifiable (albeit more subtly) during the Holocene, enabling the principal circulation changes during recent millennia to also be identified (O'Brien et al., 1995). Although such changes are defined by the ice-core geochemistry in a remote part of Greenland, there is evidence that they may have significance beyond this region because of atmospheric teleconnections with regions far from the Arctic (Mayewski et al., 1997; Stager and Mayewski, 1997).

The sequence of events from D-O 17 to D-O 8 in the NGRIP ice core was analyzed by Huber et al. (2006) who found that each abrupt warming episode lasted, on average, ~225 years during which temperatures rose 11 °C (~0.48 °C decade^{-1}). Even more remarkably, CH_4 changes were nearly synchronous with the temperature changes (lagging by $25\text{-}70 \pm 25$ years) even at the submillennial scale (Figure 5.20). Some of the warming episodes were followed abruptly by cooling of a similar magnitude, and then, warming resumed again very rapidly (e.g., D-O 13-17). It seems likely that such changes are related to changes in the extent of sea ice in the North Atlantic and associated air mass changes, bringing moisture to the Greenland Ice Sheet. This is supported by a marked decrease in deuterium excess (d) at the same times as $\delta^{18}O$ increased; conversely, higher values of d during the cold periods of a D-O cycle indicate a source region further south, where SSTs were higher (Johnsen et al., 1989). It is also significant

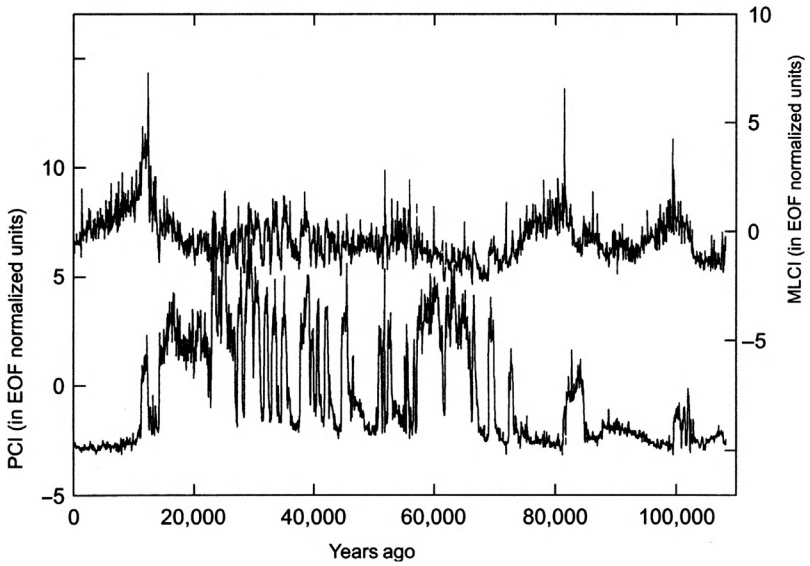


FIGURE 5.19 Variations in the two main principal components of the glaciochemistry of the GISP2 ice core over the last 110,000 years (based on covariations in sodium, potassium, ammonium, calcium, magnesium, sulfate, nitrate, and chloride ions). The lower line is interpreted as changes in the relative importance of polar/high-latitude circulation regimes and associated air masses, and the upper diagram as changes in mid-/low-latitude circulation regimes. *From Mayewski et al. (1997).*

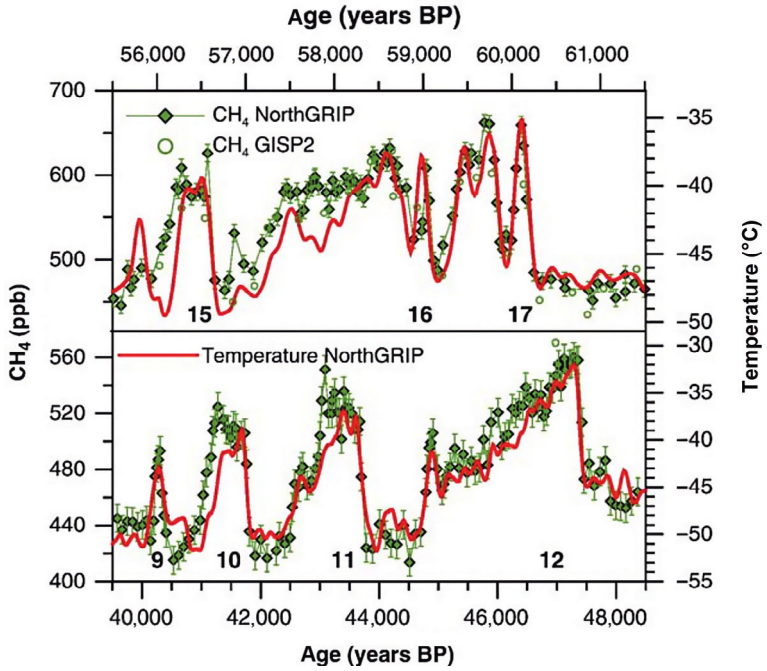


FIGURE 5.20 The temperature record from NGRIP, derived from the differential diffusion of nitrogen isotopes ($\delta^{15}N$) in the ice during periods of abrupt change, compared to the record of CH_4 in the ice. The changes in CH_4 are slightly lagged behind the isotopic/temperature changes (by 25-70 ± 25 years), but they generally track even submillennial variations in temperature. *From Huber et al. (2006).*

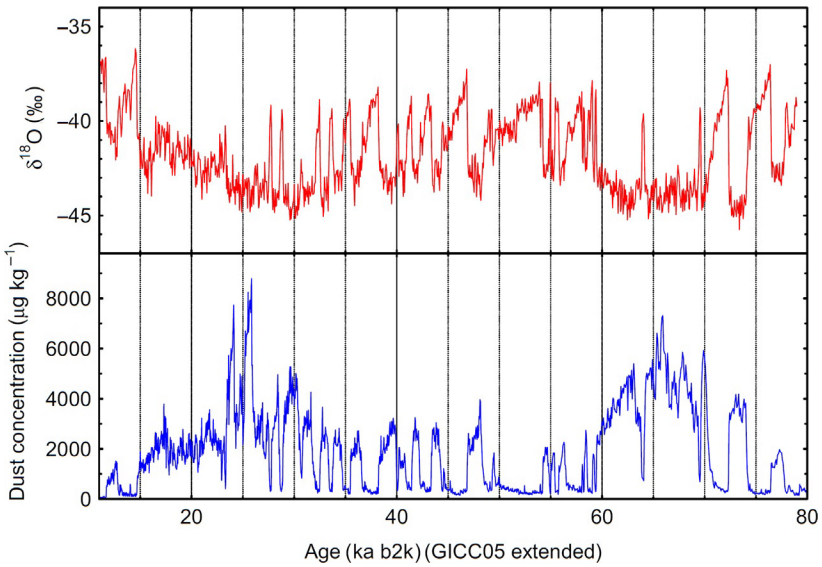


FIGURE 5.21 Dust concentration (μg kg^{-1} ice) in the NGRIP ice core (blue line) with the $\delta^{18}O$ record (red line). Dust concentration is inversely related to isotopic values, changing abruptly at (or slightly before) the isotopic transitions. *From Wolff et al. (2010b), after Ruth et al. (2007).*

that D-O events were associated with very abrupt changes in accumulation and in glaciochemistry (both dissolved ions and particulates) (Mayewski et al., 1997; Steffensen et al., 2008; Thomas et al., 2009). This is clearly seen in the record of continental dust (Figure 5.21), which indicates that environmental changes in arid source regions (mainly in East Asia) were closely in step with climate changes in Greenland. In the case of D-O 8, a decade or two before the rise in temperature, there was a major decline in most anions and cations, perhaps due to a reduction in long-distance transport of continental material (Thomas et al., 2009).

Landais et al. (2004) made a detailed study of D-O 19 and argued that the sequence of events, which characterized that event, began with a slowdown in the North Atlantic thermohaline circulation (perhaps brought about by freshwater from an extensive discharge of icebergs, calved from ice sheets in contact with the ocean). This reduction in the THC reduced the flux of heat northward, which eventually led to a slowdown or reduction in freshwater discharge to the ocean, allowing the thermohaline circulation to resume. The associated increase in heat flux to the ice sheet (the abrupt D-O warming event) was then followed by a relaxation to former values. Whether this sequence of events is directly applicable to other D-O events is debatable, given that each one has its own unique features and duration. However, the broad sequence that Landais et al. outlined could explain the characteristic isotopic signals of very abrupt change, followed by a more gradual adjustment to former values that all D-O events seem to have in common (as well as many features of the Antarctic record, as discussed later). But it does beg the question: what initiated the increase in freshwater flux? (see Chapter 6, Section 6.10 for further discussion).

Although the deep Greenland ice cores have provided remarkable details about climate variations over the last ~120,000 years, a continuous record extending back into the peak of

interglacial warmth or beyond into MIS 6 has proven to be elusive (Suwa et al., 2006). The North Greenland Eemian ice drilling project (NEEM) was specifically aimed at recovering ice from this period, by obtaining a core to bedrock in a location where it was thought that part of the Greenland Ice Sheet survived the warmest part of the last interglacial period. Earlier studies of the GRIP and GISP ice cores indicated that there were disturbances at depth in both ice cores, related to differences in the flow properties of relatively deformable glacial age ice, containing high levels of impurities, and the cleaner, more rigid interglacial ice. This gave rise to sharp discontinuities in the record that were not the result of climate change. Analysis of the NEEM core showed that although it too had disturbances at depth, sections could be matched (via globally homogeneous variations in CH_4 and $\delta^{18}O_{ATM}$) to the continuous record at EPICA DML in Antarctica, thereby transferring the timescale from that site to the Greenland record (NEEM community members, 2013). This revealed that the NEEM ice core contained an undisturbed record spanning the interval from 128.5 to 115 ka BP and possibly ice from MIS 6 and 7 as well. Melt features were common in the section from 127 to 118 ka BP, and these, together with other indicators, suggest that mean annual surface temperatures at the NEEM site were as much as 8 °C warmer at the peak of the last interglacial, somewhat higher than other estimates from the ice sheet (North Greenland Ice Core Project members, 2004).

In contrast to the widely varying isotopic record of the last glacial period, the Holocene section of Greenland ice cores is relatively flat. This has often been cited as evidence that the Holocene had an invariant climate, which (it is argued) was a necessary prerequisite for the development of agriculture and society, in general. It has even been suggested that we need to modify society's global impacts on the environment, in order that the climate might return to the benign Holocene state (e.g., Rockström et al., 2009). In reality, the Holocene was extremely variable in many regions (mainly in terms of rainfall patterns), which had major impacts on societies around the world (Oldfield, 2000), and so, the oxygen isotope record from Greenland is not representative of Holocene climate *sensu lato*. In fact, Vinther et al. (2009) showed that Holocene temperatures on the ice sheet only appear to have been invariant because the ice-sheet summit has change in elevation over the course of the Holocene. Early Holocene isotopic values have to be adjusted upward to compensate for the fact that the ice sheet was thicker in the Early Holocene (hence, isotopic values were lower than they would have been, if the ice sheet had stayed at the same size). For example, in the Early Holocene, the GISP2 and GRIP sites were 150-200 m higher than today, and Camp Century and Dye-3 were ~550 and 400 m higher, respectively. When appropriate adjustments are made for these elevation changes, it is apparent that there was a strong decline in isotopic values over the course of the Holocene, which corresponds to cooling of ~2.5 °C since ~8 ka BP (Figure 5.22). This trend is supported by physical evidence in the fabric of ice cores; melt layers in Early Holocene ice can be recognized by the presence of dense ice layers, and these provide definitive evidence that temperatures were above the freezing point at some time during summer months, conditions that were quite rare until the last few decades (Koerner and Fisher, 1990; Alley and Anandakrishnan, 1995). An analysis of these layers in ice cores from GISP2 and the Agassiz Ice Cap shows an overall decline in Holocene summer temperatures, from a time when melting at the surface was common, in the Early Holocene, to a much colder late Holocene condition. However, on the Agassiz Ice Cap, warming in the last two to three decades has led to renewed melting, at a level not seen for at least 4000 years (Figure 5.23) (Fisher et al., 2012).

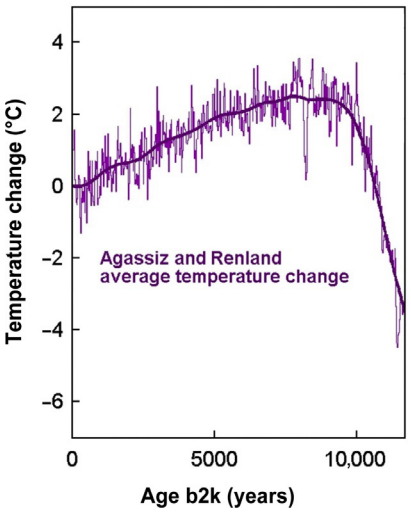


FIGURE 5.22 Mean annual temperature changes on the Agassiz and Renland Ice Caps (to the west and east of the main Greenland Ice Sheet) over the last ~12,000 years, based on oxygen isotopic data calibrated against borehole temperatures. There was an overall decline in temperature of ~2.5 °C from ~8 ka BP to the present, though note the very recent abrupt warming. *From Vinther et al. (2009).*

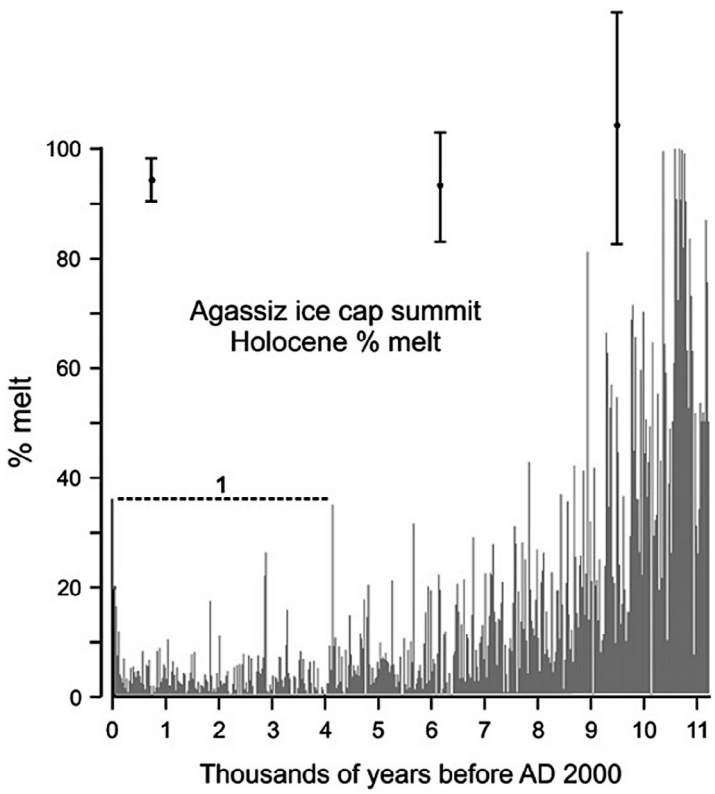


FIGURE 5.23 The Holocene record of melt in ice cores from the Agassiz Ice Cap, northern Ellesmere Island (25-year averages). Error estimates (bars) are derived from differences between nearby ice cores. Summer temperatures in the Early Holocene were much warmer than in recent years. Line 1 shows that the most recent 25-year mean was unprecedented in the last 4000 years and perhaps much longer. *From Fisher et al. (2012).*

One final point worthy of note concerning ice-core records from Greenland: remarkable records have been recovered by sampling surface ice along the ice-sheet margin, from the equilibrium line to the ice edge (Reeh et al., 1991). $\delta^{18}O$ from these "horizontal ice cores" is highly correlated with that in deep ice cores because ice flow has advected the ice originally deposited in the accumulation area to the ice-sheet margin (cf. Figure 5.16). The significance of this is that, potentially, large samples of quite old ice could be obtained by literally mining the ice margin, rather than coring the base of the ice sheet to obtain very small samples (Reeh et al., 1987). Reeh et al. (1993) noted that Summit cores yield less than 10 kg of ice per century for studies of ice older than 40,000 years BP and less than 5 kg of ice for interglacial age. Larger samples from the ice margin might permit detailed investigations of, say, dust or pollen content in the distant past.

5.4.2 Ice-Core Records from Antarctica

There are now many long ice cores from Antarctica, with the longest extending back over 800,000 years. These records are remarkable archives of many aspects of Earth's history—temperature, greenhouse gases, aerosols, sea-ice extent, explosive volcanic eruptions, solar activity, and changes in Earth's magnetic field. Furthermore, by careful synchronization with other ice cores and other long records from the northern hemisphere, we now have a much better understanding of how climatic changes across the globe were related in time and space.

The longest Antarctic ice-core record currently available is from Dome Concordia (Dome C) in East Antarctica (Figure 5.1 and Table 5.2), obtained by EPICA (the European Project for Ice Coring in Antarctica). The EPICA Dome C (EDC) ice core is 3260 m in length; the lowest ~60 m is disturbed, but the upper ~3200 m represents ~800,000 years of accumulation (equivalent to marine isotope stage 20.2) and it has thus become the *de facto* standard record of climatic changes in the region (Figure 5.24) (EPICA, 2004; Jouzel et al., 2007b). Much effort has been devoted to establishing a reliable timescale for the EDC record, leading to the most recent chronology (EDC3). This is based on an ice-flow and accumulation model, which assumes that any changes in accumulation rate over time are related to the δD record (a proxy for temperature) (Figure 5.24). Warmer conditions would have increased accumulation according to the Clausius-Clapeyron relationship, in which the water vapor content of the atmosphere increases approximately exponentially with temperature; hence, precipitation is assumed to have changed as a nonlinear function of temperature. These assumptions provided a first-order chronology that was then adjusted to accommodate a number of chronostratigraphic markers (such as volcanic sulfate horizons from eruptions of known age and a ^{10}Be excursion at the time of the Laschamp geomagnetic excursion) and by matching key features in the ice-core record to similar features in speleothems that were independently dated by U-series methods (Dreyfus et al., 2007; Parrenin et al., 2007). Variations in the elemental oxygen/nitrogen ratio ($\delta O_2/N_2$) in air bubbles in the ice also provide a check on the chronology. When firn is compressed to ice, there is a slight loss of oxygen relative to nitrogen, which is thought to be related to local insolation influencing the process of snow-firn metamorphism, and this process is subsequently captured in air bubbles at the firn-ice pore close-off. Since summer insolation is influenced by orbital variations, the $\delta O_2/N_2$ ratio can be used as a proxy for orbital forcing and thus used to tune the ice-core chronology (Bender, 2002;

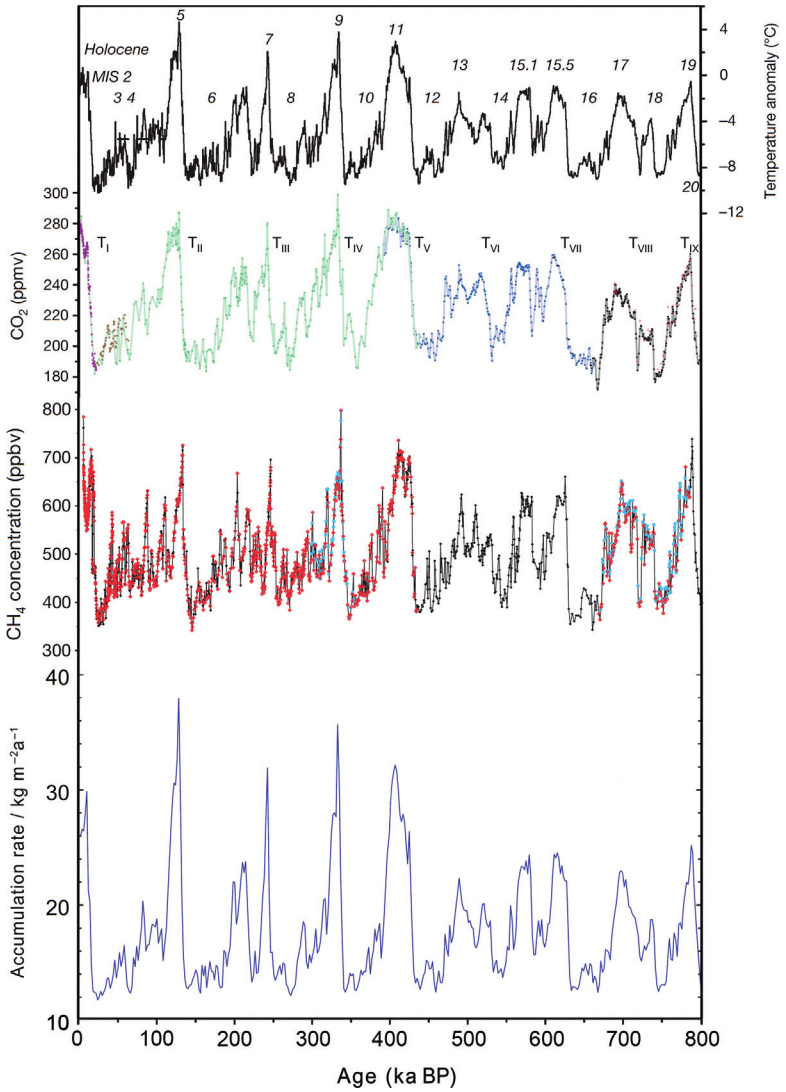


FIGURE 5.24 The EPICA Dome C δD, CO_2, CH_4, and accumulation record of the last 800,000 years (with δD interpreted in terms of mean annual temperature). Accumulation is derived from the δD record, based on the assumption that, as temperatures rose, the water vapor content of the air increased, which led to higher amounts of snowfall. This provides a first-order estimate of accumulation, though variations in Cl^- and NO_3^-, which track accumulation quite closely, suggest that accumulation may be underestimated for the period before ~450 ka BP (Wolff et al., 2010b). Marine isotope stages 1-20 are indicated and terminations (T1 to T9) are also shown. *Adapted from Lüthi et al. (2008), Loulerge et al. (2008), and Wolff et al. (2010b).*

Suwa and Bender, 2008; Landais et al., 2012). In the same way, total air content is also related to summer insolation, providing another approach to dating via orbital tuning (Raynaud et al., 2007). By these various approaches, the EDC chronology has been systematically refined, and the current iteration of the chronology (EDC3) is now considered to be accurate

to within 400 years at 14 ka, increasing to 1500 years at 40 ka and 3000 years at 100 ka BP. Below that, the uncertainty increases to ~3000-5000 years (Parrenin et al., 2007).

The Dome C ice-core record extends back in time over eight glacial-interglacial cycles (Figure 5.24). With that perspective, it is clear that δD variations in the earlier cycles, from ~800 to 430 ka BP, were lower in amplitude than those that came later. Based on the modern δD/temperature relationship (Jouzel et al., 2003), the overall range of temperature can be estimated as ~15 °C, from a maximum in MIS 5.5 (+4.5 °C) to a minimum in MIS 2 (−10.3 °C), relative to today. However, there is some evidence that this relationship has not remained constant through time and that past interglacials were even warmer, perhaps by several degrees (Sime et al., 2009). Detailed analysis of impurities in the ice reveals that there were very large changes in atmosphere dust from glacial to interglacial periods (Figure 5.25) just as in Greenland ice (Lambert et al., 2008, 2012). In the case of Antarctica, the dust originated in South America, probably from extensive glaciofluvial outwash deposits on the eastern flanks of the Patagonian Andes (Delmonte et al., 2008). Although there has been speculation that the increased dust loading of the atmosphere in glacial times could have led to iron fertilization of

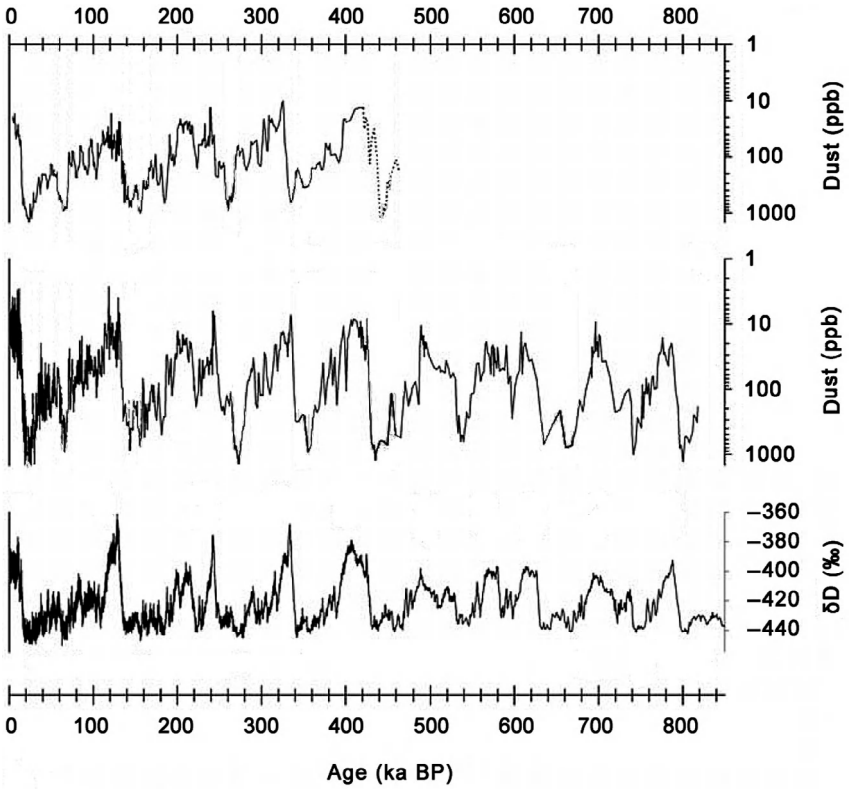


FIGURE 5.25 Dust flux in the Vostok (top) and EPICA Dome C (middle) ice cores (in μg dust per kg ice or ppb) compared to the δD record (below). Note that dust fluxes are plotted inversely with respect to δD. The dust mainly originates from the glacial outwash plains of Patagonia. Maximum dust flux corresponds to glacial periods when atmospheric dust transport was up to three orders of magnitude higher than at the height of the interglacials. *Adapted from Delmonte et al. (2008).*

photosynthetic algae in the ocean, thereby reducing atmospheric CO_2, dust flux dropped to low interglacial levels well before there was a corresponding rise in CO_2. Over the last nine terminations, dust levels declined to interglacial minima, ~4 ka before CO_2 and temperatures reached interglacial levels, indicating that there were major changes in atmospheric circulation before warming of the Southern Ocean occurred (Figure 5.26). This suggests that the dust fertilization/CO_2 drawdown mechanism was probably not the primary driver of CO_2 changes on glacial-interglacial timescales (Fischer et al., 2007; Wolff et al., 2010a).

Apart from the obvious "sawtooth" pattern of glacial-interglacial variations that characterizes the δD record in all Antarctic ice cores, there is also strong millennial-scale variability, though of a smaller amplitude than in Greenland (Wolff et al., 2010b). The question is: how are these related? The gas record in polar ice cores provides an ideal way to match the chronology of records from the two hemispheres, assuming (reasonably) that the gases are well mixed in the atmosphere. Unfortunately, CO_2 is not reliably recorded in Greenland ice (due to chemical reactions in the ice), and N_2O is also influenced by dust content. However, CH_4 has a short lifetime (<10 years), and so, changes in the sources or sinks of CH_4 are quickly registered by the level of CH_4 in the atmosphere, making it an ideal trace gas that can be used to synchronize ice-core records in both polar regions. Once this is accomplished (as discussed further, below), it is clear that Antarctic temperatures slowly increased during the cold (isotopically light) periods in Greenland, but when temperatures abruptly warmed in Greenland, Antarctic temperatures plummeted (Figure 5.27). Furthermore, the longer the duration of Greenland stadials, the more warming took place in Antarctica (EPICA community members, 2006). This is especially clear in the EPICA Dome C record (Figure 5.28), but similar relationships are seen in the ice-core data from Byrd, EPICA DML, and Dome Fuji (Lemieux-Dudon et al., 2010). This inverse relationship reinforces the concept of a "bipolar seesaw" in which changes in the thermohaline circulation trigger opposite responses in the two hemispheres (Broecker et al., 1985b; Stocker and Johnsen, 2003; Knutti et al., 2004). When there is no (or only limited) deepwater formation in the North Atlantic, heat accumulates in the southern hemisphere; the longer the shutdown of NADW formation, the more heat accumulates and the more temperatures rise in Antarctica. Once NADW formation resumes, warm water from the southern hemisphere effectively transfers heat across the equator, leading to abrupt warming in Greenland and cooling in Antarctica. Warm periods in the Antarctic ice cores are referred to as Antarctic Isotopic Maxima (AIM), and these are numbered in such a way that AIM_n corresponds to the GS preceding GI_n (EPICA community members, 2006).

Of particular interest is the two-step change in temperature that occurred during the last deglaciation, when rapidly rising temperatures were interrupted by a cooling episode, lasting ~1800 years (Figure 5.28). It is estimated that surface temperatures fell after AIM1 by ~3-4 °C at Vostok and EPICA Dome C during this "Antarctic Cold Reversal" (from ~14,500 to 12,700 cal. years BP) based on a peak to peak change in δD of 20‰, for ~25-year means (Jouzel et al., 1992; Mayewski et al., 1996). As with earlier abrupt changes, the beginning of this most recent reversal corresponds to the timing of abrupt warming in Greenland (at ~14.7 ka BP) (Lemieux-Dudon et al., 2010). Heat was then transferred to the northern hemisphere, presumably contributing to the demise of continental ice sheets and a major increase in the flux of freshwater to the North Atlantic, resulting in a reduction in (or cessation of) the Atlantic meridional overturning circulation (AMOC) at ~12.9 ka BP. This period is widely recognized in terrestrial paleoclimate records as the onset of the Younger Dryas cold period. The reduction in energy transfer via the thermohaline circulation led to the buildup of

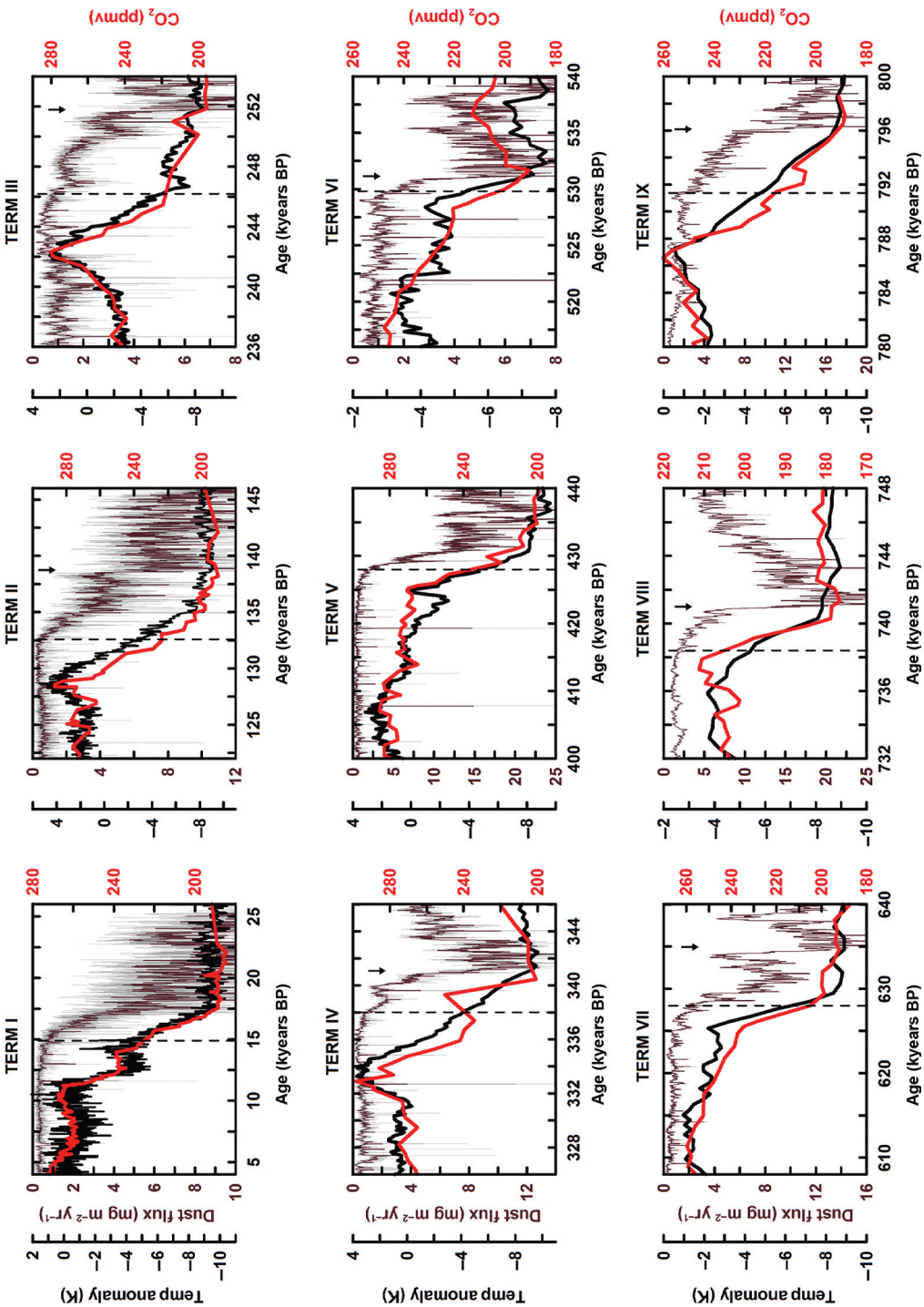


FIGURE 5.26 The sequence of changes in dust (thin brown line) CO_2 (red) and temperature at EPICA Dome C during the last nine terminations. On average, by the time dust had declined to interglacial levels (dashed line), CO_2 had risen by ~30 ppmv, indicating that dust fertilization of the ocean was not the primary driver of glacial-interglacial CO_2 changes. *From Lambert et al. (2012).*

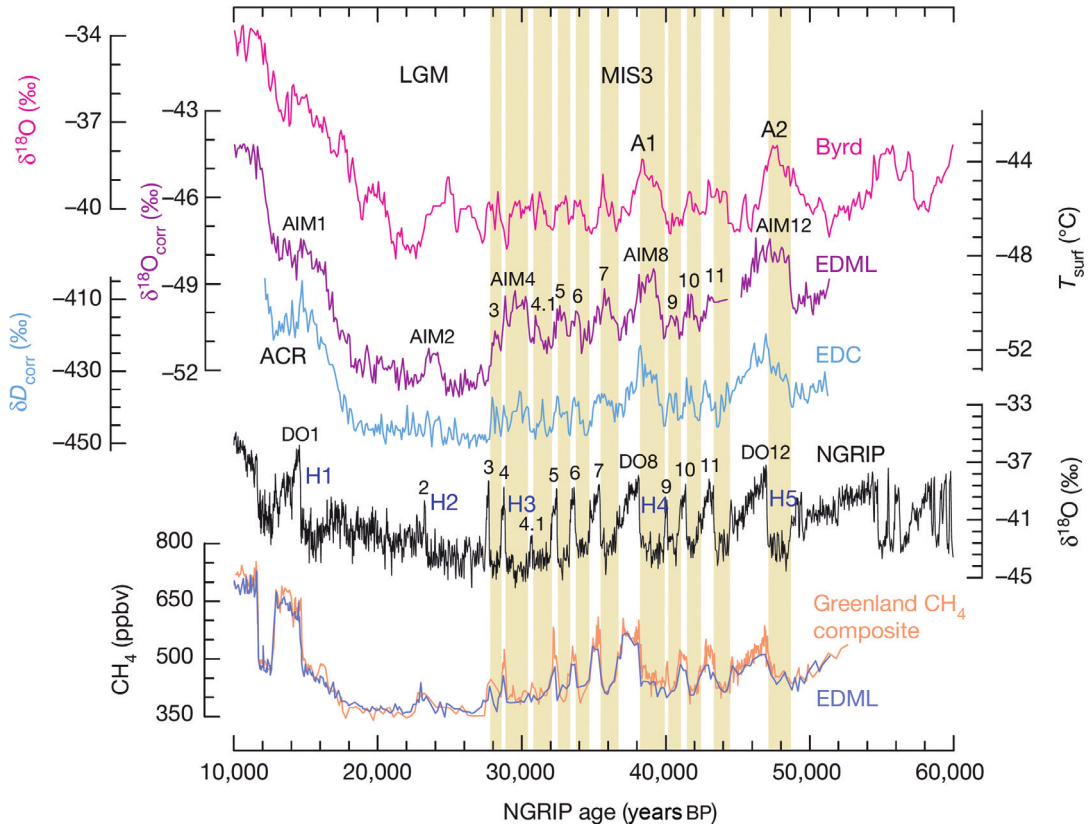


FIGURE 5.27 Hundred-year mean isotopic values from EPICA Dome C, Byrd, and EPICA DML compared to the record from NGRIP. The isotopic data have been synchronized by alignment of the common CH_4 signal in both hemispheres and by making adjustments for the gas age-ice age (Δ-age) difference (Figure 5.31). All data are plotted on the GICC05 timescale. Temperature scale on the right is based on the modern δD/temperature relationship for East Antarctica. Yellow shading shows Greenland stadials, which align with Antarctic Isotopic Maxima (AIMs). Timing of Heinrich events 1 to 5 is also shown. ACR, Antarctic Cold Reversal. *From EPICA community members (2006).*

heat in the southern ocean, and a resumption of warming in Antarctica until the AMOC became reestablished, ending the Younger Dryas interval at ~11.7 ka BP. By that time, the amount of freshwater entering the North Atlantic from melting ice sheets was no longer significant enough to trigger major changes in the AMOC, and thus, the era of major oscillations in climate, seesawing between the northern and southern hemispheres, that had characterized the preceding 80,000 years came to an end.

5.4.3 Past Atmospheric Composition from Polar Ice Cores

Ice cores are extremely important archives of past atmospheric composition. Most importantly, because bubbles of air were trapped when snow and firn became compressed into ice, ice cores can provide a continuous record of variations in the radiatively important trace

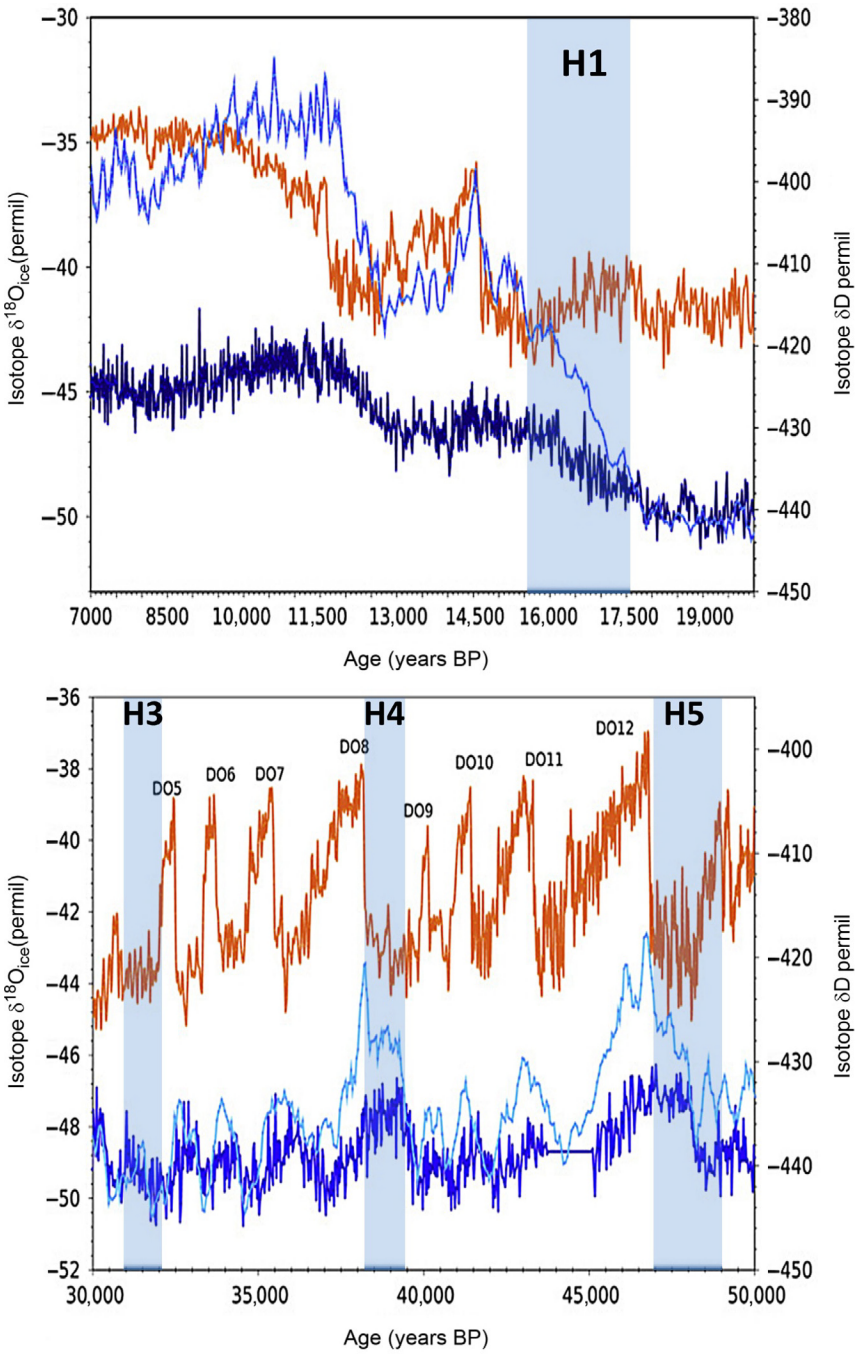


FIGURE 5.28 $\delta^{18}O_{ice}$ from NGRIP (orange) and EPICA DML (dark blue) and δD (light blue) from EPICA Dome C, after all records were chronologically aligned, using CH_4 content and other stratigraphic checks. The abrupt warming episodes in Greenland lead to cooling in Antarctica. Cold periods in Greenland are times of rising temperatures in Antarctica. *From Lemieux-Dudon et al. (2010).*

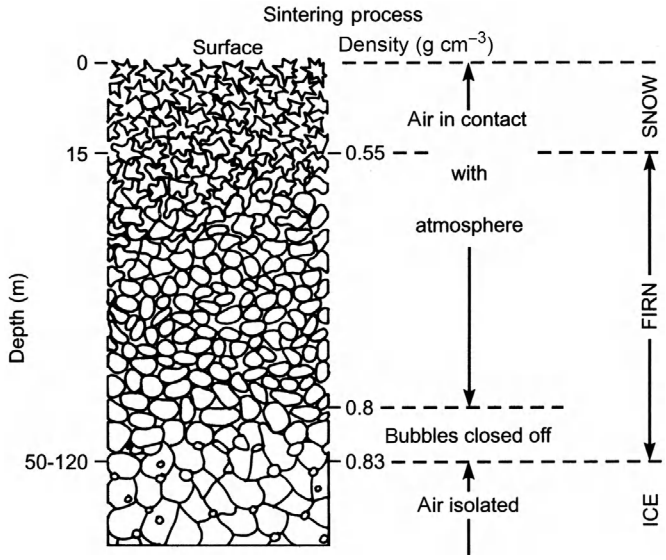


FIGURE 5.29 Schematic diagram illustrating how air is trapped in firn and ice during the process of sintering or recrystallization of snow crystals. Depending on the accumulation rate, "pore close-off" (complete isolation of air bubbles) may take up to 2500 years; this time will have varied in the past with changes in accumulation rate (see Figure 5.31). *From Raynaud (1992).*

gases—carbon dioxide, methane, and nitrous oxide (Raynaud et al., 1993). However, the air in ice bubbles is always younger than the age of the surrounding ice (Schwander and Stauffer, 1984). This is because, as snow is buried by later snowfalls and slowly becomes transformed to firn and ice, the air between the snow crystals remains in contact with the atmosphere until the bubbles or pores of air become sealed at the firn-ice transition (the "lock-in depth," LID). The sealed bubbles thus contain air that is representative of atmospheric conditions long after the time of deposition of the enclosing ice (Figure 5.29). Furthermore, since not all pores in a given stratum become sealed at the same time (perhaps closing over a period of ~50 years at Dye-3 but ~500 years at Vostok, for example), the air bubble gas record should be considered a "low-pass" filtered record, with each sample representative of gas concentrations over several tens to several hundreds of years. The highest-resolution records should therefore be found in high-accumulation-rate areas where snow is buried quickly and pore close-off is rapid. Such conditions tend to be found in warmer polar environments such as southern Greenland or in the more maritime sections of Antarctica.

Determining how the timescale of the gas record differs from that of the enclosing ice matrix is very important, or it will not be possible to tell how the two records varied with respect to each other. This becomes critical when estimating whether changes in CO_2 and other greenhouse gases were in phase with the temperature (δD) record (and thus could be considered primary forcing factors) or if they lagged behind and were thus only responding to changes in temperature that were driven by other forcing factors. However, as already noted, the timing of the lock-in depth is a complex function of the accumulation rate and temperature prevailing during the firn densification process, and finding the correct solution to determine the time difference between ice age and gas age (Δ-age) is not easy (Capron et al., 2013). The general principle that Δ-age is inversely related to temperature and accumulation rate is illustrated in Figure 5.30, but this must be considered as a model with large uncertainties (Blunier et al., 2007). For example, there is evidence that when the ice contained large

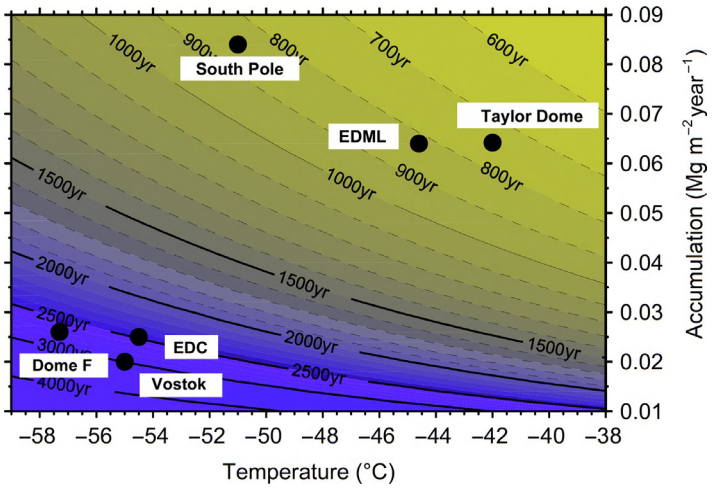


FIGURE 5.30 Δ-age (ice age-gas age) as a function of temperature and accumulation rate, based on a firn densification model. Black dots show modern conditions for several Antarctic ice core sites. Note that most Greenland sites would be off the diagram at the top right, and so, the Δ-age there (today) is considerably lower. *From Blunier et al. (2007).*

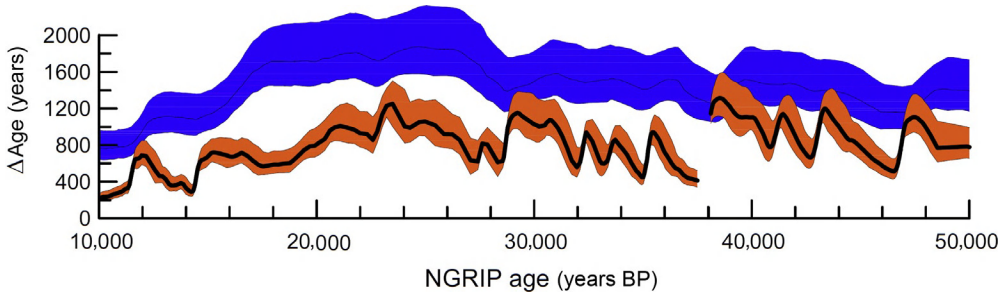


FIGURE 5.31 Estimates of Δ-age (ice age-gas age) for the last 50,000 years, for EPICA DML and NGRIP/GRIP (NGRIP before 38,000), based on the model represented in Figure 5.29. The uncertainty envelope on each record corresponds to an uncertainty of ±25% in accumulation rate or ±2% in absolute temperature. *From Blunier et al. (2007).*

amounts of impurities (as in glacial times), densification was more rapid, which would mean that estimates of the lock-in depth during glacial conditions based on modern conditions (Figure 5.31) would overestimate the value of Δ-age (Hörhold et al., 2012). Furthermore, as both temperature and accumulation have changed continually over time, so too has Δ-age, making the challenge of aligning the changes in greenhouse gases and temperature all the greater. Nevertheless, it is clear that the age differences between the isotopic record and the gas record in the ice have varied considerably: at GRIP, from ~200 years in the Holocene to as much as 2000 years during the low accumulation stadial periods, and at Vostok, from ~2500 to >5000 years (Barnola et al., 1991; Sowers et al., 1992).

In Greenland, it has been possible to directly compare the timing of abrupt changes in temperature to changes in CH_4, using changes in $\delta^{15}N$ (in gas bubbles from the same position in the ice core) as a paleotemperature indicator. When warming abruptly occurred, a temperature gradient became established in the firn, which caused the heavier isotopes of nitrogen in the air to settle to the lower layers of the firn, so that ^{15}N became enriched at pore close-off

relative to ^{14}N. With this differential locked into the ice-core record, the magnitude of the temperature change compared to any corresponding change in CH_4 can be directly compared. In the NGRIP ice core, this shows that changes in temperature and CH_4 were closely synchronized, with CH_4 only lagging behind the temperature changes by a few decades (Figure 5.20) (Huber et al., 2006). In Antarctica, it has been more challenging to obtain temperature estimates directly from $\delta^{15}N$, and so, the timing of isotopic changes relative to temperature has generally relied on using δD for paleotemperature and making appropriate adjustments for Δ-age. This approach indicated that CO_2 changes generally lagged behind the orbitally driven changes in temperature, by $\leq$800 years at termination I (e.g., Monnin et al., 2001; Loulergue et al., 2007). However, an analysis of $\delta^{15}N$ across the termination I transition suggests that there is a more direct connection between CO_2 and temperature, with essentially no lag (Parrenin et al., 2013). This is an important difference, in that it would point to CO_2 being either a direct driver of temperature changes in the Antarctic or more of a positive feedback. Further research is needed to resolve the argument, though a global stack of proxy records shows that temperature changes in Antarctica were slightly ahead of the global mean response at termination I, with a somewhat delayed increase in CO_2, resulting from degassing of the Southern Ocean as sea ice declined around Antarctica (Shakun et al., 2012).

5.4.4 Greenhouse Gas Records in Ice Cores

Instrumental measurements of greenhouse gases have a relatively brief history, generally providing a perspective on current gas concentrations of less than 60 years. These measurements reveal dramatic increases in CH_4, CO_2, N_2O, and industrial chlorofluorocarbons. Over the same period, levels of heavy metals such as lead and vanadium—as well as anthropogenic black carbon, sulfate and nitrate—also increased dramatically (though atmospheric pollution levels have declined in recent years due to clean air legislation in many countries) (Stauffer and Neftel, 1988; Mayewski et al., 1992; McConnell et al., 2007; McConnell and Edwards, 2008). Ice cores enable the short instrumental records of these contaminants to be placed in a longer-term perspective, providing some measure of the background, preindustrial levels, which prevailed before global-scale anthropogenic effects became important (e.g., Etheridge et al., 1996; Raynaud et al., 2003). Figure 5.32 shows the concentration of CH_4, N_2O, and CO_2 in Antarctic ice cores over the last 1000 years, together with recent atmospheric measurements. In 2013, CH_4 and CO_2 concentrations had reached 270% and 140% of their preindustrial levels, respectively, and N_2O was 120% of what it was 250 years ago. Collectively, these data unequivocally document the dramatic increases in greenhouse gases over the last ~200 years, to levels that are far higher than anything seen in records spanning the last 800,000 years (although older records cannot provide the same time resolution of more recent ice cores). In that regard, it is interesting to speculate on how the twentieth-century rapid rise in CO_2 would be preserved in the Vostok (low accumulation) ice core, if anthropogenic emissions were to miraculously drop to zero (Figure 5.33). Because of diffusion through the firn prior to pore close-off, the maximum level of CO_2 would not be recorded and a more smoothed record would be preserved. This effect would be less in sites where accumulation rates are higher. Of course, there is no expectation that CO_2 levels ever underwent a rapid increase in the past, analogous to the anthropogenic increase of the twentieth century, but

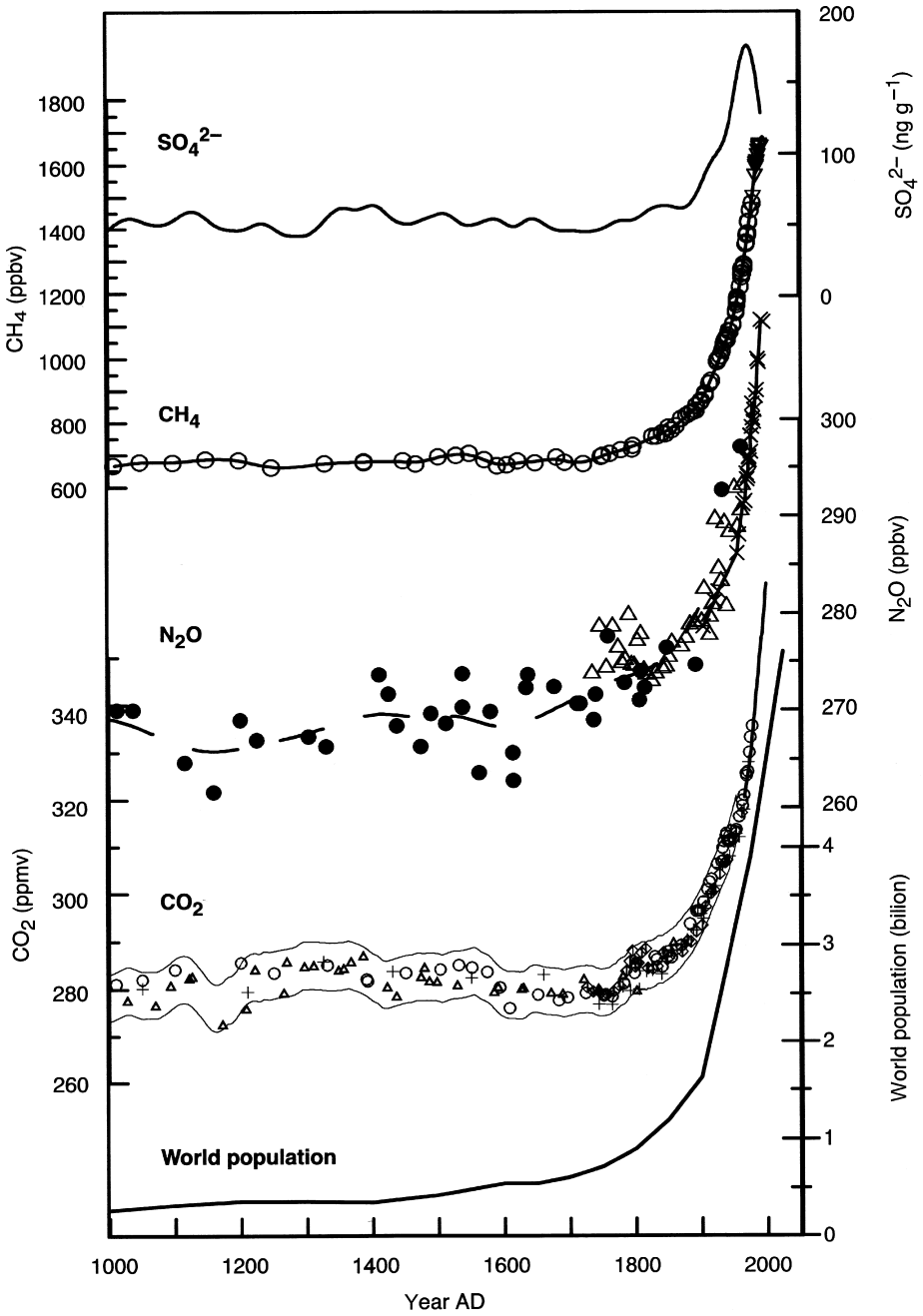


FIGURE 5.32 Ice-core records of CO_2, N_2O, and CH_4 (from high-accumulation-rate Antarctic ice cores) together with SO_4^{2-} from Greenland. Recent instrumental measurements (spanning the last few decades) have been patched on to the ice-core data. The recent decline in SO_4^{2-} is due to clean air legislation in many countries, but all of the greenhouse gases show accelerating increases, more or less coincident with the growth of world population (lower line). *From Raynaud et al. (2003).*

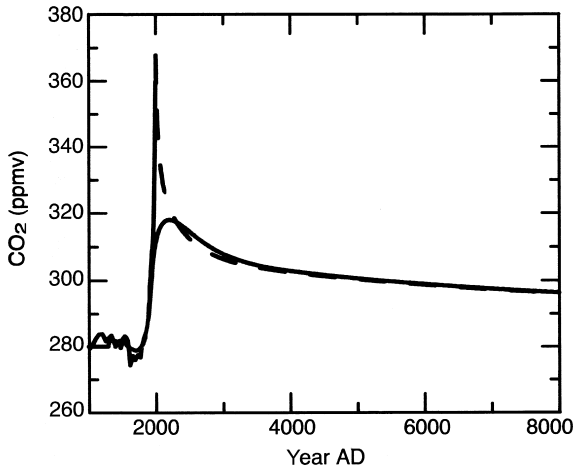


FIGURE 5.33 Hypothetical changes in the CO_2 content of an ice core from Vostok, Antarctica, assuming all anthropogenic CO_2 emissions ceased in the year 2000. Although the actual peak of CO_2 in the atmosphere reached ~370 ppmv in this example, an ice-core record recovered in the future would only register a CO_2 maximum of ~320 ppmv because of diffusion between air in the firn and air in the atmosphere before the gas bubbles become sealed off. The precise magnitude and timing of the changes depend on assumptions about the carbon cycle, the accumulation rate, and the firn densification process, but the general shape will remain the same. *From Raynaud et al. (2003).*

there has been speculation that sudden releases of CH_4 from submarine clathrate deposits may have occurred, and any signal of such changes would likely be dampened in ice-core records.

Figure 5.24 shows the CO_2 and CH_4 records over the last 800,000 years from EPICA Dome C, in comparison with the estimated temperature change in the atmosphere (above the surface inversion) derived from δD, taking into account the air-ice age difference and its changes with depth (Jouzel et al., 1993). It is clear that there is a very high correlation between the records of temperature, CO_2, and CH_4 (Loulerge et al., 2008; Lüthi et al., 2008). During glacial times, CO_2 levels were around 180-190 ppmv (with a minimum of 172 ppmv at 667 ka BP) compared to recent interglacial levels of 280 ppmv (though prior to ~450 ka BP, interglacial CO_2 levels were lower, ~240-250 ppmv). CH_4 levels were around 350-400 ppbv in glacial times versus ~700 ppbv at the height of past interglacials, changing very abruptly at each termination. The long-term record of CH_4 is broadly similar to that of CO_2 in the sense of large glacial-interglacial changes, but some important differences are nevertheless apparent (Figure 5.24). Whereas CO_2 levels slowly declined from interglacial levels to glacial minima, methane levels were generally more variable during interstadial times (Chappellaz et al., 1990; Brook et al., 1996). This reflects the fact that the primary driving forces for CO_2 and CH_4 are different. Atmospheric CO_2 levels are largely the result of oceanic changes, whereas there is relatively little CH_4 dissolved in the ocean and atmospheric levels are driven by changes in source areas on the continents. In particular, the extent of wetlands in the tropics (but also at high latitudes of the northern hemisphere) is of critical importance to CH_4 levels in the atmosphere. This points to the significance of monsoon circulations and their influence on the extent of low-latitude wetland areas over glacial-interglacial cycles (Petit-Maire et al., 1991). Taking into account that CH_4 is removed from the atmosphere by hydroxyl ion (OH^-) oxidation in the atmosphere and that it is likely that such a sink was more effective during warmer interglacial times (with more abundant water vapor in the atmosphere and more volatile organics released from forests), Raynaud et al. (1988) estimated that the global emissions of CH_4 increased by a factor of 2.3 from glacial to interglacial times. This compares with an observed increase (in the ice-core record) of 1.8. Such an increase probably resulted

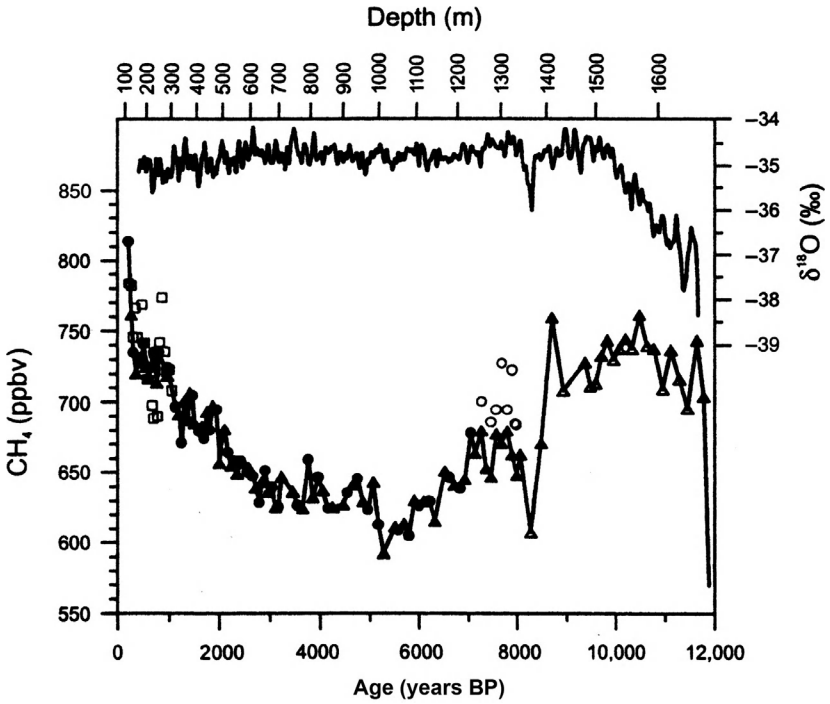


FIGURE 5.34 Methane levels in the GRIP ice core (Summit, Greenland) during the last 12,000 years. A pronounced drop in $\delta^{18}O$ at ~8250 (cal. years) BP corresponds to a sudden reduction in CH_4. The decline in CH_4 to ~5200 BP is related to a reduction in tropical wetlands. The subsequent CH_4 increase is ascribed to high-latitude peatland expansion. *From Blunier et al. (1995).*

from more extensive tropical wetlands and attendant anaerobic bacterial methanogenesis and from higher rates of bacterial activity in high-latitude peatlands during interglacials. Support for this hypothesis comes from detailed CH_4 measurements spanning the Holocene period in the GRIP (Summit) ice core from Greenland (Blunier et al., 1995). Methane levels reached a minimum of ~590 ppbv at 5200 years BP compared to Early and Late Holocene levels around 730 ppbv (Figure 5.34). This decline in CH_4 levels from the Early to Mid-Holocene corresponds to the well-recognized reduction in area of tropical wetlands over this interval with maximum aridity around 5000-6000 years BP (Street-Perrott and Perrott, 1993). By comparing the CH_4 record from ice cores in both polar regions, Chappellaz et al. (1997) were able to examine the interpolar gradient in methane concentration through time. This revealed that the Late Holocene rise in CH_4 levels was most probably due to the growth of high-latitude peatlands, while tropical regions remained relatively dry during this period.

Long-term changes in nitrous oxide (N_2O), another greenhouse gas, have also been determined from air bubbles in ice cores (Leuenberger and Siegenthaler, 1992; Sowers et al., 2003; Wolff and Spahni, 2007). As with CO_2 and CH_4, N_2O levels were also much lower in glacial times, ~30% lower than levels in the Holocene (~190 vs. ~265 ppbv). Lower atmospheric N_2O concentration probably resulted from a reduction in the production rate in the oceans

and in soils during glacial periods when the global terrestrial biomass was significantly reduced (estimated reductions range from ~20% to 60% of preindustrial conditions). N_2O also varied more or less synchronously with CH_4 on millennial timescales.

Spectral analysis of the isotopic data in Antarctic ice cores shows that variance is concentrated in the ~100, ~41, and, to a lesser extent, ~23 ka frequency bands, clearly reflecting the influence of orbital forcing (Petit et al., 1999; Jouzel et al., 2007b). In particular, in the temperature record from Vostok and EDC, there is strong power at 41 ka, which is coherent with insolation at 65°N (though see the discussion in Chapter 6, Section 6.3.4). This is also true for CO_2, but CH_4 has more variance in the precessional frequencies, reflecting the predominantly tropical source regions for that gas (Figure 5.35). The record of $\delta^{18}O_{ATM}$ ($\delta^{18}O$ of the air in gas bubbles, rather than in the ice itself) also has more variance in the precessional frequencies. $\delta^{18}O_{ATM}$ in the atmosphere today is +23.5‰ (relative to SMOW), a result of the balance between the fractionation that occurs during photosynthesis and that which occurs during respiration (the "Dole effect") (Bender et al., 1985; Sowers et al., 1991, 1993). $\delta^{18}O$ in the ocean

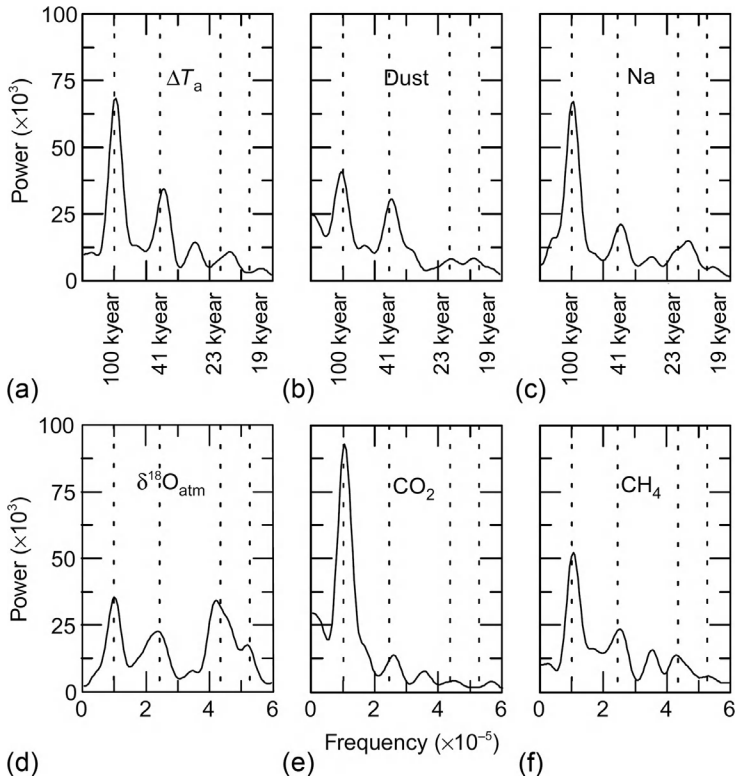


FIGURE 5.35 Spectral properties of different parameters measured on the Vostok ice core, spanning the last 420 ka (Blackman-Tukey method). (a) Air temperature (derived from δD); (b) dust; (c) Na^+ (from sea salt); (d) $\delta^{18}O$ of the atmosphere in gas bubbles; (e) CO_2; (f) CH_4. Dashed lines identify the principal frequencies associated with orbital forcing (from left to right): eccentricity (100 ka), obliquity (41 ka), and precession (23 and 19 ka). *From Petit et al. (1999).*

($\delta^{18}O_{SW}$) has changed over time due to removal of water relatively enriched in ^{16}O during times of continental ice buildup on the continents. Such changes are recorded in the $CaCO_3$ of benthic forams (see Chapter 6, Section 6.3.1). However, as the isotopic content of the ocean changed, so the oxygen isotope content of the atmosphere underwent parallel changes, since all photosynthetically derived oxygen was affected, directly or indirectly, by the changing oceanic isotopic composition (i.e., directly if the O_2 is produced by marine biota or indirectly if O_2 is produced by terrestrial biota, which are affected by isotopic changes in the hydrologic cycle). $\delta^{18}O_{ATM}$ from bubbles in the ice provides a direct measure of these changes, and the strong precessional signal in $\delta^{18}O_{ATM}$ reflects the particular importance of changes in the tropical biosphere over time.

Greenhouse gas changes are strongly correlated with temperature (δD) ($r^2 \sim 0.72$) and effectively amplified the orbitally forced changes (Genthon et al., 1987). It is possible to estimate the direct radiative effects of the glacial-interglacial changes in greenhouse gases on global temperature change from radiative-convective models; for CO_2, this is around 0.5 °C, for CH_4, 0.08 °C, and for N_2O, 0.12 °C (Leuenberger and Siegenthaler, 1992). However, the more important issue concerns the associated feedbacks, involving clouds, snow cover, sea ice, etc., which may have resulted from (and amplified) these changes. The overall (equilibrium) temperature change due to doubling of CO_2, including radiative effects and feedbacks, is referred to as the climate sensitivity and the amplification effect as the net feedback factor (f). General circulation model experiments lead to estimates of f in the range of 1-4 so that the direct radiative effects of a doubling of CO_2 levels will be increased by a factor of 1-4. Using the observed changes in greenhouse gases, dust, non-sea salt sulfate, and global ice volume, together with calculated orbitally induced changes in radiation, Lorius et al. (1990) attempted to account for the overall variance in Vostok temperature over the last glacial-interglacial cycle. Their analysis revealed that $50 \pm 10\%$ of the variance of the temperature record (~6 °C in the atmosphere above Vostok) is accounted for by greenhouse gas changes. If this figure can be applied to global glacial-interglacial temperature changes (estimated as ~4-5 °C; Rind and Peteet, 1985), then it suggests that changes in greenhouse gases were responsible for ~2 °C of the global temperature change over the last climatic cycle. Comparing this figure with the calculated direct radiative effect (0.7 °C) suggests a net feedback amplification value (f) of ~3. This is in line with model estimates, though at the high end of the general range. Possibly, this reflects a higher climate sensitivity in glacial times, when "slow feedbacks" associated with ice extent on land, and semipermanent sea ice and ice shelves, may have played a stronger role in amplifying the radiative forcing than they do at the present time.

5.4.5 Ice-Core Records from Low Latitudes

Ice caps are not confined to polar regions; they also occur at very high elevations in many mountainous regions, even near the equator (Thompson et al., 1984a; Francou and Vincent, 2011). High-elevation ice cores provide invaluable paleoenvironmental information to supplement and expand upon that obtained from polar regions (Figure 5.2 and Table 5.2). However, establishing the chronology of ice cores from low latitudes is very difficult, especially in the deeper sections. In general, accumulation rates are high, so the bulk of the ice recovered

only represents the last one or two millennia. The dating of older ice has relied on the identification of volcanic layers (such as the AD 1600 eruption of Huaynaputina in Peru) and correlation of isotopic features and/or gas content with polar ice cores or other paleoenvironmental records. This all leads to considerable uncertainty in low-latitude ice-core chronologies at depth. It is only at Sajama that a ^{14}C date of ~24 ka BP on organic material in the deepest section of the ice core provides a reliable marker in the LGM. Furthermore, thinning of the ice at depth means that the oldest sections are highly compressed. For example, in the Huascarán (Peru) and Illimani (Bolivia) ice cores (166 and 136.7 m in length, respectively), all of the pre-Holocene ice is in the lowest 2 m section, and so, it is not possible to determine in any detail the changes that occurred during that period (Thompson et al., 1995; Ramirez et al., 2003). Sajama provided more old ice at depth, so it has a more detailed LGM and late glacial record; it is also unique in that organic material (including an insect) was found in the ice at several levels, so that a chronology could be established, at least in part using radiocarbon dating (Figure 5.36). Radiocarbon dates were also obtained on organic debris in the ice core from Kilimanjaro's northern ice field, but these provided little guidance for the chronology as the resulting ages were not in stratigraphic order. Thompson et al. (2002) argued for a basal age of ~11,700 BP, based in part on a comparison with a speleothem isotopic record from Soreq Cave (Israel), but the chronology is quite uncertain and there may be discontinuities of unknown duration in the record.

In spite of these dating problems, the three long ice cores from South America provide important information about paleoclimate in the tropical Andes since the LGM (Figure 5.36) (Vimeux, 2009). LGM $\delta^{18}O$ values were more depleted by 4-6‰ relative to Holocene values, indicating that conditions at that time were wetter (assuming that the isotopes reflect an "amount effect," as shown in Figure 5.6). This finds confirmation in the more extensive playa lakes of the Altiplano and in speleothem records from Brazil, which all point to a more southerly mean position of the ITCZ and enhanced moisture flux from the Atlantic Ocean. In the Illimani and Huascarán cores, there was a shift to higher $\delta^{18}O$ beginning around 18 ka BP, which parallels changes seen in the EPICA Dome C record, with a reversal occurring after AIM1 at ~15 ka BP. At Sajama, the change to heavier isotopes is later and more abrupt; it is not clear whether such a change also occurred at Illimani and Huascarán, but if so, that detail has been lost by smoothing at depth in those highly compressed records. In any case, this change signifies a shift to drier conditions, as confirmed by an increase in Cl^- and dust in Sajama ice at that time. This may indicate that the ITCZ shifted north, before returning once again to a more southerly position during the Younger Dryas interval, when $\delta^{18}O$ once again became lower in the Andean ice cores. Finally, the Early Holocene was characterized by dry conditions and high values of $\delta^{18}O$ at Huascaran and Illimani, gradually becoming wetter in the Late Holocene. This contrasts with Sajama where the development of extensive playas in the Late Holocene led to high levels of dust reaching the ice cap.

In the Guliya ice core, from the western Qinghai-Tibetan Plateau, the ^{36}Cl profile in the core indicates that the oldest section of the record (below 300 m) may be >500,000 years old (Thompson et al., 1997). Much of the ice appears to date from the last glaciation, so details of conditions in this area at that time can be resolved in considerable detail (Thompson et al., 1997). The long-term record reveals several stadial-interstadial oscillations since the last interglacial (Figure 5.37) with $\delta^{18}O$ values in the interstadials reaching Holocene levels,

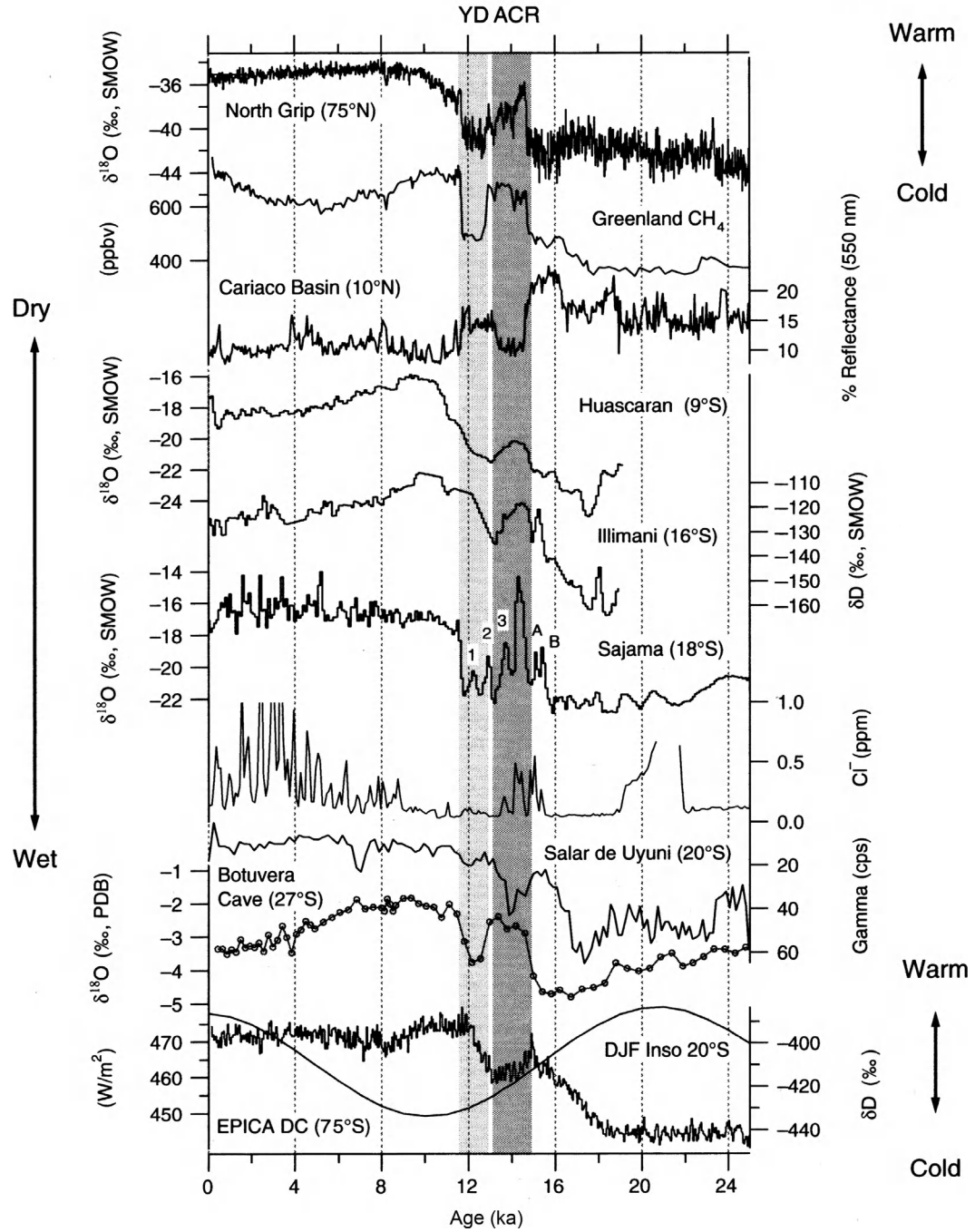


FIGURE 5.36 Records of $\delta^{18}O$ in the Huascarán (Peru) ice core, δD in Illimani (Bolivia) & $\delta^{18}O$ in Sajama (Bolivia) compared to other environmental records over the past 25,000 years: (above) NGRIP $\delta^{18}O$; Greenland CH_4; Cariaco Basin sediment reflectance. (below): chloride from Sajama ice; gamma density from the Salar de Uyuni playa lake basin sediment cores; Botuvera (Brazil) speleothem oxygen isotopes; EPICA Dome C δD, and December-February insolation at 20°S. The general interpretation of each proxy is indicated by the arrows on the left and right. The Sajama record has more ice in the LGM and late glacial section than the other tropical ice cores, and so the record is more detailed. *From Vimeux (2009).*

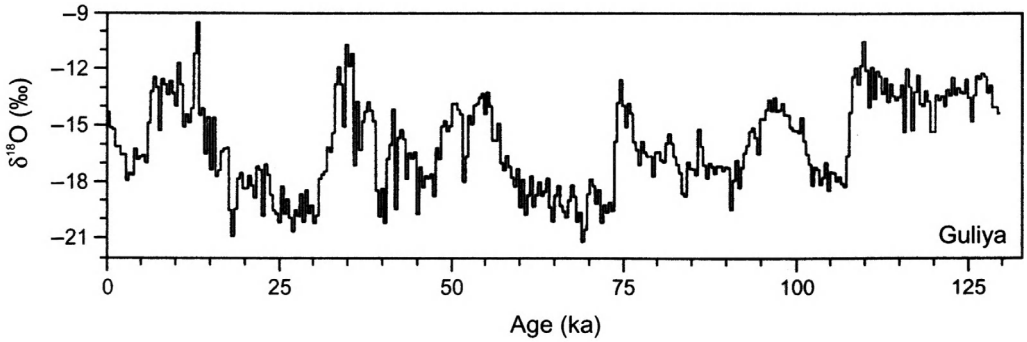


FIGURE 5.37 $\delta^{18}O$ in an ice core from Guliya Ice Cap, western Tibet (~35°N, 81°E). The 308m record was dated by correlating the CH_4 record from Vostok and GISP2 with the oscillations of $\delta^{18}O$. This assumes that the factors causing changes in $\delta^{18}O$ at Guliya would increase and decrease in phase with CH_4 (which is likely to be driven by low-latitude climatic changes). *From Thompson et al. (1997).*

around −13‰. Abrupt, high-amplitude changes in $\delta^{18}O$ occurred from ~15 to 33 ka BP, with an average length of ~200 years. These oscillations are much shorter than the Dansgaard-Oeschger oscillations seen in GISP2 and are associated with higher levels of dust, NH_4, and nitrate during higher $\delta^{18}O$ episodes (the opposite of what is seen in Greenland). This may indicate that warmer episodes occurred throughout the glacial stade, associated with less snow cover and more vegetation on the plateau.

In many ice cores from low latitudes, strong seasonal changes in dust and isotopes enable very reliable chronologies to be established for recent centuries by counting annual layers. For example, in the Quelccaya summit core (Cordillera Vilcanota, Peru: 168.68 m in length), dust levels increase in the dry season (June-September) when $\delta^{18}O$ values and conductivity levels are highest, providing a strong annual signal to a depth of 160m (AD 683 ± 5 years). A prominent conductivity peak resulting from a major eruption of the Peruvian volcano Huaynaputina (in February-March, 1600) provides an excellent chronostratigraphic check on the annual layer counts. No other ice core from the tropics has provided such a clear and detailed chronology (Thompson et al., 1986, 2013). $\delta^{18}O$ over the last 1000 years shows distinct variations in the Quelccaya core, with the lowest values from AD 1530 to 1900 (Figure 5.38). This corresponds to the "Little Ice Age" observed in many other parts of the world. Accumulation was well above average for part of this time (1530-1700) but then fell to levels more typical of the preceding 500 years. Accumulation was also slightly above the long-term mean from AD ~600 to 1000. Archeological evidence shows that there was an expansion of highland cultural groups at that time. By contrast, during the subsequent dry episode in the mountains (AD ~1040-1490), highland groups declined, while cultural groups in coastal Peru and Ecuador expanded (Thompson et al., 1988). This may reflect longer-term evidence for conditions that are common in El Niño years, when coastal areas are wet at the same time as the highlands of southern Peru are dry. Indeed, the Quelccaya record shows that El Niños are generally associated with low accumulation years (Thompson et al., 1984b). Figure 5.39 shows the correlation field between $\delta^{18}O$ at Quelccaya (1870-2009) and SSTs over the Pacific. This shows clearly that there is a strong imprint of ENSO variability on the isotopic record at Quelccaya, a point also noted by

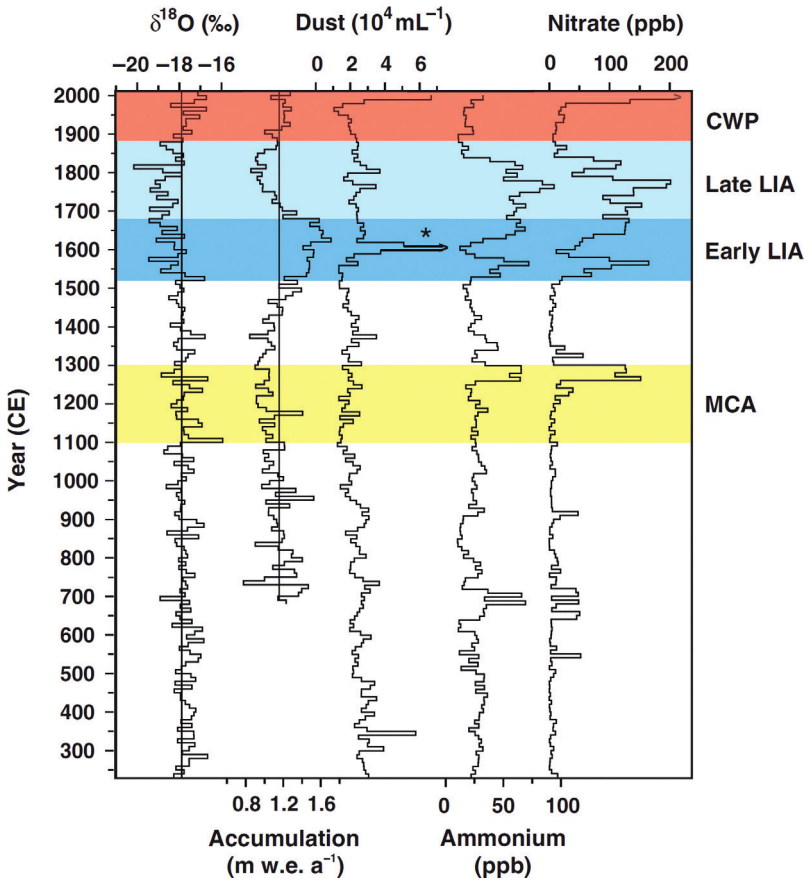


FIGURE 5.38 The record of $\delta^{18}O$, net accumulation, dust, NH_4 and NO_3 from the Quelccaya Ice Cap, southern Peru. The star on the dust profile indicates the eruption of Huaynaputina (Peru) in A.D 1600. m w.e. a^{-1}= meters of water equivalent per year. *From Thompson et al. (2013).*

Bradley et al. (2003b) and Francou et al. (2004) for Sajama Ice Cap (Bolivia) and Ecuadorian glaciers, respectively. This led Thompson to use the $\delta^{18}O$/SST regression to reconstruct Niño4 region SSTs over the last ~1500 years, which indicates that SSTs have rarely been higher than in recent years and that SSTs were 0.3-0.4 °C cooler during the Little Ice Age than in recent decades (Figure 5.39).

High-altitude regions of the tropics have experienced significant increases in temperature over the last few decades, resulting in glaciers and ice caps disappearing altogether in some places (Francou et al., 2003; Vuille et al., 2008; Braun and Bezada, 2013). At the Quelccaya Ice Cap, temperatures in the last 20 years have increased to the point that by the early 1990s, occasional surface melting had reached the Summit core site (5670 m) obscuring the detailed $\delta^{18}O$ profile that was clearly visible in cores recovered in 1976 and 1983 (Thompson et al., 1993). In the entire 1800-year record from Quelccaya, there is no comparable evidence for such melting at the Summit site. Ice cores from the Gregoriev Ice Cap (in the Pamirs) and Guliya and

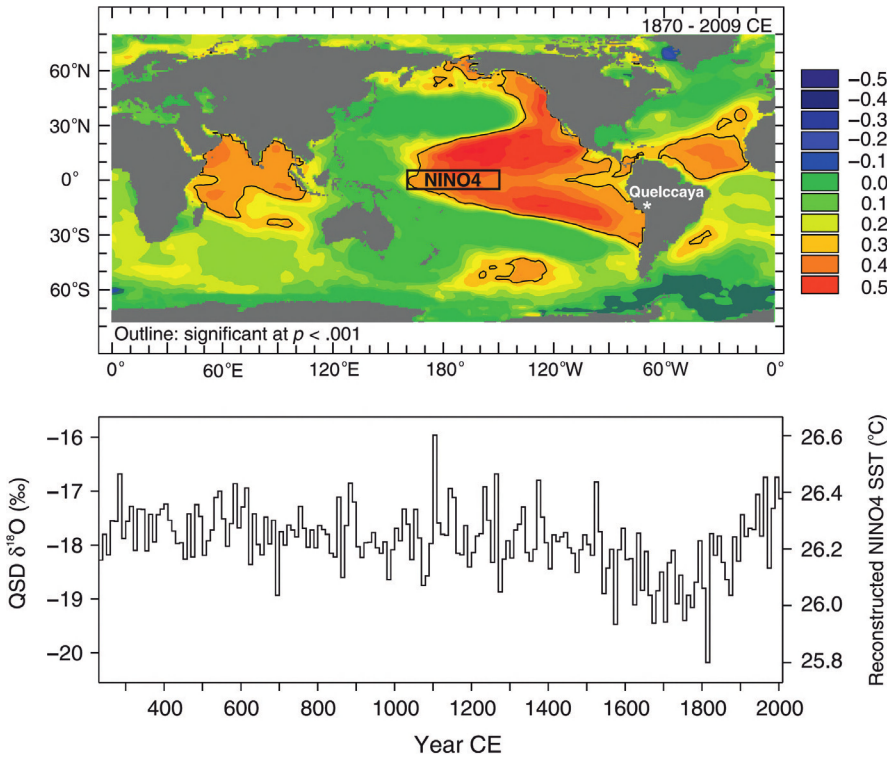


FIGURE 5.39 Map of the correlation field between $\delta^{18}O$ in the Quelccaya Summit Dome ice core and SSTs (1870-2009). This pattern shows the strong imprint of ENSO variability on the isotopic composition of the ice. The lower diagram shows reconstructed SSTs in the Niño4 area (see box on map) over the last ~1500 years, based on the $\delta^{18}O$/SST regression equation. Although the spatial correlation pattern has not remained fixed in time, the general relationship between ENSO and $\delta^{18}O$ has remained strong. The reconstruction indicates that SSTs have rarely been warmer than in recent decades, and that SSTs were persistently below average during the Little Ice Age. *From Thompson et al. (2013).*

Dundee, western China, also show evidence of recent warming (Lin et al., 1995; Yao et al., 1995). On the northern ice field of Kilimanjaro, ablation has lowered the surface by several meters over the last decade, so that ice at the surface now dates from the nineteenth century or earlier (Hardy, 2011). These records, plus other evidence from short ice cores at high-elevation sites in Africa and New Guinea (e.g., Hastenrath and Kruss, 1992), demonstrate the dramatic nature of climatic change in recent decades, prompting concern over the potential loss of these unique archives of tropical paleoenvironmental history (Thompson et al., 1993, 2006).

CHAPTER

6

Marine Sediments

OUTLINE

6.1 Introduction 196

6.2 Paleoclimatic Information from Biological Material in Ocean Cores 197

6.3 Oxygen Isotope Studies of Calcareous Marine Fauna 199
6.3.1 *Isotopic Composition of the Oceans* 201
6.3.2 *Oxygen Isotope Stratigraphy* 211
6.3.3 *Orbital Tuning* 215
6.3.4 *Orbital Forcing: Evidence from the Marine Record* 220
6.3.5 *Sea-Level Changes and $\delta^{18}O$* 222

6.4 Paleotemperatures from Relative Abundance Studies 225

6.5 Paleotemperature Reconstruction from Sediment Geochemistry 228
6.5.1 *Paleotemperatures from Alkenones* 228
6.5.2 *Paleotemperatures from TEX_{86} and Long-Chain Diols* 231
6.5.3 *IP_{25} and Related Sea-Ice Proxies* 234
6.5.4 *Paleotemperatures from Mg/Ca Ratios* 238

6.6 Oceanographic Conditions at the Last Glacial Maximum (LGM) 239

6.7 Paleoclimatic Information from Inorganic Material in Marine Sediments 244

6.8 Thermohaline Circulation of the Oceans 248
6.8.1 *Tracers in the Ocean* 252

6.9 Changes in Atmospheric Carbon Dioxide: The Role of the Oceans 258

6.10 Abrupt Climate Changes 263
6.10.1 *Heinrich Events* 267

Copyright © 2015 Raymond S. Bradley.
Published by Elsevier Inc. All rights reserved.

6.1 INTRODUCTION

Occupying more than 70% of the Earth's surface, the oceans are a very important source of paleoclimatic information. Between 6 and 11 billion metric tons of sediment accumulate in the ocean basins annually, and this provides an archive of climatic conditions near the ocean surface or on the adjacent continents. Sediments are composed of both biogenic and terrigenous materials (Figure 6.1). The biogenic component includes the remains of planktic (near surface-dwelling) and benthic (bottom-dwelling) organisms, which provide a record of past climate and oceanic circulation, in terms of surface water temperature and salinity, dissolved oxygen in deep water, nutrient or trace element concentrations, etc. (Gooday, 2003; Jorissen et al., 2007; Kucera, 2007; Rosenthal, 2007). By contrast, the nature and abundance of terrigenous material mainly provide a record of humidity-aridity variations on the continents, or the intensity and direction of winds blowing from land areas to the oceans, and other modes of sediment transport to, and within, the oceans (fluvial erosion, ice-rafting, turbidity currents, etc.). Marine sediments also contain biomarkers (organic molecules derived from terrestrial or marine organisms), which can be useful proxies of paleoceanographic conditions or of paleoenvironmental conditions on the adjacent continents (Rosell-Melé and McClymont, 2007; Eglinton and Eglinton, 2008; Gaines et al., 2009).

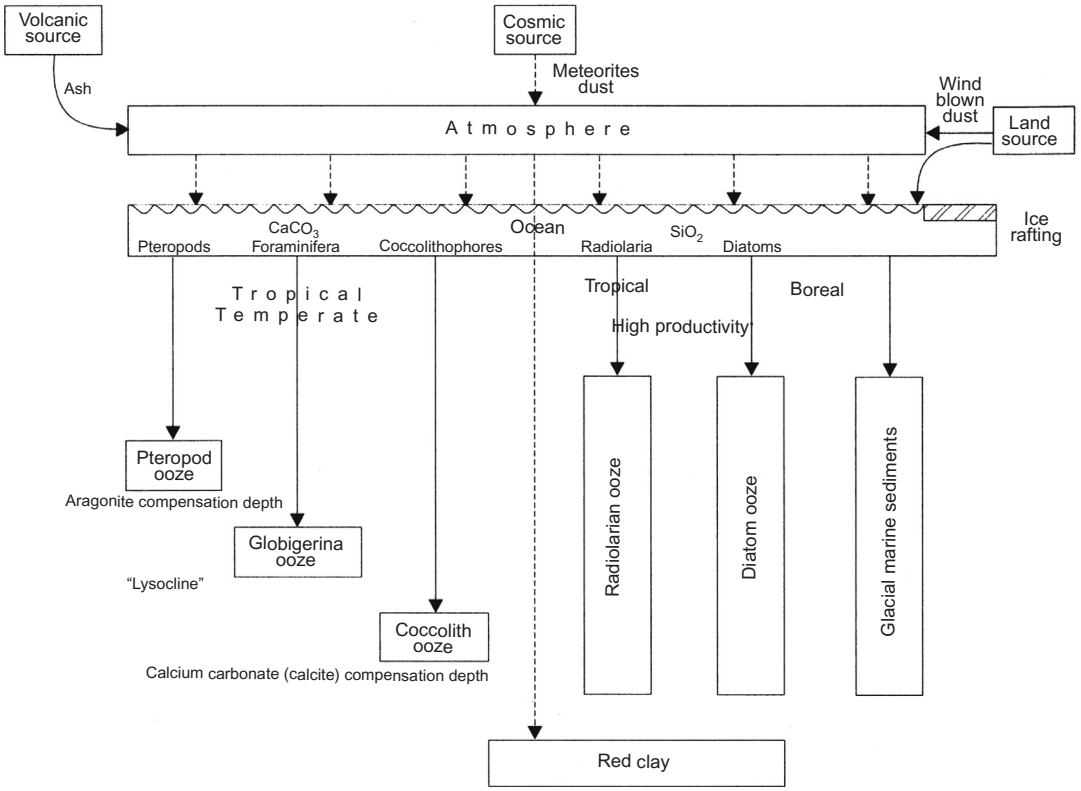


FIGURE 6.1 Pelagic sedimentation in the ocean. *After Hay (1974).*

6.2 PALEOCLIMATIC INFORMATION FROM BIOLOGICAL MATERIAL IN OCEAN CORES

Paleoclimatic inferences from biogenic material in ocean sediments derive from assemblages of dead organisms (thanatocoenoses), which make up the bulk of all but the deepest of deep-sea sediments (biogenic ooze). However, thanatocoenoses are generally not directly representative of the biocoenoses (assemblages of living organisms) in the overlying water column. Selective dissolution of thin-walled specimens at depth (see Section 6.3.1), differential removal of easily transported species by scouring bottom currents, and occasional contamination by exotic species transported over long distances by large-scale ocean currents all contribute elements of uncertainty. Because of these problems, sediments over much of the ocean floor are unsuitable for paleoclimatic reconstruction. This is illustrated in Figure 6.2 for foraminiferal studies (Ruddiman, 1977) though it should be noted that in many areas unsuitable for foraminiferal preservation, the remains of other organisms, such as diatoms or radiolarians, may provide a useful record (e.g., Sancetta, 1979; Pichon et al., 1992; Pisias et al., 1997; Crosta and Koç, 2007).

Biogenic oozes are primarily made up of the calcareous or siliceous skeletons (tests) of marine organisms. These may have been planktic (passively floating organisms living near the surface (0-200 m)) or benthic (bottom-dwelling). For paleoclimatic purposes, the most important calcareous materials are the tests of foraminifera (a form of zooplankton) (Figure 6.3) and the much smaller tests, or test fragments, of coccolithophores (unicellular algae) known informally as coccoliths. These are sometimes grouped with other minute forms

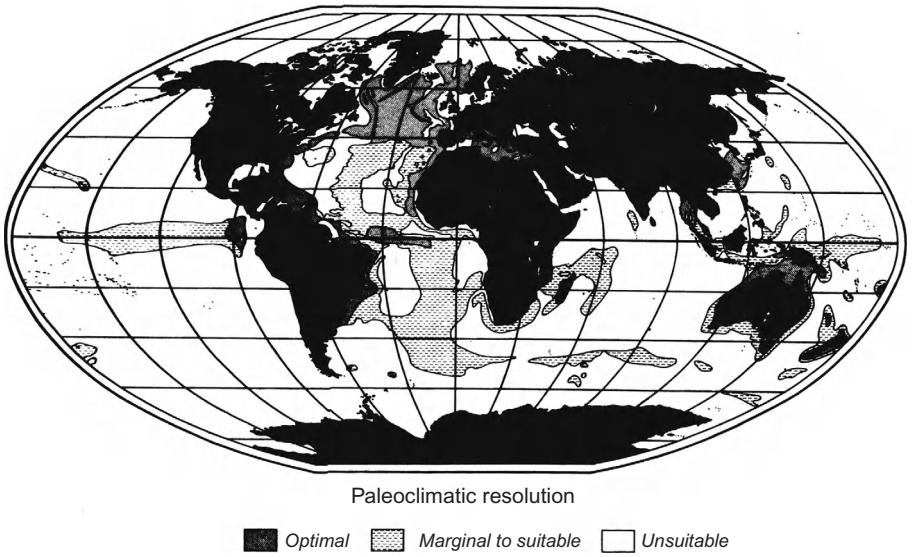


FIGURE 6.2 Regions considered to be optimal, marginally suitable, and unsuitable for accurate and detailed Quaternary paleoclimatological studies based on foraminifera. Recent cruises of the IMAGES project have targeted sites with high deposition rates on the continental shelves. Cores recovered from many of these sites provide very detailed records of past conditions that are unattainable from the deep ocean. *After Ruddiman (1977a).*

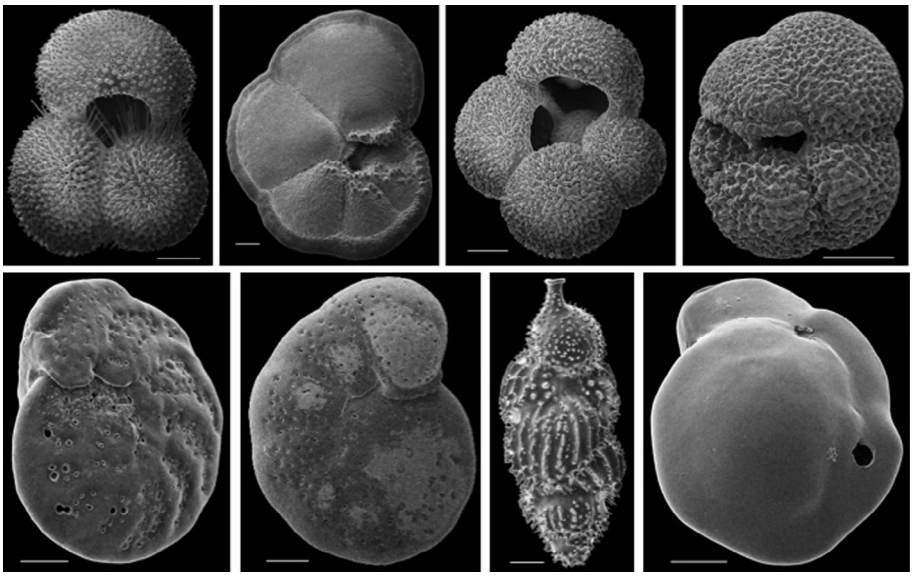


FIGURE 6.3 Some examples of planktic and benthic foraminifera that are commonly used in paleoceanographic research (left to right). Top row: tropical to subpolar planktic foraminifera (left to right): *Globigerinoides ruber*, *Globorotalia menardii*, *Globigerina bulloides*, *Neogloboquadrina incompta* (*also known as Neogloboquadrina pachyderma*, *dextral or right coiling*). Bottom row: deep-sea benthic foraminifera (left to right): *Planulina wuellerstorfi*, *Cibicidoides cicatricosus*, *Uvigerina peregrine*, *Oridorsalis umbonatus*. *Images kindly provided by Mark Leckie, University of Massachusetts.*

of calcareous fossils and referred to as calcareous nannoplankton (*nanno* = dwarf) or simply nannoliths (Haq, 1978). Organic-walled dinoflagellate cysts are another important paleoceanographic indicator of SSTs and sea ice extent in high-latitude regions (de Vernal et al., 2000, 2005; de Vernal and Marret, 2007). The most important siliceous materials are the remains of radiolarians (zooplankton), silicoflagellates, and diatoms (algae) (Haq and Boersma, 1978; Figure 6.4). By studying the morphology of the tests, individuals can often be identified to species level and their ocean floor distribution can then be related to environmental conditions (generally temperature and salinity) in the overlying water column (Figure 6.5). However, it should be noted that the species assemblage in the sediment is a composite of all the species living at different depths in the water column as well as species with only a seasonal distribution in that particular area. Phytoplankton, and zooplankton that possess symbiotic algae, are restricted to the euphotic (well-lit) zone, but some species live at different water depths at different times in their life cycles. Depth habitats are of particular significance to isotopic and geochemical studies of tests aimed at reconstructing sea-surface temperatures (SSTs). For example, oxygen isotope composition is a function of the water temperature (and to some extent salinity) at which the carbonate is secreted (Section 6.3). If test walls are secreted at varying depths through the lifespan of an individual, simple correlations with surface water temperatures and salinities may not be meaningful (Duplessy et al., 1981).

Paleoclimatic inferences from the remains of calcareous and siliceous organisms have resulted from basically four types of analyses: (a) oxygen isotopic composition, principally of calcium carbonate in foram tests (Mix, 1987; Ravelo and Hillaire-Marcel, 2007);

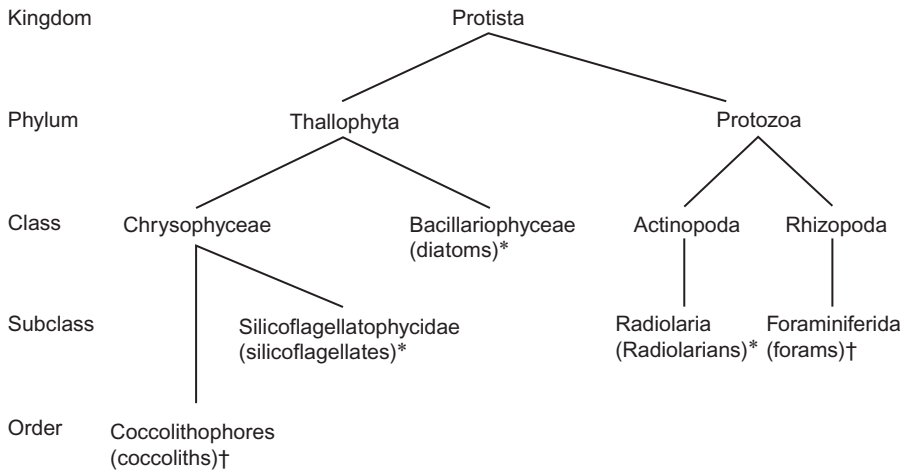


FIGURE 6.4 Taxonomic relationships of the main marine organisms used in paleoclimatic reconstructions. Asterisks indicate siliceous tests; the dagger indicates calcareous tests.

(b) quantitative interpretations of species assemblages and their spatial variations through time (Imbrie and Kipp, 1971; Molfino et al., 1982; Guiot and de Vernal, 2007); (c) Mg/Ca ratios in foram tests, which are related to temperature (Rosenthal, 2007), and (d) (of far less importance) morphological variations in a particular species resulting from environmental factors (ecophenotypic variations; Kennett, 1976; Kucera, 2007). Most of these studies have concentrated on the Foraminiferida (forams). In the following sections, therefore, the focus will be on foraminiferal studies. Paleoclimatic studies of coccoliths, radiolarians, diatoms, and silicoflagellates have mainly been in terms of changes in the relative abundance of assemblages (e.g., Pichon et al., 1992; Guiot and de Vernal, 2007) though isotopic studies of diatoms have also been carried out (e.g., Juillet-Leclerc and Labeyrie, 1987; Shemesh et al., 1992; Crosta and Koç, 2007). Oxygen isotope variations in coccoliths provide useful paleotemperature estimates and may provide even more reliable sea surface temperature data than those based on forams alone as coccoliths live exclusively in the photic zone (Margolis et al., 1975; Dudley and Goodney, 1979; Andersen and Steinmetz, 1981; Girardeau and Luc, 2007). However, there are problems in isolating sufficiently pure samples of very small microfossils such as coccoliths (or diatoms).

6.3 OXYGEN ISOTOPE STUDIES OF CALCAREOUS MARINE FAUNA

If calcium carbonate is crystallized slowly in water, ^{18}O is slightly concentrated in the calcium carbonate relative to that in the water. The process is temperature-dependent, with the concentrating effect diminishing as temperature increases. In a nutshell, this is the basis for a very important branch of paleoclimatic research—the analysis of oxygen isotopes in the calcareous tests of marine microfauna (principally foraminifera but also coccoliths). The approach was first enunciated by Urey (1947, 1948) who noted, "...if an animal deposits

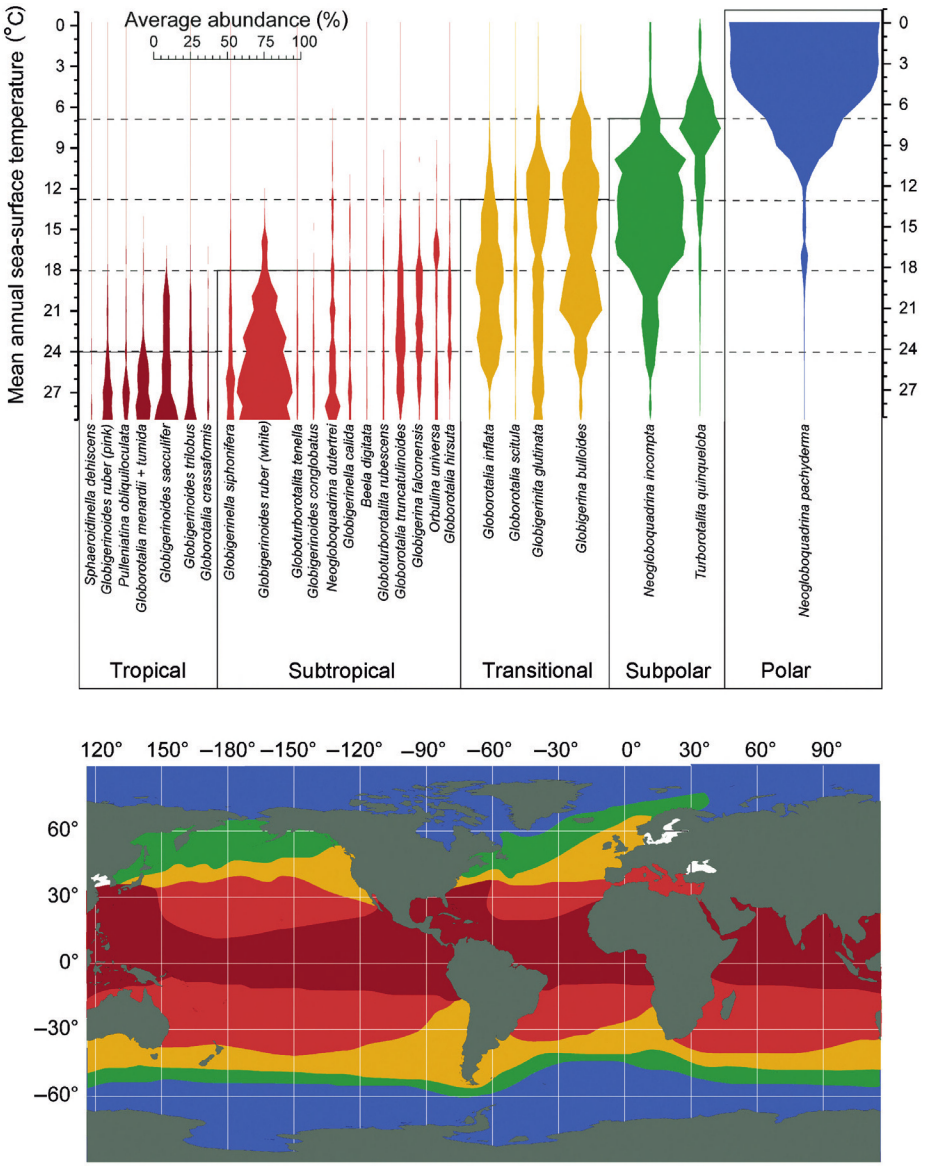


FIGURE 6.5 Examples of foraminiferal abundances in relation to SSTs (top) and distribution of the major foraminiferal provinces in the world ocean. *From Kucera (2007).*

calcium carbonate in equilibrium with the water in which it lies, and the shell sinks to the bottom of the sea. . .it is only necessary to determine the ratio of the isotopes of oxygen in the shell today in order to know the temperature at which the animal lived" (Urey, 1948). He then went on to calculate, from thermodynamic principles, the magnitude of this temperature-dependent isotopic fractionation (for equilibrium fractionation, there is a

~0.23% decrease in the $\delta^{18}O$ of calcite, for a 1 °C increase in temperature). Although the principle of Urey's argument is correct, the numerous complications that arise in the real world have made direct paleotemperature estimates rather problematical. In fact, the oxygen isotope record in marine sediments varies *locally* (with temperature and, to a lesser extent, salinity) and *globally* with variations in continental ice volume. This global signal is the single most important record of past climatic variations for the entire Cenozoic.

6.3.1 Isotopic Composition of the Oceans

The oxygen isotopic composition of a sample is generally expressed as a departure of the $^{18}O/^{16}O$ ratio from an arbitrary standard:[1]

$$\delta^{18}O = \frac{\left(^{18}O/^{16}O\right)_{\text{sample}} - \left(^{18}O/^{16}O\right)_{\text{standard}}}{\left(^{18}O/^{16}O\right)_{\text{standard}}} \times 10^3$$

The resulting values are expressed in per mil units (‰); negative values represent lower ratios in the sample (i.e., less ^{18}O than ^{16}O and therefore isotopically lighter) and positive values represent higher ratios in the sample (more ^{18}O than ^{16}O and therefore isotopically heavier).

Empirical studies relating the isotopic composition of calcium carbonate deposited by marine organisms to the temperature at the time of deposition have demonstrated a relationship that approximates the following:[2]

$$T = 16.9 - 4.38(\delta_c - \delta_w) + 0.10\,(\delta_c - \delta_w)^2$$

where T is water temperature in degrees Celsius, δ_c is the per mil difference between the sample carbonate and the SMOW standard, and δ_w is the per mil difference between the $\delta^{18}O$ of water in which the sample was precipitated and the SMOW standard (Epstein et al., 1953; Craig, 1965; Ravelo and Hillaire-Marcel, 2007).

For modern samples, δ_w can be measured directly in oceanic water samples; in fossil samples, however, the isotopic composition of the water is unknown and cannot be assumed to have been as it is at the site today. In particular, during glacial periods, the removal of isotopically light water from the oceans to form continental ice sheets (Chapter 5, Section 5.2) led to an increase in the $^{18}O/^{16}O$ ratio of the oceans as a whole by $\sim 1.0 \pm 0.10$‰ (equivalent to the mean isotopic composition of LGM ice sheets of −27‰; Lambeck and Chappell, 2001). Thus, the expected increase in δ_c of foraminiferal tests during glacial periods due to lower water temperatures is complicated by the increase in δ_w of the ocean water at these times. How much of the increase in δ_c is the result of variations in δ_w can be assessed by analyzing $\delta^{18}O$ in pore waters squeezed from sediments of last glacial age (Schrag and DePaulo, 1993; Adkins et al., 2002a) or in the tests of benthic (bottom-dwelling) foraminifera. Bottom

[1] See footnote 1, p.144; isotopic studies based on carbonate fossils use as a standard a Cretaceous belemnite from the PeeDee Formation of North Carolina (PDB-1) or a cross-referenced US National Bureau of Standards sample. Carbon dioxide released from PDB − 1 = +0.2‰ relative to CO_2 equilibrated with SMOW (Standard Mean Ocean Water) (Craig, 1961b).

[2] The precise form of the relationship depends on the particular technique used in analysis and on the temperature at which fractionation occurs (for further discussion, see Shackleton, 1974; Mix, 1987).

waters today (derived from cold, dense, polar water spreading through the deep ocean basins) are relatively close to the freezing point of seawater, so the bulk of the $\delta^{18}O$ increase in benthic forams in glacial times cannot be due to significantly lower temperatures; rather, the evidence indicates that at least 70% of the increase results from the changing isotopic composition of the oceans (Duplessy, 1978; Mix, 1987). Hence, the isotopic changes recorded in benthic foraminiferal tests are primarily a record of changing terrestrial ice volumes, or a "paleoglaciation" record (Shackleton, 1967; Dansgaard and Tauber, 1969). The benthic isotope record thus demonstrates that there have been more than 20 periods of major continental glaciation during the Quaternary, with the largest changes in ice volume (from glacials to interglacials) within the last 900,000 years (Shackleton et al., 1990; Lisiecki and Raymo, 2005). The record of changing $\delta^{18}O$ in relation to variations in continental ice volume (recorded in terms of eustatic sea level change) is discussed further in Section 6.3.5.

Changes in the isotopic composition of ocean water through time are not the only complications affecting a simple temperature interpretation of δ_c (Mix, 1987). Urey's initial hypothesis developed from a consideration of calcium carbonate precipitated inorganically, where the carbonate forms in isotopic equilibrium with the water. However, in the formation of carbonate tests by living organisms, metabolically produced carbon dioxide may be incorporated; in such cases, the carbonate would not be formed in isotopic equilibrium with the water, and the resulting isotopic composition would differ from the thermodynamically predicted value generally leading to $\delta^{18}O$ (and $\delta^{13}C$) lower than the expected equilibrium values (Duplessy et al., 1970; Shackleton et al., 1973; Vinot-Bertouille and Duplessy, 1973). This was termed the vital effect by Urey (1947). This effect differs from one species of foraminifera to another (Grossman, 1987). Modern samples of *Globigerinoides ruber*, for example, give isotopic values 0.5‰ lighter than expected from thermodynamic principles alone, which is equivalent to a temperature error of ~2.5 °C (Shackleton et al., 1973). On the other hand, not all forams exhibit this unfortunate characteristic. For example, samples of *Pulleniatina obliquiloculata* and *Uvigerina* spp. (benthic forams) appear to be in isotopic equilibrium with surrounding water (Shackleton, 1974). In other species, where isotopic equilibrium is not achieved, there is evidence that the vital effect remains constant over time (Duplessy et al., 1970). It is thus possible to circumvent this particular problem by careful selection of the species being studied or by assessing its specific vital effect and adjusting the measured isotopic values accordingly.

Another complication in calculating water temperatures from the isotopic composition of carbonate tests is the problem of variations in depth habitat of planktic foraminifera (Ravelo and Hillaire-Marcel, 2007). Even if the ice effect and vital effects are known, there is still some uncertainty as to whether foraminifera lived at the same depth from glacial to interglacial times. Water temperatures in the upper few hundred meters of the ocean change rapidly with depth, particularly outside the Tropics (Table 6.1), so small variations in depth habitat can be equivalent to a change in temperature of several degrees Celsius (i.e., a change perhaps as large as the glacial to interglacial change at the surface of the ocean). It is thus critical to know what factors control depth habitat of foraminifera and in particular the depths at which tests are secreted (Emiliani, 1971). Several studies have concluded that water density (a function of temperature and salinity; Figure 6.6) is of prime importance to individual species, since the same species may be found in different areas living at different depths but in water of the same temperature and salinity. During glacial periods, when the oceans were more saline (due to the removal of water to the continental ice sheets), foraminifera may have migrated

TABLE 6.1 Mean Vertical Temperature Distribution (°C) and Temperature Gradients in the Three Oceans Between 40°N and 40°S.

	Atlantic Ocean		Indian Ocean		Pacific Ocean		Mean	
Depth (m)	Temperature (°C)	Gradient (°C/ 100 m)	Temperature (°C)	Gradient (°C/ 100 m)	Temperature (°C)	Gradient (°C/ 100 m)	Temperature (°C)	Gradient (°C/ 100 m)
0	20.0		22.2		21.8		21.3	
		2.2		3.3		3.1		2.8
100	17.8		18.9		18.7		18.5	
		4.4		4.7[a]		4.4[a]		4.5[a]
200	13.4		14.3		14.3		14.0	
		1.8		1.6		2.6		2.0
400	9.9		11.0		9.0		10.0	
		1.5		1.2		1.2		1.3
600	7.0		8.7		6.4		7.4	
		0.7		0.9		0.65		0.75
800	5.6		6.9		5.1		5.9	
		0.35		0.7		0.4		0.5
1000	4.9		5.5		4.3		4.9	
		0.20		0.4		0.4		0.35
1200	4.5		4.7		3.5		4.2	
		0.15		0.3		0.2		0.22
1600	3.9		3.4		2.6		3.3	
		0.12		0.15		0.1		0.12
2000	3.4		2.8		2.15		2.8	
		0.08		0.09		0.05		0.07
3000	2.6		1.9		1.7		2.1	
		0.08		0.03		0.03		0.05
4000	1.8		1.6		1.45		1.6	

[a] *Maximum gradient.*
From Defant (1961).

upward in the water column, to a zone of warmer water, in order to maintain a constant-density environment. Conversely, they may have migrated downward (to cooler water) in interglacials (Figure 6.6). Clearly, such vertical migrations would result in isotopic paleotemperature estimates of glacial to interglacial temperature differences, considerably *less* than the

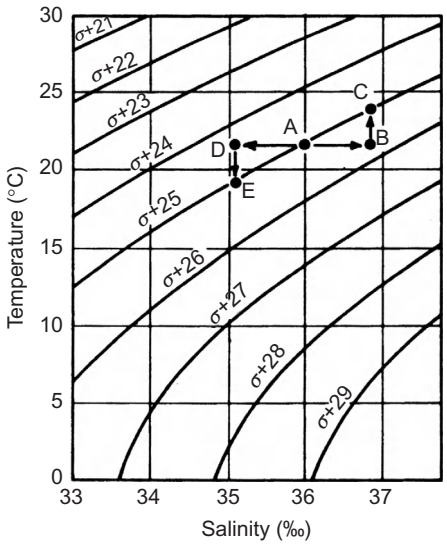


FIGURE 6.6 Temperature-salinity diagram: $\sigma = 10^3(\rho_w - 1)$, where ρ_w = water density. Density of sea water is a function of both temperature and salinity. Lines of equal density are shown. During glacial periods, when the removal of water to the continental ice sheets would have made overall oceanic salinity higher, foraminifera may have migrated to warmer water (generally upward in the water column) to maintain a constant-density environment (illustrated schematically as A-B-C). In an interglacial, the opposite situation may have prevailed and the response of foraminifera may have been to move downward in the water column to a cooler zone below (A-D-E).

changes actually occurring in the water column (Savin and Stehli, 1974). Hence, if this model is correct, any residual paleotemperature signal obtained (after correcting for ice and vital effects) would have to be considered a minimum estimate only.[3] This problem may, however, be a relatively minor one compared to the important effect of variations in depth habitat of foraminifera during their life cycle. Although the tests of living forams contain $CaCO_3$ that has been secreted in isotopic equilibrium with the upper mixed water layer, in certain species, foram tests from the sea floor are significantly enriched in ^{18}O compared to their living counterparts (Duplessy et al., 1981). This is apparently due to calcification of the tests at depths (>300 m) considerably below the upper mixed layer, during the process of gametogenesis (reproduction). Gametogenic calcification may account for ~20% of foram test weight in samples from the sea floor and, because calcium carbonate has been extracted from water which is much cooler than that nearer the surface, the overall $\delta^{18}O$ values indicate a mean temperature significantly lower than the near-surface temperature (Figure 6.7). Obviously, the rate at which the organism descends through the water column and the relative extent of gametogenic calcification will greatly influence the final isotopic composition of the test calcite. Similarly, as certain species are distinctly seasonal, the water temperature at those times will be reflected in $\delta^{18}O$. In order to use $\delta^{18}O$ in foram tests as a temperature indicator, it is necessary to establish in some way exactly which temperatures (by depth and season) are being recorded. One approach to this problem is to compare the $\delta^{18}O$ of forams in core-top assemblages or in sediment traps with oceanographic conditions in the overlying water column, to determine empirically the optimum relationship. For example, studies of $\delta^{18}O$ in forams collected in sediment traps at depth in the Sargasso Sea, compared to the temperature profile in

[3] In addition, the effects of sediment mixing (bioturbation) that tend to smooth out extremes in the record also contribute to making actual glacial-interglacial $\delta^{18}O$ differences appear smaller (Shackleton and Opdyke, 1976).

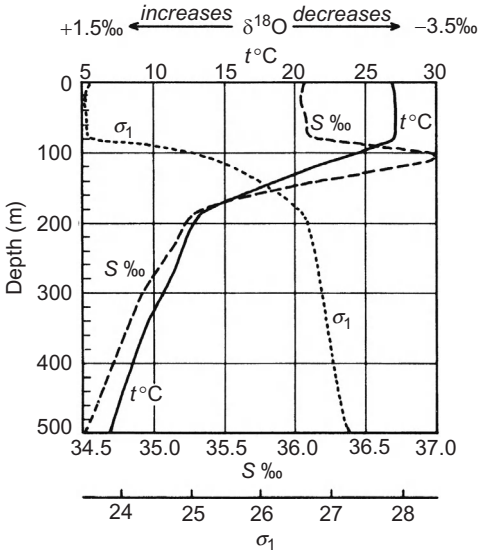


FIGURE 6.7 A typical vertical temperature, salinity, and density profile from the tropical oceans. As the amount of calcium carbonate secreted at depths below the upper mixed layer (generally ~100 m) increases, so the ^{18}O content of the test carbonate increases. Isotopic temperature estimates from foram tests that have undergone gametogenic calcification at depth are considerably lower than those obtained from living foraminifera collected in the upper mixed layer (~0.2‰ °C^{-1}).

the overlying water column, have shed light on both the seasonal occurrence of forams and the relationship between depth habitat and $\delta^{18}O$ in the foram tests (Deuser and Ross, 1989). This revealed, *inter alia*, that *Globorotalia truncatulinoides* adds calcite to its test at a depth of ~800 m, resulting in a sample mean $\delta^{18}O$ that does not correspond to SSTs but to water temperatures at ~200 m. The sediment trap data also demonstrate that many species only occur at particular times of year. For example, *P. obliquiloculata* and *Neogloboquadrina dutertrei* live in the upper 100 m and give $\delta^{18}O$ values that are representative of the winter mixed layer, whereas *G. ruber* (pink variety) that also live in the mixed layer (upper 25 m) occur only in summer months, resulting in different values of $\delta^{18}O$. This complication has some benefit; there is the potential of using seasonally occurring species of known depth habitat to reconstruct past changes in seasonality (and mixed layer depth) from foram assemblages (cf. Reynolds-Sautter and Thunell, 1989).

One additional complexity in using $\delta^{18}O$ as a paleotemperature indicator is that $\delta^{18}O$ is also strongly related to salinity (Figure 6.8). Hence, any change in salinity due to large-scale dilution effects (because of ice sheet melting) or to local changes in the precipitation-evaporation (P-E) relationship will also be recorded in foraminifera so affected (Duplessy et al., 1991). This can be put to good use in order to estimate salinity changes at the sea surface, providing all other effects can be determined independently. Thus, Duplessy et al. (1993) assessed local salinity changes near Portugal during the last deglaciation by first estimating SSTs (from micropaleontological transfer functions; see Section 6.4) and taking into account the influence of ice sheet meltwater on surface salinity and oceanic $\delta^{18}O$. By comparing the $\delta^{18}O$ record "expected" from such variations with the observed record, they argued that the resulting series of differences must be due to local changes in salinity. In spite of the uncertainties in such an approach (cf. Rohling and Bigg, 1998), the results strongly indicate that salinity was low during the time of maximum ice sheet melting (meltwater pulse 1, "MWP-IA," around 14.6-14.3 ka BP; Carlson and Clark, 2013) (Figure 6.9). Changes in ocean circulation and salinity are discussed further in Section 6.8.

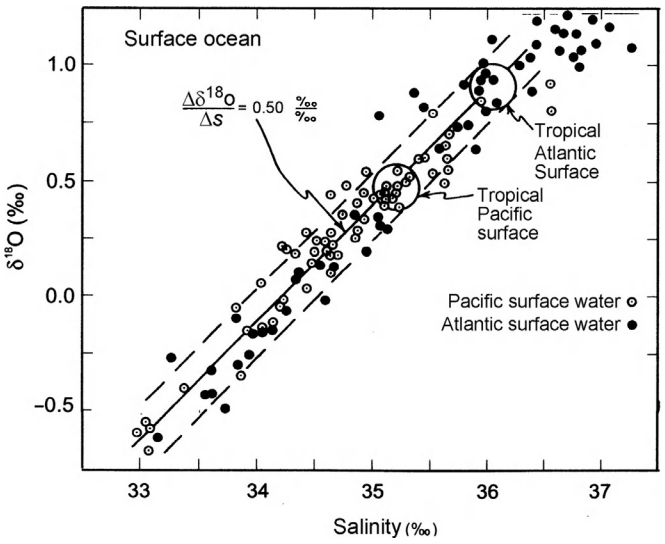


FIGURE 6.8 Relationship between $\delta^{18}O$ and salinity in oceanic surface waters, based on modern water samples. *From Broecker (1989) using data of H. Craig.*

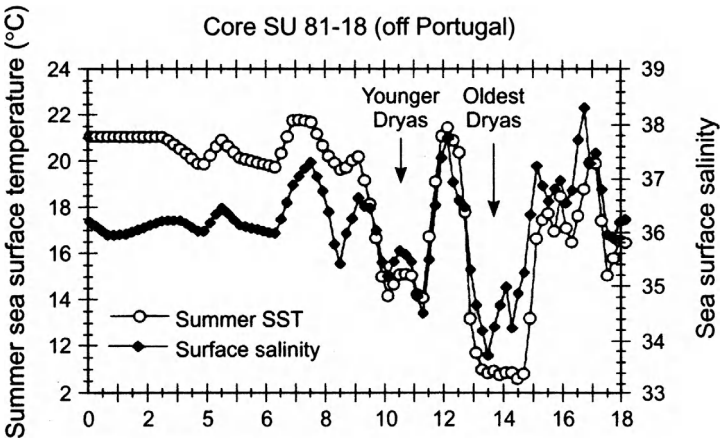


FIGURE 6.9 Estimated SST and salinity anomalies off the coast of Portugal (~38°N, 10°W). The salinity was high during times of maximum meltwater flux (primarily from the Laurentide Ice Sheet via the Mississippi drainage into the Gulf of Mexico) but low during the Oldest Dryas and Younger Dryas events (~14,500-13,000 and 11,000-10,000 ^{14}C years BP, respectively). *From Duplessy et al. (1992).*

A final problem affecting paleotemperature calculations from the isotopic composition of test carbonate concerns the effect of dissolution on species composition in the thanatocoenoses. This is a pervasive factor that has implications not only for isotopic studies of carbonate tests but also for all paleoclimatic studies based on assemblages of calcareous microfossils in marine sediments. Throughout the deep ocean basins of the world, a major factor affecting preservation of carbonate tests is the rate of dissolution at depth. The oceans are predominantly undersaturated with respect to calcium carbonate at all depths below the upper mixed layer (the zone above the thermocline; Olausson, 1965, 1967). After death, as the calcareous tests descend through the water column, dissolution occurs in the undersaturated water at depth, so that only about 25% of the carbonate flux from the mixed layer actually reaches

the ocean floor (Adelseck and Berger, 1977; Schiebel, 2002). Pteropod tests (composed of calcium carbonate in the form of aragonite) are most susceptible to solution and are the first to disappear; pteropods are thus only found in relatively shallow waters where undersaturation is not pronounced (Berner, 1977). At greater depth, dissolution of tests made of calcite (e.g., foraminifera and coccoliths) becomes apparent. The level at which calcite dissolution is at a maximum is the lysocline (Berger, 1970, 1975) generally encountered at 2500-4000 m depth in the oceans (Figure 6.10). In the Atlantic, this corresponds to the boundary between North Atlantic Deep Water and the deeper Antarctic bottom water (Berger, 1968). Below this level, calcite dissolution rates increase markedly, until at extreme depths, the water is so corrosive to calcite that virtually no tests survive to be deposited. The depth at which the dissolution rate equals the rate of supply of carbonate tests from the overlying water column is the calcite compensation depth (CCD) (Berger, 1970). This can be envisaged as analogous to a snow line on land; deep ocean basins below the compensation depth are devoid of carbonate sediments and made up primarily of clays and siliceous microfossils, whereas higher levels are increasingly blanketed by calcareous microfossil tests (Berger, 1971). Because the calcite compensation depth is a function of both the rate of supply of carbonate tests and the dissolution rate, its actual depth varies from one area to another (Figure 6.11) though generally it is <4000 m (Berger and Winterer, 1974). Since vast areas of the ocean floor are below 4000 m, particularly in the Pacific Basin, this phenomenon greatly restricts the area in which foraminiferal studies can be usefully carried out (cf. Figure 6.2). Even in less deep areas of the ocean, sediments

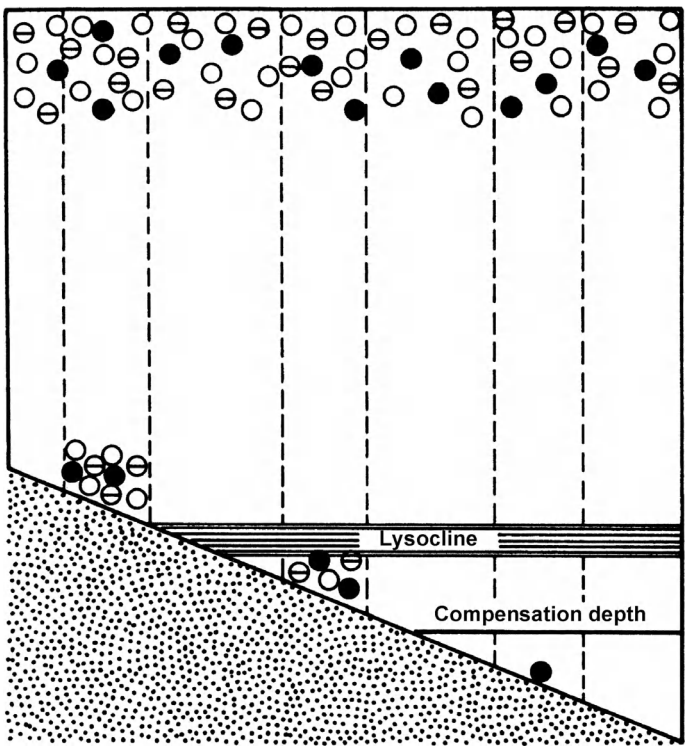


FIGURE 6.10 Schematic diagram illustrating selective dissolution of planktonic foraminiferal species at depth, due to undersaturation of the water with respect to calcium carbonate. Dark circles represent the resistant species *Globorotalia tumida*. Open circles represent *Globigerinoides ruber*, which is dissolved relatively easily. *Globigerina bulloides* (open circle with a line) is intermediate in resistance. Dissolution alters the species composition of the sediment so it may not be representative of species in the overlying water column. At depths below the compensation depth, only the occasional *Globorotalia tumida* may survive. Changes in the depth of the lysocline and compensation depth through time may alter the sediment species composition, due to differential dissolution. *After Bé (1977).*

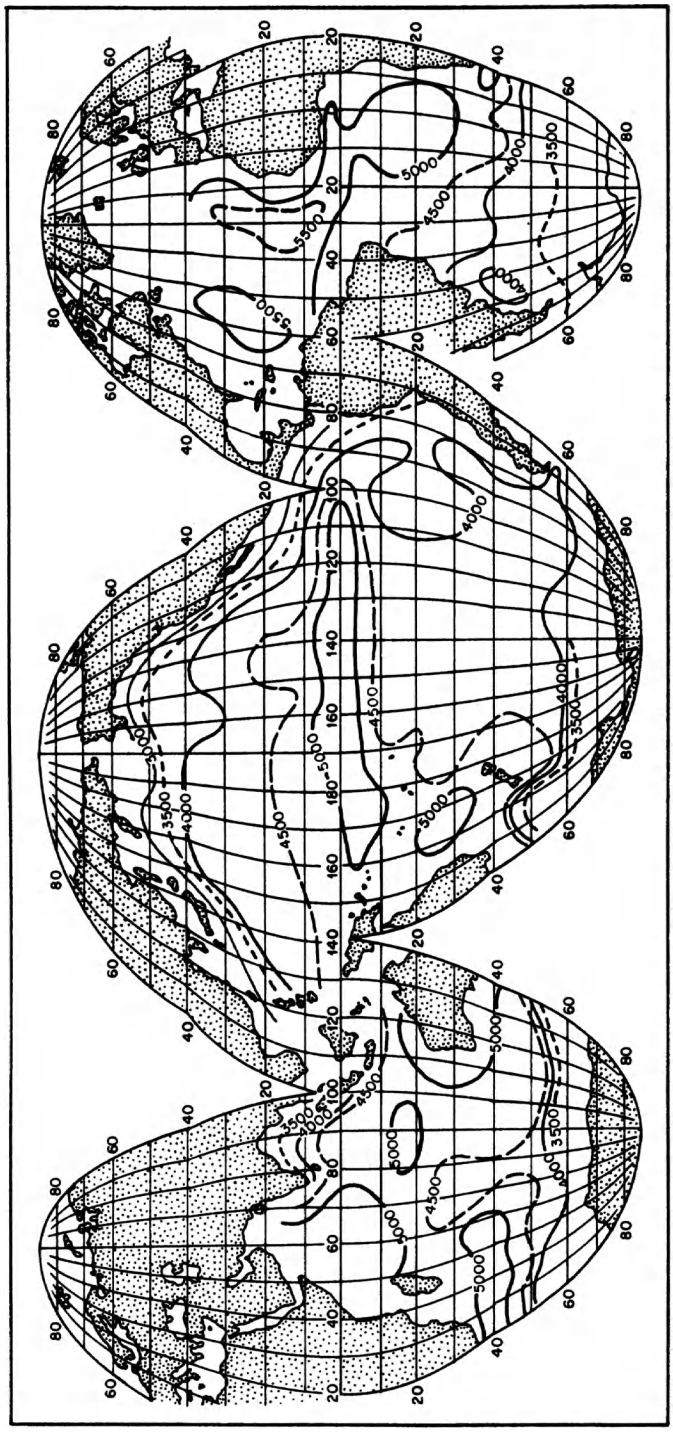


FIGURE 6.11 Distribution of calcium carbonate compensation depth. Depths in thousands of meters. *After Berger and Winterer (1974).*

accumulating below the lysocline are subject to significant dissolution. Most importantly, dissolution does not affect all species uniformly; selective removal of the more fragile, thin-walled species may significantly alter the original assemblages (biocoenoses) leaving behind thanatocoenoses that are unrepresentative of productivity in the overlying water column (Figure 6.10). Assemblages may be relatively enriched in resistant species, which tend to be deep-dwelling, secreting their relatively thick tests in water that is significantly cooler than that near the ocean surface (Ruddiman and Heezen, 1967; Berger, 1968). Similarly, in populations of a particular species, the thicker walled, more robust individuals, which are preferentially preserved, tend to build their shells in deeper, colder water and are therefore isotopically heavier than their more fragile counterparts (Hecht and Savin, 1970, 1972; Berger, 1971).

Studies of the relative abundances of different foraminiferal species, in cores from various depths, have demonstrated these effects well (Figure 6.12) and enabled species to be ranked according to their relative susceptibility to solution. Similar studies of coccoliths indicate corresponding problems, with structurally solid, cold water forms preferentially preserved in thanatocoenoses (Berger, 1973a; Kucera, 2007). Berger (1973b) suggested that the partially dissolved assemblages be designated taphocoenoses, to distinguish them clearly from assemblages more representative of the original biocoenoses. Clearly, paleoclimatic reconstructions based on taphocoenoses require careful interpretation if the rate or dissolution has changed over time, as suggested by a number of studies (Chen, 1968; Berger, 1971, 1973b; Broecker, 1971; Thompson and Saito, 1974; Berger et al., 1977; Ku and Oba, 1978). There is evidence that dissolution rates increased during interglacial times in the tropical Pacific and Indian Oceans, resulting in the removal of many less resistant species, and a relative concentration of individuals with a cold water aspect (Wu and Berger, 1989).[4] Conversely, in glacial times, dissolution rates were reduced, giving rise to assemblages of both solution-susceptible and solution-resistant forms. In short, glacial-interglacial changes may be characterized by corresponding dissolution cycles in these areas (Berger, 1973b). Such effects would result in erroneous isotopic paleotemperature estimates since interglacial-age samples would have a higher abundance of cold water individuals compared to glacial-age samples, thereby reducing the apparent glacial-interglacial temperature range (Berger, 1971; Berger and Killingley, 1977; Emiliani, 1977). Similarly, in foraminiferal assemblage studies (Section 6.4), dissolution cycles may result in taphocoenoses that lead to quite erroneous paleotemperature estimates. Thus, Berger (1971) and Ruddiman (1977) urge that all carbonate sediments be considered residual, unless easily dissolved material is present.

One interesting aspect of dissolution rate changes over time is the presence of a "deglacial preservation spike" or stratigraphic zone representing a period when dissolution rates were markedly reduced (Broecker and Broecker, 1974; Berger et al., 1977). There is evidence that, at around 14,000 years BP (and during other terminations), there was a significant worldwide drop in the aragonite compensation depth and the lysocline, lasting for only a relatively short period (perhaps <1000 years). This resulted in enhanced preservation of carbonate fossils at that time and hence a "spike" of well-preserved foraminifera and pteropods in the

[4] In the equatorial Atlantic and Gulf of Mexico, dissolution seems to have increased in glacial times (Gardner, 1975; Luz and Shackleton, 1975).

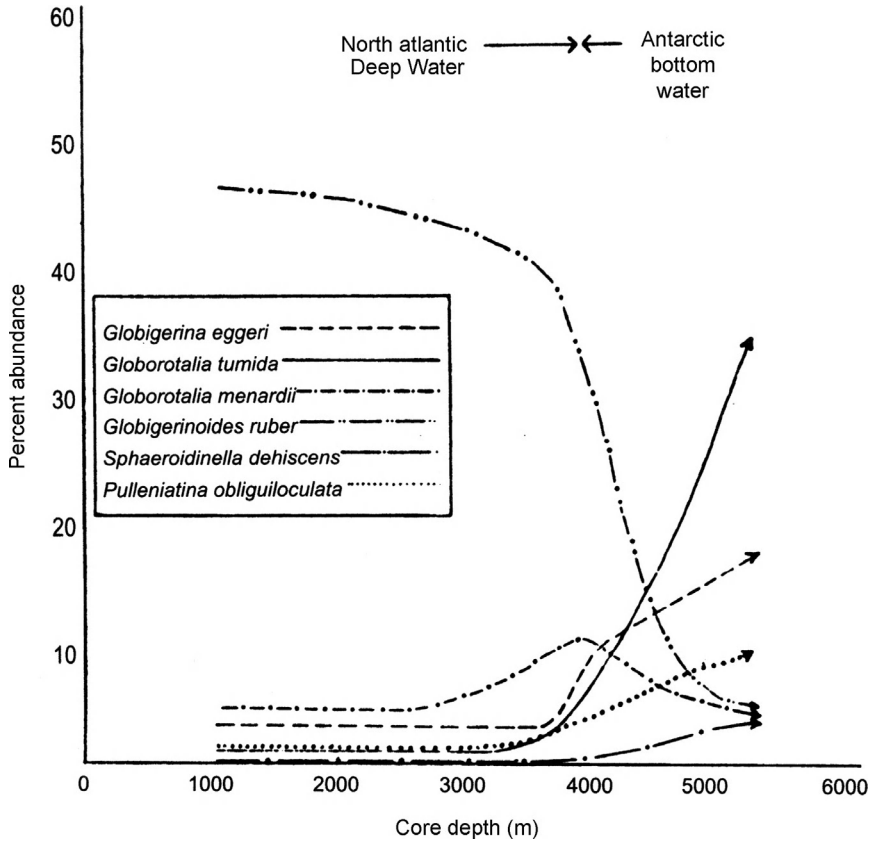


FIGURE 6.12 Changes in percentage abundance of several diagnostic planktonic foraminifera in equatorial Atlantic core tops with increasing water depths due to differential dissolution. The more corrosive Antarctica bottom water dissolves poorly resistant species (such as *Globigerinoides ruber*) so that more resistant species (such as *Globorotalia tumida*) increase in relative abundance. *After Ruddiman and Heezen (1967).*

sedimentary record (Wu et al., 1990). Indeed, the preservation spike is particularly apparent because dissolution rates appear to have been even greater at ~12,000 years BP directly following the time of the dissolution minimum (Berger and Killingley, 1977).

Another significant dissolution signal (the "Brunhes dissolution cycle") is seen in sediments from the equatorial Pacific and Indian Oceans (Wu and Berger, 1989). This is clearly shown in Figure 6.13 in which the difference in oxygen isotope stratigraphies between records from the Ontong Java Plateau is plotted; one record (V28-238) is from 3120 m and the other (V28-239) is from 3490 m water depth. A generally positive difference in $\delta^{18}O$ (of ~0.3‰) between these records is expected because the core from the deeper site has been affected by dissolution (making it isotopically heavier) and this effect is enhanced during the interglacials. However, from ~300 to 500 ka BP, the dissolution effect is systematically greater indicating some persistent influence on carbonate dissolution. This has also been seen in Indian Ocean sediments (Peterson and Prell, 1985).

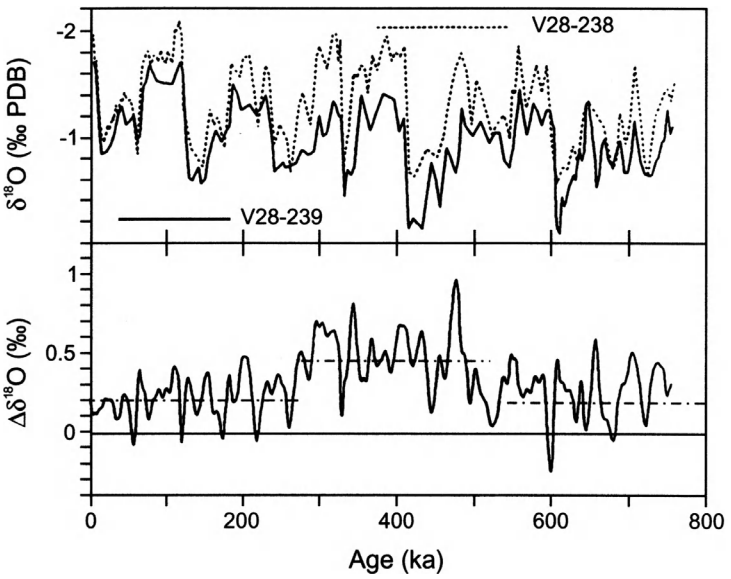


FIGURE 6.13 Two oxygen isotope records from the Ontong Java Plateau (eastern equatorial Pacific) (upper diagram) and the difference between them (V28-239 minusV28-238) (lower diagram). The V28-239 record is from 3490 m and V28-238 from 3120 m water depth. Dissolution has affected the deeper record leading to the preservation of forams with a higher ^{18}O content. In addition, a pronounced episode of enhanced dissolution is seen in the lower diagram, from ~300 to 500 ka BP. *From Wu and Berger (1989).*

The cause of these rapid shifts in compensation depth is not clear and, in fact, may result from a combination of many factors. Redeposition of carbonate from the continental shelves as sea-level rose could have increased oceanic alkalinity and thereby reduced dissolution (Berger et al., 1977). However, as the sea level rose, a low salinity upper water layer may have formed (from continental ice sheet melting), creating a lid on the North Atlantic Ocean and preventing vertical mixing (Worthington, 1968). Continued biological activity in the oceans might then have led to the accumulation of CO_2 and hence increased dissolution (Berger et al., 1977); perhaps, it is this signal that is observed following the dissolution minimum.

6.3.2 Oxygen Isotope Stratigraphy

Oxygen isotope analyses have been carried out on planktic and benthic species in sediment cores from most of the important areas of calcareous sedimentation throughout the world (Shackleton, 1977). The overwhelming conclusion from studies of isotopic changes in benthic forams (after making due allowance for variations in sedimentation rates, vital effects, and other complicating factors mentioned in the previous section) is that similar isotopic ($\delta^{18}O$) variations are recorded in all areas (Mix, 1987). This is because the primary $\delta^{18}O$ signal being recorded is that of ice volume changes on the continents and concomitant changes in the isotopic composition of the oceans (see Section 6.3.1). Indeed, such changes also affect the $\delta^{18}O$ content of the atmosphere, as recorded in air bubbles from ice cores (see Chapter 5, Section 5.4.3). Because the mixing time of the oceans is relatively short (~10^3 years), this global-scale phenomenon results in essentially synchronous isotopic variations in the sedimentary record (though bioturbation (mixing by burrowing organisms in the upper sediments) tends to smooth out fine details in the record). These synchronous variations enable correlations to be made between cores that may be thousands of kilometers apart

(Pisias et al., 1984; Prell et al., 1986; Lisiecki and Raymo, 2005). Changes in the isotopic composition of planktic forams also include this ice volume effect, but there may also have been significant influences from SST or salinity changes that would have been larger in the oceanic mixed layer than at depth.

Because there is a consistent stable isotope signal in marine sediments from around the world, universally recognizable marine isotope stages (MIS) can be defined (Emiliani, 1955, 1966; Pisias et al., 1984). Warmer periods (interglacials and interstadials) are assigned odd numbers (the present interglacial being number 1) and colder (glacial) periods are assigned even numbers (Figure 6.14). This provides a relative chronostratigraphic scheme, but absolute dating must then be based on a variety of techniques, such as radiocarbon, U-series dating, paleomagnetism (see Chapters 3 and 4), or orbital tuning (discussed further below). Commonly, it is assumed that sedimentation rates were linear between horizons of known age (such as paleomagnetic boundaries) to provide an interpolated chronology for the record. A comparison of terrestrial chronostratigraphic markers of known age with equivalent horizons in the ocean sediments enables further checks to be made on the isotopic chronology. For example, the Barbados high sea level stands (dated by uranium-series analyses of raised corals at 83,000, ~104,000, and ~125,000 years BP; Gallup et al., 1994; Stirling et al., 1995) correspond to isotopically light carbonate values in foraminiferal tests (Shackleton and Opdyke, 1973; Shackleton and Matthews, 1977) indicating that the chronology of the last interglacial-glacial cycle is well established (Figure 6.15). Tephras found in marine sediments and in Greenland ice cores (dated by counting annual layers) provide other useful markers, at least for the last glacial cycle (e.g., the ~55,500 years BP Z2 ash layer in the North Atlantic) so that they can also be used as independent chronostratigraphic markers (e.g., Kvamme et al., 1989). This is particularly important where the ash can also be found in other terrestrial deposits, such as ice cores, loess, or lake sediments, enabling direct correlation of land and marine records to be carried out (e.g., Grönvald et al., 1995).

Five stages are recognized in the isotopic record of the last ~130,000 years, with MIS 5 being subdivided into several substages, bearing the letter designations 5a to 5e. Stages 5a, 5c, and 5e were periods of reduced terrestrial ice volume and/or higher temperatures, with substage 5e being the peak of the last interglacial (Shackleton, 1969). Stages 5b and 5d were periods of cooler temperature and/or terrestrial ice growth, but on a smaller scale than occurred in stage 4. Interestingly, the change in benthic $\delta^{18}O$ commonly recorded between stages 5e and 5d is so large and so rapid that it is difficult to account for it only in terms of ice sheet growth. Ice sheets take thousands of years to grow to such a size that they affect oceanic isotopic composition (Barry et al., 1975). It seems likely that at least part of this change reflects a rapid temperature decline (of $\geq 1.5\ ^{\circ}C$) in abyssal water temperature (Shackleton, 1969, 1987). Subsequent changes in $\delta^{18}O$ (in stages 5c to 1) were then primarily the result of changing ice volumes on the continents, according to this argument. However, paleo-sea level data from New Guinea also point to a very rapid change in eustatic sea level (~60 m) between ~115,000 and ~105,000 years BP, which supports a simple ice growth interpretation of the $\delta^{18}O$ record. If this change did indeed occur, it represents an extraordinary episode in Late Quaternary history, with the water equivalent of one Greenland ice sheet being transferred from the oceans to the continents every 1000 years during this interval (see also Section 6.3.5).

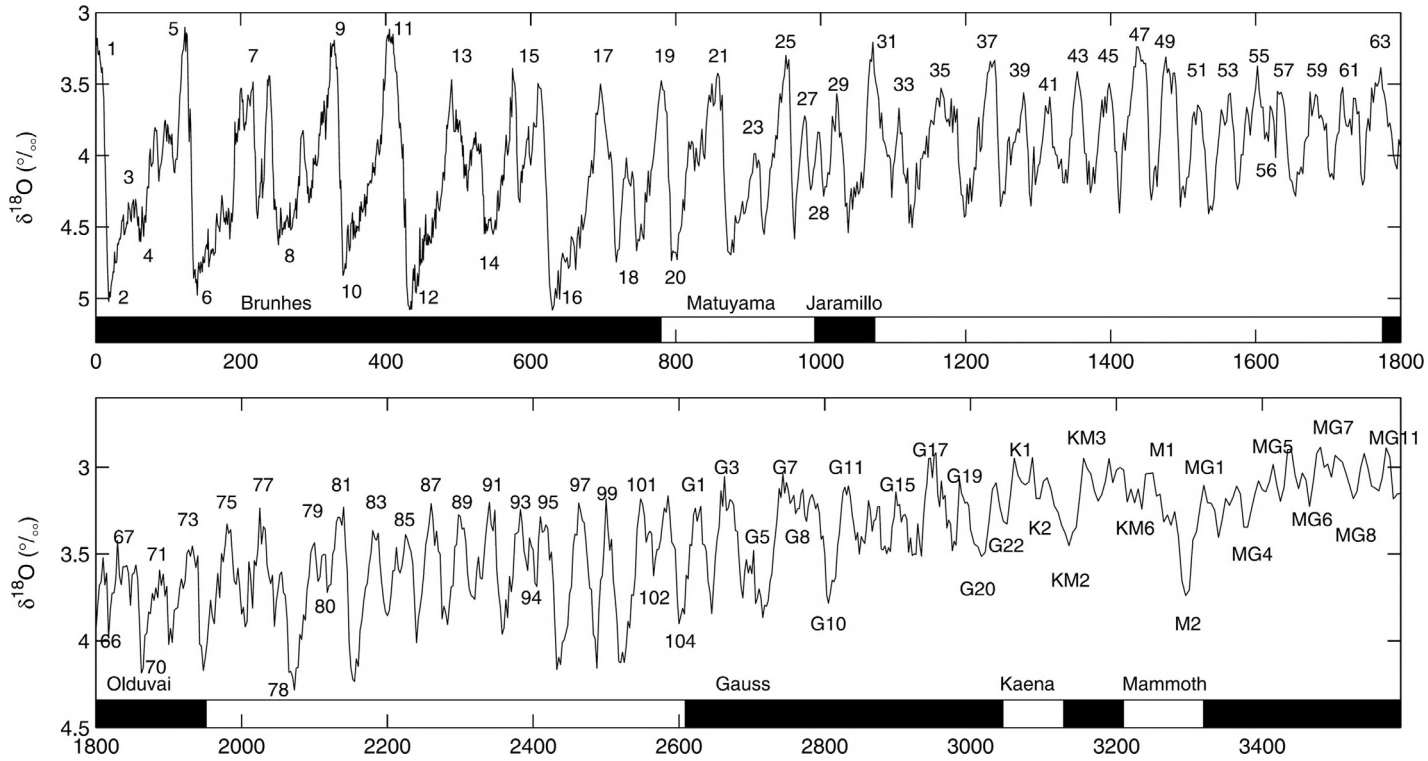


FIGURE 6.14 A composite average (or stack) of 57 benthic $\delta^{18}O$ records for the last 3.5 Ma, constructed by first correlating them all graphically, which produces a composite record that is independent of any absolute timescale. An age model was then assigned to the stacked record, based on tuning it to optimize the fit with a simple model of ice volume, while at the same time minimizing changes in the mean sedimentation rate. The model is driven by June 21st insolation changes at 65°N (which mainly reflect changes in obliquity) and incorporates a 15 ka time constant for ice sheet growth. Note that the scale of the vertical axis changes in the two panels and that the number of records in the stack becomes more limited further back in time. Thus, before 2.6 Ma BP, the average is based on less than half of the number used to construct the Late Pleistocene record. *From Lisiecki and Raymo (2005).*

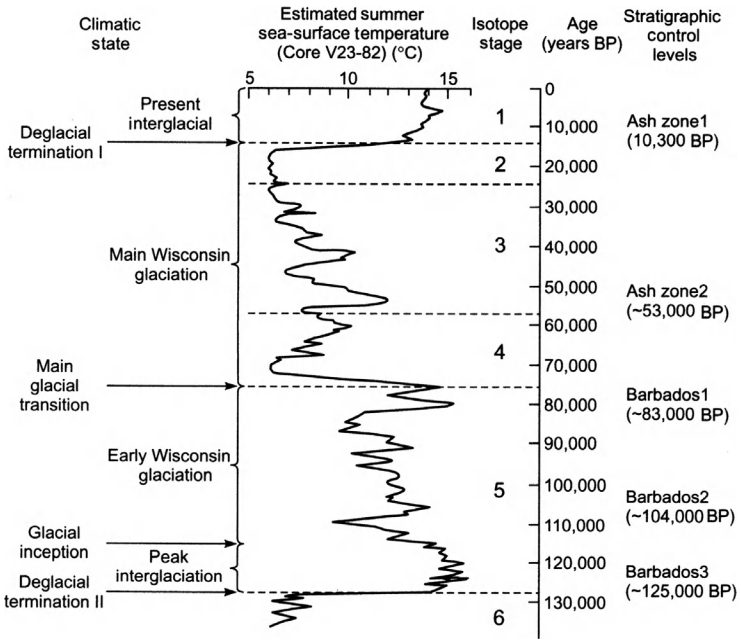


FIGURE 6.15 Summer sea-surface temperature reconstructions for the North Atlantic Ocean based on foraminiferal assemblage paleotemperature estimates, using core V23-82 from 53°N 22°W (Sancetta et al., 1973a,b). Chronological controls used in other cores are shown on the right (tephra layers and Barbados sea level stands). Isotopic stages are after Shackleton and Opdyke (1973). Generalized climatic conditions and major changes are shown at left. *After Ruddiman (1977b).*

Because the isotopic record provides an integrated summary of global ice volume changes, marine isotope stages are commonly used as standard reference units for both marine and terrestrial deposits (Shackleton and Opdyke, 1973). On the land, studies of continuous stratigraphic sequences spanning the last 150,000 years or more are rare; more often, deposits studied are discontinuous both in time and in space. In the oceans, the sedimentary record has been less disturbed so there are cogent reasons for using marine stratigraphic divisions to clarify and help understand the terrestrial record (e.g., Kukla, 1977, 1987b; Rutter et al., 1990). However, it should be emphasized that the isotopic signals in ocean cores contain both a temperature and an ice-volume component, which may not be synchronous. Furthermore, the ice-volume signal is an index of *global* ice volume and says nothing about ice extent in any one geographic area. This makes the application of a marine isotope stratigraphic frame of reference to many areas of questionable utility since the local stratigraphy may bear little relationship to the marine isotopic record (Hughes et al., 2013). For example, although there is a generally good correspondence between the marine isotope record of continental ice volume changes and glacial stratigraphy over North America, at least over the past ~1 MY (10 episodes of glaciation), there are few places in North America where the Laurentide Ice Sheet was at its maximum extent at ~21,000 cal. years BP (the marine isotope maximum; Mix et al., 2001); generally the ice sheet reached its greatest geographic extent 2000-4000 years earlier (Clark et al., 2009).

6.3.3 Orbital Tuning

An entirely different approach to dating marine sediments is to assume that orbital forcing has been the primary factor driving the growth and decay of ice sheets on land and therefore of the $\delta^{18}O$ signal in benthic marine sediments. Since the different periods associated with changes in eccentricity, precession, and obliquity are well known, this provides an opportunity to tune the chronology of $\delta^{18}O$ in marine sediments to orbital frequencies (Imbrie, 1985). This strategy developed from the discovery of a strong orbital signal in several different marine sedimentary records, with changes in the Earth's orbit acting as a "pacemaker" of ice ages (Hays et al., 1976). In orbital tuning, the astronomically driven changes (the forcing) are assumed to alter the climate system in some way, which is then registered in the proxy record (Figure 6.16). Providing the phase lag between orbital forcing and climatic response is constant (or can be estimated, if it changed over time); tuning the proxy record to the original forcing will enable an absolute chronology to be established (Martinson et al., 1987). In practice, tuning is carried out with respect to a particular frequency, such as that due to changes in obliquity, and the resulting tuned record can then be analyzed to see how changes at other orbital frequency bands are represented. If there is coherency at other orbital frequencies, this provides strong support for the tuning strategy adopted. For example, Imbrie et al. (1984) analyzed several records, in the 23,000- and 41,000-year (precession and obliquity) frequency bands, initially using a rough chronology made up of points in each record, the ages of which were approximately known (e.g., the Brunhes-Matuyama boundary, which was assumed to be at 730,000 years BP—but see discussion on p. 220—and the stage 5-6 boundary at 127,000 years BP). Assuming a time constant for large ice sheets of ~17,000 years (estimated from an ice sheet growth model), an age model was constructed to maximize the coherency between the record of orbital forcing in these frequency bands and the sedimentary $\delta^{18}O$ record. The analysis proceeded iteratively, eventually dropping the initial assumption that certain points were of known age so that the final record was entirely based on orbital tuning. The ultimate test was then to examine the coherency spectrum of the tuned record with the spectrum of orbital forcing at frequencies *other* than those used in the tuning procedure. In the tuned records obtained by Imbrie et al. (1984), coherency was very high not only in the tuning bands but also in the ~100 ka eccentricity band that was not used in tuning at all.

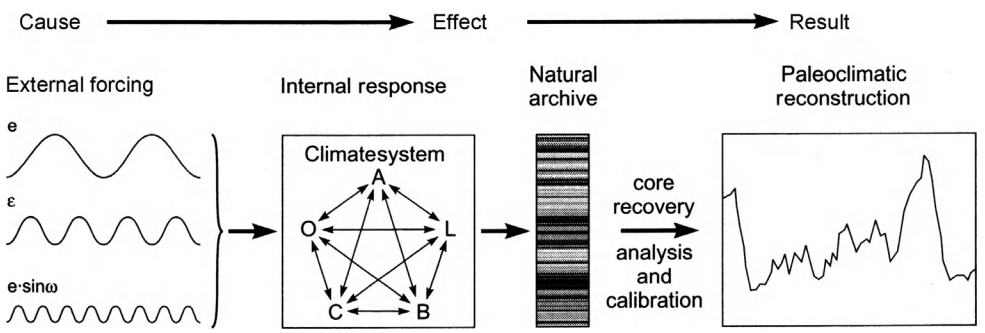


FIGURE 6.16 Schematic diagram illustrating the relationship between orbital forcing and the signal that is eventually preserved in the sedimentary record.

Orbital tuning has been extended back to 5.3 Ma years, using the average of a stack of benthic isotope data from 57 sediment cores from around the world, which were first aligned graphically, based on their characteristic temporal features (Figure 6.14) (Lisiecki and Raymo, 2005). A timescale was then assigned to the stacked record, using an ice model driven by insolation changes on June 21, at 65°N (which mainly reflects variations in obliquity) with the further constraint of trying to minimize changes in the mean sedimentation rate. A number of important features are apparent in the resulting composite record. First, from 3.6 to 2.4 Ma BP, there was a gradual increase in $\delta^{18}O$ indicating a progressive cooling, probably associated with a long-term decline in atmospheric CO_2 or slowly evolving tectonic changes that had critical effects on the global climate system (Berger et al., 1999; Ravelo et al., 2004; Mudelsee and Raymo, 2005). Around this time, uplift of the Tibetan Plateau led to increasing aridification of the Eurasian interior, which in turn greatly increased the production of atmospheric dust that could have reduced global temperatures (see Chapter 7). There was also a progressive restriction of the Indonesian seaway, through which warm water flows from the western Pacific into the Indian Ocean and the Atlantic (Cane and Molnar, 2001). A reduction in the flux of warm water through the seaway might have led to the cooling of high latitudes in the North Atlantic, favoring the growth of ice sheets. Whatever the cause, there was a gradual increase in the volume of continental ice sheets during this period, a development that was also registered by an increase in ice-rafted debris in marine sediments from the North Atlantic (Kleiven et al., 2002). The increase in benthic $\delta^{18}O$ values to levels typical of recent stadials indicates that continental ice sheets (in either the Northern or Southern Hemispheres, or both) reached a size equivalent to a drop in sea level of ~45 m (Mudelsee and Raymo, 2005). As cooling progressed, at ~2.75 Ma BP, a threshold appears to have been passed, associated with major changes in the stratification of the North Pacific Ocean. This lack of mixing with deeper water resulted in higher summer and autumn SSTs, which increased the flux of moisture to the adjacent North American continent, leading to the buildup of an ice sheet and the deposition of ice-rafted debris in the North Pacific Ocean (Haug et al., 2005).

Oxygen isotopes in benthic forams from the Pliocene and Early Pleistocene varied with obliquity (41 ka period), but beginning around 950 ka BP, there was a gradual increase in the importance of variance in the 100 ka (eccentricity) frequency band (sometimes referred to as the mid-Pleistocene transition) (Medina-Elizalde and Lea, 2005). This was associated with the growth of much larger continental ice sheets compared to the preceding period (as registered by higher levels of $\delta^{18}O$) (Figure 6.14). It seems unlikely that this was due simply to a change in the amplitude of eccentricity variations because over this interval, there was actually a shift *away* from variance in the 100 ka eccentricity frequency band and an increase in variance at lower frequencies (~412 ka) (Imbrie et al., 1993b). The 100 ka period in $\delta^{18}O$ is therefore likely to have resulted from feedbacks internal to the climate system that amplified the orbitally driven radiative forcing. From ice core records, greenhouse gases are clearly implicated in this amplification process (see Chapter 5, Section 5.4.3) though there may also have been critical effects related to the size of the ice sheets themselves, by feedbacks related to sea ice formation (Gildor and Tziperman, 2000) or to an increase in the elevation of major mountain ranges (Himalayas-Tibet and the north-south mountain ranges of western North America) (Ruddiman et al., 1986). As these ranges became higher, their effect on the general circulation would have been to establish a more meridional circulation regime, which may have favored faster ice sheet growth under certain orbitally driven radiation regimes.

There has been much discussion of why continental glaciation in its early stages might have followed a 41 ka trajectory or indeed if this is simply an artifact of the benthic record itself. Although obliquity variations dominate insolation receipts at high latitudes, summer insolation intensity (i.e., the seasonal maximum) in polar regions is strongly affected by precession (which varies with a period of 23 ka) modulated by variations in eccentricity; the influence of precession on summer insolation maxima is out of phase between the Northern and Southern Hemisphere. If ice sheet growth in one hemisphere was balanced by ice loss in the other hemisphere, this might effectively eliminate variance at the precessional frequency in the benthic isotope record (which integrates the overall effects of ice growth on the continents, regardless of where that might have occurred) (Raymo et al., 2006). The result might be a somewhat misleading signal of obliquity forcing, even if precession was driving ice sheet mass balance. However, this explanation does not square with the dominant 41 ka periodicity found in many records of North Atlantic and tropical Pacific SSTs. An alternative hypothesis was proposed by Huybers (2006) who noted that summer seasons are shorter when the Earth is closest to the Sun because the Earth accelerates along its orbit at those times. Thus, when precession coincides with Northern Hemisphere summer at the same time as perihelion, the intensity of solar radiation reaching the Earth is higher, but the duration of summer conditions in polar region is shorter. Huybers noted that cumulative summer temperatures above 0 °C in the Arctic are correlated with the total amount of energy received (integrated summer insolation) above a certain threshold (275 W m^{-2}); as the insolation forcing increases, so do summer melting degree days in the Arctic. He thus proposed an insolation index based on that threshold, finding that this index actually varies with a 41,000-year period; furthermore, it is in phase with the rate of change in ice growth (determined from the benthic isotope record) over much of the last 2 Ma (Figure 6.17). This relationship suggests that it is variations in summer melting, driven by overall summer insolation anomalies (not just insolation intensity at the peak of the summer), that affect ice sheet mass balance and concomitant changes in the isotopic composition of the oceans (cf. Huybers and Denton, 2008).

Figure 6.14 also shows that the isotopic record is made up of periods of gradually increasing $\delta^{18}O$ separated by shorter, relatively abrupt episodes when $\delta^{18}O$ values decreased; this is especially clear for the last ~1 Ma. The curve is thus "saw-toothed" in character, the slow increase in $\delta^{18}O$ resulting from the gradual buildup of ice on the continents, followed by a period of rapid deglaciation when isotopically light water was returned to the oceans. Broecker and van Donk (1970) referred to the sharp decreases in $\delta^{18}O$ as terminations, signifying the end of a glacial period, the most recent deglaciation being Termination I. The estimated ages of other terminations are shown in Table 6.2. Each termination occurred when there was a combination of high obliquity, high eccentricity, and the occurrence of Northern Hemisphere summer at perihelion (sometimes referred to as a "warm orbit"), leading to large insolation anomalies (up to 40 W m^{-2} outside the atmosphere, in summer at high latitudes) (Huybers, 2011). Interestingly, this suggests that major glaciations are unlikely to occur when eccentricity is high, as each precessional cycle will tend to limit ice sheet growth, and there is some evidence for that in the isotopic record (Huybers, 2007; Lisiecki, 2010). However, it is obliquity that mainly controls the pacing of deglaciation; times of obliquity maxima bring about large positive insolation anomalies at high latitudes (Figure 2.17), and it is this 41,000 beat that underlies the Quaternary cycles of glaciation and deglaciation (Huybers, 2007). The gradual increase in importance of the 100 ka periodicity in glaciation in the latter

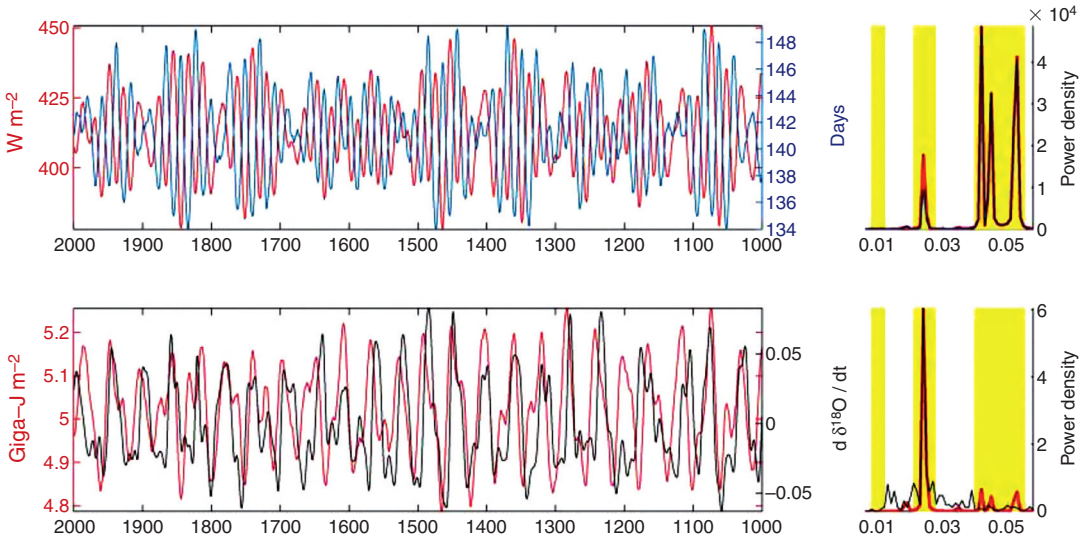


FIGURE 6.17 *Upper panel:* Number of days that insolation is above 275 W/m^2, a measure of the integrated summer energy available for melting snow and ice (blue line, right axis) and the average insolation intensity during this interval (red line, left axis). Intensity and duration are anticorrelated; when earth is closest to the sun, summers are the shortest. Spectral estimate of the duration (blue) and intensity (red), showing that the variance distribution of both series is identical and primarily concentrated at the precession periods. Shaded bands from left to right indicate the 100-ky, 41-ky (obliquity), and 21-ky (precession) bands. *Lower panel:* Summer energy (red line, left axis) and the time rate of change of $\delta^{18}O$ (black line, right axis) for the early Pleistocene (2M to 1M years ago) and the corresponding spectral estimates on the right. Positive rates of change indicate decreasing ice volume. Variability in both records is predominantly at the 41-ky obliquity period. *From Huybers (2006).*

half of the Pleistocene (the Mid-Pleistocene transition) arises from factors within the Earth's climate system (e.g., Clark et al., 1999), not simply from an increase in the importance of eccentricity variations (Ruddiman, 2006). Indeed, the gradual shift from a "41 ka world" to a "100 ka world" can be considered as simply a continuation of the 41 ka variability with occasional missing beats in that frequency (Huybers, 2007).

Finally, it is clear that $\delta^{18}O$ values over the last ~2.5 Ma have rarely been lower than Holocene levels, indicating that there have been very few occasions when there was less continental ice than there is at present; these episodes were principally in MIS 5e, 9, 11, and 31 (Raymo, 1992). There been many episodes of continental glaciation over the last ~1 MY that were comparable in magnitude to the most recent ice age (MIS 2) with benthic isotopic values exceeding ~4.7‰ (maximum values of ~5.1‰ occurred at 433 and 630 ka BP).

An important by-product of orbitally tuning the $\delta^{18}O$ record is that it provides age estimates on the timing of paleomagnetic polarity boundaries recorded within the sediments, which are independent of radiometric age determinations. Thus, Shackleton et al. (1990) pointed out that the Brunhes-Matuyama boundary occurred at ~780,000 BP (not 730 ka, as previously thought). The benthic isotope record produced by Lisiecki and Raymo (2005) confirms this assessment and indicates that the Jaramillo lasted from 1.075 to 0.991 Ma BP, the Olduvai from 1.968 to 1.781 Ma BP, and the Matuyama-Gauss boundary occurred at ~2.608 Ma BP. These dates are compatible with independent high-resolution dates on paleomagnetic reversals

TABLE 6.2 Estimated Ages of Oxygen Isotope Stage Boundaries and Terminations

		Estimated Ages ($\times 10^3$ years)				
Boundary[a]	**Termination**[b]	**A**[c]	**B**[d]	**C**[e]	**D**[f]	**E**[g]
2.0	I	14	13	11	11	12.05
3.0			32	29	27	24.11
4.0			64	61	58	58.96
5.0			75	73	72	73.91
5.1						79.25
5.2						90.95
5.3						99.38
5.4						110.79
5.5						123.82
6.0	II	130	128	127	128	129.84
7.0			195	190	188	189.61
8.0	III	243	251	247	244	244.18
8-9			297	276	279	
9-10	IV	337	347	336	334	
10-11			367	352	347	
11-12	V	424	440	453	421	
12-13			472	480	475	
13-14			502	500	505	
14-15			542	551	517	
15-16	VI	533	592	619	579	
16-17			627	649	608	
17-18			647	662	671	
18-19			688	712	724	
Brunhes-Matuyama boundary		780	700	728		
Jaramillo (top)		991		908		
Jaramillo (bottom)		1075		983		
Olduvai (top)		1781		1640		
Olduvai (bottom)		1968		1820		

[a] *Isotope boundary designation 2.0 (Pisias et al., 1984) is alternatively referred to as 1-2.*
[b] *Terminations from Broecker and Van Donk (1970). They defined terminations on the basis of their interpretation of the saw-toothed character of the oxygen isotope record.*
[c] *From Lisiecki and Raymo (2005).*
[d] *Estimates from Shackleton and Opdyke (1973) by linear interpolation in core V28-238, using a mean sedimentation rate of 1.7 cm per thousand years.*
[e] *Estimates from Hays et al. (1976), Kominz et al. (1979), and Pisias and Moore (1981) based on the assumption that variations in the tilt of the Earth's axis (obliquity) have resulted in variations of global ice volume and that the phase shift between the Earth's tilt and the 41,000 year component of the isotopic record has remained fixed with time. See Section 6.3.3 for discussion.*
[f] *Estimations from Morley and Hays (1981) based on adjustments to maintain a constant phase relationship between variations in oxygen isotope ratios and changes in obliquity and precession.*
[g] *Derived from orbital tuning by Martinson et al. (1987).*

(Tauxe et al., 1992; Chen et al., 1995). The marine isotope chronology can also be used to date other stratigraphic events, such as the level at which particular species became extinct (its last appearance datum, or LAD) (Berggren et al., 1980). These biostratigraphic events may then be used as chronostratigraphic markers in their own right, independent of both radioisotopic and stable isotope analyses on the sedimentary record in question. For example, extinction of the radiolarian *Stylatractus universus* has been found by stable isotope stratigraphy to have occurred throughout the Pacific and Atlantic Oceans at 425,000 ± 5000 years BP (Hays et al., 1976; Morley and Shackleton, 1978). Similarly, the coccolith *Pseudoemiliania lacunosa* became globally extinct in the middle of isotope stage 12, at ~458,000 years BP and the coccolith *Emiliania huxleyi* made its first appearance at ~262,000 years BP, late in isotope stage 8 (Thierstein et al., 1977).

6.3.4 Orbital Forcing: Evidence from the Marine Record

Although it is now quite clear that orbital forcing played a key role in pacing glaciations during the Quaternary period (Berger, 1980), the mechanisms involved in linking changes in insolation to changes in the climate system are not so clear. Over the last ~1 Ma, the principal periodicity in the $\delta^{18}O$ marine sediment record lies in the 100 ka band, but this has relatively little power in the insolation record (cf. Figure 2.16). Imbrie et al. (1992, 1993a) examined this matter in great detail and proposed a comprehensive model to account for this enigma. Their model builds on the earlier ideas of Weyl (1968), Broecker and van Donk (1970), and Broecker and Denton (1989). However, by focusing on how different parts of the climate system respond at the three distinct orbital frequencies (23, 41, and 100 ka), Imbrie et al. were able to demonstrate a recurrent geographic sequence of orbitally driven changes at all frequencies during the course of a glacial-interglacial cycle. By looking at the phase relationships between insolation, global ice volume, and other climate proxies, it was clear that certain parts of the climate system had a consistent early response to Northern Hemisphere high-latitude insolation changes, whereas others responded later. By mapping the geographic distribution of these responses, a mechanistic model of glacial-interglacial changes was constructed. This revealed that four key subsystems control the rate at which radiation changes are propagated through the climate system, each having a different level of inertia. Near-surface processes on the land and in the upper ocean and in the deep waters of the Southern Ocean respond quickly (in <1 ka), whereas changes involving ice sheets, displaced wind systems, and deep ocean chemistry take longer (3-5 ka). Through the interaction of these different subsystems, the sequence of events that led to glaciation and deglaciation slowly unfolded.

Like earlier workers, Imbrie et al. (1992) argued that a critical factor driving glacial-interglacial changes is salinity-controlled convection in the Icelandic, Norwegian, and Greenland (Nordic) Seas and in the Labrador Sea, which they refer to as the Nordic and Boreal heat pumps, respectively. During interglacials, both areas produced deepwater that drove the thermohaline circulation of the Atlantic and carried heat to the Southern Ocean, thereby restricting sea ice around Antarctica. With both heat pumps operating, ventilation of the deep ocean was at its maximum. As summer insolation decreased at high northern latitudes, the atmosphere and ocean surface cooled, reducing evaporation and increasing snowfall and sea ice cover. Eventually, salinity in the Nordic Seas decreased, at first slowing and then entirely eliminating convective overturning via the Nordic heat pump, drastically curtailing warm water flux to the Southern Hemisphere. However, the Boreal heat pump

continued to operate, producing intermediate water, but the net result was a dramatic reduction in thermohaline circulation and hence in the return flow of warm water to the North Atlantic. As Antarctic sea ice expanded, the northward flux of Antarctic bottom water increased and an equatorward shift in the southern westerlies led to ocean circulation changes that sequestered carbon in the Southern Ocean. This in turn led to a reduction in atmospheric CO_2 levels, which further reinforced the downward insolation trend. Further cooling in the Northern Hemisphere resulted in ice growth on land and a fall in sea level, allowing extensive marine-based ice sheets to develop in locations that were vulnerable to later sea level increases. Ice sheet growth eventually disrupted the westerly wind system causing sea ice to form over large areas of the North Atlantic that increased the production of intermediate water and caused a slight increase in NADW, leading to a minor recession in Antarctic sea ice extent. As the insolation cycle returned once more to a situation with higher Northern Hemisphere summer energy receipts, the northern oceans slowly warmed and, on the continents, snow-melted and the ice margins retreated. This allowed the zone of maximum westerly winds to shift northward, and warmer waters and subtropical air masses could then be advected from the south, causing the ice sheets to rapidly melt and sea level to rise very quickly with catastrophic collapse of marine-based ice sheets. At the same time, sea ice rapidly receded and this, together with the advected waters from the south, resulted in a sharp increase in the salinity of the North Atlantic and a resumption of the Nordic heat pump. Large-scale melting events due to the rapid melting of continental and marine-based ice sheets may have resulted in short-term reversals of these trends (as discussed in Section 6.10), but eventually, the primary sequence of events driven by orbital forcing prevailed, leading once more to a strong thermohaline circulation involving both the Boreal and the Nordic heat pump systems.

Although this sequence of events appears to be causally linked to the 23 and 41 ka precession and obliquity cycles in a simple linear relationship, most of the variance in the ice volume record over the last 1 Ma is actually in the 100 ka eccentricity cycle. Since variations in insolation due to eccentricity changes are an order of magnitude smaller than those due to precession and obliquity changes, it is difficult to understand why changes at this frequency are so large. Several models have been proposed to explain this problem. One set of models generally views the climate system as having the ability to develop internal (free) oscillations or resonance in response to some external forcing, possibly unconnected to orbital forcing. Another set views the climate system as following the same sequence of responses noted for the 23 and 41 ka cycles but in a nonlinear manner; at some point, a threshold is crossed, which then gives rise to a much larger response (Imbrie et al., 1993b). The critical factor driving this nonlinear response appears to be the size of the continental ice sheets (primarily the Laurentide Ice Sheet). Large ice sheets significantly disrupt the westerlies, leading to a strong meridional circulation, which then greatly amplifies the sequence of climate system changes associated with 23 and 41 ka cycles. So, when some combination of forcing at the 23 and 41 ka bands leads to the ice sheets exceeding a critical size, they then overtake the "normal" system response to orbital forcing. In effect, the ice sheets themselves become the principal agents driving the climate system, producing a cycle of changes with a longer (100 ka) periodicity due to the large amount of inertia associated with ice sheet growth and decay. This model provides an elegant explanation for the changes observed over the last few hundred thousand years, but why this pattern became more significant in the last million years remains to be

fully explained (Raymo and Huybers, 2008). An alternative to these hypotheses was proposed by Shackleton (2000) who argued that the 100 ka periodicity seen in marine sediments and other paleoclimate proxies is primarily due to variations in CO_2, rather than changes in ice sheet dynamics. He used the record of atmospheric $\delta^{18}O$ in ice from Vostok to separate the benthic ice volume and deepwater temperature signals, which showed that deepwater temperatures, CO_2, and Vostok air temperatures are all in phase, whereas ice volume lagged behind. A similar argument was made by Medina-Elizalde and Lea (2005) and Herbert et al. (2010) who found that Pacific SSTs led changes in ice volume. What drove CO_2 changes at the 100 ka periodicity is unclear, but it may be related to degassing of CO_2 from the Southern Ocean, modulated by changes in sea ice extent, which plays a critical role in the rate at which dissolved CO_2 is released to the atmosphere.

6.3.5 Sea Level Changes and $\delta^{18}O$

It was noted earlier that the bulk of the $\delta^{18}O$ signal in benthic foraminifera is related to changes in the isotopic composition of the oceans under the influence of changing continental ice volume. As ice sheets grow on the continents, the $\delta^{18}O$ of the ocean increased and global sea level fell. Hence, there should be some sort of relationship between $\delta^{18}O$ in forams, continental ice volume, and sea level change. However, the connections between these three phenomena are complex; the mean isotopic composition of ice sheets no doubt changed over time, depending on the ice sheet location (latitudinally) and its mean elevation. If ice sheets remained in a steady state for extended periods, the mean $\delta^{18}O$ of ice lost at the margin (representing older ice formed at lower elevations) would probably have been higher than precipitation falling later on the high-elevation accumulation zone of the ice sheet, leading to a systematic enrichment of the ocean in ^{18}O without any change in ice volume. There is therefore a nonlinear relationship between ice sheet volume and oceanic $\delta^{18}O$ composition (Mix and Ruddiman, 1984). Furthermore, the $\delta^{18}O$ of benthic forams is not only influenced by oceanic $\delta^{18}O$; if water temperature (or salinity) changed, this would have affected $\delta^{18}O$ and such effects may have been more important at certain times (and certain locations) than at others. Finally, direct estimates of paleosea level are generally based on coral reefs found on rising coastlines so that the record of former low sea level stands is now found at locations well above present sea level (Figure 6.18). Understanding how sea level at various times in the past relates to global ice volume changes requires not only a tectonic model for local uplift but also an understanding of global sea level distribution, relative to the mean geoid. Temporally synchronous sea level terraces may not be at equivalent heights above present sea level due to geophysical constraints on the distribution of water on the planet (Peltier, 1994).

Notwithstanding these difficulties, establishing a relationship between $\delta^{18}O$ and sea level offers the prospect of obtaining a long-term and continuous record that is not available from direct sea level measurements. However, given that the overall change in sea level from the last glacial maximum to the present was ~130 m and benthic isotopes changed by only ~2‰, it is clear that even a small change in deepwater temperature introduces large uncertainty into paleo-sea level estimates. Chappell and Shackleton (1986) and Shackleton (1987) estimated this effect by comparing paleo-sea level estimates from U-series-dated coral terraces on the Huon Peninsula of New Guinea (Figure 6.18) with the record of $\delta^{18}O$ in benthic foraminifera,

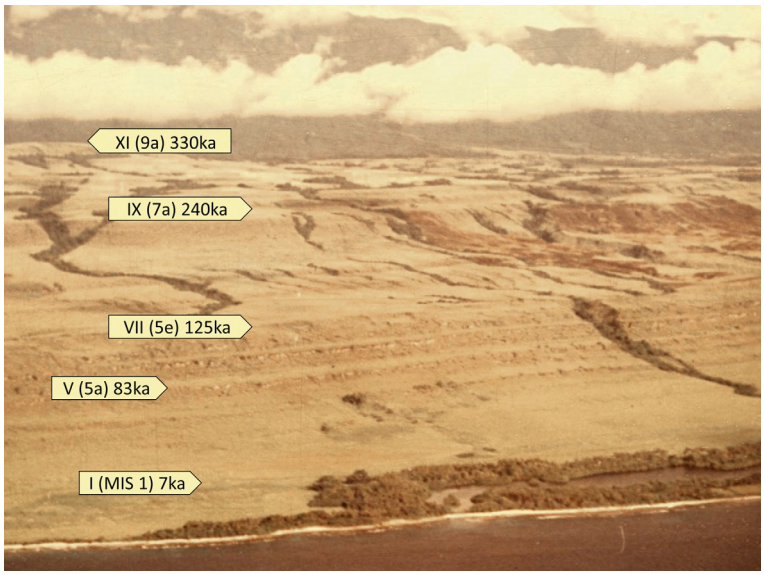


FIGURE 6.18 Raised coral terraces, indicative of former sea levels, near Kwangama on the north coast of Papua New Guinea. The coastline in this area has been continuously rising at the same time as sea level has been rising and falling due to ice volume changes on the land (eustatic sea level changes). The age of each terrace and corresponding marine isotope stages are indicated. *Photo from J. Chappell.*

concluding that in order to match these records, temperatures in the deep ocean must have been at least 1.5 °C cooler in glacial and interstadial times (~110-20 ka BP) than during interglacials (MIS 1 and 5e). Subsequent studies have confirmed their estimate (Adkins et al., 2002a). By assuming that such a change was typical of earlier glacial-interglacial cycles, Shackleton (1987) estimated (from benthic $\delta^{18}O$) the relative magnitudes of ice volume at the times of glacial and interglacial extremes back in time, for which no well-dated sea level terraces exist. This led him to conclude that continental glaciation during marine isotope stage 6 was slightly greater than in stage 2 and that in stages 12 and 16, it was even larger. Previous interglacials (MIS 7, 13, 15, 17, and 19) were significantly warmer (i.e., had much less ice remaining on the continents) than the present one. Stages 1, 5e, 9, and 11 were all similar (isotopically) though independent evidence suggests that stages 5e and 11 (at least) were somewhat warmer with sea level $\geq$6 m above present levels.

Another approach to sea level reconstruction is provided by sediments from the eastern Mediterranean and the Red Sea. The Red Sea is very sensitive to sea level changes due to its high rate of evaporation (currently ~2 m $year^{-1}$) and a shallow sill that separates it from the ocean to the south. These factors amplify the isotopic effects of sea level changes; by developing a water exchange model for the basin, a high-resolution record of sea level change has been obtained from forams in Red Sea sediments (Siddall et al., 2003; Rohling et al., 2009). The chronology of these changes has been adjusted by correlation with foraminiferal data from the eastern Mediterranean, which was in turn linked to an independently dated speleothem record from Soreq Cave, Israel (Grant et al., 2012) (Figure 6.19). These sea level

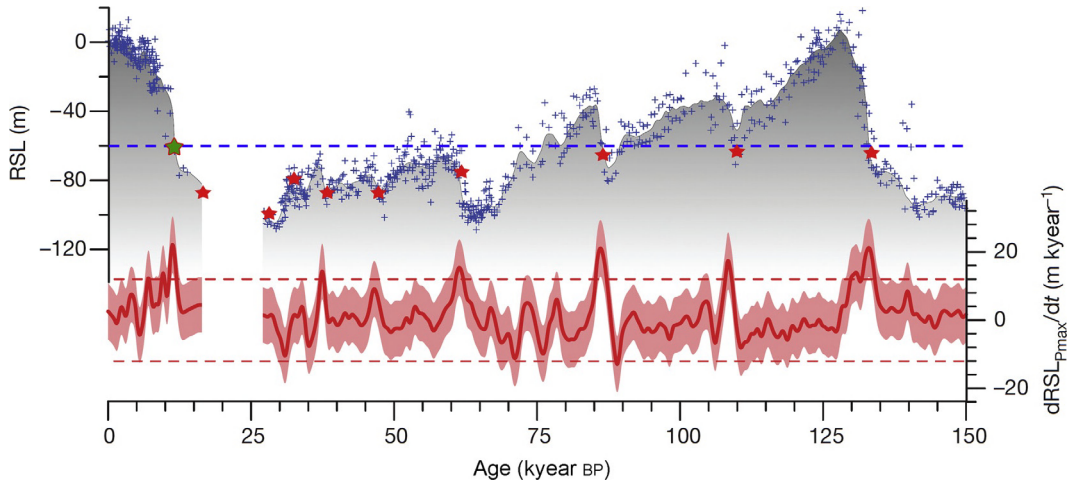


FIGURE 6.19 A high-resolution record of sea level change obtained from forams in Red Sea sediments (Siddall et al., 2003). The chronology of these changes has been adjusted by correlation with foraminiferal data from the eastern Mediterranean, which was in turn linked to an independently dated speleothem record from Soreq Cave, Israel. Blue crosses are individual data points and the gray-shaded line is the maximum probability relative sea level estimate. The lower red line shows the rate of change in sea level based on the first derivative of the gray line. Dashed lines show sea level increases of 12 m ka^{-1} (positive if rising, negative if falling). Stars demote the timing of Heinrich events. Note that Heinrich events only occur when sea level is below −60 m. This may indicate that ice sheets must be large enough to calve into the ocean to drive Heinrich events; sea level at −60 m also approximates the depth at which the Bering Strait becomes exposed, separating the Pacific from the Atlantic Ocean. *Modified from Grant et al. (2012).*

reconstructions show that sea level fell in stages from its maximum of around 6 m above present at the peak of the last interglacial, to an LGM minimum of ∼120 m below present. It is interesting that maximum rates of sea level rise (in excess of +12 m ka^{-1}) occurred around the time of Heinrich events (see Section 6.10.1). It is also notable that Heinrich events only occurred when sea level was −60 m or lower, which suggests that such events required ice sheets to be large enough to have ice streams in contact with the sea. It may also be of significance that this is the approximate depth at which the Bering Strait became exposed land, preventing the transfer of water between the Pacific and Atlantic Oceans via the Arctic Ocean.

An even longer sea level reconstruction has been made by correlating the Red Sea foram isotopic record with the Antarctic ice isotopic record (Rohling et al., 2009). The argument is that the ice core isotopic record is a proxy for global temperature and thus linked to sea level on long timescales (cf. Shackleton et al., 2000), so the chronology of the ice core can be applied to the foram record (Figure 6.20). This reconstruction confirms that sea level in the last 0.5 Ma was probably only higher than today during MIS 5e and that MIS 12 was an exceptionally severe glacial interval, with sea level possibly even lower than at the LGM. The reconstruction also reveals that there were periods of abrupt sea level changes at many times in the past—both rising and falling at very high rates (1-2 cm year^{-1}). Understanding the climatic

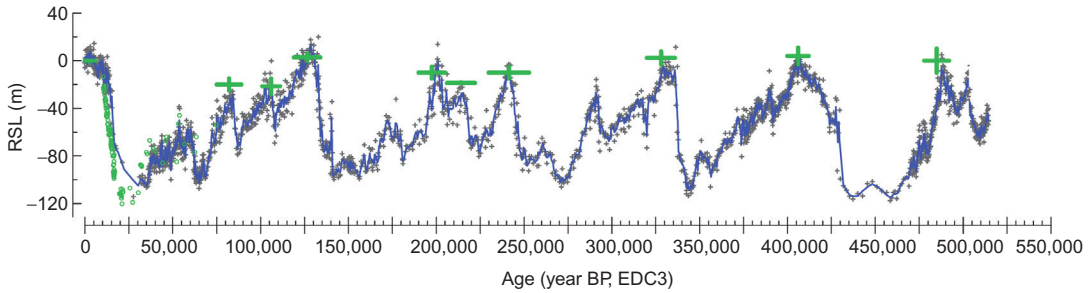


FIGURE 6.20 Estimated changes in eustatic sea level over the last 550,000 years based on carbonate $\delta^{18}O$ measurements on central Red Sea core GeoTü-KL09. The green symbols are coral and speleothem-based sea level markers. Chronology was derived from the Antarctic EPICA Dome C ice core record (which was correlated with the benthic isotopic record). *From Rohling et al. (2009).*

conditions that could have enabled such astonishing rates of continental ice sheet growth to occur (at rates comparable to those at times of ice sheet collapse) remains an enigma.

6.4 PALEOTEMPERATURES FROM RELATIVE ABUNDANCE STUDIES

The possibility of reconstructing paleoclimates by using the relative abundance of a particular species, or species assemblage, in ocean sediment cores was first proposed by Schott (1935). Schott recognized that variations in the number of *Globorotalia menardii* (a foraminifera characteristic of subtropical and equatorial waters) are indicative of alternating cold and warm intervals in the past. However, 30 years was to elapse before the availability of relatively long undisturbed cores, and improved dating techniques, enabled others to capitalize on Schott's work and to develop his ideas further. For example, Ruddiman (1971) derived time series of the ratios of all warm water species to cold water species to obtain qualitative paleotemperature estimates that showed good correlations with oxygen isotope paleoglaciation curves. Although somewhat of an improvement over earlier studies based on individual species, Ruddiman recognized that the technique was still relatively simplistic in considering all species as equally "warm" or "cold" when gradations in their individual tolerances obviously exist.

In the early 1970s, major advances in paleoclimatic and paleo-oceanographic reconstructions were made by a number of workers. Multivariate statistical analyses of modern and fossil data were used to quantify former marine conditions (marine climates) in an objective manner (Imbrie and Kipp, 1971; Hecht, 1973; Berger and Gardner, 1975; Williams and Johnson, 1975; Molfino et al., 1982). The general approach in all of these studies was to calibrate the species composition of modern (core-top) samples in terms of modern environmental parameters (such as sea-surface temperatures in February and August). This was achieved by developing empirical equations that relate the two data sets. These equations (transfer

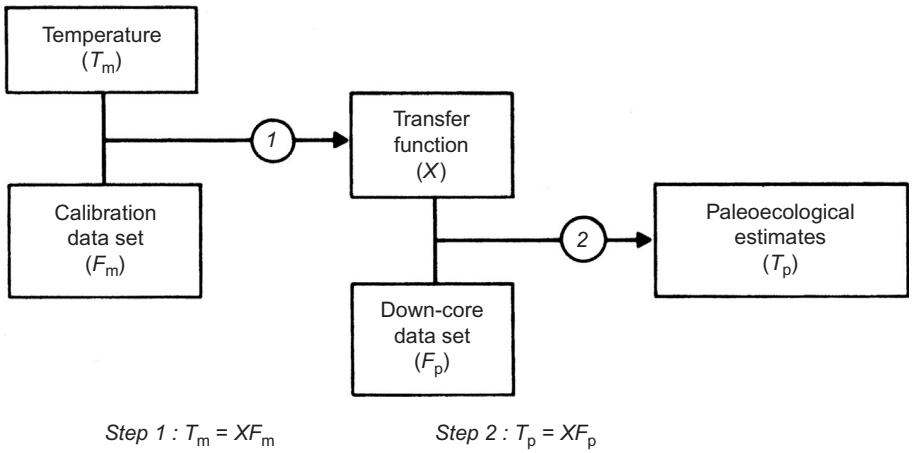


FIGURE 6.21 Schematic quantitative paleoclimatic model. In step 1, the transfer function (X) is calculated by calibration of the modern (core-top) foraminiferal data set (F_m) with modern sea-surface temperatures (T_m). In step 2, the transfer function is applied to a down-core (fossil) data set (F_p) to yield estimates of past temperatures (T_p). *After Hutson (1977).*

functions) were then applied to down-core faunal variations to reconstruct past environmental conditions (Figure 6.21). Mathematically, the procedure can be simply expressed as follows:

$$T_m = XF_m \quad \text{and} \quad T_p = XF_p$$

where T_m and T_p are modern and paleotemperature estimates, respectively, F_m and F_p are modern and fossil faunal assemblages, respectively, and X is a transfer coefficient (or set of coefficients).

A fundamental assumption in the use of transfer functions to reconstruct marine climates is that former biological and environmental conditions are within the "experience" of the modern (calibration) data set (as illustrated in Figure 6.22). If this is not so, a no-analog condition exists and erroneous paleoclimatic estimates may result (Hutson, 1977). Another important assumption is that the relationship that currently exists between marine climate and marine fauna has not altered over time due, for example, to evolutionary changes of the species in question. However, perhaps the major uncertainty in many studies is the very nature of the calibration data set itself. The "modern" faunal assemblages are generally derived from core-top samples that may represent a depositional period of several hundred, if not thousands of years, due to bioturbation and disturbance during core recovery (Emiliani and Ericson, 1991; Kucera et al., 2005a). Indeed, the chronological heterogeneity of core-top samples was considered by Imbrie and Kipp (1971) to be the largest single source of error in their paleoenvironmental reconstructions ("most [core-top samples] represent. . .the last 2000 to 4000 years and....some may contain materials deposited in the age range 4,000-8,000 years B.P."; Imbrie and Kipp, 1971).

Of all the multivariate approaches to the quantification of former marine climates, the methodology of Imbrie and Kipp (1971) has been most widely applied. In their original study, an attempt was made to reconstruct sea-surface temperature variations at a core site (V12-122) ~150 km south of Haiti. To achieve this, the species composition of core-top samples from

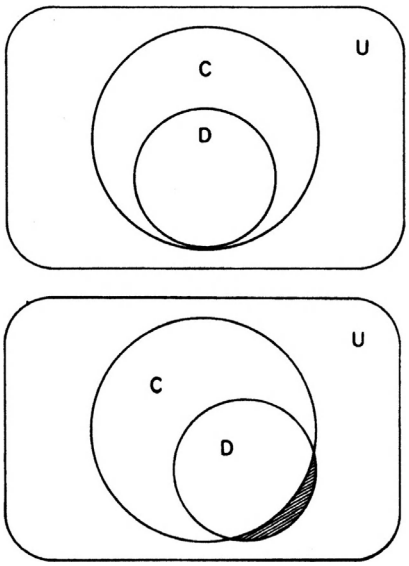


FIGURE 6.22 Venn diagram illustrating conditions that are ideal (above) and nonideal (below) for calibrating a transfer function. In an ideal situation, the calibration data set, C, encompasses the range of all biological and environmental conditions that exist in the down-core data set, D. In a nonideal situation, the calibration data set, C, does not reflect all the biological and environmental conditions that are represented within the down-core data set, D and a no-analog condition results (shaded area). U is the universe of all biological and environmental conditions both today and in the past. *After Hutson (1977).*

61 sites in the Atlantic Ocean (and part of the Indian Ocean) was used as the basic "modern fauna" data set. As a first step, Imbrie and Kipp reduced the number of independent variables in this data set by the use of principal components analysis. Principal components analysis is an objective way of combining the original variables into linear combinations (eigenvectors) that effectively describe the principal patterns of variation in a few primary orthogonal components, leaving the less coherent aspects (noise) for the last few components (Sachs et al., 1977). Thus, Imbrie and Kipp were able to condense much of the spatial variation of species abundance in 61 core-top samples from the Atlantic Ocean into five principal components or assemblages, which accounted for almost all of the variance in the original data set. By mapping the relative contribution of each component to the variance of each core-top sample, it was clear that four of these assemblages were related to temperature variations near the sea surface and could be simply described as tropical, subtropical, subpolar, and polar assemblages. A fifth assemblage was more related to oceanic circulation around the subtropical high-pressure cells and was termed the gyre margin assemblage.

The next step was to utilize the relative weightings of each assemblage (factor scores) at each site to predict sea-surface temperatures. A stepwise multiple regression procedure was used, with temperature as the dependent variable and the factor scores as independent variables (predictors). In this way, an equation was derived that parsimoniously described sea-surface temperature in terms of the relative importance of the factor scores at each site. In the case of winter temperatures, for example, the following calibration equation was derived:

$$T_w = 23.6A + 10.4B + 2.7C + 3.7D + 2.0K$$

where A, B, C, and D refer to the four major assemblages (tropical, subtropical, subpolar, and polar) and K is a constant (gyre margin assemblage was not considered in this analysis).

This equation explained 91% of variance in the modern winter sea-surface temperature observations. Having calibrated the modern faunal data set in terms of sea-surface temperatures, it was then possible to transform the fossil (down-core) faunal variations from core V12-122 into relative weightings of the major faunal assemblages already defined; these values were then entered into the calibration equation to produce paleotemperature estimates.

Since Imbrie and Kipp's pioneering work, there have been many attempts to refine and improve on their methodology (e.g., Ruddiman and Esmay, 1987; Dowsett and Poore, 1990; Guiot and de Vernal, 2007). The most widespread approach adopts a modern analog technique (MAT) to find the modern (core-top) assemblages that most closely resemble each fossil assemblage (Prell, 1985). Using a statistical measure (a similarity coefficient) to quantify how closely each modern assemblage is to the fossil one, the modern sea-surface temperatures of the "top 10" modern assemblages were then used in a weighted average, to estimate the paleo-SST. A similar approach was applied in the Atlantic Ocean, by Pflaumann et al. (1996, 2003) who demonstrated a very high degree of skill ($r^2 = 0.99$) in estimating modern SSTs for both summer and winter seasons over the entire range of Atlantic temperatures, from −1.4 °C (in winter at high latitudes) to +28.6 °C (in summer in equatorial regions). Trend-Staid and Prell (2002) also used the MAT to reconstruct LGM SSTs for the Atlantic, Pacific, and Indian Ocean Basins. For a comparison of the modern analog method with other approaches, see Kucera et al. (2005a), though different methods produce only minor differences in the overall reconstructions.

6.5 PALEOTEMPERATURE RECONSTRUCTION FROM SEDIMENT GEOCHEMISTRY

6.5.1 Paleotemperatures from Alkenones

Certain marine phytoplankton of the class Prymnesiophyceae, most notably the coccolithophorid *E. huxleyi*, respond to changes in water temperature by altering the molecular composition of their cell membranes. Specifically, as water temperature decreases, they increase the production of unsaturated ketones (alkenones). Cells contain a mixture of long-chain alkenones with 37, 38, or 39 carbon atoms (*n*-C_{37} to *n*-C_{39}), which are either di-, tri-, or tetra-unsaturated (designated, e.g., as $C_{37:2}$, $C_{37:3}$, or $C_{37:4}$, respectively). A temperature-dependent unsaturation index U^{k}_{37} is defined as

$$U^{k}_{37} = \frac{[C_{37:2}] - [C_{37:4}]}{[C_{37:2} + C_{37:3} + C_{37:4}]}$$

where $[C_{37:2}]$ represents the concentration of the di-unsaturated methyl ketone, alkadienone, containing 37 carbon atoms. The index varies from −1 (when all alkenones are $C_{37:4}$) to +1 (all $C_{37:2}$). However, since $C_{37:4}$ is absent in most marine sediments, the index can be simplified to

$$U^{k'}_{37} = \frac{[C_{37:2}]}{[C_{37:2} + C_{37:3}]}$$

Values are generally positive (~0.05-0.98) in Quaternary sediments (Brassell et al., 1986). The importance of these organic biomarkers is that they are produced by photosynthetic algae

and thus reflect conditions in the euphotic zone, and they are not influenced by changes in the salinity or isotopic composition of the ocean. They thus provide an important complement to $\delta^{18}O$ and faunal composition studies of marine paleotemperatures (Herbert, 2003; Rosell-Melé and McClymont, 2007).

Studies of the algae *E. huxleyi* in controlled growth chambers, and of sediments accumulating beneath areas with different SSTs, show a strong signal relating water temperature to $U^{k'}_{37}$ (Prahl et al., 1988; Sikes et al., 1991; Rosell-Melé et al., 1995). From a global survey of SSTs and alkenones in surface sediments (Conte et al., 2006), the $U^{k'}_{37}$-mean annual temperature relationship was found to be

$$\mathrm{MAT} = 29.876U^{k'}_{37} - 1.334, \quad r^2 = 0.97,\ n = 592$$

This relationship spans a range of temperature from ~0 to 30 °C (Figure 6.23). Although the data show a strong relationship between mean annual SSTs and alkenones in surface sediments, when compared to alkenones collected from surface waters and water temperatures in the mixed layer at the same time (integrated production temperature), there is an increasing disparity between the two data sets, which increases below ~22 °C. This may be related, in part, to the strong seasonality of alkenone production in certain areas (so that mean annual temperature is not the primary factor in production), or it could indicate that there is differential degradation of $C_{37:3}$ versus $C_{37:2}$ alkenones in the water column or in the sediments (Sachs et al., 2000; Conte et al., 2006; Rontani et al., 2013). Lateral advection of alkenones in some regions may also strongly bias the record.

Notwithstanding these issues, $U^{k'}_{37}$ is widely used as an SST paleothermometer in marine sediments. Where direct comparisons can be made, alkenones generally show similar SST estimates to those based on faunal composition (using modern analog or transfer functions) (e.g., Bard, 2000; Margo Project Members, 2009). Where differences occur, it is probably related to the fact that the two approaches are not dealing with precisely the same phenomena. Alkenone-based SSTs are derived from phytoplankton that live in the euphotic zone, particularly the upper 10 m of the water column. Furthermore, phytoplankton blooms commonly

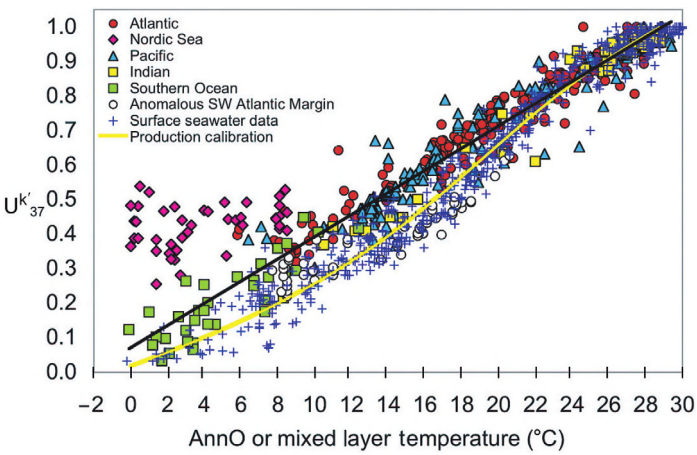


FIGURE 6.23 $U^{k'}_{37}$ in core-top sediments (colored symbols) versus mean annual surface water temperature in the overlying water column. A regression of these data is shown by the black line. The crosses (and yellow third-order polynomial regression line) show the relationship between alkenones collected from the water column and mixed layer (0-30 m) temperatures at the time of sampling (integrated production temperature). Samples from the Nordic Seas and the southwestern Atlantic Basin are affected by the advection of anomalously warm and cold water, respectively, and were not included in the regression calculation. *From Conte et al. (2006).*

occur rapidly at particular seasons, and the resulting organic sediment may thus represent a relatively short episode of only a few weeks (Sikes and Keigwin, 1994, 1996). In areas with a large annual range of SSTs, a shift in the seasonal timing of maximum phytoplankton productivity could result in different alkenone-based paleotemperatures, even without any real change in oceanographic conditions (Chapman et al., 1996). By contrast, the foram-based paleotemperatures are based on a set of different species that may reach peak abundances at different times of the year and live at different depth habitats. Consequently, such estimates are likely to represent more time- and depth-integrated measures of temperature change than those from alkenones. Furthermore, foram assemblage (and $\delta^{18}O$) data are subject to potential biases due to dissolution effects, whereas alkenone-based paleotemperatures are not (Sikes and Keigwin, 1994).

Alkenones from a Bermuda Rise sediment core (~33.6°N) provide a detailed record of SSTs for MIS 3 that reveals a remarkable similarity to the ice core oxygen isotope record from Greenland (Figure 6.24) (Sachs and Lehman, 1999). Abrupt warming from stadials to interstadials ranged from 1.7 to 5.3 °C, but during the transitions to interstadials 12 and 8, the high-resolution alkenone record shows that temperatures sharply cooled for a brief period. This has also been observed in a high-resolution oxygen isotope record from Peru (Kanner et al., 2012). Sachs and Lehman interpret the cooling as the result of cold water associated with icebergs and meltwater, which may have flooded the subtropical Atlantic during Heinrich events at those transitions (cf. Condron and Winsor, 2011).

By combining alkenone-based paleotemperature reconstructions with other approaches (such as faunal assemblage, or $\delta^{18}O$-based paleotemperature estimates), important new insights into paleoceanographic conditions can be obtained. For example, Zhao et al. (1995) studied sediments from off the northwest coast of Africa and found that paleotemperature minima at different times in the last 80 ka correspond closely to Heinrich events seen in North Atlantic sediments (see Section 6.10.1). These abrupt changes appear to represent times when cold meltwater, produced by ice-rafting events, was transferred southward by the Canary current, causing temperatures to decline by 3-4 °C in <100 years (Figure 6.25). Meltwater effects were also detected in northeastern Atlantic sediments by Sikes and Keigwin (1996) by comparing both alkenone and $\delta^{18}O$ records. This approach was used to good effect in "backing-out" past changes in salinity from an Indian Ocean sediment record by Rostek et al. (1993). They established SSTs using alkenones, then applied that to the $\delta^{18}O$ record to reconstruct paleosalinity (see also Caley et al., 2011). By subtracting the local temperature effect on $\delta^{18}O$, and knowing the effect of changing ice volume on $\delta^{18}O$, the residual change in $\delta^{18}O$ was interpreted as a record of changing salinity (Figure 6.26). High salinity (by +0.5-1‰) from 160 to 140 ka and 75 to 25 ka BP resulted from a weaker southwest monsoon (with less rainfall on the subcontinent and hence less runoff to the Bay of Bengal) and/or a stronger northeastern (counter) monsoon airflow at those times.

Other studies have applied alkenone analysis to high-resolution paleotemperature reconstruction of both recent sediments (e.g., to examine ENSO events; Kennedy and Brassell, 1992) and to periods of rapid environmental change during glacial terminations. "Younger Dryas-type" oscillations were found to have occurred during Terminations II and IV suggesting that similar mechanisms, involving rapid reorganization of North Atlantic Deep Water formation, occurred during earlier deglaciation events, as well as the most recent one (Eglinton et al., 1992).

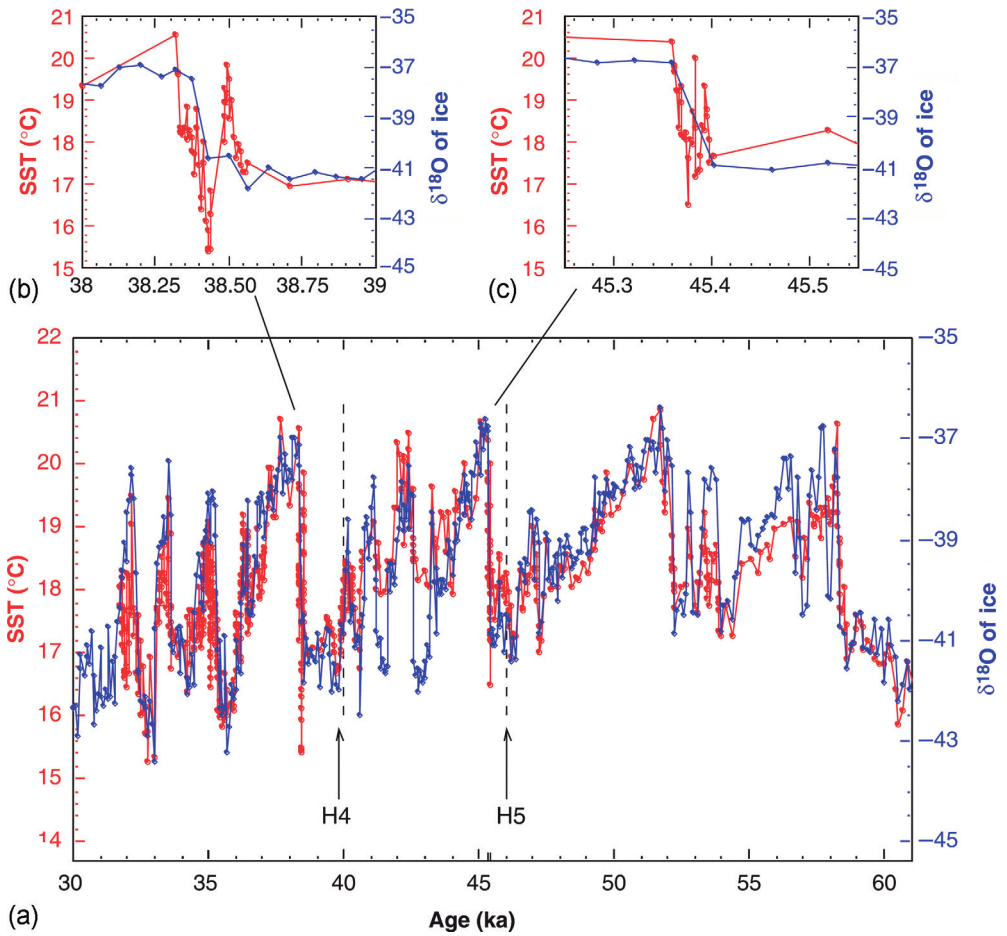


FIGURE 6.24 Alkenone-based SST reconstruction from the Bermuda Rise (red) compared to oxygen isotope data from GISP2 (blue). The timescale of the marine record has been aligned to that of the ice core record; note that this chronology has subsequently been revised (discussed in Chapter 5, Section 5.3). The transitions from stadial conditions to interstadials 12 and 8 (top right and top left, respectively) show a rapid reversal in SSTs, which may be associated with freshwater from icebergs and meltwater from the Laurentide Ice Sheet, flooding the Bermuda Rise at those times. *From Sachs and Lehman (1999).*

6.5.2 Paleotemperatures from TEX_{86} and Long-Chain Diols

Thaumarchaeota (which make up a phylum within the Archaea) are single-celled microorganisms that are ubiquitous in both marine and lacustrine environments. Thaumarchaeota have a lipid membrane that is modified in response to changes in water temperature (Schouten et al., 2013). These lipids include tetraethers with 86 carbon atoms—specifically glycerol dibiphytanyl glycerol tetraethers, or GDGTs (Figure 6.27). As temperatures increase, the Thaumarchaeota incorporate GDGTs with more cyclopentane rings into their lipid membranes (making them more rigid). Lipids extracted from

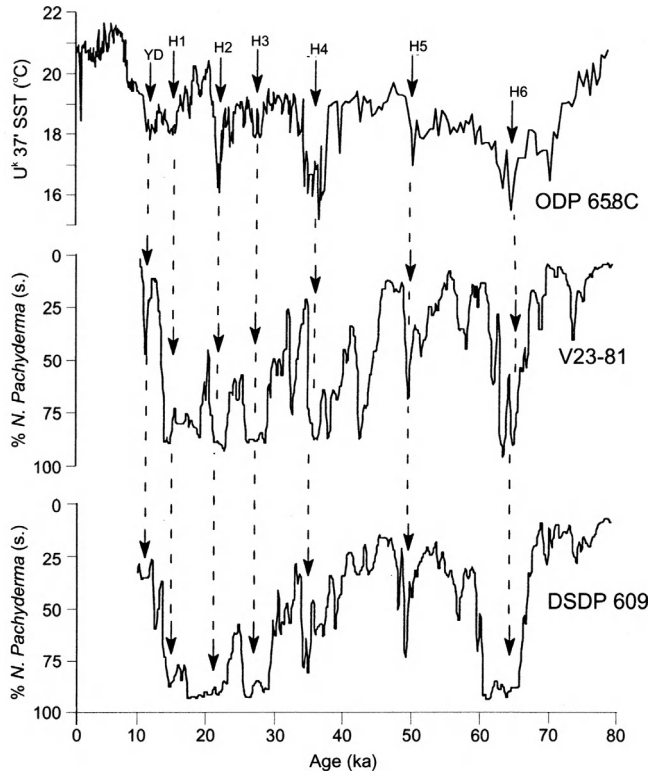


FIGURE 6.25 $U^{k'}_{37}$-based temperature reconstruction of SSTs in ODP core 658C from off the northwest coast of Africa (upper panel) compared to percentages of the cold-water foram *N. pachyderma* (s.) in two cores from the North Atlantic. The strong relationship between Heinrich events and cold water episodes in the North Atlantic with episodes of low SSTs off the African coast suggests a linkage via the cold Canary current carrying cool, low salinity meltwater southward at these times. *From Zhao et al. (1995).*

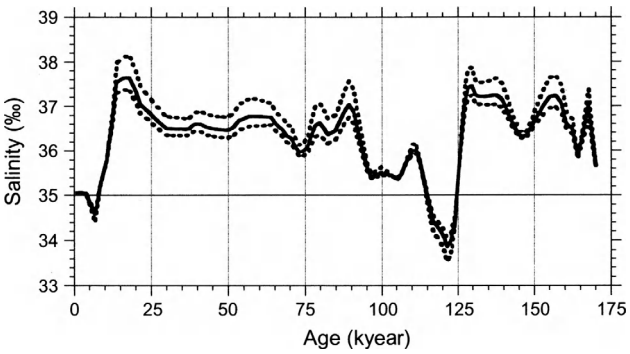


FIGURE 6.26 Paleosalinity reconstructed for the site of Indian Ocean core MD 9000963 (southwest of India). This was derived from $\delta^{18}O$ by obtaining paleotemperatures from alkenones and then adjusting the $\delta^{18}O$ record for these changes plus changes in global ice volume and salinity due to continental ice growth and decay. The residual $\delta^{18}O$ changes are interpreted as a record of paleosalinity. *From Rostek et al. (1993).*

core-top marine sediments from globally distributed samples demonstrate that the average number of cyclopentane rings in the assemblage of GDGTs is strongly (positively) related to SSTs, offering the prospect of using this as a paleotemperature proxy (Schouten et al., 2002). To that end, a tetraether index, TEX_{86}, was developed (at the Royal Netherlands Institute for Sea Research (NIOZ) in Texel) based on the relative number of cyclopentane rings in the lipid extracts:

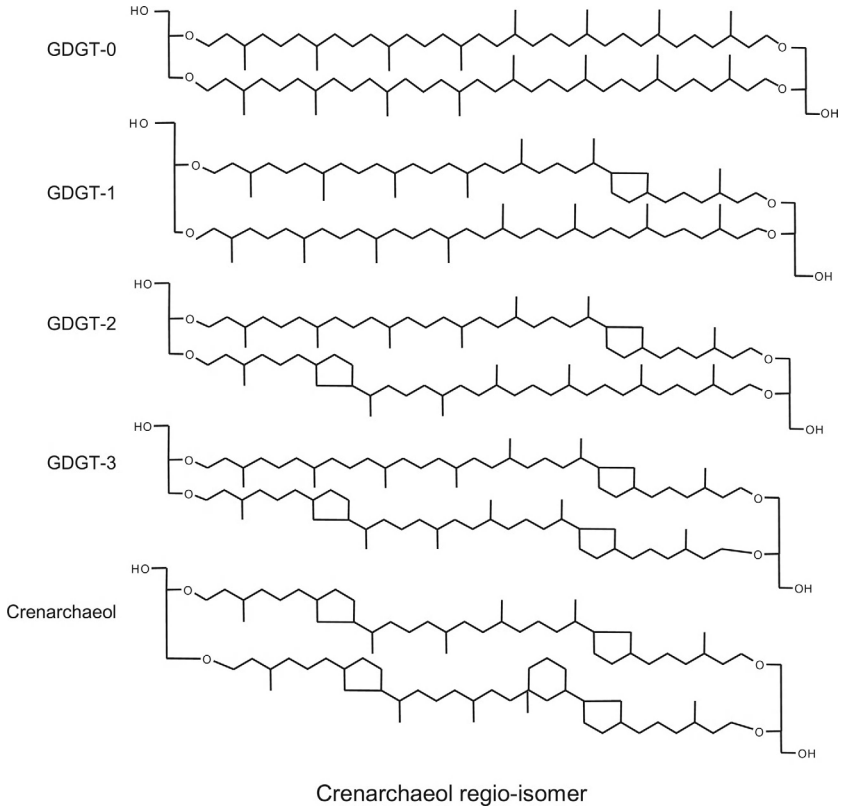


FIGURE 6.27 The chemical structure of GDGTs that are used to formulate the TEX_{86} index. The lipids are tetraethers with 86 carbon atoms and contain 1-4 cyclopentane moieties. Crenarchaeol also contains a cyclohexane moiety; in the calculation of TEX_{86}, cren′, a regio- (positional) isomer of crenarchaeol, is used. It is worth noting that in the literature, these tetraethers are commonly numbered differently, which can cause confusion. *From Kim et al. (2010).*

$$TEX_{86} = \frac{([GDGT-2] + [GDGT-3] + [cren'])}{([GDGT-1] + [GDGT-2] + [GDGT-3] + [cren'])}$$

where GDGT-1 to GDGT-3 are the amounts of GDGTs containing one to three cyclopentane moieties, respectively, and cren′ is a positional (regio-) isomer of crenarchaeol, which has 4 cyclopentane moieties and a cyclohexane ring (Figure 6.27) (Schouten et al., 2002; Kim et al., 2008).

Although there are uncertainties about precisely when (seasonally) or where (vertically) in the water column Thaumarchaeota live and biosynthesize the GDGTs (e.g., Wuchter et al., 2005; Herfort et al., 2006; Huguet et al., 2007; Turich et al., 2007; Kim et al., 2008; Shah et al., 2008), the empirical evidence relating mean annual SSTs and TEX_{86} is nevertheless quite strong (e.g., Wuchter et al., 2006), and so the index has been applied to reconstruct

paleotemperatures in a number of studies. Based on a large array of core-top samples, the following formula best describes the data (Kim et al., 2010):

$$\mathrm{SST} = 68.4^{*}\log(\mathrm{TEX}_{86}) + 38.6$$

This equation is highly significant over an SST range of ~6-30 °C; Kim et al. (2010) referred to this equation as $\mathrm{TEX}_{86}^{\mathrm{H}}$. For temperatures below ~5 °C, Kim et al. (2010) proposed eliminating cren′ from the TEX_{86} equation, to obtain a better fit to observations; they refer to this value as $\mathrm{TEX}_{86}^{\mathrm{L}}$ (and $\mathrm{SST} = 67.5^{*}\mathrm{TEX}_{86}^{\mathrm{L}} + 46.9$). TEX_{86} can complement alkenone-based and other temperature estimates, and because diagenetic changes in GDGTs appear to be minimal (unlike alkenones), there is the possibility of using TEX_{86} in pre-Quaternary sediments (e.g., Jenkyns et al., 2004; Sluijs et al., 2006). TEX_{86} applications in lakes are more complicated and are discussed in Chapter 9, Section 9.7).

Another group of lipids that appear to have potential as paleothermometers are long chain *n*-alkyl diols. These have chain lengths that vary from C_{24} to C_{36} and an alcohol group at C_1 and another position that may vary from C_{11} to C_{19}. The important diols in marine sediments for paleotemperature reconstruction are C_{28}, C_{30}, and C_{32}, specifically the diols C_{28}1,13, C_{30}1,13, and C_{30}1,15 (produced by diatoms and marine algae). Based on the analysis of core-top samples, a long-chain diol index (LDI) was found to be strongly correlated with SSTs over a temperature range of −3 to 27 °C (Rampen et al., 2012):

$$\mathrm{LDI} = \frac{F[\mathrm{C}_{30}1,\ 15-\mathrm{diol}]}{F[\mathrm{C}_{28}1,\ 13-\mathrm{diol}] + F[\mathrm{C}_{30}1,\ 13-\mathrm{diol}] + F[\mathrm{C}_{30}1,\ 15-\mathrm{diol}]}$$

where *F* indicates the fractional abundance of each diol. So far, there have only been a few studies that have examined the LDI in relation to other proxies (e.g., Naafs et al., 2012; Lopes dos Santos et al., 2013), but it appears to provide another useful method for paleotemperature estimates, providing comparable values to foraminiferal assemblage, alkenone, and TEX_{86}-based estimates. However, each of the indices may be biased toward SSTs in a particular season or toward mean annual conditions, potentially providing useful information about the seasonality of SSTs (Figure 6.28).

6.5.3 IP_{25} and Related Sea Ice Proxies

IP_{25} is a lipid biomarker produced by diatoms (mainly *Haslea* spp.) that inhabit sea ice. Thus, although not a direct indicator of SSTs, it serves as an indicator of the presence of sea ice, which is obviously related to ocean surface temperature (Belt et al., 2007, 2010). The key (ice proxy) molecule is a highly branched isoprenoid (HBI) alkene with 25 carbon atoms (Figure 6.29). Field studies of sea ice and of surface sediments in areas where sea ice ranges from only seasonally present to complete cover all year show that IP_{25} can be a very useful indicator of the presence of sea ice and its variation over time. However, it does not appear that IP_{25} is produced by sea ice algae in the Antarctic, so at present, all IP_{25} studies relate only to Arctic sea ice. A related compound (an HBI diene) may provide a comparable indicator for Southern Hemisphere sea ice variations (Massé et al., 2011). As with all biomarkers, there are many questions regarding the controls on organisms producing the compound (e.g., the influences of nutrients, light and other variables, and seasonality of production) as well as issues relating to preservation of the biomarker (degradation over time,

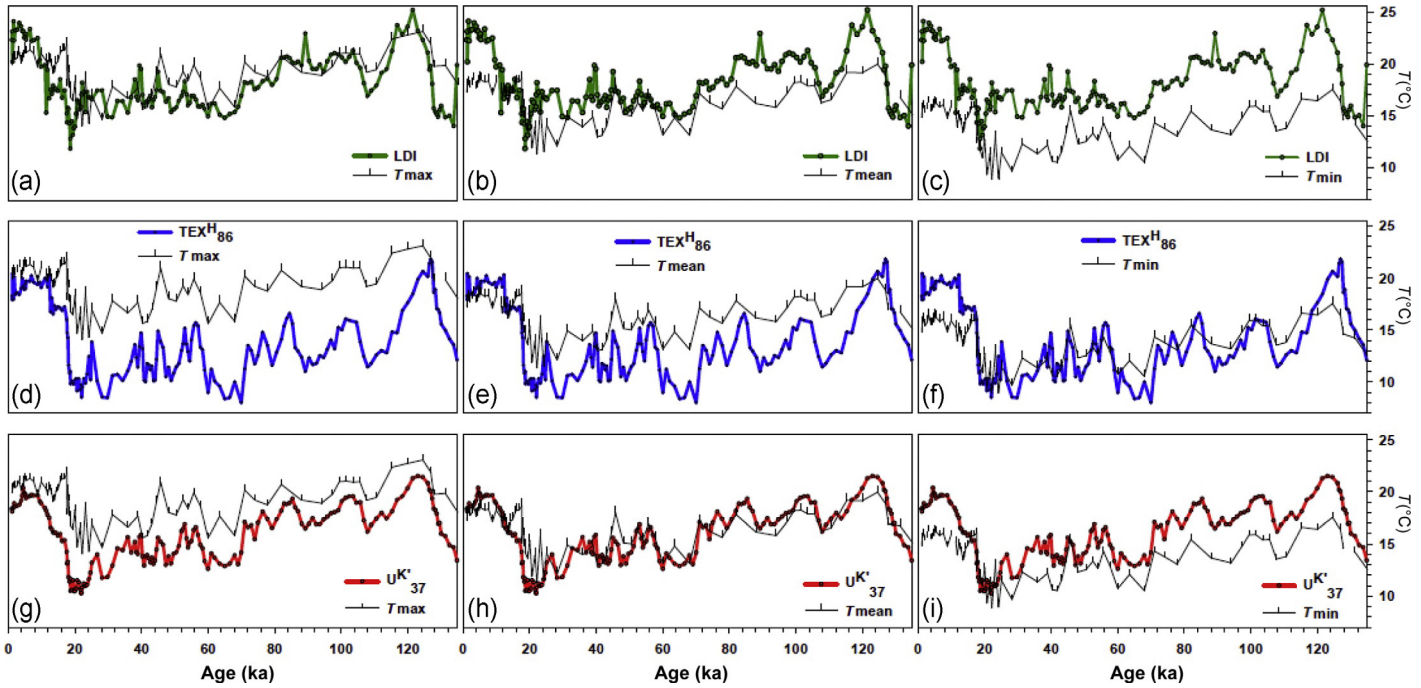


FIGURE 6.28 A comparison of paleo-SST estimates over the last 130,000 years for a site off southeastern Australia, based on faunal (foraminiferal) assemblages (derived from the modern analog technique) (narrow line in all plots) as well as from the long-chain diol index (LDI) (green, top panels), TEX^{H}_{86} (blue, middle panels), and $U^{k'}_{37}$ (red, bottom panels). The three panels show the seasonal maximum (left), annual mean (middle), and seasonal minimum (right) SST estimates from the faunal data. Assuming these are correct, in this location the LDI corresponds most closely to maximum (summer) temperatures, whereas TEX^{H}_{86} is closest to minimum (winter) temperatures, and $U^{k'}_{37}$ tracks mean annual temperatures. In this example, the TEX_{86}-based SSTs are derived from a logarithmic calibration, which optimizes the fit to data at higher temperatures (designated as TEX^{H}_{86} by Kim et al., 2010). *From Lopes dos Santos et al. (2013).*

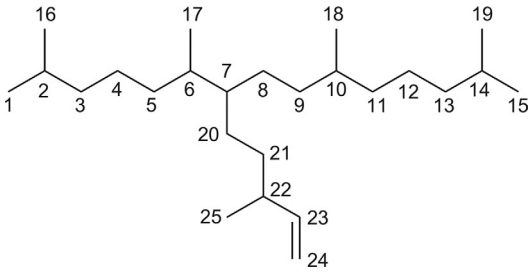


FIGURE 6.29 The structure of IP_{25}, a highly branched isoprenoid alkene with 25 carbon atoms, which is produced by diatoms that inhabit environments at the sea ice margin. *From Belt and Müller (2013).*

which is especially important where ratios of specific compounds are used, water depth, etc.) and the extent of lateral transport from the production location to the site of deposition. Nevertheless, the indications so far are that IP_{25} is an excellent proxy for Arctic sea ice conditions. This is particularly so if the IP_{25} proxy is combined with sterol biomarkers, such as dinosterol or brassicasterol, that are produced by phytoplankton in ice-free waters. Thus, Müller et al. (2011) proposed an additional index, PIP_{25}, that combines data on IP_{25} with a phytoplankton biomarker (P) indicative of ice-free conditions:

$$PIP_{25} = IP_{25}/(IP_{25} + P_c)$$

where c (the ratio of the mean IP_{25} and mean P concentration) is a factor used to compensate for the generally much higher concentrations of phytoplankton content compared to IP_{25}. Using both biomarkers, a full range of sea ice conditions may be assessed (Figure 6.30).

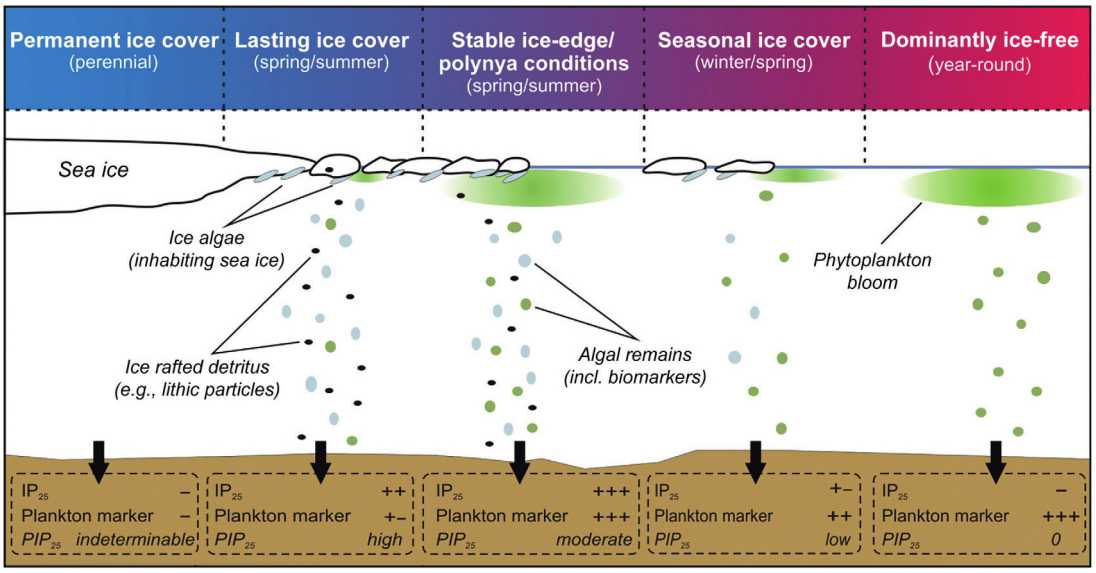


FIGURE 6.30 Changes in sea ice extent, from permanently ice-covered to predominantly ice-free conditions, can be identified by the use of the biomarker proxy IP_{25}, together with other phytoplankton biomarker indices (assuming limited lateral transport from the sea ice production location to the sediment deposition site). *From Belt and Müller (2013).*

However, sea ice diatoms also contribute to the overall sterol content of sediment, which could have a significant effect on this index (Rampen et al., 2010; Belt et al., 2013). Further research is needed to clarify the full range of attributes and limitations of these emerging new proxies, though there are a number of studies that point to their potential (e.g., Massé et al., 2008; Vare et al., 2009; Cabedo-Sanz et al., 2013). IP_{25} has been extracted from sediment cores from the interisland channels of the Canadian Arctic Archipelago to obtain a sea ice reconstruction for the Holocene. This shows that spring/early summer sea ice was limited for much of the Early to Mid-Holocene but increased after ~4000 years BP, reaching maxima around ~2300 years BP, and during recent centuries, in the Little Ice Age (Vare et al., 2009; Belt et al., 2010). Cabedo-Sanz et al. (2013) studied sediment cores spanning the Younger Dryas interval from near the coast of northwestern Norway. Using IP_{25} and phytoplankton sterols to derive a PIP_{25} index, they showed clearly that sea ice abruptly formed in that region at the onset of the Younger Dryas (having been absent before that) and disappeared once again after ~11,500 years BP (Figure 6.31). On a shorter timescale, Massé et al. (2008) reconstructed sea ice variations north of Iceland for the last millennium, showing a close

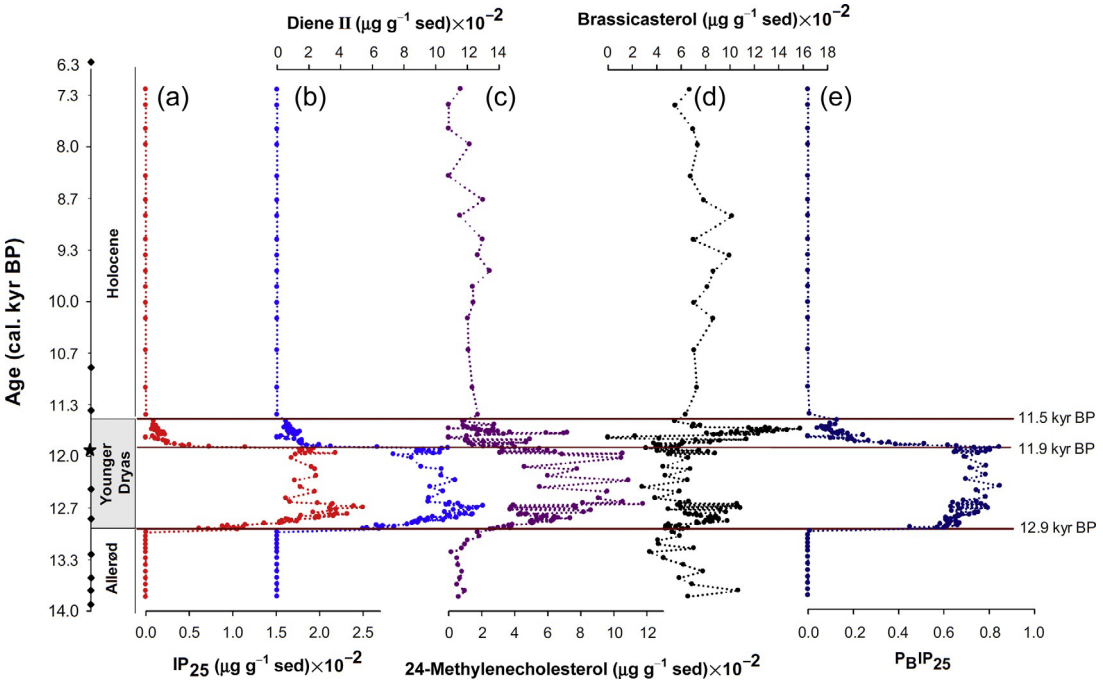


FIGURE 6.31 Concentration profiles of biomarkers in marine sediment core JM99-1200 from off the northwestern coast of Norway (at ~69°N, 16°E) (a) IP25; (b) diene II; (c) 24-methylenecholesterol; (d) brassicasterol; (e) PIP_{25} index (using brassicasterol as the phytoplankton biomarker indicative of ice-free conditions). The horizontal solid lines at 12.9 and 11.5 ka BP approximate the onset and termination of the Younger Dryas. The horizontal solid line at ca. 11.9 cal. ka BP represents a shift in sea ice conditions during the later Younger Dryas. Diamonds mark the AMS ^{14}C dates and the asterisk indicates the Vedde Ash tephra horizon used in the age model. The biomarkers indicate that sea ice was absent from this location both before and after the Younger Dryas but was present during the coldest part of the Younger Dryas interval. *From Cabedo-Sanz et al. (2013).*

correspondence with historical records of sea ice extent and with independent proxies of SSTs. These and other studies thus reveal the potential of IP_{25} and related indices to provide valuable new insights into the extent and variability of sea ice in the past.

6.5.4 Paleotemperatures from Mg/Ca Ratios

During the formation of biogenic calcium carbonate, Mg^{2+} may substitute for Ca^{2+}; this process is temperature-dependent, with greater substitution occurring as water temperatures rise (Figure 6.32). Measurements of the Mg/Ca ratio in forams can thus provide an index of water temperature at the time (and depth) of calcite formation, which can be directly compared to the oxygen isotopic composition of the same material (Barker et al., 2005; Rosenthal, 2007). Because Mg/Ca and oxygen isotopes both reflect the time that the foram test is produced, by selecting species with a particular depth habitat, paleotemperatures at those depths can be obtained. Moreover, Mg/Ca data are not affected by changes in salinity, which can influence the isotopic composition of foram tests. An interesting application of Mg/Ca ratios to obtain paleotemperature data is provided by Lea et al. (2003). They produced a high-resolution SST record from the Cariaco Basin (~11.5°N) from Mg/Ca ratios in *G. ruber* for the period spanning the LGM to the present. The oxygen isotope record from the site shows an overall decline related to the changing isotopic composition of the oceans as the continental ice sheets melted, but the Mg/Ca data provide a record of SSTs in the basin, which is strongly correlated with the oxygen isotope record from Greenland, like the alkenone-derived SSTs from the Bermuda Rise discussed earlier (see also Figure 6.52; Deplazes et al., 2013). LGM cooling in the basin was $\sim 2.6 \pm 0.5$ °C relative to today. Temperatures abruptly declined during the Younger Dryas interval, synchronous (within dating errors) with changes in the ice core $\delta^{18}O$ and with CH_4 (Figure 6.33). These connections are thought to be related to shifts in the position of the Intertropical Convergence Zone (ITCZ) during termination 1, with a more southerly position during the Younger Dryas, leading to cold and dry conditions over the Cariaco Basin and generally drier conditions across tropical wetlands (which reduced CH_4 production) (cf. Chiang and Friedman, 2012).

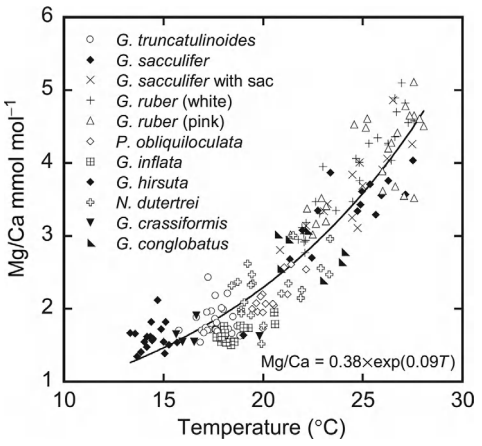


FIGURE 6.32 Relationship between Mg/Ca and temperature for different species of foraminifera, based on sediment trap collections. *From Barker et al. (2005), using data from Anand et al. (2003).*

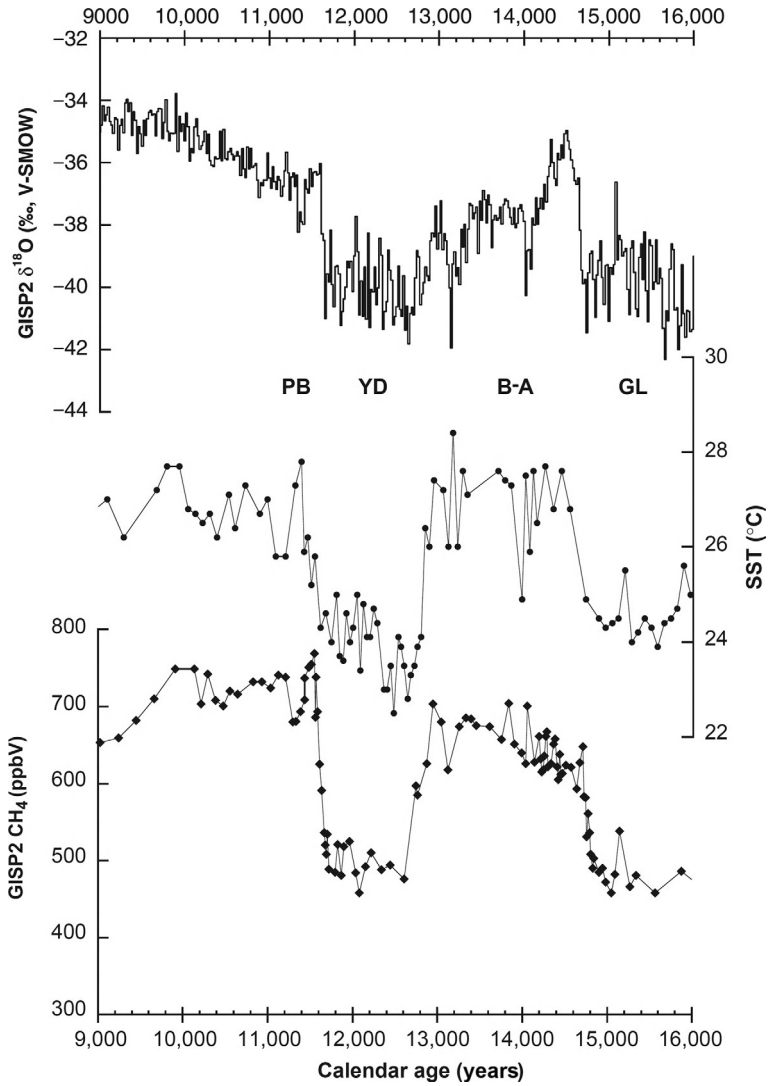


FIGURE 6.33 SSTs in the Cariaco Basin reconstructed from Mg/Ca ratios (middle) compared to GISP2 oxygen isotope data (top) and CH_4 (bottom). PB, preboreal; YD, Younger Dryas; B-A, Bølling-Allerød; GL, glacial. *From Lea et al. (2003).*

6.6 OCEANOGRAPHIC CONDITIONS AT THE LAST GLACIAL MAXIMUM (LGM)

One of the most important applications of these various quantitative paleotemperature reconstruction techniques has been the mapping of paleoceanographic conditions across the world's oceans for selected time intervals in the past. This was one of the major objectives

of the CLIMAP project (Climate: Long-range Investigation, Mapping, and Prediction), which focused attention on marine conditions at the LGM (which they defined as 18,000 ^{14}C years BP, ~21,500 cal. years BP) (CLIMAP Project Members, 1976, 1981, 1984). Using microfossil transfer functions derived for each of the major world oceans, February and August sea-surface temperatures were reconstructed for this period. Most studies relied mainly on foraminiferal assemblage data, but in areas where siliceous fossils predominate (e.g., in the South Atlantic and Antarctic Oceans), the technique was also applied to radiolarian assemblages (Lozano and Hays, 1976; Morley and Hays, 1979) and to diatoms (Koç Karpuz and Schrader, 1990; Pichon et al., 1992). In the Pacific Ocean, where preservational characteristics of carbonate and siliceous fossils vary significantly from one area to another, it was found to be advantageous to develop transfer functions based on four major microfossil groups (coccoliths, foraminifera, radiolaria, and diatoms) to achieve optimum paleotemperature reconstructions (Geitzenauer et al., 1976; Luz, 1977; Moore, 1978; Sancetta, 1979; Moore et al., 1980). These efforts contributed greatly to our understanding of past changes in ocean surface temperatures, generating many important new insights and hypotheses about orbital forcing and mechanisms of glaciation, such as the rates and timing of ice sheet growth and decay (Hays et al., 1976; McIntyre et al., 1975, 1976; Ruddiman and McIntyre, 1981). Following CLIMAP, the SPECMAP (*Spectral Mapping Project*) focused on determining the spectral characteristics of the ocean sediment-based paleoclimatic record and establishing a basic time frame for past climatic events (Imbrie et al., 1984; Martinson et al., 1987). Subsequent research has focused not only on surface water conditions but also on the three-dimensional structure of the world's oceans through time, in an effort to reconstruct the deepwater circulation that plays a critical role in energy transfer and the sequestration of carbon dioxide in the abyss. These efforts include EPILOG (Environmental Processes of the Ice Age: Land, Oceans, Glaciers), GLAMAP (Glacial Atlantic Ocean Mapping), and MARGO (Multiproxy Approach for the Reconstruction of the Glacial Ocean Surface) (Mix et al., 2001; Pflaumann et al., 2003; Sarnthein et al., 2003; Kucera et al., 2005b; MARGO Project members, 2009).

The MARGO project combined reconstructed SSTs from microfossil-based transfer functions with those based on geochemically based paleotemperature reconstructions (alkenones and Mg/Ca) to provide a comprehensive assessment of SSTs during the LGM (which they defined as 23,000-19,000 years BP). Figure 6.34 shows the global SST differences (LGM-present) for the world oceans. Several important features stand out in this analysis. As shown in the CLIMAP reconstructions, SSTs in the subtropical gyres were very similar to today, perhaps even slightly warmer in some regions. The largest change in SSTs occurred in the central North Atlantic, west of Ireland, where temperatures were ~12 °C cooler than today (Figure 6.35). Strong east-west temperature gradients were features of the tropical and equatorial seas, indicating much stronger upwelling associated with eastern boundary currents, especially in the Atlantic Basin. In the North Atlantic, there is less agreement among the different proxies (de Vernal et al., 2006), but it appears that sea ice was extensive as far south as 55°N in winter, and open water conditions occurred as far north as Svalbard (~75°N) in summer months (Figure 6.35). Although there is more variability in the geochemically based paleotemperature estimates, overall zonally averaged temperatures across the entire Tropics were generally <2 °C cooler than today (Figure 6.36). For the global oceans as a whole, SSTs were 1.9 ± 1.8 °C cooler at the LGM, with the largest changes in temperature in the North Atlantic Ocean.

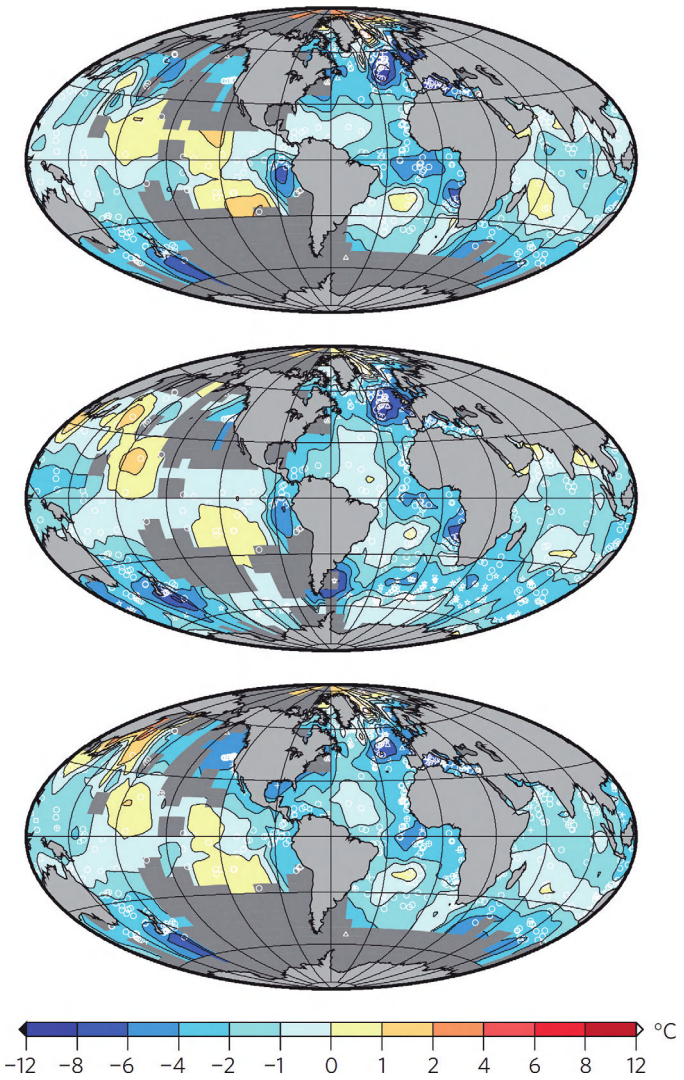


FIGURE 6.34 LGM sea-surface temperature (SST) anomalies, reconstructed from biological indicators (forams, diatoms, dinoflagellate cysts, and radiolaria) and from geochemical paleothermometry (Mg/Ca, alkenones). Anomalies are (LGM-modern World Ocean Atlas data) (1998). Top: July-September; middle: January-March; bottom: mean annual anomalies. *From MARGO Project Members (2009).*

It is particularly interesting that the cooling of ocean surface temperatures at low latitudes during the LGM was relatively small. This conclusion contrasts with some of the terrestrial evidence from the Tropics. For example, Standell et al. (2007) estimate from changes in glacier equilibrium line altitudes in the Venezuelan Andes that temperatures there were $\sim 8.8 \pm 2\,^{\circ}C$ lower at the LGM than today. Large temperature changes are also suggested by studies of noble gases in groundwater from tropical Brazil. The concentration of noble gases (Ne, Ar, Kr, and Xe) in groundwater is largely a function of the temperature at the water table where dissolution occurs. By comparing noble gas concentrations in radiocarbon-dated groundwaters of Holocene and of glacial age, a temperature difference of $5.4 \pm 0.6\,^{\circ}C$ was estimated.

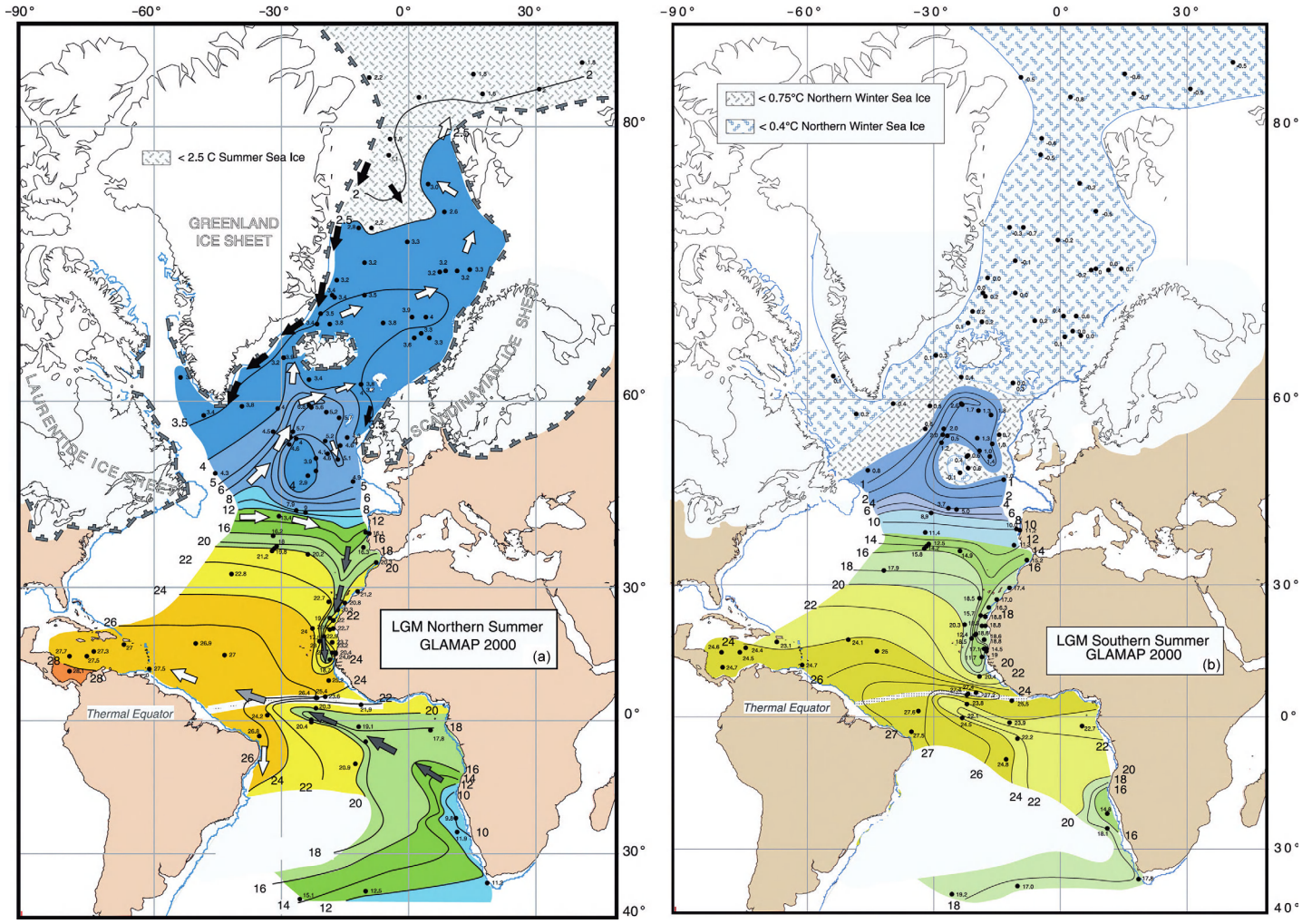


FIGURE 6.35 GLAMAP 2000 SST reconstruction of the glacial Atlantic for Northern Hemisphere summer (left) and winter (right). Arrows indicate major current directions (gray for cold, white for warm). Position of the thermal equator is shown by whitish stippled belt. Blue contours mark the position of glacial shore lines. *From Pflaumann et al. (2003).*

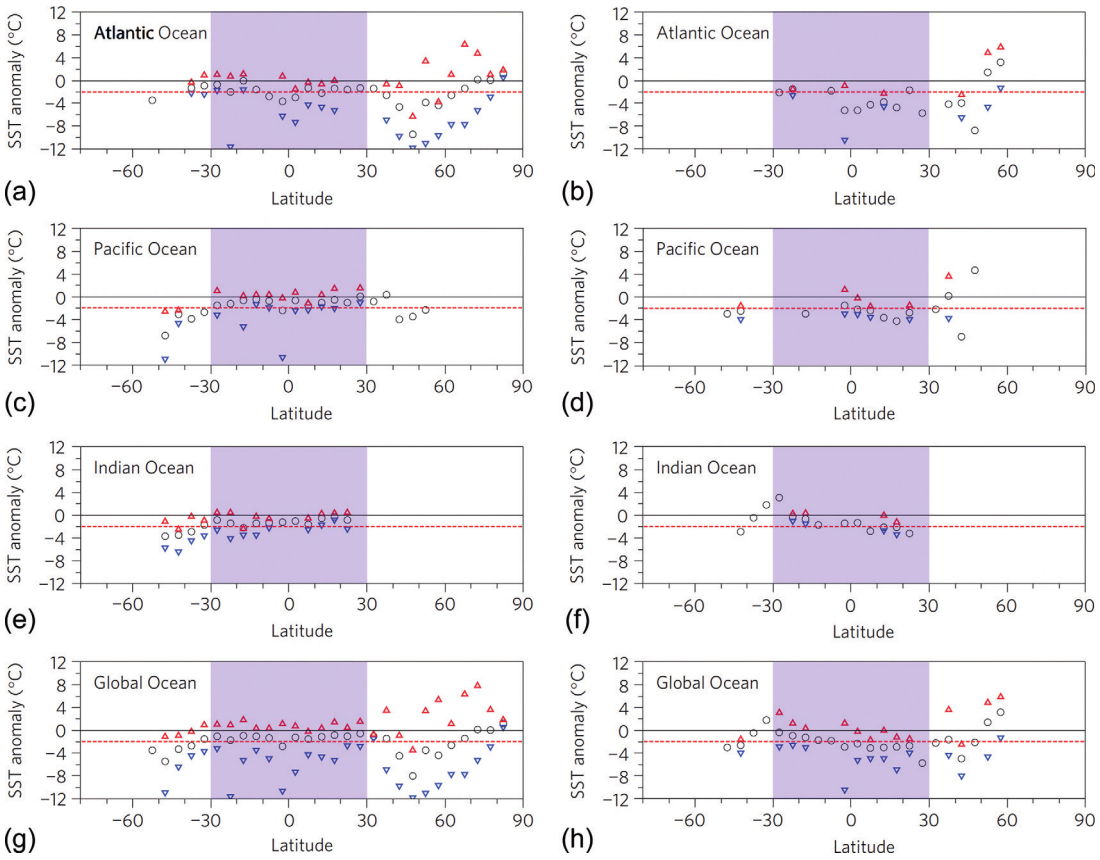


FIGURE 6.36 Zonal averages of SST anomalies (LGM-present) for different ocean basins and for the global ocean. Left panels are estimates based on foraminifera and dinocyst assemblages; the right hand panels show estimates based on alkenones and Mg/Ca estimates from foraminifera. Triangles show the upper and lower extremes of each estimate, and the circles show the averages. Red dashed line indicates anomalies of −2 °C. The gray shading shows the zone from 30°N to 30°S (which is half of the surface area of the globe). It is notable that in this region, temperatures were generally <2 °C cooler during the LGM than at the present time. *Modified from MARGO Project Members (2009).*

Miller et al. (1997) estimated that temperatures in central Australia were at least 9 °C colder in glacial times compared to the Holocene, based on the extent of racemization of amino acids in ^{14}C-dated emu eggshells. Since racemization is a function of age and temperature, by controlling for age, paleotemperatures could be calculated (see Chapter 4, Section 4.2.1.4). These diverse lines of evidence point to significantly cooler temperatures on land, in tropical and subtropical latitudes at the LGM. Such a contrast is also demonstrated in GCMs for both paleoclimate and future climate simulations, in which temperatures over land areas in the Tropics tend to change more than over the oceans (Izumi et al., 2013). However, the paleoclimatic evidence indicates that there were even larger land-ocean contrasts in the past than are shown in the model simulations.

6.7 PALEOCLIMATIC INFORMATION FROM INORGANIC MATERIAL IN MARINE SEDIMENTS

Weathering and erosion processes in different climatic zones may result in characteristic inorganic products. When these are carried to the oceans (by wind, rivers, or floating ice) and deposited in offshore sediments, they convey information about the climate of adjacent continental regions or about the oceanic and/or atmospheric circulation at the time of deposition (McManus, 1970; Kolla et al., 1979). On continental margins, the bulk of sediment is deposited by rivers, but in remote areas of the ocean, far from land areas and the influence of floating ice, very fine wind-blown material washed out of the atmosphere may form a significant proportion of the total sediment accumulation (Windom, 1975). Modern observations show that total dust flux thousands of kilometers downwind of arid regions is mainly a function of conditions in the source region, whereas variations in grain size are more related to changes in (upper level) wind speed (Rea, 1994). Thus, by examining variations in the eolian fraction of marine sediment cores, an important index of continental aridity, modulated by changes in airflow patterns, can be obtained. For example, in a sediment core 2500 km east of the Chinese Loess Plateau, Hovan et al (1989, 1991) found large variations in eolian accumulation rates that correspond to changes in the environment of the Loess Plateau. During interglacials, when loess accumulation slowed and soils formed on the plateau, eolian flux rates were low, but during glacial periods (defined by the benthic $\delta^{18}O$ record of the same core) eolian flux rates were many times higher (Figure 6.37).

Numerous studies of inorganic material in cores from off the coast of West Africa have enabled climatic fluctuations of the adjacent land mass to be deduced. In this area today, vast quantities of silt and clay-sized particles (>25 million tons per year) are transported from the Sahara desert westward across the Atlantic by the northeast trade winds (Chester and Johnson, 1971). During Late Quaternary glacial epochs, an even higher proportion of terrigenous material accumulated in the equatorial and tropical Atlantic, off West Africa due to stronger trade winds and a more extensive arid zone (Figure 6.38) (Sarnthein et al., 1981; Matthewson et al., 1995). Further support for this scenario of drier conditions during glacial episodes is provided by studies of biogenic detritus in ocean cores. The concentration of freshwater diatoms (*Melosira*) and opal phytoliths (minute silica bodies derived from epidermal cells of land plants, particularly grasses) increased during glacial periods in cores south of 20°N off the coast of West Africa. It is suggested that this results from deflation of lacustrine sediments by stronger trade winds in relatively dry glacial times, following more humid interglacial periods when (grassland) vegetation was extensive and lakes were more common (Parmenter and Folger, 1974; Pokras and Mix, 1985).

Another region of major eolian dust flux to the oceans is off the coast of the Arabian Peninsula. Today, strong northwesterly winds carrying fine-grained sediments to the Indian Ocean sweep over low level southwesterly (monsoon) winds from Somalia. In modern sediments, the 30% isoline of siliciclastic grains (>6 μm) approximates the location of the main convergence zone between the northwesterly and southwesterly airflows. Reconstructions of the position of this isoline for various time slices in the past thus track variations in this convergence zone, showing that it was further to the southeast during the LGM (i.e., stronger northwesterly airflow) but much closer to the coast 6-9 ka BP (Figure 6.39) (Sirocko and Sarnthein, 1989; Sirocko et al., 1991).

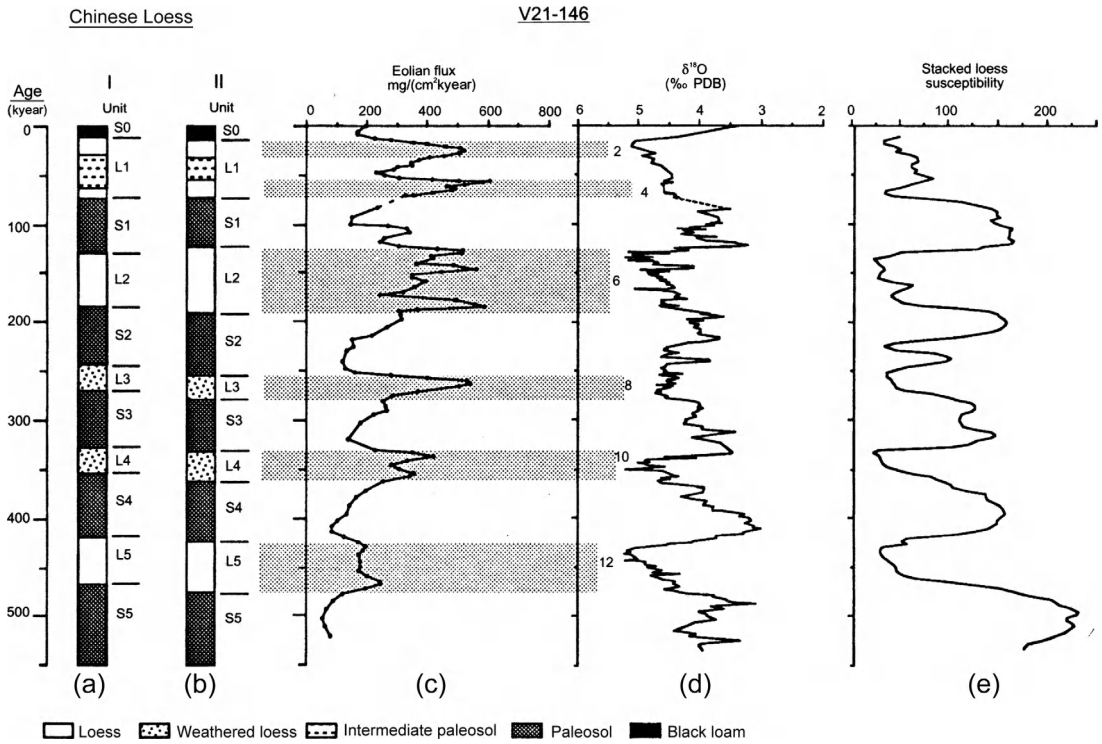


FIGURE 6.37 Eolian flux recorded in North Pacific core V21-146 (from ~38°N, 163°E) and benthic isotope record in the same core (center graphs) compared to the magnetic susceptibility of loess in a stacked set of records from the Chinese Loess Plateau (right graph). The chronology of loess and paleosol units described by Kukla (1987a) is shown on the extreme left (column I). Revised ages, based on correlations between the marine record and the loess susceptibility are shown in the second (column II). *From Hovan et al. (1991).*

A final example comes from the Southern Hemisphere where eolian sediments in the Tasman Sea record variations in aridity in southeastern Australia (Hesse, 1994). During glacial periods, dust flux increased by 50-300% and the northern boundary of the main dust plume shifted equatorward by ~350 km. This cyclical pattern of increased dust flux during glacial periods and reduced dust flux in interglacials is superimposed on a longer-term increase in overall eolian sediment that began ~350-500 ka ago, reflecting the increasing aridification of southeastern Australia.

In each of these cases, there is strong evidence that eolian dust flux to the oceans was much greater during the last glaciation, as well as during earlier glacial events. Part of this increase was probably related to a stronger pole-equator temperature gradient and higher wind speeds (cf. Wilson and Hendy, 1971), but there were also much larger arid areas in the intertropical zone during glacial times (Sarnthein, 1978). Both factors led to far higher levels of atmospheric turbidity during glacial periods, and this is well recorded in remote polar (and high elevation) ice cores as a pronounced increase in particulate matter (e.g., Petit et al., 1999; Winckler et al., 2008) (Figure 6.40). There has also been speculation that the higher

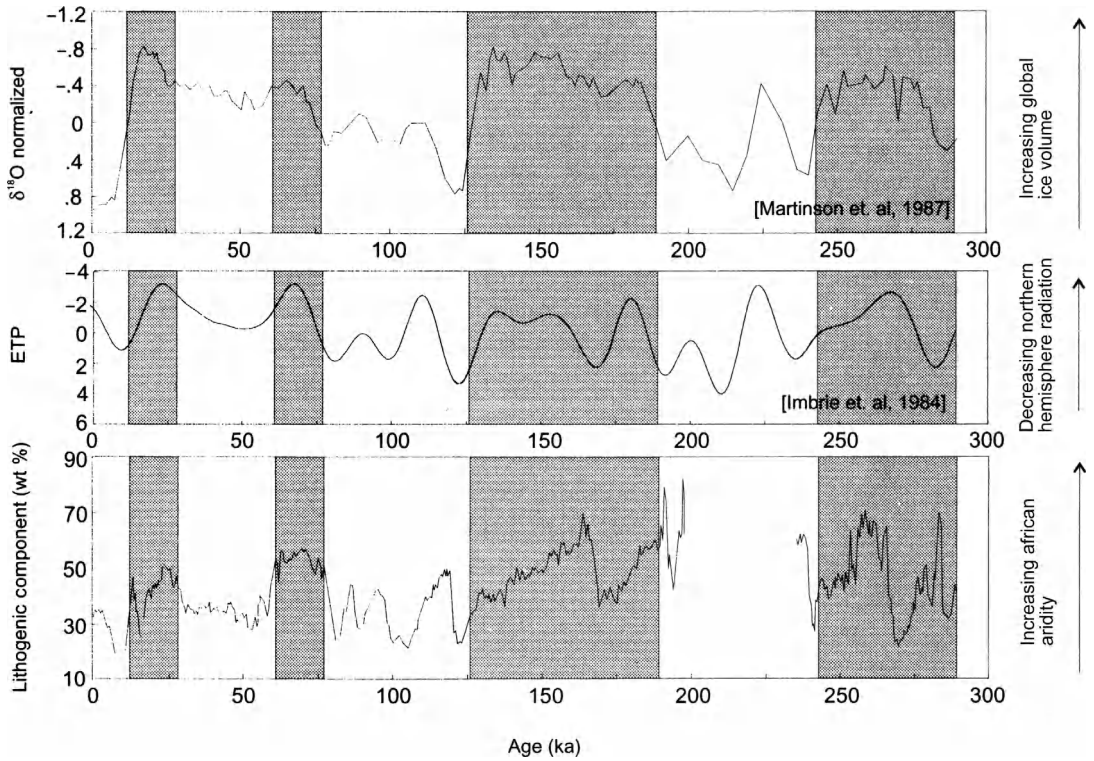


FIGURE 6.38 The lithogenic component of marine core CD53-30 (~20°N, 21°W, from off the northwest coast of Africa) (bottom panel) compared to the SPECMAP marine isotope record (upper panel) and the combined Northern Hemisphere record of precession, obliquity, and eccentricity forcing (middle panel). Glacial periods (shaded) correspond to higher levels of eolian dust flux from the Sahara to the adjacent ocean. The rapid increases in dust are generally associated with decreasing Northern Hemisphere radiation, driven by changes in precession, though the abrupt shifts in dust content suggest a nonlinear response to orbital forcing. *From Matthewson et al. (1995).*

amounts of eolian material may have played a role in controlling carbon dioxide levels in the atmosphere during glacial periods. Since biological activity (particularly in the Southern Ocean) is limited by a lack of iron, the additional iron deposited in the oceans during glacials may have increased oceanic photosynthetic activity to the point that carbon dioxide levels were reduced (Martin, 1990). Recent experiments to "seed" oligotrophic ocean areas with iron have indeed shown that productivity increases significantly when this limiting factor is removed (e.g., Coale et al., 1996; Pollard et al., 2009), but to what extent this mechanism contributed to the lower carbon dioxide levels of glacial times remains controversial.

Coarse-grained sediments found in sediment cores in remote parts of the ocean provide evidence of former ice-rafting episodes (either from icebergs or from formerly landfast sea ice). One of the most compelling lines of evidence that large-scale continental glaciation began in the early Pleistocene is based on the first appearance of ice-transported coarse sediment in cores from both the North Atlantic and the North Pacific. Shackleton et al. (1984) placed the timing of this at ~2.4-2.5 Ma ago in the North Atlantic; Haug et al. (2005) dated the onset of

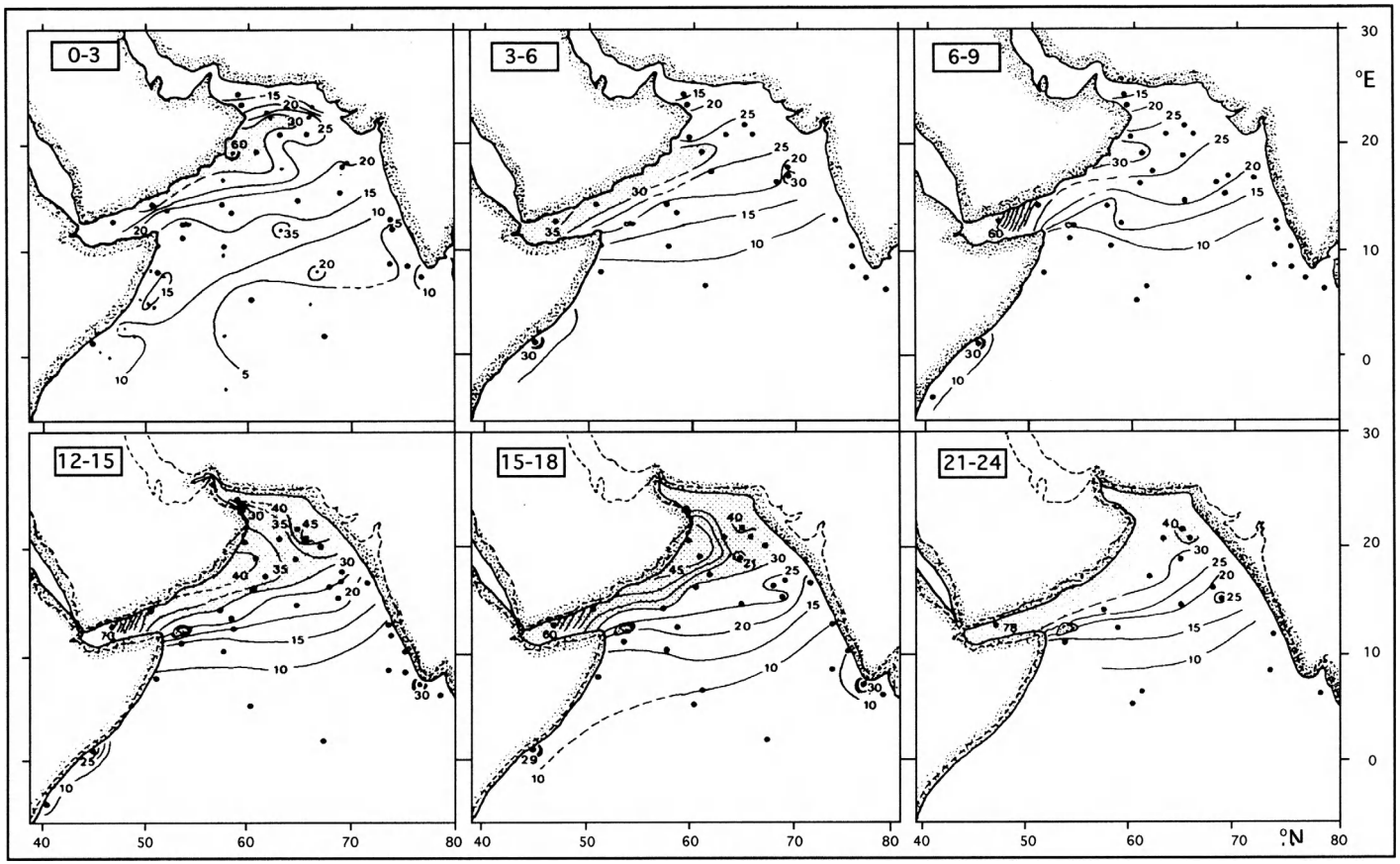


FIGURE 6.39 Percentages of siliciclastic grains >6 mm in the siliciclastic fraction of cores off the Arabian Peninsula, at 3000-year intervals from 21 to 24,000 years BP. (Bottom right) 0 to 3000 years BP (top left). The 30% isoline corresponds to the main convergence zone between northwesterly airflow carrying dust from the Arabian Peninsula and southwesterly monsoon airflow from the horn of Africa (Somalia). *From Sirocko et al. (1991).*

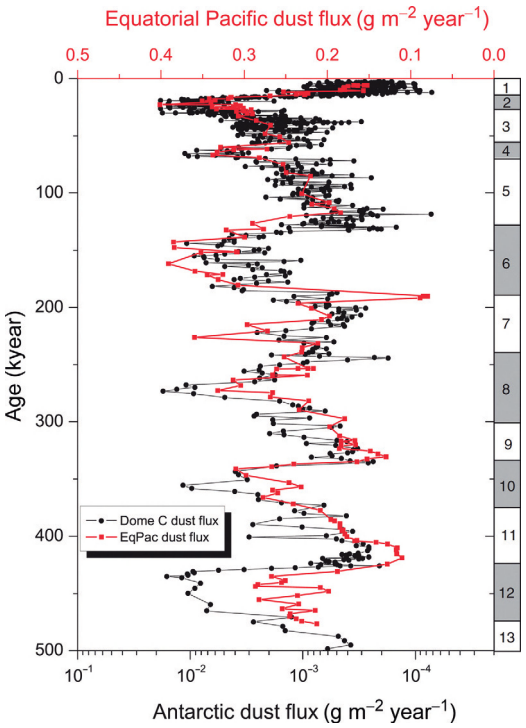


FIGURE 6.40 Changes in dust recorded in the EPICA Dome C ice core from Antarctica and in a sediment core from the central equatorial Pacific, showing synchronous changes in dust flux over the last five glacial-interglacial cycles. Each record is plotted on its own independent timescale. Marine isotope stages are shown on the right. *From Winckler et al. (2008).*

ice-rafting and stratification of the North Pacific at ~2.8 Ma ago. Subsequently, there were many other episodes of major ice-rafting in the North Atlantic (above ambient background levels); these are now termed Heinrich events (Heinrich, 1988) (see Section 6.10.1). At least some of these coarse layers contain an abundance of detrital carbonates, with a geographic distribution that indicates a source region in Foxe Basin (west of Baffin Island) or Hudson Bay. It appears that the material was transported to the North Atlantic through Hudson Strait, via icebergs that calved from a major ice stream of the Laurentide Ice Sheet (Andrews et al., 1994; Dowdeswell et al., 1995) (see Figure 6.54).

6.8 THERMOHALINE CIRCULATION OF THE OCEANS

Circulation of water at the ocean surface is largely a response to the overlying atmospheric circulation that exerts drag at the surface. However, circulation of deeper waters in the oceans of the world is a consequence of density variations, which result from differences in temperature and salinity brought about by sensible and latent heat fluxes, precipitation, and runoff at the ocean surface. This leads to the circulation of heat and salt throughout the world's oceans, which is termed the thermohaline circulation (Figure 6.41) (Rahmstorf, 2002; Wunsch, 2002). In addition, diffusive mixing and turbulent eddies also transport water masses around the globe, on an even larger scale than in the thermohaline "conveyor belt" system (Ganachaud and Wunsch, 2000; Holzer and Primeau, 2006).

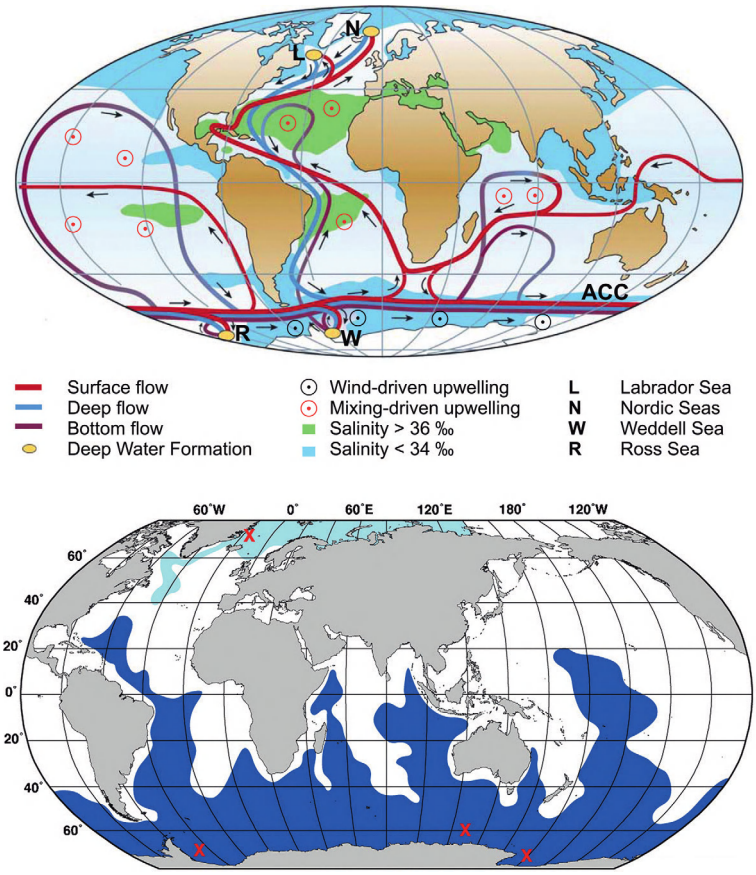


FIGURE 6.41 Upper figure: Simplified map of the modern thermohaline circulation system (conveyor belt). Near surface waters are shown in red, and deeper flows are in blue and purple. The main areas of deepwater formation in the North Atlantic are shown by the yellow ovals; no deepwater is currently formed in the North Pacific. Note that this system accounts for only part of the movement of water around the globe. Much more mixing occurs through diffusive processes and turbulence associated with large-scale eddies. Lower figure: sea ice formation and brine rejection in sub-Antarctic waters (red crosses) lead to dense water that sinks, creating Antarctic bottom water (AABW). This spreads northward, filling the deepest basins of the oceans (dark blue, the limit defined here by the 45.92 kg m^{-3} isopycnal, a surface of constant potential density). *Upper figure: from Kuhlbrodt et al. (2007); lower figure: from Talley (1999).*

In areas where surface waters become relatively dense, due to cooling and/or evaporation (thereby increasing salinity), they will sink to the level at which they reach equilibrium (neutral buoyancy) with surrounding water masses.[5] Also, areas of sea ice formation, which result in salt expulsion from the ice, produce brine that increases the water density, causing water to

[5] A water mass, like an air mass, is recognized by its distinctive physical properties (principally temperature and salinity) that enable it to be distinguished from adjacent water masses. As a water mass moves from its source region, it will slowly mix with other waters and gradually lose its original identity.

sink and form a cold dense water mass. Dense water masses flow away from their source regions as either bottom water or intermediate water, depending on their relative density (Oppo and Curry, 2012). Much of the deepest sections of the world's oceans are occupied by dense Antarctic bottom water (AABW), which originates from areas of sea ice formation adjacent to the Antarctic continent (Figure 6.41). AABW is characterized by a temperature of ~−0.4 °C and a salinity of ~34.7‰. In the Atlantic Ocean, much of the deepest sections (>2 km) are occupied by North Atlantic Deep Water (NADW) that forms mainly in the Norwegian Sea (60°N, east of Iceland) and in the Greenland Sea (north and west of Iceland) (Figure 6.42) (Kellogg, 1987; Hay, 1993). Deep water does not form at present in the North Pacific, where waters are less saline than in the North Atlantic (Emile-Geay et al., 2003).

Overlying these dense water masses (at ~l km depth) are intermediate waters, which generally have slightly lower salinities and/or higher temperatures. Much of the world ocean is occupied by Antarctic Intermediate Water (AAIW) that has a temperature of 2-4 °C and a salinity of ~34.2‰ and originates in the circum-Antarctic polar frontal zone. At high latitudes of the North Atlantic, intermediate water from the Labrador Sea (3-4 °C, 34.92‰) is found (sometimes referred to as Upper North Atlantic Deep Water or Northwestern Atlantic Deep Water) and further south saline water flowing from the Mediterranean Sea can also be traced at intermediate levels.

Changes in deepwater circulation are important for paleoclimatology since, as a result of deepwater formation and compensating fluxes of water in the upper mixed layer, large quantities of heat are carried around the globe. Of particular significance is the thermohaline

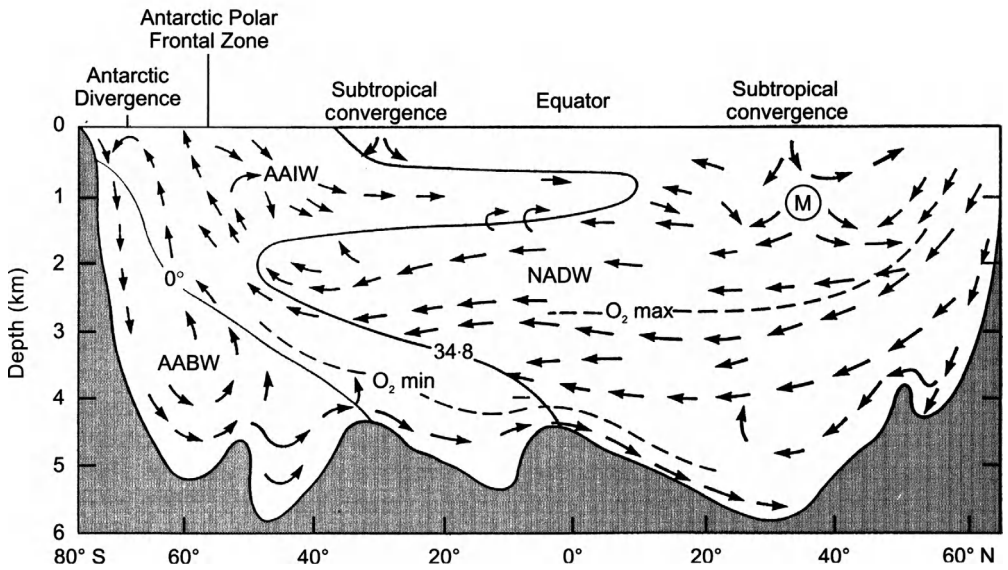


FIGURE 6.42 Meridional cross section of the Atlantic Ocean showing the principal water masses and their distribution today. NADW, North Atlantic Deep Water; AABW, Antarctic bottom water; AIW, Atlantic Intermediate Water; AAIW, Antarctic Intermediate Water. During the last glacial maximum, NADW was more limited in extent, whereas AABW penetrated further north into the deep basins of the North Atlantic (cf. Figure 6.43). *Adapted from Brown et al. (1989).*

circulation associated with the formation of North Atlantic Deep Water (Dickson and Brown, 1994). As noted earlier, NADW forms north of ~60°N as surface waters cool (by evaporation and sensible heat loss) and their salinity increases, thereby creating a dense water mass that moves southward at depth carrying saline water to the South Atlantic and other ocean basins (Figure 6.41). The loss of water in this manner is compensated for by the poleward movement of warm, saline surface waters to the North Atlantic, in the Gulf Stream and associated North Atlantic Drift. These water masses are partly responsible for the relatively mild temperatures that western Europe experiences, even in winter.

The wind-driven movement of warm salty water to high latitudes of the North Atlantic, the formation of dense NADW and the displacement of water as NADW exits from the North Atlantic (the Atlantic Meridional Overturning Circulation, or AMOC) can be considered as part of a linked conveyor belt system, involving mass transfer throughout the global ocean. Disturbances to the AMOC may involve changes in the rate of water exchange, or even a cessation of deepwater formation altogether (Broecker, 1991). In fact, models indicate that the system is quite sensitive to disturbance, particularly by freshwater inflows into the North Atlantic (Manabe and Stouffer, 1988; Rahmstorf, 1994; Weaver and Hughes, 1994). Currently, the North Atlantic Basin loses slightly more freshwater via evaporation than it gains from either precipitation or river runoff (-1.21 m a^{-1} vs. +0.87 m and 0.21 m, respectively). It is this fact, together with a flux of saline Gulf Stream water and strong cooling (especially in winter), that leads to NADW formation. However, when the major continental ice sheets melted, freshwater flux to the North Atlantic increased creating an upper, low salinity water layer that reduced NADW formation. This in turn affected the global circulation of NADW, eventually leading to a reduction in the returning northward flux of warm, salty subtropical water. With less heat transported into the North Atlantic and generally colder climatic conditions, freshwater runoff from the continental ice sheets was reduced, and the process of NADW formation was restored and the overall circulation reverted back to its former condition. Thus, the North Atlantic overturning circulation varied in strength, controlled by the relative balance of freshwater flux to the surface waters of the North Atlantic Basin (Broecker et al., 1985b, 1990a,b; Broecker and Denton, 1989; Broecker, 1994). At the extreme, if deepwater formation ceased altogether, the rate of salt export from the North Atlantic (in NADW) would be less than the rate of salt buildup resulting from evaporation and water vapor export to adjacent regions. Salinity would then gradually increase until some critical density threshold was reached at which point the AMOC would resume, bringing more saline water to the North Atlantic via the Gulf Stream. Providing that meltwater flux to the North Atlantic was less than the salt buildup, NADW would continue to form. However, if meltwater and/or salt export exceeded that threshold, NADW formation would be greatly reduced or eliminated altogether (Broecker et al., 1990a). In this way, the ocean-atmosphere-cryosphere systems are in a dynamic equilibrium, in which disturbance of one part of any system may lead to a nonlinear response in another system (Broecker and Denton, 1989).

In a reassessment of this model, Boyle and Rosener (1990) questioned whether the coupled system really has only two modes or whether in fact there have been multiple stable circulation patterns as suggested by model simulations (e.g., Rahmstorf, 1994, 1995). They suggest that rather than being controlled by an "on-off switch," the system may be considered as responding more to a "valve" whereby there are many possible quasi-stable circulation states. Unfortunately, the resolution of deep-sea sediments is frequently insufficient (because of low

sedimentation rates and bioturbation) to resolve which of these models is correct, though there is evidence that when the formation of NADW was reduced (during Heinrich events, for example), a distinct North Atlantic Intermediate Water was produced (Boyle and Keigwin, 1987; Gherardi et al., 2009). This suggests an additional scenario, perhaps the result of some balance of factors neither at one extreme nor the other. Lehman and Keigwin (1992a,b) made the argument that the formation of deepwater in the Norwegian Sea (Lower NADW) was disrupted quite often in Late Glacial times (see Section 6.10.1) but deepwater from the Labrador Sea (Upper NADW) continued to form. Another scenario was proposed by Veum et al. (1992) who suggested that deepwater was formed by brine rejection during sea ice formation in the marginal ice zone of the Greenland-Iceland-Norwegian Seas throughout the last glacial maximum, ventilating the deep basins of this region. By contrast, no deepwater formed to the south in the open North Atlantic Ocean, the deep basins of which were occupied by AABW until ~12,600 years BP. Thus, there may be many different states of deepwater circulation that have developed over time, with complete shutdown of both Lower and Upper NADW being the extreme end-members of a whole range of possible conditions.

6.8.1 Tracers in the Ocean

Before discussing further the evidence for changes in the thermohaline circulation, it is first necessary to consider the means by which changes in deepwater circulation can be identified. Each water mass has certain geochemical characteristics that can be identified by analysis of forams living in those waters. Thus, the geochemistry of benthic forams in marine sediments serves as a tracer of deepwater conditions at the time the forams were deposited. Of particular importance is the $^{13}C/^{12}C$ ratio ($\delta^{13}C$) in the carbonate tests, derived from dissolved CO_2 in the water column (Ravelo and Hillaire-Marcel, 2007). The $\delta^{13}C$ value for the atmosphere is −7.2‰; because of fractionation effects, seawater in equilibrium with the atmosphere has a $\delta^{13}C$ (dissolved inorganic carbon, DIC) value of ~+3.5‰ (at 2 °C) (Mook et al., 1974). By contrast, organic matter has a $\delta^{13}C$ of −20 to −25‰. Oxidation of organic matter falling through the water column therefore causes the $\delta^{13}C_{DIC}$ of the water to decline. If surface waters are nutrient-rich and productive, the large input of organic material to the deep ocean will result in low $\delta^{13}C_{DIC}$ and reduced oxygen levels. The low $\delta^{13}C_{DIC}$ is balanced to some extent by dissolution of the carbonate tests of planktic forams as they fall through the water column, because these have a $\delta^{13}C$ value close to that of total dissolved CO_2 (DIC) in the upper water column. Hence, the overall $\delta^{13}C$ of a water mass reflects a balance between the amount of organic matter oxidized and dissolution processes. Nevertheless, the global distribution of $\delta^{13}C_{DIC}$ strongly reflects the nutrient content and organic productivity of the water mass (Kroopnick, 1985). For example, Antarctic waters are nutrient-rich and productive, resulting in deepwater (AABW) that is relatively depleted in ^{13}C; North Atlantic Deep Water, on the other hand, has lower nutrient levels, is less productive, and has a higher $\delta^{13}C_{DIC}$ value (Duplessy and Shackleton, 1985). These characteristics, preserved in the tests of benthic forams, can be used to trace the presence and distribution of NADW and AABW over glacial-interglacial cycles (e.g., Curry et al., 1988; Raymo et al., 1990). Furthermore, in areas of deepwater formation, the vertical distribution of $\delta^{13}C_{DIC}$ is fairly homogeneous (due to convective mixing) so that the $\delta^{13}C$ signal in the calcareous tests of both benthic and planktic

foraminifera is similar. When deepwater formation ceases (or with increasing distance from areas of deepwater formation) the difference between surface and deepwater $\delta^{13}C_{DIC}$ increases, and this is reflected in the tests of deep-dwelling and surface forams (Duplessy et al., 1988). Hence $\delta^{13}C_{DIC}$ can be used to identify changes in areas of deepwater formation and to track their movement over time. For example, Anderson et al. (2009) found anomalously low $\delta^{13}C$ in forams from the eastern equatorial Pacific during the period from ~16 to 9 ka BP. This recorded the influx and upwelling of nutrient-rich deepwater from the Southern Ocean during the last deglaciation, associated with increased ventilation of the deep ocean basins around Antarctica and a rise in atmospheric CO_2 that had been sequestered at depth during glacial times.

There are two slight complications to this ingenious approach. First not all benthic foram species record the same values of $\delta^{13}C$, apparently due to a species-dependent habitat effect; this can be resolved by selecting only benthic forams (such as *Cibicidoides wuellerstorfi*), which do not show such an effect, or by using those whose effect is known (Zahn et al., 1986). Second, the global mean $\delta^{13}C$ content of the ocean was lower (by ~0.4‰) in glacial times because of the significant decrease in biomass on the continents and a remobilization of $\delta^{13}C$-depleted organic material on the exposed continental shelves (when sea level was up to 120 m lower) (Boyle and Keigwin, 1985; Curry et al., 1988; Duplessy et al., 1989; Keigwin et al., 1994). Approximately 500 Gt carbon (with a $\delta^{13}C$ of −25‰) was added to the ocean-atmosphere system at such times, lowering the ^{13}C content of the ocean accordingly (Siegenthaler, 1991). With less photosynthetic activity on land, one might expect higher pCO_2 levels during glaciations, but this was more than compensated for by enhanced CO_2 solubility (in cooler waters) and increased oceanic biological activity (i.e., greater carbon sinks). These factors affected all marine sedimentary records equally; $\delta^{13}C$ thus provides a valuable proxy indicator of water masses in the past (Figure 6.43)

Another useful tracer of deepwater is the Cd/Ca ratio in benthic foram tests (Boyle and Keigwin, 1982; Boyle, 1988). Cadmium is a proxy for oceanic nutrient levels; Antarctic bottom waters have relatively high Cd levels compared to NADW so Cd/Ca provides a useful index of these water masses (Boyle, 1992). Although Cd levels in the world ocean were higher during glacial time, sediments from the Bermuda Rise show that during the last glacial maximum (isotope stage 2) and during the Younger Dryas interval, Cd levels in the deep Atlantic Ocean increased even more, indicating that NADW flux was reduced and replaced by AABW at those times (Boyle and Keigwin, 1987). This supports the $\delta^{13}C$ data, which also points to a shift in deepwater circulation towards increased AABW flux (Figure 6.43) not only in the last glacial but also in isotope stage 6 (135 ka BP) and earlier glacial periods (Boyle and Keigwin, 1985; Duplessy and Shackleton, 1985; Oppo and Fairbanks, 1987; Curry et al., 1988; Raymo et al., 1990).

Water masses can also be traced by neodymium (Nd) isotopes in marine sediments (Claude and Hamelin, 2007). ^{143}Nd is the radioactive decay product of ^{147}Sm (samarium) and so broadly reflects the age of continental source rocks. Dissolved neodymium is transported to the oceans from the continents via rivers; as each ocean basin is surrounded by different source rocks, this imparts a specific Nd signal to the water masses emanating from the region, which persists over long distances and is recorded in both biogenic and authigenic sediments associated with the water mass. The tracer (ε_{Nd}) is expressed as the deviation of the ratio $^{143}Nd/^{144}Nd$ relative to a "bulk Earth" reference standard (0.512638 parts per 10^4).

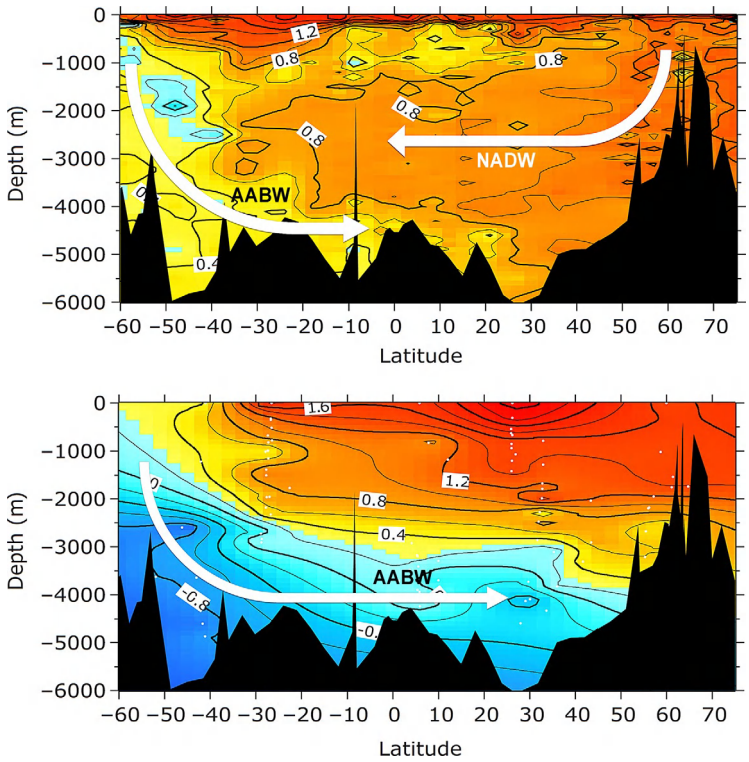


FIGURE 6.43 Cross sections of $\delta^{13}C$ along transects through the Western Atlantic Ocean, from 75°N to 60°S. Upper panel shows modern conditions (from GEOSECS measurements). Higher values of $\delta^{13}C$ characterize North Atlantic Deep Water (NADW) and lowest values are diagnostic of Antarctic bottom water (AABW). Lower panel shows conditions during the last glacial maximum, when AABW occupied much of the deep ocean. *From Oppo and Curry (2012).*

ε_{Nd} values for NADW are typically around −13.5, compared to −7 to −9 for AABW, and −2 to −3 for North Pacific Deep Water (van de Flierdt et al., 2006). Nd isotope ratios in a sediment core from the southeastern Atlantic (41°S) show large variations in ε_{Nd} that parallel changes in benthic $\delta^{13}C$ and $\delta^{18}O$ in Greenland ice cores over the past 90,000 years (Figure 6.44) (Piotrowski et al., 2005). These changes reflect the relative influence of NADW versus AABW and are consistent with inferences about variations in North Atlantic Deep Water formation derived from other tracers, as discussed earlier.

In addition to these diagnostic tracers of water masses, there are also some proxies of ocean dynamics (kinematic tracers) that may be obtained. For example, an important proxy of deep-water formation is the ratio of $^{231}Pa/^{230}Th$. Both isotopes are produced in seawater by the decay of dissolved ^{235}U and ^{234}U, respectively (François, 2007). The decay products are readily adsorbed onto particles settling through the water column, leading to the accumulation of unsupported (excess) ^{231}Pa and ^{230}Th in the sediments. However, ^{231}Pa is less easily adsorbed than ^{230}Th and so ~50% of the ^{231}Pa that is produced in the North Atlantic is transported out of the Basin by NADW. This results in a lower $^{231}Pa/^{230}Th$ ratio in the sediments than in the overlying water column. Providing that there have not been significant changes in the

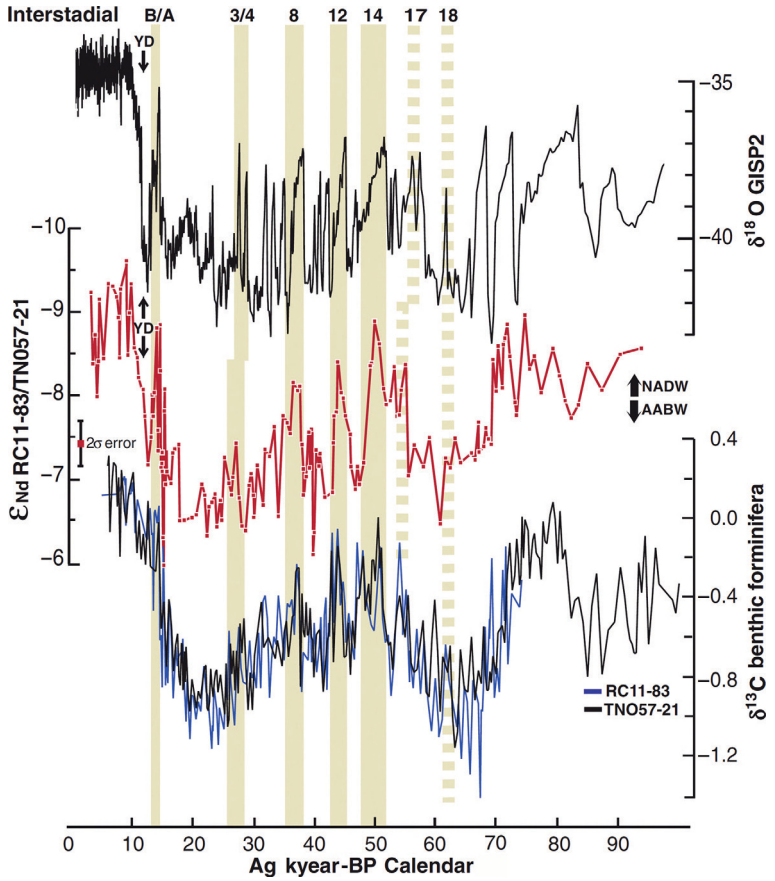


FIGURE 6.44 $\delta^{18}O$ from the GISP2 ice core, Nd isotope ratios (ε_{Nd}), benthic $\delta^{13}C$ in sediment cores from Cape Basin, southeastern Atlantic Ocean. Changes in ε_{Nd} and $\delta^{13}C$ and are indicative of the relative influence of NADW versus AABW, which vary in parallel with isotopic changes in Greenland ice. Greenland interstadial stages noted at the top, together with the Bølling-Allerød and Younger Dryas warm/cold stages. *From Piotrowski et al. (2005).*

scavenging rate by particles, tracking variations in this ratio over time provides a valuable index of the strength of the AMOC. If the AMOC is strong, more ^{231}Pa is exported, leading to low values of $^{231}Pa/^{230}Th$. If the AMOC completely stopped, the ratio would rise, approaching the mean value in seawater (0.093) for a complete cessation of deepwater production. This is exactly the situation that was found in a sediment core from the Bermuda Rise (33.7°N, 57.5°W); during Heinrich event 1, the AMOC circulation appears to have completely shut down and then abruptly resumed at the start of the Bølling-Allerød warm period (Figure 6.45). Interestingly, $^{231}Pa/^{230}Th$ ratios were not very different during the LGM compared to the Holocene (cf. Gutjahr and Lippold, 2011; Ritz et al., 2013). The AMOC also slowed during the Younger Dryas interval, before slowly becoming reestablished and rising to modern-day values during the Early Holocene (McManus et al., 2004). Similar changes in the $^{231}Pa/^{230}Th$ ratio have also been seen for earlier Heinrich events (Lippold et al., 2009). However, the

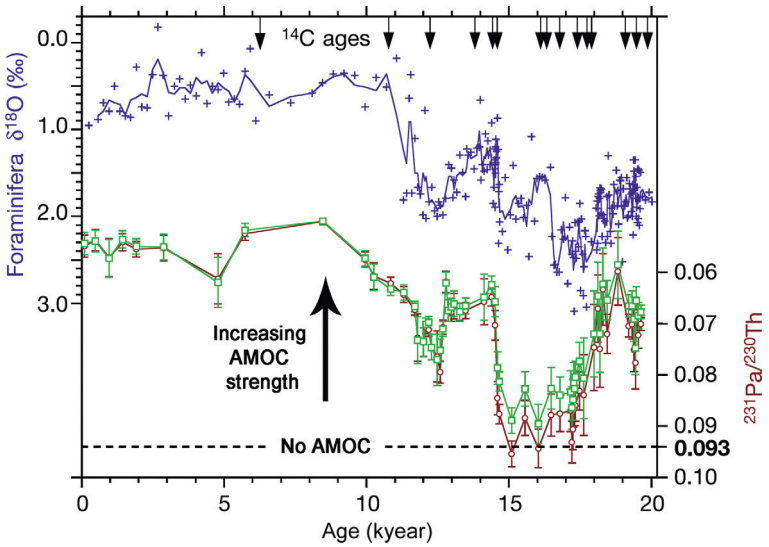


FIGURE 6.45 Stable isotopes in planktonic foraminifera (*G. inflata*) from the Bermuda Rise together with the ratio of ^{231}Pa/^{230}Th in sediments. During Heinrich event 1 (H1), there was no export of ^{231}Pa from the North Atlantic, due to a shutdown of the Atlantic Meridional Overturning Circulation (AMOC) leading to an increase in the sedimentary ^{231}Pa/^{230}Th ratio (until it approached that of seawater, 0.093). The AMOC also slowed down during the Younger Dryas interval (YD). Higher foram isotopic values indicate lower temperatures and/or higher salinity; part of the overall isotopic decrease (~1.0‰) from the LGM to the Holocene is due to continental ice volume effects on the oceanic isotopic composition. *From McManus et al. (2004).*

interpretation is not straightforward as there is also evidence for more diatoms at those times, due to an increase in silica-rich waters, which increased the rate of scavenging of ^{231}Pa, driving the ^{231}Pa/^{230}Th ratio higher (Keigwin and Boyle, 2008). But the influx of silica-rich waters may itself have resulted from a reduction in the AMOC, making the problem quite complex. Additional studies of cores from different depths provide a more nuanced interpretation of these changes. During the LGM, there was a fairly vigorous circulation of Atlantic Intermediate Water (compared to NADW) and during H1 deepwater formation may not have not completely ceased, but continued to form at a slower rate and at shallower depths (down to ~2000 m) (Gherardi et al., 2009; Lippold et al., 2012).

Another important attribute of deepwater formation is the transport of oxygen into the deep ocean basins of the world. Water at the surface is generally well oxygenated but oxygen levels decline with depth due to oxidation of organic matter falling through the water column. Deepwater formation ventilates the deep ocean by carrying oxygenated water to great depths. Ventilation rates can be estimated by measuring the radiocarbon content of the water; once water is isolated from the atmosphere, radiocarbon is no longer in equilibrium with the atmospheric reservoir and ^{14}C levels decline (see Chapter 3, Section 3.2.1.4.2). The radiocarbon age of deepwater therefore reflects the time since isolation from the surface; this obviously varies from one area to another (cf. Figure 3.9) but typically deepwater has a ^{14}C age of ~400 years in the Atlantic, ~1200 years in the Indian Ocean, and ~1600 years in the Pacific Ocean. Organisms living in upwelling areas (where they develop organic tissue in equilibrium with "old water") will have

an apparent radiocarbon age several hundred, and in some areas as much as several thousand years older than "modern" (Sikes et al., 2000; Marchitto et al., 2007). To assess whether ventilation rates have varied over time, Broecker et al. (1988a) compared planktic and benthic forams from the last glacial maximum (LGM) in Atlantic and Pacific Ocean sediments. On average, the difference between the radiocarbon age of forams in the upper and lower water columns in the North Atlantic increased during the LGM, to as much as 2000 years, compared to ~500 years in the Late Holocene, indicating that ventilation rates were significantly lower in glacial times compared to the present (Keigwin and Schlegel, 2002). A similar conclusion was reached by Bard et al. (1994) who also found evidence for reduced North Atlantic ventilation during the cold Younger Dryas oscillation. By contrast, there is considerable uncertainty about conditions in the Pacific; some studies conclude that ventilation of the North Pacific increased during the LGM, while others argue that conditions were like today, with minimal ventilation taking place (Broecker et al., 2004a,b). By compiling data from various depths through time, a picture of the changes in ventilation can be obtained. Thus, Robinson et al. (2005) were able to show that ventilation of the Atlantic increased significantly during the Bølling-Allerød interval, compared to the preceding period, and the subsequent Younger Dryas, when the overturning circulation appears to have greatly reduced ventilation of the ocean depths (Figure 6.46).

In studies of a sediment core from off the southern coast of California, Marchitto et al. (2007) found a large decrease in intermediate water $\Delta^{14}C$ from ~17.5 to 14.6 cal. years BP, and again from ~13.5 to 11 ka BP, indicating that, during those intervals, the region was affected by deep ocean water that had been isolated from the atmosphere for an extended time period. The variations in $\Delta^{14}C$ correspond closely to the postglacial rise in CO_2 recorded in the Antarctic Dome C ice core. During the LGM, extensive sea ice around the Antarctic

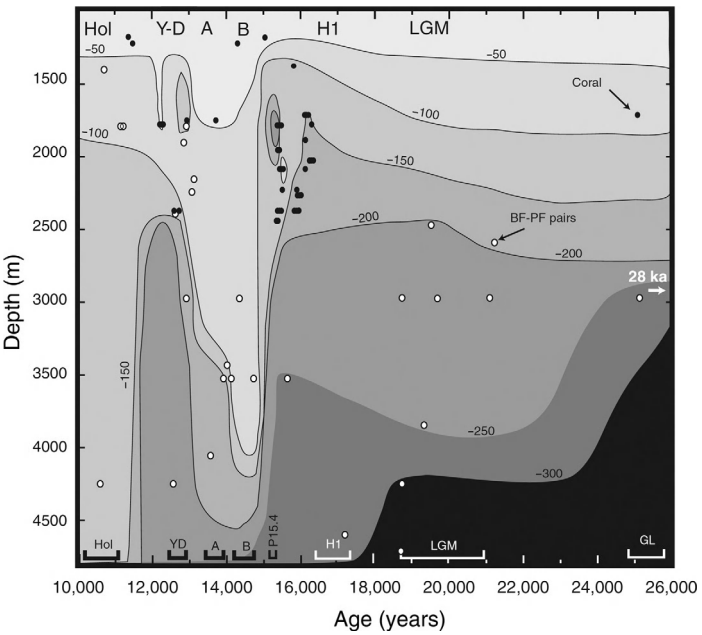


FIGURE 6.46 Schematic diagram illustrating the $\Delta^{14}C$ content of foraminifera (open circles) and corals (dark circles) from 26 to 10 ka BP, at different depths below 1000 m in the western North Atlantic. Data are plotted relative to the atmospheric record. Darker colors are low in radiocarbon, and light colors are rich in radiocarbon, indicating strong ventilation from the surface. This shows that the Atlantic Meridional Overturning Circulation (AMOC) was strong during the Bølling-Allerød (B-A) but weak before and afterwards, during Heinrich event 1 (H1) and in the Younger Dryas interval (YD). *From Robinson et al. (2005).*

continent isolated a large area of the Southern Ocean from the atmosphere, resulting in the creation of an increasingly ^{14}C-depleted carbon reservoir in Antarctic deepwater and a decline in atmospheric CO_2. At deglaciation, recession of the sea ice and a poleward shift of the westerlies led to increased upwelling in the Southern Ocean around Antarctica, causing large amounts of CO_2 from the formerly isolated water mass to be released to the atmosphere. At the same time, the upwelling transferred ^{14}C-depleted water from the abyss to Antarctic Intermediate Water, the signal of which was subsequently detected in sediments off southern California (Marchitto et al., 2007; Anderson et al., 2009). Interestingly, these changes appear to be linked to a decline in North Atlantic Deep Water production (as revealed by $^{231}Pa/^{230}Th$) supporting the hypothesis of a strong connection between NADW formation and conditions in the Southern Ocean (the bipolar seesaw).

6.9 CHANGES IN ATMOSPHERIC CARBON DIOXIDE: THE ROLE OF THE OCEANS

It is clear from ice core records that carbon dioxide levels in the atmosphere were considerably lower at the last glacial maximum than in the Holocene (by 90-100 ppmv) (see Chapter 5, Section 5.4.3). Indeed, long-term carbon dioxide changes parallel $\delta^{18}O$ in ice and must have played a role in glacial-interglacial climatic changes, either directly or indirectly. How did such changes come about? Ocean ventilation is a critical factor in determining atmospheric CO_2 concentrations because upwelling of deepwater brings nutrient-rich water to the surface, increasing biological productivity, which draws down CO_2 levels in the atmosphere as the organic tissue and carbonate shells of marine organisms are produced. When these die and fall through the water column, the carbon fixed near the surface is transferred to deeper layers of the ocean and may be deposited in the sediments. This process can be thought of as an "ocean carbon pump" whereby biological activity continually removes carbon from the ocean surface (Volk and Hoffert, 1985). However, in some upwelling areas, this process may be insufficient to overcome the transfer of CO_2 from the ocean surface to the atmosphere; in those situations, degassing of CO_2 from carbon-rich upwelling waters would lead to an increase in atmospheric CO_2 (Pedersen et al., 1991). Thus, some areas of the ocean are carbon sinks and some are carbon sources for the atmosphere. Because the ocean carbon content is 50-60 times that of the atmosphere, even relatively small changes in the rates of ocean carbon dioxide uptake or loss can have large effects on atmospheric CO_2 levels (Broecker, 1982). Changes in sea-surface temperature and salinity in glacial times (to a colder, more saline ocean) can account for ~10% of the observed pCO_2 changes (simply by the difference in CO_2 solubility under such conditions), but the bulk of the change must be related to an increase in biological productivity in the ocean during glacial periods. Factors that alter the biological productivity of surface waters and the rate of upwelling of nutrient-rich deepwater or that change the distribution of sources and sinks of carbon can therefore have a significant effect on atmospheric CO_2 levels (Ennever and McElroy, 1985).

An important index of photosynthetic activity in the surface waters of the ocean is the relative proportion of ^{12}C to ^{13}C. During photosynthesis, ^{12}C is preferentially removed from the water to produce organic material with low $\delta^{13}C$. In many regions of the ocean, productivity is limited by a lack of nutrients (particularly iron, phosphate, and nitrate). Broecker (1982)

suggested that during glacial periods, when sea level was lower, phosphates that had accumulated on the continental shelves would be eroded and dispersed into the ocean, increasing nutrient levels and hence productivity in the near-surface waters. This would have led to ^{12}C removal from near the surface causing the $\delta^{13}C$ gradient between the upper and deep ocean to increase. At the same time, higher productivity in the photic zone would have increased the rate of CO_2 removal from the ocean, thereby lowering pCO_2. Hence, there should be a record of lower atmospheric CO_2 levels preserved in the skeletal remains of organisms that lived near the surface, compared to those that lived in the deep ocean. Shackleton et al (1983) examined this proposition by measuring the difference between ^{13}C in the carbonate tests of planktic and benthic forams in an equatorial Pacific core (Figure 6.47a). The resulting record of the

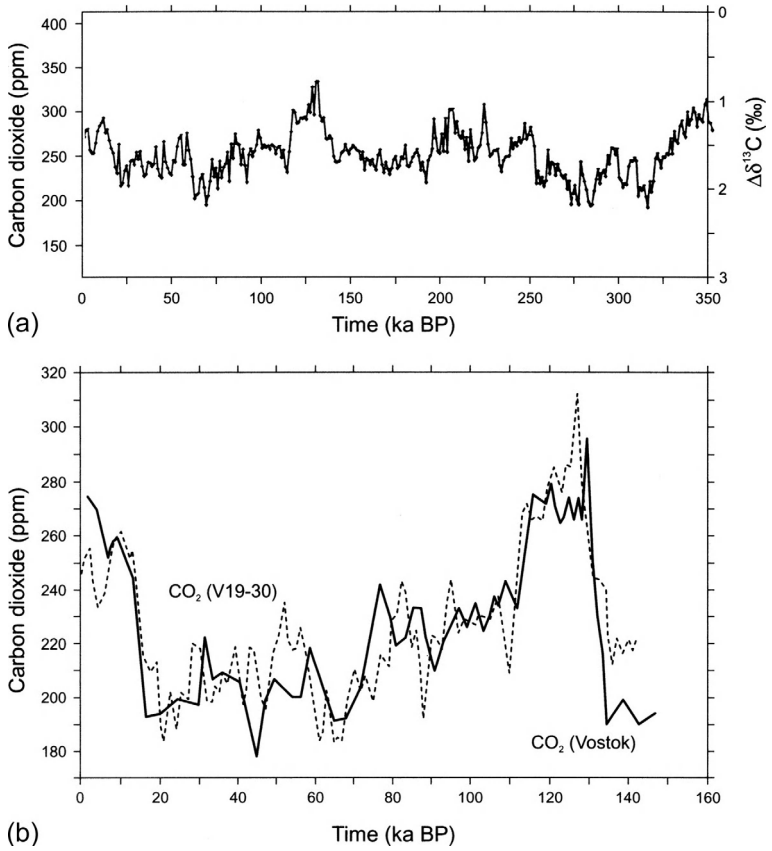


FIGURE 6.47 Upper panel: The difference between $\delta^{13}C$ in planktonic forams *Neogloboquadrina dutertrei* and in benthic forams *Uvigerina senticosa*, from equatorial Pacific core V19-30 (Shackleton and Pisias, 1985). This difference ($\Delta\delta^{13}C$) shows the relative increase in biological productivity of surface waters in glacial periods compared to deep water, which results in a higher $\delta^{13}C$ gradient at those times. Increased surface water productivity would have led to a reduction in atmospheric carbon dioxide, so the $\Delta\delta^{13}C$ can be interpreted as a paleo-CO_2 index (left scale). The *lower panel* shows the same record plotted with the Vostok ice core CO_2 record, though the exact temporal match may not be quite correct (Shackleton et al., 1992).

$\delta^{13}C$ gradient between near surface and deep waters ($\Delta\delta^{13}C$) provides a proxy of atmospheric CO_2 levels, with stronger gradients signifying increased productivity at the surface and hence lower pCO_2. This record is remarkably similar to that obtained from the Vostok ice core (Figure 6.47b) suggesting that changes in the rate at which organic carbon is sequestered in the ocean (as distinct from changes in the carbonate content, which would not affect near surface $\delta^{13}C$) have been the dominant cause of atmospheric CO_2 changes on glacial to interglacial timescales. Furthermore, spectral analysis of this record in relation to benthic $\delta^{18}O$ (a proxy of continental ice volume) shows that CO_2 changes are strongly in phase with orbital forcing but lead ice volume changes at all orbital frequencies (Shackleton and Pisias, 1985). This conclusion implies that CO_2 variations played a key role in the forcing of climatic changes involving ice sheet growth and decay, rather than passively responding to such changes (cf. Shakun et al., 2012). It also indicates that the phosphate mobilization idea of Broecker (1982) cannot be the main factor initiating productivity changes, since that mechanism is tied to sea level changes (which lag by several thousand years both the orbital forcing and CO_2 changes). It is of interest that much of the variance of the CO_2 record is in the frequency band related to obliquity, which has its main impact on radiation receipts at higher latitudes. This suggests that the subpolar ocean areas (perhaps via switches in thermohaline circulation) play a critical role in driving CO_2 changes and hence amplifying orbitally forced climatic change (cf. Wenk and Siegenthaler, 1985). This has strong support in the work of Ziegler et al. (2013). They produced a record of $\Delta^{13}C$ (benthic-planktonic $\delta^{13}C$) from a sediment core obtained from the southern Agulhas Plateau (41°S, 26°E) in the sub-Antarctic region. This record is strongly correlated with atmospheric CO_2 over the last 360,000 years (Figure 6.48). Furthermore, both the CO_2 and $\Delta^{13}C$ records vary coherently with atmospheric dust, registered in the Dome C ice core. This strongly supports the hypothesis that high levels of dust in the atmosphere during glacial times played a key role in controlling atmospheric CO_2 levels by modulating the strength of the oceanic carbon pump in the Southern Ocean. Interestingly, $\Delta^{13}C$ values were low and CO_2 levels were relatively high during North Atlantic Heinrich events, suggesting that the biological pump was weaker at those times. This conforms with the notion of a bipolar seesaw in the thermohaline circulation, such that a reduction in NADW and cooling of the Northern Hemisphere is linked to warming in the Southern Hemisphere. This warming led to a poleward shift in the southern westerlies, retreat of sea ice around Antarctica, and associated upwelling of deepwater and outgassing of CO_2 to the atmosphere. Dust flux to the Southern Ocean also declined at those times, thereby reducing its influence on biological activity, which resulted in a decline in $\Delta^{13}C$ (Figure 6.48).

An additional argument in favor of increased Southern Ocean biological activity controlling atmospheric CO_2 levels was suggested by Kumar et al. (1995) who examined "excess" $^{231}Pa/^{230}Th$ and $^{10}Be/^{230}Th$ in sub-Antarctic sediments as a measure of past biological productivity. They point out that most of the biomass initially deposited as sediment is not preserved so the measured sediment accumulation rate is not a reliable index of former productivity. As discussed earlier, the radionuclides ^{231}Pa and ^{230}Th (dispersed throughout the ocean from the decay of uranium in seawater) are removed from the water column by attachment to particles. However, ^{231}Pa is less easily removed than ^{230}Th, so as particle flux (productivity) increases the disparity in the scavenging rate of the two radionuclides increases (i.e., the $^{231}Pa/^{230}Th$ ratio increases). A similar index is provided by $^{10}Be/^{230}Th$;

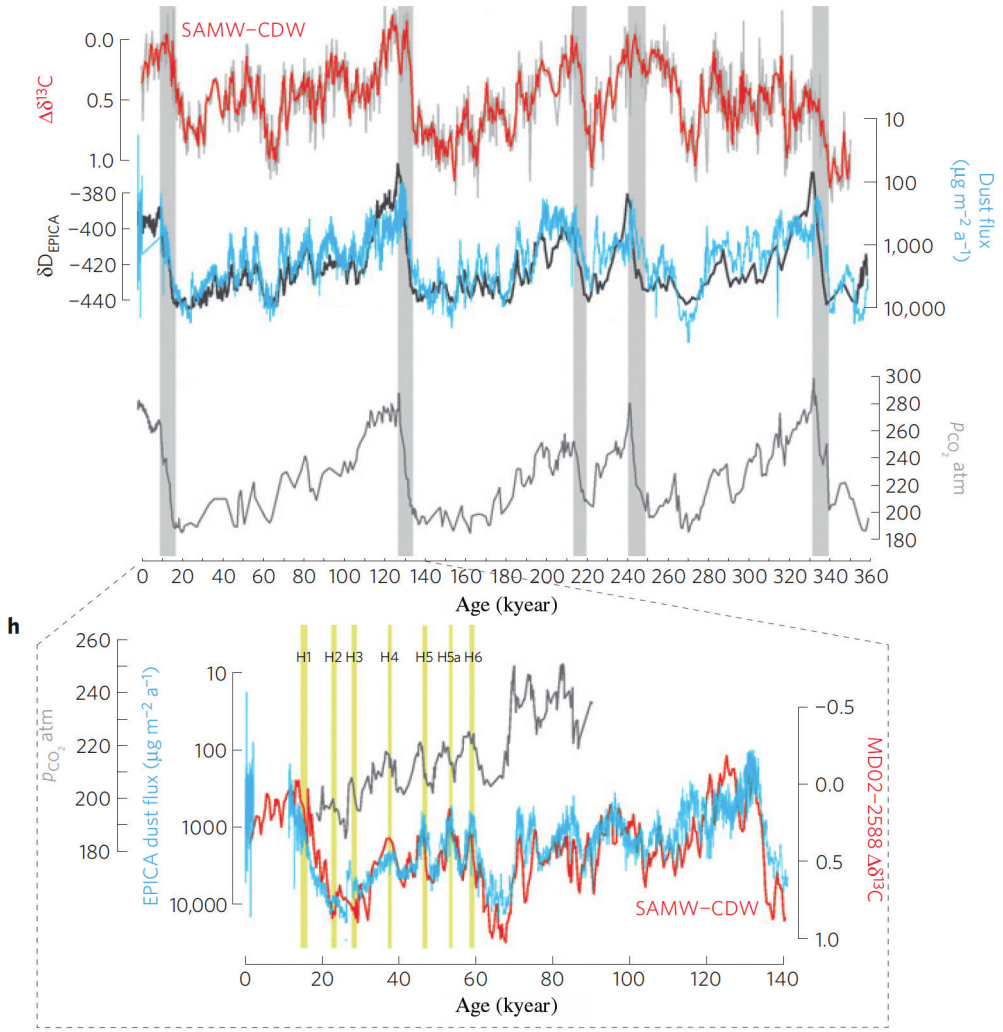


FIGURE 6.48 A 360,000-year record of $\Delta^{13}C$ (benthic $\delta^{13}C$-planktonic $\delta^{13}C$) (upper gray line with 3 point running mean in red), δD (black line), and dust flux (blue line) from the EPICA Dome C ice core and the pCO_2 record from Dome C (lower gray line). The $\Delta^{13}C$ record is from 41 °S in sub-Antarctic waters south of Africa. The lower figure shows an expanded high-resolution section from the last 140,000 years, showing the tight correlation between dust flux, pCO_2, and $\Delta^{13}C$, together with the times of Heinrich events in the North Atlantic. At those times, dust flux was reduced, the difference in $\delta^{13}C$ between the upper and lower ocean was reduced, and CO_2 levels increased. *From Ziegler et al. (2013).*

^{10}Be is a cosmogenic isotope that is widely dispersed across ocean basins, but like ^{231}Pa, it has a longer residence time than ^{230}Th. Thus, an increase in $^{10}Be/^{230}Th$ also provides a measure of particle flux. Both $^{231}Pa/^{230}Th$ and $^{10}Be/^{230}Th$ accumulate in the sediments even though the particles that transported them to the sea floor may no longer be present. An excess of these radionuclides (over that expected from a steady sedimentation rate) thus documents formerly

high productivity in the overlying water column. Studies of these and other productivity indices reveal that sub-Antarctic waters were much more productive in glacial times, but this was not the case at sites closer to the Antarctic continent (perhaps because of more extensive sea ice). Kumar et al. argue that the sediments provide evidence that 30-50% of the observed reduction in CO_2 can be explained by a more efficient biological pump in the cold waters surrounding Antarctica during glacial episodes due to iron fertilization.

Studies of nitrogen isotopes point to another mechanism that has important implications for atmospheric CO_2 changes (Altabet et al., 1995; Ganeshram et al., 1995). As noted earlier, nitrate (NO_3^-) is a key nutrient limiting biological productivity in many parts of the ocean. Oceanic nitrate concentration is the result of the balance between upwelling of nitrate-rich waters and processes of denitrification carried out by bacteria in low oxygenated zones of the ocean. Denitrification produces gaseous nitrogen and nitrous oxide that then escapes from the water column, thereby reducing the supply of fixed nitrogen available for plant growth, which in turn influences atmospheric CO_2 levels. During denitrification, fractionation results in the preferential loss of ^{14}N, enriching the waters in ^{15}N that is then incorporated into whatever organic material is forming and settling to the sea floor. Consequently, sediments from times of reduced denitrification have a lower $\delta^{15}N$, as is evident during marine isotope stages 2, 4, and 6 in cores from off the northwestern coast of Mexico (Figure 6.49) and from the Arabian Sea. Together with the eastern equatorial South Pacific, these areas are especially important for denitrification in the modern ocean, accounting for almost all of the water column denitrification going on today. The evidence for greatly reduced denitrification in glacial periods, plus the fact that lower sea level would have reduced the contribution of denitrification processes in continental shelf sediments, suggests that overall ocean nitrate levels would have been considerably higher at such times. This would have led to increased biological activity in areas of the ocean that are today relatively unproductive (oligotrophic) causing a general decline in atmospheric pCO_2. Altabet et al. (1995) also pointed out that the reduced level of greenhouse gas N_2O, observed in glacial periods in the Vostok ice core, may be a direct consequence of reduced oceanic denitrification at those times.

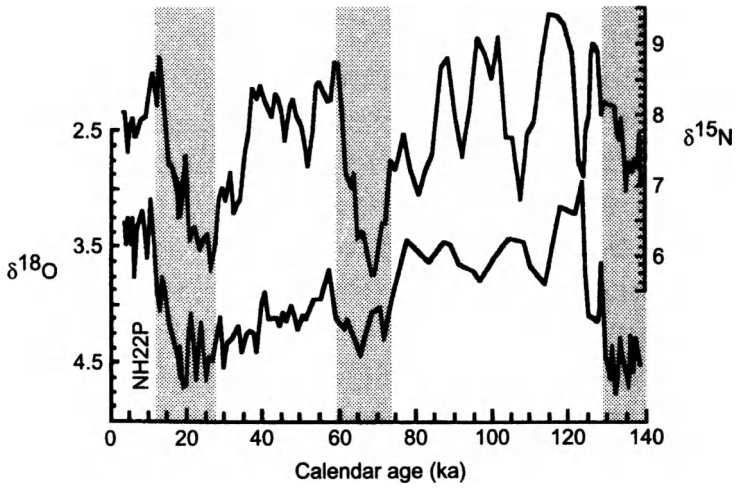


FIGURE 6.49 The record of $\delta^{18}O$ in benthic forams and $\delta^{15}N$ in bulk sediments from off the northwestern Mexican continental margin, spanning the last 140,000 years. Principal glacial stages are shaded. The benthic record shows the familiar index of continental ice growth and decay; the $\delta^{15}N$ records denitrification processes occurring in the water column. Low values of $\delta^{15}N$ indicate relatively low rates of denitrification that imply higher levels of productivity and a reduction in atmospheric CO_2 levels. *From Ganeshram et al. (1995).*

From this brief summary of various lines of evidence, it is apparent that several factors were probably operating simultaneously to lower atmospheric carbon dioxide levels during glacial periods. Collectively, these factors increased ocean productivity to the point where there was a net flux of CO_2 from the atmosphere to the ocean, eventually leading to atmospheric pCO_2 levels ~100 ppmv lower than preindustrial levels. The initial driving force for such changes seems to be orbital forcing, leading to additional feedbacks (involving, *inter alia*, a reduction in global SSTs, ice sheet growth, aridification of the continents and enhanced dust flux to the oceans, and changes in thermohaline circulation), which then amplified these changes.

6.10 ABRUPT CLIMATE CHANGES

One of the key features of the Greenland oxygen isotope records is the sequence of abrupt changes that characterize the period from 20 to 60,000 years BP (see Chapter 5, Section 5.4.1). These Dansgaard-Oeschger (D-O) events are short-lived, in some cases switching from stadial to interstadial levels and back again in less than 1000 years (e.g., D-O events 3 and 4; Figure 5.17). Understanding the cause of these large and rapid changes has been a major focus of Quaternary research over the last decade (e.g., Clark et al., 2002; Wunsch, 2006; Clement and Peterson, 2008). In many marine sediment cores, where sedimentation rates are low and bioturbation has disturbed the record, it is difficult to resolve short-term changes of this sort. However, in some locations, there is strong evidence that D-O events are mirrored by abrupt changes in the nature of sediment deposition. In the Norwegian Sea, variations in ice-rafted debris (IRD) and isotopically light excursions in both benthic and planktic forams correspond to stadial conditions in the GISP2 ice core, with larger anomalies associated with Heinrich events (discussed further in Section 6.10.1) (Figure 6.50) (Dokken and Jansen, 1999; Rasmussen and Thomsen, 2008). These changes are related to freshwater from melting ice sheets flooding the North Atlantic, resulting in extensive sea ice formation. As the sea ice formed, brine was rejected creating a dense, isotopically light water mass that sank to the ocean depths, resulting in synchronous isotopic changes in both planktic and benthic forams at those times (cf. Vidal et al., 1998). Increased IRD probably came from shore-fast ice, which carried material offshore during seasonal ice breakup. The sedimentary evidence thus implicates extensive sea ice formation in the Nordic Seas, due to freshwater anomalies, as the primary explanation for the large D-O changes seen in the Greenland ice core. GCM simulations provide strong support for this idea (Gildor and Tziperman, 2003; Kaspi et al., 2004; Li et al., 2005, 2010a,b). Sea ice can form and decay rapidly and provides a strong ice-albedo feedback to the atmosphere. Model simulations with LGM boundary conditions and (imposed) large and small sea ice limits show that changes in the extent of winter sea ice in the eastern North Atlantic (Norwegian Sea) have a strong effect on Greenland temperatures. When sea ice retreats in this region, higher temperatures and more snow accumulation occur on the Greenland ice sheet, whereas more extensive sea ice reduces Greenland temperature and snowfall rates, similar to what is seen in the ice core records (Li et al., 2010a,b; Wolff et al., 2010a). Why the extent of sea ice changed is uncertain, but it was probably linked to variations in the Atlantic meridional overturning circulation (AMOC); changes in freshwater input to the North Atlantic would have reduced deepwater formation, at the same time favoring the formation of sea ice due to lower surface water salinity. As the surface waters freshened and overturning of the water column was reduced, relatively warm

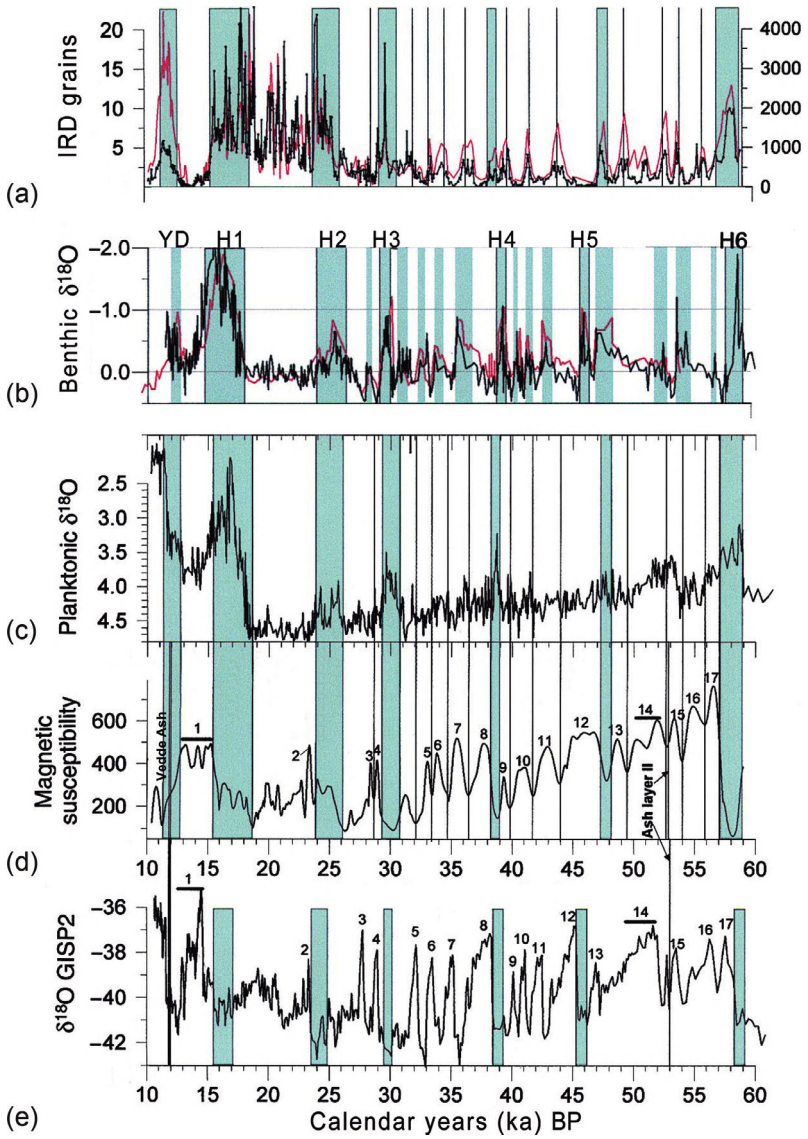


FIGURE 6.50 Changes in sediment characteristics in Norwegian Sea cores MD95-2010 (67°N, 4.5°E) and ENAM93-21 (63°N, 4°E). (a) number of IRD grains per gram of dry sediment (red, right axis = 125 μm, black, left axis = 500 μm); (b) $\delta^{18}O$ in benthic forams, corrected for global isotopic changes; (c) $\delta^{18}O$ in planktic forams; (d) magnetic susceptibility; (e) $\delta^{18}O$ in GISP2 ice core; DO events are numbered. Sediment and ice core records are plotted on their independent timescales. Green shading indicates large anomalies associated with Heinrich events. DO events are associated with isotopically light excursions in planktic and benthic forams and with IRD anomalies. The largest anomalies are due to Heinrich events. *Adapted from Dokken and Jansen (1999).*

Atlantic intermediate depth water accumulated in the subsurface of the Nordic Seas, as recorded by isotopically light benthic marine forams, with southern affinities (Elliott et al., 2002; Rasmussen and Thomsen, 2004, 2008). The fresher surface waters and sea ice cover limited mixing until a threshold was reached when the water column became unstable and warmer waters then rose to the surface. At that point, sea ice rapidly retreated, and temperatures warmed abruptly in Greenland (Figure 6.51). This hypothesis argues that the D-O variations were not primarily driven by changes in the AMOC, but modulated by changes in sea ice extent related to freshwater entering the North Atlantic. The variations in AMOC were a relatively minor player in this sequence of events. By contrast, even greater deposits of iceberg-transported IRD (Heinrich events) were associated with periods of more extensive freshwater flooding, due to the breakup of ice shelves at the margins of continental ice sheets. This resulted in major disruptions to deepwater formation and a strong reduction in the AMOC, with worldwide consequences. Thus, the global signature of Heinrich events is stronger than that of D-O events (as discussed in Section 6.10.1). In a minor amendment to this model of D-O development, Petersen et al. (2013) argued that the growth and decay of an ice shelf along the east coast of Greenland played a critical role. During warm interstadials, higher accumulation on the Greenland ice sheet led to ice sheet growth and the expansion of marine-based ice shelves into the northwestern North Atlantic (Greenland Sea). Cooling brought about by the growth of this ice mass led in turn to more sea ice and development of a cold stadial condition. The accumulation of warm water at depth then destabilized the ice shelf, leading to its breakup and eventual loss of sea ice as discussed above. Such a scenario is not strongly supported by model simulations, which show that it is the northeastern North Atlantic (Norwegian Sea), which is the more sensitive location for changes in sea ice extent to drive D-O type changes recorded in the Greenland ice cores (Li et al., 2010a,b). Nevertheless, ice shelves in the Barents Sea, at the edge of the Arctic Ocean or along the Scandinavian Ice Sheet margins, could also have played a role, together with changes in sea ice.

How did D-O changes in the North Atlantic affect other regions? Voelker (2002) provided a survey of records with high enough resolution to detect short-term changes, and these reveal that there was a global impact of D-O events. In Antarctica, careful alignment of the Greenland and Antarctic ice core records using common trace gas signals indicates that the D-O changes in Greenland were inversely correlated with isotopic changes at the EPICA Dronning Maud Land core site (Lemieux-Dudon et al., 2010). This supports the notion of a bipolar seesaw, wherein the temperature changes are linked through the thermohaline circulation, with northern cooling associated with southern warming, and vice versa. There is also compelling evidence from Cariaco Basin and Arabian Sea sediments that D-O changes in the North Atlantic affected those regions, via displacement of the ITCZ and changes in the strength of monsoon airflow over the Arabian Sea (Schulz et al., 1998; Schulte and Müller, 2001; Deplazes et al., 2013). During interstadials, a strong monsoon in the Arabian Sea and a more northerly mean position of the ITCZ over northern South America led to anoxic conditions at depth, which resulted in dark laminated sediments, in contrast to the lighter, more bioturbated sediments that were associated with stadials. Sediment color variations thus record changes in monsoon strength and the relative position of the ITCZ (Figure 6.52). Other high-resolution records also document changes associated with D-O events, indicating the global impact of the changes (e.g., Martrat et al., 2007 (Iberian margin); Kanner et al., 2012 (northern Peru); Zhao et al., 2010 (central China) and Wang et al., 2006 (southeastern Brazil)).

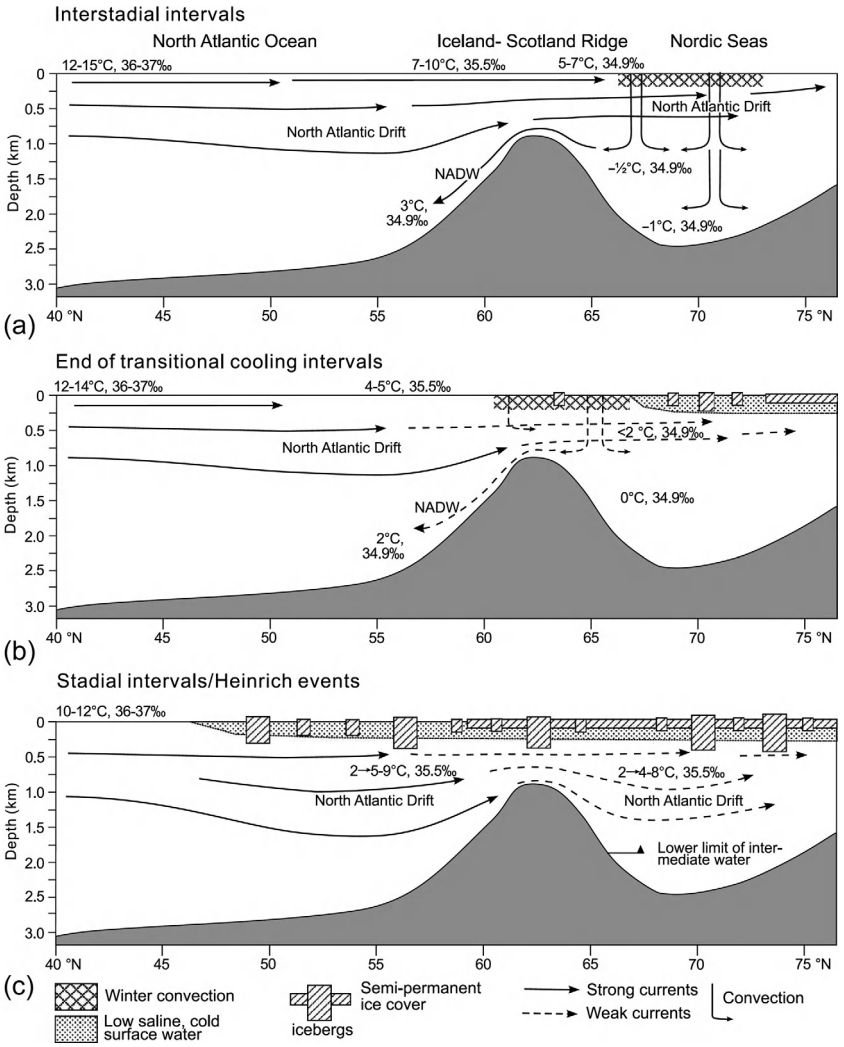


FIGURE 6.51 Schematic SSW-NNE cross-sections of the North Atlantic and Nordic Seas showing reconstructed circulation regimes and associated temperature and salinity estimates during (a) interstadials, (b) transitional cooling intervals, and (c) stadials. The salinities of the water masses are modified from modern salinities in the North Atlantic realm. During the glacial period the global salinities were probably up to one per mil higher than today. Heat accumulated in the subsurface layers of the Nordic Seas during stadial periods as the zone of deepwater formation had weakened and/or shifted southward, allowing unobstructed flow of intermediate-depth Atlantic water across the Iceland-Faeroes-Shetland Ridge. At some point, the warm water in the Nordic Seas became unstable and rose to the surface, causing rapid destruction of the overlying ice cover and abrupt warming of the North Atlantic. *From Rasmussen and Thomsen (2004).*

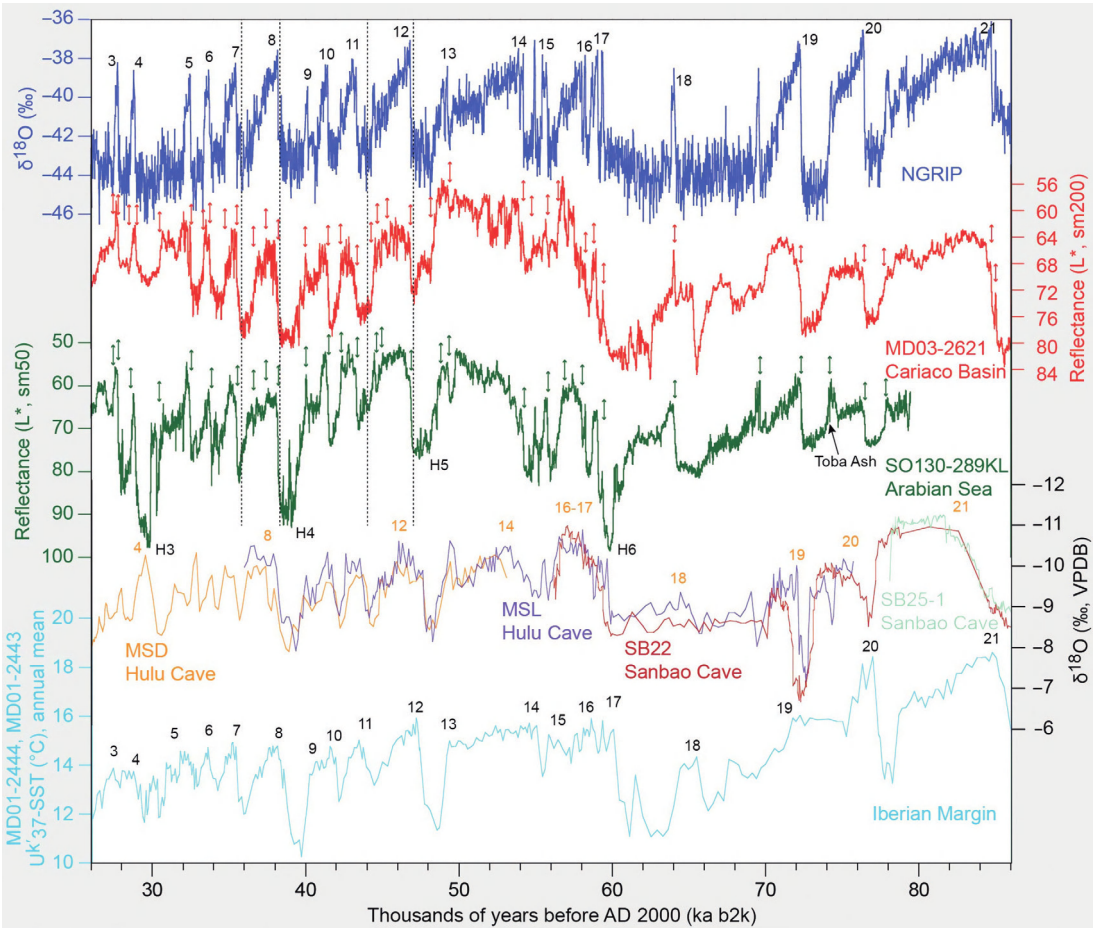


FIGURE 6.52 Correspondence between isotopic changes in the NGRIP ice core with sedimentary records from the Cariaco Basin, the Arabian Sea, and the Iberian Margin. The ice core Dansgaard-Oeschger events are numbered and chronological tie points are indicated by arrows. High reflectance values (Cariaco, Arabian Sea) indicate lighter colored sediments associated with stadials. SST estimates for the Iberian margin are based on alkenones. *From Deplazes et al. (2013).*

6.10.1 Heinrich Events

In addition to the abrupt changes in sediment cores that are associated with D-O events, less frequent but even larger anomalies have been recognized in cores from across the North Atlantic, particularly in a belt around 35-50°N. An increase in the percent of lithic materials (in the >180 μm fraction) in sediment cores from the northeastern North Atlantic during the last glacial period were first reported by Heinrich (1988) (Figure 6.53). Further studies showed that these peaks of lithic material (now known as Heinrich events) could be traced over wide

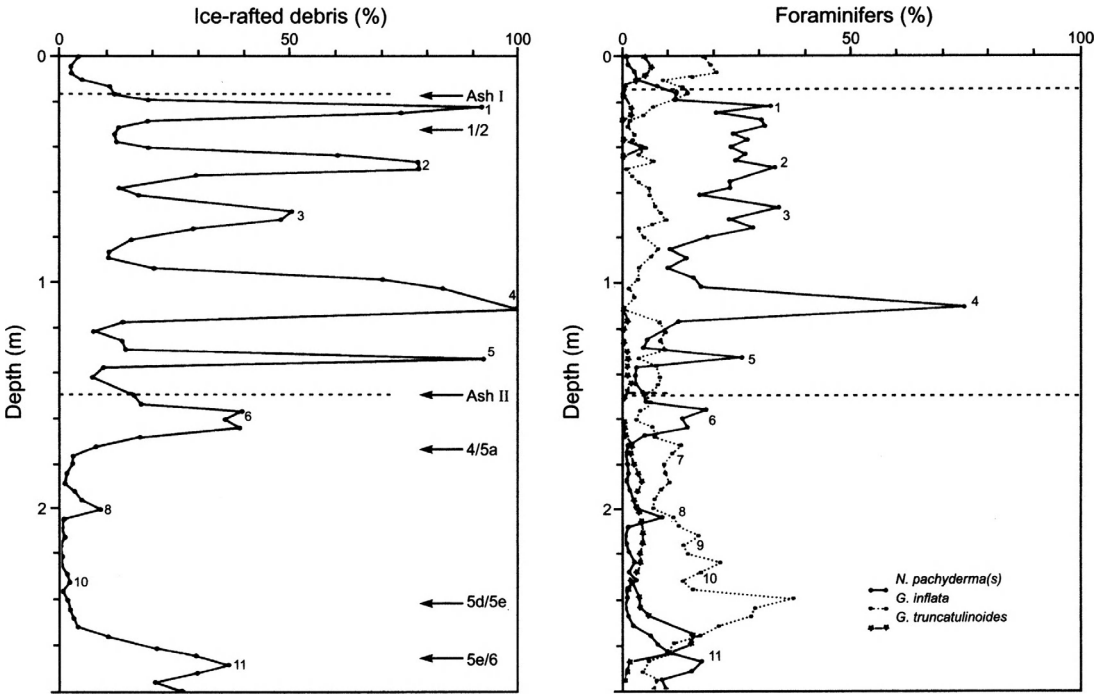


FIGURE 6.53 Ice rafted debris (IRD) as a percentage of the total number of forams + ice-rafted particles in a sediment core from the North Atlantic (~47°N, 20°W). Isotopic stage boundaries and volcanic ash layers are shown (Ash I was deposited approximately 10,800 years BP and Ash II ~54,000 BP). Times of maximum ice-rafted debris are now known as Heinrich events (cf. Table 6.3). *From Heinrich (1988).*

areas of the North Atlantic Ocean (Grousset et al., 1993; Hemming, 2004). Six events (H_1 to H_6) over the last ~70 ka have been identified in numerous sediment cores and dated by bracketing AMS ^{14}C dates or by correlation with the Greenland ice sheet isotope chronology (Table 6.3). However, while physical evidence for the start of a Heinrich event may be clear, a more gradual decline in IRD often makes the end point less easy to define. Furthermore, uncertainties related to marine reservoir correction and bioturbation have made precise dating problematical. Arguably, the best dates for these events come from U-series-dated tropical speleothems that record climate anomalies resulting from changes in the thermohaline circulation that accompanied Heinrich events, as discussed further below. Each event appears to have been an episode of very rapidly accumulating ice-rafted detritus (IRD) at times associated with a drop in foram concentration, due to lower productivity and/or increased dissolution (Broecker et al., 1992; Broecker, 1994). Heinrich events 3 and 6 differ from the others in that the two events are defined more by low percentages of forams than by a great deal of IRD, perhaps reflecting conditions when the Laurentide Ice Sheet was smaller (at the start of stages 2 and 4, respectively), so the delivery of icebergs and entrained debris was probably more limited (Gwiazda et al., 1996b). Bond et al. (1993) also identified IRD in sediments of Younger Dryas age from the Labrador Sea, which they characterized as an additional Heinrich event

TABLE 6.3 Age of Heinrich Events (ka BP)

	Marine Sediments	Sanchez-Goni and Harrison (2010)	Speleothems
H_0	11		12.5-11.5
H_1	16-17.25[a]	15.6-18.0	15.0-17.0
H_2	24-25.2[a]	24.3-26.5	23.5-24.5
H_3	31[b]	31.3-32.7	30.5-31.5
H_4	38[b]	38.3-40.2	38.5-39.5
H_5	~45[b]	47.0-50.0	47.0-49.0
H_6	~60[b]	60.1-63.2	59.5-60.5
H_7	~71		
H_8	~76		
H_9	~85		
H_{10}	~105		
H_{11}	~133		

Older events (designated here as "H_7" to "H_{11}") are based on two cores studied by McManus et al. (1994) with ages subject to uncertainties of probably ±5%.
[a] *Radiocarbon adjusted to calendar years (Hemming, 2004).*
[b] *Correlation to Greenland ice core $\delta^{18}O$ (Hemming, 2004).*

(H_0) (cf. Keigwin and Jones, 1995). However, the cause of Younger Dryas cooling was probably different from other Heinrich events, and so this should be considered as a distinct anomaly, as discussed further below. Although most studies have focused on Heinrich events during MIS 2-4, evidence for Heinrich-like IRD events has also been reported for earlier periods, from Atlantic sediment cores (e.g., Martrat et al. 2007; Hodell et al., 2008a; Stein et al., 2009; Margari et al., 2010). Hodell et al. (2008a) found little evidence for such events prior to ~640 ka BP, which they interpreted as evidence that the earlier, smaller continental ice sheets did not experience thermal instabilities and collapses (leading to calving of debris-laden icebergs) that appear to have been more common in recent glaciations.

Heinrich originally described the IRD as mainly angular quartz grains, but cores from further south and west have a relatively high percentage of distinctive limestone and dolomite in each detrital layer, suggesting a single source for these materials, possibly Paleozoic carbonates from the Hudson Bay/Hudson Strait region (Hemming, 2004). Also, Heinrich layers 1 and 2 increase in thickness westward toward the Labrador Sea, in a belt from 43 to 55°N, suggesting that material originated from the Laurentide Ice Sheet and was dispersed across the Atlantic by icebergs (Dowdeswell et al., 1995) (Figure 6.54). Isotopic studies of individual mineral grains have been carried out to try and pinpoint the provenance of material in different Heinrich events (Bond et al., 1992; Grousset et al., 1993; Andrews et al., 1994). Two

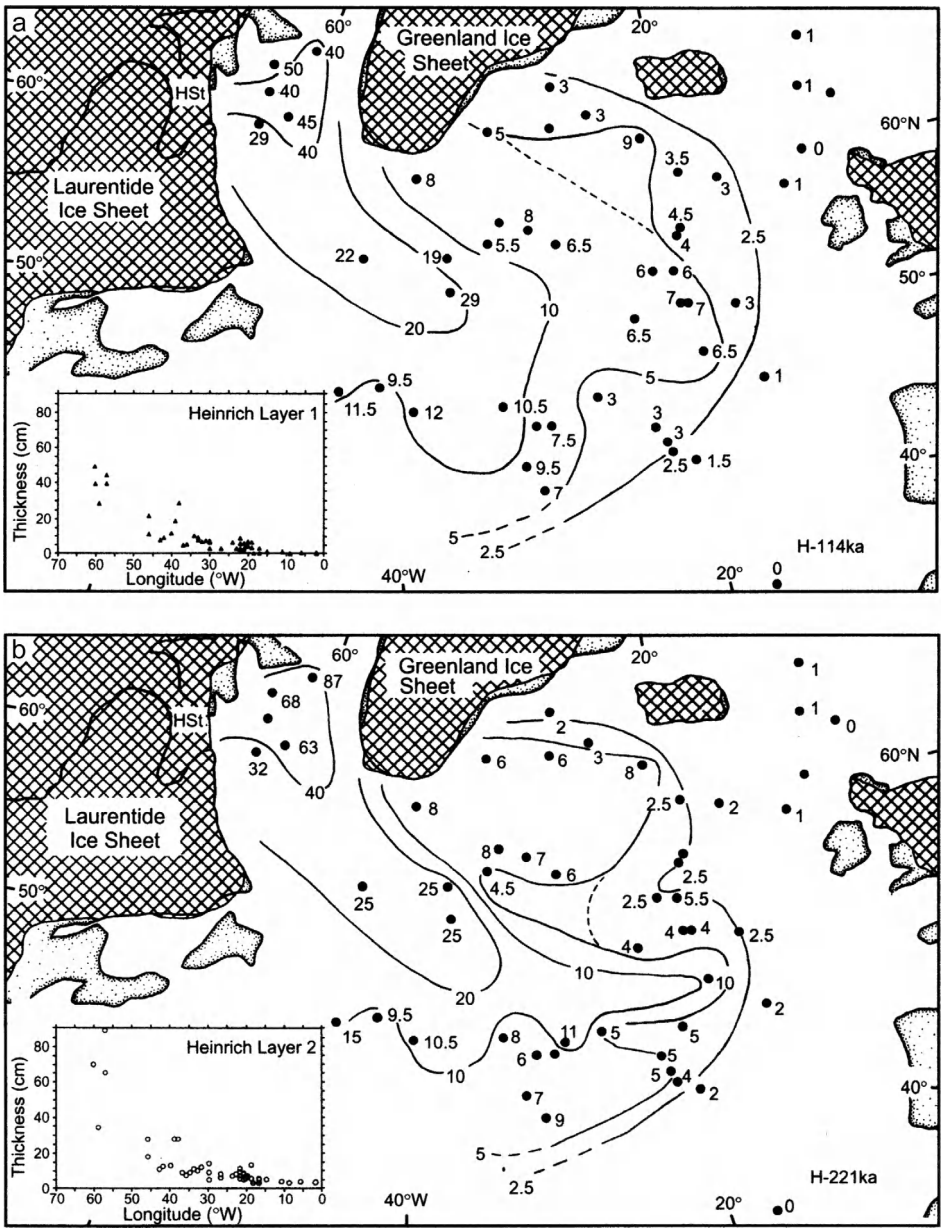


FIGURE 6.54 Thickness (cm) of Heinrich layers in North Atlantic sediments, based on whole core magnetic susceptibility data. Cross-hatching denotes major ice sheets; HSt, Hudson Strait, thought to have been the major ice stream supplying material to the North Atlantic from the Laurentide Ice Sheet. Upper figure: Heinrich event 1 (~14.3 ka ^{14}C years BP; lower figure: Heinrich event 2 (~21 ka ^{14}C years BP). *From Dowdeswell et al. (1995).*

approaches, one using lead isotopes and the other using neodymium and strontium isotope ratios and strontium concentrations, to characterize the sediments and their potential source rocks, have led to conflicting interpretations. Lead isotopic ratios point quite specifically to the Churchill Province of the Canadian Shield (northwest of Hudson Bay, Hudson Strait, and Baffin Island) as the source of debris in Heinrich event 2 (~21,000 years BP) (Gwiazda et al., 1996a). By contrast, Sr and Nd isotopes allow for the possibility of multiple sources of detrital material (including Icelandic, Fennoscandian, and British Isles Ice Sheet sources) during this and other Heinrich events, particularly for H_3 and H_6 (Grousset et al., 1993; Bond and Lotti, 1995; Revel et al., 1996; Scourse et al. 2000). These different interpretations have important implications for identifying the forcing mechanisms that led to Heinrich events. If Heinrich events only involve material from the Laurentide Ice Sheet (via Hudson Strait), this points to some sort of internal mechanism controlling ice discharge, such as the binge-purge model of MacAyeal (1993). However, if Heinrich events result from ice being discharged from ice sheets all around the North Atlantic, this suggests a more pervasive climatic forcing mechanism that could have influenced both small (Icelandic) and large (Laurentide) ice sheets more or less simultaneously (Bond and Lotti, 1995). Furthermore, calving of ice streams in one region could have led to a sea level rise that destabilized ice sheet margins elsewhere, though the magnitude of sea level changes associated with Heinrich events remains very uncertain, with estimates ranging from ~2 to 15 m (cf. Figure 6.19) (Chappell, 2002; Siddall et al., 2008; Carlson and Clark, 2013).

It may be significant that Heinrich events typically occurred at the end of prolonged cooling episodes, as recorded by increasing percentages of the cold-water foram *Neogloboquadrina pachyderma* (sinistral) leading up to the event (Figure 6.55). Furthermore, these longer-term cooling cycles can be correlated with similar variations in $\delta^{18}O$ in the GRIP Summit ice core from Greenland, indicating direct links between the ocean and atmospheric systems (which each record primarily represents) and changes in ice sheet dynamics, recorded by IRD in the Heinrich layers. Following each Heinrich event, there is an abrupt shift to warmer Atlantic surface water and higher temperatures in Greenland, which took place over just a few decades (cf. Steffensen et al., 2008).

The occurrence of Heinrich events is closely linked to changes in the Atlantic meridional overturning circulation (AMOC). Today, relatively dense saline water transported into the North Atlantic from the Tropics cools and sinks, ventilating the ocean depths as part of the thermohaline "conveyor belt" circulation (Section 6.8). A reduction in the salinity of the surface waters (buoyancy forcing) will disrupt this process, leading to a slowdown, or even a cessation, in the formation of North Atlantic Deep Water, with global effects resulting from subsequent changes in the thermohaline circulation. This was the situation at the end of the last glaciation, with a large increase in freshwater fluxes to the North Atlantic as continental ice sheets melted, leading to a slowdown in the AMOC (Clark et al., 2012). Consequently, with less North Atlantic Deep Water (NADW) being formed, there was only a limited return flow of water into the North Atlantic from the south. This led to the accumulation of heat in the Southern Hemisphere, as seen in the isotopic record from Antarctica (EPICA-DML; see Figure 5.28), as well as at depth in the North Atlantic, as recorded in Mg/Ca ratios and $\delta^{18}O$ in benthic forams in North Atlantic sediment cores (Figure 6.56) (Broecker, 1998; McManus et al., 2004; Gutjahr and Lippold, 2011; Marcott et al., 2011). Importantly, the period of warming at intermediate depths in the North Atlantic *preceded* each Heinrich event by

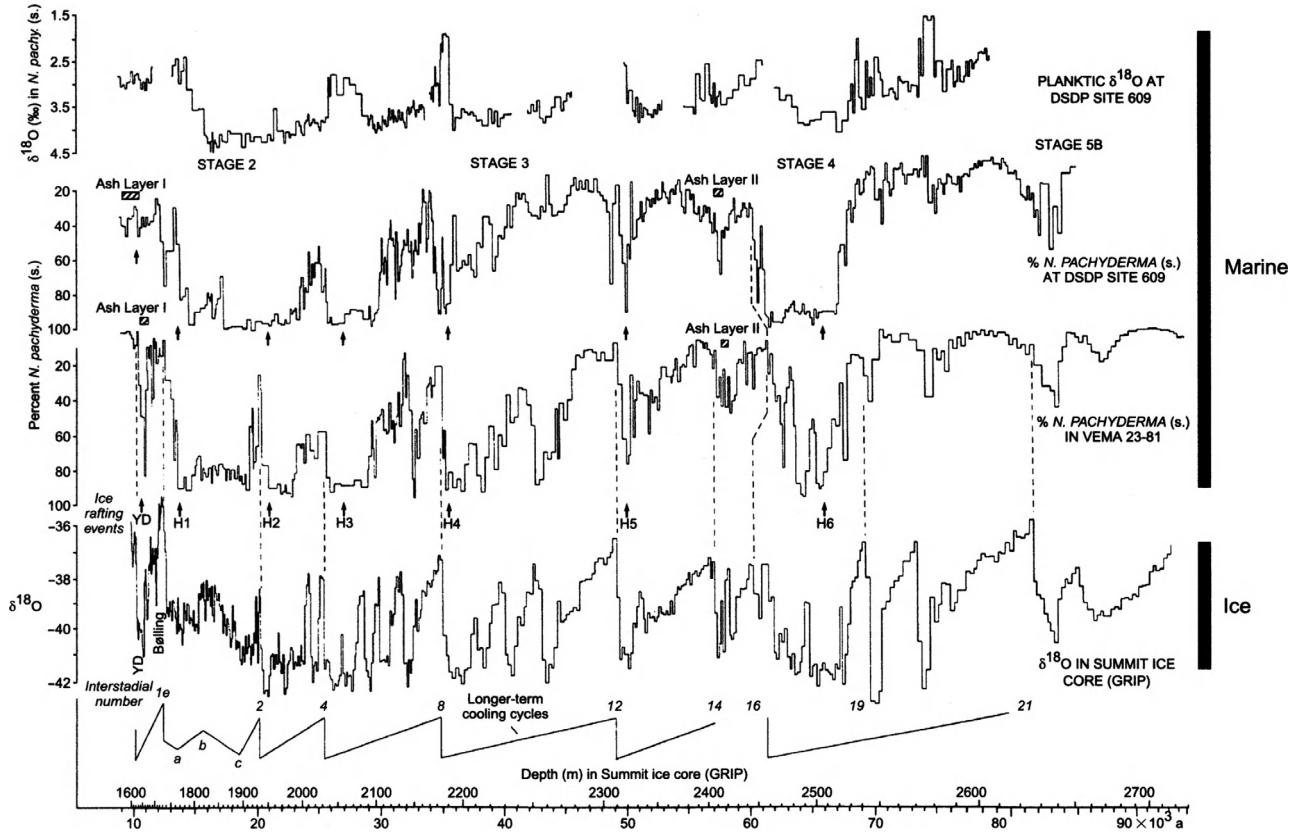


FIGURE 6.55 Comparison of $\delta^{18}O$ and percentages of the planktonic cold water foram *Neogloboquadrina pachyderma* [sinistral] in two ocean sediment cores from the North Atlantic, with the $\delta^{18}O$ record from the GRIP ice core (Summit, Greenland). Dashed lines indicate common features used to match the records, but the timescale shown is based on radiocarbon dates for the past ~35,500 years and estimated ages of Heinrich events (shown as H1 to H6) derived in other studies. The ice core record was then forced to fit the assumed sediment chronology. The records are quite similar, indicating that there were strong links between the ocean-atmosphere-cryosphere system in the North Atlantic during the time period represented here. The lower schematic diagram shows how clusters of millennium-length cycles of $\delta^{18}O$ in the ice core record (sometimes referred to as Dansgaard-Oeschger cycles) seem to form long-term cooling cycles, which terminate abruptly at irregular intervals; a similar pattern can be seen in the cold-water foram percentage data, especially in core VM23-81 (from ~55°N). *From Bond et al. (1993).*

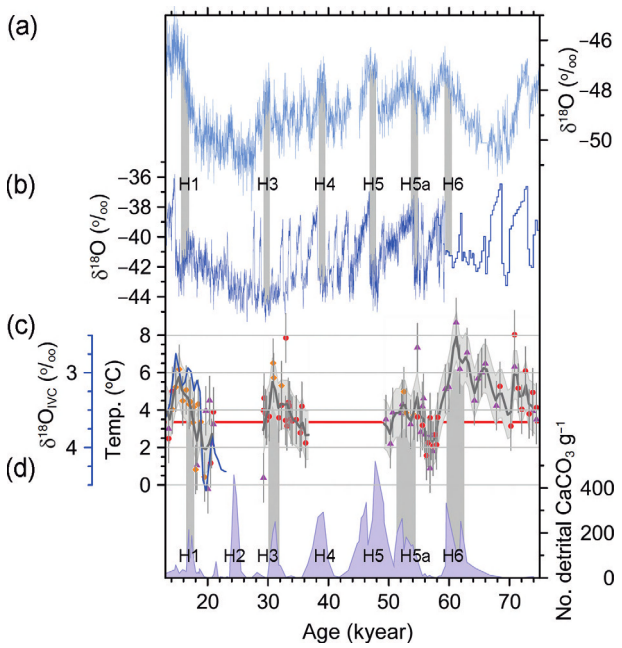


FIGURE 6.56 (a) $\delta^{18}O$ record from Antarctic EPICA-DML (European Project for Ice Coring in Antarctica Dronning Maud Land) ice core (chronology from Lemieux-Dudon et al., 2010). (b) $\delta^{18}O$ record from the North Greenland Ice Core Project ice core; chronology <60 ka from Lemieux-Dudon et al. (2010), and >60 ka from GISP2 ice core age model. (c) Mg/Ca-derived bottom water temperatures on three different species of benthic foraminifera, from North Atlantic core EW9302-2JPC (1251 m, 48°48′N, 45°05′W). 500-year Gaussian-filtered record shown by thick gray line, with a 1.3 °C error, based on analytical uncertainty. Also shown is the ice-volume corrected benthic $\delta^{18}O$ ($\delta^{18}O_{IVC}$) record from this core (blue line) during the last deglaciation. (d) Number of ice-rafted detrital $CaCO_3$ grains g^{-1} of sediment in core EW9302-2JPC, with increases in the number of these grains identifying Heinrich layers 1-6. Vertical gray bars show timing of Heinrich events on the independent ice core (a, b) and EW9302-2JPC core (c, d) chronologies. Warming in Antarctica and in the North Atlantic at depth precedes the Heinrich events, which also correspond to cold conditions in Greenland. Conditions are reversed following Heinrich events. *From Marcott et al. (2011).*

several thousand years; circulation changes prior to Heinrich events, involving an influx of water from the Southern Hemisphere, were also noted in Bermuda Rise sediments by Gutjahr and Lippold (2011). The warmer subsurface waters in the North Atlantic may have led to melting and instability at the tidewater ice margins of the Laurentide Ice Sheet, along the coast of Labrador and Hudson Strait and perhaps also along the Scandinavian Ice Sheet edge, leading to rapid disintegration of the ice (cf. Alvarez-Solas et al., 2010). Surface melting and enlargement of crevasses may also have promoted calving (Hulbe et al., 2004; see comments by Alley et al., 2005). As a result, "armadas" of icebergs would have rapidly entered the Atlantic, adding even more freshwater to the North Atlantic and leading to an abrupt collapse of the AMOC (Broecker et al., 1992; Broecker, 1994). Another possible explanation for ice sheet collapse, suggested by modeling experiments, is that ice sheets may grow to a point where they develop instabilities (due to basal ice melting) that cause rapid discharge (surges) into marine embayments via ice streams and ice shelves (MacAyeal, 1993; Alley and MacAyeal, 1994). Cold, slow-moving ice can freeze rock debris into its base, but during times of destabilization, channelized ice streams develop where frictional heating allows ice to slide over a relatively warm and wet bed. Debris-laden icebergs are generated when the surging ice streams enter the marine environment, and this continues until the ice sheets become stable once again. This "binge-purge" model could account for the quasi-periodic character of the observed record, though just what climatic conditions are needed to bring about destabilization of the ice sheets is not clear. There is a fairly delicate balance between conditions that

(a) maintain an ice sheet in a quasi-equilibrium state, (b) cause a periodic collapse but then allow recovery, and (c) cause irreversible collapse (i.e., complete deglaciation). The interplay of ocean, atmosphere, and ice with the added complexities of eustatic sea level change and glacio-isostatic adjustments as ice loads changed allows for many possible scenarios of how the observed changes may have been brought about. Whatever the mechanism for the iceberg flux associated with Heinrich events, presumably it would have been followed by a period with far less iceberg discharge and a rapid reduction in freshwater flux to the North Atlantic, allowing salinity to increase and a return to the conveyor "on" mode, with increased advection of warmer water and warmer air masses into the Greenland area (Paillard and Labeyrie, 1994).

Many model simulations have examined the effects of "freshwater forcing" from the Laurentide Ice Sheet on the thermohaline circulation. In most cases, this has been done by adding freshwater across a wide swath of the North Atlantic, usually from 50 to 70°N (hosing experiments), and comparing the result with baseline simulations. Various combinations of forcing (varying freshwater amount and duration) have been examined (Stouffer et al., 2006; Kageyama et al., 2010; Otto-Bliesner and Brady, 2010). However, recent simulations using high-resolution ocean circulation models indicate that the hosing experiments may be misguided. Freshwater entering the North Atlantic from Hudson Strait, Baffin Bay, and the Labrador coast does not spread across the North Atlantic but is restricted to the western boundary current that entrains the freshwater along the coast of North America, eventually spreading out at subtropical latitudes rather than further north (Figure 6.57) (Condron and Winsor, 2012). However, if freshwater enters the North Atlantic from the Arctic Ocean, more extensive flooding across the higher latitudes does occur. What could be the source of such a freshwater inflow? In the Condron and Winsor (2012) simulation, they examined the hypothesis that freshwater from large proglacial lakes along the southern margin of the Laurentide Ice Sheet entered the Arctic Ocean via the Mackenzie River and eventually exited the Arctic Ocean via Fram Strait, into the North Atlantic. This is the scenario that, some have argued, led to the Younger Dryas cold reversal (~12,700-11,700 years BP) (e.g., Tarusov and Peltier, 2005). However, there is little direct evidence that such flooding occurred at that time and no evidence that similar events occurred many times during MIS 2-4. However, it is quite plausible that the Arctic Ocean itself was a source of freshwater for the North Atlantic. Very thick pack ice developed over the Arctic Ocean during glacial times, when temperatures were extremely low, and there was minimal influx of warm Atlantic water beneath the ice. Snow would have accumulated *in situ* for many centuries, creating "paleocrystic floes" made up of a basal layer of sea ice, but tens of meters of freshwater on top (in the form of snow and superimposed ice) (analogous to the fringing ice shelves seen on northern Ellesmere Island today, which are over 50 m thick in places) (Bradley and England, 2008). Sedimentary evidence for such a thick and rigid ice cover is suggested by periods of nondeposition beneath the ice during the LGM (Poore et al., 1999; Polyak et al., 2004). This ice cover may have been destabilized and mobilized by warm water intrusions from the Nordic Seas during stadials, as warm intermediate-level waters penetrated northward. Benthic species normally associated with waters above 3.5 °C certainly reached beyond the Arctic Circle during stadials (Rasmussen and Thomsen, 2004). These warm water incursions may have led to breakup of the marginal Arctic Ocean ice cover, resulting in large volumes of

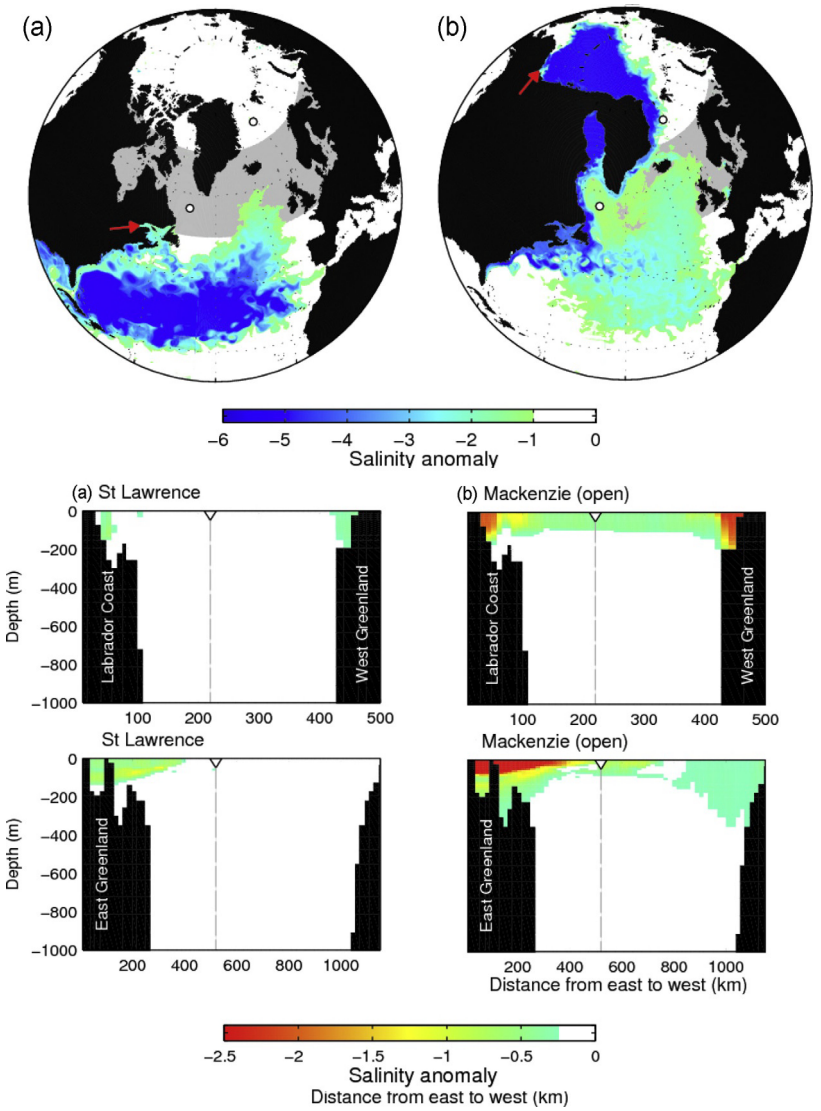


FIGURE 6.57 Top: The dispersal of meltwater in the North Atlantic. The colors (green-blue) show the difference in surface salinity (perturbation minus control simulation) in response to releasing meltwater from the (a) Gulf of St. Lawrence and (b) the Mackenzie Valley (with the Canadian Arctic archipelago closed, i.e., ice-covered). The snapshots show conditions of maximum surface freshening (32 and 56 months, respectively, after the meltwater release). Red arrows are the discharge locations. White circles are locations where open-ocean deep convection has been observed in the modern-day ocean, though the locations of deepwater formation in glacial times were probably different. The gray shading (50-70°N) is the traditional climate model meltwater "hosing" region. Below: The distribution of meltwater across the central Labrador Sea (56.5°N, 51°W) (upper panel) and Greenland Sea (~75°N, 3°W) (lower panel), corresponding to sites where open ocean deep convection has been observed in the modern era. The colors (green-red) show the difference in salinity (perturbation minus control simulation) after 10 years of model integration. Only meltwater that enters the North Atlantic from the Arctic Ocean creates a classic "freshwater cap" that inhibits open ocean deep convection (vertical dashed line, indicating the locations of deepwater formation today). The water column of the central Labrador and Greenland Seas is unaltered by meltwater discharge from the St. Lawrence Valley. *From Condron and Winsor (2012).*

relatively freshwater (as ice floes) being carried southward, directly into those areas of the North Atlantic where deepwater formed (Figure 6.57).

The changes in oceanic and atmospheric circulation that accompanied Heinrich events had dramatic worldwide consequences. As the AMOC was reduced, temperatures fell across the entire Northern Hemisphere, but rose in the Southern Hemisphere as warm water began to accumulate in the Southern Ocean (Blunier et al., 1998; Stocker and Johnsen, 2003). This stronger interhemispheric thermal gradient resulted in a southward shift in the position of the Intertropical Convergence Zone (ITCZ) and its associated belt of convective rainfall (Broccoli et al., 2006; Chiang, 2009; Chiang and Friedman, 2012). The resulting changes in rainfall are clearly seen in speleothem records from Brazil (Wang et al., 2006; cf. Figure 8.11) as well as in lake sediment records from the Bolivian Altiplano (Baker et al., 2001; Fritz et al., 2010a; Placzek et al., 2013) and in sediments from off the coast of Brazil (Figure 6.58) (Arz et al., 1998; Jennerjahn et al., 2004; Jaeschke et al., 2007). Heinrich events are also recognizable in sediments from the Arabian Sea (Schulz et al., 1998; Deplazes et al., 2013; Figure 6.52) and in loess and speleothem records from China (e.g., Figures 7.10 and 8.11) (Porter and An, 1995; Wang et al., 2006), which indicate that there was an overall reduction in monsoon strength as a result of Heinrich event-related changes in North Atlantic circulation. Similar changes associated with D-O events can also be seen in many paleoclimate records from the Tropics, though only high-resolution proxies record those more rapidly changing conditions (e.g., Kanner et al., 2012; Deplazes et al., 2013). Thus, changes in North Atlantic Deep Water formation, resulting from freshwater influx had global impacts, with particular effects on the distribution of rainfall throughout the Tropics.

In summary, Heinrich events and D-O events are both important aspects of the variability of climate in the past, and both are related to changes in the amount of freshwater entering the North Atlantic, which stabilized the water column and reduced deepwater formation, with

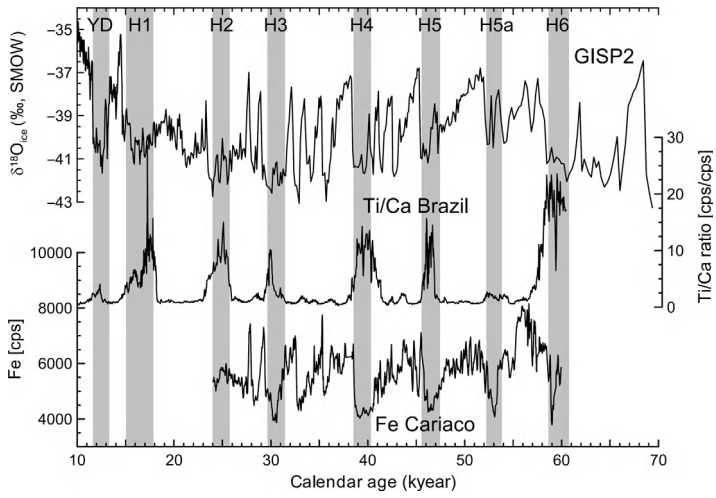


FIGURE 6.58 Variations in Ti/Ca ratio in sediment cores off the northeastern coast of Brazil (~4°S, 36°W), compared to GISP2 ice core oxygen isotopes and the record of terrestrial Fe in a core from the Cariaco Basin off the coast of Venezuela (cps, counts per second, on an XRF scanner). Both parameters are proxies for precipitation on the adjacent continent and show that as the ITCZ shifted southward during Heinrich events, rainfall increased over northeastern Brazil, but declined over the northern parts of South America (Orinoco Basin) that supply sediment to the Cariaco Basin. Hence, the two records are inversely related. It is also noteworthy that there is no strong signal of D-O events in these data. *From Jaeschke et al. (2007).*

worldwide consequences. But the causes of the two types of abrupt change are somewhat different—D-O events primarily involved the formation of extensive sea ice, which can rapidly develop but decay just as quickly. At other times, freshwater was derived from the melting of continental ice, via ice streams or ice shelves, where the ice was in contact with the ocean. Deep Water formation then declined, leading to the buildup of warm water at depth that destabilized the ice sheets further, leading to calving on a massive scale, adding large volumes of freshwater to the surface ocean as icebergs and associated sediments drifted into the sea, principally from the Laurentide Ice Sheet, leading to the ice-rafted deposits we now identify as Heinrich layers. This led to a further reduction in deepwater formation (an abrupt reduction in the AMOC) with the accumulation of more warm water at depth. Eventually, the water column became unstable bringing these warmer waters to the surface, causing sea ice to rapidly recede, leading to the abrupt isotopic changes observed in the Greenland Ice Sheet (Figure 5.28), and a resumption of deepwater formation. The prerequisites for this sequence of events were the continental and marine-based ice sheets in contact with the ocean and the ice-covered Arctic Ocean itself, adjacent to the critical zones of deepwater formation in the North Atlantic. The fact that the Bering Strait was also closed (from ~80 to 12 ka BP) may also have been a contributing factor, as this limited any export of relatively fresh surface water from the North Atlantic across the Arctic Ocean into the Pacific, thereby reinforcing the slowdown of the AMOC as freshwater would have accumulated in North Atlantic Basin (Hu et al., 2012). It is thus perhaps no surprise that it is only during the periods of major glaciation when such conditions exist that these kinds of abrupt changes have been observed in the paleoclimate record (Figure 6.19) (cf. Ganopolski and Rahmstorf, 2001).

CHAPTER

7

Loess

OUTLINE

7.1 Chronology of Loess-Paleosol Sequences 284

7.2 Paleoclimatic Significance of Loess-Paleosol Sequences 287

Loess is a deposit of wind-blown silt that blankets large areas of the continents. It is often light brown in color, consisting predominantly of quartz, feldspars, micas, and calcium carbonate (Pye, 1984, 1987). Geographically, loess is extensive in the North American Great Plains, south-central Europe, Ukraine, central Asia, China, and Argentina (Figure 7.1). In North America, loess was derived from both glacial and nonglacial sources (Bettis et al., 2003) but is commonly related to formerly extensive outwash deposits from the Laurentide ice sheet and to the floodplains of large, braided rivers; sections along the Mississippi River valley may reach 20 m in thickness (Forman et al., 1995; Oches et al., 1996). The thickest loess deposits are found in the unglaciated regions of Alaska (up to 50 m; Beget and Hawkins, 1989) and in Nebraska (up to 48 m) where the LGM (Peoria) loess was derived from bedrock sources northwest of the region (Muhs et al., 2008). In Europe, loess deposits are common in areas that lie between the former Alpine and the Scandinavian ice sheets and in regions to the east associated with major river systems (Figure 7.2) (Kukla, 1975b; Frechen et al., 2003; Smalley et al., 2009). Some of the thickest loess sections are related to formerly extensive braided rivers at a time when vegetation cover was greatly reduced (primarily grassland) (Fitzsimmons et al., 2012). Although rarely continuous, some sites have loess and paleosol sequences that extend back into the Early Pleistocene (particularly in the middle and lower Danube River Basin, e.g., at Stari Slankamen in Serbia and at Stranzendorf and Krems in Austria; Marković et al., 2011). Elsewhere, loess is related to desert conditions, especially the extensive deserts of central Asia where weathered material, transported from adjacent mountain ranges, has accumulated (Smalley et al., 2009). These vast arid areas, and the adjacent Yellow River system, are the source regions

Copyright © 2015 Raymond S. Bradley.
Published by Elsevier Inc. All rights reserved.

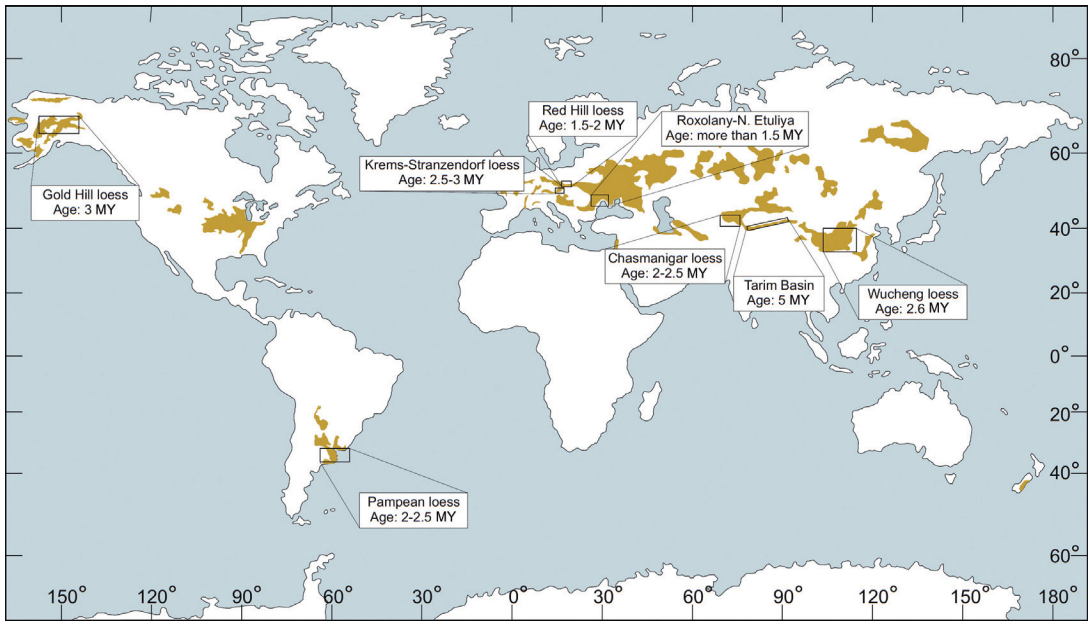


FIGURE 7.1 Global distribution of loess deposits. *Modified from Varga (2011).*

for the extensive Chinese loess deposits (Stevens et al., 2013). In north-central China (southeast of the Gobi Desert), loess deposits are extremely thick, up to 300 m in places (Figure 7.3), and completely cover the underlying topography, forming a loess plateau that extends over an area of ~500,000 km^2 (Liu et al., 1985). It is there that the most comprehensive paleoclimatic studies of loess deposits have been carried out (Kukla, 1987a; Kukla and An, 1989; Liu and Ding, 1998; An, 2000).

The characteristic stratigraphic feature of the Loess Plateau is the alternation of loess units and intervening paleosols. The loess accumulated during dry periods when dustfall was high and vegetation was predominantly short grasses. During episodes of warmer and wetter conditions, a reduction in loess deposition and *in situ* weathering of the loess already on the ground led to accretionary soil formation (Figure 7.4). Today, the alternating sequence of loess units and paleosols (Figure 7.5) forms the longest and most complete terrestrial record of Quaternary paleoclimatic conditions to be found on the continents (An et al., 1990; Ding et al., 1993). In fact, widespread loess has accumulated on the Loess Plateau for >7 Ma, and in some areas, loess deposition can be traced as a red, clay-rich deposit back to ~25 Ma ago (late Oligocene), indicating that arid source regions have existed in the continental interior for at least that long (An et al., 2001; Guo et al., 2002; Qiang et al., 2011). Further aridification of the continent resulted from uplift of the Himalayas and Tibetan Plateau during the Miocene, which isolated the Eurasian interior from moist air to the south and southeast (Liu and Yin, 2002; An et al., 2005; Guo et al., 2008). As the continent became more arid, northerly winds from strong winter Siberian-Mongolian high-pressure systems carried eolian material southward where it accumulated on the landscape. Upper-level

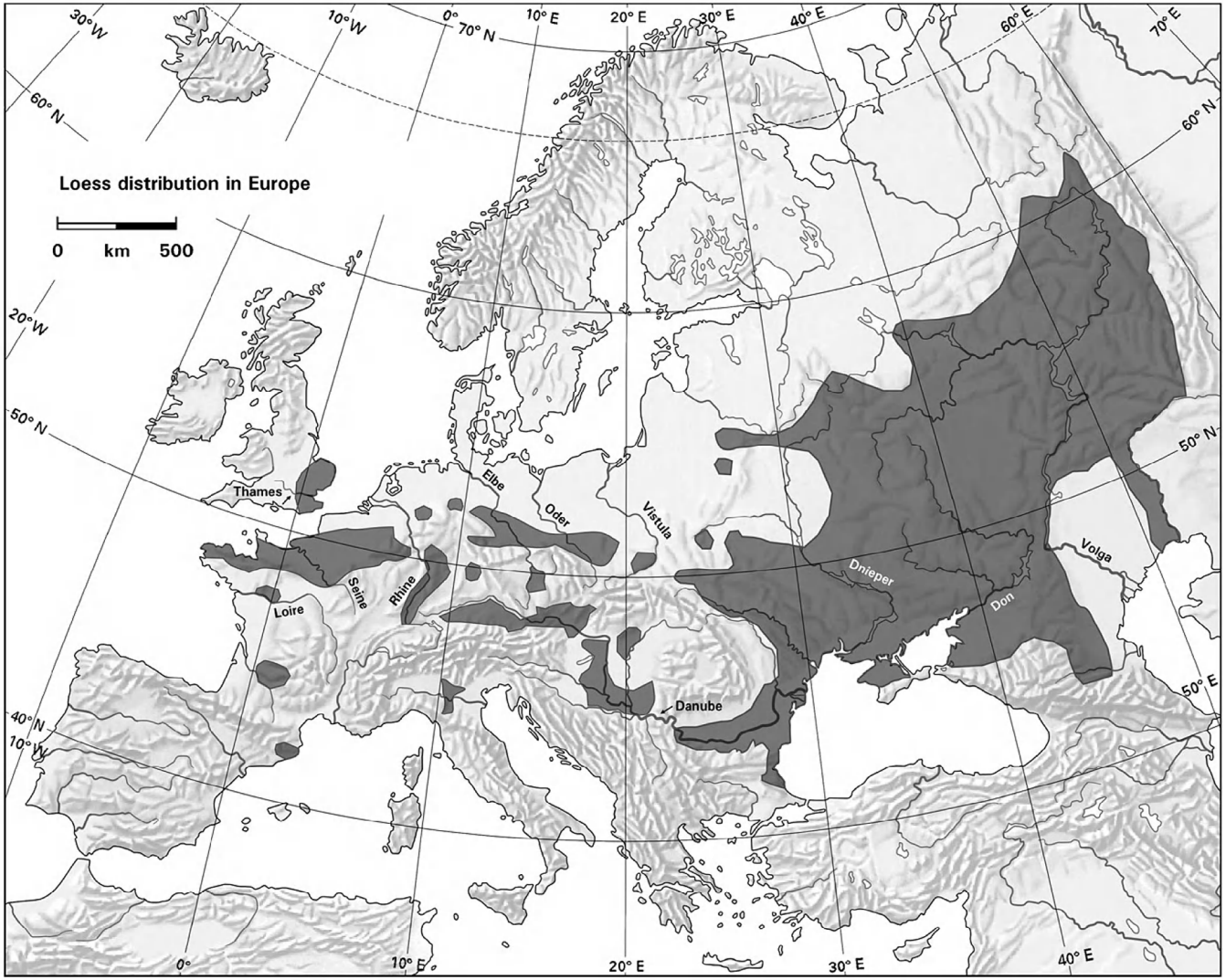


FIGURE 7.2 Loess distribution in Europe. Loess distribution is related to the former extent of ice sheets and the distribution of major river systems. *From Smalley et al. (2009).*

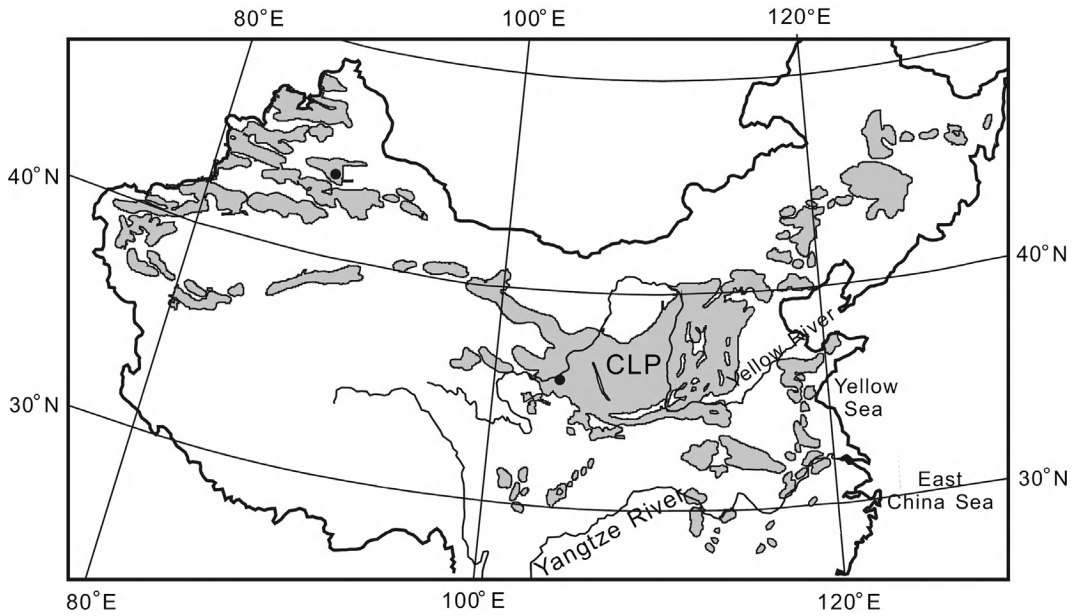


FIGURE 7.3 Distribution of loess in China. *From An (2014).*

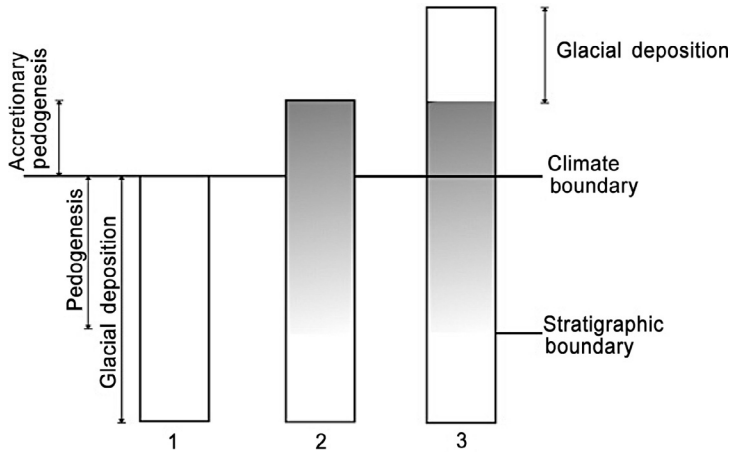


FIGURE 7.4 Conceptual model for pedogenic overprinting on previously emplaced loess. (1) Loess builds up. (2) Climate changes and loess accumulation decreases; soil forms on both newly deposited sediment and the preexisting loess. (3) Sedimentation rates increase again and pedogenesis is reduced as more loess accumulates. In this way, the climatic boundary when soil formation began has been obscured. *From Stevens et al. (2007).*

westerly winds also carried fine dust far to the east, where it was deposited in the North Pacific (Rea et al., 1998; Zheng et al., 2004). During summer months, continental heating leads to the development of low-pressure systems that draw in moist air, delivering rainfall to the continental interior. This alternation of cold, dry northerly and northwesterly winter winds and warm, moist southerly or southeasterly winds defines the classic monsoon climate of the region (An et al., 1990). On glacial-interglacial timescales, the strength of the



FIGURE 7.5 A well-exposed loess-paleosol section near Huangling, Shaanxi province, China. The upper (Holocene) soil is not visible, and most of the most recent loess unit (L1) and the last interglacial soil (S1) have been removed in this location. The very prominent S5 paleosol is easily recognized throughout the Loess Plateau. *Photograph kindly provided by Bill McCoy.*

winter and summer monsoons varied, with the glacial periods dominated by the winter monsoon circulation and minimal penetration of summer moisture into the continental interior; during interglacials, opposite conditions prevailed. Much of the eolian sediment transported during glacial periods was associated with dust storms that carried large quantities of relatively coarse-grained sediments from the arid regions. During interglacials, dust storms were less common so the mean grain size of material being deposited on the Loess Plateau was much finer (Liu et al., 1985; Zhang et al., 1999; Prins et al., 2007). Detailed geochemical and grain-size studies of the Miocene and Pliocene red clay units show that monsoon-like climatic conditions have been a feature of the Loess Plateau region for over 20 Ma, though the signal is much more subdued than in overlying Quaternary sediments that are made up of loess and paleosols (An et al., 2001; Guo et al., 2008). This may be because there was less input from dust storms or the fine-grained sediments in the red clay were strongly weathered through pedogenic processes under more humid climatic conditions in the past (Ding et al., 2000). Isolating the more resistant quartz grains reveals cyclical variations in grain size similar to Quaternary sediments, though of lower amplitude (Guo et al., 2008; Sun et al., 2010). Conditions changed significantly around 2.7 Ma BP, with a marked increase in the loess sedimentation rate, leading to a replacement of the red clay units by an alternation of loess and accretionary paleosols (Figure 7.6). This change is clearly linked to the onset of major continental glaciation in the northern hemisphere, probably coupled with the first occurrence of permanent ice cover on the Arctic Ocean. This reduced Eurasian temperatures in winter, leading to stronger northerly winds that transported increasing amounts of dust from the continental interior (Ding et al., 2000; Sun and An, 2005).

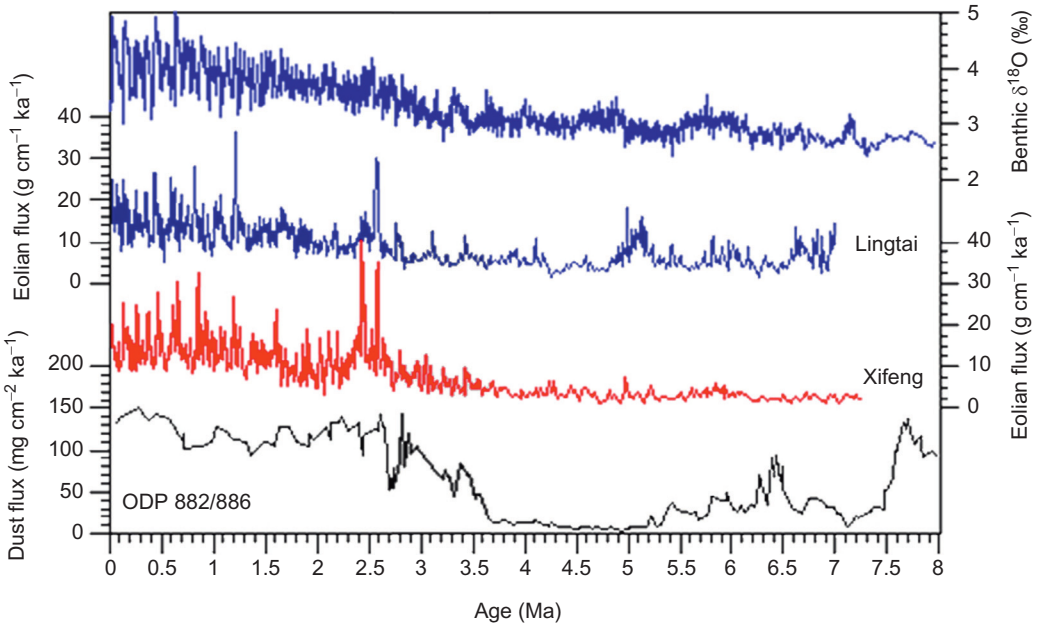


FIGURE 7.6 Comparison of dust flux on the Chinese Loess Plateau (Sun and An, 2005) and the North Pacific (Rea et al., 1998) with the benthic δ^{18}O record (Zachos et al., 2001) over the last 7 Ma. *From An (2014).*

7.1 CHRONOLOGY OF LOESS-PALEOSOL SEQUENCES

The paleomagnetic polarity timescale (see Chapter 4) provides the primary chronostratigraphic framework for dating loess (Figure 7.7) (Heller and Liu, 1984; Rolph et al., 1989; Rutter et al., 1990; Thistlewood and Sun, 1991). Reversals and excursions are clearly registered in the loess, though there are uncertainties about the amount of time it took before the magnetic signal became locked into the sediments (Zhou and Shackleton, 1999; Sun et al., 2006; Jin and Liu, 2011). A more refined chronology has been developed by starting with the basic paleomagnetic timescale and then tuning the primary indices of loess-paleosol changes—magnetic susceptibility and grain size—to the obliquity and precession orbital record. Magnetic susceptibility (χ) is considered to be an index of summer monsoon intensity (An et al., 1991), with higher values of magnetic susceptibility in paleosols than in the loess units, due to the formation of superparamagnetic grains during pedogenesis. Quartz grain size is an index of winter monsoon strength, with the highest values indicating cold and windy conditions, which carried coarse-grained particles far from the source regions (Porter and An, 1995; Xiao et al., 1995). Variations in these parameters clearly reveal the alternation of loess and paleosols back in time (Figure 7.8). Of particular note is the major paleosol, S5, which represents a long interglacial period, and major loess units at ~2.6 Ma (L33), 1.25 Ma (L15), and ~0.87 Ma BP (L9) (cf. Vandenberghe et al., 2004). Tuning these data to the obliquity and precessional time series implicitly assumes that the two measures of

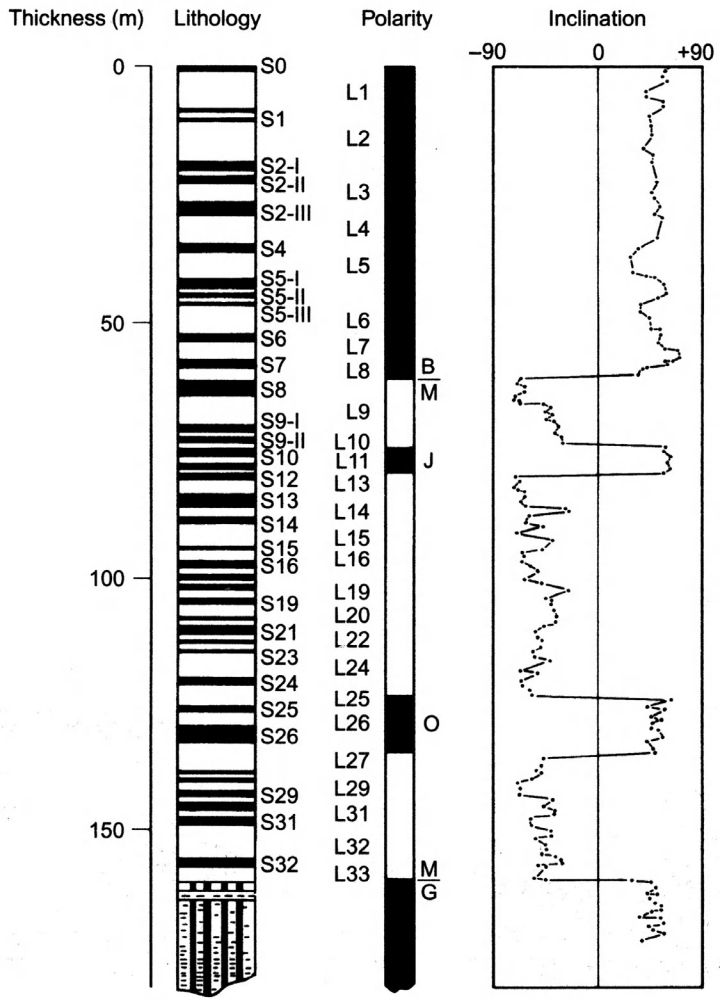


FIGURE 7.7 Magnetic stratigraphy of the loess-paleosol section at Baoji, Loess Plateau, north-central China. Major paleosols (S) and loess units (L) are numbered from the top down (Holocene soil, S_0). Changes in polarity are clearly indicated by the inclination record on the right (B/M, Brunhes-Matuyama boundary; J, Jaramillo subchron; O, Olduvai subchron; and M/G, Matuyama-Gauss boundary). Loess began to accumulate over a red clay deposit around the time of the Gauss-Matuyama transition. *From Liu et al. (1993).*

winter and summer monsoon strength are in phase with the northern hemisphere ice volume changes, which previous research has tied to orbital variations (Imbrie et al., 1984). Using the same lagged responses (8000 years from obliquity minima and 4500 years from precessional maxima), an orbitally tuned timescale for the loess records has thus been developed (Sun et al., 2006). The results show excellent correlation between different sites and similar amplitude modulation to the orbital parameters over time. Although there are benefits from tuning the grain-size and magnetic susceptibility data to phase-lagged orbital data, well-dated speleothem isotopic data do not support the notion of a lagged summer monsoon response to orbital forcing. $\delta^{18}O$ in stalagmites from eastern China (which provide an index of summer monsoon strength) shows that there was a direct response of monsoon rainfall over the last 224 ka to July 21st insolation at 65°N, which is dominated by the 23,000

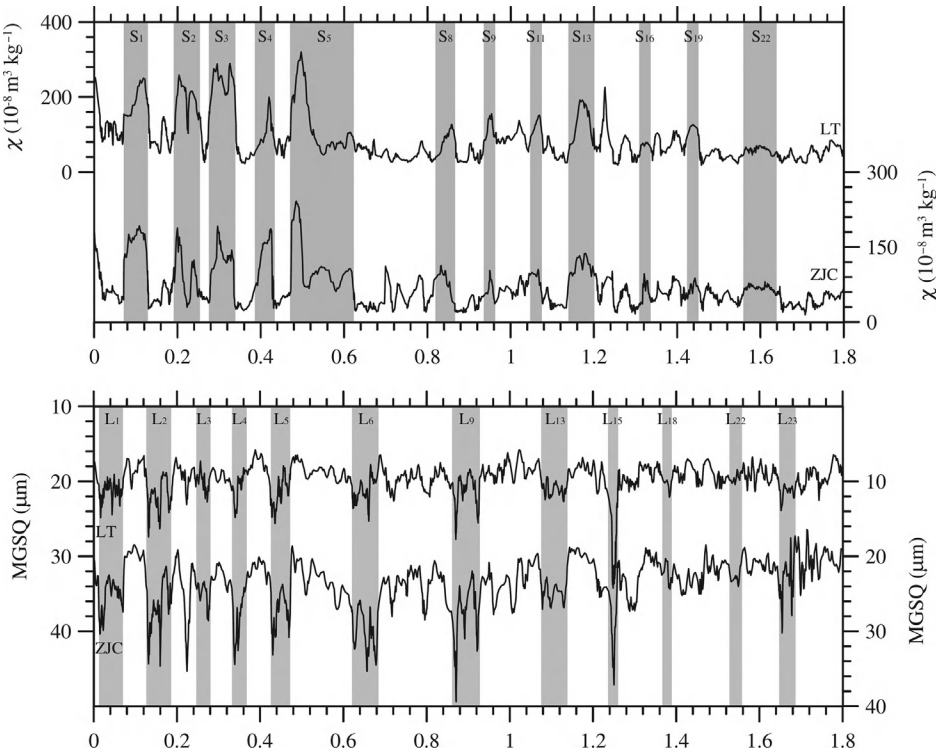


FIGURE 7.8 Correlation of the Lingtai (LT) and Zhaojiachuan (ZJC) magnetic susceptibility (χ, above) and mean grain size of quartz (MGSQ, below) for the 0-1.8 Ma time interval. Stratigraphic units are simply counted back from the Holocene soil (S_0) and the most recent loess episode (L_1), to the preceding interglacial soil (S_1) and underlying loess (L_2), and so on, down the section. In this way, 32 major loess and paleosol units have been recognized in the last ~2.7 Ma (i.e., above the red clay unit), documenting the alternation between glacial and interglacial conditions throughout the Quaternary. Here, the shaded bars indicate that the duration of major paleosols (S1, S2, etc.) and loess units (L1, L2, etc.) is well correlated between the two sections. *From Sun et al. (2006).*

precessional cycle (Wang et al., 2008). Further studies are needed to reconcile the speleothem and loess data, as they should carry a common summer monsoon signal.

Aminostratigraphic studies (on snails embedded in the loess; see Chapter 4, Section 4.2.1) have been useful in clarifying the stratigraphic relationships between different locations, which has been particularly helpful in the more spatially discontinuous European loess sections (Oches and McCoy, 1995a,b,c, 2001; Marković et al., 2007). For more detailed chronological studies over the last glacial-interglacial cycle, radiometric and luminescence dates are commonly obtained, particularly using optically stimulated luminescence techniques (OSL) (see Chapter 3). OSL dates have shown that in some locations, loess deposition is not as uniform (in time and space) as is commonly assumed (Lu et al., 2007; Stevens et al., 2007, 2008). Thus, although dating by orbital tuning provides a broad glacial-interglacial chronostratigraphic framework, this approach may lead to significant errors on shorter timescales (Stevens et al., 2008).

7.2 PALEOCLIMATIC SIGNIFICANCE OF LOESS-PALEOSOL SEQUENCES

Long-term changes in quartz grain size and magnetic susceptibility show several distinct stages over the past 3.6 Ma, beginning with an abrupt change at ~3.4 Ma when summer monsoon intensity increased but winter monsoon intensity decreased (Figure 7.9). From 3.4 to 2.72 Ma BP, the summer monsoon became stronger, while the winter monsoon remained fairly steady. From 2.72 to 1.25 Ma BP, magnetic susceptibility declined, suggesting summer monsoon rainfall decreased, but winter monsoon strength increased. This pronounced change at 2.72 Ma is associated with the red clay/loess-paleosol transition and is linked to the onset of major northern hemisphere glaciation, which is recorded in many other paleoclimatic records. At 1.25 Ma (and particularly after ~0.5 Ma BP), the variability of magnetic susceptibility and mean quartz grain size both increased, coincident with major changes in the northern hemisphere ice volume. The timing of these changes is similar to those obtained by Ding et al. (2005) who argued that desert expansion occurred at 2.6, 1.2, 0.7, and 0.2 Ma ago, based on the increased flux of coarse-grained eolian material at sites near the northwestern desert margin. They interpreted these changes as reflecting a decline in summer monsoon strength, which reduced rainfall at the margins of the Loess Plateau, allowing desert regions to expand. Deng et al. (2006) also found evidence for increasingly arid conditions over time, based on changes in the magnetic properties of sediments over the last 2.5 Ma. A steady decline in eolian and pedogenic hematite in the loess and paleosols, respectively, resulted from an increase in aridity in the source regions and a reduction in chemical weathering due to cooler conditions.

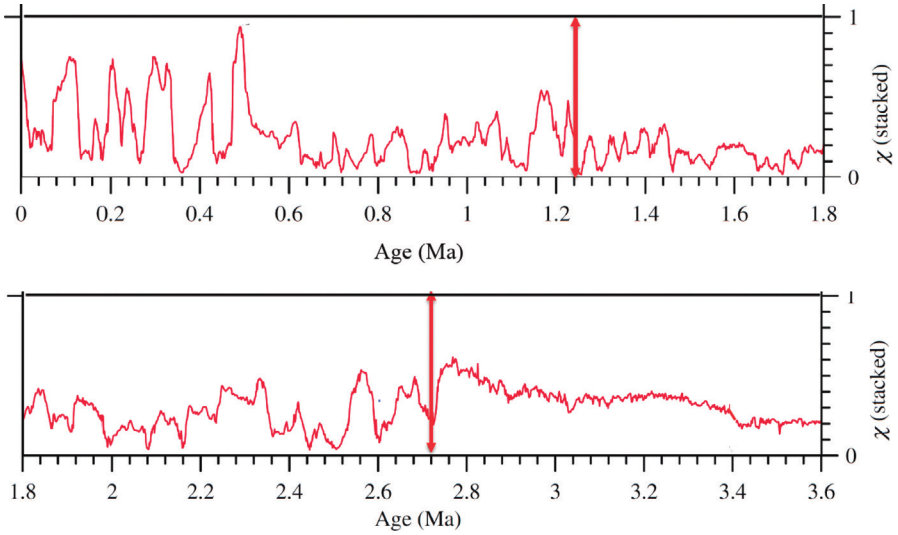


FIGURE 7.9 Temporal changes of stacked magnetic susceptibility (χ) records for the last 3.6 Ma. Susceptibility is interpreted as an index of summer monsoon strength. The "stack" is an average of normalized data from two sites: Lingtai and Zhaojiachuan on the Loess Plateau between Xi'an and Lanzhou (cf. Figure 7.8). Arrows indicate that the evolution of summer monsoons can be divided into three phases: 3.6-2.72, 2.72-1.25, and 1.25-0 Ma. *Modified, from Sun et al. (2006).*

Detailed OSL dating of loess has revealed that grain size varies in parallel with $\delta^{18}O$ in Greenland ice, for at least part of the last glacial-interglacial cycle (Liu and Ding, 1998; Sun et al., 2012) (Figure 7.10). This points to a connection between conditions in the North Atlantic and loess deposition, which was first proposed by Porter and An (1995) and discussed further by Porter and Zhou (2006). A possible explanation is provided by GCM simulations in which the North Atlantic was flooded with freshwater, which affects the state of the Atlantic Meridional Circulation (AMOC). This in turn influences the global atmospheric circulation, thereby linking climatic conditions in both Greenland and East Asia (Sun et al., 2012).

There have been surprisingly few attempts to quantify paleoclimatic conditions associated with loess deposits and paleosols. At the simplest level, modern analogs of similar soils and loess accumulation areas provide an approximation to climatic conditions prevalent at different times in the past. Thus, Liu et al. (1985) estimated that mean annual precipitation and temperature during the formation of paleosol S5 were 350 mm and 4 °C higher than today, respectively. Similarly, Ding et al. (1992) suggested that the oldest thick loess units (L33 and L32) represent mean annual temperatures 12 °C lower than today and precipitation levels less than 25% of modern values, based on the modern climate of locations thought to be

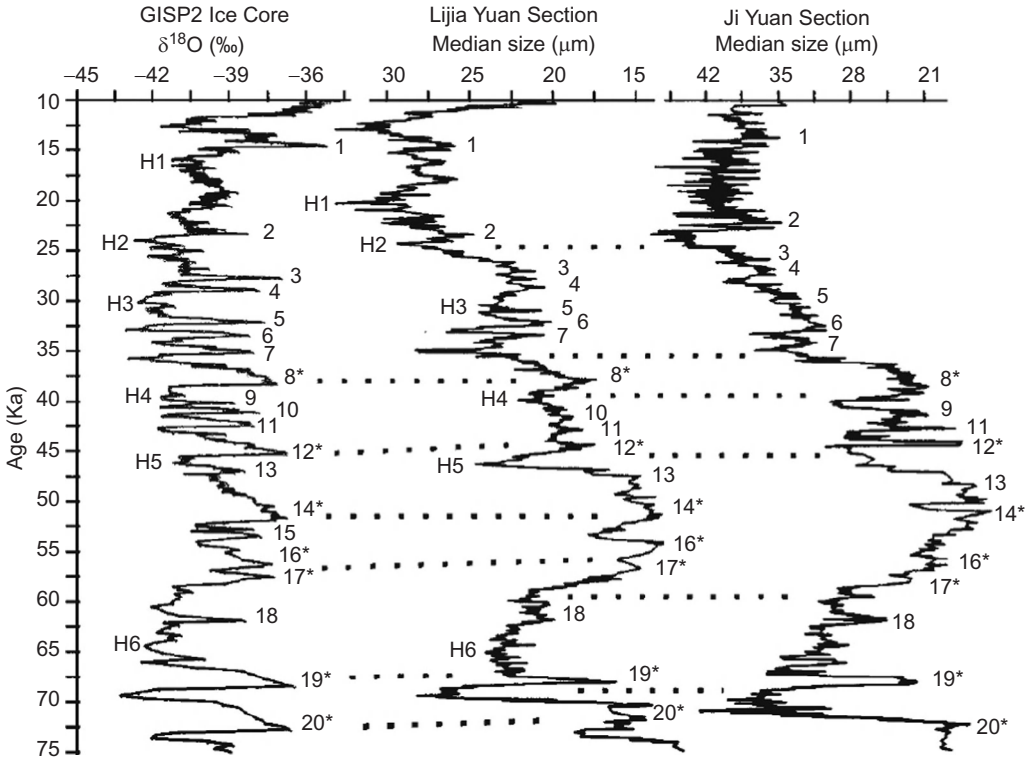


FIGURE 7.10 Correlation of the isotopic record from Greenland (GISP2) and median grain size in two locations on the Loess Plateau. Dansgaard-Oeschger cycles are numbered from 1 to 20, and correlative features in the grain size records are indicated. The interstadials marked with an asterisk are also identified in Antarctica (Bender et al., 1994). The placement of the Heinrich events (H1 to H6) is according to Bond et al. (1993). *From Liu and Ding (1998).*

analogous to conditions prevailing when the loess accumulated. Rousseau and Wu (1997, 1999) examined assemblages of snails from the last two glacial-interglacial cycles, documenting changes in the frequency of hygrophilous, xerophilous, and "oriental" fauna, the latter representing snails that are only found today in quite humid environments of southeastern China. This provided qualitative estimates of the relative changes in temperature and moisture conditions, based on modern climatic conditions associated with the distribution of snails today (though dissolution of snails during the warmest and most humid intervals led to only a limited perspective on those time periods). Wu, N.Q et al. (2007) examined snail assemblages from loess unit L5 and paleosol S4 (equivalent to MIS 12 and 11, respectively, ~480-360 ka BP). Although the benthic isotope record indicates that MIS 12 had the greatest volume of continental ice in the entire Quaternary, snail assemblages from the Loess Plateau suggest that conditions there were not especially cold, with mean annual temperatures (MAT) only 1-3 °C lower than modern conditions. Furthermore, based on the presence of hygrophilous species, it appears that the summer monsoon extended into the region from ~450 to 442 ka BP, in the middle of MIS 12. During the early part of MIS 11 (S4), climatic conditions in the northern and western Loess Plateau were similar to modern conditions in more humid regions to the southwest, with a MAT of 11-14 °C and annual precipitation as much as 30% higher, until cooler, and drier conditions prevailed after ~385 ka BP.

Maher et al. (1994) and Maher and Thompson (1995) focused on magnetic susceptibility (χ) as a proxy of rainfall. They argued that susceptibility is higher in soils due to the *in situ* formation of ultrafine (<0.02 μm) ferromagnetic (maghemite) grains by inorganic precipitation, aided by the presence of magnetotactic (iron-reducing) bacteria (cf. Maher and Thompson, 1992; Heller et al., 1993; Verosub et al., 1993; Liu et al., 1994). Alternations of wetting and drying cycles favor this process so that susceptibility profiles can be considered a proxy for past rainfall variations. They established the relationship between modern rainfall amounts and susceptibility measurements based on recent soils in different regions of the Chinese Loess Plateau but were able to confirm that a very similar relationship applies on the Russian steppes (Maher et al., 2003). Balsam et al. (2011) examined whether the link between χ and rainfall amount has a more universal application, by examining soils from Africa and from other parts of China. They concluded that below ~200 mm year^{-1}, there is simply no relationship between χ and rainfall amount, because pedogenic processes are essentially absent. Furthermore, χ may actually decline with rainfall amounts above ~1200 mm year^{-1} because of the saturation of the soils and the formation of gleys, which may decrease the rate at which ferromagnetic material is produced or even replace magnetic iron with nonmagnetic forms (Bloemendal and Liu, 2005). Although magnetic susceptibility appears to be a useful paleoprecipitation proxy, and it has been widely measured in loess, there may be other magnetic properties or measurements of specific minerals (such as goethite and hematite) that could help to further refine estimates of past rainfall amounts (cf. Balsam et al., 2004, 2011; Ji et al., 2004).

Figure 7.11 shows a reconstruction of rainfall at Xifeng for the past 1.1 Ma, based on magnetic susceptibility measurements (Maher and Thompson, 1995). Rainfall varied by a factor of ~2 over this interval (from ~400 to ~750 mm), but for 80% of the last 1.1 Ma, rainfall has been less than today. Liu et al. (1995) took a similar approach in reconstructing rainfall at Xifeng but only for the last glacial-interglacial cycle. They concluded that rainfall fell to much lower levels in glacial times (<200 mm a^{-1}) than estimated by Maher and Thompson (1995). A similar conclusion was reached by Zhou et al. (2007) who related the amount of the

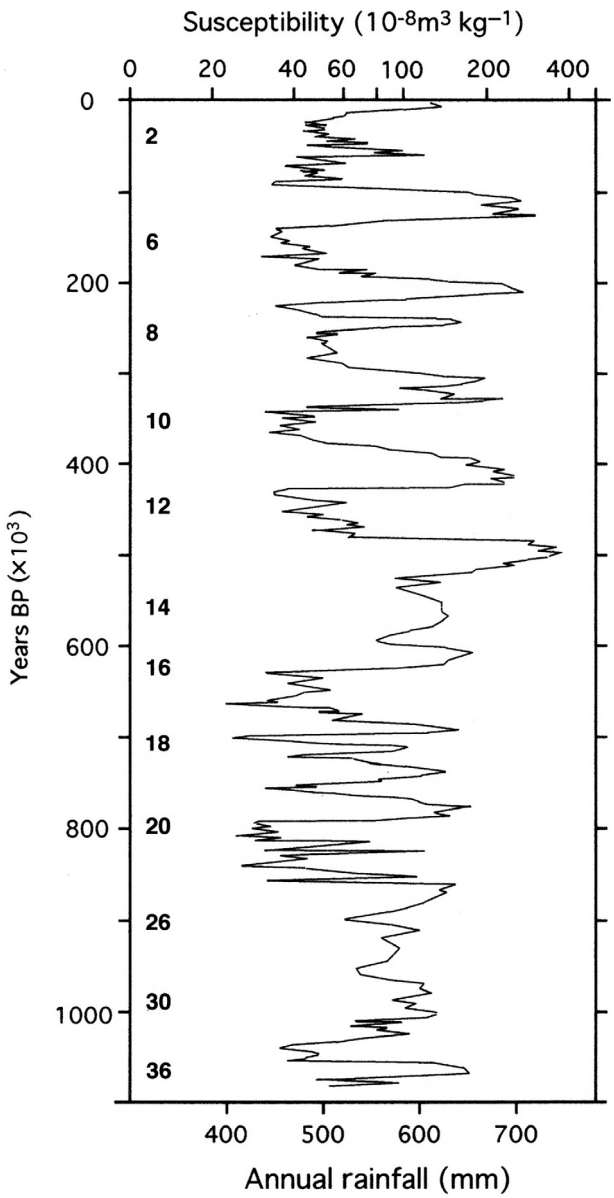


FIGURE 7.11 The record of magnetic susceptibility at Xifeng, Loess Plateau, north-central China, interpreted in terms of variations in annual rainfall. As rainfall increases, the amount of magnetic material produced by weathering processes increases, leading to higher susceptibility levels. Marine Isotope Stage numbers are indicated on the left. *From Maher and Thompson (1995).*

cosmogenic isotope ^{10}Be in loess to rainfall, based on the argument that most of the ^{10}Be results from wet deposition (precipitation scavenging in the atmosphere). By deconvolving the record to remove geomagnetic field effects, a paleoprecipitation record was extracted. They concluded that annual rainfall at Luochuan was ~200 mm year^{-1} at the height of the LGM and during MIS 4 but increased to ~600 mm year^{-1} during MIS 3 and to 800 mm year^{-1} for a brief period in the Early Holocene.

CHAPTER

8

Speleothems

OUTLINE

8.1 Isotopic Variations in Speleothems 295
8.2 Tropical and Subtropical Paleoclimate Variability from Speleothems 296
8.3 Speleothems and Glacial Terminations 299
8.4 Millennial to Centennial Scale Changes 302
8.5 Late Glacial and Holocene Records 304
8.6 Stalagmite Records of the Last Two Millennia 310
8.7 Paleoclimatic Information from Periods of Speleothem Growth 311
8.8 Speleothems as Indicators of Sea-Level Variations 315

Speleothems are mineral formations occurring in limestone caves, most commonly as stalagmites and stalactites or slablike deposits known as flowstones. Stalactites (which hang from the ceilings of caves) often have a hollow core, with growth occurring around this central orifice, whereas stalagmites are solid and grow incrementally at the drip site. Thus, stalagmites are generally selected for paleoclimatic analysis. The extensive distribution of karst landscapes (Figure 8.1) means that studies can be undertaken on a worldwide basis. Speleothems are primarily composed of calcium carbonate, precipitated from groundwater that has percolated through the adjacent carbonate host rock. Certain trace elements may also be present (often giving the deposit a characteristic color), and one of these, uranium, can be used to determine the age of a speleothem, as discussed in the text below. Seasonal variations in the trace element composition of dripwaters may also be used to identify annual layers (Treble et al., 2005a). Deposition of a speleothems results from evaporation of water or degassing of carbon dioxide from water droplets. Evaporation is normally only an important process near cave entrances; most speleothems from deep within caves therefore result from the

Copyright © 2015 Raymond S. Bradley.
Published by Elsevier Inc. All rights reserved.

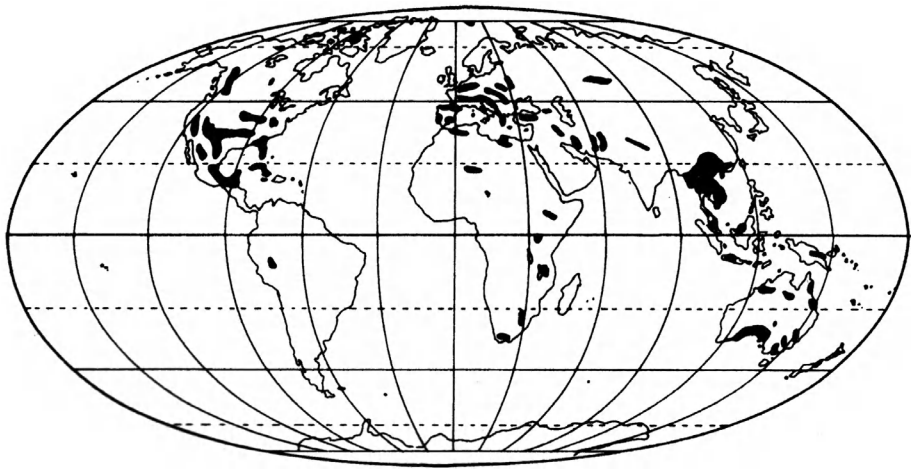


FIGURE 8.1 Distribution of karst in the world, showing the potential sources of paleoclimatic information from speleothems.

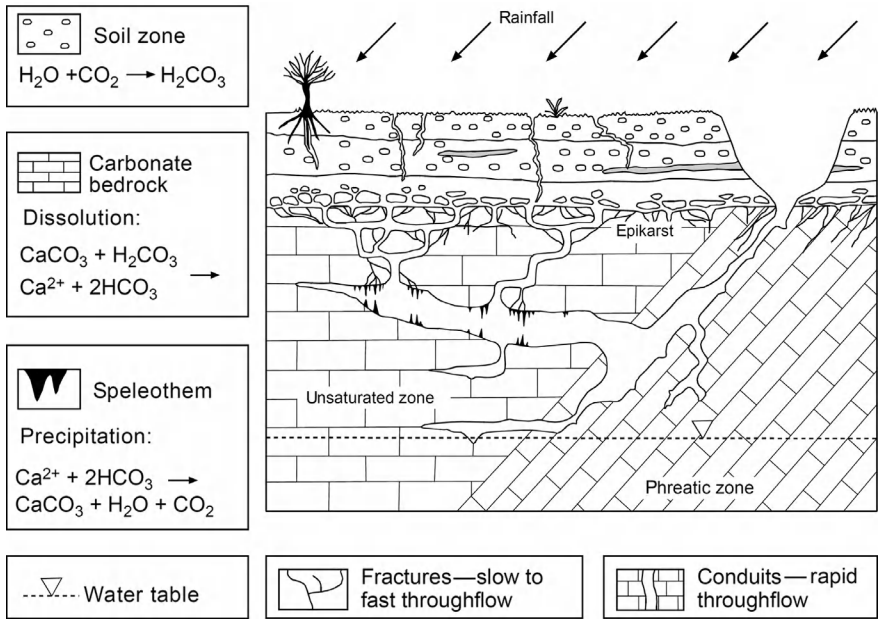


FIGURE 8.2 Schematic diagram of a cave system and carbonate dissolution and deposition (Fairchild et al., 2006).

degassing process. Water that has percolated through soil and been in contact with decaying organic matter usually accrues a partial pressure of carbon dioxide exceeding that of the cave atmosphere. Thus, when water enters the cave, degassing of carbon dioxide occurs, causing the water to become supersaturated with calcite, which is thus precipitated (Figure 8.2) (McDermott, 2004; McDermott et al., 2006; Fairchild and Baker, 2012).

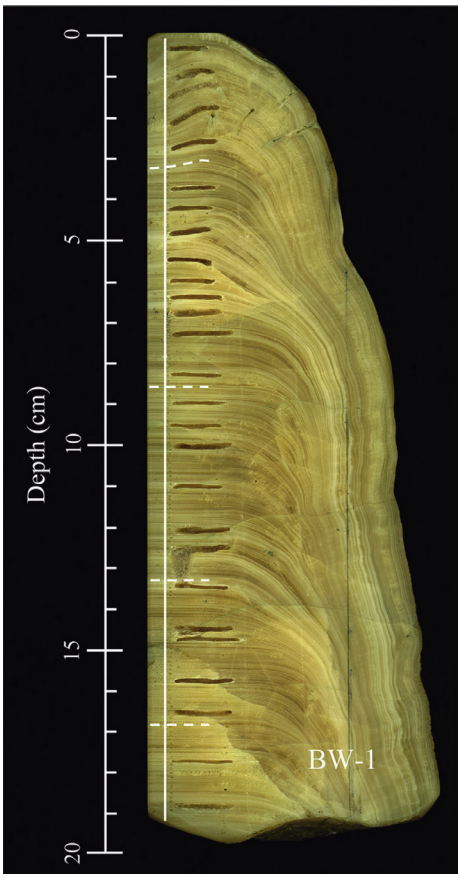


FIGURE 8.3 A polished section of a stalagmite from Kulishu Cave, near Beijing (39.6°N, 115.6°E, 610 m asl). Holes can be seen where samples were drilled for ^{230}Th dating. The white vertical line shows the track of subsamples for stable isotope analysis, and dashed lines indicate the positions of samples for Hendy test. *From Ma et al. (2012).*

There has been explosive growth in the number of paleoclimatic studies using speleothems, especially high-resolution studies of stalagmites (Figure 8.3). This has been facilitated by the development of thermal ionization mass spectrometers (TIMS) and multicollector inductively coupled plasma mass spectrometers (MC-ICP-MS) that can provide high-precision uranium-series dates (Edwards et al., 1987a; Shen et al., 2002, 2012; Richards and Dorale, 2003; Eggins et al., 2005; Cheng et al., 2012a) and improved techniques for high-resolution sampling and analysis using laser ablation mass spectrometry, ion microprobes, and micro X-ray fluorescence scanners (e.g., Baldini et al., 2002; Kolodny et al., 2003; Frisia et al., 2005; Orland et al., 2009). Hence, stalagmites can provide insight into episodes of rapid environmental change; dating of these periods can be more precise than ^{14}C dating and times of abrupt change well beyond the range of radiocarbon can be examined. However, for paleoclimatic applications, the resolution of such studies is constrained by the residence time of water in the aquifers, which link surface climatic conditions to subsurface speleothem growth. This effectively acts as a low-pass filter on the environmental record in speleothems, but generally flow rates are high enough

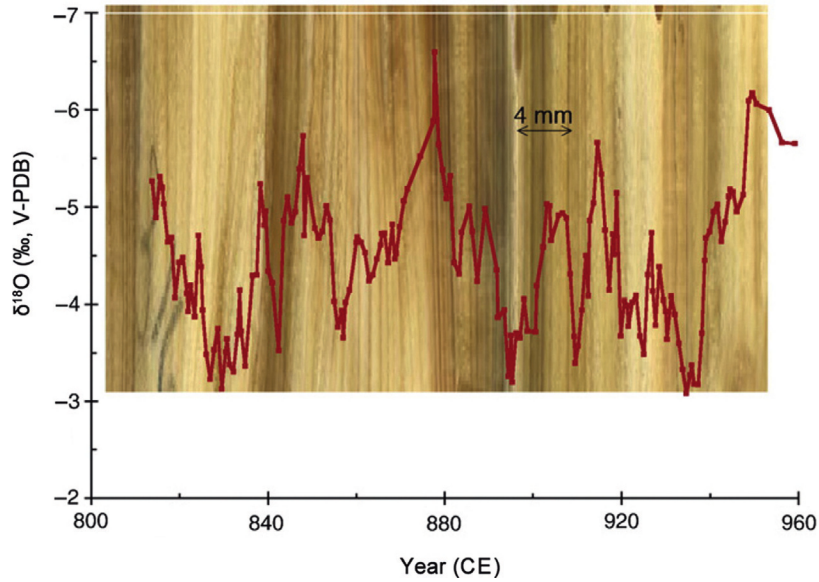


FIGURE 8.4 A cross section through the growth axis of a stalagmite from Chaac Cave, Yucatan peninsula, Mexico (21°N, 89°W), showing distinct laminations during the Mayan Terminal Classic Period. The nearest measured ^{230}Th dates to the sample interval shown in this figure occur at CE 1004 and 780; this gives an age range for the sample of 918-820 (98 years). A total of 85 ± 10 laminations were counted in this section, strongly suggesting that these laminations are annual. The error in lamination counts stems from the different number of laminations in the center of growth compared to the periphery along the same depth interval; often, a single layer observed in the center of growth appears as several bands away from the center. Superimposed on the stalagmite cross section (in red) is the δ^{18}O record showing a series of droughts (higher isotopic values) that had severe impacts on the regional population. *From Medina-Elizalde et al. (2010).*

that annual (or even subannual) variations may be resolved in some situations (Figure 8.4) (cf. Shopov et al., 1994; Baldini et al., 2002).

Speleothems are most commonly dated by uranium-series disequilibrium methods (generally ^{230}Th/^{234}U) described in Chapter 3, Section 3.2.3. Isotopes of uranium leached from the carbonate bedrock are coprecipitated as uranyl carbonate with the calcite of the speleothems. Normally, the precipitating solution contains no ^{230}Th because thorium ions either are adsorbed onto clay minerals or remain in place as insoluble hydrolysates. Thus, providing the speleothem contains no clay or other insoluble materials, which are carriers of detrital thorium, the activity ratio of ^{234}U to its decay product ^{230}Th will give the sample age (Richards and Dorale, 2003). The method is useful over the time range ~500,000-100 years BP. A number of precautions are taken to ensure a reliable age estimate, most notably that any samples containing more than 1% of acid-insoluble detritus are likely to be rejected. Also, any indication that recrystallization has occurred (suggesting that the sample may not have remained a closed system) would raise concerns. The latest analytic techniques for U-series dating require very small samples (<100 mg of calcite) and generally yield dates with a 1σ precision of <1% and in some cases as low as 0.1% (Shen et al., 2012).

8.1 ISOTOPIC VARIATIONS IN SPELEOTHEMS

Stable isotopes of oxygen and carbon provide the main basis for reconstructing the temperature or precipitation history of a site from speleothems. When air and water movement in a cave is relatively slow, a thermal equilibrium is established between the bedrock temperature and that of the air in the cave, approximating the mean annual surface temperature. During deposition of calcite from seepage (drip) water, as CO_2 is lost, fractionation of oxygen isotopes occurs at a rate that is dependent on the temperature of deposition ($-0.24‰\,^{\circ}C^{-1}$; O'Neil et al., 1969). Thus, in theory, oxygen isotopic variations in the speleothem calcite ($\delta^{18}O_c$) should provide a proxy of temperature variations through time. However, a number of other factors must also be considered (Mickler et al., 2004). First, isotopic paleotemperatures are recorded only if the calcite (or aragonite) is deposited in isotopic equilibrium with the dripwater solution. This can be assessed by determining if $\delta^{18}O_c$ is constant along a growth layer; if values vary for the same depositional interval, it indicates that deposition was affected by evaporation, not just the slow degassing of CO_2, and this would alter the simple temperature-dependent fractionation relationship. Another test of isotopic equilibrium that is commonly invoked is the so-called Hendy test. This involves comparing variations in carbon and oxygen isotopes along individual growth layers (Hendy, 1971). If a nonequilibrium situation existed, the isotopic composition would be controlled by kinetic factors and the same fluctuations would be found for both carbon and oxygen isotopes. If no correlation between these two isotopes is found, it can be assumed that the carbonate speleothem was deposited in equilibrium.

A few other factors also have to be considered in reconstructing paleotemperature from $\delta^{18}O_c$. Although the fractionation factor between calcite and water decreases with an increase in cave temperature (causing a *decrease* in $\delta^{18}O_c$ values), changes in air temperature at the surface are almost certainly accompanied by changes in the isotopic composition of precipitation, such that (in midlatitudes, at least) the $\delta^{18}O$ value of dripwater tends to *increase* with higher temperatures (see Chapter 5, Section 5.2.3). The relative importance of these opposing effects must therefore be evaluated. Also, during glacial periods, the growth of ^{18}O-depleted continental ice sheets led to an increase in $\delta^{18}O$ of oceanic water (of up to 1‰) and hence also of precipitation. Thus, for a given climatic shift, several (often opposing) factors come into play, and in some locations, it may be difficult to assess *a priori* in which direction the $\delta^{18}O_c$ might have changed (Thompson et al., 1976; Harmon et al., 1978a). Ideally, when sample resolution is comparable to that of instrumental or historical data, a direct comparison can be made during the period when records overlap. Thus, Mangini et al. (2005) used regional temperature reconstructions (from Luterbacher et al., 2004) to calibrate variations in $\delta^{18}O$ in a stalagmite from Spannagel Cave in the central Alps of Austria. They then used this regression to derive temperatures at the cave over the last 2000 years, at near-annual resolution. Similarly, Burns et al. (2002) were able to show that there was strong relationship between regional rainfall and $\delta^{18}O$ in Oman stalagmites during the twentieth century, thereby quantifying their interpretation of the longer stalagmite record in terms of rainfall variations. Direct monitoring of dripwater is also extremely useful, in order to understand the environmental factors that are important in the most recent period of deposition (e.g., Genty et al., 2001; McDonald and Drysdale, 2004; Cruz et al., 2005a; Treble et al., 2005b; Mattey et al., 2008).

In some speleothems, dripwater, trapped as tiny liquid inclusions as the speleothem grew, has been isolated to provide a more direct measure of the changing isotopic composition of rainwater (e.g., van Breukelen et al., 2008) or to extract noble gases for direct paleotemperature estimation (e.g., Kluge et al., 2008). These inclusions vary in abundance and when present in large amounts (>1% by weight) give speleothems a milky appearance (Thompson et al., 1976; Harmon et al., 1979). Because it is possible that the inclusion water may have continued to exchange oxygen isotopes with the surrounding calcite following its entrapment, it is preferable to measure the deuterium-hydrogen (D/H) ratio, since there is no hydrogen in the calcite with which hydrogen in the water might have exchanged. The relationship between δD and $\delta^{18}O$ in dripwater should approximate the Meteoric Water Line (MWL), first noted in precipitation by Craig (1961c):

$$\delta D = 8\delta^{18}O + 10$$

and

$$d = \delta D - 8\delta^{18}O$$

where d is the *deuterium excess* parameter (see Section 5.2.5). Providing this relationship (or perhaps a similar relationship, with a different d-value) has remained constant over time, the former $\delta^{18}O$ values of rainfall over very long periods of time can be estimated. Using this approach to account for the amount of rainfall-related isotopic change, McGarry et al. (2004) were then able to constrain the probable range of temperatures experienced at Soreq Cave, Israel, since the last interglacial. According to this analysis, temperatures fell from around 20 °C during marine isotope stage 5e to ~10 °C at the Last Glacial Maximum (LGM). In contrast, Fleitmann et al. (2003a) ruled out temperature changes as an explanation for the presence of much lighter hydrogen isotopes in fluid inclusions and much lighter $\delta^{18}O_c$ of the associated calcite in stalagmites from northern Oman, during the LGM and earlier glacial episodes. They argued that the changes reflect stronger monsoon rainfall in the region at those times, which brought more isotopically depleted water into the cave systems. In fact, throughout the Tropics, temperature changes on glacial-interglacial timescales have been relatively small (2-4 °C), equivalent to less than 1‰ in $\delta^{18}O_c$, and so the oxygen isotope signal in tropical speleothems is predominantly that of rainfall variations. This has proven to be a powerful tool for understanding past climatic conditions, particularly changes in monsoon circulation regimes, revealing important details about how climate changes in the Tropics and at high latitudes are dynamically linked, on both long and short timescales.

8.2 TROPICAL AND SUBTROPICAL PALEOCLIMATE VARIABILITY FROM SPELEOTHEMS

Speleothems from China have provided remarkable insights into monsoon climate variability over the last half a million years (Wang et al., 2008; Cheng et al., 2012b). As an example, Figure 8.5 shows $\delta^{18}O$ variations spanning the last 224 ka in a set of stalagmites from northeastern and central China, within an area dominated by the East Asian monsoon regime. These records are synchronous with Northern Hemisphere July insolation at 65°N, which

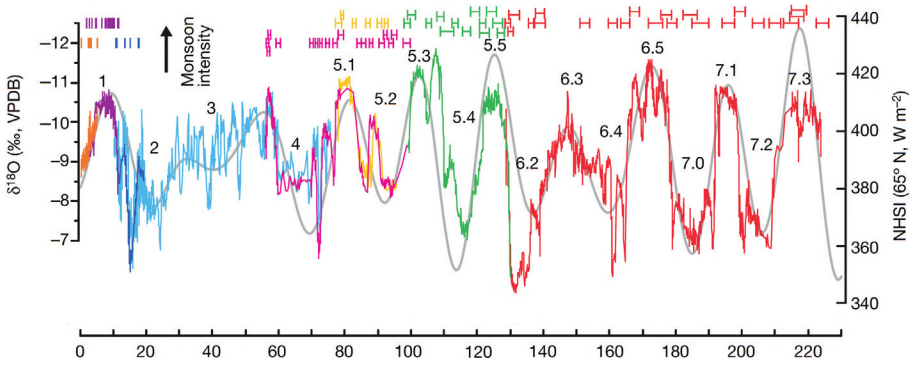


FIGURE 8.5 Oxygen isotope records from stalagmites in Hulu Cave, northeastern China (26°N, 105°E) (light blue), and various stalagmites from Sanbao Cave, central China (32°N, 110°E) (other colors). Note that isotopic values are plotted inversely, such that monsoon intensity (indicating the % of summer rainfall in the annual rainfall total) increases upward. Northern Hemisphere summer insolation (July 21) at 65°N is shown in gray. The Hulu $\delta^{18}O$ record is plotted 1.6% more negative to account for the higher values at Hulu Cave compared to Sanbao Cave. The ^{230}Th ages and errors (2σ error bars at top) are color-coded by stalagmites. Numbers indicate marine isotope stages and substages. *From Wang et al. (2008).*

is dominated by the 23 ka precessional cycle. Remarkably, stalagmites from the far western edge of China (on the border with Kazakhstan, 42°N, 81°E) also indicate that during times of insolation maxima, isotopically light summer monsoon rainfall even reached that region, well beyond the limits of monsoon airflow today (Cheng et al., 2012c). The strong precessional signal is thought to be due to direct orbital effects on the strength and duration of the Indian and South Asian monsoon systems, which advect moisture northward. Isotopic fractionation in convective clouds, which develop as air masses move inland from the tropical Indian and Pacific Ocean, leads to strong isotopic depletion of water vapor advected into the continental interior during times of insolation maxima (Lewis et al., 2010; Pausata et al., 2011). Part of the signal may also result from changes in the proportion water vapor derived from East Asian versus Indian monsoon systems, as the former is isotopically heavier (Maher, 2008). In addition, there is likely to have been a local "amount effect" in the isotopically depleted monsoon rainfall, though this relationship may not be fully linear with summer rainfall amount. There may be a threshold beyond which higher amounts of rainfall do not lead to isotopically lighter values (and perhaps vice versa) (Cheng et al., 2012b). One or more of these factors could explain why the orbital insolation maxima at MIS 5.5 and 7.3 are not matched by comparably lower isotopic values (Figure 8.5). Nevertheless, the abrupt changes in isotopic values (both increasing and decreasing) indicate a direct response of Asian monsoon rainfall to precessional (~23 ka) orbital forcing, with no significant lag overall (<1 ka). Unlike many other paleoclimatic records, including those from the Chinese Loess Plateau, the isotopic data from stalagmites show no strong 41 or 100 ka signal, suggesting that the fluctuations in summer monsoon rainfall across this region are not strongly influenced by ice volume changes on the northern continents.

Another remarkable isotopic record has been assembled from Soreq and Peqiin Caves (in central and northern Israel, respectively) using overlapping speleothems (Bar-Matthews and Ayalon, 1997, 2004; Bar-Matthews et al., 1999, 2000, 2003). Records from both sites

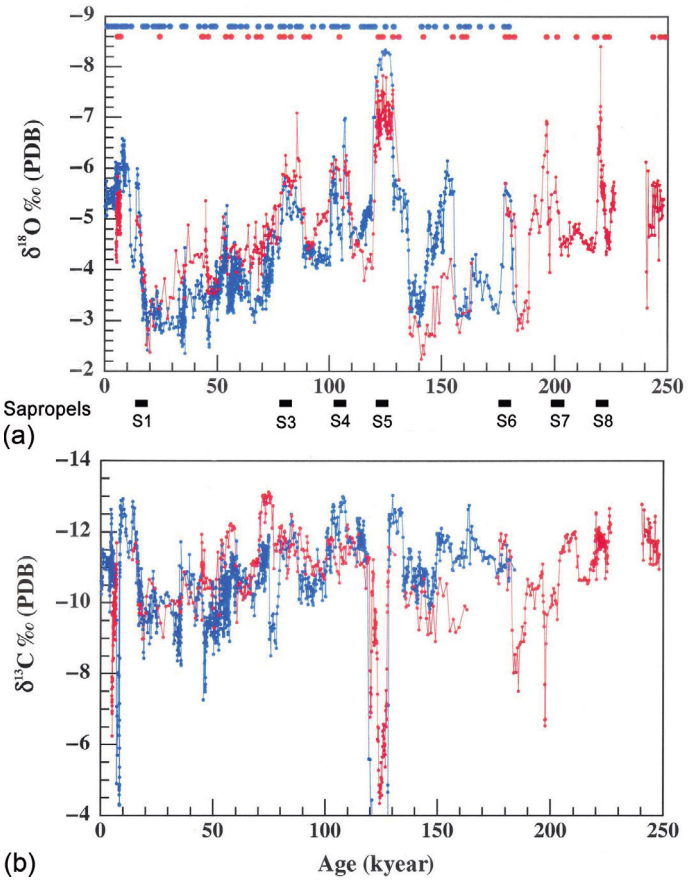


FIGURE 8.6 Composite record of oxygen and carbon isotopes from more than 20 overlapping stalagmites and stalactites from Peqiin Cave, northern Israel (red), and Soreq Cave, central Israel (blue). TIMS dates are shown by bars at top of upper diagram. Overlapping records show strong similarities and so sections with the highest-resolution analyses are used to form the composite series. Low values of $\delta^{18}O$ reflect wet conditions, but the wettest episodes are shown by exceptionally high $\delta^{13}C$ values (during the Early Holocene and in the last interglacial period). Times of sapropel formation in the eastern Mediterranean are shown by bars (Bar-Matthews et al., 2003).

are well correlated, providing a composite record that spans the last 250 ka (Figure 8.6). In this region, modern observations show that the $\delta^{18}O$ of rainfall is inversely related to rainfall amount (−1‰ per 200 mm rain) so the long record shows that glacial periods were very dry in this region (<50% of modern rainfall amounts, in MIS 2 and 6), whereas interglacials were wet. $\delta^{18}O$ was lowest around 220, 195, 128-120, and 110-100 ka BP (Figure 8.6). $\delta^{13}C$ values reflect the prevailing C3-type vegetation of the region (see Appendix A) and generally parallel $\delta^{18}O$ variations, except for two episodes when $\delta^{13}C$ was extremely high, around 128-120 and 8.5-7 ka BP. These periods were the wettest of the entire record, with the heavy rainfall passing too quickly through the overlying soils to equilibrate with the soil-derived CO_2, so the isotopic composition of the percolating waters reflects that of the atmosphere (0-2‰) rather than the isotopically lighter vegetation (Bar-Matthews et al., 1997). The exceptional nature of these periods is confirmed by geomorphological evidence of water pools within the (now dry) caves, which date from 128 to 115 ka BP (Bar-Matthews et al., 2003). Rainfall is estimated to have been double present-day amounts during these wet periods, leading to correlative highstands of Lake Lisan (the enlarged precursor of today's Dead Sea) (Bar-Matthews et al., 1997; Frumkin, 1997). In addition, there is a strong

correlation between the timing of major anoxic events in the eastern Mediterranean Sea and periods of heavier rainfall in Israel. Periods of anoxia (lack of oxygen at depth) in the eastern Mediterranean have occurred several times in the last 250 ka, approximately in phase with minima in the precessional cycle (Bar-Matthews et al., 2000). At these times, sapropels—black, organic-rich sediments—were widely deposited across the eastern Mediterranean Sea (Kallel et al., 2000, 2004). Speleothems from Soreq and Peqiin Caves clearly show that each sapropel was deposited when conditions were wetter (Figure 8.6). Heavier rainfall would have resulted in increased runoff (with increased nutrient flux and perhaps higher biological productivity) and a low salinity surface water layer across the Mediterranean Sea, reducing convection and thus ventilation of deepwater, eventually leading to anoxic conditions. TIMS dating of high $\delta^{18}O$ episodes in speleothems provides a precise chronology of these wetter episodes, during which a critical threshold of surface water salinity must have been reached, followed by deposition of the sapropels (Bar-Matthews et al., 2000). The speleothems thus provide a limiting (maximum) duration for sapropel formation (Bar-Matthews et al., 2003). Similar studies of a stalagmite from western Italy confirm that, at least at the time of sapropel 6 (~175 ka BP), wetter conditions were more widespread across the Mediterranean Basin (Bard et al., 2002a).

8.3 SPELEOTHEMS AND GLACIAL TERMINATIONS

Terminations were originally defined by Broecker and van Donk (1970) as abrupt changes in the isotopic composition of benthic forams, indicating major declines in continental ice volume at the transition from glacial to interglacial climates. Stalagmite isotopic data provide a new perspective on these intervals. Chinese stalagmites show that the Asian monsoon abruptly strengthened in each of the last four terminations (Figure 8.7). For example, in Termination II, the shift from isotopically enriched values typical of a weak monsoon regime to lighter values characteristic of strong monsoon interglacial conditions occurred within ~70 years, at 129 ± 0.8 ka BP (Yuan et al., 2004; Zhang et al., 2004; Cheng et al., 2006, 2009; Kelly et al., 2006). This is very similar to the $\delta^{18}O$ and $\delta^{13}C$ records from stalagmites in Soreq and Peqiin Caves, Israel, where the shift to wetter interglacial conditions was also extremely rapid, centered on ~130 ka BP (Bar-Matthews et al., 2003). All of these records reveal changes that were delayed with respect to insolation forcing; more than half of the glacial-interglacial increase in July insolation at 65°N had already occurred before there was a response seen in the stalagmite data. However, isotopic changes were then far more rapid than the changes in insolation, pointing to a nonlinear response to insolation forcing, perhaps indicating that there was an abrupt reorganization of global atmospheric circulation when the size of continental ice sheets, and/or sea-ice extent, fell below a critical threshold. Uplifted corals in Barbados show that sea level was only 18 ± 3 m below present at 135.8 ± 0.8 ka BP, indicating that most continental ice sheets must have melted by that time (Gallup et al., 2002). Certainly, the glacial to interglacial increase in Antarctic temperatures, most of the rise in CO_2, and much of the rise in CH_4, had already occurred before the isotopic terminations were recorded in caves across the Tropics.

The longest isotopic speleothem record currently available in the United States is from Devil's Hole, Nevada, where a calcite vein precipitated from groundwater supersaturated

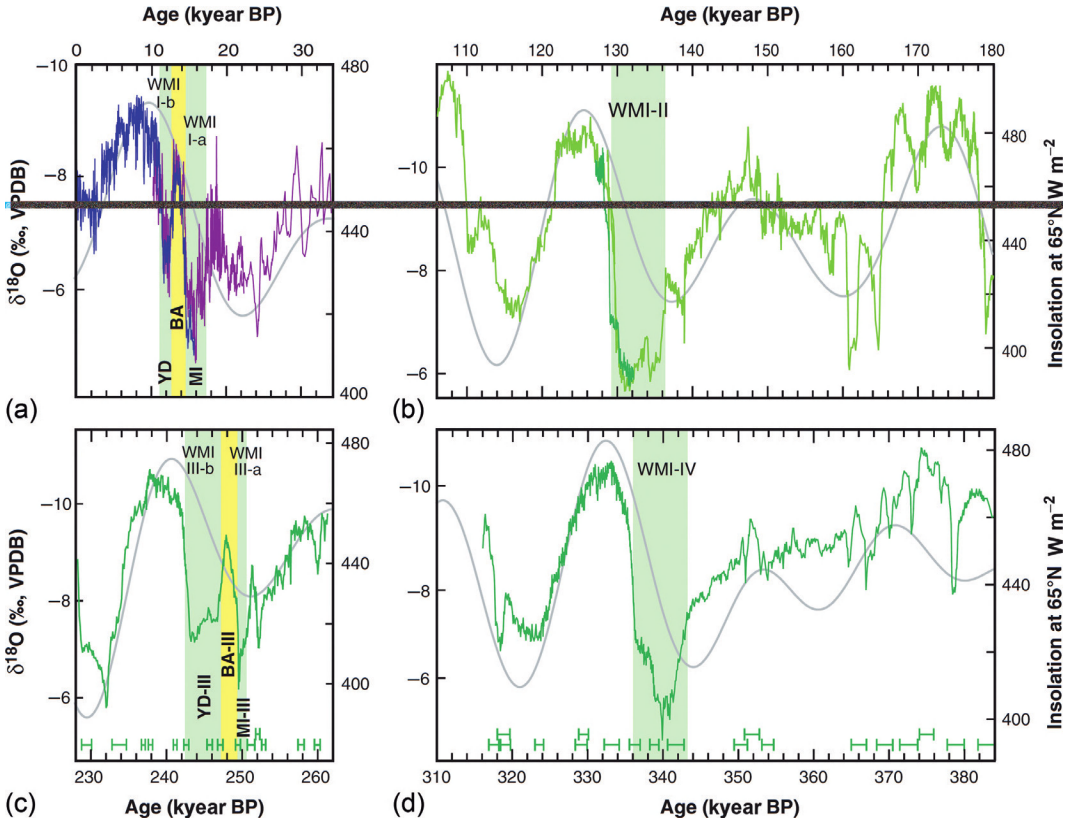


FIGURE 8.7 $\delta^{18}O$ in speleothems from (a) Hulu and Dongge Caves (northeastern and southern China) and (b-d) Sanbao Cave on the southern edge of the China Loess Plateau, and July 21 insolation at 65°N (gray line) for the last four terminations. Lower symbols show ^{230}Th dates with associated 2σ error bars. WMI indicates "weak monsoon interval." The transitions to wetter interglacial conditions are all abrupt but delayed from the rise in insolation. *From Cheng et al. (2009).*

in calcite spans almost 0.5 Ma (60 to ~560 ka BP) (Ludwig et al., 1992). In this system, $\delta^{18}O$ in calcite is considered to reflect changes in the isotopic composition of precipitation feeding the groundwater, so that higher values reflect warmer conditions (Winograd et al., 1988, 1992; see also Johnson and Wright, 1989). The record shows very similar variations to the SPECMAP marine isotope record (Figure 8.8) as well as to δD in the Vostok ice core, suggesting that the signal recorded is of more than regional significance. However, the Devil's Hole record generated considerable controversy because the timing of the transition from the penultimate glaciation to the last interglacial occurred earlier at Devil's Hole than in the marine isotope record (~150 vs. 135 ka BP) and the interglacial maximum was reached by ~135 ka BP at Devil's Hole, compared to the SPECMAP isotopic minima at ~124 ka BP. The Devil's Hole calcite is well dated (with many high-precision dates derived by TIMS), whereas the SPECMAP record was tuned to orbital frequencies, assuming orbital forcing was the dominant control

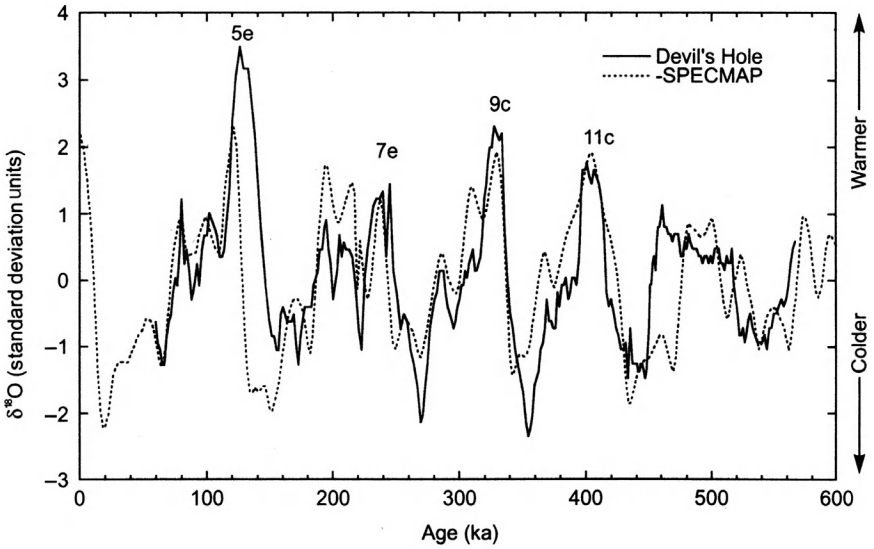


FIGURE 8.8 The $\delta^{18}O_c$ record in a calcite vein from Devil's Hole, Nevada, compared to the SPECMAP marine isotope record. Selected marine isotope substages are numbered. Values are expressed as departures from the overall mean of each series, in standard deviation units (computed over the full record). The value of zero thus represents the mean for each record. Note that the sign of the SPECMAP time series has been reversed so that interglaciations appear as peaks (Winograd et al., 1997).

on continental ice volume changes.[1] Furthermore, the Devil's Hole calcite was only deposited after precipitation had been transferred through the groundwater system, which must have taken at least several thousand years (and by some estimates >10 ka), making the discrepancy between the two records even larger (though clearly there was a lag between ice sheet demise and changes in the isotopic composition of the ocean, which is what the benthic forams record). Winograd et al. (1992) argue that the warming, which led to the last interglacial maximum (stage 5e in the marine isotope record), actually began around 150 ka BP. The critical implication of this argument is that sea level started to rise when orbitally driven Northern Hemisphere insolation anomalies were low (perhaps even when they were declining) so that the conventional view of *Northern Hemisphere* solar insolation forcing this deglaciation (at least) would not be tenable. This assault on the Milankovitch hypothesis launched numerous counterarguments, none of which have entirely settled the matter (Johnson and Wright, 1989 and reply by Winograd et al., 1988; Shackleton, 1993 and reply by Ludwig et al., 1992; Edwards and Gallup, 1993 and reply by Ludwig et al., 1992; Imbrie et al., 1993c and reply by Winograd and Landwehr, 1993). The solution may lie in the Southern Hemisphere where insolation was rising at 140 ka BP, suggesting that the onset of Northern Hemisphere

[1] However, the last interglacial isotopic minimum in marine sediments corresponds to the high sea-level stand, recorded by corals (uplifted by tectonic activity) in several locations around the world and consistently dated at ~125,000 ± 2500 years BP by U-series TIMS (cf. Gallup et al., 1994; Stirling et al., 1995). Direct U-series dating of marine sediments also confirms this time (123,500 ± 4500 years BP) as the last interglacial peak, when continental ice volume was at a minimum (Slowey et al., 1996).

deglaciation may have been triggered by events in the opposite hemisphere (cf. Weaver et al., 2003). Indeed, wetter (interglacial) conditions were already affecting northeastern Brazil (~10°S) by ~136.4 ± 1.2 ka BP (Wang et al., 2004).

Additional evidence in support of the early onset of warm conditions leading up to the last interglacial comes from a high elevation cave near Innsbruck, Austria. Modern temperature in the cave is only 1-2 °C above freezing and so past episodes of deposition were interrupted when temperatures were only slightly lower. Indeed, the cave was beneath glacial ice during the last glaciation. Several periods of calcite deposition occurred over the last 350 ka, but of particular interest is the onset of flowstone deposition at 135-137 ka BP (Spötl et al., 2002; Holzkamper et al., 2005). This clearly demonstrates that ice must have retreated from the site by ~137 ka BP and that temperatures had reached near modern levels, permitting water to percolate through the ground and into the cave. The timing of this ice recession corresponds to a minimum in Northern Hemisphere summer insolation and, like the Devil's Hole record, it is at odds with the SPECMAP age for Termination II (the midpoint of the transition from stages 6 to 5, boundary 6.0, is 128 ± 3 ka BP, according to Martinson et al., 1987; cf. Figure 6.15).

8.4 MILLENNIAL TO CENTENNIAL SCALE CHANGES

Highly resolved and well-dated speleothems from the Tropics show that climate has varied on millennial to centennial scales, with strong connections to conditions in extratropical regions. This is illustrated in Figure 8.9 that shows isotopic changes in a speleothem from Pacupahuain Cave in the central Andes of Peru (11.5°S). Abrupt changes in the stalagmite record are clearly associated with Dansgaard-Oeschger events recorded in the NGRIP ice core from Greenland (Kanner et al., 2012). Warm (isotopically heavy) events in Greenland are synchronous with isotopically enriched (relatively dry) events in the Andes, indicating a weak South American summer monsoon (SASM) at those times due to a northward shift of the Inter-Tropical Convergence Zone (ITCZ). In contrast, periods when the stalagmite calcite was relatively depleted in ^{18}O, indicating a strong SASM, correspond to Antarctic Isotope Maxima (AIM) events. At those times, the ITCZ was displaced to the south, bringing increased rainfall to the central Peruvian Andes. These relationships reflect the bipolar seesaw in which cold conditions in the North Atlantic are linked via the thermohaline circulation to warm conditions in the Southern Hemisphere, with a southward displacement of the ITCZ. This connection is also seen during Heinrich events, when large amounts of freshwater were discharged into the Atlantic, from proglacial lakes, calving icebergs, or thick Arctic sea ice (or all three). This led to significant disruption of the Atlantic Meridional Overturning Circulation (AMOC). Heinrich events are recorded in Pacupahuain Cave as relatively wet periods, again linked to a southward shift in the mean position of the ITCZ. A similar record was found in a cave from the Amazon Basin lowlands in eastern Ecuador (3°S, 78°W) where D-O events were relatively dry due to a weak SASM, whereas Heinrich events were wet (Mosblech et al., 2012). The effects of Heinrich events are also seen in stalagmites from southeastern Brazil, where they are associated with stronger monsoon rainfall resulting from increased outflow of (isotopically light) moisture from the Amazon Basin (Wang et al., 2006).

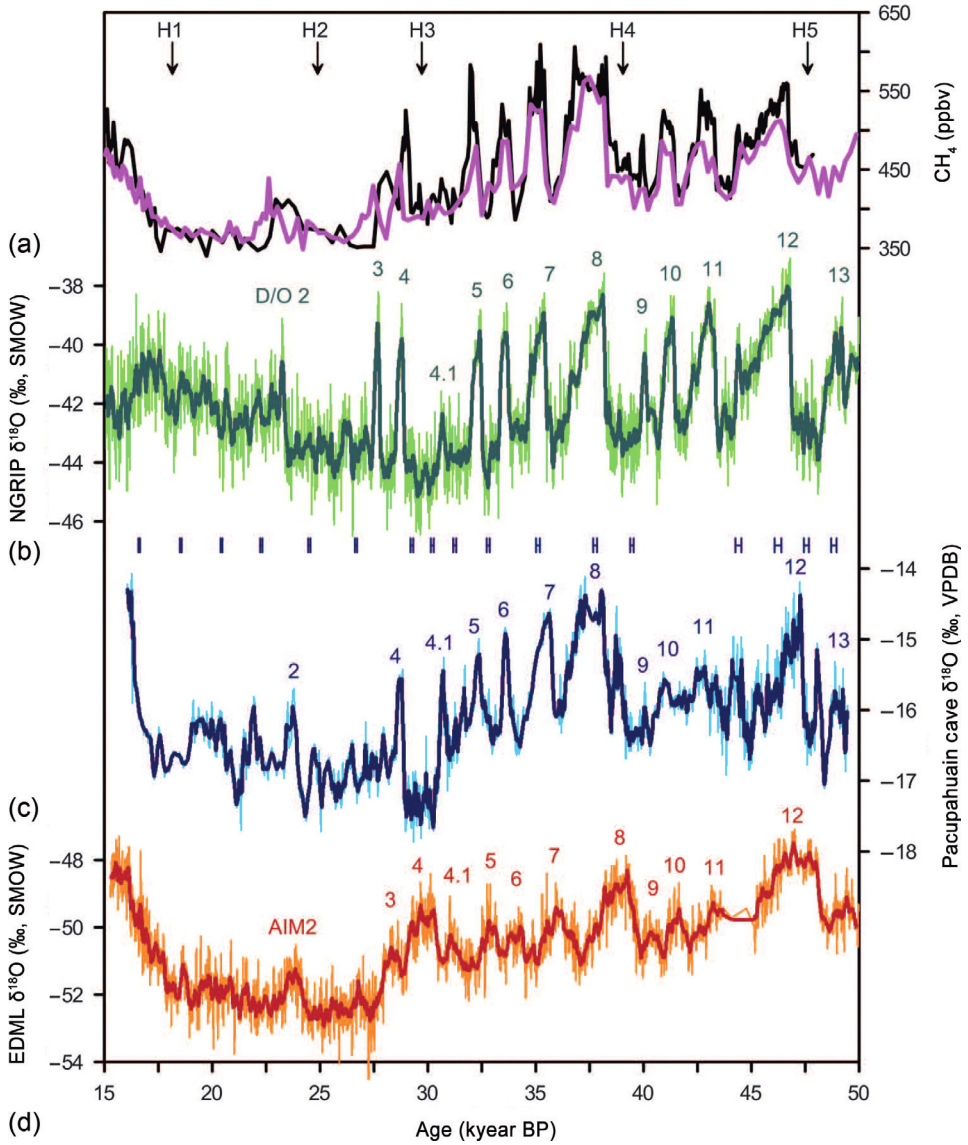


FIGURE 8.9 Oxygen isotope variations in a stalagmite from Pacupahuain Cave, central Peruvian Andes (11.5°S, 76°W) (blue line), together with $\delta^{18}O$ data from NGRIP (Greenland) and EDML (Antarctica) ice cores (green and red lines, respectively) and CH_4 data from GRIP and NGRIP. Age controls on the cave record are indicated above that record. Dansgaard-Oeschger (D-O) events are numbered, as are Heinrich events 1-5. Antarctic Isotope Maxima (AIM) events 2-12 are also shown. The more enriched (less negative) values at Pacupahuain indicate a weaker South American summer monsoon (SASM), and these correspond to warm D-O events in Greenland. CH_4 values at those times are high, due to wetter conditions in the Indian and East Asian monsoon regions. Heinrich events are associated with colder conditions in the North Atlantic, AIM maxima, and a stronger SASM, due to southward displacement of the ITCZ, which led to more rainfall in the region. *From Kanner et al. (2012).*

Abrupt millennial-scale variations are also recorded in stalagmites from caves in northeastern and southern China during marine isotope stages 2 and 3 but there, interstadial conditions in Greenland correspond to strong monsoons, whereas the most enriched isotopic values (weakest monsoon intervals) are coincident with Heinrich events in the North Atlantic (Figure 8.10) (Wang et al., 2001; Zhou et al., 2008; Zhao et al., 2010). Thus, monsoon rainfall in South America (south of the Equator) and in East Asia is remarkably out of phase on millennial timescales as clearly shown in Figure 8.11 (Wang et al., 2006). This indicates that changes in North Atlantic conditions, linked via the thermohaline circulation to conditions in the Antarctic region, have a direct impact throughout the Tropics. Cold episodes in the North Atlantic lead to the southward displacement of the ITCZ in South America, which shifts the locus of the SASM southward, towards southern Brazil. At the same time, due to the bipolar seesaw, temperatures increase around Antarctica, which weakens the Mascarene high-pressure system in the southern Indian Ocean, leading to less moisture being transported northward across the Equator into the Indian summer monsoon system (An et al., 2011). During warm D-O events, conditions were more or less reversed. Thus, tropical monsoon systems in both hemispheres were dynamically linked to conditions at higher latitudes resulting in virtually synchronous hemisphere-wide atmospheric teleconnections between monsoon Asia, South America, and the North Atlantic throughout the last ~75,000 years. It is also of interest that because of the out-of-phase relationship between the SASM and the Indian and East Asian monsoon systems, CH_4 was relatively high during D-O events (Figure 8.9). These were relatively dry periods in central Peru and in the Amazon Basin, and so the most likely source of the increased methane production was tropical wetlands in the Indian and East Asian monsoon region.

8.5 LATE GLACIAL AND HOLOCENE RECORDS

Several Chinese caves have provided an exceptionally detailed picture of climatic variations over the past ~16,000 years. Of particular note are the records from Kulishu (~40°N), Hulu (32.5°N), and Dongge Caves (25°N) in eastern China, where summer monsoon rainfall accounts for the bulk of annual rainfall totals. Stalagmites from these sites experienced very similar isotopic variations in rainfall (as did several other sites across eastern China) from ~16,000 to 10,000 years BP (Dong et al., 2010; Ma et al., 2012). Furthermore, the chronology of changes recorded in the Chinese speleothems closely matches isotopic changes seen in Greenland ice (with dry conditions in China corresponding to cold conditions in Greenland) (Dykoski et al., 2005; Wang et al., 2005). The transition to the Bølling-Allerød period occurred at 14,645 ± 60 BP in Hulu Cave and the Younger Dryas (a time of weaker monsoon conditions) began at 12,820 ± 60 BP (compared to 12,880 ± 260 BP in GISP2). This episode ended quite abruptly (in less than a few decades) at 11,560 ± 40 BP in Kulishu Cave (compared to 11,640 ± 250 in GISP2) when isotopic values sharply decreased by ~2‰; thus records from both regions suggest that the Younger Dryas interval lasted ~1250 years (Figure 8.12). A similar picture was obtained from a cave in southwestern Oregon where lower $\delta^{18}O$ from 12,840 ± 200 to 11,700 ± 260 years BP is interpreted as a period of lower temperatures in that region (Vacco et al., 2005).

Holocene records from East Asia, Arabia, and Southern Hemisphere sites in South America show a strong response to summer orbital forcing in the respective hemispheres

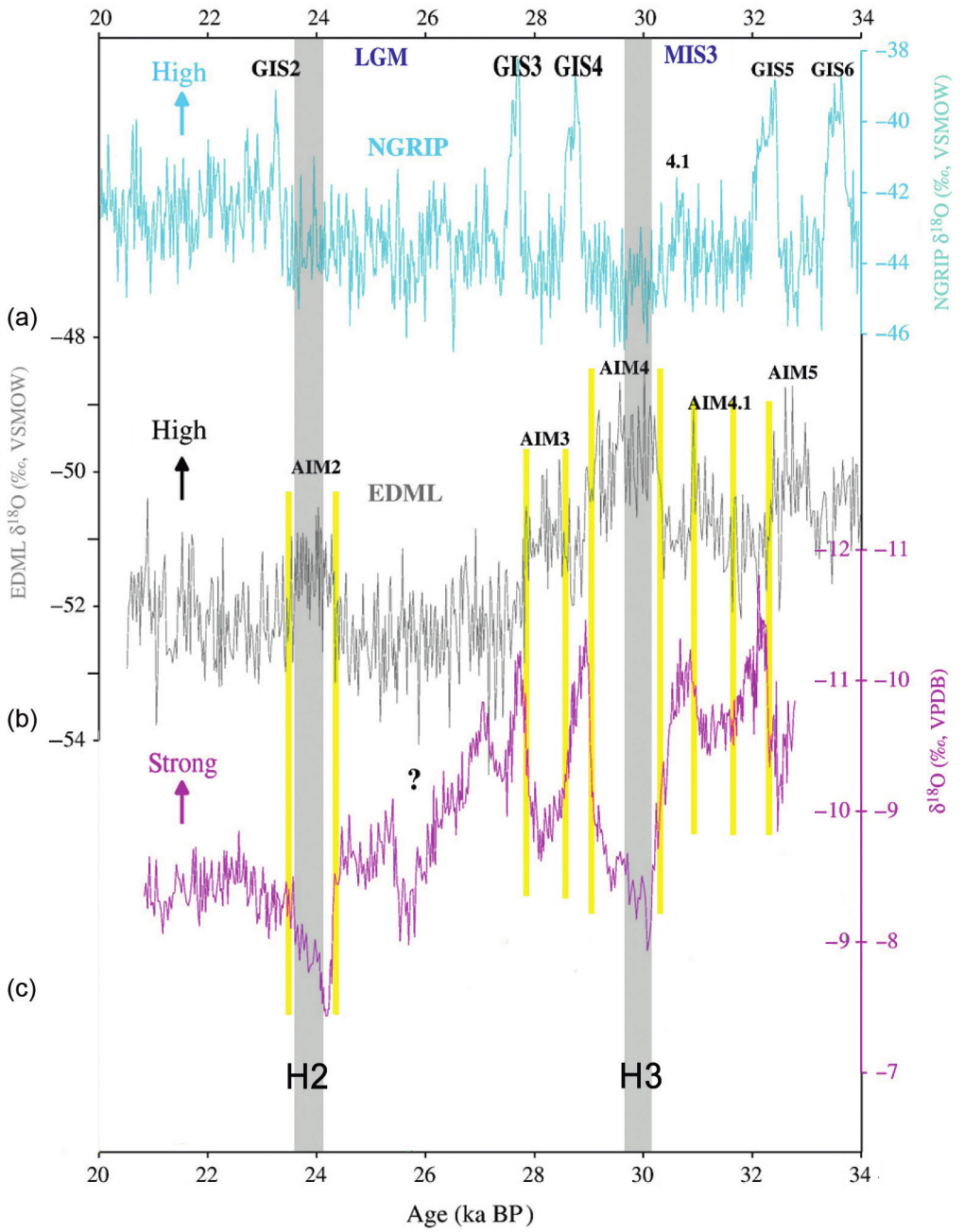


FIGURE 8.10 Comparison between high-latitude temperature records and low-latitude monsoon records. (a) $\delta^{18}O$ record of NGRIP; (b) $\delta^{18}O$ record from the EPICA Dronning Maud Land (EDML) ice core given on the GICC05 timescale. The synchronization uncertainty ranges from 400 to 800 years for all events (EPICA Community Members, 2006); (c) Composite $\delta^{18}O$ records of stalagmites from Sanbao, Hulu, and Dishibao Caves, central China. The "high" labels indicate high temperature in Greenland and Antarctica. The "strong" refers to Asian summer monsoon intensity. *From Zhao et al. (2010).*

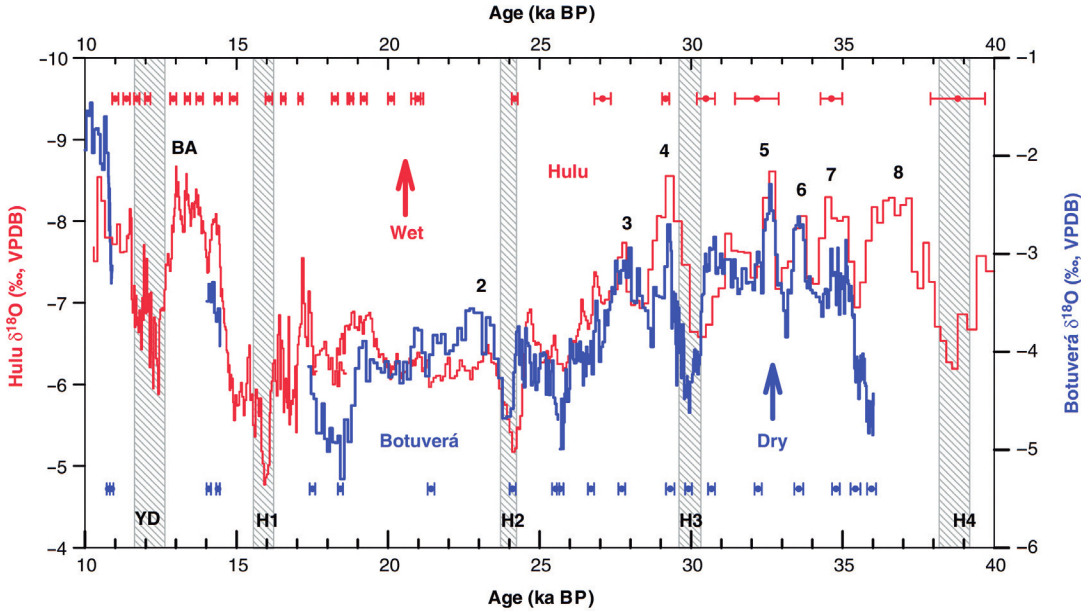


FIGURE 8.11 Oxygen isotope data from Botuverá Cave, southeastern Brazil (blue), and Hulu Cave, northeastern China (red), showing a strongly out-of-phase relationship, such that wet conditions in Brazil correspond to dry conditions in China (note that the *y*-axis for Hulu cave is inverted, so that wetter conditions are at the top). Thus, Heinrich events (shaded) are associated with a weak summer monsoon in China but wet conditions in southern Brazil due to southward displacement of the ITCZ. Age controls on the stalagmites are indicated above and below each record. *From Wang et al. (2006).*

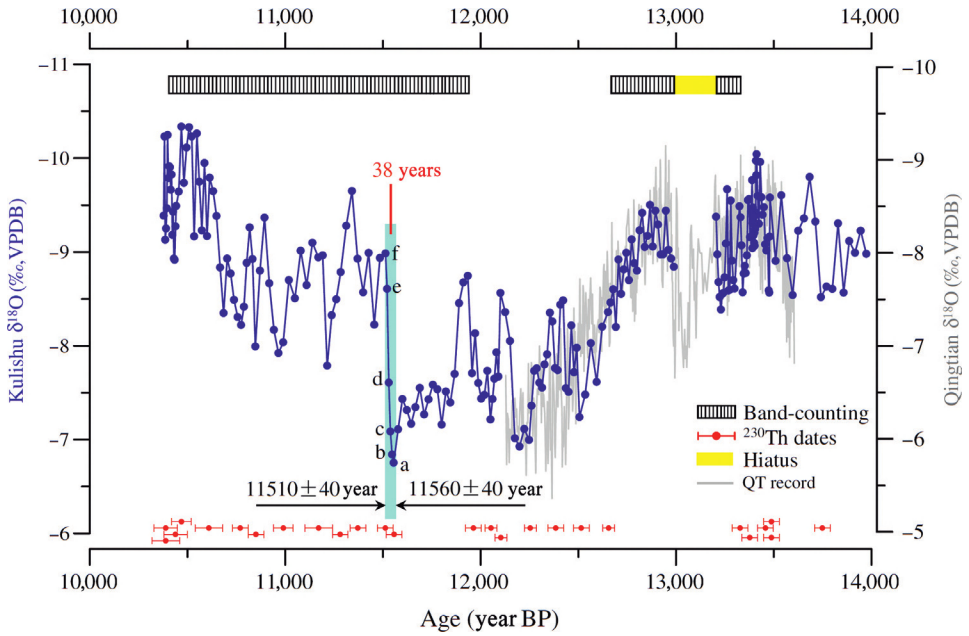


FIGURE 8.12 Oxygen isotope changes during the Younger Dryas episode as recorded in stalagmites from at Kulishu (blue) and Qingtian Caves (gray; Liu et al., 2008) eastern China. The more negative values (up) are related to stronger monsoon conditions. ^{230}Th dating errors (2σ) are indicated at the bottom. The annual-layer counting and hiatus intervals are marked by black and yellow bars at the top. The onset of the Younger Dryas was fairly gradual, extending over 350-400 years, whereas it ended abruptly (vertical light-blue bar, which has duration of <38 years as determined by the annual-layer counting). *From Ma et al. (2012).*

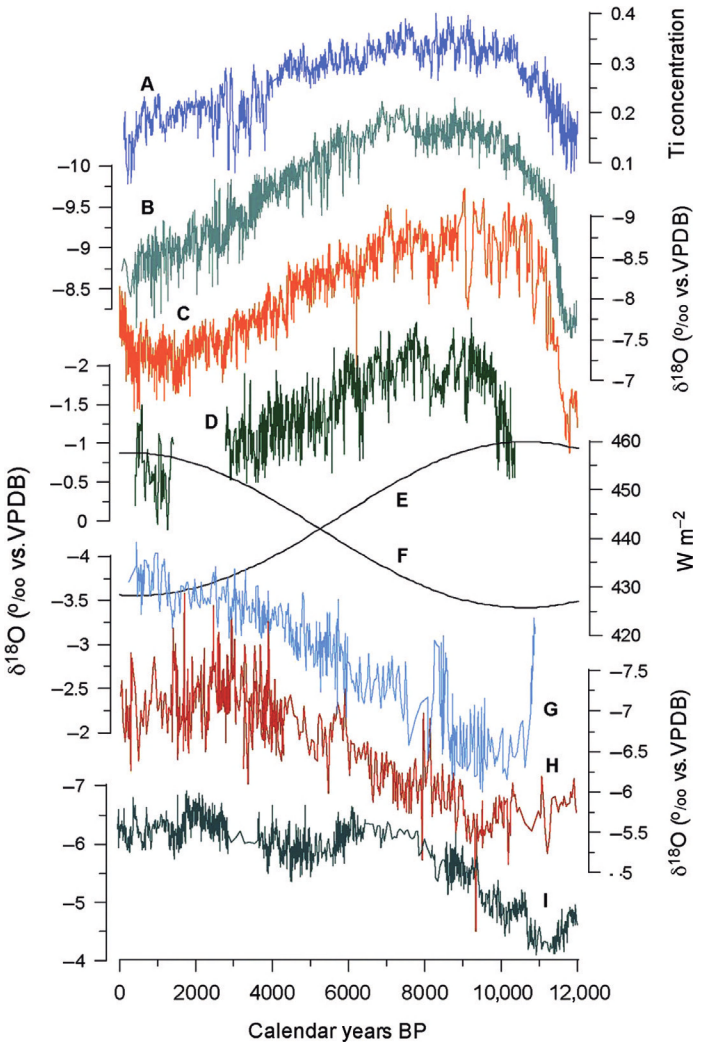


FIGURE 8.13 Oxygen isotope records from three caves in the Northern Hemisphere and three in the Southern Hemisphere, plus (a) the Cariaco Basin Ti record (Haug et al., 2001). (b) Sanbao Cave, southern China, 31°N (Dong et al., 2010); (c) Dongge Cave, central China, 25°N (Dykoski et al., 2005; Wang et al., 2005); (d) Qunf Cave, southern Oman, 17°N (Fleitmann et al., 2003b); (e) and (f) insolation curves for July at 10°N and January at 10°S, respectively; (g) Botuverá Cave, southeastern Brazil, 27°S (Wang et al., 2006); (h) Cueva del Tigre Perdido, eastern Peruvian lowlands, 7°S (van Breukelen et al., 2008); (i) Liang Luar Cave, Indonesia, 8°S (Griffiths et al., 2009). *From Burns (2011).*

(Figure 8.13). In the Early Holocene, the ITCZ migrated northward, increasing monsoon rainfall across the Indian and East Asian monsoon regions; then as insolation declined in the Late Holocene, the ITCZ migrated back southward (Fleitmann et al., 2007a). Monsoon strength is primarily related to insolation in the summer of each hemisphere, leading to the opposite trends in monsoon strength in each region. Hence, when the Indian and East Asian monsoons were strong, the South American summer monsoon was weak. A major consequence of these changes was an expansion of tropical wetlands in Asia and a higher CH_4 concentration in the atmosphere (Burns, 2011).

The Holocene record from Dongge Cave has been sampled in great detail, with a mean sample interval of 4-5 years. TIMS dates provide an extremely well-dated chronology, with 2σ errors of 50-70 years (Dykoski et al., 2005; Wang et al., 2005). As at other Asian cave sites

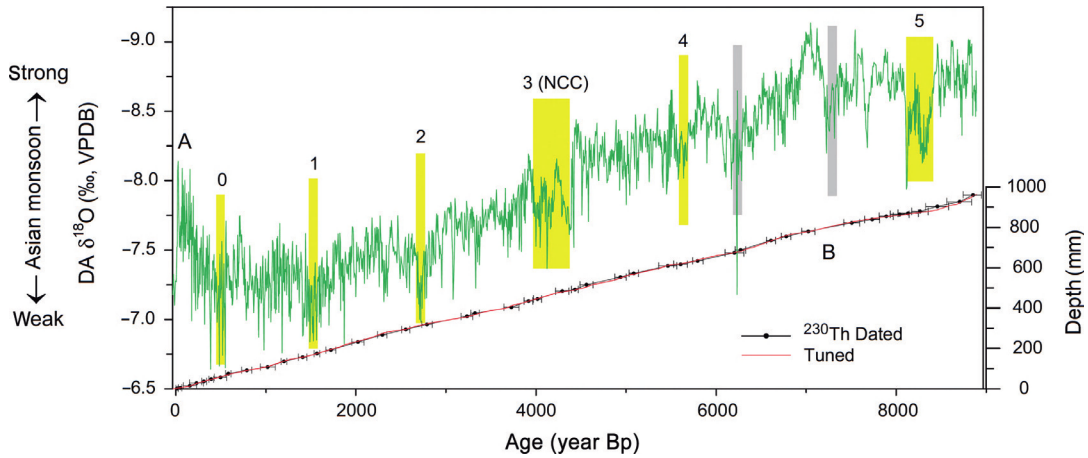


FIGURE 8.14 Stalagmite $\delta^{18}O$ record for the last 10,000 years from Dongge Cave, southern China. TIMS dates are shown at the bottom, with age model given by the solid line. The overall enrichment in $\delta^{18}O$ reflects a weakening monsoon rainfall regime over the course of the Holocene, due to orbital forcing (higher summer insolation in the Early Holocene). Superimposed on this low-frequency trend are short dry episodes (highlighted) that appear to correlate with ice rafting (Bond) events in the North Atlantic. The complex drier interval around 4-4.2 ka BP corresponds to the collapse of Neolithic cultures in China (NCC) (Wang et al., 2005).

(e.g., Cosford et al., 2008; Cai et al., 2012), the overall record (Figure 8.14) shows a decline in monsoon strength from the Early Holocene (due to orbital forcing), but this low-frequency change is punctuated by a number of episodes, lasting 100-500 years, when monsoon rainfall was reduced. These episodes—centered at 8.3, 7.2, 6.3, 5.2, 4.4, 2.7, 1.6, and 0.5 ka BP—are similar in timing to periods of weak upwelling (reduced southwestern monsoon) in the Arabian Sea (Gupta et al., 2003) and to times of increased ice rafting in the North Atlantic (Bond et al., 1997). The pronounced increase in $\delta^{18}O$ at ~8.3 ka BP may be linked to similar anomalies seen around the world at this time, perhaps reflecting the impact of a final, massive freshwater discharge from the waning Laurentide Ice Sheet on North Atlantic thermohaline circulation and related atmospheric teleconnections (Barber et al., 1999; Rohling and Pälike, 2005). Several other stalagmites record this episode in detail. In Israel, there is evidence (from a sharp drop in $\delta^{13}C$) that there was a short cold episode between 8.2 and 8.0 ka BP, within a period characterized by relatively high rainfall (Bar-Matthews et al., 1999). A similar brief cold period was seen in the isotopic record of benthic ostracods in Lake Ammersee, southern Germany, at this time (von Grafenstein et al., 1999). In Oman, there was a general increase in $\delta^{18}O$ from ~8.5 to 8.2 ka BP, reflecting a gradual reduction in southwestern (Indian Ocean) monsoon rainfall, but then a further abrupt reduction at ~8.2 ka BP, when stalagmite deposition ceased entirely for about 200 years (Fleitmann et al., 2003b, 2004). Evidence for reduced rainfall at this time is also recorded in a stalagmite from Costa Rica (Lachniet et al., 2004a). $\delta^{18}O$ began to rise around 8.4 ka BP, reaching a maximum at ~8.2 ka BP. This is interpreted as a significant reduction in rainfall that would normally be associated with the seasonal migration of the ITCZ across the region. The northward movement of the ITCZ may have been limited by a stronger subtropical Atlantic anticyclone and/or cooler subtropical Atlantic SSTs at that time. Indeed, the records from China, Oman, and Costa Rica all point to a more

limited seasonal migration of ITCZ and a significant reduction in monsoon rainfall in the Northern Hemisphere during this brief interval around 8.2 ka BP.

Higher-frequency variations in the Dongge Cave record show a strong correlation with atmospheric ^{14}C variations over the course of the Holocene, suggesting that solar forcing may have influenced the strength of the Asian monsoon on decadal to century timescales. Evidence for such a connection has also been seen in stalagmite records from Oman, where radiocarbon anomalies and $\delta^{18}O$ are strongly correlated (Neff et al., 2001; Fleitmann et al., 2003b) (Figure 8.15). As in the Dongge Cave record, low $\Delta^{14}C$ (reflecting higher solar activity)

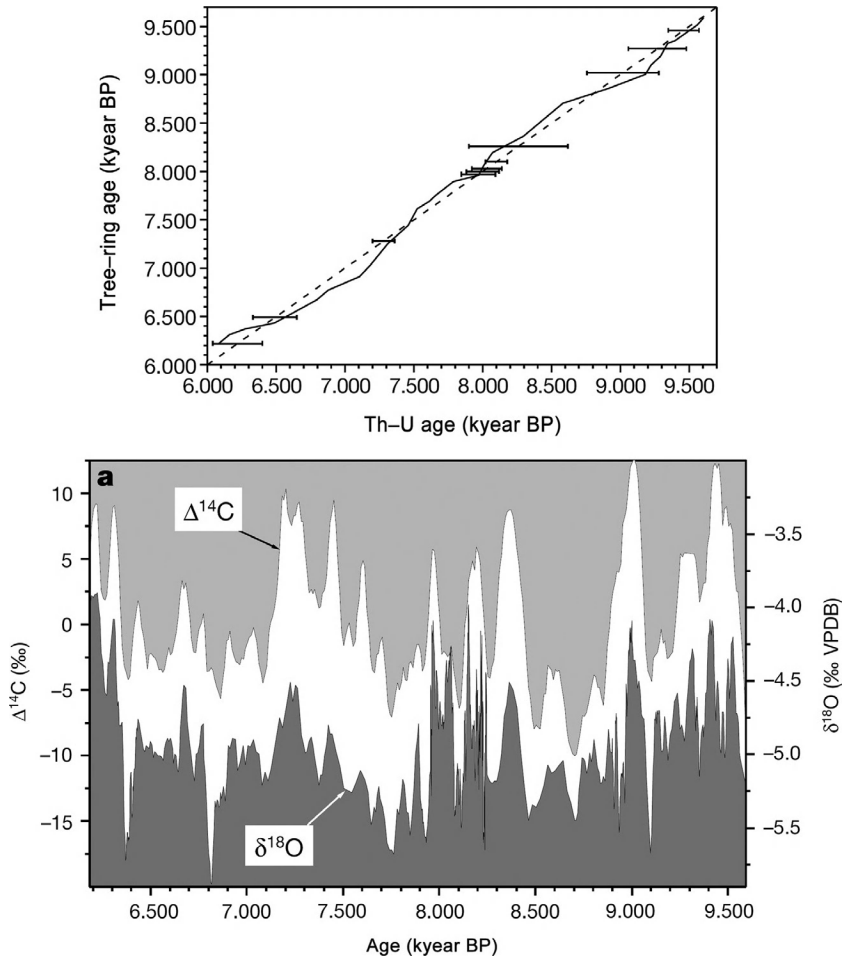


FIGURE 8.15 Oxygen isotope and $\Delta^{14}C$ record from Hoti Cave, Oman, showing a strong relationship between atmospheric radiocarbon anomalies and the isotopic composition of rainfall in this region ($r = 0.6$ in the unsmoothed data). Low $\delta^{18}O$ values are related to low radiocarbon anomalies, which are thought to result from high solar activity (reduced cosmogenic isotope production rates). The two records have been filtered and the speleothem chronology was slightly adjusted to optimize the fit between the records. The upper diagram shows that the adjustment (solid line) is well within the uncertainty of the original age model for the series (dashed line) (Neff et al., 2001).

is associated with higher rainfall (stronger monsoon and lower $\delta^{18}O$). There is also a strong correlation between $\delta^{18}O$ in a stalagmite from northwestern Germany and radiocarbon anomalies (Niggemann et al., 2003) such that increases in radiocarbon anomalies correspond to drier and warmer conditions (higher $\delta^{18}O$) in this region. This is similar to changes seen in stalagmites from northern Italy over the last few centuries (Frisia et al., 2003). Although such relationships are statistically significant and can be plausibly understood in terms of simple irradiance-climate relationships, the fact remains that there is as yet no obvious mechanism to explain how fairly small changes in solar activity might bring about quite large changes in the Earth's climate. The observed change in total irradiance over recent solar cycles is extremely small, only ~0.1% outside the atmosphere, and the evidence for larger, long-term changes in irradiance is equivocal. Indeed, how solar activity changes are related to solar irradiance changes remains unclear (Lean et al., 2002). This matter is discussed further in Chapter 2, Section 2.7.

8.6 STALAGMITE RECORDS OF THE LAST TWO MILLENNIA

At a number of sites, high-resolution studies of stalagmites provide detailed records of climate variability over the last one or two millennia, at annual or near-annual sample intervals. For example, Burns et al. (2002) identified 780 layers in a polished section of a stalagmite from Oman, and U-series dating confirmed that these layers were annual. Over 600 samples drilled from the section provided a record with a sample interval of ~1.3 years (Figure 8.16). $\delta^{18}O$, $\delta^{13}C$, and layer thickness all vary in parallel and reflect changes in rainfall since AD 1215

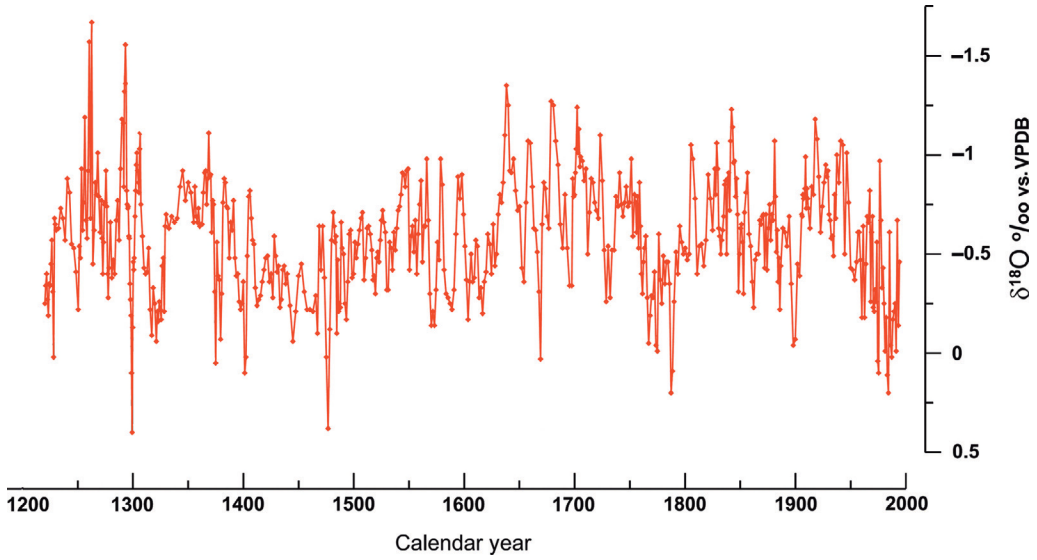


FIGURE 8.16 $\delta^{18}O$ in a stalagmite from a cave in southern Oman. Modern observations and calibration of the uppermost section with instrumental records of rainfall show that lower isotopic values are related to higher monsoon rainfall, which also leads to thicker annual layers. *Modified from Burns et al. (2002).*

(±5 years). The record greatly extends the limited perspective on climate variability available from instrumental data in the region and suggests that the strongest monsoon rainfall occurred around AD 1650-1700. In the twentieth century, the trend has been towards less rainfall, possibly related to the warming of the Indian Ocean (relative to the Asian continent), reducing the seasonal temperature gradient that drives the monsoon.

High-resolution samples from caves in eastern India and southern China, which overlap in time over the last ~1300 years, show remarkable coherence, even though they are over 3000 km apart (Figure 8.17) (Sinha et al., 2007, 2011a,b; Zhang et al., 2008). Both regions show relatively weak monsoon conditions in the Little Ice Age, with drought conditions prevalent in the late fourteenth and fifteenth centuries and in the early 1600s, far more severe than anything recorded in the last century (Sinha et al., 2011b). Tree-ring studies in southern Vietnam also point to droughts at those times, indicating large-scale regional monsoon failures over a very wide region (Buckley et al., 2010). It may be no coincidence that these drought episodes were associated with times of societal unrest and dynastic collapse in the region (Zhang et al., 2008). The reasons for such extensive rainfall anomalies are unclear but may be related to an increase in the frequency of "active break" periods in monsoon conditions, which lead to overall reductions in summer rainfall. This change in synoptic circulation patterns may be related to a southward displacement of the ITCZ and/or to a weakening of the Mascarene high-pressure zone in the southern Indian Ocean, leading to a reduction in the cross-equatorial flow of moist air into the region. It is interesting to note that rainfall variations in South and East Asia over the last millennium are inversely related to precipitation in northeastern Peru, as recorded by a stalagmite from Cascayunga Cave (Reuter et al., 2009). A very similar sequence of wet and dry intervals is also recorded in Panama (Lachniet et al., 2004b) and in the Yucatan of Mexico, where prolonged and severe droughts in the ninth century were also associated with societal collapse (Figure 8.18) (Medina-Elizalde et al., 2010). This suggests that the out-of-phase relationship between Asia and South America, observed during glacial times, discussed earlier, may also have operated on much shorter timescales, with global-scale changes in the mean position of the ITCZ once again implicated (cf. Yancheva et al., 2007).

8.7 PALEOCLIMATIC INFORMATION FROM PERIODS OF SPELEOTHEM GROWTH

The deposition of speleothems is dependent on a number of factors—geologic, hydrologic, chemical, and climatic. A change in any one of these factors could cause water percolation to cease, terminating speleothem growth at a particular drip site. However, cessation of speleothem growth over a large geographical area is more likely to be due to a climatic factor than anything else, so dating periods of speleothem growth can provide useful, albeit rather crude, paleoclimatic information (e.g., Baker et al., 1993; Zhao et al., 2001; Drysdale et al., 2004; Holzkamper et al., 2005). This is most successful when dating samples from sites that are presently marginal for speleothem growth, because they are too arid or too cold. Uninterrupted speleothem growth is recognizable in polished sections as a series of very fine growth layers; major hiatuses in deposition are usually marked by erosional surfaces, desiccation and chalkification, dirt bands, and sometimes color changes.

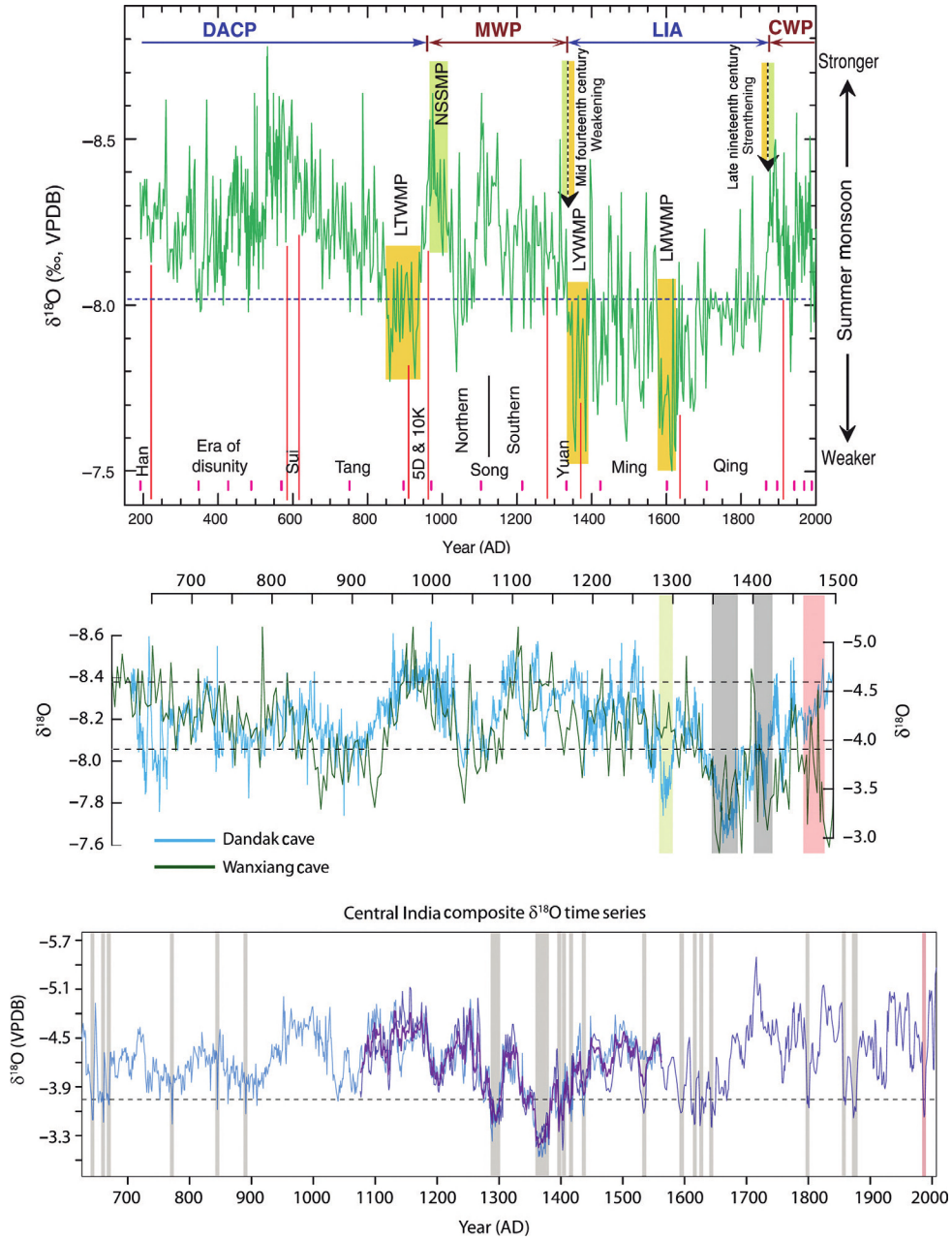


FIGURE 8.17 Isotopic record from Wanxiang Cave, southern China (33°N, 109°E), and Dandak Cave, eastern India (19.5°S, 83°E), from ~AD 600 to 1500. Although separated by ~3000 km, both records reflect variations in Indian monsoon airflow during the summer. They show a relatively weak monsoon during the early years of Little Ice Age (thirteenth to nineteenth centuries) with droughts in both regions during the late fourteenth and early fifteenth centuries. Weaker monsoon episodes were associated with the final decades of the Tang, Yuan, and Ming dynasties. In upper panel, Chinese Dynastic periods are shown at the bottom; pink marks indicate U-series dates. LYWMP = Late Yuan Weak Monsoon Period; LTWMP = Late Tang Weak Monsoon Period; LMWMP = Late Ming Weak Monsoon Period; NSSMP = Northern Song Strong Monsoon Period; DACP = Dark Ages Cold Period; MWP = Medieval Warm Period; LIA = Little Ice Age; CWP = Current Warm Period. Lower panel shows 2 records from Dandak cave (blue) and nearby Jhumar cave (purple) in eastern India (averaged records in darker color where they overlap). *Data from Zhang et al. (2008) and Sinha et al. (2011b).*

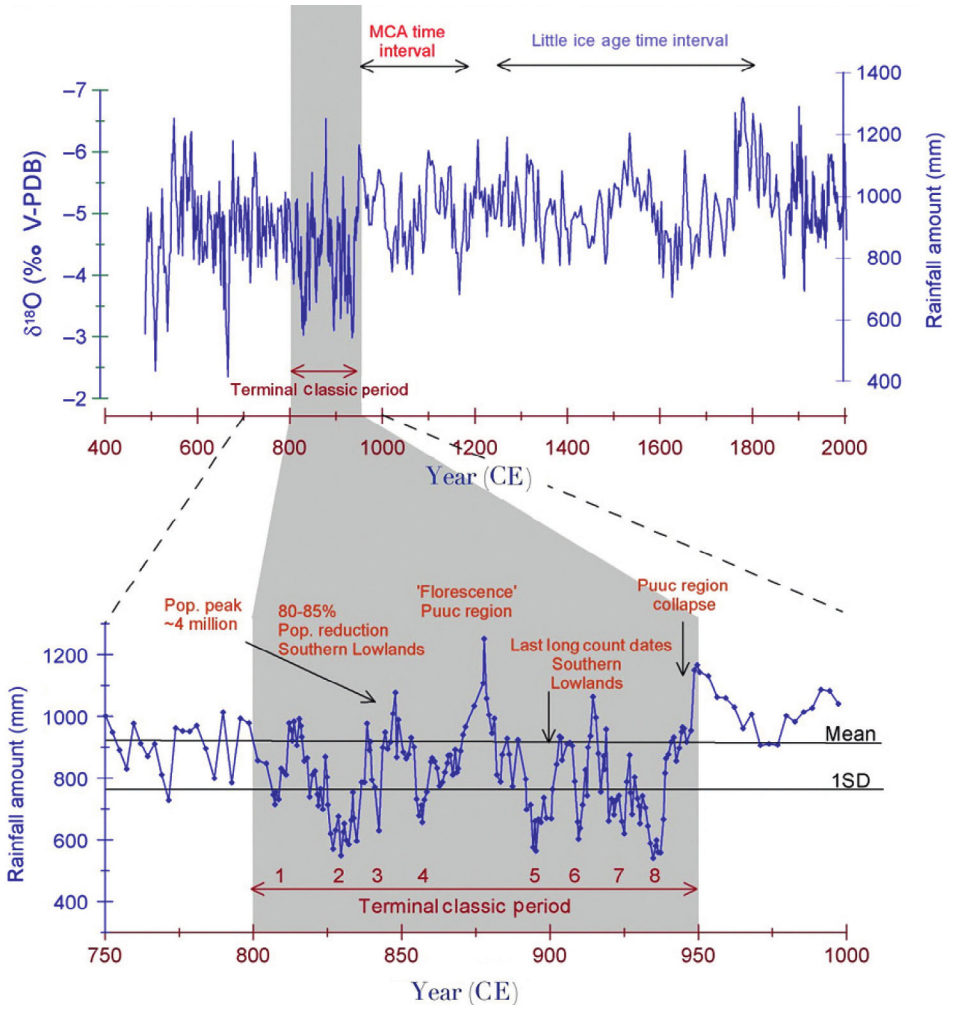


FIGURE 8.18 A $\delta^{18}O$-derived precipitation record from a stalagmite from the Yucatán Peninsula spanning the last 1500 years with an average resolution of 2.3 years. $\delta^{18}O$ was converted to precipitation by applying the calibration equation: ((annual precipitation (mm)) = $-176.47\delta^{18}O - 50.956$. The error of the estimation is ±100 mm, including calibration and sample analytic reproducibility errors (±0.1‰). The lower diagram shows an expansion of the record for the Maya Terminal Classic Period, showing a series of eight consecutive droughts from 800 to 950 CE. At this time, the resolution of the record is annual or higher, and precipitation reduction was between 36% and 51% compared to today's mean annual average (1120 mm) in the region of the cave. Some relevant Terminal Classic Period political and demographic events are indicated. *From Medina-Elizalde et al. (2010).*

Caves in northeastern Brazil are currently too dry to support the growth of speleothems, but there were intermittent periods of growth in the past when wetter conditions prevailed (Figure 8.19). Each episode was associated with orbital insolation maxima at 10°S in the Austral autumn (February to May, which is the time of maximum rainfall in the region). Insolation at this latitude is largely related to the precessional cycle (Wang et al., 2004). At times of insolation maxima, the Interropical Convergence Zone (ITCZ) was displaced further south than its modern

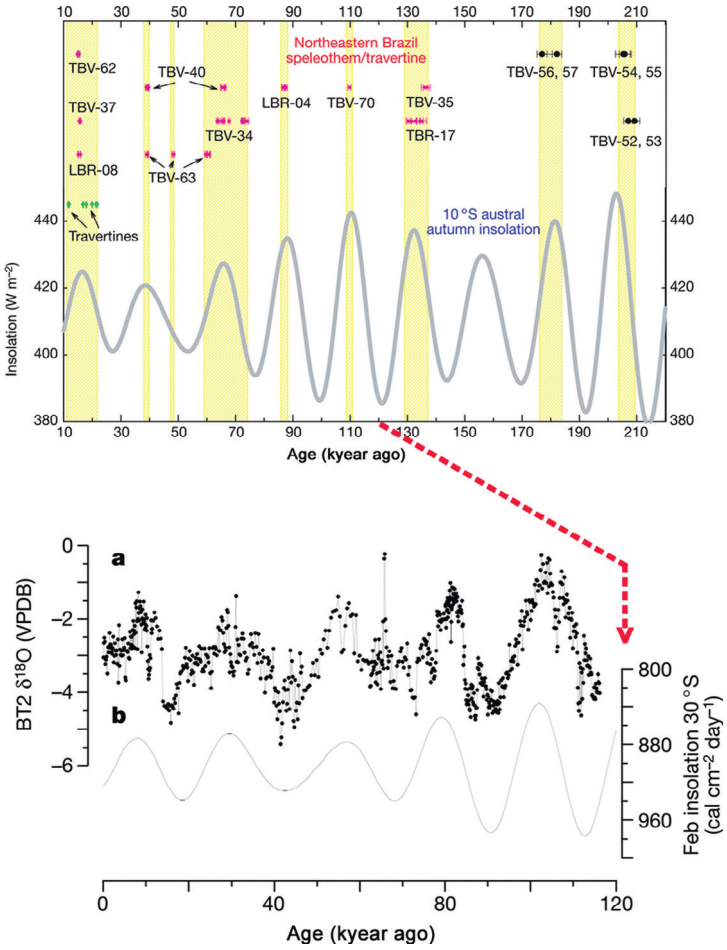


FIGURE 8.19 Comparison of growth intervals of speleothems and young travertine from northeastern Brazil and insolation variation at 10°S over the Austral autumn. Pink, black, and green dots represent, respectively, stalagmite, flowstone (a type of speleothem), and travertine. Lower diagram: Stable oxygen isotope profile from Botuverá Cave, Brazil (27°S). The BT2 profile is compared with February solar insolation at 30°S (increasing downward). *From Wang et al. (2004) and Cruz et al. (2005b).*

limits, bringing more precipitation to the region, effectively turning on depositional processes in the caves. These wetter periods correspond in time with periods of low $\delta^{18}O$ in Greenland ice (i.e., cold conditions in the North Atlantic) and enriched $\delta^{18}O$ in speleothems from southern China (i.e., a weaker East Asian monsoon). How these widely dispersed records are linked together is complex but the key may be a very strong pole-equator temperature gradient in the Northern Hemisphere at those times (driven by insolation but enhanced by the presence of high-latitude continental ice sheets), which would lead to a southward displacement of the ITCZ. Further insight is provided by speleothems from Botuverá Cave in subtropical Brazil where continuous deposition has occurred over the last 116,000 years (Cruz et al., 2005b). At this more southerly latitude (27°S), there is a strong seasonal rainfall cycle (winter and early spring from equatorward movement of midlatitude cyclonic storms and late summer/early autumn from poleward transport of moist air from the Amazon Basin). Each period of rainfall has a distinct isotopic signal (−3‰ in winter vs. −7‰ in early autumn), so the overall isotopic composition of annual rainfall reflects the relative proportion of rainfall in each season. $\delta^{18}O$ in stalagmites shows a strong relationship to precession, with lowest values from 95 to 85, 45 to 40, and 20 to 14 ka

BP when summer insolation was relatively high (Figure 8.19). At those times, the seasonal outflow of moist air from the Amazon Basin extended further south (i.e., there was a stronger South American summer monsoon and a southward displacement of the South Atlantic Convergence Zone), resulting in proportionately more isotopically light rainfall entering the caves. Conversely, when insolation was lower, an equatorward shift in these systems led to higher amounts of rainfall from Atlantic storms and the deposition of more isotopically enriched calcite in the caves.

In the arid region of Yemen, on the Arabian peninsula, ^{230}Th dates on stalagmites reveal intermittent periods of growth, at ~6-10, ~100-105, 123-130, ~195-209, ~230-245, and ~300-330 ka BP, corresponding to marine isotope (interglacial) stages 1, 5.3, 5.5, 7.1, 7.5, and 9 (Fleitmann et al., 2011). These are similar to the dates of speleothem formation in Oman (Burns et al., 2001). In between these periods, no calcite formed because conditions were too dry. By evaluating the regional pattern of stalagmite formation, Fleitmann et al. estimated that rainfall amounts must have been two to three times higher than today during the periods when stalagmites were actively forming in this region. At those times, conditions may have been wet enough to support human populations, providing "windows of opportunity" for migration across the area, from Africa into regions to the east.

In many high-latitude or mountain caves, low temperatures, less snowmelt, and more extensive permafrost during glacial periods may have resulted in a marked reduction, even a cessation, of groundwater percolation. Furthermore, decreased biotic activity may have led to a decrease in the partial pressure of carbon dioxide in the soil atmosphere and therefore less carbonate in solution; consequently, speleothem growth in such regions may have ceased (Holzkamper et al., 2005). Uranium-series dates on alpine speleothems from western Canada, collected at sites that have a surface mean annual temperature close to 0 °C and are hence marginal for speleothem growth, reveal four earlier periods of speleothem deposition when conditions for speleothem growth were favorable, from ~320 to 285, ~235 to 185, 150 to 90, and ~15 ka BP to the present (Harmon et al., 1977). These dates compare favorably with periods of speleothem growth observed in caves in Europe. In caves in central Siberia, where permafrost is sporadic today, stalagmite growth has only occurred for brief periods over the last 0.5 Ma. Each of these periods coincides with peak interglacial warmth, when water was able to percolate freely in the caves (Vaks et al., 2013).

8.8 SPELEOTHEMS AS INDICATORS OF SEA-LEVEL VARIATIONS

Speleothem growth in locations close to sea level can provide an extremely valuable indicator of former sea-level position and hence ice volume changes on land. As speleothems must form above sea level in air-filled caves, the occurrence of speleothems in caves that are presently below sea level provides an upper limit to sea level at the time of formation. Similarly, speleothems exposed today that have overgrowths of marine aragonite indicate unequivocally that sea level was formerly higher. Thus, Bard et al. (2002b) found a stalagmite 18 m below present sea level, encrusted with biogenic calcite produced by marine serpulid worms. These colonized the stalagmite surface after sea level rose, submerging the cave. TIMS dates reveal that stalagmite growth began ~206 and ended ~145 ka BP (spanning marine isotope stages 7.2 to 6), but there was a clear hiatus from ~202 to 190 ka BP when sea level was higher and serpulid worms also colonized the stalagmite surface (Figure 8.20). Although the

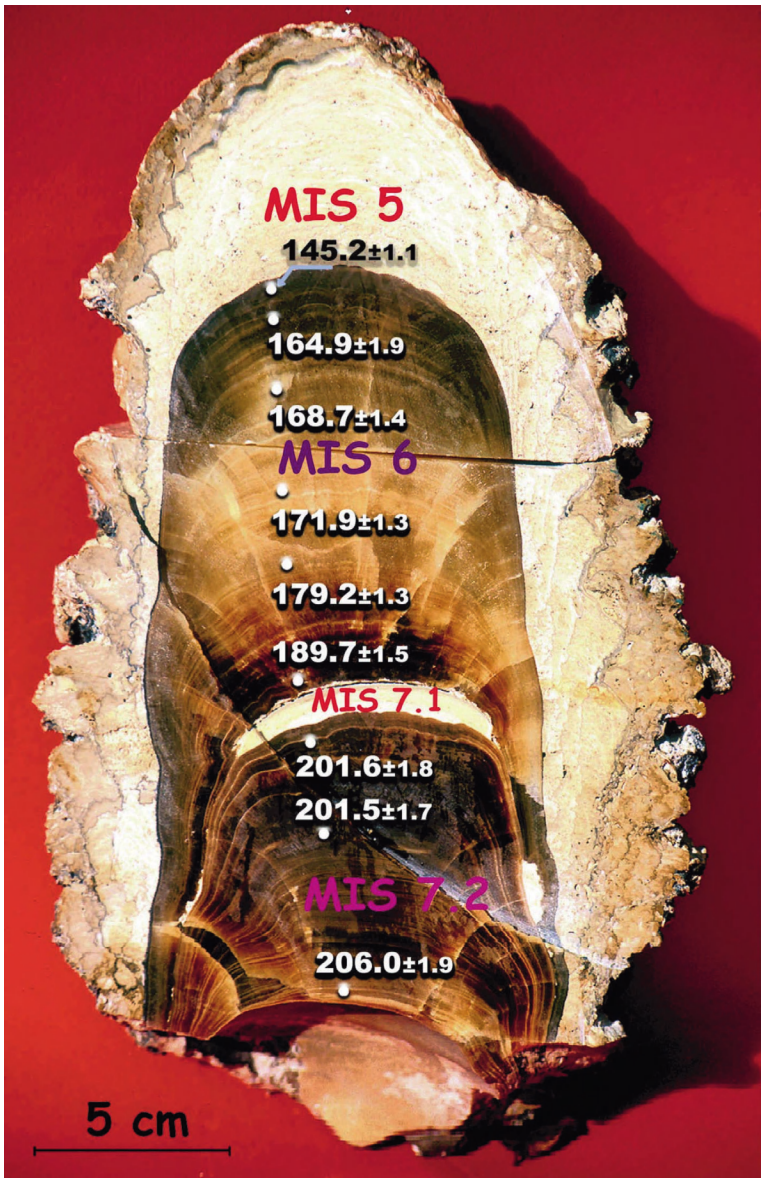


FIGURE 8.20 A cross section of a stalagmite from Argentarola Cave, west-central Italy, showing overgrowth of biogenic calcite produced by marine serpulid worms after the cave was submerged by rising sea level. The stalagmite was collected at 18 m below present sea level, in an area where the coastline has been tectonically stable. U-series dates are shown at sample locations along the stalagmite. A clear hiatus, with additional biogenic calcite encrustation interrupting stalagmite growth, between ~202 and 190 ka BP, indicates that sea level was above −18 m during that interval (Bard et al., 2002b).

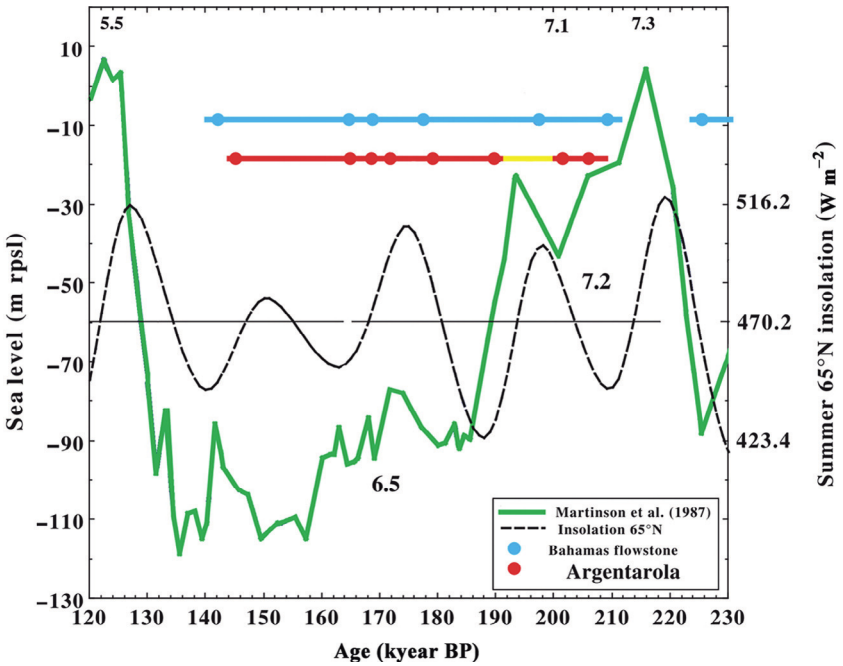


FIGURE 8.21 Speleothem growth in caves below present sea level constrains past sea-level position to have been below −18 m from ~190 to ~140 ka BP (based on Argentarola Cave stalagmite in west-central Italy). From 202 to 190 ka BP sea level was above −18 m, but below −9 m (level of dated flowstone deposit in a cave in the Bahamas). However, from ~225 to 213 ka BP, sea level may have been above −9 m, as speleothem deposition ceased during that period in the Bahamas Cave. These inferences are consistent with sea-level changes implied by the benthic foram SPECMAP record of Martinson et al. (1987) (green line) and of expectations related to orbital forcing (dashed line). The much higher sea level during stage 5.5 (~125 ka BP) suggests that other factors drove the continental ice sheet demise at that time (such as an increase in CO_2 of ~100 ppmv) in addition to orbital forcing. *After Bard et al. (2002b).*

exact sea-level position cannot be determined from this one site, another submerged speleothem from the Bahamas, at −9 m (Toscano and Lundberg, 1999), showed no growth hiatus during this interval, suggesting that eustatic sea level was between −9 and −18 m during this interval (marine isotope stage 7.1) (Figure 8.21).

Harmon et al. (1978b) were able to conclude from studies of Bermuda speleothems that interglacial conditions (high sea-level stands) occurred at around 120,000 and 97,000 years BP; between these events, a lower sea-level stand (−8 m) occurred at ~114,000 years BP. Li et al. (1989) and Lundberg and Ford (1994) extended this approach by applying high-precision (TIMS) dating to a flowstone from the Bahamas (at −15 m water depth) that revealed growth hiatuses attributable to pre-Holocene high sea-level episodes at >280, ~230, ~215, ~125, and ~100 ka BP. Not all hiatuses are attributable to sea-level rise; a reduction in precipitation could limit groundwater flow and lead to cessation of calcite deposition (Richards et al., 1994). Nevertheless, evidence of continuous speleothem growth in caves below current sea level, in areas of platform stability, is a definitive indication that sea level could not have been above the threshold level during that time. Thus, Richards et al. (1994)

were able to eliminate the possibility that sea level rose above −18 m at any time between 93 and 15 ka BP. Furthermore, their data constrain sea level at marine isotope stage 5a as having been between −15 and −18 m, based on the onset of speleothem growth at these levels at 93 and 80 ka BP, respectively. Additional (submarine) sampling of speleothems has the potential of revealing the precise magnitude of former eustatic sea-level changes over long periods of time, which has important implications for understanding ice sheet growth and decay rates in relation to insolation changes (e.g., Dutton et al., 2009).

CHAPTER

9

Lake Sediments

OUTLINE

9.1 Sedimentology and Inorganic Geochemistry 320
9.2 Varves 323
9.3 Pollen, Macrofossils, and Phytoliths 324
9.4 Ostracods 327
9.5 Diatoms 327
9.6 Stable Isotopes 330
9.7 Organic Biomarkers 338

Lakes accumulate sediments from their surrounding environment and so sediment cores recovered from lakes can provide a continuous record of environmental change (Figure 9.1) (Cohen, 2003; Smol, 2008). Accumulation rates in lakes are often high, so lake sediments offer the potential for high-resolution records of past climate, providing they can be adequately dated. However, no two lakes are identical so the environmental conditions in each lake basin, and the water properties of each lake must be carefully evaluated in order to make a meaningful paleoclimatic interpretation of the sediments. In this chapter, a variety of organic and inorganic proxies are considered, but other important proxies obtained from lake sediments (aquatic insects and pollen) are dealt with in Chapter 11, Section 11.2.2, and Chapter 12, respectively.

Lake sediments are made up of two basic components: allochthonous material, originating from outside the lake basin, and autochthonous material, produced within the lake itself. Allochthonous material is transported to lakes by rivers and streams, overland flow, eolian activity, and (in some cases) by subsurface drainage. It is made up of varying amounts of fluvial or eolian clastic sediment, dissolved salts, terrestrial macrofossils, phytoliths, pollen, charcoal from fires, etc. Autochthonous material either is biogenic in origin or may result from inorganic precipitation within the water column (often as a consequence of seasonally varying biological productivity, which can significantly alter the water chemistry). Both allochthonous and autochthonous material can be useful in paleoclimatic reconstruction.

Copyright © 2015 Raymond S. Bradley.
Published by Elsevier Inc. All rights reserved.

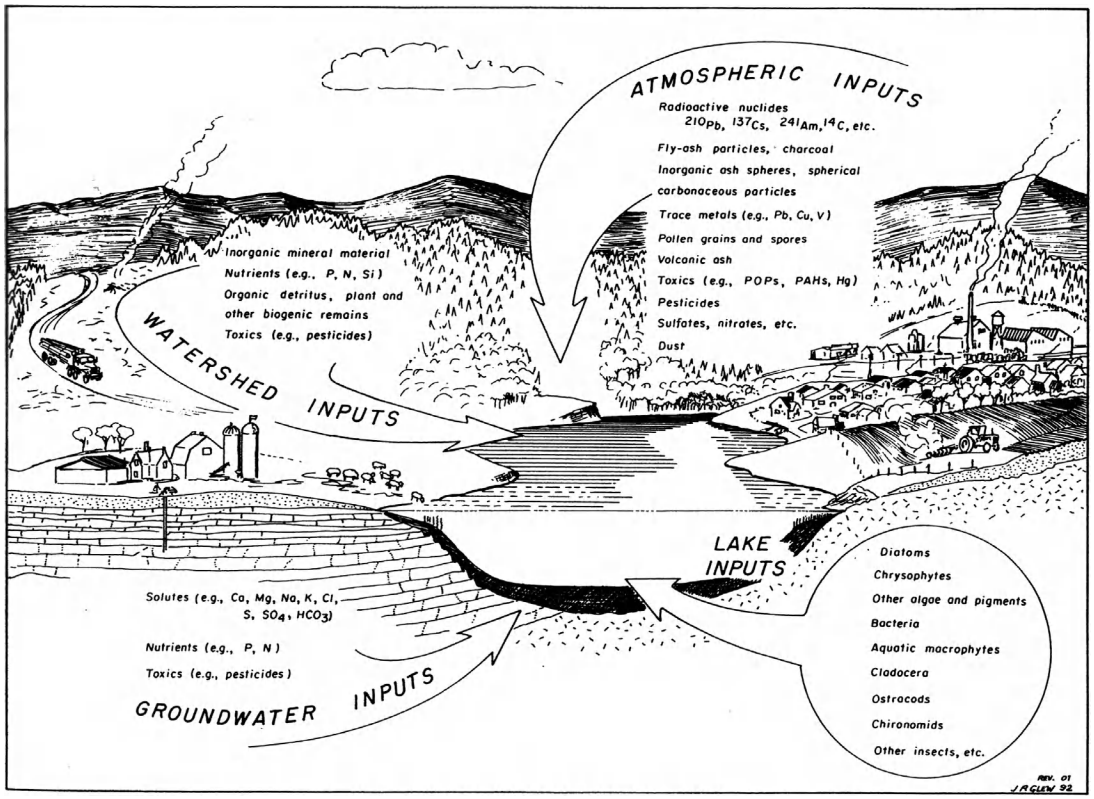


FIGURE 9.1 Schematic diagram illustrating the transfer of material from the atmosphere and the watershed to sediments in a lake (allochthonous input) and from sources within the lake itself (autochthonous input). In some cases, groundwater may also influence the transfer of dissolved materials to the sediments. *From Smol et al. (2001).*

9.1 SEDIMENTOLOGY AND INORGANIC GEOCHEMISTRY

A great deal of basic information about changes in climatic conditions can be derived from relatively simple measurements of the sedimentary and inorganic geochemical characteristics of lake sediments. For example, Nesje et al. (2000) demonstrated the usefulness of "loss on ignition" (LOI) to track the mass balance of the Jostedalsbreen Ice Cap, Norway, using LOI as an index of the relative quantities of organic matter versus inorganic clastic material in sediment cores downstream from the ice cap. The advance and retreat of glaciers is tracked quite well by the changes in LOI, because clastic sediment amount increases (and/or organic matter production decreases) during times of glacier growth. Similarly, magnetic susceptibility measurements can also document changes in the proportion of clastic material in a sediment core, and this also may reflect glacier activity in certain situations (e.g., Polissar et al., 2005). These types of measurement, together with a record of changes in other basic physical properties of lake sediments (dry bulk density, grain size variations, etc.) linked to accurate stratigraphic descriptions, provide a starting point for further paleoclimatic analysis, the exact approach depending on the type of material available and the environmental setting of the lake itself.

Of course, much more robust reconstructions are obtained through multiproxy analysis, which strengthens the interpretation provided by a single proxy (e.g., Birks et al., 2000; Caseldine et al., 2003; Lotter, 2003; McFadden et al., 2005).

Various nondestructive methods are available for sediment analysis, such as the analysis of visible light or X-ray digital images of sediment cores (Francus, 2004). Of particular importance is the acquisition of elemental data at very high resolution by scanning X-ray fluorescence analysis (Shanahan et al., 2008; Rothwell and Croudace, 2014). In many cases, the down-core record of a specific element, or elemental ratio, can provide valuable insights in past conditions. For example, Bakke et al. (2010a) examined the record of Ti, derived by XRF scanning of a sediment core from Kråkenes Lake in southern Norway. In this region, Ti reflects the erosion of Precambrian bedrock by glaciers and thus provides a proxy for glacial activity in the watershed. Ti increased at the start of the Younger Dryas interval, but after ~12.15 ka b2k, large and rapid variations in the amount of Ti in the sediment occurred (Figure 9.2). This "flickering" signal is interpreted as reflecting a highly dynamic period when the area experienced short-term fluctuations in westerly winds, driven by rapid changes in sea-ice conditions, causing large changes in glacier mass balance and sediment delivery to the lake. In Lake Huguang Maar, southern China, the Ti content provides a record of winter eolian influx to the lake (Figure 9.3). This shows an abrupt and persistent increase in winter winds at the onset of the Younger Dryas interval, which corresponds closely to the timing of a weaker summer monsoon, as recorded in the $\delta^{18}O$ of stalagmites from further north, in eastern China (Yancheva et al., 2007).

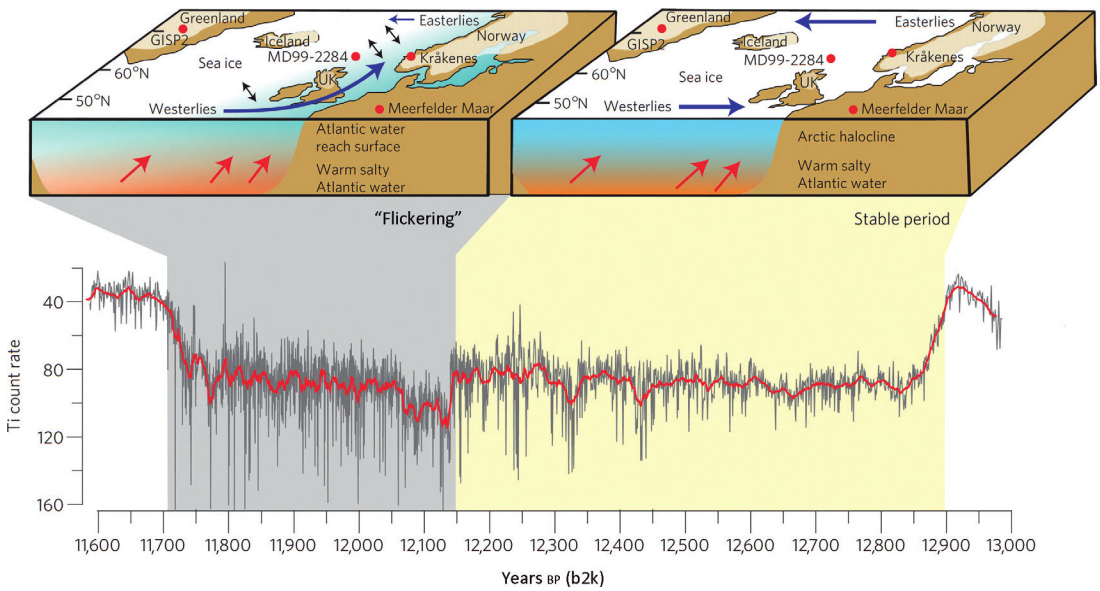


FIGURE 9.2 The Ti record from Kråkenes Lake, southwestern Norway, during the period from 13,000 to 11,600 b2k. The record shows an increase in Ti due to increased glacier erosion during the Younger Dryas interval, and rapid oscillations in sediment delivery to the lake toward the end of this period. This is interpreted as the result of changes in sea ice that affected the location and frequency of warm Atlantic water and associated westerly winds, as illustrated in the schematic diagram earlier. *From Bakke et al. (2010a).*

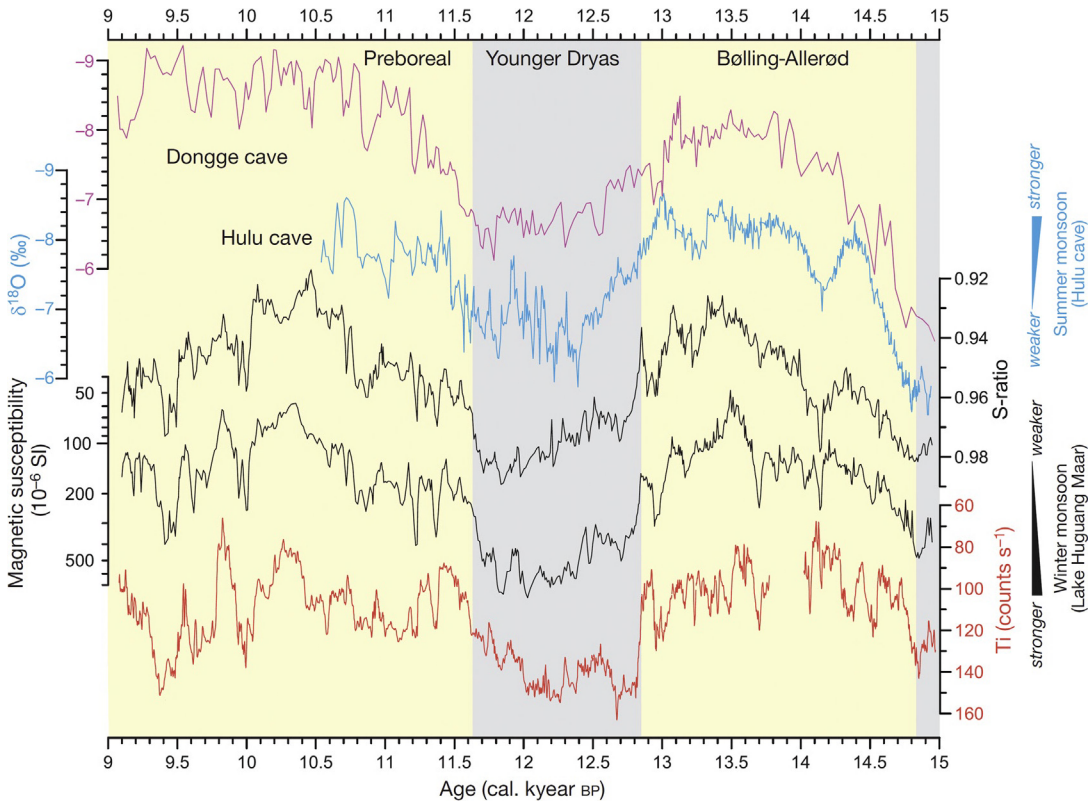


FIGURE 9.3 The record of Ti counts (from XRF analysis) together with magnetic susceptibility and S-ratio values from Lake Huguang Maar, southern China (21°N, 110°E), compared to oxygen isotopic data from stalagmites in Dongge and Hulu caves. The magnetic susceptibility and S-ratio values are indicators of the concentration of magnetic minerals and the abundance of magnetite, respectively; a high S-ratio indicates the availability of bottom-water oxygen and is interpreted to reflect wind-driven lake mixing. The variations in titanium are due to changes in winter eolian dust deposition, so that during the Younger Dryas interval, stronger winds prevailed at the same time as the summer monsoon rainfall declined (higher $\delta^{18}O$ values in the stalagmites). Magnetic susceptibility is sensitive to lake redox conditions and the eolian input, both of which are affected by wind strength (note inverted scales). *From Wang et al. (2001), Yancheva et al. (2007) and Dykoski et al. (2005).*

9.2 VARVES

In many parts of the world, the annual climatic cycle is the strongest part of the overall spectrum of climate variability and this is commonly reflected in the deposition of annually laminated sediments in lakes, known as varves[1] (Anderson and Dean, 1988; Ojala et al., 2012). Varves can result from the deposition of clastic or biogenic material or a combination of both (Figure 9.4). Varves are only rarely identifiable in lacustrine sediments because a variety of processes within lakes generally act to mix or disturb the seasonally varying flux of material

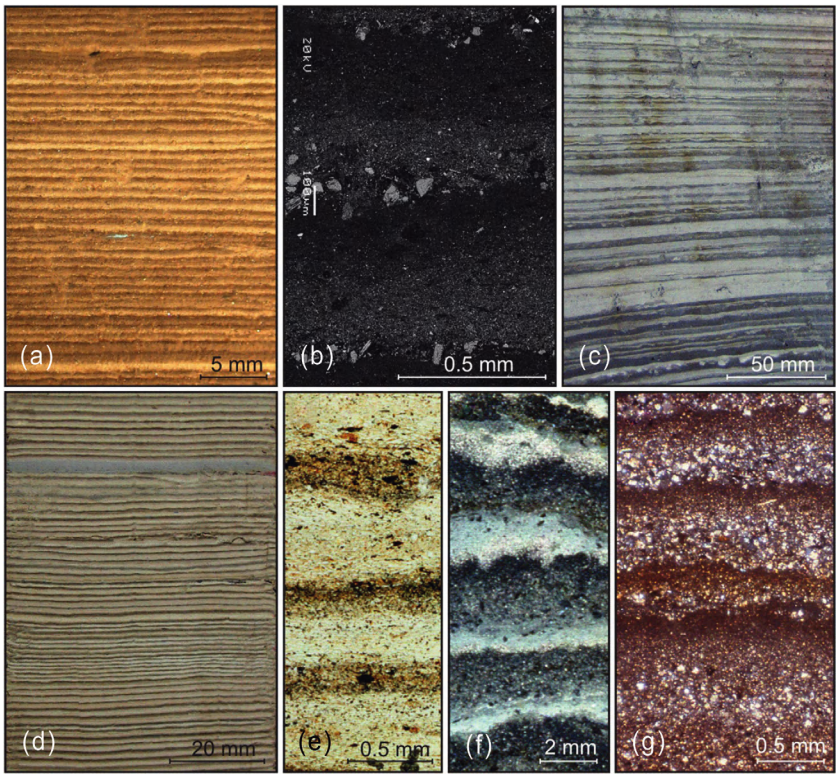


FIGURE 9.4 Examples of different types of varves. (a) Clastic-biogenic varves from Lake Nautajärvi, central southern Finland, around 2500 b2k, and (b) their scanning electron microscope image in backscattered mode. (c) Glaciolacustrine clay varves from Koria, southern Finland. (d) Carbonaceous varves from Belauer See, Northern Germany. (e) Petrographic microscope image (plain light) of organic varves from Lake Holzmaar, Westeifel Volcanic Field, Germany. (f) Petrographic microscope image (polarized light) of carbonaceous-organic varves from Sacrower See, eastern Germany. (g) Petrographic microscope image (polarized light) of nonglacial clastic varves from Lake C2, north coast of Ellesmere Island, Canadian High Arctic. *From Ojala et al. (2012).*

[1] In the marine environment, varved sediments are much rarer, but outstanding examples have been found in areas of high biological productivity (upwelling regions) and where deep anoxic basins allow sediment preservation (e.g., the Cariaco Basin off the coast of Venezuela (Hughen et al., 1996) and the Santa Barbara Basin off southern California (Sancetta, 1995; Pike and Kemp, 1996)).

to the lake floor. In particular, burrowing organisms at the sediment-water interface may mix the sediments and prevent the identification of annually deposited sequences. Varves are more common in cold-temperate environments, particularly in deep anoxic lakes that are frozen over for part of the year and where sediment input is strongly seasonal (e.g., Ojala et al., 2000). In some lakes, varved sediments have accumulated continuously for thousands of years (e.g., Elk Lake, Minnesota: Bradbury and Dean, 1993; Lakes Holzmaar and Meerfelder Maar, Germany: Zolitschka, 1998; Litt et al., 2009; Lake Gosciaz, Poland: Ralska-Jasiewiczowa et al., 1998; Central Finland lakes: Tiljander et al., 2003; Ojala and Alenius, 2005; Lake Yoa, Chad: Francus et al., 2013). This provides the opportunity to examine the sedimentary characteristics of the record in remarkable detail (Figure 9.5) (Dean et al., 1999; Shanahan et al., 2008). In exceptional circumstances, varves can be used as a chronological yardstick to calibrate the radiocarbon timescale (Staff et al., 2013) (see Chapter 3, Section 3.2.1.5).

In some cases, extreme events can be identified in varves for specific years. Thus, Besonen et al. (2008) were able to recognize the sedimentary signal of individual hurricanes that swept across the Boston area of southern New England in recent centuries and match these to the annual record of known historic events. The timing of earlier (pre-Colonial) hurricanes could then be reliably identified (Figure 9.6). This showed that hurricanes were more frequent during Medieval time (with eight hurricanes in the thirteenth century) but were much less common during the Little Ice Age (with only two in the seventeenth century).

9.3 POLLEN, MACROFOSSILS, AND PHYTOLITHS

Pollen is the most widely studied component of lake sediments and is discussed at length in Chapter 12. Pollen has provided a wealth of paleoenvironmental and paleoclimatic information and is a staple in paleoclimatic reconstructions used in verifying general circulation model simulations (Prentice et al., 1996; Bartlein et al., 1998; Bennett and Willis, 2001). Plant macrofossils (e.g., leaves, seeds, and fruits that are visible to the naked eye) can be especially helpful in corroborating vegetation reconstructions based on pollen (e.g., Hannon and Gaillard, 1997; Jackson et al., 1997). Unlike pollen, macrofossils generally stay close to the plant source and so are clearly diagnostic of local vegetation. This is a particularly useful attribute in areas subject to wide pollen dispersal (such as mountain regions) or where the overall pollen rain is low and easily biased by pollen dispersed from far distances, as in Arctic (tundra) regions (Birks, 2001; Birks and Birks, 2003). Furthermore, pollen grains are generally only identifiable to family or genus level, whereas macrofossils are commonly identifiable to species level, thereby providing more insight into climatic conditions controlling the distribution of individual species. Studies that are able to combine both pollen-based climatic interpretations with plant macrofossil data are especially insightful (e.g., Birks and Birks, 2000). For example, detailed studies of both pollen and macrofossil remains from LGM sites in Alaska suggest that the widely held, pollen-based concept of an extensive "steppe-tundra" landscape at that time is incorrect, having been biased by the presence of pollen transported over long distances. A more realistic view of the Beringian LGM paleoenvironment is that it was made up of a patchwork of boggy tundra regions, separated by drier and more open tundra, dominated by sedge, moss, and herbs (Elias, 1997; Goetcheus and Birks, 2001).

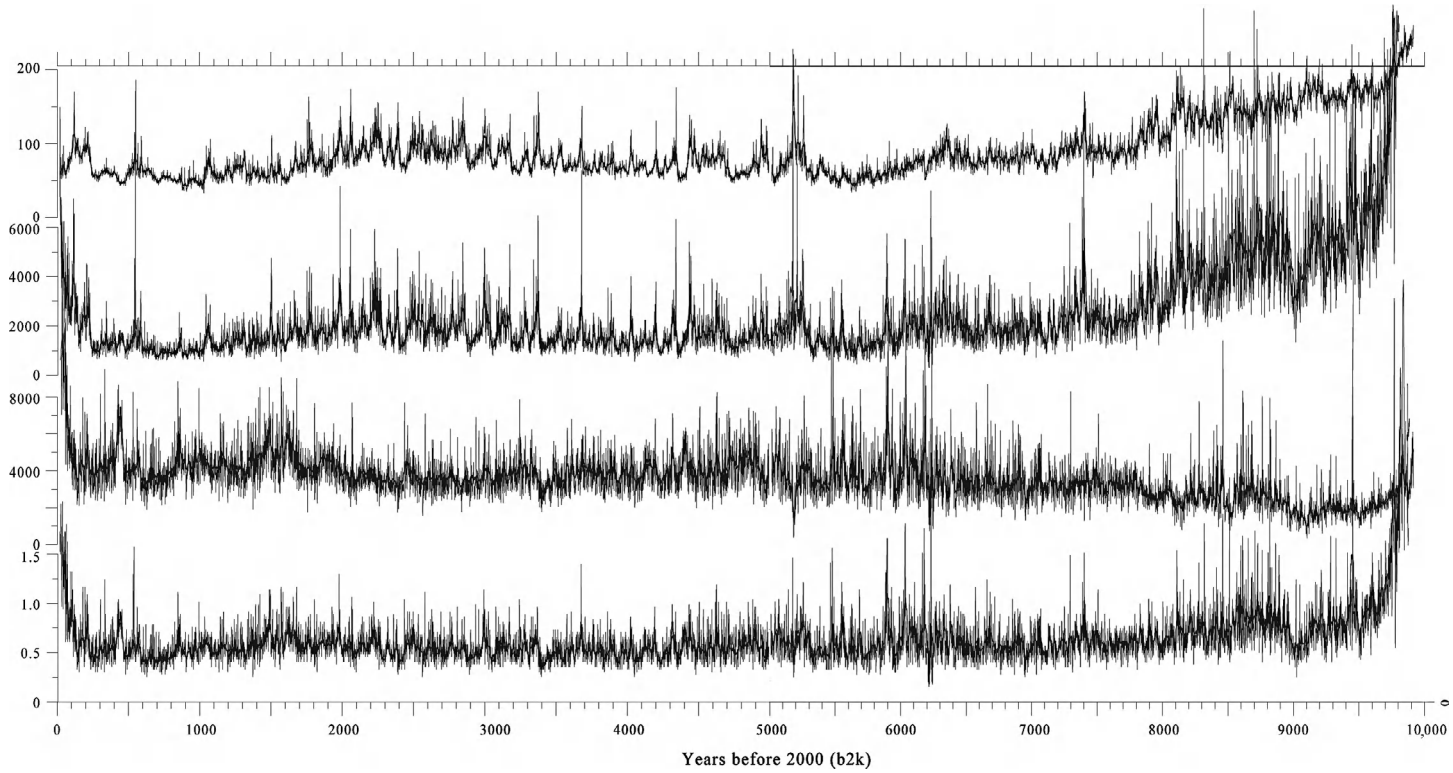


FIGURE 9.5 A varved (annually resolved) sediment record from Lake Nuutajärvi, Finland spanning the last 10,000 years. The record shows (bottom to top) total varve thickness (mm), the relative amounts of organic material, and minerogenic material in each varve, and the relative X-ray density. The organic (dark layers) and minerogenic components (light layers) are derived from the X-ray data. Increased erosion occurred from 9590 to 9530, 9450 to 9400, 9220 to 9110, 9000 to 8000, 7400 to 7200, 6400 to 6000, 4700 to 4400, and ~3500 to 1500 b2k. These intervals are interpreted as having had severe winters with increased amounts of snow. Erosion also increased after ~600 b2k, due to agricultural activity in recent centuries. *Adapted from Ojala and Alenius (2005).*

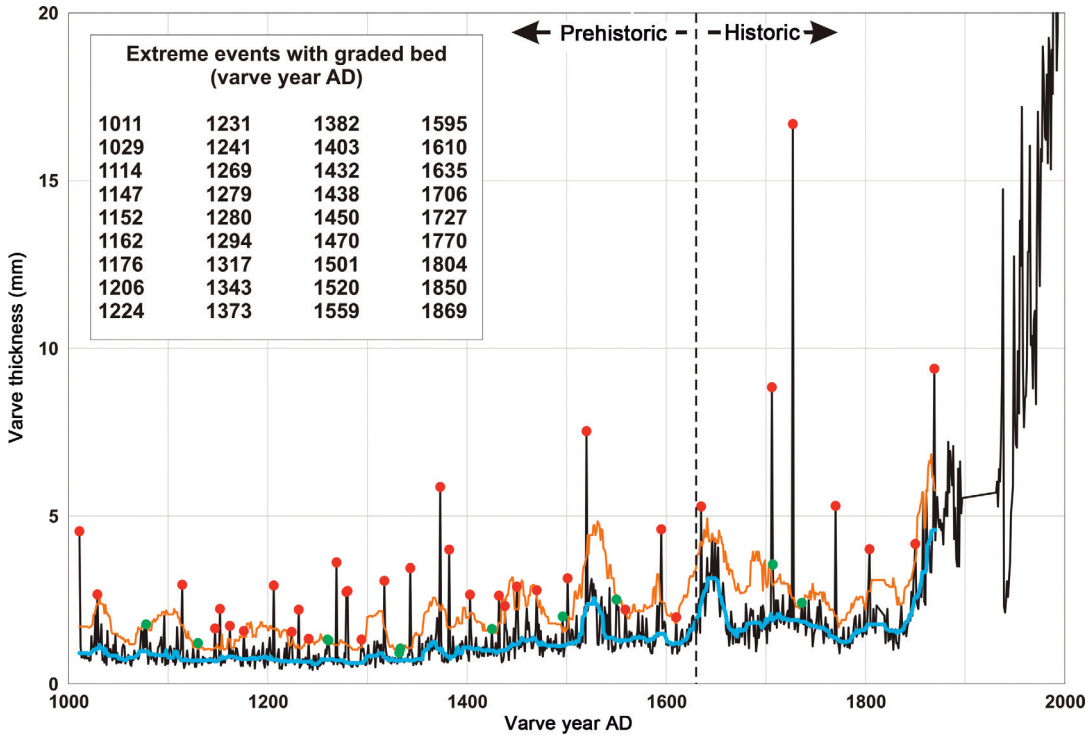


FIGURE 9.6 Varve thickness in Lower Mystic Lake, Boston, Massachusetts, from AD 1011-1870, and the years of extreme events. Varve thicknesses (mm) are plotted in the lower black line. The thickened blue line shows a robust estimate of the time-dependent background thickness based on median smoothing with a 17 year window. The upper orange line represents a statistically-determined threshold, above which varve thicknesses were classified as extremes. Of the 47 identified extreme events, the 36 which contain a graded bed (characteristic of historic hurricane events) are marked by filled black circles and listed in the inset table, and the 11 which do not contain a graded bed are marked by open black circles. The dashed vertical line at 1630 indicates the prehistoric/historic boundary for the region. *From Besonen et al. (2008).*

Phytoliths are morphological distinctive deposits of opaline silica, found in many higher plants. Because they are highly resistant, these "plant stones" remain long after the plant that secreted the phytoliths has decayed. They may then be transported by streams or the wind and deposited in lakes and marine sediments (or incorporated into terrestrial deposits, such as loess) (Piperno, 2001). Phytolith analysis is far less common than pollen analysis, but it can provide complementary data to help refine palynological interpretations that may be ambiguous or provide surrogate plant distribution data where pollen is absent or has not been well preserved (e.g., Barboni et al., 1999). Phytoliths have been especially useful in discriminating between changes in types of grassland vegetation over time (and associated climatic conditions) as different grassland types produce phytoliths with distinctive morphologies (Alexandre et al., 1997). The prospect of direct paleotemperature reconstructions from fossil phytoliths was demonstrated by Fredlund and Tieszen (1997), who showed that distinct phytolith assemblages are associated with a range of modern grasslands, spanning a temperature

gradient across the North American Great Plains. This enabled them to estimate that temperatures were 7-8 °C lower in Kansas and Nebraska during the Late Pleistocene. Quantitative estimates of climatic conditions in the South Island of New Zealand were obtained from phytoliths by Prebble et al. (2002). They developed transfer functions, based on modern climatic conditions associated with particular vegetation types that produce distinctive phytoliths, and applied these to the down-core phytolith record (Prebble and Schulmeister, 2002). In this region, effective precipitation and soil pH are the major controls on the vegetation (and associated phytolith) distribution in modern samples, rather than temperature alone.

9.4 OSTRACODS

Biological productivity in lakes is, in part, climatically dependent and so the remains of organisms that lived in the water column can be of paleoclimatic significance (Battarbee, 2000). For example, different species of ostracods (small bivalved crustaceans, typically ~0.5-2.5 mm in size) are especially common in alkaline, Ca^{2+}-rich lakes. Ostracods are sensitive to a number of variables, including water chemistry (especially anion composition), water depth, and, to some extent, temperature (Holmes, 2001; Schwalb, 2003). Determining which parameters are of importance requires detailed studies of the lake in question, and of the species of ostracods being examined, to decipher the often complex interplay of competing factors involved in ostracod ecology. Nevertheless, in some cases, ostracod assemblages have proven helpful in the interpretation of paleoclimatic conditions. For example, ostracod assemblages (which have known salinity tolerances) were identified in Late Pleistocene and Holocene sediments from the Bolivian Altiplano as diagnostic of water-level changes, from the extensive Minchin lacustrine phase of the Late Pleistocene to the isolated salar lakes of the Early Holocene (Wirrman and Mourguiart, 1995). Megalake Minchin reached over 60,000 km^2 in area and was relatively fresh, but lake levels fell by over 100 m after ~21 ka BP, leading to isolated saline lakes such as the modern-day Salar Uyuni. Similarly, Holmes (1998) found that ostracod assemblages typical of different water depth habitats could be used to determine how lake-level variations (and hence P-E) had varied over time in Wallywash Great Pond, Jamaica. Trace element chemistry of ostracod shells has also been used in paleoenvironmental studies, particularly the ratios of Sr/Ca and Mg/Ca, but the interpretation of such changes is not straightforward and may differ from one lake system to another, depending on the specific water chemistry (Holmes, 1996; Holmes and Engstrom, 2003). The most successful investigations have involved combining studies of ostracod geochemistry (including oxygen isotopes, discussed later) with ostracod trace element geochemistry and other proxies that may be available in the sediments (pollen, diatoms, chironomids, etc.) (cf. Gasse et al., 1987; Chivas et al., 1993; Holmes et al., 1997).

9.5 DIATOMS

Siliceous microfossils are an important component of many lake and wetland sediments and account for the bulk of biogenic deposition in many lakes. Siliceous organisms include diatoms, sponges, and protozoan plates, but so far, only diatoms have proven to be important

in paleoclimatic reconstructions. Diatoms are unicellular algae (of the class Bacillariophyceae) that are sensitive indicators of lake water temperature and water chemistry (pH, dissolved oxygen, salinity, and nutrient content, particularly nitrogen and phosphorus) (Battarbee et al., 2001; Mackay et al., 2003; Smol and Stoermer, 2010). Certain diatoms are especially diagnostic of changes in salinity (Gasse et al., 1997). Diatoms have very distinct morphologies that enable individuals to be identified to species level in most cases. This provides the opportunity for very powerful discrimination of the important environmental parameters to which specific diatoms respond. These responses are commonly identified through collections of surface sediments from a wide range of lakes in which different modern conditions of temperature, pH, water chemistry, etc., have also been measured (a "training data set"). Diatom assemblages are calibrated with environmental variables in the training data set to determine which factors are of primary significance (Birks, 2010; Fritz et al., 2010b; Juggins and Birks, 2012). For example, Fritz (1990) determined that salinity was the main control on diatom assemblages in a set of 55 (largely closed basin) lakes, spanning a wide range of salinity, from the northern Great Plains of the United States. Each diatom taxa had an optimum salinity tolerance. Once this was established, down-core assemblages were used to estimate paleosalinities of the lake water, by calculating a weighted mean of the optimum salinity for each taxa present in the assemblage at each level in the core. Instrumental records of salinity from Devils Lake, North Dakota, taken over the last century confirmed the validity of the reconstructions. In a similar study, Laird et al. (1998) compared their diatom-based salinity reconstruction (from Moon Lake, North Dakota) to an instrumentally derived drought index, showing a strong correlation over the last century (Figure 9.7). The Moon Lake sediments show that the lake was an open system with low salinity in the Early Holocene (characterized by the freshwater diatom, *Stephanodiscus minutulus*), but it had become an increasingly saline closed lake by ~7300 years BP dominated by the saline diatom *Cyclotella choctawhatcheeana* (Laird et al., 1996). Dry conditions continued for much of the Holocene, but it became wetter, leading to lower salinity, over the last 2500 years. High-resolution analysis of the last two millennia provides a detailed picture of drought conditions, with a sample resolution of ~5 years (Figure 9.7). This reveals that the area was relatively wet during the Little Ice Age (especially in the fourteenth and early nineteenth centuries)—perhaps wetter than at any time since the Early Holocene. Before ~AD 1200, much drier conditions prevailed, with episodes that were even drier than the "Dust Bowl" drought years of the 1930s.

Diatoms have also proven useful in paleotemperature reconstructions in areas where temperature is the dominant environmental control, such as in alpine and high-latitude regions (Pienitz et al., 1995; Lotter et al., 2010). Korhola et al. (2000) sampled 38 lakes in northern Finland, spanning a July air temperature gradient of ~6 °C. Canonical correlation analysis (CCA) was used to assess the relationship between the physical and chemical conditions in each lake, in relation to modern (core-top) diatom assemblages. This showed that temperature is the primary variable influencing diatom assemblages in the region, and the relationships so derived were then applied to Holocene sediments from Lake Tsuolbmajavri (Figure 9.8). Temperatures reached a maximum ~6200 cal. years BP, declining to low values around ~4000 years BP. There was a slight warming trend to ~1000 years BP, but much colder conditions—almost as cold as at any time in the entire record—occurred during the Little Ice Age.

In some situations, total biogenic silica (BioSi: the amorphous silica content of sediments) is used as a proxy for diatom productivity, as diatoms are generally the dominant form of

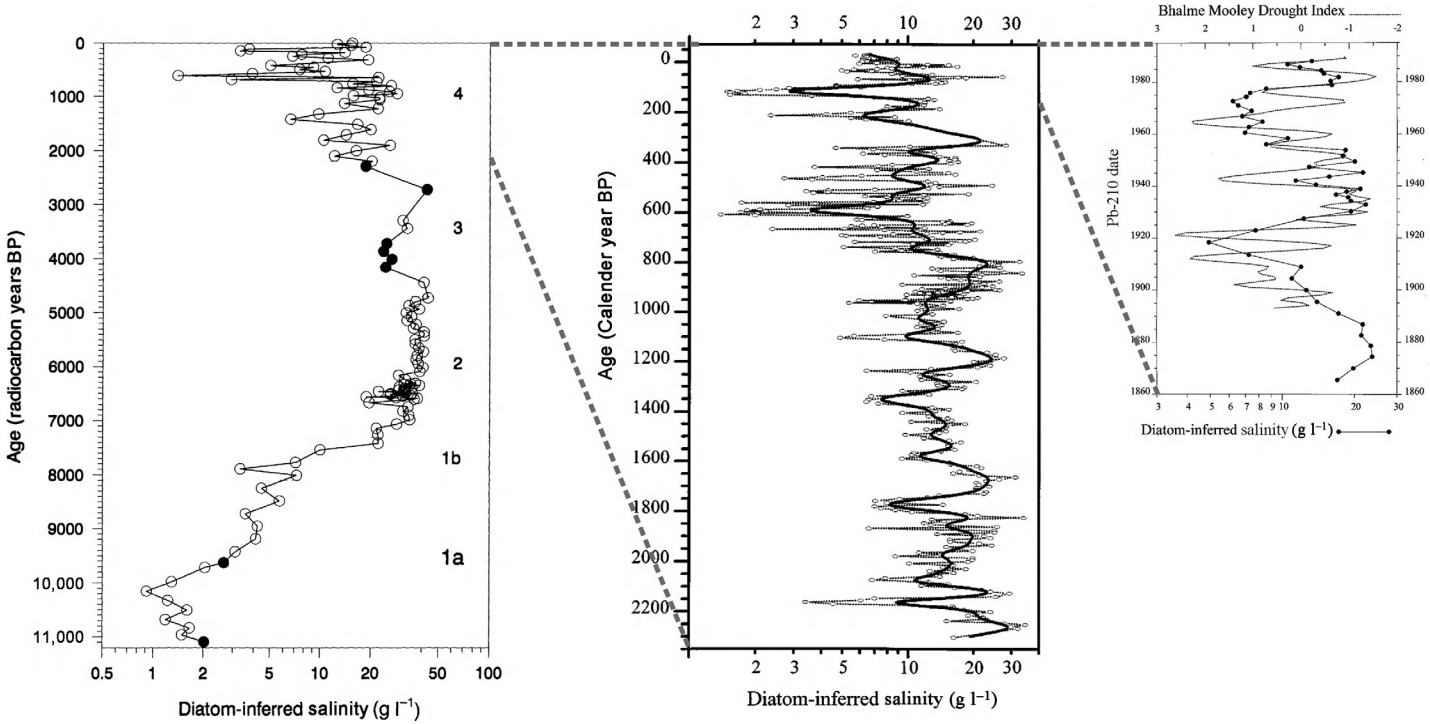


FIGURE 9.7 Diatom-based salinity reconstructions for Moon Lake, North Dakota, United States (left) record of the last 11,000 radiocarbon years, (middle) record of the last 2300 cal. years, and (right) record of the last ~100 years, compared to a drought index derived from nearby instrumental data (drought increasing to the right). *From Laird et al. (1996, 1998).*

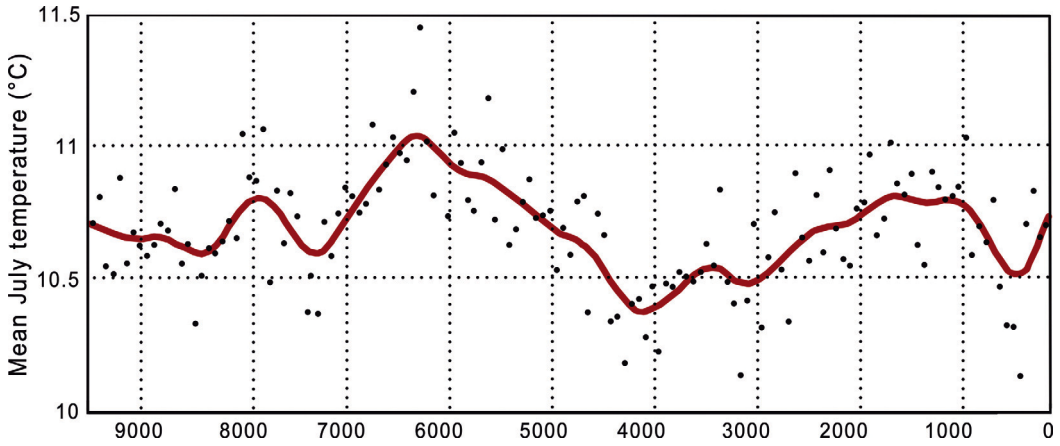


FIGURE 9.8 Reconstructed mean July temperatures at Lake Tsuolbmajavri, northwest Finland, for the last 10,000 years. The dots are average values of reconstructed temperatures produced by four different prediction models. Sample-specific prediction errors, estimated by 500 Monte Carlo simulations, ranged between 0.9 and 1.1 °C for the different models, with higher errors in the lower (older) strata. *From Korhola et al. (2000).*

biogenic silica (Conley and Schelske, 2001). In Lake Baikal, for example, dissolution of diatoms precludes a meaningful interpretation of changes in diatom assemblages in the sediments. However, dissolution is considered to have been relatively constant over time, so changes in total BioSi reflect overall changes in lake productivity (Colman et al., 1995). Figure 9.9 shows the record of biogenic silica in Lake Baikal over the last 0.8 Ma. The variations are similar to those seen in the marine benthic foram isotopic record (of global ice volume) with highest diatom productivity during interglacial times and very low productivity in glacial periods. Diatom productivity is related to the heat balance of the lake (which controls water column structure and nutrient distribution) and this in turn reflects insolation forcing (Prokopenko et al., 2001). Considering Lake Baikal's relatively high-latitude location (51.5-56°N), the record shows a surprisingly weak obliquity signal, with eccentricity and precessional frequencies dominating the record, especially over the last 400 ka (Williams et al., 1997).

Numerous other examples of the use of diatoms in paleoenvironmental and paleoclimatic reconstruction are provided in Smol et al. (2001), Pienitz et al. (2004), and Smol and Stoermer (2010). Some examples of the use of stable isotopes in diatom silica are discussed in the following section.

9.6 STABLE ISOTOPES

Isotopes of oxygen and carbon (and to a minor extent nitrogen) have provided valuable insights into paleoenvironmental and paleoclimatic conditions (Leng, 2006; Leng and Henderson, 2013). Oxygen isotopes in carbonates are especially important. These are derived either from biogenic sources (ostracods, aquatic snails, and mollusks) or from authigenic (endogenic) calcite (marl and micrite) that may be precipitated directly from the water column when it becomes saturated with respect to calcium carbonate. In closed-basin lakes,

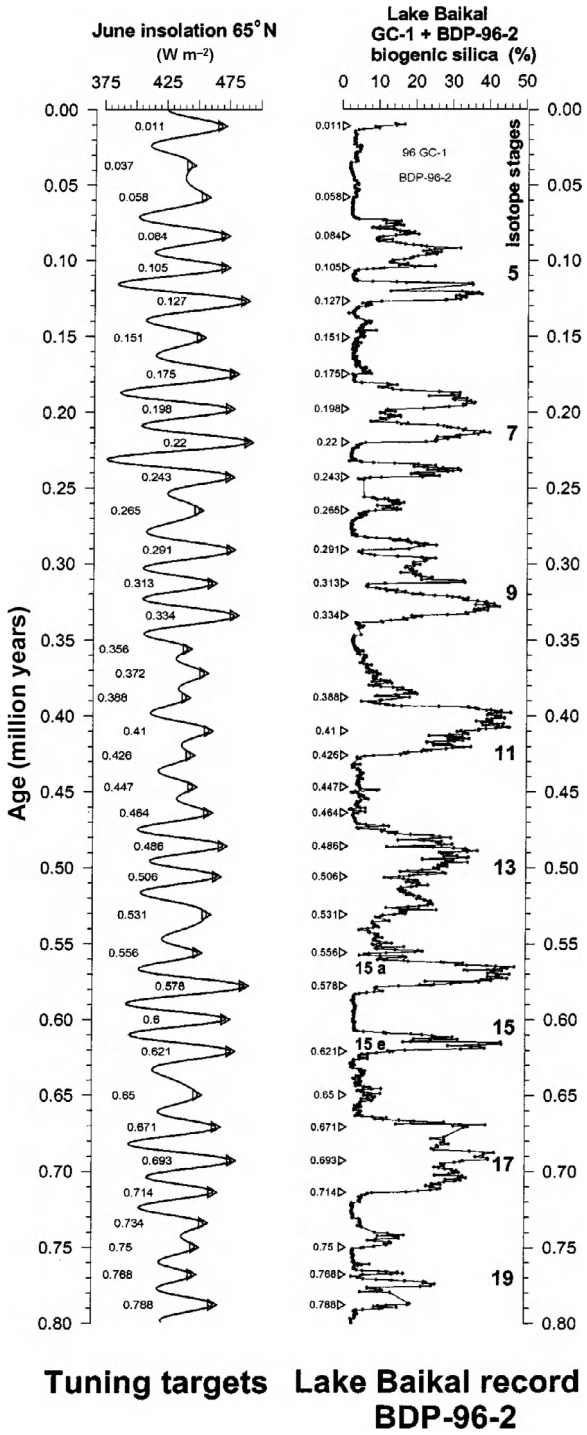


FIGURE 9.9 Biogenic silica record from Lake Baikal, Russia. The Lake Baikal sediment record was tuned to June insolation at 65°N using the corresponding warm peaks as tie points. Tie points are indicated as open arrows labeled with age in MY BP both on the insolation curve and on the tuned BioSi record. Marine isotope stages are shown on the right side of the graph. High levels of biogenic silica correspond to interstadials and interglacials. *From Prokopenko et al. (2001).*

precipitation of authigenic carbonate may occur due to evaporation, increasing the concentration of dissolved minerals, or it may result from photosynthesis by algae and macrophytes, which remove carbon dioxide, leading to supersaturation with respect to calcium carbonate. This commonly occurs due to seasonal algal blooms, which result from overturning of the water column and an increase in nutrients within the photic zone. When this happens, the increased demand for carbon dioxide leads to dissociation of calcium bicarbonate [$Ca^{2+}2HCO_3^-$] and the formation of calcite ($CaCO_3$), which is then precipitated.

The oxygen isotopic composition of calcite is a function of the isotopic composition of the water body and the water temperature at the time of calcite formation (bearing in mind that this may only occur during a particular season). Under conditions of isotopic equilibrium, $\delta^{18}O$ decreases by $\sim$0.23‰ $°C^{-1}$ increase in water temperature (it is important to determine if all the carbonate is calcite as $CaCO_3$ in the form of aragonite is enriched with respect to calcite by $\sim$0.6‰, and dolomite ($CaMgCO_3$) is enriched even more, by an additional $\sim$2.4‰).

Empirical studies indicate that temperature approximates to the following formula (Leng and Marshall, 2004):

$$T(°C) = 13.8 - 4.58(\delta_c - \delta_w) + 0.08(\delta_c - \delta_w)^2$$

where δ_c and δ_w are the $\delta^{18}O$ values of authigenic calcite and lake water, respectively. Biogenic carbonates (in ostracods and aquatic snails and mollusks) are generally formed at particular times of the year (depending on the species) and they also may have a species-specific offset (vital effect) that must be accounted for. For example, in the benthic ostracods *Candona* spp., $\delta^{18}O$ is +2.3‰ compared to calcite formed in isotopic equilibrium (von Grafenstein et al., 1994). Notwithstanding these issues, whatever the source of the calcite that is analyzed, the isotopic composition of the lake water is a critical variable. If δ_w has remained constant, temperature will be a simple function of $\delta^{18}O$ in the carbonate, but if δ_w changed, the problem is more complex. In fact, the $\delta^{18}O$ of precipitation and temperature have probably both varied over time, so obtaining a unique solution to the equation is difficult unless some independent estimate of one or the other parameter can be derived. von Grafenstein et al. (1996, 1999) solved this problem (in Lake Ammersee, Southern Germany) by analyzing benthic ostracods (*Candona* spp.), which are known to calcify in the deepwater of the lake where temperatures have remained nearly constant, close to 4 °C (the maximum density of water). Changes in $\delta^{18}O$ were thus due to variations in the $\delta^{18}O$ of inflowing water, which is almost identical to that of the local annual precipitation since the residence time of water in the lake is $<$3 years (Figure 9.10). Variations in $\delta^{18}O_p$, so derived, show a very high correlation with $\delta^{18}O$ variations in the GRIP (Greenland) ice core over the last 15,000 years, suggesting that both sites, situated on opposite sides of the North Atlantic, recorded isotopic variations that reflect large-scale changes in thermohaline (and associated atmospheric) circulation in the North Atlantic Basin (von Grafenstein et al., 1999).

In closed-basin lakes, a further complication arises because evaporation leads to the preferential removal of water containing the lighter isotope (^{16}O), leaving the residual water enriched in ^{18}O. This effect is generally assessed by plotting the ^{18}O of lake water in relation to δD. On a global scale, the relationship approximates to

$$\delta D = 8\delta^{18}O + 10$$

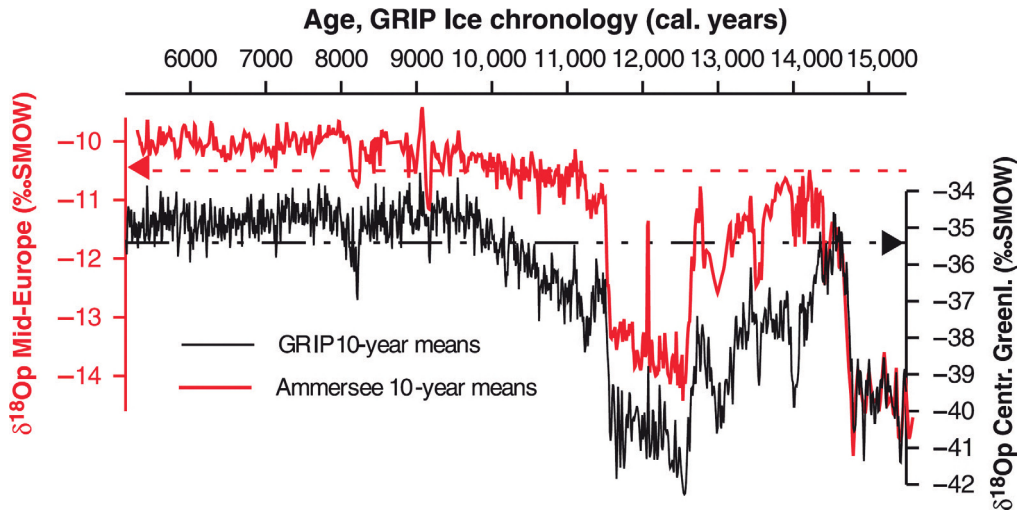


FIGURE 9.10 $\delta^{18}O$ of precipitation derived from analysis of benthic ostracods in Lake Ammersee, Southern Germany, compared to $\delta^{18}O$ in the GRIP ice core, Greenland (both records are 10-year averages). Modern $\delta^{18}O$ average (over the last 30 years) is represented by dashed lines and arrows. Similarities in the two record reflect circulation changes in the North Atlantic region that affect a wide area, though at times there were changes in Europe (e.g., at 12,000 BP) that were not recorded in Greenland, indicating a meridional contrast in North Atlantic circulation, with Europe warm, while Greenland remained cold. *von Grafenstein et al. (1999).*

which is known as the global meteoric water line (GMWL) (Ito, 2001; Leng, 2003). Evaporation leads to isotopic enrichment of both deuterium and ^{18}O, resulting in an offset (the local evaporation line, LEL) from the GMWL. The greater the amount of evaporation (interpreted as lower humidity and/or higher wind speed), the larger the offset of the LEL from the GMWL (Figure 9.11). Variations of $\delta^{18}O$ in closed-basin lakes are generally much greater than in open-system lakes, reflecting changes in local water balance (precipitation minus evaporation, P – E). For example, in Punta Laguna, a closed-basin lake in Quintana Roo, Mexico, the $\delta^{18}O$ of lake water is ~5‰ heavier than rainfall or groundwater, due to evaporative enrichment. In a sediment core from the lake, $\delta^{18}O$ in ostracods, *Cytheridella ilosvayi*, and gastropods, *Pyrgophorus coronatus*, show parallel changes over the last 3500 years, with a period of significant enrichment (more ^{18}O) from ~400 to 1100 AD (Curtis et al., 1996). This is interpreted as a time of increased evaporation and lower precipitation (i.e., lower P-E). Similar changes are seen in sediments from Lake Chichancanab (Yucatan, Mexico) where there is also an increase in gypsum precipitation (seen as an increase in % sulfur) at the time of maximum $\delta^{18}O$ values, which confirms the interpretation of more arid conditions during this interval (Figure 9.12) (Hodell et al., 1995, 2005). This is a particularly interesting time as it coincides with a dramatic reduction in the population of Yucatan (the "Mayan Collapse"), suggesting that a prolonged and unprecedented drought (unique in duration and intensity in the last 7000 years at Lake Chichancanab) was largely responsible for the sudden population demise. Records of titanium in a marine sediment core from the Cariaco Basin (~2500 km to the southeast), an index of rainfall and sediment transport from the adjacent continent, suggest that drought episodes affected a wide area and were especially intense around the ninth century AD (AD 760, 810,

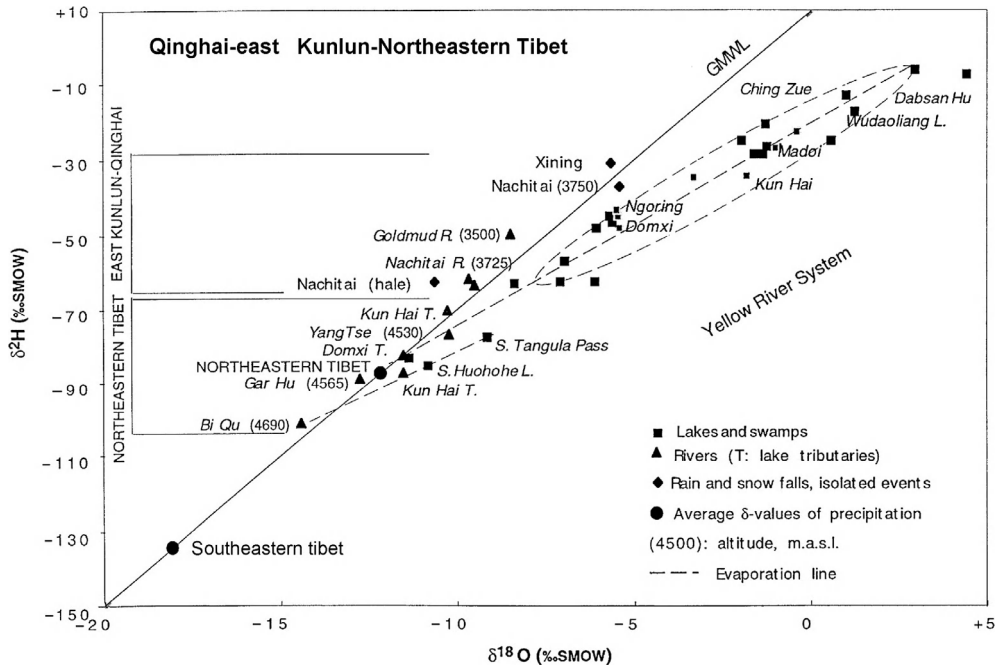


FIGURE 9.11 Isotope content (δ^2H vs. $\delta^{18}O$) of modern waters in northeastern and southeastern Tibet, the east Kunlun region, and the Qinghai Plateau. Open-system lakes plot along the global mean water line (GMWL), but in closed-basin lakes where evaporation exceeds precipitation, the isotopic composition of lake waters departs from the GMWL, defining a local evaporation line (LEL). *From Wei and Gasse (1999).*

860, and 910), which corresponds closely to the end of the Classic Maya cultural period (Haug et al., 2003; cf. Figure 8.18).

In some situations, variations in the $\delta^{18}O$ of carbonates from an open-system lake can be compared to the $\delta^{18}O$ of carbonates from a nearby closed-system lake, to obtain a time series of the differences, which should be a measure of changes in humidity (evaporation) over time. Thus, Anderson et al. (2007) examined two nearby lakes—one open and one closed basin—in the Yukon Territories of Canada that received rainfall of similar isotopic composition and were affected by similar changes in regional temperature. Subtracting isotopic values obtained from carbonates in the closed-system lake from those in the open-system lake provided a measure of changing humidity, with the smallest differences corresponding to periods when humidity was highest (and hence evaporation and isotopic enrichment in the closed lake basin had the least effect) (Figure 9.13). Similar opportunities may be available where ice cores or speleothem records provide an independent measure of the isotopic composition of rainfall over time (cf. Seltzer et al., 2000).

$\delta^{18}O$ in biogenic silica (from diatoms) has also been used to assess past changes in temperature and/or precipitation. No vital effect has been observed for diatom species, so bulk biogenic silica can be used for analysis. Since diatoms live in the photic zone of lakes, $\delta^{18}O$ in biogenic silica ($\delta^{18}O_{Si}$) reflects conditions in the epilimnia of lakes (principally in the summer growth season). $\delta^{18}O_{Si}$ changes by $-0.2‰\ ^{\circ}C^{-1}$ (Moschen et al., 2005) and

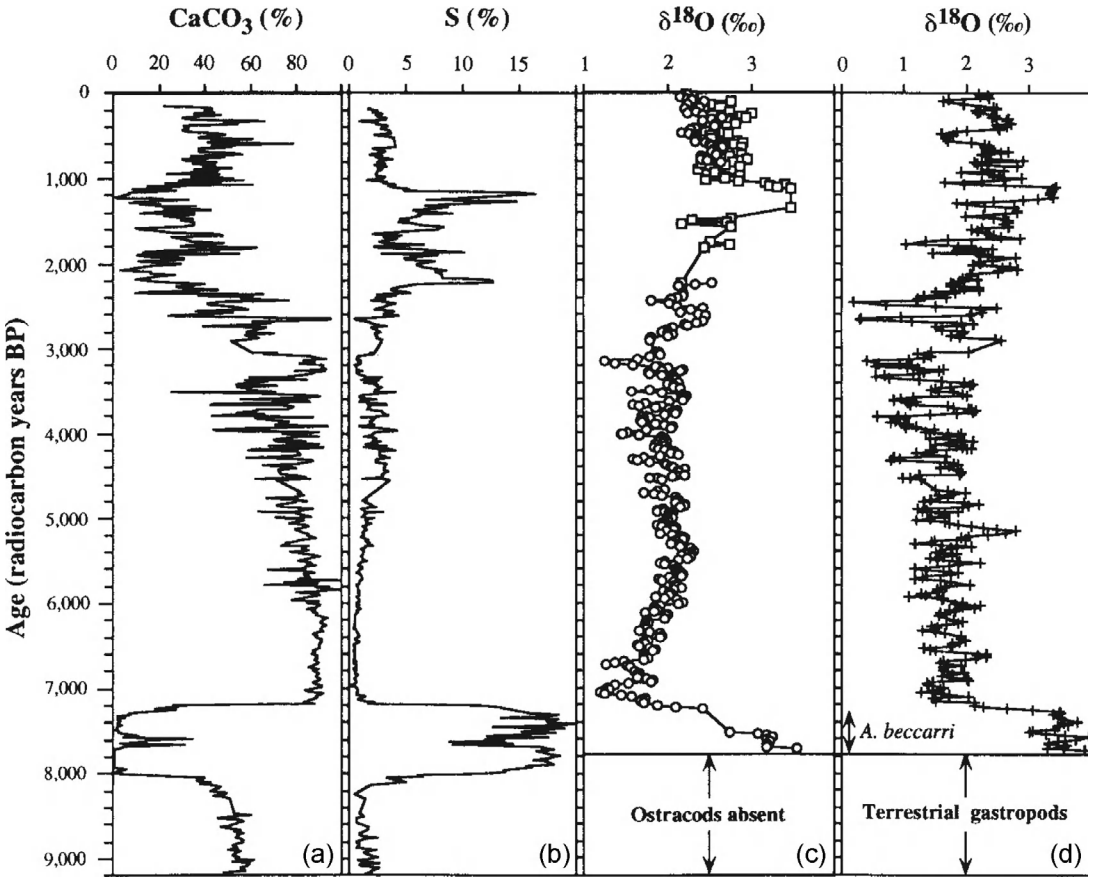


FIGURE 9.12 Sedimentary record from Lake Chichancanab, Yucatán, Mexico, for the last 7000 radiocarbon years. Columns three and four show $\delta^{18}O$ from ostracods (*Cypria ophthalmica*, circles; *Cypronotus* cf. *salinus*, squares) and aquatic gastropods (*Pyrgophorus coronatus*), respectively. Maximum $\delta^{18}O$ corresponds to high % sulfur, which is associated with gypsum deposition under low P-E (dry) conditions. The driest interval of the entire 7000-year record was centered on ~AD 850 ± 50 years, which was when the Classic Maya cultural period came to a sudden end. *From Hodell et al. (1995).*

$$T(^{\circ}\mathrm{C}) = 11.03 - 2.03\left(\delta^{18}O_{Si} - \delta^{18}O_{w} - 40\right)$$

where $\delta^{18}O_{Si}$ and $\delta^{18}O_{w}$ are the isotopic content of biogenic silica and lake water, respectively (Shemesh et al., 2001). Shemesh and Peteet (1998) estimated a decrease of up to 7 °C in surface water temperatures, based on $\delta^{18}O_{Si}$ in a lake in southern Connecticut, United States, from the Allerød to the Younger Dryas. However, this estimate is quite uncertain as changes in the frequency of precipitation from different source regions (and hence changes in $\delta^{18}O_{p}$) could have accounted for much of the change in $\delta^{18}O_{Si}$. Shemesh et al. (2001) and Rosqvist et al. (2004) faced a similar problem in studies of $\delta^{18}O_{Si}$ in lakes in northern Sweden. Independent paleotemperature estimates (from a variety of other proxies) all point to overall cooling in the Holocene, whereas the observed decrease in $\delta^{18}O_{Si}$ corresponds to a warming of at least 7 °C if

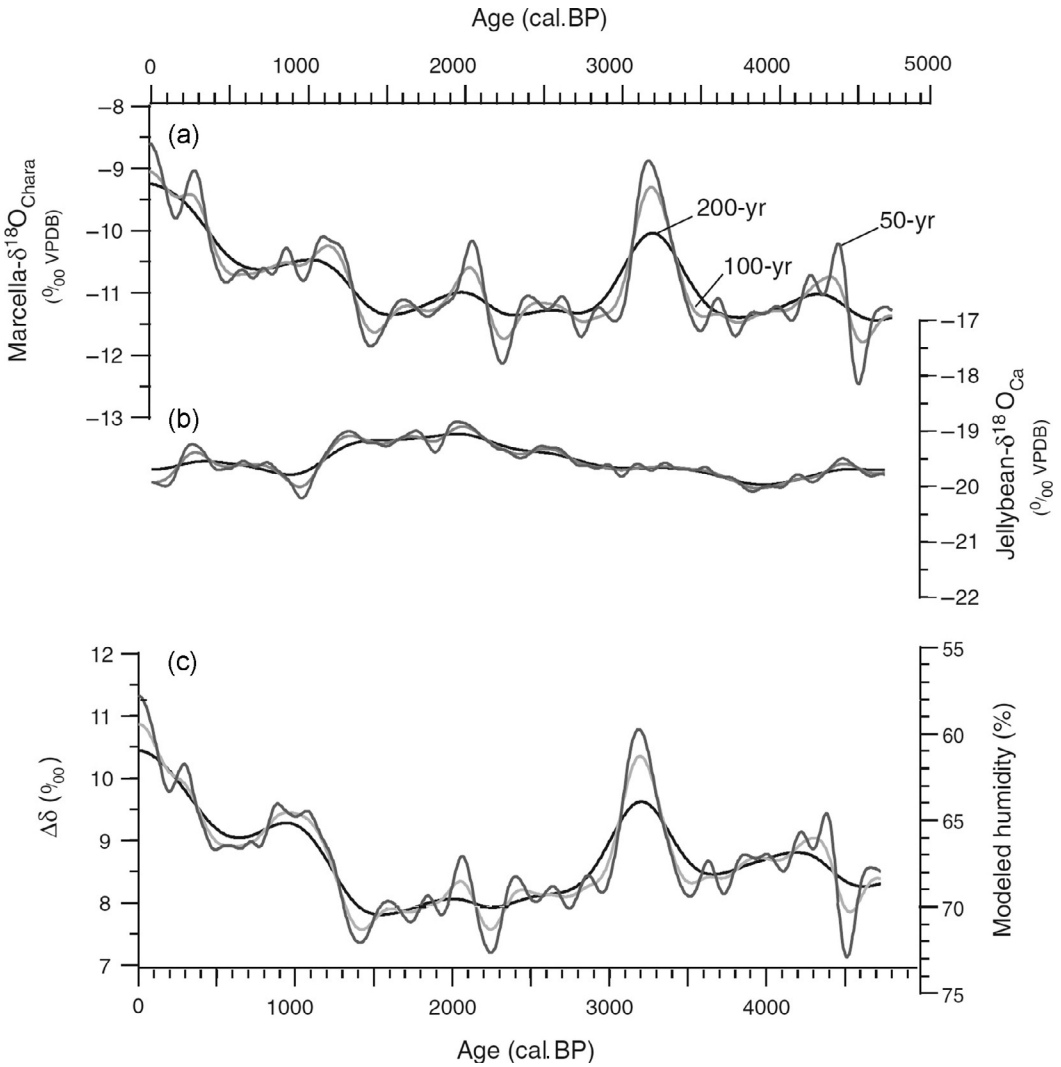


FIGURE 9.13 Oxygen isotope ratios from (a) Marcella Lake and (b) Jellybean Lake, Yukon Territory, Canada, on a calibrated age scale, (showing 200-, 100-, and 50-year smoothing). The difference between (a) and (b) is shown in (c), which reflects changes in the amount of isotopic enrichment ($\Delta\delta$) due to lower amounts of evaporation under conditions of higher humidity in the past (estimated at right, note inverted scale). Mean annual relative humidity for the site over the last 100 years is ~60%. *From Anderson et al. (2007).*

temperature was the only factor involved. They interpret the decrease in $\delta^{18}O_{Si}$ as due to an increase in the frequency of cold air masses and associated precipitation (more depleted in ^{18}O than early Holocene precipitation that originated from more southerly latitudes) (Rosqvist et al., 2004). Based on the modern relationship between $\delta^{18}O_p$ and mean annual temperature across Lapland, (1.86‰ $°C^{-1}$), Shemesh et al. (2001) estimated a cooling of ~2.5 °C, to account for the observed decrease in $\delta^{18}O_{Si}$ over the course of the Holocene.

Oxygen isotopes have also been derived from (algal) cellulose in the fine-grained organic fraction of lake sediments (Edwards, 1993; Abbott et al., 2000; Wolfe et al., 2001) and from the chitinous head capsules of chironomids (Wooller et al., 2004). In all cases, the complex relationships between the $\delta^{18}O$ of precipitation, lake water, and temperature must be carefully deciphered before a reliable paleoclimatic reconstruction can be obtained.

The isotopic composition of carbon, in organic matter and in carbonates deposited in lakes, provides additional insight into paleoclimatic and paleoenvironmental changes. Atmospheric carbon dioxide has a $\delta^{13}C$ value of −7‰ and plants acquiring CO_2 to produce cellulose via photosynthesis preferentially take up ^{12}C rather than ^{13}C. This fractionation is about −20‰ for C_3 plants (resulting in $\delta^{13}C$ of ∼ −27‰) and 4-6‰ for C_4 plants (resulting in $\delta^{13}C$ of −11‰ to −13‰). In C_4 plants that use the CAM pathway (see Appendix A, Section A.2), the fractionation can be even greater (as much as −20‰). Thus, all things being equal, a decrease in the $\delta^{13}C$ of organic matter could reflect an increase in the relative contribution of C_3 versus C_4 plant organic matter from the watershed, perhaps indicating an increase in rainfall, or P-E (Meyers and Lallier-Vergès, 1999). But algae in the lake also contribute to the organic matter in sediments; algae typically have $\delta^{13}C$ of −25‰ to −30‰ (sometimes even lower), so the percentage of aquatic versus C_3 or C_4 terrestrial material determines the overall (bulk) $\delta^{13}C$ of organic matter. Furthermore, preferential removal of ^{12}C by algae will enrich the total dissolved *inorganic* carbon (TDIC) of lake waters with ^{13}C (especially so in closed-basin lakes) and this will then be reflected in the $\delta^{13}C$ of any biogenic or authigenic carbonates produced. A further complication arises if aquatic plants utilize HCO_3^- rather than CO_2 in photosynthesis, as HCO_3^- in equilibrium with CO_2 has $\delta^{13}C$ values ∼10‰ higher than CO_2 (i.e., ∼+2‰). Thus, if there was a shift of algal utilization from CO_2 to HCO_3^- (for example, if productivity increased rapidly leading to a limitation in the CO_2 source or if pH increased, favoring HCO_3^- utilization over CO_2 in the water column), the $\delta^{13}C$ of organic matter would increase accordingly. Of course, none of these factors are known *a priori*, when considering how to interpret a sedimentary record of $\delta^{13}C$ in organic matter or in carbonates, and so other parameters must be considered to effect a meaningful interpretation. One helpful measure is the ratio of total carbon to total nitrogen (C/N). Aquatic algae have a higher nitrogen content than terrestrial plants and so a low C/N ratio indicates aquatic algae are the dominant source of carbon in the sediments. It is worth noting too that the carbon isotopic composition may vary considerably from the epilimnion of lakes to the hypolimnion (especially seasonally) so the location where biogenic or authigenic carbonates are produced (i.e., in the photic zone or at depth) can result in quite different $\delta^{13}C$ values. All in all, carbon isotopes are more difficult to interpret than oxygen isotopes, but together with other parameters, they can contribute to a more complete understanding of past climatic conditions. However, the future may hold more promise in the analysis of specific compounds extracted from organic sediments than from undifferentiated bulk samples. Lake sediments generally contain long-chain *n*-alkanes derived from the leaf wax of terrestrial vegetation. Because odd-numbered long-chain *n*-alkanes are a major component of leaf waxes, and their $\delta^{13}C$ content differs significantly between C_3 and C_4 vegetation, the $\delta^{13}C$ composition of *n*-alkanes in sediments can be used as a compound-specific index of the predominant vegetation cover and hence the precipitation-evaporation water balance in the watershed. Typically, C_3 plants have nC_{29} and nC_{31} $\delta^{13}C$ values of −35‰, versus −21‰ for C_4 plants. However, because most sediments will likely contain a mixture of *n*-alkanes from both C_3 and C_4 plants, a mixing model is required (ideally, guided by an

independent parameter, such as pollen) to estimate the relative contributions of different vegetation types (e.g., Huang et al., 2006).

Finally, the δD content of certain algal lipids in lake sediments can be used to track changes in the δD of lake water and thus (in many cases) of meteoric precipitation. In a survey of lake surface sediments across a latitudinal transect through the Eastern United States, Huang et al. (2004) found that phytols, ester-bound palmytic acid, and C_{17} *n*-alkanes were excellent recorders of lake water δD. Furthermore, there did not seem to be any significant temperature-dependent fractionation of hydrogen in the production of the lipids, so this complication is minimized compared to carbonate systems, where changes in both temperature and lake water composition must be understood. The δD of *n*-alkanes derived from terrestrial vegetation reflect (to a first order) the δD of precipitation, but the values can be significantly modified by fractionation during biosynthesis of the compound (on the order of −120‰ to −150‰, for woody vegetation and grasses, respectively; Sachse et al., 2006; Liu and Yang, 2008). Nevertheless, if such effects can be taken into account, δD in leaf wax *n*-alkanes can provide valuable insights into past changes in hydrologic conditions (e.g., Tierney et al., 2010a,b).

9.7 ORGANIC BIOMARKERS

Biomarkers are organic compounds that are produced by specific organisms; when preserved in sediments, they can provide a molecular proxy for the paleoclimatic or paleoenvironmental conditions that influenced the life of the organism (Eglinton and Eglinton, 2008; Gaines et al., 2009; Bianchi and Canuel, 2011). Some of the more important biomarkers in marine sediments are discussed in Chapter 6, Section 6.5, and some of these have also been applied to lake sediments (Castañeda and Schouten, 2011). However, because lakes vary widely in their size, vertical structure, and chemical composition, and often receive large amounts of allochthonous input from their surrounding watersheds, it is not a simple matter to interpret biomarkers from lake sediments in paleoclimatic terms, and site-specific calibrations may be required. Nevertheless, considerable progress has been made in lacustrine biomarker paleoclimatology, and the prospects for further advances seem quite bright.

An important group of lipids that may be useful paleotemperature biomarkers in lakes are the isoprenoid glycerol dialkyl glycerol tetraethers (GDGTs—tetraethers with 86 carbon atoms), which have been discussed in Chapter 6, Section 6.5.2 in the context of SST reconstructions. With an increase in temperature, the Thaumarchaeota (a phylum of single-celled organisms within the domain Archaea) produce GDGTs with more cyclopentane moieties. This provides the basis for the TEX_{86} index, which has been calibrated for SSTs using marine sediment samples from hundreds of locations, ranging from polar to tropical environments. Attempts to obtain a similar calibration from lakes have been less successful (e.g., Blaga et al., 2009; Pearson et al., 2011), though empirical studies reveal a significant relationship between the TEX_{86} indices derived from lake sediment core-top samples in large lake systems, across a wide temperature range (~5-30 °C) (Powers et al., 2010; Tierney et al., 2010a). This was used by Blaga et al. (2013) to reconstruct mean annual temperatures in Lake Lucerne, Switzerland, and similar calibrations were used by Powers et al. (2005, 2011), Woltering et al. (2011), and Tierney et al. (2008, 2010a) to reconstruct mean annual lake surface water

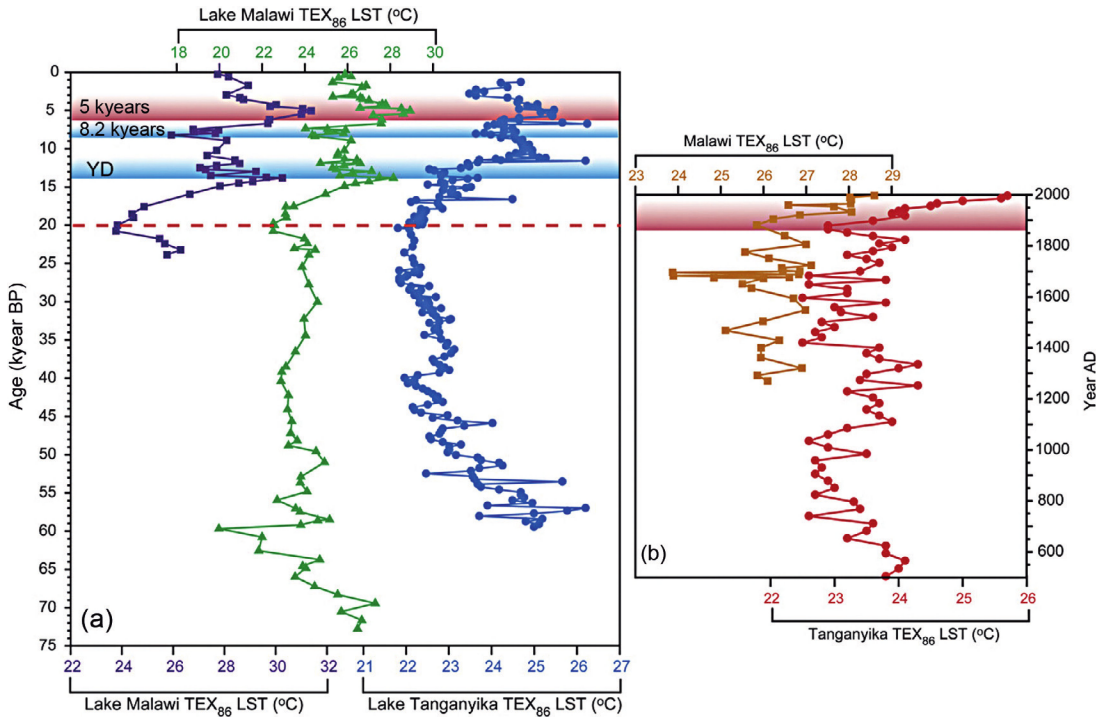


FIGURE 9.14 Lake surface, mean annual temperatures reconstructed from TEX_{86} in sediments from Lake Malawi and Lake Tanganyika. (a) Temperatures over the last 75,000 years and (b) for the last 1500 years. Note that the root mean square error on these reconstructions is ~±2.0-3.5 °C. *Data from Powers et al. (2005, 2011) and Woltering et al. (2011) (for Malawi) and Tierney et al. (2008, 2010a) (for Tanganyika), replotted and compiled by Castañeda and Schouten (2011).*

temperatures in Lake Malawi and Lake Tanganyika (Figure 9.14). The African lake reconstructions show similar features, with warming beginning around 20 ka BP and cooling during the Younger Dryas around 8.2 ka BP, followed by Mid-Holocene warming. The recent record shows significant warming over recent decades compared to the mean of previous centuries.

These reconstructions are the first to apply TEX_{86} in lakes for paleotemperature reconstruction, but there are many uncertainties that have yet to be fully resolved. In particular, methanogenic organisms that produce GDGTs may be present where anoxic conditions occur (these are common in lakes and lake sediments), thus influencing the TEX_{86} value derived from sediments. Thaumarchaeota are also not limited to the photic zone (they are thought to be chemoautotrophs) and so in lakes with a strong thermocline, the depth at which these organisms reside can greatly affect the water temperature in which they develop. Other factors such as the seasonal timing of production, lake water pH, and diagenetic effects on degradation of specific GDGTs all contribute uncertainties to the use of TEX_{86} as a paleotemperature proxy (Castañeda and Schouten, 2011). There are also potential complications related to the input of branched GDGTs from the terrestrial environment. Branched GDGTs contain *n*-alkyl side

chains with 4, 5, or 6 methyl groups and are found in peat and soils and thus may be carried into lakes via rivers and streams. To better distinguish between allochthonous and autochthonous GDGT sources, Hopmans et al. (2004) derived the BIT (branched and isoprenoid tetraether) index, which examines the amount of crenarchaeol (Figure 6.27) relative to soil-derived branched GDGTs. The index was constructed so that it ranges from 0 to 1, where zero represents a purely aquatic source of GDGTs and values >0.9 indicate only a soil source. Thus, the BIT index may be used to trace the delivery of terrestrial organic matter to a lake. However, some studies show that branched GDGTs may also be produced in lakes, which obviously complicates its value. Nevertheless, the BIT index can be a useful way of assessing if GDGTs have a large soil-derived component, and some TEX_{86} studies thus limit analyses to samples in which the BIT index is <0.5-0.6 (e.g., Tierney et al., 2010a). Other indices derived from branched GDGT ratios have also been developed, as proxies for soil pH and mean annual air temperature. The CBT index (cyclization of branched tetraethers) is exponentially negatively related to soil pH, whereas the MBT index (methylization of branched tetraethers) is correlated with mean annual air temperature and pH (Weijers et al., 2007). Initial studies using these indices have yielded mixed results, once again underlining the complex nature of GDGT production in lakes and their surrounding watersheds and highlighting the need for more research to better understand these promising proxies. Meanwhile, *in situ* calibrations and limnological monitoring programs appear to be a necessary prerequisite for reliable interpretations of the various GDGT-based indices (e.g., Sinninghe Damsté et al., 2009).

In the marine environment, SST reconstructions using the relative proportion of long-chain alkenones (C_{37}-C_{38} di- and tri-unsaturated methyl and ethyl ketones, used to derive the $U^{k'}_{37}$ index) are common and considered quite reliable (see Chapter 6, Section 6.5.1). Alkenones are also found in the sediments of many lakes (often dominated by tetra-unsaturated ketones), resulting from their production by haptophyte algae. Studies of lakes in Europe, China, and North America all suggest that alkenones can provide a paleotemperature record, as they do in the marine environment, but the alkenone-temperature relationship may be less universal, perhaps because the types of haptophytes producing alkenones are not the same in all lakes. Thus, regional or site-specific calibrations may be needed to obtain an accurate paleotemperature reconstruction (e.g., Zink et al., 2001; Chu et al., 2005; Toney et al., 2010). This approach allowed D'Andrea et al. (2011) to reconstruct a 5600 year paleotemperature record from two lakes in west Greenland (Braya Sø), which indicates that temperature changes may have played a critical role in the colonization of the Arctic by different cultural groups (Figure 9.15). More widespread use of alkenones in lake sediments for paleotemperature reconstructions requires further research on the different types of haptophyte algae and the environmental factors influencing haptophyte blooms, including their depth distribution and the seasonal timing of alkenone production. It is also important to assess whether there is differential degradation of the di-, tri-, or tetra-unsaturated ketones in the water column and sediments, which would strongly bias a U^{k}_{37} index.

Because of the time-consuming work involved in the extraction and identification of alkenones (or other organic biomarkers) in sediments, it is difficult to produce a very high-resolution record. However, if other related properties can be measured in the same sediment core at a higher resolution, it may be possible to transfer the temperature signal obtained from alkenones to the other proxy, thereby increasing the resolution of the reconstruction. Thus, von Gunten et al. (2012) measured the reflectance spectral properties of a sediment core from

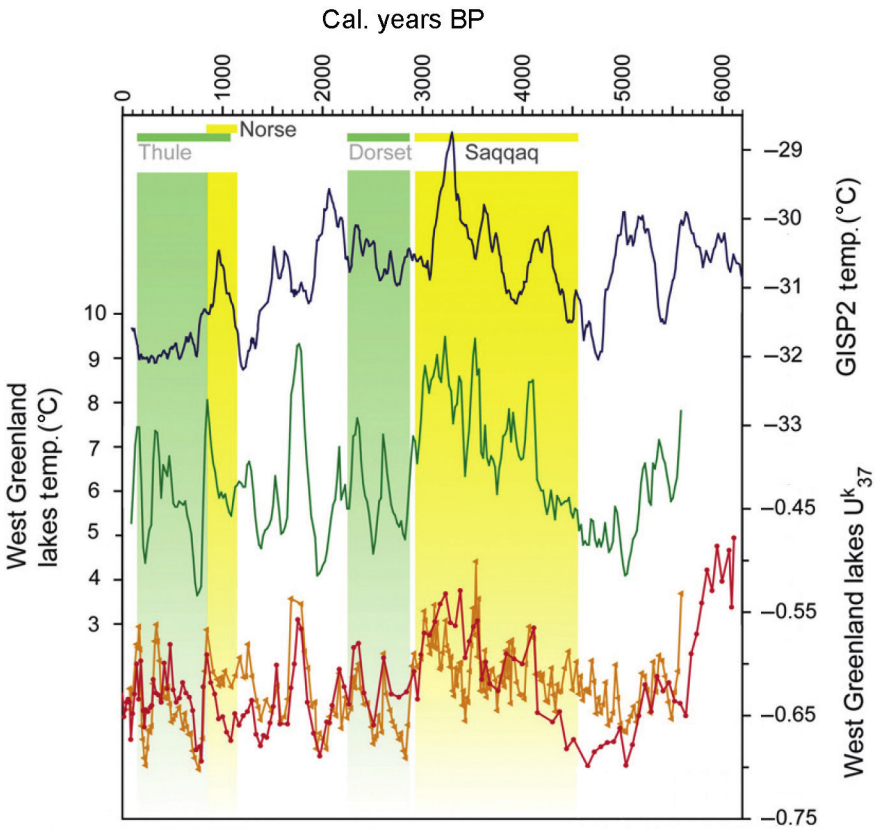


FIGURE 9.15 Late Holocene paleotemperature reconstruction from two lakes in southwestern Greenland using an alkenone unsaturation index (U^k_{37}). Lower line shows the U^k_{37} values from each lake, middle line shows temperature reconstruction, and upper line shows GISP2 temperatures derived from $\delta^{18}O$, assuming a constant relationship with temperature. The U^k_{37} temperature calibration was based on *in situ* measurements of alkenones extracted from the water column from mid-June to mid-July, regressed with the associated water temperatures, combined with a spatially based lacustrine alkenone calibration (by Zink et al., 2001), from sites containing alkenones of similar molecular composition to those in the Greenland lakes. The reconstruction is of summer water temperature, but in this area, air temperatures and lake surface water temperatures are closely correlated. At top, the presence of the principal Inuit cultural groups is noted; the Dorset culture was better adapted to hunting on sea ice and may have fared better in the colder conditions after ~3000 BP. *Data from D'Andrea et al. (2011).*

west Greenland at very high resolution (~2 mm intervals). In the visible color spectrum, chlorin produces a distinctive absorption signal in the range of 660-670 nm, and this can be used to obtain a down-core record of the amount of chlorin in the sediment (relative absorption band depth index: $RABD_{660;670}$) (Figure 9.16). Chlorin molecules are derived from chlorophyll, primarily from autochthonous primary productivity, and therefore, the sedimentary chlorin signal reflects the balance between production in the photic zone and organic matter preservation in the sediments (Rein and Sirocko, 2002; von Gunten et al., 2009). In the sediments from Braya Sø, west Greenland, the $RABD_{660;670}$ index was strongly correlated

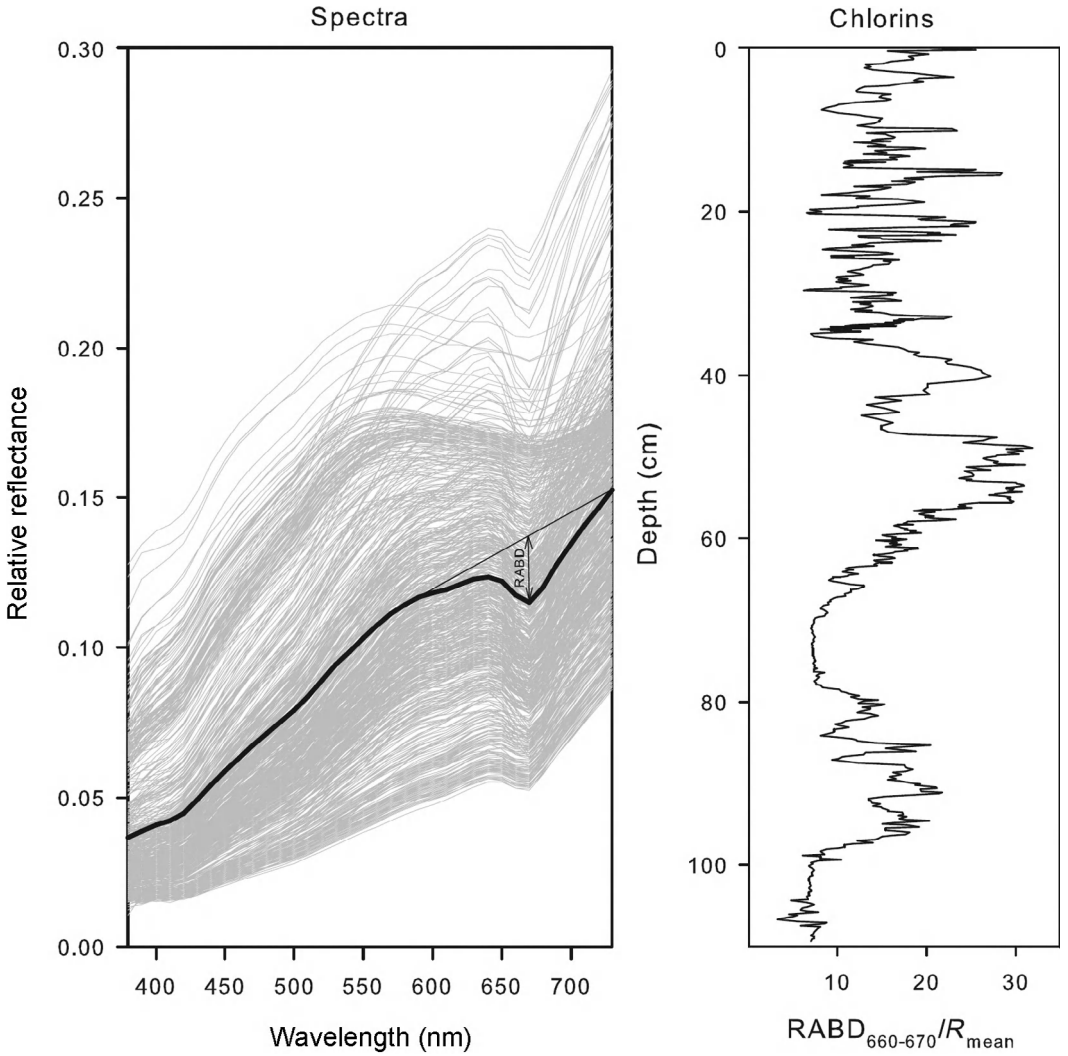


FIGURE 9.16 Visible light spectral properties of a sediment core from west Greenland (Braya Sø) showing the individual spectra from different levels in the sediment core (light gray lines, at left). The relative absorption depth at 660-670 nm ($RABD_{660;670}$) (due to chlorin) is illustrated from one depth in the record (darker line, left panel). Down-core variations in the $RABD_{660;670}$ index are shown in the right panel, indicating the relative variations in the chlorin content of the sediments. *From von Gunten et al. (2011).*

with the lower resolution alkenone paleotemperature record, and so, it was possible to use that relationship to obtain a much higher-resolution paleotemperature reconstruction than could have been obtained from the biomarker index alone (Figure 9.17). In making this proxy-to-proxy calibration, the analysis revealed a strong multidecadal signal that was not detectable from the coarser-resolution alkenone data.

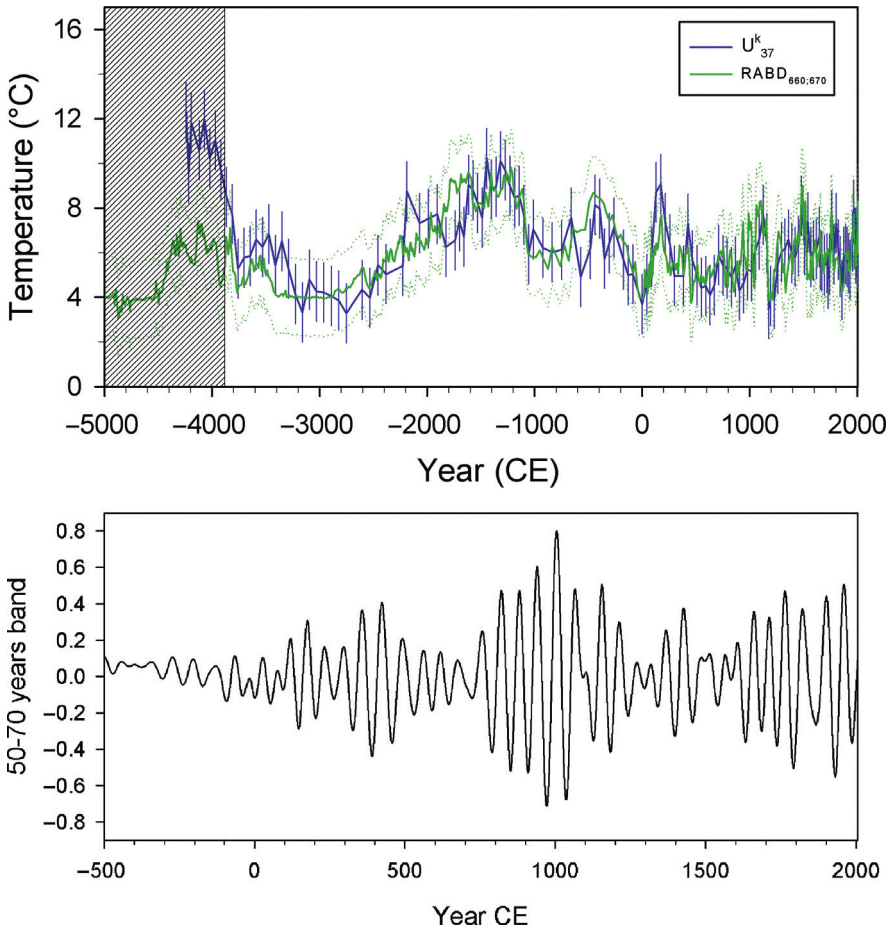


FIGURE 9.17 Temperature reconstruction for Lake Braya Sø, southwestern Greenland, based on U^k_{37} (blue line) and the more highly resolved color spectral data ($RABD_{660;670}$) (green line). The proxy-to-proxy calibration provided a higher-resolution reconstruction which revealed an oscillation at a frequency (50-70 years), which approximates the Atlantic Multidecadal Oscillation (AMO). The lower record shows the same high-resolution record filtered with a 50- to 70-year band-pass, for the last 2500 years, showing significant variations in the amplitude of this "AMO" oscillation. *From von Gunten et al. (2011).*

CHAPTER

10

Nonmarine Geologic Evidence

OUTLINE

10.1 Introduction 345

10.2 Periglacial Features 346

10.3 Snowlines and Glaciation Thresholds 351
- 10.3.1 *The Climatic and Paleoclimatic Interpretation of Snowlines and ELAs* 352
- 10.3.2 *The Age of Former Snowlines* 356

10.4 Mountain Glacier Fluctuations 358
- 10.4.1 *Evidence of Glacier Fluctuations* 359
- 10.4.2 *The Record of Glacier Front Positions* 360

10.5 Lake-Level Fluctuations 362
- 10.5.1 *Hydrologic Balance Models* 366
- 10.5.2 *Hydrologic-Energy Balance Models* 370
- 10.5.3 *Regional Patterns of Lake-Level Fluctuations* 371

10.1 INTRODUCTION

The range of nonmarine geologic studies providing information pertinent to paleoclimatology is vast; indeed, one could argue that virtually all continental sedimentary deposits convey a paleoclimatic signal to some degree. Eolian, glacial, lacustrine, and fluvial deposits are, in large part, a function of climate, though it is often difficult to identify the particular combination of climatic conditions leading to the formation of the deposit. Similarly, erosional features such as lacustrine or marine shorelines, cirques, or other features of glacially eroded landscapes indicate in a general sense a particular type of climate, but quantitative paleoclimatic reconstructions based on this kind of information present real challenges (Flint, 1976). Commonly, climatic inferences drawn from such evidence are qualitative and even dating the features may be very difficult. Nevertheless, such evidence of past changes in climate is ubiquitous, and many innovative approaches to interpreting their paleoclimatic significance have been developed.

Copyright © 2015 Raymond S. Bradley.
Published by Elsevier Inc. All rights reserved.

In this chapter, no attempt will be made to review all of the possible paleoclimate-related geologic and geomorphological phenomena. Instead, discussion will be limited to the smaller number of approaches that have either provided quantitative paleoclimatic data or helped in establishing the chronology of paleoclimatic events.

10.2 PERIGLACIAL FEATURES

The use of fossil periglacial phenomena as an index of former climatic conditions is limited by two basic problems. First, dating periglacial features directly is often difficult, if not impossible; generally, they are dated by reference to the deposits within which they are found, thereby obtaining only a maximum age for the features. Secondly, although regions of modern periglacial activity can be circumscribed by particular isotherms, the occurrence of similar activity in the past can only indicate an upper limit to temperatures at the time, not a lower limit (Williams R.B.G., 1975). Thus, in general terms, permafrost today only occurs in areas where the mean annual air temperature is $<-2\,^{\circ}C$ and it is virtually ubiquitous north of the -6 to $-8\,^{\circ}C$ isotherm in the Northern Hemisphere (Ives, 1974). Evidence of more extensive permafrost in the past, however, only demonstrates that temperatures were below these levels and provides little information on how much lower. Mapping the distribution of relict periglacial features may indicate how far the southernmost boundary of the permafrost zone was displaced, but within this zone, only the limiting maximum paleotemperature estimates are possible. Nevertheless, periglacial features are of particular interest because they provide information about the periods of extreme temperature depression during past glacial episodes. They also provide information about areas close to the ice-sheet margins, for which there are few other sources of proxy paleoclimate data.

It has already been mentioned that permafrost only occurs in areas with mean annual temperatures below a certain level, but permafrost itself may leave no morphological evidence of its former existence. Paleoclimatic inferences can only be based on features that develop in regions of permafrost and disturb the sediments in a characteristic manner. In this way, fossil or relict features can be identified and their distribution mapped (Figure 10.1). The most useful and easily identified features include fossil ice wedges, pingos, sorted polygons, stone stripes, and periglacial involutions (Washburn, 1979a). The problem is to identify those climatic factors that are necessary for the formation of the features in question; commonly, this can only be done in general terms (Table 10.1). Ice wedges, for example, result from thermal contraction at subfreezing temperatures. Winter temperatures of -15 to $-20\,^{\circ}C$ (or less) are required before active frost cracking occurs, but the exact requirements depend on the material being considered. Cracking and ice-wedge formation will occur at higher temperatures in silts and fine-grained material than in gravels where mean annual temperatures of $-12\,^{\circ}C$ may be necessary. Furthermore, the amount of snowfall is a significant factor since snow will insulate the ground surface from the effects of severe cold. This has been demonstrated in many areas where today, active ice-wedge formation does not normally occur; where snow is artificially removed (e.g., from roads or airport runways), frost cracks and ice wedges will develop. Paleoclimatic reconstructions based on such phenomena are thus subject to a certain amount of uncertainty, and similar problems have to be faced when dealing with other types of periglacial features. Nevertheless, it is possible to make conservative estimates of

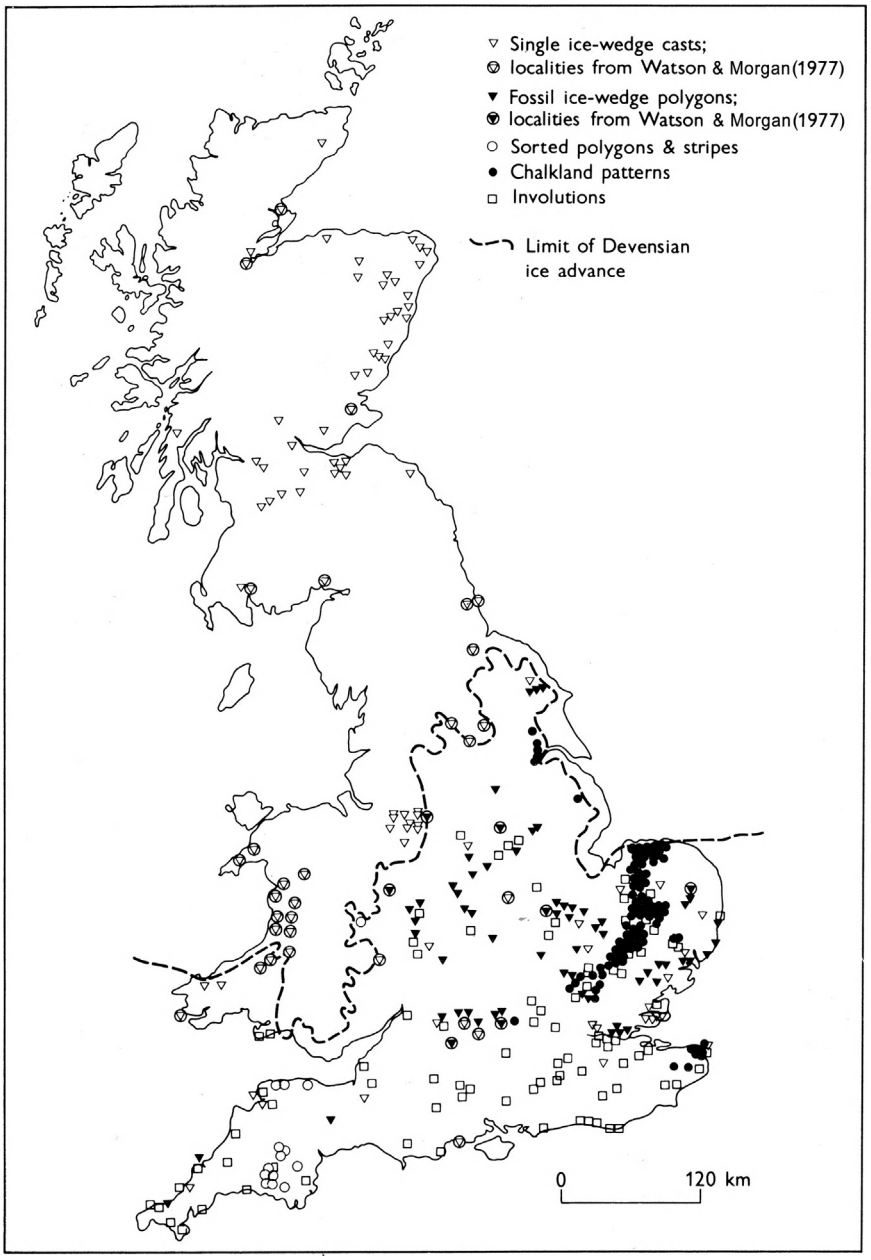


FIGURE 10.1 Distribution of patterned ground of Devensian (=Wisconsin) age in Britain. *After Washburn (1979b).*

TABLE 10.1 Climatic Threshold Values for the Distribution of Periglacial Geomorphic Features

Periglacial Geomorphic Features[a]	Climatic Threshold Values[b] MAT (°C)[c]	MAP (mm)[d]
1. Periglacial geomorphic features whose formation requires permafrost		
1.1. Features connected with continuous permafrost		
Ice-wedge polygons	<−4 to <−8 °C	>50-500 mm
	Other climatic indication: rapid temperature drops in early winter	
Sand-wedge polygons	<−12 to <−20 °C	<100 mm
Closed system pingos	<−5 °C	
1.2. Features connected with discontinuous permafrost		
Open system pingos	<−1 °C	
1.3. Features which occur in connection with continuous, discontinuous, and sporadic permafrost		
Depergelation forms (thermokarst forms, active layer and detachment failures, ground ice slumps, permafrost depressions, alas, baydjarakhs, dujodas, alas thermokarst valleys, beaded drainage, thaw and oriented lakes, thermo-erosional and thermo-abrasional niches, degradation polygons, thermokarst mounds	<−1 °C Other important indication: high ground ice content	
Seasonal frost mounds (frost blisters, hydrolaccoliths, bugors)	<−1 to <−3 °C	
Palsas	<0 to <−3 °C	
Rock glaciers	<+2 to <0 °C	<1200 mm
	Other climatic indications: continental climates with high incoming radiation, sublimation, evaporation, and little snow	
2. Features whose formation requires intense seasonally frozen ground but which also occur in connection with permafrost		
2.1. Seasonal frost-crack polygons (ground wedges)	<0 to <−4 °C; mean of coldest month <−8 °C	
2.2. Frost mounds (thufurs)		
Tundra hummocks (high latitude occurrences)	<−10 °C	
Earth hummocks (high latitude occurrences)	<−6 °C	
Earth hummocks (high altitude occurrences)	<+3 °C	
2.3. Nonsorted circles (mud boils, mud circles)	<−2 °C	>400-800 mm

TABLE 10.1 Climatic Threshold Values for the Distribution of Periglacial Geomorphic Features—cont'd

Periglacial Geomorphic Features[a]	Climatic Threshold Values[b] MAT (°C)[c]	MAP (mm)[d]
2.4. Sorted circles and stripes ($\Phi > 1$ m)[e]	<−4 °C	
2.5. Sorted circles and stripes ($\Phi < 1$ m)[e]	<+3 °C	
2.6. Gelisolifluction microforms (lobes, steps, ploughing blocks)	<−2 °C	
2.7. Nivation and cryoplanation features (nivation hollows, cryoplanation terraces, frost-riven cliffs)	<−1 °C	
3. Features linked to diurnally frozen ground and needle ice but which also occur with seasonally frozen ground and permafrost		
3.1. Miniature polygons		
3.2. Miniature sorted forms and stripes	<+1 °C	
3.3. Microhummocks		

[a] *For a description of these features, see Washburn (1979b) or French (2007).*
[b] *The thermal threshold values represent upper limits for the development of features.*
[c] *Mean annual air temperature.*
[d] *Mean annual precipitation.*
[e] $\Phi = -log_2 d$, *where* d = *sediment diameter (Krumbein's sediment size scale).*
After Karte and Liedtke (1981).

temperature change based on the former distribution of different types of periglacial features (Figure 10.2). Accuracy is really limited by our understanding of the climatic controls on similar contemporary features. From this map, it would appear that mean annual temperatures in Europe were at least 14-17 °C below recent averages during the maximum phase of the last (Wisconsin/Wurm/Weichsel) glaciation (Washburn, 1979b). Although many features used to compile the map are not well dated, and often are simply considered to reflect conditions during the maximum stage of the last glaciation, it is worth considering the point made by Dylik (1975) that maximum temperature depression was generally not coincident with the maximum extent of ice (maximum "glaciation"). Dylik considers the extent of glacier ice to be more of an index of snowfall (i.e., of cold and humid conditions) than simply of low temperatures. Periglacial features may thus achieve their maximum development during periods of minimum temperature *prior to* the maximum extent of major ice sheets; this may explain the large discrepancy between botanically derived paleotemperatures for the last glacial maximum (sometimes indicating mean annual temperatures only 3-6 °C below those of today) compared with paleotemperature estimates derived from periglacial phenomena.

Where a variety of periglacial features of varying ages can be identified in a limited area, it may be possible to reconstruct paleotemperature through time. This has been attempted by Maarleveld (1976) using observations of relict periglacial features in the Netherlands (Figure 10.3). Maarleveld associated each type of feature with particular temperature

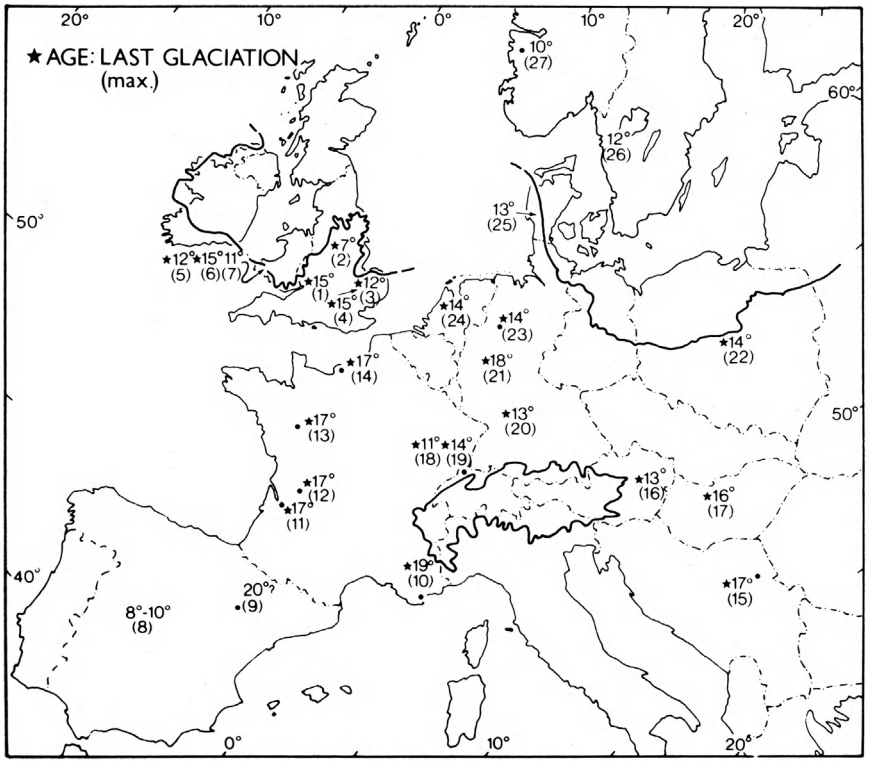


FIGURE 10.2 Temperature increases in Europe since the last glacial maximum, based on periglacial features. Increases are minimum estimates. Maximum ice limits are shown as heavy lines. *After Washburn (1979a).*

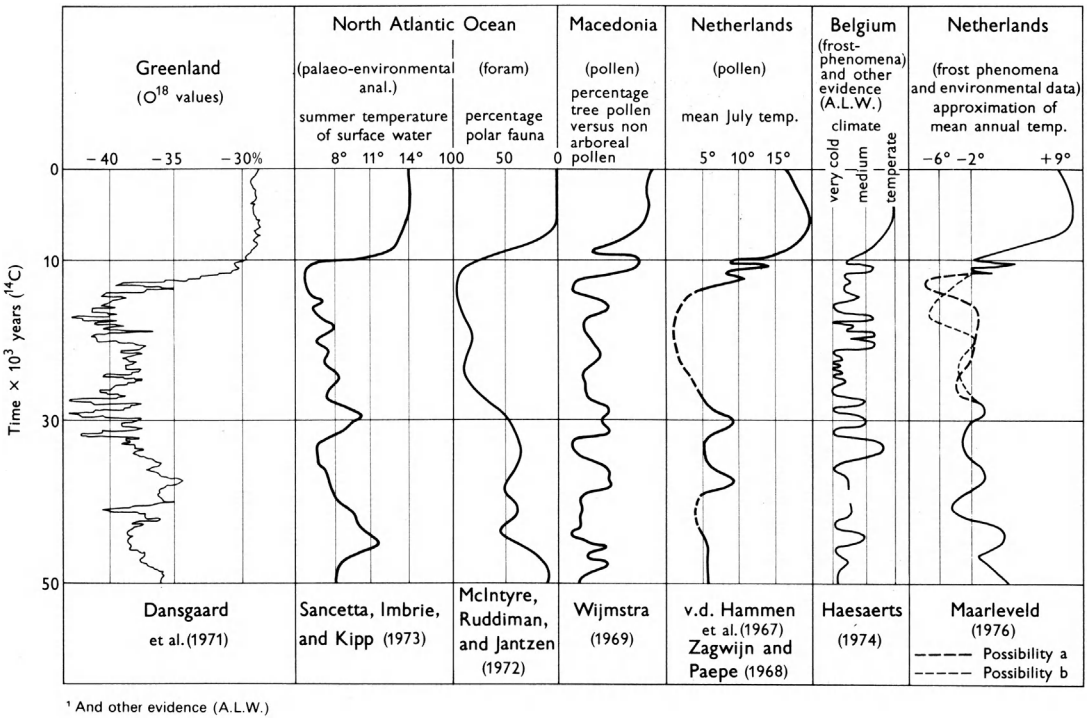


FIGURE 10.3 Paleotemperature reconstruction for Europe based on periglacial features (right column) compared to other long proxy data records. *After Maarleveld (1976).*

constraints; pingo remnants, for example, indicated maximum mean annual temperatures of −2 °C, whereas "extensive coarse snow meltwater deposits" were indicative of a range in mean annual temperature of −5 to −7 °C. Unfortunately, Maarleveld does not identify which sections of his graph are based on estimates of maximum temperature and which are based on a defined temperature range, so the graph may be more precise in some sections than in others. Nevertheless, as a first approximation to paleotemperature reconstruction through time, the results compare well with other proxy data series (Figure 10.3) and indicate the potential value of periglacial studies for paleoclimatic analysis.

10.3 SNOWLINES AND GLACIATION THRESHOLDS

In regions of permanent snow accumulation, it is possible to identify an altitudinal zone separating the lower region of seasonal snow accumulation from the upper region of permanent snow. The term zone is used because from year to year the actual boundary or snowline will vary in elevation, depending on the particular weather conditions during the accumulation and ablation seasons. On a glacier, this would be equivalent to the firn line or (on temperate glaciers where there is no superimposed ice zone) the equilibrium line altitude (ELA). If observations were made over a period of time, the average elevation of the snowline would be apparent, enabling the regional or climatic snowline to be identified (Østrem, 1974). Observations of modern glaciers indicate that the ELA approximates the height at which the accumulation area of the glacier occupies ~70% of its total area. To estimate paleosnowlines, the common practice is to reconstruct the paleo-ELA by mapping the former glacier area (from moraine positions) and then determining where the ELA would have been, based on an accumulation area ratio of ~0.7. This generally corresponds to the uppermost limit of lateral moraines. Mapping the difference between modern and paleo-ELAs constructed in this way can provide useful insights into past climatic conditions. For example, Péwé and Reger (1972) were able to demonstrate that the Arctic Ocean plays no significant role as a moisture source in the present-day glaciation of Alaska, because the snowline gradient along the north coast is not steep and the snowline does not fall to low elevations (Figure 10.4). By contrast, snowline gradients in the south, adjacent to the Gulf of Alaska, are very steep and increase in elevation rapidly away from the moisture source. A similar pattern of snowlines (though considerably lower) occurred in Late Wisconsin times, indicating that the main moisture sources then were like those of today.

A similar index is provided by glaciation levels or glaciation thresholds, which define the lowest limit at which glaciers or permanent ice fields can develop (Miller et al., 1975; Porter, 1977). This is usually determined by identifying the highest unglacierized, and the lowest glacierized, mountain summits in a region and averaging the two elevations. Both snowlines and glaciation thresholds can be used in paleoclimatic reconstructions if similar features can be mapped for periods in the past (Osmaston, 1975), though obviously they only provide information about (extreme) glacial periods and can add nothing to our knowledge of warmer intervals. Although much effort has been expended in mapping both modern and former snowlines, with only a few exceptions, paleoclimatic reconstructions have been simplistic and the results often equivocal. This is mainly due to the following problems:

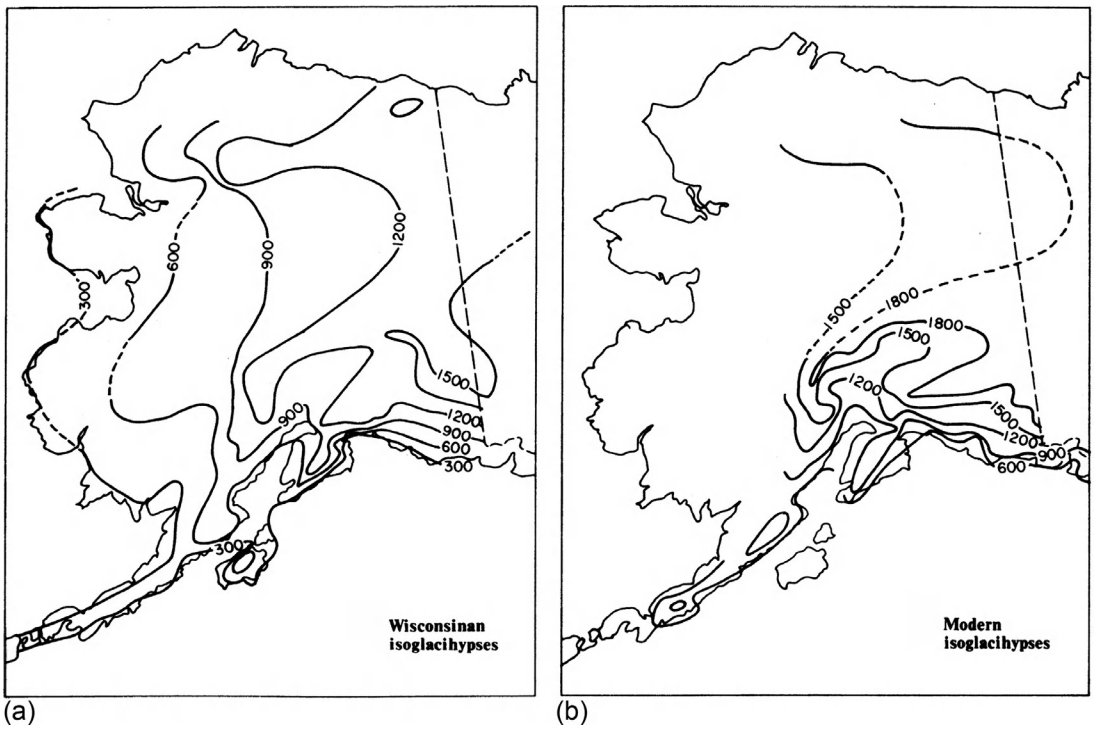


FIGURE 10.4 (a, b) Modern and Wisconsin snowlines in Alaska (in m). Snowlines today show the same pattern as glacial age snowlines, suggesting that no major change in moisture sources has occurred. The Gulf of Alaska, not the Beaufort Sea, was thus the most important source of moisture for glaciation. *After Péwé and Reger (1972).*

(a) Present-day snowlines have not been adequately studied in relation to present climate; climatic "controls" on modern snowline elevations are not well understood and cannot be assumed to be the same in all areas. Furthermore, atmospheric lapse rates have not been well documented in mountain regions and are problematic in paleotemperature reconstructions.

(b) Paleosnowline reconstructions are often based on features of varying age, possibly accounting for the large variations in estimates of past snowline lowering (e.g., Reeves, 1965; Brakenridge, 1978).

10.3.1 The Climatic and Paleoclimatic Interpretation of Snowlines and ELAs

It has commonly been assumed that snowlines are related to the height of the summer 0 °C isotherm, and indeed, Leopold (1951) demonstrated a close correspondence between the two surfaces, in the Western United States from 35 to 50°N. Paleosnowlines

approximately 1000 m lower than today were thus interpreted as indicating lower summer temperatures. Using modern free-air lapse rates of 0.6 °C per 100 m in summer months, Leopold concluded that July temperatures were 6 °C lower than today when snowlines were at the position of maximum depression. Other months were assumed to have cooled proportionately less, with midwinter (January) temperatures having remained the same as today. As a result, he concluded that mean annual temperatures had been 4-5 °C lower. Using similar logic, but an assumed lapse rate of 0.75 °C per 100 m, Reeves (1965) concluded that the 1300 m lowering of the snowline in New Mexico was equivalent to a decrease in July temperature of 10 °C and in mean annual temperature of 5.1 °C. Considerable doubt was cast on these estimates by Brakenridge (1978) who found no strong relationship between present-day snowline in the American Southwest and the July 0 °C isotherm, or indeed any July isotherm, since the latitudinal snowline gradient is considerably steeper. A better fit is obtained with the −6 °C mean annual isotherm; the "full glacial" snowline has a similar gradient, suggesting that there was a fall in mean annual temperature of 7 °C. In the central Andes (10-30 °S), snowlines are actually lower in areas with higher temperatures, because such areas have higher precipitation that compensates for the warmer conditions; highest snowlines are found in the cold, arid mountains of the western Altiplano (Sierra Occidental) (Fox, 1991).

These studies illustrate the basic problems of identifying how snowlines vary with temperature and, if they do, what lapse rate should be assumed in order to use former snowlines as an indicator of temperature change. It is probably not a reasonable assumption to use modern lapse rates in such calculations, since both temperature and moisture conditions in the past would have been different from today, perhaps resulting in lower lapse rates in many areas. However, this entire approach is extremely simplistic and neglects other important factors. Snowline not only is a function of lapse rate but also depends on the variation of accumulation with elevation (accumulation gradient) radiation balance, wind speed, humidity, and the variation of albedo with temperature (since temperature influences the frequency of snowfall versus rainfall events) (Williams R.B.G., 1975; Seltzer, 1994).

The importance of precipitation in controlling snowline elevation and spatial variation has been noted for the Cordilleran Mountains of both North and South America. In the Cascade Range of Washington, for example, 86% of the variance in glaciation thresholds is explained by accumulation season precipitation (though mean annual temperature is highly correlated with precipitation) (Porter, 1977). By assessing the amount of temperature change during the Late Wisconsin (Fraser) glaciation from palynological evidence, Porter estimated that winter precipitation was 20-30% less than today, accompanied by ablation season temperatures 5.5 ± 1.5 °C lower than at present. Extending this approach to the Rocky Mountains, Porter et al. (1983) estimated that the lower Late Pleistocene snowlines of that region required substantially lower temperatures than a simple lapse rate calculation would suggest ($\Delta T = -10$ to -15 °C vs. -6 °C) because conditions were drier at the time. Unless both temperature and precipitation changes are taken into account, erroneous conclusions would be reached. However, such an approach was seen by Seltzer (1994) as only a partial solution since there were undoubtedly also changes in incoming radiation (due to orbital forcing) and regional effects due to changes in cloudiness and hence

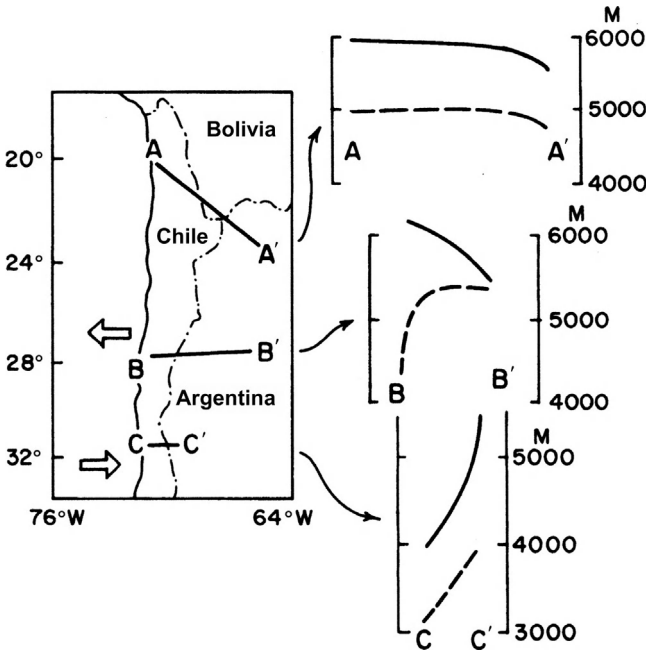


FIGURE 10.5 Modern (——) and Pleistocene (------) snowline elevations along east-west transects in the South American Andes. Principal zonal wind components today are shown by arrows at diagram on left. At the northern and southern locations, Pleistocene snowlines were uniformly lower throughout the transect. In the central location (28°S), a reversal of snowline gradient is apparent between Pleistocene and modern times. This resulted from a shift in the subtropical high-pressure cell and associated wind fields, changing from predominantly onshore flow in Pleistocene time to offshore today. *After Hastenrath (1971).*

in the overall radiation balance. He proposed a model incorporating many of these factors, but estimating how the important variables may have changed remains a major challenge.

In the Andes, snowlines are highest (>6000 m) at the latitude of maximum aridity (Figure 10.5). "Pleistocene" snowlines were lower by 650-1500 m, the depression being greatest in the hyperarid regions of southern Peru and northern Chile and least in the equatorial zone. This suggests a general temperature decrease over the entire region but substantially higher precipitation amounts in the desert zone (Hastenrath, 1967). Further insight is provided by east-west transects across the mountain barrier, which indicate a reversal of modern snowline gradients between 28 and 32°S (Figure 10.5). This is related to the prevailing circulation around subtropical high-pressure cells centered at ~30°S; prevailing winds are easterly to the north and westerly (onshore) to the south. During glacial periods, the lower snowline gradients generally parallel modern snowlines, but at 28°S, this is not the case. "Pleistocene" snowlines show a reversal of gradient, suggesting an equatorward shift of ~5° in the boundary between temperate latitude westerlies and tropical easterlies in the lower troposphere. Where westerly wind regimes became established, a marked eastward rise of Pleistocene snowline resulted (Figure 10.5). Similar reversals of firn line gradient, from modern times to glacial periods, have also been noted in parts of East Africa (Hamilton and Perrott, 1979).

From this brief survey, it is apparent that snowlines in different regions are controlled by different climatic parameters and that these must first be understood in order to use

paleosnowlines in paleoclimatic reconstructions. However, some assessment of the relative importance of different climatic variables to snowline lowering can be made by the use of an energy balance model that takes into account many of the relevant variables and the interactions between them. For example, such a model has been applied to the question of what climatic conditions were necessary to bring about extensive glacierization of Northern Canada (Williams, 1979). By calculating the regional snowline for varying climatic conditions, it was possible to determine where perennial snow cover is most likely to have developed in the past (i.e., which areas are most susceptible to glacierization) and the extent of glacierization brought about by different changes in climatic conditions. Interestingly, Williams' model indicates that a substantial fall in summer temperatures (10-12 °C) is necessary to extensively glacierize Keewatin and Labrador, though smaller changes in temperature are sufficient to glacierize Baffin Island, to the north (Figure 10.6). This confirms the view that Baffin Island is particularly sensitive to climatic fluctuations and is likely to have been a primary site for ice-sheet initiation in the past (and probably in the future also) (Tarr, 1897; Bradley and Miller, 1972; Andrews et al., 1972). It is also of interest that the model results indicate increased

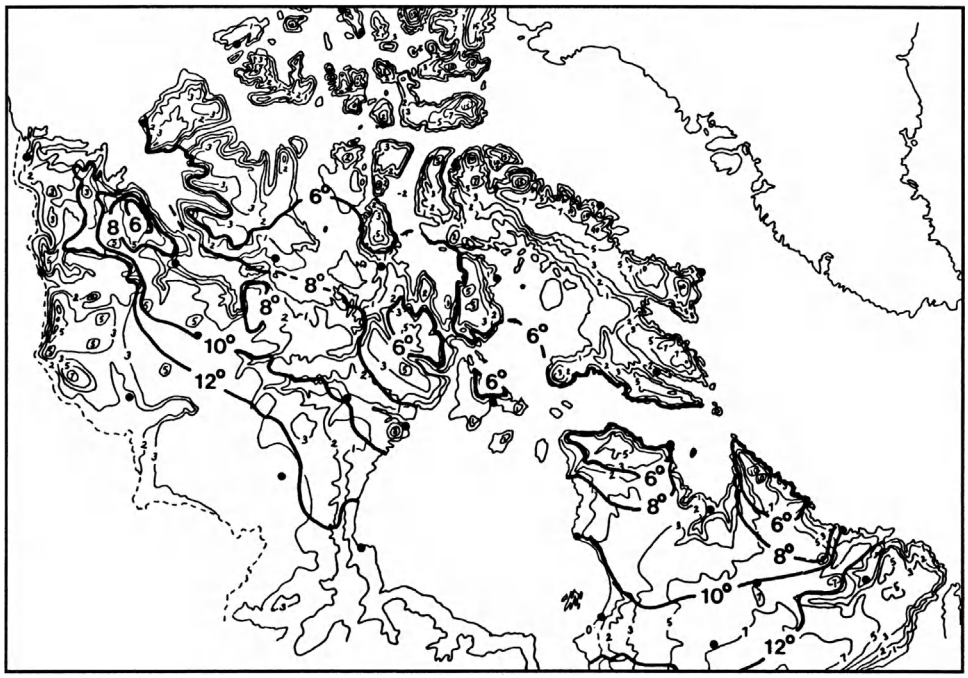


FIGURE 10.6 Boundaries of perennial snow cover predicted by an energy balance model for various amounts of uniform spring and summer temperature decrease, assuming "normal" (1931-1970) snow accumulation and Earth-orbital parameters of 116,000 years BP for 31 March. For example, with a spring-summer lowering of 6-8 °C, the perennial snow cover would have been confined mainly to the Arctic Islands and the northern tip of Labrador-Ungava; with a 10-12 °C temperature lowering, extensive areas of Keewatin and Labrador would have been glacierized. *From Williams (1979).*

snowfall has little impact on the areal extent of glacierization; temperature changes seem to be of most significance for regional snowline lowering and glacierization (Williams, 1979).

10.3.2 The Age of Former Snowlines

In the preceding section, reference has frequently been made to "former" or "Pleistocene" snowlines without qualification. However, not all paleosnowlines are defined in the same way, further confusing the paleoclimatic picture. A common method is to estimate the average elevation of cirque floors occupied by glaciers during a particular glacial period (Péwé and Reger, 1972). Alternatively, paleosnowlines may be located at the median altitude between the terminal moraine of a given advance and the highest point on the cirque headwall (Richmond, 1965). In both approaches, orientation of the cirque is an important factor, not only in terms of radiation receipts but also in terms of prevailing winds and enhanced precipitation catchment in the lee of mountain barriers. Markedly different paleosnowlines may result from studies based on different cirque populations of varying orientation. Furthermore, the use of cirque floor elevation without knowledge of the age of glacial deposits associated with the feature may lead to a mixed population of paleosnowline estimates. Thus, Hastenrath (1971) was only able to describe the paleosnowlines he mapped as "Pleistocene" and Péwé and Reger (1972) described their paleosnowlines as "generalized Wisconsin age" features. Such factors may explain the large variations in snowline depression commonly reported; in New Mexico, for example, estimates of regional snowline lowering vary from 1000 to 1500 m (Brakenridge, 1978) and even larger variations are noted in other studies (e.g., Reeves 1965). This imprecision in dating, and uncertainty over climatic controls on snowline elevation, severely limits the value of most snowline studies for paleoclimatic reconstruction. However, careful study of modern conditions and of well-dated glacial deposits can provide important insights into paleoclimatic conditions of mountain regions, as shown by Porter (1977). Indeed, there would appear to be considerable potential in a reevaluation of this subject for many mountainous parts of the world. An interesting example is provided by Dahl and Nesje (1996) in their study of Holocene paleoclimate in the mountains of southern Norway. They estimated changes in the size of Hardangerjøkulen from glaciofluvial and glaciolacustrine sediments, relying on the fact that as the outlet glacier advanced and retreated, certain thresholds were passed, which were recorded as diagnostic signatures in downstream sediments. This enabled the ice cap area to be estimated, and from that, the paleo-ELA could be calculated (Figure 10.7). Changes in the upper limit of pine (*Pinus sylvestris* L.) provided an assessment of variations in summer temperature, and from these, estimates of temperatures at the ELA could be obtained (using a lapse rate of 0.6 °C per 100 m). They then used a well-established relationship between winter accumulation (A) and temperature (t) at the equilibrium line of Norwegian glaciers ($A = 0.915\ e^{0.339t}$) to reconstruct the change in winter accumulation at the ELA (assuming this relationship has remained constant over time) (Figure 10.7). Their approach reveals that at certain times in the past (9500-8300, 7200-6200, and at ~5500 and ~4500 [calibrated ^{14}C] years BP), the ice cap grew in size due to higher winter precipitation, in spite of warmer summer temperatures. The major "Little Ice Age" advance (culminating in the eighteenth century) was unusual in resulting from both higher winter precipitation and lower summer temperatures, which perhaps explains why the ELA at that time was lower than at any other time in the Holocene.

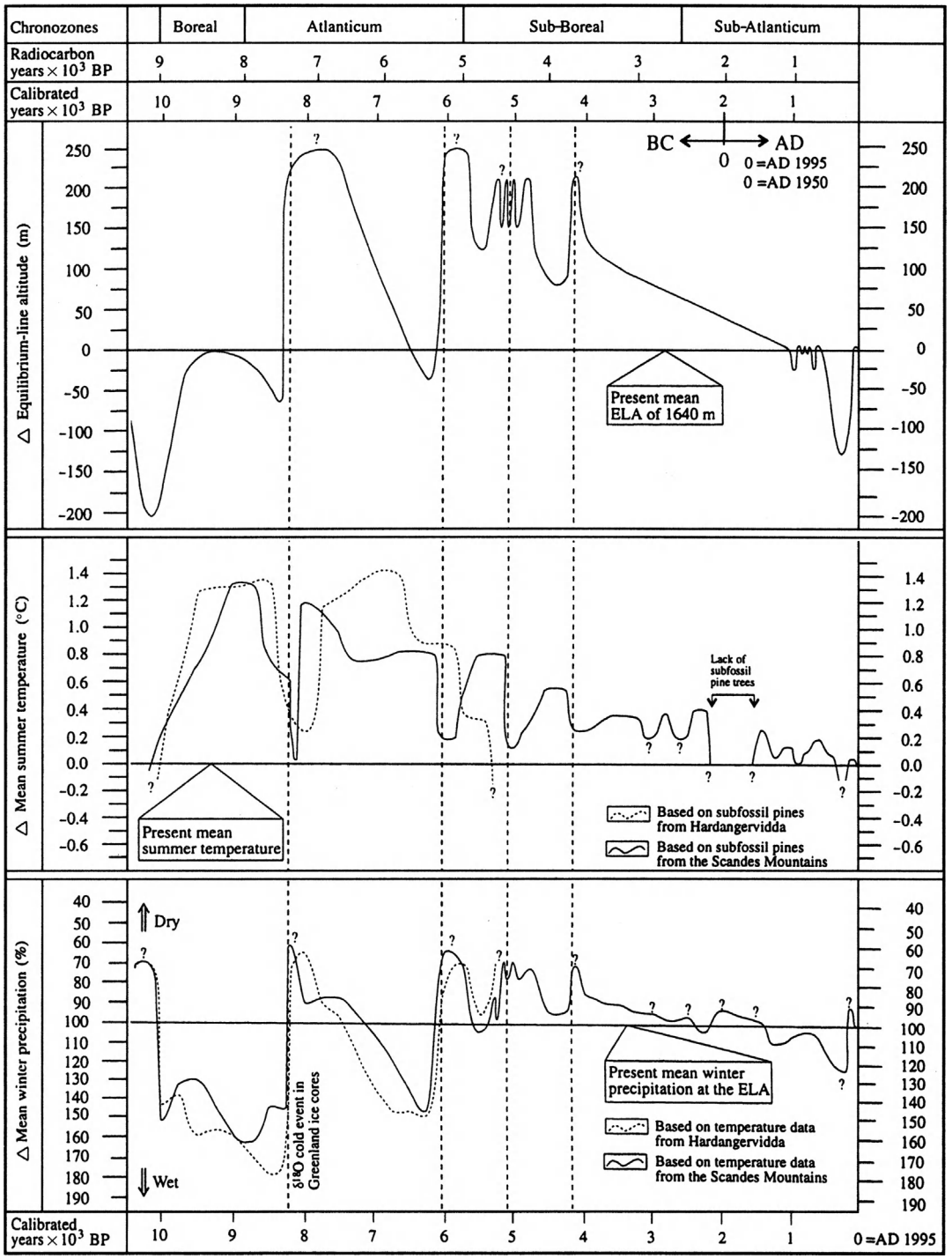


FIGURE 10.7 Variations in equilibrium line altitude (ELA) on Hardangerjøkulen, south central Norway (top panel), summer temperature based on subfossil wood (*Pinus sylvestris* L.) found above modern tree line (middle panel) and winter precipitation (accumulation) derived from modern relationships between accumulation and temperature at the ELA (lower panel: note scale is inverted). Values are expressed relative to modern conditions. Ages are given in calibrated and uncalibrated ^{14}C years at top. Summer temperatures were above present levels for most of the Holocene; glacier advances were associated with periods of higher winter accumulation. Only the "Little Ice Age" experienced both lower summer temperatures and higher winter precipitation, leading to the largest ice advance of the entire Holocene. *After Dahl and Nesje (1996).*

10.4 MOUNTAIN GLACIER FLUCTUATIONS[1]

Glacier fluctuations result from changes in the mass balance of glaciers; increases in net accumulation lead to glacier thickening, mass transfer, and advance of the glacier snout; increases in net ablation lead to glacier thinning and recession at the glacier front. A glacial advance therefore corresponds to a positive mass balance brought about by a climatic fluctuation that favors accumulation over ablation (e.g., Figure 10.8). However, there are many combinations of climatic conditions that might correspond to such a net change in mass balance (Oerlemans and Hoogendorn 1989) so that evidence of a formerly more extensive ice position does not provide an unequivocal picture of climate at the time. However, if a check on one important variable (such as temperature) is available from an independent source of paleoclimatic data, it may be possible to calculate, or model, the overall change in climate that resulted in the advance or retreat of the glacier terminus (e.g., Allison and Kruss 1977).

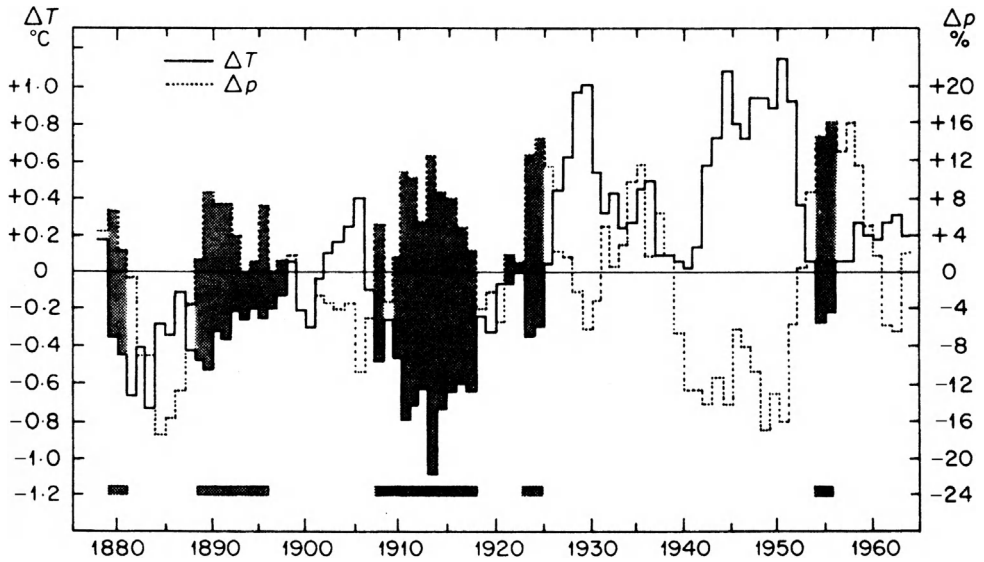


FIGURE 10.8 Mean departures (from 1851 to 1950 averages) of summer (June, July, and August) precipitation (%) and temperature (°C) at seven stations above 2000 m in the Swiss Alps. Shaded areas indicate times when precipitation was above average *and* temperatures were below average. These correspond closely to the times of principal glacier advances in the area (bars at bottom). *After Hoinkes (1968).*

[1] The growth and decay of *continental* ice sheets and associated changes in sea level and oceanic and atmospheric circulation are fundamental characteristics of the Quaternary Period (for a global overview, see *Quaternary Science Reviews*, vol. 5, 1986 and vol. 9, No. 2/3, 1990). Such studies provide important regional information on ice extent in response (implicitly) to large-scale changes in climate. Comprehensive volumes on the extent and chronology of glaciations around the world are provided by Ehlers and Gibbard (2004a,b,c; see summary in Ehlers and Gibbard, 2003).

Changes in mass balance are not transformed immediately into changes in glacier front positions. There may be a period of downwasting, during which the glacier loses mass but does not recede. For example, the lower Khumbu Glacier, in the Mount Everest massif, thinned by ~70 m between 1930 and 1956, but the glacier snout remained stationary (Müller, 1958). Even when downwasting is not a significant factor, glacier front positions will lag behind climatic fluctuations. Different glaciers have different response times to mass balance variations (Oerlemans, 1989). An increase in net mass results in a kinematic wave moving down the glacier at a rate several times faster than the normal rate of ice flow. The time it takes for this wave to reach the glacier snout is the response time of the glacier and depends on a number of factors including the glacier length, basal slope, ice thickness and temperature, and overall geometry of the glacier itself (Nye, 1965; Paterson, 1994). The South Cascade Glacier (Washington), for example, has a response time of only about 25-30 years, whereas large ice sheets have response times on the order of millennia.

There is some evidence that an excess of ablation over accumulation may cause a more rapid response, with ice recession lagging very little behind the climatic fluctuation that caused the mass loss (Karlén, 1980). Glacier front variations are thus a rather complex integration of both short- and long-term climatic fluctuations, so that one should not be surprised to see some larger glaciers advancing at the same time that smaller glaciers, with shorter response times, are retreating. Glaciers of different sizes and response times in different areas may be undergoing synchronous advances but in response to different climatic events; the largest glacier systems respond to low-frequency climatic fluctuations, whereas the smaller systems respond to higher-frequency fluctuations.

10.4.1 Evidence of Glacier Fluctuations

The complexity of climatic conditions and differing glacier response times makes glacier fluctuations, as viewed through the misty window of the paleoclimatic records, a rather complicated source of paleoclimatic data. This is compounded by the difficulties inherent in dating former glacier front positions in environments that generally have very little organic material for dating and where weathering rates are extremely slow.

A record of changes in glacier front positions is generally derived from moraines produced during glacial advances; periods of glacier recession, and the magnitude of the recession, are much harder to identify in the field, and so the record of downvalley glaciofluvial or glaciolacustrine sediments is often a much more useful paleoclimate record that can be related to glacier extent (Nesje and Dahl, 2000). Furthermore, in the right situation, the sedimentary record can be linked to changes in ELA and through that to a more direct climatic interpretation (e.g., Dahl and Nesje, 1996; Bakke et al., 2005, 2010b, 2013). The problem with the record of moraines is that they are commonly incomplete, with recent advances (which were often the most extensive) obliterating evidence of earlier, less extensive advances. However, detailed stratigraphic studies of glacial deposits may reveal buried soils and weathered profiles indicative of former subaerial surfaces, subsequently buried by more recent morainic debris (e.g., Rothlisberger, 1976; Schneebeli, 1976).

By far, the greatest difficulty in the use of glacier front positions as a paleoclimatic index is the problem of dating the glacial deposits. Radiocarbon dates may be obtained on organic

material in soils that developed on moraines, but they only provide a minimum age on the glacial advance. There may be a delay of many hundreds of years between the time a moraine becomes relatively stable and the time it takes for a mature soil profile to develop. If a soil has been buried by debris from a subsequent glacial advance, a date on the soil would provide only a maximum age on the later glacial episode because the organic material in the soil may be hundreds of years older (at least) than the subsequent ice advance (Griffey and Matthews, 1978; Matthews, 1980). Past variations in radiocarbon production rates further impede accurate dating, especially in the last 500 years or so, encompassing the critically important "Little Ice Age" glacier advances. For older glaciations in volcanic areas, tephrochronology (see Chapter 4, Section 4.3) or the dating of interstratified lava flows may assist in the interpretation of glacial events (e.g., Loffler, 1976; Porter, 1979). Elsewhere, recent advances in cosmogenic isotope dating of exposed surfaces have opened up the possibility of dating the time that has elapsed since an area was ice-covered or since a moraine became stabilized (e.g., Phillips et al., 1996) (see Chapter 3, Section 3.2.5).

Lichenometry is commonly used to date moraines (see Chapter 4, Section 4.4.1), but the technique is uncertain and probably no more reliable than ±20% before 1000 years BP; in most cases, lack of a well-dated calibration curve, or the derivation of a curve based on observations in an environment totally unlike that of the glacial valley or cirque in question, makes the uncertainties even larger. In short, the chronology of glacier fluctuations is quite uncertain in most parts of the world.

10.4.2 The Record of Glacier Front Positions

Studies of glacier fluctuations have been conducted in virtually all mountainous parts of the world (Davis et al., 2009, and associated papers in a Special Issue of *Quaternary Science Reviews*, and Thackray et al., 2008, and associated papers in a Special Issue of the *Journal of Quaternary Science*). In spite of the difficulties of dating glacial deposits, mountain regions have provided some of the most comprehensive records of repeated glaciation throughout the Quaternary Period (e.g., Thackray, 2008; Owen et al., 2008). Glacial deposits from mountain glaciers indicate there have been at least 11 episodes of major glaciation in the last 1 MY that were (broadly speaking) of global significance (Figure 10.9) as evidenced by a corresponding enrichment of the oceans in ^{18}O. However, because of the aforementioned dating problems, the most detailed work has focused on postglacial (Holocene) glacier fluctuations. Early work in the Rocky Mountains led Matthes (1940, 1942) to suggest that many alpine glaciers disappeared during a Mid-Holocene warm and dry period (which was termed the Altithermal by Antevs, 1948) only to be regenerated during subsequent cooler and/or wetter periods ("Neoglaciations"; Porter and Denton, 1967). Evidence that mountain glaciers and small ice caps may have been smaller or even disappeared entirely in the Early to Mid-Holocene is often circumstantial, but radiocarbon dates on vegetation revealed by recent ice recession provide compelling evidence that glaciers were at least the same size or smaller than today (e.g., Hormes et al., 2001; Joerin et al., 2006; Anderson et al., 2008; Thompson et al., 2013). Some of the most comprehensive studies have been carried out in Scandinavia, based on lake sediment studies and ^{14}C-dated subfossil wood from above modern tree line, which provide estimates of summer temperature for much of the Holocene (see Chapter 11,

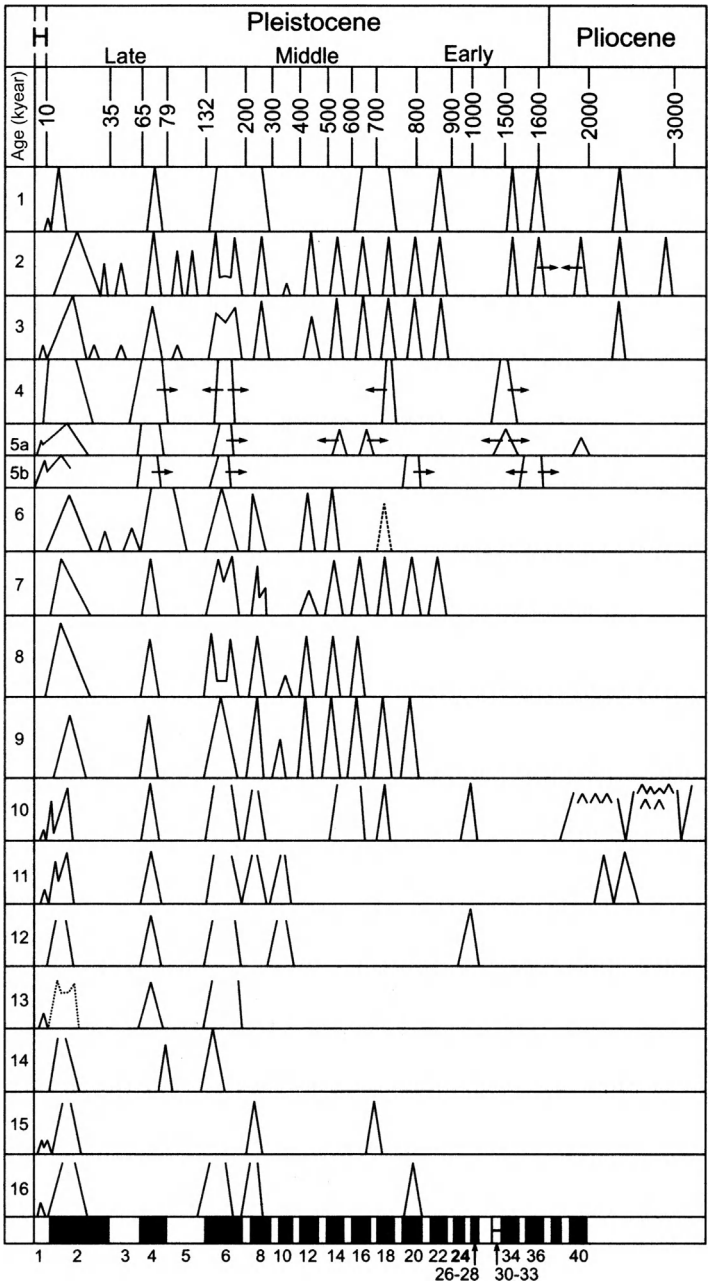


FIGURE 10.9 Summary diagram showing the principal episodes of glaciation in the Northern and Southern Hemispheres over the past ~3 MY based on glacial geologic studies in the various regions indicated. Ice advances are indicated schematically by an upward-pointing triangle, the relative dimensions of which signify the magnitude of each ice advance. Note that timescale (shown at top) is nonlinear; marine oxygen isotope stages are indicated at bottom with even-numbered stages (times of major ice accumulation on the continents) shaded (however, note that not all such stages are equal in magnitude—see Section 6.3.2). Arrows indicate dating uncertainties; in spite of these, numerous episodes of globally significant ice advances are clearly identifiable. 1 = US Cordilleran ice sheet; 2 = US mountain glaciers; 3 = US Laurentide Ice Sheet; 4 = Canadian Cordilleran Ice Sheet; 5 = Canadian Laurentide Ice Sheet (a = SW margin, b = NW margin); 6 = NE Russia; 7 = Poland/western (former) Soviet Union; 8 = NW Europe; 9 = European Alps; 10 = Southern Andes; 11 = New Zealand; 12 = Tasmania; 13 = Southern Ocean and sub-Antarctica; 14 = Antarctica (Ross Embayment); 15 = New Guinea; 16 = E. Africa. *Simplified from charts accompanying Bowen et al. (1986) and Clapperton (1990).*

Section 11.3.2). It seems likely that many alpine glaciers in the region could not have survived the warmest episodes from 8000 to 4000 years BP (Karlén, 1981; Nesje et al., 1991). Similar conclusions have been reached by other workers elsewhere (e.g., Koerner and Paterson, 1974 for Meighen Ice Cap in the Canadian High Arctic and Brown, 1990 for the equatorial glaciers of New Guinea). A post-Mid-Holocene climatic deterioration is apparent in many areas, resulting in renewed glacierization and glacier advances between 5000 and 4000 years BP (Figure 10.10). Several episodes of glaciation occurred over the following few thousand years, culminating in the most recent Neoglacial episode (between the thirteenth and mid-nineteenth century), which generally resulted in the most extensive of the Holocene glacial advances. This period is commonly referred to as the Little Ice Age (Bradley and Jones, 1993) and is particularly well documented in Western Europe (Grove, 1988, 2001a,b). In the European Alps, glacier advances can be traced through historical records, paintings, and sketches, and this has greatly facilitated the interpretation of glacial deposits in the field. Detailed reconstructions of glacier front positions over the past ~450 years have been constructed for several French, Swiss, and Austrian glaciers, most notably the Grindelwald Glacier, Switzerland (Messerli et al., 1978; Zumbühl, 1980), and the Mer de Glace, France (Nussbaumer et al., 2007). Using a variety of such sources, periods of both glacier advance and recession can be determined (e.g., Figure 10.11). However, such detailed records are rare and the advance/retreat record would have been impossible to construct with only geomorphological evidence to go on.

Because the Little Ice Age advances were most extensive (in many areas greater than at any time since the end of the last major glaciation), the record of earlier glacial events was often destroyed or buried. This has made worldwide correlations very difficult, compounded by the dating difficulties discussed earlier. Hence, whether there were globally synchronous glacial episodes is somewhat unclear. Certainly, there were many periods of alpine glacier expansion throughout the Holocene (Figure 10.10) and these varied in magnitude from one area to another. However, there is little support for the notion that Holocene glacier fluctuations were synchronous throughout the world or that advances had a regular periodicity (cf. Denton and Karlén, 1973a; Grove, 1979; Rothlisberger, 1986; Wigley and Kelly, 1990).

10.5 LAKE-LEVEL FLUCTUATIONS

Throughout the arid and semiarid part of the world, there is commonly no runoff (surface water discharge) to the oceans. Instead, surface drainage may be essentially nonexistent (in areic regions) or it may terminate in interior landlocked basins where water loss is almost entirely due to evaporation (endoreic regions). In these basins of inland drainage (Figure 10.12), changes in the hydrologic balance resulting from climatic fluctuations may have dramatic effects on water storage. During times of positive water budgets, lakes may develop and expand over large areas, only to recede and dry up during times of negative water balance. Studies of lake-level variations can thus provide important insights into paleoclimatic conditions, particularly in arid and semiarid areas. In modern lake basins, former periods of positive water balance are generally identified by abandoned wave-cut shorelines and/or beach deposits (Figure 10.13) or perched deltas from tributary rivers and streams and exposed lacustrine sediments at elevations above the present lake shoreline (e.g., Morrison, 1965; Butzer et al., 1972; Bowler, 1976). Periods of negative water balance (relative to today) are identifiable in lake sediment cores or by paleosols developed on exposed lake sediments

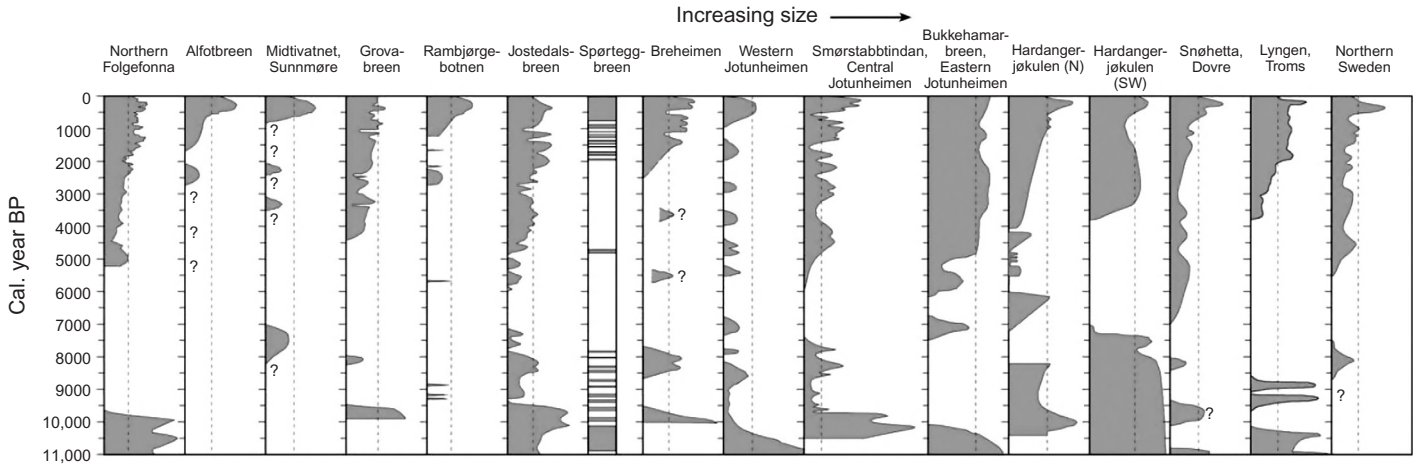


FIGURE 10.10 A summary of Holocene glacier advances for different regions of Scandinavia—one of the best-studied regions of the world. Horizontal scale is schematic and not to scale. Although these changes reflect climate fluctuations that are specific to the region, the overall pattern is similar to that seen in many other mountain ranges of the world, with more extensive glaciers in the Early Holocene, followed by recession (in some cases resulting in the complete deglacierization of some areas) and then renewed glacier advances 4000-5000 years ago, in the Neoglacial period. A series of advances and retreats characterize the most recent millennia, culminating in the Little Ice Age glacier advances of recent centuries, which were often the most extensive of the entire Holocene in many regions. Glaciers have greatly receded in recent decades due to global warming, resulting from increases in anthropogenic greenhouse gases. ? indicates that the record is uncertain. *From Nesje (2009).*

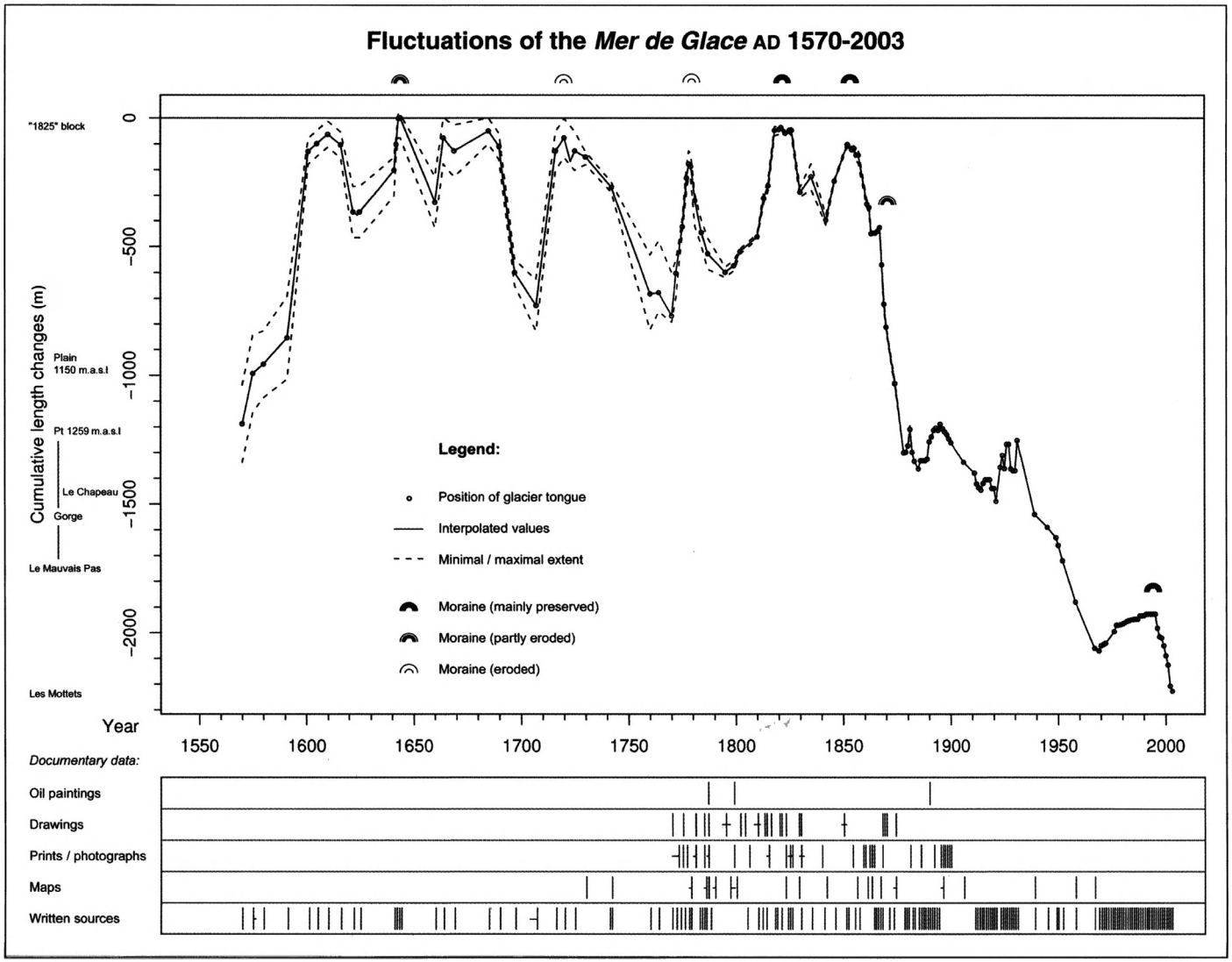


FIGURE 10.11 Fluctuations of the Mer de Glace (Mont Blanc, France) between AD1570 and 2003, relative to its maximum advance position in 1825 position. The major recession of >2 km since 1850 (with minor interruptions around 1890 and 1920) is clearly seen. Moraines are indicated by bold curves and information sources are shown in the lower part of the figure. The changes were almost identical at the Lower Grindelwald Glacier, Switzerland, which has similarly detailed historical records. *From Nussbaumer et al. (2007).*

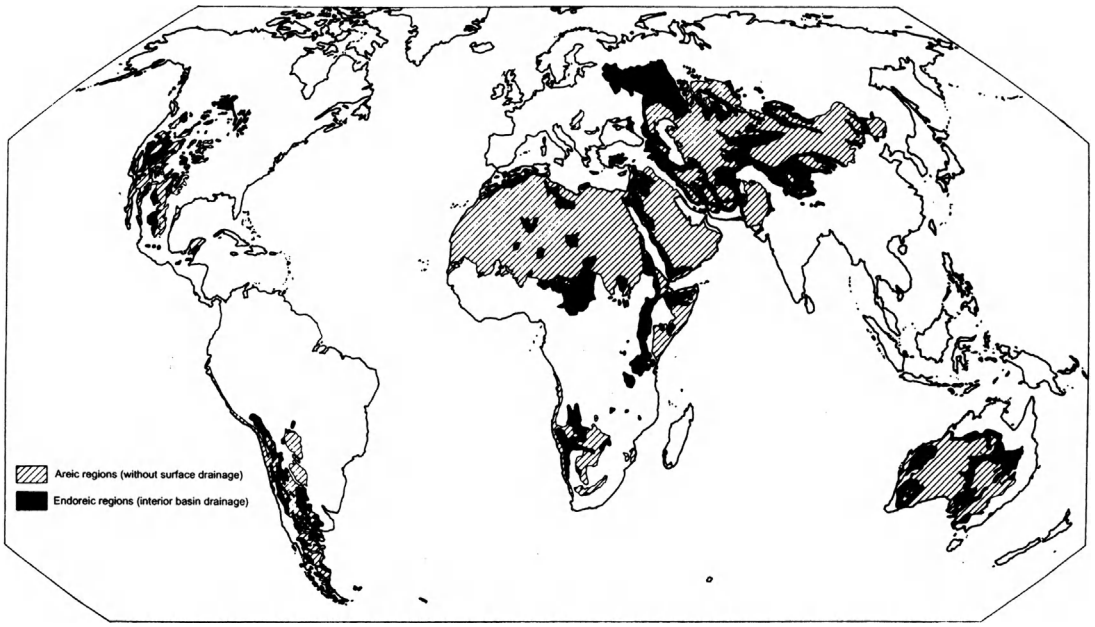


FIGURE 10.12 Areas of endoreic and areic drainage. Areic regions have no permanent surface drainage; endoreic areas are basins of inland drainage. *From Cooke and Warren (1977), after de Martonne and Aufrere (1928).*

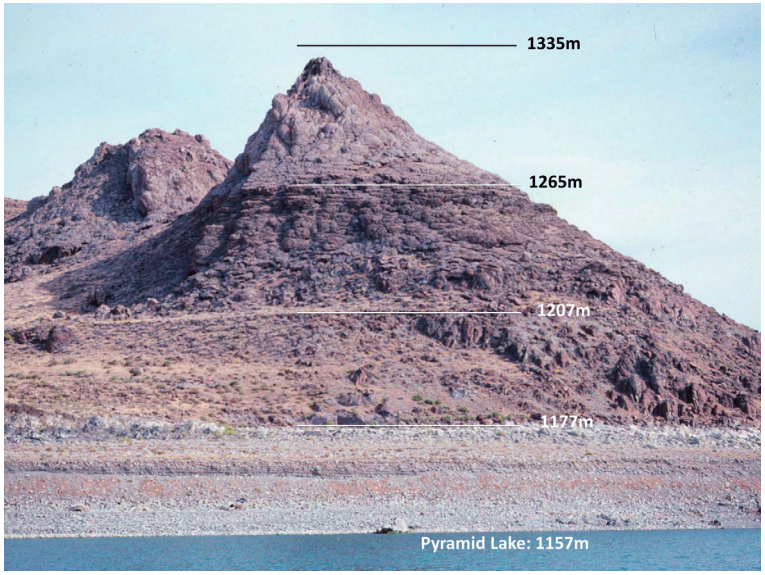


FIGURE 10.13 Paleolake shoreline terraces on Anaho Island in Pyramid Lake, Nevada. The lowest shoreline (1177 m) is Late Holocene in age (~3 ka-AD1900). The first erosional terrace (1207 m) was formed between 13.2 and 9.5 ka BP and the constructional tufa terrace (1265 m) formed 23-17 ka BP. The paleolake levels correspond to different sill elevations, at which point water was able to drain into other basins. The Lahontan highstand stood ~3 m above the top of the island. *Photograph kindly provided by Larry Benson.*

(Street-Perrott and Harrison, 1985a,b). A study of the stratigraphy, geochemistry, and microfossil content of lake sediments from closed basins may be particularly valuable in deciphering lake history (e.g., Bradbury et al., 1981, 2001).

Most of the early studies of lake-level fluctuations focused on closed lakes where changes in the precipitation-evaporation balance led to volumetric changes and consequent adjustments in lake-level elevation. Recent work has attempted to expand beyond predominantly arid and semiarid regions, where such lake systems are commonly found, to higher latitudes where open (overflowing) lake systems are more common. In open-system lakes, water balance changes are naturally compensated for by changes in outflow, but lake levels may also change somewhat, albeit far less than in closed lake systems. Where multiple sediment cores are available from a lake, it may be possible to detect in the sedimentary facies former shallow-water conditions and to thereby date periods with lower lake levels (e.g., Harrison and Digerfeldt 1993). Macrofossil and palynological evidence can also provide evidence of changes in lake level via shifts in the relative abundance of shallow and deepwater aquatic flora. Where such studies have been carried out, it may be possible to reconstruct water balance changes even in open-system lakes (some of which may, of course, have become closed systems in drier periods). Although the vast majority of open-system lake sediment studies do not have a suite of cores from deep- to shallow water, detailed studies of sedimentologic, macrofossil, diatom, and palynological data can sometimes indicate lake-level changes (Yu and Harrison, 1995; Tarusov et al., 1996). Such studies have been used for large-scale hydrologic reconstructions by Harrison (1989) and Harrison et al. (1996).

Lake-level fluctuations have been studied in dozens of closed basins throughout the world (for a list of principal works, see Street-Perrott et al., 1983). The majority of these studies are stratigraphic and provide only qualitative estimates of climatic conditions. Periods of higher lake levels are commonly described as pluvials, but the question of whether such conditions result from increased precipitation or lower temperatures and more effective precipitation (via reduced evapotranspiration) is controversial (cf. Brakenridge, 1978; Wells, 1979). In an attempt to resolve the controversy, a number of studies have attempted to use the geomorphological evidence, together with empirically derived equations relating climatic parameters today, to make quantitative estimates of paleoclimatic conditions associated with particular lake stages in the past. These can be considered in two general categories: hydrologic balance models and hydrologic-energy balance models.

10.5.1 Hydrologic Balance Models

In a closed basin, variations in lake level are a function of water volume, which is, in turn, a reflection of the balance of water supply and water loss:

$$\frac{dV}{dt} = \frac{d(P + R + U)}{dt} - \frac{d(E + O)}{dt}$$

where V is water volume in the lake; P is precipitation over the lake; R is runoff from the tributary basin, into the lake; U is underground (subsurface) inflow to the lake; E is evaporation from the lake; and O is subsurface outflow from the lake. For any particular lake stage, if the hydrologic balance is considered to be at equilibrium, such that

$$\frac{dV}{dt} = 0$$

then $P + R + U = E + O$. Generally, subsurface inflow and outflow are considered to be negligible and are omitted from the equation, even though in some cases they may be substantial; in the case of the Great Salt Lake, Utah, for example, subsurface inflow has been variously estimated at 3-15% of total lake input (Arnow, 1980). In most cases, however, the subsurface components are unknown even for modern lake levels and trying to estimate them for paleolakes would be extremely speculative. Assigning values of zero to these components, the hydrologic balance equation for a particular basin is thus

$$A_L P_L + A_T(P_T k) = A_L E_L$$

where A_L is the lake area; A_T is the area of the tributary basin from which water drains to the lake; P_T is mean precipitation per unit area over the tributary basin; k is a coefficient of runoff (hence, $P_T k$ equals the runoff per unit area, R_T, from the tributary basin); P_L is mean precipitation per unit area, over the lake; and E_L is mean evaporation per unit area, from the lake. Since only A_L and A_T are known for any given lake stage, the equation may be rearranged; thus,

$$\frac{A_L}{A_T} = \frac{P_T k}{A_L E_L}$$

A solution of the equation therefore requires knowledge of precipitation over the lake and adjacent catchment basin, runoff from the surrounding basin, and the amount of water that evaporates from the lake. All of these parameters are a function of many other variables that are also unknown, making a unique solution to the equation extremely difficult, to say the least. To illustrate the uncertainties involved, Table 10.2 lists some of the principal factors affecting evaporation and runoff. Of major importance to both parameters is temperature, and this has enabled some limits to be placed on estimates of former runoff and evaporation values when reasonably good paleotemperature estimates are available. If paleotemperatures are known, empirically derived equations relating runoff, evaporation, and temperature (e.g., Figures 10.14 and 10.15) can be used to solve the hydrologic balance equation. However, these empirical relationships are often limited

TABLE 10.2 Factors Affecting Rates of Evaporation and Runoff

Evaporation	Runoff
Temperature (daily means and seasonal range)	Ground temperature
Cloudiness and solar radiation receipts	Vegetation cover and type
Wind speed	Soil type (infiltration capacity)
Humidity (vapor pressure gradient)	Precipitation frequency and seasonal distribution
Depth of water in lake and basin morphology (water volume)	Precipitation intensity (event magnitude and duration)
Duration of ice cover	Precipitation type (rain, snow, etc.)
Salinity of lake water	Slope gradients, stream size, and number

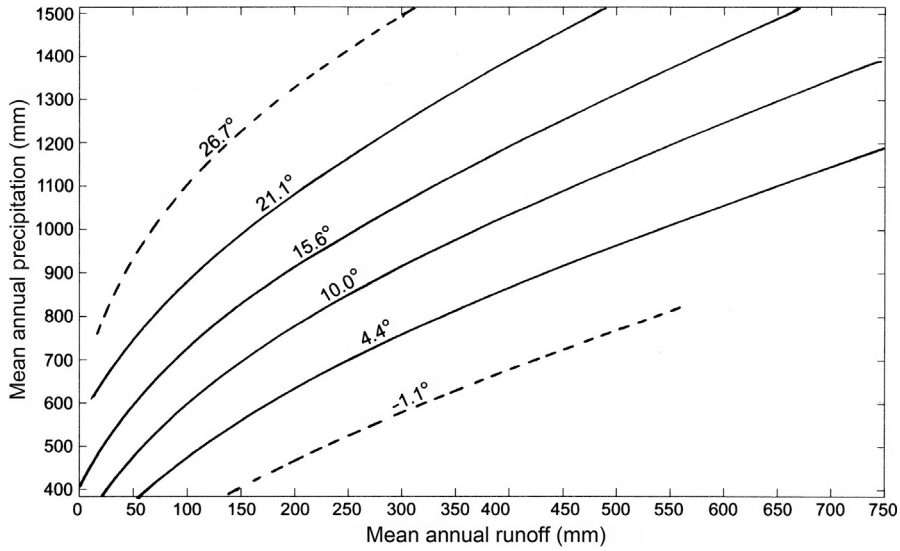


FIGURE 10.14 Relationship between mean annual runoff and mean annual precipitation for areas with different mean annual temperatures (in °C). Temperatures are weighted by dividing the sum of the products of monthly precipitation and temperature by the annual precipitation. The quotient gives a mean annual temperature in which the temperature of each month is weighted in accordance with the precipitation during that month. A weighted mean annual temperature greater than the mean that would normally be computed indicates that precipitation is concentrated in warm months (and vice versa). *After Langbein et al. (1949).*

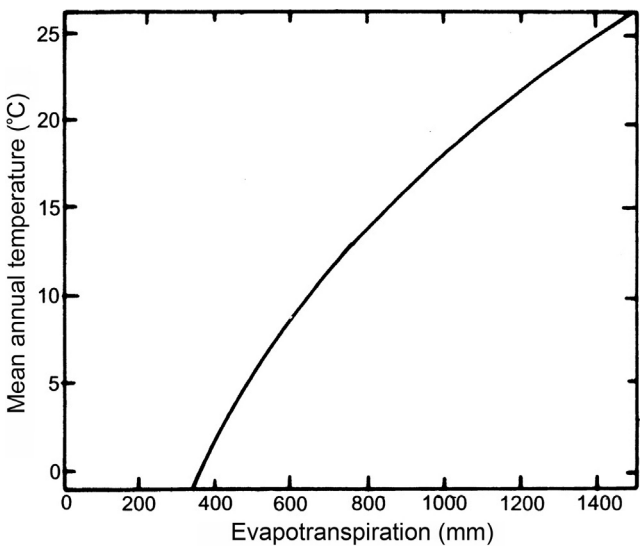


FIGURE 10.15 Relationship between mean annual temperature and evapotranspiration loss in humid areas, based on data from the eastern United States. *After Langbein et al. (1949).*

in the range of values considered and constrained by inadequate or even nonexistent data. Consider, for example, the relationship between lake evaporation and temperature. Most empirical relationships are based on standard measurements of evaporation from metal pans 1.2 m in diameter, at different temperatures; lake evaporation is assumed to be less than pan evaporation by a factor of 0.7, based on empirical studies by Kohler et al. (1966). However, evaporation rates depend on a number of factors, which have not been constant through time (Table 10.2), for example, lake volume and salinity variations. In large lakes, such as Lakes Superior and Ontario, there is a very poor correlation between monthly temperature and evaporation because much energy is used in raising the water temperature at depth (i.e., in heat storage). Evaporation is at a maximum in fall and winter months when the lake surface eventually becomes warmer than the overlying air (Morton, 1967). Such an effect would be far less significant in tropical lakes but could be important in midlatitude situations where relatively large lakes developed in the past (e.g., Lakes Bonneville and Lahontan). The formation and duration of ice cover would also significantly affect evaporation rates. At the other end of the spectrum, lakes that are drying up may have extremely high salt concentrations; as salinity increases, the evaporation rate will decline due to a lowering of vapor pressure. For example, in a lake with a salinity of 200‰, evaporation will only be 80% of that from a freshwater lake (Langbein, 1961). Such factors complicate any simple empirical relationship one might derive from instrumentally recorded data and point to the inherent difficulties involved in hydrologic balance calculations for paleolakes. Similar difficulties are encountered with precipitation-runoff relationships (Table 10.2). Even if precise empirical relationships could be demonstrated, reliable paleotemperature estimates are required. Commonly, these too are fraught with uncertainty and may, in fact, depend implicitly on assumptions about paleoprecipitation amounts. For example, paleotemperatures derived from studies of snowline depression depend on the assumption that precipitation amounts are similar to those of today. Any increase in precipitation would require a smaller fall in temperature to produce the same amount of snowline depression. Hence, the use of paleotemperature estimates based on snowline depression (e.g., Leopold, 1951; Brakenridge, 1978) leads to suspiciously circular reasoning. Without accurate paleotemperatures, quite divergent conclusions may ensue. In Table 10.3, for example, three different studies of Paleolake Estancia, New Mexico, are summarized. Although each used slightly different approaches and empirical relationships, the fundamental difference in their final paleoprecipitation estimates (ranging from 86% to 150% of today's values) lies in the different paleotemperatures assumed. The larger the change in temperature assumed, the smaller is the required increase in precipitation (cf. Benson, 1981). Given a sufficiently large decrease in temperature, values of precipitation even smaller than today can be shown to balance the hydrologic budget at times of relatively high lake levels (e.g., Galloway, 1970).

It is unlikely that controversies over paleoprecipitation estimates will be resolved unless (a) more detailed studies of modern relationships between evaporation and temperature, precipitation, and runoff are undertaken, to provide more reliable empirical equations, and (b) better (independent) paleotemperature estimates are available. Paleotemperature calculated from the extent of amino-acid epimerization in the shells of freshwater gastropods of known age is one approach to address this issue (McCoy, 1987b; Oviatt et al., 1994).

TABLE 10.3 Paleoprecipitation Estimates from Selected Western US Hydrological Balance Studies

Study Area	Paleotemperature Change Assumed (°C)		Paleoprecipitation/ Modern Precipitation	Author(s)
	July	Annual		
Lake Estancia, New Mexico	−9	−4.5	1.5	Leopold (1951)
Lake Estancia, New Mexico	−8	>−7.5	1.0	Brakenridge (1978)
Lake Estancia, New Mexico	−10	−10.5	0.86	Galloway (1970)
Spring Valley, Nevada	−7	−3.5	1.6	Snyder and Langbein (1962)
Various, in Nevada		−2.8	1.68	Mifflin and Wheat (1979)

10.5.2 Hydrologic-Energy Balance Models

An alternative to the conventional hydrologic balance models described earlier was applied by Kutzbach (1980) to Paleolake Chad in North Africa. Kutzbach utilized the climatonomic approach of Lettau (1969) by considering the hydrologic balance of a lake basin in terms of energy fluxes at the surface. In simple terms, a positive hydrologic balance results when there is insufficient energy available to evaporate precipitation falling on the basin. Instead of calculating paleoprecipitation amounts from estimates of runoff and evaporation (via paleotemperature estimates), a hydrologic-energy balance model utilizes estimates of net radiation and sensible and latent heat fluxes over the lake and tributary basin. Modern values of these components are used, based on measurements in locations that are thought to characterize the paleoenvironments of the basin being studied. Paleotemperature estimates are thus implicit in this "analogue" approach; in the Paleolake Chad study, for example, the changes in vegetation that were assumed for 5000-10,000 years BP correspond to an area-weighted difference in mean annual temperature of −1.5 °C, by analogy with areas of similar vegetation today. Precipitation was estimated to have been almost double modern values (~650 mm versus 350 mm today), a result that is similar to previous estimates of precipitation for the area at that time, based on a variety of paleoenvironmental data. Using a similar approach, but with somewhat different assumptions about the magnitude of the important parameters, Tetzlaff and Adams (1983) concluded that precipitation over the Lake Megachad Basin must have been at least three times modern values in order to produce the observed increase in lake size.

Kutzbach's approach to the quantification of past climatic conditions from paleolake studies could be applied to many other lake systems. However, whether it represents a major improvement over conventional hydrologic studies is debatable, since it involves at least as many assumptions, and may involve a good deal more (e.g., Benson 1981). Nevertheless, this kind of modeling has the merit of being able to identify, via sensitivity tests, which

climatic variables are likely to have been of most significance in bringing about the observed lake-level changes.

10.5.3 Regional Patterns of Lake-Level Fluctuations

A number of relatively well-dated stratigraphic and geomorphological studies of lake-level fluctuations have enabled maps of relative lake levels to be constructed for selected time intervals for many parts the world (Street-Perrott and Harrison, 1985a,b; Harrison, 1993; Viau and Gajewski, 2001). Although individual errors in dating lake levels no doubt occur, mapping relative lake levels for discrete time periods has the advantage that regionally coherent patterns may be discerned, even if isolated "anomalies" occur. Thus, relative lake levels in much of the arid and semiarid world can be mapped for selected time intervals over the last 25,000 years. Street-Perrot and Grove (1976, 1979) established a basic methodology that has been widely followed ever since. They identified the total range of lake-level fluctuation at each site, from the level of complete desiccation to the known maximum level (or overflow) and defined three categories: Low levels were when lakes were at no more than 15% of their maximum range, intermediate levels were when lake levels fluctuated between 15% and 70% of their range, and high levels were when lake levels exceeded 70% of the total altitudinal range. Maps were then prepared to show the spatial distribution of low, intermediate, or high lake levels, so defined, at each time interval (e.g., Figures 10.16 and 10.17). These maps demonstrate remarkable coherence in the spatial and temporal patterns of lake-level fluctuations.

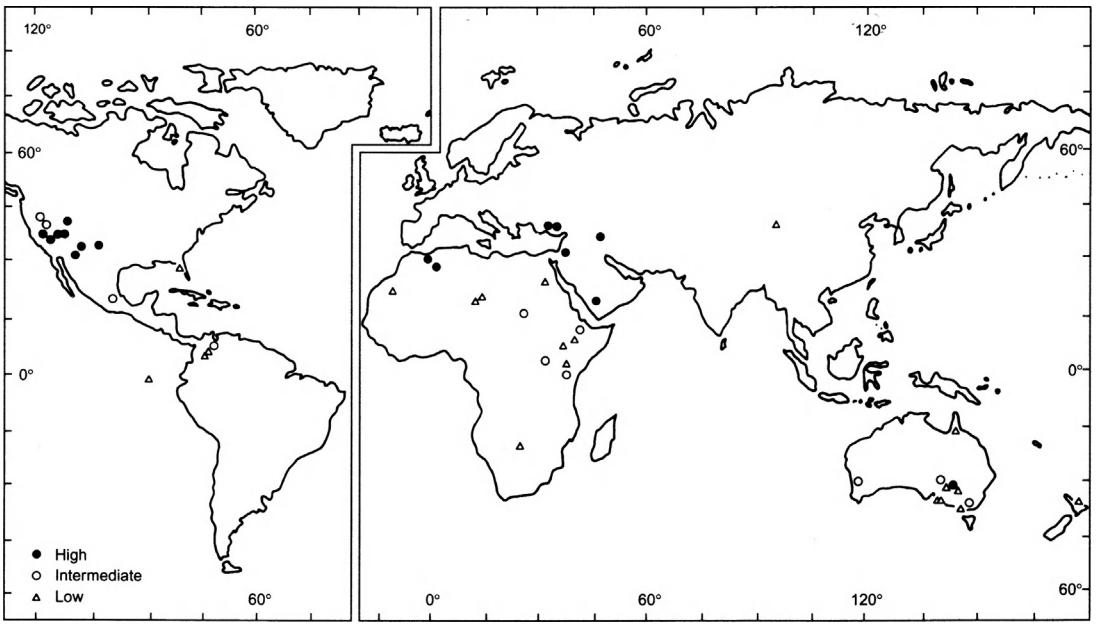


FIGURE 10.16 Lake-level status at ~18,000 years BP. Lakes were low over most of Africa but high in the Western United States. See text for definition of high, intermediate, and low lake status. *From Street-Perrott and Harrison (1985a).*

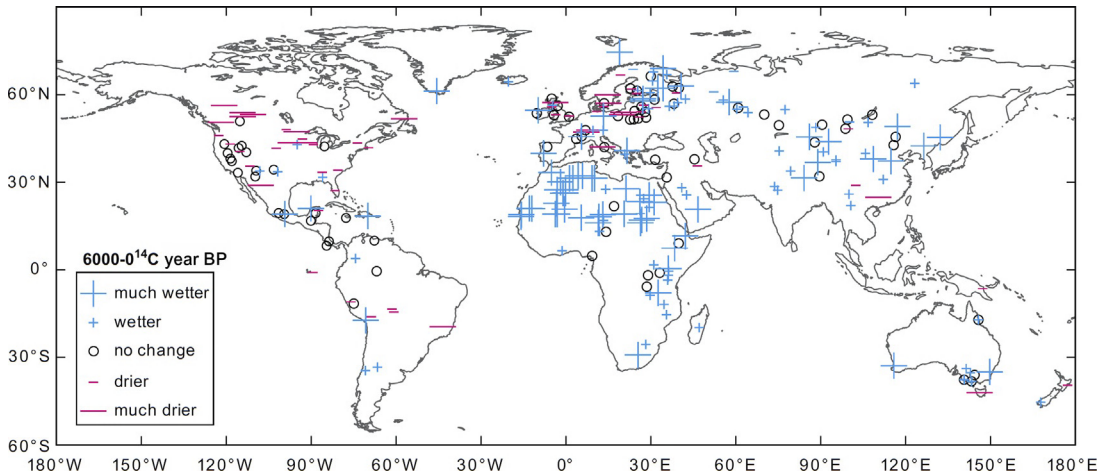


FIGURE 10.17 Change in the global lake status at 6000 ^{14}C years BP (6800 cal. years BP) compared to present. The data are derived from the Global Lake Status Data Base. *From Wanner et al. (2008), after Braconnot et al. (2004).*

During the last glacial maximum (18,000-17,000 years BP), most of the evidence from the intertropical zone (largely dominated by data from Africa) indicates that the area was relatively dry (Figure 10.16); only in extratropical regions (the North American Great Basin, in particular) is there an abundance of evidence for extensive lake stages at that time, related to the displacement of storm tracks around the southern margins of the Laurentide Ice Sheet (Webb et al. 1993a). Thus, the so-called "pluvial" climate of the Western United States at the glacial maximum is not a viable model for tropical and equatorial regions (Butzer et al., 1972; Nicholson and Flohn, 1980). During this arid phase, dune systems on the equatorward margins of the Sahara and Kalahari deserts greatly expanded (Sarnthein, 1978); in the southwestern Sahara, for example, dunes even blocked the much reduced flow of the Senegal River in Mali (Michel, 1973). Low lake levels persisted in these regions until ~12,000 years BP, when many lakes began to fill, commonly spilling over from their enclosed catchment basins and initiating new drainage systems. Maximum lake development throughout the intertropical zone peaked in the Early to Mid-Holocene (Rognon and Williams, 1977; Harrison, 1993; Figures 10.17 and 10.18) though interestingly lake levels were generally low in midlatitudes at this time, suggesting a poleward displacement of the westerlies. In sub-Saharan Africa, lake expansion was particularly spectacular, with Lake Chad expanding in area to a size comparable with the Caspian Sea today (Grove and Warren, 1968; Rognon, 1976; Street and Grove, 1976). The high lake phase continued until 4000-5000 years BP, interrupted in most of Africa, at least, by an episode of increased aridity and somewhat lower lake levels (though still relatively high) around 7500 ± 1000 years BP (Figure 10.19) (Hoelzmann et al., 2004). Profound ecological changes accompanied these periods of more effective precipitation, enabling human occupancy and cultural activities to take place in Saharan Africa at a scale that is almost inconceivable today (see Chapter 12, Section 12.5.5). Since ~4500 years BP, there has been a relatively steady decrease in lake size leading to a situation over the last 1000 years in which lakes over most of the Tropics and lower midlatitudes are virtually all at low stages

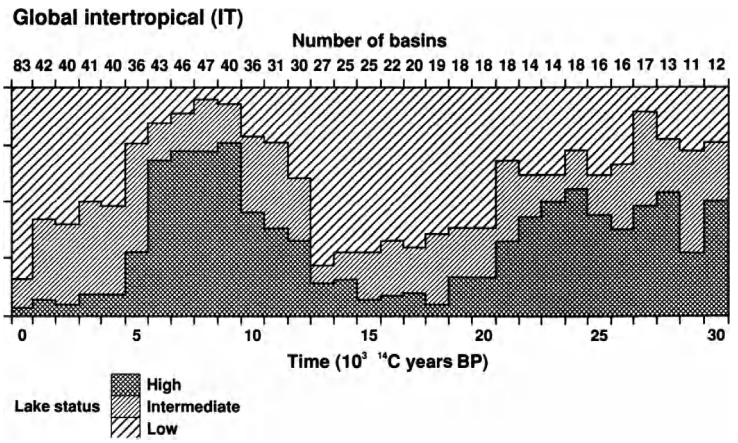


FIGURE 10.18 Histogram of lake-level status in the intertropical zone for 1000-year time periods from 30,000 years BP to the present. Based on the percentage of radiocarbon dates (shown at top of figure) relating to lake levels, which were classified as high, low, or intermediate. Most of the data relate to intertropical Africa. *After Street-Perrott and Harrison (1985b).*

(Figure 10.20). In many areas, it appears that lake levels have rarely been lower during the past 20,000 years.

In spite of the excellent spatial coherence displayed in the maps shown, caution must be used in interpreting lake-level data in this way. Once a lake has desiccated, there is no way of knowing just how much drier conditions may have been during the period of desiccation. Dry periods are thus likely to be underestimated. Comparison of lake basins of vastly different sizes can lead to erroneous conclusions. Small-volume lakes respond much more rapidly to hydrologic variations than large deepwater lakes and are likely to record higher-frequency climatic variations than large-volume lakes. A good analogy to this would be the problems encountered in trying to correlate fluctuations of a small alpine glacier with those of a large ice sheet; clearly, the response times of the two systems are different by perhaps an order of magnitude. The problem is not quite as profound in lake systems, however, since mass turnover rates in lakes are rarely longer than a few decades even for very large lakes (Langbein, 1961). Thus, providing a coarse enough time interval is used, and major low-frequency components of hydrologic changes are being considered, it should be possible to make broad regional comparisons. When regional patterns show little spatial coherence for a particular interval, it may be that the climate was fluctuating fairly rapidly over a wide range so that no major low-frequency signal dominates the record. Finally, it should be noted that the 15% and 70% category boundaries (for low and high stages) used by Street and Grove (1976, 1979) may represent quite different surface area states, depending on the morphology of the basin. Consider, for example, a lake that overflows from a deep narrow basin to a broad shallow plain at some level; the increase in lake depth represents a vastly greater change in surface area (and hence in evaporation from the surface) than a fall in lake level of comparable magnitude. When evaporation from the expanded lake area balances inflow, a new equilibrium is reached. Thus, lake surface area is the critical variable controlling lake depth, and this in turn is a function of the basin morphology. Unfortunately, such data are rare.

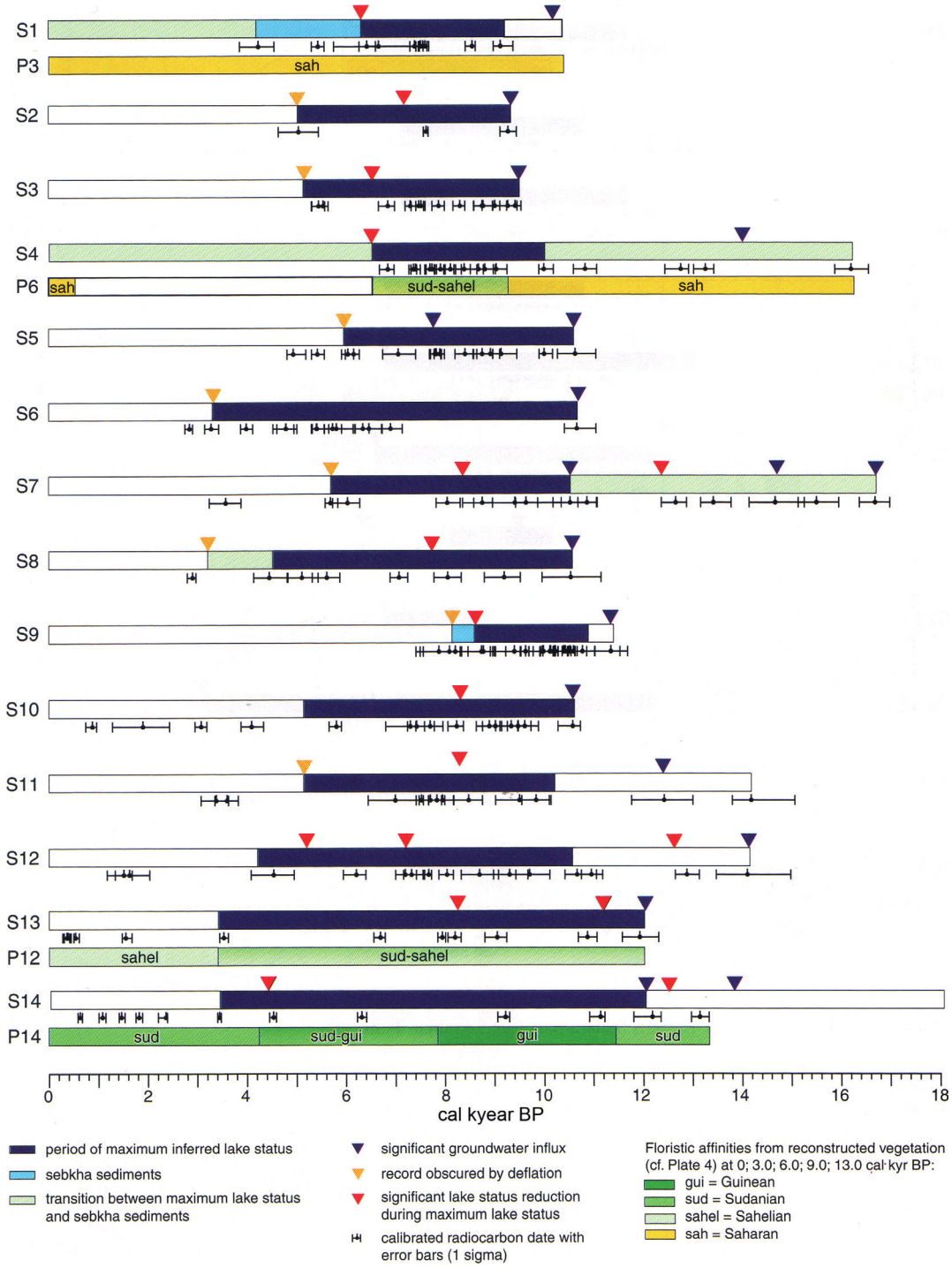


FIGURE 10.19 Paleohydrologic conditions in lakes from the Western and central Sahara, from late glacial time through the Holocene; a similar pattern is found in the eastern Sahara and Arabian Peninsula. Dark color indicates the main wet interval. Red triangles indicate a period when lakes became smaller but still remained large relative to earlier and later periods. The wet Early to Mid-Holocene enabled grazing animals to expand their ranges into the region and for people to settle in many parts of the Sahara that are uninhabitable today, due to the lack of surface water. In some regions, this occupancy is documented by pictographs on rock walls (as shown on the book cover). *From Hoelzmann et al. (2004).*

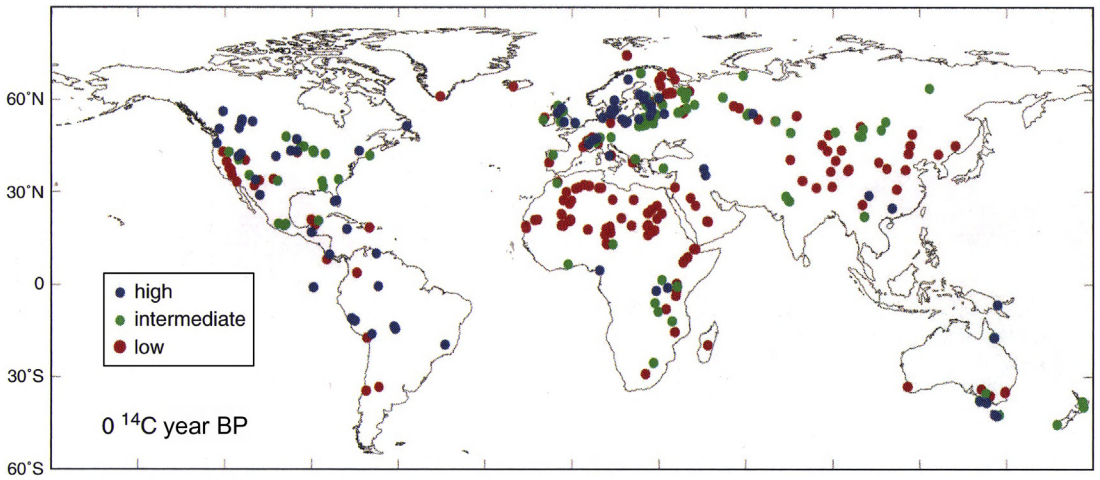


FIGURE 10.20 Modern lake-level status (see text for definition of high, intermediate, and low lake status). It is clear that over much of the intertropical zone, lake levels today are as dry as at any time in the last 25,000 years. *From Braconnot et al. (2004).*

CHAPTER

11

Insects and Other Biological Evidence from Continental Regions

OUTLINE

11.1 Introduction 377

11.2 Insects 377

11.2.1 *Paleoclimatic Reconstructions Based on Fossil Coleoptera* 379

11.2.2 *Paleoclimatic Reconstruction Based on Aquatic Insects* 384

11.3 Former Vegetation Distribution from Plant Macrofossils 388

11.3.1 *Arctic Tree Line Fluctuations* 389

11.3.2 *Alpine Tree Line Fluctuations* 392

11.3.3 *Lower Tree Line Fluctuations and Rodent Middens* 395

11.4 Peat 400

11.1 INTRODUCTION

Biological material as a proxy of climate spans a wide range of subdisciplines, of which two are so large that separate chapters are devoted to them (see Chapters 12 and 13). Here, we focus on the record provided by insects, rodent middens, and other terrestrial biological evidence.

11.2 INSECTS

Insects are the most abundant class of animals on Earth and representatives of the group can be found in virtually every type of environment, from polar desert to tropical rainforest. Naturally, this ubiquitous distribution is only possible because of the great diversity of insect types, each of which has adapted to particular environmental conditions. Of overriding significance to the distribution of an individual species is the climate and in particular the

Copyright © 2015 Raymond S. Bradley.
Published by Elsevier Inc. All rights reserved.

temperature conditions, of an area. Species that are restricted to specific climatic zones are said to be stenothermic, whereas species with less rigorous climatic requirements are eurythermic; clearly, the former group are of most value in paleoclimatic reconstructions and it is these on which paleoclimatic inferences are based. It would be unwise, however, to place too much faith in the presence of any particular individual insect as a climatic indicator, since insects are often extremely mobile and inevitably individuals will be blown far from their optimum habitat. More reliable interpretations can be placed on assemblages of insects, which are commonly found in associations characteristic of a particular climatic regime. Such assemblages are observed today and it is reasonable to assume that similar fossil assemblages represent similar climatic conditions in the past. In this respect, the approach resembles that of palynology. It is the characteristic fossil assemblage that provides the climatic information (Coope, 1967). Excellent, comprehensive guides to the study of Quaternary insects and their use in paleoenvironmental reconstruction are provided by Elias (1994, 2010).

Most paleoclimatic work utilizing insects has involved the study of fossil beetles (Coleoptera; Coope, 1977a,b), though other insects such as flies (Diptera), caddis flies (Trichoptera), and wasps and ants (Hymenoptera) have also provided additional information (Morgan and Morgan, 1979). There are more than 300,000 species of beetles, accounting for 20% of all known organisms (Elias, 2010). Insect fossils are commonly found in sedimentary deposits such as lake sediments or peat, where their exoskeletons, made of chitin (a highly resistant polysaccharide), may be extremely well preserved. This is of great value because taxonomic differentiation of the class is primarily based on exoskeleton morphology. Fossils can, therefore, often be identified down to species level by an examination of microscale features in the exoskeleton (Figure 11.1). One result of this work has been the demonstration of morphological constancy for many species throughout the Quaternary. This is considered to be evidence that they have also exhibited physiological constancy, in other words, they have not altered their ecological requirements, at least over the past 2 million years or so. Although no direct evidence of this can be obtained, the fact that fossil assemblages are often so similar to modern assemblages, in what are assumed to be similar environmental conditions, suggests that radical changes in physiological development have not occurred. This is a fundamental assumption in using fossil insects as paleoclimatic indices, since any change in their climatic tolerances would, of course, invalidate any conclusions that might be drawn from their presence. However, this problem is no different from that facing palynologists or marine microfaunal analysts, and indeed entomologists, have considerably more evidence for genotypic stability in their fossils than can be provided in many other branches of biology.

From a paleoclimatic viewpoint, one of the most important attributes of insects is their ability to occupy new territory fairly rapidly following a climatic amelioration. They thus provide a more sensitive index of climate variation than plants, which have much slower migration rates. Indeed, Coleoptera may occupy and abandon a new territory in response to a marked but brief warm interval, whereas there may be no evidence for such an event in the pollen record because of the lag in vegetation response time (Coope and Brophy, 1972; Morgan, 1973). In short, "this combination of sensitivity and rapidity of response to climatic changes, coupled with their demonstrated evolutionary stability, makes the Coleoptera one of the most climatically significant components of the whole terrestrial biota" (Coope, 1977a). Evidence for the extreme mobility of insect populations is found by comparing the modern distribution of a species with its fossil occurrence. For example, *Tachinus caelatus* has been

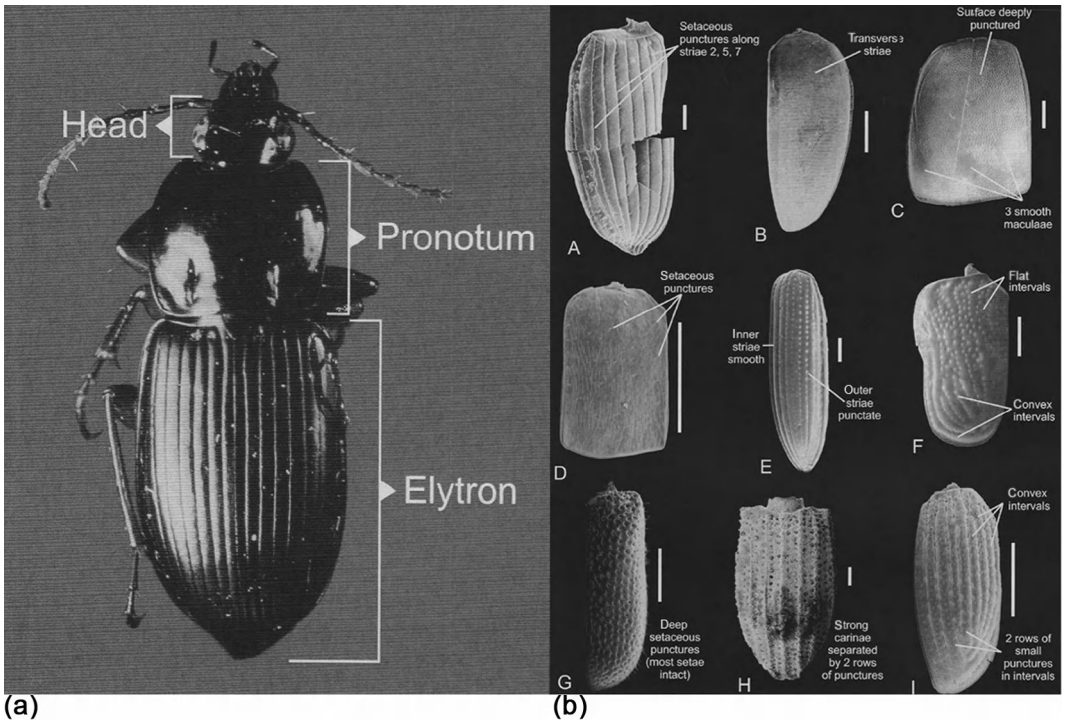


FIGURE 11.1 (a) The beetle, *Pterostichus leconteianus*, showing the principal parts that are commonly preserved in Quaternary deposits. (b) Scanning electron microscope photographs of the elytra of various beetles, showing their distinctive morphology. (A) *Selenophorus gagantinus* (Carabidae); (B) *Choleva americana* (Catopidae); (C) *Hypocaccus estriatus* (Histeridae); (D) *Tachyporus dimorphus* (Staphylinidae); (E) *Aspidoglossa subangulata* (Carabidae); (F) *Pachybrachis mitis* (Chrysomelidae); (G) *Stephanopachys sobrinus* (Bostrichidae); (H) *Rhagodera costata* (Zopheridae); (I) *Apion alaskanum* (Curculionidae). Scale bar = 0.5 mm. *Panel a: from Elias (2010). Photographs kindly provided by Scott Elias, Royal Holloway College, University of London.*

found in glacial-age sediments in Britain, but today, it appears to be restricted to the mountains of Mongolia where an extreme continental climate prevails (Coope, 1994). Numerous other species from glacial deposits in the United Kingdom are today only found in tundra regions of Siberia. By contrast, many British interglacial and interstadial deposits contain insects that are found only in southern Europe today (Figure 11.2). Thus, the insects have responded to climatic change by mass migration, effectively maintaining a more or less constant environment for themselves by shifting geographically as the global climate changes of the Quaternary ebbed and flowed around them.

11.2.1 Paleoclimatic Reconstructions Based on Fossil Coleoptera

A great deal of paleoclimatic work using insects has been carried out in Europe, especially in Britain, where the temperate assemblages of Coleoptera today were replaced in the past by an alternation of boreal or polar assemblages during glacial and stadial events and by more

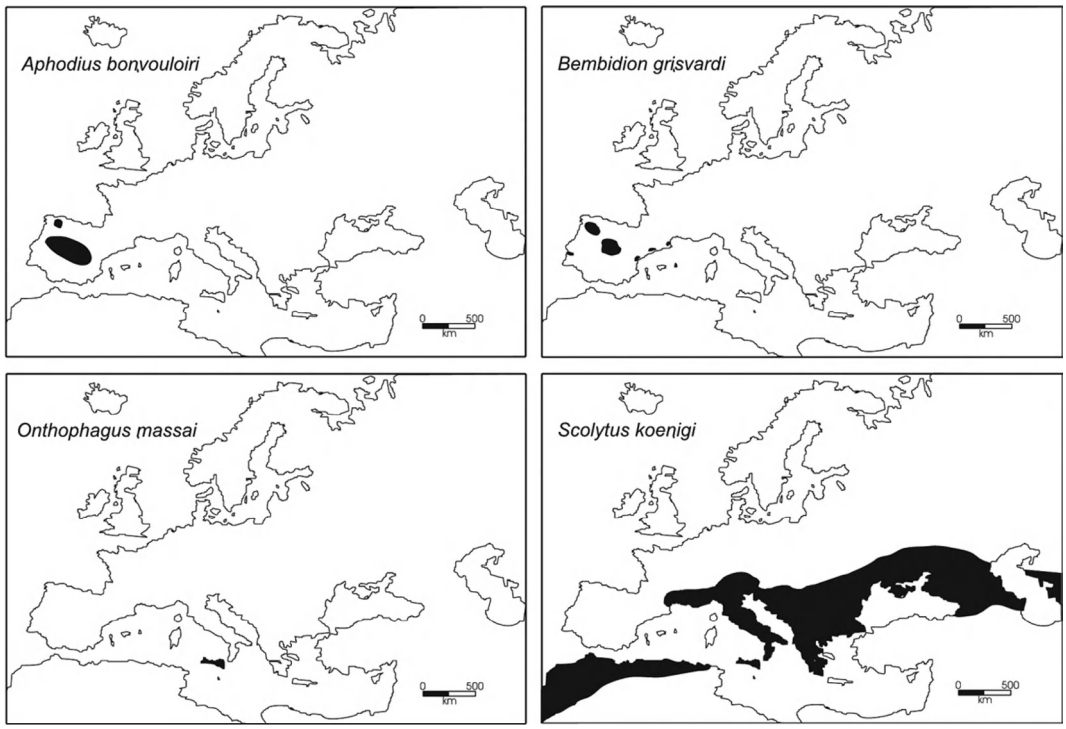


FIGURE 11.2 Modern distribution of four thermophilous beetle species found in interstadial and interglacial deposits in Britain. *From Coope (1986).*

southern or subtropical assemblages during interglacials and interstadials (Coope, 1975a, 1977b). A large number of sites have been studied, ranging in age from interglacial to postglacial (Flandrian). Figure 11.3 illustrates the estimated average July temperature record of the past 120,000 years, since the last (Ipswichian (=Sangamon=Eemian)) interglacial. July temperatures are assumed to be a major control on insect distribution since the northern limits of most thermophilous (warmth-loving) species more closely parallel July or summer season isotherms than isotherms of winter months (Morgan, 1973). Nevertheless, some estimates of winter temperatures can be made by considering the occurrence of species that are today characteristic of continental Eurasia. A species may be an arctic stenotherm (having a northern distribution) but it may live in continental areas where July temperatures are relatively high and winter temperatures extremely low. Bearing such factors in mind, and considering modern climate in areas where the (fossil) species are found today, it is possible to assess the annual temperature range at intervals in the past (Figure 11.3; Coope, 1977b).

Over the past 125,000 years, there appear to have been three distinct periods when temperatures in central England were at least as warm, or warmer, than they are at present: the Ipswichian interglacial, the Upton Warren interstadial, and the Lake Windermere interstadial. The last interglacial was, by definition, the warmest of these episodes, with Coleopteran assemblages characteristic of southern Europe today, present in lowland England; July

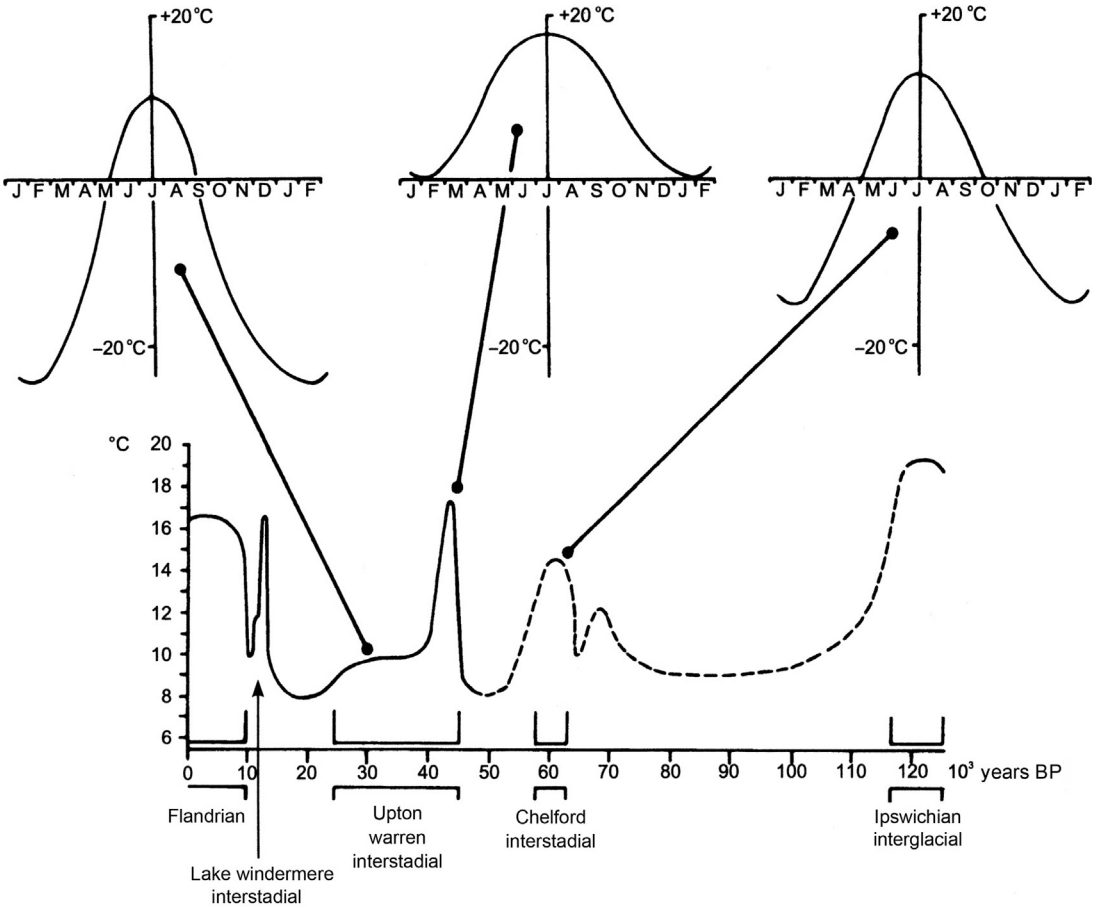


FIGURE 11.3 Reconstructed July paleotemperatures based on insect remains in areas of the southern and central British Isles since the last (Ipswichian) interglacial. Annual temperature ranges are also shown. The period before 50,000 years BP (dashed line) is very uncertain and there may have been a more gradual, monotonic decline in temperature from 120,000 to 60,000 years BP. *After Coope (1977b).*

temperatures are estimated to have been 1-3 °C higher than today (Coope, 1974). Between 50,000 and 25,000 years BP, the climate of Great Britain appears to have fluctuated rapidly between temperate and cold continental conditions. This inference is based on the occurrence of climatically contrasting Coleopteran assemblages that follow one another quite abruptly in stratigraphic sequences. The period has been termed the Upton Warren interstadial complex and includes one brief period (~43,000 years BP) when temperatures seem to have been warmer (by 1-2 °C) than the present day (Figure 11.3). The duration of this interval is uncertain (indeed uncertain radiocarbon dates, close to the limit of the method, may account for the apparently rapid temperature fluctuations of this period), but it may have lasted for 1000-2000 years, followed by a gradual fall in temperature. This cooling was accompanied by more continental conditions, as evidenced by a beetle assemblage typical of parts of Eurasia today;

average February temperatures of −20 °C and July temperatures of only +10 °C seem probable. In spite of periods of relative warmth during the "interstadial complex," central England was devoid of trees all the time and there is little palynological evidence for any climatic amelioration (Coope, 1975b). Evidently, the Coleoptera were sufficiently mobile that they could rapidly move northward as the climate improved, whereas certain plants could not migrate northward fast enough to become established in Britain before the climate once again deteriorated. A similar situation occurred at the end of the Devensian (Weichselian) cold phase when temperatures again rose abruptly, but for only a relatively short period (the Lake Windermere Interstadial; Coope and Pennington, 1977). At this time, an abrupt change from arctic to thermophilous beetle assemblages took place, with maximum warmth occurring around 12,500-12,000 years BP. Shortly thereafter (when from pollen data, it is apparent that birch began to colonize the north of England), the interstadial peak of warmth had passed and a significantly cooler episode was already beginning. The newly established birch forest declined and the thermophilous beetle assemblage was replaced by a northern assemblage typical of tundra regions today. By 9500 years BP, this sequence had been entirely reversed and thermophilous species again rapidly replaced the arctic stenotherms that had been abundant only 500 years earlier (Osborne, 1974, 1980). Again, the more mobile insects were in advance of the vegetation and provide a more accurate assessment of paleoclimatic conditions than could be obtained simply from palynological data.

It is perhaps appropriate to note that Coleopteran and palynological data do not always appear to be out of phase; such situations are probably the exception rather than the rule. The Chelford interstadial (radiocarbon-dated at ∼60,000 years BP), for example, must have lasted long enough for trees to migrate northward into Britain following the cold, Early Devensian period. Coleopteran assemblages are in complete accord with palynological evidence for a cool but quite continental climate at this time (Figure 11.3); conditions in central England were similar to those in southern Finland today (Simpson and West, 1958; Coope, 1959, 1977b).

A more rigorous, quantitative approach to paleoclimatic reconstruction has been applied to Coleopteran fauna from a set of ^{14}C-dated sites in Britain, spanning the past 22,000 years. The "mutual climatic range" method is based on climatic conditions found across the modern range of particular species, which defines their tolerance limits (cf. Grichuk, 1969). The climate of locations where several fossil species once coexisted is defined by the overlapping range of climatic conditions that is compatible with their occurrence together in one place (Figure 11.4; Elias, 1997; Marra et al., 2004). For beetles, this "mutual climatic range" is defined in terms of the mean temperature of the warmest and coldest months (Atkinson et al., 1986b, 1987). Figure 11.5 shows the temperatures reconstructed in this way for Great Britain (50-55°N) for the past 22,000 years, compared to the observed range of temperatures in central England from AD 1659 to 1980. Of particular note is the extremely low winter temperatures during the last glacial maximum (22-18 ka BP) and also from ∼14.5 to 13 ka BP, when the mean temperature of the coldest month was −16 °C and <−20 °C, respectively. Such low temperatures must certainly have been associated with extensive sea ice in the Atlantic, west of Great Britain at those times, or the oceanic influence would have produced a much more moderate climatic regime. From 13.3 to 12.5 ka BP, rapid warming took place (by +25 °C in winter and +7-8 °C in summer), indicating northward migration of the sea-ice front at that time. For a short interval around 12,000 years BP, temperatures were similar to today, but in

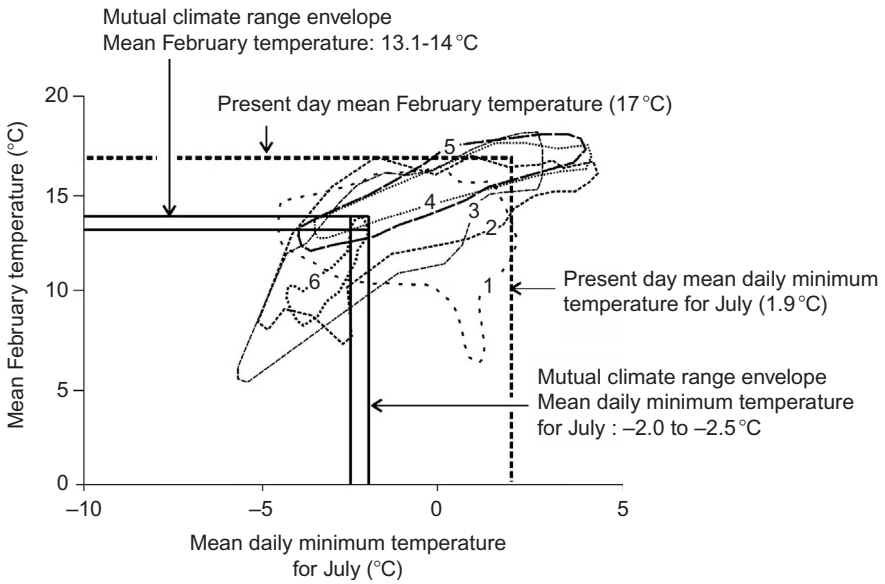
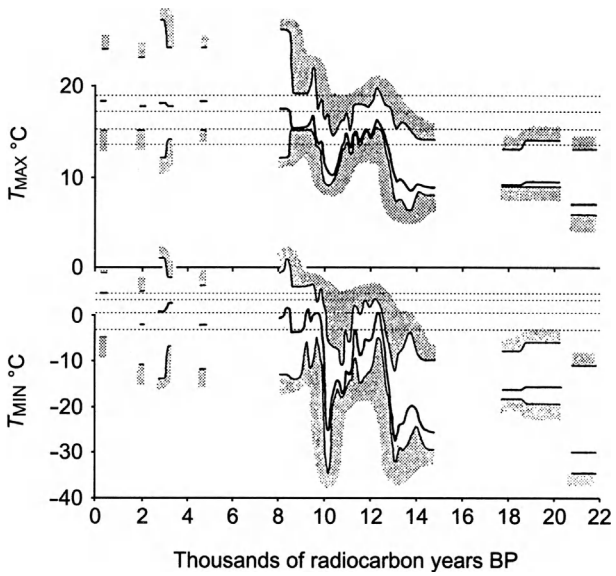


FIGURE 11.4 LGM temperature reconstruction of the lower Awatere Valley, New Zealand, using the mutual climatic range (MCR) method. Mean February and mean July minimum temperatures are derived from the intersection of the climate distributions for six beetle species. (1) *Acritelater reversus*; (2) *Notogonum ferridayi*; (3) *Bombidium hotikikensis*; (4) *Leanobium flavomaculatum*; (5) *Limnichus simplex*; (6) *Aleochara hammondi*. From Marra et al. (2004).

FIGURE 11.5 Mean temperature of the warmest and coldest months of the year (TMAX and TMIN) for intervals over the past 22,000 years, according to beetle remains in sediments from various sites across the British Isles, calibrated using the mutual climatic range method. The dark center lines give the best estimate of temperature, and the upper and lower lines, the extreme ranges of estimates (based on the average of samples of similar ages). The inner horizontal lines give the range of decadal mean temperatures, in the warmest and coldest months, recorded in central England over the interval AD 1659-1980; the outer horizontal lines give the range of warmest and coldest individual years over the same interval. *From Atkinson et al. (1987).*



the ensuing Younger Dryas cold event, the region was plunged back into glacial-like conditions, followed by abrupt warming to a more equable maritime climate by the Early Holocene. One note of caution is required regarding the apparent abrupt changes: radiocarbon "plateau" (see Chapter 3, Section 3.2.1.5) makes the definition of a precise chronology difficult at certain times (especially around 10,000 ^{14}C years BP). This may tend to exaggerate the rapidity of environmental changes at these times.

The longest insect-based paleotemperature reconstructions using the mutual climatic range approach are that of Ponel (1995) who examined insects in cores from the Grande Pile (France). This record extends back to before the last interglacial and provides insect-based paleotemperature estimates from ~135 to ~25 ka BP (cf. Figures 12.18 and 12.19). The analysis indicates that in the coldest part of the last glaciation, mean temperatures in the warmest month were ~10 °C lower than in the Eemian optimum and, in the coldest month of the year, they may have been >20 °C colder in glacial times than in the last interglacial.

The mutual climatic range approach has not yet been widely employed beyond Europe, though applications to other regions data have made (summarized in Elias, 2010). However, it has rarely been possible to reconstruct long-term temperature variations in any detail, as Coope has done for Great Britain. This is primarily because the insect fauna of many regions is not as well studied as that of Europe and the distribution and ecology of modern insects are often not well known (Ashworth, 1980; Morgan and Morgan, 1981). Consequently, it is more difficult to accurately reconstruct paleoenvironmental conditions by fossil insect faunal assemblages. As more studies of both modern and fossil assemblages are carried out, this situation should improve significantly, and important results are nevertheless possible in some areas. For example, studies of late glacial sites in Chile suggest that there was no Younger Dryas episode in that area, shedding new light on an ongoing controversy (Hoganson and Ashworth, 1992).

11.2.2 Paleoclimatic Reconstruction Based on Aquatic Insects

In studies of lake sediments, certain aquatic insects have proven useful in paleoclimatic reconstruction. Nonbiting midges (Order, Diptera; Family, Chironomidae) are of particular importance. These freshwater insects (a type of two-winged fly) have an aquatic larval stage in their life cycle. The head capsules of the larvae are chitinous and thus commonly preserved in lake sediments. These capsules have characteristic morphologies that enable them to be identified to genus and often to species level (Figure 11.6). Since the midges are sensitive to air temperature (and the larvae to water temperature), chironomid remains have proven to be extremely good indicators of paleotemperatures (Brooks, 2003, 2006; Porinchu and MacDonald, 2003). Furthermore, chironomids have a short life cycle and thus provide an essentially instantaneous response to changes in their environment (Hofmann, 1986; Walker, 1987).

Many studies have been carried out to determine which environmental factors influence the modern distribution of chironomids (e.g., Walker et al., 1997; Lotter et al., 1999; Brooks and Birks, 2001; Larocque et al., 2001; Porinchu et al., 2002; Francis, 2004). These span a wide range of geographic settings, but all point to midsummer temperature (of the air and/or water) as the primary factor influencing species distribution. Other factors, such as pH, salinity, oxygen content of the water, and water depth, may also be important in some circumstances, but temperature is generally the overriding variable (Walker and Cwynar, 2006). This



FIGURE 11.6 Head capsule of the larvae of the chironomid *Abiskomyia*. The characteristic morphology allows this specimen to be identified to the genus level, though in some cases, chironomid remains can be identified to species level. *Photomicrograph courtesy of Donna Francis, University of Massachusetts, Amherst.*

has led to a number of paleotemperature reconstructions based on chironomid larval remains in lake sediments. As an example, Figure 11.7 shows a chironomid stratigraphy from Whitrig Bog (southeastern Scotland) for the late glacial-Early Holocene transition, arranged by the chironomid temperature preferences. Using a modern data set that relates chironomid taxa presence in more than 100 lake surface sediments to mean July air temperature, the paleomidge data can be converted to a paleotemperature record (Figure 11.8; Brooks et al., 1997; Brooks and Birks, 2000, 2001). Temperatures rose from ~6 °C at the start of the record to around 11 °C during an early interstadial phase, before dropping 3-4 °C during the Younger Dryas episode, then returning to warmer conditions in the Early Holocene. Short cold events during the early warm period are clearly distinguished. The resulting reconstruction mirrors

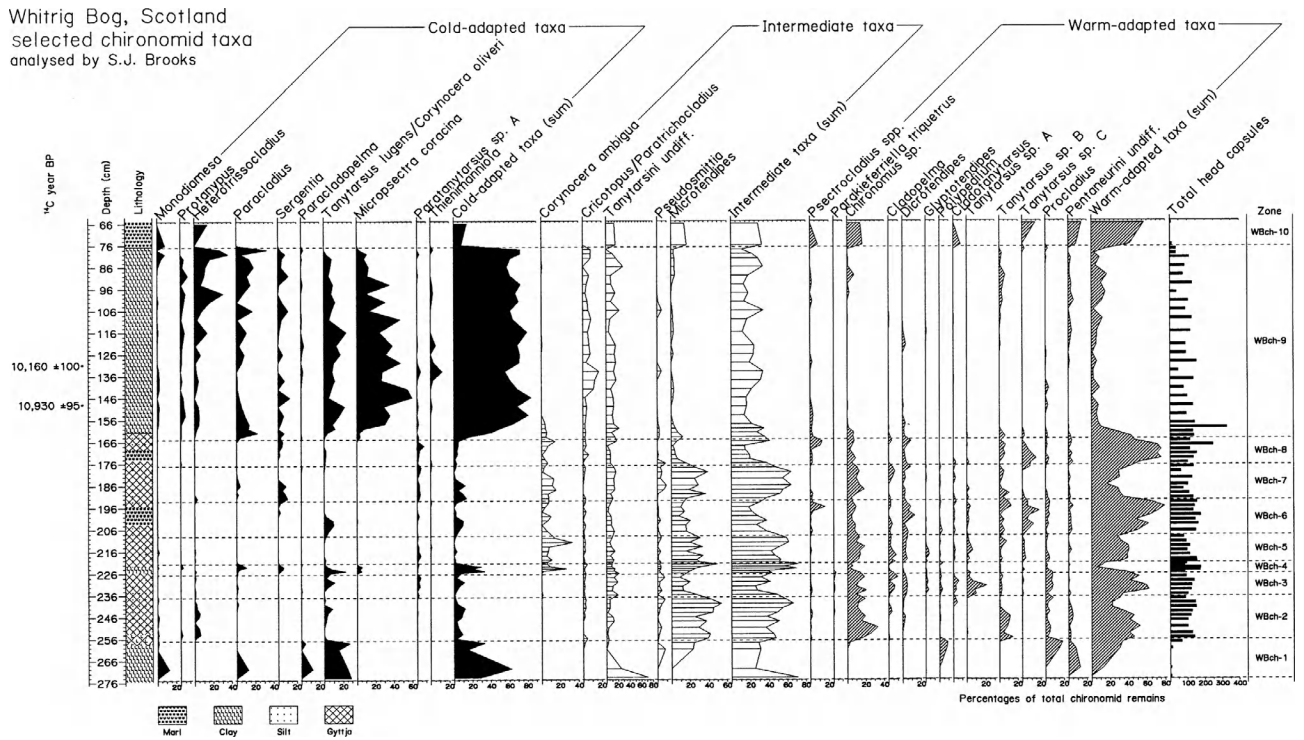


FIGURE 11.7 Late glacial chironomid stratigraphy from Whitrig Bog, southeast Scotland, with the cold-intermediate and warm-adapted taxa grouped, from left to right. A clear change occurred at 166 cm depth, at the onset of the Younger Dryas interval, from warm- and intermediate- to cold-adapted taxa. *From Brooks and Birks (2001).*

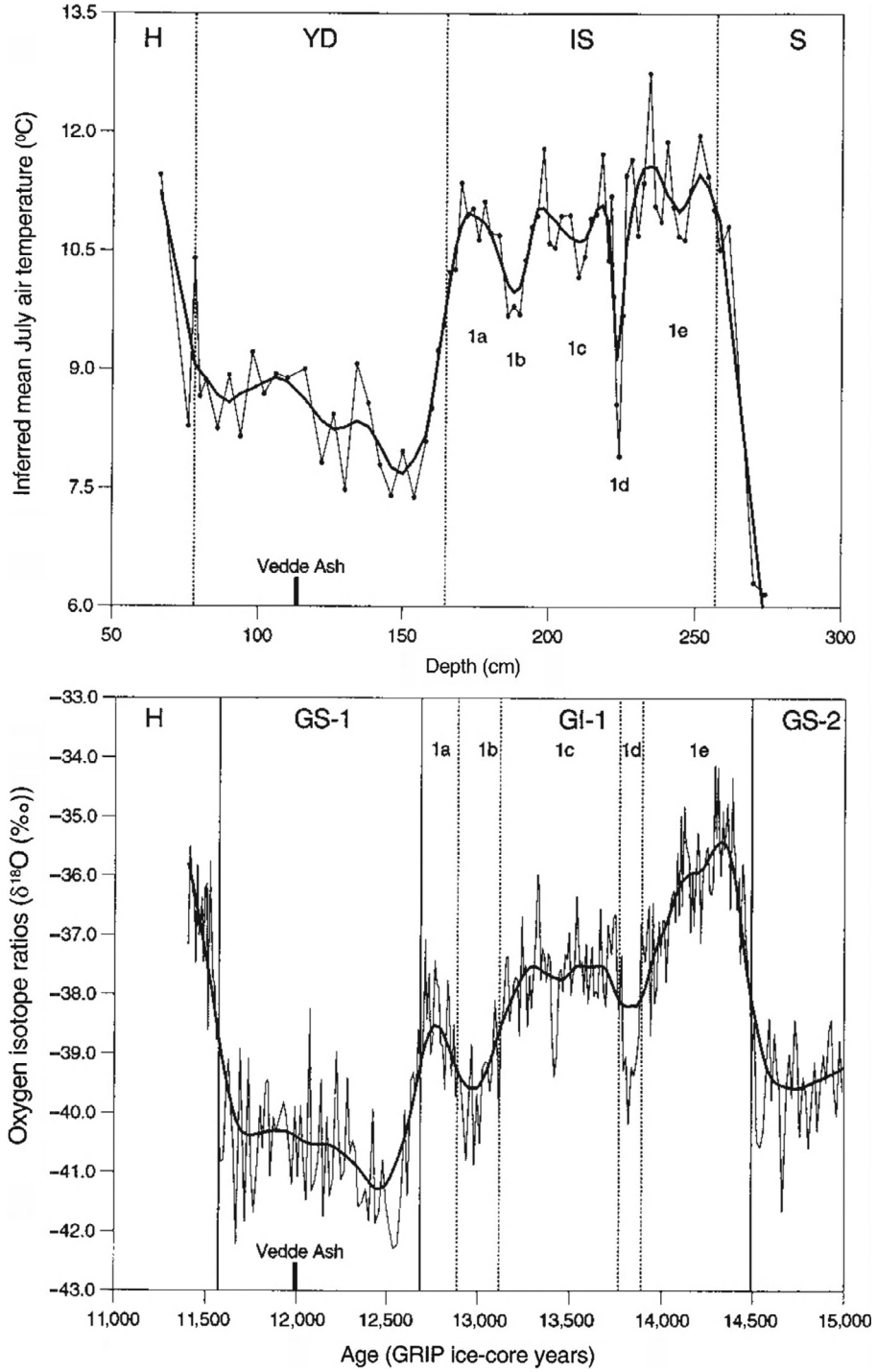


FIGURE 11.8 (a) The late glacial and Earliest Holocene chironomid-inferred mean July air temperature reconstruction (°C) at Whitrig Bog compared with (b) the GRIP oxygen isotope data. From Johnsen et al. (1992) and Dansgaard et al. (1993). The GRIP timescale is in GRIP ice-core years BP. The occurrence of the Vedde volcanic ash is marked in both plots and a tentative correlation between the GRIP isotope stratigraphy (events Holocene, GS-1, GI-1, GS-2, and episodes GI-1a to GI-1e), and the chironomid-inferred temperature is shown. *From Brooks (2006).*

extremely well the oxygen isotope stratigraphy of the Greenland Ice Sheet—so well, in fact that the "event stratigraphy" from GRIP (Björck et al., 1998) can be transposed to the Whitrig Bog record to provide a chronology for the chironomid-based temperature variations (Figure 11.8). Interestingly, a few studies have explored the possibility of using oxygen isotopes in the chitinous head capsules of chironomids (as well as in chitin from beetles; discussed in Elias, 2010) as a direct measure of past temperature. This relies on the relationship between temperature and the isotopic composition of precipitation (or lake water, assuming no enrichment due to evaporation) as the line of argument (e.g., Wooller et al., 2004; Wang et al., 2009).

In some situations, chironomids can provide a record of paleosalinity, related to changes in the water balance (or depth) of lakes (Walker et al., 1995; Eggermont et al., 2006). Thus, Verschuren et al. (2001) used chironomids (together with other evidence) to infer lake-level variations over the past 1100 years at Lake Naivasha, close to the equator in Kenya. This showed the freshest waters, associated with a highstand of the lake, in the seventeenth and eighteenth century and saline conditions from ~AD 1000 to 1270, when the lake fell to its lowest level of the last millennium. Hence, in areas where pronounced changes in salinity are likely to have occurred, chironomids may be useful paleoecological indicators. However, in most situations, they will be of secondary importance to diatoms, which are more diagnostic of salinity conditions (e.g., Fritz et al., 1991).

Apart from chironomids, the use of aquatic insects in paleoenvironmental reconstruction has been somewhat exploratory. Williams and Eyles (1995) suggested that the occurrence of different caddis flies (Trichoptera) in deposits of the last interglacial and Early Wisconsin age from near Toronto indicates a change in temperature of 4-5 °C from 80 to 55 ka BP. This estimate is based on modern climatic conditions in the present-day distribution of the different species identified. Such studies provide complementary information to support more comprehensive paleoenvironmental reconstructions (e.g., Williams, N.E. et al., 1981).

11.3 FORMER VEGETATION DISTRIBUTION FROM PLANT MACROFOSSILS

It is not uncommon for plant macrofossils to be found far beyond the range of the particular species today. Where climatic controls on present-day plant distributions are known, their former distribution may be interpreted paleoclimatically, from dated macrofossils. Fluctuations of three major biogeographic boundaries have been studied in considerable detail using macrofossils: the arctic tree line, the alpine tree line, and the lower or "dryness" tree line of semiarid and arid regions. In each case, the precise definition of tree line poses considerable problems since there is rarely a clearly demarcated boundary. Commonly, there is a gradual transition from mature dense forest through more open, discontinuous woodland to isolated trees or groups of trees, which may include dwarf or krummholz (deformed) forms, particularly in the alpine case (LaMarche and Mooney, 1972). Topoclimatic factors are particularly important in determining the precise limit of trees. It is not necessary to dwell on this at length here, but sufficient to note that the location of the modern tree line is itself often problematical and may make the interpretation of macrofossils somewhat difficult. Furthermore, tree line position today may not be in equilibrium with modern climate, but reflect conditions in the past when seedlings were able to become established. For further discussion of the problem, see Larsen (1974), Wardle (1974), and Holtmeier (2000).

11.3.1 Arctic Tree Line Fluctuations

Macrofossil evidence of formerly more extensive boreal forests has been found throughout the Northern Hemisphere, in tundra regions of Alaska, northern Canada, and the USSR (e.g., Miroshnikov, 1958; Tikhomirov, 1961; McCulloch and Hopkins, 1966; Ritchie, 1987). In addition, paleopodzols (relict forest soils) and charcoal layers (relating to forest fire episodes) have been found in many tundra areas of Keewatin, north-central Canada (Bryson et al., 1965; Sorenson and Knox, 1974). In most areas, the macrofossil evidence is episodic in nature, made up of radiocarbon dates on isolated tree stumps located north of the modern tree line. In Keewatin, a number of dates (also on organic material in paleopodzols and on charcoal layers) have enabled a time series of the forest/tundra boundary during the latter part of the Holocene to be constructed (Figure 11.9; Sorenson, 1977). According to these data, the northern tree line was 250 km or more north of the modern tree line between 6000 and 3500 years BP (cf. Moser and MacDonald, 1990; Gajewski and Garralla, 1992). Less extensive northward migrations occurred around 2700-2200 and 1600-1000 years BP. By contrast, the presence of arctic brown paleosols (relict tundra soils), buried beneath more recent podzols south of the modern tree line, suggests that the tree line was at least 80 km further south around 2900, 1800, and 800 years BP. In Eurasia, MacDonald et al. (2000) were able to map the extent of different tree taxa based on macrofossils found north of their present limits. From 8000 to 5000 years BP, trees were found close to the (present-day) shores of the Arctic Ocean in areas that are now tundra (Figure 11.10).

What paleoclimatic significance can be ascribed to such fluctuations? Several authors have noted the correspondence of northern tree lines with isotherms of summer or July mean temperatures (Larsen, 1974), so a northward migration of the ecotone may indicate warmer

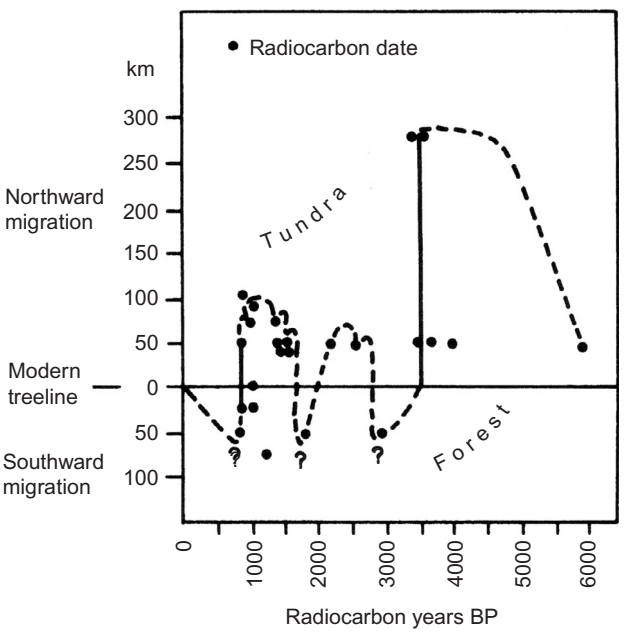


FIGURE 11.9 A reconstruction of Holocene tree line fluctuations in southwestern Keewatin, northwest Territories, Canada. Tree line position is based on radiocarbon-dated tree macrofossils *in situ* north of the present tree line and on dates on buried forest and tundra soils north and south of the modern tree line. *After Sorenson and Knox (1974).*

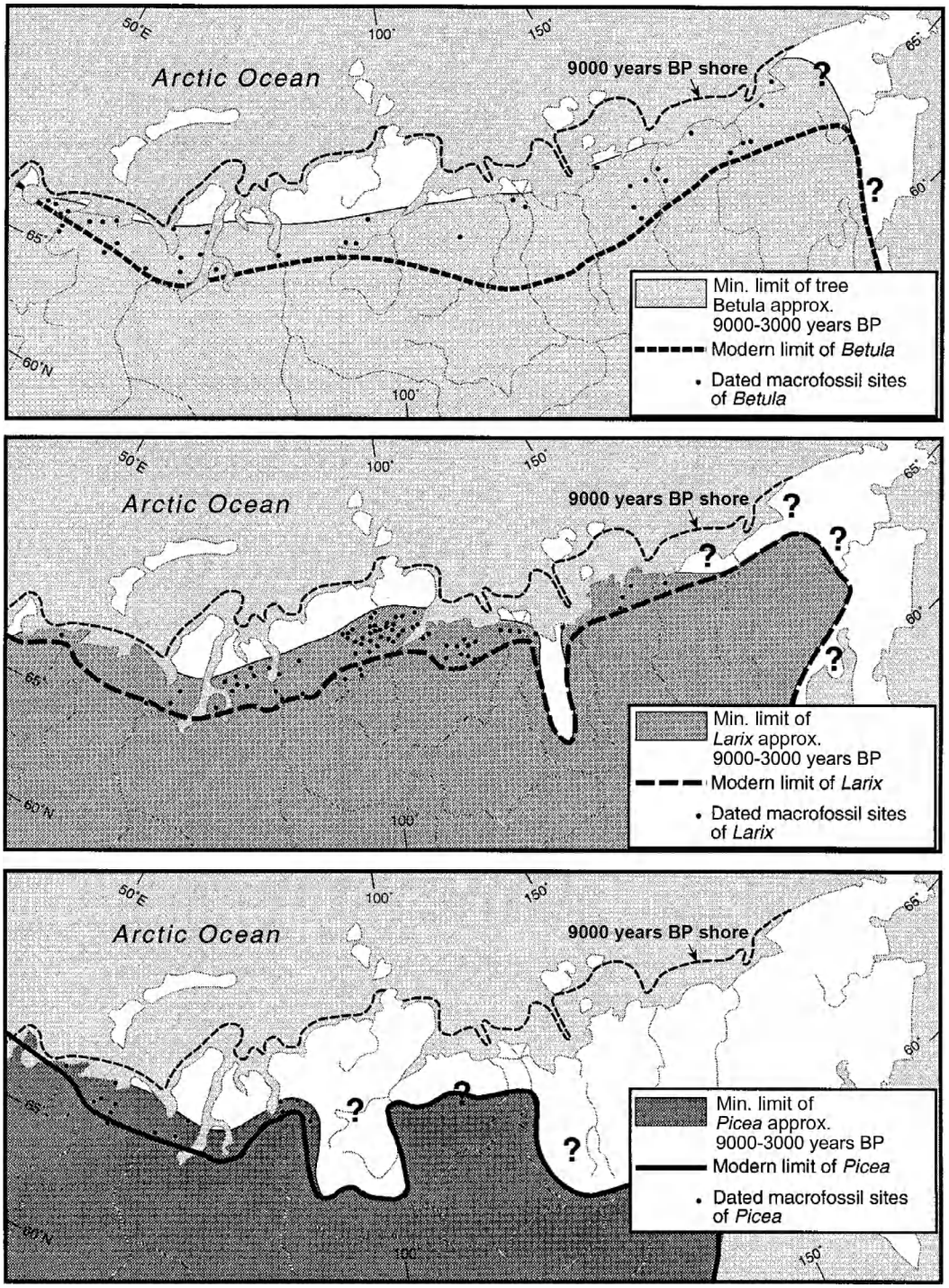


FIGURE 11.10 The latitudinal pattern of boreal forest development across northern Russia in the Early to Mid-Holocene based upon the distribution of radiocarbon-dated wood macrofossils, compared to modern limits. The maps show the northern limits of tree genera (*Betula*, birch; *Larix*, larch; and *Picea*, spruce) between ~9 and 3 ka BP. The inferred location of the Arctic coastline of Eurasia at 9 ka BP (which approximates the present 25 m bathymetric contours) is also indicated. *From MacDonald et al. (2000).*

summer conditions. A tentative calibration of tree line migration in terms of July temperatures was made by Nichols (1967). Nichols assumed that, when the forest limit moved northward 250 km, July temperatures at the modern tree line were similar to locations 250 km south of the tree line today. In this way, July paleotemperatures were reconstructed for Keewatin, using paleosol, macrofossil, and palynological evidence. Modern tree line is also closely related spatially to the mean or modal position of the Arctic front in summer over North America and the median front position over northern Eurasia (Figure 11.11; Bryson, 1966; Krebs and Barry, 1970). Whether this is a causative factor in the location of the northern forest border or whether the vegetation boundary itself largely determines the climatic differences noted across the vegetation boundary is difficult to assess though general circulation model experiments show the tree line has strong feedback effects on climate (Foley et al., 1994). Mid-Holocene warming of the 60-90°N zone, due to orbital forcing alone, was about 2 °C, but experiments with a more extensive boreal forest zone show an additional warming of 1 °C (in summer) and 4 °C in spring. This was the result of higher net radiation due to lower albedo under forest cover (compared to tundra) that was especially critical in the snow-covered spring season.

If air mass boundaries are a determinant of the forest border, then, mapping paleoforest limits may provide an important insight into the dynamic climatology of the past (e.g.,

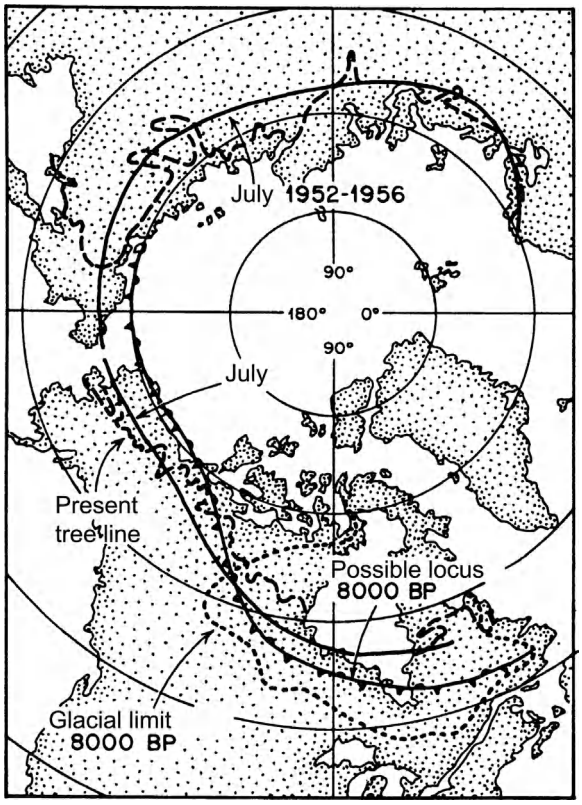


FIGURE 11.11 Modern tree line in relation to modal, mean, or median position of Arctic front in recent years (for definitions of positions, see Krebs and Barry (1970) and Bryson (1966)). Proposed location of front at 8 ka BP is shown, based on macrofossil and palynological evidence. The 8 ka BP position implies a higher-amplitude upper-level westerly flow pattern at that time. *After Ritchie and Hare (1971).*

Ritchie and Hare, 1971). Unfortunately, a number of factors make such interpretations difficult. Northward tree line migration during a climatic amelioration is more rapid than southward tree line migration in response to a climatic deterioration. Once established, trees may survive periods of adverse climate, and the tree line will only slowly "recede" as the trees that die are not replaced (cf. alpine tree lines; LaMarche and Mooney, 1967). This process may differ from one location to another. For example, in the forest-tundra zone of northeastern Quebec (east of Hudson Bay), charcoal from formerly extensive coniferous forests indicates that the tree line (i.e., the limit of continuous forest) does not appear to have migrated north-south en masse. Rather, the evidence suggests that the modern tundra-forest ecotone in this area is the product of a formerly more extensive (mid-Holocene) forest that experienced lower temperatures and periodic destruction by fire in the Late Holocene, leading to the predominantly treeless landscape, with isolated stands of trees seen today (Payette and Gagnon, 1985). Trees were unable to reproduce in the cooler conditions after 3000 year BP (and especially from ~650 to 450 years BP), so the forest-tundra boundary seen today reflects the combined influence of climate and fire history (Payette and Morneau, 1993). Furthermore, detailed studies show the importance of changing growth form in response to climatic change, particularly changes in snow depth. Black spruce (*Picea mariana*) at the northern tree line in Quebec can grow in both upright and prostrate (krummholz) forms, as is typical of many species at their arctic and alpine range limits. In the warmer interval from ~AD 1435 to 1570, spruce was mainly growing as erect trees, but after 1570, cold conditions led to stem dieback so only the snow-protected krummholz forms survived (Payette et al., 1989). Milder temperatures (and possibly heavier snowfall) in the eighteenth century allowed more shoots to form, but very severe winters from ~1801 to 1880 again killed many exposed stems (Lavoie and Payette, 1992). Thus, trees at the northern forest boundary may adapt to cooler climatic conditions by adopting a more prostrate growth form, until more favorable conditions allow them to assume erect growth. In such areas, the idea of a north-south migration of tree line is clearly too simplistic (cf. Holtmeier, 2000). No doubt further studies of ^{14}C-dated macrofossils, paleosols, growth form analysis, and tree-ring variations will produce a more coherent picture of paleoclimate at this important ecotone.

11.3.2 Alpine Tree Line Fluctuations

In a survey of temperatures at alpine tree line sites around the world, from 68°N to 42°S, Körner and Paulsen (2004) found that the upper limits of tree growth had a common thermal limit, with most tree lines having a mean ground temperature of 6.7 °C (~1 °C higher in temperate and Mediterranean regions and ~1 °C lower in equatorial zones). There is thus a broad biogeographic relationship between temperature and the upper limit of tree growth (although mean temperatures are only a convenient proxy for the actual controls, which probably involve the frequency and timing of extreme events; Tranquillini, 1993; Holtmeier, 1994). Furthermore, topoclimatic factors (particularly aspect, shading and cold air drainage), as well as the effects of grazing by herbivores, and past fire history have affected tree line position in many places (Holtmeier, 2000). In the arid subtropics, tree line is influenced by both temperature and the availability of moisture. In the humid tropics, where seasonal temperature

differences are extremely small, the transition to a treeless zone is generally much more abrupt. In mid to high latitudes (particularly in the Northern Hemisphere), tree lines are often more diffuse, reflecting strong topoclimatic controls.

Evidence of higher tree line in the past is commonly interpreted as indicating warmer summer temperatures, using a lapse rate of 0.6-0.7 °C per 100 m to assess the magnitude of temperature change. For example, Dahl and Nesje (1996) estimated that summer temperatures in northern Sweden have varied by ~1.5 °C over the Holocene, based on tree line variations of <220 m (Figure 11.12). However, there are a number of problems in interpreting such data (Karlén, 1976). In particular, the macrofossil record may be incomplete; the highest trees may not have been found or indeed may not have been preserved. Furthermore, in some areas, mountain summits may not extend far enough beyond the modern tree line to give a maximum estimate on former tree line extent (e.g., LaMarche, 1973). In those situations, paleotreeline evidence would only provide a minimum paleotemperature estimate. Finally, present tree line may not be in equilibrium with modern climate; a recent history of fire, overgrazing, avalanches, gales, or insect infestation may have resulted in a tree line well

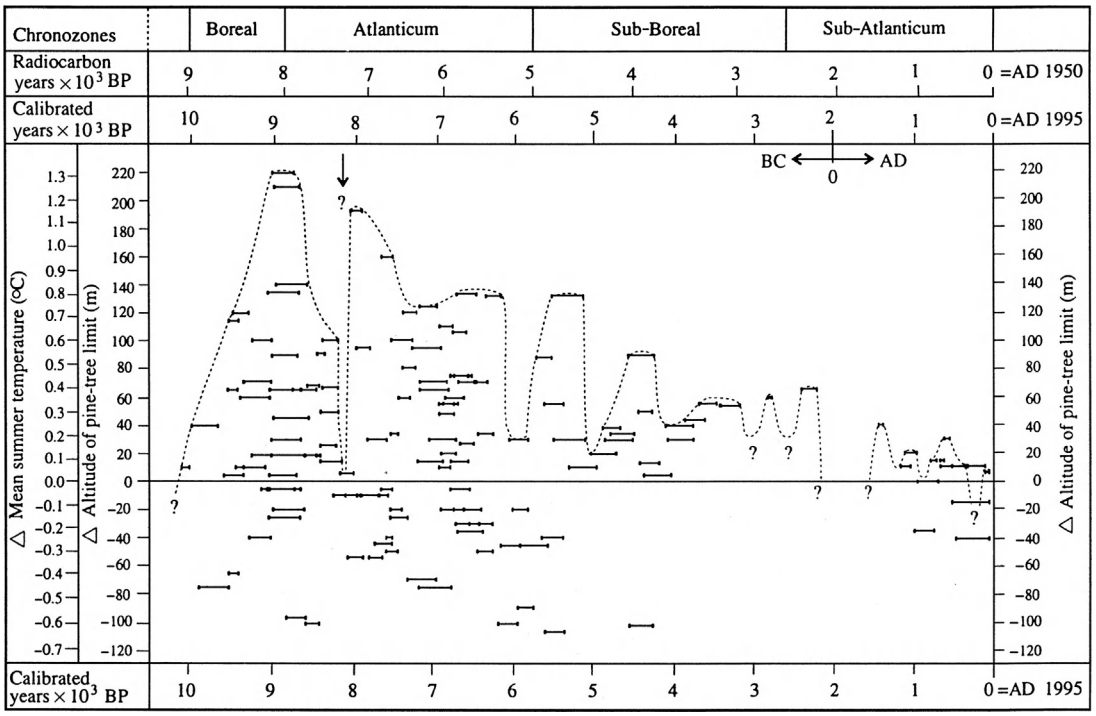


FIGURE 11.12 Elevation of ^{14}C-dated subfossil pine wood samples (*Pinus sylvestris* L.) in the Scandes Mountains, central Sweden (black bars), relative to modern pine limit in the region (after adjustment for isostatic rebound during the Holocene). Upper limit of pine growth is indicated by the dashed line. Changes in temperature are estimated by assuming a lapse rate of 0.6 °C/100 m. Wood samples were ^{14}C-dated close to the core, to obtain an age near the time of germination. *From Dahl and Nesje (1996), based on samples collected by L. Kullman and G. and J. Lundqvist.*

below the potential maximum for modern climatic conditions (Holtmeier, 2000). Trees take many years to become established during periods of favorable climate and may not have reached their highest position until after the temperature maximum; again, this would tend to give a minimum paleotemperature estimate based on tree line fluctuations. It is also worth noting that the time of tree line establishment may be of more significance than the time of tree death (which may not have been climatically related). Ideally, then, one should attempt to date the innermost wood fraction by either radiocarbon analysis or dendrochronology or both (LaMarche and Mooney, 1967, 1972), though often the inner wood has weathered away or decayed, making this impossible and providing only a minimum estimate on the timing of alpine tree line advances. Karlén (1976) considers that higher tree lines in the past probably indicate mean temperatures above contemporary values for periods of 50-100 years, in order for young seedlings to become established and for the tree line as a whole to "advance." Once established, trees can survive periods of adverse climate, perhaps equally as long; thus, tree line variations could be considered as providing a low-frequency record of past climate that is biased toward recording warmer intervals of >50 years in duration.

Bearing all these factors in mind, it is perhaps not surprising to find that the alpine tree line record, considered on a worldwide basis, is extremely complex. Nevertheless, there is evidence that tree lines were higher during the Early to Mid-Holocene in many areas, perhaps reflecting a globally extensive warmer interval. The most comprehensive studies have been carried out in Scandinavia where hundreds of birch, alder, and pine macrofossils from above modern tree line have been ^{14}C-dated. These show unequivocally that the altitudinal limit of trees was well above modern tree line elevation from soon after deglaciation of the mountains (~9000 years BP) to the Mid-Holocene. In northern Fennoscandia, the maximum extent of pine was ~5 ka BP, becoming lower especially after ~3.5 ka BP (Eronen and Huttunen, 1987; Karlén, 1993). In central Sweden (Figure 11.12), pine grew at least 220 m above its mid-twentieth century limit from 9 to 7 ka BP but was replaced by birch as the highest elevation species around 6 ka. At that time, pine reached its maximum Holocene abundance, and birch forest extended 200 m above modern limits (Kullman, 1989, 1993). This suggests July temperatures were ~1-2 °C above mid-twentieth century levels (using a lapse rate of ~0.65 °C/100 m). Cooling set in after ~3500 BP, at which time many glaciers that had completely disappeared in the Early Holocene reformed (Karlén, 1993; Kvamme, 1993; Matthews, 1993). This marked the first of several neoglaciation episodes, culminating in the most recent cold episode from the sixteenth to nineteenth century AD (the "Little Ice Age"). Detailed studies of dead larch trees above modern tree line in the northern Urals showed that prior to the Little Ice Age, trees grew 60-80 m above the modern limit (from the ninth to the thirteenth century AD), but nothing was established after that date until the mid-twentieth century (Shiyatov, 1993). Trees from this medieval warm period did survive into the subsequent colder period, but many died in the late thirteenth and early fourteenth century, in the early 1500s, and in the early and late nineteenth century (cf. Kullman, 1987). This pattern echoes the views of many paleoclimatologists that there was an earlier onset to the Little Ice Age (in the fourteenth century) and that the subsequent 500 years experienced a succession of both mild and sharply colder episodes, culminating in the coldest period, in the early nineteenth century (Bradley and Jones, 1992b, 1993; Jones and Bradley, 1992; Mann et al., 1998).

Alpine tree line studies elsewhere mirror to a large extent the picture emerging from Scandinavia (e.g., the parallel changes found in the Carpathian Mountains by Rybnfckova and Rybnfcek, 1993, and in the Swiss Alps by Tinner et al., 1996). Similarly, in western North America, several studies indicate tree line was above modern limits in the Early Holocene. In the San Juan Mountains, Carrara et al. (1991) dated >50 macrofossils of conifer wood from above tree line and found evidence for trees up to 140 m above modern limits from 9600 to 5400 years BP, indicating July temperatures were up to 0.9 °C warmer than present. From 5400 to 3500, tree line was near modern limits and, then, a climatic deterioration led to a decline in tree line after 3500 BP. This is similar to evidence from the Canadian Rockies (Luckman and Kearney, 1986; Clague and Mathewes, 1989) and from other parts of the western United States (Rochefort et al., 1994). In some areas, the absence of radiocarbon-dated wood at certain intervals suggests brief colder episodes within the Early Holocene but more extensive sampling may revise that picture (cf. Kullman, 1988). Macrofossil evidence is a rather blunt instrument and apparent "data gaps" are difficult to interpret. Karlén (1993) supports his interpretation of cooler episodes with lake sediment evidence, and this points to the need for integration of many different proxies to fully comprehend the complexity of Holocene climates in mountain areas.

11.3.3 Lower Tree Line Fluctuations and Rodent Middens

Throughout the arid and semiarid regions of the southwestern United States, there is an altitudinal zonation of vegetation with xerophytic desert scrub (commonly sagebrush, evergreen creosote bush, and evergreen blackbrush) at lower elevations, grading into mesophytic woodland (juniper, piñon pine, and live oak) at successively higher elevations (Figure 11.13).

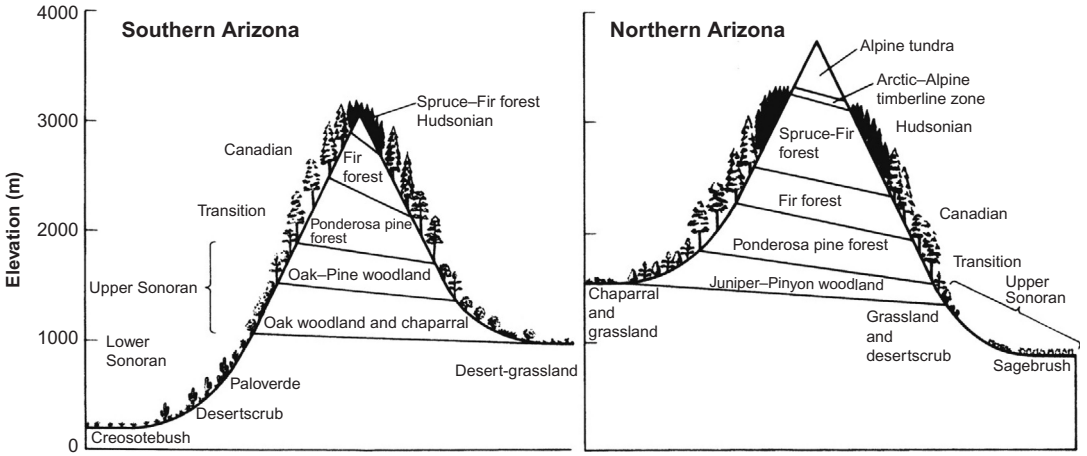


FIGURE 11.13 Transect through mountains of the southwestern United States to show vegetation change with elevation. During glacial times, vegetation boundaries were generally lower due to increased effective moisture (resulting from lower temperatures and/or higher precipitation).

The precise elevation of the woodland/desert scrub boundary varies more or less with latitude, being lowest in the Chihuahuan Desert of Mexico and highest in the interior Great Basin of Nevada. This elevational gradient, decreasing to the south, is related to distance from the source of summer moisture (the Gulf of Mexico and the tropical Pacific); the interior Great Basin is both furthest from these source regions of tropical maritime air and isolated from temperate Pacific moisture sources by the mountain ranges to the west (Wells, 1979). The lower tree line elevational gradient thus strongly reflects the importance of moisture for tree growth, and for this reason, it is sometimes referred to as the "dryness tree line."

Our understanding of fluctuations in the lower tree line has been greatly facilitated by the analysis of fossil middens of the pack rat (genus *Neotoma*) from caves throughout the southwestern United States (Wells and Jorgensen, 1964; Wells and Berger, 1967; Betancourt et al., 1990). Studies of rat middens in other arid and semiarid regions of the world have also provided remarkable insights into past vegetation distribution and associated climatic variations (Pearson and Dodson, 1993; Pearson, 1999; Betancourt et al., 2000; Chase et al., 2011, 2012). Pack rats forage incessantly within a very limited range (~1 ha) of their dens, which are constructed of plant material from the surrounding site. Because of the rats' propensity for collecting items at random, and not simply food stocks, the dens or middens effectively provide a remarkably complete inventory of the local flora (Wells, 1976; Spaulding et al., 1990; Vaughan, 1990). Middens are cemented together into hard, fibrous masses by a dark brown, varnish-like coating of dried *Neotoma* urine (known as amberat). The amberat cements the deposit to rocky crevices in caves and prevents its destruction by fungi and bacteria. Because the cave sites are so dry, *Neotoma* middens may remain preserved for tens of thousands of years; in fact, over a thousand macrofossils from *Neotoma* middens in the western United States have so far been dated, ranging in age from the Late Holocene to >40,000 years BP (Webb and Betancourt, 1990).

Middens are constructed until the rock crevice is filled, so they generally represent samples of vegetation near the site, from discrete time intervals in the past. Many are essentially nests, providing just a short time capsule of the past environment, but some South African *Hyrax* middens have been occupied continuously for long periods of time, preserving a more or less continuous stratigraphic record of vegetation history (Chase et al., 2012). Macrofossils recovered include branches, twigs, leaves, bark, seeds, fruits, grasses, invertebrates such as snails and beetles, and even the bones of vertebrate animals. Such prolific inventories of macrofossils have enabled quite detailed pictures of the local vegetation around the midden site to be reconstructed, though the material collected may not represent a random sample of plants in the area. Because pack rats may collect certain types of material preferentially, middens do not necessarily give a complete picture of the relative abundance of plants in the collection area. Furthermore, different species of pack rat have different collection preferences, so sequential occupancy of the same site by different species might give the erroneous impression of a change in local vegetation (Dial and Czaplewski, 1990).

In spite of these potential problems, regional comparisons of *Neotoma* midden composition across the southwestern United States for different time intervals have enabled the broadscale patterns of vegetation change since the last glaciation to be established. Most significantly, the results demonstrate a dramatic increase in the area of piñon-juniper woodland throughout

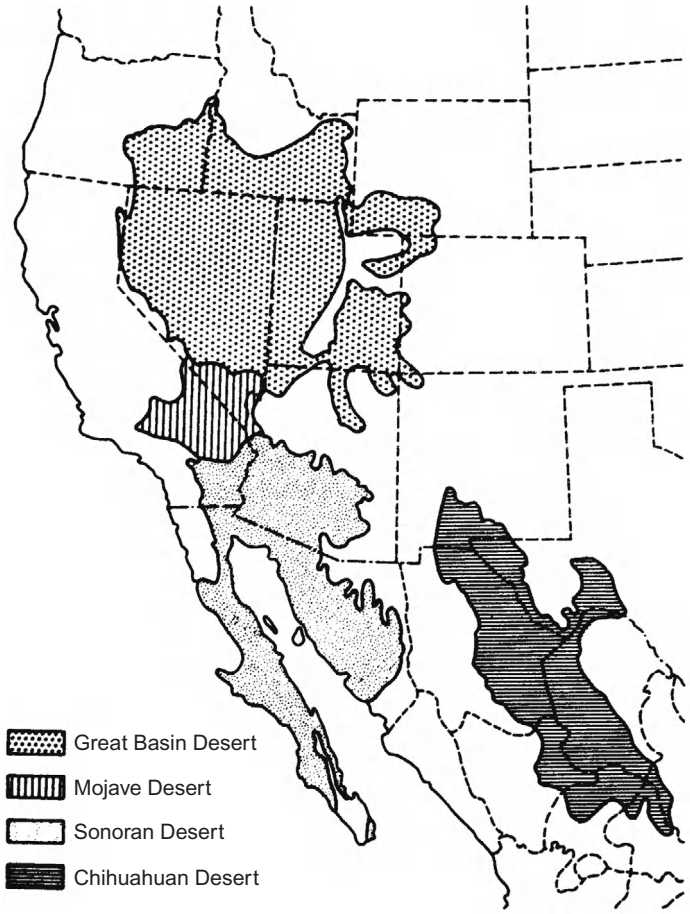


FIGURE 11.14 Desert areas of the western United States. Changing altitudinal vegetation zonation within desert areas is recorded in fossil pack rat middens.

the South during the Late Wisconsin period of maximum glaciation (Van Devender and Spaulding, 1979; Van Devender, 1990a). In the Great Basin, Mohave, Sonoran, and Chihuahuan deserts of today (Figure 11.14), such woodlands are restricted to higher elevations, often on isolated peaks surrounded by vast areas of desert scrubland. However, over periods ranging from >40,000 to ~12,000 years BP, *Neotoma* middens from currently hyperarid sites document the presence of juniper or piñon-juniper woodlands over a vastly enlarged area. In the Great Basin, forest vegetation (now restricted to isolated mountain peaks) extended well below its present range; for example, subalpine conifers grew as much as 1000 m below modern limits (Thompson, 1990). In the Mojave Desert, piñon-juniper woodland occupied terrain down to ~900 m, in areas that today only support thermophilous desert scrub. Similarly, in the Sonoran and Chihuahuan Desert, piñon-juniper-oak woodland extended down to 500-600 m into areas that are extensive deserts today (Van Devender, 1990a,b). Interestingly,

TABLE 11.1 Estimates of Climatic Conditions in the Western and Southwestern United States During the Last Glacial Maximum, Relative to Today, Based on Fossils Found in Packrat Middens

Location	ΔT (°C)	Rainfall	Notes	Sources
Colorado Plateau	>6.3 (Su)	Higher (Wi.)	Drier summers	Betancourt (1990)
Grand Canyon	~6.7 (Ann)	+24-41%	Winter rainfall max	Cole (1990)
Great Basin	10 (Ann)	Higher		Thompson (1990)
Sonoran Desert	8 (July)	+50%	Winter rainfall max	Van Devender (1990b)
Chihuahuan Desert	Strong summer cooling	Higher	Winter rainfall regime; few freezes	Van Devender (1990a)
Mojave Desert	6 (Ann)	+<40%	Winter rainfall max	Spaulding (1990)

in these southern desert regions, the vegetation communities that predominated have no modern analog in the region today, consisting of both forest vegetation and frost-sensitive desert succulents. This suggests a lower frequency of winter cold air outbreaks leading to killing frosts; possibly, the forest cover also helped by reducing nighttime radiational cooling.

The patterns of glacial period vegetation change in the region all indicate lower summer temperatures, by 6-10 °C, reduced evaporation, and enhanced winter rainfall (by up to 50%) (Table 11.1). This is related to the displacement of winter storms southward into the region and a reduction in summer monsoon airflow from the Gulf of Mexico. Such conditions appear to have prevailed, with little change, from at least 22,000 to 12,000 years BP. Rapid changes in climate and vegetation took place in the following few thousand years, so that by 8-9000 years BP, vegetation patterns had begun to look more like modern conditions; the winter rainfall regime had ended, temperatures had risen to within a few degrees of modern levels, and rainfall was largely delivered by summer monsoons (Figure 11.15). Maximum aridity appears to have occurred in the mid-Holocene in some areas (e.g., the Grand Canyon and Mojave Deserts; Cole, 1990; Spaulding, 1990, 1991), but elsewhere, there is evidence for a stronger mid-Holocene monsoon rainfall regime, with drier conditions and the most extensive desert vegetation developing later in the Holocene (Van Devender, 1990a; Van Devender, et al., 1994). In the Mojave Desert, evidence for increased effective moisture in the Late Holocene (3.8-1.5 ka BP) suggests a "neopluvial" of cooler and/or wetter conditions, perhaps correlative with neoglacial episodes in the mountains to the north and east (Spaulding, 1990).

Rat middens from the margins of the hyperarid Atacama Desert in Chile reveal quite dramatic changes in the past climate of the region (Betancourt et al., 2000). Today, vegetation around the midden sites consists of only a few species of grass, but between 11.8 and 10.5 ka BP, the wettest period of the past 22,000 years, a rich flora of shrubs and perennial grasses carpeted the region (Latorre et al., 2002). This evidence is supported by

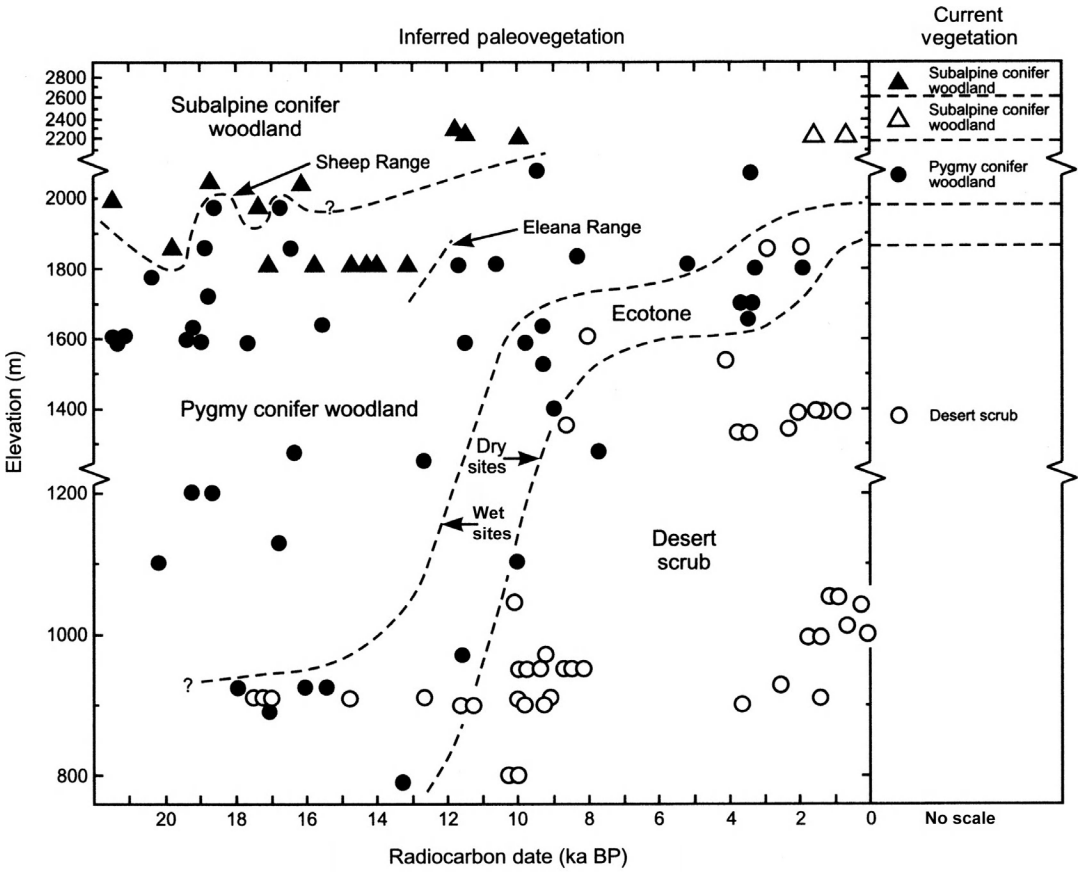


FIGURE 11.15 Changes in major vegetation zones in rocky areas of central-south Nevada over the past 22,000 years, as recorded by macrofossils in the middens of pack rats. Dashed lines indicate the approximate elevation of ecotones. The pygmy conifer (piñon-juniper) woodland/desert scrub transition varied from wet to dry sites, as indicated by the broad ecotone. *After Spaulding (1990).*

geomorphological evidence of high lake level stands across the region and by lake sediment studies that all indicate much wetter conditions, beginning around 15.5 ka BP (Grosjean and Veit, 2005). Betancourt et al. (2000) suggest that the wetter conditions in late glacial and Early Holocene resulted from more La Niña-like conditions, which is associated with a stronger Bolivian high-pressure system, and increased moisture flux up the eastern slopes of the Andes.

In South Africa, middens of the rock hyrax *Procavia capensis* provide continuous records of vegetation from the LGM through the Holocene (Scott and Woodborne, 2007; Chase et al., 2009, 2011, 2012). Analysis of the stable isotopes of nitrogen ($\delta^{15}N$) and carbon ($\delta^{13}C$) provides a record of rainfall through time. During dry periods, ^{15}N is enriched in vegetation, and this is

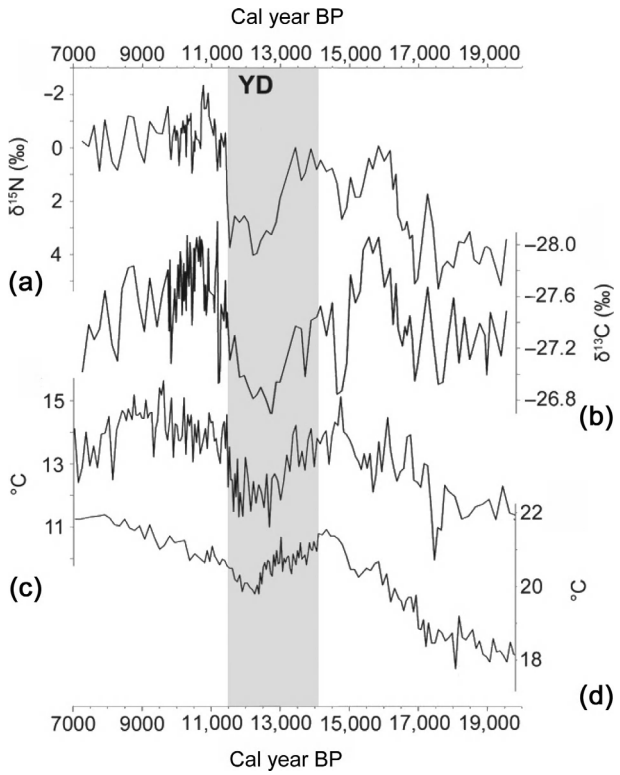


FIGURE 11.16 The record of (a) $\delta^{15}N$ and (b) $\delta^{13}C$ in the midden of a rock hyrax, from the Cederberg Mountains (southwestern tip of South Africa). Higher values of these isotopes reflect drier conditions. (c) and (d) are SSTs from ODP core 1084B and GeoB1023-5, respectively. These indicate increased upwelling of cooler water in late glacial times and during the Younger Dryas period (YD). *From Chase et al. (2011).*

then reflected in the hyrax urine that cements the middens together. A similar signal is seen in $\delta^{13}C$. In this region, the vegetation is predominantly made up of C_3 plants (see Appendix A) with variations in $\delta^{13}C$ reflecting changes in water-use efficiency in the plant leaves (greater enrichment during dry conditions). Together, the $\delta^{15}N$ and $\delta^{13}C$ records provide a coherent picture of rainfall changes through time (Figure 11.16). These reveal dry conditions during the late glacial period, followed by increasingly wetter conditions, but this trend was abruptly interrupted during the Younger Dryas period, when drier conditions resumed. The dry Younger Dryas was associated with cooler sea surface temperatures offshore in the southeast Atlantic. These resulted from upwelling of cooler waters caused by stronger southeast trade winds; cooler subsurface waters offshore were a consequence of a reduction in the warm Agulhas current around South Africa, as the oceanic subtropical front south of the continent shifted toward the equator.

11.4 PEAT

Peat that has accumulated in bogs (acidic mires) has already been mentioned as a natural archive from which tephra and pollen can be recovered, but studies of the peat itself have also provided valuable paleoclimatic information (Barber, 1981; Chambers and Charman, 2004;

Charman et al., 2009; Chambers et al., 2012). Mires are extensive in boreal regions, particularly in areas where drainage is poor due to permafrost impeding groundwater drainage (Figure 11.17). There are also extensive peat deposits in the Tropics, especially in southeast Asia and in the Amazon Basin (Strack, 2008). Most of the boreal peat found today began to accumulate after the last glacial period, whereas tropical peat has accumulated since the Late Pleistocene. Because peatlands occupy such vast areas of the world, they offer rich opportunities for paleoclimatic reconstruction using both paleoecological and geochemical approaches.

Ombrotrophic ("cloud-fed") bogs are of particular significance for paleoclimate reconstructions, as hydrological conditions are directly controlled by the rainfall-evaporation balance. The accumulation or organic matter (principally *Sphagnum* moss, as well as grasses, and dwarf shrubs such as Ericaceae and *Empetrum*) is favored by waterlogged conditions, providing excellent preservation of macrofossils that can be used to reconstruct vegetation history (Barber and Charman, 2003; Barber et al., 2003). Total peat accumulation is largely a function of the rate of decay of the vegetation, rather than overall vegetative productivity. Decay occurs in the upper oxygenated zone (the acrotelm), whereas organic matter accumulates in the waterlogged anoxic zone beneath (the catotelm) (Mäkilä and Saarnisto, 2008). Thus, changes in the height of the water table can have direct effects on the preservation of organic material, which can be measured by analyzing the degree of humification with depth. This is generally done by colorimetric methods, digesting the peat with an alkaline solution and measuring the color of the resulting liquid. Darker colors signify strong humification (a higher level of humic material) when the vegetation was exposed to oxidation (indicating

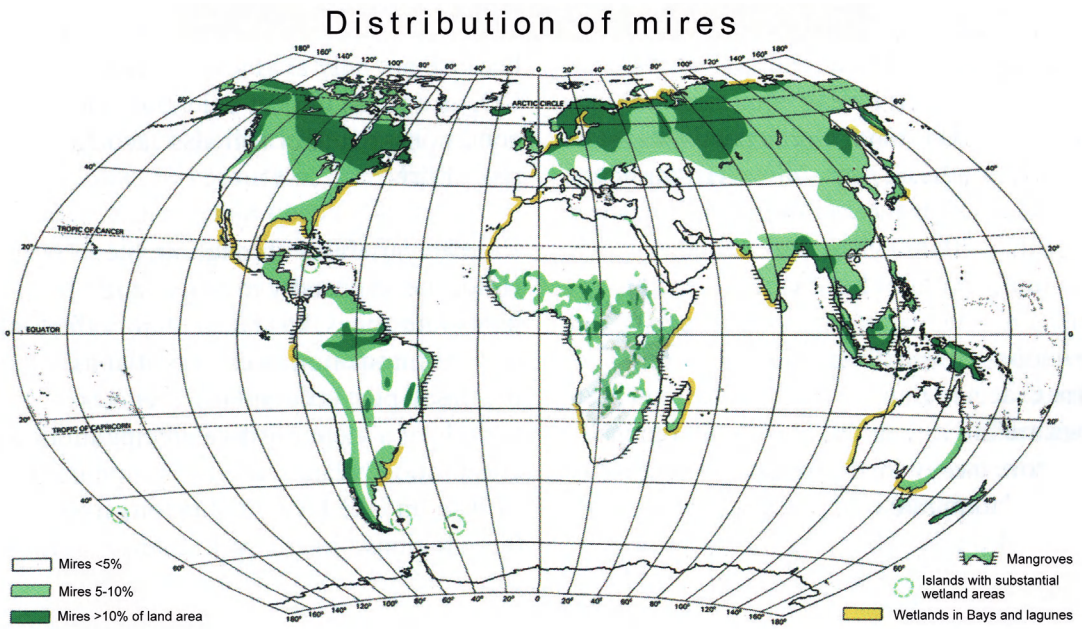


FIGURE 11.17 Global distribution of peatland mires. *From Strack (2008).*

generally dry conditions), and lighter colors point to wetter periods and less humification when the water table was higher. Thus, Vorren et al. (2012) measured the Mid- to Late Holocene record of peat humification in a peat bog in northwestern Norway, identifying 19 episodes when wet intervals were recorded in the peat, some of which appear to have been of wide geographical significance (Figure 11.18). However, the balance of P-E can also be affected by temperature changes, and cool periods (perhaps associated with more snowfall, or longer-lasting snow cover) may also result in wet conditions, so other paleoclimatic indicators such as chironomids may be needed to determine to what extent the hydrological balance is driven by precipitation alone, or by a combination of temperature and precipitation (Charman et al., 2009). Vorren et al. (2012) argued that the changes in bog wetness were strongly related to solar activity variations (using $\Delta^{14}C$ as a proxy for irradiance changes). This link between bog surface wetness and solar activity is a theme that runs through many peat studies, particularly those from western Europe (e.g., Mauquoy et al., 2002; Blaauw et al., 2004; Borgmark, 2005). GCM simulations by Shindell et al. (2001) do indicate that a reduction in irradiance might lead to cooler mean annual temperatures across Europe, with the atmospheric circulation in a more negative North Atlantic Oscillation mode (resulting in wetter conditions across much of western Europe, but leaving Scandinavia with less rainfall). How this would lead to a common signal across widely dispersed sites (even those in southern Chile; van Geel et al., 2000) remains somewhat of an enigma. Certainly, there are other proxies that appear to have registered a solar irradiance signal (e.g., Neff et al., 2001; Niggemann et al., 2003; Wang et al., 2005b), but there is as yet no comprehensive theory that can explain how very small changes in solar activity could affect climate over wide areas of the globe (see Chapter 2, Section 2.7).

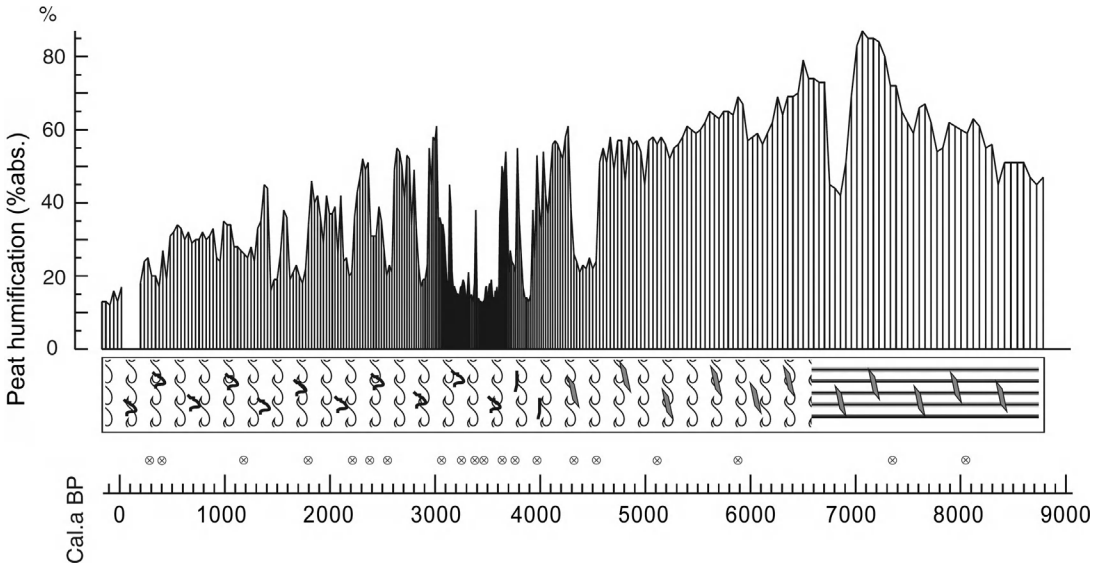


FIGURE 11.18 Humification index in peat from Rystad mire, Lofoten, northwestern Norway, based on colorimetric measurements of humic material extracted from the peat. Low values indicate wet conditions when the water table was high. *From Vorren et al. (2012).*

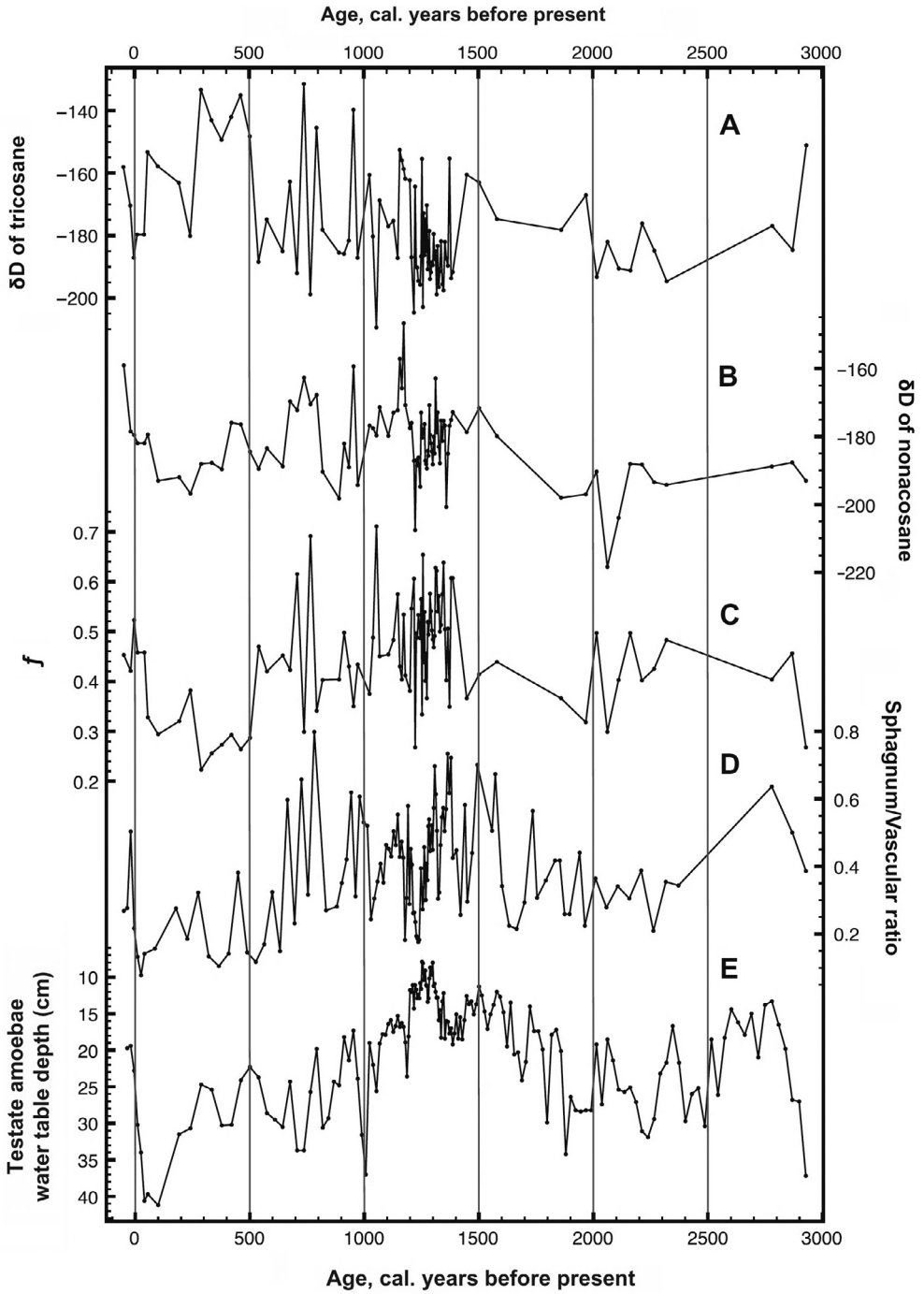


FIGURE 11.19 Various measures of water balance (P-E) over the last 3000 years, derived from Minden Bog in Michigan, USA (A) δD in C_{23} *n*-alkanes from *Sphagnum*; (B) δD in C_{29} *n*-alkanes from vascular plants; (C) *f*, the fraction of water remaining at the bog surface, after evaporation, transpiration, and infiltration; (D) the Sphagnum/Vascular Ratio (SVR) showing the relative abundance of *n*-alkanes from *Sphagnum* and from vascular plants, and (E) Water table depth reconstruction from testate amoebae. All of the indices point to wetter conditions from 1200 to 1500 years BP. *From Nichols et al. (2012).*

A key indicator of hydrological conditions in mires are testate amoeba, which can be extracted from peat. These are a diverse group of protozoans with morphologically distinctive tests (Charman, 2001). Different communities of testate amoeba are characteristic of varying bog surface wetness (principally the duration of any summer moisture deficit). Although testate amoebae are also influenced by pH, in ombrotrophic bogs pH is generally uniform and so bog surface wetness is the primary control on their community structure. Downcore profiles of testate amoeba assemblages, calibrated with modern data, can thus provide a reconstruction of past hydrological conditions.

Organic matter from peat provides an excellent target for organic biomarker studies, as macrofossils are commonly well preserved in peat and individual species can often be identified. *n*-Alkanes from leaf waxes vary between *Sphagnum* (which only thrives in wet conditions, since it has no vascular system that can supply water from deeper zones in the peat) and vascular plants (that favor drier conditions as they do not survive well in waterlogged areas). The average *n*-alkane chain length for vascular plants is around C_{29}-C_{31} compared to C_{23} for *Sphagnum* (Nichols et al., 2006, 2009). This allowed Nichols et al. (2009) to derive a *Sphagnum*/vascular plant ratio moisture balance index, for a bog in northwestern Norway, based on the ratio of C_{23} to C_{29} *n*-alkanes, which indicated an abrupt shift to drier conditions occurred at around 8000 years BP. Peat from ombrotrophic bogs also offers the prospect of obtaining reliable estimates of the hydrogen isotopic content of rainfall from compound-specific (e.g., *n*-alkane) isotope studies. By separating δD in C_{23} *n*-alkanes derived from *Sphagnum*, from δD in C_{29} *n*-alkanes derived from vascular plants, Nichols et al. (2010) derived an evaporation index based on the idea that vascular plants can tap into water from below the surface (and so are not greatly affected by evaporative losses), whereas *Sphagnum* must rely on rainfall for its moisture, and so is potentially subjected to strong evaporative losses. The difference in the δD values derived from vascular plants and from *Sphagnum* thus provides a measure of the relative impact of changes in hydrological conditions (P-E) (Figure 11.19).

CHAPTER

12

Pollen

OUTLINE

12.1 Introduction 405

12.2 The Basis of Pollen Analysis 406
- 12.2.1 *Pollen Grain Characteristics* 408
- 12.2.2 *Pollen Productivity and Dispersal: The Pollen Rain* 410
- 12.2.3 *Sources of Fossil Pollen* 410
- 12.2.4 *Preparation of the Samples* 411
- 12.2.5 *Pollen Analysis of a Site: The Pollen Diagram* 411
- 12.2.6 *Zonation of the Pollen Diagram* 414

12.3 Pollen Rain as a Representation of Vegetation Composition and Climate 414
- 12.3.1 *Maps of Modern Pollen Data* 416
- 12.3.2 *Mapping Vegetation Change: Isopolls and Isochrones* 418
- 12.3.3 *How Rapidly Does Vegetation Respond to Changes in Climate?* 422

12.4 Quantitative Paleoclimatic Reconstructions Based on Pollen Analysis 425

12.5 Paleoclimatic Reconstruction from Long Quaternary Pollen Records 434
- 12.5.1 *Europe* 434
- 12.5.2 *Sabana de Bogotá, Colombia* 438
- 12.5.3 *Central American Lowlands* 441
- 12.5.4 *Amazonia* 443
- 12.5.5 *Equatorial and Sub-Saharan Africa* 445
- 12.5.6 *Northeastern Siberia* 449

12.1 INTRODUCTION

Every year, millions of tons of organic material are dispersed into the atmosphere by flowering plants and cryptogams (plants without true flowers or seeds) in an effort to reproduce. The higher plants (angiosperms and gymnosperms) produce pollen grains containing the male genetic material; sexual reproductive success is assured only if this material reaches a female receptacle of the same plant species. The lower plants or cryptogams produce

Copyright © 2015 Raymond S. Bradley.
Published by Elsevier Inc. All rights reserved.

spores that contain the necessary genetic material for the growth of an independent generation of plants. Pollen grains and spores are the basis of an important aspect of paleoclimatic reconstruction—pollen analysis, or palynology, the study of pollen and spores.[1] Where pollen has been preserved over time, in lakes, bogs, estuaries, etc., it provides a record of past vegetation changes that may be due to changes of climate. Pollen analysis is one of the most important branches of Quaternary paleoclimatology, providing information from the continents to compliment that derived from marine sediments and ice cores.[2] Pollen records from some sites span the entire Quaternary; more commonly they span the Holocene and/or late glacial period. Since pollen records from lakes and bogs are more or less ubiquitous, they can provide an important link between the higher-resolution tree-ring records of the Late Holocene and other longer but lower resolution records from the land and oceans (see Table 12.1).

An important consideration in pollen analysis is the concept of scale (Webb, 1991; Bradshaw, 1994). Vegetation changes occur on a variety of scales (both temporal and spatial). Not all such changes are necessarily due to a change in climate; fire, insect infestation, plant successional changes, and interference by man, as well as changes in factors leading to the accumulation and preservation of the fossil material itself, often make interpretation of the pollen record complex. However, by selecting the appropriate spatial and temporal scale for analysis, pollen studies can isolate the important climatic signal from the nonclimatic noise (Figure 12.1).

This chapter focuses on some of the methods used to achieve the goal of quantitative paleoclimatic reconstruction from pollen, preserved mainly in lakes and bogs. Studies that pertain to the reconstruction of past vegetation composition or plant succession *sensu stricto* are not dealt with in any detail (cf. Huntley and Webb, 1988; Jackson, 1994). The chapter concludes with some examples of palynological studies from different regions that have shed light on important paleoclimatic problems. The emphasis in this final section is on long records that provide information about past climatic changes on the continents, for comparison with long ice core and marine sedimentary records.

12.2 THE BASIS OF POLLEN ANALYSIS

Paleoclimatic reconstruction by pollen analysis is possible, thanks to four basic attributes of pollen grains: (1) They possess morphological characteristics that are specific to a particular genus or species of plant; (2) they are produced in vast quantities by wind-pollinated plants and are distributed widely from their sources; (3) they are extremely resistant to decay in certain sedimentary environments; and (4) they reflect the natural vegetation at the time of

[1] As pollen grains have been studied far more than spores for reconstructing past climates (i.e., the emphasis has been on higher plants; Table 12.1), the following sections will focus on pollen grains. However, from a methodological viewpoint, most of the problems of studying pollen grains apply equally to the study of spores.

[2] In some cases, pollen extracted from marine sediments has enabled direct correlations to be made between terrestrial and marine records, providing a check on the terrestrial chronologies (e.g., Hooghiemstra et al., 1992, 1993). Pollen has also aided in the chronological interpretation of tropical ice cores (e.g., Liu et al., 2005, 2007).

TABLE 12.1 Some Important Plant Taxa in North American and European Quaternary Palynology (see Figure 12.1)

Genus	Family	Common Name
Abies		Fir
Acer		Maple
Alnus		Alder
Ambrosia		Ragweed
Artemisia		Wormwood/Sage
Betula		Birch
Carpinus[a]		Ironwood
Carya		Hickory
	Chenopodiaceae	Goosefoot
Corylus		Hazel
	Cyperaceae	Sedges
Ephedra		Horsetail
Eucalyptus[b]		Eucalyptus
Fagus		Beech
Fraxinus		Ash
	Gramineae	Grasses
Juglans		Walnut
Juniperus		Juniper
Larix		Larch
Liquidambar		Sweet gum
Lycopodium[b]		Clubmoss
Nyssa		Tupelo
Ostrya		Hornbeam
Picea		Spruce
Pinus		Pine
Populus		Poplar
Pseudotsuga		Douglas fir
Quercus		Oak
Salix		Willow
Taxodium		Bald cypress
Taxus		Yew
Tilia		Basswood/lime
Tsuga		Hemlock
Ulmus		Elm

[a]Ostrya *and* Carpinus *pollen are indistinguishable and are generally considered together.*
[b]*Exotic pollen added to samples for pollen influx calculations (see Section 12.2.4).*

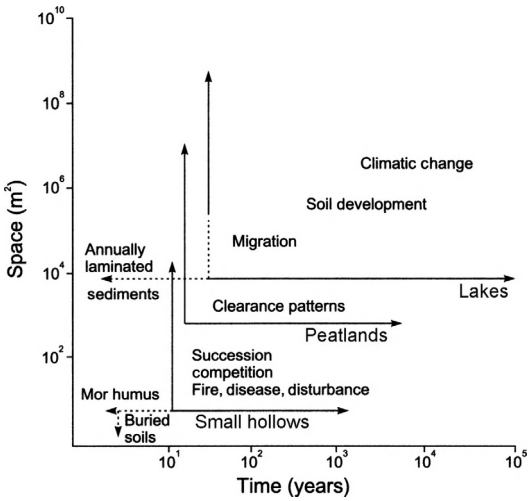


FIGURE 12.1 Scale is important in defining the information that can be obtained from pollen analysis. Information about climate is obtained at the larger temporal and spatial scales, mainly from lakes and peatlands. At smaller spatial and temporal scales, nonclimatic effects dominate the pollen signal. *From Bradshaw (1994).*

pollen deposition, which (if viewed at the right scale) can yield information about past climatic conditions.

12.2.1 Pollen Grain Characteristics

Pollen grains range in size from 10 to 150 μm and are protected by a chemically resistant outer layer, the exine. Because pollen grains of many plant families are different morphologically, they can be recognized by their distinct shape, size, sculpturing, and number of apertures (Punt et al., 2007; Figure 12.2). The exine is made of sporopollenin, a complex polymer (a β-carotenoid ester) resistant to all but the most extreme oxidizing or reducing agents. Thus, the organic or inorganic matrix in which the pollen grains are trapped can be removed by chemical means without destroying the pollen itself. There is some evidence, however, that in certain sedimentary environments, not all pollen grains will be equally well preserved (Cushing, 1967). For example, pollen grains are more subject to corrosion in moss peat than in silt deposits, and this may be due to the activities of phycomycetes, bacteria, and other microorganisms. Furthermore, the pollen of some species (e.g., *Populus*) may begin to disintegrate even before reaching a deposition site (Davis, 1973).

Generally, identification of pollen grains is only to the genus or family level, but in some cases, particular species can be resolved (Faegri and Iversen, 1975; Moore and Webb, 1978). Great strides have been made in compiling pollen atlases especially for tropical regions, and these have helped to expand and improve pollen analysis in those areas (Hooghiemstra and van Geel, 1998). Some progress has also been made in automating pollen identification by image analysis (e.g., Holt et al., 2011), but most studies still rely on painstaking manual identification by analysts at the microscope. Exploratory studies of the stable isotopic composition of the pollen grain exine have been carried out, but so far, this approach has not been widely applied (Loader and Hemming, 2004).

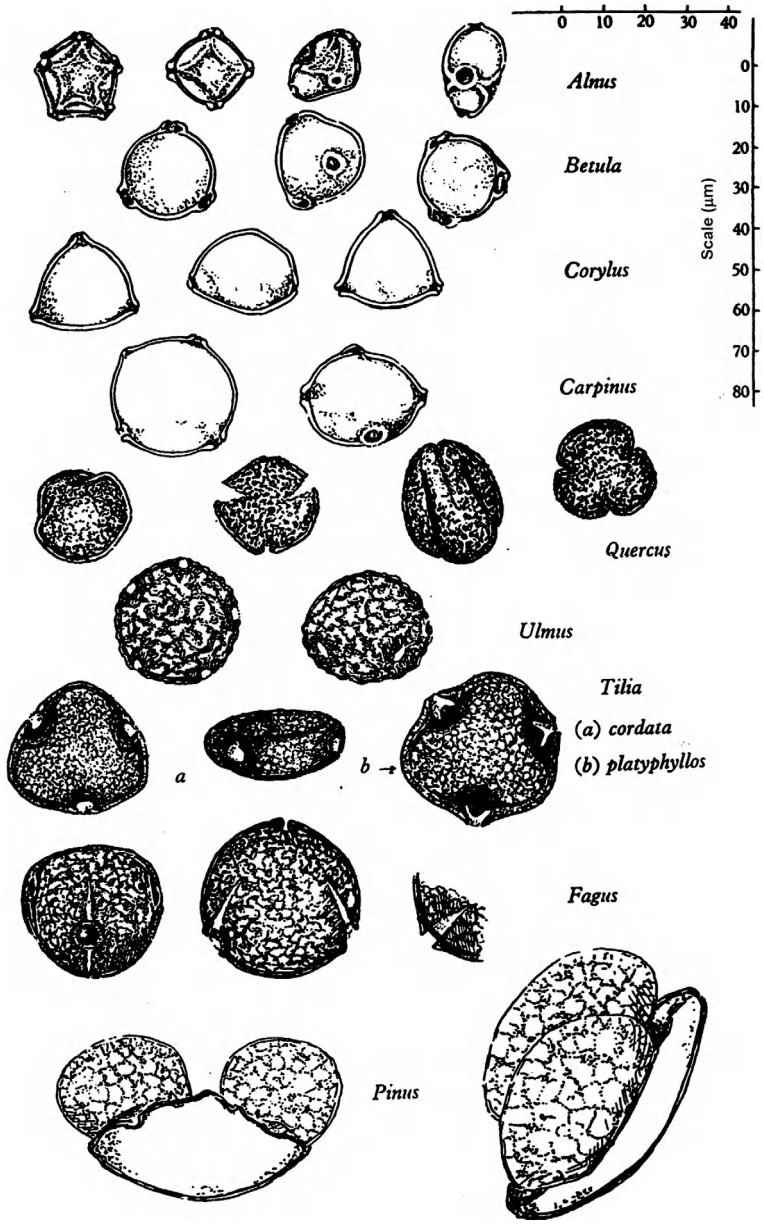


FIGURE 12.2 Some of the principal pollen types in British Holocene deposits, drawn to the same scale. Common names of plants are given in Table 9.1. *From Godwin (1956).*

12.2.2 Pollen Productivity and Dispersal: The Pollen Rain

All plants that participate in sexual reproduction produce pollen grains, dispersing them by various mechanisms in an endeavor to reach and fertilize the female reproductive organs of other plants. The amount of pollen produced is generally inversely proportional to the probability of success in fertilization; thus, plants using insects or animals as a dispersal agent (entomophilous or zoophilous species) produce orders of magnitude less pollen than those dispersing pollen by wind (anemophilous species). By the same token, plants that are self-fertilizing (autogamous or cleistogamous species) produce only minute quantities of pollen compared to anemophilous species. Because of these facts, even though the vast majority of flowering plants are insect pollinated, the accumulation of pollen grains at any given site will usually be dominated by pollen of anemophilous species. A single oak tree may produce and disperse by wind more than 10^8 pollen grains per year, and hence, the pollen from an entire forest (the pollen rain) assumes astronomical proportions. Pollen accumulation in a northern hardwood forest may reach 80 kg ha^{-1} a^{-1} (Faegri and Iversen, 1975). Pollen production by entomophilous species is generally several orders of magnitude lower, and autogamous species produce even less. In some cases, an entomophilous species, such as *Tilia*, may produce fairly large amounts of pollen, but the relatively efficient dispersal mechanism (via insects) means that pollen grains are rarely found in large numbers, even in forests where *Tilia* is abundant (Janssen, 1966).

12.2.3 Sources of Fossil Pollen

Since pollen is an aeolian sediment, pollen falling on sites where organic or inorganic sediments are accumulating will become part of the stratigraphic record (Traverse, 1994). Pollen has thus been recovered from peat, lake sediments, alluvial deposits, estuarine and marine sediments, and glacial ice. Pollen has also been recovered from archaeological sites (Dimbleby, 1985), rat middens (King and Van Devender, 1977), and coprolites (fossilized fecal matter of animals; Martin et al., 1961). In Quaternary palynology, the principal sources of paleoclimatic information are peat from bogs and marshes, and sediments from relatively shallow lakes (Jacobson and Bradshaw, 1981). In many lakes, sedimentation rates are often quite high, providing an opportunity to recover samples with a high temporal resolution, generally an order of magnitude greater than in marine sediments, where pollen concentrations decline rapidly away from the coast (e.g., Montade et al., 2011). Terrestrial pollen studies can thus provide a temporal perspective on climatic changes rarely possible in a marine setting.

The vast majority of pollen grains dispersed by wind are not carried more than 0.5 km beyond their source. Dispersal by wind is a function of grain size, the larger and heavier grains falling to the ground sooner than the smaller, lighter grains (Dyakowska, 1936). Pollen grains of beech (*Fagus*) and larch (*Larix*), for example, are relatively heavy and settle out close to their source. Consequently, the occurrence of fossil beech or larch grains in a deposit would indicate the former growth of a species in the immediate vicinity of the site. Field measurements of pollen dispersal from artificial sources and from isolated stands of vegetation indicate that pollen produced by an individual plant is not identifiable above background levels (the regional pollen rain) beyond a few hundred meters. This is also indicated by theoretical dispersal models (Tauber, 1965). Many investigators thus favor the analysis of sediments from fairly large lakes (>1 km^2) because they act as catchment basins for the regional pollen rain and are not unduly influenced by vegetation in the immediate vicinity of the sampling site (Prentice, 1985).

Much work has been conducted on the problems of pollen transport and sedimentation in lake basins (Pennington, 1973; Holmes, 1994). Just as in the atmosphere, differential settling of pollen grains occurs in water also, with the result that the original ratios in which pollen enters the lake from the air may be distorted, with the lighter pollen grains preferentially deposited in the littoral zone. Pollen is also concentrated in lake basins by inflowing streams, especially during periods of heavy runoff. Furthermore, resuspension and redeposition of pollen grains during periods of turbulent mixing, particularly in shallow water, also occur, thereby smoothing out yearly variations in pollen and sediment inputs to the lake. Further smoothing may result from the activities of burrowing worms and other mud dwellers (Davis, 1974). Thus, very high-resolution studies (annual to decadal) are not practicable except perhaps in annually laminated (varved) sediments (e.g., Swain, 1978). In any case, this temporal scale is not appropriate for climatic reconstruction from pollen, since the climatic signal (recorded through changes in vegetation) will not be strong at this scale. Other nonclimatic factors would likely overwhelm any climatic signal. As the sampling timescale increases, the climatic signal begins to predominate over nonclimatic noise (Bradshaw, 1994). By careful interpretation of the record at the appropriate temporal scale and aggregation of data at the regional scale, the fundamental climatic signal can be distilled from the array of other factors affecting the accumulation of pollen in lakes.

12.2.4 Preparation of the Samples

In order to isolate pollen grains and spores from the matrix of organic or inorganic sediment, rigorous chemical treatment by hydrochloric, sulfuric, and hydrofluoric acid is generally required, as well as acetolysis by a mixture of acetic anhydride and sulfuric acid (for details, see Moore and Webb, 1978 or Faegri et al., 1989). Removal of the matrix enables the remaining pollen grains and spores to be seen clearly when stained and mounted on slides for microscopic analysis. Generally, the original core is sampled at intervals of a few centimeters (depending on the sedimentation rate), and slides of pollen and spores at each level are prepared. These are then examined and the number of different grains in each sample is noted. The total number of grains counted at each level would depend on the purpose of the study and the source of material being studied (Moore and Webb, 1978), but usually, at least 200 grains are counted.

For pollen flux density calculations (Section 12.2.5), the number of pollen grains counted on each the slide must be related to the total pollen content of the sample from the level being considered. The most widely used method is to add a known quantity of exotic pollen or spores (e.g., *Eucalyptus* or *Lycopodium*) to the sample initially and then to count the number of these grains that occur on the final slide preparation. The ratio of exotic pollen counted to the number of exotic pollen added originally can be used to estimate the total pollen content of the original sample (Stockmarr, 1971; Bonny, 1972).

12.2.5 Pollen Analysis of a Site: The Pollen Diagram

Pollen data from a stratigraphic sequence are generally presented in the form of a pollen diagram composed of "pollen spectra" from each level sampled (Figure 12.3). A pollen spectrum consists of the number of different pollen grains at a particular level expressed as a percentage of the total pollen count (the pollen sum). Actually, the pollen sum is not always made up of all pollen types counted. For paleoclimatic purposes, the objective of the analysis

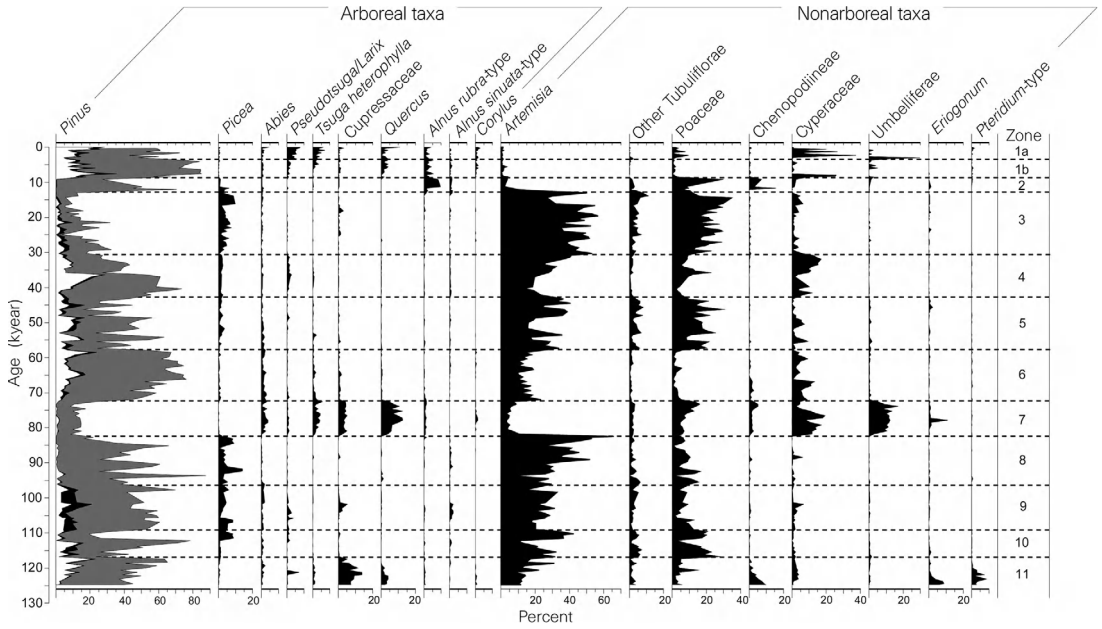


FIGURE 12.3 Pollen diagram from Carp Lake, Oregon, spanning the past 125,000 years, showing 11 distinct zones, which were derived objectively from the spectrum of pollen represented. Three types of pine are recorded in the first column: *P. contorta* or *P. ponderosa* (white), *P. monticola or P. albicaulis* (black), and indeterminate (shaded). *From Whitlock and Bartlein (1997).*

is to depict climatically significant regional vegetation change, so both arboreal and nonarboreal (shrub and herb) species are included in the pollen sum. Species that commonly grow in wet (lowland) environments around the sample site are usually excluded, though difficulties arise when a particular genus has different species (not easily distinguished by their pollen) that grow in both wet lowland and drier upland environments (e.g., *Picea mariana*, black spruce, and *Picea glauca*, white spruce, respectively; Wright and Patten, 1963).

In the pollen diagram, changes in the percentage of one species are assumed to reflect similar changes in the vegetation composition (due consideration being given to the factors of over- and underrepresentation discussed in the preceding text). The problem with this is that apparent changes in one species occurrence may occur in the percentage data as a result of changing receipts of pollen from other species because the total must always equal 100% (what Prentice and Webb, 1986, call the "Fagerlind effect"). The following example from Faegri and Iversen (1975, p. 160) succinctly summarizes the difficulty:

> If we visualize a forest consisting of equal parts of oak and pine, and we use the pollen production figures quoted, we find that the corresponding spectrum will contain 15 percent oak, 85 percent pine. If beech is substituted for pine (apart from the botanical improbability of that succession) the same quantity of oak will give 60 percent of the pollen as against 40 percent beech. If the beech is then replaced by a tree, e.g. *Acer* spp. or *Populus balsamifera*, which is scarcely, or not at all, registered in the spectra, we shall find almost 100 percent oak pollen, although the quantity of oak has not changed at all. It is necessary to take into account not only the curve under discussion, but the others as well.

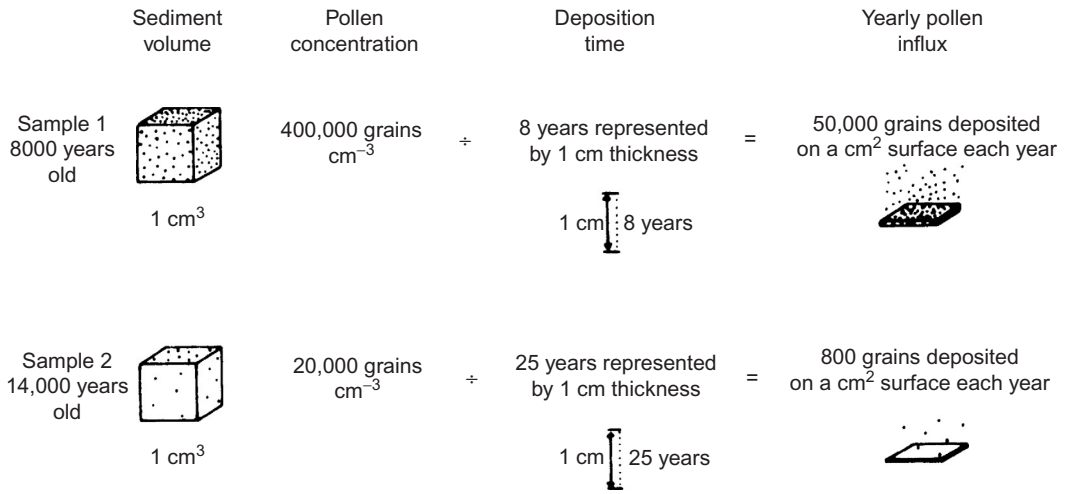


FIGURE 12.4 Examples of pollen influx (pollen flux density) calculations from measurements of pollen concentration and the rate of accumulation of the sediment matrix. *After Davis (1963).*

To circumvent such problems, palynologists may calculate pollen flux density (sometimes, incorrectly, called absolute pollen influx values), which is the number of grains accumulating on a unit of the sediment surface per unit time (Figure 12.4). However, to do this, the sediment accumulation rates must be known. Generally, samples are ^{14}C dated at close intervals to establish a mean sedimentation rate. In North America, the rise of *Ambrosia* (ragweed) pollen at the time of colonial settlement (when forests were being cleared and herbaceous plants were increasing rapidly in numbers) is clearly seen in lake sediments; because the dates of settlement are known, sedimentation rates since then are readily calculated (Bassett and Terasmae, 1962; McAndrews, 1966; Davis et al., 1973). Clearly, the latter method is only useful for obtaining modern pollen flux statistics, whereas ^{14}C dating enables influx to be calculated over earlier periods.

Pollen flux values can often clarify a stratigraphic record, but they have some important disadvantages too. Sediment focusing in lakes may result in unrealistically high values of total pollen flux, leading to erroneous conclusions. Most importantly, flux calculations require that sediments be closely and accurately dated so that reliable sedimentation rates can be obtained. Relatively few records are sufficiently well dated, and for large regional climate reconstructions, in which dozens if not hundreds of sites are used, percentage pollen values are always employed. There is strong evidence that in spite of their inherent limitations, such data provide reliable, reproducible, and verifiable paleoclimate reconstructions (e.g., Webb et al., 1993a). Consequently, pollen flux density studies have taken a back seat to pollen percentages in most modern paleoclimatic studies.

In some situations, in addition to pollen counts of individual taxa, pollen ratios may be included in a pollen diagram, as useful indices of broad changes in vegetation and climate (Li et al., 2010b). For example, the ratio of arboreal to nonarboreal pollen (AP/NAP) is commonly included to summarize changes from forested conditions to grassland or tundra. Similarly, in more arid environments, the ratio of *Artemisia* to Chenopodiaceae pollen (A/C) may

be calculated as an indicator of water availability, since *Artemisia* (typical of steppe vegetation) requires more moisture than Chenopodiaceae (drought-tolerant vegetation) (El-Moslimany, 1990). Other useful but less commonly used indices, and their limitations, are discussed by Li et al. (2010a).

The interpretation of pollen diagrams can often be significantly improved if macrofossil evidence (leaves, seeds, etc.) can be located at a site, since this may help to refine the taxonomic identification of local vegetation and identify some species that produce very little pollen. This is of particular importance in tundra environments (e.g., during glacial conditions) and at sites near the limit of trees (in the sub-Arctic and in high mountains) where arboreal pollen may be transported across this important ecotone (Jackson et al., 1997; Birks and Birks, 2000; Barkenow and Sandgren, 2001).

12.2.6 Zonation of the Pollen Diagram

Pollen diagrams contain a large amount of information on the covariance of different pollen types through time. In order to facilitate comparison between different sites, the stratigraphic record in pollen diagrams is commonly subdivided into pollen zones; these are biostratigraphic units defined on the basis of the characteristic fossil pollen assemblage (Figure 12.3). Generally, pollen zones contain a homogeneous assemblage of pollen and spores, but some investigators may recognize a zone that is characterized by abrupt changes. Needless to say, the definition of what constitutes a zone is a rather subjective decision and may not be agreed upon by different scientists (Tzedakis, 1994). Human nature also compels us to look for correlations with zonations previously "identified," thereby reinforcing systems that may not justify such blind faith! To avoid these problems, a number of more objective, computer-based methods have been suggested (Birks and Gordon, 1985). These are capable of identifying both major and minor zone boundaries (i.e., of defining zones and subzones) and permit objective comparisons to be made between sites. Objective computer-based zonation, or change-point analysis, can also be applied to other variables in a sedimentary sequence (e.g., macrofossils, diatoms, and sediment characteristics) to shed further light on the major climate-related features of the stratigraphic record (Birks, 1978; Birks and Birks, 1980). If similar local pollen assemblage zones can be identified over a large geographic area, it may be possible to define regional vegetation changes of broad paleoclimatic significance (Gordon and Birks, 1974; Birks and Berglund, 1979). However, given that pollen identification is generally limited to the genus/family level, pollen assemblages will not capture the much greater diversity of plant communities that ecologists would recognize, for example, in a modern landscape (Seppä and Bennett, 2003).

12.3 POLLEN RAIN AS A REPRESENTATION OF VEGETATION COMPOSITION AND CLIMATE

Differences in pollen productivity and dispersal rates pose a significant problem for the reconstruction of vegetation composition because the relative abundance of pollen grains in a deposit cannot be directly interpreted in terms of species abundance in the area. It is

necessary to know the relationship between plant frequency in an area and the total pollen rain from that plant species in order to use pollen data to calculate the actual composition of the surrounding vegetation. For example, a vegetation community composed of 10% pine, 35% maple, and 65% beech may be represented in a deposit by approximately equal amounts of pine, maple, and beech pollen, because of the differences in their pollen productivity and dispersal rates. However, for paleoclimatic reconstruction, these matters are of less significance. What the paleoclimatologist needs to know is whether there are *patterns* in the pollen data that can be calibrated in terms of climate. Again, the question comes down to the appropriate scale of analysis. At the smallest spatial scale, and the shortest temporal scale, the signal represented by pollen will be dominated on the one hand by short-term (synoptic scale) factors affecting dispersal of pollen and on the other by local factors affecting plant growth. Stepping back from this complexity reveals the desired climate information.

Palynologists adopt the uniformitarian principle: the present is the key to the past. By using spatial relationships in modern pollen distribution and their relationship to modern climate as a guide to interpreting pollen patterns recorded in the past, paleoclimatic reconstructions can be made. Modern vegetation communities can be considered as analogs of former vegetation cover; if pollen assemblages in the modern pollen rain resemble fossil pollen assemblages, the former vegetation and its associated climate is assumed to be similar to that in the analog region today. If similar pollen assemblages cannot be found today, presumably no modern analog for the former vegetation cover and climate exists (e.g., Ritchie, 1976). The main problem with this approach is the difficulty of sampling the vast array of possible vegetation assemblages in the modern landscape in order to find a good analog and the fact that much "natural vegetation" in both the Old and New Worlds has been destroyed or greatly modified. Nevertheless, even in such modified environments, on the regional scale ($\sim 10^3$ km), modern pollen still contains a climatic signal that allows differentiation of *regional-scale* climatic conditions.

Pollen rain in mountainous regions poses particular problems of interpretation, because vegetation communities may be confined to narrow climatic zones along mountainsides (Maher, 1963). In parts of South America, for example, vegetation may grade all the way from equatorial rain forest below 500 m to tundra-like páramo (or the drier puña) above 3500 m, over a horizontal distance of less than 100 km. Ideally, the identification of vegetation changes close to the tree line is greatly improved if pollen can be supplemented with macrofossil evidence (Birks and Birks, 2000). Nevertheless, modern pollen rain studies demonstrate that in many situations, good discrimination between different vegetation zones is possible, even where complex spatial interfingering of different vegetation communities occurs (Salgado-Labouriau, 1979; Gaudreau et al., 1989; Lynch, 1996; Hicks, 2001). In the mountains of East Africa, pollen from high elevations is not dispersed very far beyond the high-altitude vegetation zone from which it is derived (Hamilton and Perrott, 1980). Pollen from lower vegetation zones is commonly carried upward to higher elevations by daytime upslope winds. However, with increasing elevation, gradient winds predominate, so that there may be an upper limit to upslope pollen transport (Markgraf, 1980). In Colombia, for example, arboreal pollen from below the tree line (~3200-3500 m) becomes insignificant above 3700 m (Marchant et al., 2001). Characteristic pollen rain assemblages corresponding to different elevations can thus be identified and used to reconstruct altitudinal changes in vegetation through time (e.g., Salgado-Labouriau et al., 1978). Such changes may be converted to

paleoclimatic estimates if modern climatic controls on the altitudinal limits of different taxa are known, though consideration must be given to constraints imposed on vegetation by changing CO_2 levels during glacial periods (Jolly and Haxeltine, 1997; Boom et al., 2001). At those times, vegetation may have changed more in response to CO_2 levels than to a simple drop in temperature.

12.3.1 Maps of Modern Pollen Data

Extensive studies of modern pollen rain and modern vegetation have been made for North America (e.g., Davis and Webb, 1975; Webb and McAndrews, 1976; Webb et al., 1978; Delcourt et al., 1984) and for Europe by Huntley and Birks (1983). In these studies, the amount of modern pollen of a particular genus was expressed as a percentage of the total pollen accumulation at each site; isopolls (lines of equal percentage pollen representation) were then mapped for each major genus and superimposed on maps of the regional vegetation (Figure 12.5). Often, the zero isopoll corresponds well with the range limit of the taxa (though

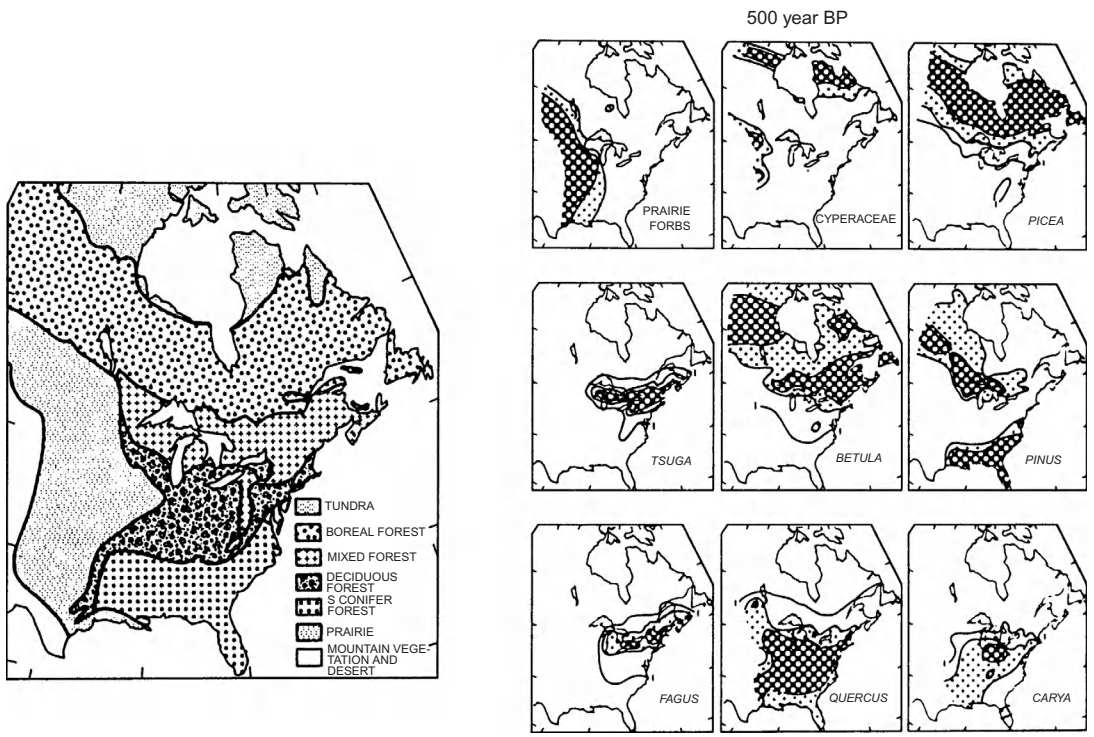


FIGURE 12.5 Generalized vegetation map of eastern North America and isopoll maps of selected taxa and groups of taxa at 500a BP. Contours shown are 5% and 10% for forbs; 1%, 5%, and 10% for Cyperaceae, *Fagus*, and *Tsuga*; 1%, 5%, and 20% for *Picea* and *Quercus*; 1%, 10%, and 20% for Betula; 20% and 40% for *Pinus*; and 1%, 3%, and 6% for *Carya*. Forb pollen is the sum of *Ambrosia*, *Artemisia*, and other Compositae, Chenopodiaceae, and Amaranthaceae pollen. *From Webb (1988).*

this varies by genus), and isopoll maxima coincide with the zone of maximum frequency of the taxa in the vegetation. However, the exact isopoll corresponding to the limits of a particular taxa needs to be determined by detailed regional studies as it may vary from one area to another. For example, the limit of *Picea* in the boreal forest of northeastern North America corresponds to the 20% isopoll because spruce pollen is carried far north of the forest limit by frequent southwesterly winds. In northern Alaska, the limit of *Picea* corresponds to the 10% isopoll; there, the Brooks Range creates a strong topographic barrier to spruce growth further north, and prevailing westerly winds reduce the spread of pollen northward. Spruce distribution in both areas is related to similar climatic controls, but the same isopolls do not provide that information (Anderson et al., 1991).

One of the most convincing demonstrations of the correspondence between modern vegetation and modern pollen is that of Webb (1974) who compared pollen content in the upper 2 cm of 64 lake sediment cores from throughout Lower Michigan with detailed forest inventory records. Maps showing the percentage distribution of individual tree genera were compared with corresponding isopoll maps (Figure 12.6). Clearly, the spatial distribution of

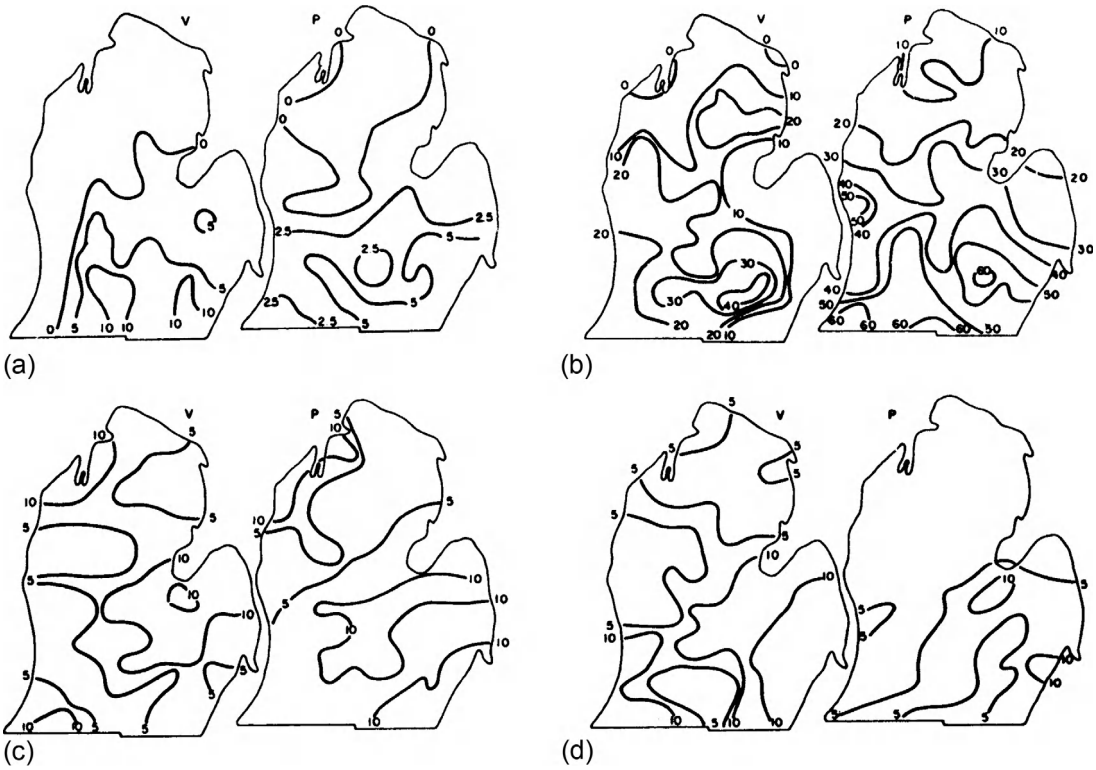


FIGURE 12.6 Maps of the percentages of (a) hickory, (b) oak, (c) elm, and (d) ash in the vegetation of Michigan (V) compared to the percentages of pollen (P) from the same trees in the modern pollen rain (based on arboreal pollen sum). Modern pollen data based on analysis of uppermost lake sediments. *From Webb (1974).*

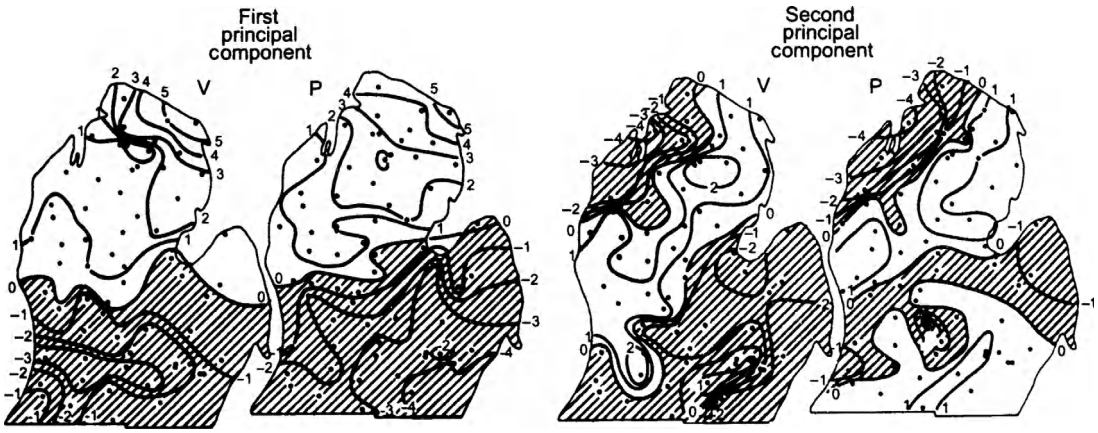


FIGURE 12.7 Map of the first two principal components (PC) of vegetation percentages (V) and pollen type percentages (P) in Michigan. The principal components of vegetation reflect major vegetation formations in the state. PC1 has a distribution reflecting the change from deciduous forest in the south to mixed coniferous-hardwood forest in the north. It accounts for 25% of variance in the original data set. PC2 depicts primary divisions within the two major vegetation formations, differentiating the northern hardwoods from the pine-birch-aspen forests in the north and the beech-maple and elm-ash-cottonwood forests from the oak-hickory forests in the south. It accounts for a further 35% of variance in the original data set. The first two principal components of pollen mirror the principal components of vegetation, indicating that the spatial pollen data may be used as a reliable indicator of vegetation distribution. Lakes shown by dots. *After Webb (1974).*

pollen of each genus closely resembles the percentage cover of that genus in the state (cf. Prentice, 1978; Solomon and Webb, 1985). Furthermore, the forest composition (i.e., the covariation of individual genera) when summarized by principal components is also revealed by principal component analysis of the pollen rain data (Figure 12.7). In this analysis, the first principal component reflects the dominant climatic control on vegetation (and hence pollen), and the second principal component reflects regional variations in soil type.

These studies clearly indicate that in spite of the problems involved in pollen dispersal, preservation, and accumulation (see Sections 12.2.2 and 12.2.3), the broad geographic patterns of vegetation are closely mirrored by the composition and amount of the pollen rain. Thus, at this scale of analysis, fossil pollen has much to offer for reconstructing paleoclimatic conditions.

12.3.2 Mapping Vegetation Change: Isopolls and Isochrones

Studies of modern pollen rain and the distribution of different taxa in the landscape today indicate that there is a fairly good spatial correspondence between them. Maps of modern pollen data can reproduce broadscale patterns of individual taxa over large areas (Davis and Webb, 1975; Webb and McAndrews, 1976; Huntley and Birks, 1983; Delcourt et al., 1984). Studies such as these paved the way for synoptic mapping of vegetation distribution at discrete periods in the past. This approach was first suggested by Szafer (1935) who defined the term isopoll as lines of equal percentage representation of a particular pollen type in the pollen sum. Using isopolls, Szafer constructed maps showing the distribution of beech and

spruce across East Germany and Poland at five intervals from late glacial to late Holocene time. However, Szafer's time framework was speculative since, at that time, there was no means of accurately dating organic material. It was only with the extensive use of ^{14}C dating that identical stratigraphic horizons could be identified (by interpolation between dates) at sites over large geographic areas, thus facilitating the preparation of time-sequential maps, such as those compiled by Huntley and Birks (1983), Delcourt et al. (1984), Jacobsen et al. (1987), and Williams et al. (2004). As an example, Figure 12.8 shows isopolls of spruce (*Picea*), pine (*Pinus*), and oak (*Quercus*) over eastern North America at intervals from 18 ka BP to the present (Webb et al., 1993a). These maps indicate the vegetation response to warming and to the retreat of the Laurentide ice sheet, with rapid migration of individual taxa in the period from 12 ka to 9 ka BP. By 9 ka BP, the principal features of the modern pollen distribution (0 ka) can be seen for the first time, and by 6 ka BP, most taxa had achieved their northernmost postglacial limit. Note however that spruce pollen percentages show a small

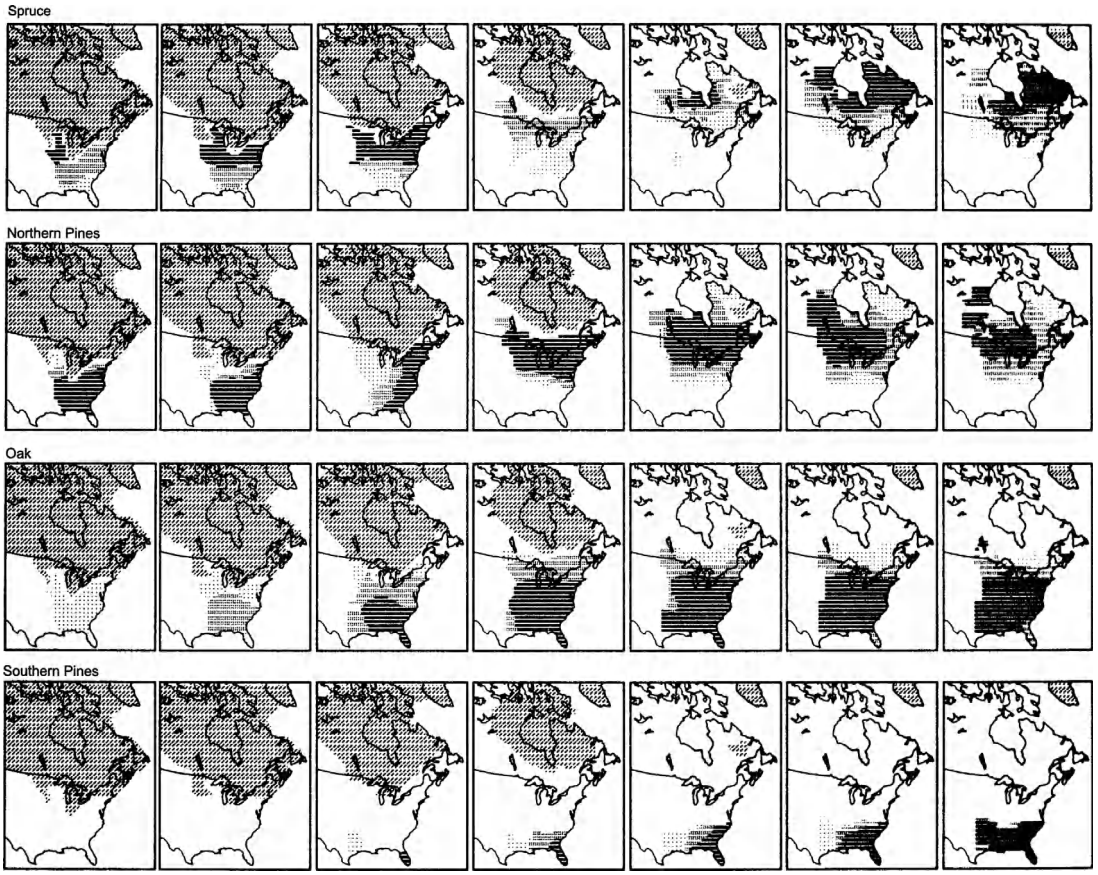


FIGURE 12.8 Isopoll maps of observed pollen data at 3-ka year intervals, from 18 ka BP (leftmost column) to the present (at right). Three levels of shading indicate pollen percentages: >1% (lightest), >5%, and >20% (darkest). *From Webb et al. (1987).*

southward shift after 6 ka BP, possibly reflecting a change to higher levels of available soil moisture in the northeastern United States (which favors spruce over pine) after the Early Holocene (Webb et al., 1993b).

Isopoll maps can be reinterpreted to show the migration of a particular genus or ecotone through time by isochrones (equal time lines). Figure 12.9a, for example, shows the location of the 15% spruce isopoll at intervals from 11,500 to 8000 years BP, a line thought to approximate the southern boundary of the late glacial boreal forest in this area. Similarly, Figure 12.9b shows the position of the conifer-hardwood/deciduous forest ecotone derived by analogy with modern pollen, which indicates that this boundary coincides with the 20-30% isopolls for oak and pine. Both maps indicate a rapid northward migration of forests in late glacial times. A final map, Figure 12.9c, illustrates the position of the "prairie border," the grassland/forest ecotone of midwestern North America based on 30% isopolls for herb pollen. Following rapid eastward shift in the Early Holocene, this boundary regressed

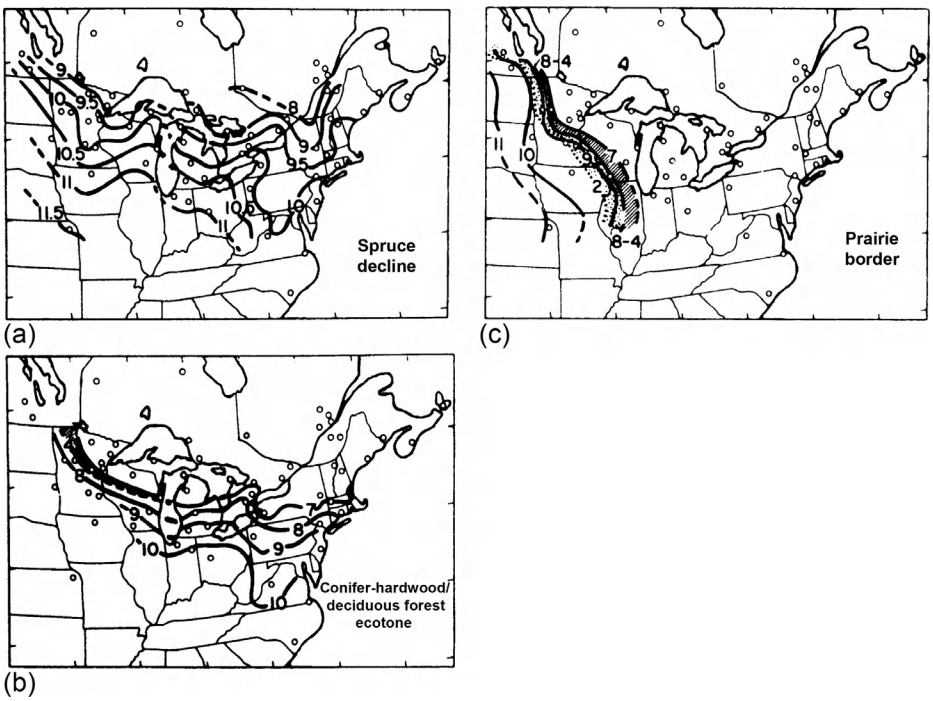


FIGURE 12.9 Isochrones (in thousands of years) on the migration of various vegetation taxa or ecotones, based on the position of diagnostic isopolls considered to be characteristic of the vegetation boundary. For example, in the modern boreal forest, isopolls of spruce exceed 15%. In (a), isochrones indicate the position of the 15% spruce isopoll at different times and are considered to reflect the southern margin of the boreal forest as it migrated northward. In (b), the conifer-hardwood/deciduous forest ecotone is identified by the 20% isopoll for pine and the 30% isopoll for oak, reflecting a change from dominance of oak to dominance of pine (in a northward direction). In (c), the "prairie border" is delimited by the 30% isopoll for herbaceous pollen. Shading indicates the area across which the prairie border first expanded (to 7000 years BP) then retreated (westward) as conditions became more moist in the region in the Mid- to Late Holocene. *After Bernabo and Webb (1977).*

westward after ~7000 years BP, indicating that the period of minimum precipitation and maximum warmth in the area had already passed.

Isopoll maps of individual taxa implicitly acknowledge that vegetation formations as we now know them have been impermanent features of the landscape (as discussed in Section 12.3.3). This is clearly illustrated by Huntley (1990b) who shows maps of "vegetation units," identified by associations of different pollen taxa at times in the past. Many of the vegetation units typical of western Europe today did not exist in Europe before the Early Holocene, and indeed, even as recently as 1 ka BP, there were areas of vegetation that have no analog in the modern vegetation formations of Europe (Huntley, 1990a,b).

Isopoll and isochrone maps depicting former vegetation patterns provide a qualitative perspective on past climate since vegetation formations on a broad scale (biomes) are clearly determined by climate (Prentice et al., 1992). To formalize this, palynologists have adopted the concept of "plant functional types" (PFTs)—groups of plants that have similar ecological requirements—to define biomes (Cramer, 1997; Harrison et al., 2009). Plants within the same PFT group are similar in stature (e.g., tree- or shrub-like), have similar types of leaves (needle- or broad-leaved), have similar phenological requirements (deciduous or evergreen), and thus have broadly similar adaptations to climate but may differ in the precise assemblage of species from one region to another. Table 12.2 shows the European pollen taxa that are associated with major plant functional types, as defined by Prentice et al. (1996). These PFTs (and their associated pollen) could then be grouped together to characterize the major biomes of the region (Table 12.3). Pollen from the uppermost surfaces of bogs and lake sediment cores were classified into PFTs, and then biomes, to compare with modern biome distribution. This showed good spatial correspondence, confirming that pollen data organized in this way can provide useful large-scale information about vegetation patterns and their changes through time (Prentice et al., 1992, 1996). However, the biome concept implicitly assumes uniformity of vegetation within each biome unit, whereas in reality, there are generally continuous vegetation gradients across biomes. Thus, a focus on biomes may underestimate the important dynamic changes in vegetation that took place within biomes, in response to climatic fluctuations. Furthermore, as discussed in the next section, plants migrate as individuals, not simply as parts of large-scale units, and so, inevitably, there were times in the past when the transient movement of plants in response to climate change led to unique biomes that have no modern counterpart.

The PFT/biome approach has been used to reconstruct the changing pattern of vegetation across North America every few thousand years since the LGM (Figure 12.10; Williams et al., 2004). This reveals the former importance of biomes that no longer exist, such as mixed parkland in the northcentral United States from ~16,000 to ~13,000 years BP. Taiga quickly spread into areas formerly occupied by ice, and cool mixed forest was replaced by warm mixed forest across much of the eastern United States once the ice sheet disappeared in the Early Holocene. There has also been a global-scale project to map the distribution of the world's major biomes from pollen data at 6000 and 18,000 years BP, providing a synoptic view of global vegetation patterns at the LGM and in the Mid-Holocene (Jolly et al., 1998; Prentice and Webb III; 1998; Williams et al., 1998; Edwards et al., 2000; Prentice et al., 2000; Takahara et al., 2000; Tarusov et al., 2000; Thompson and Anderson, 2000; Yu et al., 2000; Williams et al., 2000, 2004; Bartlein et al., 2011). One of the motivations for this approach was to be able to compare GCM simulations of past climatic conditions with the observed paleoclimatic data as a test of model

TABLE 12.2 Plant Functional Types (PFTs) and the Pollen Taxa Assigned to Them, Based on an Assessment of European Flora (Prentice et al., 1996)

Trees		
Boreal evergreen conifer	[bec]	*Abies*, *Picea*, *Pinus* (*haploxylon*)
Boreal summer green	[bs]	*Alnus*, *Betula*, *Larix*, *Populus*, *Salix*
Cool-temperate conifer	[ctc]	*Abies*
Intermediate-temperate conifer	[ctc_1]	*Cedrus*, *Taxus*
Eurythermic conifer	[ec]	*Juniperus*, *Pinus (diploxylon)*
Temperate summer green	[ts]	*Acer*, *Alnus*, *Fraxinus [excelsior type]*
		Populus, *Quercus* (deciduous), *Salix*
Cool-temperate summer green	[ts_1]	*Carpinus*, *Corylus*, *Fagus*, *Frangula*, *Tilia*, *Ulmus*
Warm-temperate summer green	[ts_2]	*Castanea*, *Fraxinus ornus*, *Juglans*, *Ostrya*, *Platanus*, *Rhamnus*, *Vitis*
Warm-temperate broad-leaved evergreen	[wte]	*Quercus* (evergreen)
Cool-temperate broad-leaved evergreen	[wte_1]	*Buxus*, *Hedera*, *Ilex*
Shrubs		
Warm-temperate sclerophyllous shrub	[wte_2]	*Olea*, *Phillyrea*, *Pistacia*
Others		
Steppe forb	[sf]	*Artemisia*, Chenopodiaceae
Desert forb	[df]	*Ephedra*
Arctic-Alpine dwarf shrub	[aa]	*Alnus*, *Betula*, *Salix*
Grass	[g]	Poaceae
Sedge	[s]	Cyperaceae
Heath	[h]	Ericales

veracity. Since plants have specific climatic tolerances, these can be defined from modern distributions, and then, model-derived distributions can be reconstructed from these known limits. This is discussed further in Section 12.4.

12.3.3 How Rapidly Does Vegetation Respond to Changes in Climate?

An important question that relates to current concerns over rapid anthropogenic climate change is as follows: what is the lag response of vegetation to climate change? Can the pollen record provide information on short-period, large-amplitude changes in climate, or to put the question more generally: what are the frequency response characteristics of the pollen record? Davis and Botkin (1985) attempted to answer this question by the use of a forest growth model

TABLE 12.3 Characteristic PFTs Within the Major Biomes of Europe (cf. Table 12.2)

Cold deciduous forest	bs, ec (h)
Taiga	bs, bec, ec, (h)
Cold mixed forest	bs, ctc, (ctc_1), ec, (ts,), (h)
Cool conifer forest	bs, bec, ctc, ec, (ts_1), (h)
Temperate deciduous forest	bs, ctc, (ctc_1), ec, ts, ts_1, (ts_2), (wte_1), (h)
Cool mixed forest	bs, bec, ctc, ec, ts, ts_1, (h)
Broad-leaved evergreen/warm mixed forest	ec, ts, (ts_1), (ts_2), wte, (wte_1), (h)
Xerophytic woods/scrub	ec, wte, wte_2
Steppe	sf, g
Desert	sf, dr, g
Tundra	aa, g, s, (h)

Those in parentheses are restricted to part of the biome.
From Prentice et al. (1996).

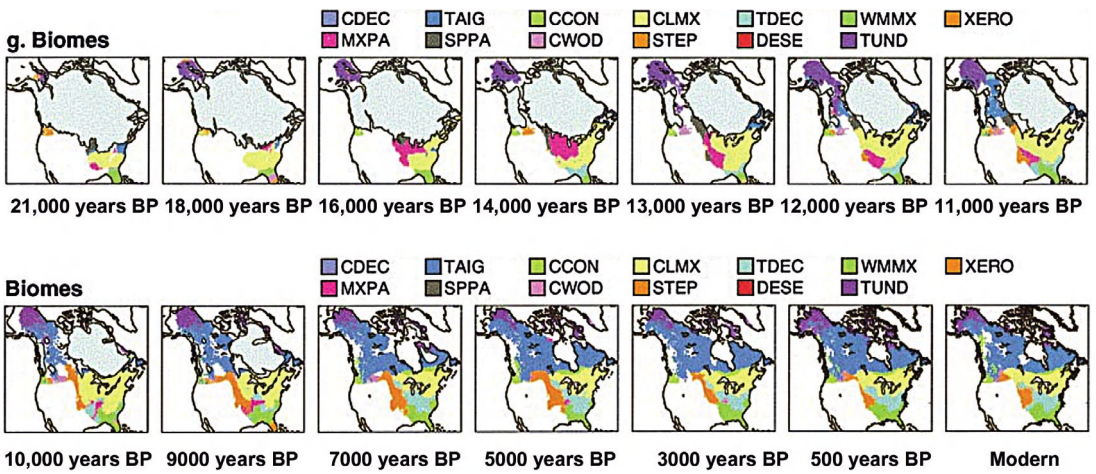


FIGURE 12.10 Inferred biome distribution across North America at the times indicated. CCON, cool conifer forest; CDEC, cold deciduous forest; CLMX, cool mixed forest; CWOD, conifer woodland; DESE, desert; MXPA, mixed parkland; SPPA, spruce parkland; STEP, steppe; TAIG, taiga; TDEC, temperate deciduous forest; TUND, tundra; WMMX, warm mixed forest; XERO, xerophytic scrub (Williams et al., 2004).

to simulate changes in forest composition (basal areas of particular tree species) after steplike changes in temperature. They compared large-amplitude, short-duration events with smaller-amplitude, longer-term changes and concluded that the forest response to climatic cooling lagged 100-150 years behind, due to "community inertia." There is a natural delay in colonization by new species, mainly due to the shading effects of mature canopy trees.

Consequently, they anticipate that changes in forest composition in response to the warming from ~1850 to 1990 will continue for at least another century (cf. Overpeck et al., 1990). They also found that vegetation responses to large, short events were similar to those that resulted from longer-, smaller-amplitude changes (Figure 12.10). The smallest change necessary for a detectable forest response was a ~50-year change in mean annual temperature of 2 °C, or a 1 °C change sustained over ~200 years. In short, these model experiments suggest that one should not expect the pollen record of (midlatitude forest) vegetation to resolve the influence of climatic changes "more closely than within a century or two"; rather it provides a "running mean of climatic variation" (Davis and Botkin, 1985). This appears to be confirmed by studies of the vegetation response to abrupt climatic events, such as the onset and termination of the Younger Dryas and the cooling that was widespread around 8.2 ka BP (Williams et al., 2002; Pross et al., 2009). In various sites across North America and Europe, vegetation lags following climate changes were generally <200 years and often <100 years. However, other studies reveal much more rapid changes in vegetation (~10 years) (in areas of high topographic relief (where distances between ecotones are short) during these periods (Ammann et al., 2000; Tinner and Lotter, 2001). This implies that some areas may soon witness significant changes in vegetation in response to current anthropogenic climate changes.

The question of vegetation response to climatic change also involves the notion of ecosystems: have they always been the same as we see them in the landscape today? Webb (1988), Huntley and Webb (1989), and Huntley (1990a) provide persuasive arguments that modern vegetation should not be viewed as fixed units with a constant composition, which moved regimentally across a region in response to changes in climate. Rather, individual taxa respond differently, leading to a constant change in vegetation composition, at times producing vegetation formations with no modern analogs (e.g., in late glacial time in much of western Europe; Huntley, 1990b). This is partly not only due to the individualistic responses of taxa to climatic changes and their different abilities to migrate but also due to the fact that Late Pleistocene and Early Holocene climates were in many areas quite unlike anything seen today (COHMAP members, 1988). According to Webb (1988), "ecosystems and plant assemblages are to the biosphere what clouds, fronts and storms are to the atmosphere . . . features that come and go . . . [with] . . . internal dynamics . . . [but] . . . not of sufficient strength to overcome major changes from the outside." Thus, snapshots of the past would reveal biomes varying in composition over time, rather than simply migrating as fixed entities. This has important implications for anticipating future changes in ecosystems that may accompany global warming. New communities may well be unlike those of today or those in the past (Overpeck et al., 1990; Davis, 1991).

With such a view of vegetation change, we inevitably turn to the controversial issue of whether vegetation can ever be considered "in equilibrium" with climate. This seems to be very much a question of one's definition of equilibrium and the scale at which one examines the question. Webb (1986, 1987, 1988) argues that vegetation is in *dynamic equilibrium* with climate; on the timescale of 10^3-10^5 years, climate has changed continuously, and vegetation (viewed on subcontinental scales, at ~10^3 year intervals) has kept pace with these changes. Changing the temporal and spatial focus to shorter intervals and smaller areas would no doubt reveal "disequilibria" related to migrational, successional, or edaphic influences (Davis et al., 1986; Prentice, 1986). However, this issue is further complicated by differences related to particular types of vegetation or environment (e.g., in a forest environment, if a

species can tolerate shade by canopy trees or if the landscape being invaded is open). In particular, the extent of disturbance in an ecosystem can have an important effect on the ability of a species to occupy new environments even under the pressure of a change in climate (Davis, 1991). Furthermore, in some environments such as desert and semiarid regions, where vegetation has adapted to a high variability of rainfall, a sustained change in precipitation may generate an almost immediate response in vegetation cover[3] (Ritchie, 1986). Finally, evidence of seemingly fast migration rates from the paleorecord may be overestimated if small isolated plant populations were present beyond the main species limit (perhaps not clearly visible in isopoll maps). These populations may then have been able to rapidly expand into new territory, giving rise to overestimates of migration rates (from the main vegetation boundary) (e.g., Stewart and Lister, 2001; Anderson et al., 2006). Notwithstanding these specific problems, the evidence is that in midlatitudes, at least, a synoptic view of vegetation at ~2000- to 3000-year intervals reveals changes that are consistent with the changes that occurred in climate as we currently understand them (Webb et al., 1987).

As a test of the hypothesis that vegetation is in dynamic equilibrium with climate, Bartlein et al. (1986) and Webb et al. (1987) used equations that relate modern pollen rain to contemporary climate (see Section 12.4) and applied them to climatic conditions in the past (derived from a general circulation model) to predict what the pollen rain should have been if vegetation was in equilibrium with climate. This approach assumes (a) the equations adequately characterize the pollen-climate relationship and (b) the models accurately reconstructed past climate. The results show fairly good correspondence between the simulated and observed pollen rain, demonstrating that vegetational lags are not significant on the space and timescales being considered. In another approach, Prentice et al. (1991) used "response surfaces" (see Section 12.4) to predict climate (from 18 to 3 ka BP) directly from the fossil pollen data. The results were compared with (independently derived) model-simulated climate, and good agreement was found. Since there were no major anomalies between the pollen-derived climate and that derived from the model, they concluded that "continental scale vegetation patterns have responded to continuous climatic changes during the past 18 ka, with lags no greater than ~1500 years" (Prentice et al., 1991). In fact, as noted in the preceding text, vegetation (as tracked by pollen) can clearly change over much shorter intervals. It seems safe to conclude that in many locations, pollen can be a sensitive indicator of abrupt, short-lived climatic changes.

12.4 QUANTITATIVE PALEOCLIMATIC RECONSTRUCTIONS BASED ON POLLEN ANALYSIS

Paleoclimatic reconstruction from fossil pollen spectra is based on the notion that, since vegetation distribution is largely determined by climate, it should be possible to use that distribution (as represented in the fossil pollen spectra) to reconstruct past climate. Large

[3] This has implications for vegetation-induced changes in trace gas concentrations (CH_4, CO_2), albedo, and hydrology in relation to climatic forcings, since a rapid response in vegetation over large areas (such as the tropical desert margins) could have more or less immediate feedback effects on the climate system (cf. Petit-Maire et al., 1990).

databases of surface pollen samples (generally from the surface sediments of lakes) are now available for many parts of the world, and these have enabled pollen assemblages to be calibrated directly in terms of climate (Bartlein et al., 2011). Even though in many regions natural vegetation has been dramatically reduced, the broadscale relationships between pollen rain and climate are sufficiently robust that they can be used to make reliable paleoclimatic reconstructions. This has been demonstrated several times (e.g., Bartlein et al., 1984; Huntley, 1990b; Huntley and Prentice, 1993) though Guiot (1990) believes this factor (the reduction in natural vegetation) creates a great deal of noise in paleoclimate estimates (see discussion below).

Many different statistical methods have been used to interpret fossil pollen spectra in terms of past climatic conditions (for a brief review, see Bartlein et al., 2011). All involve first establishing the relationship between modern pollen data and climatic parameters across as wide a geographic region as possible. These observed relationships are then applied to the fossil data. The simplest approach is multiple linear regression, such that

$$C_m = T_m P_m$$

where C_m is the modern climatic data, P_m is the modern pollen rain, and T_m is a functional coefficient or set of coefficients (transfer functions) derived from the relationship between modern climate and pollen data. Former climatic conditions (C_f) are then derived by using the fossil pollen assemblage (P_f) and the modern transfer function (T_m). In studies of pollen-climate relationships in eastern North America, the equations were derived for different regions, defined in such a way that a "clear and monotonic" relationship could be recognized between climate and pollen percentages (generally using a pollen sum of the major forest taxa, plus Cyperaceae and prairie forbs (herbs)) (Bartlein and Webb, 1985). Those species associated with human settlement (e.g., *Ambrosia*) are eliminated to minimize anthropogenic influences on the pollen sum. Scatter plots of pollen percentages and climate variables (e.g., % oak and July mean temperature across a region) commonly show nonlinear relationships between the pollen percentage and the climate variable. Such nonlinearities can often be resolved by transforming the pollen data by some power function (Figure 12.11). The transformed data are then used in developing an equation in which climate is the dependent variable and pollen percentages are the independent (predictor) variables. Thus, for the US New England region, the following equation was constructed ($R^2 = 0.77$) (Bartlein and Webb, 1985):

$$\begin{aligned}\text{July } T_{\text{mean}}(^\circ\text{C}) = {} & 17.76 + 1.73\ (Quercus)^{0.25} + 0.09\ (Juniperus) + 0.51\ (Tsuga)^{0.25} \\ & - 0.41\ (Pinus)^{0.5} - 0.12\ (Acer) - 0.04\ (Fagus)\end{aligned}$$

Using this approach, Bartlein and Webb (1985) estimated that at 6 ka BP, July temperatures over the northcentral and eastern United States, and southern Canada were 1-2 °C warmer than modern temperatures. Using a very similar approach, Huntley and Prentice (1988) estimated July temperatures in central and southern Europe were as much as 4 °C warmer at 6 ka BP compared to modern climate. The assumptions underlying this method (both ecological and statistical) are discussed at length in Howe and Webb (1983). Most important is the key uniformitarian assumption that any changes seen in pollen percentages of the past can be interpreted in terms of modern climate-pollen relationships. Indeed, this assumption underlies almost all paleoclimatic research involving calibration of paleorecords by means of

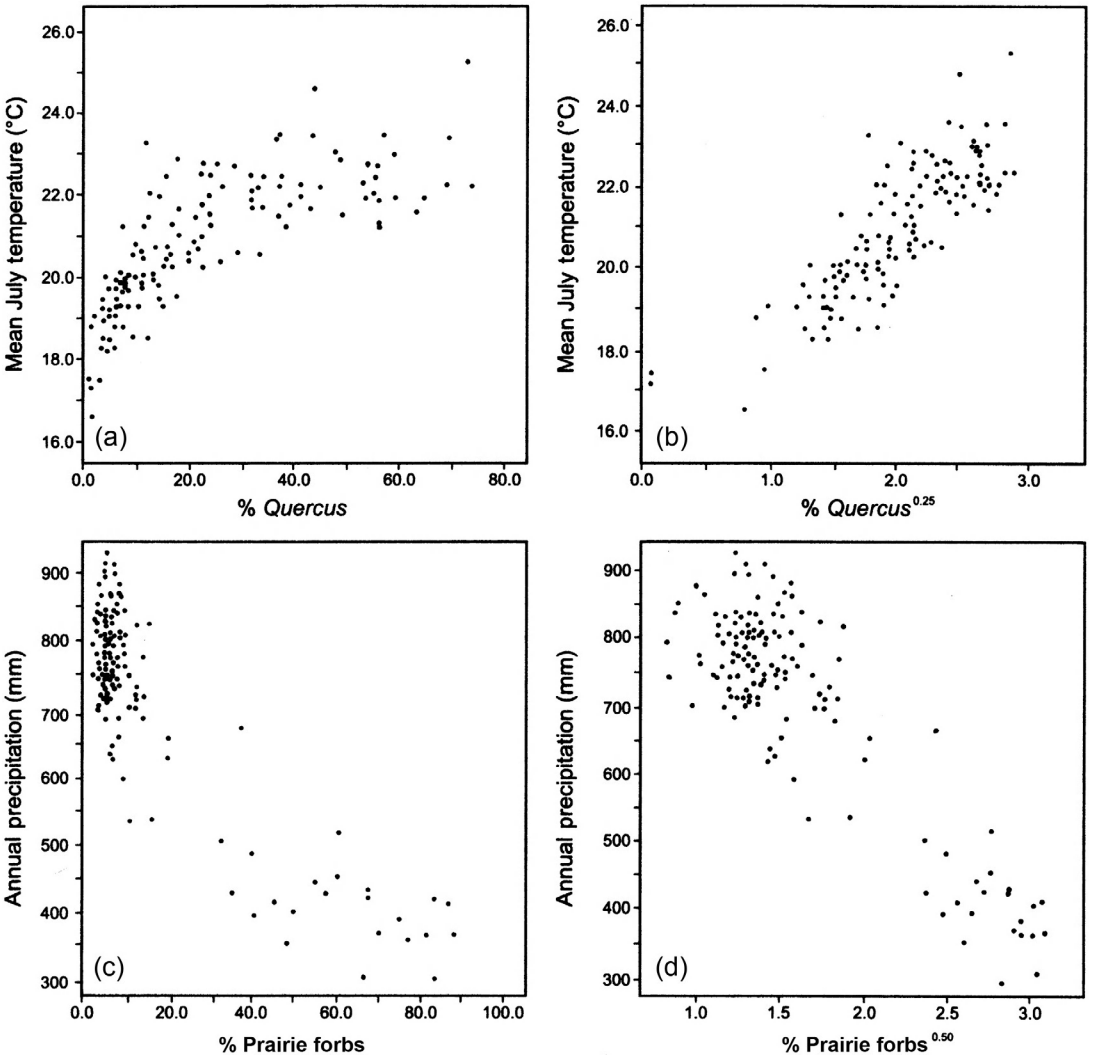


FIGURE 12.11 Scatter diagrams for (a) July mean temperature versus the percentages of *Quercus* (oak) pollen; (b) July mean temperature versus the percentages of *Quercus* pollen raised to the 0.25 power; (c) annual precipitation versus the percent of prairie-forb pollen (excluding *Ambrosia*); and (d) annual precipitation versus the percent of prairie-forb pollen raised to the 0.5 power. *From Bartlein et al. (1984).*

modern data (Jackson and Williams, 2004). One must also accept that paleoclimatic reconstructions based on transfer functions are only reliable if the modern calibration data set is extensive enough to be representative of all (or nearly all) conditions occurring in the past; otherwise, unwarranted extrapolations may be made. Hence, transfer functions will not help to explain in climatic terms fossil pollen assemblages in the past that bear no relation to modern experience (the no-analog situations; Williams and Jackson, 2007), though new

approaches to improving the climatic interpretation of such periods have been proposed (e.g., Gonzales et al., 2009).

The no-analog problem was encountered by Overpeck et al. (1985) who quantified the relationship between modern pollen rain and fossil pollen spectra by calculating "dissimilarity coefficients" for each level in a pollen diagram (cf. Prell, 1985; Bartlein and Whitlock, 1993). By matching the locations that were most similar (or least dissimilar) to a given pollen spectra in the past, they were able to characterize Holocene vegetation change in the eastern United States in terms of modern analogs. Then, using modern climatic data from the modern pollen analog sites, they could make deductions about former climatic conditions. This approach worked well for most Holocene samples, but for the period from ~11 to 9 ka in the Upper Midwest of the United States, no close analogs could be found in the modern pollen rain. This was probably because at that time, climate was rapidly changing and individual species responded to those changes at different rates, creating transient ecosystems not observed today.

Another multivariate approach to paleoclimatic reconstruction involves the computation of "response surfaces." Pollen distribution is considered as occupying "climate space" defined by a three-dimensional array of climate variables (Bartlein et al., 1986). Figure 12.12a–c illustrates the concept, beginning with simple bivariate graphs, relating spruce (*Picea*) pollen percentages to mean January and July temperatures and to annual precipitation. The graphs are based on over 1000 modern pollen samples from across northern North America and Greenland and climatic data from the nearest weather stations (Anderson et al., 1991). Clearly, it would be difficult to use any one of these graphs alone in interpreting pollen data. By plotting spruce pollen percentages in relation to both January and July mean temperatures (Figure 12.12d), a more coherent picture emerges with the highest pollen percentages associated with mean July temperatures of 12-15 °C and mean January temperatures of −17 to −20 °C. Similarly, maximum spruce pollen percentages are found where annual precipitation is around 900 mm and July temperatures are 11-13 °C. Spruce pollen percentages thus vary within the three-dimensional "climate space" defined by the two monthly temperatures and annual precipitation. This can be envisaged by considering how pollen percentages vary in relation to both January and July temperatures, as annual precipitation changes along a third axis—represented in Figure 12.13 as a series of slices at selected precipitation intervals. Spruce pollen is highest in areas with July temperatures around 10-13 °C, January temperatures of −12 to −18 °C, and annual precipitation of 880-1600 mm. These figures show schematically that the pollen percentage data define a body of variable density (i.e., the % data) suspended in climate space (Prentice et al., 1991). Response surfaces are mathematical expressions of these relationships, obtained by locally weighted regression techniques. Each pollen taxon is described in this way so that with a set of several equations, it is possible to define the combination of climatic conditions to which a given pollen spectra (made up of many different pollen types) correspond. This is made clear by considering what climatic conditions might be represented (in a fossil pollen spectra) by, say, 20% spruce. Clearly, there are many possible combinations of climate variables where 20% spruce pollen would be expected (Figure 12.13d). But those options would be more limited if the spectra had 20% spruce and 10% pine (which has its own constraints in climate space), and as more pollen types are added, each one uniquely delimited in climate space, the number of possible options becomes more and more limited. Eventually, the appropriate climatic conditions

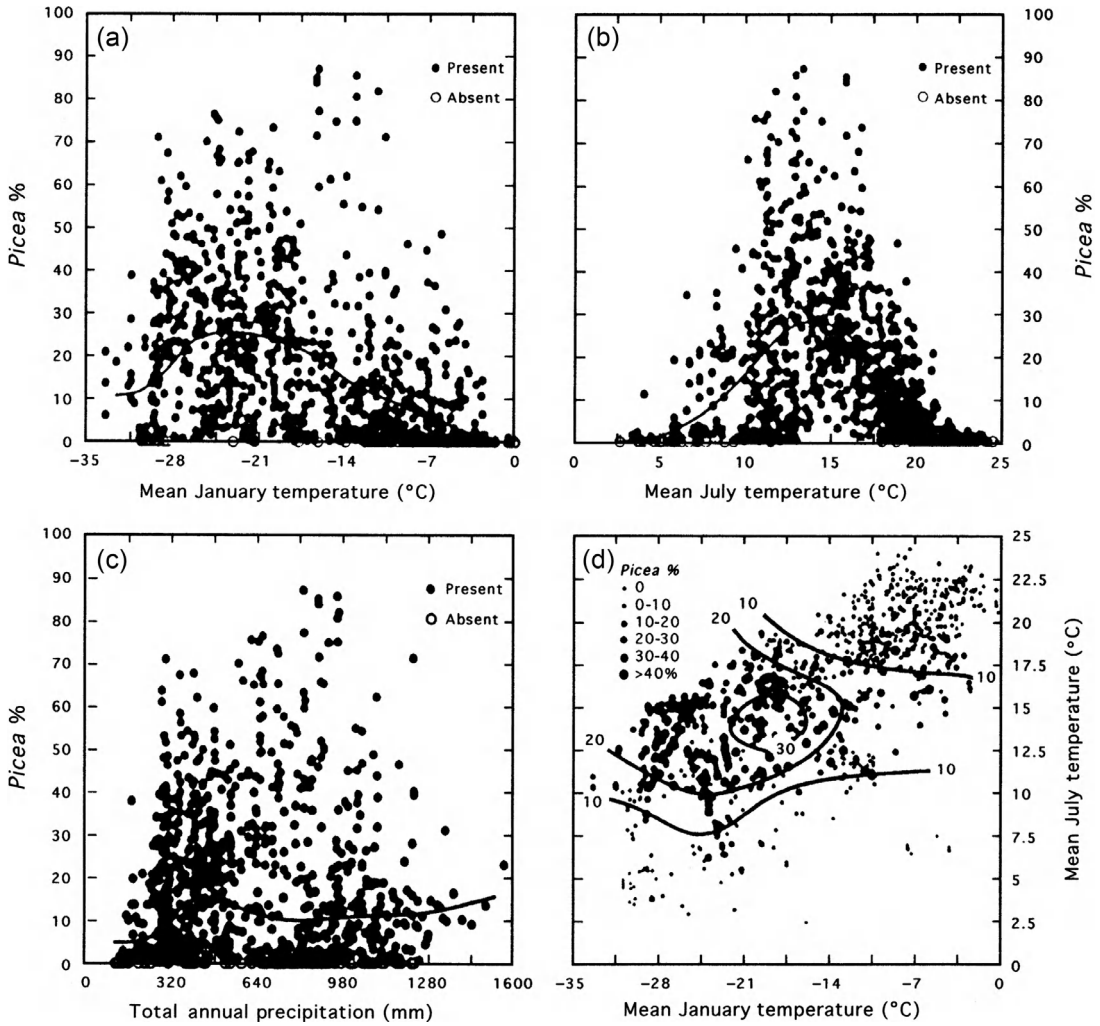


FIGURE 12.12 Scatter diagrams and response surfaces of *Picea* (spruce) pollen percentages and (a) mean January temperature, (b) mean July temperature, (c) total annual precipitation, and (d) mean July temperature and mean January temperature. *From Anderson et al. (1991).*

corresponding to the combination of pollen types are isolated, or at least the range of options is minimized, and the centroid of the final climate space, so defined, could be taken as the best estimate of the climate. Prentice et al. (1991) demonstrate that, in eastern North America, at least six major pollen taxa (spruce, birch, northern pines, southern pines, oak, and prairie forbs) are needed to avoid nonunique or indeterminate solutions. These six types are sufficient to define past climatic conditions at fossil pollen sites across eastern North America (Figure 12.14) though it must be recognized that not all values on the map are as reliable as others; this depends on the goodness of fit of the response surface for the modern

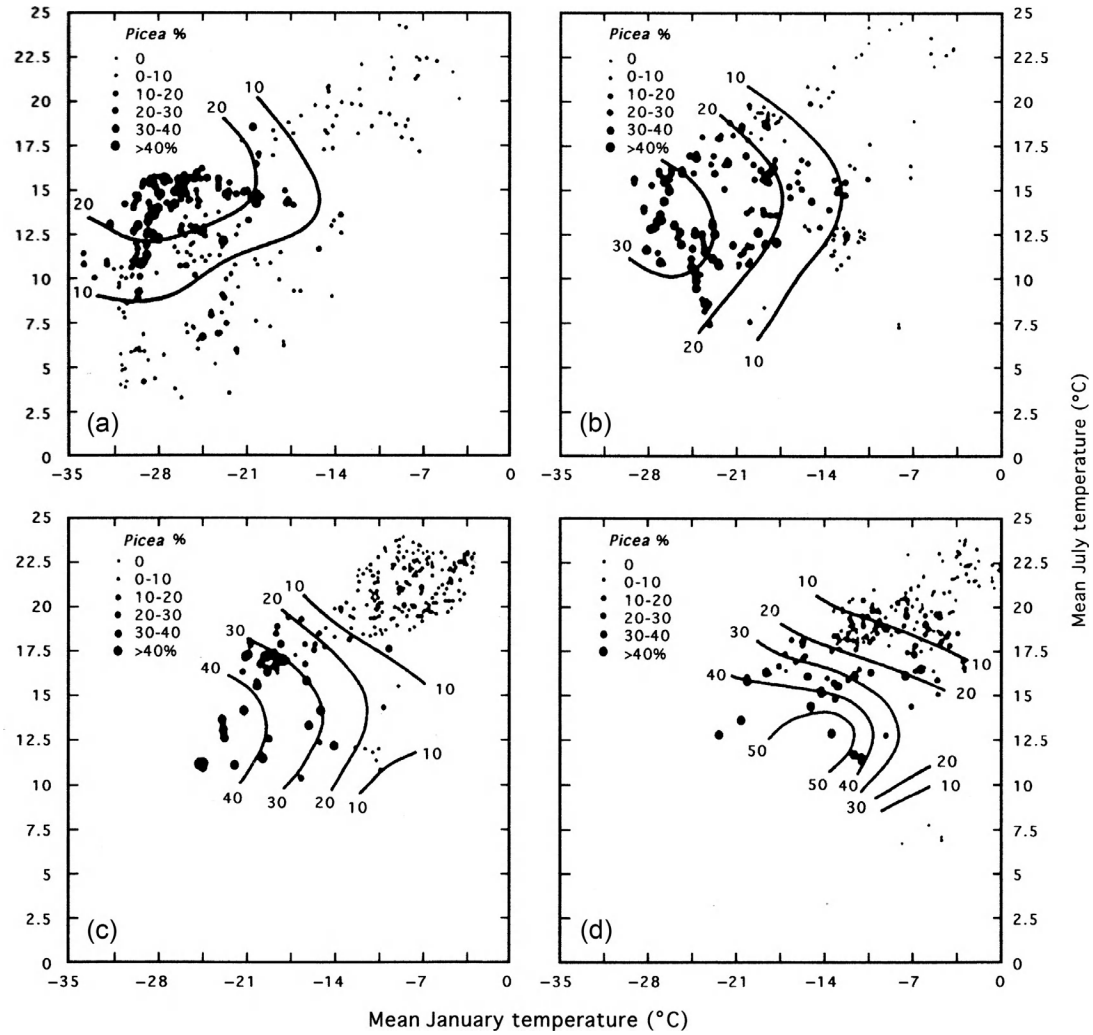


FIGURE 12.13 Scatter diagrams and response surfaces of *Picea* (spruce) pollen percentages as a function of mean July and January temperatures for four ranges of annual precipitation: 0-400 mm (top left), 400-640 mm (top right), 640-880 mm (bottom left), and 880-1600 mm (bottom right). *From Anderson et al. (1991).*

climate-pollen relationship and the "size" of the area in climate space to which the fossil pollen spectra correspond. The maps would be improved if some indication of relative error or reliability was represented (in time and space). Using more taxa should decrease the uncertainty in the paleoclimatic estimates (cf. Webb et al., 1993a, who used 14 taxa). In the example given, pollen rain is assumed to reflect January and July mean temperatures and annual precipitation. However, other parameters such as soil moisture or an index of continentality might be more discriminating variables. For example, Webb et al. (1993b) used a soil moisture index to define response surfaces and then reconstructed soil moisture changes over the

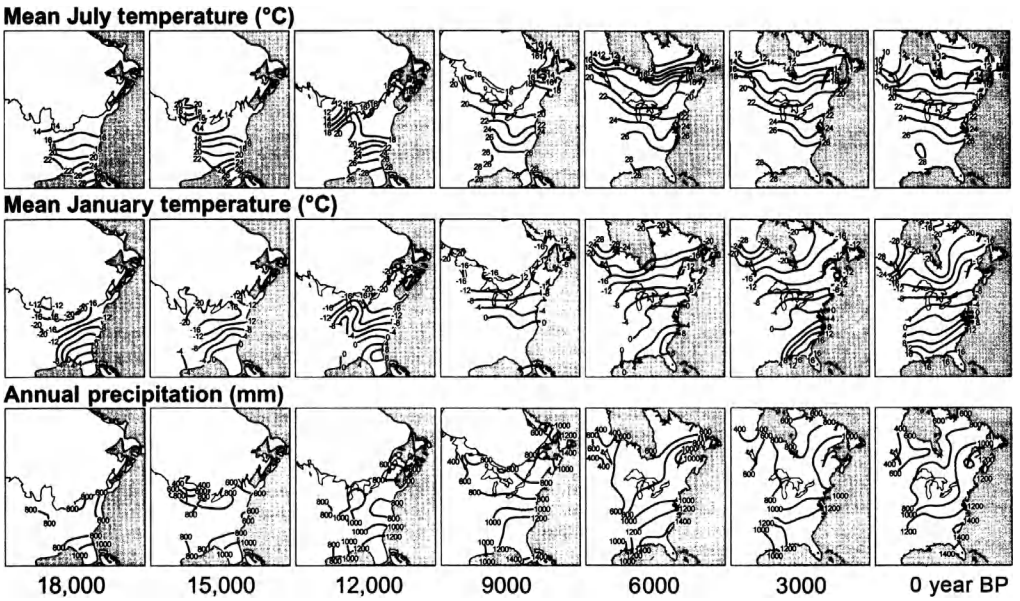


FIGURE 12.14 Climatic conditions at 3 ka intervals from 18 ka BP to the present inferred from fossil pollen and the modern abundances of six pollen types (spruce, birch, northern pines, southern pines, oak, and prairie forbs) using response surfaces. The blank area is the Laurentide ice sheet. *From Prentice et al. (1991).*

northeastern United States since 12 ka BP. Changes in precipitation were obtained from another set of response functions. This analysis revealed that although precipitation was lowest at 12 ka BP, effective soil moisture was lowest at 9 ka BP, a time when pine became most abundant in this region. The reconstruction is supported by lake level data, which points to the Early Holocene as a time of significantly drier conditions.

Although paleoclimatic reconstructions using pollen data have often used different statistical approaches to calibration, the good news is that they appear to give quite similar results, at least in terms of overall large-scale climatic patterns. This allowed Bartlein et al. (2011) to combine the results of many different reconstructions, to map climatic anomalies at 6000 and 21,000 calendar years BP (e.g., Figure 12.15). This showed that, at 6 ka BP, temperatures of the warmest month (and growing degree days) were higher across much of western Europe, though in regions near the Mediterranean, cooler conditions prevailed. It was also wetter across most of western Europe at that time, and thus, the moisture available to plants (the ratio of actual to potential evapotranspiration, α) was also higher. The pattern of temperature and precipitation changes was less coherent over North America, though the northeastern section of the continent generally had a higher number of growing degree days and drier conditions overall.

One of the inherent problems of producing a reliable paleoclimate reconstruction is related to the way in which the modern landscape has been transformed by human activity. Guiot (1987) argues that in many areas (such as in Europe), the variable topography and a long history of human impact make it very difficult to capture, in the contemporary pollen rain, all the information necessary to interpret fossil pollen spectra. These problems introduce

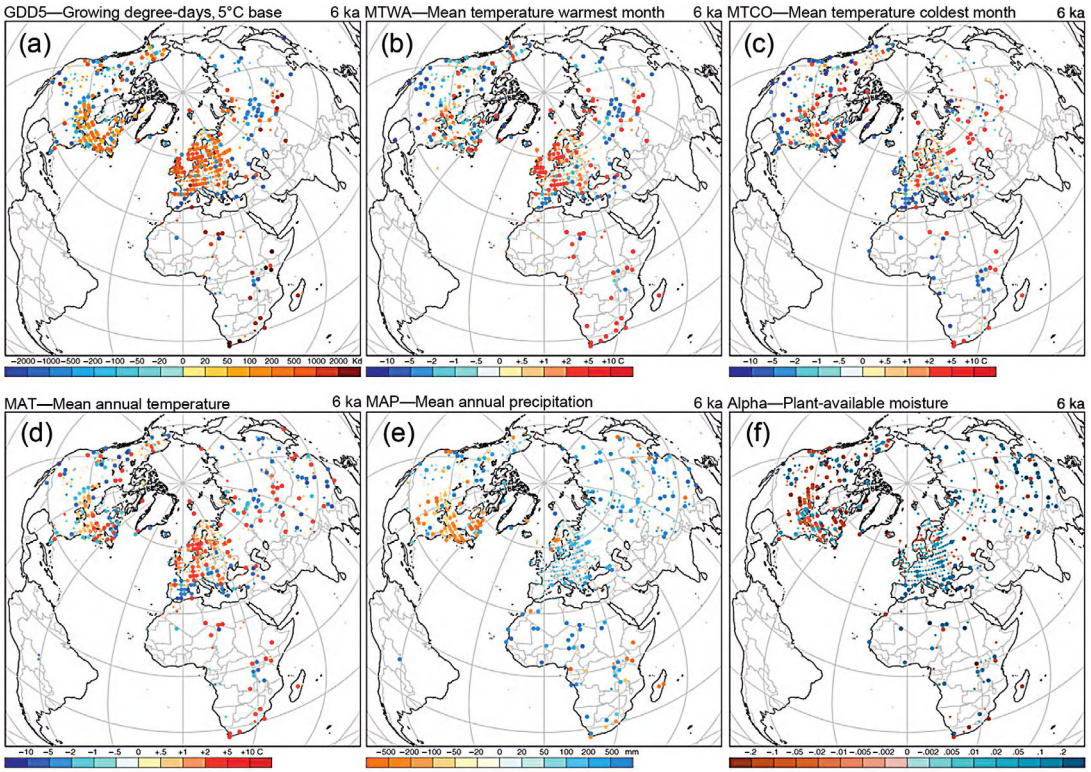


FIGURE 12.15 Reconstructed anomalies (relative to 1961-1990 averages) of (a) growing degree days (5 °C base), (b) mean temperature of the warmest month, (c) mean temperature of the coldest month, (d) mean annual temperature, (e) mean annual precipitation, and (f) alpha (ratio of actual to potential evapotranspiration) at 6 ka. Data are derived from many reconstructions that used different statistical approaches to the calibration of modern pollen data. Large symbols indicate grid points with significant anomalies (i.e., those that exceed twice the pooled standard error of the reconstructions); small symbols indicate anomalies that are not significant by this measure. Note that the anomaly patterns are spatially coherent and include areas with both significant and not significant values. *From Bartlein et al. (2011).*

considerable noise into paleoclimate estimates. Furthermore, the response of vegetation to a given change in climate will not always be represented in the pollen spectra in the same way; it will depend on the preceding vegetation state. There will be a certain autocorrelation in the pollen series that is not accommodated by the transfer or response function approaches (though Webb et al. (1987) and Prentice et al. (1991) implicitly take this into account by reconstructing climate only at 3 ka intervals). Guiot proposes a method to reduce the variability (noise) in a paleoclimate reconstruction based on transfer or response functions (which he terms "analog climates"). First, the changes in fossil pollen spectra from a limited region are analyzed to extract those variations that are common to the different locations. This is achieved by a method akin to principal components analysis. The main component might account for, say, 80% of the common variance in two or more records, and it is assumed that this common signal (termed the "paleobioclimate") represents the overriding influence of

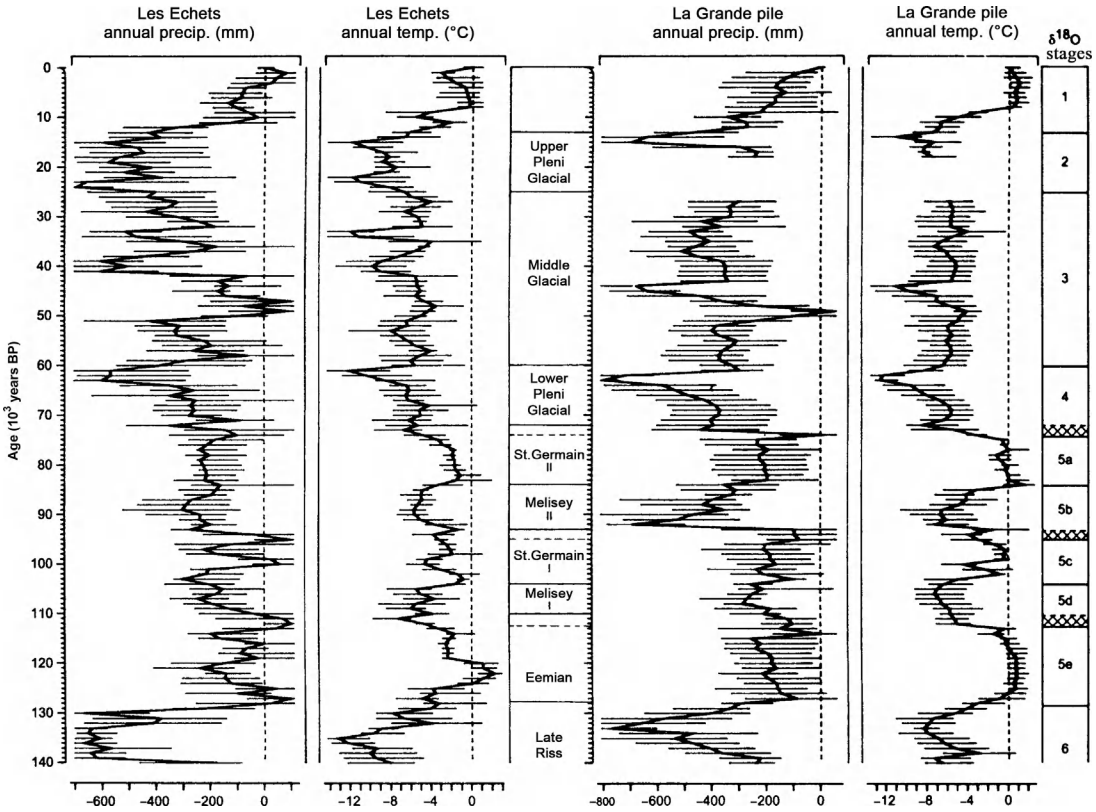


FIGURE 12.16 Reconstructions of mean annual temperature and annual precipitation at Les Échets (left) and La Grande Pile, France (right) (for locations, see Figure 12.17). Values are expressed as deviations from modern values (9.5 °C and 1080 mm at La Grande Pile and 11 °C and 800 mm at Les Échets). Error bars are computed by Monte Carlo simulation. The chronology is approximate before the Upper Pleniglacial, being dated by correlation with the SPECMAP marine isotope record, shown on the right (cf. Section 6.3.3). *After Guiot et al. (1989). Compare this with Figure 12.18.*

climatic variations on vegetation changes at all the sites. This series is then used in identifying the most appropriate modern analog climate, based on a measure of similarity between fossil and modern pollen spectra (Guiot et al., 1989). By reducing what is assumed to be nonclimatic noise in the original series, the final paleoclimate estimates have a larger climate signal-to-noise ratio than would otherwise be obtained. Using this approach, Guiot et al. (1989) were able to estimate mean annual temperature and precipitation variations over the past 140,000 years at two sites in France (Figure 12.16). These show temperatures similar to or slightly higher than Holocene levels at the height of the last interglacial in Europe (the Eemian); two subsequent interstadials (St. Germain I and II) were almost as warm. Extremely cold and dry conditions were first experienced around ~65 ka BP. Three or four other cold, dry intervals occurred in the main (Würm/Weichselian) glacial period, followed by a change to much warmer and wetter conditions in the Holocene. These reconstructions, and their limitations, are discussed further in Section 12.5.1.

12.5 PALEOCLIMATIC RECONSTRUCTION FROM LONG QUATERNARY POLLEN RECORDS

There are now numerous palynological records that span the Late Quaternary and in some cases extend back continuously into the Pliocene. Dating is, of course, problematical beyond the range of radiocarbon dating (~40,000 years in most cases), and often, the records are simply assumed to extend back to the last interglacial and beyond, based on the character of the pollen record itself. In some cases, correlation with marine oxygen isotope stratigraphy, either directly (in marine sedimentary records) or indirectly (by comparisons between terrestrial and nearby marine records), can prove helpful in constructing a chronology. Here, a selected number of long palynological records from different areas of the world are presented to provide an overview of how such records, even if not well dated or calibrated quantitatively, can reveal important paleoclimatic changes of large-scale significance. They provide important insights into changes in terrestrial climates on timescales comparable to the important ice core, loess, and marine sedimentary records, thereby completing the global picture of climatic variations over the Quaternary period.

12.5.1 Europe

Several long records extending >100 ka have been recorded from lakes and bogs in Europe (Figure 12.17). Of these, La Grande Pile in the French Vosges mountains has been studied in the most detail, with over 20 cores recovered for pollen, plant macrofossils, sedimentologic and faunal (insect) analysis (Woillard, 1978; Woillard and Mook, 1982; de Beaulieu and Reille, 1992; Guiot et al., 1992, 1993; Pons et al., 1992; Seret et al., 1992; Ponel, 1995). The pollen record from this location is well documented, enabling the overall sequence of vegetation changes over the last interglacial-glacial cycle to be established (Figure 12.18). The penultimate glaciation (Riss) was characterized by an open grassland with few trees. The transition to peak interglacial conditions in the Eemian is marked by a clear sequence of taxa,[4] first *Juniperus*, then *Pinus*, and *Betula*, *Ulmus*, and *Quercus*, with *Corylus* and finally *Taxus* indicative of the interglacial climatic optimum. Subsequent climatic deterioration is marked by a rise in *Abies* and *Carpinus*, then *Picea*, *Pinus*, *Betula*, and *Juniperus* once again. This short cool episode is the first of two such periods (termed Melisey I and II) separated by more temperate conditions (St. Germain I and II). This is clearly seen in the relative proportions of arboreal to non-arboreal pollen (AP/NAP) with the colder periods characterized by sharp increases in the NAP fraction of the pollen sum. The onset of full-glacial conditions (the Pleniglacial) began ~70 ka BP when *Artemisia* and other cool steppe taxa increased in abundance. The following 50 ka was dominated by NAP, though occasional fluctuations in the abundance of arboreal taxa suggest that conditions were not completely static. Coldest and driest conditions occurred in the late glacial (Tardiglacial) as shown by lowest NAP values and highest levels of *Artemisia* (Figure 12.18).

These interpretations have been quantified by Guiot et al. (1989, 1992) as discussed earlier (cf. Figure 12.16) based on calibration with modern pollen assemblages. However, the

[4] For common names, see Table 12.1.

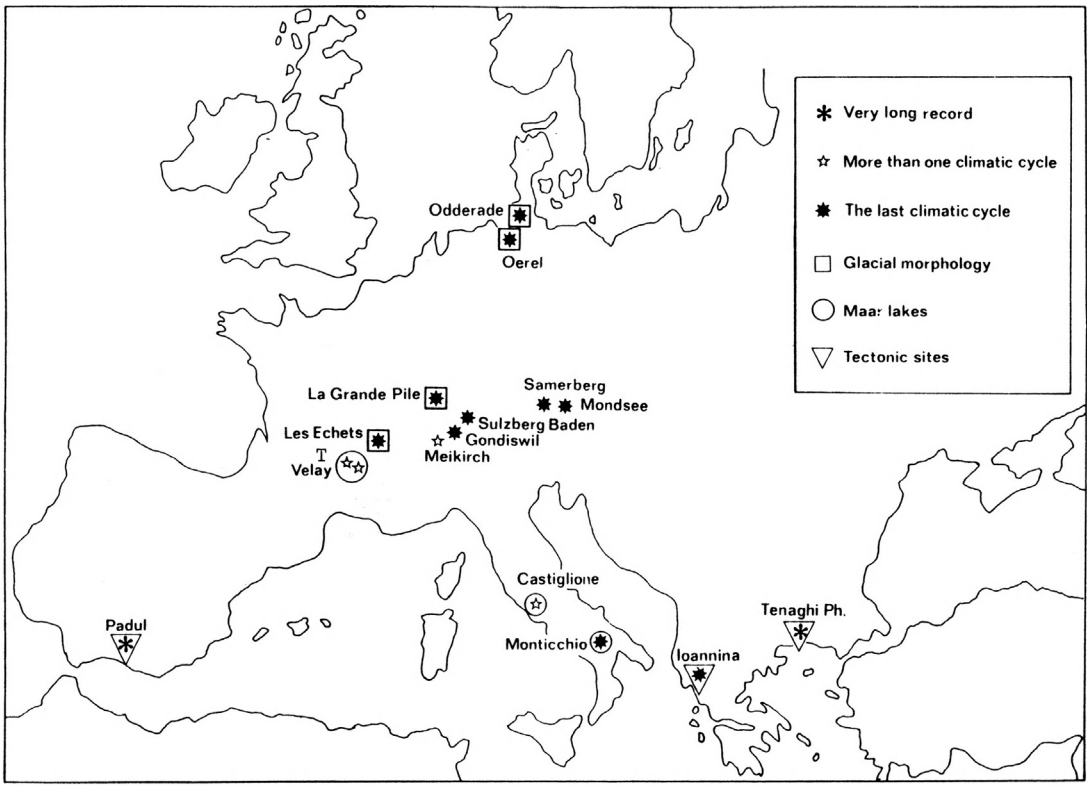


FIGURE 12.17 Location of the longest European pollen records that span at least the last glacial-interglacial cycle. *From Guiot et al. (1993).*

reconstructions are problematical because there are no good modern analogs (at least not in Europe) for pollen assemblages recorded in the coldest parts of the last glaciation. Indeed, the full-glacial vegetation assemblage may have more in common with the cold, arid steppes of interior Asia and Tibet today than anywhere in Europe. Furthermore, periods of rapid change may not be adequately recorded in the pollen record because the overall inertia in vegetation assemblages makes pollen a poor indicator of short, abrupt climatic changes. These concerns have led to the incorporation of other climatic indicators, such as sedimentary characteristics (Seret et al., 1992) and insects (Guiot et al., 1993; Ponel, 1995) together with pollen in recent reconstructions. For example, the loess content of the sediment is highest and organic matter content is lowest during the coldest intervals of the Pleniglacial. Taking such factors into account results in significant differences of interpretation (up to 6 °C) with more variability of temperature during the full-glacial period. Further studies have combined pollen with the insect fauna to refine the reconstruction of mean annual temperature (Figure 12.19). Insects respond quickly to climatic fluctuations (see Section 11.2) and so are especially useful in a period when climate is unstable (Ponel, 1995). Combining both insect and pollen data reveals many rapid changes in climate during the Pleniglacial, some of which correspond to

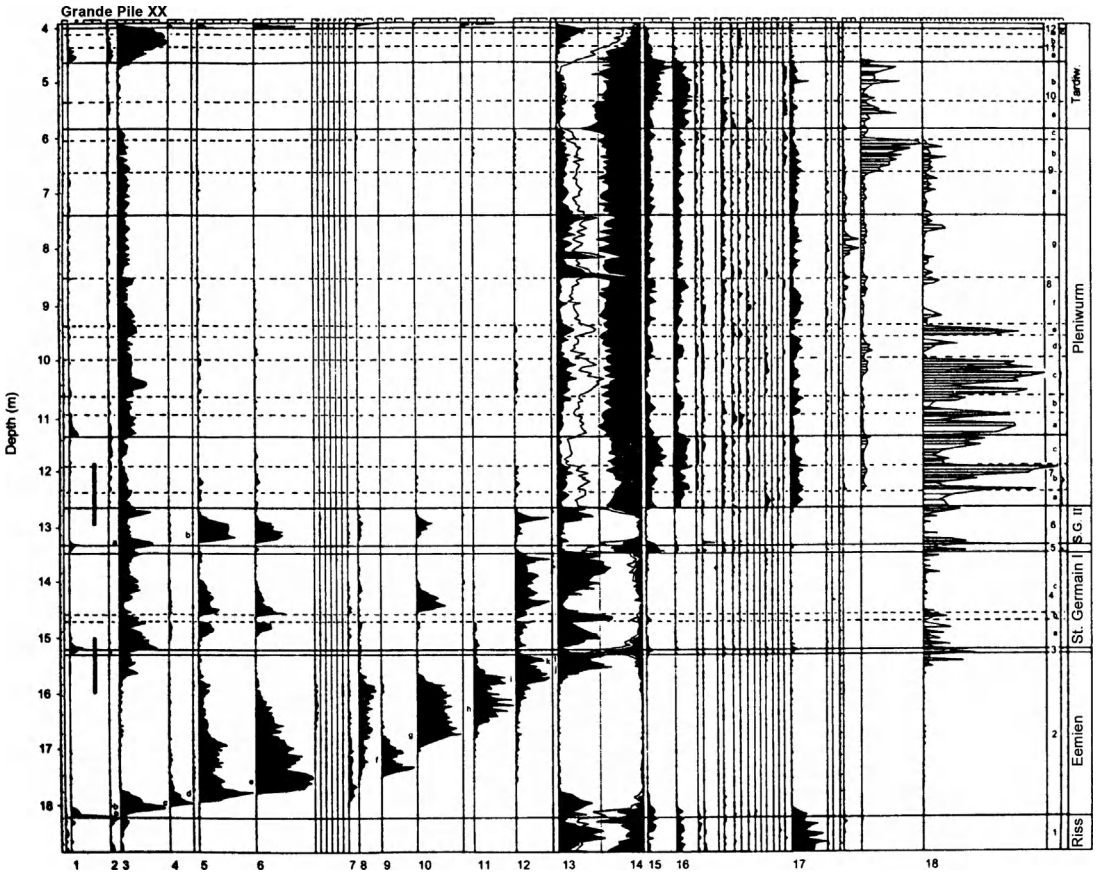


FIGURE 12.18 Pollen diagram from La Grande Pile, Vosges, France, representing changes from the penultimate glaciation (Riss) to the late glacial ("TardiWürm"—see pollen zones indicated on the right). Numbers across bottom correspond to principal pollen types; the sequential change in vegetation during a complete glacial-interglacial cycle is clearly seen. 1 = *Juniperus*; 2 = *Salix*; 3 = *Betula*; 4 = *Ulmus*; 5 = deciduous *Quercus*; 6 = *Corylus*; 7 = *Fraxinus*; 8 = *Alnus*; 9 = *Taxus*; 10 = *Carpinus*; 11 = *Abies*; 12 = *Picea*; 13 = *Pinus*; 14 = Poaceae; 15 = *Artemisia*; 16 = heliophytes (various); 17 = Cyperaceae; 18 = *Isoetes*. The thin line between 13 and 14 represents the overall arboreal/nonarboreal pollen ratio, with arboreal pollen increasing to the right. *From de Beaulieu and Reille (1992).*

Dansgaard-Oeschger oscillations seen in the Greenland ice cores and possibly also to North Atlantic Heinrich events. This multivariate approach to paleoclimate reconstruction has much to offer since it is clear that no one variable can provide an accurate view of past climate in Europe during full-glacial conditions. By pooling the information each proxy provides, a more reliable reconstruction can be obtained.

The longest continuous pollen record in Europe is from Tenaghi Philippon (Macedonia, Greece) where a ~200 m sequence of peat, gyttja, lake marls, and clays provides a unique picture of vegetation changes in southern Europe for the last 1.3 Ma. Although this record has been known for a long time, dating has always been problematical. Tzedakis et al. (2003, 2006) revised earlier chronologies, using a combination of ^{14}C, paleomagnetic data, and observed

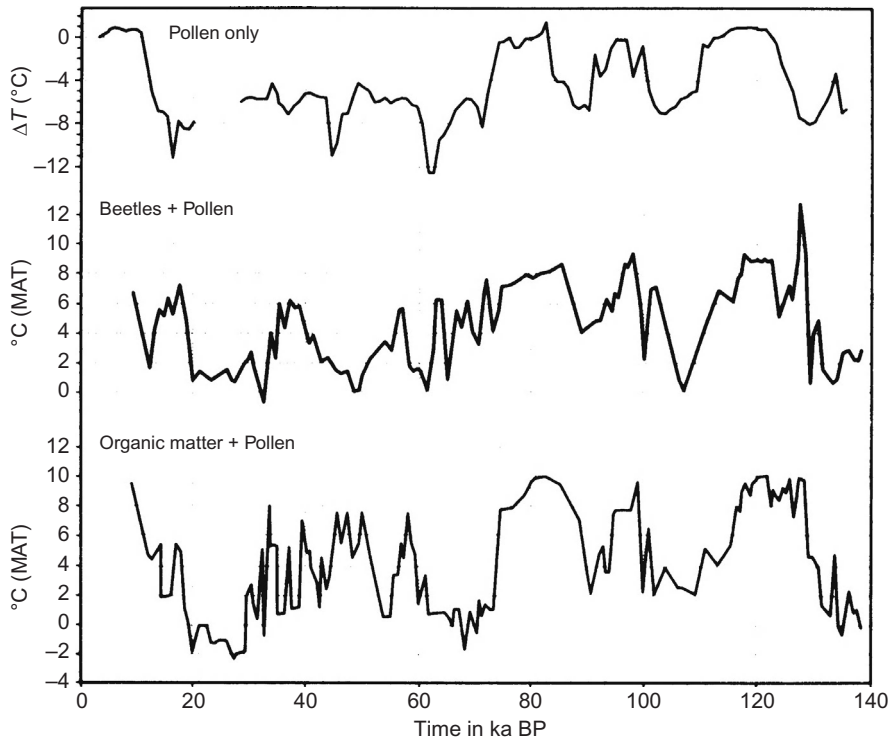


FIGURE 12.19 Mean annual temperature at La Grande Pile over the past 140,000 years, reconstructed from pollen alone (top) and pollen constrained by the additional consideration of organic matter variations (lower diagram) or insects (Coleoptera) (middle) (cf. Figure 9.15). Modern pollen analogs are not good descriptors of climatic conditions during the main glacial phase (~70-20 ka BP) or when climate changed abruptly. By considering insect fauna and sedimentologic changes, additional constraints on paleotemperature estimates are introduced. *From Guiot et al. (1993).*

correlations between vegetation changes and precessional variations. Noting that tree population dropped rapidly, due to cold and dry conditions, when perihelion occurred in March, and Mediterranean-type vegetation expanded, due to hot and dry conditions, when perihelion occurred in June, they tuned the pollen record accordingly, revealing a much longer series than had hitherto been recognized. This provides a fascinating long-term perspective on vegetation changes, summarized in Figure 12.20 by the variations in arboreal pollen (AP) percentages. Expansion and contraction of forest vegetation (from close to 0% to almost 100% AP) tracked the decay and growth of global ice volume (as registered by the benthic ^{18}O record shown in Figure 12.20), but there were other suborbital-scale variations that appear to track wet-dry oscillations unrelated to glacial-interglacial variability. Large shifts in forest vegetation also occurred in the pre-Brunhes period, when glacial-interglacial changes were smaller than for the last ~0.5 Ma, dominated by the 41 ka obliquity changes, rather than the ~100 ka variability seen later. Of particular interest is MIS 16 (~630-680 ka BP), when tree population remained low throughout this long interval. This period appears to have had an enduring effect of the vegetation of the region. Prior to MIS 16, a taxonomically diverse flora

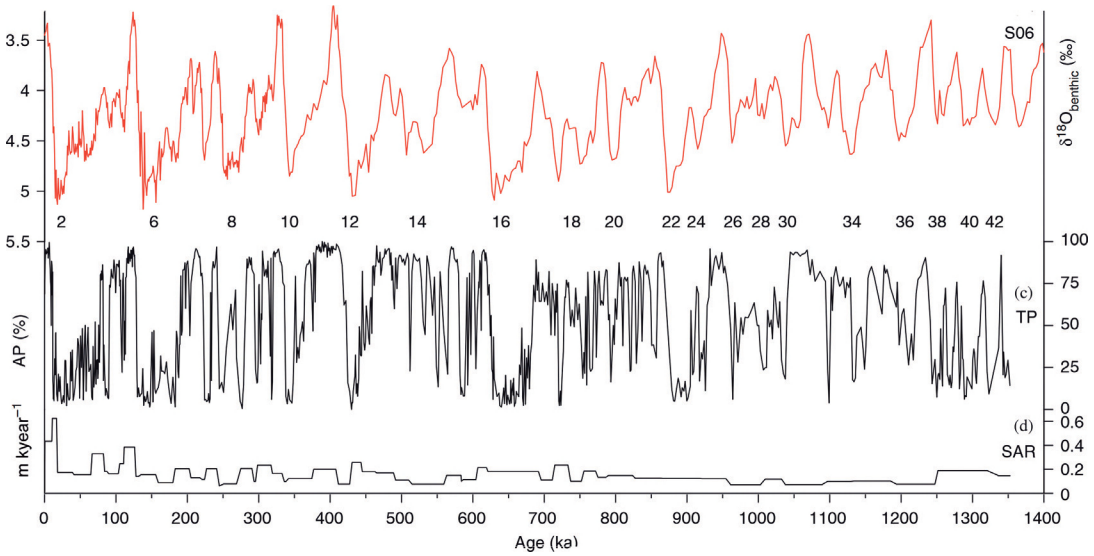


FIGURE 12.20 Tenaghi Philippon arboreal pollen (AP) percentages plotted on the pollen-orbital-calibrated time-scale (below) and the S06 (equatorial Pacific) benthic $\delta^{18}O$ composite record (above) for the last 1.4 Ma. Lowest line shows the resultant sediment accumulation rates (SARs). Inflections of the SAR curve show the location of the control points. *From Tzedakis et al. (2006).*

existed, but after MIS 16, the tree flora became more restricted, with the remaining species somewhat more drought-tolerant than those species that disappeared. Whether this reflects drier interglacials following MIS 16, local hydrologic changes, or that the prolonged cold interval led to the extirpation of many taxa is not entirely clear. Nevertheless, this pattern of species loss has been noted in other parts of Europe, with more cold-tolerant taxa surviving in northern regions and more drought-tolerant species surviving in the south, indicative of the overall shift toward more extreme temperature and moisture conditions over time.

12.5.2 Sabana de Bogotá, Colombia

The longest continuous sedimentary record from South America comes from a mountain-rimmed basin in the Colombian Andes (Hooghiemstra, 1984). Known as the Sabana de Bogotá, it is a former lake basin, currently at ~2550 m above sea level. More than 580 m of sediment has been recovered but dating the record has been challenging; it is now thought to extend back through the Early Quaternary (Torres et al., 2013). Vegetation in the area is zoned altitudinally, ranging from tropical forest below ~1000 m to Andean forest above ~2300 m, to páramo above ~3500 m (Figure 12.21). At the highest elevations, perennial snow is found. Pollen has been analyzed throughout the period of record but in remarkable detail (~60-year resolution) for the last 284 ka (Groot et al., 2011). Of particular interest is the percentage of arboreal pollen (AP%), which is strongly correlated with temperature-driven changes in the upper forest limit. Regional studies indicate that a 10% change in AP%

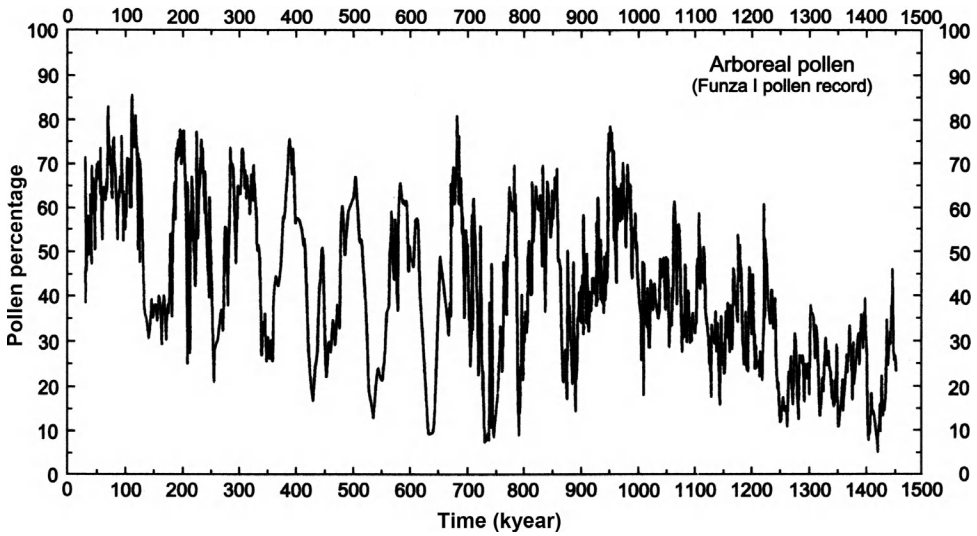


FIGURE 12.21 Fluctuations of arboreal pollen (AP) sum at the Funza site, Sabana de Bogotá, Colombia, over the past 1.46 Ma. The former lake of Bogota desiccated at ~27 ka BP, terminating this sequence. The development of a pronounced ~100 ka climatic cycle within the last 1 Ma is clearly seen. *After Hooghiemstra and Ran (1994).*

corresponds to a change in mean annual temperature of 1.3 ± 0.3 °C (assuming a steeper lapse rate during glacial times; Wille et al., 2001). Spectral analysis of the AP% in the record indicates that there are two strong periodicities, which appear to reflect the 41 ka (obliquity) and ~100 ka (eccentricity) signals. The complete record was thus tuned to match the 41 ka frequency recorded in benthic marine isotopic records, which ties changes in the AP% to the orbitally induced glacial-interglacial changes seen in the marine record (implicitly taking into account an assumed 6-8 ka lag between the orbital forcing and ice volume changes). With these assumptions, the base of the Funza record is ~2.25 Ma BP (Groot et al., 2011; Torres et al., 2013). With the timescale resolved, the long-term history of vegetation changes and climatic implications can be explored. Over the last 284 ka, AP% has varied from ~10% to >90%, indicating that temperatures in the Funza basin have varied from ~6 °C during glacial maximum conditions to ~17 °C at the peak of interglacial warmth (Figure 12.22). Of particular interest are the very rapid changes in forest cover that occurred at glacial terminations, suggesting that temperatures increased by $\sim 10 \pm 2$ °C within a matter of centuries. There were also rapid changes that occurred at other times, associated with D-O and Heinrich events in the North Atlantic, pointing to strong links between conditions in the North Atlantic and in the high mountains of South America (cf. Kanner et al., 2012; Placzek et al., 2013). Interpreting the longer record of arboreal pollen in terms of temperature is more problematical, as there was no oak (*Quercus*) in the region prior to ~0.5 Ma BP, and no alder (*Alnus*) before ~1 Ma BP, so the forest composition was quite different, with no modern analog (Figure 12.23). Nevertheless, for the last million years, the percentage of all the other arboreal pollen (excluding *Quercus* and *Alnus*) has varied in parallel to those taxa, suggesting that the long-term responses to temperature changes on glacial-interglacial timescales have been similar to those reconstructed for the last ~280 ka, when the forest composition was similar to today. It is

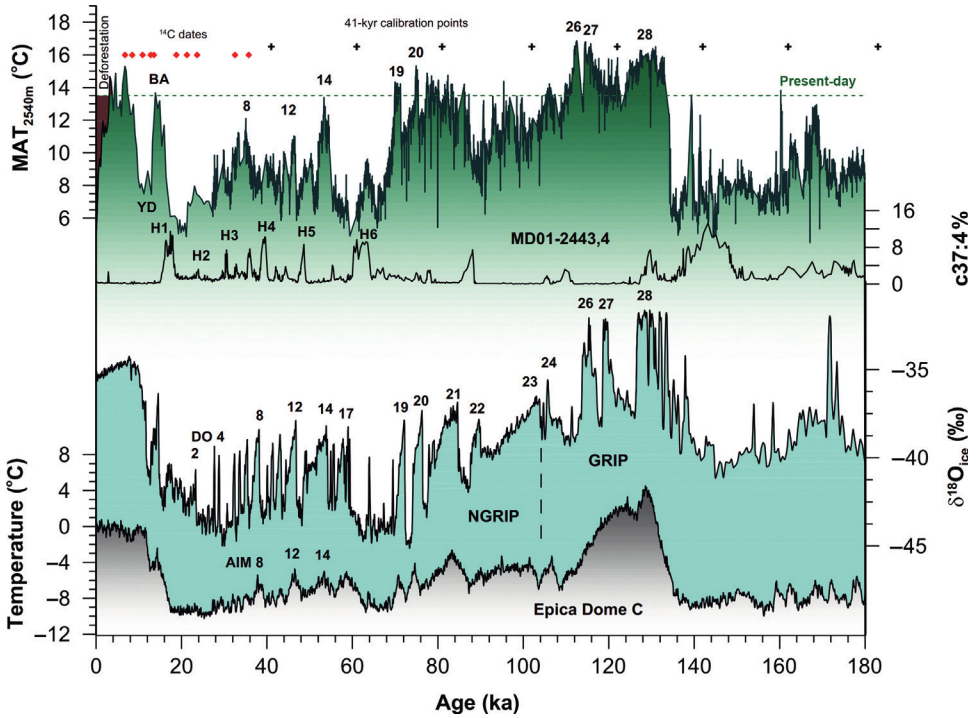


FIGURE 12.22 Reconstructed mean annual temperatures (MATs) at Lake Fúquene, the C37:4 alkenone record from the Iberian margin (indicating the timing of Heinrich events; Martrat et al., 2007), the Greenland $\delta^{18}O$ ice core record (Anklin et al., 2003), and the estimated temperature record of EPICA Dome C (Jouzel et al., 2007b; Parrenin et al., 2007). D-O numbers indicate Dansgaard-Oeschger cycles and AIM are the Antarctic Isotope Maxima. H1-H6 correspond to the Heinrich events, BA = Bølling-Allerød interstadial, and YD = Younger Dryas. The combined Greenland $\delta^{18}O$ record includes (1) the Greenland Ice Core Chronology 2005 (GICC05) (North Greenland Ice Core Project Members, 2004) based on annual layer counting for the past 60 ka, (2) the original NGRIP data (North Greenland Ice Core Project Members, 2004; Svensson et al., 2008) between 60 and 103 ka, and (3) the data of GRIP below 103 ka (see Chapter 5, Section 5.3.2). *From Groot et al. (2011).*

also of interest that the overall record indicates a shift in the frequency of climatic change occurred around 1 Ma BP, from relatively low-amplitude high-frequency variations to higher-amplitude fluctuations with a period close to 100 ka (cf. Figure 12.23) (Hooghiemstra et al., 1993; Torres et al., 2013).

One further complication in interpreting the AP% changes simply, in terms of temperature, relates to the changing concentration of CO_2 on glacial to interglacial timescales. Elsewhere, studies of vegetation change in montane environments suggest that the lower concentrations of carbon dioxide in glacial times may have had a particularly strong impact on vegetation at high elevations. Ice core evidence indicates CO_2 levels were ~100 ppm lower at the last glacial maximum compared to preindustrial levels, so that at high elevations the partial pressure of CO_2 may have prevented C_3 plants, such as trees, from surviving (Street-Perrott, 1994; Street-Perrott et al., 1997, 1998). Lower carbon dioxide levels cause an increase in stomatal gas exchange, thereby raising transpiration rates and drought stress on plants (Jolly and Haxeltine, 1997). C_4 plants such as grasses are generally more efficient in utilizing CO_2

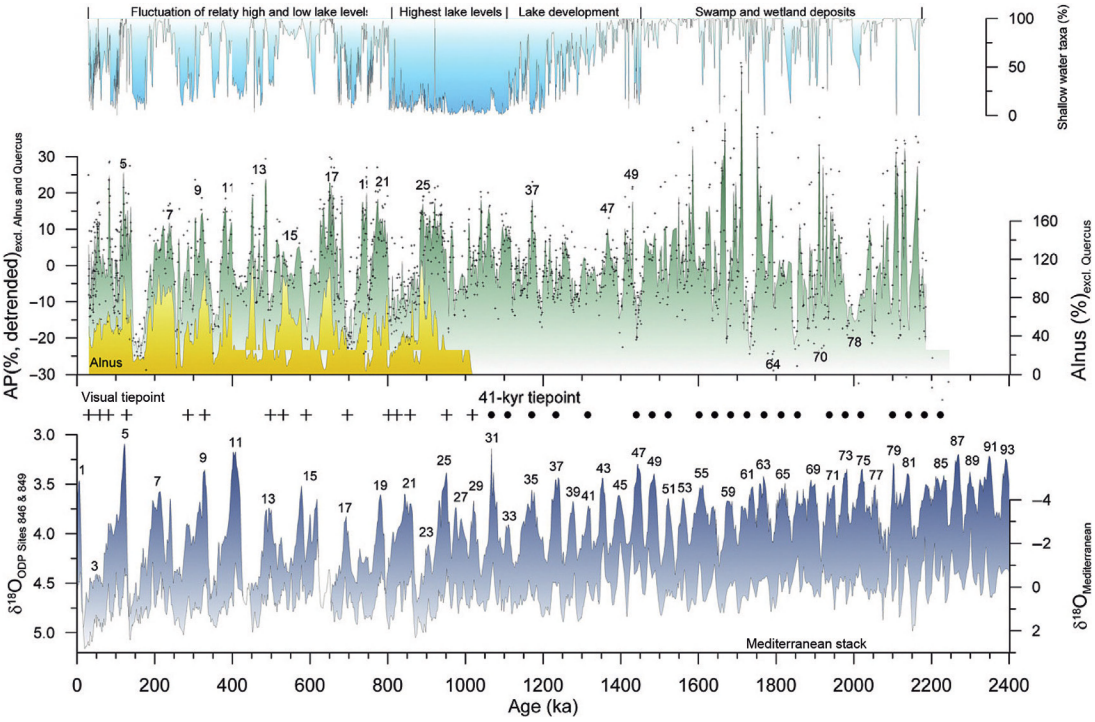


FIGURE 12.23 Pleistocene evolution of montane forest and páramo biomes in the Sabana de Bogotá, Columbia, after tuning the AP% record to obliquity forcing. *Upper panel* shows the development of hydrologic conditions in the basin over time, based on the percentage ratio of the aquatic fern Isoetes (reflecting water up to 8 m deep) versus aquatics reflecting shallow water. *Central panel* shows % *Alnus* record (yellow) and % total arboreal pollen (AP), excluding *Quercus* and *Alnus* (green). *Lower panel* shows a benthic $\delta^{18}O$ stacked record from ODP eastern equatorial Pacific Sites 846 and 849 (green) and a Mediterranean planktic $\delta^{18}O$ stacked record (white). *From Torres et al. (2013).*

and water, so the evidence for lower tree lines and more extensive páramo vegetation may, in part, be related to changes in CO_2 levels.

12.5.3 Central American Lowlands

Lake Petén Itzá is a closed basin lake in the lowlands of northern Guatemala from which a sediment core spanning the last ~83 ka was recovered (Hodell et al., 2008b). The climate at this latitude (~17°N) is subtropical (mean annual temperature of ~25 °C) with a strong seasonal cycle of rainfall related to the migration of the intertropical convergence zone (ITCZ) and associated convective activity toward the lake in summer months and much drier conditions, linked to subtropical divergence, in winter months when the ITCZ moves southward. Changes in the mean position of the ITCZ are strongly linked to the Atlantic meridional overturning circulation (AMOC). In the past, when the AMOC was weak, the ITCZ shifted southward, leading to drier conditions in Guatemala, with direct effects on lake level, water chemistry, and vegetation across the region. The strength of the AMOC is influenced by precession, and this has been the low-frequency driver of ecological and hydrologic changes

across Central America during the Late Quaternary. Superimposed on precessional effects were more abrupt changes related to Heinrich events in the North Atlantic (reductions in strength of the AMOC due to large inflows of freshwater from melting icebergs close to the source regions of North Atlantic deepwater formation) (Correa-Metrio et al., 2012a). When the AMOC was weak, the ITCZ was displaced to the south, leading to drier conditions in Central America, resulting in lower lake levels (up to 56 m lower at Lake Petén Itzá) and the deposition of authigenic gypsum ($CaSO_4$).

These changes are clearly registered in the pollen record from Lake Petén Itzá. The relative abundance of certain pollen types is strongly related to temperature allowing Correa-Metrio et al. (2011) to create "synthetic assemblages" as models of different temperature conditions, from ~13.5 to 26 °C. They then compared the down-core assemblages to these models to identify the closest fit to the synthetic data and thereby obtain an optimum paleotemperature reconstruction (Figure 12.24; Correa-Metrio et al., 2012a). This reveals gradual cooling from 83 ka BP to the LGM, with the coldest period from ~22 to 14.5 ka BP, when temperatures were

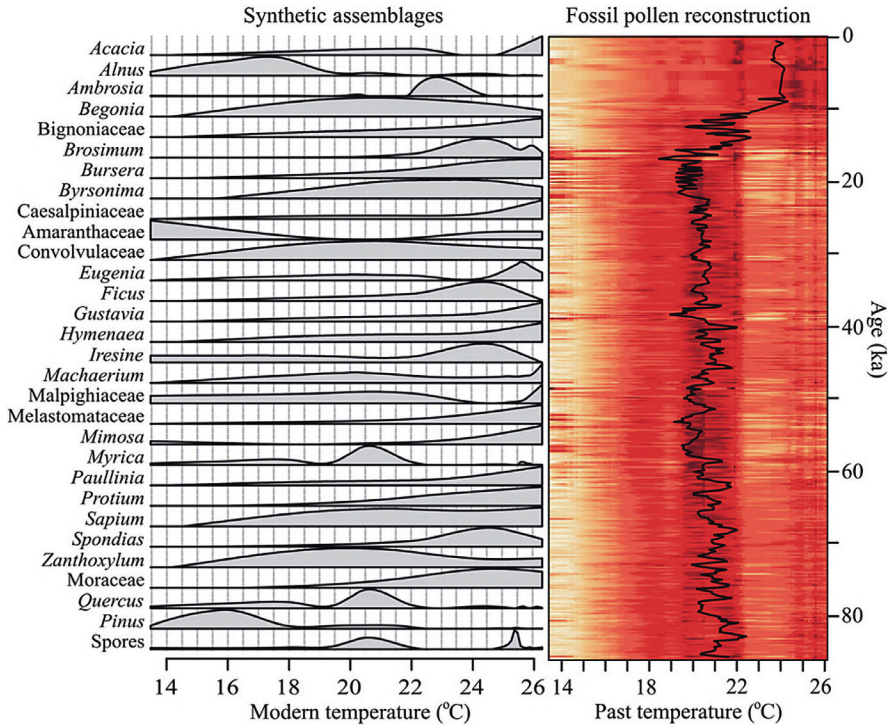


FIGURE 12.24 Pollen-based temperature reconstruction from Lake Petén Itzá, northern Guatemala, using synthetic assemblages. *Left panel*: Distribution of each taxon along the observed modern temperature gradient with abundances scaled to a uniform size for illustration purposes (Correa-Metrio et al., 2011). Gray shapes represent relative abundance of pollen across the temperature gradient at 0.5 °C temperature increments, although 0.25 °C increments were used for the calculations. *Right panel*: Temperature reconstruction. The darker the red shading, the smaller the distance of fossil samples from the ideal pollen synthetic assemblages shown in the left panel. *From Correa-Metrio et al. (2012a).*

4-5 °C lower than today. Although there were periods of abrupt temperature change, even the most rapid rate of change was an order of magnitude smaller than that expected over the next century due to anthropogenic climate change. In the past such rapid changes resulted in "no-analog" vegetation assemblages, suggesting that the future climate in this region will also lead to unique vegetation communities, with local extinctions probable.

During the LGM (23-18 ka BP), vegetation in the region was a pine-oak forest dominated by high elevation taxa that migrated downslope as temperatures declined, a pattern also seen in pollen data from Panama (Bush and Colinvaux, 1990). Nothing comparable to that forest composition can be seen in the region today. Relatively wet conditions prevailed, indicating that either the ITCZ extended north across the region or winter cold air outbreaks and associated rainfall were more common. Embedded within this pattern of long-term cooling were rapid changes in vegetation that occurred during Heinrich events (HE) when temperate woodlands (dominated by pine and oak) were quickly replaced by xeric shrublands with only scattered trees and a high proportion of grasses. This change was related to lower temperatures (by 1.5-2.5 °C) and much drier conditions at those times, with a strongly seasonal pattern of rainfall. Vegetation communities returned to their pre-Heinrich composition shortly after HEs, but some species lagged behind others, so that it took centuries to millennia before the full pre-HE community structure was restored (Correa-Metrio et al., 2012b).

12.5.4 Amazonia

Although it is commonly assumed that the large numbers of species of flora and fauna in the equatorial lowlands of South America are the result of long periods of stable climate, a number of biogeographic studies have cast doubt on that assumption. In a comprehensive study of different species of birds in and around the Amazon Basin, Haffer (1969, 1974) identified a number of regions that he considered had been refugia for groups of birds during drier periods in the past when the extensive tropical forests of today were reduced to discrete forest enclaves separated by savanna vegetation. Forest-dwelling species, which were isolated in this way, differentiated (developed new species) independently from members of the same species that had been separated into *other* forest enclaves. Haffer argued that when wetter conditions returned and the forests reoccupied the savanna region, forest-dwelling species also expanded their ranges, coming into contact with other population groups in the intervening areas. In these areas of "secondary contact," hybridization of species took place so that the discrete morphological characteristics of species that had evolved within the forest refugia were no longer obvious.

According to proponents of the refuge hypothesis, the results of these changes can be seen today in contemporary biogeographic distribution patterns. Within the extensive tropical forests, zones of relatively high species diversity (i.e., zones containing extreme concentrations of different plant and animal species) can be identified. These are sometimes referred to as centers of endemism (Brown and Ab'Saber, 1979). Within these zones, individual species may exhibit very uniform morphological characteristics (Vanzolini and Williams, 1970). Such regions are considered by many to be the former forest refuges that served as survival centers for forest dwellers during drier intervals. Between these centers of endemism, contact areas or "suture zones" are found, characterized by far fewer species than in the refuges and by more diverse morphological characteristics in the population of a particular species.

The refuge hypothesis has been controversial, but the tide has now turned toward a view of far less dramatic changes in Amazonian climate (Bush, 2005; Colinvaux, 2007). On the one hand, there is considerable biogeographic evidence that there are indeed certain regions where species diversity is extraordinarily high. Such regions are generally identified by first mapping the ranges of individual species, then superimposing the distributions, and selecting those areas that exhibit very high levels of species diversity (Haffer, 1982). In this way, studies of rain forest trees, butterflies, and lizards have been undertaken, and all reveal geographically similar core areas to those suggested by Haffer (1974) on the basis of his detailed studies of tropical birds (cf. Vanzolini and Williams, 1970; Vanzolini, 1973; Brown et al., 1974; Prance, 1974, 1982; Brown, 1982). There is even linguistic and ethnographic evidence that points to the existence of similarly distributed forest refuges in prehistoric Amazonia (Meggers, 1982; Migliazza, 1982). The general coincidence of all these regions is quite impressive, considering the range of evidence involved. However, it could be argued that the distribution patterns observed do not reflect former refugia at all, but merely reflect modern ecological units that have evolved together in response to contemporary edaphic and climatic conditions, the uniqueness of which may or may not be immediately obvious (Endler, 1982; Colinvaux, 1996). Similarly, zones of "secondary contact" may simply reflect significant environmental gradients (Benson, 1982).

Clearly, these arguments could only be satisfactorily resolved by well-dated stratigraphic evidence demonstrating that certain areas contained savanna *at the same time* as other areas (i.e., the postulated refugia) were under forest cover (Livingstone, 1982) and there are now many lines of evidence indicating that the lowland Amazon Basin has, in fact, remained extensively forested throughout the past 40,000 years (at least). For example, a long pollen record from the lowlands of northwestern Brazil, in the heart of the dense tropical rain forest ecosystem (*selva*) is continuous for >40,000 years and shows no evidence for any savanna phase in this area; arboreal pollen remained at 70-90% of the pollen sum throughout the period (Colinvaux et al., 1996a). Interestingly, the pollen record shows an increase in montane species, such as *Podocarpus*, in the last glacial period (marine isotope stage 2) so at that time, a unique forest assemblage made up of both lowland and montane elements was present. There is no analog for such an assemblage today; it seems to represent a migration of montane plants into a lowland environment that was cooler than today by 5-6 °C (based on a descent of *Podocarpus* by ~ 800-1000 m and assuming an adiabatic lapse rate of 0.6 °C 100 m^{-1}). Several other studies support the idea of cooler, not drier conditions, at least in the core of the evergreen tropical forest zone. In eastern Ecuador, a section dating from the last glaciation also shows an unusual mixture of montane and lowland rain forest pollen types, as well as associated macrofossils. In this area, trees such as *Alnus* and *Podocarpus* occurred ~1500 m below their modern range limits (Liu and Colinvaux, 1985; Bush et al., 1990). Such evidence has also been found in Panama, where oak trees (*Quercus*) grew 1000 m lower than today in glacial times (Bush and Colinvaux, 1990). In southeastern Brazil, palynological data also suggest cooler, wetter conditions during the last glacial maximum, with temperatures lower by 6-9 °C. Similar conditions were reconstructed for the Peruvian Amazon, from ~48 to 19 ka BP (Bush et al., 2004). Collectively, such evidence provides a compelling argument for an extensive lowland rain forest throughout the last glacial period and into the Holocene, albeit a forest that had a quite different composition than today in some areas (Colinvaux et al., 1996b). That is not to say that some peripheral areas that currently experience seasonal moisture deficits

were not drier (cf. Markgraf, 1989; Vander Hammen and Absy, 1994). For example, in the seasonally dry forests of southeastern Bolivia, conditions were both cooler and drier from 50 to 12 ka BP, which was probably related to less summer convection and/or a more limited southward migration of the ITCZ seasonally (Punyasena et al., 2008). Furthermore, speleothem records from Brazil show that pronounced changes in precipitation did occur in relation to precessional forcing (see Chapter 8, Section 8.2), so it is likely that parts of the Amazon Basin did experience lower rainfall totals when the seasonal migration of the ITCZ was more limited. Nevertheless, although there are still very few records from this vast region, there is currently very little stratigraphic evidence to support the idea that *most* of the Amazon Basin was occupied by savanna in glacial times (cf. Clapperton, 1993a,b; Anhuf et al., 2006). Indeed, recent studies of pollen in marine sediments from off the mouth of the Amazon reveal little change in arboreal pollen percentages throughout the past 100,000 years; if savanna had been extensive, there ought to be a clear signal in the pollen carried down the Amazon and deposited offshore, but there is not (Haberle, 1997). It therefore seems likely that the centers of endemism noted in so many biogeographic studies reflect a complex of conditions (climatic, topographic, geologic, geomorphological, etc.), which have distinguished these regions over long periods of time, even as climate fluctuated from cooler glacial to warmer interglacial conditions.

12.5.5 Equatorial and Sub-Saharan Africa

As in South America, biogeographers have long held the view that the extensive tropical forests of the Congo Basin and adjacent coastal regions in the Gulf of Guinea were formerly more limited in extent, confined to areas where climatic conditions have remained favorable over long periods of time. These refugia are recognized today by the high number of endemic taxa and rich species diversity compared to other areas (e.g., Hamilton, 1976; Sosef, 1991; Maley, 1996). Unlike South America, there is considerable evidence in support of the biogeographic arguments, provided by palynological data from lake sediments (Anhuf, 1997, 2000). In Ghana, a 27,000-year-long record from crater Lake Bosumtwi shows clearly that the semideciduous equatorial forests that have occupied this area for most of the Holocene were not present in glacial times (Figure 12.25). From 19 to 15 ka BP, arboreal pollen fell to as low as 5% of the pollen sum (compared to >75% today) and herbaceous plants (grasses and sedges) occupied the area. This is confirmed by $\delta^{13}C$ in sediment cores; values were −10 to −20‰ during the time when levels of Gramineae pollen were high (consistent with the dominance of C_4 plants) compared to Holocene values of −28‰, typical of forest (C_3) plants (Talbot and Johannessen, 1992; see also Giresse et al., 1994). Certain montane plants (such as mountain olive, *Olea hochstetteri*) also migrated into the area; today they are only found far to the west, above ~1200 m, suggesting temperatures were cooler by 3-4 °C during glacial times. Similar evidence has been reported from sites in West Cameroon, Plateau Batéké in Congo, and further east in Burundi where data of the modern pollen rain were used to quantify paleotemperature changes (Figure 12.26) (Maley, 1991; Bonnefille et al., 1992). Figure 12.27 shows the limits of lowland rain forest refugia in equatorial Africa during the Last Glacial Maximum compared to modern conditions. This comparison reveals how dramatically different the region was in glacial time, with savanna and grasslands covering vast areas that are forested

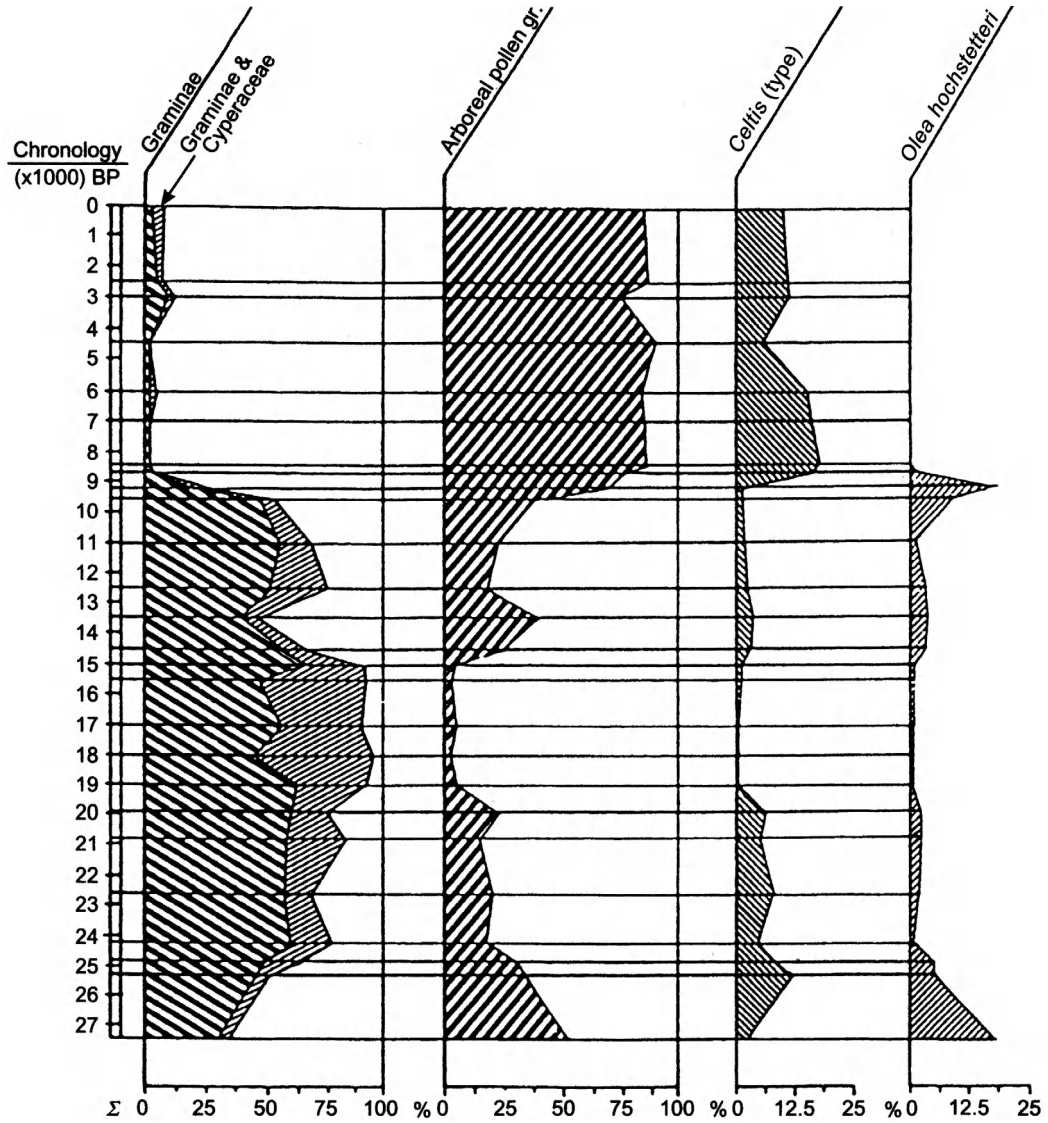


FIGURE 12.25 Summary of the important pollen variations in Lake Bosumtwi, Ghana, over the past 27,000 years. Prior to ~10 ka BP, grasses (Gramineae) characteristic of open savanna environments dominated this location, and arboreal pollen was low, especially from ~19 to 15.5 ka BP. The presence of mountain olive (*Olea hochstetteri*) in this lowland environment indicates cooler conditions prevailed during glacial times. *From Maley (1996).*

today. The total area of tropical humid forest was reduced by ~74% (Anhuf et al., 2006). Conditions changed abruptly at ~9500 years BP with the rapid expansion of the rain forest to cover an area even larger than today within 2 ka (Maley, 1991, 1996). This change is thought to be related to rapid warming of SSTs in the Gulf of Guinea (as a result of reduced upwelling) leading to a longer wet season and higher total rainfall amounts (Maley, 1989a) but dramatic

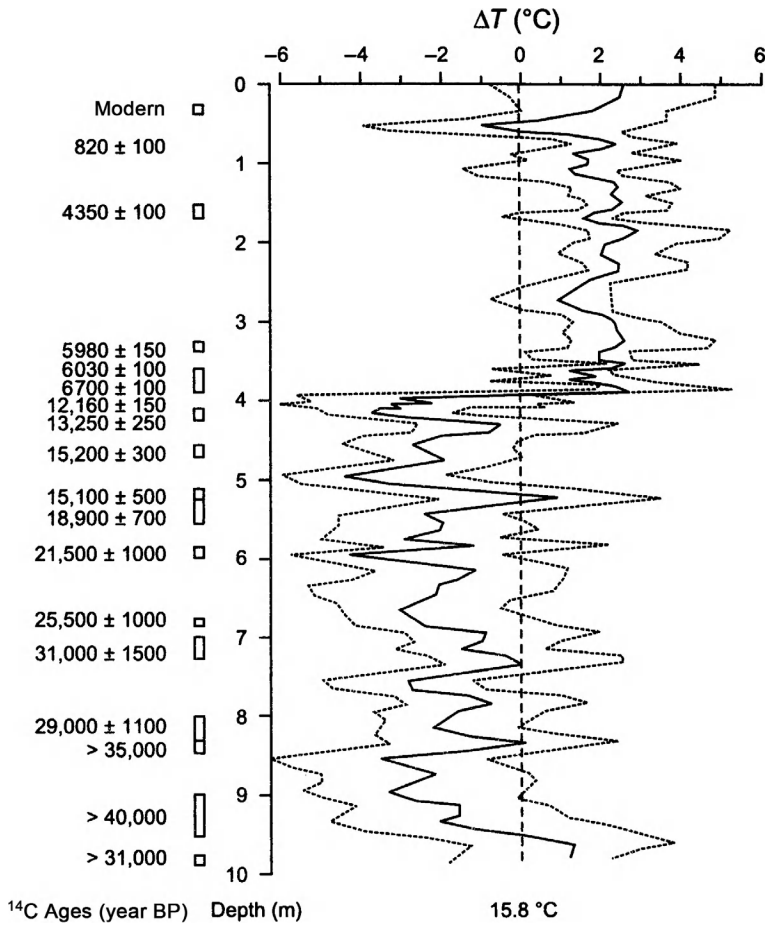


FIGURE 12.26 Mean annual temperature departures (relative to the present-day temperature of 15.8 °C) derived from pollen in a peat bog at Kashiru, Burundi, East Africa. The site is at 2240 m in the humid montane forest. Paleotemperature estimates were obtained using a network of modern pollen rain samples over a wide area of East Africa, calibrated against modern climatic data from the region. Dashed lines indicate confidence interval. ^{14}C dates are shown on the left (note that the data are plotted linearly with respect to depth, not age). Paleotemperature estimates from the surface samples are affected by human-induced changes in vegetation, and hence, the modern pollen spectrum provides a temperature estimate warmer than the instrumentally recorded value. *From Bonnefille et al. (1992).*

changes also occurred in East Africa around this time (Figure 12.26). Jolly and Haxeltine (1997) argued that significant changes in tropical vegetation would have occurred (even at low elevations) regardless of changes in temperature due to the lower CO_2 levels during glacial times, which favored grasses and sedges (C_4 plants) over trees, but detailed pollen analysis indicates that precipitation changes were the primary factor in driving regional vegetation changes (Wu et al., 2007a,b).

At the same time as lowland forest vegetation was expanding in the Early Holocene, climatic conditions in sub-Saharan Africa became less arid, enabling the semiarid savanna

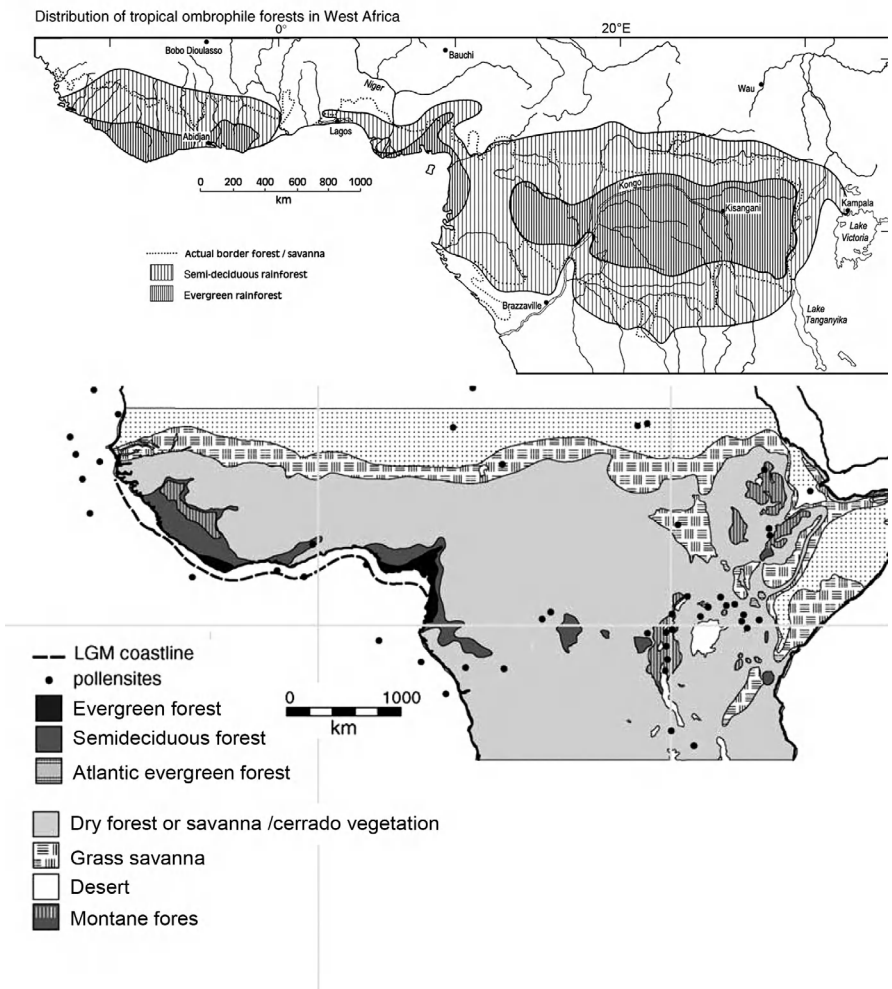


FIGURE 12.27 Distribution of tropical humid forests in equatorial West Africa today (top) compared to vegetation at the last glacial maximum (below). More than 70% of the humid forest that covers the region today was replaced by savanna vegetation at the LGM. *Modified from Anhuf et al. (2006).*

vegetation belt to extend farther northward (cf. Section 10.4.3). As a result, the range of large herbivores (such as giraffe, elephant, hippopotamus, and gazelle) was also more extensive, and today, the bleached bones of these animals provide a mute reminder of the remarkably different climatic conditions that existed there in the Early Holocene. Accompanying the animal migration into sub-Saharan Africa were aboriginal hunters who recorded their way of life on magnificent rock paintings and carvings (Lhote, 1959; Lajoux, 1963; Monod, 1963). These are found today, hundreds of kilometers from the nearest permanent settlements.

Of particular significance during the period of more extensive savanna and tropical forests were the much more extensive riverine and lacustrine environments, which effectively

provided water connections across the entire sub-Saharan region, from the Nile to Senegal (Beadle, 1974). Fauna of the Lake Chad Basin, for example, provide unequivocal evidence for recent connections, not only with the Niger and Congo Basins but also with the Nile drainage system over 1000 km to the east. Even today, relict populations of animals and plants are found isolated in topographically favorable environments, far removed from their nearest adjacent populations. For example, the Eurasian green frog (*Rana ridibunda*) has been found in the streams of the Ahaggar Mountains at least 1000 km from adjacent population groups. Furthermore, and perhaps most remarkably, a Nile crocodile (*Crocodylus niloticus*) was found in a pool in the Tassili n'Ajjer Mountains, separated by vast stretches of desert from major population centers to the east (Seurat, 1934; Beadle, 1974). Such disjunct species bring climatic changes to life.

Subtropical Africa is probably more arid today than it has been during most of the Holocene and was only more arid during the Late Wisconsin glacial maximum (cf. Figures 10.16–10.19). However, the record is still far from complete in both time and space, so brief periods of relatively moist or even drier conditions (on the order of 10^2 years) may have occurred. Indeed, lake level evidence does show that abrupt changes in climate (probably related to upwelling) did occur in the Late Holocene (e.g., ~3500-4000 years BP, as recorded by lake level changes in Lake Bosumtwi), but these oscillations did not persist and no significant change in forest cover resulted (Talbot and Delibrias, 1977; Maley, 1991). Nevertheless, such episodes may have had significant consequences for human populations in the region (Maley, 1989b, 1997).

12.5.6 Northeastern Siberia

Lake El'gygytgyn (Lake E) in Chukotka, northeastern Siberia, was created by a meteorite striking the earth ~3.58 Ma ago. As this part of the Arctic was never glaciated, sediments in the lake provide a unique paleoenvironmental record extending back into the Late Pliocene (Melles et al., 2012). Today, the lake is surrounded by tundra, and the nearest tree line is 150 km to the south, though the nearest continuous forest is ~300 km away. Pollen analysis shows quite different conditions in the region around Lake E during the Pliocene, with forests of spruce, fir, larch, and hemlock compared to the shrub tundra that occurs today (Brigham-Grette et al., 2013; Lozhkin and Anderson, 2013). Using the best modern analog approach, which finds the optimum fit between the pollen spectrum in the core and that from present-day environments, the mean temperature of the warmest month is estimated to have been ~15-16 °C, with 600 mm of annual precipitation (compared to ~8 °C and 200 mm today). Conditions changed quite dramatically around 2.74 Ma ago, with the loss of spruce and pine in the landscape. By 2.63 Ma BP, vegetation was predominantly larch, birch, and shrubby alder as precipitation fell to near modern levels, and summer temperatures declined. This change may be linked to the establishment of a permanent Arctic Ocean ice cover at the onset of the Quaternary, limiting moisture flux from the north, although model simulations do not fully support that view (Melles et al., 2012). After this time, colder conditions became increasingly more common, with shrub-tundra vegetation dominating the landscape over much of the last ~2 Ma, with a few notable exceptions that correspond to past interglacials in the marine isotope record (Figure 12.28). These periods are marked by high levels of

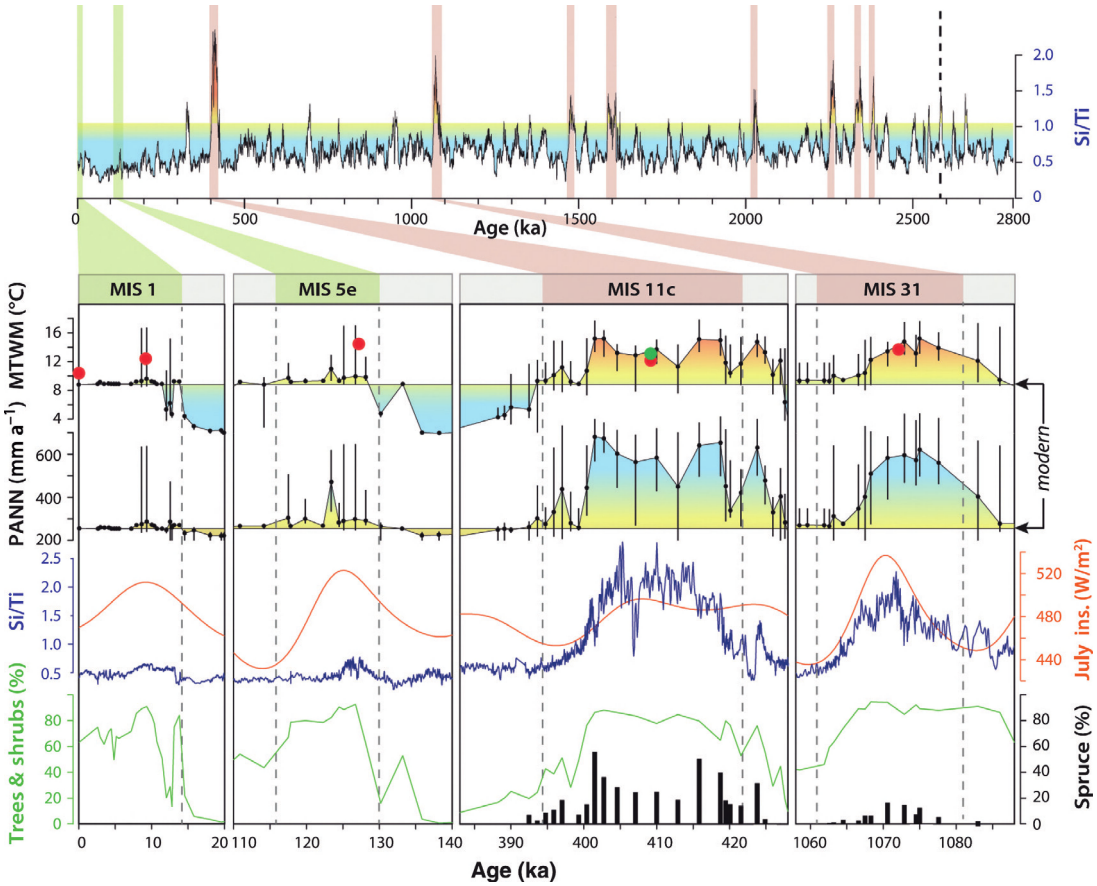


FIGURE 12.28 Quaternary record of the Si/Ti ratio from Lake El'gygytgyn, northeastern Siberia (top), with periods of exceptional warmth marked. High levels of biogenic silica production reflect enhanced primary productivity in the lake when ice cover was minimal and nutrient flux to the lake (due to enhanced weathering) was at a maximum. For the last four of these periods, the percentage of trees and shrubs and % spruce is shown (bottom) with inferred annual precipitation (PANN) and the mean temperature of the warmest month (MTWM) shown above, relative to modern values, based on the total pollen assemblage. MIS 5e was only slightly warmer and wetter than in the Holocene, but MIS 11c and MIS 31 were much warmer and wetter, despite similar July insolation anomalies (bottom panel, orange lines). The red and green dots denote model-based temperature estimates based on simulations in which orbital and greenhouse gas forcing was changed. *From Melles et al. (2012).*

biogenic silica production, which are interpreted as reflecting enhanced primary productivity in the lake when ice cover was minimal and nutrient flux to the lake (due to enhanced weathering) was at a maximum. Pollen from these intervals suggest that the Early Holocene and preceding interglacial warm period (MIS 5.5) were slightly warmer and wetter than today (1-2 °C and +20-50 mm precipitation), but earlier interglacials were quite different. MIS 11c (~395-422 ka BP) and MIS 31 (~1060-1080 ka BP) were "super interglacials" during which coniferous forests migrated northward, so that Lake E pollen at those times included spruce,

pine, birch, alder, and larch (Lozhkin and Anderson, 2013). Temperatures during the warmest month were 4-5 °C above MIS 5.5, and precipitation was ~300 mm higher. Interestingly, orbital conditions at those times (high obliquity, perihelion during the Northern Hemisphere summer and high eccentricity, or a so-called warm orbit) were similar during MIS 5e and MIS 31, yet climatic conditions at Lake E were quite different. CO_2 levels were slightly higher 1 Ma ago (~325 ppmv), but it seems unlikely that this can account for the different conditions observed, and a good explanation has yet to be found (Melles et al., 2012).

CHAPTER

13

Tree Rings

OUTLINE

13.1 Introduction 453

13.2 Fundamentals of Dendroclimatology 454
- 13.2.1 *Sample Selection* 456
- 13.2.2 *Cross Dating* 458
- 13.2.3 *Standardization of Ring-Width Data* 463
- 13.2.4 *Divergence* 469
- 13.2.5 *Calibration of Tree-Ring Data* 470
- 13.2.6 *Verification of Climatic Reconstructions* 476

13.3 Dendroclimatic Reconstructions 480
- 13.3.1 *Reconstructions of Temperatures over the Northern Hemisphere* 480
- 13.3.2 *Drought Reconstruction* 481
- 13.3.3 *Reconstruction of Atmospheric Circulation Modes* 487
- 13.3.4 *Wildfires and Dendroclimatology* 490

13.4 Isotopic Dendroclimatology 493
- 13.4.1 *$\delta^{18}O$ and $\delta^{2}H$* 493
- 13.4.2 *$\delta^{13}C$* 495

13.1 INTRODUCTION

Variations in tree-ring widths from one year to the next have long been recognized as an important source of chronological and climatic information. In Europe, studies of tree rings as a potential source of paleoclimatic information go back to the early eighteenth century when several authors commented on the narrowness of tree rings (some with frost damage) dating from the severe winter of 1708-1709. In North America, Twining (1833) first drew attention to the great potential of tree rings as a paleoclimatic index (for historical reviews, see Studhalter, 1955; Robinson et al., 1990; Schweingruber, 1996, p. 537; Speer, 2010). However, in the English-speaking world, the "father of tree-ring studies" is generally considered to be Douglass, an astronomer who was interested in the relationship between sunspot activity and rainfall. To test the idea of a sunspot-climate link, Douglass needed long climatic records and he recognized

Copyright © 2015 Raymond S. Bradley.
Published by Elsevier Inc. All rights reserved.

that ring-width variations in trees of the arid southwestern United States might provide a long, proxy record of rainfall variation (Douglass, 1914, 1919). His efforts to build long-term records of tree growth were facilitated by the availability of wood from archaeological sites, as well as from modern trees (Robinson, 1976). Douglass' early work was crucial for the development of dendrochronology (the use of tree rings for dating; see Chapter 3, Section 3.2.1.5) and for dendroclimatology (the use of tree rings as a proxy indicator of climate).

13.2 FUNDAMENTALS OF DENDROCLIMATOLOGY

A cross section of most temperate forest trees will show an alternation of lighter and darker bands, each of which is usually continuous around the tree circumference. These are seasonal growth increments produced by meristematic tissues in the cambium of the tree (Vaganov et al., 2006). When viewed in detail (Figure 13.1), it is clear that they

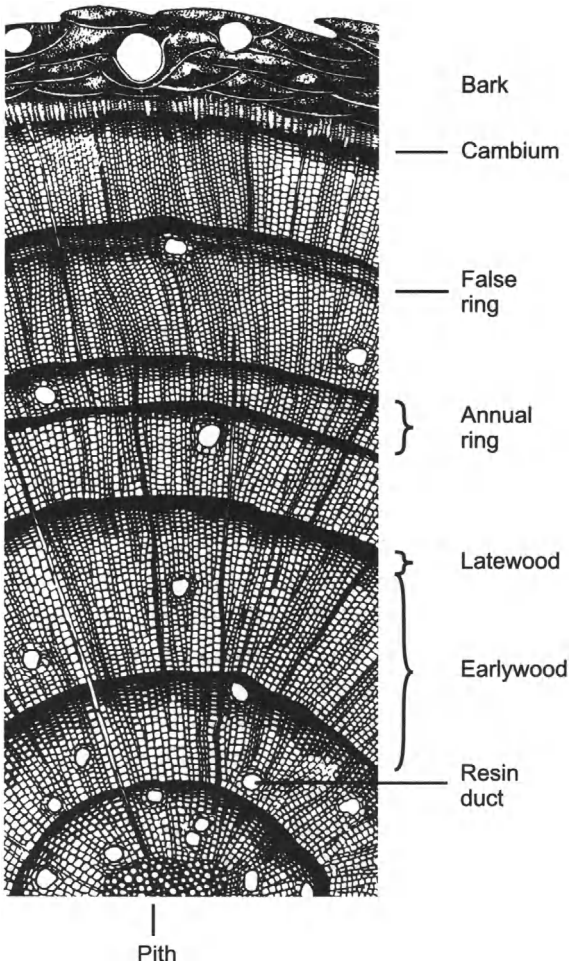


FIGURE 13.1 Drawing of cell structure along a cross section of a young stem of a conifer. The earlywood is made up of a large and relatively thin-walled cells (tracheids); latewood is made up of small, thick-walled tracheids. Variations in tracheid thickness may produce false rings in either earlywood or latewood. *After Fritts (1976).*

are made up of sequences of large, thin-walled cells (earlywood) and more densely packed, thick-walled cells (latewood). Collectively, each couplet of earlywood and latewood comprises an annual growth increment, more commonly called a tree ring. The mean width of a ring in any one tree is a function of many variables, including the tree species, tree age, availability of stored food within the tree and of important nutrients in the soil, and a whole complex of climatic factors (sunshine, precipitation, temperature, wind speed, humidity, and their distribution through the year) (Vaganov et al., 2011). The problem facing dendroclimatologists is to extract whatever climatic signal is available in the tree-ring data and to distinguish this signal from the background noise. Furthermore, the dendroclimatologist must know precisely the age of each tree ring if the climatic signal is to be chronologically useful. From the point of view of paleoclimatology, it is perhaps useful to consider the tree as a filter or transducer that, through various physiological processes, converts a given climatic input signal into a certain ring-width output that is stored and can be studied in detail, even thousands of years later (e.g., Fritts, 1976; Schweingruber, 1988, 1996; Hughes, 2011).

Climatic information has most often been gleaned from interannual variations in ring width, but there has also been a great deal of work carried out on the use of density variations, both inter- and intra-annually (densitometric dendroclimatology). Wood density is an integrated measure of several properties including cell wall thickness, lumen diameter, size and density of vessels or ducts, and proportion of fibers (Polge, 1970; Schweingruber, 1996). Tree rings are made up of both earlywood and latewood, which vary markedly in average density, and these density variations can be used, like ring-width measurements, to identify annual growth increments and to cross-date samples (Parker, 1971). It has also been shown empirically that density variations contain a strong climatic signal and can be used to estimate long-term climatic variations over wide areas (Schweingruber et al., 1979, 1993). Density variations are measured on X-ray negatives of prepared core sections (Figure 13.2), and the optical density of the negatives is inversely proportional to wood density (Schweingruber et al., 1978).

Density variations are particularly valuable in dendroclimatology because they have a relatively simple growth function (often close to linear with age). Hence, standardization of density data may allow more low-frequency climatic information to be retained than is the case with standardized ring-width data (see Section 13.2.3). Generally, two values are measured in each growth ring: minimum density and maximum density (representing locations within the earlywood and latewood layers, respectively) though maximum density seems to be a better climatic indicator than minimum density values. For example, Schweingruber et al. (1993) showed that maximum density values were strongly correlated with April-August mean temperature in trees across the entire boreal forest, from Alaska to Labrador, whereas minimum and mean density values and ring widths had a much less consistent relationship with summer temperature at the sites sampled (cf. D'Arrigo et al., 1992). Maximum latewood density values are calibrated in the same way as with the ring-width data using the statistical procedures described in Section 13.2.5. However, optimum climatic reconstructions may be achieved by using both ring widths and densitometric data to maximize the climatic signal in each sample (e.g., Briffa et al., 1995).

Isotopic variations in wood have been studied as a possible proxy of temperature or precipitation variations through time, but the complexities of fractionation both within the hydrologic system and in the trees themselves make simple interpretations quite difficult.

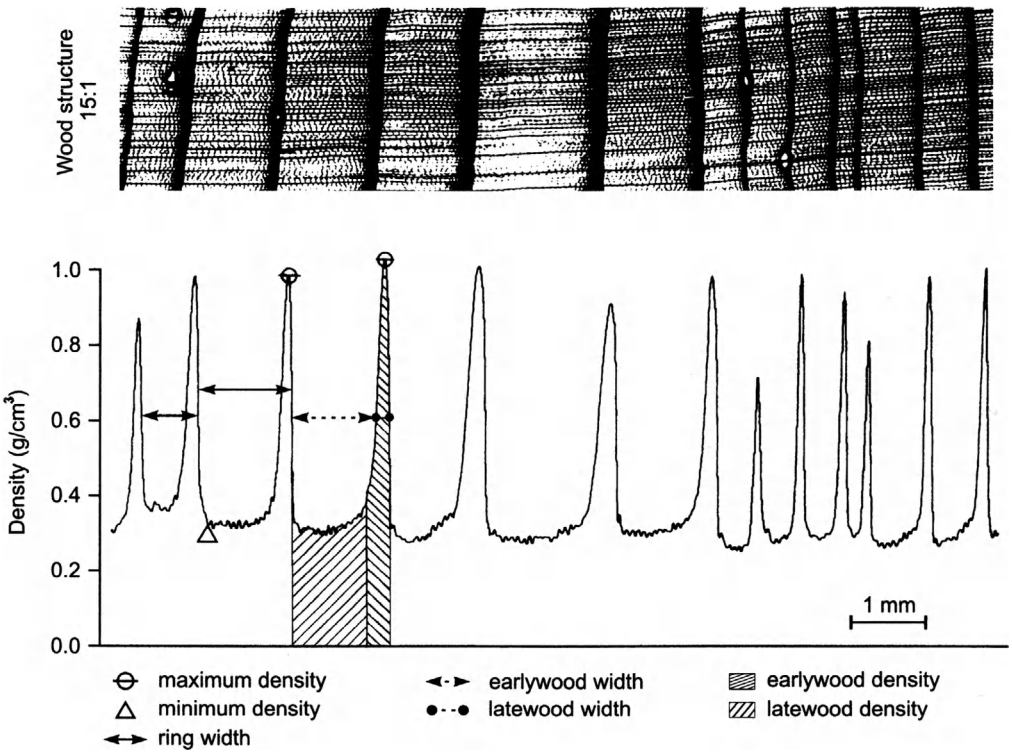


FIGURE 13.2 Example of a tree-ring density plot based on an X-ray negative of a section of wood (in the preceding text). Minimum and maximum densities in each annual ring are clearly seen, enabling the annual ring width to be measured as well as the width of both the earlywood and latewood. *Courtesy of F. Schweingruber.*

Nevertheless, detailed isotopic analysis of wood from tropical trees, in which distinct annual rings may not be clearly visible, has provided new insights into growth rates and climatic variations over recent centuries (Evans and Schrag, 2004). This is discussed further in Section 13.4. Ring-width, densitometric, and isotopic approaches to paleoclimatic reconstruction are complementary and, in some situations, could be used independently to check paleoclimatic reconstructions based on only one of the methods or collectively to provide more accurate reconstructions (e.g., Briffa et al., 1992a; McCarroll et al., 2003, 2011).

13.2.1 Sample Selection

In conventional dendroclimatological studies, where ring-width variations are the source of climatic information, trees are sampled in sites where they are under stress; commonly, this involves selection of trees that are growing close to their extreme ecological range. In such situations, climatic variations will greatly influence annual growth increments, and the trees are said to be sensitive. In more beneficent situations, perhaps nearer the middle of a species range or in a site where the tree has access to abundant groundwater, tree growth may not be noticeably influenced by climate, and this will be reflected in the low interannual variability of ring widths (Figure 13.3). Such tree rings are said to be complacent. There is thus a

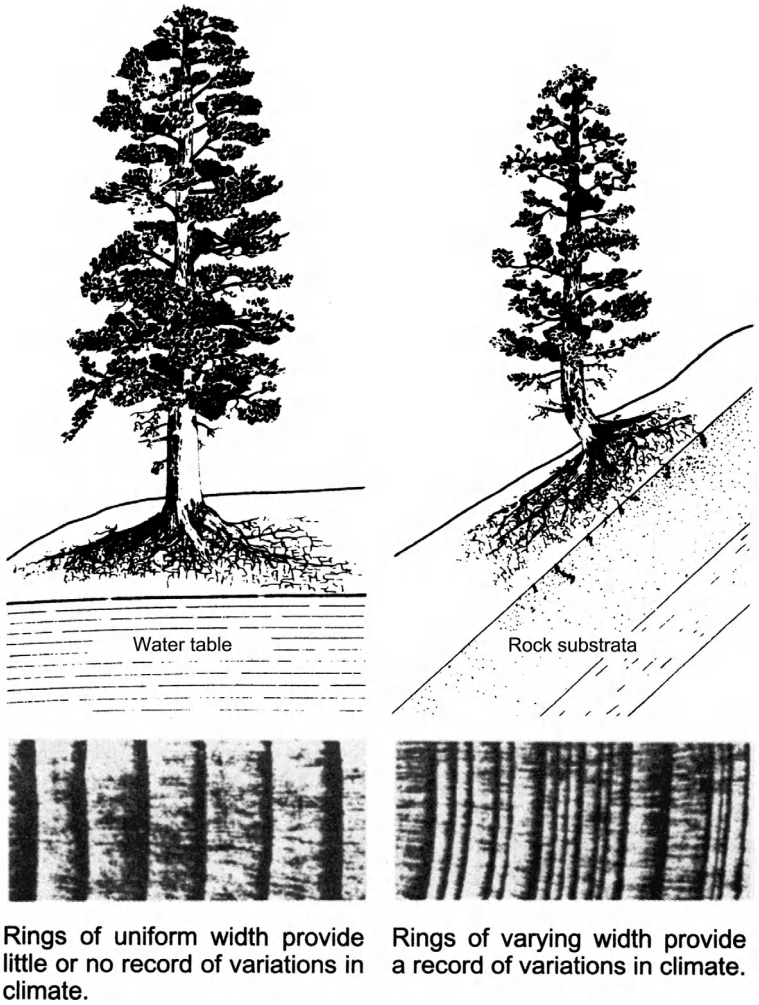


FIGURE 13.3 Left: Trees growing on sites where climate seldom limits growth processes produce rings that are uniformly wide. Such rings provide little or no record of variations in climate and are termed *complacent*. Right: Trees growing on sites where climatic factors are frequently limiting produce rings that vary in width from year to year depending on how severely limiting climate has been to growth. These are termed *sensitive*. *From Fritts (1971).*

spectrum of possible sampling situations, ranging from those where trees are extremely sensitive to climate to those where trees are virtually unaffected by interannual climatic variations. Clearly, for useful dendroclimatic reconstructions, samples close to the sensitive end of the spectrum are favored as these would contain the strongest climatic signal. Often therefore, tree-ring studies at the range limit of trees are favored (e.g., alpine or Arctic tree line sites). However, climatic information may also be obtained from trees that are not under such obvious climatic stress, providing the climatic signal common to all the samples can be successfully isolated (LaMarche, 1982). For example, ring widths of bald cypress trees from swamps in the southeastern United States have been used to reconstruct the drought and

precipitation history of the area over the last 1000 years or more (Stahle et al., 1988, 2012; Stahle and Cleaveland, 1992). Paleoclimatic reconstructions have also been achieved using teak from equatorial forests in Indonesia (D'Arrigo et al., 1994) as well as from mesic forest trees in Tasmania (Cook et al., 1992; see also Jones et al., 2009). For isotope dendroclimatic studies (see Section 13.4), the sensitivity requirement does not seem to be as critical, and it may, in fact, be preferable to use complacent tree rings for analysis (Gray and Thompson, 1978). Sensitivity is also less significant in densitometric studies, and good relationships between maximum latewood density and temperature have been found in "normal" trees that are growing on both moist and well-drained sites (Schweingruber et al., 1991, 1993).

In marginal environments, commonly two types of climatic stress are recognized, moisture stress and temperature stress. Trees growing in semiarid areas are frequently limited by the availability of water, and ring-width variations primarily reflect this variable. Trees growing near to the latitudinal or altitudinal tree line are mainly under growth limitations imposed by temperature, and hence, ring-width variations in such trees contain a strong temperature signal. However, other climatic factors may be indirectly involved. Biological processes within the tree are extremely complex and similar growth increments may result from quite different combinations of climatic conditions. Furthermore, climatic conditions prior to the growth period may "precondition" physiological processes within the tree and hence strongly influence subsequent growth. For the same reason, tree growth and food production in 1 year may influence growth in the following year and lead to a strong serial correlation or autocorrelation in the tree-ring record. Tree growth in marginal environments is thus commonly correlated with a number of different climatic factors in both the growth season (year t_0) and the preceding months, as well as with the record of prior growth itself (generally in the preceding growth years, t_{-1} and t_{-2}). Indeed, in some dendroclimatic reconstructions, tree growth in subsequent years (t_{+1}, t_{+2}, etc.) may also be included since they also contain climatic information about year t_0.

Trees are sampled radially using an increment borer, which removes a core of wood (generally 4-5 mm in diameter) leaving the tree unharmed. It is important to realize that dendroclimatic studies are unreliable unless an adequate number of samples are recovered; two or three cores should be taken from each tree, and at least 20 trees should be sampled at an individual site, though this is not always possible (Speer, 2010). Eventually, as discussed in the succeeding text, all the cores are used to compile a master chronology of ring-width variation for the site, and it is this that is used to derive climatic information.

13.2.2 Cross Dating

For tree-ring data to be used for paleoclimatic studies, it is essential that the age of each ring be known precisely. This is necessary in constructing the master chronology from a site where ring widths from modern trees of similar age are being compared and equally necessary when matching up sequences of overlapping records from living trees, dead tree stumps, or archaeological specimens to extend the chronology back in time (Figure 13.4; Stokes and Smiley, 1968). Great care is needed because occasionally trees will produce false rings or intra-annual growth bands, which may be confused with the actual earlywood/latewood transition (Figure 13.5). Furthermore, in extreme years, some trees may not produce an annual growth layer at all, or it may be discontinuous around the tree or so thin as to be indistinguishable

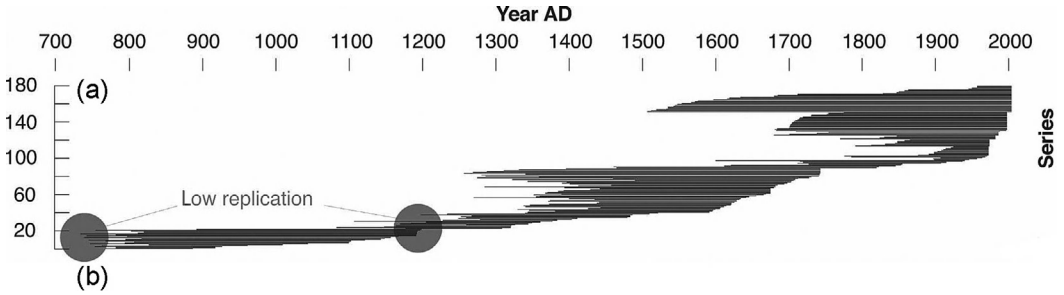


FIGURE 13.4 Samples of wood from living trees are matched with older samples from dead trees, using cross dating of ring-width or density variations. In this case, maximum latewood density was measured on more than 180 samples, and the composite record then extended back to AD 755. The two periods circled had only minimal sample overlap, but this was sufficient to extend the overall chronology back in time. *From Büntgen et al. (2006).*

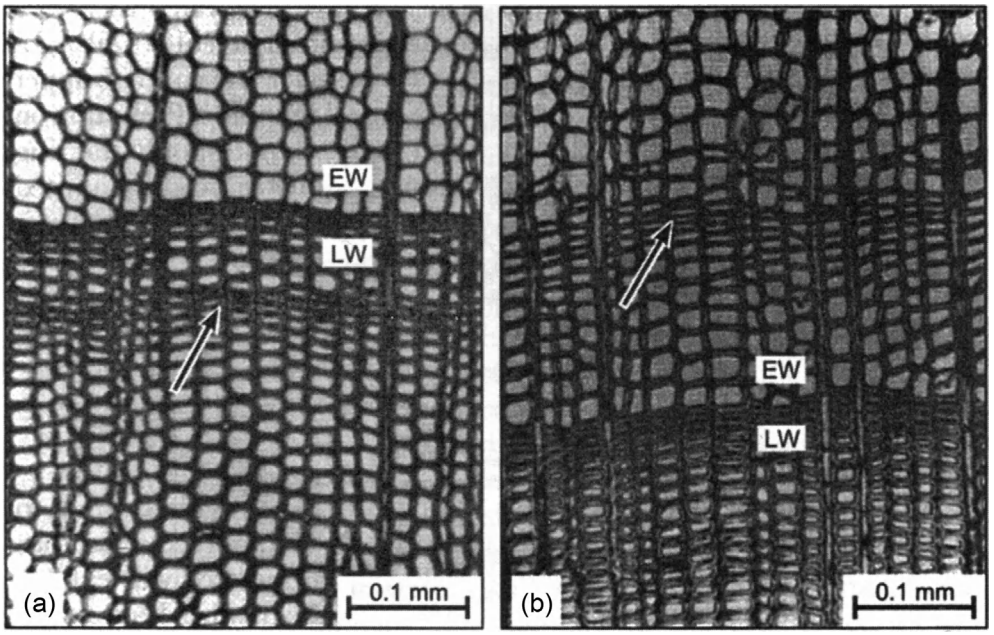


FIGURE 13.5 Annual growth increments or rings are formed because the wood cells produced early in the growing season (earlywood, EW) are large, thin-walled, and less dense, while the cells formed at the end of the season (latewood, LW) are smaller, thick-walled, and more dense. An abrupt change in cell size between the last-formed cells of one ring (LW) and the first-formed cells of the next (EW) marks the boundary between annual rings. Sometimes, growing conditions temporarily become severe before the end of the growing season and may lead to the production of thick-walled cells within an annual growth layer (arrows). This may make it difficult to distinguish where the actual growth increment ends, which could lead to errors in dating. Usually these intra-annual bands or false rings can be identified, but where they cannot, the problem must be resolved by cross dating. *After Fritts (1976).*

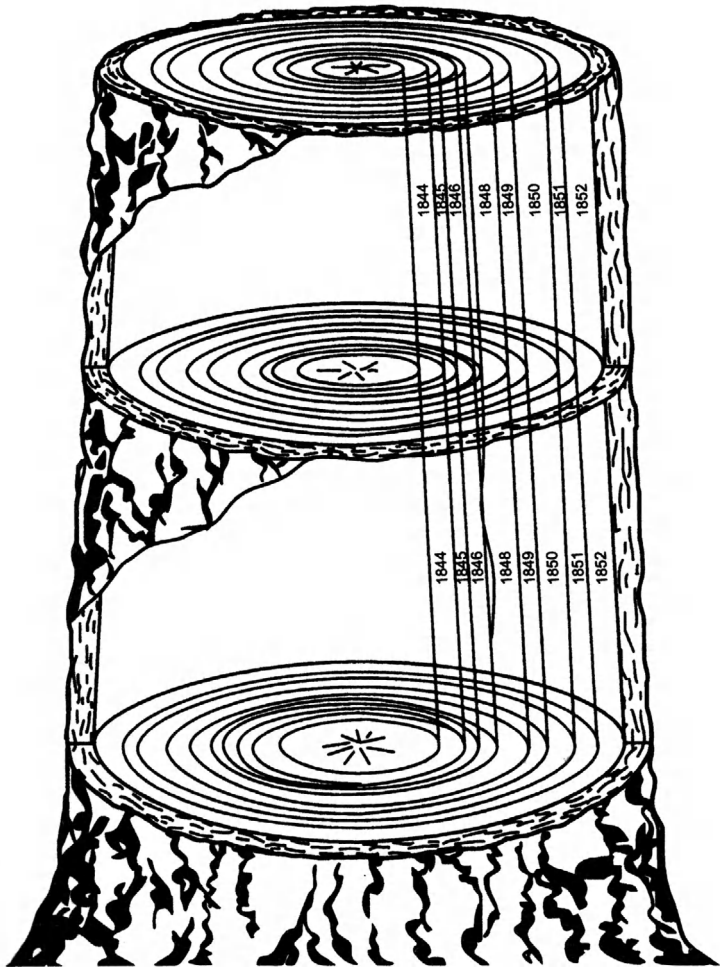


FIGURE 13.6 Schematic diagram illustrating the potential difficulty presented by the formation of a partial ring (in 1847). In the lowest two sections, the ring might not be sampled by an increment borer that removes only a narrow wood sample. In the upper section, the ring is thin but presents all around the tree circumference. Such missing or partially absent rings are identified by careful cross dating of multiple samples. *From Glock (1937).*

from adjacent latewood (i.e., a partial or missing ring) (Figure 13.6). Clearly, such circumstances would create havoc with climatic data correlation and reconstruction, so careful cross dating of tree-ring series is necessary. This involves comparing ring-width sequences from each core so that characteristic patterns of ring-width variation (ring-width "signatures") are correctly matched (Figure 13.7). If a false ring is present, or if a ring is missing, it will thus be immediately apparent (Holmes, 1983; Speer, 2010). The same procedure can be used with archaeological material; the earliest records from living trees are matched or cross-dated with archaeological material of the same age that may, in turn, be matched with older material. This procedure is repeated many times to establish a thoroughly reliable chronology. In the southwestern United States, the ubiquity of beams or logs of wood used in Indian pueblos has enabled chronologies of up to 2000 years to be constructed in this way. In fact,

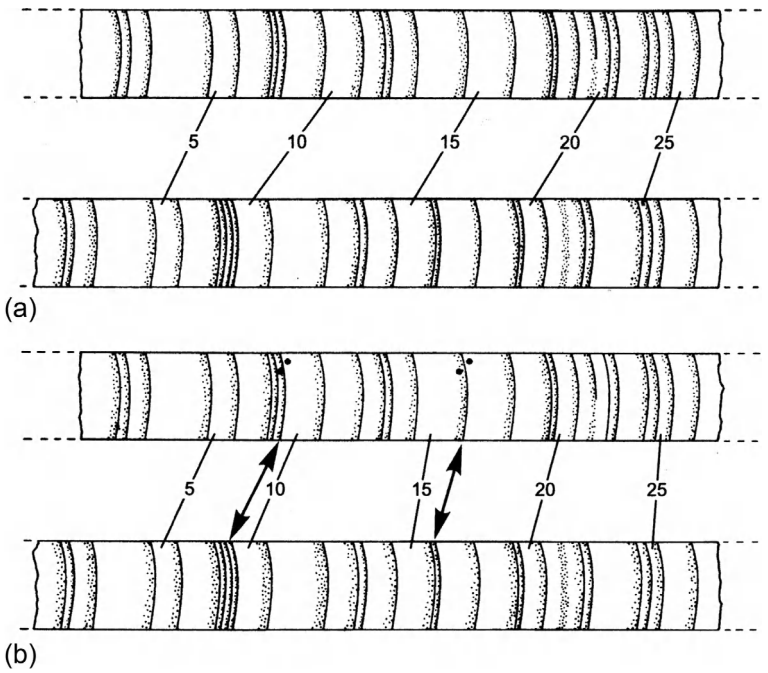


FIGURE 13.7 Cross dating of tree rings. Comparison of tree-ring widths makes it possible to identify false rings or where rings are locally absent. For example, in (a), strict counting shows a clear lack of synchrony in the patterns. In the lower specimen of (a), rings 9 and 16 can be seen as very narrow, and they do not appear at all in the upper specimen. Also, rings 21 (lower) and 20 (upper) show intra-annual growth bands. In (b), the positions of inferred absence are designated by dots (upper section), the intra-annual band in ring 20 is recognized, and the patterns in all ring widths are synchronously matched. *After Fritts (1976).*

accomplished dendrochronologists can quickly pinpoint the age of a dwelling by comparing the tree-ring sequence in supporting timbers with master chronologies for the area (Robinson, 1976). Similarly, archaeologically important chronologies have been established in western Europe. Hoffsummer (1996), for example, used beams of wood from buildings in southeastern Belgium to establish an oak chronology extending back to AD 672, and in several regions of France, chronologies of over 1000 years in length have been assembled from construction timbers (Lambert et al., 1996). Dendrochronological studies have also been used in studies of important works of art, for example, in dating wooden panels used for paintings, furniture, and even the cover boards of early books (Eckstein et al., 1986; Lavier and Lambert, 1996). Finally, tree stumps recovered from alluvial sediments and bogs have been cross-dated to form composite chronologies extending back continuously through the entire Holocene (e.g., Eckstein et al., 2009; Kromer, 2009). Long tree-ring series such as these are so accurate that they are used to calibrate the radiocarbon timescale (see Chapter 3, Section 3.2.1.5). In some locations, subfossil wood buried in sedimentary deposits can be cross-dated, but the wood is older than the continuously cross-dated sequences that have been painstakingly constructed in Europe and thus "floating" in time (Figure 13.8). However, when multiple radiocarbon dates on the wood are plotted versus the floating chronology, they can often

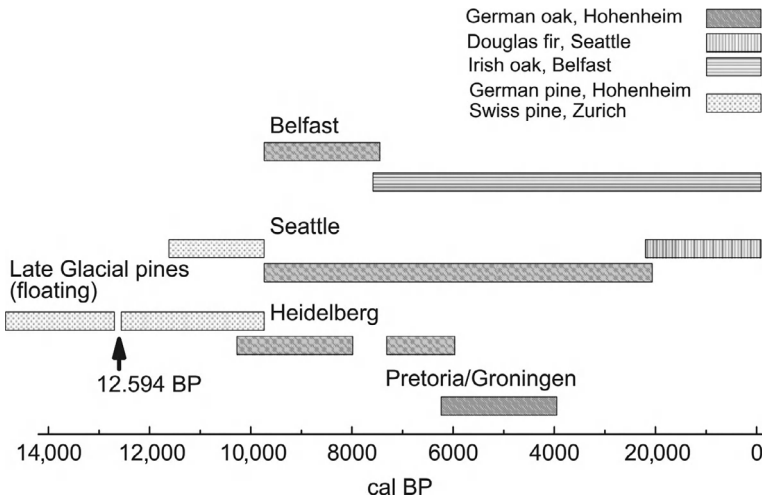


FIGURE 13.8 Tree-ring-based ^{14}C data series obtained from three tree-ring chronologies. The names of the ^{14}C labs are given above the bars. The species and the tree-ring laboratories are shown in the legend. *From Kromer (2009).*

be used to fix the sequence in time by "wiggle-matching" the radiocarbon variations that have occurred with the radiocarbon master chronology (Figure 13.9). In this way, floating chronologies may be closely (but not absolutely) fixed in time (e.g., Kromer et al., 2004; Friedrich et al., 2006; Schaub et al., 2008a,b). Subfossil can wood samples also be valuable in constraining the older section of the radiocarbon calibration curve, which is largely based on marine samples for which the radiocarbon marine reservoir corrections are quite uncertain, particularly during periods of rapid climatic and oceanographic change in the period from 60 to 10 ka BP (Turney et al., 2010).

Tree rings are unique among paleoclimatic proxies in that, through cross dating of multiple cores extending continuously back in time from the present day, the absolute age of a sample can be established. This attribute distinguishes tree rings from other high-resolution proxies (ice cores, varved sediments, corals, banded speleothems, etc.) because in such proxies, comparable replication of records and cross dating of many samples across multiple sites are rarely possible. Consequently, with the exception of specific marker horizons (e.g., those associated with a volcanic event of known age), dating of such proxies is always more uncertain than in dendroclimatic studies (Stahle, 1996).

Once the samples have been cross-dated and a reliable chronology has been established, there are three important steps to produce a dendroclimatic reconstruction:

(1) Standardization of the tree-ring parameters to produce a site chronology
(2) Calibration of the site chronology with instrumentally recorded climatic data and production of a climatic reconstruction based on the calibration equations
(3) Verification of the reconstruction with data from an independent period not used in the initial calibration

In the next three sections, each of these steps is discussed in some detail.

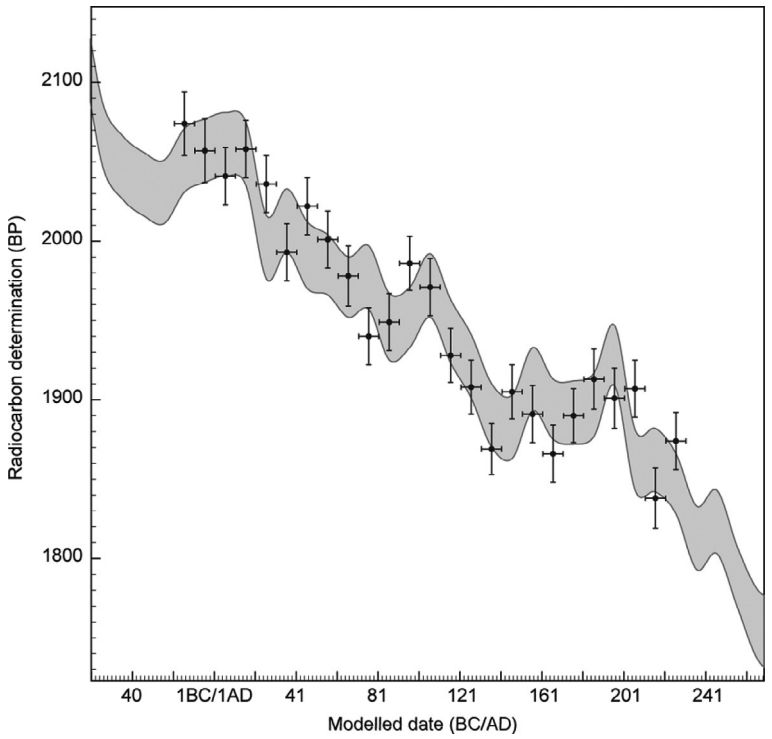


FIGURE 13.9 An example of "wiggle-matched" tree-ring data; high-precision ^{14}C determinations ($\pm 1\sigma$) on a "floating chronology" of *Phyllocladus trichomanoides* wood samples, from a New Zealand buried forest fitted to a calibration data set for the period 60 BC to AD 270. By matching to variations in both series, the floating data set can be fixed in time quite precisely. *From Hogg et al. (2012).*

13.2.3 Standardization of Ring-Width Data

Once the chronology for each core has been established, individual ring widths are measured and plotted to establish the general form of the data (Figure 13.10). It is common for time series of ring widths to contain a low-frequency component resulting entirely from the tree growth itself, with wider rings generally produced during the early life of the tree. In order that ring-width variations from different cores can be compared, it is first necessary to remove the growth function peculiar to that particular tree. Only then can a master chronology be constructed from multiple cores. Growth functions are removed by fitting a curve to the data and dividing each measured ring-width value by the "expected" value on the growth curve (Figure 13.11). Commonly, a negative exponential function or a low-pass digital filter is applied to the data. Cook et al. (1990) recommend that a cubic-smoothing spline be used, in which the 50% frequency response equals ~75% of the record length (n). This means that low-frequency variations in the data (with a period $>0.75n$) are largely removed from the standardized data, so the analyst then has an explicit understanding of the frequency domain that the resulting series represents (Cook and Peters, 1981).

Whatever method is used to remove the biological growth function, the standardization procedure leads to a time series of ring-width indices, with a mean of one and a variance that

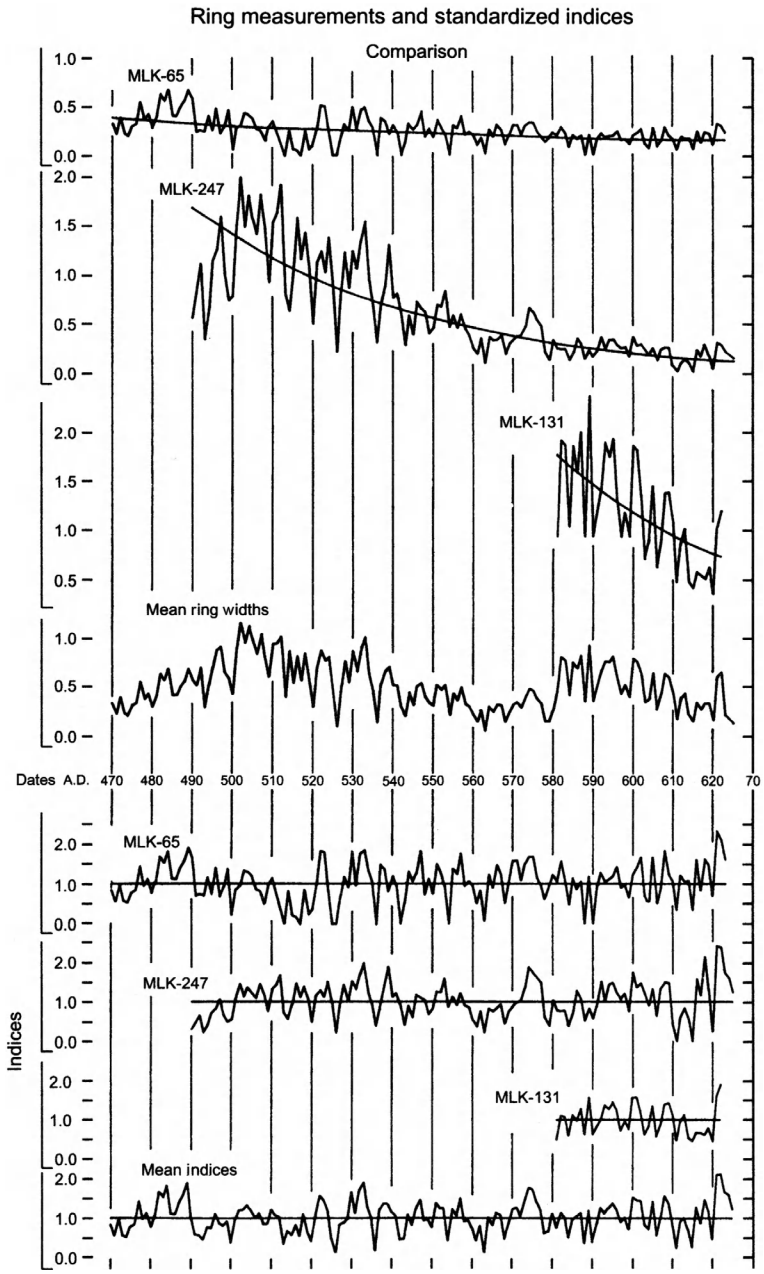


FIGURE 13.10 Standardization of ring-width measurements is necessary to remove the decrease in size associated with increasing age of the tree. If the ring widths for the three specimens shown in the upper figure are simply averaged by year, without removing the effect of the tree's age, the mean ring-width chronology shown below them exhibits intervals of high and low growth, associated with the varying age of the samples. This age variability is generally removed by fitting a curve to each ring-width series and dividing each ring width by the corresponding value of the curve. The resulting values, shown in the lower half of the figure, are referred to as indices and may be averaged among specimens differing in age to produce a mean chronology for a site (lowermost record). *From Fritts (1971).*

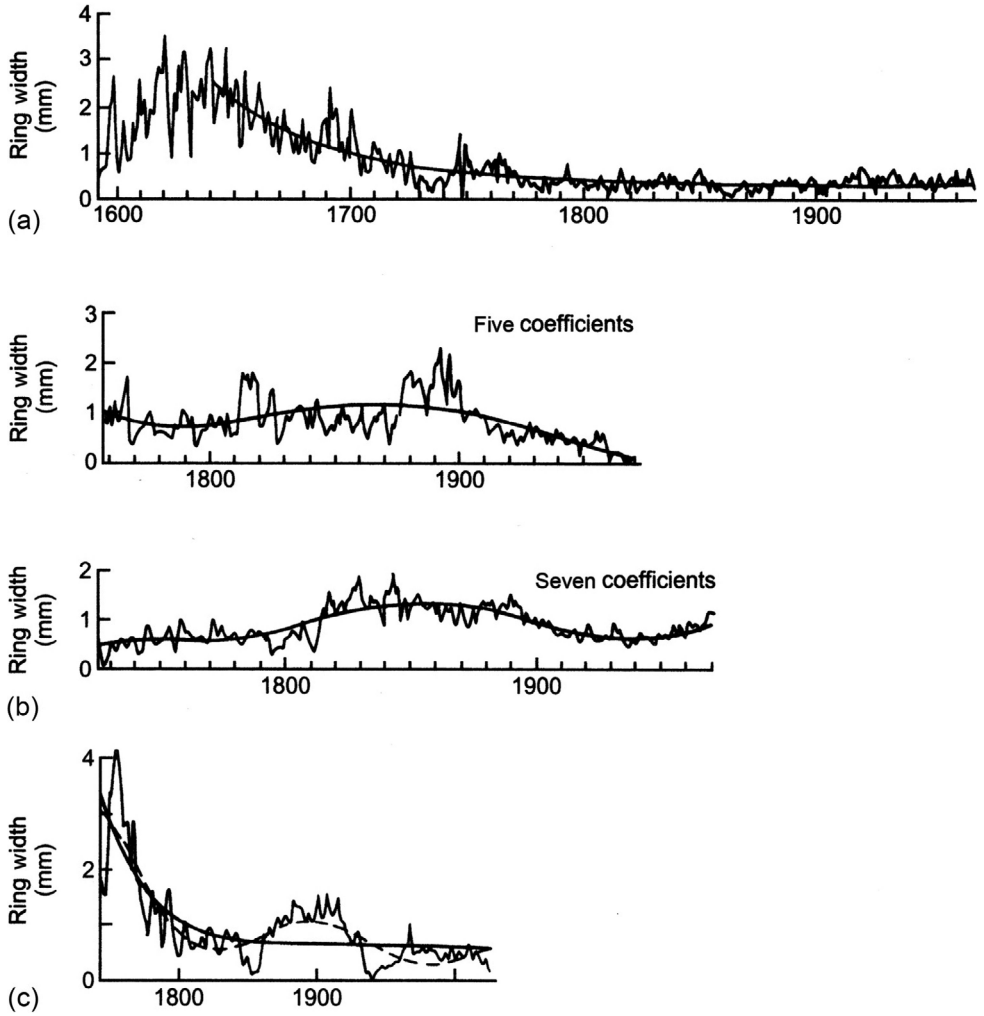


FIGURE 13.11 Some examples of potential problems in standardization of ring widths. In (a), most of the tree-ring series can be fitted by the exponential function shown. However, the early part of the record must be discarded. In (b), the two ring-width series required higher-order polynomials to fit the lower-frequency variations of each record (the greater the number of coefficients for each equation, the greater the degree of complexity in the shape of the curve). In (c), the series could be standardized using either a polynomial (dashed) or exponential function (solid line). Depending on the function selected and its complexity, low-frequency climatic information may be eliminated. The final ring-width indices depend very much on the standardization procedure employed. Examples selected from Fritts (1976).

is fairly constant through time (Fritts, 1971). Ring-width indices from individual cores are then averaged, year by year, to produce a master chronology of mean indices for the sample site, independent of growth function and differing sample age (Figure 13.10, lowest graph). Averaging the standardized indices also increases the (climatic) signal-to-noise ratio. This is because climatically related variance, common to all records, is not lost by averaging, whereas nonclimatic "noise," which varies from tree to tree, will be partially canceled in the averaging

process. It is thus important that a large enough number of cores be obtained initially to help enhance the climatic signal common to all the samples (Cook et al., 1990).

Standardization is an essential prerequisite to the use of ring-width data in dendroclimatic reconstruction, but it poses significant methodological problems. Consider, for example, the ring-width chronologies shown in Figure 13.11. Drought-sensitive conifers from the southwestern United States characteristically show ring-width variations like those in Figure 13.11a. For most of the chronology, a negative exponential function, of the form $y = ae^{-bt} + k$, fits the data well. However, this is not the case for the early section of the record, which must be either discarded or fitted by a different mathematical function. Obviously, the precise functions selected will have an important influence on the resulting values of the ring-width indices (see also Section 13.2.4). In the case of trees growing in a closed-canopy forest, the growth curve is often quite variable and unlike the negative exponential values characteristic of arid-site conifers. Periods of growth enhancement or suppression related to nonclimatic factors such as competition, management, and insect infestation are often apparent in the records. In such cases (Figure 13.11b), some other function might be fitted to the data, and individual ring widths would then be divided by the local value of this curve to produce a series of ring-width indices. Care must be exercised not to select a function (such as a complex polynomial), which describes the raw data too precisely, or *all* of the (low-frequency) climatic information may be removed; most analysts select the simplest function possible to avoid this problem, but inevitably the procedure selected is somewhat arbitrary. In densitometric or isotope dendroclimatic studies, there is generally less of a growth trend in density and isotope data; hence, these approaches may yield more low-frequency climatic information than is possible in the measurement of ring widths alone (cf. Schweingruber and Briffa, 1996).

It is clear that standardization procedures are not easy to apply and may actually remove important low-frequency climatic information. It is not possible, *a priori*, to decide if part of the long-term change in ring width is due to a coincident climatic trend. The problem is exacerbated if one is attempting to construct a long-term dendrochronological record, when only tree fragments or historical timbers spanning limited time intervals are available, and the corresponding growth function may not be apparent. The consequences of different approaches to standardization are well illustrated by the studies of long tree-ring series (Scots pine, *Pinus sylvestris*) from northern Fennoscandia by Briffa et al. (1990, 1992a). In order to produce a long dendroclimatic reconstruction extending over 1500 years, Briffa et al. (1990) constructed a composite chronology made up of many overlapping cores that varied in their individual length from less than 100 to more than 200 years (Figures 13.12). In the shorter segments, the growth function is significant over the entire segment length, but in longer segments, the growth factor becomes less significant (cf. Figure 13.10, upper panel). In Briffa et al. (1990), each segment was standardized individually (the procedure commonly used in dendroclimatic studies) in this case by the use of a cubic spline function that retains variance at periods less than $\sim 2/3$ of the record length. Thus, in a 100-year segment, variance at periods >66 years would be removed, whereas in a 300-year segment, variance at periods up to 200 years would be retained. All standardized cores were then averaged together, producing the record shown in Figure 13.13c. This shows considerable interannual- to decadal-scale variability but little long-term low-frequency variability. In fact, since the mean segment length varies over time (Figure 13.12), so too will the low-frequency variance represented in the composite series.

In Briffa et al. (1992a), the standardization procedure was revised by first aligning all core segments by their relative age and then averaging them (i.e., all values of the first year in

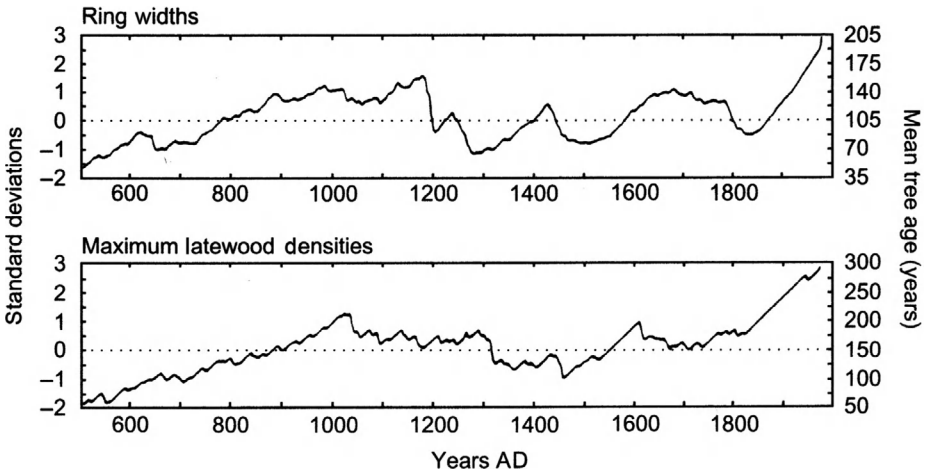


FIGURE 13.12 Average age of the core segments used to produce a 1500-year composite chronology from trees in northern Fennoscandia. Samples representing the recent period are generally longest because samples are usually selected from the oldest living trees, whereas older samples (from dead tree stumps) may be from trees of any age. *From Briffa et al. (1992a).*

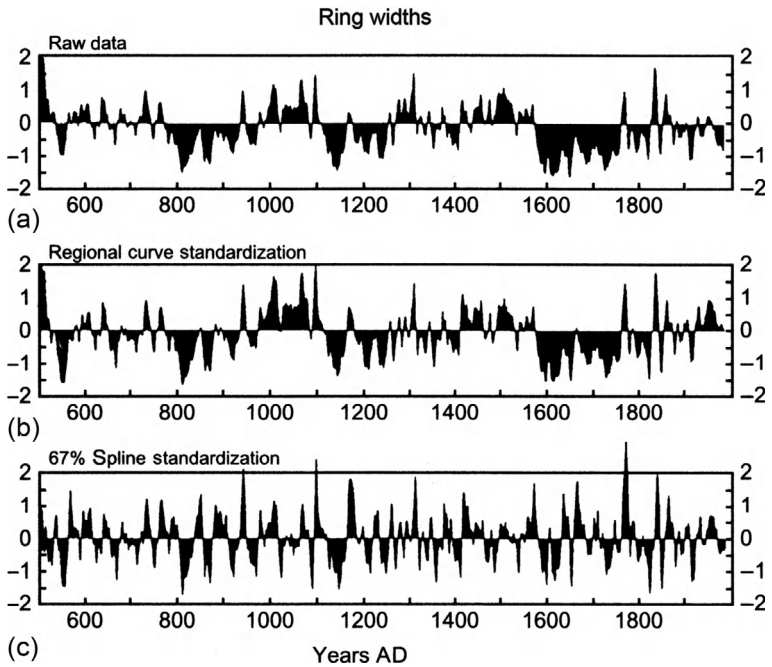


FIGURE 13.13 Ring-width data from trees in northern Fennoscandia showing (a) the mean indices, without any standardization (b) indices derived from standardization using the regional curve standardization or (c) indices derived from standardization using a cubic-smoothing spline function (see text for discussion). *From Briffa et al. (1992a).*

each segment (t_1) were averaged and then all values of $t_2, t_3, \ldots, t_n$). This assumes that in each segment used, t_1 was at, or very close to, the center of the tree and that there is a tree-growth function (dependent only on biological age), which is common to all samples. The resulting "regional curve" provided a target for deriving a *mean* growth function that could be applied to all of the individual core segments, regardless of length (Figure 13.14). Averaging together the core segments, standardized in this way by the regional curve, produced the record shown in Figure 13.13b. This has far more low-frequency information than the record produced from individually standardized cores (Figure 13.13c) and retains many of the characteristics seen in the original data (Figure 13.13a). From this series, low growth from the late 1500s to the early 1800s is clearly seen, corresponding to other European records that record a "Little Ice Age" during this interval. Also seen is a period of enhanced growth from ~950 to 1100 AD, during a period that Lamb (1965) characterized as the "Medieval Warm Epoch." It is apparent from a comparison of Figure 13.13b and c that any conclusions drawn about which were the warmest or coldest years and decades of the past can be greatly altered by the standardization procedure employed. All of the high-frequency variance of Figure 13.13c is still represented in the record produced by *regional curve standardization* (RCS), but potentially important climatic information at lower frequencies is also retained.

The problem of extracting low-frequency climatic information from long composite records made up of many individual short segments is addressed explicitly by Briffa et al. (1996) and Cook et al. (1995) who refer to this as the "segment length curse"! RCS was developed to address this problem, but it is not a complete panacea for retaining low-frequency climatic information and may in fact result in "end-effect" anomalies, which could be misinterpreted as true climate signals (Esper and Frank, 2009; Briffa and Melvin, 2011) (see Section

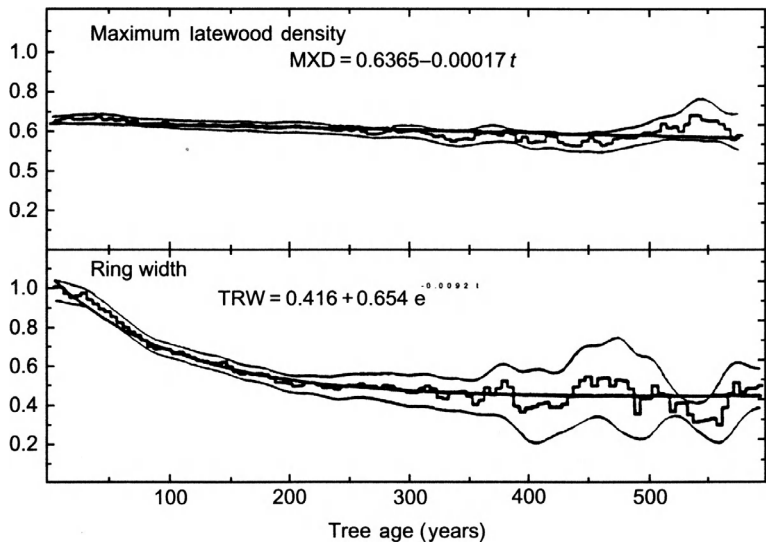


FIGURE 13.14 Regional curve standardization (RCS) of tree-ring samples from northern Fennoscandia based on a least squares fit to the mean values of all series, after they were aligned according to their biological age. Ring-width data commonly have a more pronounced growth function than maximum latewood density data. *From Briffa et al. (1992a).*

13.2.4). Some of the limitations of RCS, and additional approaches to standardization, are discussed by Melvin and Briffa (2008) and Briffa and Melvin (2011). Retention of low-frequency climate signals is of particular concern in dendroclimatology, but it is also an important problem in any paleoclimatic reconstructions that utilize limited duration records to build up a longer composite series (e.g., historical data).

13.2.4 Divergence

One issue that has received much attention in recent years is the so-called divergence problem in tree-ring data. This refers to the fact that in some locations, the strong relationship between temperature and tree-ring widths that was apparent for the past few hundred years appears to have deteriorated over recent decades (D'Arrigo et al., 2008). This divergence or nonlinearity in the expected relationship is particularly vexing as analysts would like to place the unusual recent changes in climate in a long-term perspective, and, if the tree-ring proxy no longer tracks temperature, this may not be possible. It also implies that if tree growth does not keep pace with rising temperatures, boreal forests may become less effective sinks for carbon dioxide in the future. Furthermore, it raises the question as to whether the tree ring-temperature relationship also broke down during similarly warm periods in the past, thus casting doubt on paleotemperature reconstructions.

The divergence problem was first noted in studies of tree-ring widths and maximum latewood density in white spruce from northern and central Alaska (Jacoby and D'Arrigo, 1995). It was attributed to increased moisture stress on trees under the particularly warm conditions of recent years, which was also a period of relatively low precipitation in this region. The problem was highlighted further by Briffa et al. (1998a,b) who found the same divergence pattern in maximum latewood densities over a much wider region, extending across the northern boreal forests of North America and Eurasia, as well as higher-elevation regions of the western United States, Canada, and the European Alps (Figure 13.15). Importantly, no evidence for a breakdown in the relationship between interannual variability and tree

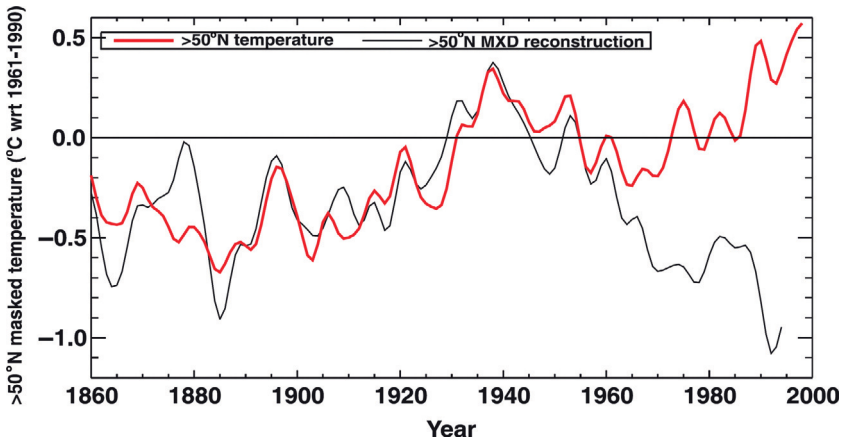


FIGURE 13.15 Instrumental temperatures (red) and tree-ring density reconstructions of temperature (black) averaged over all land grid boxes north of 50°N, smoothed with a 5-year low-pass filter. *From Briffa et al. (2004).*

growth was found; the divergence was confined to decadal-scale variability, especially since the 1960s and 1970s. Because of the widespread extent of the phenomena, the possibility that all areas had experienced drought stress seemed implausible, and so Briffa et al. suggested that large-scale factors, such as a reduction in solar irradiance or an increase in UV B radiation due to stratospheric ozone depletion, might be responsible (Briffa et al., 2004). These results led to numerous other studies, some of which confirmed that divergence in recent decades has occurred (e.g., Barber et al., 2000; Lloyd and Fastie, 2002; D'Arrigo et al., 2004, 2009; Driscoll et al., 2005), while others determined that the problem does not exist if the tree-ring data are carefully selected and appropriately analyzed (Wilson et al., 2007; Büntgen et al., 2008; Esper et al., 2009). In a short review of the issue, Esper and Frank (2009) note that data standardization is a critical factor that may explain many cases where divergence has been noted. If the method used to remove the growth function in a record is not well chosen, the lower-frequency characteristics (particularly at the end of the record) may appear as anomalies when the record is standardized. This might explain why interannual variability is not affected, and recent divergence at the decadal scale would thus be considered to be merely an artifact of data processing. However, this argument has not been universally accepted (Briffa et al., 1998a; D'Arrigo et al., 2008, 2009). Others have suggested that divergence mainly affects a particular species (e.g., spruce not tracking temperatures as consistently as larch) or reflects poor sample selection or that climatic data are inadequate for proper calibration. In remote northern and Alpine regions, meteorological stations are often very sparse, requiring dendroclimatologists to calibrate tree-ring data with instrumental data from hundreds of kilometers away or from locations at much lower elevations than the tree-growth locations, which may not properly capture local conditions at the tree-growth site (cf. Bunn et al., 2011). Calibrations based on mean monthly or seasonal temperatures might also miss the important physiological factors influencing tree growth in these marginal environments. There may be nonlinearities or thresholds in growth response to temperature that have now been exceeded in many regions.

Divergence thus remains as a somewhat enigmatic problem in dendroclimatology. In some cases, detailed local studies in regions where the divergence problem was originally thought to be an issue have found that the problem essentially disappears when samples are carefully selected for temperature sensitivity, and the data are appropriately detrended to optimize the low-frequency characteristics of the record (e.g., Wilson et al., 2007; Briffa et al., 2008; Büntgen et al., 2008; Esper et al., 2009). Initial concerns that tree growth during earlier periods of warmth might also have been decoupled from temperature have been examined, and there is no compelling evidence that this was the case; the recent period of warming appears to be unique in the last millennium. More generally, the problem has highlighted the difficulties of data calibration in remote regions and the limits to our understanding of physiological controls on tree growth, particularly the interactions between drought, temperature, and other parameters (snow cover and the timing of snowmelt, soil moisture, solar radiation, etc.) in areas with very short growing seasons (cf. Lloyd and Bunn, 2007; Porter and Pisaric, 2011).

13.2.5 Calibration of Tree-Ring Data

Once a master chronology of standardized ring-width indices has been obtained, the next step is to develop a model relating variations in these indices to variations in climatic data. This process is known as calibration, whereby a statistical procedure is used to find the

optimum solution for converting growth measurements into climatic estimates. If an equation can be developed that accurately describes instrumentally observed climatic variability in terms of tree growth over the same interval, then paleoclimatic reconstructions can be made using only the tree-ring data. In this section, a brief summary of the methods used in tree-ring calibration is given. For a more exhaustive treatment of the statistics involved, with examples of how they have been used, the reader is referred to Hughes et al. (1982), Fritts et al. (1990), and Cook and Kairiukstis (1990).

The first step in calibration is the selection of the climatic parameters that primarily control tree growth. This procedure, known as response function analysis, involves regression of tree-ring data (the predictand) against monthly climatic data (the predictors, usually temperature and precipitation) to identify which months, or combination of months, are most highly correlated with tree growth (Briffa et al., 2008). Usually months during and prior to the growing season are selected, but the relationship between tree growth in year t_0 and year t_{-1} may also be examined since tree growth in year t_0 is influenced by conditions in the preceding year. If a sufficiently long set of climatic data is available, the analysis may be repeated for two separate intervals to determine if the relationships are similar in both periods. This then leads to the selection of the month or months on which the tree-ring records are dependent and which the tree rings can therefore be expected to usefully reconstruct. For example, Büntgen et al. (2006) found that maximum density of larch (*Larix decidua* Mill) in the Swiss Alps is strongly related to June-September mean temperatures (Figure 13.16), enabling them to reconstruct temperatures for this season back to AD 755.

Once the climatic parameters that influence tree rings have been identified, tree-ring data can be used as predictors of these conditions. Various levels of complexity may be involved in

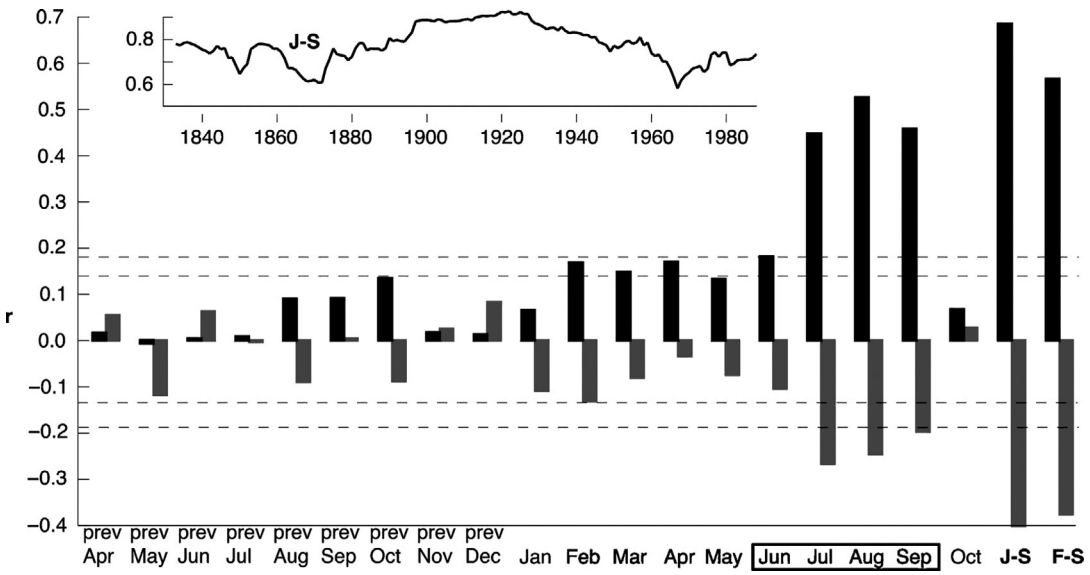


FIGURE 13.16 Climate response of the RCS-MXD chronology from the Swiss Alps. (a) Correlations with high-elevation monthly mean temperatures (black) and precipitation (gray) of the previous and current year (1818-2003). Horizontal dashed lines denote 95% and 99% significance levels, corrected for lag-1 autocorrelation. *Inset plot*: Moving 31-year correlations with June-September mean temperatures. *Modified from Büntgen et al. (2006).*

TABLE 13.1 Different Levels of Complexity in the Methods Used to Determine Relationship Between Tree-Ring Parameter and Climate

Level	Number of Variables		Main Statistical Procedures Used
	Tree Growth	Climate	
I	1	1	Simple linear regression analysis
IIa	*n*	1	Multiple linear regression (MLR)
IIb	*n*P	1	Principal components analysis (PCA)
IIIa	*n*P	*n*P	Orthogonal spatial regression (PCA and MLR)
IIIb	*n*P	*n*P	Canonical regression analysis (with PCA)

1 = a temporal array of data.
n = a spatial and temporal array of data.
*n*P = number of variables after discarding unwanted ones from PCA.
From Bradley and Jones (1995).

the reconstructions (Table 13.1). The basic level uses simple linear regression in which variations in growth indices at a single site are regressed, or simply scaled, against a single climatic parameter such as mean summer temperature or total summer precipitation. An example of this approach is the work of Cleaveland and Duvick (1992) who reconstructed July hydrologic drought indices for Iowa from a single regional chronology, which was an average of 17 site chronologies of the same species. More commonly, multivariate regression is used to define the relationship between the selected climate variables and a set of tree-ring chronologies within a geographic area where there is a common climate signal. The tree-ring data may include both ring widths and density values. Equations that relate tree rings (the predictors) to climate (the predictand) are termed transfer functions with a basic form (assuming linear relationships) of

$$y_t = a_1 x_{1t} + a_2 x_{2t} + a_3 x_{3t} + \cdots + a_m x_{mt} + b + e_t,$$

where y_t is the climate parameter of interest (for year t), $x_{1t}, \ldots, x_{mt}$ are tree-ring variables (e.g., from different sites) in year t, $a_1, \ldots, a_m$ are weights or regression coefficients assigned to each tree-ring variable, b is a constant, and e_t is the error or residual. In effect, the equation is simply an expansion of the linear equation, $y_t = ax_t + b + e_t$, to incorporate a larger number of terms, each additional variable accounting for more of the variance in the climate data (Ferguson, 1977). Theoretically, it would be possible to construct an equation to predict the value of y_t precisely. However, adding too many coefficients simply widens the confidence limits about the reconstruction estimates so that eventually the uncertainty becomes so large that the reconstruction is virtually worthless. What is needed is an equation that uses the minimum number of tree-ring variables to account for the maximum amount of variance in the climate record. Commonly, the procedure of stepwise multiple regression is used to achieve this aim (Fritts, 1962, 1965). From a matrix of potentially influential predictor variables, the one that accounts for most of the climate variance is selected; next, the predictor that accounts for the largest proportion of the remaining climatic variance is identified and added to the

equation; and so on in a stepwise manner. Tests of statistical significance, as each variable is selected, enable the procedure to be terminated when a further increase in the number of variables in the equation results in an insignificant increase in variance explanation. In this way, only the most important variables are selected, objectively, from the large array of potential predictors. An example of this approach is the reconstruction of drought in Southern California by Meko et al. (1980).

A major problem with stepwise regression is that intercorrelations between the tree-ring predictors can lead to instability in the prediction equation. In statistical terms, this is referred to as multicollinearity. To overcome this, a common procedure is to transform the predictor variables into their principal components (or empirical orthogonal functions, EOFs) and use them as predictors in the regression procedure. Principal components analysis involves mathematical transformations of the original data set to produce a set of orthogonal (i.e., uncorrelated) eigenvectors that describe the main modes of variance in the multiple parameters making up the data set (Grimmer, 1963; Stidd, 1967; Daultrey, 1976; Richman, 1986). Each eigenvector is a variable that expresses part of the overall variance in the data set. Although there are as many eigenvectors as original variables, most of the original variance will be accounted for by only a few of the eigenvectors. The first eigenvector represents the primary mode of distribution of the data set and accounts for the largest percentage of its variance (Mitchell et al., 1966). Subsequent eigenvectors account for smaller and smaller amounts of the remaining variance (Figure 13.17). Usually, only the first few eigenvectors are considered, since they will have captured most of the total variance. The value or amplitude of each eigenvector varies from year to year, being highest in the year when that particular combination of conditions represented by the eigenvector is most apparent. Conversely, it will be lowest in the year when the inverse of this combination is most apparent in the data. Eigenvector amplitudes can then be used as orthogonal predictor variables in the regression procedure, generally accounting for a higher proportion of the dependent data variance with fewer variables than would be possible using the "raw" data themselves. A time series of eigenvector values (amplitudes) is referred to as a principal component (PC), the dominant eigenvector being PC1, the next most common pattern PC2, etc.

Apart from reducing the number of potential predictors, principal components analysis also simplifies multiple regression considerably. It is not necessary to use the stepwise procedure because the new potential predictors are all orthogonal. This approach was used in the reconstruction of July drought in New York's Hudson Valley by Cook and Jacoby (1979). They selected series of ring-width indices from six different sites and calculated eigenvectors of their principal characteristics. These were then used as predictors in a multiple regression analysis with Palmer Drought Severity Indices (see Section 13.3.2; Palmer, 1965) as the dependent variable. The resulting equation, based on climatic data for the period 1931-1970, was then used to reconstruct Palmer indices back to 1694 when the tree-ring records began (Figure 13.18). This reconstruction showed that the drought of the early 1960s, which affected the entire northeastern United States, was the most severe the area has experienced in the last three centuries.

Simple univariate transfer functions express the relationship between one climatic variable and multiple tree-ring variables. A more complex step is to relate the variance in multiple growth records to that in a multiple array of climatic variables (e.g., summer temperature over a large geographic region) (Table 13.1). To do so, each matrix of data (representing variations in both time and space) is converted into its principal components; these are then

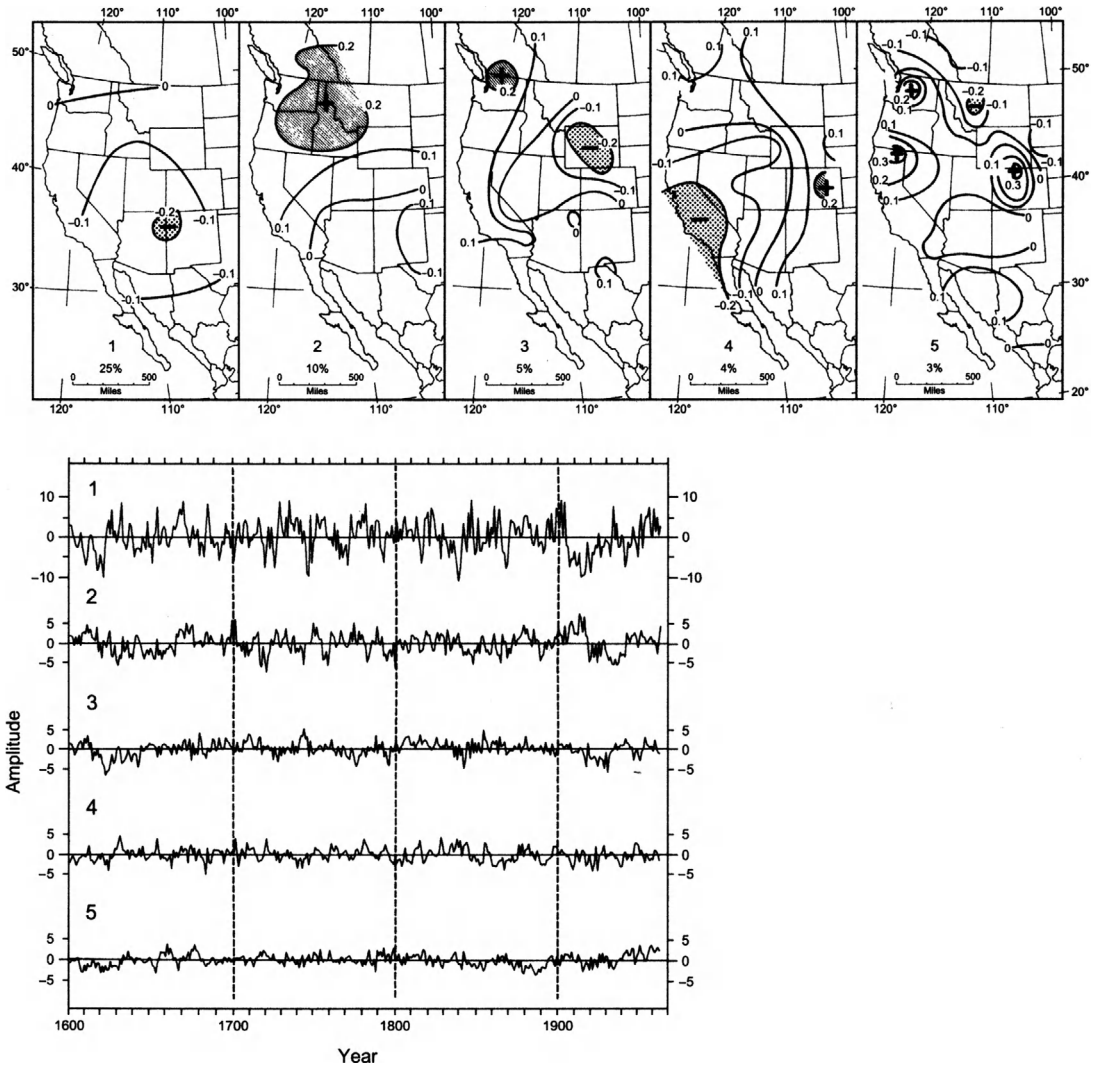


FIGURE 13.17 The first five eigenvectors of tree-ring widths based on a network of 65 chronologies distributed across the western United States, northern Mexico, and southwestern Canada. These represent the major patterns of growth anomalies in the region. Eigenvector 1 accounts for 25% of the overall variance; each subsequent eigenvector accounts for progressively less. The lower diagram shows the relative amplitudes of these five eigenvectors since AD 1600 (i.e., the principal components, [PCs] 1-5). These and other PCs were used in canonical regressions with gridded temperature, precipitation, and pressure data, first to calibrate the tree-ring data and then to reconstruct maps of each climatic parameter back to AD 1600. *From Fritts (1991).*

related using canonical regression or orthogonal spatial regression techniques (Clark, 1975; Cook et al., 1994). These techniques involve identifying the variance that is common to individual eigenvectors of the two different data sets and defining the relationship between them. The techniques are important in that they allow spatial arrays (maps) of tree-ring indices to be

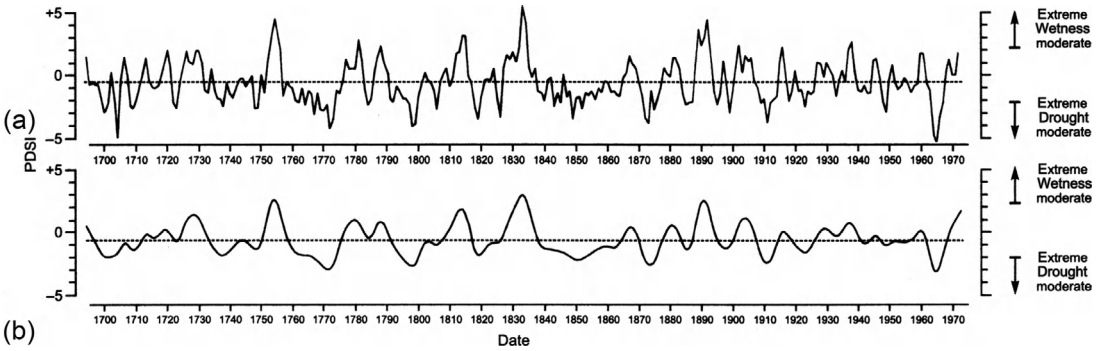


FIGURE 13.18 July Palmer drought indices for the Hudson Valley, New York, from 1694 to 1972 reconstructed from tree rings. (a) Unsmoothed estimates and (b) a low-pass-filtered version of the unsmoothed series that emphasizes periods of $\geq$10 years. *After Cook and Jacoby (1979).*

used to reconstruct maps of climatic variation through time (Fritts et al., 1971; Fritts, 1991; Briffa et al., 1992b; Fritts and Shao, 1992). Briffa et al. (1988), for example, use orthogonal spatial regression to reconstruct April to September temperatures over Europe west of 30°E using densitometric information from conifers over Europe. In their procedure, both the spatial array of temperature and the spatial array of densitometric data were first reduced to their principal components. Only significant components in each set were retained. Each retained PC of climate was then regressed in turn against the set of retained densitometric PCs. This procedure can be thought of as repeating the level IIb approach (Table 13.1) m times, where m is the number of retained climate PCs. Having found all the significant regression coefficients, the set of equations relating the climate PCs to the tree-growth PCs were then transformed back to original variable space, resulting in an equation for each temperature location in terms of all the densitometric chronologies. A similar approach was used by Schweingruber et al. (1991) and Briffa and Schweingruber (1992) to derive temperature reconstructions for Europe and by Briffa et al. (1992b) who derived temperature anomaly maps for the western United States from a network of tree-ring density data. Figure 13.19 shows some examples of these reconstructions in comparison with instrumental data for the same years, which gives a qualitative impression of how good the reconstructions might be. In fact, verification statistics over an independent period are generally good, providing a more quantitative assessment that earlier reconstructions are likely to be reliable. Of particular interest is the reconstruction of temperatures in the early nineteenth century, around the time of the eruption of Tambora (Figure 13.20). Tambora (8°S, 118°E) exploded in April 1815; it is considered to have been the largest eruption in the last thousand years if not the entire Holocene (Rampino and Self, 1982; Stothers, 1984). Contemporary accounts document the severe climatic conditions that were experienced in western Europe and in the eastern United States in the following year that became known as "the year without a summer" (Harington, 1992). The dendroclimatic reconstruction for summer temperatures (April-September) in western Europe indeed shows extremely cold conditions in 1816 with cold summers also in 1817 and 1818 over most of western Europe (and northwestern Russia; cf. Shiyatov, 1996) continuing into 1819 in southern Europe. Over most of the western United States and Alaska, 1816 was not cold, but the

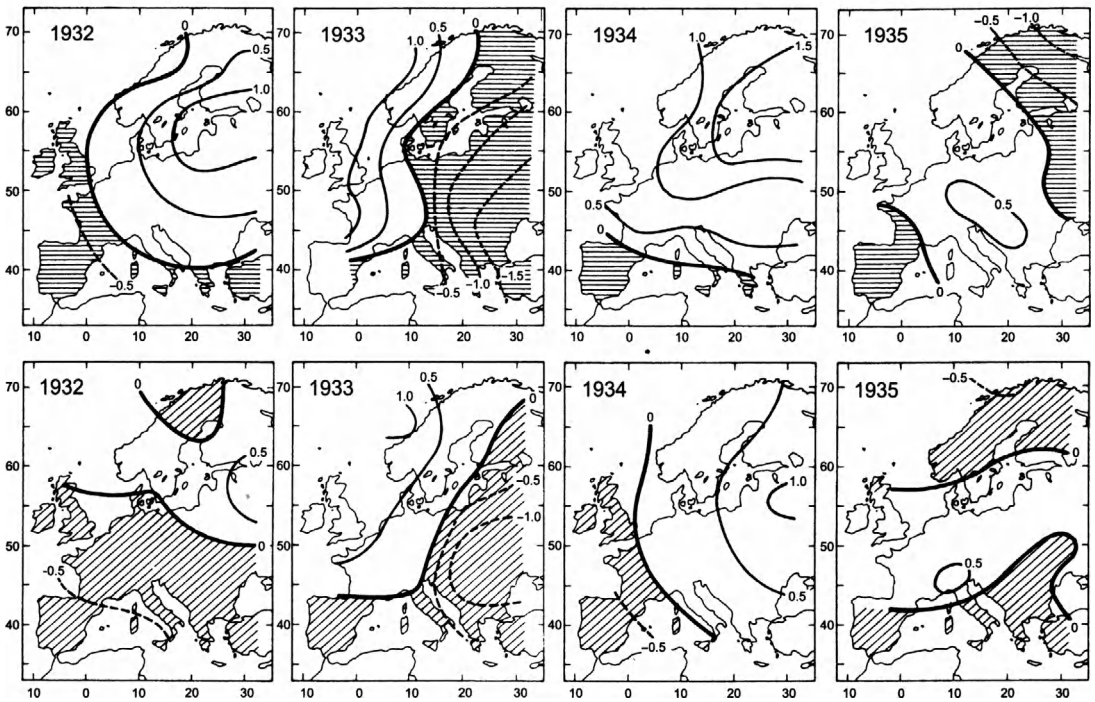


FIGURE 13.19 Observed April-September mean temperature anomalies in the summers of the early 1930s (expressed as departures from the 1951 to 1970 mean) compared with (in the succeeding text) the corresponding reconstruction based on a tree-ring density network made up of 37 chronologies distributed across the region. *From Schweingruber et al. (1991).*

following four summers were uniformly cooler than the 1951-1970 reference period. The coldest summer in the last few centuries in the western United States (1601) was also associated with an eruption, probably Huaynaputina in Peru (Briffa et al., 1992b, 1994). Temperatures across the region averaged 2.2 °C below the 1881-1982 mean as a result of that event.

Before concluding this section on calibration, it is worth noting that tree-ring indices need not be calibrated only with climatic data. The ring-width variations contain a climatic signal, and this may also be true of other natural phenomena that are dependent in some way on climate. It is thus possible to calibrate such data directly with tree rings and to use the long tree-ring records to reconstruct the other climate-related series. In this way, dendroclimatic analysis has been used to reconstruct runoff records (e.g., Woodhouse et al., 2006) and glacier mass balance variations (Watson and Luckman, 2004).

13.2.6 Verification of Climatic Reconstructions

An essential step in dendroclimatic analysis (indeed in all paleoclimatic studies) is to test or verify the paleoclimatic reconstruction in some way. The purpose of verification is to test if the transfer function model (derived from data in the calibration period) is stable over

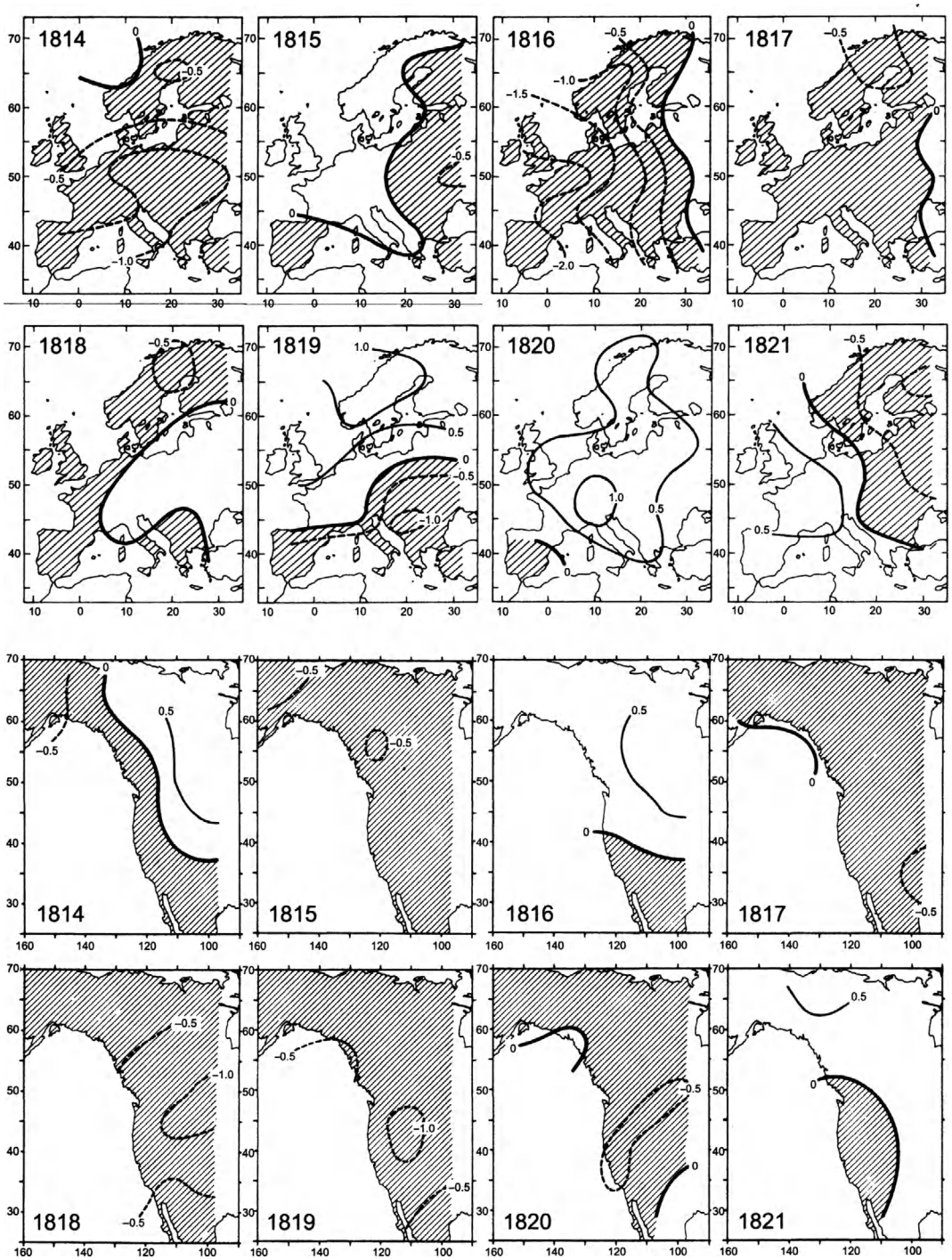


FIGURE 13.20 Reconstructed summer (April-September) temperature anomalies (from 1951 to 1970 means) for western Europe and western North America for the early nineteenth century based on a 37-site tree-ring density network in Europe and a 53-site density network in North America. Conditions were cold in both regions in the years following the eruption of Tambora, though 1816 itself was mostly warm in western North America. *From Schweingruber et al. (1991).*

time, usually by comparing part of the reconstruction with independent data from a different period. Inevitably, when the prediction estimates are tested against independent data set, the amount of explained variance will almost always be less than in the calibration period. To quantify how good the reconstruction is, in comparison with independent data, various statistical tests are generally performed (Gordon, 1982; Fritts et al., 1990, Appendix 1 of Fritts, 1991). These statistics then provide some level of confidence in the rest of the reconstruction; the performance of the transfer function over the verification period is the best guide to the likely quality of the reconstruction for periods when there are simply no instrumental data.

Two approaches to verification are generally adopted. First, when calibrating the tree-ring data, very long instrumental records for the area are sought. Only part of these records are then used in the calibration, leaving the remaining early instrumental data as an independent check on the dendroclimatic reconstruction. If the reconstruction is in the form of a map, several records from different areas may be used to verify the reconstruction, perhaps indicating geographic regions where the reconstructions appear to be most accurate (e.g., Briffa et al., 1992b). This approach is difficult in some areas where tree-ring studies have been carried out (e.g., the western USA and northern tree lines) because these are areas with very few early instrumental records (Bradley, 1976). Dendroclimatic studies in western Europe (Briffa and Schweingruber, 1992; Serre-Bacher et al., 1992) can be more exhaustively tested because of the much longer instrumental records in that area. Indeed, it is sometimes possible to conduct two calibrations with tree-ring and climatic data from different time periods and to compare the resulting dendroclimatic reconstructions for earlier periods derived independently from the two data sets (e.g., Briffa et al., 1988). This provides a vivid illustration of the stability of the derived paleoclimatic reconstructions (Figure 13.21).

A second approach is to use other proxy data as a means of verification. This may involve comparisons with historical records or with other climate-dependent phenomena such as glacier advances (LaMarche and Fritts, 1971) or pollen variations in varved lake sediments (Fritts et al., 1979). It may even be possible to use an independent tree-ring data set to compare observed growth anomalies with those expected from paleoclimatic reconstructions. Blasing and Fritts (1975), for example, used a network of trees from an area between northern Mexico and southern British Columbia to reconstruct maps of sea-level pressure anomalies over the eastern Pacific and western North America. A separate temperature-sensitive data set from Alaska and the Northwest Territories of Canada was then used to test the reconstructions. Periods of anomalously low growth in the northern trees were associated with increased northerly airflow as predicted by the pressure reconstructions.

In all verification tests, one is inevitably faced with two questions:

(a) If the verification is poor, does the fault lie with the dendroclimatic reconstruction (and hence the model from which it was derived) or with the proxy or instrumental data used as a test (which may itself be of poor quality and subject to different interpretations)? In such cases, reevaluation of the tree-ring data, the model, and the test data must be made before a definitive conclusion can be reached.

(b) Is the dendroclimatic reconstruction for the period when no independent checks are possible as reliable as for the period when verification checks can be made? This might seem an insoluble problem, but it is particularly important when one considers the

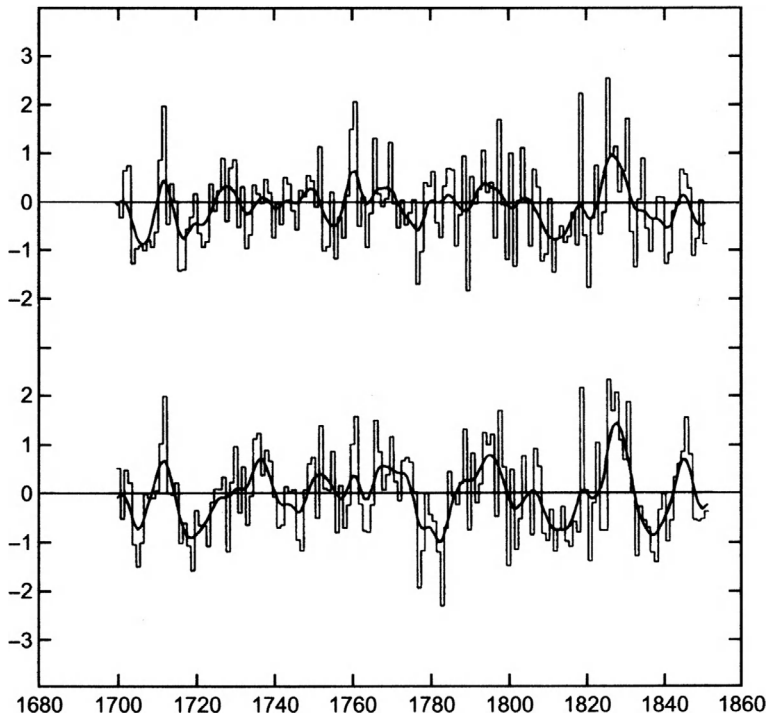


FIGURE 13.21 Two reconstructions of northern Fenno-Scandinavian temperatures for July-August using the same transfer function model, but with calibration based on 1852-1925 in the upper diagram and 1891-1964 in the lower diagram. Ordinate axis is in standard deviation units with one unit equal to ~1 °C. The two calibrations accounted for 69% and 56% of the variance of instrumental temperature over the same (calibration) interval, respectively. Both gave statistically significant statistics when verified against data from the other "independent" interval. Thus, both reconstructions could be viewed as statistically reliable. Although the two series are strongly correlated ($r = 0.87$), there are important differences between them, which warns against overinterpreting the reconstructions for individual years. For example, the lower diagram shows an extreme in 1783 that does not appear in the upper diagram, and even the lower-frequency variations show important differences requiring careful examination of the regression weights going in to each reconstruction. *From Briffa et al. (1988).*

standardizing procedure employed in the derivation of tree-growth indices (Section 13.2.3). Errors are most likely to occur in the earliest part of the record, whereas tests using instrumental data are generally made near the end of the tree-growth record (where replication is generally highest and the slope of the standardization function is generally lowest) and least likely to involve the incorporation of large error. The optimum solution is for both instrumental and proxy data checks to be made on reconstructions at intervals throughout the record, thereby increasing confidence in the overall paleoclimatic estimates.

Dendroclimatologists have set the pace for other paleoclimatologists by developing methods for rigorously testing their reconstructions of climate. Many other fields would benefit by adopting similar procedures.

13.3 DENDROCLIMATIC RECONSTRUCTIONS

The following sections provide selected examples of how tree rings have been used to reconstruct climatic parameters in different regions of the world. This is not by any means an exhaustive review, and for further information, the reader should examine the books edited by Dean et al. (1996) and Hughes et al. (2011).

13.3.1 Reconstructions of Temperatures over the Northern Hemisphere

As concerns have grown over the rise in global mean temperatures, many questions have arisen about the long-term context of recent global warming: How unique has the warming been, when did it begin, and what other forcing factors besides anthropogenic greenhouse gases may have been responsible for the observed changes? In the parlance of the Intergovernmental Panel on Climate Change (IPCC), these are questions of attribution—what forcing factors could have brought about the recent changes? Instrumental temperature records provide a reliable picture of global temperature variations back to around 1850 (Brohan et al., 2005) but to extend the record further back in time, an extensive network of temperature-sensitive paleoclimate proxies is required. Many studies have shown that tree growth at the northern tree line and at the upper limit of trees in mountain regions is limited by temperature; consequently, networks of tree-ring data (ring widths or density) from those regions can be used to reconstruct past changes in temperature. Several studies have produced reconstructions of Northern Hemisphere temperatures spanning the last 1000-1200 years based exclusively on such tree-ring data (there are insufficient data from the Southern Hemisphere to do a similar reconstruction for that region) (e.g., Briffa et al., 2001; Esper et al., 2002; Cook et al., 2004a; Osborn and Briffa, 2006; Wilson et al., 2007). Other studies have combined tree-ring data with other high-resolution proxies, but commonly, tree-ring data still make up a large proportion of the overall data used (e.g., Mann et al., 1998, 1999, 2008; Crowley and Lowery, 2000; Moberg et al., 2005; Ljungqvist, 2009, 2010; Frank et al., 2010a,b). All of the tree-ring reconstructions use data from outside the Tropics, and so, they provide a record of temperature variations in the extratropical region. Furthermore, although tree growth may be influenced by climatic conditions during the preceding seasons, the ring width and density data mainly reflect summer growing season conditions (Cook et al., 2004a). Nevertheless, on multidecadal to centennial timescales, summer and annual variations are likely to be quite similar. Careful selection and processing of tree-ring data must be carried out to preserve the low-frequency aspects of the data. As an example, Figure 13.22 shows a temperature reconstruction for the Northern Hemisphere extratropical region, based on a network of over 1200 ring width chronologies from 14 high-latitude and high-elevation sites from North America and Eurasia (Esper et al., 2002). Although the number of chronologies available per year declined back in time, careful assessment by Cook et al. (2004a) indicates that this had minimal effect on the reconstruction. The mean tree-ring indices, smoothed to emphasize variability at periods >20 years in duration, were calibrated with similarly processed instrumental data for the land areas 30-70°N. This shows that the period around AD 1000 ± 50 years was the warmest period prior to the twentieth century, though arguably not as warm as in recent decades (Frank et al., 2007). This is the same conclusion reached by many other

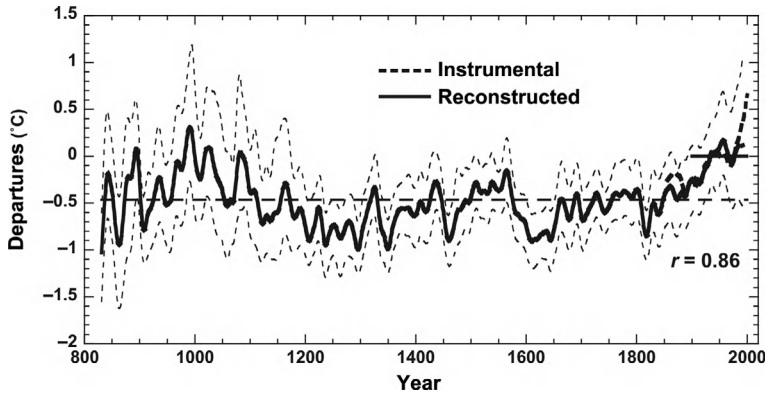


FIGURE 13.22 The temperature-calibrated mean RCS tree-ring chronology, AD 831-1990 (thick solid curve) for the extratropical Northern Hemisphere (30-70°N), land only, 20-year low-pass-filtered. The thin dashed curves are bootstrap 95% confidence intervals, and the thick dashed curve represents the instrumental data up to 2000. The temperature values are anomalies from the full twentieth-century instrumental mean anomaly (1900-1999). The difference between the twentieth-century zero anomaly and the long-term anomaly mean (~0.47 °C) is indicated by the long-term mean (thick dashed horizontal line). *From Cook et al. (2004a).*

reconstructions, though the lack of proxy data for the most recent years, and potential divergence problems (Section 13.2.4) make this a controversial matter and one that is difficult to unequivocally resolve (cf. Mann et al., 1999; Moberg et al., 2005; Osborn and Briffa, 2006; Wilson et al., 2007; Ljungqvist, 2010). The coldest intervals of the last millennium were from ~1250 to 1400, in the early 1600s and in the early 1800s. Attribution studies suggest that these colder periods were strongly related to explosive volcanism, perhaps reinforced by snow and sea-ice feedbacks, which reduced temperatures sharply not only after each eruption but also more generally throughout much of the last millennium (Figure 13.23) (cf. Miller et al., 2012). By contrast, the warmest period in medieval time was a period of relative quiescence in explosive volcanic activity. It has been suggested that solar forcing may have played an additional role in modulating temperatures over this period, but our current understanding is that total solar irradiance (TSI) change over the last thousand years was less than ±0.2%, and thus, it is unlikely that it had a major influence on global temperatures, though such changes may have been of regional significance due to changes in atmospheric circulation (Wang, Y.-M. et al., 2005). The most recent warming cannot be explained by observed changes in irradiance or volcanic activity and was driven by the increase in atmospheric greenhouse gases, propelling Northern Hemisphere and global mean temperatures to levels not experienced for the last 1000 years (Jansen et al., 2007).

13.3.2 Drought Reconstruction

The growth of many trees is limited by the availability of moisture rather than temperature, providing dendroclimatologists with the opportunity to extend the limited instrumental records of precipitation (or moisture balance) far back in time. This has greatly expanded our understanding of drought history and its societal impact in many regions and given new insights into the atmospheric conditions that lead to drought conditions.

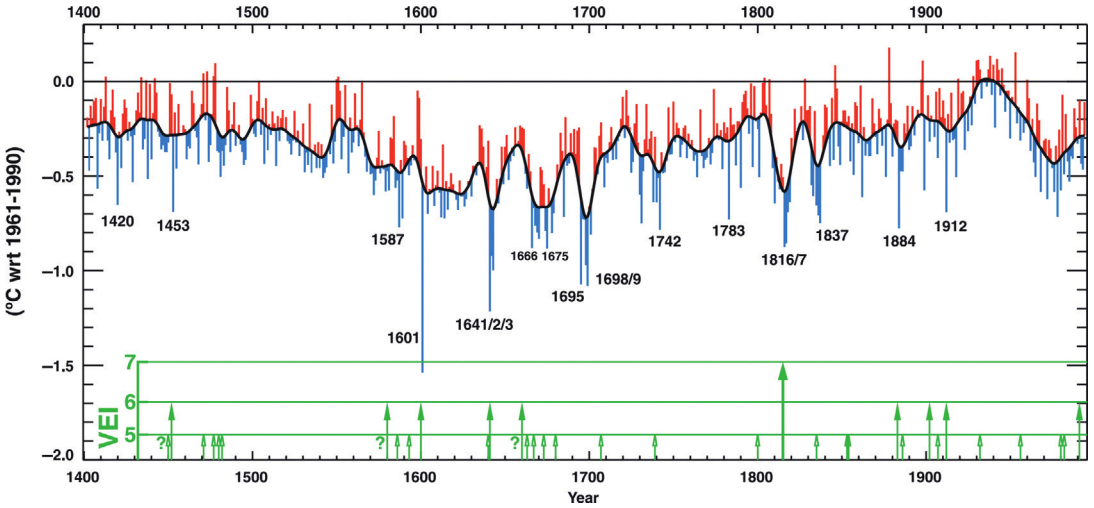


FIGURE 13.23 Estimates of warm-season temperature (°C anomalies from the 1961 to 1990 mean) for land areas north of 20°N. The smoothed curve is the 25-year low-pass-filtered reconstruction produced using the age-band decomposition approach of Briffa et al. (2001). The Volcanic Explosivity Index (VEI) is indicated by the arrows at the bottom; "?" marks those eruptions whose date is uncertain. *From Briffa et al. (2004).*

A network of 835 drought-sensitive tree-ring chronologies has been developed for North America, most of them extending back at least 500 years, with a smaller network covering the last 1200 years (Cook et al., 1996, 1999). Ongoing studies of long-lived swamp cedars from the southeastern United States and Mexico will no doubt add to this network in the future (Stahle et al., 2012). All of these records have been calibrated against the Palmer Drought Severity Index (PDSI) that has become, *de facto*, the index of choice for characterizing drought (Dai et al., 2004). Palmer indices are measures of the relative intensity of precipitation abundance or deficit and take into account soil-moisture storage and evapotranspiration as well as prior precipitation history (Palmer, 1965). Thus, they provide, in one variable, an integrated measure of many complex climatic factors, somewhat weighted by antecedent conditions. They are scaled from +4 or more (extreme wetness) to −4 or less (extreme drought) and are widely used by agronomists in the United States as a guide to climatic conditions relevant to crop production. Cook et al. (1996) calculated PDSI values for North America from twentieth-century instrumental data and interpolated these to a uniform 2.5×2.5 grid. Then, EOFs of tree-ring data within a specified circle around each point were obtained to capture the principal modes of variability in the adjacent tree-ring network, and these were regressed against the PDSI data, point by point (Cook et al., 1996). The resulting equations were then used to calculate PDSI values back in time for each location, and verification statistics indicate that the reconstructions at all grid points are statistically significant back to AD 1300 and as far back as AD 800 at 75% of the network (Herweijer et al., 2007).

The gridded set of drought reconstructions (the "North American Drought Atlas"; Cook and Krusic, 2004; Cook et al., 2010a) is a tremendous resource for examining the frequency and duration of droughts in the past (as well as pluvial episodes) and comparing them with wet and dry periods experienced in the twentieth century. Over the last century, the most

severe and widespread drought episode affecting North America was in the 1930s (~1929-1940), commonly referred to as the "Dust Bowl years" due to widespread wind erosion of topsoil over vast areas of the Great Plains (Egan, 2006). The tree-ring data capture the spatial dimensions of the observed drought quite well (although not the severity of drought in all areas), and the Drought Atlas provides a long-term perspective on earlier periods when similarly extensive droughts occurred (Figure 13.24). This reveals that although many areas have experienced prolonged droughts in the past, the drought of the 1930s was the most extreme in the last 500 years in terms of its overall geographic extent, duration, and magnitude (Fye et al., 2003). However, there have been a number of even longer droughts that have affected the United States ("megadroughts"; Stahle et al., 2000), particularly in the western and southwestern states. The most remarkable of these occurred in the late 1500s, beginning first in Mexico in the 1530s and 1540s, then extending into the southwestern United States by the 1570s, and gradually drifting in geographic focus to other regions further north and east (Stahle and Dean, 2011). In fact, there is compelling evidence that drought affected the eastern seaboard of the United States in the 1560-1580s, leading to severe hardship for colonial settlers in South Carolina and Virginia, resulting in many deaths and the eventual abandonment of their first settlements in those regions (Stahle et al., 1998, 2000). But the human consequences of drought were vastly more profound in Mexico, where millions of people are thought to have died in the sixteenth century as a result of drought-induced famine, social collapse,

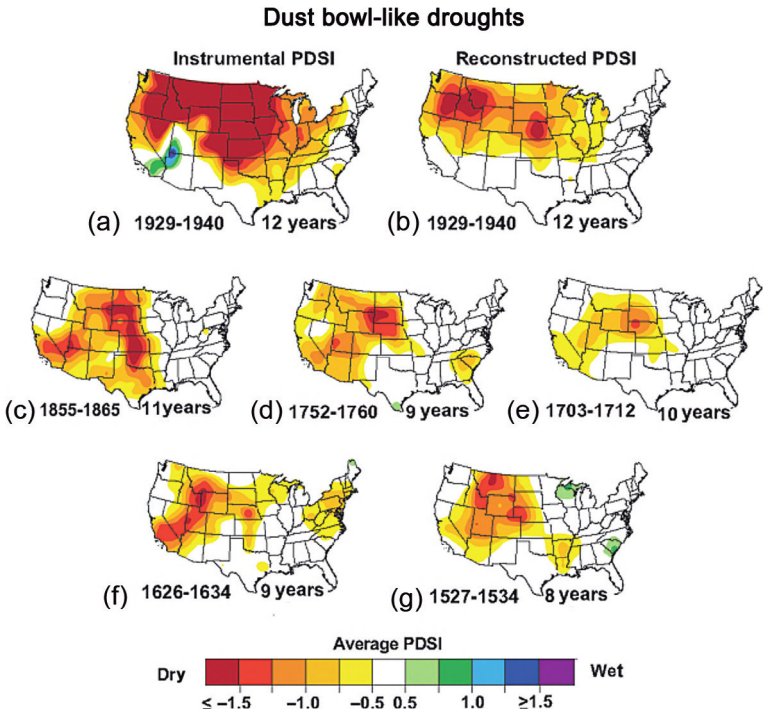


FIGURE 13.24 The Dust Bowl drought of the 1930s and its analogs. (a) and (b) Mean instrumental and reconstructed summer PDSI for the period 1929-1940; (c)–(g) reconstructed summer PDSI averaged and mapped for the drought periods shown. *From Fye et al. (2003).*

and an epidemic of hantavirus (known locally as *cocoliztli*) spread via the excreta of rats that invaded the living areas of communities, as the rat population exploded in the years immediately after the drought (Acuña-Soto et al., 2002; Stahle et al., 2011).

In the western United States, a set of especially long tree-ring chronologies have enabled drought history (defined as PDSI ≤ 1) to be examined since AD 800 (Cook et al., 2004b). Overall, the period from AD 900 to 1300 was drier than the following 600 years, with four periods having particularly extensive areas of drought, centered on AD 936, 1034, 1150, and 1253 (Figure 13.25). In the twelfth century, more than 50% of the region was experiencing unusually dry conditions. A tree-ring reconstruction of the flow of the Upper Colorado River clearly shows the exceptional nature of the period from AD 1130 to 1154, when the mean annual runoff was 80% of the twentieth-century average, with flow continuously low from AD 1143 to 1155 (Figure 13.26; Meko et al., 2007). Similar results were found in a reconstruction of runoff in the Sacramento River basin of California (Meko et al., 2001; Meko and Woodhouse, 2005). Clearly, if such a severe and prolonged drought was to occur again, the consequences for the southwestern United States would be catastrophic, and so understanding the circulation patterns that gave rise to this anomalous situation is of great importance.

Analysis of twentieth-century droughts centered over the southwestern United States reveals a strong link to sea surface temperature anomaly patterns in the Pacific (Cole and Cook, 1998; Cook et al., 2007). In particular, "La Niña-like" conditions, wherein eastern

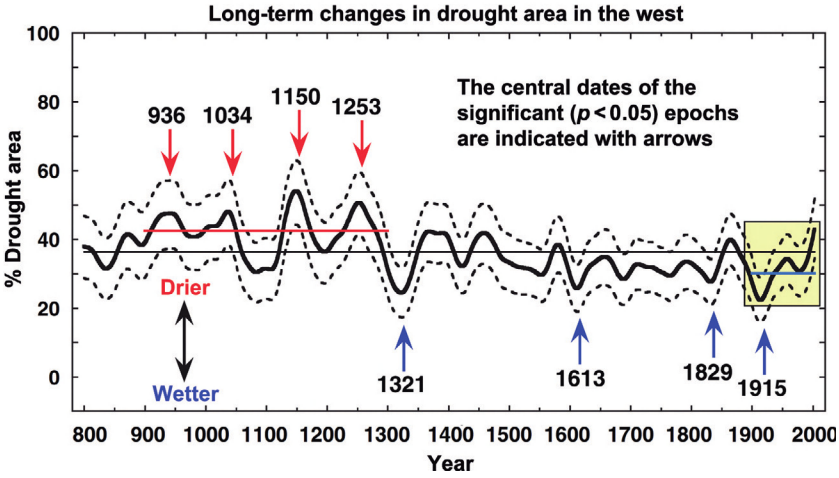


FIGURE 13.25 Smoothed Drought Area Index reconstruction (solid black curve) for the West, showing two-tailed 95% bootstrap confidence intervals (dashed black curves) and the long-term mean (thin horizontal black line). Sixty-year smoothing was applied to highlight the multidecadal to centennial changes in aridity. The four driest epochs were before AD 1300, whereas the four wettest epochs occurred after that date. The difference between the means of the AD 900-1300 period (red line, 42.4%) and AD 1900-2003 period (blue line, 30%) is also apparent. The 12.4% difference between the two periods translates into an average drought area increase of 41.3% in the West during the earlier period. This difference is statistically significant; however, some of the AD 900 to 1300 period PDSI estimates are extrapolations, because they fall outside the range of the instrumental PDSI data in the AD 1928-1978 calibration period, though they are still based on the actual growth histories of highly drought-sensitive trees. *From Cook et al. (2004b).*

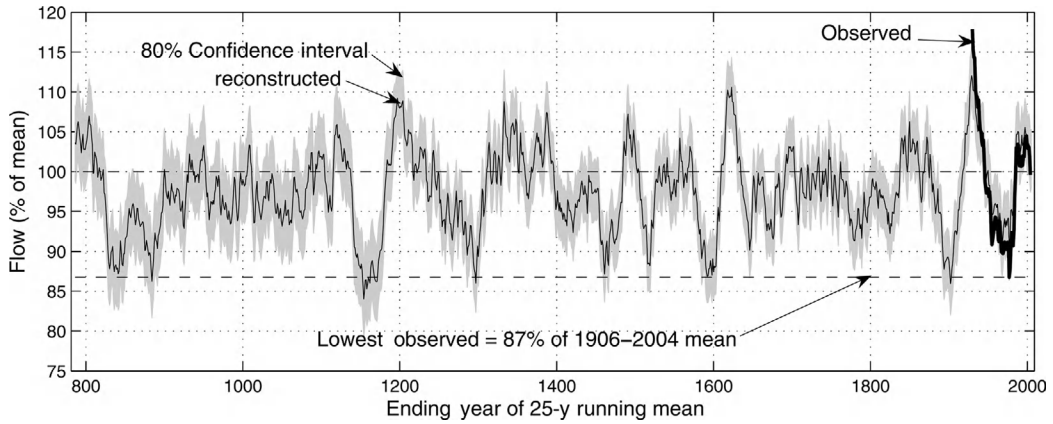


FIGURE 13.26 Reconstructed flows for the Sacramento River, California (25-year running means). Flows are plotted as a percentage of the 1906-2004 mean of observed natural flows (18.53 billion cubic meters, or 15.03 million acre-feet). Confidence interval is shaded. Horizontal dashed line is the lowest 25-year running mean of observed flows (1953-1977). *From Meko et al. (2007).*

equatorial Pacific SSTs are below average, lead to displacement of the mid-latitude jet stream to the north, so that precipitation is greatly reduced over the southwestern and southern states of the United States. Conditions during El Niños are more or less the opposite, with above average rainfall amounts across the southern tier of states and drier conditions to the north. In the twentieth century, the spectrum of ENSO variability has involved an oscillation between El Niños and La Niñas on a 3- to 7-year timescale, which is not conducive to droughts lasting for one or more decades (Cole et al., 2002). Thus, the overall drier conditions in the western United States from AD 900 to 1300 suggest that although ENSO variations may still have occurred, the SST pattern may have been more "La Niña-like," with a persistent shift in circulation toward that which we typically associate with La Niñas today (Cook et al., 2007). This period remains as somewhat of a puzzle, but one thing is clear: the twentieth-century instrumental record does not capture the full spectrum of ENSO variability that the paleoclimatic data represent. This presents a real challenge in trying to prepare for future changes in a region where population pressure and the demand for water are at an all-time high (Woodhouse et al., 2010).

Interestingly, the 1930s Dust Bowl drought does not appear to have been a simple La Niña-driven event. Drought conditions extended far into the northwest and the northern Great Plains, so the situation was different from that of the mid- to late sixteenth-century megadrought. It may be that unusually warm SSTs in the North Atlantic played an additional role in the 1930s drought, but statistical analysis suggests that there were also other important factors in play, perhaps involving aerosol feedbacks that reinforced the widespread warm and dry conditions across the central United States (the so-called Charney feedbacks; Charney et al., 1975; Cook et al., 2011). To what extent regional land disturbance, resulting from poor agricultural practices that were common at that time, contributed to the exceptional drought of the 1930s remains an open question.

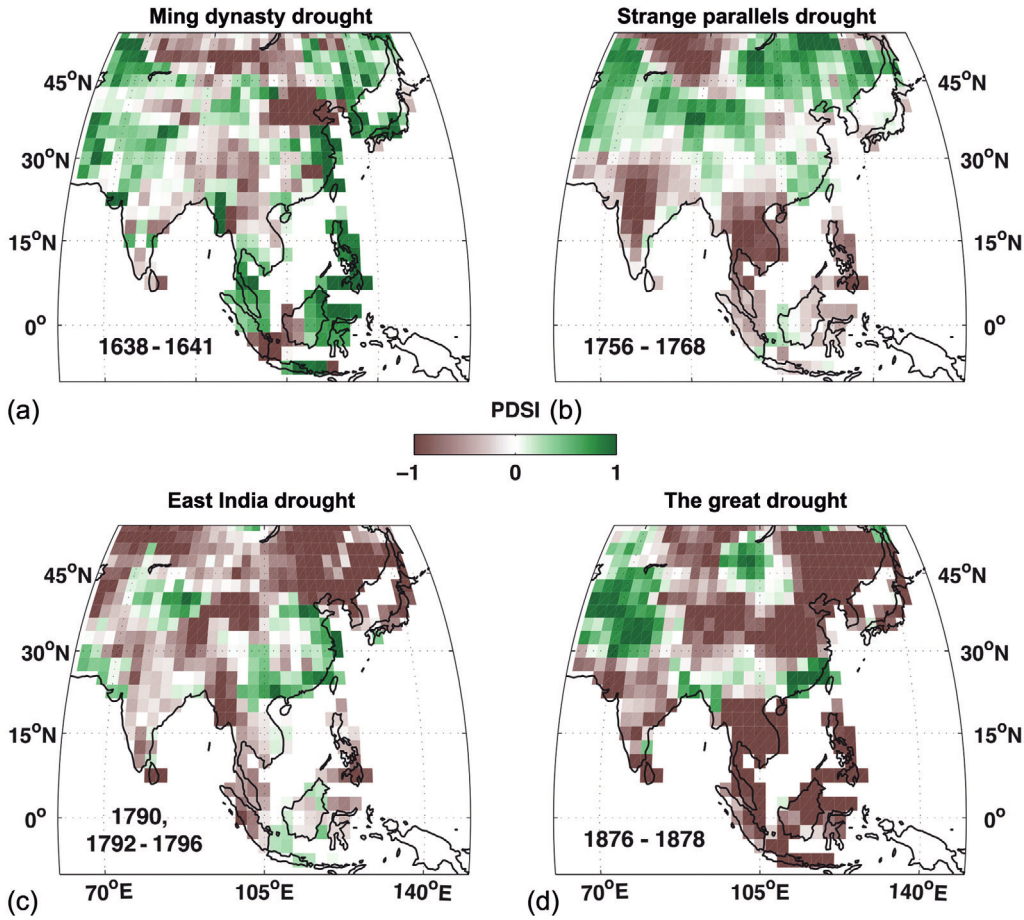


FIGURE 13.27 Spatial drought patterns during four historical Asian droughts. Mean PDSI over each of four regional droughts identified from the historical record. (a) The Ming Dynasty drought (1638-1641). (b) The "Strange Parallels" drought (1756-1768). (c) The East India drought of the late eighteenth century (1790 and 1792-1796). In 1791, much of India appears to have been slightly wet, except for the region around Chennai where the drought persisted. (d) The late Victorian Great Drought (1876-1878). *From Cook et al. (2010b).*

Drought history has also been the focus of tree-ring research in East and Southeast Asia, using a similar methodology to that employed for North America (Cook et al., 2010b). This reveals the extent and magnitude of several major regional-scale droughts (Figure 13.27), the most severe of which occurred from 1750 to 1768, affecting India, Southeast Asia, and Indonesia (cf. Buckley et al., 2007). A shorter, but devastating, drought was associated with a strong El Niño event in 1876-1878; more than 30M people are thought to have died as a result of crop failures during this period. The link between droughts in Southeast Asia and El Niños was first suggested by Berlage (1931) who noted the connection through his studies of tree rings in teak (*Tectona grandis*) from Indonesia. More recently, D'Arrigo et al. (2006a) have

expanded upon this work, reconstructing Palmer Drought Severity Indices for Java and Sulawesi back to 1787. These demonstrate a strong negative correlation with central Pacific SSTs (Niño 3.4 region); during El Niños, the main zone of convective rainfall shifts eastward, and high pressure persists over Indonesia, leading to drought. Interestingly, the tree-ring PDSI reconstruction also reveals extreme droughts followed major explosive eruptions in the Tropics (e.g., in 1810 and 1815-1818). As it is common for El Niños to follow major equatorial eruptions, this may be the mechanism, though cooler SSTs in the Indonesian warm pool may also been a factor (D'Arrigo et al., 2006b).

It is often claimed that severe and persistent droughts were the root cause of societal collapse in many regions. Certainly, climate is not constant in any region, and in areas that are marginal for agriculture, prolonged and unexpected droughts can exacerbate vulnerabilities (Weiss and Bradley, 2001). But, many other factors can contribute to societal disruption, and so establishing the climatic conditions during which societal changes may have occurred provides essential context for discussion. Tree-ring-based drought reconstructions have provided spatial and temporal perspectives on many cases where drought has led to severe impacts on societies (e.g., Therrell et al., 2004) and may even have been a decisive a factor in the collapse of a particular cultural regime. For example, in China, the end of the Ming Dynasty in AD 1644 may have been driven, in part, by crop failures and societal unrest as a result of a severe drought that became progressively worse and expanded in area, from AD 1638 to 1641 (Shen et al., 2007; Cook et al., 2010b). This appears to have been the most severe drought of the last millennium in northeastern China, leading to a complete cessation of runoff in the lower Yellow River and the drying up of wells across the region. In this case, there is a compelling argument that societal disruption was driven by the drought, leading inexorably to the end of Ming rule. In the western United States, the demise of Anasazi culture was certainly associated with drought in the thirteenth century (AD 1276-1297), but anthropological and archaeological evidence suggests that other cultural and demographic factors may have played as significant a role in the societal changes that occurred (Stahle and Dean, 2011). Tree-ring data clearly show that the thirteenth-century drought was centered over the Anasazi cultural heartland, but migration from the region was already under way prior to the critical period of drought, so other factors appear to have played an equally important role in driving societal changes at that time. Tree-ring reconstructions also suggest that climate played a role in the decline of the kingdom of Angkor in Cambodia, in the late fourteenth century, though it was perhaps not the defining factor that led to major societal disruptions (Buckley et al., 2010). Angkor was highly dependent on a complex hydraulic engineering system, and tree-ring reconstructions for the region indicate that significant hydrologic variability involving droughts followed by strong monsoon rainfall and catastrophic flooding may have contributed to partial destruction of the water system, with consequent societal impacts.

13.3.3 Reconstruction of Atmospheric Circulation Modes

One of the most important developments in dendroclimatology over the last 20 years has been the establishment of extensive networks of tree-ring data sets and associated climate reconstructions (e.g., Cook and Krusic, 2004; Cook et al., 2010a,b; Villalba et al., 2011; Stahle et al., 2012). This has enabled large-scale modes of climate variability to be constrained in

time and space, providing a long-term perspective on the most important regional circulation patterns and an understanding of how variability of these modes may be related to forcing factors. However, these reconstructions assume the observed anomaly pattern associated with a particular mode of circulation in the twentieth century has not varied significantly over time, and this may not have been the case. Here, three examples are discussed.

In section 13.3.2, the relationship between regional droughts in the southwestern and western United States and ENSO variability was discussed. Precipitation and temperature anomalies over large parts of the globe are affected as the ENSO system shifts from an El Niño to a La Niña phase, and the pattern of these teleconnections can be used to extend the limited instrumental record of ENSO variability back in time. However, these anomaly patterns are often complex due to the influence of other circulation patterns (e.g., in the North Atlantic or Indian Ocean, for example) so that not all El Niños have identical anomaly fields (indeed, not all El Niños have the same characteristic pattern or magnitude of anomalies in SSTs), and this introduces uncertainty into all ENSO reconstructions (Cole and Cook, 1998; Wilson et al., 2010). Bearing in mind these potential problems, a network of tree-ring data from moisture-sensitive sites in the southwestern United States and Mexico has been used to reconstruct an index of sea surface temperatures in the central Pacific (the Niño 3.4 region, 5°N-5°S, 120-170°W), which is commonly used as a proxy for the entire ENSO system. Principal components of the tree-ring data were regressed against the instrumental SST record of Niño 3.4, and the resulting equation was then used to reconstruct a Niño 3.4 index back to the fifteenth century. This shows strong variability in the ~4- and ~5-year frequency bands over the last 600 years, which is also seen in the shorter instrumental record. However, a comparison with other ENSO reconstructions, which include coral proxies of SSTs from the across the Pacific, provides little comfort that the tree-ring reconstruction from the American Southwest provides a completely reliable record of ENSO variability. Though all reconstructions appear to track ENSO variability quite well in the twentieth century, they differ significantly in earlier periods. This may reflect that fact that "typical" El Niños in the twentieth century were different in the past, or the associated teleconnection patterns have not been as stable in time as assumed. To try and resolve these difficulties, McGregor et al. (2010) extracted the first principal component from a set of 10 separate reconstructions of ENSO, derived from different networks of tree-ring and other paleoclimate proxies from around the Pacific Basin (Figure 13.28). This "unified ENSO

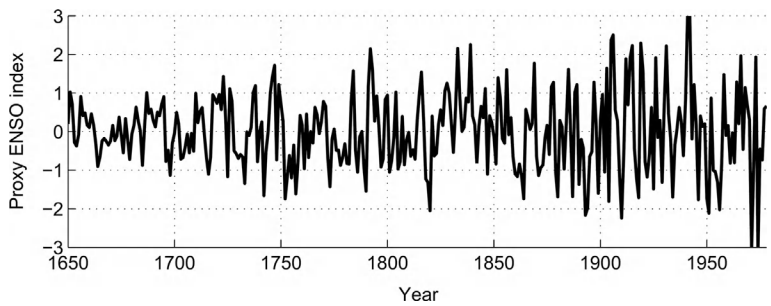


FIGURE 13.28 A "unified ENSO proxy" (UEP) for 1650-1978. *From McGregor et al. (2010).*

proxy" (UEP) stands up quite well to independent verification and thus may be the best reconstruction currently available to examine long-term ENSO variability. It reveals a strong increase in ENSO variability through time, with recent extremes surpassing those of earlier centuries. There is also evidence for significant decadal-scale variability over the last few centuries, which may be linked to conditions in the North Pacific (discussed below). It has been suggested that periods of low radiative forcing due to volcanic eruptions or reduced solar irradiance might lead to El Niño conditions, and this has indeed been observed following a number of recent major volcanic events (Adams et al., 2003; Mann et al., 2005; Emile-Geay et al., 2008). Despite the uncertainties of long-term ENSO reconstructions, all reconstructions so far do show a tendency for a shift to El Niño-like conditions in the year following major explosive volcanic eruptions.

The Pacific decadal oscillation (PDO) involves a large-scale shift in North Pacific circulation, with important implications for both marine ecosystems and climate in northwestern North America. The PDO (defined as the leading principal component of Pacific sea surface temperatures, north of 20°N; Figure 13.29) has two modes, involving a change in the intensity and position of the Aleutian Low and associated airflow and ocean currents (Trenberth, 1990; Mantua et al., 1997; Hare and Mantua, 2000). Instrumental data are only available to examine the frequency characteristics of the PDO for the last century or so, but long-term variability of the PDO has been reconstructed for the last 300 years using a network of tree-ring data from regions of western North America that are affected by rainfall and temperature anomalies associated with different modes of the PDO (Biondi et al., 2001; D'Arrigo et al., 2001;

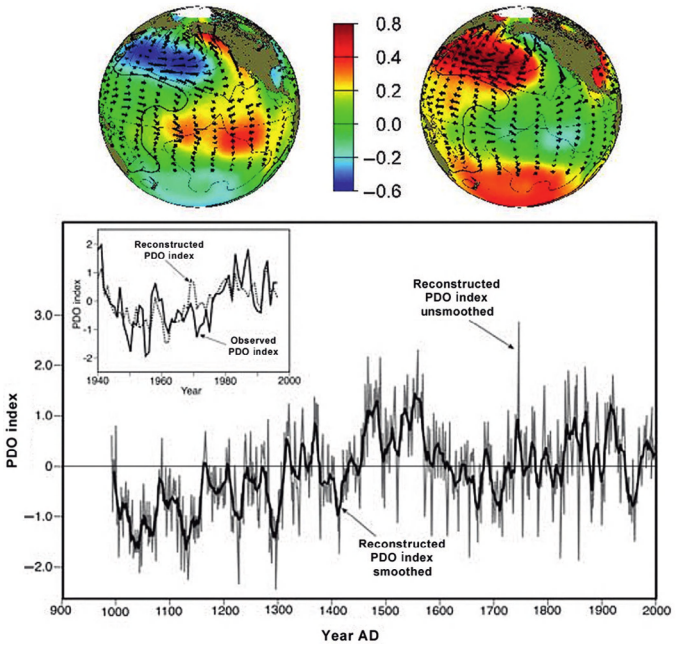


FIGURE 13.29 Upper panel: Phases of the PDO: left, "warm" or positive phase; right, "cold" or negative phase. Shading indicates sea surface temperature anomalies, and arrows are wind field anomalies (from http://jisao.washington.edu/pdo/). Lower panel: Reconstructed annual PDO compared to observed annual PDO (Mantua et al., 1997) (insert) and reconstructed annual PDO index from AD 993 to 1996. The heavy line is the index smoothed using an 11-year moving average. *From MacDonald and Case (2005).*

MacDonald and Case, 2005). This reveals the timing of a number of transitions in the PDO that occurred in the past, though few have been as significant as the shift in circulation between the 1940s and 1950s (Figure 13.29b). Interestingly, the PDO appears to have been predominantly in a negative mode from ~ AD 1000 to 1300, which corresponds to the period with greatest drought area over a wide region of the western United States (Cook et al., 2004a; cf. Figure 13.25). In fact, aridity was far more extensive at that time than would be expected from a "typical" negative PDO state, and this suggests that a quite different circulation mode, for which we may have no modern analog, was in operation at that time. From ~1450 to 1600, the PDO was strongly positive, and apart from a period from ~1630 to 1730, it has remained generally positive since that time. It appears that the behavior of the PDO that has typified the last century may not be typical of longer timescales (MacDonald and Case, 2005).

In the Atlantic, the dominant interannual mode of circulation is the North Atlantic oscillation (NAO). This refers to a dipole pressure gradient across the North Atlantic, from Iceland to the Azores, which has its strongest expression in winter months (Hurrell, 1995). The NAO index is based on the normalized pressure difference between the Azores High and the Icelandic Low, from December to March. In its positive phase, pressure is anomalously low in the north, but higher in the south, associated with displacement of storm tracks (and associated above average precipitation and temperature) across the North Atlantic into northern Scandinavia and western Siberia, with relatively dry and cold conditions further south. In its negative phase, storm tracks are displaced to the south, resulting in higher than normal precipitation and cooler conditions across western and central Europe (Figure 13.30). Like the other reconstructions discussed in this section, reconstruction of the NAO is not based on the pressure gradient itself, but on the pattern of temperature and precipitation anomalies that result from the oscillation. Thus, by assembling a network of tree-ring data (plus a few additional ice core isotopic proxies), Cook et al. (2002) were able to capture much of the structure of the NAO variability back to AD 1400, via its expression in the associated climate anomaly field (Figure 13.30). Instrumental and historical data from Europe indicate that this reconstruction is well validated back to AD 1500 (Luterbacher et al., 2002; Pinto and Raible, 2012). Spectral analysis of the record shows a strong periodicity at ~4 years, as well as strong biennial variability. The NAO was highly variable but generally in a positive phase from the late fifteenth through early seventeenth centuries, whereas variability was lower during the eighteenth and nineteenth centuries. NAO variability increased again in the twentieth century but may have been modulated by low-frequency variability not seen in earlier centuries (the Atlantic multidecadal oscillation, AMO), arguably related to the increasing effects of anthropogenic greenhouse gas forcing on the climate system.

13.3.4 Wildfires and Dendroclimatology

Wildfires have played an important role in the development of ecosystems in many parts of the world. In the western United States, dry winters and warm springs lead to early snowmelt in the mountains and thus reduced soil moisture, setting the scene for

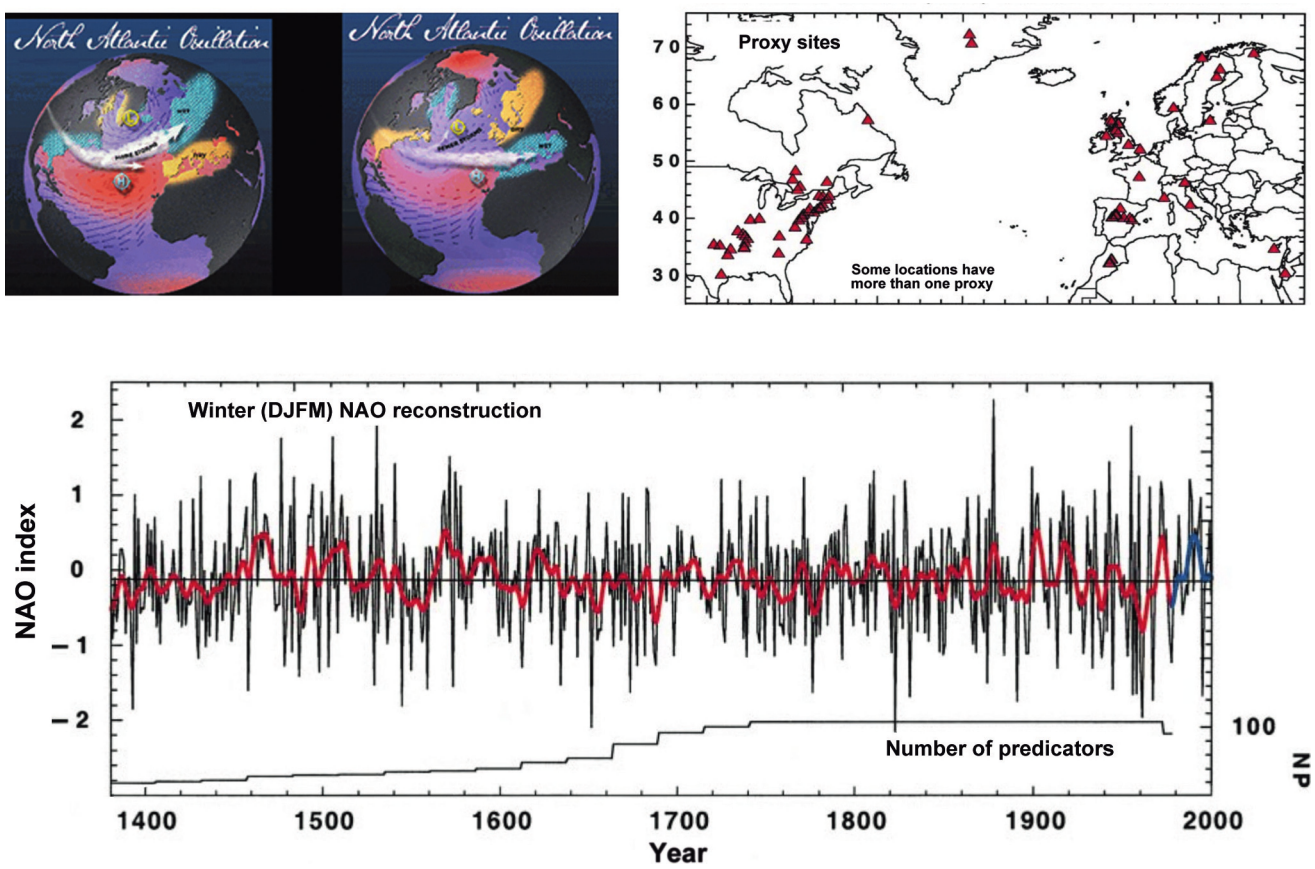


FIGURE 13.30 Top left: Major features of the North Atlantic Oscillation; positive phase (left) and negative phase (right). Top right: Location of tree-ring chronologies (and two Greenland ice core oxygen isotope data sets) used to reconstruct the NAO; below: NAO index reconstructed back to AD 1400. *From Cook et al. (2002).*

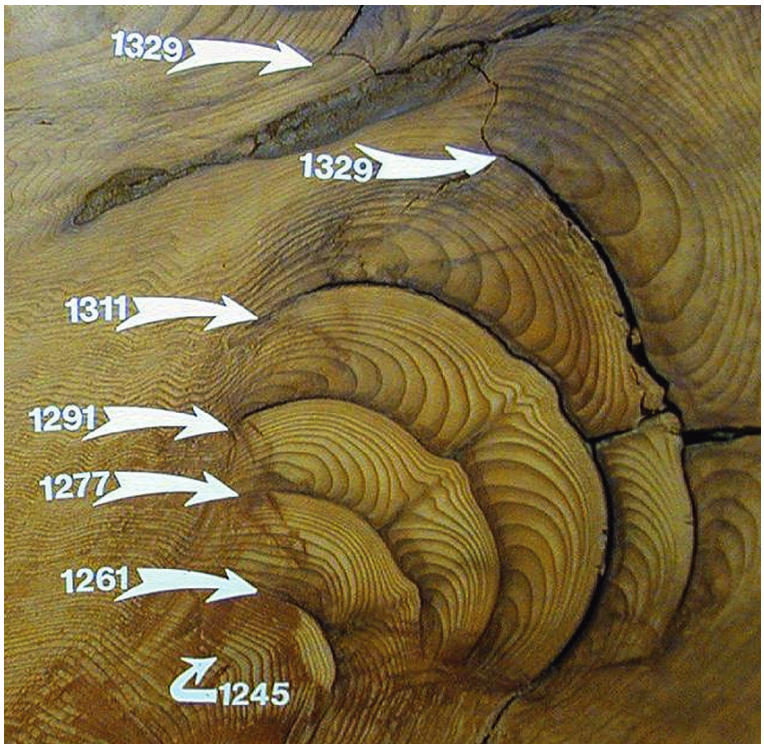


FIGURE 13.31 Fire scars in giant sequoias from the Sierra Nevada of California and the dates of each fire, as determined dendrochronologically. *Photograph kindly provided by Tom Swetnam, University of Arizona.*

lightning-induced fires (Westerling et al., 2006). During droughts, wildfires are especially common, and since droughts tend to be linked to ENSO variability in this region, so too is the history of wildfires (Swetnam and Betancourt, 1990, 1992). Trees often survive fires but may suffer damage to part of the cambial layer, leading to fire scars within the woody tissue (Figure 13.31). These then provide a record of fire history when dated dendrochronologically (Schweingruber, 1996). By compiling such data from trees over a wide region of the southwestern United States, years with widespread fire occurrence have been identified and compared to years when fires were far less extensive (Figure 13.32). This shows the very strong relationship between fire extent and the phase of ENSO, with the most extensive regional droughts almost all associated with La Niña years (Swetnam and Brown, 2011). Analysis of a much longer record of fire history, from giant sequoias (*Sequoiadendron giganteа*) in California, reveals that fire frequency was higher from ~ AD 800 to 1300, the driest interval of the last 2000 years in the Sierra Nevada (Swetnam et al., 2009) and a time of widespread drought across the western United States (Cook et al., 2004a,b). These records all point to the very strong regional-scale ecological impacts of large-scale modes of climate variability in the Pacific on large areas of the western and southwestern United States (Swetnam and Brown, 2011).

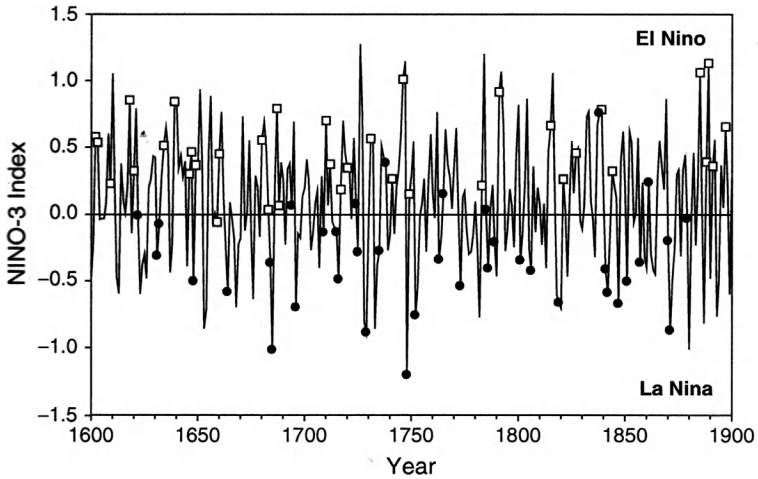


FIGURE 13.32 Tree-ring reconstructed Niño-3 index of sea surface temperatures (from Cook, 2000) shown with the largest (black dots) and smallest (open squares) regional fire years in a 120-site fire-scar network from the southwestern United States. "Large" and "small" fires designate >20 or <4 sites affected by fire, respectively. *From Swetnam and Brown (2011).*

13.4 ISOTOPIC DENDROCLIMATOLOGY

Many studies have demonstrated empirically that variations in the isotopic content of tree rings ($\delta^{13}C$, $\delta^{18}O$, and $\delta^{2}H$)[1] are in some way related to climate. In the past, such studies have often relied simply on statistical relationships, but physiological studies now provide a strong theoretical basis for understanding the processes within plants that lead to the fractionation of different isotopes during the process of wood formation (Farquhar et al., 1989; McCarroll and Loader, 2006; Barbour, 2007).

13.4.1 $\delta^{18}O$ and $\delta^{2}H$

In mid- and high latitudes, there is a positive relationship (*sensu lato*) between the oxygen and hydrogen isotopic composition of rainfall and temperature, whereas in the Tropics, there is generally no correlation between isotopes and temperature, but a strong negative relationship with precipitation amount (Rozanski et al., 1993; cf. Chapter 5, Figure 5.6). It is therefore reasonable to expect that the oxygen (or hydrogen) isotopic content of wood in trees might preserve a record of past temperature or rainfall amounts in such regions, through the uptake of soil water with a specific isotopic signature. The problem is that

[1] To avoid the difficulties of chemical heterogeneity in wood samples, a single component, α-cellulose (polymerized glucose), is extracted for isotopic analysis; α-cellulose contains both carbon-bound and oxygen-bound (hydroxyl) hydrogen atoms, but the latter exchange readily within the plant. It is therefore necessary to remove all hydroxyl hydrogen atoms (by producing nitrated cellulose) to avoid problems of isotopic exchange since the initial period of biosynthesis. For a discussion of isotopes, deuterium/hydrogen (D/H) and $^{18}O/^{16}O$ ratios, see Sections 5.2.1 and 5.2.2.

additional isotopic fractionation occurs within trees during the synthesis of woody material and these biological and kinetic fractionations are themselves dependent on many factors, including temperature, relative humidity, and wind speed (evapotranspiration effects) (Gagen et al., 2011). In particular, evaporative enrichment occurs within leaves, so the duration and amount of evapotranspiration modulates the isotopic content of the soil water. Also, if the tree has deep roots and taps into groundwater that is more isotopically homogeneous, it will be difficult to detect interannual changes in isotopes within the wood (cf. Darling, 2004).

These are just some of the many factors that influence the resulting oxygen isotopic content of woody tissue, but with careful sample selection, the overall climate signal may outweigh other complications. For example, Treydte et al. (2006) produced a 1000-year oxygen isotope-based precipitation reconstruction from Juniper trees in the mountains of northern Pakistan. In this region, precipitation is derived from storms embedded in the westerlies, with most of the annual totals accumulating as snow in winter months. Wet conditions reduce evapotranspiration (and thus enrichment of ^{18}O) in the needles, leading to relatively low values of ^{18}O in woody tissues when precipitation is high. Results indicate that snowfall for most of the last thousand years was much lower than in the twentieth century, with particularly low amounts in the 1790s and 1890s—both periods when large-scale famine is known to have affected the region.

The vast majority of dendroclimatic reconstructions have come from trees in mid- to high-latitude locations, where strong seasonality in temperature gives rise to well-developed annual rings. In the Tropics, most trees do not produce annual rings, as seasonal temperature changes are minimal (though there are exceptions; see Worbes, 2002). However, many tropical forests do experience a strong seasonal change in rainfall amount and evaporation rate, which has a significant effect on the physiology of tree growth and the oxygen isotopic content of the wood produced over the course of each year. Such changes have been modeled using observed environmental data as the drivers, and the simulated isotopic variations closely match those observed in actual wood samples (e.g., Roden et al., 2000; Evans and Schrag, 2004). Tests on samples from across the Tropics demonstrate that a clear seasonal isotopic cycle can often be detected, enabling annual growth increments to be identified and measured, even in the absence of annual rings (Poussart and Schrag, 2005; see also Poussart et al., 2006, who report on other seasonal changes in wood chemistry). Furthermore, variations around the mean annual isotopic cycle reflect seasonal changes in factors affecting ^{18}O, namely, evaporative enrichment of leaf water oxygen isotopes (mainly during the dry season) and an enhanced amount effect that leads to isotopic depletion of ^{18}O when convective rainfall amounts are especially high (Figure 13.33). Thus, Anchukaitis and Evans (2010) were able to identify a strong ENSO signal in *Pouteria* trees from the Monteverde cloud forests of Costa Rica. During El Niño years, rainfall in this region is low, leading to evaporative enrichment of leaf water, so that wood produced in those periods was isotopically heavier than in wetter years. A similar effect was observed in different tree species from Java (Indonesia) where El Niños are also associated with drought (Poussart et al., 2004). This suggests that oxygen isotope data from a network of trees across the tropical Pacific region might provide a valuable long-term record of ENSO variability (Evans, 2004).

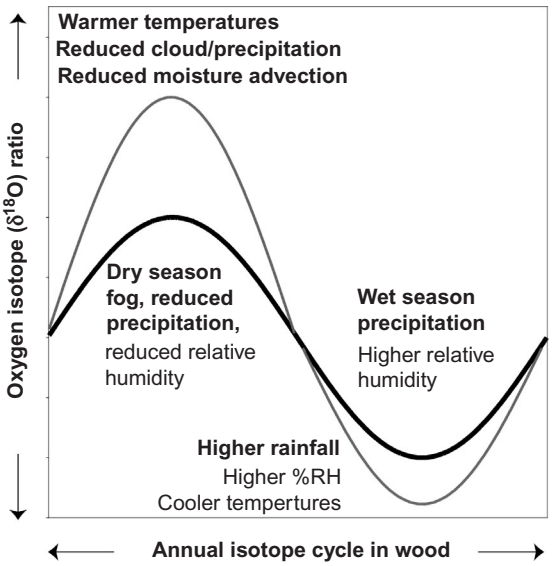


FIGURE 13.33 Conceptual model of climatic controls on the annual and interannual patterns of stable oxygen isotope ratios in the of cloud forest tree radial growth. The annual cycle is generated primarily by the seasonal change in the $\delta^{18}O$ of rainfall, the use of cloud water by trees in the dry season, and the isotopic enrichment of source water by evapotranspiration during the dry season. Interannual variability in annual maximum values is expected to be related to temperature, relative humidity, cloudiness, and moisture advection during the dry season. Anomalies in the annual minima are probably related primarily to wet season precipitation amounts. *From Anchukaitis et al. (2008).*

13.4.2 $\delta^{13}C$

All of the carbon in wood derives from atmospheric carbon dioxide, which is converted to carbohydrates in the leaves of plants through photosynthesis. $\delta^{13}C$ in the atmosphere today is −8‰ (~1.6‰ lower than in preindustrial time, due to the input of isotopically light CO_2 from fossil fuel combustion), but plants discriminate against ^{13}C during photosynthesis; as a result, the $\delta^{13}C$ of wood is generally in the −20 to −30 range. Variations in the $\delta^{13}C$ values of wood from year to year reflect changes in the extent of this discrimination. A critical parameter in the fractionation of ^{13}C is the CO_2 concentration in the intercellular space within leaves. If this is low (perhaps due to a high rate of photosynthesis when growing season temperatures or sunshine totals are high), it leads to a *reduction* in isotopic discrimination, so ^{13}C values remain relatively high. Conversely, if photosynthesis rates are low, and intracellular CO_2 levels remain high, the resulting photosynthates will be more depleted in ^{13}C (Farquhar et al., 1982, 1989; Schleser et al., 1999; McCarroll and Loader, 2004). Thus, $\delta^{13}C$ of wood from mid- and high-latitude trees is generally positively correlated with summer temperature and sunshine duration (Treydte et al., 2007). Similarly, drought conditions cause plants to close stomata (to conserve water), and this also results in a relatively low CO_2 concentration in leaves. Consequently, both warm conditions and dry conditions (which, of course, commonly occur together) will lead to relatively high values of $\delta^{13}C$ in wood. Thus, Kress et al. (2010) found that $\delta^{13}C$ of wood from relatively xeric Alpine sites in the Lötschental of Switzerland was strongly correlated with both temperature and sunshine duration, but negatively related to precipitation amount, so that a composite drought index best captured the overall controls on carbon isotopic fractionation. This enabled a long-term drought reconstruction to be obtained (Figure 13.34). One characteristic of carbon isotope values that could be of great importance is the apparent lack of a biological growth

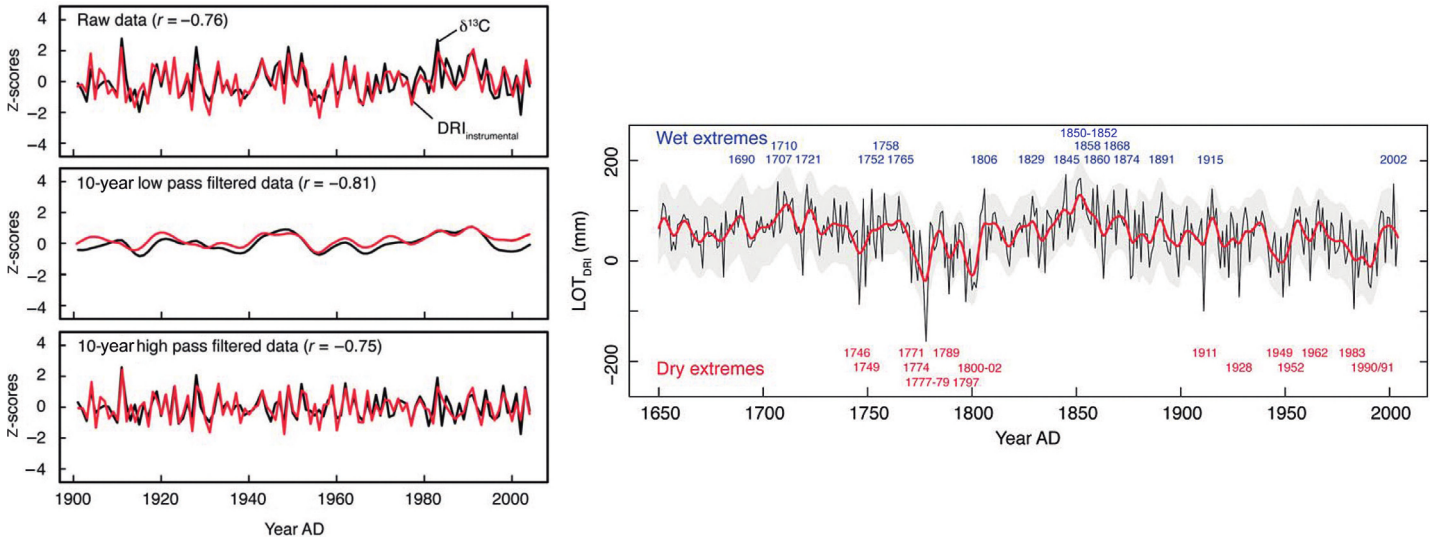


FIGURE 13.34 Left: Carbon isotope series (black) and July-August drought index (DRI) calculated from instrumental temperature and precipitation data (red) for AD 1901-2004. Right: Annually resolved $\delta^{13}C$ drought reconstruction for the Lötschental, Switzerland. 10-year low-pass-filtered record is shown by the bold line, and the gray shadow indicates the estimated error margin. The 20 wettest and driest years are indicated. *From Kress et al. (2010).*

function that affects long-term climate reconstructions from tree-ring widths and (to a lesser extent) latewood density (Gagen et al., 2007). As the processes of isotopic fractionation are not age-dependent, there is no need to remove a low-frequency growth function (the "segment length curse" described by Cook et al., 1995). Carbon isotopes do tend to be low during the first few decades of a tree's growth (due to canopy effects on early tree growth), but this problem is easily overcome by simply eliminating those data values. Furthermore, it appears that interannual carbon isotope variations are highly coherent from tree to tree within a region, so that a regional signal is easily obtained from a small number of samples (i.e., the signal/noise ratio is high). This implies that long-term climate reconstructions, which rely on overlapping wood fragments, may not require a large number of samples to produce a reliable picture of regional isotopic changes over time (McCarroll and Loader, 2004).

Isotopic dendroclimatology is still in its early stages, but the availability of new instruments (such as laser ablation ICP-MS) that will allow a large number of wood samples to be analyzed quickly will likely spur many more studies and provide a more secure footing for this field. It may fulfill its greatest promise in tropical dendroclimatology, and in multiproxy studies that combine several isotopes, and in combination with conventional (ring width and density) dendroclimatology (McCarroll et al., 2003; Gagen et al., 2011).

CHAPTER

14

Corals

OUTLINE

14.1 Coral Records of Past Climate 499
14.2 Paleoclimate from Coral Growth Rates 506
14.3 Luminescence in Corals 506
14.4 $\delta^{18}O$ in Corals 507
14.5 $\delta^{13}C$ in Corals 510
14.6 $\Delta^{14}C$ in Corals 510
14.7 Trace Elements in Corals 511
14.8 Fossil Coral Records 512

Corals have played an important role in paleoclimatology by providing dateable material associated with former sea-level positions. In some areas, reefs have been tectonically uplifted above present sea level (Figure 6.18), providing detailed records of former sea-level position, if the uplift history can be estimated (e.g., Chappell, 2002; Cutler et al., 2003). Questions related to stratigraphy, dating, diagenetic changes, etc., add additional uncertainties (Medina-Elizalde, 2013). Nevertheless, with appropriate sample selection, corals can provide independent checks on the timing and magnitude of sea-level changes, as reconstructed from marine sediments (e.g., Siddall et al., 2003; Rohling et al., 2009; Grant et al., 2012). Sea-level changes are discussed further in Chapter 6, Section 6.3.5. Here, the focus is on the paleoclimatic record captured during growth of the corals.

14.1 CORAL RECORDS OF PAST CLIMATE

The term "coral" is generally applied to members of the order Scleractinia, which have hard calcareous skeletons supporting softer tissues (Wood, 1983; Veron, 1993). For paleoclimatic studies, the important subgroups are the reef-building, massive corals (Figure 14.1) in

Copyright © 2015 Raymond S. Bradley.
Published by Elsevier Inc. All rights reserved.

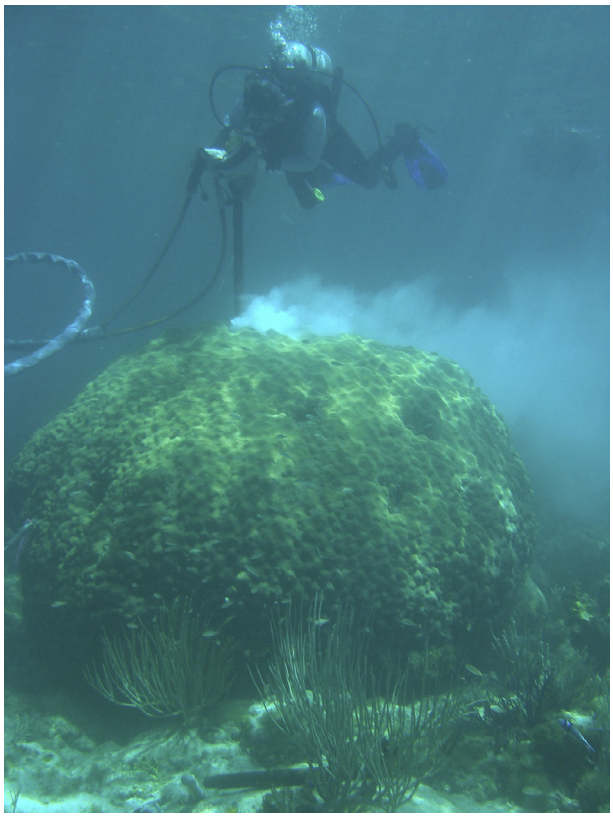


FIGURE 14.1 Drilling a core from large *Montastraea faveolata* colonies in the Dry Tortugas, National Park, the westernmost Florida Key. *Photograph kindly provided by Kristine DeLong and the USGS Coastal and Marine Science Center, St. Petersburg, Florida.*

which the coral polyp lives symbiotically with unicellular algae (zooxanthellae); these are known as hermatypic corals (as opposed to ahermatypic, which contain no algal symbionts and are not reef builders). The algae produce carbohydrates by photosynthesis and thus are affected by the availability of light, which varies with water depth (most growing between 0 and 20 m), water turbidity, and cloudiness. Much of the organic carbon fixed by the algae diffuses from the algal cells, providing food for the coral polyps that, in turn, provide a protective environment for the algae. Reef-building corals are limited mainly by temperature and most are found within the 18 °C mean annual sea-surface temperature (SST) isotherm (generally between 30°N and 30°S). When temperatures fall below 18 °C, the rate of calcification (skeletal growth) is significantly reduced and sustained lower temperatures may lead to death of the colony. Sclerosponges (calcareous sponges, such as *Ceratoporella nicholsoni*) from well below the ocean surface have also been analyzed to obtain a record of past changes in water temperature at depth (e.g., Haase-Schramm et al., 2003). Outside of the Tropics, deep-sea corals have been recovered, and these can provide unique high-resolution windows into oceanographic conditions, such as ventilation rates or water mass movements in the past (e.g., Adkins et al., 2002b, 2004; Robinson and van der Flierdt, 2008; Colin et al., 2010; Copard et al., 2012). In the following section, the focus is on reef-building corals from the Tropics,

most commonly colonies of the boulder-like *Porites* or *Montastraea*, though several other species are emerging as good proxies, namely, *Siderastrea siderea*, *Diploria strigosa*, *Diploria labyrinthiformis*, and *Diploastrea heliopora*.

New carbonate is added to the surface of a coral colony each year, incorporating isotopic and geochemical tracers that reflect the ambient environmental conditions (Felis and Pätzold, 2004; Lough, 2010). Coral growth rates (typically ~0.5-2 cm/year) vary over the course of a year; when sectioned and X-rayed, an alteration of high- and low-density bands can be seen, representing an annual growth increment (Figure 14.2). High-density layers are produced during times of highest SSTs (Fairbanks and Dodge, 1979; Lough and Barnes, 1990), providing a chronological framework for subsequent analyses. Dating in this way is fairly accurate as shown by the close correspondence between large excursions in $\delta^{18}O$ and known El Niño/Southern Oscillation (ENSO) events (Cole et al., 1992) and by very close similarity between annual counts and precise ^{230}Th dates on individual bands (Dunbar et al., 1994; Shen et al., 2008). However, significant improvements in the reliability of chronologies and an increase in the signal/noise ratio of paleoclimate signals in corals are obtained by cross dating multiple coral records, following well-tested methods in dendrochronology (e.g., Hendy et al., 2003; DeLong et al., 2013).

Samples for analysis are microdrilled from the coral slab or core at regularly spaced intervals along the growth axis or along particular skeletal elements. Assigning the precise seasonal time to each sample can be problematical and is usually done by assuming a linear growth rate between the more dense marker bands, the edge of which is assigned to the "onset" of high SSTs, to produce a "mean annual" signal. However, if coral extension (growth) is nonlinear, detailed sampling (6-12 samples per year) is required or the samples may not recover the entire seasonal range and provide only minimum estimates on total interannual variability. Furthermore, under extreme conditions (often associated with major El Niño/-Southern Oscillation (ENSO) events), coral growth in some areas may even cease, so that the real extremes may go unrecorded in corals from those regions.

Coral studies have focused mainly on the environmental record in coral growth rates, isotopes, and trace elements incorporated into the coral structure (Corrège, 2006; Grottoli and Eakin, 2007). This has led to new information about paleo-SSTs, rainfall, river runoff, ocean circulation, and modes of ocean-atmospheric circulation, such as ENSO or the Indian Ocean Dipole. Many studies have been based on relatively short periods of time (the last few decades) to provide a better understanding or calibration of the parameter being analyzed, thereby increasing confidence in the paleoreconstructions (e.g., Lough and Barnes, 1997; Quinn and Sampson, 2002; Smith et al., 2006; Goodkin et al., 2007; McGregor et al., 2011). So far, only a few studies spanning more than the last 200 years have been published (Table 14.1; Figure 14.3); to reduce analytical costs, many other studies have just examined short windows of time within the last few centuries (e.g., Winter et al., 2000; Zinke et al., 2004). Besides these studies of relatively modern corals, corals dating back to the last interglacial, or even earlier, are often found in raised marine terraces throughout the Tropics. Providing diagenetic changes in the coral aragonite have not occurred (Bar-Matthews et al., 1993), it may be possible to reconstruct SSTs (and annual variations in SSTs) for selected intervals in the past (e.g., Gagan et al., 2000; Cobb et al., 2003).

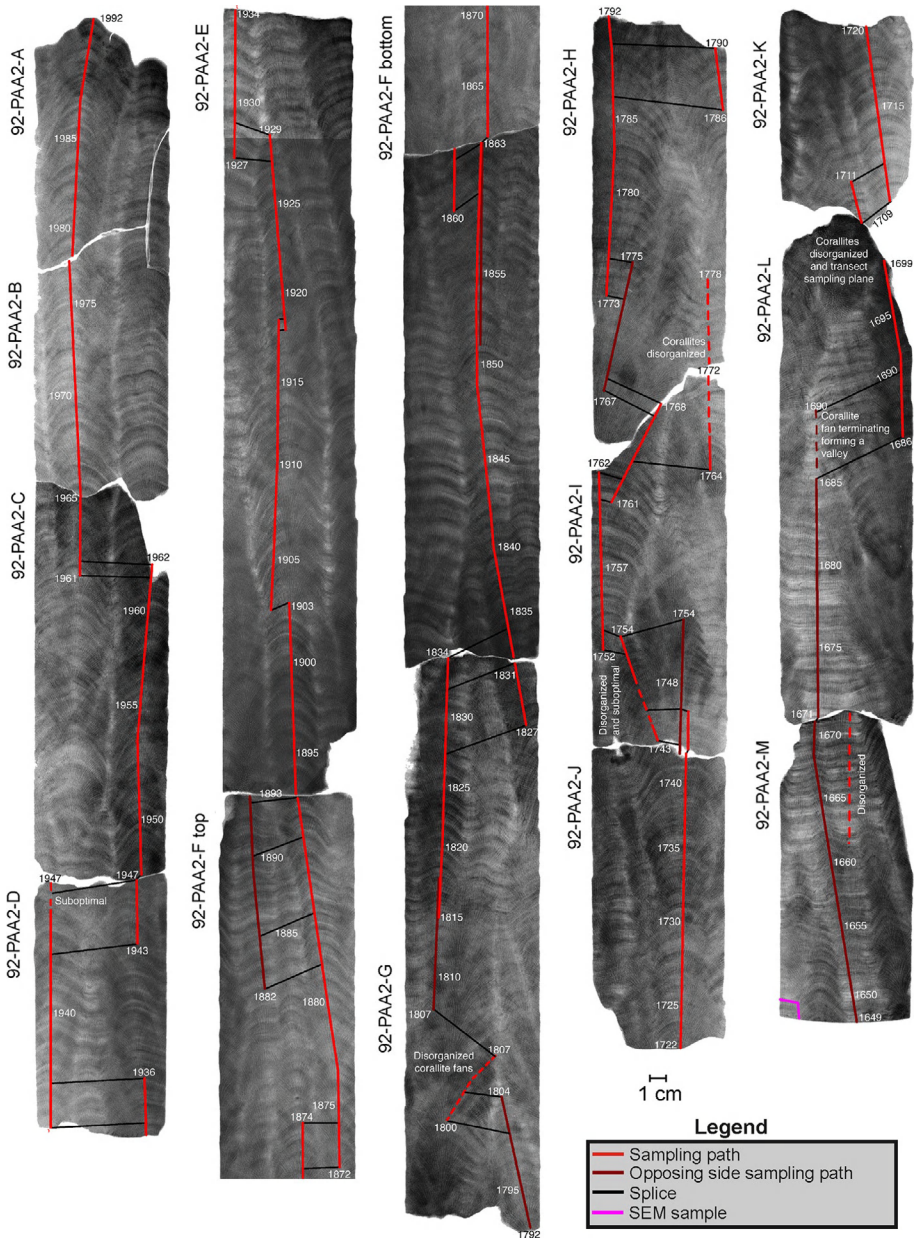


FIGURE 14.2 Positive X-radiograph of a coral slab of *Porites lutea* from Amédée Island, New Caledonia (22.5°S and 166.5°E). Denser layers appear darker. Red lines show sampling trajectories, and years counted are shown by the dates in white. *From DeLong et al. (2013).*

TABLE 14.1 Coral-Based Records of Past Climate that Continuously Span the Last 200 Years or More

Location	Latitude, Longitude	Record Length	Parameter	Indicator of	References
Bermuda	32°N, 65°W	~1180-1986	Growth rate	SST/upwelling	Pätzold et al. (1999), Berger et al. (2002)
Red Sea	28°N, 38°E	1751-1994	$\delta^{18}O$	SST, NAO/AO	Felis et al. (2000)
S. Florida	25°N, 80°W	1745-1986	$\delta^{18}O$	Rainfall/runoff	Swart et al. (1996)
Yucatan	21°N, 87°W	1773-2009	Growth rate	SST	Vasquez-Bedoya et al. (2012)
N.W. Jamaica	19°N, 78°W	1356-1991	Sr/Ca[a]	Temperature	Haase-Schramm et al. (2003)
Bahamas	18°N, 88°W	1552-2001	Growth rate	SST	Saenger et al. (2009)
Guam	14°N, 145°E	1790-2000	$\delta^{18}O$	SST, SSS, ENSO	Asami et al. (2005)
Gulf of Chiriquí, Panama	8°N, 82°W	1707-1984	$\delta^{18}O$	Rainfall/ITCZ position	Linsley et al. (1994)
Isabel Island	0.4°S, 91°W	1587-1953	$\delta^{18}O$	SST	Dunbar et al. (1994)
Galápagos			$\Delta^{14}C$	Upwelling	Druffel et al. (2007)
Malindi, Kenya	3°S, 41°E	1705-1997	Ba/Ca	River runoff/erosion	Fleitmann et al. (2007b)
Bali	8°S, 116°E	1783-1990	$\delta^{18}O$	SST, IOD	Charles et al. (2003)
Great Barrier Reef, NE Queensland	17-23°S, 46-151°E	1631-1957	Luminescence	River runoff/flooding	Lough (2007, 2011)
Abraham Reef	22°S, 167°E	1479-1985	Growth rate	SST	Lough and Barnes (1997)
Rarotonga	22°S, 160°E	1726-2000	Sr/Ca	SST, PDO	Linsley et al. (2000, 2006)
					Ren et al. (2002)
New Caledonia	22°S, 166°E	1658-1993	$\delta^{18}O$, $\delta^{13}C$	SST	Quinn et al. (1998)
New Caledonia	23°S, 167°E	1649-1999	Sr/Ca	SST	DeLong et al. (2012)
Great Barrier Reef, Australia	22°S, 153°E	1635-1957	$\Delta^{14}C$	Oceanic advection and/or upwelling	Druffel and Griffin (1993)

Continued

TABLE 14.1 Coral-Based Records of Past Climate that Continuously Span the Last 200 Years or More—cont'd

Location	Latitude, Longitude	Record Length	Parameter	Indicator of	References
Abrolhos Is., W. Australia	29°S, 114°E	1795-1993	$\delta^{18}O$, $\delta^{13}C$	SST	Kuhnert et al. (1999)
Fiji	17°S, 179°E	1617-2001	$\delta^{18}O$	SST	Linsley et al. (2008)
Tonga	20°S, 175°W	1650-2004	$\delta^{18}O$	SST	Linsley et al. (2004)
Ifaty, Madagascar	23°S, 44°E	1659-1995	$\delta^{18}O$	SST, IOD	Zinke et al. (2004, 2005)
Great Barrier Reef	18°S, 146°E	1612-1985	$\delta^{18}O$, Sr/Ca	SST, salinity	Hendy et al. (2002)
Bermuda	32°N, 64°W	1781-1988	Sr/Ca $\delta^{18}O$	SST, salinity	Goodkin et al. (2005, 2008)
			$\delta^{13}C$ $\Delta^{14}C$	Ocean mixing	Goodkin et al. (2012)
Puerto Rico	17°N, 67°W	1751-2004	Sr/Ca $\delta^{18}O$,	SST	Kilbourne et al. (2007, 2008, 2010)
			$\Delta^{14}C$	Ocean mixing	
Puerto Rico	17°N, 69°W	1700-1989	Luminescence	SST, hurricanes	Nyberg et al. (2007)
Great Barrier Reef	18°S, 146°E	1644-1986	Fluorescence	River runoff	Isdale et al. (1998)
Great Barrier Reef	18°S, 146°E	1572-2001	Extension rate, density (calcification)	SST?, stress	De'Ath et al. (2009)
Bali	8°S, 115°'E	1782-1990	$\delta^{18}O$	SST, ENSO, monsoon	Charles et al. (2003)
Coral Sea	18°S, 148°E	1708-1992	Sr/Ca $\delta^{18}O$	Salinity, IPO	Calvo et al. (2007)
Bahamas	25°N, 78°W	1552-1991	Linear growth	SST	Saenger et al. (2009)
Fiji	16°S, 178°W	1617-2004	$\delta^{13}C$	Suess effect	Dassié et al. (2013)
Ha'afera, Tonga	20'S, 175°W	1793-2004	Sr/Ca $\delta^{18}O$	Salinity, SPCZ	Wu et al. (2013)

ENSO, El Niño/Southern Oscillation; IOD, Indian Ocean Dipole; PDO, Pacific Decadal Oscillation; NAO, North Atlantic Oscillation; AO, Arctic Oscillation, IPO, Interdecadal Pacific Oscillation; SPCZ, South Pacific Convergence Zone.
[a]*Sclerosponge from −20 m.*

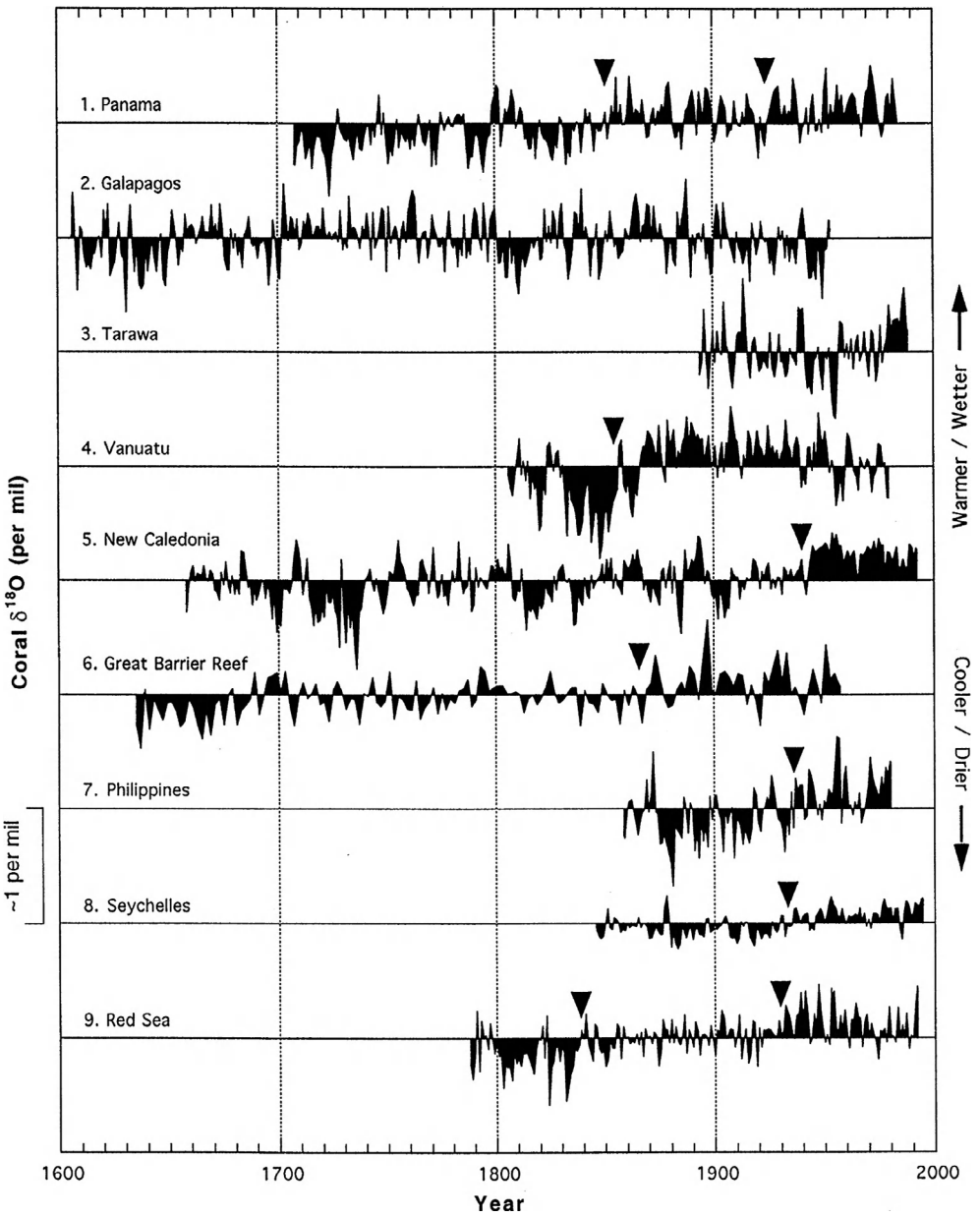


FIGURE 14.3 A selection of recent coral $\delta^{18}O$ records from the Atlantic, Pacific and Indian Ocean, and the Red Sea. Lower values of $\delta^{18}O$ result from warmer and or wetter conditions. *From Gagan et al. (2000).*

14.2 PALEOCLIMATE FROM CORAL GROWTH RATES

Coral growth rates are dependent on a variety of factors, including SSTs and nutrient availability (Lough et al., 1996; Lough and Cooper, 2011). The longest record of coral growth rate variations is an 800-year record from a massive coral head (*Montastraea cavernosa*) in Bermuda (Pätzold et al., 1999; Berger et al., 2002). In this region, growth rates are inversely related to SST, since cool upwelling water is nutrient-rich, causing coral growth to increase. The record shows that SSTs were generally above the long-term mean from ~1250 to 1470. Coolest conditions were experienced from ~1470 to 1710 and from ~1760 to the end of the nineteenth century, followed by twentieth-century warming. Growth rates were also used as a proxy for SSTs in a study of corals from the Bahamas (Saenger et al., 2009). They found that the lowest temperatures of the last ~450 years were from ~AD 1650 to 1730, when SSTs were ~1 °C lower than in the twentieth century. These studies reveal overall changes in SSTs that are broadly similar to estimates of Northern Hemisphere summer temperature change over the same period of time (Bradley et al., 2003b; Mann et al., 2009). Placing coral growth parameters (skeletal density, linear extension, and calcification rates) in a long-term context is especially important today, in view of concerns about the viability of coral colonies under the dual anthropogenic threats of rising ocean temperatures and ocean acidification. Indeed, the evidence so far is not encouraging, with significant declines in coral growth in recent years in many parts of the Tropics (Cooper et al., 2008; Cantin et al., 2010; Lough and Cooper, 2011).

14.3 LUMINESCENCE IN CORALS

In some regions, exceptional runoff events from adjacent continents are recorded by fluorescent bands in corals (visible under UV light) (Isdale, 1984; Hendy et al., 2003). These bands result from terrestrially derived fulvic acid being incorporated into the coral structure (Boto and Isdale, 1985). Luminescence can thus be used as a proxy for river runoff (Lough, 2007). Since runoff into the coastal waters of the Great Barrier Reef is largely derived from summer rainfall from tropical cyclones, Lough (2011) used the luminescence signal calibrated against rainfall amount, to reconstruct northeastern Queensland summer rainfall totals back to AD 1685 (Figure 14.4). This showed that rainfall was generally below the 1901-1980 mean from ~AD 1760 to 1850 and became more variable thereafter. A strong correlation with ENSO was detected; wet periods generally correspond to La Niña events, which are often associated with an increase in the frequency of tropical cyclones affecting the region. Luminescence in corals was also used as an indicator of hurricane frequency (which strongly affects coastal runoff) in the northern Caribbean (Nyberg et al., 2007). This suggests that hurricane frequency in this region steadily declined over the period ~AD 1750-1995. Finally, Grove et al. (2013) examined luminescence in corals from the coast of northeastern Madagascar, spanning the last ~300 years. After correcting for anthropogenic effects on runoff, due to deforestation, they concluded that rainfall in the region is strongly modulated by the Pacific Decadal Oscillation (PDO), with positive phases of the PDO associated with increased rainfall and associated runoff in the region.

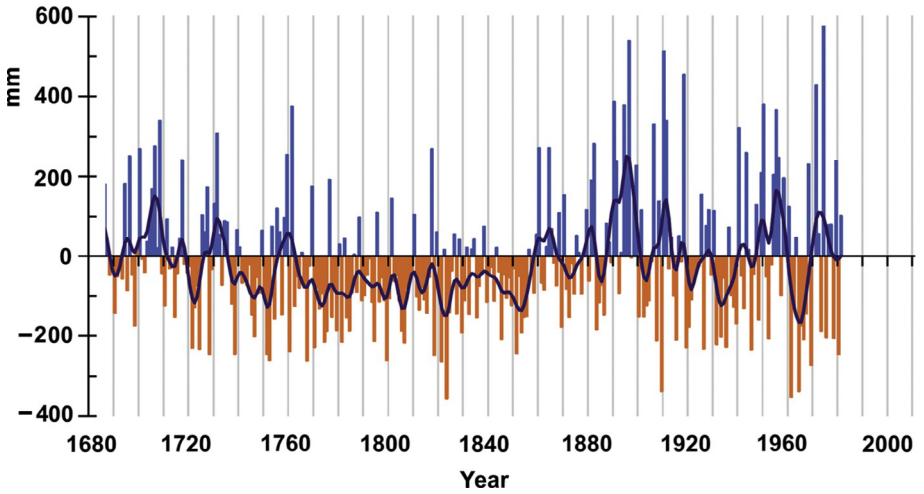


FIGURE 14.4 A reconstruction of northeastern Queensland (Australia) summer rainfall totals based on the luminescence signal in a set of corals from the Great Barrier Reef. Anomalies are expressed relative to the 1901-1980 (calibration period) average. *From Lough (2011).*

14.4 δ^{18}O IN CORALS

It has long been known that a temperature-dependent fractionation of oxygen isotopes occurs when biological carbonate is precipitated from solution (Epstein et al., 1953). δ^{18}O decreases by ~0.22‰ for each 1 °C increase in temperature. Seasonal variations in δ^{18}O along the growth axis of a coral and their relationship to seasonal SST variations were first reported by Emiliani et al. (1978) and Fairbanks and Dodge (1979). Subsequently, Dunbar and Wellington (1981) also showed that, if finely sampled, coral δ^{18}O can provide an intra-annual record of SST changes (Figure 14.5). Offsets from predicted equilibrium values may be caused by vital effects (cf. Section 6.3.1) but these are constant for a given genus (Weber and Woodhead, 1972). δ^{18}O in Caribbean coral samples for selected time intervals during the last few centuries were compared with recent values by Winter et al. (2000), suggesting that temperatures were 2-3 °C cooler in the late eighteenth and early nineteenth centuries compared to the 1980s (Figure 14.6). These estimates are supported by other reconstructions using Mg/Ca (Watanabe et al., 2001) and Sr/Ca and δ^{18}O (Kilbourne et al., 2008, 2010). The lower temperatures were likely brought about by more frequent cold air outbreaks from the North American continent during the Little Ice Age and/or a southward shift in the ITCZ (Kilbourne et al., 2010).

In those areas of the Tropics, such as the equatorial regions, where seasonal temperature variability is low, a simple SST-δ^{18}O relationship may not be not found. In areas with seasonally heavy rainfall, which is depleted in δ^{18}O during convective activity, the ocean surface mixed layer becomes isotopically light during the wet season, producing a pronounced seasonal signal in coral δ^{18}O (Cole and Fairbanks, 1990; Linsley et al., 1994). In some regions, this effect is brought about, or enhanced, by flooding of near-coastal waters by isotopically light river water discharged from the continents (McCulloch et al., 1994). Conversely during prolonged hot, dry conditions, surface evaporation can increase sea-surface salinity (SSS) and

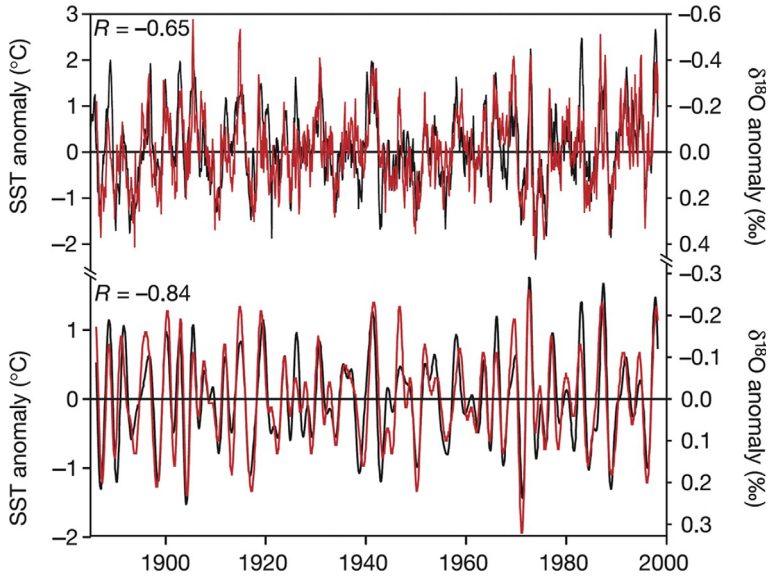


FIGURE 14.5 The relationship between $\delta^{18}O$ in modern corals (red) from Palmyra Island, southwest Pacific (6°N and 162°W) and the instrumental record of SSTs in the Niño 3.4 region of the central Pacific (5°N-5°S and 120°-170°W) (black). In the lower diagram, a 2-7-year band-pass filter has been applied to the data. A highly significant correlation between $\delta^{18}O$ and temperature is seen, such that higher temperature anomalies correspond to more negative $\delta^{18}O$ values. *From Cobb et al. (2003).*

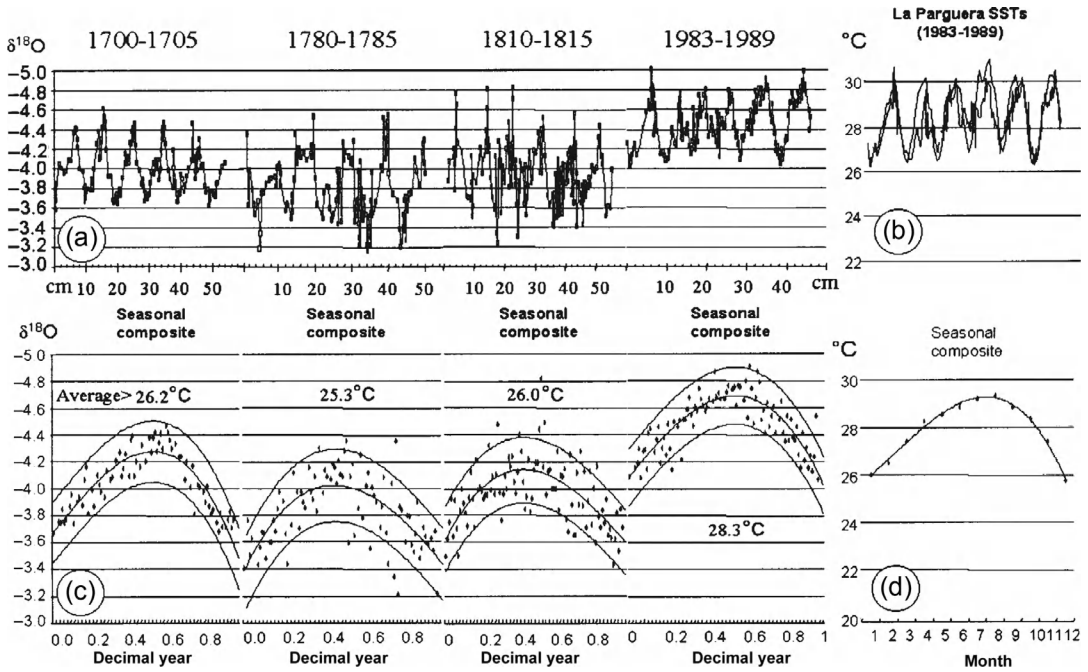


FIGURE 14.6 (a) $\delta^{18}O$ measured in coral samples from off the southwestern coast of Puerto Rico for selected time intervals during the Little Ice Age, compared to recent values (1983-1989); (b) measured SSTs from the region; (c) average seasonal ranges derived from the values shown in (a); (d) Seasonal variation in SSTs. A regression of $\delta^{18}O$ on temperature indicates that the mean temperatures during the selected time windows were 2-3 °C cooler than in the 1980s, as indicated in (c). *From Winter et al. (2000).*

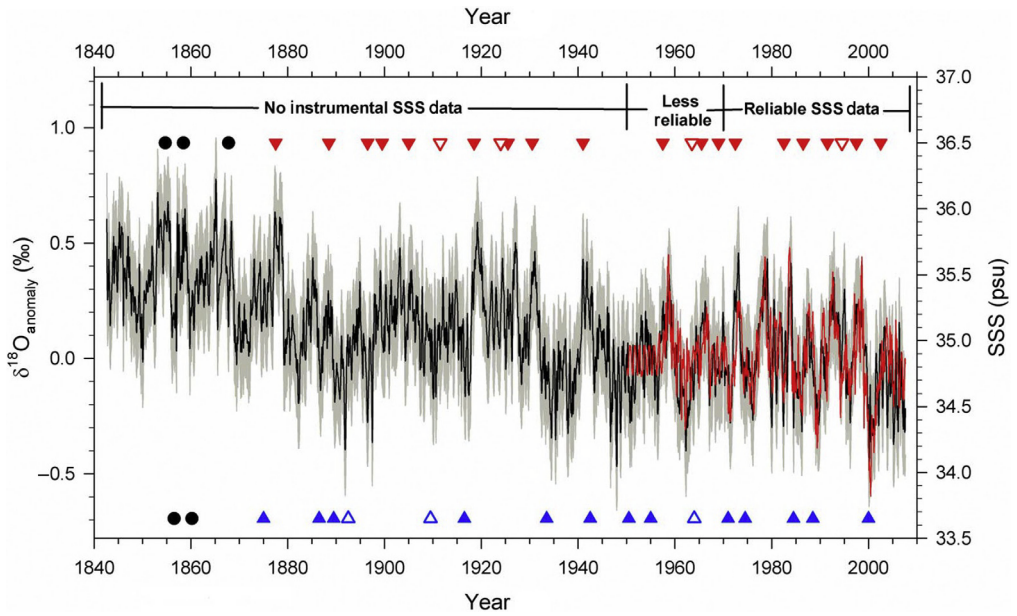


FIGURE 14.7 Sea-surface salinity reconstruction from Vanuatu, in the South West Pacific (black line) and observed salinity record (red line). La Niñas in this region (blue triangles) are associated with low salinity and El Niños with high salinity (red triangles). Open triangles show those events not recorded by the coral reconstruction; black dots show ENSO events that were identified in the preobservational period. The long-term trend is thought to be related to interdecadal changes in surface water advection. *From Gorman et al. (2012).*

lead to isotopic enrichment (higher values of $\delta^{18}O$) due to the preferential removal of ^{16}O. Ideal locations would thus be where there are either large annual changes in rainfall (e.g., Cole et al., 1993; Linsley et al., 1994) or large SST changes with little change in SSS (e.g., Dunbar et al., 1994), or where warm-wet and cold-dry seasons occur (resulting in an additive effect on coral $\delta^{18}O$) (e.g., Cahyarini et al., 2008). For example, in parts of the western Pacific, El Niños are associated with unusually heavy rainfall. At Tarawa Atoll (1°N and 172°E), negative $\delta^{18}O$ excursions of 0.6 ± 0.1‰ occur during ENSO events as a result of dilution of the mixed layer by isotopically depleted rainfall (Cole and Fairbanks, 1990). In this region, the anomalies provide a diagnostic signal of ENSO events in the past (Figure 14.7) (Gorman et al., 2012). By identifying the appropriate regional ENSO signal in different parts of the Pacific Ocean, it is possible to reconstruct the spatial and temporal characteristics of ENSO events (both "warm" and "cold") far back in time (Cole et al., 1992; Cobb et al., 2013; Hereid et al., 2013).

In areas that experience extreme SST anomalies during ENSO events, $\delta^{18}O$ in corals may provide a unique record of such occurrences and provide a longer perspective on ENSO variability than can be obtained from the short period of instrumental records (e.g., Carriquiry et al., 1994). Using the coral *Pavona clavus* from the Galápagos Islands, Dunbar et al. (1994) reconstructed SST variations over the past 380 years from the $\delta^{18}O$ record. This shows that of the 100 largest negative $\delta^{18}O$ anomalies over the last 350 years (indicating extremely high SSTs in the region), 88 corresponded (± 1 year) to Quinn's (1992) chronology of El Niño events,

derived from historical sources. Dunbar et al. then examined the changing pattern of dominant periodicities in the record using evolutionary spectral analysis. This involved applying spectral analysis to the data sequentially, in overlapping intervals of time (in this case, 120-year intervals, from 1610-1730 to 1862-1982) in order to map out the time/frequency response of SSTs in this area. The analysis revealed several shifts in the dominant frequency modes; in the early 1700s, the quasiperiodic El Niño events shifted from the 4.6-7-year band to 4.6 and 3 years. A second shift occurred in the mid-1800s to a predominant period around 3.5 years (cf. Braganza et al., 2009). Similarly timed changes in the dominant lower-frequency variance are also seen, especially in the mid-1800s, from ~33 to ~17 years. It is interesting that a pronounced change (toward warmer and/or dryer conditions) also occurred in the mid- to late 1800s across South Pacific, as recorded by a number of coral records from the region (Quinn et al., 1993; Hendy et al., 2002; Linsley et al., 2004).

14.5 $\delta^{13}C$ IN CORALS

$\delta^{13}C$ in coralline carbonates is affected by a variety of factors, including the $\delta^{13}C$ of seawater (related, in part, to the relative contributions of surface and upwelled waters), the fractionation of carbon isotopes during algal photosynthesis and physiological processes within corals. Since algae preferentially take up ^{12}C from dissolved inorganic carbon (DIC) in ocean waters, higher rates of photosynthesis lead to DIC becoming enriched in ^{13}C (less negative $\delta^{13}C$), which in turn affects the $\delta^{13}C$ of the skeletal carbonate being constructed (McConnaughey, 1989). Several studies have shown that $\delta^{13}C$ declines with water depth (e.g., Fairbanks and Dodge, 1979) and during cloudy months (i.e., as photosynthesis rates are reduced) (e.g., Shen et al., 1992a; Quinn et al., 1993), suggesting $\delta^{13}C$ in coral bands might provide a long-term index of cloudiness. However, complications related to coral geometry (varying growth rates and photosynthetic activity around a coral head) and possible nonlinear photosynthetic responses to changing light levels have generally assigned $\delta^{13}C$ records a backseat to $\delta^{18}O$ in stable isotope paleoclimatic reconstructions from corals. However, $\delta^{13}C$ in corals does appear to be an important tracer of the oceanic uptake of anthropogenic CO_2 (and thus ocean acidification) by tracking the $\delta^{13}C$ composition of dissolved inorganic carbon in surface waters of the ocean (Swart et al., 2010).

14.6 $\Delta^{14}C$ IN CORALS

Changes in oceanic mixed layer $\Delta^{14}C$ (i.e., ^{14}C anomalies from long-term trends) are related to either changes in atmospheric ^{14}C levels or to upwelling of ^{14}C-depleted waters from the deep ocean. $\Delta^{14}C$ anomalies are also recorded in tree rings, and, therefore, changes observed in corals that are not seen in tree rings are presumably related to changes in oceanic circulation, indicating either coral upwelling or advection of ^{14}C depleted (or enriched) waters from other regions. Thus, Druffel and Griffin (1993) related unusually large excursions of $\Delta^{14}C$ values in corals from the southwestern Great Barrier Reef between 1680 and 1730 to changes in the relative contributions of waters from the South Equatorial Current ($\Delta^{14}C \sim -60‰$) and the East Australia current ($\Delta^{14}C \sim -38‰$). Similarly, Druffel et al. (2007) found intervals of

low $\Delta^{14}C$ in corals from the Galápagos and suggested that those were periods when strongly depleted Subantarctic waters were entrained into the equatorial undercurrent that crosses the Pacific from west to east. This water eventually upwelled around Galápagos Archipelago, as recorded by $\Delta^{14}C$ in the corals. Corals from southwestern Puerto Rico were used by Kilbourne et al. (2007) to decipher variations in equatorial waters (depleted in ^{14}C) versus subtropical waters (relatively enriched in ^{14}C) over the last 250 years. They found that quite large changes in the proportions of these different water masses have occurred, on both interannual and interdecadal timescales.

14.7 TRACE ELEMENTS IN CORALS

Because certain elements (Sr, Ba, Mn, Cd, and Mg) are chemically similar to Ca, trace amounts of these elements may be found in coral skeletal carbonate. Many studies have shown that the relative concentration of such elements (expressed as the ratio of the trace element to calcium) often provides a paleoclimatic or paleoceanographic signal (Shen and Sanford, 1990). For example, because Cd levels are generally much higher below the mixed layer, Cd/Ca ratios in Galápagos corals increase in association with seasonal upwelling (Shen et al., 1987). Ba/Ca ratios are inversely related to SSTs (Lea et al., 1989) so low Cd/Ca and Ba/Ca ratios provide a useful index of El Niño events (in the Galápagos area) because such events are associated with very high SSTs and minimal upwelling. Mn/Ca ratios also provide valuable information in some regions; for example, in the west-central Pacific, Mn is remobilized from lagoonal sediments during strong episodes of equatorial westerly winds (associated with El Niños), and thus large Mn/Ca ratios in corals are indicative of such conditions (Shen et al., 1992a,b). Elsewhere, Mn/Ca (and perhaps also Ba/Ca) ratios may provide information on runoff from continental regions since terrestrial material is rich in Mn and Ba compared to ambient levels in the oceanic mixed layer. For example, Fleitmann et al. (2007b) examined Ba/Ca ratios for the last ~300 years in a coral from off the coast of Kenya as an index of soil-derived sediments from the adjacent land areas. This revealed individual annual anomalies that could be related to heavy rainfall episodes, but an overall long-term increase in Ba/Ca was ascribed to increased soil erosion due to poor agricultural practices rather than a systematic increase in rainfall.

Sr/Ca ratios (and to a lesser extent, Mg/Ca and U/Ca) are important paleotemperature indicators in corals (Figure 14.8) (McCulloch et al., 1994; Min et al. 1995; Mitsuguchi et al., 1996). Sr/Ca and observed SSTs are often strongly correlated providing a reliable basis for paleotemperature reconstructions (Quinn and Sampson, 2002). However, Sr/Ca (and perhaps Mg/Ca) ratios may be dependent on coral growth rate in some slower-growing species or in slower-growing regions of a colony (DeLong et al., 2013). This may lead to lower paleotemperature estimates in coral sections with low growth rates (below the species-specific threshold) compared to those derived from faster-growing sections of the same coral. To take this into account, Goodkin et al. (2007) used a combination of samples from different slow-growing *D. labyrinthiformis* coral colonies, combined with growth rate and Sr/Ca data, to establish a strong calibration between Sr/Ca and SSTs that could be widely applied across different sites. However, colonies with faster growth rates of the same genera (*D. strigosa*) exhibit no growth-related dependence in coral Sr/Ca (Giry et al., 2010).

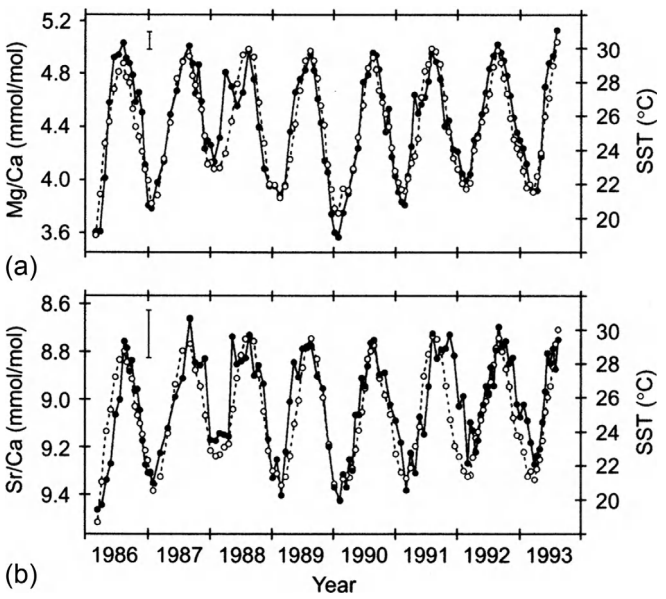


FIGURE 14.8 Comparison between recorded SSTs (3-week averages of daily temperatures) at a tidal station on the Ryukyu Islands, Japan (dashed lines), and geochemical variations in a nearby coral: (a) Mg/Ca ratios ($r = 0.92$); (b) Sr/Ca ratios ($r = 0.85$). Analytical error bars are indicated; these amount to $\pm 0.5^\circ$ and $\pm 1.6^\circ$ C, respectively. *From Mitsuguchi et al. (1996).*

DeLong et al. (2012) analyzed a number of corals from New Caledonia in the southwestern Pacific in great detail (~12 Sr/Ca samples per year), spanning the period from 1649 to 1999. Observed SSTs over recent decades, and Sr/Ca ratios were highly correlated enabling a 350-year SST reconstruction to be produced (Figure 14.9). This shows that temperature gradually declined from the mid-seventeenth century to a minimum in the mid-nineteenth century before gradually increasing to the present. Strong multidecadal scale variability superimposed on those trends is related to the large-scale South Pacific Decadal Oscillation (perhaps a low-frequency manifestation of ENSO variability) that has been recognized in SST and rainfall patterns across the region (Shakun and Shaman, 2009; Hsu and Chen, 2011).

14.8 FOSSIL CORAL RECORDS

It is clear from Table 14.1 that the number of long coral records extending back continuously from the present day is quite limited, but in some areas fossil coral, samples have been collected, providing snapshots of past conditions that can be compared with data from modern samples (Gagan et al., 2000). For example, Cobb et al. (2003) obtained fossil corals from Palmyra Island (6°N, 162°W) in the central Pacific. At this location, SSTs are strongly correlated with ENSO variations; El Niños are associated with warm and wet conditions, which are recorded as negative $\delta^{18}O$ anomalies in the coral. The age range of the fossil samples was delimited by U/Th dates, and then high-resolution sampling was conducted for $\delta^{18}O$ analysis. This revealed common interannual to multidecadal-scale oscillations in corals that overlapped in age. Splicing many records together then produced a long-term perspective on SST/salinity variations in the central Pacific over the last millennium, from AD 982 to 1998 (Figure 14.10). This showed that El Niños and La Niñas in the late seventeenth century

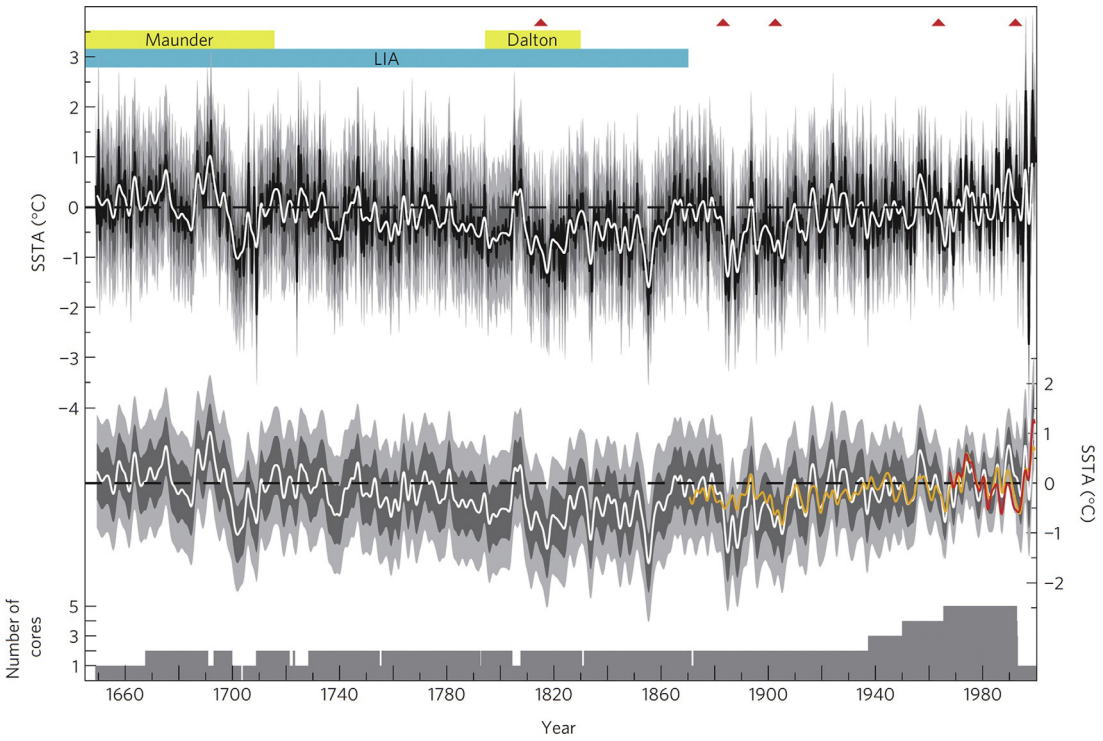


FIGURE 14.9 Upper graph: Monthly sea-surface temperature anomalies from 1667 to 1992 (relative to the 1961-1990 mean) reconstructed from more than 14,000 Sr/Ca measurements in corals from New Caledonia in the southwestern Tropical Pacific. Black and white lines are 7- and 36-month low-pass filtered data, respectively. Lower graph: The 36-month filtered data shown with estimated 1 and 2 SD errors (gray shading). Red and orange lines show instrumentally recorded SSTs. Histogram below shows the number of cores used in the analysis. Periods of reduced solar activity are shown in yellow; major explosive eruptions are indicated by the red triangles. *From DeLong et al. (2012).*

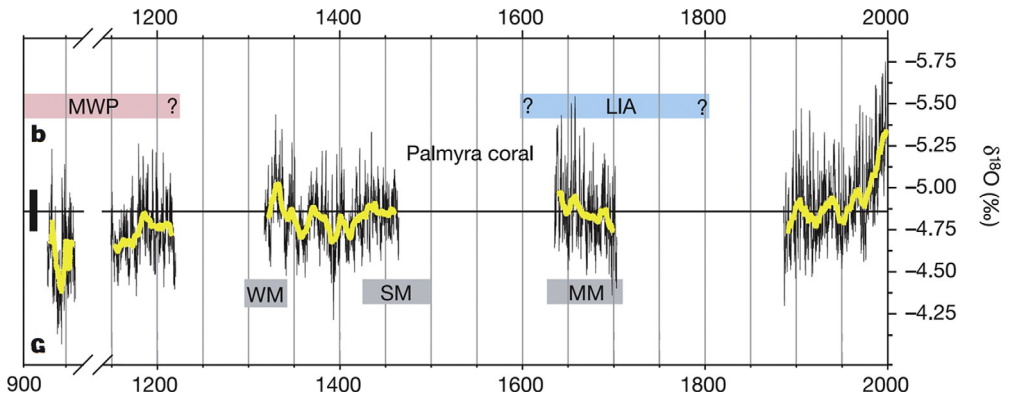


FIGURE 14.10 Oxygen isotopes in modern and fossil corals from Palmyra Island, southwestern Pacific. Less negative values (plotted inversely) are indicative of cooler and/or drier conditions in the past. Such conditions in this region are commonly associated with La Niñas. *From Cobb et al. (2003).*

were more frequent and of greater amplitude than the region has experienced in the twentieth century. By contrast, ENSO variability in the twelfth and mid-fourteenth century was quite subdued. The overall record also indicates that there have only been small changes in SSTs on the centennial scale (after estimating the effects of salinity changes) but conditions in the tenth century were likely to have been significantly cooler and/or drier than in the late twentieth century, suggesting more La Niña-like conditions at that time.

Many other short fossil records, extending back to 350 ka BP in absolute age, have been analyzed (Table 14.2). Sr/Ca in corals from the Great Barrier Reef of Australia showed that

TABLE 14.2 Some Examples of Fossil Coral Records

Site	Parameter	Sample age (ka BP)	References
Bermuda	$\delta^{18}O$	AD 1520-1603	Kuhnert et al. (2002)
Misima Island, Papua New Guinea	$\delta^{18}O$, Sr/Ca	AD 1411-1644	Hereid et al. (2012)
Palmyra Island	$\delta^{18}O$	0.25-1.0	Cobb et al. (2003)
Northern Line Islands (Fanning, Christmas Is.)	$\delta^{18}O$	1.3-6.9	Cobb et al. (2013)
Bonaire, Caribbean	Sr/Ca	1.8-6.2	Giry et al. (2012)
	$\delta^{18}O$, Sr/Ca	1.8-6.2	Giry et al. (2013)
Red Sea	$\delta^{18}O$, Sr/Ca	2.9 and 122	Felis et al. (2004)
Vanuatu	Sr/Ca, U/Ca	4.15	Corrège et al. (2000)
Mentawai Islands, W. Indonesia	Sr/Ca, $\delta^{18}O$	4.16-6.57	Abram et al. (2007)
Vanuatu	Sr/Ca	4.2-10.3	Beck et al. (1997)
Hainan Island, South China Sea	$\delta^{18}O$	4.4	Sun et al. (2005)
Eilat, Red Sea	$\delta^{18}O$	4.5-6	Moustafa et al. (2000)
Dominican Republic	$\delta^{13}C$, $\delta^{18}O$	5.2-7.2	Greer and Swart (2006)
Great Barrier Reef, Australia	Sr/Ca, $\delta^{18}O$	5.35	Gagan et al. (1998, 2000)
New Caledonia	Sr/Ca, Ba/Ca	5.5	Lazareth et al. (2013)
Tahiti	$\delta^{18}O$, Sr/Ca	9.5	DeLong et al. (2010)
Tahiti	Mg/Ca, Ba/Ca, U/Ca, and Cd	9-15	Inoue et al. (2010)
Tahiti	$\delta^{18}O$, Sr/Ca	12.4 and 14.2	Asami et al. (2009)
Tahiti	$\delta^{18}O$, Sr/Ca	15	Felis et al. (2012)
Papua New Guinea	$\delta^{18}O$	Various[a]	Tudhope et al. (2001), Brown et al. (2006)
Vanuatu	$\delta^{18}O$, Sr/Ca	350	Kilbourne et al. (2004)

[a] *Various samples, dated ~2.3, 6.5, 38-42, 85, 112, and 118-128 ka BP.*

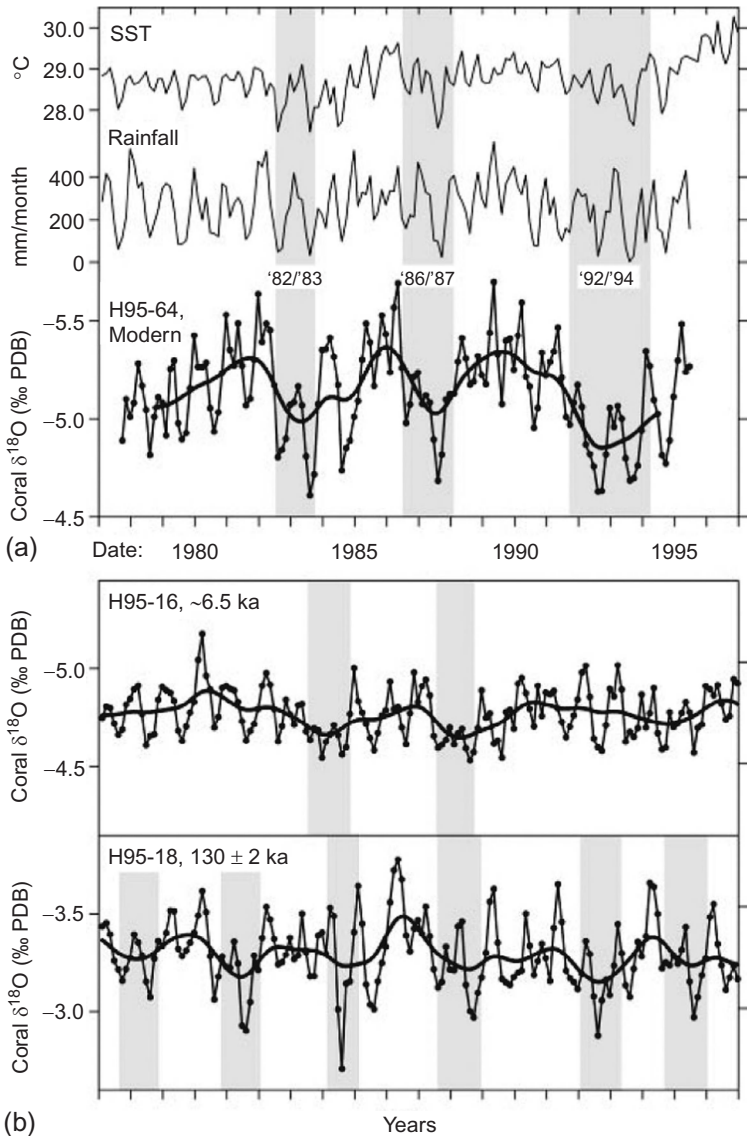


FIGURE 14.11 Oxygen isotope variations in modern corals from the northern coast of Papua New Guinea (upper panel, shown with recorded SSTs and rainfall, from 1978 to 1997) and in fossil coral samples, dated ~6500 years BP (middle panel), and ~130,000 years BP (lower panel). El Niño events in the 1980s and early 1990s are shaded in the upper panel. They are generally dry and cool in this region, resulting in relatively enriched $\delta^{18}O$ values (note inverted scale). El Niño-like variations are also seen in the fossil samples (shaded), though the amplitudes are less than in modern corals. *From Tudhope et al. (2001).*

temperatures were ~1.2 °C higher in the mid-Holocene than in the early 1990s (Gagan et al., 1998). By also analyzing $\delta^{18}O$ in the same samples, they were able to then remove the temperature signal from the $\delta^{18}O$ to obtain the change in salinity. This showed an enrichment in ^{18}O, indicating that salinity was higher, due to a greater rate of evaporation, resulting from the higher SSTs. If such a pattern had been widespread across the Tropics in the mid-Holocene, it could have significantly increased the water vapor content of the atmosphere and the export of latent heat into extratropical latitudes.

A number of fossil coral studies have focused on the nature of ENSO variability in the past. In general, these studies demonstrate that the ENSO system has been a long-term feature of the climate system throughout the last glacial-interglacial cycle, though with changes in strength (amplitude) and frequency at different times. For example, in corals from the north coast of Papua New Guinea, Tudhope et al. (2001) found evidence that ENSO variability (expressed in that region by cooler and drier conditions, hence recorded in corals by isotopically heavy—less negative—values of $\delta^{18}O$) was similar in both glacial and interglacial periods (Figure 14.11). In studies of fossil corals from the southwestern Pacific, Cobb et al. (2013) determined that ENSO variability changed very little during the Holocene, though recent decades were characterized by higher amplitude events than were typical in the past. With additional sampling, it is reasonable to expect that enough fossil corals will eventually be found to provide a more or less continuous picture of tropical oceanic conditions extending well back into the LGM, at least for some regions.

CHAPTER

15

Historical Documents

OUTLINE

15.1 Introduction 517

15.2 Historical Records and Their Interpretation 519
- 15.2.1 *Historical Weather Observations* 524
- 15.2.2 *Historical Records of Weather-Dependent Natural Phenomena* 526
- 15.2.3 *Phenological and Biological Records* 534

15.3 Regional Studies Based on Historical Records 538
- 15.3.1 *East Asia* 540
- 15.3.2 *Europe* 544

15.4 Records of Climate Forcing Factors 545

15.5 Climate Paradigms for the Last Millennium 548

15.1 INTRODUCTION

Some of the most diverse and invaluable sources of proxy data are historical records. These data are particularly important since they deal with short-term (high-frequency) climatic fluctuations during the most recent past. In terms of the climatic future, it is this timescale and frequency domain that is often of most interest to planners and decision makers. A great deal can be learned about the probability of extreme events by reference to historical records, and this provides a more realistic perspective on the likelihood of similar events recurring in the future (Ingram et al., 1978; Pfister and Brázdil, 1999). An excellent overview of the topic, with many examples from Europe, is provided by Brázdil et al. (2005).

The use of historical records to reconstruct past climates is intimately linked with the debate over the extent to which climate and climatic fluctuations have played a role in human history. Several volumes devoted to climate and history address this issue (LeRoy Ladurie, 1971; Delano Smith and Parry, 1981; Rotberg and Rabb, 1981; Wigley et al., 1981; Pfister et al., 1999; Jones et al., 2001). Much of the discussion in these volumes revolves around the effects

Copyright © 2015 Raymond S. Bradley.
Published by Elsevier Inc. All rights reserved.

(if any) that climate and climatic variations have had on various aspects of human activity, particularly agricultural and economic activity and their social and political consequences (Ingram et al., 1981a; Salvesen, 1992; Bauernfeind and Woitek, 1999). For the purposes of this chapter, it is not necessary to review the arguments *pro* or *con*, except to note the danger of using historical data as a proxy for climate when no cause and effect relationship has been clearly demonstrated. Usually this problem is tackled empirically by establishing a relationship between the historical time series and a brief record of overlapping climatic data. However, without a model demonstrating the logic of such a relationship, erroneous conclusions may result (de Vries, 1981). Models should be comprehensive, recognizing not just the role of climate but also the potential significance of other nonclimatic factors (Parry, 1981). In this way, there will be not only a stronger basis for historical paleoclimatic reconstruction but also a better understanding of the role of climate and climatic fluctuations in history.

Paleoclimatic data from historical sources rely, of course, on written observations or inscriptions. This means that certain parts of the world have been endowed with a much richer heritage of historical paleoclimatic information than other regions (Table 15.1). The longest records come from Egypt, where stone inscriptions relating to the Nile flood levels are available from mid-Holocene times (~5000 years BP), indicating higher rainfall amounts from East African summer monsoons at that time (Bell, 1970; Henfling and Pflaubaum, 1991). Arabic chronicles also provide intermittent observations (mainly on rainfall) in other parts of the Middle East (Iraq, Syria, and Palestine) going back over 1000 years (Grotzfeld, 1991). In China, the earliest inscriptions on oracle bones date back to the time of the Shang Dynasty (~3700-3100 years BP) when conditions appear to have been slightly warmer than in modern times (Wittfogel, 1940; Chu, 1973; Zhang, 2004, vol. 1). Such records are, of course, few and far between and for the vast majority of the continental land areas, as well as the oceans, historical observations are generally only available for the last few centuries.

Historical data can be grouped into four major categories. First, there are observations of weather phenomena *per se*, for example, the frequency and timing of frosts or the occurrence

TABLE 15.1 Earliest Historical Records of Climate

Area	Earliest Written Evidence (Approximate Dates)
Egypt	3000 BC
China	1750 BC
Southern Europe	500 BC
Northern Europe	0
Japan	AD 500
Iceland	AD 1000
North America	AD 1500
South America	AD 1550
Australia	AD 1800

Modified after Ingram et al. (1978).

of snowfall recorded by early diarists. Secondly, there are records of weather-dependent natural phenomena (sometimes termed parameteorologic phenomena) such as droughts, floods, and lake or river freeze-up and breakup. Thirdly, there are phenological records, which deal with the timing of recurrent weather-dependent biological phenomena, such as the dates of flowering of shrubs and trees or the arrival of migrant birds in the spring. We will include in this group of records observations of the former spatial extent of particular climate-dependent species. A fourth category involves records of forcing factors that may have had an influence on climatic conditions in the past. Within each of these categories, there is a wide range of potential sources and an equally wide range of possible climate-related phenomena. These are discussed in more detail in the following sections.

15.2 HISTORICAL RECORDS AND THEIR INTERPRETATION

Potential sources of historical paleoclimatic information include (a) ancient inscriptions; (b) annals, chronicles, etc.; (c) governmental records; (d) private estate records; (e) maritime and commercial records; (f) personal papers, such as diaries or correspondence; and (g) scientific or proto-scientific writings, such as (noninstrumental) weather journals (Ingram et al., 1978). In all these sources, the historical climatologist is faced with the difficulty of ascertaining exactly what the qualitative description of the past is equivalent to in terms of modern-day observations. What do the terms "drought," "frost," and "frozen over" really mean? How can qualifying terms (e.g., "extreme" frost) be interpreted? Baker (1932), for example, notes that one seventeenth-century diarist recorded three droughts of "unprecedented severity" in the space of only 5 years! An approach to solving this problem has been to use content analysis (Baron, 1982) to assess in quantitative terms, and as rigorously as possible, climatic information in the historical source. Historical sources are examined for the frequency with which key descriptive words were used (e.g., "snow," "frost," and "blizzard") and the use which the writer may have made of modifying language (e.g., "severe frost," "devastating frost," and "mild frost"). In this way, an assessment can be made of the range of descriptive terms that were used, so they can be ranked in order of increasing severity as perceived by the original writer. The ranked terms may then be given numerical values so that statistical analyses can be performed on the data. This may involve simple frequency counts of one variable (e.g., snow) or more complex calculations using combinations of variables. The original qualitative information may thus be transformed into more useful quantitative data on the climate of different periods in the past. Nonclimatic information is often required to interpret the climatic aspects of the source: Where did the event take place (was the event only locally important; was the diarist itinerant or sedentary?) and precisely when did it occur and for how long? This last question may involve difficulties connected with changing calendar conventions (van Engelen et al., 2001) and trying to define what is meant by terms such as "summer" or "winter" and what time span might be represented by a phrase such as "the coldest winter in living memory." Not all of these problems may be soluble, but content analysis can help to isolate the most pertinent and unequivocal aspects of the historical source (Moody and Catchpole, 1975).

Historical sources rarely give a complete picture of former climatic conditions. More commonly, they are discontinuous observations, very much biased toward the recording of

extreme events, and even these may pass unrecorded if they fail to impress the observer. Furthermore, long-term trends may go unnoticed since they are beyond the temporal perspective of one individual. In a sense, the human observer acts as a high-pass filter, recording short-term fluctuations about an ever-changing norm (Ingram et al., 1981b). Nevertheless, long-term records of natural phenomena (such as the freezing of a lake) can convey relevant low-frequency information even if the time series is made up of many short-term observations.

Historical records that appear to be rich in parameteorologic information were probably not produced with the historical climatologist in mind, and care must be taken to assess the purpose of the writer in making the record. For example, Chinese dynastic histories contain abundant references to floods and droughts, but the purpose of the notation was not to record the vagaries of climate, but to make a record of human suffering and damage caused by changes in rainfall. Such events were considered to convey a supernatural warning to the Emperor of the day (Yao, 1944). Because of this, there is a strong seasonal bias toward reporting flood and drought events in the vitally important growing season, as well as a spatial bias in the data, toward settled areas with large populations. For example, in the Ming Dynasty (1368-1643), the number of recorded droughts and floods in the metropolitan province exceeds that of any other province (Chu, 1926; Yao, 1943). Also, because floods and droughts resulted in tax exemptions in the region afflicted, it is not unlikely that local officials may have been tempted to exaggerate the severity of extreme events. This, of course, is true of many areas throughout history.

References to unusual temperatures may be strongly skewed, depending on the perspective of the author. This bias poses a difficult challenge to reconstructing reliable paleotemperature estimates. For example, in the more than 20,000 "climatic calamities" noted in Chinese documents, only 100 concerned warm anomalies (Wang, 1991a,b). Cold episodes were mentioned in 35% of years, but warm episodes only figured in 5% of the years. This bias reflects the significance of cold conditions to agricultural activities in China. In cooler climates, it is warm conditions that are of particular significance; Icelandic archives commonly record mild spells and these characterized the warm decades of the 1570s, 1640-1650s, and 1700s (Figure 15.1) (Ogilvie, 1992).

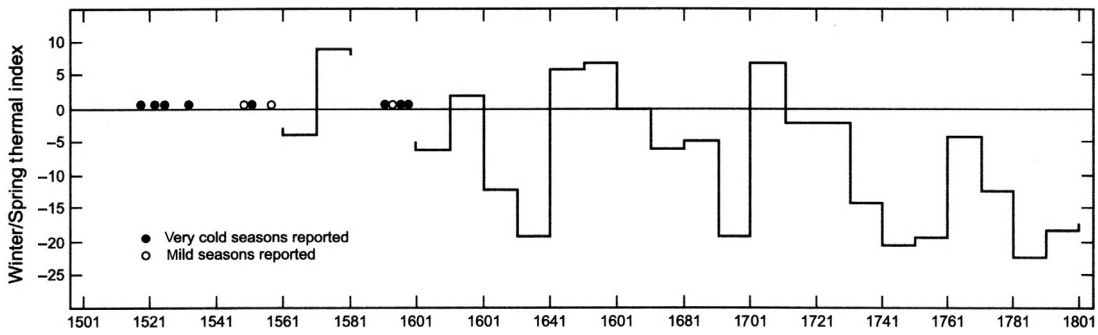


FIGURE 15.1 Winter-spring thermal index for Iceland 1501-1801 based on content analysis of historical documents (annals, correspondence, and diaries). Isolated reports of very cold or very mild seasons are also shown. *From Ogilvie (1992).*

Finally, it is worth noting that not all historical sources are equally reliable. It may be difficult in some cases to determine if the author is writing about events of which he has first-hand experience or if events have been distorted by rumor or the passage of time. Ideally, sources should be original documents rather than compilations; many erroneous conclusions about past climate have resulted from climatologists relying on poorly compiled secondary sources that have proved to be quite erroneous when traced back to the original data (Bell and Ogilvie, 1978; Wigley, 1978; Ingram et al., 1981b). Nevertheless, some major compilations such as the voluminous Chinese encyclopedia, the *T'u-shu Chi-cheng*, have proved to be invaluable sources of paleoclimatic information (Chu, 1926, 1973; Yao, 1942, 1943).

Some observations may not need direct calibration if comparable contemporary observations are available. This applies to such things as rain/snow frequency, dates of first and last snowfall, and river freeze/thaw dates, providing urban heat island effects or technological changes (such as river canalization) have not resulted in a nonhomogeneous record. However, if historical observations can be calibrated in terms of recorded temperature, more quantitative comparisons with recent data are then possible. This may be done by utilizing early instrumental data that overlap with the proxy record, to develop an equation relating the two data sets (e.g., Dobrovolný et al., 2010). Thus, Bergthorsson (1969) regressed observations of sea-ice frequency off the coast of Iceland with mean annual temperatures during the nineteenth century and then used the resulting equation to reconstruct long-term temperature fluctuations over the preceding 300 years from sea-ice observations. Similarly, observations of Dutch canal freezing frequencies were calibrated with instrumentally recorded winter temperature data by de Vries (1977) (Figure 15.2). The calibration equations were then used to reconstruct paleotemperatures prior to the period of instrumental records in each area (though higher temperatures, when canals remained unfrozen or sea ice was absent, cannot be reconstructed in these cases).

In many locations, precipitation occurrence (daily frequency) was recorded together with remarks on rainfall intensity, rather than the rainfall totals. In China, a remarkably comprehensive system was established from 1736 (lasting until 1911) in which daily records of rainfall and snowfall were maintained at 273 locations across 18 provinces of eastern and southern China (Ge et al., 2005). These were known as *Yu Xue Fen Cun* (*Yu* = rainfall, *Xue* = snowfall, *Fen* = a measurement unit, ~0.32 cm, and *Cun* = 10 Fen), and the data were transmitted to the Emperor on a regular basis to inform him of meteorologic conditions that might affect agricultural production and perhaps (if the news was bad) the potential for social unrest. Interestingly, data were reported in terms of the type and duration of precipitation and the depth to which rainfall penetrated into the ground (infiltration depth)—which was of primary agricultural importance—or the cumulative snowfall depth. As infiltration of rainfall very much depends on local soil type, prior soil moisture conditions, rainfall duration, and intensity, Ge et al. (2005) undertook field experiments, artificially recreating varying rainfall amounts and intensities and then measuring infiltration depths in order to quantify the historical descriptive terms. In this way, they were able to reconstruct daily precipitation totals at Shijiazhuang (south of Beijing) and sum those for months and seasons (Figure 15.3). It appears that winter precipitation was higher than in the twentieth century prior to 1825, declining thereafter over the course of the nineteenth century. In summers, rainfall was highest in the late eighteenth and early nineteenth centuries (~1785-1815).

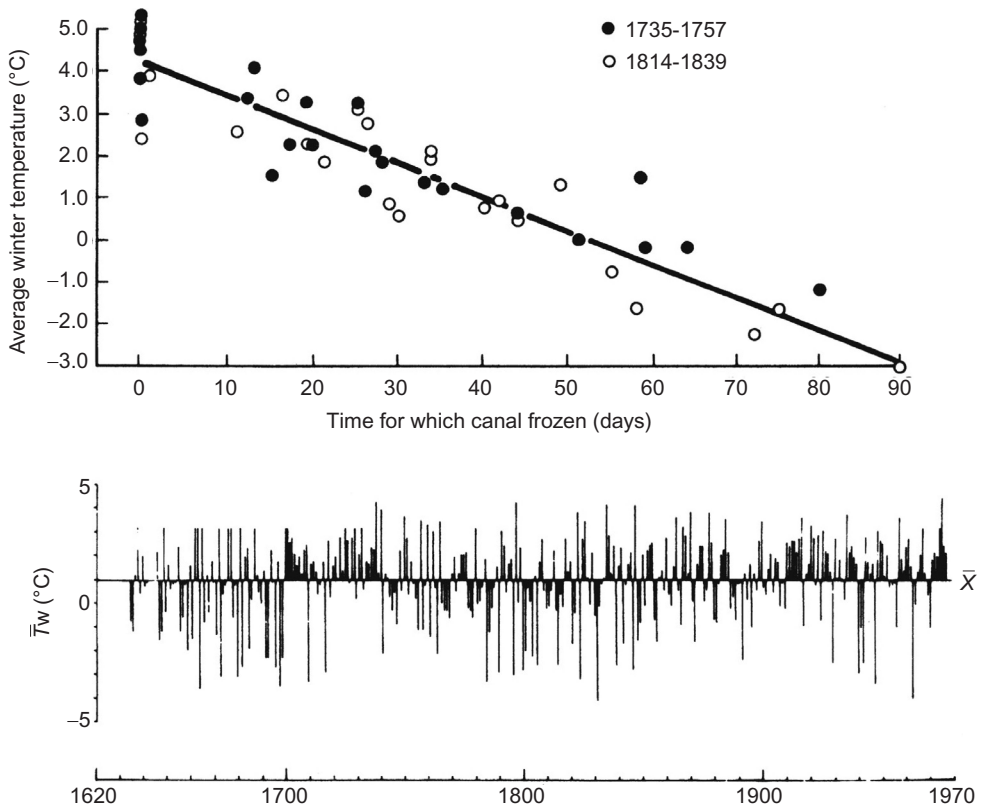


FIGURE 15.2 Upper diagram: Relationship between the number of days per winter with a canal frozen between Haarlem and Leiden (Holland) and average winter temperatures. The best-fit linear regression line is shown. Lower diagram: Reconstructed winter temperatures at De Bilt, Holland, expressed as departures from the long-term average (+2 °C) based on regression shown and historical records of canal freezing frequencies. *After van den Dool et al. (1978).*

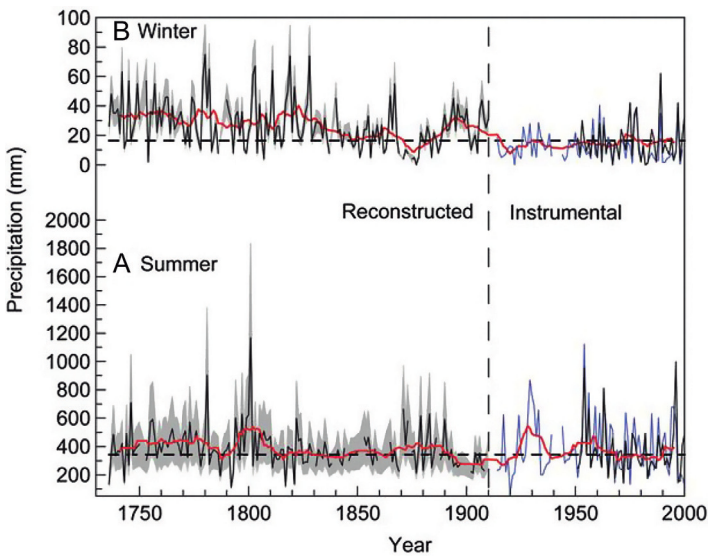


FIGURE 15.3 Reconstructed (1736-1911) and instrument-measured (1951-2000) (a) summer and (b) winter precipitation (black line) at Shijiazhuang, near Beijing, China. The red line represents 11-year running mean values, while the horizontal dashed line is the mean annual value for 1961-1990. The shading indicates the 95% confidence limits. Because measurements at Shijiazhuang were missing for 1911-1950, these were replaced by data from nearby Baoding (the blue line). *From Ge et al. (2005).*

Several studies have shown that statistically significant relationships exist between rainfall frequency (and/or rainfall duration) and daily rainfall amounts, enabling estimates of daily rainfall to be made and then for monthly and seasonal totals to be accumulated. In the lower Yangtze River valley of eastern China, for example, local officials maintained detailed weather observations during the Qing Dynasty (1636-1910). This set of records (*Qing Yu Lu*, the "Clear and Rain Records") provides daily records on sky conditions, wind directions, precipitation type (rain or snow, light, heavy, torrential, etc.), and the duration of precipitation events (Wang and Zhang, 1988). By relating precipitation totals to precipitation frequency and intensity during recent decades (using instrumental data), Wang and Zhang (1992) were able to establish regression equations that could then be applied to the historical data to reconstruct precipitation amounts in the past. Others have noted that rainfall frequency (number of rainy days and/or the length of rainy episodes) is often inversely related to temperature because cloud cover tends to reduce direct radiation and rainfall itself will lead to evaporative cooling. Wang et al. (1992) applied this line of reasoning to the *Qing Yu Lu*, to extend the instrumental record of summer temperature in Beijing from 1855 back to 1724. Mikami (1992b) also noted the strong relationship between the number of rain days in parts of Japan and summer temperature (based on instrumental data). Using diaries kept by generations of the Ishikawa family from 1721 (which fortunately overlapped with the period of instrumental records), he calibrated the number of rainy days with July temperature during the overlapping period and then used this relationship to reconstruct temperature from 1721, using the historical records of rainfall frequency (Figure 15.4) (Mikami, 2008).

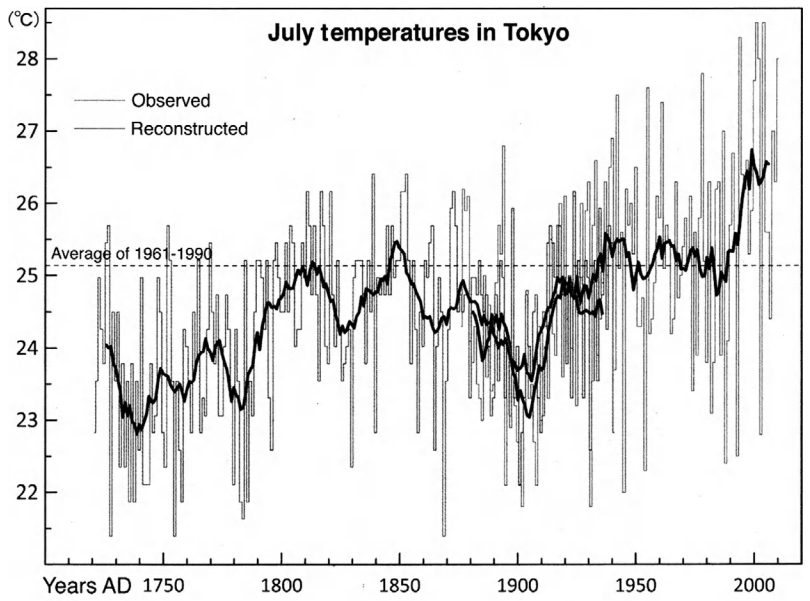


FIGURE 15.4 Combined time series of reconstructed (broken line) and observed (solid line) July temperatures in Tokyo for 1721-1995. The reconstructed values are based on a calibration of the number of rainy days and July temperatures in the period of overlap between observed and recorded data. *From Mikami (2008).*

15.2.1 Historical Weather Observations

The most widely recorded meteorologic phenomenon in historical documents is snow, in terms of the date of the first and last snowfalls of each year or the number of days with snow on the ground or the frequency of days with snowfall. Some of the earliest snowfall observations are from Hangchow, China, for the period AD 1131-1210, when discontinuous records were made of the dates of the last snowfall in spring. Comparison with Hangchow records for the period 1905-1914 indicates that snowfalls commonly occurred 3-4 weeks later in the spring months during the twelfth century than was typical of the early twentieth century (Chu, 1926). This suggests a more prolonged, and probably more severe, winter during the Southern Song Dynasty (AD 1127-1279).

More modern but more complete records of snowfall (dates of first and last occurrences) were compiled for the London area by Manley (1969). These extend back to 1811 and indicate a reduction in the snow season of approximately 6 weeks between 1811-1840 and 1931-1960, though most of this change has occurred during the twentieth century, perhaps due to a marked increase in the urban heat island effect. A similar problem may have affected recent observations of first snow cover in the Tokyo area. During the period from 1632-1633 to 1869-1870, the average date of the first snow cover was January 6, whereas from 1876-1877 to 1954-1955, the mean was January 15 (Arakawa, 1956a). For both periods, the standard deviations were similar (approximately 20 days). How much of the change is due to a warmer Tokyo metropolitan area is difficult to assess and points to the particular value of data from more rural locations. Pfister, for example, has compared the number of days with snow cover (extensive snow on the ground) at various places with similar elevations on the upper and lower plateaus of Switzerland. During the eighteenth century, snow cover was often far more persistent than in even the harshest winter of the twentieth century, 1962-1963 (Table 15.2), and this provides strong support for the record of "days with snow lying" in the Zurich-Winterthur area (Figure 15.5). These data point to the decade 1691-1700 as having had the highest number of days with snow on the ground (>65 annually) compared to recent averages of only half that number (Pfister, 1985). It is also of significance that this decade was the coldest in central England, according to long-term instrumental records of temperature (Manley, 1974). Thus, urban growth effects, while undoubtedly exerting a progressive influence on temperature, cannot account for all the marked changes observed.

TABLE 15.2 Number of Days with Snow Cover per Year (March to May Values in Parentheses) for Selected Localities in Switzerland

Winter of	Lower Plateau	Upper Plateau
1769-1770		126 (45)
1784-1785	134 (51)	154 (60)
1788-1789	112 (35)	
1962-1963[a]	59 (0)	86 (12)

[a]*Harshest winter of the twentieth century. Severe winters were also noted in 1684-1685, 1715-1716, 1730-1731, and 1969-1970. After Pfister (1978a).*

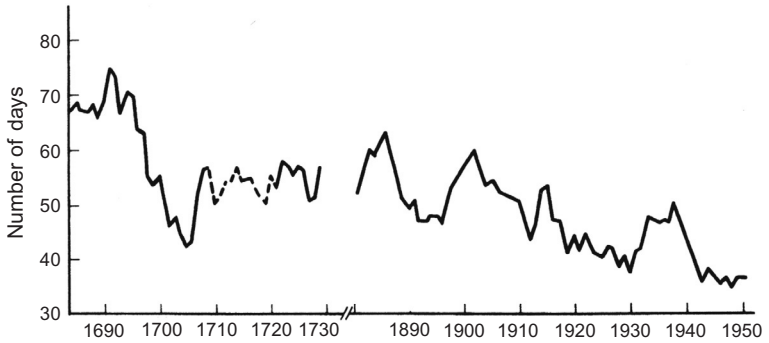


FIGURE 15.5 Fluctuations in the number of days with snow lying in Zürich (note break in abscissa scale). Prior to 1800, figures have been estimated based on daily noninstrumental observations. Observations for 1721-1738 made in Winterthur, 20 km northeast of Zürich. Value plotted as 10-year running means with value at year n corresponding to the decade n to $(n+9)$. *From Pfister et al. (1978).*

An interesting method of assessing past winter temperatures has been demonstrated by Flohn (1949) who observed that the ratios of snow days to rain days in winter months correlate well with winter temperatures during the instrumental period. Using sixteenth-century observations of Tycho Brahe in Hven, Denmark (1582-1597), and of Wolfgang Haller in Zurich (1546-1576), Flohn was able to show that winters after 1564 were increasingly severe, leading to a marked increase in glacial advances in the Alps in the early seventeenth century. At Hven, winter temperatures from 1582 to 1597 averaged 1.5 °C below those around the early twentieth century. It is also interesting that sixteenth-century weather singularities (synoptic events that recur at the same time each year) continue to be observed in the twentieth century, indicating an underlying cyclicity in the general circulation that has persisted in spite of fundamental changes in the climate of the region.

In the Kanazawa area of Japan (west-central Honshu), historical records of snowfall were maintained by the ruling Maeda family from 1583 to ~1870. Based on detailed analysis of these and subsequent records, Yamamoto (1971) constructed an index of snowfall variation that corresponds reasonably well with instrumentally recorded winter temperatures in recent years. Although no precise calibration has been attempted, the index gives an overall impression of snowier winters, particularly in the first half of the nineteenth century, and this conclusion seems to be supported by other snowfall indices derived from Japanese historical sources.

Another observation frequently noted in historical records is the incidence of frost during the growing season, an occurrence of particular significance to agriculturalists. As with snowfall, long records of frost occurrence are available from China, in particular from the farming regions of the mid and lower sections of the Yellow River (Huang He). Higher frequencies of frost were recorded during the periods 1551-1600, 1621-1700, 1731-1780, and 1811-1910. However, the range is small (from one to six events per decade) and the significance of such changes in the frequency of extremes for the overall growing season temperature is not clear. Other historical records indicate that the *frost-free* period in Inner Mongolia and northeastern China from 1440 to 1900 was ~2 months shorter on average than during the twentieth century. Similarly, in southern China the frost-free season in recent decades has been 5-6 weeks longer than the long-term mean from 1440 to 1900 (Zhang and Gong, 1979).

European historical archives have provided a variety of noninstrumental records of value to the climatologist. Many of these sources were evaluated by H. H. Lamb to produce an index of winter severity and summer wetness spanning the last 1000 years (Lamb, 1961, 1963, 1977). Lamb concluded that the period AD 1080-1200 was characterized by dry summers throughout Europe, the like of which has not been seen since. He therefore designated this interval the "Medieval Warm Epoch" (Lamb, 1965, 1988). This has generated considerable interest as a possible analog for future, greenhouse gas-induced climates. However, subsequent studies have provided mixed support for this concept (Hughes and Diaz, 1994; Bradley et al., 2003c; Mann et al., 2008, 2009; Jones et al., 2009; Diaz et al., 2011; Graham et al., 2011); the available evidence is limited (geographically) and equivocal. A number of records do indeed show evidence for warmer conditions at some time during this interval, especially in the eleventh and twelfth centuries in parts of Europe, as Lamb pointed out. However, other records show no such evidence or indicate that warmer conditions prevailed, but at different times. Indeed, not all seasons may have been warm; for example, winters at this time were relatively harsh in western Europe, at least until ~AD 1170 (Alexandre, 1977). This rather incoherent picture may be due to an inadequate number of records, and a clearer picture may emerge as more and better calibrated proxy records are produced. However, multiproxy temperature reconstructions do not support the notion that Lamb's MWE was of global significance (Mann et al., 2009).

One of the most interesting and unusual studies of historical material is that of Neuberger (1970) who examined the changing climate of the "Little Ice Age (LIA)" (sixteenth-nineteenth centuries) in western Europe through artists' perceptions of their climatic environment, as depicted in contemporary paintings (see also Zerefos et al., 2007). Neuberger examined over 12,000 paintings from the period 1400 to 1967, and wherever possible, the intensity of the blue sky, visibility depicted, percentage cloudiness, and cloud type were categorized for each painting. More than half of the paintings contained some sort of meteorological information and the basic characteristics were averaged for different periods within the last 570 years, as shown in Figure 15.6. During the period 1400-1549, paintings have a high percentage of blue sky, good visibility, and little cloud cover. Paintings completed during the next 300 years were generally darker, with less blue sky, showed lower visibilities, and had a much higher percentage of cloud cover and a greater frequency of low-and convective-type clouds. Over the last 100 years, there was some reduction in cloudiness depicted and a drop in low and convective cloud frequency, though visibilities remained low, perhaps reflecting increasing atmospheric turbidity due to industrial and agricultural activity. It is remarkable that, in spite of many changes in style, the artists have captured in their paintings a significant record of climatic variation through time. Perhaps this perceptual record, more than any cold statistic, indicates the degree to which life during the "Little Ice Age" was affected by a deteriorating climate.

15.2.2 Historical Records of Weather-Dependent Natural Phenomena

Of all the weather-related natural catastrophes, floods and droughts appear to have had the most widespread and persistent impact on human communities, as records of these events are found in historical documents from all over the world (e.g., Pfister and Hachler,

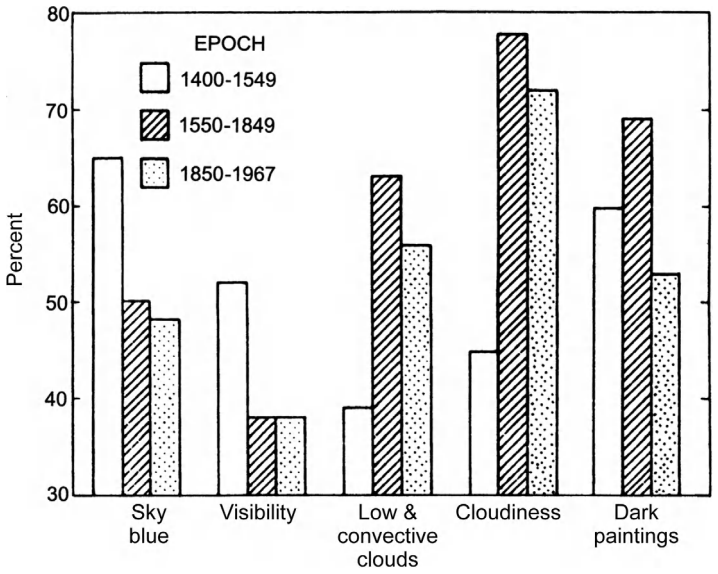


FIGURE 15.6 Changes in the frequency of certain characteristics of European paintings in the periods 1400-1549, 1550-1849, and 1850-1967. *After Neuberger (1970).*

1991; Pavese et al., 1992; Barriendos, 1997; Jacobeit et al., 2003; Brázdil et al., 2006, 2012; Glaser et al., 2010; Wetter et al., 2011). Extreme conditions often caused tremendous hardship on agricultural communities, and in some regions, the level of concern about these impacts can be traced in local ecclesiastical records. Rogation ceremonies (*rogativas*) were held by the Catholic Church to pray for relief from periods of bad weather, and these ceremonies steadily became more elaborate if the conditions persisted, often culminating in processions through the streets, carrying images or reliquaries containing the bones of locally venerated saints (Barriendos, 1997). Fifty such processions were recorded in Erice (western Sicily) between AD 1568 and 1913, generally associated with prolonged dry conditions in spring months (Piervitali and Colacino, 2001).

The longest and most detailed records of floods and droughts come from China, where regional gazetteers and other records have been kept in many provinces and districts since the tenth century and many records are available for the last 2000 years (Chu, 1973; Zhang, 2004, 2005). Each of these gazetteers recorded local facts of historical or geographic interest and climatological events of significance to agriculture and the local economy (for example, droughts, floods, severe cold snaps, heavy snowfalls, and unseasonable frosts). Not surprisingly, the gazetteers have been the focus of much interest, though there are often many difficulties in interpreting the data (see Section 15.2). In particular, technological improvements such as the building of irrigation channels or drainage ditches may drastically reduce the frequency of climatological disasters. For example, the Chinese province of Sichuan is unusual in that recorded occurrences of floods are rare, yet droughts are common. Usually, one finds over long periods of time a similar number of extremely wet and extremely dry events. The reason for this anomaly appears to be the particularly efficient flood-control measures introduced by the administrator Li Ping 2100 years ago, which were able to reduce flood hazards but did little to alleviate the perils of droughts (Yao, 1943).

In a similar way, the rise in flood and drought frequency during the Yuan Dynasty (AD 1234-1367) may be partly due to the destruction of irrigation and drainage systems by the Mongol invaders of the time (Chu, 1926).

A detailed spatial-temporal database of floods and droughts in China over the last 500 years was compiled by the State Meteorological Administration (1981) and later extended back to AD 980 (Zhang, 2005). For each of the last 500 years, each regional record was classified into one of five anomaly classes (wet to dry). Wang and Zhao (1981) subjected these matrices to principal components analysis. One hundred and eighteen stations from almost the whole of eastern China were used in the analysis of data from 1470 to 1977. The resulting eigenvectors indicated broad-scale patterns of "precipitation anomalies," and these were then compared with eigenvectors derived from instrumentally recorded summer precipitation data for the period 1951-1974 (Figure 15.7). Summer was chosen because it is the time corresponding to most recorded droughts and floods (Yao, 1942). Similarities between the principal modes of precipitation anomaly in both the instrumental and the historical periods indicate strongly that the historical records can indeed provide a valuable proxy of the patterns of summer precipitation variation over long periods of time.

Zhang (2005) identified the most severe droughts affecting northeastern China over the last millennium, when drought conditions persisted for 3 or more years across 4 or more provinces. Of these, the most severe, in area and duration, were between AD 1585-1590 and AD 1637-1643, when lakes, rivers, springs, and wells dried up over large areas, leading to mass starvation and social unrest (Figure 15.8) (Shen et al., 2007). In 1588 and 1589, Lake Taihu, the third-largest lake in China, dried up and in 1640, the lower Yellow River and some of its tributaries were dry, conditions not seen in the last century. Drought conditions spread from north to south across eastern China, which is a pattern commonly seen (Figure 15.9). These droughts are clearly related to a failure of the summer monsoon, but the exact cause (whether it is related to unusual ENSO, or PDO conditions, or related to major volcanic eruptions at those times) is unclear (Shen et al., 2007). It is interesting that the 1587-1589 period was also exceptionally dry in the western United States, which suggests a link to anomalous ENSO conditions (Stahle et al., 2007).

Apart from floods and droughts, the parameteorologic phenomenon, which seems to have attracted most attention in historical records, is the freezing of lakes, rivers, canals, and bays. Koslowski and Glaser (1999) reconstructed the record of freezing conditions in the southwestern Baltic Sea near Denmark using a variety of ship and coastal records, which noted disruptions to coastal shipping and information about traveling conditions across frozen straits. This enabled them to construct an annual ice severity index back to AD 1501; over the last 500 years, particularly severe ice conditions were experienced from 1554 to 1576, 1593 to 1630, 1655 to 1710, and 1763 to 1860. Considering the atmospheric circulation that favors the persistently cold conditions that lead to coastal freezing, they suggest that these periods were characterized by frequent anticyclonic (blocking) and weak westerly airflow (i.e., the negative phase of the North Atlantic Oscillation; Wanner et al., 2001).

The longest continuous series of lake freezing dates is that of Lake Suwa (near Kyoto) in Japan. Records of the date when this small ($\sim$15 km^2) lake became completely frozen over have been kept since the fifteenth century, though the dates are not very reliable from 1680 to 1740 (Arakawa, 1954, 1957). A comparison of these dates with meteorological

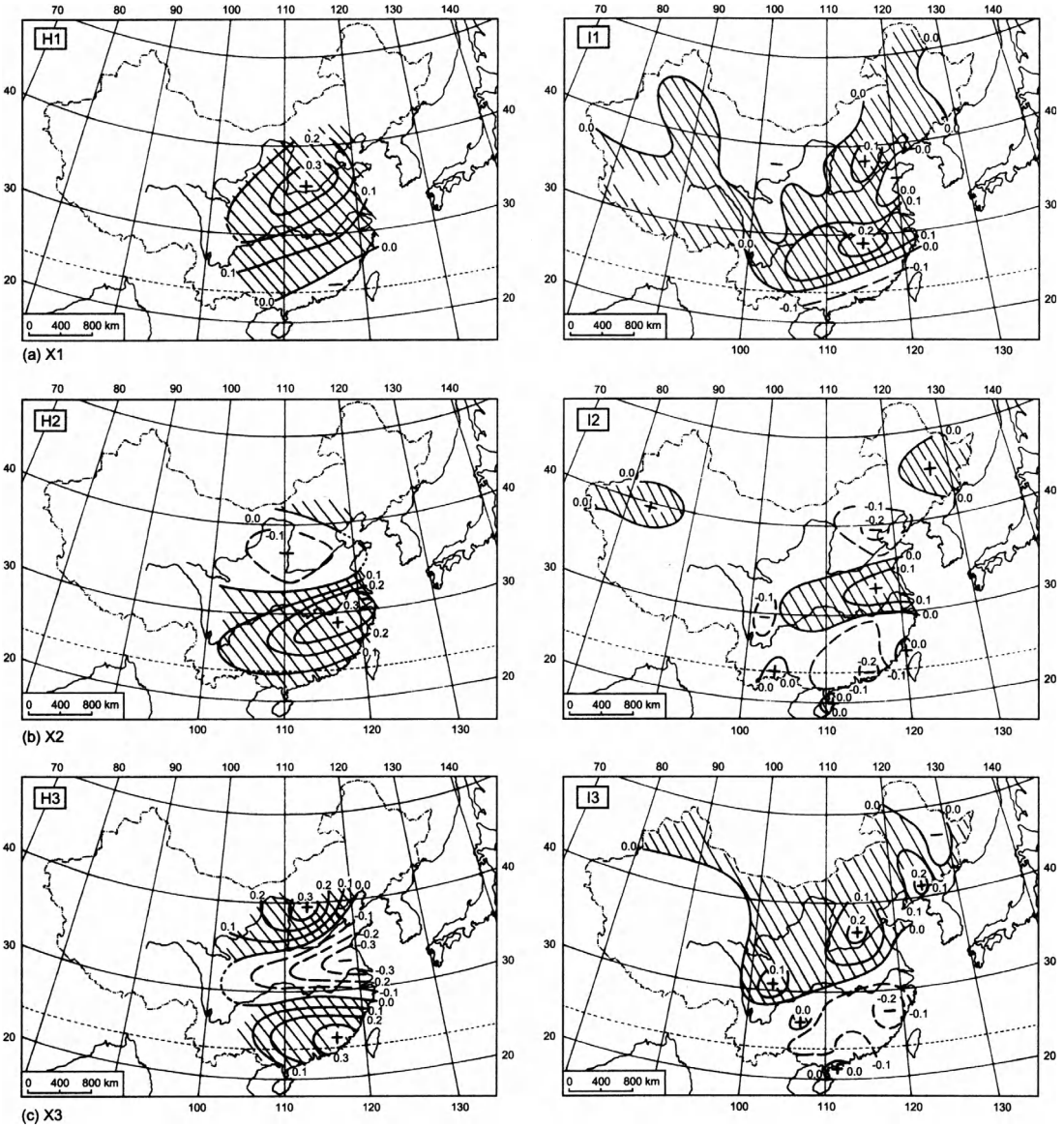


FIGURE 15.7 Eigenvectors of drought and flood data using historical records for AD 1470-1977 (left) and instrumentally recorded precipitation data from 1951 to 1974 (right). The first three eigenvectors of historical data (H1 to H3) account for 15%, 11%, and 7% of variance in the data, respectively. The first three eigenvectors of instrumental data (I1 to I3) account for 18, 13, and 11 and of variance in the data, respectively. Eigenvectors H1 and I1 are similar; so are H2 and I3 and H3 and I2 (inverse patterns). This indicates that historical data can be reliable indicators of climatic anomaly patterns. *After Wang and Zhao (1981).*

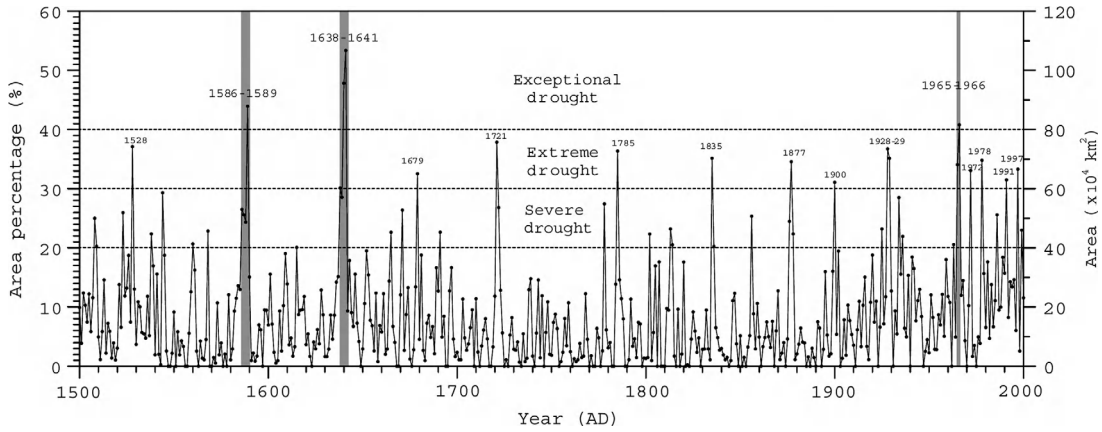


FIGURE 15.8 Area of eastern China in very dry conditions (severe drought or worse) during the last five centuries based on the network of drought/flood indices in China. Thresholds of severe, extreme, and exceptional drought were defined by comparison with the occurrence rates of droughts in these categories in the drought classification scheme used by the US National Drought Mitigation Center. The drought of greatest extent occurred in the later 2 years of the 1638-1641 event, peaking at about 50%; the second (~44%) occurred in 1589 of the 1586-1589 event, and the third peak (~41%) in 1966. *From Shen et al. (2007).*

measurements from 1945 to 1990 provides a calibration in terms of December-January mean temperatures (Figure 15.10). This indicates that the lowest temperatures were in the early 1600s, with generally colder conditions than in the twentieth century from the mid-fifteenth to mid-seventeenth centuries (Mikami, 2008).

Long historical records of river and lake freezings are also available from China. Using local gazetteers and diaries, Zhang and Gong (1979) compiled records of the frequency of freezings of lakes in the mid and lower reaches of the Yangtze River, freezings of rivers and wells in the lower Yellow River Basin, the occurrence of sea ice in the Gulf of Chihli and Jiangsu Province (31-41°N), and snowfall in tropical areas of southern China. Using all this information, they calculated the number of exceptionally cold winters per decade from 1500 to 1978. The highest frequency of cold winters occurred during the periods 1500-1550, 1601-1720, and 1830-1900, with the decade 1711-1720 being the most severely cold period in the last 480 years. By mapping the areas most affected by severe winters, it was also possible to recognize two main patterns of the anomaly—periods when cold winters predominated east of ~115°E and periods when areas to the west were colder. From modern meteorologic studies, it appears that such large-scale anomaly patterns result from changes in the position of the upper-level trough over East Asia. When the trough is in a more westerly position and fairly deep, cold air sweeps down more frequently over the area west of 115°E. When the trough is weaker and less extensive, westerly flow prevails leading to milder conditions in the west, with cold air outbreaks more common to the east. Generally speaking, the colder periods had more frequent cold outbreaks west of 115°E, indicating that such periods were characterized by a strongly developed upper air trough over eastern Asia. Conversely, the warmer periods were times of stronger westerly flow in winter and weaker upper-level trough development (Zhang and Gong, 1979).

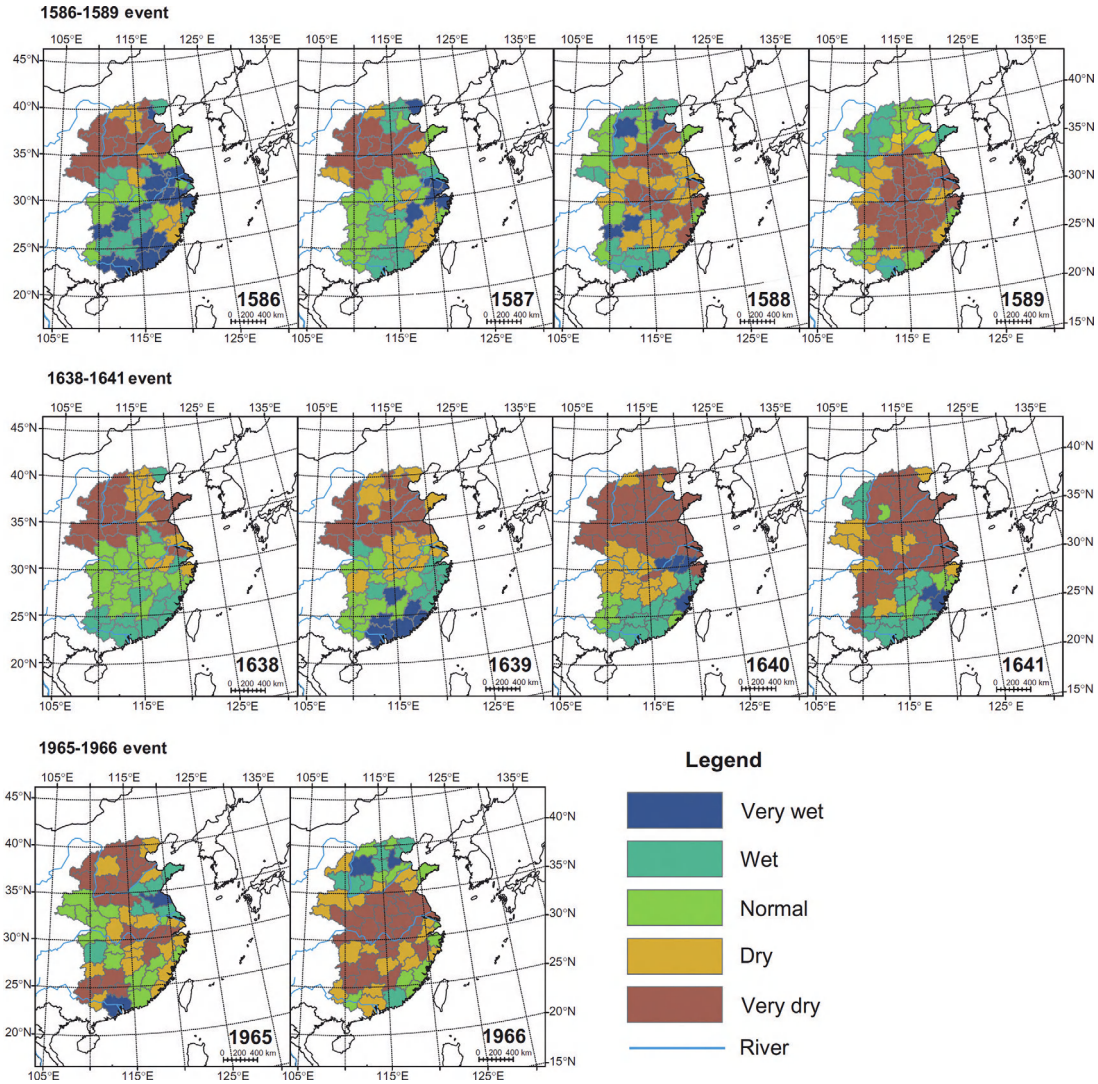


FIGURE 15.9 Spatial pattern and temporal evolution of climatic conditions during three exceptional drought events in eastern China. The center of the drought was located in northern China initially and then moved southward to the middle and lower Yangtze River valley and beyond, to reach its maximum spatial coverage in the later stages. *From Shen et al. (2007).*

Historically, one of the most important effects of severe winter temperatures was on water transportation systems, and many records exist regarding the disruptions caused by canals and rivers freezing over for prolonged periods. In the Netherlands, for example, canals were built in the early seventeenth century to connect major cities, and records of transportation on the canals, including times of freezing over, have been kept since 1633 (de Vries, 1977). Using instrumental winter temperature data from De Bilt (Labrijn, 1945), the number of days on

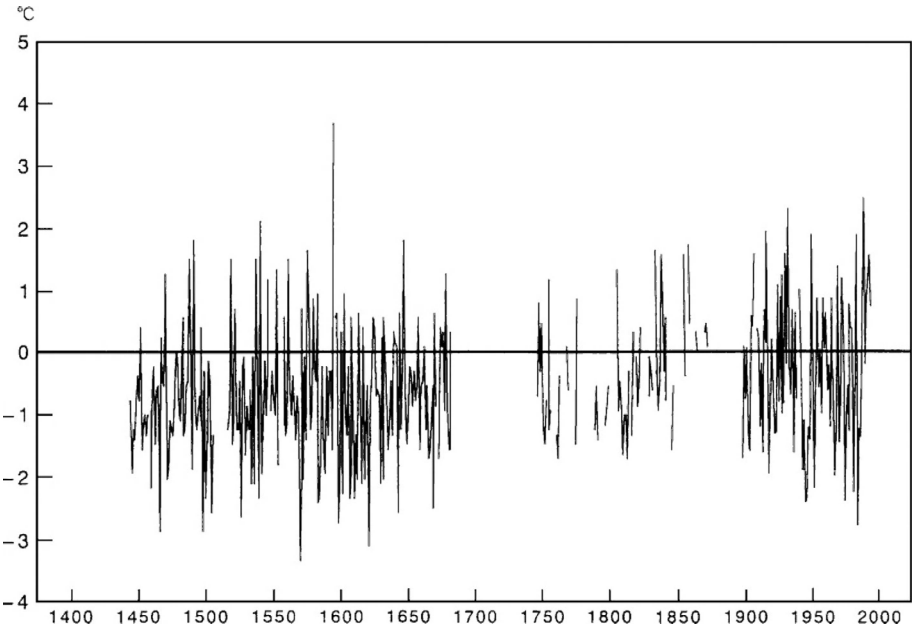


FIGURE 15.10 Variations in December/January temperatures at Suwa during the period 1444-1870 (reconstructed) and 1891-1995 (observed). *From Mikami (2008).*

which the Haarlem-Leiden canal was frozen each winter was calibrated (Figure 15.2, upper diagram), enabling De Bilt winter temperatures to be reconstructed back to 1657. Further temperature estimates, back to 1634, were possible by calibration of the canal freezing data with barge trip frequency between Haarlem and Amsterdam (1634-1682), a service which was commonly suspended due to ice cover on the canal (van den Dool et al., 1978). In this way, a complete winter temperature reconstruction for De Bilt has been obtained back to 1634 (Figure 15.2). Note however that this record conveys no information about how warm winters may have been in years when the record shows only that the canal was never frozen over.

In more northern latitudes, rivers freeze over every year, and in historical time, the dates of freeze-up and breakup were both economically and psychologically important. Consequently, diaries and journals from these regions commonly contain frequent reference to the state of icing on nearby rivers and estuaries. Ironically, remote regions of northern Canada are relatively well endowed with historical records, thanks to the efforts of Hudson's Bay Company managers at various company posts around Hudson's Bay and points to the west (Ball, 1992). A valuable analysis of such data from western Hudson's Bay has been made by Catchpole et al. (1976). Using content analysis, they analyzed journals kept by Hudson's Bay Company, trading post managers from the early eighteenth to the late nineteenth century. Although reference to the state of ice on nearby rivers and estuaries was often imprecise, content analysis enabled quite reliable estimates to be made of the dates of freeze-up and breakup (Figure 15.11) and these provide a unique index of overall "winter duration" in this remote region (Moody and Catchpole, 1975). The prolonged period of both early freeze-up and late

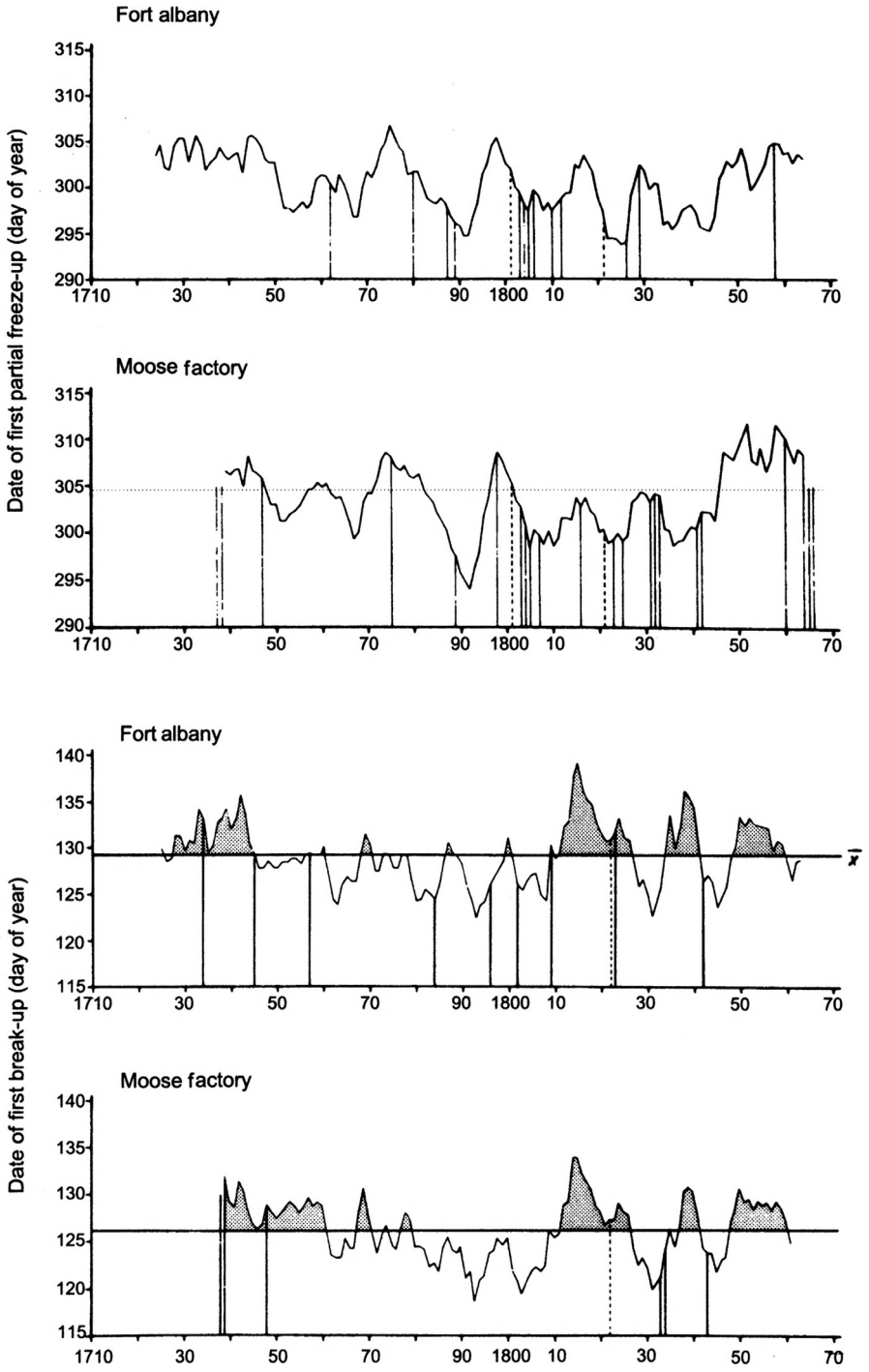


FIGURE 15.11 Seven-year running means of dates of first partial freezing (above) and first breaking (below) of ice in estuaries at the locations indicated (all on west coast of Hudson's Bay, Canada). Data obtained by content analysis of historical sources. See also Table 15.3. Comparable dates for modern conditions shown as horizontal lines. Dates are given in days after December 31. *After Catchpole et al. (1976).*

TABLE 15.3 Comparison of Historical (H) and Modern (M) Dates of Freeze-Up and BreakUp (in Days After December 31)

	First Partial Freezing (H) or First Permanent Ice (M)			First Complete Freezing (H) or Complete Freezing (M)			First Breaking (H) or First Deterioration of Ice (M)		
Site	**Earliest**	**Mean**	**Latest**	**Earliest**	**Mean**	**Latest**	**Earliest**	**Mean**	**Latest**
Churchill River at Churchill (M)	273	291	318	288	319	336	141	160	169
Fort Prince of Wales	273	292	319	295	321	345	150	168	187
Hudson Bay at Churchill (M)	292	305	319	313		340	124	159	180
Moose Factory (H)	281	304	335	290	319	341	105	126	145
Moose River at Moosonee (M)	304	316	331	217	330	347	103	116	126

After Catchpole et al. (1976).

breakup in the early part of the nineteenth century is particularly noteworthy. Comparisons with modern data are difficult because the sites are no longer inhabited, but where comparisons can be made, it appears that the "freeze season" (the time between freeze-up and breakup) averaged 2-3 weeks longer during the eighteenth and nineteenth centuries than in recent years (Table 15.3).

15.2.3 Phenological and Biological Records

In this section, consideration will be given to purely phenological data, that is, data on the timing of recurrent biological phenomena (such as the blossoming and leafing of plants, crop maturation, animal migrations, etc.) and historical observations on the former distribution of particular climate-sensitive plant species. In China, phenological observations have been made for thousands of years, with the first "phenological calendar," showing the annual cycle of nature, dating to the eleventh century BC (Yoshino, 2004). Phenology in Europe dates from the eighteenth century, when Linnaeus began to keep notes on plant leafing and flowering dates, the timing of seed production, etc., in Sweden (Freer, 2003). Phenological networks are now well established in many countries (for a summary, see Rutishauser, 2007).

The value of phenological records as a proxy of climate is illustrated in Figure 15.12. From 1923 to 1953, the flowering dates of 51 different species of plants in a Bluffton, Indiana, garden were noted. For each species, the average date of flowering was computed and individual years expressed as a departure from the 30-year mean (Lindsey and Newman, 1956). Yearly departure values for all species were then averaged to give an overall departure index for the 51 species; in Figure 15.12, this is plotted against the mean temperature of the period March 1 to May 16 (i.e., the start of the growth period). Clearly, the phenological data are an excellent index of spring temperatures; cool periods corresponding closely to late flowering dates and *vice versa*. This example illustrates well the potential paleoclimatic value of long-term

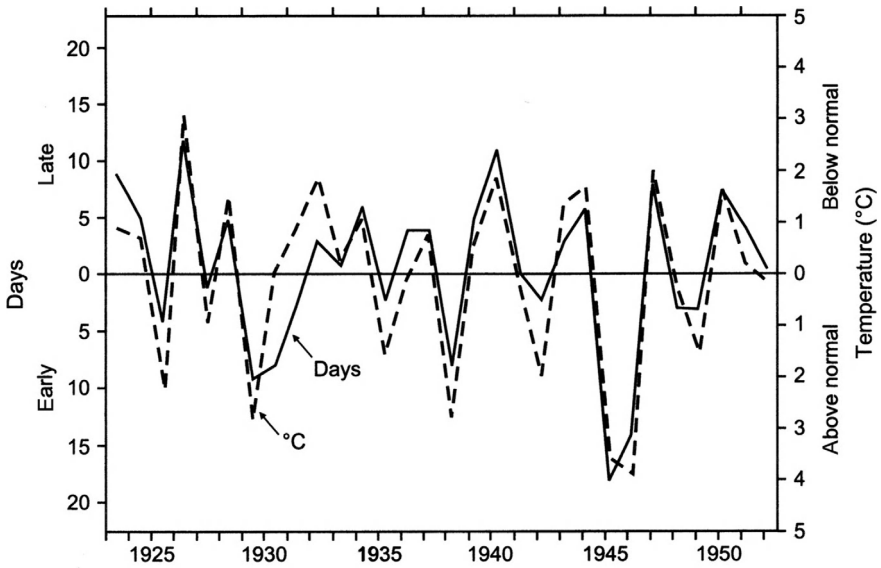


FIGURE 15.12 Phenological data as a climatic index. Solid line shows the average number of days per year in which the flowering dates of 51 species were earlier (below zero, left ordinate) or later (above zero, left ordinate) than the average. The dashed line shows the average departure of mean daily temperature from March 1 to May 16 for each year (right ordinate scale). Observations from Bluffton, Indiana. *After Lindsey and Newman (1956).*

phenological observations; if they can be calibrated, they may provide an excellent proxy record of past climatic variation (Sparks and Carey, 1995; Primack et al., 2004; Rutishauser et al., 2007; Schleip et al., 2008).

One of the longest and best known phenological records comes, like so many other long historical records, from the Far East. At Kyoto (the capital of Japan from AD 784 to 1869), the governor or emperor used to hold a party under the flowering cherry blossoms of his estate, when they were in full bloom, and so extensive records of these events exist (Arakawa, 1956b, 1957; Sekiguti, 1969). The blooming dates can be considered as an index of spring warmth (February and March) when the flower buds develop (Aono and Kazui, 2008; Primack et al., 2009; Aono and Saito, 2010). Higher spring temperatures result in earlier blooming dates. The Kyoto record is extremely sparse before AD 1100, but nevertheless, it is of interest as it spans such a long period of time (Figure 15.13). The date of flowering in individual years has varied by as much as a month, but it is difficult to detect any significant long-term trend in the data, other than the obvious warming (earlier flowering dates) since the early twentieth century, which is probably related (at least in part) to the urban heat island effect in Kyoto. The coldest periods were from 1330 to 1350, 1520 to 1550, and 1670 to 1700 (Aono and Kazui, 2008). The late seventeenth century was notably cold and snowy in Japan, as also noted in historical records by Maejima and Tagami (1983).

The most important phenological records from Europe concern harvest dates such as the beginning of the rye harvest (Tarand and Kuiv, 1994) and, most importantly, the timing of grape harvests (Le Roy Ladurie et al., 2006; Meier et al., 2007). Grape harvests are, of course, determined not only by climatic factors but also by economic considerations. For example,

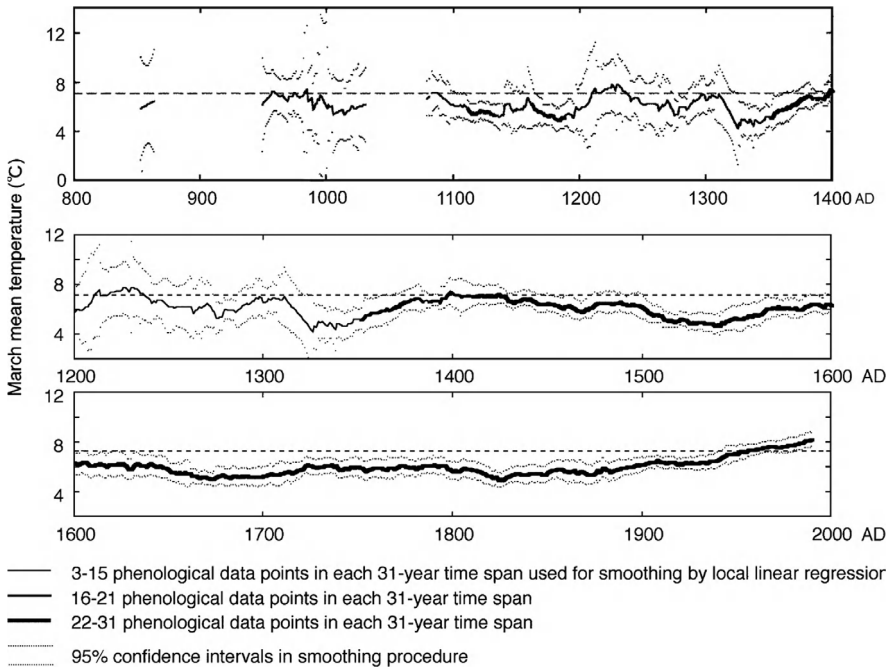


FIGURE 15.13 March mean temperature at Kyoto, based on dates of the year when the cherry tree (*Prunus serrulata* var. *spontanea also known as Prunus jamasakura*), was in full flower at Kyoto, Japan, according to old diaries and chronicles. The dates of the year were calibrated against March mean temperature in the instrumental period. Different curve thicknesses indicate differences in the number of phenological data points in each 31-year span used by the local linear regression procedure. Confidence intervals (95%) on the smoothed value are also shown in dotted lines. For the period in the upper panel, additional data from the flowering dates of wisteria (*W. floribunda*) were used, based on a regression between cherry and wisteria blooming dates. Current mean temperature for March, after adjusting for the urban heat island, is 7.1 °C (dashed line). Note the different timescale for the upper panel. *From Aono and Kazui (2008) and Aono and Saito (2010).*

an increasing demand for brandy may cause the vineyard owner to delay the harvest in order to obtain a liquor richer in sugar and more desirable from the point of view of spirits production. However, such factors are unlikely to be of general significance, and providing variation in the dates of grape harvests show regional similarities, it is reasonable to infer that climate is a controlling factor. Thus, Chiune et al. (2004) calculated the median date of the pinot noir grape harvest at different sites in Burgundy (northeastern France) back to AD 1370 and then converted the dates to mean temperature estimates for April-August using a process-based model of pinot noir grape growth (Figure 15.14). This indicates that warm periods, comparable to the end of the twentieth century, occurred in the 1380s, 1420s, and between 1630 and 1680. The record also clearly shows the remarkable warmth that the region experienced in the summer of 2003 was truly exceptional (cf. Luterbacher et al., 2004; Schär et al., 2004). These results extend the work of LeRoy Ladurie and Baulant (1981) who produced a regionally homogeneous index of grape harvest dates for central and northern France, based on over 100 local harvest date series, extending back

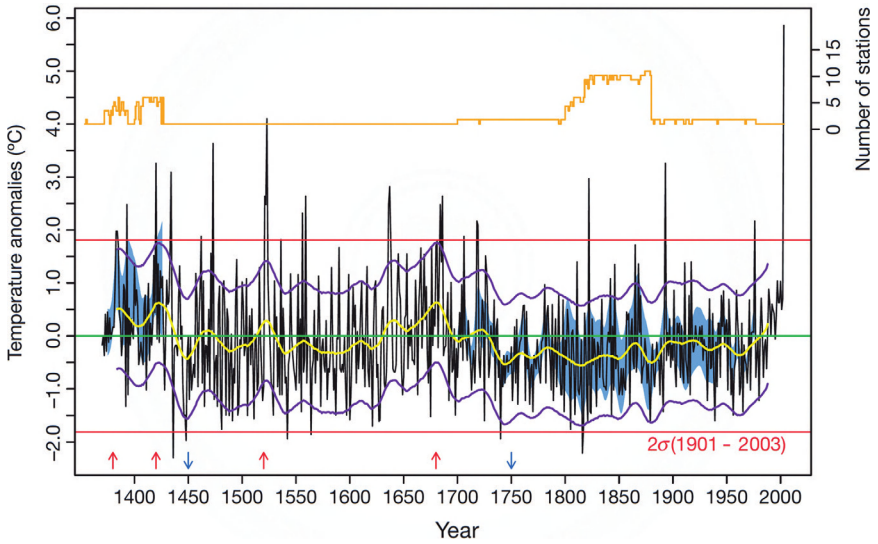


FIGURE 15.14 April-August temperature anomalies in Burgundy, France, as reconstructed from grape harvest dates from 1370 to 2003. Yearly anomalies are in black and the 30-year Gaussian filter is in yellow. Confidence intervals, due to vineyard differences (when there were more than three available observations in a year), are shaded in blue. Orange line (number of stations) represents the number of observed harvest dates for each year. Confidence intervals (with two standard errors), based on the regression between observed and reconstructed temperature in Dijon, 1880-2000, are in purple. Green horizontal (zero) line is the 1960-1989 reference period. Red horizontal lines represent the 2σ interval of the reconstructed temperature for the twentieth century (1901-2003). Vertical arrows indicate warm or cold decadal periods (red or blue) that were above the 90th percentile or below the 10th percentile. *From Chiune et al. (2004).*

to 1484. For the period of overlap with instrumental records from Paris (1797-1879), this index had a correlation coefficient with mean April to September temperatures of +0.86, indicating that it provides a good proxy of the overall warmth of the growth season (LeRoy Ladurie, 1971). Indeed, Bray (1982) showed that the reconstructed summer paleotemperatures also have a strong correlation with the record of alpine glacier advances in western Europe. Periods characterized by temperatures consistently below the median value were generally followed by glacier advances.

The deterioration of climate during the LIA also had important geographic consequences for plants and animals, particularly in marginal environments. In the Lammermuir Hills of southeastern Scotland, for example, oats were cultivated up to elevations of over 450 m during the warm interval from AD 1150 to AD 1250. However, by AD 1300, the *uppermost* limit had fallen to 400 m and by AD 1600 to only ~265 m, more than doubling the area of uncultivable land (Parry, 1975, 1981). These changes probably resulted from reduced summer warmth, wetter conditions, and earlier snowfalls in winter months, factors which all combined to increase the probability of crop failure from only 1 year in 20 in the Middle Ages to 1 year in two or three during the LIA. The abandonment of upland field cultivation was also accompanied by the abandonment of upland settlements and resulted in a considerable redistribution of population in the area.

Former plant and animal distributions can provide useful indices of climatic fluctuations. For example, Parmesan and Yohe (2003) have documented widespread changes in the distribution of flora and fauna in the twentieth century as a result of global warming. These changes have affected marine and terrestrial species. Trading post records of marine mammals and other species around the coasts of Greenland also point to the close dependence of animal populations on climatic fluctuations and associated changes in the distribution of sea ice over the last century (Vibe, 1967). However, such records rarely extend back beyond the mid-nineteenth century and merely point to the biological significance of climatic fluctuations, which instrumental records have documented in considerable detail. Nevertheless, there is great potential in using historical records of former plant and animal distributions, the timing of migrations, etc., to document climatic variations during periods for which no instrumental records exist. The possible value of such work is well illustrated by the wide-ranging surveys of former plant and animal populations in China reported by Chu (1973) and Ge et al. (2003).

15.3 REGIONAL STUDIES BASED ON HISTORICAL RECORDS

Historical records of unusual weather events in key parts of the world have been used to reconstruct extreme ENSO (El Niño/Southern Oscillation) events (Quinn, 1992, 1993; Quinn and Neal, 1992; Mabres et al., 1993; Ortlieb, 2000; García-Herrera et al., 2008). El Niños are characterized by unusually warm water off the coast of Ecuador and northern Peru, especially in December, and are associated with circulation anomalies resulting from the redistribution of atmospheric mass across the South Pacific (the Southern Oscillation). Oscillations of this coupled ocean-atmosphere system generally occur over a 3- to 7-year period with above-average sea surface temperatures along the eastern equatorial Pacific later replaced by below-average temperatures (La Niñas). ENSOs result in global temperature and precipitation anomalies (Bradley et al., 1987) and worldwide disruptions of the climate system, with certain regions being particularly affected (Diaz and Kiladis, 1992). During strong El Niños, heavy rains are common in coastal regions of southern Ecuador and northern Peru, often causing floods and landslides, whereas across the Pacific, El Niños are associated with droughts in Indonesia and northeastern Australia, often leading to widespread brush fires. Because weather conditions can often be quite extreme during both El Niño and La Niña events (depending on the location), historical documents reporting on these events can be used to piece together when they occurred and to rank them in terms of their overall magnitude. This has proven useful in interpreting and verifying other proxy records of ENSO events, such as those derived from corals, tree rings, and multiproxy reconstructions (e.g., Cook et al., 2000; Mann et al., 2000; D'Arrigo et al., 2005; McGregor et al., 2010; Fowler et al., 2012; Hereid et al., 2012). However, early work on this topic (Quinn, 1992, 1993; Quinn and Neal, 1992) has been extensively revised because the reconstructions did not rely on primary documentary sources, and El Niños were often identified by anomalies in far-flung regions that are sometimes (but not always) linked by atmospheric teleconnections to El Niño events. Thus, García-Herrera et al. (2008) consider that all previous studies (including Ortlieb, 2000) have overestimated the frequency of El Niño events. Their chronology is based only on primary sources from Trujillo, northern Peru, where the most robust and consistent signal of El Niño occurrence (i.e., unusually heavy rainfall in what is normally an

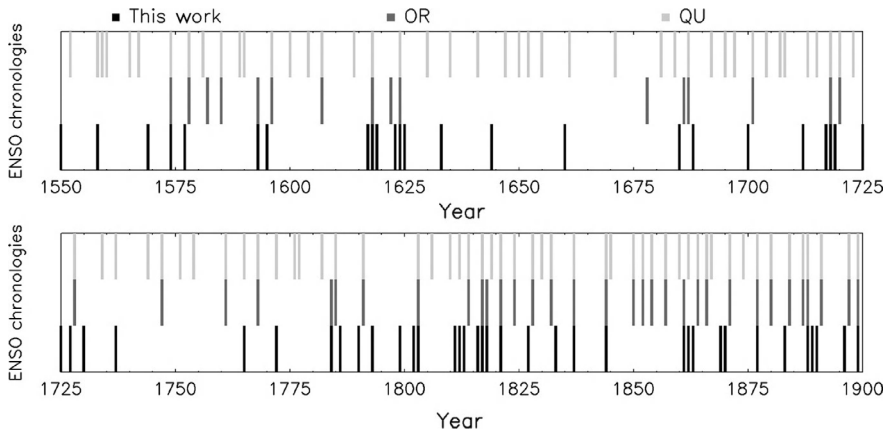


FIGURE 15.15 A comparison of the years when El Niños occurred in the 1550-1900 period, according to the reconstructions of Quinn (1992) (top), Ortlieb (2000) (middle), and García-Herrera et al. (2008) (bottom). Ortlieb reassessed Quinn's work and confirmed only a small number of events. García-Herrera et al. rely only on primary sources from a location with a clear and unequivocal link to El Niños. *From García-Herrera et al. (2008).*

extremely arid location) is well documented. Figure 15.15 provides a summary of these different interpretations.

There is an increasing number of studies from the Caribbean region and Central and South America, which have extensive historical records dating from colonial time (e.g., Chenoweth, 2003; Endfield, 2007; Mendoza et al., 2007; Prieto, 2007; Neukom et al., 2009; Prieto and García-Herrera, 2009). Of particular note are studies of hurricanes and severe storms in the Caribbean and adjacent tropical Atlantic that were often clearly described in historical reports (García-Herrera et al., 2004, 2005, 2007). From these studies, it appears that there was an above-average number of hurricanes from 1766 to 1780, which may indicate that there were relatively warm sea surface temperatures in the tropical Atlantic at that time, and (perhaps) few El Niños (Figure 15.15), which tend to be associated with strong upper-level winds across the tropical Atlantic that disrupt hurricane development.

Apart from land-based observations of meteorologic conditions, there are vast archives of marine records in many libraries; ships' logs contain valuable information about wind direction, wind speed, cloud cover, and other parameters. The CLIWOC project (*Climatological Database for the World's Oceans, 1750-1850*) (Wheeler et al., 2006) focused attention on the importance of these records, but there are many more that can yield valuable information (e.g., Frich and Freyendahl, 1994; García-Herrera et al., 2004; Wheeler and Suarez-Dominguez, 2005). At higher latitudes, ships' logs can also provide much information about sea-ice conditions and the presence of icebergs, which were a significant threat in polar waters (Catchpole, 1992; Prieto et al., 2004).

One of the most fascinating studies of ships' voyages is that of Garcia et al. (2001) who examined the time it took for Spanish galleons to cross the Pacific from Acapulco to Embarcadero de San Bernardino (at the southeastern tip of Luzon Island) en route to Manila in the Philippines. Between 1585 and 1815, ships regularly undertook this voyage at latitudes 10-15°N, taking advantage of the northeast trade winds, carrying merchandise between the two Spanish colonial empires. By examining records in the *Archivo General de Indias* (in Seville, Spain), Garcia et al. found that the galleons generally set sail between mid-March

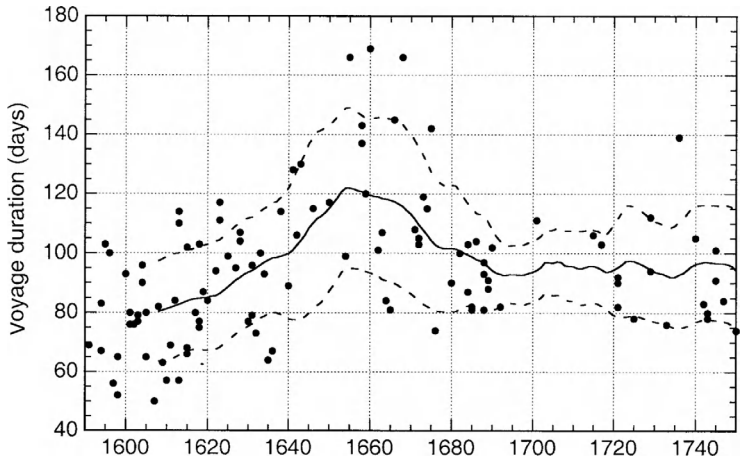


FIGURE 15.16 Number of days taken by Spanish galleons sailing from Acapulco, Mexico, to reach Embarcadero de San Bernardino (at the southeastern edge of Luzon, in the Philippines) en route to Manila, 1591-1750. Solid line, 30-year running mean; dashed lines, ±1 standard deviation. *From Garcia et al. (2001).*

and mid-April, and the duration of each voyage varied considerably from year to year, averaging about 3 months. However, significant decadal-scale differences were also apparent (Figure 15.16) with voyages taking much longer between 1640 and 1670. By looking at the westward progression of the galleons, it became clear that most of this difference was related to changes in the position and strength of the western Pacific monsoon trough, which appears to have been positioned further east from ~1640 to ~1670. This literally took the wind out of the ships' sails because the easterly trades were replaced by more southerly and southwesterly winds associated with the monsoon-trade wind convergence zone.

15.3.1 East Asia

Dynastic records, local histories, and diaries from China, Korea, and Japan are valuable sources of information about past weather events and their impacts on these largely agricultural societies (Kim, 1987; Wang and Zhang, 1988; Batten, 2009). Numerous investigators have sifted through these enormous archives to extract weather-related information (see, for example, the volumes edited by Zhang, 1988; Mikami, 1992a; Zhang, 2004) and many climate reconstructions based on these records have been published (Table 15.4).

In China, most studies have been carried out on records from the lower Yangtze River Basin and regions to the north (Wang and Wang, 1989; Wang and Wang 1990; Wang, 1991a,b; Wang et al., 1991; Wang et al., 1991; Ge et al., 2003). Phenological records from across east-central China, together with data on the number of snow days per year at Hefei (in the lower Yangtze River valley), were calibrated with seasonal temperatures at nearby stations to reconstruct winter half-year temperature anomalies over the past two millennia (Figure 15.17) (Ge et al., 2003). When averaged over the region, this indicates that temperatures were lowest in the fifth century and then slowly increased to reach highest levels in the tenth and thirteenth centuries. Temperatures then declined to low levels again in the early nineteenth century, with another particularly cold interval in the mid-seventeenth century when killing frosts severely damaged

TABLE 15.4 Paleoclimate Series Constructed for East Asia Based on Historical Records

	Region	Sp	Su	Fa	Wi	Ann	Record of	Interval	Ref. Period	Period	Source
1	East China	x	x	x	x	x	Temperature anomalies	10	1470-1980	1470-1980	Wang and Wang (1990, 1991), Wang (1991b)
2	North China	x	x	x	x	x	Temperature anomalies	10	1470-1980	1470-1980	Wang and Wang (1990, 1991), Wang (1991a,b)
3	South China (five regions[a])				x		Temperature anomalies	10	1470-1970s		Zhang (1980), Zhang (1988)
4	China				x		Number of cold winters	10		1500-1970s	Zhang and Gong (1979)
5	Lower Yellow River					x	Number of frosts	10		1440-1940s	Zhang and Gong (1979)
6	Shandong province				x		Cold winter index	10		1500-1970s	Zheng and Zheng (1992)
7	Southeast China (Shanghai)	x	x	x	x	x	Temperature anomalies	10	1950-1979	1470-1970s	Wang et al. (1991)
8	Mid and South China (S. of 35°N)				x		Temperature anomalies	10	1951-1980	1470-1970s	Wang and Wang (1989)
9	China				x		Thunder events	30		190 BC-1920	Wang (1980)
10	Middle and Lower Yangtze					x	Temperature indices	10		1470-1970s	Zheng and Feng (1986)
11	Eastern China					x	"Dust Rain" events	1		<300 BC-1933	Zhang (1983)
12	Beijing	x	x				Mean temperatures	1		1724-1986	Wang et al. (1992)
13	S. China				x		Frost, snow (irregular)	1		1488-1900	Li (1992)
14	China				x		Winter monsoon index	10		1390-1980	Guo (1992)
15	Korea					x	Number of cold events	50		1392-1900	Kim (1984)
16	Hirosaki, Japan	x	x	x	x	x	Maximum temperature	20-40	1661-1870	1661-1870	Maejima and Tagami (1983)

Continued

TABLE 15.4 Paleoclimate Series Constructed for East Asia Based on Historical Records—cont'd

	Region	Sp	Su	Fa	Wi	Ann	Record of	Interval	Ref. Period	Period	Source
17	Japan		x		x		Temperature index	10		601-1900	Maejima and Tagami (1986)
18	Japan		x				Temperature	1	1950-1970	1771-1840	Mikami (1992a,b)
19	C. Japan		x		x		Temperature, precipitation	1		1801-1870	Mizukoshi (1992)
20	C. and S. Japan		x		x		Snow/rain ratio; summer rainfall	1		1670-1860	Tagami and Fukaishi (1992)
21	C. and S. Japan				x		Synoptic type frequency	1		1720-1869	Fukaishi and Tagami (1992)

[a]*Region I, eastern part of Changjiang River Basin; Region II, central part of Changjiang River Basin; Region III, Hunan and Jiangxi provinces; Region IV, southeastern provinces; Region V, Guangdong and Guangxi provinces.*

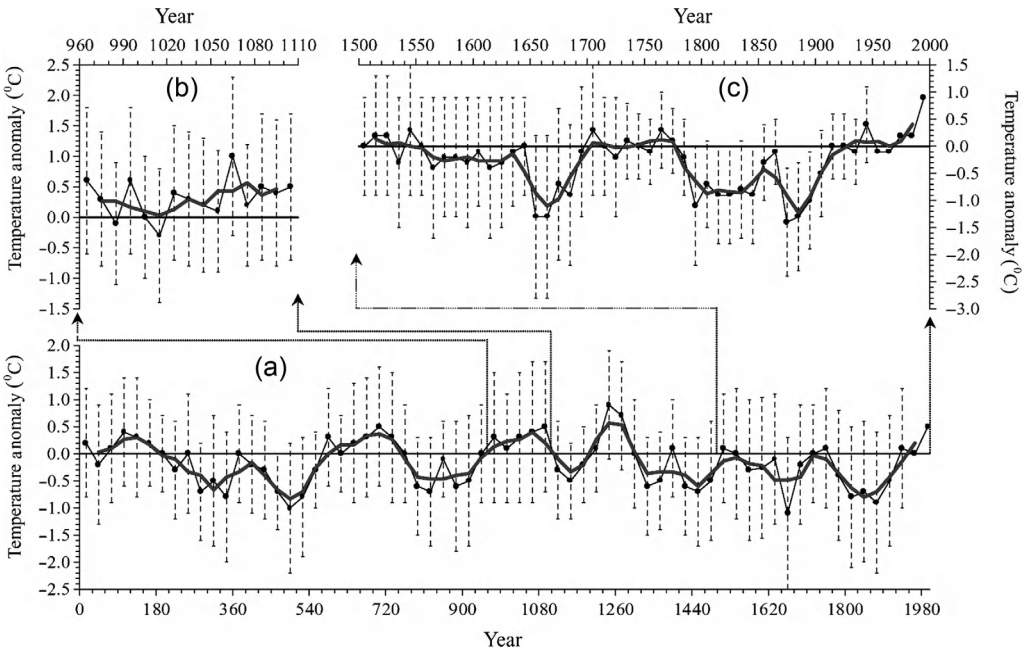


FIGURE 15.17 Winter half-year temperature anomalies from the 1951 to 1980 mean, averaged over 20 sites in eastern China. Averages have a 30-year resolution during (a) the past 2000 years and 10-year resolution during (b) AD 961-1110 and (c) 1501-1999. Black line with dots shows the winter half-year temperature anomalies; darker line is a three-point running mean. Dashed lines show error bars for each 10- or 30-year average. *From Ge et al. (2003).*

vegetation as far south as 20°N (Li, 1992). The 1650s were also exceptionally cold in Korea (Kim, 1984, 1987). Indeed, Kim and Choi (1987) believe that summers in Korea in the period 1631-1740 were the coldest of the past 1000 years. During both of the cold periods, in the seventeenth and nineteenth centuries, the frequency of floods and droughts in China increased, suggesting greater instability in climate during those times (Zheng and Feng, 1986).

In Japan, many documents dating from the Edo era (late seventeenth to early nineteenth centuries) contain records of daily weather conditions (Figure 15.18). This has enabled monthly climatological maps to be constructed for 1700-1870, using daily synoptic

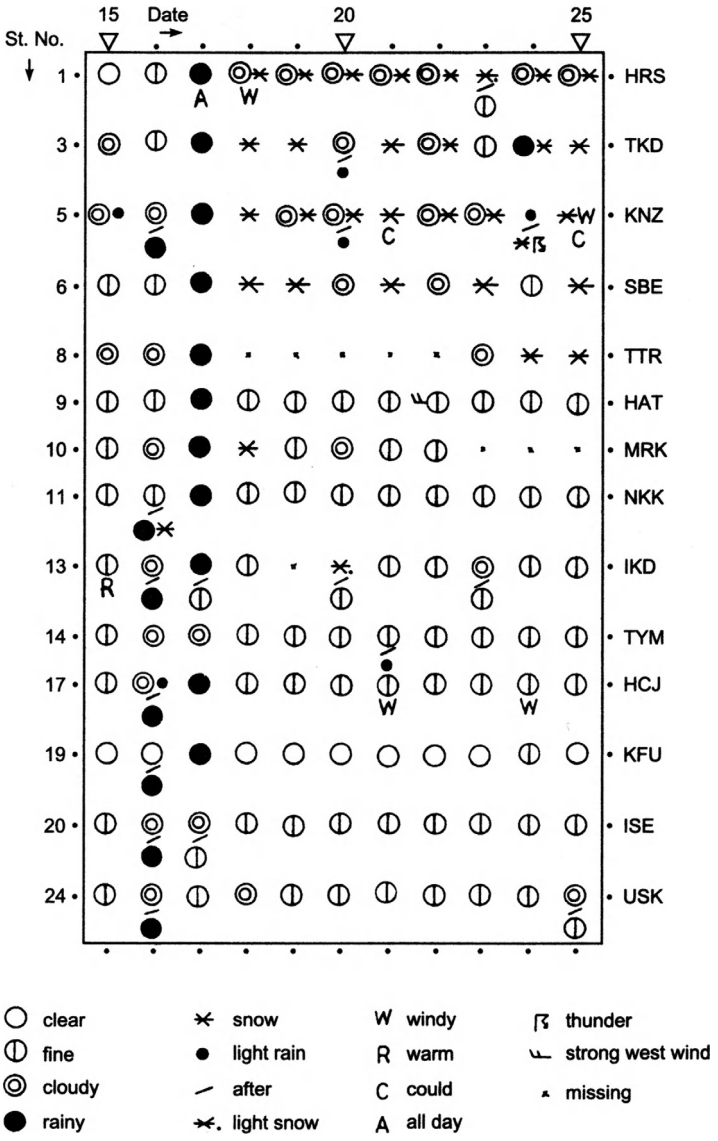


FIGURE 15.18 An example of coded weather data for January 15-25, 1754, derived from diaries kept by feudal clans in 14 different locations throughout Japan. *From Fukaishi and Tagami (1992).*

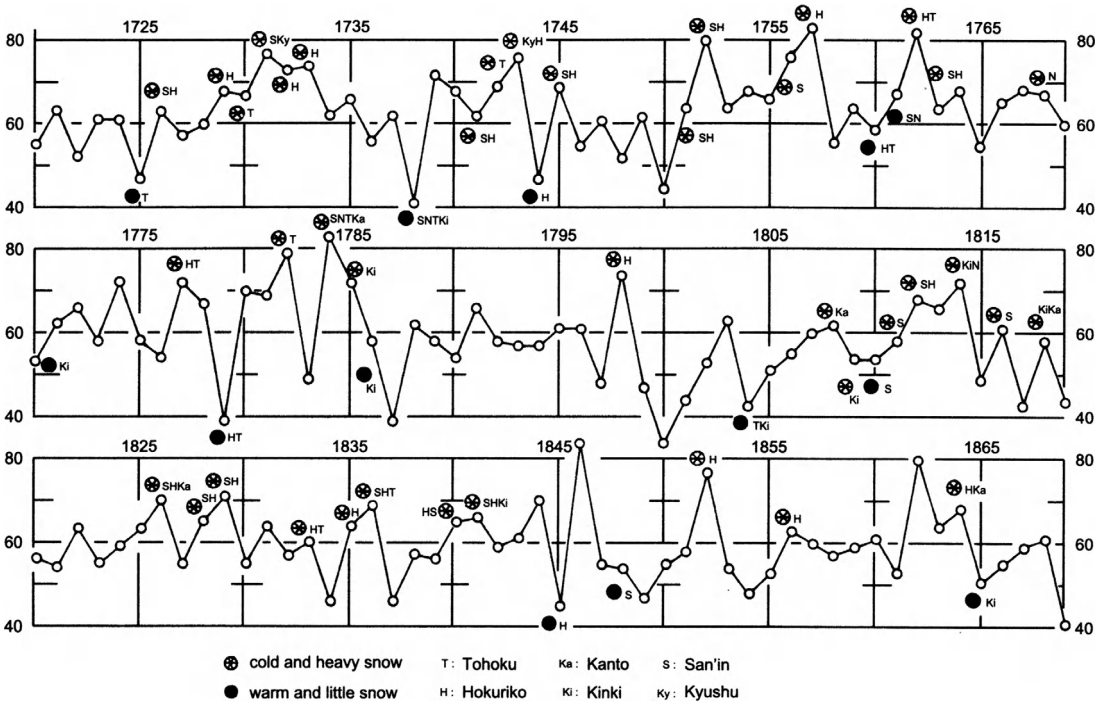


FIGURE 15.19 Annual number of days with a "winter-like" pressure pattern across Japan (high pressure in the west and low pressure in the east) for the period November 1-March 31 each year from 1720 to 1869, based on an interpretation of mapped weather information obtained from diaries. *From Fukaishi and Tagami (1992).*

information provided by the network of early observers (Yoshimura, 1996). All of the information has been coded and digitized for computer-based analysis (Yoshimura, 1992). These historical records have provided a wealth of information about the climate of Japan during the last 250 years (Mizukoshi, 1992; Murata, 1992; Tagami and Fukaishi, 1992). For example, Fukaishi and Tagami (1992) classified the observations into those patterns that are typical of characteristic "winter-like" pressure patterns, with high pressure in the west and low pressure in the east. Figure 15.19 shows the number of days with this pattern during the November-March period of each year, from 1720 to 1869. Unusually cold conditions with heavy snow were common in the years when this pressure pattern prevailed (e.g., 1726-1733, 1777-1785, 1808-1819, and 1826-1836).

15.3.2 Europe

Evidence for significant changes in the climate of Europe over the last few centuries is abundant (Frenzel et al., 1992; Pfister, 1992) and several major summaries have been published focusing on specific regions (Pfister, 1984, 1999; Brázdil and Kotyza, 1995-2000; Buisman and van Engelen, 1995-2000; Rácz, 1999; Glaser, 2001). This has led to quantitative regional reconstructions of temperature and precipitation that enable the more recent instrumental period to be placed in a longer-term perspective. For example, Dobrovolný

et al. (2010) calibrated documentary material from Switzerland, Germany, and the Czech Republic with overlapping instrumental temperature data to reconstruct monthly temperature anomalies back to AD 1500 (Figure 15.20). This showed that the period since 1988 was the warmest of the entire record. A similar conclusion was reached by van Engelen et al. (2001) and Shabalova and van Engelen (2003) for the Low Countries, with the last 25 years of the twentieth century warmer, in both winter and summer seasons, than any comparable period in the last millennium. Region-wide reconstructions, combining documentary data with tree ring and instrumental data, also confirm the unusual nature of recent decades (Luterbacher et al., 2004, 2007; Xoplaki et al., 2005). Precipitation is more variable but large-scale anomalies have been reconstructed (Pauling et al., 2006). Both the temperature and precipitation fields point to the importance of the North Atlantic Oscillation (NAO) in determining strong regional anomaly patterns. Winter sea-level pressure patterns have also been reconstructed for the last 500 years, based on statistically derived relationships between temperature, precipitation, and pressure anomalies at specific locations in the instrumental period and observed pressure fields across the North Atlantic and Europe. The resulting equations (transfer functions) were then applied to climatic data derived from documentary data to reconstruct sea-level pressure back to AD 1500 (Luterbacher et al., 2002). Figure 15.21 shows the two leading EOFs of sea-level pressure during the period AD 1500 to 1999, based on this analysis. EOF 1 accounts for 55% of the variance and represents a dipole pattern reminiscent of the NAO. EOF 2 shows a pattern typical of anticyclonic blocking situations over western Europe. The time series of EOF 1 shows that the recent expression of this pattern is unprecedented in the last 500 years.

15.4 RECORDS OF CLIMATE FORCING FACTORS

Historical observations have been important in documenting the occurrence of major explosive volcanic eruptions and in tracking indices of solar variability (indicative of changes in irradiance). Unusual postsunset sky colors were commonly recorded by astute observers of the heavens, and many such observations can be linked to large explosive volcanic eruptions, which lofted sulfur-rich gases and particulate matter high into the stratosphere. Scattering of solar radiation by these particles can reduce direct radiation and cause dramatic early morning or late evening sky colors (Meinel and Meinel, 1983). For example, Chinese chroniclers reported that, in the reign of Emperor Ling Ti (AD 168-189), "several times the sun rose in the east red as blood and lacking light. . .only when it had risen to an elevation of more than two zhàng [24°] was there any brightness. . ." At the same time, Roman observers noted, "before the war of the deserter [A.D. 186] the heavens were ablaze....stars were seen all the day long. . . hanging in the air which was a token of a cloud. . ." (Wilson et al., 1980). These are typical descriptions of the sky following major explosive volcanic eruptions; it seems likely that this particular event was related to eruptions in Alaska (White River ash), which have been radiocarbon dated to around that time. Lamb (1970, 1977, 1983) used these kinds of observations as the basis for constructing a chronology of explosive volcanism over the past ~500 years, which he termed the Dust Veil Index (DVI) (Figure 15.22). This proved to be invaluable in interpreting the acidity record of ice cores, which is also a register of explosive volcanic events (see Section 5.3.2). Many studies have used the DVI to assess the impact of

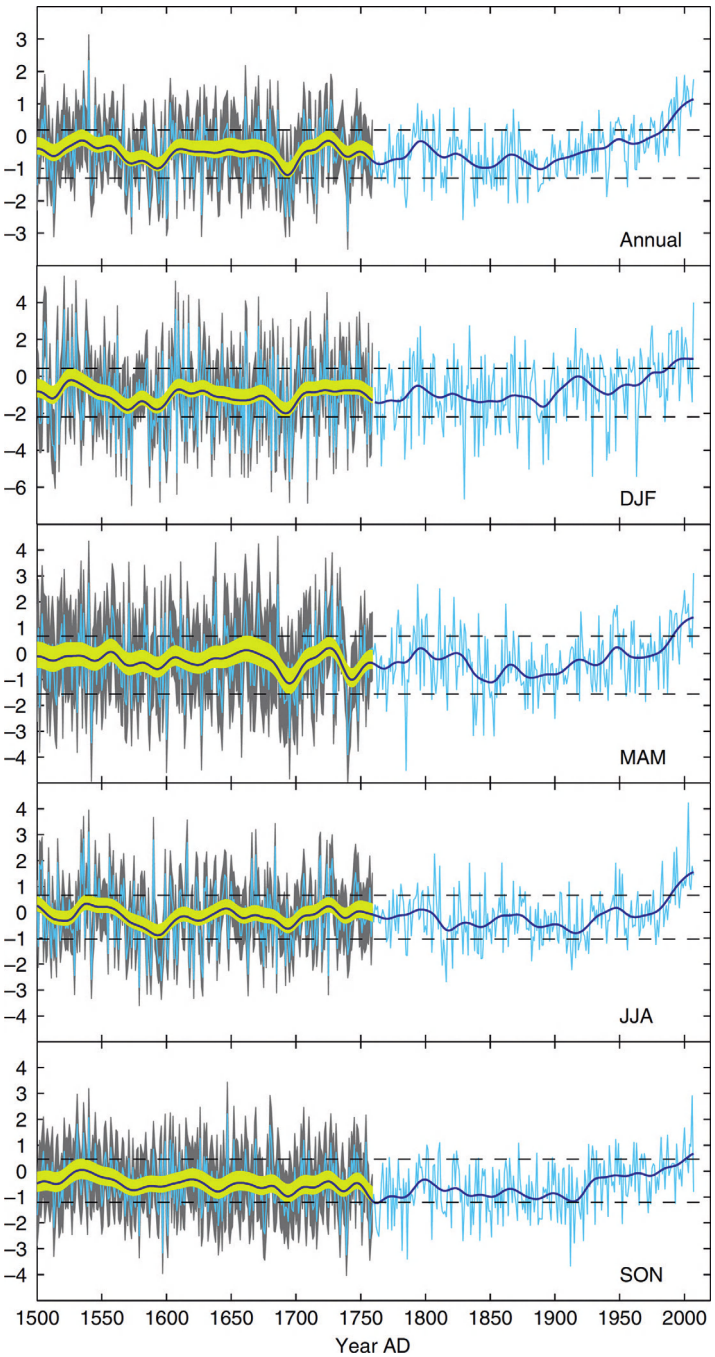


FIGURE 15.20 Spliced Central European temperature reconstructions AD 1500-2007 (based on variance and mean-adjusted proxy data for 1500-1759 and instrumental data for 1760-2007), expressed as anomalies from the 1961 to 1990 average, with Gaussian low-pass-filtered data approximately corresponding to 20-year moving averages. The error bands are ~95% confidence intervals. Dashed horizontal lines show the highest and lowest level for the low-frequency error bars. *From Dobrovolny et al. (2010).*

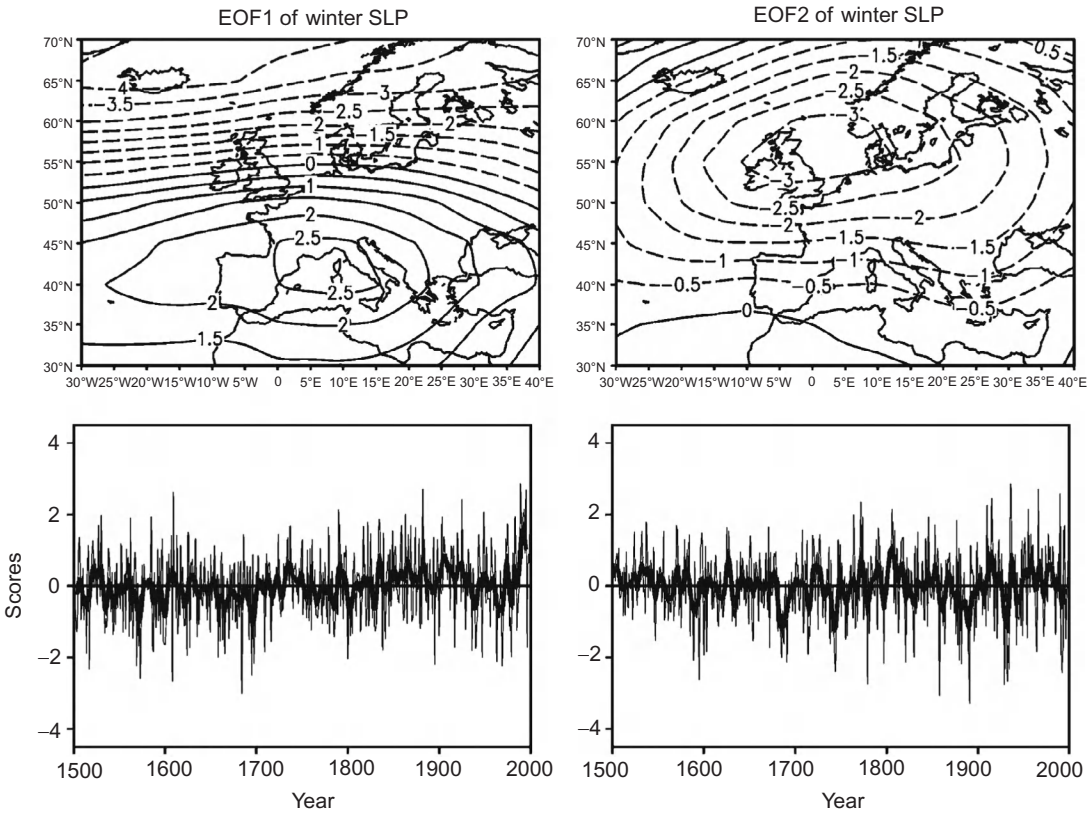


FIGURE 15.21 Top: Patterns of the first two EOFs of winter sea-level pressure (SLP) anomalies 1500-1999 (anomalies in hPa; contour interval 0.5 hPa). The last nine winters are from reanalysis data. The first EOF accounts for 55%, and the second 23%, of the winter SLP variance. Solid lines indicate positive values, and dashed lines mark negative values. Below: Corresponding normalized time components (scores) of the first two EOFs. The thick line is the nine-point low-pass filtered time series. *From Luterbacher et al. (2002).*

explosive volcanism on temperature variations (e.g., Sear et al., 1987) though glaciochemical data from ice cores are now used more commonly to assess the history and magnitude of explosive volcanism (Robock and Free, 1996; Robock, 2000; Gao et al., 2008). Historical records have also been useful in documenting the regional climatic effects of specific eruptions, such as the Lakagígar (Laki) fissure eruption in Iceland (1783-1784) (Stothers, 1996; Demarée and Ogilvie, 2001) and other similar "dry fog" events (Camuffo and Enzi, 1994, 1995). Of particular interest is the eruption of Tambora (Indonesia) in April 1815, which was one of the largest eruptions in the late Holocene and had global climatic effects (Harington, 1992; Stothers, 1984). This event led to cold conditions in many areas the following year, which became known as *the year without a summer*. Historical records have also been valuable in revealing the worldwide effects of a massive explosive eruption in AD 1257 (from Mount Rinjani, Lombok Island, Indonesia) that has been identified in ice cores from both Greenland and Antarctica (Palais et al., 1992; Stothers, 2000; Lavigne et al., 2013).

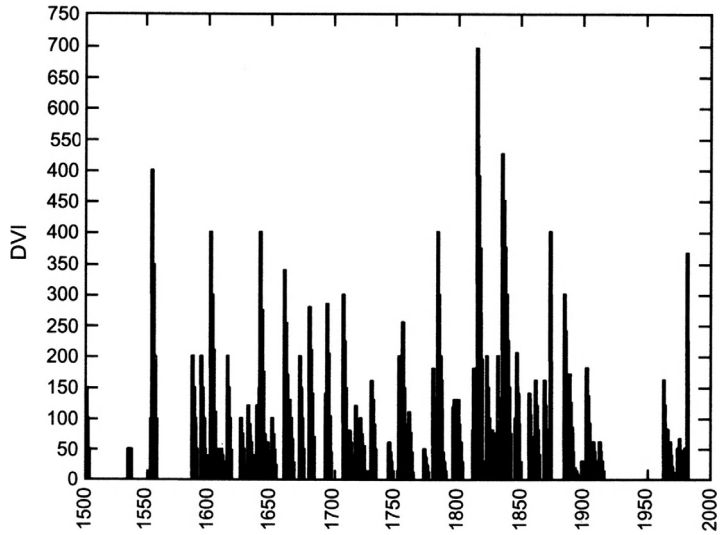


FIGURE 15.22 A Dust Veil Index (DVI) for the Northern Hemisphere, assuming dust from an individual eruption, is apportioned over 4 years, with 40% of each DVI assigned to year 1, 30% to year 2, 20% to year 3, and 10% to year 4. Thus, the 1883 eruption of Krakatau (DVI = 1000) results in values of 400 in 1883, declining to 100 in 1886. It is further assumed that all dust from eruptions poleward of 20°N remained in the Northern Hemisphere. For eruptions equatorward of 15°N, the dust was assigned equally between the two hemispheres, and for eruptions between 15°N and 20°N and 15°S and 20°S, it was assumed that two-thirds of the material remained in the hemisphere of the eruption, and one-third was dispersed to the other hemisphere. *From Bradley and Jones (1992b); DVI values from Lamb (1970, 1977, 1983).*

Early observations of the sun noted dark spots on the photosphere, and astronomical records of these sunspots extend back to the early seventeenth century (Hoyt and Schatten, 1997). Naked-eye sunspot observations and records of auroras have provided clues about solar variability over even longer time periods (Vaquero and Vásquez, 2009; Vaquero and Trigo, 2012). These long-term sunspot observations demonstrate a periodic variation in solar activity with a mean cycle length of ~11 years, though the amplitude of each cycle has changed over time and a prolonged episode of little or no sunspot activity (the Maunder Minimum) occurred from ~1675 to 1715 (Figure 2.25) (Eddy, 1976). Satellite observations of the last few solar cycles show that these involve changes in the solar constant (total irradiance outside the atmosphere) of ~0.1% from sunspot maximum to sunspot minimum. What the longer-term changes in solar cycle magnitude represent in terms of total or spectral irradiance is uncertain, but current estimates are that the overall change in cycle-averaged total irradiance during this period has been ~0.1%; changes in UV radiation may have been greater (Lean, 2000; Wang et al., 2005a,b).

15.5 CLIMATE PARADIGMS FOR THE LAST MILLENNIUM

Conventional wisdom has it that the climate of the last millennium followed a simple sequence—a "Medieval Warm Epoch" (MWE), a "Little Ice Age" (LIA) and then globally extensive warming. This view has its roots in the early work of H. H. Lamb (1963, 1965) but

more recent research has reassessed this paradigm. Lamb defined the MWE as a period of unusual warmth in the eleventh to thirteenth centuries AD, based almost exclusively on evidence from western Europe and the North Atlantic region. His studies predated modern quantitative paleoclimatology, so the values of temperature change that he attributed to this period are essentially anecdotal and based largely on his own estimates and personal perspective. In revisiting the concept of a MWE, Hughes and Diaz (1994) reviewed a wide range of paleoclimatic data, much of it reported since Lamb's classic work (Lamb, 1965). They concluded that "it is impossible at present to conclude from the evidence gathered here that there is anything more significant than the fact that in some areas of the globe, for some part of the year, relatively warm conditions may have prevailed." Thus, they found no clear support for there having been a globally extensive warm epoch in the MWE or indeed within a longer interval stretching from the ninth to the early fifteenth centuries. Certainly, there is little evidence that global or hemispheric mean temperatures were higher during the MWE than in the latter half of the twentieth century (Bradley et al., 2003c,d), yet this notion has somehow become entrenched as common lore. This is unfortunate as it does not help our understanding of natural climate variability and its causes. Perhaps of greater significance is that there were significant precipitation anomalies during the period of the "MWE"; in particular, many areas experienced protracted drought episodes and these were far beyond the range of anything recorded within the period of instrumental records (Figure 15.23). For example, Stine (1994) describes compelling evidence that prolonged drought affected many parts of the western United States (especially eastern California and the western Great Basin) from (at least) AD 910 to ~AD 1110 and from (at least) AD 1210 to ~AD 1350. There is also strong evidence that prolonged drought affected Patagonia during the earlier of these episodes. This led Stine to argue

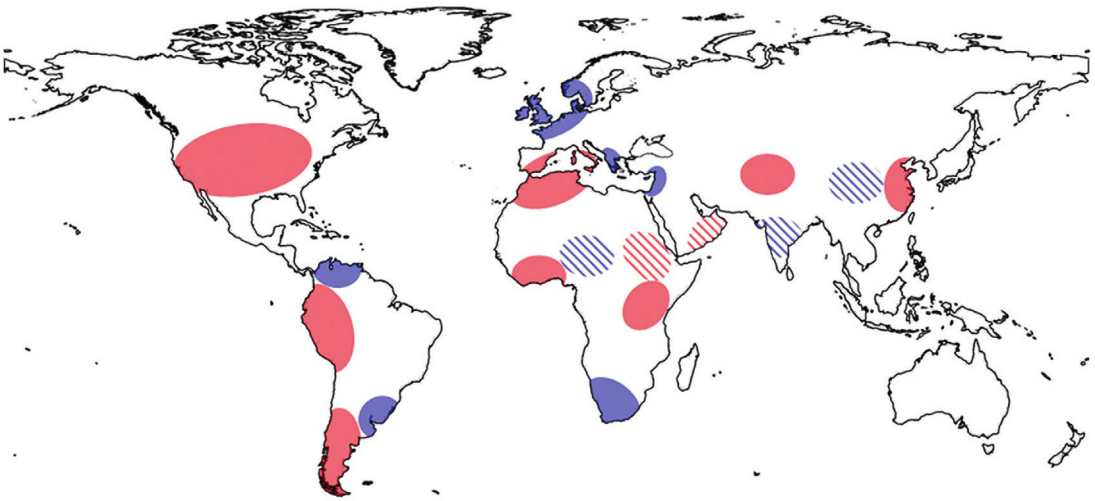


FIGURE 15.23 Hydroclimatic anomalies during the period from AD 950 to 1400. Pink areas indicate anomalously dry conditions during this interval, (relative to twentieth century averages) though droughts generally did not last for the entire period; blue areas indicate wet conditions. Hatching indicates areas where there is more uncertainty. *From Diaz et al. (2011).*

that a better term for the overall period was the "Medieval Climatic Anomaly" (MCA), which removes the emphasis on temperature as its defining characteristic (Stine, 1998). The widespread nature of hydrologic anomalies during the MCA suggests that changes in the frequency or persistence of particular circulation regimes (e.g., NAO and ENSO) may account for the unusual nature of the period, and naturally, this may have led to anomalous warmth in some (but not all) regions. Recent discussions on climate in Medieval times include Mann et al. (2009), Ge et al. (2010), Graham et al. (2011), and Diaz et al. (2011).

Numerous studies provide strong evidence that cooler conditions characterized the ensuing few centuries, and the term "Little Ice Age" is commonly applied to this period (Figure 15.24). The environmental consequences of the Little Ice Age climate are well illustrated in many wonderful paintings of alpine glaciers (far in advance of their current positions) (Zumbühl, 1980; Grove, 1988). Similar glacial evidence is available from virtually all mountainous parts of the world, indicating that the changes were brought about by large-scale forcing factors. Unfortunately, the term "Little Ice Age" is often used without clarity; some authors consider the LIA began in the thirteenth century; others date it as starting in the fifteenth century. In reality, this deterioration was one of several Late-Holocene cool episodes (neoglacials) that led Matthes (1940) to introduce the LIA term. He wrote "We are living in an epoch of renewed but moderate glaciation – a 'little ice age' that already has lasted about 4,000 years... glacier oscillations of the last few centuries have been among the greatest that have occurred during the 4,000 year period... the greatest since the end of the Pleistocene ice age." It is this latest and most dramatic episode of neoglaciation to which the term "Little Ice Age" is now generally applied. In fact, there were a series of post-Medieval cool events, beginning in the thirteenth century (Grove, 2001a,b) and varying in intensity from one region to another, but there seems to have been a more widespread climatic deterioration after $\sim 1510 \pm 50$ (Bradley and Jones, 1992b). There is general agreement that the LIA came to an abrupt end in the mid to late nineteenth century ($\sim$1850-1890), only a few decades after some of the coldest conditions of the last 500 years were experienced. Most of our longest instrumental temperature records began during this time, and much of the warming registered since then represents a recovery from that low point in the early nineteenth century, largely as a result of the buildup of greenhouse gases in the atmosphere.

Just how the LIA is defined is illustrated by several estimates of northern hemisphere mean annual temperature for the last 1000 years, which show a gradual decline in temperature over the first half of the last millennium, rather than a sudden "onset" of a "LIA" (Figure 15.25) (Jansen et al., 2007). Furthermore, it is clear that within the period 1550-1850, there was a great deal of temperature variation both in time and space. Some areas were warm at times when others were cold and vice versa, and some seasons may have been relatively warm, while other seasons in the same region were anomalously cold (Luterbacher et al., 2004; Xoplaki et al., 2005; Mann et al., 2008, 2009). No doubt the complexity or structure that we see in the climate of the LIA is a reflection of the (relative) wealth of information that paleoclimate archives (tree rings, corals, varved sediments, ice cores, historical records, etc.) have provided for this period. Having said that, when viewed over the long term, this overall interval was undoubtedly one of the coldest in the entire Holocene.

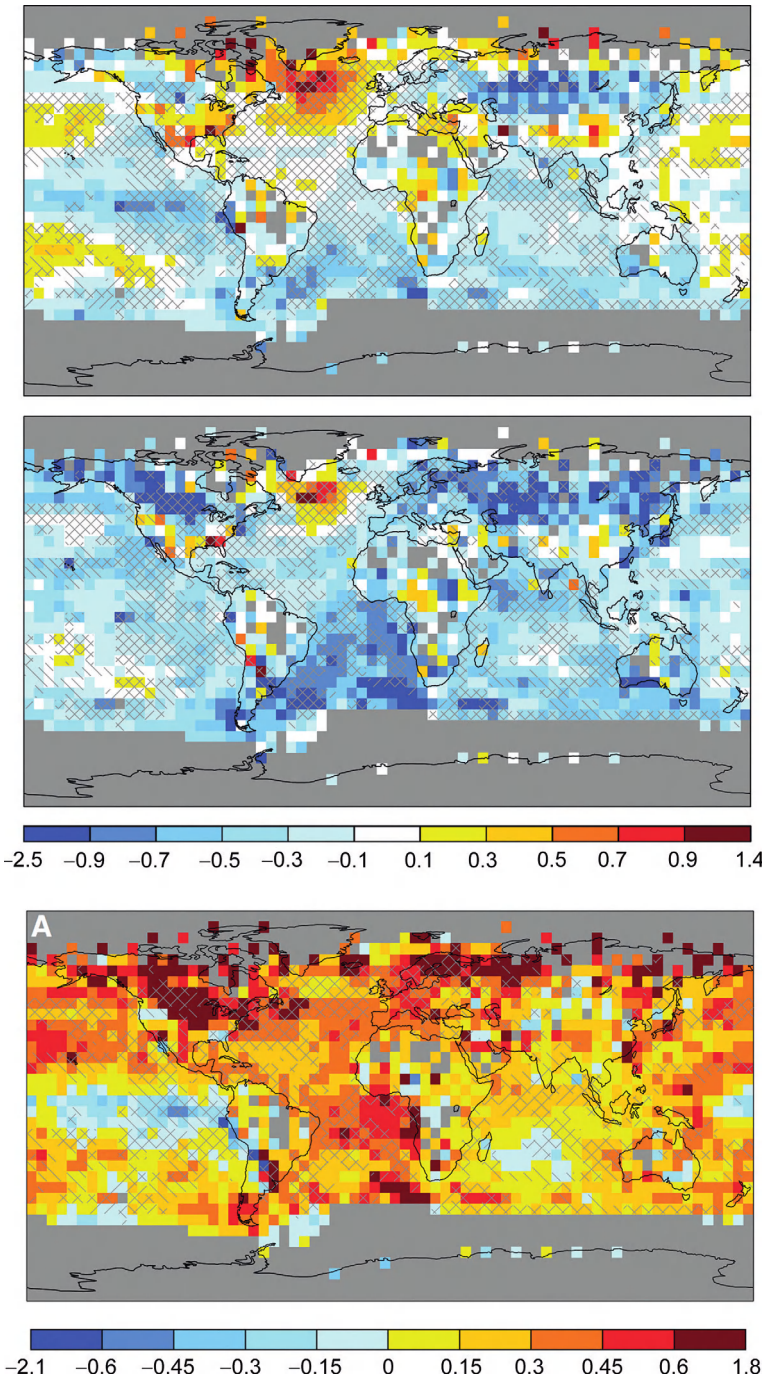


FIGURE 15.24 Reconstructed temperature anomalies (relative to the mean for 1961-1990) for the periods AD 950-1250 (above) and AD 1400-1700 (middle). Lower panel shows the difference between the two periods (Medieval and LIA). The reconstructions are based on a network of proxy records, principally comprised of tree-ring width and density data, coral, lake sediment, and ice core geochemical data and historical documentary sources. Areas covered by hatching indicate that the reconstruction passed one or more tests of statistical significance. Gray areas (mainly in the polar regions) have insufficient records to make a meaningful temperature estimate. *From Mann et al. (2009).*

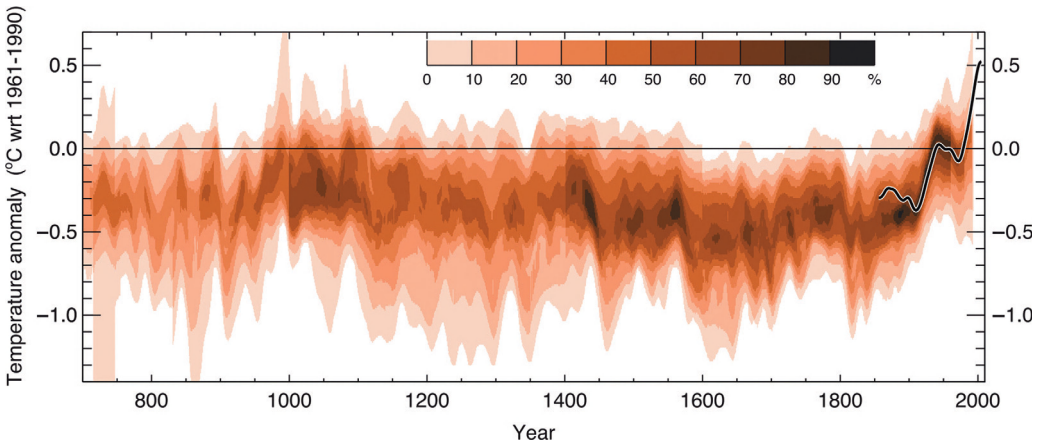


FIGURE 15.25 Northern Hemisphere temperatures (mean annual or summer) from 10 reconstructions using a variety of proxy data. The color-coding represents the extent to which the records agree on a multidecadal timescale, with a score of 100% when temperatures fall within ±1 standard error of all 10 reconstructions and 5% when values fall within the 5-95% range. Thus, the darkest colors indicate where the different reconstructions are in close agreement, while the lighter shading indicates periods of wider disagreement. All series were smoothed by a Gaussian-weighted filter to remove fluctuations on timescales of less than 30 years, and all temperatures are expressed as departures from the 1961 to 1990 average. The HadCRUT2v instrumental mean annual temperature record is shown by the black line. *From Jansen et al. (2007).*

APPENDIX

A

Further Considerations on Radiocarbon Dating

A.1 CALCULATION OF RADIOCARBON AGE AND STANDARDIZATION PROCEDURE

Although it is not necessary for a user of radiocarbon dates to know, in detail, how the actual value is arrived at, some understanding of the procedure is enlightening, particularly when considering adjustments for ^{14}C fractionation effects (see Section 3.2.1.4.3). The whole subject is a complex sequence of calibrations, adjustments, and corrections (see Olson, 2009 for the history of these procedures). The following brief explanation is offered for the adventurous.

In order to make dates from different laboratories comparable, a standard material is used by all laboratories for the measurement of "modern" carbon isotope concentrations. This standard used to be "US National Bureau of Standards oxalic acid I" (Ox I) prepared from West Indian sugar cane grown in 1955. Ninety-five percent of the ^{14}C activity of this material is equivalent to the ^{14}C activity of wood grown in 1890, so by this devious means, all laboratories standardized their results to a material which had not been contaminated by "atomic bomb" ^{14}C. Because the original standard has now been exhausted, another oxalic acid standard (Ox II) is used with the old standard equivalent to [0.7459 Ox II]. By convention, all dates are given in "years before 1950" (years BP, "Before Present" or "before physics" (i.e. atmospheric nuclear bomb tests, which contaminated the atmosphere with ^{14}C)) so dates are adjusted to this temporal standard, rather than the possibly more logical time of 1890. A second adjustment is needed to correct for the fact that oxalic acid undergoes variable ^{13}C and ^{14}C fractionation effects during analysis. To make interlaboratory comparisons of samples possible, standardization is necessary to take these fractionation effects into account. Fortunately, the fractionation effect of ^{14}C is extremely close to twice that of ^{13}C, which is far more abundant and can be measured easily in a mass spectrometer.[1]

[1] $\delta^{14}C = 2\delta^{13}C + 10^{-3} (\delta^{13}C)^2$.

The necessary standardization is thus achieved by measuring ^{13}C rather than ^{14}C. Following the detailed analysis of oxalic acid samples by Craig (1961a), it was agreed that all standard samples should be adjusted to a ^{13}C value of $-19.3‰$, where

$$\delta^{13}C = \left(^{13}C/^{12}C\right)_{ox} - \left(^{13}C/^{12}C\right)_{PDB} \div \left(^{13}C/^{12}C\right)_{PDB} \times 10^3 \quad (A.1)$$

C_{ox} refers to the oxalic acid standard, and C_{PDB} refers to another reference standard, a Cretaceous belemnite (*Belemnitella americana*) from the Peedee Formation of South Carolina (Craig, 1957). Recent updates to the reference standards are discussed by Coplen (1996).

Standardization of the ^{14}C activity in the oxalic acid reference sample is achieved thus:

$$0.95A_{ox} = 0.95A_{1ox}\left[1 - \left(\left(2\delta^{13}C_{ox} + 19\right) \div 1000\right)\right] \quad (A.2)$$

where A_{1ox} is the ^{14}C activity of the reference oxalic acid and $^{13}C_{ox}$ is the ^{13}C of the reference oxalic acid (Equation A.1). The value of $0.95A_{ox}$ then becomes the universal ^{14}C standard activity from which all dates are calculated.

The procedure normally adopted for calculating the radiocarbon date of a sample can be summarized in three equations:

(a) The activity of the sample is expressed as a departure from the reference standard:

$$\delta^{14}C = A_{sample} - 0.95A_{ox} \div 0.95A_{ox} \times 10^3$$

where A_{sample} is the ^{14}C activity of the sample, corrected for background radiation, and A_{ox} is the 1950 activity of NBS oxalic acid I (or equivalent), corrected for background and isotope fractionation.

(b) The activity of the sample is corrected for fractionation by normalizing to $\delta^{13}C = -25‰$ PDB, which is the average for wood (see below for discussion):

$$\Delta = \delta^{14}C - \left(2\left[\delta^{13}C + 25\right]\right)\left(1 + \left(\delta^{14}C \div 1000\right)\right)$$

where $\delta^{13}C = [((^{13}C/^{12}C)_{sample} - (^{13}C/^{12}C)_{PDB}) \div (^{13}C/^{12}C)_{PDB}] \times 10^3$.

(c) Age (T) is then calculated using the "Libby" half-life of 5570 years:

$$T = 8033 \log_e(1 + (\Delta/1000))^{-1}.$$

A.2 FRACTIONATION EFFECTS

Because isotopic fractionation occurs to differing extents during plant photosynthesis and during shell carbonate deposition, it is necessary to know the magnitude of the effect so that dates on different materials can be compared. Lerman (1972) and Troughton (1972) have studied fractionation effects in modern plants and found a trimodal distribution; the magnitude of fractionation seems to be related to the particular biochemical pathway evolved by different plant species for photosynthesis. Thus, highest ^{13}C depletion corresponds to so-called C_3 plants which utilize the Calvin photosynthetic cycle (CAL) and lowest depletion occurs in C_4 plants utilizing the Hatch-Slack (HS) cycle. Succulents utilize a third metabolic pathway

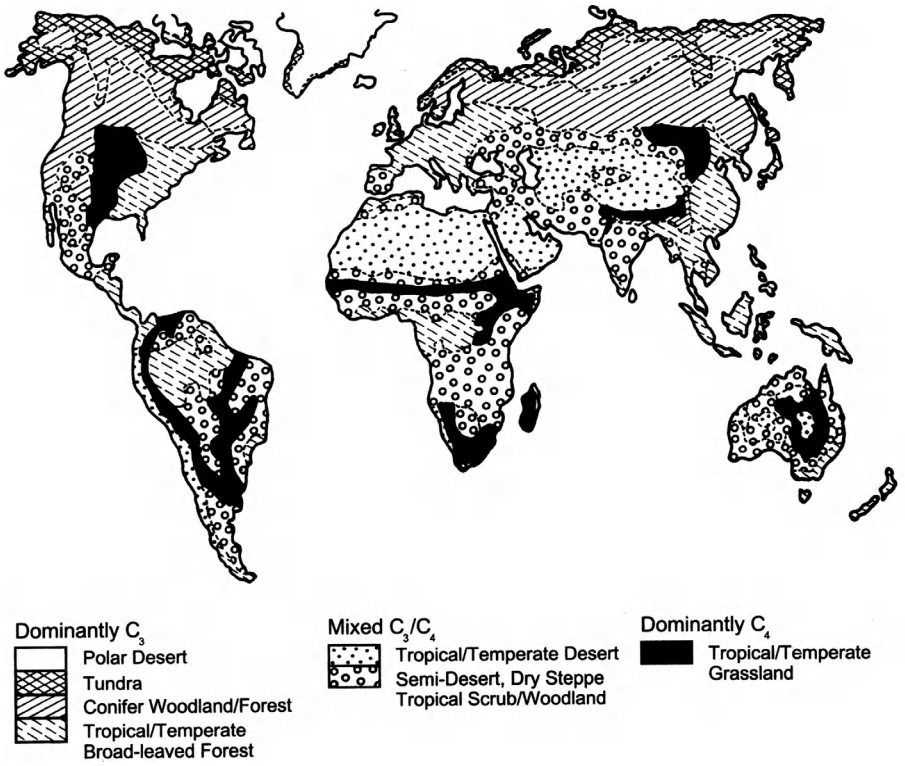


FIGURE A.1 Distribution of major ecosystems dominated by C_3 or C_4 vegetation. The northern limits of temperate grasslands in North America and Asia include a significant proportion of C_3 plants due to the cool growing season. *From Cerling and Quade (1993).*

(crassulacean acid metabolism, CAM) and may fix carbon by either the HS or CAL pathways depending on temperature and photoperiod; they thus form a third group. Figure A.1 shows the large-scale distribution of ecosystems dominated by C_3 or C_4 plants. The implications for dating are that samples containing, say, a high proportion of HS plants would show $^{14}C/^{12}C$ ratios characteristic of these less depleted plants (Figure A.2). An uncorrected date on such material would thus appear younger than a stratigraphically equivalent sample comprising predominantly CAL-type plants. Similar problems presumably exist in dating animal remains that feed predominantly on plants using one or another photosynthetic pathway, though this question has not been studied in detail.

By international agreement, all ^{14}C dates are corrected for fractionation effects by standardization to a $\delta^{13}C$ value of $-25‰$, the average value for wood. This results in relatively small "corrections" for CAL plants but larger corrections for HS and CAM plants, freshwater and marine shells, and aquatic plants. In particular, corrections of up to 450 years may be necessary in the case of marine shells because they produce carbonate in equilibrium with ocean water that is relatively enriched in ^{13}C. Table A.1 indicates the magnitude of corrections necessary to standardize ^{14}C dates for fractionation effects. Where no such adjustment was made in a dated sample, these values may act as a guide to the appropriate correction needed.

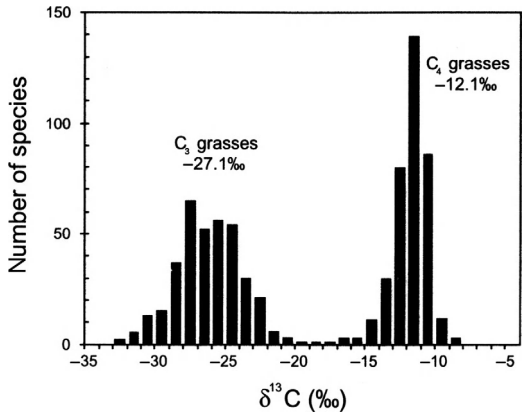


FIGURE A.2 $\delta^{13}C$ values (‰) for C_3 and C_4 grasses. *From Cerling and Quade (1993).*

TABLE A.1 Radiocarbon Fractionation Errors.

	Dating Material	Photosynthetic Pathway	$\delta^{13}C$ (‰)	Years to Add to Uncorrected Date
1.	Wood and wood charcoal	(C_3) CAL	-25 ± 5	0 ± 80
2.	Tree leaves	(C_3) CAL	-27 ± 5	-30 ± 80
3.	Peat, humus, soil[a]	(C_3) CAL	-27 ± 7	-30 ± 110
4.	Grains[b]	(C_3) CAL	-23 ± 4	$+30 \pm 60$
5.	Leaves and straw of grasses and sedges (e.g., totora)[b]	(C_3) CAL	-27 ± 4	-30 ± 60
6.	Bones (European)		-20 ± 4	$+80 \pm 60$
7.	Grains[c]	(C_4) HS	-10 ± 3	$+240 \pm 50$
8.	Leaves and straw of grasses and sedges (e.g., papyrus)	(C_4) HS	-13 ± 4	$+200 \pm 60$
9.	Succulents[d]	CAM	-17 ± 8	$+130 \pm 120$
10.	Aquatic plants (freshwater)		-8 to -24	
	Aquatic plants (marine)		-8 to -17	
11.	Fresh and brackish water shells		0 to -12	
12.	Marine shells		$+3$ to -2	

CAL, Calvin metabolic pathway; HS, Hatch-Slack metabolic pathway; CAM, crassulacean acid metabolism.
[a]*Most nordic and temperate peats, humus, and soils are of C-type. Others must be considered as unidentified.*
[b]*Wheat, oats, barley, rice rye, and related grasses.*
[c]*Maize, sorghum, millet, panic, and related grasses.*
[d]*Cactus, agave, pineapple,* Tillandsia, *etc.*
(After Lerman (1972))

APPENDIX

B

Internet Resources in Paleoclimatology

The internet offers enormous resources for those interested in paleoclimatology, including databases, GCM paleoclimate simulations, useful software, information about organizations, and newsletters. Many of these are well maintained, and others may be more transient. Readers can consult the Paleoclimate Resources Web Page at the University of Massachusetts Climate System Research Center, where I will attempt to maintain a comprehensive and up-to-date set of links:

www.geo.umass.edu/climate/paleo.html

References: Where references include a URL, beginning with: dx.doi.org/. . ., this will provide a link to the Abstract. A search on Google Scholar can often provide a link to a .pdf of a paper that is listed in the references, or search for the author's Web site where the publication may be found. If you don't have access to a particular journal, I suggest emailing the author to request a .pdf copy.

Data: For access to data sets, consult the World Data Center for Paleoclimatology and the European Pangaea Web sites:

NOAA Paleoclimatology Program (World Data Center A for Paleoclimatology)

www.ngdc.noaa.gov/paleo/paleo.html

Pangaea: A data publisher for earth and environmental science (registration is required):

www.pangaea.de

References

Abbott, P.M., Davies, S.M., 2012. Volcanism and the Greenland ice-cores: the tephra record. Earth-Sci. Rev. 115, 173–191.

Abbott, M.B., Wolfe, B.B., Aravena, R., Wolfe, A.P., Seltzer, G.O., 2000. Holocene hydrological reconstructions from stable-isotopes and palaeolimnology, Cordillera Real, Bolivia. Quat. Sci. Rev. 19, 1801–1820.

Abbott, P.M., Davies, S.M., Steffensen, J.P., Pearce, N.J.G., Bigler, M., Johnsen, S.J., Seierstad, I.K., Svensson, A., Wastegård, S., 2012. A detailed framework of Marine Isotope Stages 4 and 5 volcanic events recorded in two Greenland ice cores. Quat. Sci. Rev. 36, 59–77.

Abram, N.J., Gagan, M.K., Liu, Z.Y., Hantoro, W.S., McCulloch, M.T., Suwargadi, B.W., 2007. Seasonal characteristics of the Indian Ocean Diploe during the Holocene epoch. Nature. 445, 299–302.

Acuña-Soto, R., Stahle, D.W., Cleaveland, M.K., Therrell, M.D., 2002. Megadrought and megadeath in 16th century Mexico. Emerg. Infect. Dis. 8, 360–362.

Adams, J.B., Mann, M.E., Ammann, C.M., 2003. Proxy evidence for an El Niño-like response to volcanic forcing. Nature. 426, 274–278.

Adelseck, C.G., Berger, W.H., 1977. On the dissolution of planktonic foraminifera and associated microfossils during settling and on the sea floor. In: Sliter, W.V., Bé, A.W.H., Berger, W.H. (Eds.), Dissolution of Deep-Sea Carbonates. Special Publication No. 13, Cushman Foundation for Foraminiferal Research, Washington, DC, pp. 70–81.

Adkins, J.F., Boyle, E.A., 1997. Changing atmospheric $\Delta^{14}C$ and the record of deep water paleoventilation ages. Paleoceanography. 12, 337–344.

Adkins, J.F., McIntyre, K., Schrag, D.P., 2002a. The salinity, temperature and $\delta^{18}O$ of the Glacial Deep Ocean. Science. 298, 1769–1773.

Adkins, J.F., Cheng, H., Boyle, E.A., Druffel, E.R.M., Edwards, R.L., 2002b. Deep-sea coral evidence for rapid change in ventilation of the deep North Atlantic 15,400 years ago. Science. 280, 725–728.

Adkins, J.F., Henderson, G.M., Wang, S.L., O'Shea, S., Mokadem, F., 2004. Growth rates of the deep-sea scleractinia *Desmophyllum cristagalli* and *Enallopsammia rostrata*. Earth Planet. Sci. Lett. 227, 481–490.

Aharon, P., Chappell, J., 1986. Oxygen isotopes, sea level changes and the temperature history of a coral reef environment in New Guinea over the last 10^5 years. Palaeogeogr. Palaeoclimatol. Palaeoecol. 56, 337–379.

Aitken, M.J., 1974. Physics and Archaeology. Clarendon Press, Oxford, 291 pp.

Aitken, M.J., 1985. Thermoluminescence Dating. Academic Press, London.

Aitken, M.J., 1998. An Introduction to Optical Dating. Oxford University Press, Oxford, 267 pp.

Aldahan, A., Possnert, G., 1998. A high-resolution ^{10}Be profile from deep sea sediment covering the last the last 70 ka: indication for globally synchronized environmental events. Quat. Sci. Rev. 17, 1023–1032.

Aldaz, L., Deutsch, S., 1967. On a relationship between air temperature and oxygen isotope ratio of snow and firn in the South Pole region. Earth Planet. Sci. Lett. 3, 267–274.

Alexandre, P., 1977. Les variations climatiques au Moyen Age (Belgique, Rhenanie, Nord de la France). Ann: Econ. Soc. Civ. 32, 183–197.

Alexandre, A., Meunier, J.-D., Lezine, A.-M., Vincens, A., Schwartz, D., 1997. Phytoliths: indicators of grassland dynamics during the late Holocene in intertropical Africa. Palaeogeogr. Palaeoclimatol. Palaeoecol. 136, 213–229.

Alley, R.B., 2002. The Two-mile Time Machine: Ice cores, Abrupt Climate Change and the Future. Princeton University Press, Princeton, 240 pp.

Alley, R.B., Anandakrishnan, S., 1995. Variations in melt-layer frequency in the GISP2 ice core: implications for Holocene summer temperatures in central Greenland. Ann. Glaciol. 21, 64–70.

Alley, R.B., Cuffey, K.M., 2001. Oxygen- and hydrogen-isotopic ratios of water in precipitation: beyond paleothermometry. Rev. Mineral. Geochem. 43, 527–553.

Alley, R.B., MacAyeal, D., 1994. Ice-rafted debris associated with the binge-purge oscillations of the Laurentide Ice Sheet. Paleoceanography. 9, 503–511.

Alley, R.B., Perepezko, J.H., Bentley, C.R., 1988. Long-term climate changes from crystal growth. Nature. 332, 592–593 (and reply by Petit, J.P., Duval, P., Lorius, C., p. 593).
Alley, R.B., Gow, A.J., Johnsen, S.J., Kipfstuhl, J., Meese, D.A., Thorsteinsson, T., 1995. Comparison of deep ice cores. Nature. 373, 393–394.
Alley, R.B., Shuman, C.A., Meese, D.A., Gow, A.J., Taylor, K.C., Cuffey, K.M., Fitzpatrick, J.J., Grootes, P.M., Zielinski, G.A., Ram, M., Spinelli, G., Elder, B., 1997a. Visual-stratigraphic dating of the GISP2 ice core: basis, reproducibility and application. J. Geophys. Res. 102C, 26367–26381.
Alley, R.B., Gow, A., Meese, D.A., Fitzpatrick, J.J., Waddington, E.D., Bolzan, J.F., 1997b. Grain-scale processes, folding and stratigraphic disturbance in the GISP2 ice core. J. Geophys. Res. 102C, 26819–26830.
Alley, R.B., Mayewski, P.A., Sowers, T., Stuiver, M., Taylor, K.C., Clark, P.U., 1997c. Holocene climatic instability: a prominent, widespread event 8200 yr ago. Geology. 25, 483–486.
Alley, R.B., Marotzke, J., Nordhaus, W.D., Overpeck, J.T., Peteet, D.M., Pielke Jr., R.A., Pierrehumbert, R.T., Rhines, R.B., Stocker, T.F., Talley, L.D., Wallace, J.M., 2002. Abrupt climate change. Science. 299, 2005–2009.
Alley, R.B., Andrews, J.T., Barber, D.C., Clark, P.U., 2005. Comment on "Catastrophic ice shelf breakup as the source of Heinrich event icebergs" by C.L. Hulbe et al. Paleoceanography. 20, PA1009, dx.doi.org/10.1029/2004PA001086.
Alley, R.B., Shuman, C.A., Meese, D.A., Gow, A.J., Taylor, K.C., Cuffey, K.M., Fitzpatrick, J.J., Grootes, P.M., Zielinski, G.A., Ram, M., Spinelli, G., Elder, B., 2007. Visual-stratigraphic dating of the GISP2 ice core: basis, reproducibility and application. J. Geophys. Res. 102C, 26367–26381.
Allison, I., Kruss, P., 1977. Estimation of recent climatic change in Irian Jaya by numerical modelling of its tropical glaciers. Arct. Alp. Res. 9, 49–60.
Altabet, M.A., Francois, R., Murray, D.W., Prell, W.L., 1995. Climate-related variations in denitrification in the Arabian Sea from sediment 15N/14N ratios. Nature. 373, 506–509.
Alvarez-Solas, J., Charbit, S., Ritz, C., Paillard, D., Ramstein, G., Dumas, C., 2010. Links between ocean temperature and iceberg discharge during Heinrich events. Nat. Geosci. 3, 122–126.
Alverson, K., Oldfield, F., Bradley, R.S. (Eds.), 1999. Past Global Changes and Their Significance for the Future. Elsevier, Amsterdam, 479 pp.
Alverson, K., Bradley, R.S., Pedersen, T.F. (Eds.), 2003. Paleoclimate, Global Change and the Future. Springer Verlag, Berlin, 220 pp.
Amason, B., 1969. The exchange of hydrogen isotopes between ice and water in temperate glaciers. Earth Planet. Sci. Lett. 6, 423–430.
Ambach, W., Dansgaard, W., Eisner, H., Moller, J., 1968. The altitude effect on the isotopic composition of precipitation and glacier ice in the Alps. Tellus. 20, 595–600.
Ammann, B., Birks, H.J.B., Brooks, S.J., Eicher, U., von Grafenstein, U., Hofmann, W., Lemdahl, G., Schwander, J., Tobolski, K., Wick, L., 2000. Quantification of biotic responses to rapid climatic changes around the Younger Dryas—a synthesis. Palaeogeogr. Palaeoclimatol. Palaeoecol. 159, 313–347.
Ammann, C.M., Meehl, G.A., Washington, W.M., Zender, C.S., 2003. A monthly and latitudinally varying volcanic forcing dataset in simulations of 20th century climate. Geophys. Res. Lett. 30, 1657. dx.doi.org/10.1029/2003GL016875.
Ammann, C.M., Joos, F., Schimel, D.S., Otto-Bliesner, B.L., Tomas, R.A., 2007. Solar influence on climate during the past millennium: results from transient simulations with the NCAR Climate System Model. Proc. Natl. Acad. Sci. U. S. A. 104, 3713–3718.
An, Z.S., 2000. The history and variability of the East Asian paleomonsoon climate. Quat. Sci. Rev. 19, 171–187.
An, Z.S. (Ed.), 2014. Late Cenozoic Climate Change in Asia. Springer, Berlin.
An, Z., Liu, T., Lu, Y., Porter, S.C., Kukla, G., Wu, X., Hua, Y., 1990. The long term paleomonsoon variation recorded by the loess paleosol sequence in central China. Quat. Int. 718, 91–95.
An, Z.S., Kukla, G.J., Porter, S.C., Xiao, J., 1991. Magnetic susceptibility evidence of monsoon variation on the Loess Plateau of central China during the last 130,000 years. Quat. Res. 36, 29–36.
An, Z.S., Kutzbach, J.E., Prell, W.L., Porter, S.C., 2001. Evolution of Asian monsoons and phased uplift of the Himalaya–Tibetan Plateau since late Miocene times. Nature. 411, 62–66.
An, Z.S., Huang, Y.S., Liu, W.G., Guo, Z.T., Clemens, S., Li, L., Prell, W., Ning, Y.F., Cai, Y.J., Zhou, W.J., Lin, B.H., Zhang, Q.L., Cao, Y.N., Qiang, X.K., Chang, H., Wu, Z.K., 2005. Multiple expansions of C_4 plant biomass in East Asia since 7 Ma coupled with strengthened monsoon circulation. Geology. 33, 705–708.
An, Z.S., Clemens, S.C., Shen, J., Qiang, X.K., Jin, Z.D., Sun, Y.B., Prell, W.L., Luo, J.J., Wang, S.M., Xu, H., Cai, Y.J., Zhou, W.J., Liu, X.D., Liu, W.G., Shi, Z.G., Yan, L.B., Xian, X.Y., Chang, H., Wu, F., Ai, L., Lu, F.Y., 2011. Glacial-interglacial Indian summer monsoon dynamics. Science. 333, 719–723.

Anand, P., Elderfield, H., Conte, M.H., 2003. Calibration of Mg/Ca thermometry in planktonic foraminifera from a sediment trap time series. Paleoceanography. 18. dx.doi.org/10.1029/2002PA000846.

Anchukaitis, K., Evans, M.N., 2010. Tropical cloud forst climate variability and the demise of the Monteverde golden toad. Proc. Natl. Acad. Sci. U. S. A. 107, 5036–5040.

Anchukaitis, K., Evans, M.N., Wheelwright, N.T., Schrag, D.P., 2008. Stable isotope chronology and signal calibration in neotropical cloud forest trees. J. Geophys. Res. 113, G03030. dx.doi.org/10.1029/2007JG000613.

Andersen, T.F., Steinmetz, J.C., 1981. Isotopic and biostratigraphical records of calcareous nannofossils in a Pleistocene core. Nature. 294, 741–744.

Andersen, K.K., Svensson, A., Johnsen, S.J., Rasmussen, S.U., Bigler, M., Rothlisberger, R., Ruth, U., Siggard-Andersen, M.-L., Steffensen, J.P., Dahl-Jensen, D., Vinther, B.M., Clausen, H.B., 2006a. The Greenland Ice Core Chronology 2005, 15–42ka. Part 1: constructing the time scale. Quat. Sci. Rev. 25, 3246–3257.

Andersen, K.K., Ditlevsen, P.D., Rasmussen, S.O., Clausen, H.B., Vinther, B.M., Johnsen, S.J., Steffensen, J.P., 2006b. Retrieving a common accumulation record from Greenland ice cores for the past 1800 years. J. Geophys. Res. 111. D15106, dx.doi.org/10.1029/2005JD006765.

Anderson, R.Y., Dean, W.L., 1988. Lacustrine varve formation through time. Palaeogeogr. Palaeoclimatol. Palaeoecol. 62, 215–235.

Anderson, D.M., Prell, W.L., Barratt, N.J., 1989. Estimates of sea surface temperature in the Coral Sea at the last glacial maximum. Paleoceanography. 4, 615–627.

Anderson, P.M., Bartlein, P.J., Brubaker, L.B., Gajewski, K., Ritchie, J.C., 1991. Vegetation-pollen-climate relationships for the arcto-boreal regions of North America and Greenland. J. Biogeogr. 18, 565–582.

Anderson, L.L., Hu, F.S., Nelson, D.M., Petit, R.J., Palge, K.N., 2006. Ice-age endurance: DNA evidence of a white spruce refugium in Alaska. Proc. Natl. Acad. Sci. U. S. A. 103, 12447–12450.

Anderson, L., Abbott, M.B., Finney, B.P., Burns, S.J., 2007. Late Holocene moisture balance variability in the southwest Yukon Territory, Canada. Quat. Sci. Rev. 26, 130–141.

Anderson, R.K., Miller, G.H., Briner, J.P., Lifton, N.A., DeVogel, S.B., 2008. A millennial perspective on Arctic warming from ^{14}C in quartz and plants emerging beneath ice caps. Geophys. Res. Lett. 35, L01502, dx.doi.org/10.1029/GL032057.

Anderson, R.F., Ali, S., Bradtmiller, L.I., Nielsen, S.H.H., Fleisher, M.Q., Anderson, B.E., Burckle, L.H., 2009. Wind-driven upwelling in the Southern Ocean and the deglacial rise in atmospheric CO_2. Science. 323, 1443–1448.

Andrée, M., Beer, J., Loetscher, H.P., Moor, E., Oeschger, H., Bonani, G., Hoffman, H.J., Morenzoni, E., Ness, M., Suter, M., Wolfli, W., 1986. Dating polar ice by ^{14}C accelerator mass spectrometry. Radiocarbon. 28, 417–423.

Andrews, J.T., Barry, R.G., Bradley, R.S., Miller, G.H., Williams, L.D., 1972. Past and present glaciological responses to climate in eastern Baffin Island. Quat. Res. 2, 303–314.

Andrews, J.T., Davis, P.T., Wright, C., 1976. Little Ice Age permanent snowcover in the eastern Canadian Arctic: extent mapped from Landsat-1 satellite imagery. Geogr. Ann. 58A, 71–81.

Andrews, J.T., Erlenkeuser, H., Tedesco, K., Aksu, A., Jull, A.J.T., 1994. Late Quaternary (Stage 2 and 3) meltwater and Heinrich Events, northwest Labrador Sea. Quat. Res. 41, 26–34.

Andriessen, P.A.M., Helmens, K.F., Hooghiemstra, H., Riezobos, P.A., Van der Hammen, T., 1993. Absolute chronology of the Pliocene-Quaternary sediment sequence of the Bogota area, Colombia. Quat. Sci. Rev. 12, 483–501.

Anhuf, D., 1997. Palaeovegetation in west Africa for 18,000 B.P. and 8500 B.P. Eiszeit. Gegenw. 47, 112–119.

Anhuf, D., 2000. Vegetation history and climate changes in Africa north and south of the Equator (10N-10S) during the Last Glacial Maximum (LGM). In: Smolka, P., Volkheimer, W. (Eds.), Southern Hemisphere Paleo- and Neoclimate. Springer, Berlin, pp. 225–248.

Anhuf, D., Ledru, M.P., Behling, H., Da Cruz Jr., F.W., Cordeiro, R.C., Van der Hammen, T., Karmann, I., Marengo, J.A., De Oliveira, P.E., Pessenda, L., Siffedine, A., Albuquerque, A.L., Da Silva Dias, P.L., 2006. Paleo-environmental change in Amazonian and African rainforest during the LGM. Palaeogeogr. Palaeoclimatol. Palaeoecol. 239, 510–527.

Anklin, M., Barnola, J.M., Beer, J., Blunier, T., Chappellaz, J., Clausen, H.B., Dahl-Jensen, D., Dansgaard, W., De Angelis, M., Delmas, R.J., 1993. Climate instability during the last interglacial period recorded in the GRIP ice core. Nature. 364, 203–207.

Antevs, E., 1948. Climatic changes and pre-white man. Univ. Utah Bull. 36, 168–191.

Aono, Y., Kazui, K., 2008. Phenological data series of cherry tree flowering in Kyoto, Japan, and its application to reconstruction of springtime temperature since the 9th century. Int. J. Climatol. 25, 905–914.

Aono, Y., Saito, S., 2010. Clarifying springtime temperature reconstructions of the Medieval period by gap-filling the cherry blossom phonological data series at Kyoto, Japan. Int. J. Biometeorol. 54, 211–219.
Appleby, P.G., 2001. Chronostratigraphic techniques in recent sediments. In: Last, W.M., Smol, J.P. (Eds.), Tracking Environmental Change Using Lake Sediments. Basin Analysis, Coring and Chronological Techniques, vol. 1. Kluwer, Dordrecht, pp. 171–203.
Appleby, P.G., Oldfield, F., 1978. The calculation of ^{210}Pb dates assuming a constant rate of supply of unsupported ^{210}Pb to the sediment. Catena. 5, 1–8.
Appleby, P.G., Oldfield, F., 1983. The assessment of ^{210}Pb data from sites with varying sediment accumulation rates. Hydrobiology. 103, 29–35.
Arakawa, H., 1954. Fujiwhara on five centuries of freezing dates of Lake Suwa in central Japan. Arch. Meteorol. Geophys. Bioklimatol. B6, 152–166.
Arakawa, H., 1956a. Dates of first or earliest snow covering for Tokyo since 1632. Quart. J. Roy. Meteorol. Soc. 82, 222–226.
Arakawa, H., 1956b. Climatic change as revealed by the blooming dates of the cherry blossoms at Kyoto. J. Meteorol. 13, 599–600.
Arakawa, H., 1957. Climatic change as revealed by the data from the Far East. Weather. 12, 46–51.
Arguez, A., Vose, R.S., 2011. The definition of the standard WMO climate normal. Bull. Am. Meteorol. Soc. 92, 699–704.
Arnow, T., 1980. Water budget and water-surface fluctuations of Great Salt Lake. Utah Geol. Miner. Surv. Bull. 116, 255–263.
Arz, H.W., Pätzold, J., Wefer, G., 1998. Correlated millennial-scale changes in surface hydrography and terrigenous sediment yield inferred from Last Glacial marine deposits off northeastern Brazil. Quat. Res. 50, 157–166.
Asami, R., Yamada, T., Iryu, Y., Quinn, T.M., Meyer, C.P., Paulay, G., 2005. Interannual and decadal variability of the western Pacific sea surface condition for the years 1787–2000: reconstruction based on stable isotope record from a Guam coral. J. Geophys. Res. 110, C05018, dx.doi.org/10.1029/2004JC002555.
Asami, R., Felis, T., Deschamps, P., Hanawa, K., Iryu, Y., Bard, E., Durand, N., Murayama, M., 2009. Evidence for tropical South Pacific climate change during the Younger Dryas and the Bølling-Allerød from geochemical records of fossil Tahiti corals. Earth Planet. Sci. Lett. 288, 96–107.
Ashworth, A.C., 1980. Environmental implications of a beetle assemblage from the Gervais formation (Early Wisconsinan?), Minnesota. Quat. Res. 13, 200–212.
Atkinson, T.C., Lawson, T.J., Smart, P.L., Harmon, R.S., Hess, J.W., 1986a. New data on speleothem deposition and palaeoclimate in Britain over the last forty thousand years. J. Quat. Sci. 1, 67–72.
Atkinson, T.C., Briffa, K.R., Coope, G.R., Joachim, M., Perry, D.W., 1986b. Climatic calibration of coleopteran data. In: Berglund, B. (Ed.), Handbook of Holocene Palaeoecology and Palaeohydrology. Wiley, New York, pp. 851–858.
Atkinson, T.C., Briffa, K.R., Coope, G.R., 1987. Seasonal temperatures in Britain during the last 22,000 years, reconstructed using beetle remains. Nature. 325, 587–592.
Austin, W.E.N., Bard, E., Hunt, J.B., Kroon, D., Peacock, J.D., 1995. The ^{14}C age of the Icelandic Vedde ash: implications for Younger Dryas marine reservoir age corrections. Radiocarbon. 37, 53–62.
Bada, J.L., 1985. Amino acid racemization dating of fossil bones. Annu. Rev. Earth Planet. Sci. 13, 241–268.
Bada, J.L., Schroeder, R.A., 1975. Amino acid racemization reactions and their geochemical implications. Naturwissenschaften. 62, 71–79.
Bada, J.L., Protsch, R., Schroeder, R.A., 1973. The racemization reaction of isoleucine used as a palaeotemperature indicator. Nature. 241, 394–395.
Baker, J.N.L., 1932. The climate of England in the 17th century. Quart. J. Roy. Meteorol. Soc. 58, 421–436.
Baker, A., Smart, P.L., Ford, D.C., 1993. Northwest European paleoclimate as indicated by growth frequency variations of secondary calcite deposits. Palaeogeogr. Palaeoclimatol. Palaeoecol. 100, 291–301.
Baker, P., Seltzer, G.O., Fritz, S.C., Dunbar, R.B., Grove, M.J., Tapia, P.M., Cross, S.L., Rowe, H.D., Broda, J.P., 2001. The history of South American tropical precipitation for the past 25,000 years. Science. 291, 640–643.
Bakke, J., Lie, Ø., Nesje, A., Dahl, S.O., Paasche, Ø., 2005. Utilizing physical sediment variability in glacier-fed lakes for continuous glacier reconstructions during the Holocene, northern Folgefonna, western Norway. The Holocene. 15, 161–176.
Bakke, J., Lie, Ø., Heegaard, E., Dokken, T., Haug, G.H., Birks, H.J.B., Dulski, P., Nilsen, T., 2010a. Rapid oceanic and atmospheric changes during the Younger Dryas cold period. Nat. Geosci. 2, 202–205.
Bakke, J., Dahl, S.O., Paasche, O., Simonsen, J., Kvisvik, B., Bakke, K., Nesje, A., 2010b. A complete record of Holocene glacier variability at Austre Okstindbreen, northern Norway: an integrated approach. Quat. Sci. Rev. 29, 1246–1262.

Bakke, J., Trachsel, M., Kvisvik, B.C., Nesje, A., Lysså, A., 2013. Numerical analyses of a multi-proxy data set from a distal glacier-fed lake, Sørsendalsvatn, western Norway. Quat. Sci. Rev. 73, 182–185.
Baksi, A.K., Hsu, V., McWilliams, M.O., Farrar, E., 1992. $^{40}Ar/^{39}Ar$ dating of the Brunhes-Matuyama geomagnetic field reversal. Science. 256, 356–357.
Balco, G., 2011. Contributions and unrealized potential contributions of cosmogenic-nuclide exposure dating to glacier chronology, 1990-2010. Quat. Sci. Rev. 30, 3–27.
Baldini, J.U.L., McDermott, F., Fairchild, I.J., 2002. Structure of the 8200-year cold event revealed by a speleothem trace element record. Science. 296, 2203–2206.
Baldwin, M.P., Dunkerton, T.J., 2001. Stratospheric harbingers of anomalous weather regimes. Science. 294, 581–584.
Balescu, S., Lamothe, M., 1994. Comparison of TL and IRSL age estimates of feldspar coarse grains from waterlain sediments. Quat. Geochronol. (Quat. Sci. Rev.). 13, 437–444.
Ball, T., 1992. Historical and instrumental evidence of climate: western Hudson Bay, Canada 1714-1850. In: Bradley, R.S., Jones, P.D. (Eds.), Climate Since A.D. 1500. Routledge, London, pp. 40–73.
Balsam, W., Ji, J.F., Chen, J., 2004. Climatic interpretation of the Luochuan and Lingtai loess sections, China, based on changing iron oxide mineralogy and magnetic susceptibility. Earth Planet. Sci. Lett. 223, 335–348.
Balsam, W.L., Ellwood, B.B., Williams, E.R., Long, X.Y., El Hassani, A., 2011. Magnetic susceptibility as a proxy for rainfall: worldwide data from tropical and temperate climate. Quat. Sci. Rev. 30, 2732–2744.
Barber, K.E., 1981. Peat Stratigraphy and Climatic Change: A Palaeoecological Test of the Theory of Cyclic Peat Bog Regeneration. Balkema, Rotterdam.
Barber, K.E., Charman, D.J., 2003. Holocene palaeoclimate records from peatlands. In: Mackay, A.W., Battarbee, R.W., Birks, H.J.B., Oldfield, F. (Eds.), Global Change in the Holocene. Arnold, London, pp. 10–226.
Barber, D.C., Dyke, A., Hillaire-Marcel, H., Jennings, A.E., Andrews, J.T., Kerwin, M.W., Bilodeau, G., McNeely, R., Southon, J., Morehead, M.D., Gagnon, J.-M., 1999. Forcing of the cold event of 8200 years ago by catastrophic drainage of Laurentide lakes. Nature. 400, 344–348.
Barber, V., Juday, G., Finney, B., 2000. Reduced growth of Alaska white spruce in the twentieth century from temperature-induced drought stress. Nature. 405, 668–672.
Barber, K.E., Chambers, F.M., Maddy, D., 2003. Holocene palaeoclimates from peat stratigraphy: macrofossil proxy climate records from three oceanic raised bogs in England and Ireland. Quat. Sci. Rev. 22, 521–539.
Barboni, R., Bonnefille, R., Alexandre, A., Meunier, J.D., 1999. Phytoliths as paleoenvironmental indicators, West Side Middle Awash Valley, Ethiopia. Palaeogeogr. Palaeoclimatol. Palaeoecol. 152, 87–100.
Barbour, M.M., 2007. Stable oxygen isotope composition of plant tissue: a review. Funct. Plant Biol. 34, 83–94.
Bard, E., 1988. Correction of accelerator mass spectrometry ^{14}C ages measured in planktonic foraminifera: paleoceanographic implications. Paleoceanography. 3, 635–645.
Bard, E., 2000. Comparison of alkenone estimates with other paleotemperature proxies. Geochem. Geophys. Geosyst. 2. dx.doi.org/10.1029/2000GC000050.
Bard, E., Frank, M., 2006. Climate change and solar variability: what's new under the Sun? Earth Planet. Sci. Lett. 248, 480–493.
Bard, E., Fairbanks, R.G., Arnold, M., Maurice, P., Duprat, J., Moyes, J., Duplessy, J.C., 1989. Sea-level estimates during the last deglaciation based on $\delta^{18}O$ and accelerator mass spectrometry ^{14}C ages measured in *Globigerina bulloides*. Quat. Res. 31, 381–391.
Bard, E., Hamelin, B., Fairbanks, R.G., Zindler, A., 1990. Calibration of the ^{14}C timescale over the last 30,000 years using mass spectrometric U-Th ages from Barbados corals. Nature. 345, 405–410.
Bard, E., Arnold, M., Fairbanks, R., Hamelin, B., 1993. ^{230}Th-^{234}U and ^{14}C age, obtained by mass spectrometry on corals. Radiocarbon. 35, 191–199.
Bard, E., Arnold, M., Mangerud, J., Paterne, M., Labeyrie, L., Duprat, J., Mélières, M.A., Sønstegaard, E., Duplessy, J.C., 1994. The North Atlantic atmosphere-sea surface ^{14}C gradient during the Younger Dryas climatic event. Earth Planet. Sci. Lett. 126, 275–287.
Bard, E., Hamelin, B., Arnold, M., Montaggioni, L., Cabioch, G., Faure, G., Rougerie, F., 1996. Deglacial sea-level record from Tahiti corals and the timing of global meltwater discharge. Nature. 382, 241–244.
Bard, E., Rostek, F., Sonzogni, C., 1997. Interhemispheric synchrony of the last deglaciation inferred from alkenone palaeothermometry. Nature. 385, 707–710.
Bard, E., Raisbeck, G., Yiou, F., Jouzel, J., 2000. Solar irradiance during the last 120 years based on cosmogenic nuclides. Tellus. 52B, 985–992.

Bard, E., Delaygue, G., Rostek, F., Antonioli, F., Silenzi, S., Schrag, D.P., 2002a. Hydrological conditions over the western Mediterranean basin during the deposition of the cold Sapropel 6 (ca 175 kyr BP). Earth Planet. Sci. Lett. 202, 481–494.

Bard, E., Antonioli, F., Silenzi, S., 2002b. Sea-level during the penultimate interglacial period based on a submerged stalagmite from Argentarola Cave (Italy). Earth Planet. Sci. Lett. 196, 135–146.

Barkenow, L., Sandgren, P., 2001. Paleoclimate and tree-line changes during the Holocene based on pollen and plant macrofossils records from six lakes at different altitudes in northern Sweden. Rev. Palaeobot. Palynol. 117, 109–118.

Barker, S., Cacho, I., Benway, H., Tachikawa, K., 2005. Planktonic foraminiferal Mg/Ca as a proxy for past ocean temperatures: a methodological overview and data compilation for the Last Glacial Maximum. Quat. Sci. Rev. 24, 821–834.

Barletta, F., St-Onge, G., Stoner, J.S., Lajeunesse, P., Locat, J., 2010. A high-resolution Holocene paleomagnetic secular variation and relative paleointensity stack from eastern Canada. Earth Planet. Sci. Lett. 298, 162–174.

Bar-Matthews, M., Ayalon, A., 1997. Late Quaternary paleoclimate in the eastern Mediterranean region from stable isotope analysis of speleothems at Soreq Cave, Israel. Quat. Res. 47, 155–168.

Bar-Matthews, M., Ayalon, A., 2004. Speleothems as palaeoclimate indicators, a case study from Soreq Cave located in the eastern Mediterranean region, Israel. In: Battarbee, R.W., Gasse, F., Stickley, C.E. (Eds.), Past Climate Variability through Europe and Africa. Springer, Dordrecht, pp. 363–391.

Bar-Matthews, M., Wasserburg, G.J., Chen, J.H., 1993. Diagenesis of fossil coral skeletons: correlation between trace elements, textures and $^{234}U/^{238}U$. Geochim. Cosmochim. Acta. 57, 257–276.

Bar-Matthews, M., Ayalon, A., Kaufman, A., Wasserburg, G.J., 1999. The eastern Mediterranean paleoclimate as a reflection of regional events: Soreq Cave, Israel. Earth Planet. Sci. Lett. 166, 85–95.

Bar-Matthews, M., Ayalon, A., Kaufman, A., 2000. Timing and hydrological conditions of Sapropel events in the estern Mediterranean, as evident from speleothems, Soreq cave, Israel. Chem. Geol. 169, 145–156.

Bar-Matthews, M., Ayalon, A., Gilmour, M., Matthews, A., Hawkesworth, C.J., 2003. Sea-land oxygen isotopic relationships from planktonic foraminifera and speleothems in the eastern Mediterranean region and their implications for paleorainfall during interglacial intervals. Geochim. Cosmochim. Acta. 67, 3181–3199.

Barnola, J.-M., Raynaud, R., Korotkevich, Y.S., Lorius, C., 1987. Vostok ice core provides 160,000 year record of atmospheric $\delta^{18}O$. Nature. 329, 408–414.

Barnola, J.-M., Pimienta, P., Raynaud, D., Korotkevich, Y.S., 1991. CO_2-climate relationship as deduced from the Vostok ice core: a re-examination based on new measurements and on a re-evaluation of the air dating. Tellus. B43, 83–90.

Baron, W.R., 1982. The reconstruction of eighteenth century temperature records through the use of content analysis. Clim. Chang. 4, 385–398.

Barriendos, M., 1997. Climatic variations in the Iberian Peninsula during the late Maunder Minimum (A.D. 1675-1715): an analysis of data from rogation ceremonies. The Holocene. 7, 105–111.

Barry, R.G., Andrews, J.T., Mahaffy, M.A., 1975. Continental ice sheets: conditions for growth. Science. 190, 979–981.

Bartlein, P.J., Webb III, T., 1985. Mean July temperature at 6000 B.P. in eastern North America: regression equations for estimates from fossil-pollen data. In: Harington, C.R. (Ed.), Climatic Change in Canada 5. Syllogeus No. 55, National Museum of Canada, Ottawa, pp. 301–342.

Bartlein, P.J., Whitlock, C., 1993. Paleoclimatic interpretation of the Elk Lake pollen record. In: Bradbury, J.P., Dean, W.E. (Eds.), Elk Lake, Minnesota: Evidence for Rapid Climate Change in the North-Central United States. Special Paper 276, Geological Society of America, Boulder, pp. 275–293.

Bartlein, P.J., Webb III, T., Fieri, E., 1984. Holocene climatic change in the northern midwest: pollen-derived estimates. Quat. Res. 22, 361–374.

Bartlein, P.J., Prentice, I.C., Webb III, T., 1986. Climatic response surfaces from pollen data for some eastern North American taxa. J. Biogeogr. 13, 35–57.

Bartlein, P.J., Edwards, M.E., Shafer, S.L., Barker Jr., E.D., 1995. Calibration of radiocarbon ages and the interpretation of paleoenvironmental records. Quat. Res. 44, 417–424.

Bartlein, P.J., Anderson, K.H., Anderson, P.M., Edwards, M.E., Mock, C.J., Thompson, R.S., Webb, R.S., Webb III, T., Whitlock, C., 1998. Paleoclimate simulations for North America over the past 21,000 years: features of the simulated climate and comparisons with paleoenvironmental data. Quat. Sci. Rev. 17, 549–585.

Bartlein, P.J., Harrison, S.P., Brewer, S., Connor, S., Davis, B.A.S., Gajewski, K., Guiot, J., Harrison-Prentice, T.I., Henderson, A., Peyron, O., Prentice, I.C., Scholze, M., Seppä, H., Shuman, B., Sugita, S., Thompson, R.S., Viau, A.E., Williams, J., Wu, H., 2011. Pollen-based continental climate reconstructions at 6 and 21ka: a global synthesis. Clim. Dyn. 37, 775–802.

Bassett, I.J., Terasmae, J., 1962. Ragweeds, *Ambrosia* species in Canada and their history in postglacial time. Can. J. Bot. 40, 141–150.

Bassinot, F.C., Labeyrie, L.D., Vincent, E., Quidelleur, X., Shackleton, N.J., Lancelot, Y., 1994. The astronomical theory of climate and the age of the Brunhes-Matuyama magnetic reversal. Earth Planet. Sci. Lett. 126, 91–108.

Battarbee, R.W., 2000. Paleolimnological approaches to climate change, with special regard to the biological record. Quat. Sci. Rev. 19, 107–124.

Battarbee, R.W., Jones, V.J., Flower, R.J., Cameron, N.G., Bennion, H., Carvalho, L., Juggins, S., 2001. Diatoms. In: Smol, J.P., Birks, H.J.B., Last, W.M. (Eds.), Tracking Environmental Change Using Lake sediments, vol. 3. Kluwer Academic, Dordrecht, pp. 155–202.

Batten, B.L., 2009. Climate Change in Japanese History and Prehistory. Occasional Papers 2009–01, E.O. Reischauer Institute of Japanese Studies, Harvard University, Cambridge, 77 pp.

Bauernfeind, W., Woitek, U., 1999. The influence of climatic change on price fluctuations in Germany during the 16th century. Clim. Chang. 43, 303–321.

Baumgartner, A., 1979. Climatic variability and forestry. In: Proceedings of the World Climate Conference. WMO Publication No. 537, World Meteorological Organization, Geneva, pp. 581–607.

Baumgartner, T.R., Michaelsen, J., Thompson, L.G., Shen, G.T., Soutar, A., Casey, R.E., 1989. The recording of interannual climatic change by high resolution natural systems: tree rings, coral bands, glacial ice layers and marine varves. In: Peterson, D. (Ed.), Climatic Change in the Eastern Pacific and Western Americas. American Geophysical Union, Washington, DC, pp. 1–14.

Baumgartner, S., Beer, J., Masarik, J., Wagner, G., Meynadier, L., Synal, H.-A., 1998. Geomagnetic modulation of the ^{36}Cl flux in the GRIP ice core, Greenland. Science. 279, 1330–1332.

Bé, A.W.H., 1977. An ecological, zoogeographic and taxonomic review of recent planktonic foraminifera. In: Ramsay, A.T.S. (Ed.), Oceanic Micropalaeontology. Academic Press, London, pp. 1–88.

Bé, A.W.H., Damuth, J.E., Lott, L., Free, R., 1976. Late Quaternary climatic record in western equatorial Atlantic sediment. In: Cline, R.M., Hays, J.D. (Eds.), Investigation of late Quaternary Paleooceanography and Paleoclimatology. Memoir No. 145, Geological Society of America, Boulder, pp. 165–200.

Beadle, L.C., 1974. The Inland Waters of Tropical Africa. Longmans, London.

Beck, J.W., Récy, J., Taylor, F., Edwards, R.L., Cabioch, G., 1997. Abrupt changes in Holocene tropical sea surface temperature derived from coral records. Nature. 385, 705–707.

Becker, B., 1993. An 11,000 year German oak and pine dendrochronology for radiocarbon calibration. Radiocarbon. 35, 201–213.

Becker, B., Kromer, B., Trimlorn, P., 1991. A stable isotope tree-ring timescale of the late glacial/Holocene boundary. Nature. 353, 647–649.

Beer, J., Mende, W., Stellmacher, R., White, O.R., 1996. Intercomparisons of proxies for past solar variability. In: Jones, P.D., Bradley, R.S., Jouzel, J. (Eds.), Climatic Variations and Forcing Mechanisms of the Last 2000 Years. Springer, Berlin, pp. 501–517.

Beer, J., Mende, W., Stellmacher, R., 2001. The role of the sun in climate forcing. Quat. Sci. Rev. 19, 403–415.

Beget, J.E., 1994. Tephochronology, lichenometry and radiocarbon dating at Gulkana glacier, central Alaska Range, USA. The Holocene. 4, 307–313.

Beget, J.E., Hawkins, D.B., 1989. Influence of orbital parameters on Pleistocene loess deposition in central Alaska. Nature. 337, 151–153.

Beget, J.E., Machida, H., Lowe, D. (Eds.), 1996. Climatic Impact of Explosive Volcanism: Recommendations for Research. IGBP PAGES Workshop Report 96-1, Bern, 11.

Bell, B., 1970. The oldest records of the Nile floods. Geogr. J. 136, 569–573.

Bell, W.T., Ogilvie, A.E.J., 1978. Weather compilations as a source of data for the reconstruction of European climate during the Medieval Period. Clim. Chang. 1, 331–348.

Belt, S.T., Müller, J., 2013. The Arctic sea-ice biomarker IP_{25}: a review of current understanding, recommendations for future research and applications in palaeo sea ice reconstructions. Quat. Sci. Rev. 79, 9–25.

Belt, S.T., Massé, G., Rowland, S.J., Poulin, M., Michel, C., LeBlanc, B., 2007. A novel chemical fossil of palaeo sea ice: IP_{25}. Org. Geochem. 38, 16–27.
Belt, S.T., Vare, L.L., Massé, G., Manners, H.R., Price, J.C., MacLachlan, S.E., Andrews, J.T., Schmidt, S., 2010. Striking similarities in temporal changes to seasonal sea ice conditions across the central Canadian Arctic Archipelago over the last 7,000 years. Quat. Sci. Rev. 29, 3489–3504.
Belt, S.T., Brown, T.A., Ringrose, A.E., Cabedo-Sanz, P., Mundy, C.J., Gosselin, M., Poulin, M., 2013. Quantitative measurement of the sea ice diatom biomarker IP_{25} and sterols in Arctic sea ice and underlying sediments: further considerations for palaeo sea ice reconstruction. Org. Geochem. 62, 33–45.
Bender, M., Sowers, T., Dickson, M.-L., Orchado, J., Grootes, P., Mayewski, P.A., Meese, D.A., 1994. Climate correlations between Greenland and Antarctica during the past 100,000 years. Nature. 327, 663–666.
Bender, M.L., 2002. Orbital tuning chronology for the Vostok climate record supported by trapped gas composition. Earth Planet. Sci. Lett. 204, 275–289.
Bender, M.L., 2013. Paleoclimate. Princeton University Press, Princeton, 306 pp.
Bender, M.L., Labeyrie, L.D., Raynaud, D., Lorius, C., 1985. Isotopic composition of atmospheric oxygen in ice linked with deglaciation and global primary productivity. Nature. 318, 349–352.
Benedict, J.B., 1967. Recent glacial history of an alpine area in the Colorado Front Range, USA. I. Establishing a lichen growth curve. J. Glaciol. 6, 817–832.
Benedict, J.B., 1993. A 2000-year lichen snow-kill chronology for the Colorado Front Range, USA. The Holocene. 3, 27–33.
Bennett, K.D., Willis, K.J., 2001. Pollen. In: Smol, J.P., Birks, H.J.B., Last, W.M. (Eds.), Tracking Environmental Change Using Lake sediments, vol. 3. Kluwer Academic, Dordrecht, pp. 5–32.
Benson, C.S., 1961. Stratigraphic studies in the snow and firn of the Greenland Ice Sheet. Folia Geogr. Dan. 9, 13–37.
Benson, L.V., 1981. Paleoclimatic significance of lake-level fluctuations in the Lahontan Basin. Quat. Res. 16, 390–403.
Benson, W.W., 1982. Alternative models for infrageneric diversification in the humid Tropics: tests with Passion Vine Butterflies. In: Prance, G.T. (Ed.), Biological Diversification in the Tropics. Columbia University Press, New York, pp. 608–640.
Berger, W.H., 1968. Planktonic foraminifera: selective solution and paleoclimatic interpretation. Deep-Sea Res. 15, 31–43.
Berger, W.H., 1970. Planktonic foraminifera: selective solution and lysocline. Mar. Geol. 8, 111–138.
Berger, W.H., 1971. Sedimentation of planktonic foraminifera. Mar. Geol. 11, 325–358.
Berger, W.H., 1973a. Deep-Sea carbonates: evidence for a coccolith lysocline. Deep-Sea Res. 20, 917–921.
Berger, W.H., 1973b. Deep-Sea carbonates: pleistocene dissolution cycles. J. Foram. Res. 3, 187–195.
Berger, W.H., 1975. Deep-Sea carbonates: dissolution profiles from foraminiferal preservation. In: Sliter, W.V., Bé, A.W.H., Berger, W.H. (Eds.), Dissolution of Deep-Sea Carbonates. Special Publication No. 13, Cushman Foundation for Foraminiferal Research, Washington, DC, pp. 82–86.
Berger, A., 1977a. Long-term variations of the Earth's orbital elements. Celest. Mech. 15, 53–74.
Berger, A., 1977b. Support for the astronomical theory of climatic change. Nature. 269, 44–45.
Berger, W.H., 1977c. Deep-Sea carbonate and the deglaciation preservation spike in pteropods and foraminifera. Nature. 269, 301–304.
Berger, A., 1978. Long-term variations of caloric insolation resulting from the Earth's orbital elements. Quat. Res. 9, 139–167.
Berger, A., 1979. Insolation signatures of Quaternary climatic changes. Il Nuovo Cimento. 2C, 63–87.
Berger, A., 1980. The Milankovitch astronomical theory of paleoclimates. A modern review. Vistas Astron. 24, 103–122.
Berger, A., 1988. Milankovitch theory and climate. Rev. Geophys. 26, 624–657.
Berger, A., 1990. Testing the astronomical theory with a coupled climate-ice-sheet model. Glob. Planet. Chang. 3, 25–141.
Berger, W.H., Gardner, J.V., 1975. On the determination of Pleistocene temperatures from planktonic foraminifera. J. Foram. Res. 5, 102–113.
Berger, W.H., Killingley, J.S., 1977. Glacial-Holocene transition in deep-sea carbonates: selective dissolution and the stable isotope signal. Science. 197, 563–566.
Berger, A., Loutre, M.F., 1991. Insolation values for the climate of the last 10 million years. Quat. Sci. Rev. 10, 297–318.

Berger, W.H., Wefer, G., 1991. Productivity of the glacial ocean: discussion of the iron hypothesis. Limnol. Oceanogr. 36, 1899–1918.

Berger, W.H., Winterer, E.L., 1974. Plate stratigraphy and the fluctuating carbonate line. In: Hsu, K.J., Jenkins, H. (Eds.), Pelagic Sediments on Land and in the Ocean. Special Publication No. 1, International Association of SedimentologistsBlackwell Scientific, Oxford, pp. 11–48.

Berger, R., Homey, A.G., Libby, W.F., 1964. Radiocarbon dating of bone and shell from their organic components. Science. 144, 999–1001.

Berger, W.H., Johnson, R.F., Killingley, J.S., 1977. "Unmixing" of the deep-sea record and the deglacial meltwater spike. Nature. 269, 661–663.

Berger, A., Gallée, H., Loutre, M.F., 1991. The earth's future climate at the astronomical timescale. In: Goodess, C.M., Palutikof, J.P. (Eds.), Future Climate Change and Radioactive Waste Disposal. Climatic Research Center, University of East Anglia, Norwich, pp. 148–165.

Berger, A., Loutre, M.F., Laskar, J., 1992a. Stability of the astronomical frequencies over the Earth's history for paleoclimatic studies. Science. 255, 560–566.

Berger, G.W., Pillans, B.J., Palmer, A.S., 1992b. Dating loess up to 800 ka by thermoluminescence. Geology. 20, 403–406 (see also comment by Wintle et al., 1993. Geology 21, 568).

Berger, A., Li, X.S., Loutre, M.F., 1999. Modelling northern hemisphere ice volume over the last 3Ma. Quat. Sci. Rev. 18, 1–11.

Berger, W.H., Pätzold, J., Wefer, G., 2002. Times of quiet, times of agitation: Sverdrup's conjecture and the Bermuda coral record. In: Wefer, G., Berger, W., Behre, K.-E., Jansen, E. (Eds.), Climate Development and History of the North Atlantic Realm. Springer, Berlin, pp. 89–99.

Berggren, W.A., Burckle, L.H., Cita, M.B., Cooke, H.B.S., Funnell, B.M., Gartner, S., Hays, J.D., Kennett, J.P., Opdyke, N.D., Pastouret, L., Shackleton, N.J., Takayanagi, I.Y., 1980. Towards a Quaternary time scale. Quat. Res. 13, 277–302.

Berggren, W.A., Kent, D.V., Swisher III, C.C., Aubry, M.P., 1995. A revised Cenozoic geochronology and chronostratigraphy. In: Beggren, W.A., Kent, D.V., Aubry, M.P., Hardenbol, J. (Eds.), Geochronology Time Scales and Global Stratigraphic Correlation. Special Publication No. 54, Society for Sedimentary Geology, Tulsa, Oklahoma, pp. 129–212.

Berggren, A.-M., Beer, J., Possnert, G., Aldahan, A., Kubik, P., Christl, M., Johnsen, S.J., Abreu, J., Vinther, B.M., 2009. A 600-year annual ^{10}Be record from the NGRIP ice core, Greenland. Geophys. Res. Lett. 36, L11801, dx.doi.org/10.1029/2009GL038004.

Bergthorsson, P., 1969. An estimate of drift ice and temperature in Iceland in 1000 years. Jøkull. 19, 94–101.

Berkelhammer, M., Sinha, A., Stott, L., Cheng, H., Pausata, F.S.R., Yoshimura, K., et al., 2012. An abrupt shift in the Indian Monsoon 4000 years ago. In: Giosan, L., Fuller, D.Q., Nicoll, K., Flad, R.K., Clift, P.D. (Eds.), Climates, Landscapes and Civilisations. Geophysical Monograph Series, vol. 198. American Geophysical Union, Washington, DC, pp. 75–87.

Berlage, H., 1931. Over het verband tusschen de dikte der jaarringen van djatdibonem (*Tectona grandis* L.F.) en den regenval op Java [On the relation between the width of annual rings of *Tectona grandis* and the rainfall in Java]. Tectona. 24, 939–953.

Bernabo, J.C., Webb III, T., 1977. Changing patterns in the Holocene pollen record of northeastern North America: a mapped summary. Quat. Res. 8, 69–96.

Berner, R.A., 1977. Sedimentation and dissolution of pteropods in the ocean. In: Anderson, N.R., Malahoff, A. (Eds.), The Fate of Fossil Fuel CO_2 in the Ocean. Plenum Press, New York, pp. 243–260.

Beschel, R., 1961. Dating rock surfaces by lichen growth and its application in glaciology and physiography (lichenometry). In: Raasch, G.O. (Ed.), Geology of the Arctic, II. University of Toronto Press, Toronto, pp. 1044–1062.

Besonen, M.R., Bradley, R.S., Mudelsee, M., Abbott, M., Francus, P., 2008. A 1,000 year record of hurricane activity from Boston, Massachusetts. Geophys. Res. Lett. 35, L14705, dx.doi.org/10.1029/2008GL033950.

Betancourt, J.L., 1990. Late Quaternary biogeography of the Colorado Plateau. In: Betancourt, J.L., Van Devender, T.R., Martin, P.S. (Eds.), Packrat Middens: The Last 40,000 Years of Biotic Change. University of Arizona Press, Tucson, pp. 259–292.

Betancourt, J.L., Van Devender, T.R., Martin, P.S. (Eds.), 1990. Packrat Middens: The Last 40,000 Years of Biotic Change. University of Arizona Press, Tucson.

Betancourt, J.L., Latorre, C., Rech, J.A., Quade, J., Rylander, K.A., 2000. A 22,000-year record of monsoonal precipitation from Northern Chile's Atacama Desert. Science. 289, 1542–1546.
Bettis III, E.A., Muhs, D.R., Roberts, H.M., Wintle, A.G., 2003. Last glacial loess in the conterminous USA. Quat. Sci. Rev. 22, 1907–1946.
Bianchi, T.S., Canuel, E.A., 2011. Chemical Biomarkers in Aquatic Systems. Princeton University Press, Princeton, 396 pp.
Bickerton, R., Matthews, J.A., 1992. On the accuracy of lichenometric dates: an assessment based on the 'Little Ice Age' moraine sequence of Nigardsbreen, southern Norway. The Holocene. 2, 227–237.
Bigler, M., Röthlisberger, R., Lambert, F., Wolff, E.W., Castellano, E., Udisti, R., Stocker, T.F., Fischer, H., 2009. Atmospheric decadal variability from high-resolution Dome C ice core records of aerosol constituents beyond the Last Interglacial. Quat. Sci. Rev. 29, 324–337.
Biondi, F., Gershunov, A., Cayan, D.R., 2001. North Pacific decadal climate variability since 1661. J. Clim. 14, 5–10.
Birks, H.J.B., 1978. Numerical methods for the zonation and correlation of biostratigraphical data. In: Berglund, B.E. (Ed.), Palaeohydrological Changes in the Temperate Zone in the Last 15,000 Years. 1, International Geological Correlation Program, Project 158B, Subproject B, University of Lund, Sweden, pp. 99–119.
Birks, H.H., 2001. Plant macrofossils. In: Smol, J.P., Birks, H.J.B., Last, W.M. (Eds.), Tracking Environmental Change Using Lake sediments, vol. 3. Kluwer Academic, Dordrecht, pp. 49–74.
Birks, H.J.B., 2010. Numerical methods for the analysis of diatom assemblage data. In: Smol, J.P., Stoermer, E.F. (Eds.), The Diatoms: Applications for the Environmental and Earth Sciences. Cambridge University Press, Cambridge, pp. 23–54.
Birks, H.J.B., Berglund, B.E., 1979. Holocene pollen stratigraphy of southern Sweden: a reappraisal using numerical methods. Boreas. 8, 257–279.
Birks, H.J.B., Birks, H.H., 1980. Quaternary Palaeoecology. Arnold, London.
Birks, H.H., Birks, H.J.B., 2000. Future uses of pollen analysis must include plant macrofossils. J. Biogeogr. 27, 31–35.
Birks, H.H., Birks, H.J.B., 2003. Reconstructing Holocene climates from pollen and plant macrofossils. In: Mackay, A., Battarbee, R., Birks, H.J.B., Oldfield, F. (Eds.), Global Change in the Holocene. Arnold, London, pp. 342–357.
Birks, H.J.B., Birks, H.H., 2008. Biological responses to rapid climate change at the Younger Dryas-Holocene transition at Kråkenes, western Norway. The Holocene. 18, 19–30.
Birks, H.J.B., Gordon, A.D., 1985. Numerical Methods in Quaternary Pollen Analysis. Academic Press, London.
Birks, H.H., Gulliksen, S., Haflidason, H., Mangerud, J., Possnert, G., 1996. New radiocarbon dates for the Vedde ash and the Saksunarvatn ash from western Norway. Quat. Res. 45, 119–127.
Birks, H.H., Battarbee, R.W., Birks, H.J.B., 2000. The development of the aquatic ecosystem at Kråkenes Lake, western Norway, during the late-glacial and early-Holocene—a synthesis. J. Paleolimnol. 23, 91–114.
Björck, S., Walker, M.J.C., Cwynar, L.C., Johnsen, S., Knudsen, K.-L., Lowe, J.J., Wohlfarth, B., 1998. An event stratigraphy for the last termination in the North Atlantic region based on the Greenland ice-core record: a proposal by the INTIMATE group. J. Quat. Sci. 13, 283–292.
Blaauw, M., van Geel, B., van der Plicht, J., 2004. Solar forcing of climatic change during the mid-Holocene: indications from raised bogs in The Netherlands. The Holocene. 14, 35–44.
Black, D.E., Peterson, L.C., Overpeck, J.T., Kaplan, A., Evans, M.N., Kashgarian, M., 1999. Eight centuries of North Atlantic Ocean atmosphere variability. Science. 286, 1709–1713.
Blackwell, B., Schwarcz, H.P., 1995. The uranium series disequilibrium dating methods. In: Rutter, N.W., Catto, N.R. (Eds.), Dating Methods for Quaternary Deposits. Geological Association of Canada, St. John's, pp. 167–208.
Blaga, C.I., Reichart, G.-J., Heiri, O., Sinninghe Damsté, J.S., 2009. Tetraether membrane lipid distributions in water-column particulate matter and sediments: a study of 47 European lakes along a north-south transect. J. Paleolimnol. 41, 523–540.
Blaga, C.I., Reichart, G.-J., Lotter, A.F., Anselmetti, F.S., Sinninghe Damsté, J.S., 2013. A TEX86 lake record suggests simultaneous shifts in temperature in Central Europe and Greenland during the last deglaciation. Geophys. Res. Lett. 40, 948–953. dx.doi.org/10.1002/GRL.50181.
Blasing, T.J., Fritts, H.C., 1975. Past climate of Alaska and northwestern Canada as reconstructed from tree-rings. In: Weller, G., Bowling, S.A. (Eds.), Climate of the Arctic. University of Alaska Press, Fairbanks, pp. 48–58.

Blinman, E., Mehringer, P.J., Sheppard, J.C., 1979. Pollen influx and the deposition of Mazama and Glacier Peak tephras. In: Sheets, P.D., Grayson, D.K. (Eds.), Volcanic Activity and Human Ecology. Academic Press, New York, pp. 393–425.

Blockley, S.P.E., Lane, C.S., Hardiman, M., Rasmussen, S.O., Seierstad, I.K., Steffensen, J.P., Svensson, A., Lotter, A.F., Turney, C.S.M., Bronk Ramsey, C., INTIMATE members, 2012. Synchronisation of palaeoenvironmental records over the last 60,000 years, and an extended INTIMATE event stratigraphy to 48,000 b2k. Quat. Sci. Rev. 36, 2–10.

Bloemendal, J., Liu, X.M., 2005. Rock magnetism and geochemistry of two Plio-Pleistocene Chinese loess-palaeosol sequences—implications for quantitative palaeoprecipitation reconstruction. Palaeogeogr. Palaeoclimatol. Palaeoecol. 226, 149–166.

Blunier, T., Chappellaz, J., Schwander, J., Stauffer, B., Raynaud, D., 1995. Variations in atmospheric methane concentration during the Holocene epoch. Nature. 374, 46–49.

Blunier, T., Chappellaz, J., Schwander, J., Dallenbach, A., Stauffer, B., Stocker, T.F., Raynaud, D., Jouzel, J., Clausen, H.B., Hammer, C.U., Johnsen, S.J., 1998. Asynchrony of Antarctic and Greenland climate change during the last glacial period. Science. 394, 739–743.

Blunier, T., Spahni, R., Barnola, J.-M., Chappellaz, J., Loulergue, L., Schwander, J., 2007. Synchronization of ice core records via atmospheric gases. Clim. Past. 3, 325–330.

Boersma, A., 1978. Foraminifera. In: Haq, B.U., Boersma, A. (Eds.), Introduction to Marine Micropaleontology. Elsevier/North Holland, New York, pp. 19–77.

Bonan, G.B., 2008. Forests and climate change: forcings, feedbacks, and the climate benefits of forests. Science. 320, 1444–1449.

Bond, G.C., Lotti, R., 1995. Iceberg discharges into the North Atlantic on millennial time scales during the Last Glaciation. Science. 267, 1005–1010.

Bond, G., Heinrick, H., Broecker, W., Labeyrie, L., McManus, J., Andrews, J., Huon, S., Jantschik, R., Clausen, S., Simet, C., Tedesco, K., Klas, M., Bonani, G., Ivy, S., 1992. Evidence for massive discharges of icebergs into the North Atlantic Ocean during the last glacial period. Nature. 360, 245–249.

Bond, G., Broecker, W., Johnsen, S., McManus, J., Labeyrie, L., Jouzel, J., Bonani, G., 1993. Correlations between climate records from North Atlantic sediment and Greenland ice. Nature. 365, 143–147.

Bond, G., Showers, W., Cheseby, M., Lotti, R., Almasi, P., deMenocal, P., Priore, P., Cullen, H., Hajdas, I., Bonani, G., 1997. A pervasive millennial-scale cycle in North Atlantic Holocene and Glacial climates. Science. 278, 1257–1266.

Bond, G., Kromer, B., Beer, J., Muscheler, R., Evans, M.N., Showers, W., Hoffmann, S., Lotti-Bond, R., Hajdas, I., Bonani, G., 2001. Persistent solar influence on North Atlantic climate during the Holocene. Science. 294, 2130–2136.

Bonfils, C., de Noblet-Ducoudré, N., Guiot, J., Bartlein, P., 2004. Some mechanisms of mid-Holocene climate change in Europe, inferred from comparing PMIP models to data. Clim. Dyn. 23, 79–98.

Bonnefille, R., Chalie, F., Guiot, J., Vincens, A., 1992. Quantitative estimates of full glacial temperatures in equatorial Africa from palynological data. Clim. Dyn. 6, 251–257.

Bonny, A.P., 1972. A method for determining absolute pollen frequencies in lake sediments. New Phytol. 71, 391–403.

Boom, A., Mora, G., Cleef, A.M., Hooghiemstra, H., 2001. High altitude C_4 grasslands in the northern Andes: relicts from glacial conditions? Rev. Palaeobot. Palynol. 115, 147–160.

Booth, R.K., Jackson, S.T., Forman, S.L., Kutzbach, J.E., Bettis III, E.A., Kreig, J., Wright, D.K., 2005. A severe centennial-scale drought in mid-continental North America 4200 years ago and apparent global linkages. The Holocene. 15, 321–328.

Borgmark, A., 2005. Holocene climate variability and periodicities in south-central Sweden, as interpreted from peat humification analysis. The Holocene. 15, 387–395.

Borisenkov, Y.P., Tsvetkov, A.V., Agaponov, S.V., 1983. On some characteristics of insolation changes in the past and future. Clim. Chang. 5, 237–244.

Borisenkov, Y.P., Tsvetkov, A.V., Eddy, J.A., 1985. Combined effect of earth orbit perturbations and solar activity on terrestrial insolation. Part I. Sample days and annual mean values. J. Atmos. Sci. 42, 933–940.

Boto, K., Isdale, P., 1985. Fluorescent bands in massive corals result from terrestrial fulvic acid inputs to nearshore zone. Nature. 315, 396–397.

Bowen, D.Q., Richmond, G.M., Fullerton, D.S., Sibrava, V., Fulton, R.J., Velichko, A.A., 1986. Correlation of Quaternary glaciations in the Northern Hemisphere. Quat. Sci. Rev. 5, 509–510 (plus chart).

Bowen, D.Q., Hughes, S., Sykes, G.A., Miller, G.H., 1989. Land-sea correlations in the Pleistocene based on isoleucine epimerization in non-marine molluscs. Nature. 340, 49–51.

Bowler, J.M., 1976. Aridity in Australia: age origins and expression in aeolian landforms and sediments. Earth-Sci. Rev. 12, 279–310.
Boyle, E.A., 1988. Cadmium: chemical tracer of deepwater paleoceanography. Paleoceanography. 3, 471–490.
Boyle, E.A., 1992. Cadmium and $\delta^{13}C$ paleochemical ocean distributions during the stage 2 glacial maximum. Annu. Rev. Earth Planet. Sci. 20, 245–287.
Boyle, E.A., 1997. Cool tropical temperatures shift the global $\delta^{18}O$-T relationship: an explanation for the ice core $\delta^{18}O$ borehole temperature conflict? Geophys. Res. Lett. 24, 273–276.
Boyle, E.A., Keigwin, L.D., 1982. Deep circulation of the North Atlantic over the past 200,000 years: geochemical evidence. Science. 218, 784–787.
Boyle, E.A., Keigwin, L.D., 1985. Comparison of Atlantic and Pacific paleochemical records for the last 215,000 years: changes in deep ocean circulation and chemical inventories. Earth Planet. Sci. Lett. 76, 135–150.
Boyle, E.A., Keigwin, L.D., 1987. North Atlantic thermohaline circulation during the past 20,000 years linked to high-latitude surface temperature. Nature. 330, 35–40.
Boyle, E.A., Rosener, P., 1990. Further evidence for a link between Late Pleistocene North Atlantic surface temperatures and North Atlantic Deep-Water production. Palaeogeogr. Palaeoclimatol. Palaeoecol. (Glob. Planet. Change Sect.). 89, 113–124.
Braconnot, P., Harrison, S.P., Joussaume, S., Hewitt, C.D., Kitoh, A., Kutzbach, J.E., Liu, Z., Otto Bliesner, B., Syktus, J., Weber, S.L., 2004. Evaluation of PMIP coupled ocean-atmosphere simulations of the mid-Holocene. In: Battarbee, R.W., Gasse, F., Stickley, C.E. (Eds.), Past Climate Variability through Europe and Africa. Springer, Dordrecht, pp. 515–534.
Braconnot, P., Otto-Bliesner, B., Harrison, S., Joussaume, S., Peterchmitt, J.-Y., Abe-Ouchi, A., Crucifix, M., Driesschaert, E., Fichefet, Th., Hewitt, C.D., Kageyama, M., Kitoh, A., Loutre, M.-F., Marti, O., Merkel, U., Ramstein, G., Valdes, P., Weber, L., Yu, Y., Zhao, Y., 2007. Results of PMIP2 coupled simulations of the Mid-Holocene and Last Glacial Maximum. Part 1: experiments and large-scale features. Clim. Past. 3, 261–262.
Braconnot, P., Harrison, S.P., Kageyama, M., Bartlein, P.J., Masson-Delmotte, V., Abe-Ouchi, A., Otto-Bliesner, B., Zhao, Y., 2012. Evaluation of climate models using palaeoclimatic data. Nat. Clim. Chang. 2, 417–424.
Bradbury, J.P., Dean, W.E. (Eds.), 1993. Elk Lake, Minnesota: Evidence for Rapid Climatic Change in the North-central United States. Special Paper 276, Geological Society of America, Boulder, 336 pp.
Bradbury, J.P., Leyden, B., Salgado-Labouriau, M., Lewis, W.M., Schubert, C., Binford, M.W., Frey, D.G., Whitehead, D.R., Weibezahn, F.H., 1981. Late Quaternary environmental history of Lake Valencia, Venezuela. Science. 214, 1299–1305.
Bradbury, J.P., Grosjean, M., Stine, S., Sylvestre, F., 2001. Full and Late Glacial lake records along the PEP1 transect: their role in developing interhemispheric paleoclimate interactions. In: Markgraf, V. (Ed.), Interhemispheric Climate Linkages. Academic Press, San Diego, pp. 265–291.
Bradley, R.S., 1976. Precipitation History of the Rocky Mountain States. Westview Press, Boulder, Colo..
Bradley, R.S., 1988. The explosive volcanic eruption signal in northern hemisphere continental temperature records. Clim. Chang. 12, 221–243.
Bradley, R.S., 1991. Instrumental records of past global change: lessons for the analysis of non-instrumental data. In: Bradley, R.S. (Ed.), Global Changes of the Past. University Corporation for Atmospheric Research, Boulder, pp. 103–116.
Bradley, R.S., 2003. Climate forcing during the Holocene. In: Mackay, A.W., Battarbee, R.W., Birks, H.J.B., Oldfield, F. (Eds.), Global Change in the Holocene: Approaches to Reconstructing Fine-resolution Climate Change. Arnold, London, pp. 10–19.
Bradley, R.S., 2008. Holocene perspectives on future climate change. In: Battarbee, R.W., Binney, H.A. (Eds.), Natural Climate Variability and Global Warming: A Holocene Perspective. Wiley-Blackwell, Chichester, pp. 254–268.
Bradley, R.S., Eddy, J.A., 1991. Records of past global changes. In: Bradley, R.S. (Ed.), Global Changes of the Past. University Corporation for Atmospheric Research, Boulder, pp. 5–9.
Bradley, R.S., England, J., 2008. The Younger Dryas and the Sea of Ancient Ice. Quat. Res. 70, 1–10.
Bradley, R.S., Jones, P.D. (Eds.), 1992a. Introduction. Climate Since A.D. 1500, Routledge, London, pp. 1–16.
Bradley, R.S., Jones, P.D., 1992b. When was the “Little Ice Age”? In: Mikami, T. (Ed.), Proceedings of the International Symposium on the Little Ice Age Climate. Department of Geography, Tokyo Metropolitan University, Tokyo, pp. 1–4.

Bradley, R.S., Jones, P.D. (Eds.), 1992c. Records of explosive volcanic eruptions over the last 500 years. Climate Since A.D. 1500, Routledge, London, pp. 606–622.
Bradley, R.S., Jones, P.D., 1993. "Little Ice Age" summer temperature variations: their nature and relevance to recent global warming trends. The Holocene. 3, 367–376.
Bradley, R.S., Jones, P.D. (Eds.), 1995. Climate Since A.D. 1500. revised ed. Routledge, London.
Bradley, R.S., Miller, G.H., 1972. Recent climatic change and increased glacierization in the eastern Canadian Arctic. Nature. 237, 385–387.
Bradley, R.S., Diaz, H.F., Kiladis, G.N., Eischeid, J.K., 1987. ENSO signal in continental temperature and precipitation records. Nature. 327, 497–501.
Bradley, R.S., Bard, E., Farquhar, G., Joussaume, S., Lautenschlager, M., Molfino, B., Raschke, E., Shackleton, N.J., Sirocko, F., Stauffer, B., White, J., 1993. Evaluating strategies for reconstructing past global changes-what and where are the gaps? In: Eddy, J.A., Oeschger, H. (Eds.), Global Changes in the Perspective of the Past. Wiley, Chichester, pp. 145–171.
Bradley, R.S., Alverson, K., Pedersen, T.F., 2003a. Challenges of a changing earth: past perspectives, future concerns. In: Alverson, K.D., Bradley, R.S., Pedersen, T.F. (Eds.), Paleoclimate, Global Change and the Future. Springer Verlag, Berlin, pp. 163–167.
Bradley, R.S., Vuille, M., Hardy, D.R., Thompson, L.G., 2003b. Low latitude ice cores record Pacific sea surface temperatures. Geophys. Res. Lett. 30, 1174–1177. dx.doi.org/10.1029/2002GL016546.
Bradley, R.S., Hughes, M.K., Diaz, H.F., 2003c. Climate in Medieval time. Science. 302, 404–405.
Bradley, R.S., Briffa, K.R., Cole, J., Hughes, M.K., Osborn, T.J., 2003d. The climate of the last millennium. In: Alverson, K., Bradley, R.S., Pedersen, T.F. (Eds.), Paleoclimate, Global Change and the Future. Springer Verlag, Berlin, pp. 105–141.
Bradshaw, R.H.W., 1994. Quaternary terrestrial sediments and spatial scale: the limits to interpretation. In: Traverse, A. (Ed.), Sedimentation of Organic Particles. Cambridge University Press, Cambridge, pp. 239–252.
Braganza, K., Gergis, J.L., Power, S.B., Risbey, J.S., Fowler, A.M., 2009. A multiproxy index of the El Niño-Southern Oscillation, A.D. 1525-1982. J. Geophys. Res. Atmos. 114. dx.doi.org/10.1029/2008JD010896.
Brakenridge, G.R., 1978. Evidence for a cold, dry full-glacial climate in the American Southwest. Quat. Res. 9, 22–40.
Brassell, S.C., Eglinton, G., Marlowe, I.T., Pflaumann, U., Sarnthein, M., 1986. Molecular stratigraphy: a new tool for climatic assessment. Nature. 320, 129–133.
Braun, C., Bezada, M., 2013. The history and disappearance of glaciers in Venezuela. J. Latin Am. Geogr. 12, 85–124.
Bray, J.R., 1974. Glacial advance relative to volcanic activity since AD 1500. Nature. 248, 42–43.
Bray, J.R., 1979. Surface albedo increase following massive Pleistocene explosive eruptions in western North America. Quat. Res. 12, 204–211.
Bray, J.R., 1982. Alpine glacier advance in relation to a proxy summer temperature index based mainly on wine harvest dates, AD 1453-1973. Boreas. 11, 1–10.
Brázdil, R., 1996. Reconstructions of past climate from historical sources in Czech lands. In: Jones, P.D., Bradley, R.S., Jouzel, J. (Eds.), Climatic Variations and Forcing Mechanisms of the Last 2000 Years. Springer-Verlag, Berlin, pp. 409–431.
Brázdil, R., Pfister, C., Wanner, H., von Storch, H., Luterbacher, J., 2005. Historical climatology: the state of the art. Clim. Chang. 70, 363–430.
Brázdil, R., Kundzewicz, Z.W., Benito, G., 2006. Historical hydrology for studying flood risk in Europe. Hydrol. Sci. J. 51, 739–764.
Brázdil, R., Kundzewicz, Z.W., Benito, G., Demarée, G., MacDonald, N., Roald, L.A., 2012. Historical floods in Europe in the past millennium. In: Kundzewicz, Z.W. (Ed.), Changes of Flood Risk in Europe. IAHS Special Publication 10 IAHS Press, Wallingford, pp. 121–166.
Briffa, K.R., Melvin, T.M., 2011. A closer look at regional curve standardization of tree-ring records: justification of the need, a warning of some pitfalls and suggested improvements in its application. In: Hughes, M.K., Swetnam, T.W., Diaz, H.F. (Eds.), Dendroclimatology: Progress and Prospects. Springer, Dordrecht, pp. 113–145.
Briffa, K.R., Schweingruber, F.H., 1992. Recent dendroclimatic evidence of northern and central European summer temperatures. In: Bradley, R.S., Jones, P.D. (Eds.), Climate Since A.D. 1500. Routledge, London, pp. 366–392.
Briffa, K.R., Jones, P.D., Pilcher, J.R., Hughes, M.K., 1988. Reconstructing summer temperatures in northern Fennoscandia back to A.D. 1700 using tree-ring data from Scots Pine. Arct. Alp. Res. 20, 385–394.

Briffa, K.R., Bartholin, T.S., Eckstein, D., Jones, P.D., Karlen, W., Schweingruber, F.H., Zetterberg, P., 1990. A 1400-year tree-ring record of summer temperatures in Fennoscandia. Nature. 346, 434–439.
Briffa, K.R., Jones, P.D., Bartholin, T.S., Eckstein, D., Schweingruber, F.H., Karlen, W., Zetterberg, P., Eronen, M., 1992a. Fennoscandian summers from A.D. 500: temperature changes on short and long timescales. Clim. Dyn. 7, 111–119.
Briffa, K.R., Jones, P.D., Schweingruber, F.H., 1992b. Tree-ring density reconstructions of summer temperature patterns across western North America since 1600. J. Clim. 5, 735–754.
Briffa, K.R., Jones, P.D., Schweingruber, F.H., 1994. Summer temperatures across northern North America: regional reconstructions from 1760 using tree-ring indices. J. Geophys. Res. 99D, 25835–25844.
Briffa, K.R., Jones, P.D., Schweingruber, F.H., Shiyatov, S.G., Cook, E.R., 1995. Unusual twentieth century warmth in a 1,000-year temperature record from Siberia. Nature. 376, 156–159.
Briffa, K.R., Jones, P.D., Schweingruber, F.H., Karlen, W., Shiyatov, S.G., 1996. Tree-ring variables as proxy climate indicators: problems with low-frequency signals. In: Jones, P.D., Bradley, R.S., Jouzel, J. (Eds.), Climate Variations and Forcing Mechanisms of the Last 2000 Years. Springer-Verlag, Berlin, pp. 9–41.
Briffa, K., Schweingruber, F., Jones, P., Osborn, T., 1998a. Reduced sensitivity of recent tree growth to temperature at high northern latitudes. Nature. 391, 678–682.
Briffa, K., Schweingruber, F., Jones, P., Osborn, T., Harris, I., Shiyatov, S., Vaganov, A., Grudd, H., 1998b. Trees tell of past climates: but are they speaking less clearly today? Philos. Trans. R. Soc. Lond. B. 353, 65–73.
Briffa, K.R., Osborn, T.J., Schweingruber, F.H., Harris, I.C., Jones, P.D., Shiyatov, S.G., Vaganov, E.A., 2001. Low frequency temperature variations from a northern tree ring density network. J. Geophys. Res. 106, 2929–2941.
Briffa, K., Osborn, T., Schweingruber, F., 2004. Large-scale temperature inferences from tree rings: a review. Glob. Planet. Chang. 40, 11–26.
Briffa, K., Shishov, V.V., Melvin, T.M., Vaganov, A., Grudd, H., Hantemirov, R.M., Eronen, M., Nauerzbaev, M.M., 2008. Trends in recent temperature and radial tree growth spanning 2000 years across northwest Eurasia. Phil. Trans. R. Soc. Lond. B. 363, 2271–2284.
Brigham-Grette, J., Melles, M., Minyuk, P., Andreev, A., Tarasov, P., DeConto, R., Koenig, S., Nowaczyk, N., Wennrich, V., Rosén, P., Haltia, E., Cook, T., Gebhardt, C., Meyer-Jacob, C., Snyder, J., Herzschuh, U., 2013. Pliocene Warmth, polar amplification, and stepped Pleistocene cooling recorded in NE Arctic Russia. Science. 340, 1421–1427.
Broccoli, A.J., Dahl, K.A., Stouffer, R.J., 2006. Response of the ITCZ to Northern Hemisphere cooling. Geophys. Res. Lett. 33, L01702. dx.doi.org/10.1029/2005GL024546.
Broecker, W., 1971. Calcite accumulation rates and glacial to interglacial changes in oceanic mixing. In: Turekian, K.K. (Ed.), The Late Cenozoic Glacial Ages. Yale University Press, New Haven, pp. 239–265.
Broecker, W.S., 1982. Ocean chemistry during glacial time. Geochim. Cosmochim. Acta. 46, 1689–1705.
Broecker, W.S., 1987. Unpleasant surprises in the greenhouse? Nature. 328, 123–126.
Broecker, W.S., 1989. The salinity contrast between the Atlantic and Pacific Oceans during glacial time. Paleoceanography. 4, 207–212.
Broecker, W.S., 1991. The great ocean conveyor. Oceanography. 4, 79–89.
Broecker, W.S., 1994. Massive iceberg discharges as triggers for global climate change. Nature. 372, 421–424.
Broecker, W.S., 1997. Thermohaline circulation, the Achilles heel of our climate system: will man-made CO2 upset the current balance? Science. 278, 1582–1588.
Broecker, W.S., 1998. Paleocirculation during the last deglaciation: a bipolar seesaw? Paleoceanography. 13, 119–121. dx.doi.org/10.1029/97PA03707.
Broecker, W.S., 2009. The mysterious ^{14}C decline. Radiocarbon. 51, 109–119.
Broecker, W.S., Barker, S.A., 2007. 190‰ drop in atmosphere's $\Delta^{14}C$ during the "Mystery Interval" 17.5 to 14.5 kyr. Earth Planet. Sci. Lett. 256, 90–99.
Broecker, W.S., Bender, M.L., 1972. Age determinations on marine strandlines. In: Bishop, W.W., Miller, J.A. (Eds.), Calibration of Hominoid Evolution. Scottish Academic Press, Edinburgh, pp. 19–38.
Broecker, W.S., Broecker, S., 1974. Carbonate dissolution on the eastern flank of the East Pacific Rise. In: Hay, W.W. (Ed.), Studies in Paleo-oceanography. Special Publication No. 20, Society of Economic Paleontologists and Mineralogists, Tulsa, pp. 44–58.
Broecker, W.S., Denton, G.H., 1989. The role of ocean-atmosphere reorganizations in glacial cycles. Geochim. Cosmochim. Acta. 53, 2465–2501.
Broecker, W.S., van Donk, J., 1970. Insolation changes, ice volumes and the ^{18}O record in deep-sea cores. Rev. Geophys. Space Phys. 8, 169–198.

Broecker, W.S., Thurber, D.L., Goddard, J., Ku, T.L., Matthews, R.K., Mesolella, K.J., 1968. Milankovitch hypothesis supported by precise dating of coral reefs and deep-sea sediments. Science. 159, 297–300.
Broecker, W.S., Peng, T.-H., Ostlund, G., Stuiver, M., 1985a. The distribution of bomb radiocarbon in the ocean. J. Geophys. Res. 90, 6953–6970.
Broecker, W.S., Peteet, D., Rind, D., 1985b. Does the ocean-atmosphere have more than one stable mode of operation? Nature. 315, 21–25.
Broecker, W.S., Andrée, M., Bonani, G., Wolfli, W., Oeschger, H., Klas, M., Mix, A., Curry, W., 1988. Preliminary estimates for the radiocarbon age of deep water in the glacial ocean. Paleoceanography. 3, 659–669.
Broecker, W.S., Bond, G., Klas, M., Bonani, G., Wolfli, W., 1990a. A salt oscillator in the glacial Atlantic? 1. The concept. Paleoceanography. 5, 469–477.
Broecker, W.S., Peng, T.-H., Jouzel, J., Russell, G., 1990b. The magnitude of global fresh-water transports of importance to ocean circulation. Clim. Dyn. 4, 73–79.
Broecker, W.S., Bond, G., Klas, M., Clark, E., McManus, J., 1992. Origin of the northern Atlantic's Heinrich events. Clim. Dyn. 6, 265–273.
Broecker, W.S., Clark, E., Hajdas, I., Bonani, G., 2004a. Glacial ventilation rates for the deep Pacific Ocean. Paleoceanography. 19, PA2002. dx.doi.org/10.1029/2003PA000974.
Broecker, W.S., Barker, S., Clark, E., Hajdas, I., Bonani, G., Stott, L., 2004b. Ventilation of the glacial deep Pacific Ocean. Science. 306, 1169–1172.
Broecker, W.S., Clark, E., Barker, S., 2008. Near constancy of the Pacific Ocean surface to mid-depth radiocarbon-age difference over the last 20 kyr. Earth Planet. Sci. Lett. 274, 322–326.
Brohan, P., Kennedy, J.J., Harris, I., Tett, S.F.B., Jones, P.D., 2005. Uncertainty estimates in regional and global observed temperatures: a new data set from 1850. J. Geophys. Res. 111, D12106. dx.doi.org/10.1029/2005JD006548.
Bromwich, D.H., Weaver, C.J., 1983. Latitudinal displacement of the main moisture source controls $\delta^{18}O$ of snow in coastal Antarctica. Nature. 301, 145–147.
Bronk Ramsey, C.B., Staff, R.A., Bryant, C.L., Brock, F., Kitagawa, H., van der Plicht, J., Schlolaut, G., Marshall, M.H., Brauer, A., Lamb, H.J., Payne, R.L., Tarasov, P.E., Haraguchi, T., Gotanda, K., Yonenobu, H., Yokohama, Y., Tada, R., Nakagawa, T., 2012. A complete terrestrial radiocarbon record for 11.2 to 52.8 kyr BP. Science. 338, 370–374.
Brook, E.J., Sowers, T., Orchado, J., 1996. Rapid variations in atmospheric methane concentration during the past 110,000 years. Science. 273, 1087–1091.
Brooks, S.J., 2003. Chironomid analysis to interpret and quantify Holocene climatic change. In: Mackay, A., Battarbee, R., Birks, H.J.B., Oldfield, F. (Eds.), Global Change in the Holocene. Arnold, London, pp. 328–341.
Brooks, S.J., 2006. Fossil midges (Diptera: Chironomidae) as paleoclimatic indicators for the Eurasian region. Quat. Sci. Rev. 25, 1894–1910.
Brooks, S.J., Birks, H.J.B., 2000. Chironomid-inferred late-glacial air temperatures at Whitrig Bog, southeast Scotland. J. Quat. Sci. 15, 759–764.
Brooks, S.J., Birks, H.J.B., 2001. Chironomid-inferred air temperatures from Lateglacial and Holocene sites in northwest Europe: progress and problems. Quat. Sci. Rev. 20, 1723–1741.
Brooks, S.J., Mayle, F.E., Lowe, J.J., 1997. Chironomid-based Late Glacial climatic reconstruction for southeast Scotland. J. Quat. Sci. 12, 161–167.
Brown, K.S., 1982. Paleoecology and regional patterns of evolution in Neotropical forest butterflies. In: Prance, G.T. (Ed.), Biological Diversification in the Tropics. Columbia University Press, New York, pp. 255–308.
Brown, I.M., 1990. Quaternary glaciations of New Guinea. Quat. Sci. Rev. 9, 273–280.
Brown, K.S., Ab'Saber, A.N., 1979. Ice-age forest refuges and evolution in the Neotropics: correlation of paleoclimatological, geomorphological and pedological data with modern biological endemism. Paleoclimas. 5, 1–30.
Brown, K.S., Sheppard, P.M., Turner, J.R.G., 1974. Quaternary refugia in tropical America: evidence from race formation in Heliconius butterflies. Proc. R. Soc. Lond. B. 187, 369–378.
Brown, J.S., Colling, A., Park, D., Phillips, J., Rothery, D., Wright, J., 1989. Ocean Circulation. The Open University, Milton Keynes, 238 pp.
Brown, T.A., Farwell, G.W., Grootes, P.M., Schmidt, F.H., 1992. Radiocarbon AMS dating of pollen extracted from peat samples. Radiocarbon. 34, 550–556.
Brown, J., Collins, M., Tudhope, A., 2006. Coupled model simulations of mid-Holocene ENSO and comparisons with coral oxygen isotope records. Adv. Geosci. 6, 29–33.

Bryson, R.A., 1966. Air masses, streamlines and the boreal forest. Geogr. Bull. 8, 228–269.
Bryson, R.A., Murray, T.J., 1977. Climates of Hunger. University of Wisconsin Press, Madison.
Bryson, R.A., Irving, W.N., Larsen, J.A., 1965. Radiocarbon and soil evidence of former forest in the southern Canadian forest. Science. 147, 46–48.
Buckley, B.M., Palakit, K., Duangsathaporn, K., Sanguantham, P., Prasomin, P., 2007. Decadal scale droughts over northwestern Thailand over the past 448 years: links to the tropical Pacific and Indian Ocean sectors. Climate Dynam. 29, 63–71.
Buckley, B.M., Anchukaitis, K.J., Penny, D., Fletcher, R., Cook, E.R., Sano, M., Nam, L.C., Wichienkeeo, A., Minh, T.T., Hong, T.M., 2010. Climate as a contributing factor in the demise of Angkor, Cambodia. Proc. Natl. Acad. Sci. U. S. A. 107, 6748–6752.
Budyko, M.I., 1978. The heat balance of the earth. In: Gribbin, J. (Ed.), Climatic Change. Cambridge University Press, Cambridge, pp. 85–113.
Buisman, J., 1995. Duizend Jaar Weer, Wind en Water in de Lage Landen [A Thousand years, Wind and Water in the Low Countries], 4 vols (vol. 1, up to 1300; vol. 2, 1300–1450; vol. 3, 1450–1575; vol. 4, 1575–1675). Uitgerverij Van Wijnen, Fraenker.
Bunn, A.G., Hughes, M.K., Salzer, M.W., 2011. Topographically modified tree-ring chronologies as a potential means to improve paleoclimate inference. Clim. Chang. 105, 627–634.
Büntgen, U., Frank, D., Nievergelt, D., Esper, J., 2006. Summer temperature variations in the European Alps, A.D. 755–2004. J. Clim. 19, 5606–5623.
Büntgen, U., Frank, D., Wilson, R., Carrer, M., Urbinati, C., Esper, J., 2008. Testing for tree-ring divergence in the European Alps. Glob. Chang. Biol. 14, 2443–2453.
Burbank, D.W., 1981. A chronology of Late Holocene glacier fluctuations on Mount Rainier, Washington. Arct. Alp. Res. 13, 369–381.
Burga, C., 1988. Swiss vegetation history during the past 18,000 years. New Phytol. 110, 581–602.
Burns, S.J., 2011. Speleothem records of changes in tropical hydrology over the Holocene and possible implications for atmospheric methane. The Holocene. 21, 735–741.
Burns, S.J., Fleitmann, D., Matter, A., Neff, U., Mangini, A., 2001. Speleothem evidence from Oman for continental pluvial events during interglacial periods. Geology. 29, 623–626.
Burns, S.J., Fleitmann, D., Mudelsee, M., Neff, U., Matter, A., Mangini, A., 2002. A 780-year annually resolved record of Indian Ocean monsoon precipitation from a speleothem from south Oman. J. Geophys. Res. 107 (D20), 4434. dx.doi.org/10.1029/2001JD001281.
Burrows, C.J., Burrows, V.L., 1976. Procedures for the study of snow avalanche chronology using growth layers of woody plants. INSTAAR Occasional Paper No. 23, University of Colorado INSTAAR, Boulder.
Bush, M.B., 2005. Of orogeny, precipitation, precession and parrots. J. Biogeogr. 32, 1301–1302.
Bush, M.B., Colinvaux, P.A., 1990. A pollen record of a complete glacial cycle from lowland Panama. J. Veg. Sci. 1, 105–118.
Bush, M.B., Colinvaux, P.A., Weimann, M.C., Piperno, D.R., Liu, K.-B., 1990. Late Pleistocene temperature depression and vegetation change in Ecuadorian Amazonia. Quat. Res. 34, 330–345.
Bush, M.B., Silman, M.R., Urrego, D.H., 2004. 48,000 years of climate and forest change in a biodiversity hotspot. Science. 303, 827–829.
Butzer, K.W., Isaac, G.L., Richardson, J.L., Washbourn-Kamau, C., 1972. Radiocarbon dating of East African lake levels. Science. 175, 1069–1076.
Cabedo-Sanz, P., Belt, S.T., Knies, J., Husum, K., 2013. Identification of contrasting seasonal sea ice conditions during the Younger Dryas. Quat. Sci. Rev. 79, 74–86.
Cahyarini, S.Y., Pfeiffer, M., Timm, O., Dullo, W.-C., Schönberg, D.G., 2008. Reconstructing seawater $\delta^{18}O$ from paired coral $\delta^{18}O$ and Sr/Ca ratios: methods, error analysis and problems, with examples from Tahiti (French Polynesia) and Timor (Indonesia). Geochim. Cosmochim. Acta. 72, 2841–2853.
Cai, Y.J., Zhang, H.W., Cheng, H., An, Z.S., Edwards, R.L., Wang, X.F., Tan, L.C., Liang, F.Y., Wang, J., Kelly, M., 2012. The Holocene Indian monsoon variability over the southern Tibet plateau and its teleconnections. Earth Planet. Sci. Lett. 335–336, 135–144.
Caley, T., Kim, J.H., Malaizé, B., Giraudeau, J., Laepple, T., Caillon, N., Charlier, K., Rebaubier, H., Rossignol, L., Castañeda, I., Schouten, S., Sinninghe Damsté, J.S., 2011. High-latitude obliquity as a dominant forcing in the Agulhas current system. Clim. Past. 7, 1285–1296.

Calkin, P.E., Ellis, J.M., 1980. A lichenometric dating curve and its application to Holocene glacier studies in the Central Brooks Range, Alaska. Arct. Alp. Res. 12, 245–264.
Calvo, E., Marshall, J.F., Pelejero, C., McCulloch, M.T., Gagan, M.K., Lough, J.M., 2007. Interdecadal climate variability in the Coral Sea since 1708 A.D. Palaeogeogr. Palaeoclimatol. Palaeoecol. 248, 190–201.
Camuffo, D., Enzi, S., 1994. Chronology of 'Dry Fogs' in Italy, 1374–1891. Theor. Appl. Climatol. 50, 31–33.
Camuffo, D., Enzi, S., 1995. Impact of the clouds of volcanic aerosols in Italy during the last 7 centuries. Nat. Hazards. 11, 135–161.
Cande, S.C., Kent, D.V., 1992. A new geomagnetic polarity time scale for the late Cretaceous and Cenozoic. J. Geophys. Res. 97B, 13917–13951.
Cande, S.C., Kent, D.V., 1995. Revised calibration of the geomagnetic polarity time scale for the late Cretaceous and Cenozoic. J. Geophys. Res. 100, 6093–6095.
Cane, M.A., Molnar, P., 2001. Closing of the Indonesian seaway as a precursor to East African aridification around 3-4 million years ago. Nature. 411, 157–162.
Cantin, N.E., Cohen, A.L., Karnauskas, K.B., Tarrant, A.M., McCorkle, D.C., 2010. Ocean warming slows coral growth in the central Red Sea. Science. 329, 322–325.
Cao, L., Fairbanks, R.G., Mortlock, R.A., Risk, M.J., 2007. Radiocarbon reservoir age of high latitude North Atlantic surface water during the last deglacial. Quat. Sci. Rev. 26, 732–742.
Capron, E., Landais, A., Chappellaz, J., Schilt, A., Buiron, D., Dahl-Jensen, D., Johnsen, S.J., Jouzel, J., Lemieux-Dudon, B., Loulergue, L., Leuenberger, M., Masson-Delmotte, V., Meyer, H., Oerter, H., Stenni, B., 2010. Millennial and sub-millennial scale climatic variations recorded in polar ice cores over the last glacial period. Clim. Past. 6, 345–365.
Capron, E., Landias, A., Buiron, D., Cauquoin, A., Chappellaz, J., Debret, M., Jouzel, J., Leuenberger, M., Martinerie, P., Masson-Delmotte, V., Mulvaney, R., Parrenin, F., Prié, F., 2013. Glacial-interglacial dynamics of Antarctic firn columns: comparison between simulations and ice core air-δ^{15}N measurements. Clim. Past. 9, 983–999.
Carlson, A.E., Clark, P.U., 2013. Ice sheet sources of sea level rise and freshwater sources during the last deglaciation. Rev. Geophys. 50, RG4007. dx.doi.org/10.1029/2011RG000371.
Carrara, P.E., 1979. The determination of snow avalanche frequency through tree-ring analysis and historical records at Ophir, Colorado. Geol. Soc. Am. Bull. 1 (90), 773–780.
Carrara, P.E., Trimble, D.A., Rubin, M., 1991. Holocene treeline fluctuations in the northern San Juan mountains, Colorado, U.S.A., as indicated by radiocarbon-dated conifer wood. Arct. Alp. Res. 23, 233–246.
Carriquiry, J.D., Risk, M.J., Schwarcz, H.P., 1994. Stable isotope geochemistry of corals from Costa Rica as proxy indicator of El Niño-Southern Oscillation (ENSO). Geochim. Cosmochim. Acta. 58, 335–352.
Carslaw, K.S., Boucher, O., Spracklen, D.V., Mann, G.W., Rae, J.G.L., Woodward, S., Kulmala, M., 2010. A review of natural aerosol interactions and feedbacks within the Earth system. Atmos. Chem. Phys. 10, 1701–1737.
Caseldine, C.R., Geirsdóttir, A., Langdon, P., 2003. Efstadalsvatn—a multi-proxy study of a Holocene lacustrine sequence from NW Iceland. J. Paleolimnol. 30, 55–73.
Castañeda, I., Schouten, S., 2011. A review of molecular organic proxies for examining modern and ancient lacustrine environments. Quat. Sci. Rev. 30, 2851–2891.
Castellano, E., Becagli, S., Hansson, M., Hutterli, M., Petit, J.R., Rampino, M.R., Severi, M., Steffensen, J.P., Traversi, R., Udisti, R., 2005. Holocene volcanic history as recorded in the sulfate stratigraphy of the European Project for Ice Coring in Antarctica Dome C (EDC96) ice core. J. Geophys. Res. 110, D06114. dx.doi.org/10.1029/2004JD005259.
Catchpole, A.J.W., 1992. Hudson's Bay Company ships' log-books as sources of sea ice data, 1751-1870. In: Bradley, R.S., Jones, P.D. (Eds.), Climate Since A.D. 1500. Routledge, London, pp. 17–39.
Catchpole, A.J.W., Moodie, D.W., Milton, D., 1976. Freeze-up and break-up of estuaries on Hudson Bay in the 18th and 19th centuries. Can. Geogr. 20, 279–297.
Cerling, T.E., Quade, J., 1993. Stable carbon and oxygen isotopes in soil carbonates. In: Swart, P.K., Lohmann, K.C., McKenzie, J., Savin, S. (Eds.), Climate Change in Continental Isotopic Records. American Geophysical Union, Washington, DC, pp. 217–231.
Chambers, F.M., Charman, D.J., 2004. Holocene environmental change: contributions from the peatland archive. The Holocene. 14, 1–6.
Chambers, F.M., Booth, R.K., De Vleeschouwer, F., Lamentowicz, M., Le Roux, G., Mauquoy, D., Nichols, J.E., van Geel, B., 2012. Development and refinement of proxy-climate indicators from peats. Quat. Int. 268, 21–33.

Channell, J.E.T., Hodell, D.A., Curtis, J.H., 2012. ODP Site 1063 (Bermuda Rise) revisited: oxygen isotopes, excursions and paleointensity in the Brunhes Chron. Geochem. Geophys. Geosyst. 13, Q02001. doi.org/10.1029/2011GC003897.

Chapman, M.R., Shackleton, N.J., Zhao, M., Eglinton, G., 1996. Faunal and alkenone reconstructions of sub-tropical North Atlantic surface hydrography and paleotemperature over the last 28 kyrs. Paleoceanography. 11, 343–358.

Chappell, J., 2002. Sea level changes forced ice breakouts in the Last Glacial cycle: new results from coral terraces. Quat. Sci. Rev. 21, 1229–1240.

Chappell, J.M.A., Polach, H.A., 1972. Some effects of partial recrystallisation on ^{14}C dating of late Pleistocene corals and molluscs. Quat. Res. 2, 244–252.

Chappell, J.M.A., Shackleton, N.J., 1986. Oxygen isotopes and sea level. Nature. 324, 137–138.

Chappellaz, J., Barnola, J.M., Raynaud, D., Korotkevich, Y.S., Lorius, C., 1990. Ice core record of atmospheric methane over the last 160,000 years. Nature. 345, 127–131.

Chappellaz, J., Blunier, T., Kints, S., Dällenbach, A., Barnola, J.-M., Schwander, J., Raynaud, D., Stauffer, B., 1997. Changes in the atmospheric CH_4 gradient between Greenland and Antarctica during the Holocene. J. Geophys. Res. 102 (D13), 15987–15997.

Charles, C.D., Rind, D., Jouzel, J., Koster, R.D., Fairbanks, R.G., 1994. Glacial-interglacial changes in moisture sources for Greenland: influences on the ice core record of climate. Science. 263, 508–511.

Charles, C.D., Cobb, K., Moore, M.D., Fairbanks, R.G., 2003. Monsoon-tropical ocean interaction in a network of coral records spanning the 20th century. Mar. Geol. 201, 207–222. dx.doi.org/10.1016/s0025-3227(03)00217-2.

Charman, D.J., 2001. Biostratigraphic and palaeoenvironmental applications of testate amoebae. Quat. Sci. Rev. 20, 1753–1764.

Charman, D.J., Barber, K.E., Blaauw, M., Langdon, P.G., Mauquoy, D., Daley, T.J., Hughes, P.D.M., Karofeld, E., 2009. Climate drivers for peatland palaeoclimate records. Quat. Sci. Rev. 28, 1811–1819.

Charney, J.G., Stone, P.H., Quirk, W.J., 1975. Drought in the Sahara: a biogeophysical feedback mechanism. Science. 187, 434–435.

Chase, B.M., Meadows, M.E., Scott, L., Thomas, D.S.G., Marais, E., Sealy, J., Reimer, P.J., 2009. A record of rapid Holocene climate change preserved in hyrax middens from southwestern Africa. Geology. 37, 703–706.

Chase, B.M., Quick, L.J., Meadows, M.E., Scott, L., Thomas, D.S., Reimer, P.J., 2011. Late glacial interhemispheric climate dynamics revealed in South African hyrax middens. Geology. 39, 19–22.

Chase, B.M., Scott, L., Meadows, M.E., Gil-Romera, G., Boom, A., Carr, A.S., Reimer, P.J., Truc, L., Valsecchi, V., Quick, L.J., 2012. Rock hyrax middens: a palaeoenvironmental archive for southern African drylands. Quat. Sci. Rev. 56, 107–125.

Chen, C., 1968. Pleistocene pteropods in pelagic sediments. Nature. 219, 1145–1147.

Chen, J., Farrell, J.W., Murray, D.W., Prell, W.L., 1995. Timescale and paleoceanographic implications of a 3.6 m.y. oxygen isotope record from the northeast Indian Ocean (Ocean Drilling Program site 758). Paleoceanography. 10, 21–47.

Cheng, H., Edwards, R.L., Wang, Y.J., Kong, X.G., Ming, Y.F., Kelly, M.J., Wang, X.F., Gallup, C.D., Liu, W.G., 2006. A penultimate glacial monsoon record from Hulu Cave and two-phase glacial terminations. Geology. 34, 217–220.

Cheng, H., Edwards, R.L., Broecker, W.S., Denton, G.H., Kong, X.G., Wang, Y.J., Zhang, R., Wang, X.F., 2009. Ice age terminations. Science. 326, 248–252.

Cheng, H., Edwards, R.L., Shen, C.C., Polyak, V.J., Asmerom, Y., Woodhead, J., Hellstrom, J., Wang, Y., Kong, X., Spötl, C., Wang, X., Alexander, E.C., 2012a. Improvements in ^{230}Th dating, ^{230}Th and ^{234}U half-life values, and U–Th isotopic measurements by multi-collector inductively coupled plasma mass spectroscopy. Earth Planet. Sci. Lett. 371–372, 82–91.

Cheng, H., Sinha, A., Wang, X.F., Cruz, F.W., Edwards, R.L., 2012b. The global paleomonsoon as seen through speleothem records from Asia and the Americas. Clim. Dyn. 39, 1045–1062. dx.doi.org/10.1007/s00382-012-1363-7.

Cheng, H., Zhang, P.Z., Spötl, C., Edwards, R.L., Cai, Y.J., Zhang, D.Z., Sang, W.C., Tan, M., An, Z.S., 2012c. The climatic cyclicity in semiarid-arid central Asia over the past 500,000 years. Geophys. Res. Lett. 39, L01705. dx.doi.org/10.1029/2011GL050202.

Chenoweth, M., 2003. The 18th Century Climate of Jamaica, Derived from the Journals of Thomas Thistlewood, 1750–1786. American Philosophical Society, Philadelphia, 153 pp.

Chester, R., Johnson, L.R., 1971. Atmospheric dusts collected off the Atlantic coasts of North Africa and the Iberian Peninsula. Mar. Geol. 11, 251–260.

Chiang, J.C.H., 2009. The Tropics in paleoclimate. Annu. Rev. Earth Planet. Sci. 37, 263–297.

Chiang, J.C.H., Friedman, A.R., 2012. Extratropical cooling, interhemispheric thermal gradients, and Tropical climate change. Annu. Rev. Earth Planet. Sci. 40, 383–412.
Chiang, J.C.M., Biasutti, M., Battisti, D.S., 2003. Sensitivity of the Atlantic Inter-Tropical Convergence Zone to Last Glacial Maximum boundary conditions. Paleoceanography. 18, 1094. dx.doi.org/10.1029/2003PA000916.
Chinn, T.J.H., 1981. Use of rock weathering-rind thickness for Holocene absolute age-dating in New Zealand. Arct. Alp. Res. 13, 33–45.
Chiu, T.-C., Fairbanks, R.G., Mortlock, R.A., Bloom, A.L., 2005. Extending the radiocarbon calibration beyond 26,000 years before present using fossil corals. Quat. Sci. Rev. 24, 1797–1808.
Chiu, T.-C., Fairbanks, R.G., Cao, L., Mortlock, R.A., 2007. Analysis of the atmospheric ^{14}C record spanning the past 50,000 years derived from high-precision $^{230}Th/^{234}U/^{238}U$, $^{231}Pa/^{235}U$ and ^{14}C dates on fossil corals. Quat. Sci. Rev. 26, 18–36.
Chiune, I., Yiou, P., Viovy, N., Seguin, B., Daux, V., Le Roy Ladurie, E., 2004. Grape ripening as a past climate indicator. Nature. 432, 289–290.
Chivas, A.R., De Decker, P., Cali, J.A., Chapman, A., Kiss, E., Shelley, J.M.G., 1993. Coupled stable-isotope and trace-element measurements of lacustrine carbonates as paleoclimatic indicators. In: Swart, P.K., Lohmann, K.C., McKenzie, J., Savon, S. (Eds.), Climate Change in Continental Isotopic Records. American Geophysical Union, Washington, DC, pp. 113–121.
Chu, K'o-chen, 1926. Climate pulsations during historical times in China. Geogr. Rev. 16, 274–282.
Chu, K'o-chen, 1973. A preliminary study on the climatic fluctuations during the last 5000 years in China. Sci. Sinica. 16, 226–256.
Chu, G.Q., Sun, Q., Li, S.Q., Zheng, M.P., Jia, X.X., Lu, C.F., Liu, J.Q., Liu, T.S., 2005. Longchain alkenone distributions and temperature dependence in lacustrine surface sediments from China. Geochim. Cosmochim. Acta. 69, 4985–5003.
Clague, J.J., Mathewes, R.W., 1989. Early Holocene thermal maximum in western North America: new evidence from Castle Peak, British Columbia. Geology. 17, 277–280.
Clapperton, C.M., 1990. Quaternary glaciations in the southern hemisphere: an overview. Quat. Sci. Rev. 9, 299–304 (plus chart).
Clapperton, C.M., 1993a. Quaternary Geology and Geomorphology of South America. Elsevier, Amsterdam.
Clapperton, C.M., 1993b. Nature of environmental changes in South America at the Last Glacial Maximum. Palaeogeogr. Palaeoclimatol. Palaeoecol. 101, 189–208.
Clark, D., 1975. Understanding Canonical Correlation Analysis. Concepts and Techniques in Modern Geography No. 3, University of East Anglia, Norwich.
Clark, P.U., Alley, R.B., Pollard, D., 1999. Northern hemisphere ice-sheet influences on global climate change. Science. 286, 1104–1111.
Clark, P.U., Pisias, N.G., Stocker, T.F., Weaver, A.J., 2002. The role of the thermohaline circulation in abrupt climate change. Nature. 415, 863–869.
Clark, P.U., Dyke, A.S., Shakun, J.D., Carlson, A.E., Clark, J., Wohlfarth, B., Mitrovica, J.X., Hostetler, S.W., McCabe, A.M., 2009. The Last Glacial Maximum. Science. 325, 710–714.
Clark, P.U., Shakun, J.D., Baker, P.A., Bartlein, P.J., Brewer, S., Brook, E., Carlson, A., Cheng, H., Kaufman, D.S., Liu, Z.Y., Marchitto, T.M., Mix, A.L., Morrill, C., Otto-Bliesner, B.L., Pahnke, K., Russell, J.M., Whitlock, C., Adkins, J.F., Blois, J.L., Clark, J., Colman, S.M., Curry, W.B., Flower, B.P., He, F., Johnson, T.C., Lynch-Stieglitz, J., Markgraf, V., McManus, J., Mitrovica, J.X., Moreno, P.I., Williams, J.W., 2012. Global climate evolution during the last deglaciation. Proc. Natl. Acad. Sci. U. S. A. 109, E1134–E1142.
Clarke, M.L., Wintle, A.G., Lancaster, N., 1996. Infra-red stimulated luminescence dating of sands from the Cronese Basins, Mojave Desert. Geomorphology. 17, 199–205.
Claude, C., Hamelin, B., 2007. Isotopic tracers of water masses and deep currents. In: Hillaire-Marcel, C., de Vernal, A. (Eds.), Proxies in Late Cenozoic Paleoceanography. Elsevier, Amsterdam, pp. 645–679.
Clausen, H.B., Hammer, C.U., 1988. The Laki and Tambora eruptions as revealed in Greenland ice cores from 11 locations. Ann. Glaciol. 10, 16–22.
Claussen, M., 2009. Late Quaternary vegetation-climate feedbacks. Clim. Past. 5, 203–216.
Cleaveland, M.K., Duvick, D.N., 1992. Iowa climate reconstructed from tree-rings, 1640-1982. Water Resour. Res. 28, 2607–2615.

Clement, A.C., Peterson, L.C., 2008. Mechanisms of abrupt climate change of the last glacial period. Rev. Geophys. 46. dx.doi.org/10.1029/RG000204.
CLIMAP Project Members, 1976. The surface of the ice-age Earth. Science. 191, 1131–1144.
CLIMAP Project Members, 1981. Seasonal reconstructions of the Earth's surface at the last glacial maximum. Geol. Soc. Am. Map Chart Ser. MC-36, .
CLIMAP Project Members, 1984. The last interglacial ocean. Quat. Res. 21, 123–224.
Coale, K.H., Johnson, K.S., Fitzwater, S.E., Gordon, R.M., Tanner, S., Chavez, F.P., Ferioli, L., Sakamoto, C., Rogers, P., Millero, F., Steinberg, P., Nightingale, P., Cooper, D., Cochlan, W.P., Landry, M.R., Constantinou, J., Rollwagen, G., Trasvina, A., Kudela, R., 1996. A massive phytoplankton bloom induced by an ecosystem-scale iron fertilization experiment in the equatorial Pacific Ocean. Nature. 383, 495–501.
Cobb, K.M., Charles, C.D., Cheng, H., Edwards, R.L., 2003. El Niño/Southern Oscillation and tropical Pacific climate during the last millennium. Nature. 424, 271–276.
Cobb, K.M., Westphal, N., Sayani, H.R., Watson, J.T., Di Lorenzo, E., Cheng, H., Edwards, R.L., Charles, C.D., 2013. Highly variable El Niño-Southern Oscillation throughout the Holocene. Science. 339, 67–70.
Coe, R.S., Liddicoat, J.C., 1994. Overprinting of natural magnetic remanance in lake sediments by a subsequent high-intensity field. Nature. 367, 57–59.
Cohen, A.S., 2003. Paleolimnology: The History and Evolution of Lake Systems. Oxford University Press, Oxford, 500 pp.
COHMAP Members, 1988. Climatic changes of the last 18,000 years: observations and model simulations. Science. 241, 1043–1052.
Cole, K.L., 1990. Late Quaternary vegetation gradients through the Grand Canyon. In: Betancourt, J.L., Van Devender, T.T., Martin, P.S. (Eds.), Packrat Middens: The Last 40,000 Years of Biotic Change. University of Arizona Press, Tucson, pp. 240–258.
Cole, J.E., Cook, E.R., 1998. The changing relationship between ENSO variability and moisture balance in the continental United States. Geophys. Res. Lett. 25, 4529–4532.
Cole, J.E., Fairbanks, R.G., 1990. The Southern Oscillation recorded in the oxygen isotopes of corals from Tarawa Atoll. Paleoceanography. 5, 669–683.
Cole, J.E., Shen, G.T., Fairbanks, R.G., Moore, M., 1992. Coral monitors of El Niño/Southern Oscillation dynamics across the equatorial Pacific. In: Diaz, H.F., Markgraf, V.K. (Eds.), El Niño: Historical and Paleoclimatic Aspects of the Southern Oscilllation. Cambridge University Press, Cambridge, pp. 349–376.
Cole, J.E., Fairbanks, R.G., Shen, G.T., 1993. Recent variability in the Southern Oscillation: isotopic results from a Tarawa atoll coral. Science. 260, 1790–1793.
Cole, J.E., Overpeck, J.T., Cook, E.R., 2002. Multiyear La Niña events and persistent drought in the contiguous United States. Geophys. Res. Lett. 29, 1647. http://dx.doi.org/10.1029/2001GL013561.
Cole-Dai, J., Thompson, L.G., Mosley-Thompson, E., 1995. A 485 year record of at mospheric chloride, nitrate and sulfate: results of chemical analysis of ice cores from Dyer Plateau, Antarctic Peninsula. Ann. Glaciol. 21, 182–188.
Colin, C., Frank, N., Copard, K., Douville, E., 2010. Neodymium isotopic composition of deep-sea corals from the NE Atlantic: implications for past hydrological changes during the Holocene. Quat. Sci. Rev. 29, 2509–2517.
Colinvaux, P.A., 1996. Quaternary environmental history and forest diversity in the Neotropics. In: Jackson, J., Coates, A. (Eds.), Environmental and Biological Change in Neogene and Quaternary Tropical America. Chicago University Press, Chicago.
Colinvaux, P.A., 2007. Amazon Expeditions: My Quest for the Ice-Age Equator. Yale University Press, New Haven, 328 pp.
Colinvaux, P.A., De Oliveira, P.E., Moreno, J.E., Miller, M.C., Bush, M.B., 1996a. A long pollen record from lowland Amazonia: forest and cooling in Glacial times. Science. 274, 85–88.
Colinvaux, P.A., Liu, K.-B., De Oliveira, P., Bush, M.B., Miller, M.C., Steinitz-Kannon, M., 1996b. Temperature depression in the lowland Tropics in Glacial time. Clim. Chang. 32, 19–33.
Colman, S.M., Dethier, D.P. (Eds.), 1986. Rates of Chemical Weathering of Rocks and Minerals. Academic Press, Orlando.
Colman, S.M., Pierce, K.L., 1981. Weathering rinds on andesitic and basaltic stones as a Quaternary age indicator, western United States. U.S. Geological Survey Prof. Paper 1210.
Colman, S.M., Pierce, K.L., Birkeland, P.W., 1987. Suggested terminology for Quaternary dating methods. Quat. Res. 28, 314–319.

Colman, S.M., Peck, J.A., Karabanov, E.B., Carter, S.J., Bradbury, J.P., King, J.W., Williams, D.F., 1995. Continental climate response to orbital forcing from biogenic silica records in Lake Baikal. Nature. 378, 769–771.

Condomes, M., Moraud, P., Camus, G., Duthon, L., 1982. Chronological and geochemical study of lavas from the Chaine des Puys, Massif Central, France: evidence for crustal contamination. Contrib. Mineral. Petrol. 81, 296–303.

Condron, A., Winsor, P., 2011. A subtropical fate awaited freshwater discharged from glacial Lake Agassiz. Geophys. Res. Lett. 38, L03705. dx.doi.org/10.1029/2010GL046011.

Condron, A., Winsor, P., 2012. Meltwater routing and its ability to trigger the Younger Dryas. Proc. Natl. Acad. Sci. U. S. A. 109, 19928–19933.

Conley, D.J., Schelske, C.L., 2001. Biogenic silica. In: Smol, J.P., Birks, H.J.B., Last, W.M. (Eds.), Tracking Environmental Change Using Lake sediments, vol. 3. Kluwer Academic, Dordrecht, pp. 281–293.

Conte, M.H., Sicre, M.-A., Rühlemann, C., Weber, J.C., Schulte, S., Schulz-Bull, D., Blanz, T., 2006. Global temperature calibration of the alkenone unsaturation index (Uk'37) in surface waters and comparison with surface sediments. Geochem. Geophys. Geosyst. 7. dx.doi.org/10.1029/2005GC001054.

Cook, E.R., Jacoby, G.C., 1979. Evidence for the quasi-periodical July drought in the Hudson Valley, New York. Nature. 282, 390–392.

Cook, E.R., Kairiukstis, L.A. (Eds.), 1990. Methods of Dendrochronology. Kluwer, Dordrecht, 394 pp.

Cook, E.R., Krusic, P.J., 2004. North American summer PDSI reconstructions. In: IGBP PAGES/World Data Center for Paleoclimatology Data Contribution Series No. 2004-045, NOAA/NGDC Paleoclimatology Program, Boulder, CO, 24 pp.

Cook, E.R., Peters, K., 1981. The smoothing spline: a new approach to standardizing forest-interior tree-ring width series for denroclimatic studies. Tree Ring Bull. 41, 45–53.

Cook, E.R., Briffa, K., Shiyatov, S., Mazepa, V., 1990. Tree-ring standardization and growth-trend estimation. In: Cook, E.R., Kariukstis, L.A. (Eds.), Methods of Dendrochronology: Applications in the Environmental Sciences. Kluwer, Dordrecht, pp. 104–123.

Cook, E.R., Bird, T., Peterson, M., Barbetti, M., Buckley, B.M., D'Arrigo, R., Francey, R., 1992. Climatic change over the last millennium in Tasmania reconstructed from tree rings. The Holocene. 2, 205–217.

Cook, E.R., Stahle, D.W., Cleaveland, M.K., 1992a. Dendroclimatic evidence from eastern North America. In: Bradley, R.S., Jones, P.D. (Eds.), Climate Since A.D. 1500. Routledge, London, pp. 331–348.

Cook, E.R., Briffa, K.R., Jones, P.D., 1994. Spatial regression methods in dendroclimatology: a review and comparison of two techniques. Int. J. Climatol. 14, 379–402.

Cook, E.R., Briffa, K.R., Meko, D.M., Graybill, D.A., Funkhauser, G., 1995. The 'segment length curse' in long tree-ring chronology development for paleoclimatic studies. The Holocene. 5, 229–237.

Cook, E.R., Meko, D.M., Stahle, D.W., Cleaveland, M.K., 1996. Tree-ring reconstructions of past drought across the coterminous United States: tests of a regression method and calibration/verification results. In: Dean, J.S., Meko, D.M., Swetnam, T.W. (Eds.), Tree Rings, Environment and Humanity. Radiocarbon, University of Arizona, Tucson, pp. 1–24.

Cook, E.R., Meko, D.M., Stahle, D.W., Cleaveland, M.K., 1999. Drought reconstructions for the continental United States. J. Clim. 12, 1145–1162.

Cook, E.R., D'Arrigo, R.D., Cole, J.E., Stahle, D.W., Villalba, R., 2000. Tree-ring records of past ENSO variability and forcing. In: Diaz, H.F., Markgraf, V. (Eds.), El Niño and the Southern Oscillation: multiscale variability and global and regional impacts. Cambridge University Press, Cambridge, pp. 297–323.

Cook, E.R., D'Arrigo, R.D., Mann, M.E., 2002. A well-verified, multiproxy reconstruction of the North Atlantic Oscillation since A.D. 1400. J. Clim. 15, 1754–1764.

Cook, E.R., Esper, J., D'Arrigo, R., 2004a. Extra-tropical northern hemisphere land temperature variability over the past 1000 years. Quat. Sci. Rev. 23, 2063–2074.

Cook, E.R., Woodhouse, C.A., Eakin, C.M., Meko, D.M., Stahle, D.W., 2004b. Long-term aridity changes in the western United States. Science. 306, 1015–1018.

Cook, E.R., Seager, R., Cane, M.A., Stahle, D.W., 2007. North American drought: reconstructions, causes and consequences. Earth-Sci. Rev. 81, 93–134.

Cook, E.R., Seager, R., Heim, R.R., Vose, R.S., Herweijer, C., Woodhouse, C., 2010a. Megadroughts in North America: placing IPCC projections of hydroclimatic change in a long-term palaeoclimate context. J. Quat. Sci. 25, 48–61.

Cook, E.R., Anchukaitis, K., Buckley, B.M., D'Arrigo, R.D., Jacoby, G.C., Wright, W.E., 2010b. Asian monsoon failure and megadrought during the last millennium. Science. 328, 486–489.

Cook, B.I., Cook, E.R., Anchukaitis, K., Seager, R., Miller, R.L., 2011. Forced and unforced variability of twentieth century North American droughts and pluvials. Clim. Dyn. 37, 1097–1110.
Cooke, R.U., Warren, A., 1977. Geomorphology in Deserts. University of California Press, Berkeley.
Coope, G.R., 1959. A late Pleistocene insect fauna from Chelford, Cheshire. Proc. R. Soc. Lond. B. 151, 70–86.
Coope, G.R., 1967. The value of Quaternary insect faunas in the interpretation of ancient ecology and climate. In: Cushing, E.J., Wright, H.E. (Eds.), Quaternary Paleoecology. Yale University Press, New Haven, pp. 359–380.
Coope, G.R., 1974. Interglacial coleoptera from Bobbitshole, Ipswich. J. Geol. Soc. Lond. 130, 333–340.
Coope, G.R., 1975a. Climatic fluctuations in north-west Europe since the last Interglacial, indicated by fossil assemblages of coleoptera. In: Wright, A.E., Moseley, F. (Eds.), Ice Ages Ancient and Modern. Geological Journal Special Issue No. 6, Liverpool University Press, Liverpool, pp. 153–168.
Coope, G.R., 1975b. Mid-Weichselian climatic changes in western Europe, reinterpreted from coleopteran assemblages. Bull. R. Soc. N. Z. 13, 101–110.
Coope, G.R., 1977a. Quaternary coleoptera as aids in the interpretation of environmental history. In: Shotton, F.W. (Ed.), British Quaternary Studies. Clarendon Press, Oxford, pp. 55–68.
Coope, G.R., 1977b. Fossil coleopteran assemblages as sensitive indicators of climatic changes during the Devensian (Last) cold stage. Proc. R. Soc. Lond. B. 280, 313–337.
Coope, G.R., 1986. Coleoptera analysis. In: Berglund, B.E. (Ed.), Handbook of Holocene Palaeoecology and Palaeohydrology. Wiley, New York, pp. 703–713.
Coope, G.R., 1994. The response of insect faunas to glacial-interglacial climatic fluctuations. Philos. Trans. R. Soc. Lond. 344B, 19–26.
Coope, G.R., Brophy, J.A., 1972. Late glacial environmental changes indicated by a coleopteran succession from North Wales. Boreas. 1, 97–142.
Coope, G.R., Pennington, W., 1977. The Windermere interstadial of the late Devensian. Philos. Trans. R. Soc. Lond. B208, 337–339.
Cooper, T.F., De'ath, G., Fabricius, K.E., Lough, J.M., 2008. Declining coral calcification in massive *Porites* in two nearshore regions of the northern Great Barrier Reef. Glob. Chang. Biol. 14, 529–538.
Copard, K., Colin, C., Henderson, G.M., Scholten, J., Douville, E., Sicre, M.-A., Frank, N., 2012. Late Holocene intermediate water variability in the northeastern Atlantic as recorded by deep-sea corals. Earth Planet. Sci. Lett. 313–314, 34–44.
Coplen, T.B., 1996. More uncertainty than necessary. Paleoceanography. 11, 369–370.
Correa-Metrio, A., Bush, M.B., Pérez, L., Schwalb, A., Cabrera, K.R., 2011. Pollen distribution along climatic and biogeographic radients in northern Central America. The Holocene. 21, 681–692.
Correa-Metrio, A., Bush, M.B., Cabrerea, K.R., Sully, S., Brenner, M., Hodell, D.A., Escobar, J., Guilderson, T., 2012a. Rapid climate change and no-analog vegetation in lowland Central America during the last 86,000 years. Quat. Sci. Rev. 38, 63–75.
Correa-Metrio, A., Bush, M.B., Hodell, D.A., Brenner, M., Escobar, J., Guilderson, T., 2012b. The influence of abrupt climate change on the ice-age vegetation of the Central American lowlands. J. Biogeogr. 39, 497–509.
Corrège, T., 2006. Sea surface temnperature and salinity reconstructions from coral geochemical tracers. Palaeogeogr. Palaeoclimatol. Palaeoecol. 232, 408–428.
Corrège, T., Delcroix, T., Récy, J., Beck, W., Cabioch, G., Le Cornec, F., 2000. Evidence for stronger El Niño-Southern Oscillation (ENSO) events in a mid-Holocene massive coral. Paleoceanography. 15, 465–470.
Cosford, J., Qing, H.R., Eglington, B., Mattey, D., Yuan, D.X., Zhang, M.L., Chang, H., 2008. East Asian monsoon variability since the mid-Holocene recorded in a high-resolution absolute-dated aragonite speleothem from eastern China. Earth Planet. Sci. Lett. 275, 296–307.
Coulter, S.E., Pilcher, J.R., Plunkett, G., Baillie, M., Hall, V.A., Steffensen, J.P., Vinther, B.M., Clausen, H.B., Johnsen, S.J., 2012. Holocene tephras highlight complexity of volcanic signals in Greenland ice cores. J. Geophys. Res. 117, D21303. dx.doi.org/10.1029/2012JD017698.
Cox, A., 1969. Geomagnetic reversals. Science. 163, 237–245.
Craig, H., 1953. The geochemistry of the stable carbon isotopes. Geochim. Cosmochim. Acta. 3, 53–92.
Craig, H., 1957. Isotopic standards for carbon and oxygen and correction factors for mass spectrometric analysis of CO_2. Geochim. Cosmochim. Acta. 12, 133–149.
Craig, H., 1961a. Mass spectrometer analysis of radiocarbon standards. Radiocarbon. 3, 1–3.

Craig, H., 1961b. Standard for reporting concentrations of deuterium and oxygen-18 in natural waters. Science. 133, 1833–1834.
Craig, H., 1961c. Isotopic variations in meteoric waters. Science. 133, 1702–1703.
Craig, H., 1965. The measurement of oxygen isotope paleotemperature. In: Proceedings of the Spoleto Conference on Stable Isotopes in Oceanographic Studies and Paleotemperatures. Consiglio Nazionale delle Ricerche Laboratorio di Geologia Nucleare, Pisa, pp. 3–24.
Cramer, W., 1997. Using plant functional types in a global vegetation model. In: Woodward, F.I. (Ed.), Plant Functional Types: Their Relevance to Ecosystem Properties and Global Change. Cambridge University Press, Cambridge, pp. 271–288.
Croll, J., 1867a. On the eccentricity of the Earth's orbit and its physical relations to the glacial epoch. Philos. Mag. 33, 119–131.
Croll, J., 1867b. On the change in the obliquity of the ecliptic, its influence on the climate of the polar regions and on the level of the sea. Philos. Mag. 33, 426–445.
Croll, J., 1875. Climate and Time. Appleton and Co., New York.
Cronin, T.M., 2009. Paleoclimates. Columbia University Press, New York, 441 pp.
Crosta, X., Koç, N., 2007. Diatoms: from micropaleontology to isotope geochemistry. In: Hillaire-Marcel, C., de Vernal, A. (Eds.), Proxies in Late Cenozoic Paleoceanography. Elsevier, Amsterdam, pp. 327–370.
Crowley, T.J., 1994. Pleistocene temperature changes. Nature. 371, 664.
Crowley, T.J., 2000. Causes of climate change over the past 1000 years. Science. 289, 270–277.
Crowley, T.J., Kim, K.-Y., 1999. Modeling the temperature response to forced climate change over the last six centuries. Geophys. Res. Lett. 26, 1901–1904.
Crowley, T.J., Lowery, T., 2000. How warm was the Medieval Warm Period? A comment on "man-made versus natural climate change" Ambio. 29, 51–54.
Crozaz, G., Picciotto, E., De Breuck, W., 1964. Antarctic snow chronology with Pb-210. J. Geophys. Res. 69, 2597–2604.
Crozaz, G., Langway Jr., C.C., Picciotto, E., 1966. Artificial radioactivity reference horizons in Greenland firn. Earth Planet. Sci. Lett. 1, 42–48.
Crucifix, M., 2006. Does the Last Glacial Maximum constrain climate sensitivity? Geophys. Res. Lett. 33, L18701dx.doi.org/10.1029/2006GL027137.
Crucifix, M., Loutre, F.M., Berger, A., 2006. The climate response to the astronomical forcing. Space Sci. Rev. 125, 213–226.
Crutzen, P.J., 2002. The geology of mankind. Nature. 415, 23.
Crutzen, P.J., Steffen, W., 2003. How long have we been in the Anthropocene Era? Clim. Chang. 61, 251–257.
Cruz Jr., F.W., Karmann, I., Viana Jr., O., Burns, S.J., Ferrari, J.A., Vuille, M., Sial, A.N., Moreira, M.Z., 2005a. Stable isotope study of cave percolation waters in subtropical Brazil: implications for paleoclimate inferences from speleothems. Chem. Geol. 220, 245–262.
Cruz Jr., F.W., Burns, S.J., Karmann, I., Sharp, W., Vuille, M., Cardoso, A.O., Ferrari, J.A., Silva Dias, P.L., Viana Jr., O., 2005b. Insolation-driven changes in atmospheric circulation over the past 116,000 years in subtropical Brazil. Nature. 434, 63–66.
Cuffey, K.M., Paterson, W.S.B., 2010. The Physics of Glaciers. Elsevier, Amsterdam, 693 pp.
Cuffey, K.M., Alley, R.B., Grootes, P.M., Bolzan, J.M., Anandakrishnan, S., 1994. Calibration of the $\delta^{18}O$ isotopic paleothermometer for central Greenland, using borehole temperatures. J. Glaciol. 40, 341–350.
Cuffey, K.M., Clow, G.D., Alley, R.B., Stuiver, M., Waddington, E.D., Saltus, R.W., 1995. Large Arctic temperature change at the Wisconsin-Holocene transition. Science. 270, 455–458.
Cunningham, J., Waddington, E.D., 1990. Boudinage: a source of stratigraphic disturbance in glacial ice in central Greenland. J. Glaciol. 36, 269–272.
Curry, R.R., 1969. Holocene climatic and glacial history of the Sierra Nevada, California. Geol. Soc. Am. Spec. Pap. 123, 1–47.
Curry, W.B., Duplessy, J.-C., Labeyrie, L.D., Shackleton, N.J., 1988. Quaternary deep water circulation changes in the distribution of $\delta^{13}C$ of Deep water: ΣCO_2 between the last glaciation and the Holocene. Paleoceanography. 3, 317–342.
Curtis, G.H., 1975. Improvements in potassium-argon dating, 1962-1975. World Archaeol. 7, 198–207.
Curtis, J.H., Hodell, D.A., Brenner, M., 1996. Climate variability on the Yucatan Peninsula (Mexico) during the past 3500 years, and implications for Maya cultural evolution. Quat. Res. 46, 37–47.

Cushing, E.J., 1967. Evidence for differential pollen preservation in late Quaternary sediments in Minnesota. Rev. Palaeobot. Palynol. 4, 87–101.
Cutler, K.B., Edwards, R.L., Taylor, F.W., Cheng, H., Adkins, J., Gallup, C.D., Cutler, P.M., Burr, G.S., Bloom, A.L., 2003. Rapid sea-level fall and deep-ocean temperature change since the last interglacial period. Earth Planet. Sci. Lett. 206, 253–271.
Cwynar, L.C., Levesque, A.J., 1995. Chironomid evidence for late-glacial climatic reversals in Maine. Quat. Res. 43, 405–413.
D'Andrea, W.J., Huang, Y., Fritz, S.C., Anderson, N.J., 2011. Abrupt Holocene climate change as an important factor for human migration in West Greenland. Proc. Natl. Acad. Sci. U. S. A. 108, 9765–9769.
D'Arrigo, R.D., Jacoby, G.C., Free, R.M., 1992. Tree-ring width and maximum late wood density at the North American treeline: parameters of climatic change. Can. J. For. Res. 22, 1290–1296.
D'Arrigo, R.D., Jacoby, G.C., Krusic, P.J., 1994. Progress in dendroclimatic studies in Indonesia. Terr. Atmos. Ocean. Sci. 5, 349–363.
D'Arrigo, R.D., Villalba, R., Wiles, G., 2001. Tree-ring estimates of Pacific decadal climate variability. Clim. Dyn. 18, 219–224.
D'Arrigo, R., Kaufmann, R., Davi, N., Jacoby, G., Laskowski, C., Myneni, R., Cherubini, P., 2004. Thresholds for warming-induced growth decline at elevational treeline in the Yukon Territory, Canada. Glob. Biogeochem. Cycles. 18, GB3021. dx.doi.org/10.1029/2004GB002249.
D'Arrigo, R., Cook, E.R., Wilson, R.J., Allan, R., Mann, M.E., 2005. On the variability of ENSO over the past six centuries. Geophys. Res. Lett. 32, L03711.
D'Arrigo, R., Wilson, R., Palmer, J., Krusic, P., Curtis, A., Sakulich, J., Bijaksana, S., Ngkoimani, L.O., 2006a. Monsoon drought over Java, Indonesia, during the past two centuries. Geophys. Res. Lett. 33, L04709. dx.doi.org/10.1029/2005GL025465.
D'Arrigo, R.D., Wilson, R., Palmer, J., Krusic, P., Curtis, A., Sakulich, J., Bijaksana, S., Zulaikah, S., Ngkoimani, L.O., Tudhope, A., 2006b. The reconstructed Indonesian warm pool sea surface temperatures from tree-rings and corals: linkages to Asian monsoon drought and El Niño-Southern Oscillation. Paleoceanography. 21. dx.doi.org/10.1029/2005PA001256.
D'Arrigo, R., Wilson, R., Liepert, B., Cherubini, P., 2008. On the "Divergence Problem" in northern forests: a review of the tree-ring evidence and possible causes. Glob. Planet. Chang. 60, 289–305.
D'Arrigo, R., Jacoby, G., Buckley, B., Sakulich, J., Frank, D., Wilson, R., Curtis, A., Anchukaitis, K., 2009. Tree growth and inferred temperature variability at the North American treeline. Glob. Planet. Chang. 65, 71–82.
Dahl, S.O., Nesje, A., 1996. A new approach to calculating Holocene winter precipitation by combining glacier equilibrium line altitudes and pine-tree limits: a case study from Hardangerjokulen, central south Norway. The Holocene. 6, 381–398.
Dahl-Jensen, D., Johnsen, S.J., Hammer, C.U., Clausen, H.B., Jouzel, J., 1993. Past accumulation rates derived from observed annual layers in the GRIP ice core from Summit, Greenland. In: Peltier, W. (Ed.), Ice in the Climate System, Springer-Verlag, Berlin, pp. 517–532.
Dahl-Jensen, D., Mosegaard, K., Gundestrup, N., Clow, G.D., Johnsen, S.J., Hansen, A.W., Balling, N., 1998. Past temperatures directly from the Greenland Ice Sheet. Science. 282, 269–291.
Dai, A., Trenberth, K.E., Qian, T., 2004. A global data set of Palmer Drought Severity index for 1870-2002: relationship with soil moisture and effects of global warming. J. Hydrometeorol. 5, 1117–1130.
Dalfes, H.N., Kukla, G., Weiss, H. (Eds.), 1997. Third Millennium B.C. Climate Change and Old World Collapse. Springer, Berlin, 728 pp.
Dalrymple, G.B., Lanphere, M.A., 1969. Potassium-Argon Dating: Principles, Techniques and Applications to Geochronology. W.H. Freeman, San Francisco.
Damon, P.E., 1970. Radiocarbon as an example of the unity of science. In: Olsson, I.U. (Ed.), Radiocarbon Variations and Absolute Chronology. Wiley, New York, pp. 641–644.
Damon, P.E., Lerman, J.C., Long, A., 1978. Temporal fluctuations of atmospheric ^{14}C: causal factors and implications. Annu. Rev. Earth Planet. Sci. 6, 457–494.
Dansgaard, W., 1961. The isotopic composition of natural waters with special reference to the Greenland Ice Cap. Meddelelser øm Gronland. 165, 1–120.
Dansgaard, W., 1964. Stable isotopes in precipitation. Tellus. 16, 436–468.
Dansgaard, W., 2004. Frozen Annals: Greenland Ice Sheet Research. Aage V. Jenkins Fonde, Copenhagen, 122 pp.

Dansgaard, W., Johnsen, S.J., 1969. A flow model and a time scale for the ice core from Camp Century. J. Glaciol. 8, 215–223.
Dansgaard, W., Tauber, H., 1969. Glacier oxygen-18 content and Pleistocene ocean temperatures. Science. 166, 499–502.
Dansgaard, W., Johnsen, S.J., Moller, J., Langway Jr., C.C., 1969. One thousand centuries of climatic record from Camp Century on the Greenland ice sheet. Science. 166, 377–381.
Dansgaard, W., Johnsen, S.J., Clausen, H.B., Langway, C.C., 1971. Climatic record revealed by the Camp Century ice core. In: Turekian, K.K. (Ed.), The Late Cenozoic Ice Ages. Yale University Press, New Haven, pp. 37–56.
Dansgaard, W., Johnsen, S.J., Clausen, H.B., Gundestrup, N., 1973. Stable isotope glaciology. Meddelelser øm Gronland. 197, 1–53.
Dansgaard, W., Clausen, H.B., Gundestrup, N., Hammer, C.U., Johnsen, S.F., Kristinsdottir, P.M., Reeh, N., 1982. A new Greenland deep ice core. Science. 218, 1273–1277.
Dansgaard, W., Johnsen, S.J., Clausen, H.B., Dahl-Jensen, D., Gundestrup, N., Hammer, C.U., Oeschger, H., 1984. North Atlantic climatic oscillations revealed by deep Greenland ice cores. In: Hansen, J.E., Takahashi, T. (Eds.), Climate Processes and Climate Sensitivity. American Geophysical Union, Washington, DC, pp. 288–298.
Dansgaard, W., Johnsen, S.J., Clausen, H.B., Dahl-Jensen, D., Gundestrup, N.S., Hammer, C.U., Hvidberg, C.S., Steffensen, J.P., Sveinbjornsdottir, A.E., Jouzel, J., Bond, G., 1993. Evidence for general instability of past climate from a 250-kyr ice-core record. Nature. 364, 218–220.
Darling, W.G., 2004. Hydrological factors in the interpretation of stable isotope proxy data present and past: a European perspective. Quat. Sci. Rev. 23, 743–770.
Darling, W.G., Bath, A.H., Gibson, J.J., Rozanski, K., 2006. Isotopes in water. In: Leng, M.J. (Ed.), Isotopes in Palaeoenvironmental Research. Springer, Dordrecht, pp. 1–66.
Dassié, E.P., Lemlety, G.M., Linsley, B.K., 2013. The Suess effect in Fiji coral $\delta^{13}C$ and its potential as a tracer of anthropogenic CO_2 uptake. Palaeogeogr. Palaeoclimatol. Palaeoecol. 370, 30–40.
Daultrey, S., 1976. In: Principal Components Analysis. Concepts and Techniques in Modern Geography No. 8, University of East Anglia, Norwich.
Davies, S.M., Wastegard, S., Abbott, P.M., Barbante, C., Bigler, M., Johnsen, S.J., Rasmussen, T.L., Steffensen, J.P., Svensson, A., 2010. Tracing volcanic events in the NGRIP ice-core and synchronising North Atlantic marine records during the last glacial period. Earth Planet. Sci. Lett. 294, 69–79.
Davis, M.B., 1963. On the theory of pollen analysis. Am. J. Sci. 261, 899–912.
Davis, M.B., 1973. Redeposition of pollen grains in lake sediment. Limnol. Oceanogr. 18, 44–52.
Davis, R.B., 1974. Stratigraphic effects of tubificids in profundallake sediments. Limnol. Oceanogr. 19, 466–488.
Davis, M.B., 1991. Research questions posed by the paleoecological record of global change. In: Bradley, R.S. (Ed.), Global Changes of the Past. University Corporation for Atmospheric Research, Boulder, pp. 385–396.
Davis, M.B., Botkin, D.B., 1985. Sensitivity of cool-temperate forests and their fossil pollen record to rapid temperature change. Quat. Res. 23, 327–340.
Davis, R.B., Webb III, T., 1975. The contemporary distribution of pollen in eastern North America: a comparison with the vegetation. Quat. Res. 5, 395–434.
Davis, M.B., Brubaker, L.B., Webb III, T., 1973. Calibration of absolute pollen influx. In: Birks, H.J.B., West, R.G. (Eds.), Quaternary Plant Ecology. Blackwell Scientific Publications, Oxford, pp. 9–25.
Davis, M.B., Woods, K.D., Webb, S.L., Futyua, R.B., 1986. Dispersal versus climate: expansion of *Fagus* and *Tsuga* into the upper Great Lakes region. Vegetatio. 69, 93–103.
Davis, P.T., Menounos, B., Osborn, G., 2009. Holocene and latest Pleistocene alpine glacier fluctuations. Quat. Sci. Rev. 28, 2021–2033.
Dean, J.S., Meko, D.M., Swetnam, T.W. (Eds.), 1996. Tree Rings, Environment and Humanity. Radiocarbon, University of Arizona, Tucson 889 pp.
Dean, J.M., Kemp, A.E.S., Bull, D., Pike, J., Patterson, G., Zolitschka, B., 1999. Taking varves to bits: scanning electron microscopy in the study of laminated sediments and varves. J. Paleolimnol. 22, 121–136.
Dean, W., Anderson, R., Bradbury, J.P., Anderson, D., 2002. A 1500-year record of climatic and environmental change in Elk Lake, Minnesota I: varve thickness and gray-scale density. J. Paleolimnol. 27, 287–299.
De'Ath, G., Lough, J.M., Fabricius, K.E., 2009. Declining coral calcification on the Great Barrier Reef. Science. 323, 116–119.
de Beaulieu, J., Reille, M., 1992. The last climatic cycle at La Grande Pile (Vosges, France). A new pollen profile. Quat. Sci. Rev. 11, 431–438.

DeConto, R.M., Pollard, D., Wilson, P.A., Pälike, H., Leare, C.H., Pagani, M., 2008. Thresholds for Cenozoic bipolar glaciation. Nature. 455, 652–657.
Deevey, E.S., Flint, R.F., 1957. Postglacial Hypsithermal interval. Science. 125, 1824.
Defant, A., 1961. Physical Oceanography, vol. 1. Pergamon/Macmillan, New York.
de Jong, A.F.M., Mook, W.G., Becker, B., 1980. Confirmation of the Suess wiggles, 3200-3700 BP. Nature. 280, 48–49.
Delano Smith, C., Parry, M. (Eds.), 1981. Consequences of Climatic Change. Department of Geography, University of Nottingham, Nottingham.
Delcourt, P.A., Delcourt, H.R., Webb, I.I.I.T., 1984. In: Atlas of mapped distributions of dominance and modern pollen percentages for important tree taxa of Eastern North America. Contribution Series 14, American Association of Stratigraphy Palynologists, Dallas.
Delmas, R.J., 1992. Environmental information from ice cores. Rev. Geophys. 30, 1–21.
Delmas, R.J., Petit, J.R., 1994. Present Antarctic aerosol composition: a memory of ice age atmospheric dust. Geophys. Res. Lett. 21, 879–882.
Delmas, R.J., Legrand, M., Aristarain, A.J., Zanolini, F., 1985. Volcanic deposits in Antarctic snow and ice. J. Geophys. Res. 90D, 12901–12920.
Delmas, R.J., Kirchner, S., Palais, J.M., Petit, J.R., 1992. 1000 years of explosive volcanism recorded at the South Pole. Tellus. 44B, 335–350.
Delmonte, B., Andersson, P.S., Hansson, M., Schoberg, H., Petit, J.R., Basile-Doelsch, I., Maggi, V., 2008. Aeolian dust in East Antarctica (EPICA-Dome C and Vostok): provenance during glacial ages over the last 800 kyr. Geophys. Res. Lett. 35, L07703. dx.doi.org/10.1029/2008GL033382.
DeLong, K.L., Quinn, T.M., Shen, C.-C., Lin, K., 2010. A snapshot of climate variability at Tahiti 9.5 ka using a fossil coral from IODP expedition 310. Geochem. Geophys. Geosyst. 11, Q06005. http://dx.doi.org/10.1029/2009GC002758.
DeLong, K.L., Quinn, T.M., Taylor, F.W., Lin, K., Shen, C.C., 2012. Sea surface temperature variability in the southwest tropical Pacific since AD 1649. Nat. Clim. Chang. 2, 799–804.
DeLong, K.L., Quinn, T.M., Taylor, F.W., Shen, C.C., Lin, K., 2013. Improving coral-based paleoclimate reconstructions by replicating 350 years of coral Sr/Ca variations. Palaeogeogr. Palaeoclimatol. Palaeoecol. 373, 6–24.
Demarée, G.R., Ogilvie, A.E.J., 2001. *Bons Baisers d'Islande*: climatic, environmental and human dimensions impacts of the Lakagígar eruption (1873-1784) in Iceland. In: Jones, P.D., Ogilvie, A.E.G., Davies, T.D., Briffa, K.R. (Eds.), History and Climate: Memories of the Future?. Kluwer, New York, pp. 219–246.
de Martonne, E., Aufrere, L., 1928. L'extension des regions privées d'écoulement vers l'ocean. Ann. Geophys. 38, 1–24.
Deng, C.L., Shaw, J., Liu, Q.S., Pan, Y.X., Zhu, R.X., 2006. Mineral magnetic variation of the Jingbian loess/paleosol sequence in the northern Loess Plateau of China: implications for the Quaternary development of Asian aridification and cooling. Earth Planet. Sci. Lett. 241, 248–259.
Denton, G.H., Karlén, W., 1973a. Holocene climatic variations—their pattern and possible cause. Quat. Res. 3, 155–205.
Denton, G.H., Karlén, W., 1973b. Lichenometry: its application to Holocene moraine studies in southern Alaska and Swedish Lapland. Arct. Alp. Res. 5, 347–372.
Deplazes, G., Lückge, A., Peterson, L.C., Timmermann, A., Hamann, Y., Hughen, K.A., Röhl, U., Laj, C., Cane, M.A., Sigman, D.M., Haug, G.H., 2013. Links between tropical rainfall and North Atlantic climate during the last glacial period. Nat. Geosci. 6, 213–217.
Deuser, W.G., Ross, E.H., 1989. Seasonally abundant planktonic foraminifera of the Sargasso Sea: succession, deep-water fluxes, isotopic compositions and paleoceanographic implications. J. Foram. Res. 19, 268–293.
de Vernal, A., Marret, F., 2007. Organic-walled dinoflaggellate cysts: tracers of sea-surface conditions. In: Hillaire-Marcel, C., de Vernal, A. (Eds.), Proxies in Late Cenozoic Paleoceanography. Elsevier, Amsterdam, pp. 371–408.
de Vernal, A., Londeix, L., Mudie, P.J., Harland, R., Morzadec-Kerfourn, M.T., Turon, J.-L., Wrenn, J.H., 1992. Quaternary organic-walled dinoflagellate cysts of the North Atlantic Ocean and adjacent Seas: ecostratigraphy and biostratigraphy. In: Head, M.J., Wrenn, J.H. (Eds.), Neogene and Quaternary Dinoflagellate Cysts and Acritarchs. American Association of Stratigraphic Palynologists Foundation, Dallas, pp. 289–328.

de Vernal, A., Hillaire-Marcel, C., Thuron, J.-L., Matthiessen, J., 2000. Reconstruction of sea-surface temperature, salinity and sea-ice cover in the northern Atlantic during the last glacial maximum based on dinocyst assemblages. Can. J. Earth Sci. 37, 725–750.

de Vernal, A., Eynaud, F., Henry, M., Hillaire-Marcel, C., Londeix, L., Mangin, S., Matthiessen, J., Marret, F., Radi, T., Rochon, A., Solignac, S., Turon, J., 2005. Reconstruction of sea-surface conditions at middle to high-latitudes of the Northern Hemisphere during the Last Glacial Maximum (LGM) based on dinoflagellate cyst assemblages. Quat. Sci. Rev. 24, 897–924.

de Vernal, A., Rosell-Melé, A., Kucera, M., Hillaire-Marcel, C., Eynaud, F., Weinelt, M., Dokken, T., Kageyama, M., 2006. Comparing proxies for the reconstruction of LGM sea-surface temperature conditions in the northern North Atlantic. Quat. Sci. Rev. 25, 2820–2834.

Devine, J.D., Sigurdsson, H., Davis, A.N., Self, S., 1984. Estimates of sulfur and chlorine yield to the atmosphere from volcanic eruptions and potential climatic effects. J. Geophys. Res. 89B, 6309–6325.

de Vries, H.L., 1958. Variation in concentration of radiocarbon with time and location on earth. Proc. Konikl. Nederl. Akad. Wetenschap. B61, 94–102.

de Vries, J., 1977. Histoire du climat et économie: des faits nouveaux, une interpretation différente. Ann: Econ. Soc. Civ. 32, 198–228.

de Vries, J., 1981. Measuring the impact of climate on history: the search for appropriate methodologies. In: Rotberg, R.I., Rabb, T.K. (Eds.), Climate and History: Studies in Interdisciplinary History. Princeton University Press, Princeton, pp. 19–50.

Dial, N.P., Czaplewski, N.J., 1990. Do woodrat middens accurately represent the ani mals' environments and diets? The Woodhouse Mesa Study. In: Betancourt, J.L., Van Devender, T.R., Martin, P.S. (Eds.), Packrat Middens: The Last 40,000 Years of Biotic Change. University of Arizona Press, Tucson, pp. 43–58.

Diaz, H.F., Kiladis, G., 1992. Atmospheric teleconnections associated with the extreme phase of the Southern Oscillation. In: Diaz, H.F., Markgraf, V. (Eds.), El Niño: Historical and Paleoclimatic Aspects of the Southern Oscillation. Cambridge University Press, Cambridge, pp. 7–28.

Diaz, H.F., Trigo, R., Hughes, M.K., Mann, M.E., Xoplaki, E., Barriopedro, D., 2011. Spatial and temporal characteristics of climate in medieval times revisited. Bull. Am. Meteorol. Soc. 92, 1487–1500.

Dibb, J.E., Clausen, H.B., 1997. A 200-year ^{210}Pb record from Greenland. J. Geophys. Res. 102D, 4325–4332.

Dickson, R.R., Brown, J., 1994. The production of North Atlantic Deep Water: sources rates and pathways. J. Geophys. Res. 99C, 12319–12341.

Dimbleby, G.W., 1985. The Palynology of Archeological Sites. Academic Press, London.

Ding, Z., Rutter, N., Han, J., Liu, T., 1992. A coupled environmental system formed at about 2.5 Ma in East Asia. Palaeogeogr. Palaeoclimatol. Palaeoecol. 94, 223–242.

Ding, Z., Rutter, N.W., Liu, T.S., 1993. Pedostratigraphy of Chinese loess deposits and climatic cycles in the last 2.5 Ma. Catena. 20, 73–91.

Ding, Z.L., Rutter, N.W., Sun, J.M., Yang, S.L., Liu, T.S., 2000. Re-arrangement of atmospheric circulation at about 2.6 Ma over northern China: evidence from grain size records of loess-paleosol and red clay sequences. Quat. Sci. Rev. 19, 547–558.

Ding, Z.L., Derbyshire, E., Yang, S.L., Sun, J.M., Liu, T.S., 2005. Stepwise expansion of desert environment across northern China in the past 3.5 Ma and implications for monsoon evolution. Earth Planet. Sci. Lett. 237, 45–55.

Dobrovolný, P., Moberg, A., Brázdil, R., Pfister, C., Glaser, R., Wilson, R., van Engelen, A., Limanówka, D., Kiss, A., Halíčková, M., Macková, J., Riemann, D., Luterbacher, J., Bohm, R., 2010. Monthly, seasonal and annual temperature reconstructions for Central Europe derived from documentary evidence and instrumental records since A.D. 1500. Clim. Chang. 101, 69–107.

Dokken, T.M., Jansen, E., 1999. Rapid changes in the mechanism of ocean convection during the last glacial period. Nature. 401, 458–461.

Dong, W.Y., Wang, Y.J., Cheng, H., Hardt, B., Edwards, R.L., Kong, X.G., Wu, J.Y., Chen, S.T., Liu, D.B., Jiang, X.Y., Zhao, K., 2010. A high resolution stalagmite record of the Holocene East Asian monsoon from Mt Shennongjia, central China. The Holocene. 20, 257–264.

Douglass, A.E., 1914. A method of estimating rainfall by the growth of trees. In: Huntingdon, E. (Ed.), The Climatic Factor. Publication No. 192, Carnegie Institution of Washington, Washington, DC, pp. 101–122.

Douglass, A.E., 1919. Climatic Cycles and Tree Growth, vol. 1. Carnegie Institution of Washington, Washington, DC, Publication No. 289.

Dowdeswell, J.A., Maslin, M.A., Andrews, J.T., McCave, L.N., 1995. 1ceberg production, debris rafting and the extent and thickness of Heinrich layers (H-1, H-2) in North Atlantic sediments. Geology. 23, 301–304.

Dowsett, H.J., Poore, R.Z., 1990. A new planktic foraminifer transfer function for esti mating Plio-Holocene paleoceanographic conditions in the North Atlantic. Mar. Micropaleontol. 16, 1–23.

Dreyfus, G.B., Parrenin, F., Lemieux-Dudon, B., Durand, G., Masson-Delmotte, V., Jouzel, J., Barnola, J.-M., Panno, L., Spahni, R., Tisserand, A., Siegenthaler, U., Leuenberger, M., 2007. Anomalous flow below 2700m in the EPICA Dome C ice core detected using $\delta^{18}O$ of atmospheric oxygen measurements. Clim. Past. 3, 341–353.

Driscoll, W., Wiles, G., D'Arrigo, R., Wilmking, M., 2005. Divergent tree growth response to recent climate warming, Lake Clark National Park and Preserve, Alaska. Geophys. Res. Lett. 32, L20703. dx.doi.org/1029/2005GL024258.

Druffel, E.R.M., Griffin, S., 1993. Large variations of surface ocean radiocarbon: evidence of circulation changes in the southwestern Pacific. J. Geophys. Res. 98C, 20,249–20,259.

Druffel, E.R.M., Griffin, S., Beaupré, S.R., Dunbar, R.B., 2007. Oceanic climate and circulation changes during the past four centuries from radiocarbon in corals. Geophys. Res. Lett. 34, L09601. dx.doi.org/10.1029/2006GL028681.2007.

Drysdale, R.N., Zanchetta, G., Hellstrom, J.C., Fallick, A.E., Zhao, J.X., Bruschi, G., 2004. Paleoclimatic implications of the growth history and stable isotope ($\delta^{18}O$ and δ13C) geochemistry of a Middle to Late Pleistocene stalagmite from central-western Italy. Earth Planet. Sci. Lett. 227, 215–229.

Dudley, W.C., Goodney, D.E., 1979. Stable isotope analysis of calcareous nannoplankton: a paleo-oceanographic indicator of surface water conditions. In: Evolution des Atmospheres Planetaires et Climatologie de Ia Terre. Centre National d'Etudes Spatiales, Toulouse, pp. 133–148.

Duller, G.A.T., 1995. Luminescence dating using single aliquots: methods and applications. Radiat. Meas. 24, 217–226.

Duller, G.A.T., 1996. Recent developments in luminescence dating of Quaternary sediments. Prog. Phys. Geogr. 20, 127–145.

Duller, G.A.T., 2004. Luminescence dating of Quaternary sediments: recent advances. J. Quat. Sci. 19, 183–192.

Dumitru, T.A., 2000. Fission-track geochronology. In: Noller, J.S., Sowers, J.M., Lettis, W.R. (Eds.), Quaternary Geochronology: Methods and Applications. American Geophysical Union, Washington, DC, pp. 131–156.

Dunai, T., 2000. Scaling factors for production rates of in situ produced cosmogenic nuclides: a critical reevaluation. Earth Planet. Sci. Lett. 176, 157–169.

Dunai, T., 2010. Cosmogenic Nuclides: Principles, Concepts, and Applications in the Earth Surface Sciences. Cambridge University Press, Cambridge.

Dunbar, R.B., Cole, J.E., 1993. Coral records of ocean-atmosphere variability. Special Report No. 10, NOAA Climate and Global Change Program, Washington, DC.

Dunbar, R.B., Wellington, G.M., 1981. Stable isotopes in a branching coral monitor seasonal temperature variation. Nature. 293, 453–455.

Dunbar, R.B., Wellington, G.M., Colgan, M.W., Glynn, P.W., 1994. Eastern Pacific sea surface temperature since 1600 A.D.: the ^{18}O record of climate variability in Galapagos corals. Paleoceanography. 9, 291–315.

Dunbar, R.B., Linsley, B.K., Wellington, G.M., 1996. Eastern Pacific corals monitor El Niño/Southern Oscillation, precipitation and sea surface temperature variability over the past 3 centuries. In: Jones, P.D., Bradley, R.S., Jouzel, J. (Eds.), Climate Variations and Forcing Mechanisms of the Last 2,000 years. Springer-Verlag, Berlin, pp. 373–405.

Duplessy, J.-C., 1978. Isotope studies. In: Gribbin, J. (Ed.), Climatic Change. Cambridge University Press, Cambridge, pp. 46–67.

Duplessy, J.-C., Maier-Reimer, E., 1993. Global ocean circulation changes. In: Eddy, J.A., Oeschger, H. (Eds.), Global Changes in the Perspective of the Past. Wiley, Chichester, pp. 199–220.

Duplessy, J.-C., Shackleton, N.J., 1985. Response of global deep-water circulation to earth's climatic change 135,000-107,000 years ago. Nature. 316, 500–507.

Duplessy, J.-C., Lalou, C., Vinot, A.C., 1970. Differential isotopic fractionation in benthic foraminifera and paleotemperatures re-assessed. Science. 168, 250–251.

Duplessy, J.-C., Blanc, P.-L., Bé, A.W.H., 1981. Oxygen-18 enrichment of planktonic foraminifera due to gametogenic calcification below the euphotic zone. Science. 213, 1247–1250.

Duplessy, J.-C., Shackleton, N.J., Fairbanks, R.G., Labeyrie, L., Oppo, D., Kallel, N., 1988. Deep-water source variations during the last climatic cycle and their impact on the global deep water circulation. Paleoceanography. 3, 343–360.

Duplessy, J.-C., Arnold, M., Bard, E., Juillet-Leclerc, A., Kallel, N., Labeyrie, L., 1989. AMS ^{14}C study of transient events and of the ventilation rate of the Pacific Intermediate Water during the last deglaciation. Radiocarbon. 31, 493–502.

Duplessy, J.-C., Labeyrie, L., Juillet-LeClerc, A., Maitre, F., Duprat, J., Sarnthein, M., 1991. Surface salinity reconstruction of the North Atlantic Ocean during the last glacial maximum. Oceanol. Acta. 14, 311–324.

Duplessy, J.-C., Labeyrie, L., Arnold, M., Paterne, M., Duprat, J., van Weering, T.C.E., 1992. Changes in surface salinity of the North Atlantic during the last deglaciation. Nature. 358, 486–488.

Duplessy, J.-C., Bard, E., Labeyrie, L., Duprat, J., Moyes, J., 1993. Oxygen isotope records and salinity changes in the northeastern Atlantic Ocean during the last 18,000 years. Paleoceanography. 8, 341–350.

Dutton, A., Bard, E., Antonioli, F., Esat, T.M., Lambeck, K., McCulloch, M.T., 2009. Phasing and amplitude of sea-level and climate change during the penultimate interglacial. Nat. Geosci. 2, 355–358.

Dyakowska, J., 1936. Researches on the rapidity of the falling down of pollen of some trees. Bull. Int. Acad. Pol. Sci. Lett. B1, 155–168.

Dykoski, C.A., Edwards, R.L., Cheng, H., Yuan, D.X., Cai, Y.J., Zhang, M.L., Lin, Y.S., Qing, J.M., An, Z.S., Revenaugh, J., 2005. A high-resolution, absolute-dated Holocene and deglacial Asian monsoon record from Dongge Cave, China. Earth Planet. Sci. Lett. 233, 71–86.

Dylik, J., 1975. The glacial complex in the notion of the late Cenozoic cold ages. Biul. Peryglac. 24, 219–231.

Eckstein, D., Wazny, T., Blauch, J., Klein, P., 1986. New evidence for the dendrochronological dating of Netherlandish paintings. Nature. 320, 465–466.

Eckstein, J., Leuschner, H.H., Bauerochse, A., Sass-Klaassen, U., 2009. Subfossil bog-pine horizons document climate and ecosystem changes during the Mid-Holocene. Dendrochronologia. 27, 129–146.

Eddy, J.A., 1976. The Maunder Minimum. Science. 192, 1189–1202.

Eddy, J.A., 1977. Climate and the changing sun. Clim. Chang. 1, 173–190.

Edwards, T.W.D., 1993. Interpreting past climate from stable isotopes in continental organic matter. In: Swart, P.K., Lohmann, K.C., McKenzie, J., Savon, S. (Eds.), Climate Change in Continental Isotopic Records. American Geophysical Union, Washington, DC, pp. 333–341.

Edwards, R.L., Gallup, C.D., 1993. Dating of the Devils Hole calcite vein. Science. 259, 1626 (see also reply by Ludwig, K.R., et al., 1626–1627).

Edwards, R.L., Chen, J.H., Wasserburg, G.J., 1987a. ^{238}U-^{234}U-^{230}Th-^{232}Th systematics and the precise measurement of time over the past 500,000 years. Earth Planet. Sci. Lett. 81, 175–192.

Edwards, R.L., Chen, J.H., Ku, T.-L., Wasserburg, G.J., 1987b. Precise timing of the last interglacial period from mass spectrometric determination of ^{230}Th in corals. Science. 236, 1547–1553.

Edwards, R.L., Beck, J.W., Burr, G.S., Donahue, D.J., Chappell, J.M.A., Bloom, A.L., Druffel, E.R.M., Taylor, F.W., 1993. A large drop in atmospheric 14C/12C and reduced melting in Younger Dryas, documented with 230Th ages of corals. Science. 260, 962–967.

Edwards, M.E., Anderson, P.M., Brubaker, L.B., Ager, T.A., Andreev, A.A., Bigelow, N.H., Cwynar, L.C., Eisner, W.R., Harrison, S.P., Hu, F.-S., Jolly, D., Lozhkin, A.V., MacDonald, G.M., Mock, C.J., Ritchie, J.C., Sher, A.V., Spear, R.W., Williams, J.W., Yu, G., 2000. Pollen-based biomes for Beringia 18,000, 6000 and 0 ^{14}C BP. J. Biogeogr. 27, 521–554.

Egan, T., 2006. The Worst Hard Time. Mariner Books, Boston, 340 pp.

Eggermont, H., Heiri, O., Verschuren, D., 2006. Fossil Chironomidae (Insecta: Diptera) as quantitative indicators of past salinity in African lakes. Quat. Sci. Rev. 25, 1966–1994.

Eggins, S.M., Grun, R., McCulloch, M.T., Pike, A.W.G., Chappell, J., Kinsley, L., Mortimer, G., Shelley, M., Murray-Wallace, C.V., Spötl, C., Taylor, L., 2005. In situ U-series dating by laser-ablation multi-collector ICPMS: new prospects for Quaternary geochronology. Quat. Sci. Rev. 24, 2523–2538.

Eglinton, T.I., Eglinton, G., 2008. Molecular proxies for paleoclimatology. Earth Planet. Sci. Lett. 275, 1–16.

Eglinton, G., Stuart, A.B., Rosell, A., Sarnthein, M., Pflaumann, U., Tiedeman, R., 1992. Molecular record of secular sea surface temperature changes on 100-year timescales for glacial terminations I, II and IV. Nature. 356, 423–426.

Eglinton, T.I., Aluwihare, L.I., Bauer, J.E., Druffel, E.R.M., McNichol, A.P., 1996. Gas chromatographic isolation of individual compounds from complex matrices for radiocarbon dating. Anal. Chem. 68, 904–912.

Eglinton, T.I., Benitez-Nelson, B.C., Pearson, A., McNichol, A.P., Bauer, J.E., Druffel, E.R.M., 1997. Variability in radiocarbon ages of individual organic compounds from marine sediments. Science. 277, 796–799.

Ehlers, J., Gibbard, P.L., 2003. Extent and chronology of glaciations. Quat. Sci. Rev. 22, 1561–1568.
Ehlers, J., Gibbard, P.L. (Eds.), 2004a. Quaternary Glaciations: Extent and Chronology. Part I: Europe. Elsevier, Amsterdam.
Ehlers, J., Gibbard, P.L. (Eds.), 2004b. Quaternary Glaciations: Extent and Chronology. Part II: North America. Elsevier, Amsterdam.
Ehlers, J., Gibbard, P.L. (Eds.), 2004c. Quaternary Glaciations: Extent and Chronology. Part III: South America, Asia, Africa, Australia, Antarctica. Elsevier, Amsterdam.
Eichler, A., Olivier, S., Henderson, K., Laube, A., Beer, J., Papina, T., Gäggeler, H., Schwikowski, M., 2009. Temperature response in the Altai region lags solar forcing. Geophys. Res. Lett. 36, L01808. dx.doi.org/10.1029/2008GL035930.
Elias, S., 1994. Quaternary Insects and Their Environments. Smithsonian Institution Press, Washington, DC.
Elias, S.A., 1997. The mutual climatic range method of palaeoclimate reconstruction based on insect fossils: new application and interhemispheric comparisons. Quat. Sci. Rev. 16, 1217–1225.
Elias, S.A., 2010. Advances in Quaternary Entomology. Developments in Quaternary Sciences, vol. 12. Elsevier, Amsterdam, 288 pp.
Elliott, M., Labeyrie, L., Duplessy, J.-C., 2002. Changes in North Atlantic deepwater formation associated with the Dansgaard-Oeschger temperature oscillations (60-10ka). Quat. Sci. Rev. 21, 1153–1165.
Elmore, S., Phillips, F.M., 1987. Accelerator mass spectrometry for measurement of long-lived radioisotopes. Science. 236, 543–550.
El-Moslimany, A.P., 1990. Ecological significance of common non-arboreal pollen: examples from drylands of the Middle East. Rev. Palaeobot. Palynol. 64, 343–350.
Emile-Geay, J., Cane, M.A., Naik, N., Seager, R., Clement, A.C., van Geen, A., 2003. Warren revisited: Atmospheric freshwater fluxes and "Why is no deep water formed in the North Pacific" J. Geophys. Res. 108, 3178.
Emile-Geay, J., Seager, R., Cane, M.A., Cook, E.R., Haug, G., 2007. Volcanoes and ENSO over the past millennium. J. Clim. 21, 3134–3138.
Emile-Geay, J., Seager, R., Cane, M.A., Cook, E.R., Haug, G., 2008. Volcanoes and ENSO over the past millennium. J. Clim. 21, 3134–3148.
Emiliani, C., 1955. Pleistocene temperatures. J. Geol. 63, 538–578.
Emiliani, C., 1966. Paleotemperature analysis of Caribbean cores, P6304-8 and P6304-9 and a generalized temperature curve for the past 425,000 years. J. Geol. 74, 109–126.
Emiliani, C., 1971. Depth habitats of growth stages of pelagic foraminifera. Science. 173, 1122–1124.
Emiliani, C., 1977. Oxygen isotopic analysis of the size fraction between 62 and 250 micrometers in Caribbean cores P6304–8 and p 6304–9. Science. 198, 1255–1256.
Emiliani, C., Ericson, D.B., 1991. The glacial/interglacial temperature range of the surface water of the oceans at low latitudes. In: Taylor Jr., H.P., O'Neil, J.R., Kaplan, I.R. (Eds.), Stable Isotope Geochemistry: A Tribute to Samuel Epstein. Special Publication No. 3, The Geochemical Society, St. Louis, pp. 223–228.
Emiliani, C., Hudson, J.H., Shinn, E.A., George, R.Y., 1978. Oxygen and carbon isotopic growth record in a reef coral from the Florida Keys and a deep-sea coral from Blake Plateau. Science. 202, 627–629.
Endfield, G.H., 2007. Archival explorations of climate variability and social vulnerability in colonial Mexico. Clim. Chang. 83, 9–38.
Endler, J.A., 1982. Pleistocene forest refuges: fact or fancy. In: Prance, G.T. (Ed.), Biological diversification in the Tropics. Columbia University Press, New York, pp. 641–657.
Ennever, F.K., McElroy, M.B., 1985. Changes in CO_2: factors regulating the glacial to interglacial transition. In: Sundquist, E.T., Broecker, W.S. (Eds.), The Carbon Cycle and Atmospheric CO_2: Natural Variations, Archean to Present. American Geophysical Union, Washington, DC, pp. 154–162.
EPICA community members, 2004. Eight glacial cycles from an Antarctic ice core. Nature. 429, 623–628.
EPICA community members, 2006. One-to-one coupling of glacial climate variability in Greenland and Antarctica. Nature. 444, 195–198.
Epstein, S., Mayeda, T., 1953. Variation of ^{18}O content of waters from natural sources. Geochim. Cosmochim. Acta. 4, 213–224.
Epstein, S., Sharp, R.P., 1959. Oxygen isotope variations in the Malaspina and Saskatchewan glaciers. J. Geol. 67, 88–102.

Epstein, S., Yapp, C.J., 1976. Climatic implications of the DIH ratio of hydrogen in C/H groups in tree cellulose. Earth Planet. Sci. Lett. 30, 252–266.
Epstein, S., Buchsbaum, R., Lowenstam, H.A., Urey, H.C., 1953. Revised carbonate-water isotopic temperature scale. Bull. Geol. Soc. Am. 64, 1315–1326.
Eronen, M., Huttunen, P., 1987. Radiocarbon dated sub-fossil pine from Finnish Lapland. Geogr. Ann. 69A, 297–304.
Esper, J., Frank, D., 2009. Divergence pitfalls in tree-ring research. Clim. Chang. 94, 261–266.
Esper, J., Cook, E.R., Schweingruber, F.H., 2002. Low-frequency signals in long tree-ring chronologies for reconstructing past temperature variability. Science. 295, 2250–2253.
Esper, J., Frank, D., Büntgen, U., Verstage, A., Hantemirov, R.M., Kidyanov, A.V., 2009. Trends and uncertainties in Siberian indicators of 20th century warming. Glob. Chang. Biol. 16, 386–398. dx.doi.org/10.1111/j.1365-2486.2009.01913.x.
Etheridge, D.M., Steele, L.P., Langenfelds, R.L., Francey, R.J., Barnola, J.-M., Morgan, V.I., 1996. Natural and anthropogenic changes in atmospheric CO_2 over the last 1000 years from air in Antarctic ice and firn. J. Geophys. Res. 101, 4115–4128.
Evans, M.N., 2007. Toward forward modeling for paleoclimate proxy signal calibration: a case study with oxygen isotope composition of tropical woods. Geochem. Geophys. Geosyst. 8, Q07008. dx.doi.org/10.1029/2006GC001406.
Evans, M.E., Heller, F., 2003. Environmental Magnetism: Principles and Applications of Enviromagnetics. Academic Press, San Diego, 293 pp.
Evans, M.N., Schrag, D.P., 2004. A stable isotope-based approach to tropical dendroclimatology. Geochim. Cosmochim. Acta. 68, 3295–3305.
Evans, M.N., Tolwinski-Ward, S.E., Thompson, D.M., Anchukaitis, K.J., 2013. Applications of proxy system modeling in high resolution paleoclimatology. Quat. Sci. Rev. 76, 16–28.
Faegri, K., Iversen, J., 1975. Textbook of Pollen Analysis, third ed. Hafner Press, New York.
Faegri, K., Kaland, P.E., Krzywinski, K., 1989. Textbook of Pollen Analysis, fourth ed. Wiley, Chichester.
Fairbanks, R.G., 1989. A 17,000 year glacio-eustatic sea level record: influence of glacial melting rates on the Younger Dryas event and deep ocean circulation. Nature. 342, 637–642.
Fairbanks, R.G., 1990. The age and origin of the "Younger Dryas Climate Event" in Greenland ice cores. Paleoceanography. 5, 937–948.
Fairbanks, R.G., Dodge, R.E., 1979. Annual periodicity of the O-18/O-16 and C-13/C-12 ratios in the coral *Montastrea annularis*. Geochim. Cosmochim. Acta. 43, 1009–1020.
Fairbanks, R.G., Mortlock, R.A., Chiu, T.-C., Cao, L., Kaplan, A., Guilderson, T.P., Fairbanks, T.W., Bloom, A.L., Grootes, P.M., Nadeau, M.-J., 2005. Radiocarbon calibration curve spanning 0 to 50,000 years BP based on paired $^{230}Th/^{234}U/^{238}U$ and ^{14}C dates on pristine corals. Quat. Sci. Rev. 24, 1781–1796.
Fairchild, I.J., Baker, A., 2012. Speleothem Science: From Process to Past Environments. Wiley-Blackwell, Oxford, 432 pp.
Fairchild, I.J., Smith, C.L., Baker, A., Fuller, L., Spötl, C., Mattey, D., McDermott, F., 2006. Modification and preservation of environmental signals in speleothems. Earth-Sci. Rev. 75, 105–153.
Farquhar, G.D., O'Leary, M.H., Berry, J.A., 1982. On the relationship between carbon isotope discrimination and intercellular carbon dioxide concentration in leaves. Aust. J. Plant Physiol. 9, 121–137.
Farquhar, G.D., Ehleringer, J., Hubick, K., 1989. Carbon isotope discrimination and photosynthesis. Annu. Rev. Plant Physiol. Plant Mol. Biol. 40, 503–537.
Fattahi, M., Stokes, S., 2003. Dating volcanic and related sediments by luminescence methods: a review. Earth-Sci. Rev. 62, 229–264.
Faul, H., Wagner, G.A., 1971. Fission track dating. In: Michael, H.N., Ralph, E.K. (Eds.), Dating Techniques for the Archaeologist. MIT Press, Cambridge, pp. 152–156.
Felis, T., Pätzold, J., 2004. Climate reconstructions from annually banded corals. In: Shiyomi, M. (Ed.), Global Environmental Change in the Oceans and on Land. Terrapub, Tokyo, pp. 205–227.
Felis, T., Pätzold, J., Loya, Y., Fine, M., Nawar, A.H., Wefer, G., 2000. A coral oxygen isotope record from the northern Red Sea documenting NAO, ENSO, and North Pacific teleconnections on Middle East climate variability since the year 1750. Paleoceanography. 15, 679–694.

Felis, T., Lohmann, G., Kuhneret, H., Lorenz, S.J., Scholz, D., Pätzold, J., Al-Rousan, S.A., Moghrabi, S.M., 2004. Increased seasonality in Middle East temperatures during the last interglacial period. Nature. 429, 164–168.

Felis, T., Merkel, U., Asami, R., Deschamps, P., Hathorne, E.C., Kölling, M., Bard, E., Cabioch, G., Durand, N., Prange, M., Schulz, M., Cahyarini, S.Y., Pfeiffer, M., 2012. Pronounced interannual variability in tropical South Pacific temperatures during Heinrich Stadial 1. Nat. Commun. 3, 965–971.

Ferguson, R., 1977. Linear Regression in Geography. Concepts and Techniques in Modern Geography No. 15, University of East Anglia, Norwich.

Fischer, H., Siggaard-Andersen, M.L., Ruth, U., Rothlisberger, R., Wolff, E.W., 2007. Glacial-interglacial changes in mineral dust and sea salt records in polar ice cores: sources, transport, deposition. Rev. Geophys. 45, RG1002 dx.doi.org/10.1029/2005RG000192.

Fisher, D.A., 1991. Remarks on the deuterium excess in precipitation in cold regions. Tellus. 43B, 401–407.

Fisher, D.A., 1992. Stable isotope simulations using a regional stable isotope model coupled to a zonally averaged global model. Cold Reg. Sci. Technol. 21, 61–77.

Fisher, D.A., Koerner, R.M., Reeh, N., 1995. Holocene climatic records from the Agassiz Ice Cap, Ellesmere Island, N.W.T., Canada. The Holocene. 5, 19–24.

Fisher, D.A., Osterburg, E., Dyke, A., Dahl-Jensen, D., Demuth, D., Zdanowicz, C., Bourgeois, J., Koerner, R.M., Mayewski, P., Wake, C., Kreutz, K., Steig, E., Zheng, J., Yalcin, K., Goto-Azuma, K., Luckman, B., Rupper, S., 2008. The Mt Logan Holocene-late Wisconsinan isotope record: Tropical Pacific-Yukon connections. The Holocene. 18, 667–678.

Fisher, D.A., Zheng, J., Burgess, D., Zdanowicz, C., Kinnard, C., Sharp, M., Bourgeois, J., 2012. Recent melt rates of Canadian arctic ice caps are the highest in four millennia. Glob. Planet. Chang. 84–85, 3–7.

Fitch, J.R., 1972. Selection of suitable material for dating and the assessment of geological error in potassium-argon age determination. In: Bishop, W.W., Miller, J.A. (Eds.), Calibration of Hominoid Evolution. Scottish Academic Press, Edinburgh, pp. 77–91.

Fitzsimmons, K.E., Marković, S.B., Hambach, U., 2012. Pleistocene environmental dynamics recorded in the loess of the middle and lower Danube basin. Quat. Sci. Rev. 41, 104–118.

Fleischer, R.L., 1975. Advances in fission track dating. World Archaeol. 7, 136–150.

Fleischer, R.L., Hart, H.R., 1972. Fission track dating techniques and problems. In: Bishop, W.W., Miller, J.A. (Eds.), Calibration of Hominoid Evolution. Scottish Academic Press, Edinburgh, pp. 135–170.

Fleitmann, D., Burns, S.J., Neff, U., Mangini, A., Matter, A., 2003a. Changing moisture sources over the last 330,000 years in Northern Oman from fluid-inclusion evidence in speleothems. Quat. Res. 60, 223–232.

Fleitmann, D., Burns, S.J., Mudelsee, M., Neff, U., Kramers, J., Mangini, A., Matter, A., 2003b. Holocene forcing of the Indian monsoon recorded in a stalagmite from southern Oman. Science. 300, 1737–1739.

Fleitmann, D., Burns, S.J., Neff, U., Mudelsee, M., Mangini, A., Matter, A., 2004. Palaeoclimatic interpretation of high-resolution oxygen isotope profiles derived from annually laminated speleothems from Southern Oman. Quat. Sci. Rev. 23, 915–945.

Fleitmann, D., Burns, S.J., Mangini, A., Mudelsee, M., Kramer, J., Villa, I., Neff, U., Al-Subbary, A.A., Buettner, A., Hippler, D., Matter, A., 2007a. Holocene ITCZ and Indian monsoon dynamics recorded in stalagmites from Oman and Yemen (Socotra). Quat. Sci. Rev. 26, 170–188.

Fleitmann, D., Dunbar, R.B., McCulloch, M., Mudelsee, M., Vuille, M., McClanahan, T.R., Cole, J.E., Eggins, S., 2007b. East African soil erosion recorded in a 300 year old coral colony from Kenya. Geophys. Res. Lett. 34, L04401. dx.doi.org/10.1029/20006GL028525.

Fleitmann, D., Burns, S.J., Pekala, M., Mangini, A., Al-Subbary, A., Al-Aowah, M., Kramers, J., Matter, A., 2011. Holocene and Pleistocene pluvial periods in Yemen, southern Arabia. Quat. Sci. Rev. 30, 783–787.

Fleming, S., 1976. Dating in Archaeology: A Guide to Scientific Techniques. J.M. Dent, London.

Flint, R.F., 1971. Glacial and Quaternary Geology. Wiley, New York.

Flint, R.F., 1976. Physical evidence of quaternary climatic change. Quat. Res. 6, 519–528.

Flock, J.W., 1978. Lichen-bryophyte distribution along a snow-cover/soil-moisture gradient, Niwot Ridge, Colorado. Arct. Alp. Res. 10, 31–47.

Flohn, H., 1949. Klima und Witterungsablauf in Zurich im 16 Jahrhundert. Vierteljahresheft der Naturf. Gesell. Zurich. 94, 28–41.

Flohn, H., 1978. Comparison of Antarctic and Arctic climate and its relevance to climate evolution. In: Van Zinderen Bakker, E.M. (Ed.), Antarctic Glacial History and World Palaeoenvironments. A.A. Balkema, Rotterdam, pp. 3–13.
Foley, J.A., Kutzbach, J.E., Coe, M.T., Levis, S., 1994. Feedbacks between climate and boreal forests during the Holocene epoch. Nature. 371, 52–54.
Forman, S.L., 1991. Late Pleistocene chronology of loess deposition near Luochuan, China. Quat. Res. 36, 19–28.
Forman, S.L., Lepper, K., Pierson, J., 1994. Limitations of infra-red stimulated luminescence in dating High Arctic marine sediments. Quat. Geochronol. (Quat. Sci. Rev.). 13, 545–550.
Forman, S.L., Oglesby, R., Markgraf, V., Stafford, T., 1995. Paleoclimatic significance of Late Quaternary eolian deposition on the Piedmont and High Plains, central United States. Glob. Planet. Chang. 11, 35–55.
Forster, P., Ramaswamy, V., Artaxo, P., Berntsen, T., Betts, R., Fahey, D.W., Haywood, J., Lean, J., Lowe, D.C., Myhre, G., Nganga, J., Prinn, R., Raga, G., Schulz, M., van Dorland, R., 2007. Changes in atmospheric constituents and in radiative forcing. In: Solomon, S., Qin, D., Manning, M., Chen, Z., Marquis, M., Averyt, K.B., Tignor, M., Miller, H.L. (Eds.), Climate Change 2007: The Physical Science Basis. Cambridge University Press, Cambridge, pp. 129–234.
Fowler, A.M., Boswijk, G., Lorrey, A.M., Gergis, J., Pirie, M., McCloskey, S.P., Palmer, J.G., Wunder, J., 2012. Multicentennial tree-ring record of ENSO-related activity in New Zealand. Nat. Clim. Chang. 2, 172–176.
Fox, A.N., 1991. A quantitative model of Alpine snowline variations in the central Andes. In: Boletim IC-USP. Publicação Especial, No. 8, Instituto de Geosciências, Universidad de São Paulo, Brazil, pp. 75–88.
Frakes, L.A., Francis, J.E., Syktus, J.I., 1992. Climate Modes of the Phanerozoic. Cambridge University Press, Cambridge.
Francis, D.R., 2004. Distribution of midge remains (Diptera: Chironomidae) in surficial lake sediments in New England. Northeast. Nat. 11, 459–478.
François, R., 2007. Paleoflux and paleocirculation from sediment ^{230}Th and ^{231}Pa/^{230}Th. In: Hillaire-Marcel, C., de Vernal, A. (Eds.), Proxies in Late Cenozoic Paleoceanography. Elsevier, Amsterdam, pp. 681–716.
Francou, B., Vincent, C., 2011. Les Glaciers a l'epreuve du Climat. IRD Orstom.
Francou, B., Vuille, M., Wagnon, P., Mendoza, J., Sicart, J.-E., 2003. Tropical climate change recorded by a glacier in the central Andes during the last decades of the twentieth century: Chacaltaya, Bolivia, 16°S. J. Geophys. Res. 108, D4154. dx.doi.org/10.1029/2002JD002959.
Francou, B., Vuille, M., Favier, V., Cáceres, B., 2004. New evidence for an ENSO impact on low latitude glaciers: Antizana 15, Andes of Ecuador, 0°28'S. J. Geophys. Res. 109, D18106; dx.doi.org/10.1029/2003JD004484.
Francus, P. (Ed.), 2004. Image Analysis, Sediments and Paleoenvironments. Springer, Berlin, 330 pp.
Francus, P., von Suchodoletz, H., Dietze, M., Donner, R.V., Bouchard, F., Roy, A.-J., Fagot, M., Verschuren, D., Kröpelin, S., 2013. Varved sediments of Lake Yoa (Ounianga Kebir, Chad) reveal progressive drying of the Sahara during the last 6100 years. Sedimentology. 60, 911–934.
Frank, D., Esper, J., Cook, E.R., 2007. Adjustment for proxy number and coherence in a large-scale temperature reconstruction. Geophys. Res. Lett. 34, L16709. dx.doi.org/10.1029/2007GL030571.
Frank, D., Esper, J., Zorita, E., Wilson, R., 2010a. A noodle, hockey stick, and spaghetti plate: a perspective on high-resolution paleoclimatology. Wiley Interdiscip. Rev. Clim. Chang. 1, 507–516.
Frank, D., Esper, J., Raible, C.C., Buntgen, U., Trouet, V., Stocker, B., Joos, F., 2010b. Ensemble reconstruction constraints on the global carbon cycle sensitivity to climate. Nature. 463, 527–530.
Frechen, M., Oches, E.A., Kohfeld, K.E., 2003. Loess in Europe—mass accumulation rates during the Last Glacial Period. Quat. Sci. Rev. 22, 1835–1857.
Fredlund, G.G., Tieszen, L.L., 1997. Calibrating grass phytolith assemblages in climatic terms: application to late Pleistocene assemblages from Kansas and Nebraska. Palaeogeogr. Palaeoclimatol. Palaeoecol. 136, 199–211.
Free, M., Robock, A., 1999. Global warming in the context of the Little Ice Age. J. Geophys. Res. 104, 19057–19070.
Freer, S., 2003. Linnaeus' Philosophia Botanica. Oxford University Press, New York, 402 pp.
French, H.M., 2007. The Periglacial Environment. Wiley, Chichester, 475 pp.
Frenzel, B., Pfister, C., Glaser, B. (Eds.), 1992. European Climate Reconstructed from Documentary Data: Methods and Results. Gustav Fischer Verlag, Stuttgart.
Frenzel, B., Pfister, C., Glaser, B. (Eds.), 1994. Climatic Trends and Anomalies in Europe 1675-1715. Gustav Fischer Verlag, Stuttgart.

Frich, P., Freyendahl, K., 1994. The summer climate in the Øresund region of Denmark. In: Frenzel, B., Pfister, C., Glaser, B. (Eds.), Climatic Trends and Anomalies in Europe 1675-1715. Gustav Fischer, Stuttgart, pp. 33–41.
Friedrich, M., Remmele, S., Kromer, B., Hofmann, J., Spurk, M., Kaiser, K.F., Orcel, C., Küppers, M., 2004. The 12,460-year Hohenheim oak and pine tree-ring chronology from central Europe—a unique annual record for radiocarbon calibration and paleoenvironment reconstructions. Radiocarbon. 46, 1111–1121.
Friedrich, W.L., Kromer, B., Friedrich, M., Heinemeier, J., Pfeiffer, T., Talamo, S., 2006. Santorini eruption radiocarbon dated to 1627–1600 B.C. Science. 312, 548.
Frisia, S., Borsato, A., Preto, N., McDermott, F., 2003. Late Holocene annual growth in three Alpine stalagmites records the influence of solar activity and the North Atlantic Oscillation on winter climate. Earth Planet. Sci. Lett. 216, 411–424.
Frisia, S., Borsato, A., Fairchild, I.J., Susini, J., 2005. Variations in atmospheric sulfate recorded in stalagmites by synchrotron micro-XRF and XANES analyses. Earth Planet. Sci. Lett. 235, 729–740.
Fritts, H.C., 1962. An approach to dendroclimatology screening by means of multiple regression techniques. J. Geophys. Res. 67, 1413–1420.
Fritts, H.C., 1965. Tree-ring evidence for climatic changes in western North America. Mon. Weather Rev. 93, 421–443.
Fritts, H.C., 1971. Dendroclimatology and dendroecology. Quat. Res. 1, 419–449.
Fritts, H.C., 1976. Tree Rings and Climate. Academic Press, London.
Fritts, H.C., 1991. Reconstructing Large Scale Climatic Patterns from Tree-Ring Data. University of Arizona Press, Tucson.
Fritts, H.C., Blasing, T.J., Hayden, B.P., Kutzbach, J.E., 1971. Multivariate techniques for specifying tree-growth and climate relationships and for reconstructing anomalies in paleoclimate. J. Appl. Meteorol. 10, 845–864.
Fritts, H.C., Lofgren, G.R., Gordon, G.A., 1979. Variations in climate since 1602 as reconstructed from tree rings. Quat. Res. 12, 18–46.
Fritts, H.C., Guiot, J., Gordon, G.A., Schweingruber, F., 1990. Methods of calibration, verification and reconstruction. In: Cook, E.R., Kariukstis, L.A. (Eds.), Methods of Dendrochronology: Applications in the Environmental Sciences. Kluwer, Dordrecht, pp. 163–217.
Fritz, S.C., 1990. Twentieth century salinity and water-level fluctuations in Devils Lake, North Dakota: test of a diatom-based transfer function. Limnol. Oceanogr. 35, 1771–1781.
Fritts, H.C., Shao, X.M., 1992. Mapping climate using tree-rings from western North America. In: Bradley, R.S., Jones, P.D. (Eds.), Climate Since A.D. 1500. Routledge, London, pp. 269–295.
Fritz, S., Juggins, S., Batterbee, R.W., Engstrom, D.R., 1991. Reconstruction of past changes in salinity and climate using a diatom-based transfer function. Nature. 352, 706–708.
Fritz, S.C., Baker, P.A., Ekdahl, E., Seltzer, G.O., Stevens, L.R., 2010a. Millennial-scale climate variability during the Last Glacial period in the tropical Andes. Quat. Sci. Rev. 29, 1017–1024.
Fritz, S.C., Cumming, B.F., Gasse, F., Laird, K.R., 2010b. Diatoms as indicators of hydrologic and climatic change in saline lakes. In: Smol, J.P., Stoermer, E.F. (Eds.), The Diatoms: applications for the environmental and earth sciences. Cambridge University Press, Cambridge, pp. 186–208.
Fronval, T., Jansen, E., Bloemendal, J., Johnsen, S., 1995. Oceanic evidence for coherent fluctuations in Fennoscandian and Laurentide ice sheets on millennium timescales. Nature. 374, 443–445.
Frumkin, A., 1997. The Holocene history of the Dead Sea levels. In: Niemi, T.N., Ben-Avraham, Z., Gat, J.R. (Eds.), The Dead Sea: The Lake and its Setting. Oxford University Press, Oxford, pp. 237–248.
Fukaishi, K., Tagami, Y., 1992. An attempt of reconstructing the winter weather situations from 1720 to 1869 by the use of historical documents. In: Mikami, T. (Ed.), Proceedings of the International Symposium on the Little Ice Age Climate. Department of Geography, Tokyo Metropolitan University, Tokyo, pp. 194–201.
Fye, F.K., Stahle, D.W., Cook, E.R., 2003. Paleoclimatic analogs to twentieth-century moisture regimes across the United States. Bull. Am. Meteorol. Soc. 84, 901–909.
Gagan, M.K., Ayliffe, L.K., Hopley, D., Cali, J.A., Mortimer, G.E., Chappell, J., McCulloch, M.T., Head, M.J., 1998. Temperature and surface-ocean water balance of the mid-Holocene tropical western Pacific. Science. 279, 1014–1018.
Gagan, M.K., Ayliffe, L.K., Beck, J.W., Cole, J.E., Druffel, E.R.M., Dunbar, R.B., Schrag, D.P., 2000. New views of tropical paleoclimates from corals. Quat. Sci. Rev. 19, 45–64.
Gagen, M., McCarroll, D., Loader, N.J., Robertson, I., Jalkanen, R., Anchukaitis, K., 2007. Exorcising the "segment length curse": summer temperature reconstruction since A.D. 1640 using non-detrended stable carbon isotope ratios from pine trees in northern Finland. The Holocene. 17, 435–446.

Gagen, M., McCarroll, D., Loader, N.J., Robertson, I., 2011. Stable isotopes in dendroclimatology: moving beyond "potential" In: Hughes, M.K., Swetnam, T.W., Diaz, H.F. (Eds.), Dendroclimatology: Progress and Prospects. Springer, Dordrecht, pp. 147–172.

Gaggeler, H.W., VonGunten, H.R., Rossler, E., Oeschger, H., Schotterer, U., 1983. ^{210}Pb-dating of cold alpine firn/ice cores from Colle Gnifetti, Switzerland. J. Glaciol. 29, 165–177.

Gaines, S.M., Eglinton, G., Rullkötter, J., 2009. Echoes of Life: What Fossil Molecules Reveal About Earth History. Oxford University Press, Oxford, 357 pp.

Gajewski, K., Garralla, S., 1992. Holocene vegetation histories from three sites in the tundra of northwestern Quebec, Canada. Arct. Alp. Res. 24, 329–336.

Galloway, R.W., 1970. The full glacial climate in the southwestern United States. Ann. Assoc. Am. Geogr. 60, 245–256.

Gallup, C.D., Edwards, R.L., Johnson, R.G., 1994. The timing of sea levels over the past 200,000 years. Science. 263, 796–800.

Gallup, C.D., Cheng, H., Taylor, F.W., Edwards, R.L., 2002. Direct determination of the timing of sea level change during Termination II. Science. 295, 310–313.

Ganachaud, A., Wunsch, C., 2000. Improved estimates of global ocean circulation, heat transport and mixing from hydrographic data. Nature. 408, 453–457.

Ganeshram, R.S., Pedersen, T.F., Calvert, S.E., Murray, J.W., 1995. Large changes in oceanic nutrient inventories from glacial to interglacial periods. Nature. 376, 755–758.

Ganopolski, A., Rahmstorf, S., 2001. Rapid changes of glacial climate simulated in a coupled climate model. Nature. 409, 153–158.

Gao, C.C., Oman, L., Robock, A., Stenchikov, G.L., 2007. Atmospheric volcanic loading derived from bipolar ice cores: accounting for the spatial distribution of volcanic deposition. J. Geophys. Res. 112, D09109. dx.doi.org/10.1029/2006JD007461.

Gao, C.C., Robock, A., Ammann, C., 2008. Volcanic forcing of climate over the past 1500 years: an improved ice core-based index for climate models. J. Geophys. Res. 113. D23111. dx.doi.org/10.1029/2008JD010239.

Garcia, R., Díaz, H.F., García-Herrera, R., Eischeid, J., Prieto, M.R., Hernández, E., Gimeno, L., Durán, F.R., Buscary, A.M., 2001. Atmospheric circulation changes in the tropical Pacific inferred from the voyages of the Manila galleons in the sixteenth-eighteenth centuries. Bull. Am. Meteorol. Soc. 82, 2435–2455.

García-Herrera, R., Rubio, F., Wheeler, D., Hernández, E., Prieto, M.R., Gimeno, L., 2004. The use of Spanish and British documentary sources in the investigation of Atlantic hurricanes in historical times. In: Murnane, R., Liu, K.-B. (Eds.), Hurricanes: Present and Past. Columbia University Press, New York, pp. 149–176.

García-Herrera, R., Gimeno, L., Ribera, P., Hernández, E., 2005. New records of Atlantic hurricanes from Spanish documentary sources. J. Geophys. Res. Atmos. 110, D03109. dx.doi.org/10.1029/2004JD005272.

García-Herrera, R., Gimeno, L., Ribera, P., Hernández, E., González, E., Fernández, G., 2007. Identification of Caribbean basin hurricanes from Spanish documentary sources. Clim. Change 83, 55–85.

García-Herrera, R., Barriopedro, D., Hernández, E., Diaz, H.F., Garcia, R.R., Prieto, M.R., Moyano, R., 2008. A chronology of El Niño events from primary documentary sources in northern Peru. J. Clim. 21, 1948–1962.

Gardner, J.V., 1975. Late Pleistocene carbonate dissolution cycles in the eastern Equatorial Atlantic. In: Sliter, W.V., Bé, A.W.H., Berger, W.H. (Eds.), Dissolution of Deep-sea Carbonates. Special Publication No. 13, Cushman Foundation for Foraminiferal Research, Washington, DC, pp. 129–141.

Gasse, F., Fontes, J.C., Plaziat, J.C., Carbonel, P., Maczmarska, I., De Decker, P., Soulie-Marsche, I., Callot, Y., Dupeuple, P.A., 1987. Biological remains, geochemistry and stable isotopes for the reconstruction of environmental and hydrological changes in the Holocene lakes from North Sahara. Palaeogeogr. Palaeoclimatol. Palaeoecol. 60, 1–46.

Gasse, F., Barker, P., Gell, P.A., Fritz, S.C., Chalié, F., 1997. Diatom-inferred salinity in palaeolakes: an indirect tracer of climate change. Quat. Sci. Rev. 16, 547–563.

Gates, W.L., 1976. The numerical simulation of ice-age climate with a global general circulation model. J. Atmos. Sci. 33, 1844–1873.

Gaudreau, D.C., Jackson, S.T., Webb III, T., 1989. Spatial scale and sampling strategy in paleoecological studies of vegetation patterns in mountainous terrain. Acta Bot. Neerlandica. 38, 369–390.

Ge, Q.S., Zheng, J.Y., Fang, X.Q., Man, Z.M., Zhang, X.Q., Zhang, P.Y., Wang, W.C., 2003. Winter half-year temperature reconstruction for the middle and lower reaches of the Yellow River and Yangtze River, China, during the past 2000 years. The Holocene. 13, 933–940.

Ge, Q.S., Zhang, J.Y., Hao, Z.X., Zhang, P.Y., Wang, W.C., 2005. Reconstruction of historical climate in China: high-resolution precipitation data from Qing Dynasty archives. Bull. Am. Meteorol. Soc. 86, 671–679.

Ge, Q.S., Zheng, J.Y., Hao, Z.X., Shao, X.M., Wang, W.C., Luterbacher, J., 2010. Temperature variation through 2000 years in China: an uncertainty analysis of reconstruction and regional difference. Geophys. Res. Lett. 37. L03703. dx.doi.org/10.1029/2009GL041281.

Gehrels, A., Newnham, R.M., Lowe, D.J., Wynne, S., Hazell, Z.J., Caseldine, C., 2008. Towards rapid assay of cryptotephra in peat cores: review and evaluation of various methods. Quat. Int. 178, 68–84.

Geitzenauer, K.R., Roche, M.B., Mcintyre, A., 1976. Modern Pacific coccolith assemblages: derivation and application to late Pleistocene paleotemperature analysis. In: Cline, R.M., Hays, J.D. (Eds.), Investigation of Late Quaternary Paleooceanography and Paleoclimatology. Memoir 145, Geological Society of America, Boulder, pp. 423–448.

Genthon, C., Barnola, J.M., Raynaud, D., Lorius, C., Jouzel, J., Barkov, N.L., Korotkevich, Y.S., Kotlyakov, V.M., 1987. Vostok ice core: climatic response to CO_2 and orbital forcing changes over the last climatic cycle. Nature. 329, 414–418.

Genty, D., Baker, A., Vokal, B., 2001. Intra- and inter-annual growth rate of modern stalagmites. Chem. Geol. 176, 191–212.

Geyh, M.A., Schleicher, H., 1990. Absolute Age Determination: Physical and Chemical Dating Methods and Their Application. Springer-Verlag, Berlin.

Gherardi, J.M., Labeyrie, L., Nave, S., François, R., McManus, J.F., Cortijo, E., 2009. Glacial-interglacial circulation changes inferred from $^{231}Pa/^{230}Th$ sedimentary record in the North Atlantic region. Paleoceanography. 24. PA2204. dx.doi.org/10.1029/2008PA001696.

Gildor, H., Tziperman, E., 2000. Sea ice as the glacial cycles climate switch: role of seasonal and orbital forcing. Paleoceanography. 15, 605–615.

Gildor, H., Tziperman, E., 2003. Sea-ice switches and abrupt climate change. Philos. Trans. R. Soc. Lond. Ser. A. 361, 1935–1944.

Gillot, P.Y., Labeyrie, J., Laj, C., Valladas, G., Guerin, G., Poupeau, G., Delibrias, G., 1979. Age of the Laschamp paleomagnetic excursion revisited. Earth Planet. Sci. Lett. 42, 444–450.

Girardeau, J., Luc, B., 2007. Coccolithophores: from extant populations to fossil assemblages. In: Hillaire-Marcel, C., de Vernal, A. (Eds.), Proxies in Late Cenozoic Paleoceanography. Elsevier, Amsterdam, pp. 409–440.

Giresse, P., Maley, J., Brenac, P., 1994. Late Quaternary palaeoenvironments in the Lake Barombi Mbo (West Cameroon) deduced from pollen and carbon isotopes of organic matter. Palaeogeogr. Palaeoclimatol. Palaeoecol. 107, 65–78.

Giry, C., Felis, T., Kölling, M., Scheffers, S., 2010. Geochemistry and skeletal structure of *Diploria strigosa*, implications for coral-based climate reconstruction. Palaeogeography, Palaeoclimatology, Palaeoecology. 298, 378–387.

Giry, C., Felis, T., Kölling, M., Scholz, D., Wei, W., Lohmann, G., Scheffers, S., 2012. Mid- to late Holocene changes in tropical Atlantic temperature seasonality and interannual to multidecadal variability documented in southern Caribbean corals. Earth Planet. Sci. Lett. 331–332, 187–200.

Giry, C., Felis, T., Kölling, M., Wei, W., Lohmann, G., Scheffers, S., 2013. Controls of Caribbean surface hydrology during the mid- to late Holocene: insights from monthly resolved corals. Clim. Past. 9, 841–858.

Glaser, R., 2001. Klimageschichte Mitteleuropas. [Climate History of Central Europe]. Primus-Verlag, Darmstadt, 227 pp.

Glaser, R., Riemann, D., Schönbein, J., Barriendos, M., Brázdil, R., Bertolin, C., Camuffo, D., Deutsch, M., Dobrovolný, P., van Engelen, A., Enzi, S., Halíčková, M., Koenig, S.J., Kotzya, O., Limanówka, D., Macková, J., Sghedoni, M., Martin, B., Himmelsbach, I., 2010. The variability of European floods since A.D. 1500. Clim. Dyn. 101, 235–256.

Glock, W., 1937. Principles and Methods of Tree-Ring Analysis. Carnegie Institution, Washington, DC.

Godfrey-Smith, D.I., Huntley, D.J., Chen, W.H., 1988. Optical dating studies of quartz and feldspar sediment extracts. Quat. Sci. Rev. 7, 373–380.

Godwin, H., 1956. The History of the British Flora. Cambridge University Press, Cambridge.

Godwin, H., 1962. Half-life of radiocarbon. Nature. 195, 984.

Goetcheus, V.G., Birks, H.H., 2001. Full-glacial upland tundra vegetation preserved under tephra in the Beringia National Park, Seward Peninsula, Alaska. Quat. Sci. Rev. 20, 135–147.

Gonzales, L.M., Williams, J.M., Grimm, E.C., 2009. Expanded response-surfaces: a new method to reconstruct paleoclimates from fossil pollen assemblages that lack modern analogues. Quat. Sci. Rev. 28, 3315–3332.

Gooday, A., 2003. Benthic foraminifera (Protists) as tools in paleoceanography: environmental influences on faunal characteristics. Adv. Mar. Biol. 46, 1–90.
Goodfriend, G.A., 1991. Patterns of racemization and epimerization of amino acids in land snail shells over the course of the Holocene. Geochim. Cosmochim. Acta. 55, 293–302.
Goodfriend, G.A., 1992. Rapid racemization of aspartic acid in molluscan shells and potential for dating over recent centuries. Nature. 357, 399–401.
Goodfriend, G.A., Meyer, V.R., 1991. A comparative study of the kinetics of amino acid racemization/epimerization in fossil and modern mollusk shells. Geochim. Cosmochim. Acta. 55, 3355–3367.
Goodfriend, G.A., Hare, P.E., Druffel, E.R.M., 1992. Aspartic acid racemization and protein diagenesis in corals over the last 350 years. Geochim. Cosmochim. Acta. 56, 3847–3850.
Goodfriend, G.A., Brigham-Grette, J., Miller, G.H., 1996. Enhanced age resolution of the marine Quaternary record in the Arctic using aspartic acid racemization dating of bivalve shells. Quat. Res. 45, 176–187.
Goodkin, N.F., Hughen, K., Cohen, A.C., Smith, S.R., 2005. Record of Little Ice Age sea surface temperatures at Bermuda using a growth-dependent calibration of coral Sr/Ca. Paleoceanography. 20. PA4016. dx.doi.org/10.1029/2005PA001140.
Goodkin, N.F., Hughen, K.A., Cohen, A.L., 2007. A multicoral calibration method to approximate a universal equation relating Sr/Ca and growth rate to sea surface temperature. Paleoceanography. 22. PA1214. dx.doi.org/10.1029/2006PA001312.
Goodkin, N.F., Hughen, K.A., Curry, W.B., Doney, S.C., Ostermann, D.R., 2008. Sea surface temperature and salinity variability at Bermuda during the end of the Little Ice Age. Paleoceanography. 23. PA3203. dx.doi.org/10.1029/2007PA001532.
Goodkin, N.F., Druffel, E.R.M., Hughen, K.A., Doney, S.C., 2012. Two centuries of limited variability in subtropical North Atlantic thermocline variability. Nat. Commun. 3. dx.doi.org/10.1038/ncomms1811.
Goosse, H., Renssen, H., Timmermann, A., Bradley, R.S., 2005. Internal and forced climate variability during the last millennium: a model-data comparison using ensemble simulations. Quat. Sci. Rev. 24, 1345–1360.
Gordon, G.A., 1982. Verification of dendroclimatic reconstructions. In: Hughes, M.K., Kelley, P.M., Pilcher, J.R., LaMarche, V.C. (Eds.), Climate from Tree Rings. Cambridge University Press, Cambridge.
Gordon, A.D., Birks, H.J.B., 1974. Numerical methods in Quaternary paleoecology II. Comparison of pollen diagrams. New Phytol. 73, 221–249.
Gorman, M.K., Quinn, T.M., Taylor, F.W., Partin, J.W., Cabioch, G., Austin, J.A., Pelletier, B., Ballu, C., Maes, C., Saustrup, S., 2012. A coral-based reconstruction of sea surface salinity at Sabine Bank, Vanuatu from 1842 to 2007 CE. Paleoceanography. 27. dx.doi.org/10.1029/2012PA002302.
Goslar, T., Arnold, M., Bard, E., Kuc, T., Pazdur, M., Ralska-Jasiewiczowa, M., Rozanski, K., Tisnerat, N., Walanus, A., Wicik, B., Wieckowski, K., 1995. High concentration of atmospheric ^{14}C during the Younger Dryas cold episode. Nature. 377, 414–417.
Gow, A.J., Epstein, S., Sheehy, W., 1979. On the origin of stratified debris in ice cores from the bottom of the Antarctic Ice Sheet. J. Glaciol. 23, 185–192.
Gow, A.J., Meese, D.A., Alley, R.B., Fitzpatrick, J.J., Anandakrishnan, S., Woods, G.A., Elder, B.C., 1997. Physical and structural properties of the GISP2 ice core: a review. J. Geophys. Res. 102C, 26559–26575.
Graham, N.E., Ammann, C.M., Fleitmann, D., Cobb, K.M., Luterbacher, J., 2011. Support for global climate reorganization during the "Medieval Climate Anomaly. Clim. Dyn. 37, 1217–1245.
Grant, K.M., Rohling, E.J., Bar-Matthews, M., Ayalon, A., Medina-Elizalde, M., Bronk Ramsey, C., Satow, C., Roberts, A.P., 2012. Rapid coupling between ice volume and polar temperature over the past 150,000 years. Nature. 491, 744–747.
Grant-Taylor, T.L., 1972. Conditions for the use of calcium carbonate as a dating material. In: Proceedings of the 8th International Conference on Radiocarbon Dating, vol. 2. Royal Society of New Zealand, Wellington, pp. 592–596.
Gray, B.M., 1974. Early Japanese winter temperatures. Weather. 29, 103–107.
Gray, J., Thompson, P., 1978. Climatic interpretation of $\delta^{18}O$ and δD in tree rings. Nature. 271, 93–94.
Greer, L., Swart, P.K., 2006. Decadal cyclicity of regional mid-Holocene precipitation: evidence from Dominican coral proxies. Paleoceanography. 21. PA2020. dx.doi.org/10.1029/2005PA001166.
Grichuk, V.P., 1969. An attempt to reconstruct certain elements of the climate of the northern hemisphere in the Atlantic period of the Holocene. In: Neishtadt, M.I. (Ed.), Golotsen.8th INQUA Congress, Izd-vo Nauka,

Moscow, pp. 41–57 (in Russian; translated by Peterson, G.M. Center for Climatic Research, University of Wisconsin, Madison).
Griffey, N.J., Matthews, J.A., 1978. Major neoglacial glacier expansion episodes in southern Norway: evidence from moraine ridge stratigraphy with ^{14}C dates on buried palaeosols and moss layers. Geogr. Ann. 60A, 73–90.
Griffiths, M.L., Drysdale, R.N., Gagan, M.K., Zhao, J.X., Ayliffe, L.K., Hellstrom, J.C., Hantoro, W.S., Frisia, S., Feng, Y.X., Cartright, I., St Pierre, E., Fisher, M.J., Suwargardi, B.W., 2009. Increasing Australian-Indonesian monsoon rainfall linked to early Holocene sea-level rise. Nat. Geosci. 2, 636–639.
Grimm, E.C., Jacobson Jr., G.L., Watts, W.A., Hansen, B.C.S., Maasch, K.A., 1993. A 50,000-year record of climate oscillations from Florida and its temporal correlation with the Heinrich events. Science. 261, 198–200.
Grimmer, M., 1963. The space-filtering of monthly surface temperature data in terms of pattern, using empirical orthogonal functions. Quart. J. Roy. Meteorol. Soc. 39, 395–408.
Groisman, P.Ya., 1992. Possible regional climatic consequences of Pinatubo eruption. Geophys. Res. Lett. 19, 1603–1606.
Groisman, P.Ya., Karl, T.R., Wright, R.W., 1994a. Observed impact of snow cover on the heat balance and the rise of continental spring temperatures. Science. 263, 198–200.
Groisman, P.Ya., Karl, T.R., Wright, R.W., Stenchikov, G.L., 1994b. Changes of snow cover, temperature and the radiative heat balance over the northern hemisphere. J. Clim. 7, 1633–1656.
Grönvald, K., Óskarsson, N., Johnsen, S.J., Clausen, H.B., Hammer, C.U., Bond, G., Bard, E., 1995. Ash layers from Iceland in the Greenland GRIP ice core correlated with oceanic and land sediments. Earth Planet. Sci. Lett. 135, 149–155.
Groot, M.H.M., Bogota, R.G., Lourens, L.J., Hooghiemstra, H., Vriend, M., Berrio, J.C., Tuenter, E., Van der Plicht, J., Van Geel, B., Ziegler, M., Weber, S.L., Betancourt, A., Contreras, L., Gaviria, S., Giraldo, C., Gonzalez, N., Jansen, J.H.F., Konert, M., Ortega, D., Rangel, O., Sarmiento, G., Vandenberghe, J., Van der Hammen, T., Van der Linden, M., Westerhoff, W., 2011. Ultra-high resolution pollen record from the northern Andes reveals rapid shifts in montane climates within the last two glacial cycles. Clim. Past. 7, 299–316.
Grootes, P.M., Stuiver, M., Thompson, L.G., Mosley-Thompson, E., 1989. Oxygen isotope changes in tropical ice, Quelccaya, Peru. J. Geophys. Res. 94D, 1187–1194.
Grootes, P.M., Stuiver, M., White, J.W.C., Johnsen, S., Jouzel, J., 1993. Comparison of oxygen isotope records from the GISP2 and GRIP Greenland ice cores. Nature. 366, 552.
Grosjean, M., Veit, H., 2005. Water resources in the arid mountains of the Atacama Desert (Northern Chile): past climate changes and modern conflicts. In: Huber, U.M., Bugmann, H.K.M., Reasoner, M.A. (Eds.), Global Change and Mountain Regions. Springer, Dordrecht, pp. 93–104.
Grossman, E.L., 1987. Stable isotopes in benthic foraminifera: a study of vital effect. J. Foram. Res. 17, 48–61.
Grottoli, A.G., Eakin, C.M., 2007. A review of modern coral $\delta^{18}O$ and $\Delta^{14}C$ proxy records. Earth-Sci. Rev. 81, 67–91.
Grotzfeld, H., 1991. Klimageschichte des Vorderen Orients 800-1800 A.D. nach arabischen Quellen. Wiirzburger Geographische Arbeiten. 80, 21–43.
Grousset, F.E., Labeyrie, L., Sinko, J.A., Cremer, M., Bond, G., Duprat, J., Cortijo, E., Huon, S., 1993. Patterns of ice-rafted detritus in the glacial North Atlantic (40-55° N). Paleoceanography. 8, 175–192.
Grousset, F.E., Pujol, C., Labeyrie, L., Auffret, G., Boelaert, A., 2000. Were the North Atlantic Heinrich Events triggered by the behavior of the European ice sheets? Geology. 28, 123–126.
Grove, J.M., 1979. The glacial history of the Holocene. Prog. Phys. Geogr. 3, 1–54.
Grove, J.M., 1988. The Little Ice Age. Methuen, London.
Grove, J.M., 2001a. The onset of the Little Ice Age. In: Jones, P.D., Ogilvie, A.E.G., Davies, T.D., Briffa, K.R. (Eds.), History and Climate: Memories of the Future?. Kluwer, New York, pp. 153–185.
Grove, J.M., 2001b. The initiation of the "Little Ice Age" in regions round the North Atlantic. Clim. Chang. 48, 53–82.
Grove, A.T., Warren, A., 1968. Quaternary landforms and climate on the south side of the Sahara. Geogr. J. 134, 194–208.
Grove, C.A., Zinke, J., Peeters, F., Park, W., Scheufen, T., Kasper, S., Randriamanantsoa, B., McCulloch, M.T., Brummer, G.-J.A., 2013. Madagascar corals reveal a multidecadal signature of rainfall and river runoff since 1708. Clim. Past. 9, 641–656.
Guiot, J., 1987. Late Quaternary climatic change in France estimated from multivariate pollen time series. Quat. Res. 28, 100–118.
Guiot, J., 1990. Methodology of paleoclimatic reconstruction from pollen in France. Palaeogeogr. Palaeoclimatol. Palaeoecol. 80, 49–69.

Guiot, J., de Vernal, A., 2007. Transfer functions: methods for quantitative paloceanography based on microfossils. In: Hillaire-Marcel, C., de Vernal, A. (Eds.), Proxies in Late Cenozoic Paleoceanography. Elsevier, Amsterdam, pp. 523–563.
Guiot, J., Pons, A., de Beaulieu, J.L., Reille, M., 1989. A 140,000 year climatic reconstruction from two European pollen records. Nature. 338, 309–313.
Guiot, J., de Beaulieu, J.L., Reille, M., Pons, A., 1992. Calibration of the climatic signal in a new pollen sequence from La Grande Pile. Clim. Dyn. 6, 259–264.
Guiot, J., de Beaulieu, J.L., Cheddadi, R., David, F., Ponel, P., Reille, M., 1993. The climate in western Europe during the last Glacial/Interglacial cycle derived from pollen and insect remains. Palaeogeogr. Palaeoclimatol. Palaeoecol. 103, 73–93.
Guo, Q., 1992. Winter monsoon over East Asia during the Little Ice Age. In: Mikami, T. (Ed.), Proceedings of the International Symposium on the Little Ice Age Climate. Department of Geography, Tokyo Metropolitan University, Tokyo, pp. 227–232.
Guo, Z.T., Ruddiman, W.F., Hao, Q.Z., Wu, H.B., Qiao, Y.S., Zhu, R.X., Peng, S.Z., Wei, J.J., Yuan, B.Y., Liu, T.S., 2002. Onset of Asian desertification by 22 Myr ago inferred from loess deposit in China. Nature. 416, 159–163.
Guo, Z.T., Sun, B., Zhang, Z.S., Peng, S.Z., Xiao, G.Q., Ge, J.Y., Hao, Q.Z., Qiao, Y.S., Liang, M.Y., Liu, J.F., Yin, Q.Z., Wei, J.J., 2008. A major reorganization of Asian climate by the early Miocene. Clim. Past. 4, 153–174.
Gupta, A.K., Anderson, D.M., Overpeck, J.T., 2003. Abrupt changes in the Asian southwest monsoon during the Holocene and their links to the North Atlantic Ocean. Nature. 421, 354–357.
Gutjahr, M., Lippold, J., 2011. Early arrival of Southern Source Water in the deep North Atlantic prior to Heinrich event 2. Paleoceanography. 26. dx.doi.org/10.1029/2011PA002114.
Guyodo, Y., Valet, J.-P., 1999. Global changes in intensity of the Earth's magnetic field during the past 800 kyr. Nature. 399, 249–252.
Gwiazda, R.H., Hemming, S.R., Broecker, W.S., 1996a. Tracking the sources of icebergs with lead isotopes: the provenance of ice-rafted debris in Henrich layer 2. Paleoceanography. 11, 77–93.
Gwiazda, R.H., Hemming, S.R., Broecker, W.S., 1996b. Provenance of icebergs during Heinrich event 3 and the contrast to their sources during other Heinrich episodes. Paleoceanography. 11, 371–378.
Haase, D., Fink, J., Haase, G., Ruske, R., Pécsi, M., Richter, H., Altermann, M., Jäger, K.-D., 2007. Loess in Europe—its spatial distribution based on a European Loess Map, scale 1:2,500,000. Quat. Sci. Rev. 26, 1301–1312.
Haase-Schramm, A., Böhm, F., Eisenhauer, A., Dullo, W.-C., Joachimski, M.M., Hansen, B., Reitner, J., 2003. Sr/Ca ratios and oxygen isotopes from sclerosponges: temperature history of the Caribbean mixed layer and thermocline during the Little Ice Age. Paleoceanography. 18, dx.doi.org/10.1029/2002PA000830.
Haberle, S., 1997. Late Quaternary vegetation and climate history of the Amazon Basin: correlating marine and terrestrial pollen records. In: Flood, R.D., Piper, D.J.W., Klaus, A., Peterson, L.C. (Eds.), Proceedings of the Ocean Drilling Program, Scientific Results, vol. 155. pp. 381–396.
Haesaerts, P., 1974. Séquence paléoclimatique du Pléistocène supérieur du bassin de la Haine (Belgique). Ann. Soc. Géol. Belg. 97, 105–137.
Haffer, J., 1969. Speciation in Amazonian forest birds. Science. 165, 131–137.
Haffer, J., 1974. Avian speciation in tropical South America. Publication No. 14, Nuttall Ornithological Club, Cambridge, Massachusetts.
Haffer, J., 1982. General aspects of the refuge theory. In: Prance, G.T. (Ed.), Biological Diversification in the Tropics. Columbia University Press, New York, pp. 6–24.
Hagstrum, J.T., Blinman, E., 2010. Archeomagnetic dating in western North America: an updated reference curve based on paleomagnetic and archeomagnetic data sets. Geochem. Geophys. Geosyst. 11, Q06009. dx.doi.org/10.1029/2009GC002979.
Haigh, J.D., 1996. The impact of solar variability on climate. Science. 272, 981–984.
Haigh, J.D., 2005. The Earth's climate and its response to solar variability. In: Haigh, J.D., Lockwood, M., Giampapa, M.S. (Eds.), The Sun, Solar Analogs and the Climate. Springer, Berlin, pp. 1–107.
Halme, E., 1952. On the influence of climatic variation on fish and fishery. Fennia. 75, 89–96.
Hamilton, A.C., 1976. The significance of patterns of distribution shown by forest plants and animals in tropical Africa for the reconstruction of upper Pleistocene palaeoenvironments: a review. Palaeoecol. Afr. 9, 63–97.
Hamilton, A.C., Perrott, R.A., 1979. Aspects of the glaciation of Mt Elgon, East Africa. Palaeoecol. Afr. 11, 153–162.

Hamilton, A.C., Perrott, R.A., 1980. Modern pollen deposition on a tropical African mountain. Pollen Spores. 22, 437–468.
Hammer, C.U., 1977. Past volcanism revealed by Greenland ice sheet impurities. Nature. 270, 482–486.
Hammer, C.U., 1980. Acidity of polar ice cores in relation to absolute dating, past volcanism and radio echoes. J. Glaciol. 25, 359–372.
Hammer, C.U., 1984. Traces of Icelandic eruptions in the Greenland ice sheet. Jökull. 34, 51–65.
Hammer, C.U., 1989. Dating by physical and chemical seasonal variations and reference horizons. In: Oeschger, H., Langway Jr., C.C. (Eds.), The Environmental Record in Glaciers and Ice Sheets. Wiley, Chichester, pp. 99–121.
Hammer, C.U., Clausen, H.B., Dansgaard, W., Gundestrup, N., Johnsen, S.J., Reeh, N., 1978. Dating of Greenland ice cores by flow models, isotopes, volcanic debris and continental dust. J. Glaciol. 20, 3–26.
Hammer, C.U., Clausen, H.B., Dansgaard, W., 1980. Greenland ice sheet evidence of post-glacial volcanism and its climatic impact. Nature. 288, 230–255.
Hammer, C.U., Clausen, H.B., Langway Jr., C.C., 1997. 50,000 years of recorded global volcanism. Clim. Chang. 35, 1–15.
Hann, B.J., Walker, B.G., Warwick, W.F., 1992. Aquatic invertebrates and climate change: a comment on Walker *et al.* 1991. Can. J. Fish. Aquat. Sci. 49, 1274–1276 (see also, Reply, 1276–1280).
Hannon, G.E., Gaillard, M.-J., 1997. The plant-macrofossil record of past lake-level changes. J. Paleolimnol. 18, 15–28.
Hansen, J.E., Lacis, A., Rind, D., Russell, G., Stone, P., Fung, I., Ruedy, R., Lerner, J., 1984. Climate sensitivity: analysis of feedback mechanisms. In: Hansen, J.E., Takahashi, T. (Eds.), Climate Processes and Sensitivity. American Geophysical Union, Washington, DC, pp. 130–163.
Hansen, J.E., et al., 1996. A Pinatubo climate modelling investigation. In: Fiocco, G., Fina, D., Visconti, G. (Eds.), The Mount Pinatubo Eruption: Effects on the Atmosphere and Climate. Springer-Verlag, New York.
Hansen, J., Ruedy, R., Sato, M., Lo, K., 2012. Global surface temperature change. Rev. Geophys. 48, RG4004. dx.doi.org/10.1029/2010RG000345.
Haq, B.U., 1978. Calcareous nannoplankton. In: Haq, B.U., Boersma, A. (Eds.), Introduction to Marine Micropaleontology. Elsevier/North Holland, New York, pp. 79–107.
Haq, B.U., Boersma, A. (Eds.), 1978. Introduction to Marine Micropaleontology. Elsevier/North Holland, New York.
Hardy, D.R., 2011. Kilimanjaro. In: Singh, V.P., Singh, P., Haritashya, U.K. (Eds.), Encyclopedia of Snow, Ice and Glaciers. Springer, Dordrecht, pp. 672–679.
Hare, F.K., 1979. Climatic variation and variability: empirical evidence from meteorological and other sources. In: Proceedings of World Climate Conference. Publication No. 537 World Meteorological Organization, Geneva, pp. 51–87.
Hare, S.R., Mantua, N.J., 2000. Empirical evidence for North Pacific regime shifts in 1977 and 1989. Prog. Oceanogr. 47, 103–146.
Hare, P.E., Mitterer, R.M., 1968. Laboratory simulation of amino acid diagenesis in fossils. Carnegie Inst. Wash. Yearbook. 67, 205–208.
Harington, C.R. (Ed.), 1992. 1816. The Year Without a Summer? Canadian Museum of Nature, Ottawa.
Harland, W.B., Armstrong, R.L., Cox, A.V., Craig, L.E., Smith, A.G., Smith, D.G., 1990. A Geologic Time Scale 1989. Cambridge University Press, Cambridge.
Harmon, R.S., Thompson, P., Schwarcz, H.P., Ford, D.C., 1975. Uranium-series dating of speleothems. National Speleological Society Bulletin. 37, 21–33.
Harmon, R.S., Ford, D.C., Schwarcz, H.P., 1977. Interglacial chronology of the Rocky and Mackenzie mountains based on ^{230}Th and ^{234}U dating of calcite speleothems. Can. J. Earth Sci. 14, 2543–2552.
Harmon, R.S., Thompson, P., Schwarcz, H.P., Ford, D.C., 1978a. Late Pleistocene paleoclimates of North America as inferred from stable isotope studies of speleothems. Quat. Res. 9, 54–70.
Harmon, R.S., Schwarcz, H.P., Ford, D.C., 1978b. Late Pleistocene sea level history of Bermuda. Quat. Res. 9, 205–218.
Harmon, R.S., Schwarcz, H.P., O'Neil, J.R., 1979. D/H ratios in speleothem fluid inclusions: a guide to variations in the isotopic composition of meteoric precipitation? Earth Planet. Sci. Lett. 41, 254–266.
Harper, F., 1961. Changes in climate, faunal distribution and life zones in the Ungava Peninsula. Polar Notes. 20–41, Dartmouth College, N.H. No. III.
Harrison, S.P., 1989. Lake-levels and climatic changes in eastern North America. Clim. Dyn. 3, 157–167.
Harrison, S.P., 1993. Late Quaternary lake-level changes and climates of Australia. Quat. Sci. Rev. 12, 211–231.

Harrison, S.P., Digerfeldt, G., 1993. European lakes as palaeohydrological and palaeoclimatic indicators. Quat. Sci. Rev. 12, 233–248.
Harrison, S.P., Tarasov, P.E., 1996. Late Quaternary lake-level records from northern Eurasia. Quat. Res. 45, 138–159.
Harrison, S.P., Yu, Ge, Tarasov, P.E., 1996. Late Quaternary lake-level record from northern Eurasia. Quat. Res. 45, 138–159.
Harrison, S.P., Prentice, I.C., Barboni, D., Kohfeld, J.E., Ni, J., Sutra, J.-P., 2009. Ecophysiological and bioclimatic foundations for a global plant functional classification. J. Veg. Sci. 21, 30–317.
Hastenrath, S., 1967. Observations on the snow line in the Peruvian Andes. J. Glaciol. 6, 541–550.
Hastenrath, S., 1971. On the Pleistocene snow line depression in the arid regions of the South American Andes. J. Glaciol. 10, 255–267.
Hastenrath, S., Kruss, P.D., 1992. The dramatic retreat of Mount Kenya's glaciers 1963-87: greenhouse forcing. Ann. Glaciol. 16, 127–133.
Haug, G.H., Hughen, K.A., Sigman, D.M., Peterson, L.C., Röhl, U., 2001. Southward migration of the Intertropical Convergence Zone through the Holocene. Science. 293, 1304–1308.
Haug, G.H., Gunther, D., Peterson, L.C., Sigman, D.M., Hughen, K.A., Aeschlimann, B., 2003. Climate and the collapse of Maya civilization. Science. 299, 1731–1735.
Haug, G.H., Ganopolski, A., Sigman, D.M., Rosell-Melé, A., Swann, G.E., Tiedemann, R., Jaccard, S.L., Bollman, J., Maslin, M.A., Leng, M.J., Eglinton, G., 2005. North Pacific seasonality and the glaciation of North America 2.7 million years ago. Nature. 433, 821–825.
Hay, W.W., 1974. Introduction. In: Hay, W.W. (Ed.), Studies in Paleoceanography. Special Publication No. 20Society of Economic Paleontologists and Mineralogists, Tulsa, pp. 1–5.
Hay, W.H., 1993. The role of polar deep water formation in global climate change. Annu. Rev. Earth Planet. Sci. 21, 227–254.
Hays, J.D., Imbrie, J., Shackleton, N.J., 1976. Variations in the earth's orbit: pacemaker of the ice ages. Science. 194, 1121–1132 (see also Science 198, 528–530).
Head, M.J., Gibbard, P., Salvador, A., 2008. The Quaternary: its character and definition. Episodes. 38 (31), 234–238.
Hecht, A., 1973. A model for determining Pleistocene paleotemperatures from planktonic foraminiferal assemblages. Micropalaeontology. 19, 68–77.
Hecht, A.D., Savin, S.M., 1970. Oxygen-18 studies of recent planktonic foraminifera: comparisons of phenotypes and of test parts. Science. 170, 69–71 (see also Science 173, 167–169).
Hecht, A.D., Savin, S.M., 1972. Phenotypic variation and oxygen isotope ratios in recent planktonic foraminifera. J. Foram. Res. 2, 55–67.
Hecht, A., Barry, R.G., Fritts, H.C., Imbrie, J., Kutzbach, J., Mitchell Jr., J.M., Savin, S.M., 1979. Paleoclimatic research: status and opportunities. Quat. Res. 12, 6–17.
Heinrich, M., 1988. Origin and consequences of cyclic ice rafting in the northeast Atlantic Ocean during the past 130,000 years. Quat. Res. 29, 143–152.
Heller, F., Liu, T., 1984. Magnetism of Chinese loess deposits. Geophys. J. Roy. Astron. Soc. 77, 125–141.
Heller, F., Shen, C.-D., Beer, J., Liu, X.-M., Liu, T.-S., Bronger, A., Suter, M., Bonani, G., 1993. Quantitative estimates of pedogenic ferromagnetic mineral formation in Chinese loess and paleoclimatic implications. Earth Planet. Sci. Lett. 114, 385–390.
Helsen, M.M., van de Wal, R.S.W., van den Broeke, M.R., 2007. The isotopic composition of present-day Antarctic snow in a Lagrangian atmospheric simulation. J. Clim. 20, 739–756.
Hemming, S., 2004. Heinrich events: massive Late Pleistocene detritus layers of the North Atlantic and their global climate impact. Rev. Geophys. 42, RG1005.
Hendy, C., 1971. The isotopic geochemistry of speleothems: I. The calculation of the effects of different modes of formation on the isotopic composition of speleothems and their applicability as paleoclimatic indicators. Geochim. Cosmochim. Acta. 35, 801–824.
Hendy, E.J., Gagan, M.K., Alibert, C.A., McCulloch, M.T., Lough, J.M., Isdale, P.J., 2002. Abrupt decrease in tropical Pacific sea surface salinity at the end of the Little Ice Age. Science. 295, 1511–1514.
Hendy, E.J., Gagan, M.K., Lough, J.M., 2003. Chronological control of coral records using luminescent lines and evidence for non-stationary ENSO teleconnections in northeast Australia. The Holocene. 13, 187–199.

Henfling, E., Pflaubaum, H., 1991. Neue Aspekte zur klimatischen Interpretation der hohen pharaonischen Nilflutmarken am 2. Katarakt aus ägyptologischer und geomorphologischer Sicht. Würzburger Geographische Arbeiten. 80, 87–109.
Herbert, T.D., 2003. Alkenone paleotemperature determinations. In: Elderfield, H., Turekian, K.K. (Eds.), Treatise in Marine Geochemistry. Elsevier, Amsterdam, pp. 391–432.
Herbert, T.D., Peterson, L.C., Lawrence, K.T., Liu, Z., 2010. Tropical ocean temperatures over the past 3.5 million years. Science. 328, 1530–1534.
Hereid, K.A., Quinn, T.M., Taylor, F.W., Shen, C.-C., Edwards, R.L., Cheng, H., 2012. Coral record of reduced El Niño activity in the early 15th to middle 17th century. Geology. 41, 51–54.
Hereid, K.A., Quinn, T.M., Okumura, Y.M., 2013. Assessing spatial variability in El Niño-Southern Oscillation event detection skill using coral geochemistry. Paleoceanography. 28, 14–23.
Herfort, L., Schouten, S., Boon, J.P., Sinninghe Damsté, J.S., 2006. Application of the TEX_{86} temperature proxy to the southern North Sea. Org. Geochem. 37, 1715–1726.
Herron, S., Langway Jr., C.C., 1979. The debris-laden ice at the bottom of the Greenland Ice Sheet. J. Glaciol. 23, 193–207.
Herron, M.M., Langway, C.C., 1980. Firn densification: an empirical model. J. Glaciol. 25, 373–386.
Herweijer, C., Seager, R., Cook, E.R., Emile-Geay, E., 2007. North American droughts of the last millennium from a gridded network of tree-ring data. J. Clim. 20, 1353–1376.
Hesse, P.P., 1994. The record of continental dust from Australia in Tasman Sea sediments. Quat. Sci. Rev. 13, 257–272.
Hicks, S., 2001. The use of annual arboreal pollen deposition values for delimiting tree-lines in the landscape and exploring models of pollen dispersal. Rev. Palaeobot. Palynol. 117, 1–29.
Hilgen, F.J., 1991. Astronomical calibration of Gauss to Matuyama sapropels in the Mediterranean and implications for the geomagnetic polarity time scale. Earth Planet. Sci. Lett. 104, 226–244.
Hodell, D.A., Curtis, J.H., Brenner, M., 1995. Possible role of climate in the collapse of Classic Maya civilization. Nature. 375, 391–394.
Hodell, D.A., Brenner, M., Curtis, J.H., Guilderson, T., 2001. Solar forcing of drought frequency in the Maya Lowlands. Science. 292, 1367–1370.
Hodell, D.A., Brenner, M., Curtis, J.H., 2005. Terminal Classic drought in the northern Maya lowlands inferred from multiple sediment cores in Lake Chichancanab (Mexico). Quat. Sci. Rev. 24, 1413–1427.
Hodell, D.A., Channell, J.E.T., Curtis, J.H., Romero, O.E., Röhl, U., 2008a. Onset of "Hudson Strait" Heinrich events in the eastern North Atlantic at the end of the middle Pleistocene transition (~640ka)? Paleoceanography. 23. PA4218. dx.doi.org/10.1029/2008PA001591.
Hodell, D.A., Anselmetti, F.S., Ariztegui, D., Brenner, M., Curtis, J.H., Gilli, A., Grzesik, D.A., Guilderson, T.J., Müller, A.D., Bush, M.B., Correa-Metrio, A., Escobar, J., Kutterolf, S., 2008b. An 85-ka record of climate change in lowland Central America. Quat. Sci. Rev. 27, 1152–1165.
Hoelzmann, P., Jolly, D., Harrison, S.P., Laarif, F., Bonnefille, R., Pachur, H.-J., 1998. Mid-Holocene land-surface conditions in northern Africa and the Arabian Peninsula: a data set for the analysis of biogeophysical feedbacks in the climate system. Glob. Biogeochem. Cycles. 12, 35–51.
Hoelzmann, P., Gasse, F., Dupont, L.M., Salzmann, U., Staubwasser, M., Leuschner, D.C., Sirocko, F., 2004. Palaeoenvironmental changes in the arid and subarid belt (Sahara-Sahel-Arabian Peninsula) from 150kyr to present. In: Battarbee, R.W., Gasse, F., Stickley, C.E. (Eds.), Past Climate Variability through Europe and Africa. Springer, Berlin, pp. 219–256.
Hoffsummer, P., 1996. Dendrochronology and the study of roof-framing in Belgium. In: Dean, J.S., Meko, D.M., Swetnam, T.W. (Eds.), Tree Rings, Environment and Humanity. University of Arizona, Tucson, pp. 525–531.
Hofmann, W., 1986. Chironomid analysis. In: Berglund, B.E. (Ed.), Handbook of Holocene Palaeoecology and Palaeohydrology. Wiley, Chichester, pp. 715–727.
Hoganson, J.W., Ashworth, A.C., 1992. Fossil beetle evidence for climatic change, 18,000-10,000 years B.P. in south-central Chile. Quat. Res. 37, 101–116.
Hogg, A., Lowe, D.J., Palmer, J., Boswijk, G., Bronk Ramsey, C., 2011. Revised calendar date for the Taupo eruption derived by ^{14}C wiggle-matching using a New Zealand kauri ^{14}C calibration data set. The Holocene. 22, 439–449.
Hoinkes, H.C., 1968. Glacier variation and weather. J. Glaciol. 7, 3–19.

Holdsworth, G., Peake, E., 1985. Acid content of snow from a mid-troposphere sampling site on Mount Logan, Yukon Territory, Canada. Ann. Glaciol. 7, 153–160.
Hollin, J.T., Schilling, D.H., 1981. Late Wisconsin-Weichselian mountain glaciers and small ice caps. In: Denton, G.H., Hughes, T.J. (Eds.), The Last Great Ice Sheets. Wiley, New York, pp. 179–206.
Holmes, R.L., 1983. Computer-assisted quality control in tree-ring dating and measurement. Tree-Ring Bull. 44, 69–75.
Holmes, P.L., 1994. The sorting of spores and pollen by water: experimental and field evidence. In: Traverse, A. (Ed.), Sedimentation of Organic Particles. Cambridge University Press, Cambridge, pp. 9–32.
Holmes, J.A., 1996. Trace-element and stable-isotope geochemistry of non-marine ostracod shells in Quaternary paleoenvironmental reconstruction. J. Paleolimnol. 15, 223–225.
Holmes, J.A., 1998. A late Quaternary ostracod record from Wallywash Great Pond, a Jamaican marl lake. J. Paleolimnol. 19, 115–128.
Holmes, J.A., 2001. Ostracoda. In: Smol, J.P., Birks, H.J.B., Last, W.M. (Eds.), Tracking Environmental Change Using Lake sediments, vol. 4. Kluwer Academic, Dordrecht, pp. 125–151.
Holmes, J.A., Engstrom, D.R., 2003. Non-marine ostracod records of Holocene environmental change. In: Mackay, A., Battarbee, R., Birks, H.J.B., Oldfield, F. (Eds.), Global Change in the Holocene. Arnold, London, pp. 310–327.
Holmes, J.A., Street-Perrott, F.A., Allen, M.J., Fothergill, P.A., Harkness, D., Kroon, D., Perrott, R.A., 1997. Holocene paleolimnology of Kajemarum Oasis, northern Nigeria: an isotopic study of ostracodes, bulk carbonate and organic carbon. J. Geol. Soc. 154, 311–319.
Holt, K., Allen, G., Hodgson, R., Marsland, S., Flenley, J., 2011. Progress towards an automated trainable pollen location and classifier system for use in the palynology laboratory. Rev. Palaeobot. Palynol. 167, 175–183.
Holtmeier, F.-K., 1994. Ecological aspects of climatically-caused timberline fluctuations. In: Beniston, M. (Ed.), Mountain Environments in Changing Climates. Routledge, London, pp. 220–233.
Holtmeier, F.-K., 2000. Mountain Timberlines. Kluwer, Dordrecht, 369 pp.
Holzer, M., Primeau, F.W., 2006. The diffusive ocean conveyor. Geophys. Res. Lett. 33. dx.doi.org/10.1029/2006GL026232.
Holzkamper, S., Spötl, C., Mangini, A., 2005. High-precision constraints on timing of Alpine warm periods during the middle to late Pleistocene using speleothem growth periods. Earth Planet. Sci. Lett. 236, 751–764.
Hooghiemstra, H., 1984. Vegetational and climatic history of the high plain of Bogota, Colombia: a continuous record of the last 3.5 million years. Dissertationes Botanicae No. 79, J. Cramer, Vaduz.
Hooghiemstra, H., Ran, E.T.H., 1994. Pliocene-Pleistocene high resolution pollen sequence of Colombia: an overview of climatic change. Quat. Int. 21, 63–80.
Hooghiemstra, H., van Geel, B., 1998. World list of pollen and spore atlases. Rev. Palaeobot. Palynol. 104, 157–182.
Hooghiemstra, H., Stalling, H., Agwu, C.O.C., Dupont, L.M., 1992. Vegetational and climatic changes at the northern fringe of the Sahara 250,000-5,000 years B.P.: evidence from 4 marine pollen records located between Portugal and the Canary Islands. Rev. Palaeobot. Palynol. 74, 1–53.
Hooghiemstra, H., Melice, J.L., Berger, A., Shackleton, N.J., 1993. Frequency spectra and paleoclimatic variability of the high resolution 30-1450 kyr Funza I pollen record (eastern Cordillera, Colombia). Quat. Sci. Rev. 12, 141–156.
Hopmans, E.C., Weijers, J.W.H., Schefuss, E., Herfort, L., Sinninghe Damsté, J.S., Schouten, S., 2004. A novel proxy for terrestrial organic matter in sediments based on branched and isoprenoid tetraether lipids. Earth Planet. Sci. Lett. 224, 107–116.
Hörhold, M.W., Laepple, T., Freitag, J., Bigler, M., Fischer, H., Kipfstuhl, S., 2012. On the impact of impurities on the densification of polar firn. Earth Planet. Sci. Lett. 325–326, 93–99.
Hormes, A., Müller, B.U., Schlüchter, S., 2001. The Alps with little ice: evidence for eight Holocene phases of reduced glacier extent in the central Swiss Alps. The Holocene. 11, 255–264.
Hostetler, S.W., Giorgi, F., Bates, G.T., Bartlein, P.J., 1994. Lake-atmosphere feedbacks associated with paleolakes Bonneville and Lahontan. Science. 263, 665–668.
Hovan, S.A., Rea, D.K., Pisias, N.G., Shackleton, N.J., 1989. A direct link between the China loess and marine $\delta^{18}O$ records: aeolian flux to the north Pacific. Nature. 340, 296–298.
Hovan, S.A., Rea, D.K., Pisias, N.G., 1991. Late Pleistocene continental climate and oceanic variability recorded in Northwest Pacific sediments. Paleoceanography. 6, 349–370.
Howe, S.E., Webb III, T., 1983. Calibrating pollen data in climatic terms: improving the methods. Quat. Sci. Rev. 2, 17–51.
Hoyt, D.V., Schatten, K.H., 1997. The Role of the Sun in Climate Change. Oxford University Press, Oxford. 279 pp.

Hsu, H.H., Chen, Y.L., 2011. Decadal to bi-decadal rainfall variation in the western Pacific: a footprint of South Pacific decadal variability? Geophys. Res. Lett. 38. L03703. dx.doi.org/10.1029/2010GL046278.
Hu, A.X., Meehl, G.A., Han, W.Q., Timmermann, A., Otto-Bliesner, B., Liu, Z.Y., Washington, W.M., Large, W., Abe-Ouchi, A., Kimoto, M., Lambeck, K., Wu, B.Y., 2012. Role of the Bering Strait on the hysteresis of the ocean conveyor belt circulation and glacial climate stability. Proc. Natl. Acad. Sci. U. S. A. 109, 6417–6422.
Huang, Y., Shuman, B., Wang, Y., Webb III, T., 2004. Hydrogen isotope ratios of individual lipids in lake sediments as novel tracers of climatic and environmental change: a surface sediment test. J. Paleolimnol. 31, 363–375.
Huang, Y., Shuman, B., Wang, Y., Webb III, T., Grimm, E.C., Jacobson, J., 2006. Climatic and environmental controls on the variation of C3 and C4 plant abundances in central Florida for the past 62,000 years. Palaeogeogr. Palaeoclimatol. Palaeoecol. 237, 428–435.
Huber, B.T., McLeod, K.G., Wing, S.L., 2000. Warm Climates in Earth History. Cambridge University Press, Cambridge, UK, 465 pp.
Huber, C., Leuenberger, M., Spahni, R., Flückiger, J., Schwander, J., Stocker, T.F., Johnsen, S., Landais, A., Jouzel, J., 2006. Isotope calibrated Greenland temperature record over Marine Isotope Stage 3 and its relation to CH_4. Earth Planet. Sci. Lett. 243, 504–519.
Hughen, K.A., Overpeck, J.T., Peterson, L.C., Anderson, R.F., 1996. The nature of varved sedimentation in the Cariaco Basin, Venezuela and its paleoclimatic significance. In: Kemp, A.E.S. (Ed.), Palaeoclimatology and Palaeoceanography from Laminated Sediments. Special Publication No. 116, The Geological Society, London, pp. 171–183.
Hughen, K.A., Overpeck, J.T., Lehman, S.J., Kashgarian, M., Southon, J., Peterson, L.C., Alley, R., Sigman, D.M., 1998. Deglacial changes in ocean circulation from an extended radiocarbon calibration. Nature. 391, 65–68.
Hughen, K.A., Southon, J.R., Lehman, S.J., Overpeck, J.T., 2000. Synchronous radiocarbon and climate shifts during the last deglaciation. Science. 290, 1951–1954.
Hughen, K., Lehman, S., Southon, J., Overpeck, J., Marchal, O., Herring, C., Turnbull, J., 2004. ^{14}C activity and global carbon cycle changes over the past 50,000 years. Science. 30, 202–207.
Hughen, K., Southon, J., Lehman, S., Bertrand, C., Turnbull, J., 2006. Marine-derived ^{14}C calibration and activity record for the past 50,000 years updated from the Cariaco Basin. Quat. Sci. Rev. 25, 3216–3227.
Hughes, M.K., 2011. Dendroclimatology in high-resolution paleoclimatology. In: Hughes, M.K., Swetnam, T.W., Diaz, H.F. (Eds.), Dendroclimatology: Progress and Prospects. Springer, Dordrecht, pp. 17–34.
Hughes, M.K., Diaz, H.F., 1994. Was there a "Medieval Warm Period" and if so, where and when? Clim. Chang. 26, 109–142.
Hughes, T.J., Denton, G.H., Anderson, B.G., Schilling, D.H., Fastook, J.L., Lingle, C.S., 1981. The last great ice sheets: a global view. In: Denton, G.H., Hughes, T.J. (Eds.), The Last Great Ice Sheets. Wiley, New York, pp. 275–318.
Hughes, M.K., Kelley, P.M., Pilcher, J.R., LaMarche, V.C., 1982. Climate from Tree Rings. Cambridge University Press, Cambridge.
Hughes, M.K., Swetnam, T.W., Diaz, H.F. (Eds.), 2011. Dendroclimatology: Progress and Prospects. Springer, Dordrecht, 365 pp.
Hughes, P.D., Gibbard, P.L., Ehlers, J., 2013. Timing of glaciation during the last glacial cycle: evaluating the concept of a global 'Last Glacial Maximum' (LGM). Earth-Sci. Rev. 125, 171–198.
Huguet, C., Schimmelmann, A., Thunell, R., Lourens, L.J., Sinninghe Damsté, J.S., Schouten, S., 2007. A study of the TEX86 paleothermometer in the water column and sediments of the Santa Barbara Basin, California. Paleoceanography. 22. PA3203. dx.doi.org/10.1029/2006PA001310.
Hulbe, C.L., MacAyeal, D.R., Denton, G.H., Kleman, J., Lowell, T.V., 2004. Catastrophic ice shelf breakup as the source of Heinrich event icebergs. Paleoceanography. 19. PA1004. dx.doi.org/10.1029/2003PA000890.
Hummel, J., Reck, R., 1979. A global surface albedo model. J. Appl. Meteorol. 18, 239–253.
Hunt, J.B., Hill, P.G., 1993. Tephra geochemistry: a discussion of some persistent analytical problems. The Holocene. 3, 271–278 (See also discussion in, The Holocene 4, 435–438).
Huntley, B., 1990a. European vegetation history: palaeovegetation maps from pollen data –13,000 B.P. to present. J. Quat. Sci. 5, 103–122.
Huntley, B., 1990b. Dissimilarity mapping between fossil and contemporary pollen spectra in Europe for the past 13,000 years. Quat. Res. 33, 360–376.
Huntley, B., Birks, H.J.B., 1983. An Atlas of Past and Present Pollen Maps for Europe, 0-13,000 Years Ago. Cambridge University Press, Cambridge.
Huntley, B., Prentice, I.C., 1988. July temperatures in Europe from pollen data, 6000 years before present. Science. 241, 687–690.

Huntley, B., Prentice, I.C., 1993. Holocene vegetation and climates in Europe. In: Wright Jr., H.E., Kutzbach, J.E., Webb III, T., Ruddiman, W.F., Street-Perrott, F.A., Bartlein, P.J. (Eds.), Global Climates Since the Last Glacial Maximum. University of Minnesota Press, Minneapolis, pp. 136–168.
Huntley, B., Webb III, T., 1988. Vegetation History. Kluwer, Dordrecht.
Huntley, B., Webb III, T., 1989. Migration: species' response to climatic variations caused by changes in the earth's orbit. J. Biogeogr. 16, 5–19.
Huntley, D.J., Godfrey-Smith, D.I., Thewalt, M.L.W., 1985. Optical dating of sediments. Nature. 313, 105–107.
Hurford, A.J., Green, P.F., 1982. A user's guide to fission track dating calibration. Earth Planet. Sci. Lett. 59, 343–354.
Hurrell, J.W., 1995. Decadal trends in the North Atlantic oscillation. Science. 269, 676–679.
Hutson, W.H., 1977. Transfer functions under no-analog conditions: experiments with Indian Ocean planktonic foraminifera. Quat. Res. 3, 355–367.
Hütt, G., Jaek, H.I., Tchonka, J., 1988. Optical dating: K-feldspars optical response stimulation spectra. Quat. Sci. Rev. 7, 381–385.
Huxtable, J., Aitken, M.J., Bonhommet, N., 1978. Thermoluminescence dating of sediment baked by lava flows of the Chaine des Puys. Nature. 275, 207–209.
Huybers, P., 2006. Early Pleistocene glacial cycles and the integrated summer insolation forcing. Science. 313, 508–511.
Huybers, P., 2007. Glacial variability over the last two million years: an extended depth-derived age model, continuous obliquity pacing, and the Pleistocene progression. Quat. Sci. Rev. 26, 37–55.
Huybers, P., 2011. Combined obliquity and precession forcing of Late Pleistocene deglaciations. Nature. 480, 229–232.
Huybers, P., Curry, W., 2006. Links between annual, Milankovitch and continuum temperature variability. Nature. 441, 329–332.
Huybers, P., Denton, G.H., 2008. Antarctic temperature at orbital timescales controlled by local summer duration. Nat. Geosci. 1, 787–792.
Imbrie, J., 1985. A theoretical framework for the Pleistocene ice ages. J. Geol. Soc. Lond. 142, 417–432.
Imbrie, J., Imbrie, K.P., 1979. Ice Ages: Solving the Mystery. Macmillan, London.
Imbrie, J., Kipp, N.G., 1971. A new micropalaeontological method for quantitative paleoclimatology: application to late Pleistocene Caribbean core V28-238. In: Turekian, K.K. (Ed.), The Late Cenozoic Glacial Ages. Yale University Press, New Haven, pp. 77–181.
Imbrie, J., van Donk, J., Kipp, N.G., 1973. Paleoclimatic investigation of a late Pleistocene Caribbean deep-sea core: comparison of isotopic and faunal methods. Quat. Res. 3, 10–38.
Imbrie, J., Hays, J.D., Martinson, D.G., Mcintyre, A., Mix, A., Morley, J.J., Pisias, N.G., Prell, W., Shackleton, N.J., 1984. The orbital theory of Pleistocene climate: support from a revised chronology of the marine $\delta^{18}O$ record. In: Berger, A., Hays, J., Kukla, G., Saltzman, B. (Eds.), Milankovitch and Climate. Reidel, Dordrecht, pp. 269–305.
Imbrie, J., Berger, A., Boyle, E.A., Clemens, S.C., Duffy, A., Howard, W.R., Kukla, G., Kutzbach, J., Martinson, D.G., Mcintyre, A., Mix, A.C., Molfino, B., Morley, J.J., Peterson, L.C., Pisias, N.G., Prell, W.L., Raymo, M.E., Shackleton, N.J., Toggweiler, J.R., 1992. On the structure and origin of major glaciation cycles, 1. Linear responses to Milankovitch forcing. Paleoceanography. 7, 701–738.
Imbrie, J., Berger, A., Boyle, E.A., Clemens, S.C., Duffy, A., Howard, W.R., Kukla, G., Kutzbach, J., Martinson, D.G., Mcintyre, A., Mix, A.C., Molfino, B., Morley, J.J., Peterson, L.C., Pisias, N.G., Prell, W.L., Raymo, M.E., Shackleton, N.J., Toggweiler, J.R., 1993a. On the structure and origin of major glaciation cycles, 2. The 100,000-year cycle. Paleoceanography. 8, 699–735.
Imbrie, J., Berger, A., Shackleton, N.J., 1993b. Role of orbital forcing: a two million year perspective. In: Eddy, J.A., Oeschger, H. (Eds.), Global Changes in the Perspective of the Past. Wiley, Chichester, pp. 263–277.
Imbrie, J., Mix, A.C., Martinson, D.G., 1993c. Milankovitch theory viewed from Devil's Hole. Nature. 363, 531–533 (see also reply by Winograd, I.C., Landwehr, J.M., 1993).
Ineson, S., Scaife, A.A., Knight, J.R., Manners, J.C., Dunstone, N.J., Gray, L.J., Haigh, J.D., 2011. Solar forcing of winter climate variability in the Northern hemisphere. Nat. Geosci. 4, 753–757.
Ingalls, A.E., Pearson, A., 2005. Ten years of compound-specific radiocarbon dating. Oceanography. 18, 18–31.
Ingram, M.J., Underhill, D.J., Wigley, T.M.L., 1978. Historical climatology. Nature. 276, 329–334.
Ingram, M.J., Farmer, G., Wigley, T.M.L., 1981a. Past climates and their impact on Man: a review. In: Wigley, T.M.L., Ingram, M.J., Farmer, G. (Eds.), Climate and History. Cambridge University Press, Cambridge, pp. 3–50.

Ingram, M.J., Underhill, D.J., Farmer, G., 1981b. The use of documentary sources for the study of past climates. In: Wigley, T.M.L., Ingram, M.J., Farmer, G. (Eds.), Climate and History. Cambridge University Press, Cambridge, pp. 180–213.

Innes, J.L., 1982. Lichenometric use of an aggregated *Rhizocarpon* "species. Boreas. 11, 53–58.

Inoue, M., Yokoyama, Y., Harada, M., Suzuki, A., Kawahata, H., Matsuzaki, H., Iryu, Y., 2010. Trace element variations in fossil corals from Tahiti collected by IODP expedition 310: reconstruction of marine environments during the last deglaciation (15 to 9ka). Mar. Geol. 271, 303–306.

Isdale, P.J., 1984. Fluorescent bands in massive corals record centuries of coastal rainfall. Nature. 310, 378–379.

Isdale, P.J., Stewart, B.J., Tickle, K.S., Lough, J.M., 1998. Palaeohydrological variation in a tropical river catchment: a reconstruction using fluorescent bands in corals of the Great Barrier Reef, Australia. The Holocene. 8, 1–8.

Ito, E., 2001. Application of stable isotope techniques to inorganic and biogenic carbonates. In: Smol, J.P., Birks, H.J.B., Last, W.M. (Eds.), Tracking Environmental Change Using Lake sediments. Physical and Geochemical Methods, vol. 2. Kluwer Academic, Dordrecht, pp. 351–371.

Ivanovich, M., Harmon, R.S., 1982. Uranium Series Disequilibrium: Applications to Environmental Problems. Clarendon Press, Oxford.

Ives, J.D., 1974. Permafrost. In: Ives, J.D., Barry, R.G. (Eds.), Arctic and Alpine Environments. Methuen, London, pp. 159–194.

Ives, J.D., Andrews, J.T., Barry, R.G., 1975. Growth and decay of the Laurentide Ice Sheet and comparisons with Fenno-Scandinavia. Naturwissenschaften. 61, 118–125.

Izett, G.A., Obradovich, J.D., 1994. $^{40}Ar/^{39}Ar$ age constraints for the Jaramillo Normal Subchron and the Matuyama-Brunhes geomagnetic reversal. J. Geophys. Res. 99B, 2925–2934.

Izumi, K., Bartlein, P.J., Harrison, S.P., 2013. Consistent large-scale temperature responses in warm and cold climates. Geophys. Res. Lett. 40, 1817–1823. dx.doi.org/10.1002/grl.50350.

Jackson, S.T., 1994. Pollen and spores in Quaternary lake sediments as sensors of vegetation composition: theoretical models and empirical evidence. In: Traverse, A. (Ed.), Sedimentation of Organic Particles. Cambridge University Press, Cambridge, pp. 253–286.

Jackson, S.T., Williams, J.W., 2004. Modern analogs in Quaternary paleoecology: here today, gone yesterday, gone tomorrow? Annu. Rev. Earth Planet. Sci. 32, 495–537.

Jackson, S.T., Overpeck, J.T., Webb III, T., Keattch, S.E., Anderson, K.H., 1997. Mapped plant-macrofossils and pollen records of late Quaternary vegetation in eastern North America. Quat. Sci. Rev. 16, 1–70.

Jacobeit, J., Glaser, R., Luterbacher, J., Wanner, H., 2003. Links between flood events in Central Europe since AD 1500 and large-scale atmospheric circulation modes. Geophys. Res. Lett. 30, 1172. dx.doi.org/10.1029/2002GL016433.

Jacobsen, G.L., Webb III, T., Grimm, E.C., 1987. Patterns and rates of vegetation change during the deglaciation of eastern North America. In: Ruddiman, W.F., Wright, H.E. (Eds.), North America and Adjacent Oceans During the Last Deglaciation. The Geology of North America, vol. K-3. Geological Society of America, Boulder, pp. 277–288.

Jacobson, G.L., Bradshaw, R., 1981. The selection of sites for paleovegetational studies. Quat. Res. 16, 80–96.

Jacoby, G.C., D'Arrigo, R.D., 1995. Tree ring width and density evidence of climatic and potential forest change in Alaska. Glob. Biogeochem. Cycles. 9, 227–234.

Jaeschke, A., Rühlemann, C., Arz, H., Heil, G., Lohmann, G., 2007. Coupling of millennial-scale changes in sea surface temperature and precipitation off northeastern Brazil with high-latitude climate shifts during the glacial period. Paleoceanography. 22. PA4206. dx.doi.org/10.1029/2006PA001391.

Jansen, E., Overpeck, J., Briffa, K.R., Duplessy, J.-C., Joos, F., Masson-Delmotte, V., Olago, D., Otto-Bliesner, B., Peltier, W.R., Rahmstorf, S., Ramesh, R., Raynaud, D., Rind, D., Solomina, O., Villalba, R., Zhang, D., 2007. Palaeoclimate. In: Solomon, S., Qin, D., Manning, M., Chen, Z., Marquis, M., Averyt, K.B., Tignor, M., Miller, H.L. (Eds.), Climate Change 2007: The Physical Science Basis. Contribution of Working Group I to the Fourth Assessment of the Intergovernmental Panel on Climate Change. Cambridge University Press, Cambridge, pp. 433–497.

Janssen, C.R., 1966. Recent pollen spectra from the deciduous and coniferous-deciduous forests and northeastern Minnesota: a study in pollen dispersal. Ecology. 47, 804–825.

Jenk, T.M., Szidat, S., Bolius, D., Sigl, M., Gäggeler, H., Wacker, L., Ruff, M., Barbante, C., Boutron, C.F., Schwikowski, M., 2009. A novel radiocarbon dating technique applied to an ice core from the Alps indicating late Pleistocene ages. J. Geophys. Res. 114, D14305. dx.doi.org/10.1029/2009JD011860.

Jenkyns, H.C., Forster, A., Schouten, S., Sinninghe Damsté, J.S., 2004. High temperatures in the Late Cretaceous Arctic Ocean. Nature. 432, 888–892.
Jennerjahn, T.C., Ittekkot, V., Arz, H.W., Behling, H., Patzold, J., Wefer, G., 2004. Asynchronous terrestrial and marine signals of climate change during Heinrich events. Science. 306, 2236–2239.
Ji, J.F., Chen, J., Balsam, W., Lu, H.Y., Sun, Y.B., Xu, H.F., 2004. High resolution hematitite/goethite records from Chinese loess sequences for the last glacial-interglacial cycle: rapid climatic response of the Aast Asian Monsoon to the tropical Pacific. Geophys. Res. Lett. 31, L03207. dx.doi.org/10.1029/2003GL018975.
Jin, C.S., Liu, Q.S., 2011. Revisiting the position of the Brunhes-Matuyama geomagnetic polarity boundary in Chinese loess. Palaeogeogr. Palaeoclimatol. Palaeoecol. 299, 309–317.
Jochimsen, M., 1973. Does the size of lichen thalli really constitute a valid measure for dating glacial deposits? Arct. Alp. Res. 5, 417–424.
Joerin, U.E., Stocker, T.F., Schluchter, C., 2006. Multicentury glacier fluctuations in the Swiss Alps during the Holocene. The Holocene. 16, 697–704.
Johnsen, S.J., 1977. Stable isotope profiles compared with temperature profiles in firn and with historical temperature records. In: Proceedings of Symposium on Isotopes and Impurities in Snow and Ice. International Association of Hydrological Sciences Publication. 118, Washington, D.C, pp. 388–392.
Johnsen, S.J., Dansgaard, W., 1992. On flow model dating of stable isotope records from Greenland ice cores. In: Bard, E., Broecker, W. (Eds.), The Last Deglaciation: Absolute and Radiocarbon Chronologies. Springer-Verlag, Berlin, pp. 13–24.
Johnsen, S.J., Dansgaard, W., Clausen, H.B., Langway Jr., C.C., 1972. Oxygen isotope profiles through the Antarctic and Greenland ice sheets. Nature. 235, 429–434 (see also, Nature 236, 249).
Johnsen, S.J., Dansgaard, W., White, J.W.C., 1989. The origin of Arctic precipitation under glacial and interglacial conditions. Tellus. 41B, 452–468.
Johnsen, S.J., Clausen, H.B., Dansgaard, W., Fuhrer, K., Gundestrup, N., Hammer, C.U., Iversen, P., Jouzel, J., Stauffer, B., Steffensen, J.P., 1992. Irregular glacial interstadials recorded in a new Greenland ice core. Nature. 359, 311–313.
Johnsen, S.J., Clausen, H.B., Dansgaard, W., Gundestrup, N., Hammer, C.U., Tauber, H., 1995. The Eem stable isotope record along the GRIP ice core and its interpretation. Quat. Res. 43, 117–124.
Johnsen, S.J., Dahl-Jensen, D., Gundestrup, N., Steffensen, J.P., Clausen, H.B., Miller, H., Masson-Delmotte, V., Sveinbjornsdottir, A.E., White, J., 2001. Oxygen isotope and palaeotemperature records from six Greenland ice-core stations: Camp Century, Dye-3, GRIP, GISP2, Renland and NGRIP. J. Quat. Sci. 16, 299–307.
Johnson, R.G., 1982. Brunhes-Matuyama reversal dated at 790,000 yr B.P. by marine and astronomical correlation. Quat. Res. 17, 135–147.
Johnson, R.G., Wright Jr., H.E., 1989. Great Basin calcite vein and the Pleistocene time scale: comment. Science. 246, 262 (see also reply by Winograd, I.C., Coplen, T.B., 262–263).
Jolly, D., Haxeltine, A., 1997. Effect of low glacial atmospheric CO_2 on tropical African montane vegetation. Science. 276, 786–788.
Jolly, D., Prentice, I.C., Bonnefille, R., Ballouche, A., Bengo, M., Brenac, P., Buchet, G., Burney, D., Cazet, J.-P., Cheddadi, R., Edorh, T., Elenga, H., Elmoutaki, S., Guiot, J., Laarif, F., Lamb, H., Lezine, A.-M., Maley, J., Mbenza, M., Peyron, O., Reille, M., Reynaud-Farrera, I., Riollet, G., Ritchie, J.C., Roche, E., Scott, L., Ssemmanda, I., Straka, H., Umer, M., Van Campo, E., Vilimumbalo, S., Vincens, A., Waller, M., 1998. Biome reconstruction from pollen and plant macrofossil data for Africa and the Arabian Peninsula and 0 and 6000 years. J. Biogeogr. 25, 1007–1027.
Jones, P.D., Bradley, R.S., 1992. Climatic variations over the last 500 years. In: Bradley, R.S., Jones, P.D. (Eds.), Climate Since A.D. 1500. Routledge, London, pp. 649–665.
Jones, P.D., Bradley, R.S., Jouzel, J. (Eds.), 1996. Climate Variations and Forcing Mechanisms of the Last 2000 years. Springer-Verlag, Berlin.
Jones, P.D., Ogilvie, A.E.G., Davies, T.D., Briffa, K.R. (Eds.), 2001. History and Climate: Memories of the Future?. Kluwer, New York, 295 pp.
Jones, P.D., Briffa, K.R., Osborn, T.J., Lough, J.M., van Ommen, T.D., Vinther, B.M., Luterbacher, J., Wahl, E.R., Zwiers, F.W., Mann, M.E., Schmidt, G.A., Ammann, C.M., Buckley, B.M., Cobb, K.M., Esper, J., Goosse, H., Graham, N., Jansen, E., Kiefer, T., Kull, C., Küttel, M., Mosley-Thompson, E., Overpeck, J.T., Riedwyl, N., Schulz, M., Tudhope, A.W., Villalba, R., Wanner, H., Wolff, E.,

Xoplaki, E., 2009. High-resolution palaeoclimatology of the last millennium: a review of current status and future prospects. The Holocene. 19, 3–49.
Jorissen, F.J., Fontanier, C., Thomas, E., 2007. Paleoceanographic proxies based on deep-sea benthic foraminiferal assemblage characteristics. In: Hillaire-Marcel, C., de Vernal, A. (Eds.), Proxies in Late Cenozoic Paleoceanography. Elsevier, Amsterdam, pp. 263–325.
Joussaume, S., Jouzel, J., 1993. Paleoclimatic tracers: an investigation using an atmospheric general circulation model under ice age conditions. 2. Water isotopes. J. Geophys. Res. 98D, 2807–2830.
Joussaume, S., Jouzel, J., Sadorny, R., 1984. A general circulation model of water isotope cycles in the atmosphere. Nature. 311, 24–29.
Jouzel, J., 1991. Paleoclimatic tracers. In: Bradley, R.S. (Ed.), Global Changes of the Past. University Corporation for Atmospheric Research, Boulder, pp. 449–476.
Jouzel, J., Merlivat, L., 1984. Deuterium and oxygen-18 in precipitation: modeling of the isotopic effects during snow formation. J. Geophys. Res. 89D, 11749–11757.
Jouzel, J., Masson-Delmotte, V., 2010. Deep ice cores: the need for going back in time. Quat. Sci. Rev. 29, 3683–3689.
Jouzel, J., Merlivat, L., Lorius, C., 1982. Deuterium excess in an East Antarctic ice core suggests higher relative humidity at the oceanic surface during the last glacial maximum. Nature. 299, 688–691.
Jouzel, J., Merlivat, L., Petit, J.R., Lorius, C., 1983. Climatic information over the last century deduced from a detailed isotopic record in the South Pole snow. J. Geophys. Res. 88C, 2693–2703.
Jouzel, J., Lorius, C., Merlivat, L., Petit, J.R., 1987a. Abrupt climatic changes: the Antarctic ice record during the late Pleistocene. In: Berger, W.H., Labeyrie, L.D. (Eds.), Abrupt Climatic Change: Evidence and Implications. D. Reidel, Dordrecht, pp. 235–245.
Jouzel, J., Lorius, C., Petit, J.R., Genthon, C., Barkov, N.J., Kotlyakov, V.M., Petrov, V.N., 1987b. Vostok ice core: a continuous isotope temperature record over the last climatic cycle 160,000 years. Nature. 329, 403–408.
Jouzel, J., Raisbeck, G., Benoist, J.P., Yiou, F., Lorius, C., Raynaud, D., Petit, J.R., Barkov, N.I., Korotkevich, Y.S., Kotlyakov, V.M., 1989a. A comparison of deep Antarctic ice cores and their implications for climate between 65,000 and 15,000 years ago. Quat. Res. 31, 135–150.
Jouzel, J., Barkov, N.I., Barnola, J.M., Genthon, C., Korotkevich, Y.S., Kotlyakov, V.M., Legrand, M., Lorius, C., Petit, J.P., Petrov, V.N., Raisbeck, G., Raynaud, D., Ritz, C., Yiou, F., 1989b. Global changes over the last climatic cycle from the Vostok ice core record, Antarctica. Quat. Int. 2, 15–24.
Jouzel, J., Koster, R.D., Suozzo, R.J., Russell, G.L., White, J.W.C., Broecker, W.S., 1991. Simulations of the HDO and $H_2^{18}O$ atmospheric cycles using the NASA GISS general circulation model: sensitivity experiments for present day conditions. J. Geophys. Res. 96D, 7495–7507.
Jouzel, J., Petit, J.R., Barkov, N.I., Barnola, J.M., Chappellaz, J., Ciais, P., Kotlyakov, V.M., Lorius, C., Petrov, V.N., Raynaud, D., Ritz, C., 1992. The last deglaciation in Antarctica: further evidence of a "Younger Dryas" type climatic event. In: Bard, E., Broecker, W. (Eds.), The Last Deglaciation: Absolute and Radiocarbon Chronologies. Springer-Verlag, Berlin, pp. 229–266.
Jouzel, J., Joussaume, S., Koster, R.D., 1993. Use of general circulation models to follow climatic tracers on a global scale. In: Eddy, J.A., Oeschger, H. (Eds.), Global Changes in the Perspective of the Past. Wiley, Chichester, pp. 133–142.
Jouzel, J., Koster, R.D., Suozzo, R.J., Russell, G.L., 1994. Stable water isotope behavior during the last glacial maximum: a general circulation model analysis. J. Geophys. Res. 99D, 25791–25801.
Jouzel, J., Stiévenard, M., Johnsen, S.J., Landais, A., Masson-Delmotte, V., Sveinbjornsdottir, A., Vimeux, F., von Grafenstein, U., White, J.W.C., 2007a. The GRIP deuterium-excess record. Quat. Sci. Rev. 26, 1–17.
Jouzel, J., Masson-Delmotte, V., Cattani, O., Dreyfus, G., Falourd, S., Hoffmann, G., Minster, B., Nouet, J., Barnola, J.M., Chappellaz, J., Fischer, H., Gallet, J.C., Johnsen, S., Leuenberger, M., Loulergue, L., Luethi, D., Oerter, H., Parrenin, F., Riasbeck, G., Raynaud, D., Schilt, A., Schwander, J., Selmo, E., Souchez, R., Spahni, R., Stauffer, B., Steffensen, J.P., Stenni, B., Stocker, T.F., Tison, J.L., Werner, M., Wolff, E.W., 2007b. Orbital and millennial Antarctic climate variability over the past 800,000 years. Science. 317, 793–796.
Jouzel, J., Vimeux, F., Caillon, N., Delaygue, G., Hoffmann, G., Masson-Delmotte, V., Parrenin, F., 2003. Magnitude of isotope/temperature scaling for interpretation of central Antarctic ice cores. J. Geophys. Res. [Atmos.] 108. dx.doi.org/10.1029/2002JD002677.
Jouzel, J., Lorius, C., Raynaud, D., 2013. The White Planet: The Evolution and Future of Our Frozen World. Princeton University Press, Princeton, 306 pp.

Juggins, S., Birks, H.J.B., 2012. Quantitative environmental reconstructions from biological data. In: Birks, H.J.B., Lotter, A.F., Juggins, S., Smol, J.P. (Eds.), Tracking Environmental Change Using Lake Sediments. Data Handling and Numerical Techniques, Vol. 5. Springer, Berlin, pp. 431–494.
Juillet-LeClerc, A., Labeyrie, L.D., 1987. Temperature-dependence of the oxygen isotope fractionation between diatom silica and water. Earth Planet. Sci. Lett. 84, 69–74.
Kageyama, M., Paul, A., Roche, D.M., Van Meerbeeck, C.J., 2010. Modelling glacial climatic millennial-scale variability related to changes in the Atlantic meridional overturning circulation: a review. Quat. Sci. Rev. 29, 2931–2956.
Kalela, O., 1952. Changes in the geographic distribution of Finnish birds and mammals in relation to recent changes in climate. Fennia. 75, 38–51.
Kållberg, P., Berrisford, P., Hoskins, B., Simmons, A., Uppala, S., Lamy-Thépaut, S., Hine, R., 2005. ERA-40 Atlas. ERA-40 Project Report Series 19European Centre for Medium Range Weather Forecasting, Reading, 191 pp.
Kallel, N., Duplessy, J.-C., Labeyrie, L., Fontugne, M., Paterne, M., Montacer, M., 2000. Mediterranean pluvial periods and sapropel formation over the last 200,000 years. Palaeogeogr. Palaeoclimatol. Palaeoecol. 157, 45–58.
Kallel, N., Duplessy, J.-C., Labeyrie, L., Fortugne, M., Paterne, M., 2004. Mediterranean Sea paleohydrology and pluvial periods during the Late Quaternary. In: Battarbee, R.W., Gasse, F., Stickley, C.E. (Eds.), Past Climate Variability through Europe and Africa. Springer, Dordrecht, pp. 307–324.
Kanner, L.C., Burns, S.J., Cheng, H., Edwards, R.L., 2012. High-latitude forcing of the South American summer monsoon during the Last Glacial. Science. 335, 570–573.
Kapsner, W.R., Alley, R.B., Shuman, C.A., Anandakrishnan, S., Grootes, P.M., 1995. Dominant influence of atmospheric circulation on snow accumulation in Greenland over the past 18,000 years. Nature. 373, 52–54.
Karl, T., 1993. Missing pieces of the puzzle. Natl Geogr. Res. Explor. 12, 234–249.
Karlén, W., 1976. Lacustrine sediments and tree-limit variations as indicators of Holocene climatic fluctuations in Lappland, northern Sweden. Geogr. Ann. 58A, 1–34.
Karlén, W., 1979. Glacier variations in the Svartisen area, northern Norway. Geogr. Ann. 61A, 11–28.
Karlén, W., 1980. Reconstruction of past climatic conditions from studies of glacier-front variations. World Meteorol. Organ. Bull. 29, 100–104.
Karlén, W., 1981. Lacustrine sediment studies. Geogr. Ann. 63A, 273–281.
Karlén, W., 1993. Glaciological, sedimentological and palaeobotanical data indicating Holocene climatic change in Northern Fennoscandia. In: Frenzel, B., Eronen, M., Vorren, K.D., Glaser, B. (Eds.), Oscillations of the Alpine and Polar Tree Limits in the Holocene. Gustav Fischer Verlag, Stuttgart, pp. 69–83.
Karrow, P.F., Anderson, T.W., 1975. Palynological studies of lake sediment profiles from SW New Brunswick: discussion. Can. J. Earth Sci. 12, 1808–1812.
Karte, J., Liedtke, H., 1981. The theoretical and practical definition of the term "periglacial" in its geographical and geological meaning. Biuletyn Periglacjalny. 28, 123–135.
Kaspi, Y., Sayag, R., Tziperman, E., 2004. A "triple sea-ice state" mechanism for the abrupt warming and synchronous ice sheet collapses during Heinrich events. Paleoceanography. 19, PA3004. dx.doi.org/10.1029/2004PA0011009.
Kato, K., 1978. Factors controlling oxygen isotope composition of fallen snow in Antarctica. Nature. 272, 46–48.
Kaufman, D.S., Sejrup, H.P., 1995. Isoleucine epimerization in the high-molecular weight fraction of Pleistocene Arctica. Quat. Sci. Rev. (Quat. Geochronol.) 14, 337–350.
Kaufman, A., Broecker, W.S., Ku, T.L., Thurber, D.L., 1971. The status of U-series methods of mollusc dating. Geochim. Cosmochim. Acta. 35, 1155–1183.
Keigwin, L.D., 1996. The Little Ice Age and Medieval Warm Period in the Sargasso Sea. Science. 274, 1504–1508.
Keigwin, L.D., Boyle, E.A., 2008. Did North Atlantic overturning halt 17,000 years ago? Paleoceanography. 23, PA1101. dx.doi.org/10.1029/2007PA001500.
Keigwin, L.D., Jones, G.A., 1994. Western North Atlantic evidence for millennial-scale changes in ocean circulation and climate. J. Geophys. Res. C99, 12397–12410.
Keigwin, L.D., Jones, G.A., 1995. The marine record of deglaciation from the continental margin off Nova Scotia. Paleoceanography. 10, 973–985.
Keigwin, L.D., Schlegel, M.A., 2002. Ocean ventilation and sedimentation since the glacial maximum at 3 km in the western North Atlantic. Geochem. Geophys. Geosyst. 3, 1–14. dx.doi.org/10.1029/2001GC000283.
Keigwin, L.D., Curry, W.B., Lehman, S.J., Johnsen, S., 1994. The role of the deep ocean in North Atlantic climate change between 70 and 130 kyr ago. Nature. 371, 323–326.
Kellogg, T.B., 1987. Glacial-interglacial changes in global deepwater production. Paleoceanography. 2, 259–272.

Kelly, M.J., Edwards, R.L., Cheng, H., Yuan, D.Z., Cai, Y.J., Zhang, M.L., Lin, Y.S., An, Z.S., 2006. High resolution characterization of the Asian Monsoon between 146,000 and 99,000 years B.P. from Dongge Cave, China and global correlation of events surrounding Termination II. Palaeogeogr. Palaeoclimatol. Palaeoecol. 236, 20–38.
Kemp, A.E., 1996. Palaeoclimatology and Palaeoceanography from Laminated Sediments. Special Publication No. 116, Geological Society of London, 272 pp.
Kennedy, J.A., Brassell, S.C., 1992. Molecular records of twentieth century El Niño events in laminated sediments from the Santa Barbara basin. Nature. 357, 62–64.
Kennett, J.P., 1976. Phenotypic variation in some recent and late Cenozoic planktonic foraminifera. In: Hedley, R.H., Adams, C.G. (Eds.), Foraminifera, vol. 2. Academic Press, New York, pp. 111–170.
Kiehl, J.T., Trenberth, K.E., 1997. Earth's annual global mean energy budget. Bull. Am. Meteorol. Soc. 78, 197–208.
Kilbourne, K.H., Quinn, T.M., Taylor, F.W., 2004. A fossil coral perspective on western tropical Pacific climate 350ka. Paleoceanography. 19, PA1019. dx.doi.org/10.1029/2003PA000944.
Kilbourne, K.H., Quinn, T.M., Guilderson, T.P., Webb, R.S., Taylor, F.W., 2007. Decadal- to interannual-scale source water variations in the Caribbean Sea recorded by Puerto Rican coral radiocarbon. Clim. Dyn. 29, 51–62.
Kilbourne, K.H., Quinn, T.M., Webb, R., Guilderson, T., Nyberg, J., Winter, A., 2008. Paleoclimate proxy perspective on Caribbean climate since the year 1751: evidence of cooler temperatures and multidecadal variability. Paleoceanography. 23, PA3220. dx.doi.org/10.1029/2008PA001598.
Kilbourne, K.H., Quinn, T.M., Webb, R., Guilderson, T., Nyberg, J., Winter, A., 2010. Coral windows onto seasonal climate variability in the northern Caribbean since 1479. Geochem. Geophys. Geosyst. 11. dx.doi.org/10.1029/2010GC003171.
Kim, Y.O., 1984. The Little Ice Age in Korea: an approach to historical climatology. Geogr.-Educ. 14, 1–16 (in Korean with English abstract. Department of Geography, College of Education, Seoul National University).
Kim, Y.O., 1987. Climatic environment of Chosun Dynasty 1392-1910) based on historical records. J. Geogr. (Seoul). 14, 411–423 (in Korean with English abstract. Department of Geography, Seoul National University).
Kim, G.S., Choi, I.S., 1987. A preliminary study on long-term variation of unusual climate phenomena during the past 1000 years in Korea. In: Ye, D., Fu, C., Chao, J., Yoshino, M. (Eds.), The Climate of China and Global Climate. China Ocean Press, Beijing, pp. 30–37.
Kim, J.-H., Schouten, S., Hopmans, E.C., Donner, B., Sinninghe Damsté, J.S., 2008. Global sediment core-top calibration of the TEX_{86} paleothermometer in the ocean. Geochim. Cosmochim. Acta. 72, 1154–1173.
Kim, J.-H., van der Meer, J., Schouten, S., Helmke, P., Wilmott, V., Sangiorgi, F., Koç, N., Hopmans, E.C., Sinninghe Damsté, J.S., 2010. New indices and calibrations derived from the distribution of crenarchaeal isoprenoid tetraether lipids: implications for past sea surface temperature reconstructions. Geochim. Cosmochim. Acta. 74, 4639–4654.
King, L., Lehmann, R., 1973. Beobachtung zur oekologie und morphologie von *Rhizocarpon Geographicum* (L) D.C. und *Rhizocarpon Alpicola* (Hepp.) Rabenh. in gletschervorfeld des steingletschers. Ber. Schweizer. Bot. Ges. 83, 139–146.
King, K., Neville, C., 1977. Isoleucine epimerization for dating marine sediments: the importance of analyzing monospecific samples. Science. 195, 1333–1335.
King, J.E., Van Devender, T.R., 1977. Pollen analysis of fossil packrat middens from the Sonoran Desert. Quat. Res. 8, 191–204.
Kittleman, L.R., 1979. Geologic methods in studies of Quaternary tephra. In: Sheets, D.D., Grayson, D.K. (Eds.), Volcanic Activity and Human Ecology. Academic Press, New York, pp. 49–82.
Kleiven, H.F., Jansen, E., Fronval, T., Smith, T.M., 2002. Intensification of Northern Hemisphere glaciations in the circum-Atlantic region (3.5–2.4 Ma)—ice-rafted detritus evidence. Palaeogeogr. Palaeoclimatol. Palaeoecol. 184, 213–223.
Kluge, T., Marx, T., Scholz, D., Niggemann, S., Mangini, A., Aeschbach-Hertig, W., 2008. A new tool for palaeoclimate reconstruction: noble gas temperatures from fluid inclusions in speleothems. Earth Planet. Sci. Lett. 269, 408–415.
Knudsen, M.F., Riisager, P., Donadini, F., Snowball, I., Muscheler, R., Korhonen, K., Pesonen, L.J., 2008. Variations in the geomagnetic dipole moment during the Holocene and the past 50 kyr. Earth Planet. Sci. Lett. 272, 319–329.
Knutti, R., Hegerl, G.C., 2008. The equilibrium sensitivity of the Earth's temperature to radiation changes. Nat. Geosci. 1, 735–743.
Knutti, R., Fluckinger, J., Stocker, T.F., Timmermann, A., 2004. Strong hemispheric coupling of glacial climate through freshwater discharge and ocean circulation. Nature. 430, 851–856.

Koç Karpuz, N., Schrader, H., 1990. Surface sediment diatom distribution and Holocenepalotemperature variations in the Greenland, Iceland and Norwegian Sea. Paleoceanography. 5, 557–580.
Koerner, R.M., 1977. Devon Island Ice Cap: core stratigraphy and paleoclimate. Science. 196, 15–18.
Koerner, R.M., 1979. Accumulation, ablation and oxygen isotope variations on the Queen Elizabeth Islands Ice Caps, Canada. J. Glaciol. 22, 25–41.
Koerner, R.M., 1980. The problem of lichen-free zones in Arctic Canada. Arct. Alp. Res. 12, 87–94.
Koerner, R.M., 1989. Ice core evidence for extensive melting of the Greenland Ice Sheet in the last interglacial. Science. 244, 964–968.
Koerner, R.M., Fisher, D.A., 1979. Discontinuous flow, ice texture and dirt content in the basal layers of the Devon Island Ice Cap. J. Glaciol. 23, 209–222.
Koerner, R.M., Fisher, D.A., 1990. A record of Holocene summer climate from a Canadian high-Arctic ice core. Nature. 343, 630–631.
Koerner, R.M., Paterson, W.S.B., 1974. Analysis of a core through the Meighen Ice Cap, Arctic Canada and its paleoclimatic implications. Quat. Res. 4, 253–263.
Koerner, R.M., Russell, R.P., 1979. δ18O variations in snow on the Devon Island Ice Cap, North West Territories, Canada. Can. J. Earth Sci. 16, 1419–1427.
Koerner, R.M., Taniguchi, H., 1976. Artificial radioactivity layers in the Devon Island Ice Cap, North West Territories. Can. J. Earth Sci. 13, 1251–1255.
Kohler, M.A., Nordenson, T.J., Baker, D.R., 1966. Evaporation maps for the United States. US Weather Bureau Technical Paper No. 37, US Department of Commerce, Washington, DC.
Köhler, P., Bintanja, R., Fischer, H., Joos, F., Knutti, R., Lohmann, G., Masson-Delmotte, V., 2010. What caused Earth's temperature variations during the last 800,000 years? Data-based evidence on radiative forcing and constraints on climate sensitivity. Quat. Sci. Rev. 29, 129–145.
Koide, M., Goldberg, E.D., 1985. The historical record of artificial radioactive fallout from the atmosphere in polar glaciers. In: Langway Jr., C.C., Oeschger, H., Dansgaard, W. (Eds.), Greenland Ice Core: Geophysics, Geochemistry and the Environment. American Geophysical Union, Washington, DC, pp. 95–100.
Kolla, V., Biscaye, P.E., Hanley, A.F., 1979. Distribution of quartz in late Quaternary Atlantic sediments in relation to climate. Quat. Res. 11, 261–277.
Kolodny, Y., Bar-Matthews, M., Ayalon, A., McKeegan, K.D., 2003. A high spatial resolution $\delta^{18}O$ profile of a speleothem using an ion microprobe. Chem. Geol. 197, 21–28.
Kominz, M.A., Heath, G.R., Ku, T.-L., Pisias, N.G., 1979. Brunhes time scales and the interpretation of climatic change. Earth Planet. Sci. Lett. 45, 394–410.
Kopp, G., Lean, J.L., 2011. A new, lower value of total solar irradiance: evidence and climate significance. Geophys. Res. Lett. 38. L01706. dx.doi.org/10.1029/2010GL045777.
Koren, J.H., Svendsen, J.I., Mangerud, J., Furnes, H., 2008. The Dimna Ash—a 12.8 14C kyr old volcanic ash in western Norway. Quat. Sci. Rev. 27, 85–94.
Korff, H.C.I., Flohn, H., 1969. Zusammenhang zwischen dem Temperaturgefälle Äquator Pol und den planetarischen Luftdruckgurteln. Ann. Meteorol. 4, 163–164.
Korhola, A., Weckström, J., Holmström, L., Erästö, P., 2000. A quantitative Holocene climatic record from diatoms in northern Fennoscandia. Quat. Res. 54, 284–294.
Körner, C., Paulsen, J., 2004. A world-wide study of high altitude tree-line temperatures. J. Biogeogr. 31, 713–732.
Korte, M., Constable, C., Donadini, F., Holme, R., 2011. Reconstructing the Holocene geomagnetic field. Earth Planet. Sci. Lett. 312, 497–505.
Koslowski, G., Glaser, R., 1999. Variations in reconstructed ice winter severity in the western Baltic from 1501-1995, and their implications for the North Atlantic Oscillation. Clim. Chang. 41, 175–191.
Koster, R.D., Jouzel, J., Souzzo, R.J., Russell, G.L., 1992. Origin of July precipitation and its influence on deuterium content: a GCM analysis. Clim. Dyn. 7, 195–203.
Krebs, J.S., Barry, R.G., 1970. The arctic front and the tundra-taiga boundary in Eurasia. Geogr. Rev. 60, 548–554.
Kress, A., Sauer, M., Siegwolf, R.T.W., Frank, D.C., Esper, J., Bugmann, H., 2010. A 350 year drought reconstruction from Alpine tree ring stable isotopes. Glob. Biogeochem. Cycles. 24. GB2011. dx.doi.org/10.1029/2009GB003613.
Kromer, B., 2009. Radiocarbon and dendrochronology. Dendrochronologia. 27, 15–19.
Kromer, B., Becker, B., 1993. German oak and pine ^{14}C calibration, 7200-9439 B.C. Radiocarbon. 35, 125–135.

Kromer, B., Friedrich, M., Hughen, K.A., Kaiser, F., Remmele, S., Schaub, M., Talamo, S., 2004. Late Glacial ^{14}C ages from a floating 1382-ring pine chronology. Radiocarbon. 46, 1203–1209.
Kroopnick, P.M., 1985. The distribution of ^{13}C in the world oceans. Deep-Sea Res. 32, 57–84.
Ku, T.-L., 1976. The uranium series method of age determination. Annu. Rev. Earth Planet. Sci. 4, 347–380.
Ku, T.-H., 2000. Uranium-series methods. In: Noller, J.S., Sowers, J.M., Lettis, W.R. (Eds.), Quaternary Geochronology: methods and applications. American Geophysical Union, Washington, DC, pp. 101–114.
Ku, T.-L., Oba, T., 1978. A method for quantitative evaluation of carbonate dissolution in deep-sea sediments and its application to paleooceanographic reconstruction. Quat. Res. 10, 112–129.
Kucera, M., 2007. Planktonic foraminifera as tracers of past oceanic conditions. In: Hillaire-Marcel, C., de Vernal, A. (Eds.), Proxies in Late Cenozoic Paleoceanography. Elsevier, Amsterdam, pp. 213–262.
Kucera, M., Weinelt, M., Kiefer, T., Pflaumann, U., Hayes, A., Weinelt, M., Chen, M.-T., Mix, A.C., Barrows, T.T., Cortijo, E., Duprat, J., Juggins, S., Waelbroeck, C., 2005a. Reconstruction of sea-surface temperatures from assemblages of planktonic foraminifera: multi-technique approach based on geographically constrained calibration data sets and its application to glacial Atlantic and Pacific Oceans. Quat. Sci. Rev. 24, 951–998.
Kucera, M., Rosell-Melé, A., Schneider, R., Waelbroeck, C., Weinelt, M., 2005b. Multi-proxy approach for the reconstruction of the glacial ocean surface (MARGO). Quat. Sci. Rev. 24, 813–819.
Kuhlbrodt, T., Griesel, A., Montoya, M., Levemann, A., Hofmann, M., Rahmstorf, S., 2007. On the driving processes of the Atlantic meridional overturning circulation. Rev. Geophys. 45, RG2001. dx.doi.org/8755-1209/07/2004RG000166.
Kuhnert, H., Patzold, J., Hatcher, B., Wyrwoll, K.H., Eisenhauer, A., Collins, L.B., Zhu, Z.R., Wefer, G., 1999. A 200-year coral stable oxygen isotope record from a high-latitude reef off western Australia. Coral Reefs. 18, 1–12. dx.doi.org/10.1007/s003380050147.
Kuhnert, H., Pätzold, J., Schnetger, B., Wefer, G., 2002. Sea-surface temperature variability in the 16th century at Bermuda inferred from coral records. Palaeogeogr. Palaeoclimatol. Palaeoecol. 179, 159–171.
Kukla, G.J., 1975a. Missing link between Milankovitch and climate. Nature. 253, 600–603.
Kukla, G.J., 1975b. Loess stratigraphy of central Europe. In: Butzer, K.W., Isaac, G.L. (Eds.), After the Australopithecenes. Mouton, The Hague, pp. 99–188.
Kukla, G.J., 1977. Pleistocene land-sea correlations. I. Europe. Earth-Sci. Rev. 13, 307–374.
Kukla, G.J., 1978. Recent changes in snow and ice. In: Gribbin, J. (Ed.), Climatic Change. Cambridge University Press, Cambridge, pp. 114–130.
Kukla, G.J., 1979. Climatic role of snow covers. In: Sea level, Ice and Climatic Change. Publication No. 131, International Association of Scientific Hydrology, Washington, DC, pp. 79–107.
Kukla, G.J., 1987a. Loess stratigraphy in central China. Quat. Sci. Rev. 6, 191–220.
Kukla, G.J., 1987b. Pleistocene climates in China and Europe compared to oxygen isotope record. Paleoecol. Afr. 18, 37–45.
Kukla, G.J., An, Z., 1989. Loess stratigraphy in central China. Palaeogeogr. Palaeoclimatol. Palaeoecol. 72, 203–225.
Kukla, G.J., Robinson, D., 1980. Annual cycle of surface albedo. Mon. Weather Rev. 108, 56–68.
Kukla, G.J., An, Z., Melice, J.L., Gavin, J., Xiao, J.L., 1990. Magnetic susceptibilty record of Chinese loess. Trans. R. Soc. Edinb. Earth Sci. 81, 263–288.
Kullman, L., 1987. Long-term dynamics of high-altitude populations of *Pinus sylvestris* in the Swedish Scandes. J. Biogeogr. 14, 1–8.
Kullman, L., 1988. Holocene history of the forest-alpine tundra ecotone in the Scandes Mountains (central Sweden. New Phytol. 108, 101–110.
Kullman, L., 1989. Tree-limit history during the Holocene in the Scandes Mountains, Sweden inferred from sub-fossil wood. Rev. Paleobot. Palynol. 58, 163–171.
Kullman, L., 1993. Dynamism of the altitudinal margin of the boreal forest in Sweden. In: Frenzel, B., Eronen, M., Vorren, K.D., Glaser, B. (Eds.), Oscillations of the Alpine and Polar Tree Limits in the Holocene. Gustav Fischer Verlag, Stuttgart, pp. 41–55.
Kumar, N., Anderson, R.F., Mortlock, R.A., Froelich, P.N., Kubik, P., Dittrich-Hannen, D., Suter, M., 1995. Increased biological productivity and export production in the glacial Southern Ocean. Nature. 378, 675–680.
Kuniholm, P.I., Kromer, B., Manning, S.W., Newton, M., Latini, C.E., Bruce, M.J., 1996. Anatolian tree rings and the absolute chronology of the eastern Mediterranean, 2220-718 B.C. Nature. 381, 780–783.

Kurek, J., Cwynar, L.C., Ager, T.A., Abbott, M.B., Edwards, M.E., 2009. Late Quaternary paleoclimate of western Alaska inferred from fossil chironomids and its relation to vegetation histories. Quat. Sci. Rev. 28, 799–811.
Kutterolf, S., Jegen, M., Mitrovica, J.X., Kwasnitchka, T., Freundt, A., Huybers, P.J., 2012. A detection of Milankovitch frequencies in global volcanic activity. Geology. 41, 227–230.
Kutzbach, J.E., 1974. Fluctuations of climate-monitoring and modelling. World Meteorol. Organ. Bull. 23, 155–163.
Kutzbach, J.E., 1976. The nature of climate and climatic variations. Quat. Res. 6, 471–480.
Kutzbach, J.E., 1980. Estimates of past climate at Paleolake Chad, North Africa, based on a hydrological and energy balance model. Quat. Res. 14, 210–223.
Kutzbach, J.E., 1983. Monsoon rains of the late Pleistocene and early Holocene: patterns, intensity and possible causes of changes. In: Street-Perrott, E.A., Beran, M., Ratcliffe, R. (Eds.), Variations in the Global Water Budget. D. Reidel, Dordrecht, pp. 371–389.
Kutzbach, J.E., Liu, X., Liu, Z., Chen, G., 2008. Simulation of the evolutionary response of global summer monsoons to orbital forcing over the past 280,000 years. Clim. Dyn. 30, 567–579.
Kvamme, M., 1993. Holocene forest limit fluctuations and glacier development in the mountains of southern Norway and their relevance to climate history. In: Frenzel, B., Eronen, M., Vorren, K.D., Glaser, B. (Eds.), Oscillations of the Alpine and Polar Tree Limits in the Holocene. Gustav Fischer Verlag, Stuttgart, pp. 99–113.
Kvamme, T., Mangerud, J., Fumes, H., Ruddiman, W.F., 1989. Geochemistry of Pleistocene ash zones in cores from the North Atlantic. Nor. Geol. Tidsskr. 69, 251–272.
Labeyrie, L., Duplessy, J.-C., Blanc, P.L., 1987. Variations in mode of formation and temperature of oceanic waters over the past 125,000 years. Nature. 327, 477–482.
Labrijn, A., 1945. Het Klimaat van Nederland gedurende de laatste twee en een halve eeuw. Mededelingen en Verhandlingen. 49, 11–105 (Koninklijk Nederlands Met. lnst. No. 102).
Lachniet, M.S., Asmerom, Y., Burns, S.J., Patterson, W.P., Polyak, V.J., Seltzer, G.O., 2004a. Tropical response to the 8200 B.P. cold event? Speleothem isotopes indicate a weakened early Holocene monsoon in Costa Rica. Geology. 32, 957–960.
Lachniet, M.S., Burns, S.J., Piperno, J., Asmerom, Y., Polyak, V.J., Moy, C.M., Christenson, K., 2004b. A 1500-year El Niño/Southern Oscillation and rainfall history for the Isthmus of Panama from speleothem calcite. J. Geophys. Res. 109. D20177. dx.doi.org/10.1029/2004JD004694.
Laird, K.R., Fritz, S.C., Grimm, E.C., Mueller, P.G., 1996. Century-scale reconstruction from Moon Lake, a closed basin lake in the northern Great Plains. Limnol. Oceanogr. 41, 890–902.
Laird, K.R., Fritz, S.C., Cumming, B.F., 1998. A diatom-based reconstruction of drought intensity, duration and frequency from Moon Lake, North Dakota: a sub-decadal record of the last 2300 years. J. Paleolimnol. 19, 161–179.
Laj, C., Channell, J.E.T., 2007. Geomagnetic excursions. In: Kono, M. (Ed.), Geomagnetism. Treatise on Geophysics, vol. 5. Elsevier, Amsterdam, pp. 373–416.
Laj, C., Kissel, C., Mazaud, A., Channell, J.E.T., Beer, J., 2000. North Atlantic palaeointensity stack since 75ka (NAPIS-75) and the duration of the Laschamp event. Philos. Trans. R. Soc. Lond. A. 358, 1009–1025.
Lajoux, J.-D., 1963. The Rock Paintings of the Tassili. Thames and Hudson, London.
Lal, D., 1991. Cosmic ray labeling of erosion surfaces: in situ nuclide production rates and erosion models. Earth Planet. Sci. Lett. 104, 424–439.
Lal, D., Charles, C., 2007. Deconvolution of the atmospheric radiocarbon record in the last 50,000 years. Earth Planet. Sci. Lett. 258, 550–560.
LaMarche, V.C., 1973. Holocene climatic variations inferred from treeline fluctuations in the White Mountains, California. Quat. Res. 3, 632–660.
LaMarche, V.C., 1982. Sampling strategies. In: Hughes, M.K., Kelly, P.M., Pilcher, J.R., LaMarche, V.C. (Eds.), Climate from Tree Rings. Cambridge University Press, Cambridge, pp. 2–6.
LaMarche, V.C., Fritts, H.C., 1971. Tree rings, glacial advance and climate in the Alps. Z. Gletscherk. Glazialgeol. 7, 125–131.
LaMarche, V.C., Mooney, H.A., 1967. Altithermal timberline advance in western United States. Nature. 213, 980–982.
LaMarche, V.C., Mooney, H.A., 1972. Recent climatic change and development of the bristlecone pine (*P. longaeva* Bailey) Krummholz zone, Mt. Washington, Nevada. Arct. Alp. Res. 4, 61–72.
Lamb, H.H., 1961. Climatic change within historical time as seen in circulation maps and diagrams. Ann. N. Y. Acad. Sci. 95, 124–161.

Lamb, H.H., 1963. On the nature of certain climatic epochs which differed from the modern 1900-1939) normal. In: Changes of Climate. Proceedings of the WMO-UNESCO Rome 1961 Symposium on Changes of Climate. UNESCO Arid Zone Research Series XX, UNESCO, Paris, pp. 125–150.
Lamb, H.H., 1965. The early Medieval warm epoch and its sequel. Palaeogeogr. Palaeoclimatol. Palaeoecol. 1, 13–37.
Lamb, H.H., 1970. Volcanic dust in the atmosphere; with a chronology and assessment of its meteorological significance. Philos. Trans. R. Soc. Lond. A266, 425–533.
Lamb, H.H., 1977. Climate, Present, Past and Future, vol. 2 Methuen, London.
Lamb, H.H., 1983. Update of the chronology of assessments of the volcanic dust veil index. Clim. Monit. 12, 79–90.
Lamb, H.H., 1988. Climate and life during the Middle Ages, studied especially in the mountains of Europe. In: Weather, Climate and Human Affairs. Routledge, London, pp. 40–74.
Lambeck, K., Chappell, J., 2001. Sea level change through the last glacial cycle. Science. 292, 679–686.
Lambert, G.-N., Bernard, V., Doncerain, C., Girardclos, O., Lavier, C., Szepertisky, B., Trenard, Y., 1996. French regional oak chronologies spanning more than 1000 years. In: Dean, J.S., Meko, D.M., Swetnam, T.W. (Eds.), Tree Rings, Environment and Humanity. University of Arizona, Tucson, pp. 821–832.
Lambert, F., Delmonte, B., Petit, J.R., Bigler, M., Kaufmann, P.R., Hutterli, M.A., Stocker, T.F., Ruth, U., Steffensen, J.P., Maggi, V., 2008. Dust-climate couplings over the past 800,000 years from the EPICA Dome C ice core. Nature. 452, 616–619.
Lambert, F., Bigler, M., Steffensen, J.P., Hutterli, M., Fischer, H., 2012. Centennial mineral dust variability in high-resolution ice core data from Dome C, Antarctica. Clim. Past. 8, 609–623.
Lamothe, M., Balescu, S., Auclair, M., 1994. Natural IRSL intensities and apparent luminescence ages of single feldspar grains extracted from partially bleached sediments. Radiat. Meas. 23, 555–561.
Landais, A., Barnola, J.M., Masson-Delmotte, V., Jouzel, J., Chappellaz, J., Caillon, N., Huber, C., Leuenberger, M., Johnsen, S.J., 2004. A continuous record of temperature evolution over a sequence of Dansgaard-Oeschger events during Marine Isotope Stage 4 (76 to 62 kyr B.P.). Geophys. Res. Lett. 31. L22211. dx.doi.org/10.1029/2004GL021193.
Landais, A., Masson-Delmotte, V., Jouzel, J., Raynaud, D., Johnsen, S., Huber, C., Leuenberger, M., Schwander, J., Minster, B., 2006. The glacial inception as recorded in the North-GRIP Greenland ice core: timing, structure and associated abrupt temperature changes. Clim. Dyn. 26, 273–284.
Landais, A., Dreyfus, G., Capron, E., Pol, K., Loutre, M.F., Raynaud, D., Lipenkov, V.Y., Arnaud, L., Masson-Delmotte, V., Paillard, D., Jouzel, J., Leuenberger, M., 2012. Towards orbital dating of the EPICA Dome C ice core using $\delta O_2/N_2$. Clim. Past. 8, 191–203.
Langbein, W.B., 1961. Salinity and Hydrology of Enclosed Lakes. US Geological Survey Professional Paper 412US Geological Survey, Washington, DC.
Langbein, W.B., et al., 1949. Annual runoff in the United States. US Geological Survey Circular 52, US Geological Survey, Washington, DC.
Larkin, A., Haigh, J.D., Djavidnia, S., 2000. The effect of solar UV irradiance variations on the earth's atmosphere. Space Sci. Rev. 94, 199–214.
Larocque, I., Hall, R.I., Grahn, E., 2001. Chironomids as indicators of climate change: a 100-lake training set from a subarctic region of northern Sweden (Lapland). J. Paleolimnol. 26, 307–322.
Larsen, J.A., 1974. Ecology of the northern continental forest border. In: Ives, J.D., Barry, R.G. (Eds.), Arctic and Alpine Environments. Methuen, London, pp. 341–369.
Laskar, J., Joutel, F., Boudin, F., 1993. Orbital, precession and insolation quantities for the Earth from -20 Myr to +10Myr. Astron. Astrophys. 270, 522–533.
Latorre, C., Betancourt, J.L., Rylander, K.A., Quade, J., 2002. Vegetation invasions into absolute desert: a 45,000 yr rodent midden record from the Calama–Salar de Atacama basins, northern Chile (lat 22°–24°S). Geol. Soc. Am. Bull. 114, 349–366.
Lauritzen, S.E., Haugen, J.E., Lovlie, R., Gilje-Nielson, H., 1994. Geochronological potential of isoleucine epimerization in calcite speleothems. Quat. Res. 41, 52–58.
Lavier, C., Lambert, G.-N., 1996. Dendrochronology and works of art. In: Dean, J.S., Meko, D.M., Swetnam, T.W. (Eds.), Tree Rings, Environment and Humanity. University of Arizona, Tucson, pp. 543–556.
Lavigne, F., Degeai, J.-P., Komorowski, J.-C., Guillet, S., Robert, V., Lahitte, P., Oppenheimer, C., Stoffel, M., Vidai, C.M., Surono, Pratomo, I., Wassmer, P., Hajdas, I., Hadmoko, D.S., de Belizai, E., 2013. Source of the great

A.D. 1257 mystery eruption unveiled, Samalas volcano, Rinjani Volcanic Complex, Indonesia. Proceedings of the National Academy of Sciences. dx.doi.org/10.1073/pnas.1307520110.
Lavoie, C., Payette, S., 1992. Black spruce growth forms as a record of a changing winter environment at treeline, Quebec, Canada. Arct. Alp. Res. 24, 40–49.
Lawrence, J.K., Ruzmaikin, A.A., 1998. Transient solar influence on terrestrial temperature fluctuations. Geophys. Res. Lett. 25, 159–162.
Lawrence, J.R., White, J.W.C., 1991. The elusive climate signal in the isotopic composition of precipitation. In: Taylor Jr., H.P., O'Neil, J.R., Kaplan, I.R. (Eds.), Stable Isotope Geochemistry: a Tribute to Samuel Epstein. Special Publication No. 3, The Geochemical Society, St. Louis, pp. 169–185.
Lazareth, C.E., Rosell, M.G.B., Turcq, B., Le Cornec, F., Mandeng-Yogo, M., Caquineau, S., Cabioch, G., 2013. Mid-Holocene climate in New Caledonia (southwest Pacific): coral and PMIP models monthly resolved results. Quat. Sci. Rev. 69, 83–97.
Lea, D.W., Shen, G.T., Boyle, E.A., 1989. Coralline barium records temporal variability in equatorial Pacific upwelling. Nature. 340, 373–376.
Lea, D.W., Pak, D.K., Peterson, L.C., Hughen, K.A., 2003. Synchroneity of tropical and high-latitude Atlantic temperatures over the Last Glacial Termination. Science. 301, 1361–1364.
Lean, J., 1994. Solar forcing of global change. In: Nesme-Ribes, E. (Ed.), The Solar Engine and its Influence on Terrestrial Atmosphere and Climate. Springer-Verlag, New York, pp. 163–184.
Lean, J.L., 2000. Evolution of the Sun's spectral irradiance since the Maunder Minimum. Geophys. Res. Lett. 27, 2425–2428.
Lean, J.L., 2010. Cycles and trends in solar irradiance and climate. Wiley Interdiscip. Rev. Clim. Chang. 1, 111–122.
Lean, J., Rind, D., 1994. Solar variability: implications for global change. Eos. Trans. Am. Geophys. Union. 75, 1, 5–7.
Lean, J., Skumanich, A., White, O.R., 1992. Estimating the Sun's radiative output during the Maunder Minimum. Geophys. Res. Lett. 19, 1591–1594.
Lean, J., Beer, J., Bradley, R.S., 1995. Reconstruction of solar irradiance since A.D. 1600 and implications for climate change. Geophys. Res. Lett. 22, 3195–3198.
Lean, J., Wang, Y.M., Sheeley Jr., N.R., 2002. The effect of increasing solar activity on the Sun's total and open magnetic flux during multiple cycles: implications for solar forcing of climate. Geophys. Res. Lett. 29, 2224. dx.doi.org/10.1029/2002GL015880.
LeGrande, A.N., Schmidt, G.A., 2008. Ensemble, water-isotope enabled, coupled general circulation modeling insights into the 8.2-kyr event. Paleoceanography. 23, PA3207.
LeGrande, A.N., Schmidt, G.A., 2009. Sources of Holocene variability of oxygen isotopes in paleoclimate archives. Clim. Past. 5, 441–455.
Lehman, S.J., Keigwin, L.D., 1992a. Sudden changes in North Atlantic circulation during the last deglaciation. Nature. 356, 757–762.
Lehman, S.J., Keigwin, L.D., 1992b. Deep circulation revisited. Nature. 358, 197–198.
Lemieux-Dudon, B., Blayo, E., Petit, J.-R., Waelbroeck, C., Svensson, A., Ritz, C., Barnola, J.-M., Narcisi, B.M., Parrenin, F., 2010. Consistent dating for Antarctic and Greenland ice cores. Quat. Sci. Rev. 29, 8–20.
Leng, M.J., 2003. Stable-isotopes in lakes and lake sediment archives. In: Mackay, A., Battarbee, R., Birks, H.J.B., Oldfield, F. (Eds.), Global Change in the Holocene. Arnold, London, pp. 124–139.
Leng, M.J. (Ed.), 2006. Isotopes in Palaeoenvironmental Research. Springer, Dordrecht, 307 pp.
Leng, M.J., Henderson, A.C.G., 2013. Recent advances in isotopes as palaeolimnological proxies. J. Palaeolimnol. 49, 481–496.
Leng, M.J., Marshall, J.D., 2004. Paleoclimatic interpretation of stable isotope data from lake sediment archives. Quat. Sci. Rev. 23, 811–831.
Leonard, E.M., 1997. The relationship between glacial activity and sediment production: evidence from a 4450-year varve record of neoglacial sedimentation in Hector Lake, Alberta, Canada. J. Paleolimnol. 17, 319–330.
Leopold, L.B., 1951. Pleistocene climate in New Mexico. Am. J. Sci. 249, 152–168.
Le Quéré, C., Raupach, M.R., Canadell, J.G., Marland, G., 2009. Trends in the sources and sinks of carbon dioxide. Nat. Geosci. 2, 831–836.
Lerbemko, J.F., Westgate, J.A., Smith, D.G.W., Denton, G.H., 1975. New data on the character and history of the White River volcanic eruption, Alaska. In: Suggate, R.P., Cresswell, M.M. (Eds.), Quaternary Studies. Bulletin No. 13, Royal Society of New Zealand, Wellington, pp. 203–209.

Lerman, J.C., 1972. Carbon-14 dating: origin and correction of isotope fractionation errors in terrestrial living matter. In: Proceedings of 8th International Conference on Radiocarbon Dating, vol. 2. Royal Society of New Zealand, Wellington, pp. 613–624.
LeRoy Ladurie, E., 1971. Times of Feast, Times of Famine. Doubleday, New York.
LeRoy Ladurie, E., Baulant, M., 1981. Grape harvests from the fifteenth through the nineteenth centuries. In: Rotberg, R.I., Rabb, T.K. (Eds.), Climate and History: Studies in Interdisciplinary History. Princeton University Press, Princeton, pp. 259–269.
Le Roy Ladurie, E., Daux, V., Luterbacher, J., 2006. Le climat de Bourgogne et d'ailleurs. Hist. Econ. Soc. 25, 421–436.
Letreguilly, A., Reeh, N., Huybrechts, P., 1991. The Greenland Ice Sheet through the last glacial-interglacial cycle. Glob. Planet. Chang. 90, 385–394.
Lettau, H., 1969. Evapotranspiration climatonomy, I. A new approach to numerical prediction of monthly evapotranspiration, runoff and soil moisture storage. Mon. Weather Rev. 97, 691–699.
Leuenberger, M., Siegenthaler, U., 1992. Ice-age atmospheric concentration of nitrous oxide from an Antarctic ice core. Nature. 360, 449–451.
Levi, S., Karlin, R., 1989. A sixty thousand year paleomagnetic record from Gulf of California sediments: secular variation, late Quaternary excursions and geomagnetic implications. Earth Planet. Sci. Lett. 92, 219–233.
Levi, S., Gudmunsson, H., Duncan, R.A., Kristjansson, L., Gillot, P.V., Jacobsson, S.P., 1990. Late Pleistocene geomagnetic excursion in Icelandic lavas: confirmation of the Laschamp excursion. Earth Planet. Sci. Lett. 96, 443–457.
Lewis, S.C., LeGrande, A.N., Kelley, M., Schmidt, G.A., 2010. Water vapour source impacts on oxygen isotope variability in tropical precipitation during Heinrich events. Clim. Past. 6, 325–343.
Lézine, A.M., Hély, C., Grenier, C., Braconnot, P., Krinner, G., 2011. Sahara and Sahel vulnerabilkity to climate changes, lessons from Holocene hydrological data. Quatern. Sci. Rev. 30, 3001–3012.
Lhote, H., 1959. The Search for the Tassili Frescoes. Hutchinson, London.
Li, P., 1992. South China climate change during the Little Ice Age 16th-19th century. In: Mikami, T. (Ed.), Proceedings of the International Symposium on the Little Ice Age Climate. Department of Geography, Tokyo Metropolitan University, Tokyo, pp. 138–142.
Li, W.-X., Lundberg, J., Dickin, A.P., Ford, D.C., Schwarcz, H.P., McNutt, R., Williams, D., 1989. High precision mass spectrometric uranium-series dating of cave deposits and implications for paleoclimate studies. Nature. 339, 534–536.
Li, C., Battisti, D.S., Schrag, D.P., Tziperman, E., 2005. Abrupt climate shifts in Greenland due to displacements of the sea ice edge. Geophys. Res. Lett. 32, L19702. dx.doi.org/10.1029/2005GL023492.
Li, C., Battisti, D.S., Bitz, C.M., 2010a. Can North Atlantic sea ice anomalies account for Dansgaard-Osechger climate signals? J. Clim. 23, 5457–5475.
Li, F., Sun, J., Zhao, Y., Guo, X., Zhao, W., Zhang, K., 2010b. Ecological significance of common pollen ratios: a review. Front. Earth Sci. China. 4, 253–258.
Lian, O.B., Roberts, R.G., 2006. Dating the Quaternary: progress in luminescence dating of sediments. Quat. Sci. Rev. 25, 2449–2468.
Libby, W.F., 1955. Radiocarbon Dating. University of Chicago Press, Chicago.
Libby, W.F., 1970. Radiocarbon dating. Philos. Trans. R. Soc. Lond. A269, 1–10.
Lieth, H., 1975. Primary productivity in ecosystems: comparative analysis of global patterns. In: van Dobben, W.H., Lowe-McConnell, R.H. (Eds.), Unifying Concepts in Ecology: Report of Plenary Sessions, 1st International Congress on Ecology. Dr W. Junk BV, The Hague, pp. 67–88.
Lin, P.-N., Thompson, L.G., Davis, M.E., Mosley-Thompson, E., 1995. 1000 years of climatic change in China: ice-core $\delta^{18}O$ evidence. Ann. Glaciol. 21, 189–195.
Lindsey, A.A., Newman, J.E., 1956. Use of official data in spring time temperature analysis of Indiana phenological record. Ecology. 37, 812–823.
Linsley, B.K., 1996. Oxygen-isotope record of sea level and climate variations in the Sulu Sea over the past 150,000 years. Nature. 380, 234–237.
Linsley, B.K., Dunbar, R.B., Wellington, G.M., Mucciarone, D.A., 1994. A coral-based reconstruction of Inter-Tropical Convergence Zone variability over central America since 1707. J. Geophys. Res. 99C, 9977–9994.
Linsley, B.K., Wellington, G.M., Schrag, D.P., 2000. Decadal sea surface temperature variability in the subtropical South Pacific from 1726–1997 A.D. Science. 290, 1145–1148.

Linsley, B.K., Wellington, G.M., Schrag, D.P., Ren, L., Salinger, M.J., Tudhope, A.W., 2004. Geochemical evidence from corals for changes in the amplitude and spatial pattern of South Pacific interdecadal climate variability over the last 300 years. Clim. Dyn. 22, 1–11.

Linsley, B.K., Kaplan, A., Gouriou, Y., Salinger, J., Demenocal, P.B., Wellington, G.M., Howe, S.S., 2006. Tracking the extent of the South Pacific Convergence Zone since the early 1600s. Geochem. Geophys. Geosyst. 7, Q05003. dx.doi.org/10.1029/2005GC001115.

Linsley, B.K., Zhang, P., Kaplan, A., Howe, S.S., Wellington, G.M., 2008. Interdecadal-decadal climate variability from multicoral oxygen isotope records in the South Pacific Convergence Zone region since 1650 A.D. Paleoceanography. 23. dx.doi.org/10.1029/2007PA001539.

Lippold, J., Grützner, G., Winter, D., Lahaye, Y., Mangini, A., Christl, M., 2009. Does sedimentary 231Pa/230Th from the Bermuda Rise monitor past Atlantic Meridional Overturning Circulation? Geophys. Res. Lett. 36, L12601. dx.doi.org/10.1029/2009GL038068.

Lippold, J., Luo, Y.M., François, R., Allen, S.E., Gherardi, J., Pichat, S., Hickey, B., Schulz, H., 2012. Strength and geometry of the glacial Atlantic Meridional Overturning Circulation. Nat. Geosci. 5, 813–816.

Lisiecki, L.E., 2010. Links between eccentricity forcing and the 100,000-year glacial cycle. Nat. Geosci. 3, 349–352.

Lisiecki, L.E., Raymo, M.E., 2005. A Pliocene-Pleistocene stack of 57 globally-distributed benthic δ18O records. Paleoceanography. 20, PA1003. dx.doi.org/10.1029/2004PA001071.

Litherland, A.E., Beukens, R.P., 1995. Radiocarbon dating by atom counting. In: Rutter, N.W., Catto, N.R. (Eds.), Dating Methods for Quaternary Deposits. Geological Association of Canada, St. John's, pp. 117–123.

Litt, T., Schölzel, C., Kühl, N., Brauer, A., 2009. Vegetation and climate history in the Westeifel Volcanic Field (Germany) during the past 11000 years based on annually laminated lacustrine maar sediments. Boreas. 38, 679–690.

Liu, K.-B., Colinvaux, P.A., 1985. Forest changes in the Amazon Basin during the last glacial maximum. Nature. 318, 556–557.

Liu, T.S., Ding, Z.L., 1998. Chinese loess and the paleomonsoon. Annu. Rev. Earth Planet. Sci. 26, 111–145.

Liu, W.G., Yang, H., 2008. Multiple controls for the variability of hydrogen isotopic compositions in higher plant *n*-alkanes from modern ecosystems. Glob. Chang. Biol. 14, 2166–2177.

Liu, X.D., Yin, Z.Y., 2002. Sensitivity of East Asian monsoon climate to the uplift of the Tibetan Plateau. Palaeogeogr. Palaeoclimatol. Palaeoecol. 183, 223–245.

Liu, X.D., Yin, Z.Y., 2011. Forms of the Tibetan Plateau uplift and regional differences of the Asian monsoon-arid environmental evolution—a modeling perspective. J. Earth Environ. 2, 401–416.

Liu, T.S., et al., 1985. Loess and the Environment. China Ocean Press, Beijing.

Liu, T.S., Ding, Z., Yu, Z., Rutter, N., 1993. Susceptibility time series of the Baoji section and the bearings on paleoclimatic periodicities in the last 2.5 Ma. Quat. Int. 17, 33–38.

Liu, X., Rolph, T., Bloemendal, J., Shaw, J., Liu, T., 1994. Remanence characteristics of different magnetic grain size categories at Xifeng, central Chinese Loess Plateau. Quat. Res. 42, 162–165.

Liu, X., Rolph, T., Bloemendal, J., Shaw, J., Liu, T., 1995. Quantitative estimates of palaeoprecipitation at Xifeng, in the Loess Plateau of China. Palaeogeogr. Palaeoclimatol. Palaeoecol. 113, 243–248.

Liu, K.-B., Yao, Z., Thompson, L.G., 1998. A pollen record of Holocene climatic changes from the Dunde ice cap, Qinghai-Tibetan Plateau. Geology. 26, 135–138.

Liu, K.-B., Reese, C.A., Thompson, L.D., 2005. Ice-core pollen record of climatic changes in the central Andes during the last 400 yr. Quat. Res. 64, 272–278.

Liu, K.-B., Reese, C.A., Thompson, L.D., 2007. A potential pollen proxy for ENSO derived from the Sajama ice core. Geophys. Res. Lett. 34, L09504. dx.doi.org/10.1029/2006GL0298018.

Liu, D.B., Wang, Y.J., Cheng, H., Edwards, R.L., Kong, X.G., Wang, X.F., Wu, J.Y., Chen, S.T., 2008. A detailed comparison of Asian monsoon intensity and Greenland temperature during the Allerød and Younger Dryas events. Earth Planet. Sci. Lett. 272, 691–697.

Livingstone, D.A., 1982. Quaternary geography and Africa and the refuge theory. In: Prance, G.T. (Ed.), Biological Diversification in the Tropics. Columbia University Press, New York, pp. 523–536.

Ljungqvist, F.C., 2009. Temperature proxy records covering the last two millennia: a tabular and visual overview. Geogr. Ann. 91A, 11–29.

Ljungqvist, F.C., 2010. A new reconstruction of temperature variability in the extra-tropical northern hemisphere during the last two millennia. Geogr. Ann. 92A, 339–351.

Lloyd, A.H., Bunn, A.G., 2007. Responses of the circumpolar boreal forest to 20th century climate variability. Environ. Res. Lett. 2, 045013.
Lloyd, A.H., Fastie, C., 2002. Spatial and temporal variability in the growth and climate response of treeline trees in Alaska. Clim. Chang. 58, 481–509.
Loader, N.J., Hemming, D.L., 2004. The stable isotope analysis of pollen as an indicator of terrestrial palaeoenvironmental change: a review of progress and recent developments. Quat. Sci. Rev. 23, 893–900.
Locke, C.W., Locke, W.W., 1977. Little ice age snow-cover extent and paleoglaciation thresholds: north-central Barfin Island, NWT, Canada. Arct. Alp. Res. 9, 291–300.
Locke, W.W., Andrews, J.T., Webber, P.J., 1979. A Manual for Lichenometry. British Geomorphological Research, Group, Technical Bulletin No. 26University of East Anglia, Norwich.
Loffler, E., 1976. Potassium-argon dates and pre-Würm glaciations of Mount Giluwe volcano, Papua, New Guinea. Z. Gletscherk. Glazialgeol. 12, 55–62.
Lopes dos Santos, R.A., Spooner, M.I., Barrows, T.T., De Decker, P., Sinninghe Damsté, J.S., Schouten, S., 2013. Comparison of organic (Uk'37, TEXH86, LDI) and faunal proxies (foraminiferal assemblages) for reconstruction of late Quaternary sea-surface temperature variability from offshore southeastern Australia. Paleoceanography. 28, dx.doi.org/10.1002/palo.20035.
Lorenz, E.N., 1968. Climatic determinism. Meteorol. Monogr. 8, 1–3.
Lorenz, E.N., 1970. Climatic change as a mathematical problem. J. Appl. Meteorol. 9, 235–239.
Lorenz, E.N., 1976. Non-deterministic theories of climatic change. Quat. Res. 6, 495–507.
Lorius, C., 1991. Polar Ice cores: a record of climatic and environmental changes. In: Bradley, R.S. (Ed.), Global Changes of the Past. University Corporation for Atmospheric Research, Boulder, pp. 261–294.
Lorius, C., Jouzel, J., Ritz, C., Merlivat, L., Barkov, N.I., Korotkevich, Y.S., Kotlyakov, V.M., 1985. A 150,000 year climatic record from Antarctic ice. Nature. 316, 591–596.
Lorius, C., Barkov, N.I., Jouzel, J., Korotkevich, Y.S., Kotlyakov, V.M., Raynaud, D., 1988. Antarctic ice core CO_2: and climatic change over the last climatic cycle. EOS. 69, 681, and 683–684.
Lorius, C., Jouzel, J., Raynaud, D., Hansen, J., Le Treut, H., 1990. The ice core record: climate sensitivity and future greenhouse warming. Nature. 347, 139–145.
Lotter, A.F., 1991. Absolute dating of the late-Glacial period in Switzerland using annually laminated sediments. Quat. Res. 35, 321–330.
Lotter, A.F., 2003. Multi-proxy climatic reconstructions. In: Mackay, A., Battarbee, R., Birks, H.J.B., Oldfield, F. (Eds.), Global Change in the Holocene. Arnold, London, pp. 373–383.
Lotter, A.F., Ammann, B., Sturm, M., 1992. Rates of change and chronological problems during the late-glacial period. Clim. Dyn. 6, 233–239.
Lotter, A.F., Walker, I.R., Brooks, S.J., Hofmann, W., 1999. An intercontinental comparison of chironomid palaeotemperature inference models: Europe vs North America. Quat. Sci. Rev. 18, 717–735.
Lotter, A.F., Pienitz, R., Schmidt, R., 2010. Diatoms as indicators of environmental change in subarctic and alpine regions. In: Smol, J.P., Stoermer, E.F. (Eds.), The Diatoms: Applications for the Environmental and Earth Sciences. Cambridge University Press, Cambridge, pp. 231–248.
Lough, J.M., 1992. An index of the Southern Oscillation reconstructed from western North America tree-ring chronologies. In: Diaz, H.F., Markgraf, V. (Eds.), El Niño: Historical and Paleoclimatic Aspects of the Southern Oscillation. Cambridge University Press, Cambridge, pp. 215–226.
Lough, J.M., 2007. Tropical river flow and rainfall reconstruction from coral luminescence: Great Barrier Reef, Australia. Paleoceanography. 22, PA2218. dx.doi.org/10.1029/2006PA001377.
Lough, J.M., 2010. Climate records from corals. Wiley Interdiscip. Rev. Clim. Chang. 1, 318–331.
Lough, J.M., 2011. Great Barrier Reef coral luminescence reveals rainfall variability over northeastern Australia since the 17th century. Paleoceanography. 26. dx.doi.org/10.1029/2010PA002050.
Lough, J.M., Barnes, D.J., 1990. Intra-annual timing of density band formation of *Porites* coral from the central Great Barrier Reef. J. Exp. Mar. Biol. Ecol. 135, 35–57.
Lough, J.M., Barnes, D.J., 1997. Several centuries of variation in skeletal extension, density and calcification in massive Porites colonies from the Great Barrier Reef: A proxy for seawater temperature and a background of variability against which to identify unnatural change. J. Exp. Mar. Biol. Ecol. 211, 29–67.
Lough, J.M., Cooper, T.F., 2011. New insights from coral growth band studies in an era of raoid environmental change. Earth-Sci. Rev. 108, 170–184.

Lough, J.M., Barnes, D.J., Taylor, R.B., 1996. The potential of massive corals for the study of high resolution climate variation in the past millennium. In: Jones, P.D., Bradley, R.S., Jouzel, J. (Eds.), Climatic Variations and Forcing Mechanisms of the Last 2000 Years. Springer-Verlag, Berlin, pp. 355–371.

Loulerge, L., Schilt, A., Spahni, R., Masson-Delmotte, V., Blunier, T., Lemieux, B., Barnola, J.-M., Raynaud, D., Stocker, T.F., Chappellaz, J., 2008. Orbital and millennial-scale features of atmospheric CH_4 over the past 800,000 years. Nature. 453, 383–386.

Loulergue, L., Parrenin, F., Blunier, T., Barnola, J.-M., Spahni, R., Schilt, A., Raisbeck, G., Chappellaz, J., 2007. New constraints on the gas age-ice age difference along the EPICA ice cores, 0-50kyr. Clim. Past. 3, 527–540.

Loutre, M.-F., Berger, A., Bretagnon, P., Blanc, P.-L., 1992. Astronomical frequencies for climatic research at the decadal to century time scale. Clim. Dyn. 7, 181–194.

Lowe, J.J., Rasmussen, S.O., Björck, S., Hoek, W.Z., Steffensen, J.P., Walker, M.J.C., Yu, Z.C., the INTIMATE group, 2008. Synchronisation of palaeoenvironmental events in the North Atlantic region during the Last Termination: a revised protocol recommended by the INTIMATE group. Quat. Sci. Rev. 27, 6–17.

Lozano, J.A., Hays, J.D., 1976. Relationship of radiolarian assemblages to sediment types and physical oceanography in the Atlantic and western Indian Ocean sectors of the Antarctic Ocean. In: CLine, R.M., Hays, J.D. (Eds.), Investigation of Late Quaternary Paleooceanography and Paleoclimatology. Memoir 145, Geological Society of America, Boulder, pp. 303–336.

Lozhkin, A.V., Anderson, P.M., 2013. Vegetation response to interglacial warming in the Arctic: examples from Lake El'gygytgyn, Far East Russian Arctic. Clim. Past. 9, 1211–1219.

Lu, Y.C., Wang, X.L., Wintle, A.G., 2007. A new OSL chronology for dust accumulation in the last 130,000 yr for the Chinese Loess Plateau. Quat. Res. 67, 152–160.

Lückge, A., Doose-Rolinski, H., Khan, A.A., Schulz, H., von Rad, U., 2001. Monsoonal variability in the northeastern Arabian Sea during the past 5000 years: geochemical evidence from laminated sediments. Palaeogeogr. Palaeoclimatol. Palaeoecol. 167, 273–286.

Luckman, B.H., 1988. Dating the moraines and recession of Athabasca and Dome glaciers, Alberta, Canada. Arct. Alp. Res. 20, 40–54.

Luckman, B.H., 1994. Evidence for climatic conditions between 900-1300 A.D. in the southern Canadian Rockies. Clim. Chang. 26, 171–182.

Luckman, B.H., 1995. Calendar-dated, early 'Little Ice Age' glacier advance at Robson glacier, British Columbia, Canada. The Holocene. 5, 149–159.

Luckman, B.H., 1996. Reconciling the glacial and dendrochronological records for the last millennium in the Canadian Rockies. In: Jones, P.D., Bradley, R.S., Jouzel, J. (Eds.), Climatic Variations and Forcing Mechanisms of the Last 2000 Years. Springer, Berlin, pp. 85–108.

Luckman, B.H., Kearney, M.S., 1986. Reconstruction of Holocene changes in alpine vegetation and climate in the Maligne Range, Jasper National Park, Alberta. Quat. Res. 26, 244–261.

Ludwig, K.R., Simmons, K.R., Szabo, B., Winograd, I.J., Landwehr, J.M., Riggs, A.C., Hoffman, R.J., 1992. Mass spectrometric ^{230}Th-^{234}U-^{238}U dating of the Devil's Hole calcite vein. Science. 258, 284–287.

Lund, S.P., Banderjee, S.K., 1979. Paleosecular geomagnetic variations from lake sediments. Rev. Geophys. Space Phys. 17, 244–249.

Lundberg, J., Ford, D.C., 1994. Late Pleistocene sea level change in the Bahamas from mass spectrometric U-series dating of submerged speleothem. Quat. Sci. Rev. 13, 1–14.

Luterbacher, J., Rickli, R., Xoplaki, E., Tinguely, C., Beck, C., Pfister, C., Wanner, H., 2001. The Late Maunder Minimum (1675–1715) – a key period for studying decadal scale climatic change in Europe. Climatic Change. 49, 441–462.

Luterbacher, J., Xoplaki, E., Dietrich, D., Rickli, R., Jacobeit, J., Beck, C., Gyalistras, D., Schmutz, C., Wanner, H., 2002. Reconstruction of sea level pressure fields over the eastern North Atlantic and Europe back to 1500. Clim. Dyn. 18, 545–561.

Luterbacher, J., Dietrich, D., Xoplaki, E., Grosjean, M., Wanner, H., 2004. European seasonal and annual temperature variability, trends and extremes since 1500. Science. 303, 1499–1503.

Luterbacher, J., Liniger, M.A., Menzel, A., Estrella, N., Della-Marta, P.M., Pfister, C., Rutishauser, T., Xoplaki, E., 2007. The exceptional European warmth of Autumn 2006 and Winter 2007: historical context, the underlying dynamics and its phenological impacts. Geophys. Res. Lett. 34, L12704.

Lüthi, D., Le Floch, M., Bereiter, B., Blunier, T., Barnola, J.-M., Siegenthaler, U., Raynaud, D., Jouzel, J., Fischer, H., Kawamura, K., Stocker, T.F., 2008. High-resolution carbon dioxide concentration record 650,000-800,000 years before present. Nature. 435, 379–382.

Luz, B., 1977. Paleoclimates of the South Pacific based on statistical analysis of planktonic foraminifers. Palaeogeogr. Palaeoclimatol. Palaeoecol. 22, 61–78.

Luz, B., Shackleton, N.J., 1975. $CaCO_3$ solution in the tropical East Pacific during the past 130,000 years. In: Sliter, W.V., Bé, A.W.H., Berger, W.H. (Eds.), Dissolution of Deep-sea Carbonates. Special Publication No. 13, Cushman Foundation for Foraminiferal Research, Washington, DC, pp. 142–150.

Lynch, E.A., 1996. The ability of pollen from small lakes and ponds to sense fine-scale vegetation patterns in the central Rocky Mountains, U.S.A. Rev. Palaeobot. Palynol. 94, 197–210.

Lynch, T.F., Stevenson, C.M., 1992. Obsidian hydration dating and temperature controls in the Punta Negra region of northern Chile. Quat. Res. 37, 117–124.

Lyons, W.B., Mayewski, P.A., Spencer, M.J., Twickler, M.S., Graedel, T.E., 1990. A northern hemisphere volcanic chemistry 1869-1984) and climatic implications using a South Greenland ice core. Ann. Glaciol. 14, 176–182.

Ma, Z.B., Cheng, H., Tan, M., Edwards, R.L., Li, H.C., You, C.F., Duan, W.H., Wang, X., Kelly, M.J., 2012. Timing and structure of the Younger Dryas event in northern China. Quat. Sci. Rev. 41, 83–93.

Maarleveld, G.C., 1976. Periglacial phenomena and the mean annual temperature during the last glacial time in the Netherlands. Biul. Peryglac. 26, 57–78.

Mabres, A., Woodman, R., Zeta, R., 1993. Algunos puntos historicos adicionales sobre la cronologia de El Niño. Bull. Inst. Fr. Etudes Andines. 22, 395–406.

MacAyeal, D., 1993. Binge/purge oscillations of the Laurentide Ice Sheet as a cause of the North Atlantic's Heinrich events. Paleoceanography. 8, 775–784.

MacDonald, G.M., Case, R.A., 2005. Variations in the Pacific Decadal Oscillation over the past millennium. Geophys. Res. Lett. 32, L08703. dx.doi.org/10.1029/2005GL022478.

MacDonald, G.M., Velichko, A.A., Kremenetski, C.V., Borisova, O.K., Goleva, A.A., Andreev, A.A., Cwynar, L.C., Riding, R.T., Forman, S.L., Edwards, T.W.D., Aravena, R., Hammarlund, D., Szeicz, J.C., Gattaulin, V.N., 2000. Holocene treeline history and climate change across northern Eurasia. Quat. Res. 53, 302–311.

Mackay, A., Jones, V.J., Battarbee, R.W., 2003. Approaches to Holocene climate reconstruction using diatoms. In: Mackay, A., Battarbee, R., Birks, H.J.B., Oldfield, F. (Eds.), Global Change in the Holocene. Arnold, London, pp. 294–309.

Mackereth, F.H., 1971. On the variation in direction of the horizontal component of remanent magnetization in lake sediments. Earth Planet. Sci. Lett. 12, 332–338.

Madureira, L.A.S., van Kreveld, S.A., Eglinton, G., Conte, M.H., Ganssen, G., van Hinte, J.E., Ottens, J.J., 1997. Late Quaternary high-resolution biomarker and other sedimentary climate proxies in a northeast Atlantic core. Paleoceanography. 12, 255–269.

Maejima, I., Tagami, Y., 1983. Climate of Little Ice Age in Japan. Geogr. Rep. Tokyo Metropol. Univ. 21, 157–171.

Maejima, I., Tagami, Y., 1986. Climatic change during historical times in Japan: reconstruction from climatic hazards records. Geogr. Rep. Tokyo Metropol. Univ. 21, 157–171.

Magny, M., 1993. Solar influences on Holocene climatic changes. Quat. Res. 40, 1–9.

Maher, L.J., 1963. Pollen analyses of surface materials from the southern San Juan Mountains, Colorado. Geol. Soc. Am. Bull. 74, 1485–1504.

Maher, B.A., 2008. Holocene variability of the East Asian summer monsoon from Chinese cave records: a re-assessment. The Holocene. 18, 861–866.

Maher, B.A., Thompson, R., 1992. Paleoclimatic significance of the mineral magnetic record of the Chinese loess and paleosols. Quat. Res. 37, 155–170.

Maher, B.A., Thompson, R., 1995. Paleorainfall reconstructions from pedogenic magnetic susceptibility variations in the Chinese loess. Quat. Res. 44, 383–391.

Maher, B.A., Thompson, R. (Eds.), 1999. Quaternary Climates, Environments and Magnetism. Cambridge University Press, Cambridge, 390 pp.

Maher, B.A., Thompson, R., Zhou, L.P., 1994. Spatial and temporal reconstructions of changes in the Asian paleomonsoon: a new mineral magnetic approach. Earth Planet. Sci. Lett. 44, 383–391.

Maher, B.A., Alekseev, A., Alekseeva, T., 2003. Magnetic mineralogy of soils across the Russian Steppe: climatic dependence of pedogenic magnetite formation. Palaeogeogr. Palaeoclimatol. Palaeoecol. 201, 321–341.

Mäkilä, M., Saarnisto, M., 2008. Carbon accumulation in boreal peatlands during the Holocene—impacts of climate variations. In: Strack, M. (Ed.), Peatlands and Climate Change. International Peat Society, Jyvaskyla, pp. 24–43.
Maley, J., 1989a. Late Quaternary climatic changes in the African rain forest: forest refugia and the major role of sea-surface temperature variations. In: Leinen, M., Sarnthein, M. (Eds.), Paleoclimatology and Paleometeorology: Modern and Past Patterns of Global Atmospheric Transport. Kluwer Academic, Dordrecht, pp. 585–616.
Maley, J., 1989b. L'importance de la tradition orale et des donées historiques pour Ia reconstruction paleoclimatique du dernier millenaire sur l'Afrique nord-tropicale. In: Sud Sahara, Sahel Nord. Le Centre Culturel Français d'Abidjan, pp. 53–57.
Maley, J., 1991. The African rain forest and palaeoenvironments during Late Quaternary. Clim. Chang. 19, 79–98.
Maley, J., 1996. The African rainforest-main characteristics of changes in vegetation and climate from the Upper Cretaceous to the Quaternary. Proc. Roy. Soc. Edinburgh. 104B, 31–73.
Maley, J., 1997. Middle to Late Holocene changes in Tropical Africa and other continents. Paleomonsoon and sea surface temperature variations. In: Dalfes, H.N., Kukla, G., Weiss, H. (Eds.), Third Millennium B.C. Climate Change and Old World Collapse. Kluwer Academic, Dordrecht, pp. 611–640.
Manabe, S., Stouffer, R., 1988. Two stable equilibria of a coupled ocean-atmosphere model. J. Clim. 1, 841–866.
Manabe, S., Stouffer, R., 1997. Coupled ocean-atmosphere model response to freshwater input: comparison to Younger Dryas event. Paleoceanography. 12, 321–336.
Mangerud, J., 1972. Radiocarbon dating of marine shells including a discussion of apparent age of recent shells from Norway. Boreas. 1, 143–172.
Mangerud, J., Andersen, S.T., Berglund, B.E., Donner, J.J., 1974. Quaternary stratigraphy of Norden, a proposal for terminology and classification. Boreas. 3, 109–128.
Mangerud, J., Lie, S.E., Furnes, H., Kristiansen, I.L., Lømo, L., 1984. A Younger Dryas ash bed in western Norway, and its possible correlations with tephra in cores from the Norwegian Sea and the North Atlantic. Quat. Res. 21, 85–104.
Mangini, A., Spötl, C., Verdes, P., 2005. Reconstruction of temperature in the Central Alps during the past 2000 yr from a $\delta^{18}O$ stalagmite record. Earth Planet. Sci. Lett. 235, 741–751.
Manley, G., 1969. Snowfall in Britain over the past 300 years. Weather. 24, 428–437.
Manley, G., 1974. Central England temperatures: monthly means 1659 to 1973. Quart. J. Roy. Meteorol. Soc. 100, 389–405.
Mann, M.E., Park, J., Bradley, R.S., 1996. Global inter-decadal and century-scale climate oscillations during the past five centuries. Nature. 378, 266–270.
Mann, M.E., Bradley, R.S., Hughes, M.K., 1998. Global scale temperature patterns and climate forcing over the past six centuries. Nature. 392, 779–788 (also Science 280, 2029–2030).
Mann, M.E., Bradley, R.S., Hughes, M.K., 1999. Northern Hemisphere temperatures during the past millennium: inferences, uncertainties, and limitations. Geophys. Res. Lett. 26, 759–762.
Mann, M.E., Bradley, R.S., Hughes, M.K., 2000. Long-term variability in the El Niño/Southern Oscillation and associated teleconnections. In: Diaz, H.F., Markgraf, V. (Eds.), El Niño and the Southern Oscillation: multiscale variability and global and regional impacts. Cambridge University Press, Cambridge, pp. 357–412.
Mann, M.E., Cane, M.A., Zebiak, S.E., Clement, A., 2005. Volcanic and solar forcing of the tropical Pacific over the past 1000 years. J. Clim. 18, 447–456.
Mann, M.E., Zhang, Z., Hughes, M.K., Bradley, R.S., Miller, S., Rutherford, S., Ni, F., 2008. Proxy-based reconstructions of hemispheric and global surface temperature variations over the past two millennia. Proc. Natl. Acad. Sci. U. S. A. 105, 13252–13257.
Mann, M.E., Zhang, Z., Rutherford, S., Bradley, R.S., Hughes, M.K., Shindell, D., Ammann, C., Faluvegi, G., Ni, F., 2009. Global signatures and dynamical origins of the "Little Ice Age" and "Medieval Climate Anomaly". Science. 326, 1256–1260.
Mantua, N.J., Hare, S.R., Zhang, Y., Wallace, J.M., Francis, R.C., 1997. A Pacific interdecadal climate oscillation with impacts on salmon production. Bull. Am. Meteorol. Soc. 78, 1069–1079.
Marchant, R., Berrio, J.C., Cleef, A., Duivenvoorden, J., Helmens, K., Hooghiemstra, H., Kuhry, P., Melief, B., Schreve-Brinkman, E., Van Geel, B., Van Reenen, G., Van der Hammen, T., 2001. A reconstruction of Colombian biomes derived from modern pollen data along an altitude gradient. Rev. Palaeobot. Palynol. 117, 79–92.
Marchitto, T.M., Lehman, S.J., Ortiz, J.D., Flückiger, J., van Geen, A., 2007. Marine radiocarbon evidence for the mechanism of deglacial atmospheric CO_2 rise. Science. 316, 1456–1459.

Marcott, S.A., Clark, P.U., Padman, L., Klinkhammer, G.P., Springer, S.R., Liu, Z.Y., Otto-Bliesner, B.L., Carlson, A.E., Ungerer, A., Padman, J., He, F., Cheng, J., Schmittner, A., 2011. Ice-shelf collapse from subsurface warming as a trigger for Heinrich events. Proc. Natl. Acad. Sci. U. S. A. 108, 13415–13419.
Margari, V., Skinner, L.C., Tzedakis, P.C., Ganapolski, A., Vautravers, M., Shackleton, N.J., 2010. The nature of millennial scale climate variations during the last two glacial periods. Nat. Geosci. 3, 127–131.
MARGO Project Members, 2009. Constraints on the magnitude and patterns of ocean cooling at the Last Glacial Maximum. Nat. Geosci. 2, 127–132.
Margolis, S.V., Kroopnick, P.M., Goodney, D.E., Dudley, W.C., Mahoney, M.E., 1975. Oxygen and carbon isotopes from calcareous nannofossils as paleo-oceanographic indicators. Science. 189, 555–557.
Markgraf, V., 1980. Pollen dispersal in a mountain area. Grana. 19, 127–146.
Markgraf, V., 1989. Palaeoclimates in Central and South America since 18,000 B.P. based on pollen and lake-level records. Quat. Sci. Rev. 8, 1–24.
Marković, S.B., Oches, E.A., McCoy, W.D., Frechen, M., Gaudenyi, T., 2007. Malacological and sedimentological evidence for "warm" glacial climate from the Irig loess sequence, Vojvodina, Serbia. Geochem. Geophys. Geosyst. 8, Q09008. dx.doi.org/10.1029/2006GC001565.
Marković, S.B., Hambach, U., Stevens, T., Kukla, G.J., Heller, F., McCoy, W.D., Oches, E.A., Buggle, B., Zöller, L., 2011. The last million years recorded at the Stari Slankamen (Northern Serbia) loess-palaeosol sequence: revised chronostratigraphy and long-term environmental trends. Quat. Sci. Rev. 30, 1142–1154.
Marra, M.J., Smith, E.G.C., Shulmeister, J., Leschen, R., 2004. Late Quaternary climate change in the Awatere Valley, South Island, New Zealand using a sine model with a maximum likelihood envelope on fossil beetle data. Quat. Sci. Rev. 23, 1637–1650.
Martin, J.H., 1990. Glacial-interglacial CO_2 change: the iron hypothesis. Paleoceanography. 5, 1–13.
Martin, P.S., Sabel, B.E., Shutler Jr., D., 1961. Rampart cave coprolite and ecology of the Shasta ground sloth. Am. J. Sci. 259, 102–127.
Martinson, D.G., Pisias, N.G., Hays, J.D., Imbrie, J., Moore, T.C., Shackleton, N.J., 1987. Age dating and the orbital theory of the ice ages: development of a high resolution 0 to 300,000-year chronostratigraphy. Quat. Res. 27, 1–29.
Martrat, B., Grimalt, J.O., Shackleton, N., De Abreu, L., Hutterli, M.A., Stocker, T.F., 2007. Four climate cycles of recurring deep and surface water destabilizations on the Iberian Margin. Science. 317, 502–507.
Masarik, J., Frank, M., Schäfer, J., Wieler, R., 2001. Correction of in situ cosmogenic nuclide production rates for geomagnetic field intensity variations during the past 800,000 years. Geochim. Cosmochim. Acta. 65, 2995–3003.
Massé, G., Rowland, S.J., Sicre, M.-A., Jacob, J., Jansen, E., Belt, S.T., 2008. Abrupt climate changes for Iceland during the last millennium: evidence from high resolution sea ice reconstructions. Earth Planet. Sci. Lett. 269, 565–569.
Massé, G., Belt, S.T., Crosta, X., Schmidt, S., Snape, I., Thomas, D.N., Rowland, S.J., 2011. Highly branched isoprenoids as proxies for variable sea ice conditions in the Southern Ocean. Antarct. Sci. 1, 1–12.
Masson-Delmotte, V., Jouzel, J., Landais, A., Stievenard, M., Johnsen, S.J., White, J.W.C., Werner, M., Sveinbjornsdottir, A., Fuhrer, K., 2005. GRIP deuterium excess reveals rapid and orbital-scale changes in Greenland moisture origin. Science. 309, 118–121.
Masson-Delmotte, V., Hou, S., Ekaykin, A., Jouzel, J., Aristarain, A., Bernardo, R.T., Bromwich, D., Cattani, O., Delmotte, M., Falourd, S., Frezotti, M., Gallee, H., Genoni, L., Isakkson, E., Landais, A., Helsen, M.M., Hoffmann, G., Lopez, J., Morgan, V., Motoyama, H., Noone, D., Oerter, H., Petit, J.R., Poyer, A., Uemura, R., Schmidt, G.A., Schlosser, E., Simões, J., Steig, E.J., Stenni, B., Stievenard, M., van den Broeke, M.R., van de Wal, R.S.W., van de Berg, W.J., Vimeux, F., White, J.W.C., 2008. A review of Antarctic surface snow isotopic composition: observations, atmospheric circulation, and isotopic modeling. J. Clim. 21, 3359–3387.
Mattey, D., Lowry, D., Duffet, J., Fisher, R., Hodge, E., Frisia, S., 2008. A 53 year seasonally resolved oxygen and carbon isotope record from a modern Gibraltar speleothem: reconstructed drip water and relationship to local precipitation. Earth Planet. Sci. Lett. 269, 80–95.
Matthes, F.E., 1940. Report of the Committee on glaciers. Trans. Am. Geophys. Union. 21, 396–406.
Matthes, F.E., 1942. Glaciers. In: Meinzer, O.E. (Ed.), Hydrology. Dover/McGraw-Hill, New York, pp. 149–219.
Matthews, J.A., 1980. Some problems and implications of ^{14}C dates from a podzol buried beneath an end moraine at Haugabreen, southern Norway. Geogr. Ann. 62A, 185–208.
Matthews, J.A., 1993. Deposits indicative of Holocene climatic fluctuations in the timberline areas of northern Europe: some physical proxy data sources and research approaches. In: Frenzel, B., Eronen, M., Vorren, K.D., Glaser, B.

(Eds.), Oscillations of the Alpine and Polar Tree Limits in the Holocene. Gustav Fischer Verlag, Stuttgart, pp. 85–97.
Matthewson, A.P., Shimmield, G.B., Kroon, D., Fallick, A.E., 1995. A 300 kyr high resolution aridity record of the North African continent. Paleoceanography. 10, 677–692.
Mauquoy, D., van Geel, B., Blaauw, M., van der Plicht, J., 2002. Evidence from northwest European bogs shows 'Little Ice Age' climatic changes driven by variations in solar activity. The Holocene. 12, 1–6.
Mayewski, P.A., White, F., 2002. The Ice Chronicles: The Quest to Understand Global Change. University Press of New England, Hanover, 233 pp.
Mayewski, P.A., Lyons, W.B., Spencer, M.J., Twickler, M., Dansgaard, W., Koci, B., Davidson, C.I., Honrath, R.E., 1986. Sulfate and nitrate concentrations from a South Greenland ice core. Science. 232, 975–977.
Mayewski, P.A., Spencer, M.J., Lyons, W.B., 1992. A review of glaciochemistry with particular emphasis on the recent record of sulfate and nitrate. In: Moore III, B., Schimel, D. (Eds.), Trace Gases and the Biosphere. University Corporation for Atmospheric Research, Boulder, pp. 177–199.
Mayewski, P.A., Meeker, L.D., Whitlow, S., Twickler, M.S., Morrison, M.C., Bloomfield, P., Bond, G.C., Alley, R.B., Gow, A.J., Grootes, P.M., Meese, D.A., Ram, M., Taylor, K.C., Wumkes, W., 1994. Changes in atmospheric circulation and ocean ice cover over the North Atlantic during the last 41,000 years. Science. 263, 1747–1751.
Mayewski, P.A., Twickler, M.S., Whitlow, S.I., Meeker, L.D., Yang, Q., Thomas, J., Kreutz, K., Grootes, P.M., Morse, D.L., Steig, E.J., Waddington, E.D., Saltzman, E.S., Whung, P.-Y., Taylor, K.C., 1996. Climate change during the last deglaciation in Antarctica. Science. 272, 1636–1638.
Mayewski, P.A., Meeker, L.D., Twickler, M.S., Whitlow, S., Yang, Q., Prentice, M., 1997. Major features and forcing of high latitude northern hemisphere atmospheric circulation using a 110,000 year long glaciochemistry series. J. Geophys. Res. 102C, 26345–26366.
McAndrews, J.H., 1966. Postglacial history of prairie, savanna and forest in northwestern Minnesota. Mem. Torrey Bot.l Club. 22, 1–72.
McCarroll, D., 1994. A new approach to lichenometry: dating single-age and diachronous surfaces. The Holocene. 4, 383–396.
McCarroll, D., Loader, N.J., 2004. Stable isotopes in tree rings. Quat. Sci. Rev. 23, 771–801.
McCarroll, D., Loader, N.J., 2006. Isotopes in tree rings. In: Leng, M.J. (Ed.), Isotopes in Palaeoenvironmental Research. Springer, Dordrecht, pp. 67–116.
McCarroll, D., Jalkanen, R., Hicks, S., Tuovinen, M., Gagen, M., Pawallek, F., Eckstein, D., Scvhmitt, U., Autio, J., Heikkinen, O., 2003. Multiproxy dendroclimatology: a pilot study in northern Finland. The Holocene. 13, 829–838.
McCarroll, D., Tuovinen, M., Campbell, R., Gagen, M., Grudd, H., Jalkanen, R., Loader, N.J., Robertson, I., 2011. A critical evaluation of multi-proxy dendroclimatology in northern Finland. J. Quat. Sci. 26, 7–14.
McCarthy, D.P., Luckman, B.H., 1993. Estimating ecesis for tree-ring dating of moraines: a comparative study from the Canadian cordillera. Arct. Alp. Res. 25, 63–68.
McConnaughey, T.A., 1989. C-13 and O-18 isotopic disequilibria in biological carbonates: I. Patterns. Geochim. Cosmochim. Acta. 53, 151–162.
McConnell, J.R., Edwards, R., 2008. Coal burning leaves toxic heavy metal legacy in the Arctic. Proc. Natl. Acad. Sci. U. S. A. 105, 12140–12144.
McConnell, J.R., Edwards, R., Kok, G.L., Flanner, M.G., Zender, C.S., Saltzman, E.S., Banta, J.R., Pasteris, D.R., Carter, M.M., Kahl, J.D., 2007. 20th-century industrial black carbon emissions altered arctic climate forcing. Science. 317, 1381–1384.
McCormac, F.G., Baillie, M.G.L., 1993. Radiocarbon to calendar date conversion: calendrical bandwidths as a function of radiocarbon precision. Radiocarbon. 35, 311–316.
McCoy, W.D., 1987a. The precision of amino acid geochronology and paleothermometry. Quat. Sci. Rev. 6, 43–54.
McCoy, W.D., 1987b. Quaternary aminostratigraphy of the Bonneville Basin, western United States. Geol. Soc. Am. Bull. 98, 99–112.
McCulloch, D., Hopkins, D., 1966. Evidence for an early recent warm interval in northwestern Alaska. Geol. Soc. Am. Bull. 77, 1089–1108.
McCulloch, M.T., Mortimer, G.E., 2008. Applications of the ^{238}U-^{230}Th decay series to dating of fossil and modern corals using MC-ICPMS. Aust. J. Earth Sci. 55, 955–965.
McCulloch, M.T., Gagan, M.K., Mortimer, G.E., Chivas, A.R., Isdale, P.J., 1994. A high resolution Sr/Ca and δ^{18}O coral record from the Great Barrier Reef, Australia and the 1982-1983 El Niño. Geochim. Cosmochim. Acta. 58, 2747–2754.

McDermott, F., 2004. Palaeo-climate reconstructions from stable isotope variations in speleothems: a review. Quat. Sci. Rev. 23, 901–918.
McDermott, F., Schwarcz, H.P., Rowe, P.J., 2006. Isotopes in speleothems. In: Leng, M.J. (Ed.), Isotopes in Palaeoenvironmental Research. Springer, Dordrecht, pp. 185–225.
McDonald, J., Drysdale, R., 2004. The 2002–2003 El Niño recorded in Australian cave drip waters: implications for reconstructing rainfall histories using stalagmites. Geophys. Res. Lett. 31, L22202. dx.doi.org/10.1029/2004GL020859.
McDougall, I., 1995. Potassium-argon dating in the Pleistocene. In: Rutter, N.W., Catto, N.R. (Eds.), Dating Methods for Quaternary Deposits. Geological Association of Canada, St. John's, pp. 1–14.
McDougall, I., Brown, F.H., 2006. Precise 40Ar/39Ar geochronology for the upper Koobi Fora Formation, Turkana Basin, northern Kenya. J. Geol. Soc. 163, 205–220.
McDougall, I., Harrison, T.M., 1999. Geochronology and Thermochronology by the $^{40}Ar/^{39}Ar$ Method, second ed. Oxford University Press, Oxford, 288 pp.
McElhinny, M.W., McFadden, P.L., 2000. Paleomagnetism. Academic Press, San Diego.
McFadden, M.A., Patterson, W.P., Mullins, H.T., Anderson, W.T., 2005. Multi-proxy approach to long- and short-term Holocene climate-change: evidence from eastern Lake Ontario. J. Paleolimnol. 33, 371–391.
McGarry, S., Bar-Matthews, M., Matthews, A., Vaks, A., Schilman, B., Ayalon, A., 2004. Constraints on hydrological and paleotemperature variations in the eastern Mediterranean region in the last 140ky given by the δD values of speleothem fluid inclusions. Quat. Sci. Rev. 23, 919–934.
McGregor, S., Timmermann, A., Timm, O., 2010. A unified proxy for ENSO and PDO variability since 1650. Clim. Past. 6, 1–17.
McGregor, H.V., Fischer, M.J., Gagan, M.K., Fink, D., Woodroffe, C.D., 2011. Environmental control of the oxygen isotope composition of *Porites* coral microatolls. Geochim. Cosmochim. Acta. 75, 3930–3944.
McIntyre, A., Molfino, B., 1996. Forcing of Atlantic equatorial and subpolar millennia) cycles by precession. Science. 274, 1867–1870.
McIntyre, A., Ruddiman, W.F., Jantzen, R., 1972. Southward penetrations of the North Atlantic Polar Front: faunal and floral evidence of large-scale surface water mass movements over the last 225,000 years. Deep Sea Res. 19, 61–77.
McIntyre, A., Bé, A.W.H., Hays, J.D., Gardner, J.V., Lozano, J.A., Molfino, B., Prell, W., Thierstein, H.R., Crowley, T., Imbrie, J., Kellogg, T., Kipp, N., Ruddiman, W.F., 1975. Thermal and oceanic structures of the Atlantic through a glacial-interglacial cycle. In: Proceedings of WMO Symposium on Long-term Climatic Fluctuations. World Meteorological Organization, Geneva, pp. 75–80, WMO No. 421.
McIntyre, A., Kipp, N.G., Bé, A.W.H., Crowley, T., Kellogg, T., Gardner, J.V., Prell, W., Ruddiman, W.F., 1976. Glacial North Atlantic 18 000 years ago: a CLIMAP reconstruction. In: Cline, R.M., Hays, J.D. (Eds.), Investigation of Late Quaternary Paleooceanography and Paleoclimatology. Geological Society of America, Boulder, pp. 43–76, Memoir 145.
McManus, D.A., 1970. Criteria of climatic change in the inorganic components of marine sediments. Quat. Res. 1, 72–102.
McManus, J.F., Bond, G.C., Broecker, W.S., Johnsen, S., Labeyrie, L., Higgins, S., 1994. High-resolution climate records from the North Atlantic during the last interglacial. Nature. 371, 326–329.
McManus, J.F., Francois, R., Gherardi, J.-M., Keigwin, L.D., Brown-Leger, S., 2004. Collapse and rapid resumption of Atlantic meridional circulation linked to deglacial climate changes. Nature. 428, 834–837.
Medina-Elizalde, M., 2013. A global compilation of coral sea-level benchmarks: implications and new challenges. Earth Planet. Sci. Lett. 362, 310–318.
Medina-Elizalde, M., Lea, D.W., 2005. The mid-Pleistocene transition in the Tropical Pacific. Science. 310, 1009–1012.
Medina-Elizalde, M., Burns, S.J., Lea, D.W., Asmerom, Y., Von Gunten, L., Polyak, V., Vuille, M., Karmalkar, A., 2010. High resolution stalagmite record from the Yucatán peninsula spanning the Maya terminal classic period. Earth Planet. Sci. Lett. 298, 255–262.
Meehl, G.A., Stocker, T.F., Collins, W.D., Friedlingstein, P., Gaye, A.T., Gregory, J.M., Kitoh, A., Knutti, R., Murphy, J.M., Noda, A., Raper, S.C.B., Watterson, I.G., Weaver, A.J., Zhao, Z.C., 2007. Global climate projections. In: Solomon, S., Qin, D., Manning, M., Chen, Z., Marquis, M., Averyt, K.B., Tignor, M., Miller, H.L. (Eds.), Climate Change 2007: The Physical Science Basis. Cambridge University Press, Cambridge, pp. 747–845.

Meehl, G.A., Arblaster, J.M., Matthes, K., Sassi, F., van Loon, H., 2009. Amplifying the Pacific climate system response to a small 11-year solar cycle forcing. Science. 325, 1114–1118.
Meese, D.A., Gow, A.J., Grootes, P., Mayewski, P.A., Ram, M., Stuiver, M., Taylor, K.C., Waddington, E.D., Zielinski, G.A., 1994. The accumulation record from the GISP2 core as an indicator of climate change throughout the Holocene. Science. 266, 1680–1682.
Meese, D.A., Gow, A.J., Alley, R.B., Zielinski, G.A., Grootes, P.M., Ram, M., Taylor, K.C., Mayewski, P.A., Bolzan, J.F., 1997. The GISP2 depth-age scale: methods and results. J. Geophys. Res. 102C, 26411–26423.
Meggers, B.J., 1982. Archeological and ethnographic evidence compatible with the model of forest fragmentation. In: Prance, G.T. (Ed.), Biological Diversification in the Tropics. Columbia University Press, New York, pp. 483–496.
Meier, N., Rutishauser, T., Pfister, C., Wanner, H., Luterbacher, J., 2007. Grape harvest dates as a proxy for Swiss April to August temperature reconstructions back to AD 1480. Geophys. Res. Lett. 34, L20705. dx.doi.org/10.1029/2007GL031381.
Meinel, A., Meinel, M., 1983. Sunsets, Twilights and Evening Skies. Cambridge University Press, Cambridge.
Meko, D.M., Woodhouse, C.A., 2005. Tree-ring footprint of joint hydrologic drought in Sacramento and upper Colorado River basins, western USA. J. Hydrol. 308, 196–213.
Meko, D.M., Stockton, C.W., Boggess, W.R., 1980. A tree-ring reconstruction of drought in southern California. Water Resour. Res. 16, 594–600.
Meko, D.M., Therrell, M.D., Baisan, C.H., Hughes, M.K., 2001. Sacramento River flow reconstructed to A. D. 869 from tree rings. J. Am. Water Resour. Assoc. 37, 1029–1040.
Meko, D.M., Woodhouse, C.A., Baisan, C.A., Knight, T., Lukas, J.J., Hughes, M.K., Salzer, M.W., 2007. Medieval drought in the upper Colorado River Basin. Geophys. Res. Lett. 34, L10705. dx.doi.org/10.1029/2007GL029988.
Melles, M., Brigham-Grette, J., Minyuk, P.S., Nowaczyk, N.R., Wennrich, V., DeConto, R.M., Anderson, P.M., Andreev, A.A., Coletti, A., Cook, T.L., Haltia-Hovi, E., Kukkonen, M., Lozhkin, A.V., Rosén, P., Tarasov, P., Vogel, H., Wagner, B., 2012. 2.8 Million Years of Arctic climate change from Lake El'gygytgyn, NE Russia. Science. 337, 315–320.
Melvin, T.M., Briffa, K.R., 2004. A "signal-free" approach to dendroclimatic standardisation. Dendrochronologia. 26, 71–86.
Mendoza, B., García-Acosta, V., Velasco, V., Jáuregui, E., Diaz-Sandoval, R., 2007. Frequency and duration of historical droughts from the 16th to the 19th centuries in the Mexican Maya lands, Yucatan Peninsula. Clim. Chang. 83, 151–168.
Mesolella, K.J., Matthews, R.K., Broecker, W.S., Thurber, D.L., 1969. The astronomical theory of climatic change: Barbados data. J. Geology. 77, 250–274.
Messerli, B., Messerli, P., Pfister, C., Zumbuhl, H.J., 1978. Fluctuations of climate and glaciers in the Bernese Oberland, Switzerland and their geological significance, 1600–1975. Arct. Alp. Res. 10, 247–260.
Metz, B., Davidson, O.R., Bosch, P.R., Dave, R., Meyer, L.A. (Eds.), 2007. Mitigation of Climate Change. Cambridge University Press, Cambridge, 851 pp.
Meyer, C.E., Sarna-Wojcicki, A.M., Hillhouse, J.W., Woodward, M.J., Slate, J.L., Sorg, D.H., 1991. Fission-track age (400,000 yr) of the Rockland tephra, based on inclusion of zircon grains lacking fossil fission tracks. Quat. Res. 35, 367–382.
Meyers, P.A., Lallier-Vergès, E., 1999. Lacustrine sedimentary organic matter records of Late Quaternary paleoclimates. J. Paleolimnol. 21, 345–372.
Michel, P., 1973. Les bassins des Fleuves Senegal et Gambie: Etude Geomorphologie. Memoires no. 63, Office de Ia Recherche Scientifique et Technique d'Outre-mer, Paris.
Michels, J.W., Bebrich, C.A., 1971. Obsidian hydration dating. In: Michael, H.N., Ralph, E.K. (Eds.), Dating Techniques for the Archaeologist. MIT Press, Cambridge, pp. 164–221.
Mickler, P.J., Banner, J.L., Stern, L., Asmerom, Y., Edwards, R.L., Ito, E., 2004. Stable isotope variations in modern tropical speleothems: evaluating equilibrium vs. kinetic isotope effects. Geochim. Cosmochim. Acta. 68, 4381–4393.
Mifflin, M.D., Wheat, M.M., 1979. Pluvial lakes and estimated pluvial climates of *Nevada*. Bulletin 94, Nevada Bureau of Mines and GeologyUniversity of Nevada, Reno.
Migliazza, E.C., 1982. Linguistic prehistory and the refuge model in Amazonia. In: Prance, G.T. (Ed.), Biological Diversification in the Tropics. Columbia University Press, New York, pp. 497–519.
Mignot, J., Ganapolski, A., Levermann, A., 2007. Atlantic subsurface temperatures: response to a shutdown of the overturning circulation and consequences for its recovery. J. Clim. 20, 4884–4898.

Mikami, T. (Ed.), 1992a. Proceedings of International Symposium on the Little Ice Age Climate. Department of Geography, Tokyo Metropolitan University, Tokyo.
Mikami, T. (Ed.), 1992b. Climate variations in Japan during the Little Ice Age. Proceedings of the International Symposium on the Little Ice Age Climate. Department of Geography, Tokyo Metropolitan University, Tokyo, pp. 176–181.
Mikami, T., 1999. Quantitative climate reconstruction in Japan based on historical documents. Bull. Natl. Mus. Jpn. Hist. 81, 41–50.
Mikami, T., 2008. Climatic variations in Japan reconstructed from historical documents. Weather. 63, 190–193.
Milankovitch, M.M., 1941. Canon of Insolation and the Ice-age Problem. Koniglich Serbische Akademie, Beograd (English translation by the Israel Program for Scientific Translations, published for the US Department of Commerce and the National Science Foundation, Washington, DC. 1969).
Miller, J.A., 1972. Dating Holocene and Pleistocene strata using the potassium argon and argon-40/argon-39 methods. In: Bishop, W.W., Miller, J.A. (Eds.), Calibration of Hominoid Evolution. Scottish Academic Press, Edinburgh, pp. 63–73.
Miller, G.H., 1973. Variations in lichen growth from direct measurements: preliminary curves for *Alectoria minuscula* from eastern Baffin Island, NWT, Canada. Arct. Alp. Res. 5, 333–339.
Miller, G.H., Andrews, J.T., 1973. Quaternary history of northern Cumberland Peninsula, east Baffin Island, NWT, Canada, Part VI. Preliminary lichen growth curve for *Rhizocarpon geographicum*. Geol. Soc. Am. Bull. 83, 1133–1138.
Miller, G.H., Brigham-Grette, J., 1989. Amino acid geochronology: resolution and precision in carbonate fossils. Quat. Int. 1, 111–128.
Miller, G.H., Hare, P.E., 1975. Use of amino acid reactions in some arctic marine fossils as stratigraphic and geochronologic indicators. Carnegie Inst. Wash. Yearbook. 74, 612–617.
Miller, G.H., Hare, P.E., 1980. Amino acid geochronology: integrity of the carbonate matrix and potential of molluscan fossils. In: Hare, P.E., Hoering, T.C., King Jr., K. (Eds.), Biogeochemistry of Amino Acids. Wiley, New York, pp. 415–443.
Miller, G.H., Mangerud, J., 1985. Aminostratigraphy of European marine interglacial deposits. Quat. Sci. Rev. 4, 215–278.
Miller, G.H., Bradley, R.S., Andrews, J.T., 1975. Glaciation level and lowest equilibrium line altitude in the High Canadian Arctic: maps and climatic interpretation. Arct. Alp. Res. 7, 155–168.
Miller, G.H., Hollin, J.T., Andrews, J.T., 1979. Aminostratigraphy of UK Pleistocene deposits. Nature. 281, 539–543.
Miller, G.H., Magee, J.W., Jull, A.J.T., 1997. Low-latitude glacial cooling in the southern hemisphere from amino-acid racemization in emu eggshells. Nature. 385, 241–244.
Miller, G.H., Geirsdóttir, A., Zhong, Y., Larsen, D.J., Otto-Bliesner, B.L., Holland, M.M., Bailey, D.A., Refsynder, K.A., Lehman, S.J., Southon, J.R., Anderson, C., Bjornsson, H., Thordarson, T., 2012. Abrupt onset of the Little Ice Age triggered by volcanism and sustained by sea-ice/ocean feedbacks. Geophys. Res. Lett. 39, L02708. dx.doi.org/10.1029/2011GL05016.
Min, G.R., Edwards, R.L., Taylor, F.W., Récy, J., Gallup, C.D., Beck, J.W., 1995. Annual cycles of U/Ca in coral skeletons and U/Ca thermometry. Geochim. Cosmochim. Acta. 59, 2025–2042.
Miroshnikov, L.D., 1958. Ostatki drevney lesnoy rastitel'nosti na Taymyrskom poluostrove. Priroda, Moskva. 2, 106–107.
Mitchell, J.M., 1976. An overview of climatic variability and its causal mechanisms. Quat. Res. 6, 481–493.
Mitchell, J.M., Dzerdzeevski, B., Flohn, H., Hofmeyr, W.L., Lamb, H.H., Rao, K.N., Wallén, C.C., 1966. Climate Change. World Meteorological Organization, Geneva, WMO Technical Note No. 79.
Mitsuguchi, T., Matsumoto, E., Abe, O., Uechida, T., Isdale, P.J., 1996. Mg/Ca thermometry in coral skeletons. Science. 274, 961–963.
Mix, A.C., 1987. The oxygen-isotope record of glaciation. In: Ruddiman, W.F., Wright Jr., H.E. (Eds.), North America and Adjacent Oceans During the Last Deglaciation. The Geology of North America, vol. K-3. Geological Society of America, Boulder, pp. 111–135.
Mix, A.C., Ruddiman, W.F., 1984. Oxygen isotope analyses and Pleistocene ice volumes. Quat. Res. 21, 1–20.
Mix, A.C., Bard, E., Schneider, R., 2001. Environmental processes of the ice ages: land, oceans, glaciers (EPILOG). Quat. Sci. Rev. 20, 627–657.
Mizukoshi, M., 1992. Climatic reconstruction in central Japan during the Little Ice Age based on documentary sources. In: Mikami, T. (Ed.), Proceedings of the International Symposium on the Little Ice Age Climate. Department of Geography, Tokyo Metropolitan University, Tokyo, pp. 182–187.

Moberg, A., Sonechkin, D.M., Holmgren, K., Datsenko, N.M., Karlén, W., 2005. Highly variable northern hemisphere temperatures reconstructed from low- and high-resolution proxy data. Nature. 433, 613–617.

Molfino, B., Kipp, N.G., Morley, J.J., 1982. Comparison of foraminiferal, coccolithophorid and Radiolarian paleotemperature equations: assemblage coherency and estimate concordancy. Quat. Res. 17, 279–313.

Mollenhauer, G., Kienast, M., Lamy, F., Meggers, H., Schneider, R.R., Hayes, J.M., Eglinton, T.I., 2005. An evaluation of ^{14}C age relationships between co-occurring foraminifera, alkenones, and total organic carbon in continental margin sediments. Paleoceanography. 20, PA1016. dx.doi.org/10.1029/2004PA001103.

Monnin, E., Indermühle, A., Dällenbach, A., Flückiger, J., Stauffer, B., Stocker, T.F., Raynaud, D., Barnola, J.-M., 2001. Atmospheric CO_2 concentrations over the last glacial termination. Science. 291, 112–114.

Monod, Th., 1963. The late Tertiary and Pleistocene in the Sahara. In: Howell, F.C., Bouliere, F. (Eds.), African Ecology and Human Evolution. Viking Publications in Anthropology No. 36, Wenner-Gren Foundation, New York, pp. 117–229.

Montade, V., Combourieu Nebout, N., Kissel, C., Mulsow, S., 2011. Pollen distribution in marine surface sediments from Chilean Patagonia. Mar. Geol. 282, 161–168.

Moody, D.W., Catchpole, A.J.W., 1975. Environmental Data from Historical Documents by Content Analysis: Freeze-up and Break-up of Estuaries on Hudson Bay, 1714-1871. Manitoba Geographical Studies No. 5, University of Winnipeg, Winnipeg.

Mook, W.G., Bommerson, J.C., Stoverman, W.H., 1974. Carbon isotope fractionation between dissolved bicarbonate and gaseous carbon dioxide. Earth Planet. Sci. Lett. 22, 169–176.

Moore, T.C., 1978. The distribution of radiolarian assemblages in the modern and ice-age Pacific. Mar. Micropaleontol. 4, 229–266.

Moore, P.D., Webb, J.A., 1978. An Illustrated Guide to Pollen Analysis. Hodder and Stoughton, London.

Moore, T.C., Burckle, L.H., Geitzenauer, K., Luz, B., Molina-Cruz, A., Robertson, J.H., Sachs, H., Sancetta, C., Thiede, J., Thompson, P., Wenkam, C., 1980. The reconstruction of sea surface temperatures in the Pacific Ocean of 18,000 BP. Mar. Micropaleontol. 5, 215–247.

Moore, J.C., Narita, H., Maeno, N., 1991. A continuous 770-year record of volcanic acidity from East Antarctica. J. Geophys. Res. 96, 17353–17359.

Morgan, A., 1973. Late Pleistocene environmental changes indicated by fossil insect faunas of the English Midland. Boreas. 2, 173–212.

Morgan, V.I., 1982. Antarctic Ice Sheet surface oxygen isotope values. J. Glaciol. 28, 315–323.

Morgan, A.V., Morgan, A., 1979. The fossil coleoptera of the Two Creeks forest bed, Wisconsin. Quat. Res. 12, 226–240.

Morgan, A.V., Morgan, A., 1981. Paleoentomological methods of reconstructing paleoclimate with reference to interglacial and interstadial insect faunas of southern Ontario. In: Mahaney, W.C. (Ed.), Quaternary Paleoclimate. University of East Anglia, Norwich, pp. 173–192.

Morley, J.J., Hays, J.D., 1979. Comparison of glacial and interglacial oceanographic conditions in the South Atlantic from variations in calcium carbonate and radiolarian distributions. Quat. Res. 12, 396–408.

Morley, J.J., Hays, J.D., 1981. Towards a high-resolution, global, deep-sea chronology for the last 750,000 years. Earth Planet. Sci. Lett. 53, 279–295.

Morley, J.J., Shackleton, N.J., 1978. Extension of the radiolarian *Stylatractus universus* as a biostratigraphic datum to the Atlantic Ocean. Geology. 6, 309–311.

Morrison, R., 1965. Quaternary geology of the Great Basin. In: Wright, H.E., Frey, D.G. (Eds.), The Quaternary of the United States. Princeton University Press, Princeton, pp. 265–286.

Mortensen, A.K., Bigler, M., Grönvold, K., Steffensen, J.P., Johnsen, S.J., 2005. Volcanic ash layers from the Last Glacial Termination in the NGRIP ice core. J. Quat. Sci. 20, 209–219.

Morton, F.I., 1967. Evaporation from large deep lakes. Water Resour. Res. 3, 181–200.

Mosblech, N.A.S., Bush, M.B., Gosling, W.D., Hodell, D., Thomas, L., van Calsteren, P., Correa-Metrio, A., Valencia, B.G., Curtis, J., van Woesik, R., 2012. North Atlantic forcing of Amazonian precipitation during the last ice age. Nat. Geosci. 5, 817–820.

Moschen, R., Lücke, A., Schleser, G.H., 2005. Sensitivity of biogenic oxygen isotopes to changes in surface water temperature and paleoclimatology. Geophys. Res. Lett. 32, http://dx.doi.org/10.1029/2004GL022167 L07708.

Moser, K.A., MacDonald, G.M., 1990. Holocene vegetation change at treeline north of Yellowknife, Northwest Territories. Quat. Res. 34, 227–239.

Mott, R.J., 1975. Palynological studies of lake sediment profiles from southwestern New Brunswick. Can. J. Earth Sci. 12, 273–288.
Moustafa, Y.A., Pätzold, J., Loya, Y., Wefer, G., 2000. Mid-Holocene stable isotope record of corals from the northern Red Sea. Int. J. Earth Sci. 88, 742–751.
Mudelsee, M., Raymo, M.E., 2005. Slow dynamics of Northern Hemisphere glaciation. Paleoceanography. 20, PA4022. dx.doi.org/10.1029/2005PA001153.
Muhs, D.R., Bettis, E.A., Aleinikoff, J.N., McGeehin, J.P., Beann, J., Skipp, G., Marshall, B.D., Roberts, H.M., Johnson, W.C., Benton, R., 2008. Origin and paleoclimatic significance of late Quaternary loess in Nebraska: evidence from stratigraphy, chronology, sedimentology, and geochemistry. Geol. Soc. Am. Bull. 120, 1378–1407.
Müller, F., 1958. Eight months of glacier and soil research in the Everest region. In: Barnes, M. (Ed.), The Mountain World. Harper and Bros, New York, pp. 191–208.
Muller, R.A., 1977. Radioisotope dating with a cyclotron. Science. 196, 489–494.
Muller, R.A., MacDonald, G.J., 1997. Glacial cycles and astronomical forcing. Science. 277, 215–218.
Müller, P.J., Kirst, G., Ruhland, G., von Storch, I., Rosell-Melé, A., 1998. Calibration of the alkenone paleotemperature index $U^{K'}_{37}$ based on core-tops from the eastern South Atlantic and the global ocean (60°N-60°S). Geochim. Cosmochim. Acta. 62, 1757–1772.
Müller, J., Wagner, A., Fahl, K., Stein, R., Prange, M., Lohmann, G., 2011. Towards quantitative sea ice reconstructions in the northern North Atlantic: a combined biomarker and numerical modelling approach. Earth Planet. Sci. Lett. 306, 137–148.
Mullineaux, D.R., 1974. Pumice and Other Pyroclastic Deposits in Mount Rainier National Park, Washington. Bulletin 1326, US Geological Survey, Washington, DC.
Mulvaney, R., Peel, D.A., 1987. Anions and cations in ice cores from Dolleman Island and the Palmer Land plateau, Antarctic Peninsula. Ann. Glaciol. 10, 121–125.
Murata, A., 1992. Reconstruction of rainfall variation of the Baiu in historical times. In: Bradley, R.S., Jones, P.D. (Eds.), Climate Since A.D. 1500. Routledge, London, pp. 224–245.
Murray, A.S., Wintle, A.G., 2000. Luminescence dating of quartz using an improved regenerative-dose protocol. Radiat. Meas. 32, 57–73.
Muscheler, R., Kromer, B., Bjorck, S., Svensson, A., Friedrich, M., Kaiser, K.F., Southon, J., 2008. Tree rings and ice cores reveal ^{14}C calibration uncertainties during the Younger Dryas. Nat. Geosci. 1, 263–267.
Naafs, B.D.A., Hefter, J., Stein, R., 2012. Application of the long chain diol index (LDI) paleothermometer to the early Pleistocene (MIS 96). Org. Geochem. 49, 83–85.
Naeser, C.W., Naeser, N.D., 1988. Fission track dating of Quaternary events. In: Easterbrook, D.J. (Ed.), Dating Quaternary Sediments. Special Paper 227Boulder Geological Society of America, pp. 1–11.
Naeser, C.W., Briggs, N.D., Obradovich, J.D., Izett, G.A., 1981. Geochronology of tephra deposits. In: Self, S., Sparks, R.J.S. (Eds.), Tephra StudiesD. Reidel, Dordrecht, pp. 13–47.
National Research Council, 2002. Abrupt Climate Change: Inevitable Surprises. National Academy Press, Washington, DC, 230 pp.
National Research Council, 2003. Understanding Climate Change Feedbacks. National Academies Press, Washington D.C. 152 pp.
Naurzbaev, M.M., Vaganov, E.A., 2000. Variation of early summer and annual temperature in east Taymir and Putoran (Siberia) over the last two millennia inferred from tree rings. J. Geophys. Res. 16 (D6), 7317–7326.
NEEM community members, 2013. Eemian intereglacial reconstructed from a Greenland folded ice core. Nature. 493, 489–494.
Neff, U., Burns, S.J., Mangini, A., Mudelsee, M., Fleitmann, D., Matter, A., 2001. Strong coherence between solar variability and the monsoon in Oman between 9 and 6 kyr ago. Nature. 411, 290–293.
Neftel, A., Oeschger, H., Stauffer, B., 1988. CO_2 record in the Byrd ice core 50,000-5,000 years B.P. Nature. 331, 609–611.
Nelson, D.E., 1990. A new method for carbon isotopic analysis of protein. Science. 251, 552–554.
Nelson, D.E., Korteling, R.G., Stott, W.R., 1977. Carbon-14: direct detection at natural concentrations. Science. 198, 507–508.
Nesje, A., 2009. Latest Pleistocene and Holocene alpine glacier fluctuations in Scandinavia. Quat. Sci. Rev. 28, 2119–2136.
Nesje, A., Dahl, S.O., 2000. Glaciers and Environmental Change. Arnold, London, 203 pp.

Nesje, A., Kvamme, M., Løvlie, R., 1991. Holocene glacial and climate history of the Jostedalsbreen region, western Norway: evidence from lake sediments and terrestrial deposits. Quat. Sci. Rev. 10, 87–114.
Nesje, A., Dahl, S.O., Andersson, C., Matthews, J.A., 2000. The lacustrine sedimentary sequence in Sygneskardvatnet, western Norway: a continuous, high-resolution record of the Jostedalsbreen ice cap during the Holocene. Quat. Sci. Rev. 19, 1047–1065.
Neuberger, H., 1970. Climate in art. Weather. 25, 46–56.
Neukom, R., Prieto, M.R., Moyano, R., Luterbacher, J., Pfister, C., Villalba, R., Jones, P.D., Wanner, H., 2009. An extended network of documentary data from South America and its potential for quantitative precipitation reconstructions back to the 16th century. Geophys. Res. Lett. 36, L12703. dx.doi.org/10.1029/2009GL038351.
Newell, R.E., Chiu, L.S., 1981. Climatic changes and variations: a geophysical problem. In: Berger, A. (Ed.), Climate Variations and Variability: Facts and Theories. Reidel, Dordrecht, pp. 21–61.
Newhall, C.G., Self, S., 1982. The Volcanic Explosivity Index (VEl): an estimate of explosive magnitude for historical volcanism. J. Geophys. Res. 87C, 1231–1238.
Nichols, H., 1967. The postglacial history of vegetation and climate at Ennadai Lake, Keewatin and Lynn Lake, Manitoba. Eiszeit. Gegenw. 18, 176–197.
Nichols, J.E., Booth, R.K., Jackson, S.T., Pendall, E.G., Huang, Y., 2006. Palohydrologic reconstruction based on n-alkane distributions in ombrotrophic peat. Org. Geochem. 37, 1505–1513.
Nichols, J.E., Walcott, M., Bradley, R.S., Pilcher, J., Huang, Y., 2009. Quantitative assessment of precipitation seasonality and summer surface wetness using ombrotrophic sediments from an Arctic Norwegian peatland. Quat. Res. 73, 443–451.
Nichols, J.E., Booth, R.K., Jackson, S.T., Pendall, E.G., Huang, Y., 2010. Differential hydrogen isotopic ratios of *Sphagnum* and vascular plant biomarkers in ombrotrophic peatlands as a quantitative proxy for precipitation-evaporation balance. Geochim. Cosmochim. Acta. 74, 1407–1416.
Nicholson, S., Flohn, H., 1980. African environmental and climatic changes and the general circulation in late Pleistocene and Holocene. Clim. Chang. 2, 313–348.
Niggemann, S., Mangini, A., Richter, D.K., Wurth, G., 2003. A paleoclimate record of the last 17,600 years in stalagmites from the B7 cave, Sauerland, Germany. Quat. Sci. Rev. 22, 555–567.
Nix, H.A., Kalma, J.D., 1972. Climate as a dominant control in the biogeography of northern Australia and New Guinea. In: Walker, D. (Ed.), Bridge and Barrier: the Natural and Cultural History of Torres Strait. Publication No. BG3Department of Biogeography and Geomorphology, Australian National University, Canberra, pp. 61–91.
Noller, J.S., Sowers, J.M., Lettis, W.R. (Eds.), 2000. Quaternary geochronology: methods and applications. American Geophysical Union, Washington D.C, 581 pp.
North Greenland Ice Core Project members, 2004. High resolution record of Northern Hemisphere climate extending into the last interglacial period. Nature. 431, 147–151.
Nowaczyk, N.R., Arz, H.W., Frank, U., Kind, J., Plessen, B., 2012. Dynamics of the Laschamp geomagnetic excursion from Black Sea sediments. Earth Planet. Sci. Lett. 351–352, 54–69.
Nussbaumer, S.U., Zumbühl, H.J., Steiner, D., 2007. Fluctuations of the "Mer de Glace" (Mont Blanc area, France) AD 1500-2050: an interdisciplinary approach using new historical data and neural network simulations. Z. Gletscherk. Glazialgeol. 40, 3–183.
Nyberg, J., Malmgren, B.A., Winter, A., Jury, M.R., Kilbourne, K.H., Quinn, T.M., 2007. Low Atlantic hurricane activity in the 1970s and 1980s compared to the past 270 years. Nature. 447, 698–702.
Nye, J.F., 1965. A numerical method of inferring the budget history of a glacier from its advance and retreat. J. Glaciol. 5, 589–607.
O'Brien, S.R., Mayewski, P.A., Meeker, L.D., Meese, D.A., Twickler, M.S., Whitlow, S.I., 1995. Complexity of Holocene climate as reconstructed from a Greenland ice core. Science. 270, 1962–1964.
Oches, E.A., McCoy, W.D., 1995a. Aminostratigraphic evaluation of conflicting age estimates for the "Young Loess" of Hungary. Quat. Res. 44, 160–170.
Oches, E.A., McCoy, W.D., 1995b. Aminostratigraphy of central European loess cycles: introduction and data. Geolines (Praha). 2, 34–86.
Oches, E.A., McCoy, W.D., 1995c. Amino acid geochronology applied to the correlation and dating of central European loess deposits. Quat. Sci. Rev. 14, 767–782.

Oches, E.A., McCoy, W.D., 2001. Historical development and recent advances in amino acid geochronology applied to loess research: examples from North America, Europe, and China. Earth-Sci. Rev. 54, 173–192.
Oches, E.A., McCoy, W.D., Clark, P.U., 1996. Amino acid estimates of latitudinal temperature gradients and geochronology of loess deposition during the last glaciation, Mississippi Valley, United States. Geol. Soc. Am. Bull. 108, 892–903.
Oerlemans, J., 1989. On the response of valley glaciers to climatic change. In: Oerlemans, J. (Ed.), Glacier Fluctuations and Climatic ChangeKluwer, Dordrecht, pp. 353–371.
Oerlemans, J., Hoogendorn, N.C., 1989. Mass balance gradients and climatic change. J. Glaciol. 35, 399–405.
Oeschger, H., Langway Jr., C.C. (Eds.), 1989. The Environmental Record in Glacier and Ice Sheets. Wiley, Chichester.
Ogilvie, A., 1992. Documentary evidence for changes in the climate of Iceland, A.D. 1500-1800. In: Bradley, R.S., Jones, P.D. (Eds.), Climate Since A.D. 1500. Routledge, London, pp. 92–117.
Ohkouchi, N., Eglinton, T.I., Keigwin, L.D., Hayes, J.M., 2002. Spatial and temporal offsets between proxy records in sediment drifts. Science. 298, 1224–1227.
Ojala, A.E.K., Alenius, T., 2005. 10,000 years of interannual sedimentation recorded in the Lake Nautajarvi (Finland) clastic-organic varves. Palaeogeogr. Palaeoclimatol. Palaeoecol. 219, 285–302.
Ojala, A.E.K., Saarinen, T., Salonen, V.-P., 2000. Preconditions for the formation of annually laminated lake sediments in southern and central Finland. Boreal Environ. Res. 5, 243–255.
Ojala, A.E.K., Francus, P., Zolitschka, B., Besonen, M., Lamoureux, S., 2012. Characteristics of sedimentary varve chronologies—a review. Quat. Sci. Rev. 43, 45–60.
Okazaki, Y., Timmermann, A., Menviel, L., Harada, N., Abe-Ouchi, A., Chikamoto, M.O., Mouchet, A., Asahi, H., 2010. Deepwater formation in the North Pacific during the Last Glacial Termination. Science. 329, 200–204.
Olausson, E., 1965. Evidence of climatic changes in deep sea cores with remarks on isotopic palaeotemperature analysis. Prog. Oceanogr. 3, 221–252.
Olausson, E., 1967. Climatological, geoeconomical and paleooceanographical aspects of carbonate deposition. Prog. Oceanogr. 4, 245–265.
Oldfield, F., 2000. Paleoclimatology: out of Africa. Nature. 403, 370–371.
Olley, J., Caitcheon, G., Murray, A., 1998. The distribution of apparent dose as determined by optically stimulated luminescence in small aliquots of fluvial quartz: implications for dating young sediments. Quat. Geochronol. 17, 1033–1040.
Olson, I.U., 2009. Radiocarbon dating history: early days, questions, and problems met. Radiocarbon. 51, 1–43.
Olsson, I.U., 1968. Modern aspects of radiocarbon dating. Earth-Sci. Rev. 4, 203–218.
Olsson, I.U., 1974. Some problems in connection with the evaluation of 14C dates. Geol. Fören. Stockh. Förh. 96, 311–320.
Olsson, I.U., Eriksson, K.G., 1972. Fractionation studies of the shells of Foraminifera. In: Etudes sur le Quaternaire dans le Monde.Proceedings, Congress INQUA, Paris, pp. 921–923.
Olsson, I.U., Osadebe, F.A.N., 1974. Carbon isotope variations and fractionation corrections in ^{14}C dating. Boreas. 3, 139–146.
Olsson, I.U., El-Daoushy, M.F.A.F., Abd-El-Mageed, A.I., Klasson, M., 1974. A comparison of different methods for pretreatment of bones I. Geol. Fören. Stockh. Förh. 96, 171–181.
O'Neil, J.R., Clayton, R.N., Mayeda, T.K., 1969. Oxygen isotope fractionation in divalent metal carbonates. J. Chem. Phys. 51, 5547–5558.
Opdyke, N.D., 1972. Paleomagnetism of deep-sea cores. Rev. Geophys. Space Phys. 101, 213–249.
Opdyke, N.D., Channell, J.E.T., 1996. Magnetic Stratigraphy. Academic Press, San Diego.
Oppo, D.W., Curry, W.B., 2012. Deep Atlantic circulation during the Last Glacial Maximum and deglaciation. Nat. Educ. Knowl. 3, 1–6.
Oppo, D.W., Fairbanks, R.G., 1987. Variability in the deep and intermediate water circulation of the Atlantic Ocean during the past 25,000 years: northern hemisphere modulation of the Southern Ocean. Earth Planet. Sci. Lett. 86, 1–15.
Orland, I.J., Bar-Matthews, M., Kita, N.T., Ayalon, A., Matthews, A., Valley, J.W., 2009. Climate deterioration in the eastern Mediterranean as revealed by ion microprobe analysis of a speleothem that grew from 2.2-0.9 ka in Soreq cave, Israel. Quat. Res. 71, 27–35.
Ortlieb, L., 2000. The documented historical record of El Niño events in Peru: an update of the Quinn record (sixteenth through nineteenth centuries). In: Diaz, H.F., Markgraf, V. (Eds.), El Niño and the Southern Oscillation: multiscale variability and global and regional impacts. Cambridge University Press, Cambridge, pp. 207–295.

Osborn, T.J., Briffa, K.R., 2006. The spatial extent of 20th-century warmth in the context of the past 1200 years. Science. 311, 841–844.
Osborne, P.J., 1974. An insect assemblage of early Handrian age from Lea Marston, Warwickshire and its bearing on the contemporary climate and ecology. Quat. Res. 4, 471–486.
Osborne, P.J., 1980. The late Devensian-Flandrian transition depicted by serial insect faunas from West Bromwich, Staffordshire, England. Boreas. 9, 139–147.
Osmaston, H.A., 1975. Models for the estimation of firnlines of present and Pleistocene glaciers. In: Peel, R.F., Chisholm, M., Haggett, P. (Eds.), Processes in Physical and Human Geography: Bristol Essays. Heinemann, London, pp. 218–245.
Østrem, G., 1974. Present alpine ice cover. In: Ives, J.D., Barry, R.G. (Eds.), Arctic and Alpine *Environments*. Methuen, London, pp. 225–250.
Otto-Bliesner, B.L., Brady, E.C., 2010. The sensitivity of the climate response to the magnitude and location of freshwater forcing: last glacial maximum experiments. Quat. Sci. Rev. 29, 56–73.
Otto-Bliesner, B., Schneider, R., Brady, E.C., Kucera, M., Abe-Ouchi, A., Bard, E., Braconnot, P., Crucifix, M., Hewitt, C.D., Kageyama, M., Marti, O., Paul, A., Rosell-Melé, A., Waelbroeck, C., Weber, S.L., Weinelt, M., Yu, Y., 2009. A comparison of PMIP2 model simulations and the MARGO proxy reconstruction for tropical sea surface temperatures at last glacial maximum. Clim. Dyn. 32, 799–815.
Overpeck, J.T., Webb III, T., Prentice, I.C., 1985. Quantitative interpretation of fossil pollen spectra: dissimilarity coefficients and the method of modern analogs. Quat. Res. 23, 87–108.
Overpeck, J.T., Rind, D., Goldberg, R., 1990. Climate-induced changes in forest disturbance and vegetation. Nature. 343, 51–53.
Overpeck, J.T., Rind, D., Lacis, A., Healey, R., 1996. Possible role of dust-induced regional warming in abrupt climate change during the last glacial period. Nature. 384, 447–449.
Overpeck, J.T., Whitlock, C., Huntley, B., 2003. Terrestrial biosphere dynamics in the climate system: past and future. In: Alverson, K.D., Bradley, R.S., Pedersen, T.F. (Eds.), Paleoclimate, Global Change and the Future. Springer, Berlin, pp. 81–103.
Oviatt, C.G., McCoy, W.D., Nash, W.P., 1994. Sequence stratigraphy of lacustrine deposits: a Quaternary example from the Bonneville Basin, Utah; with Suppl. Data 9402. Geol. Soc. Am. Bull. 106, 133–144.
Owen, L.A., Caffee, M.W., Finkel, R.C., Seong, Y.B., 2008. Quaternary glaciation of the Himalayan-Tibetan orogeny. J. Quat. Sci. 23, 513–531.
Pagani, M., Zachos, J.C., Freeman, K.H., Tripple, B., Bohaty, S., 2005. Marked decline in atmospheric carbon dioxide concentrations during the Paleogene. Science. 309, 600–603.
Paillard, D., Labeyrie, L., 1994. Role of the thermohaline circulation in the abrupt warming after Heinrich events. Nature. 372, 162–164. Palaeoclimatol. Palaeoecol. 298, 378–387.
PALAEOSENS Project Members, 2012. Making sense of palaeoclimate sensitivity. Nature. 491, 683–691.
Palais, J.M., Germani, M.S., Zielinski, G.A., 1992. Inter-hemispheric transport of volcanic ash from a 1259 A.D. volcanic eruption to the Greenland and Antarctic ice sheets. Geophys. Res. Lett. 19, 801–804.
Palmer, W.C., 1965. Meteorological Drought. Research Paper No. 45, US Weather Bureau, Washington, DC.
Parker, M.L., 1971. Dendrochronological Techniques used by the Geological Survey of Canada, Paper 71–25. Geological Survey of Canada, Ottawa.
Parker, M.L., Hennoch, W.E.S., 1971. The use of Engelmann spruce latewood density for dendrochronological purposes. Can. J. For. Res. 1, 90–98.
Parmenter, C., Folger, D.W., 1974. Eolian biogenic detritus in deep sea sediments: a possible index of Equatorial Ice Age aridity. Science. 185, 695–698.
Parmesan, C., Yohe, G., 2003. A globally coherent fingerprint of climate change impacts across natural systems. Nature. 421, 37–42.
Parrenin, F., Barnola, J.-M., Beer, J., Blunier, T., Castellano, E., Chappellaz, J., Dreyfus, G., Fischer, H., Fujita, S., Jouzel, J., Kawamura, K., Lemieux-Dudon, B., Loulergue, L., Masson-Delmotte, V., Narcisi, B., Petit, J.-R., Raisbeck, G., Raynaud, D., Ruth, U., Schwander, J., Severi, M., Spahni, R., Steffensen, J.P., Svensson, A., Udisti, R., Waelbroeck, C., Wolff, E., 2007. The EDC3 chronology for the EPICA Dome C ice core. Clim. Past. 3, 485–497.
Parrenin, F., Barker, S., Blunier, T., Chappellaz, J., Jouzel, J., Landais, A., Masson-Delmotte, V., Schwander, J., Veres, D., 2012. On the gas-ice depth difference (Δ depth) along the EPICA Dome C ice core. Clim. Past. 8, 1239–1255.

Parrenin, F., Masson-Delmotte, V., Köhler, P., Raynaud, D., Paillard, D., Schwander, J., Barbante, C., Landais, A., Wegner, A., Jouzel, J., 2013. Synchronous change of atmospheric CO_2 and Antarctic temperature during the last deglacial warming. Science. 339, 1060–1063.
Parry, M.L., 1975. Secular climatic change and marginal agriculture. Trans. Inst. Br. Geogr. 64, 1–13.
Parry, M.L., 1981. Climatic change and the agricultural frontier: a research strategy. In: Wigley, T.M.L., Ingram, M.J., Farmer, G. (Eds.), Climate and History. Cambridge University Press, Cambridge, pp. 319–336.
Parry, M.L., Canziani, O., Palutikof, J., van der Linden, P., Hanson, C. (Eds.), 2007. Climate Change 2007: Impacts, Adaptation and Vulnerability. Cambridge University Press, Cambridge, 976 pp.
Paterson, W.S.B., 1994. The Physics of Glaciers, third ed. Pergamon, Oxford.
Pätzold, J., 1986. Temperature and CO_2 changes in tropical surface waters of the Philippines during the past 120 years: record in the stable isotopes of hermatypic corals. Berichte. 12, 1–82, Kiel: Geologisches/Palaontologisches Institut der Universitat Kiel.
Pätzold, J., Wefer, G., 1992. Bermuda coral reef record of the last 1,000 years. In: Proceedings of Fourth International Conference on Paleoceanography, Kiel, pp. 224–225.
Pätzold, J., Bickert, T., Flemming, B., Grobe, H., Wefer, G., 1999. Holozänes Klima des Nordatlantiks rekonstruiert aus massiven Korallen von Bermuda. Nat. Mus. 129, 165–177.
Pauling, A., Luterbacher, J., Casty, C., Wanner, H., 2006. Five hundred years of gridded high-resolution precipitation reconstructions over Europe and the connection to large-scale circulation. Clim. Dyn. 26, 387–405.
Paulson, D.E., Li, H.C., Ku, T.L., 2003. Climate variability in central China over the last 1270 years revealed by high-resolution stalagmite records. Quat. Sci. Rev. 22, 691–701.
Pausata, F.S.R., Battisti, D.S., Nisancioglu, K.H., Bitz, C.M., 2011. Chinese stalagmite $\delta^{18}O$ controlled by changes in the Indian monsoon during a simulated Heinrich event. Nat. Geosci. 4, 474–480.
Pavese, M.P., Banzon, V., Colacino, M., Gregori, G.P., Pasqua, M., 1992. Three historical data series on floods and anomalous climatic events in Italy. In: Bradley, R.S., Jones, P.D. (Eds.), Climate Since A.D. 1500. Routledge, London, pp. 155–170.
Payette, S., Gagnon, R., 1985. Late Holocene deforestation and tree regeneration in the forest-tundra of Quebec. Nature. 313, 570–572.
Payette, S., Morneau, C., 1993. Holocene relict woodlands at the eastern Canadian treeline. Quat. Res. 39, 84–89.
Payette, S., Filion, L., Delwaide, A., Bégin, C., 1989. Reconstruction of treeline vegetation response to long-term climate change. Nature. 341, 429–432.
Pearce, N.J.G., Denton, J.S., Perkins, W.T., Westgate, J.A., Alloway, B.V., 2007. Correlation and characterisation of individual glass shards from tephra deposits using trace element laser ablation ICP-MS analyses: current status and future potential. J. Quat. Sci. 22, 721–736.
Pearson, S., 1999. Late Holocene biological records from the middens of stick-nest rats in the central Australian arid zone. Quat. Int. 59, 39–46.
Pearson, S., Dodson, J.R., 1993. Stick-nest rat middens as sources of paleoecological data in Australian deserts. Quat. Res. 39, 347–354.
Pearson, G.W., Stuiver, M., 1993. High-precision bidecadal calibration of the radiocarbon time scale, 500-2500 B.C. Radiocarbon. 35, 25–33.
Pearson, G.W., Becker, B., Qua, F., 1993. High precision ^{14}C measurement of German and Irish oaks to show the natural ^{14}C variations from 7890 to 500 B.C. Radiocarbon. 35, 93–104.
Pearson, E.J., Juggins, S., Talbot, H.M., Weckström, J., Rosén, P., Ryves, D.B., Roberts, S.J., Schmidt, R., 2011. A lacustrine GDGT-temperature calibration from the Scandinavian Arctic to Antarctic: renewed potential for the application of GDGT-paleothermometry in lakes. Geochim. Cosmochim. Acta. 75, 6225–6238.
Pécsi, M., 1992. Loess of the last glaciation. In: Frenzel, B., Pecsi, M., Velichko, A. (Eds.), Atlas of Paleoclimates and Paleoenvironments of the Northern Hemisphere. Geographical Research Institute, Hungarian Academy of Sciences, Budapest, pp. 110–119.
Pedersen, T.F., Nielsen, B., Pickering, M., 1991. Timing of late Quaternary productivity pulses in the Panama Basin and implications for atmospheric CO_2. Paleoceanography. 6, 657–678.
Pedersen, T.F., Francois, R., Francois, L., Alverson, K., McManus, J., 2003. The Late Quaternary history of biogeochemical cycling of carbon. In: Alverson, K.D., Bradley, R.S., Pedersen, T.F. (Eds.), Paleoclimate, Global Change and the Future. Springer, Berlin, pp. 64–79.
Peel, D.A., Mulvaney, R., Davison, B.M., 1988. Stable-isotope/air-temperature relationships in ice cores from Dolleman Island and the Palmer Land plateau, Antarctic Peninsula. Ann. Glaciol. 10, 130–136.
Peixoto, J.P., Oort, A., 1992. The Physics of Climate. American Institute of Physics, New York.

Peltier, R., 1994. Ice Age paleotopography. Science. 265, 195–201.
Peng, T.-H., Broecker, W.S., 1995. Reconstruction of radiocarbon distribution in the Glacial Ocean. In: Taylor, R.E., Long, A., Kra, R.S. (Eds.), Radiocarbon After Four Decades. Springer-Verlag, New York, pp. 75–92.
Peng, C.H., Guiot, J., Van Campo, E., 1998. Estimating changes in terrestrial vegetation and carbon storage using palaeoecological data and models. Quat. Sci. Rev. 17, 719–735.
Pennington, W., 1973. Absolute pollen frequencies in the sediments of lakes of different morphometry. In: Birks, H.J.B., West, R. (Eds.), Quaternary Plant Ecology. Blackwell Scientific Publications, Oxford, pp. 79–104.
Petersen, G.M., Webb III, T., Kutzbach, J.E., van der Hammen, T., Wijmstra, T.A., Street, F.A., 1979. The continental record of environmental conditions at 18 000 yr BP: an initial evaluation. Quatern. Res. 12, 47–82.
Petersen, S.V., Schrag, D.P., Clark, P.U., 2013. A new mechanism for Dansgaard-Oeschger cycles. Paleoceanography. 28, 1–7.
Peterson, L.C., Prell, W.L., 1985. Carbonate preservation and rates of climatic change: an 800 kyr record from the Indian Ocean. In: Sundquist, E.T., Broecker, W.S. et al., (Eds.), American Geophysical Union, Washington, DC, pp. 251–269.
Petit, J.R., Duval, P., Lorius, C., 1987. Long-term climatic changes indicated by crystal growth in polar ice. Nature. 326, 62–64.
Petit, J.R., White, J.W.C., Young, N.W., Jouzel, J., Korotkevich, Y.S., 1991. Deuterium excess in recent Antarctic snow. J. Geophys. Res. 96D, 5113–5122.
Petit, J.R., Basile, I., Leruyuet, A., Raynaud, D., Lorius, C., Jouzel, J., Stievenard, M., Lipenkov, Y.Y., Barkov, N.I., Kudryashov, B.B., Davis, M., Saltzman, E., Kotlyakov, V., 1997. Four climate cycles in Vostok ice core. Nature. 387, 359–360.
Petit, J.R., Jouzel, J., Raynaud, D., Barkov, N.I., Barnola, J.-M., Basile, I., Bender, M., Chappellaz, J., Davis, M., Delaygue, G., Delmotte, M., Kotlyakov, V.M., Legrand, M., Lipenkov, V.Y., Lorius, C., Pépin, L., Ritz, C., Saltzman, E., Stievenard, M., 1999. Climate and atmospheric history of the past 420 000 years from the Vostok ice core, Antarctica. Nature. 399, 429–436.
Petit-Maire, N., Fontugne, M., Rouland, C., 1991. Atmospheric methane ratio and environmental changes in the Sahara and Sahel during the last 130 kyr. Palaeogeogr. Palaeoclimatol. Palaeoecol. 86, 197–204.
Péwé, T.L., Reger, R.D., 1972. Modern and Wisconsinan snowlines in Alaska. In: Proceedings No. 24, Section 12, Quaternary Geology. International Geological Congress, Montreal, pp. 187–197.
Pfister, C., 1978a. Climate and economy in eighteenth century Switzerland. J. Interdiscip. Hist. 9, 223–243.
Pfister, C., 1978b. Fluctuations in the duration of snow-cover in Switzerland since the late seventeenth century. In: Frydendahl, K. (Ed.), Proceedings of Nordic Symposium on Climatic Changes and Related Problems. Climatological Papers No. 4, Danish Meteorological Institute, Copenhagen, pp. 1–6.
Pfister, C., 1984. Klimageschichte der Schweiz 1525–1860. Das Klima der Schweiz von 1525–1860 und seine Bedeutung in der Geschichte von Belvolkerung und Landwirschaft, 2 vols. Paul Haupt, Bern.
Pfister, C., 1985. Snow cover, snowlines and glaciers in Central Europe since the 16th century. In: Tooley, M.J., Sheail, G.M. (Eds.), The Climatic Scene. Allen and Unwin, London.
Pfister, C., 1992. Monthly temperature and precipitation in central Europe 1525-1979: quantifying documentary evidence on weather and its effects. In: Bradley, R.S., Jones, P.D. (Eds.), Climate Since A.D. 1500. Routledge, London, pp. 118–142.
Pfister, C., 1999. Wetternachhersage. 500 Jahre Klimavariationen und Naturkatastrophen 1496–1995 [Weather Hindcast. 500 years of climate variability and natural disasters, 1496–1995]. Haupt, Bern, 304 pp.
Pfister, C., Brázdil, R., 1999. Climate variability in sixteenth century Europe and its social dimension: a synthesis. Clim. Chang. 43, 5–53.
Pfister, C., Hachler, S., 1991. Überschwemmungskatastrophen im Schweizer Alpenraum seit dem Spätmittelalter. Wurzburger Geographische Arbeiten. 80, 127–148.
Pfister, C., Messerli, B., Messerli, P., Zumbuhl, H., 1978. Die Rekonstruktion des Klima- und Witterungsverlaufes der letzten Jahrhunderte mit Hilfe verscheidener Datentypen. In: Jahrbuch der Schweizerischen Naturforschenden Gesellschaft. Birkhauser, Zurich, pp. 89–105.
Pfister, C., Brázdil, R., Glaser, R., 1999. Climatic variability in sixteenth-century Europe and its social dimension (Special Issue). Clim. Chang. 43, 1–351.
Pflaumann, U., Duprat, J., Pujol, C., Labeyrie, L.D., 1996. SIMMAX: a modern analog technique to deduce Atlantic sea surface temperatures from planktonic foraminifera in deep-sea sediments. Paleoceanography. 11, 15–35.
Pflaumann, U., Sarnthein, M., Chapman, M., d'ABREU, L., Funnell, B., Huels, M., Kiefer, T., Maslin, M., Schulz, H., Swallow, J., van Kreveld, S., Vautravers, M., Vogelsang, E., Weinelt, M., 2003. Glacial North Atlantic: sea-surface conditions reconstructed by GLAMAP 2000. Paleoceanography. 18. dx.doi.org/10.1029/2002PA000774.

Phillips, F.M., Zreda, M.G., Benson, L.V., Plummer, M.A., Elmore, D., Sharma, P., 1996. Chronology for fluctuations in Late Pleistocene Sierra Nevada glaciers and lakes. Science. 274, 749–751.
Picciotto, E., De Maere, X., Friedman, I., 1960. Isotopic composition and temperature of formation of Antarctic snows. Nature. 187, 857–859.
Picciotto, E., Crozaz, G., De Breuck, W., 1971. Accumulation on the South Pole-Queen Maud Land Traverse 1964–1968. In: Crary, A.P. (Ed.), Antarctic Snow and Ice Studies II. Antarctic Research SeriesAmerican Geophysical Union, Washington, DC, pp. 257–316.
Pichon, J.J., Labeyrie, L.D., Bareille, G., Labracherie, M., Duprat, J., Jouzel, J., 1992. Surface water temperature changes in the high latitudes of the southern hemisphere over the last glacial-interglacial cycle. Paleoceanography. 7, 289–318.
Pienitz, R., Smol, J.P., Birks, H.J.B., 1995. Assessment of freshwater diatoms as quantitative indicators of past climate change in the Yukon and Northwest Territories. J. Paleolimnol. 13, 21–49.
Pienitz, R., Douglas, M.V., Smol, J.P., 2004. Long-term Environmental Change in Arctic and Antarctic Lakes. Springer, Berlin, 562 pp.
Pierce, K.L., Friedman, I., 2000. Obsidian hydration dating of Quaternary events. In: Noller, J.S., Sowers, J.M., Lettis, W.R. (Eds.), Quaternary Geochronology: Methods and Applications. American Geophysical Union, Washington, DC, pp. 223–240.
Pierce, K.L., Obradovich, J.D., Friedman, I., 1976. Obsidian hydration dating and correlation of Bull Lake and Pinedale Glaciations near west Yellowstone, Montana. Geol. Soc. Am. Bull. 87, 703–710.
Piervitali, E., Colacino, M., 2001. Evidence of drought in western Sicily during the period 1565-1915 from liturgical offices. Clim. Chang. 49, 225–238.
Pike, J., Kemp, A.E.S., 1996. Records of seasonal flux in Holocene laminated sediments, Gulf of California. In: Kemp, A.E.S. (Ed.), Palaeoclimatology and Palaeoceanography from Laminated Sediments. Special Publication No. 116The Geological Society, London, pp. 157–169.
Pilcher, J.R., Hall, V.A., McCormac, F.G., 1995. Dates of Holocene Icelandic volcanic eruptions from tephra layers in Irish peats. The Holocene. 5, 103–110.
Pilcher, J., Bradley, R.S., Francus, P., Anderson, L., 2005. A Holocene tephra record from the Lofoten Islands, Arctic Norway. Boreas. 34, 136–156.
Pillow, M.Y., 1931. Compression wood records hurricane. J. Forest. 29, 575–578.
Pinto, J., Raible, C.C., 2012. Past and recent changes in the NAO. Interdiscip. Rev. Clim. Change. 3, 79–90.
Piotrowski, A.M., Goldstein, S.L., Hemming, S.R., Fairbanks, R.G., 2005. Temporal relationships of carbon cycling and ocean circulation at Glacial boundaries. Science. 307, 1933–1938.
Piperno, D., 2001. Phytoliths. In: Smol, J.P., Birks, H.J.B., Last, W.M. (Eds.), Tracking Environmental Change Using Lake sediments, vol. 3. Kluwer Academic, Dordrecht, pp. 235–251.
Pisias, N.G., Moore, T.C., 1981. The evolution of Pleistocene climate: a time series approach. Earth Planet. Sci. Lett. 52, 450–458.
Pisias, N.G., Martinson, D.G., Moore Jr., T.C., Shackleton, N.J., Prell, W., Hays, J., Boden, G., 1984. High resolution stratigraphic correlation of benthic oxygen isotopic records spanning the last 300,000 years. Mar. Geol. 56, 119–136.
Pisias, N.G., Roelofs, A., Weber, M., 1997. Radiolarian-based transfer functions for estimating mean surface ocean temperature and seasonal range. Paleoceanography. 12, 365–379.
Placzek, C.J., Quade, J., Patchett, P.J., 2013. A 130 ka reconstruction of rainfall on the Bolivian Altiplano. Earth Planet. Sci. Lett. 363, 97–108.
Pokras, E.M., Mix, A.C., 1985. Eolian evidence for spatial variability of late Quaternary climates in tropical Africa. Quat. Res. 24, 137–149.
Polge, H., 1970. The use of X-ray densitometric methods in dendrochronology. Tree Ring Bull. 30, 1–10.
Polissar, P., Abbott, M.B., Wolfe, A.P., Bezada, M., Rull, V., Bradley, R.S., 2005. Solar modulation of Little Ice Age climate in the Tropical Andes. Proc. Natl. Acad. Sci. U. S. A. 103, 8937–8942.
Pollard, D., DeConto, R.M., 2005. Hysteresis in Cenozoic Antarctic ice-sheet variations. Glob. Planet. Chang. 45, 9–21.
Pollard, R.T., Salter, I., Sanders, R.J., Lucas, M.I., Moore, C.M., Mills, R.A., Statham, P.J., Allen, J.T., Baker, A.R., Bakker, D.C.E., Charette, M.A., Fielding, S., Fones, G.R., French, M., Hickman, A.E., Holland, R.J., Hughes, J.A., Jickells, T.D., Lampitt, R.S., Morris, P.J., Nédeléc, F.H., Nielsdóttir, M., Planquette, H., Popova, E.E., Poulton, A.J., Read, J.F., Seeyave, S., Smith, T., Stinchcombe, M., Taylor, S., Thomalla, S.,

Venables, H.J., Williamson, R., Zubkov, M.V., 2009. Southern Ocean deep-water carbon export enhanced by natural iron fertilization. Nature. 457, 577–580.
Polyak, L., Curry, W.B., Darby, D.A., Bischof, J., Cronin, T.M., 2004. Contrasting glacial/interglacial regimes in the western Arctic Ocean as exemplified by a sedimentary record from the Mendeleev Ridge. Palaeogeogr. Palaeoclimatol. Palaeoecol. 203, 73–94.
Ponel, P., 1995. Rissian, Eemian and Würmian Coleoptera assemblages from La Grande Pile (Vosges, France. Palaeogeogr. Palaeoclimatol. Palaeoecol. 114, 1–41.
Pons, A., Guiot, J., de Beaulieu, J.L., Reille, M., 1992. Recent contributions to the climatology of the Last Glacial-Interglacial cycle based on French pollen sequences. Quat. Sci. Rev. 11, 439–448.
Poore, R.Z., Osterman, L., Curry, W.B., Phillips, R.L., 1999. Late Pleistocene and Holocene meltwater events in the western Arctic Ocean. Geology. 27, 759–762.
Porinchu, D.F., MacDonald, G.M., 2003. The use and application of freshwater midges (Chironomidae: Insecta: Diptera) in geographical research. Prog. Phys. Geogr. 27, 378–422.
Porinchu, D.F., MacDonald, G.M., Bloom, A.M., Moser, K.A., 2002. The modern distribution of chironomid sub-fossils (Insecta: Diptera) in the Sierra Nevada, California: potential for paleoclimatic reconstructions. J. Paleolimnol. 28, 355–375.
Porter, S.C., 1977. Present and past glaciation thresholds in the Cascade Range, Washington, USA: topographic and climatic controls and paleoclimatic implications. J. Glaciol. 18, 101–116.
Porter, S.C., 1979. Hawaiian glacial ages. Quat. Res. 12, 161–187.
Porter, S.C., 1981a. Glaciological evidence of Holocene climatic change. In: Wigley, T.M.L., Ingram, M.J., Farmer, G. (Eds.), Climate and History. Cambridge University Press, Cambridge, pp. 82–110.
Porter, S.C., 1981b. Tephrochronology in the Quaternary geology of the United States. In: Self, S., Sparks, R.J.S. (Eds.), Tephra Studies. D. Reidel, Dordrecht, pp. 135–160.
Porter, S.C., 1981c. Lichenometric studies in the Cascade Range of Washington: establishment of *Rhizocarpon geographicurn* growth curves at Mount Rainier. Arct. Alp. Res. 13, 11–23.
Porter, S.C., 1986. Pattern and forcing of Northern Hemisphere glacier variations during the last millennium. Quat. Res. 26, 27–48.
Porter, S.C., An, Z., 1995. Correlation between climate events in the North Atlantic and China during the last glaciation. Nature. 375, 305–308.
Porter, S.C., Denton, G.H., 1967. Chronology of neoglaciation in the North American Cordillera. Am. J. Sci. 265, 177–210.
Porter, T.J., Pisaric, M.F.J., 2011. Temperature-growth divergence in white spruce forests of Old Crow Flats, Yukon Territory, and adjacent regions of northwestern North America. Glob. Chang. Biol. 17, 3418–3430.
Porter, S.C., Zhou, W.J., 2006. Synchronism of Holocene East Asian monsoon variations and North Atlantic drift tracers. Quat. Res. 65, 443–449.
Porter, S.C., Pierce, K.L., Hamilton, T.D., 1983. Late Pleistocene glaciation in the western United States. In: Porter, S.C. (Ed.), Late Quaternary Environments of the United States. University of Minnesota Press, Minneapolis, pp. 71–111.
Potter, N., 1969. Tree-ring dating of snow avalanche tracks and the geomorphic activity of avalanches, northern Absaroka Mountains, Wyoming. In: Schumm, S.A., Bradley, W.C. (Eds.), US Contributions to Quaternary Research. Special Paper 123, Geological Society of America, Boulder, pp. 141–165.
Poussart, P.F., Schrag, D.P., 2005. Seasonally resolved stable isotope chronologies from northern Thailand deciduous trees. Earth Planet. Sci. Lett. 235, 752–765.
Poussart, P.F., Evans, M.N., Schrag, D.P., 2004. Resolving seasonality in tropical trees: multi-decade, high resolution oxygen and carbon isotope records from Indonesia and Thailand. Earth Planet. Sci. Lett. 218, 301–316.
Poussart, P.F., Myneni, S.C.B., Lanzarotti, A., 2006. Tropical dendrochemistry: a novel approach to estimate age and growth from ringless trees. Geophys. Res. Lett. 33, L17711. dx.doi.org/10.1029/2006GL026929.
Povinec, P.P., Litherland, A.E., von Reden, K.F., 2009. Developments in radiocarbon technologies: from the Libby counter to compound-specific AMS analyses. Radiocarbon. 51, 45–78.
Powers, L.A., Johnson, T.C., Werne, J.P., Castañada, I.S., Hopmans, E.C., Sinninghe Damsté, J.S., Schouten, S., 2005. Large temperature variability in the southern African tropics since the Last Glacial Maximum. Geophys. Res. Lett. 32, L08706. dx.doi.org/10.1029/2004GL022014.

Powers, L.A., Werne, J.P., Sinninghe Damsté, J.S., Hopmans, E.C., Schouten, S., 2010. Applicability and calibration of the TEX_{86} paleothermometer in lakes. Org. Geochem. 41, 404–413.
Powers, L.A., Johnson, T.C., Werne, J.P., Castañeda, I.S., Hopmans, E.C., Sinninghe Damsté, J.S., Schouten, S., 2011. Organic geochemical records of environmental variability in Lake Malawi during the last 700 years, Part I: the TEX86 temperature record. Palaeogeogr. Palaeoclimatol. Palaeoecol. 303, 133–139.
Prahl, F.G., Muehlhausen, L.A., Zahnle, D.L., 1988. Further evaluation of long-chain alkenones as indicators of paleoceanographic conditions. Geochim. Cosmochim. Acta. 51, 2303–2310.
Prance, G.T., 1974. Phytogeographic support for the theory of Pleistocene forest refuges in the Amazon Basin, based on evidence from distribution patterns in Caryocaraceae, Chrysobalanaceae, Dichapetalaceae and Lecythidaceae. Acta Amazon. 3, 5–26.
Prance, G.T., 1982. Forest refuges: evidence from woody angiosperms. In: Prance, G.T. (Ed.), Biological Diversification in the Tropics. Columbia University Press, New York, pp. 137–158.
Prebble, M., Schulmeister, J., 2002. An analysis of phytolith assemblages for the quantitative reconstruction of late Quaternary environments of the Lower Taieri Plain, Otago, South Island, New Zealand. II. Paleoenvironmental reconstruction. J. Paleolimnol. 27, 415–427.
Prebble, M., Schallenberg, M., Carter, J., Schulmeister, J., 2002. An analysis of phytolith assemblages for the quantitative reconstruction of late Quaternary environments of the Lower Taieri Plain, Otago, South Island, New Zealand. I. Modern assemblages and transfer functions. J. Paleolimnol. 27, 393–413.
Preiss, N., Mélières, M.-A., Pourchet, M., 1996. A compilation of data on lead-210 concentration in surface air and fluxes at the air-surface and water-sediment interfaces. J. Geophys. Res. 101, 28847–28862.
Prell, W.L. 1985. The stability of low-latitude sea-surface temperature: an evaluation of the CLIMAP reconstruction with emphasis on the positive SST anomalies. Dept. Energy Tech Report TR-025, Washington, DC.
Prell, W.L., Imbrie, J., Martinson, D.G., Morley, J.J., Pisias, N.G., Shackleton, N.J., Streeter, H.F., 1986. Graphic correlation of oxygen isotope stratigraphy: application to the Late Quaternary. Paleoceanography. 1, 137–162.
Prentice, I.C., 1978. Modern pollen spectra from lake sediments in Finland and Finnmark, North Norway. Boreas. 7, 131–153.
Prentice, I.C., 1985. Pollen representation, source area and basin size: toward a unified theory of pollen analysis. Quat. Res. 23, 76–86.
Prentice, I.C., 1986. Vegetation responses to past climate variation: mechanisms and rates. Vegetatio. 67, 131–141.
Prentice, I.C., Webb III, T., 1986. Pollen percentages, tree abundances and the Fagerlind effect. J. Quat. Sci. 1, 35–43.
Prentice, I.C., Bartlein, P.J., Webb III, T., 1991. Vegetation and climate change in eastern North America since the last glacial maximum. Ecology. 72, 2038–2056.
Prentice, I.C., Cramer, W., Harrison, S.P., Leemans, R., Monserud, R.A., Solomon, A.M., 1992. A global biome model based on plant physiology and dominance, soil properties and climate. J. Biogeogr. 19, 117–134.
Prentice, I.C., Guiot, J., Huntley, B., Jolly, D., Cheddadi, R., 1996. Reconstructing biomes from palaeoecological data: a general method and its application to European pollen data at 0 and 6 ka. Clim. Dyn. 12, 185–194.
Prentice, I.C., Webb III, T., 1998. BIOME 6000: reconstructing global mid-Holocene vegetation patterns from palaeoecological records. J. Biogeogr. 25, 997–1005.
Prentice, I.C., Jolly, D., BIOME 6000 participants, 2000. Mid-Holocene and glacial-maximum vegetation geography of the northern continents and Africa. J. Biogeogr. 27, 507–519.
Prescott, J.R., Robertson, G.B., 2008. Luminescence dating: an Australian perspective. Aust. J. Sci. 55, 997–1007.
Prieto, M.R., 2007. ENSO signals in South America: rains and floods in the Paraná River region during colonial times. Clim. Chang. 83, 39–54.
Prieto, M.R., García-Herrera, R., 2009. Documentary sources from South America: potential for climate reconstruction. Palaeogeogr. Palaeoclimatol. Palaeoecol. 281, 196–209.
Prieto, M.R., García-Herrea, R., Hernández, E., 2004. Early records of icebergs in the South Atlantic Ocean from Spanish documentary sources. Clim. Chang. 66, 29–48.
Primack, D., Imbres, C., Primack, R.B., Miller-Rushing, A., Del Tredici, P., 2004. Herbarium specimens demonstrate earlier flowering times in response to warming in Boston. Am. J. Bot. 91, 1260–1264.
Primack, R.B., Higuchi, H., Miller-Rushing, S.J., 2009. The impact of climate change on cherry trees and other species in Japan. Biol. Conserv. 142, 1943–1949.

Prins, M.A., Vriend, M., Nugteren, G., Vandenberghe, J., Lu, H.Y., Zheng, H.B., Ao, H., Dong, J.B., Weltje, G.J., 2007. Late Quaternary Aeolian dust input variability on the Chinese Loess Plateau: inferences from unmixing of loess grain-size records. Quat. Sci. Rev. 26, 230–242.

Prokopenko, A.A., Karabanov, E.B., Williams, D.F., Kuzmin, M.I., Shackleton, N.J., Crowhurst, S.J., Peck, J.A., Gvozdkov, A.N., King, J.W., 2001. Biogenic silica record of the Lake Baikal response to climatic forcing during the Brunhes. Quat. Res. 55, 123–132.

Pross, J., Kotthoff, U., Muller, U.C., Peyron, O., Dormoy, I., Schmiedl, G., Kalaitzidis, S., Smith, A.M., 2009. Massive perturbation in terrestrial ecosystems of the Eastern Mediterranean region associated with the 8.2ky B.P. climatic event. Geology. 37, 887–890.

Punt, W., Hoen, P.P., Blackmore, S., Nilsson, S., Le Thomas, A., 2007. Glossary of pollen and spire terminology. Rev. Palaeobot. Palynol. 143, 1–81.

Punyasena, S.W., Mayle, F.E., McElwain, J.C., 2008. Quantitative estimates of glacial and Holocene temperature and precipitation in lowland Amazonian Bolivia. Geology. 36, 667–670.

Pye, K., 1984. Loess. Prog. Phys. Geogr. 8, 176–217.

Pye, K., 1987. Aeolian Dust and Dust Deposits. Academic Press, London.

Pyne-O'Donnell, S.D.F., 2007. Three new distal tephras in sediments spanning the Last Glacial-Interglacial transition in Scotland. J. Quat. Sci. 22, 559–570.

Qiang, X.K., An, Z.S., Song, Y.G., Chang, H., Sun, Y.B., Liu, W.G., Ao, H., Dong, J.B., Fu, C.F., Wu, F., Lu, F.Y., Cai, Y.J., Zhou, W.J., Cao, J.J., Xu, X.W., Ai, L., 2011. New eolian red clay sequence on the western Chinese Loess Plateau linked to onset of Asian desertification about 25 Ma ago. Sci. China Earth Sci. 54, 136–144.

Qin, Dahe, Petit, J.R., Jouzel, J., Stievenard, M., 1994. Distribution of stable isotopes in surface snow along the route of the 1990) International Trans-Antarctica Expedition. J. Glaciol. 40, 107–118.

Quinn, W.H., 1992. A study of Southern Oscillation-related climatic activity for A.D. 622-1990 incorporating Nile River flood data. In: Diaz, H.F., Markgraf, V. (Eds.), El Niño: Historical and Paleoclimatic Aspects of the Southern Oscillation. Cambridge University Press, Cambridge, pp. 119–149.

Quinn, W.H., 1993. The large-scale ENSO event, the El Niño and other important regional features. Bull. Inst. Fr. Etudes Andines. 22, 13–34.

Quinn, W.H., Neal, V.T., 1992. The historical record of El Niño events. In: Bradley, R.S., Jones, P.D. (Eds.), Climate Since A.D. 1500. Routledge, London, pp. 623–648.

Quinn, T.M., Sampson, D.E., 2002. A multiproxy approach to reconstructing sea surface conditions using coral skeleton geochemistry. Paleoceanography. 17. dx.doi.org/10.1029/2000PA000528.

Quinn, T.M., Taylor, F.W., Crowley, T.J., 1993. A 173 year stable isotope record from a tropical South Pacific coral. Quat. Sci. Rev. 12, 407–418.

Quinn, T.M., Taylor, F.W., Crowley, T.J., Link, S.M., 1996. Evaluation of sampling resolution in coral stable isotope records: a case study using monthly stable isotope records from New Caledonia and Tarawa. Paleoceanography. 11, 529–542.

Quinn, T.M., Crowley, T.J., Taylor, F.W., Henin, C., Joannot, P., Join, Y., 1998. A multicentury stable isotope record from a New Caledonia coral: interannual and decadal sea surface temperature variability in the southwest Pacific since 1657 A.D. Paleoceanography. 13, 412–426. dx.doi.org/10.1029/98PA00401.

Rácz, L., 1999. Climate History of Hungary Since 16th Century: Past, Present and Future. Centre for Regional Studies of the Hungarian Academy of Sciences, Pécs, 158 pp.

Rahmstorf, S., 1994. Rapid climate transitions in a coupled ocean-atmosphere model. Nature. 372, 82–85.

Rahmstorf, S., 1995. Bifurcations of the Atlantic thermohaline circulation in response to changes in the hydrological cycle. Nature. 378, 145–149.

Rahmstorf, S., 2002. Ocean circulation and climate during the past 120,000 years. Nature. 419, 207–214.

Rahmstorf, S., Alley, R., 2002. Stochastic resonance in glacial climate. EOS Trans. Am. Geophys. Union. 83, 129, 135.

Raisbeck, G.M., Yiou, F., Jouzel, J., Petit, J.R., Barkov, N.I., Bard, E., 1992. ^{10}Be deposition at Vostok, Antarctica during the last 50,000 years and its relationship to possible cosmogenic production variations during this period. In: Bard, E., Broecker, W.S. (Eds.), The Last Deglaciation: Absolute and Radiocarbon Chronologies. Springer Verlag, Berlin, pp. 127–139.

Raisbeck, G.M., Yiou, F., Cattani, O., Jouzel, J., 2006. ^{10}Be evidence for the Matuyama-Brunhes geomagnetic reversal in the EPICA Dome C ice core. Nature. 444, 82–84.

Raisbeck, G.M., Yiou, F., Jouzel, J., Stocker, T.F., 2007. Direct north-south synchronization of abrupt climate change record in ice cores using Beryllium 10. Clim. Past. 3, 541–547.

Ralska-Jasiewiczowa, M., Goslar, T., Madeyska, T., Starkel, L. (Eds.), 1998. Lake Gościąż, Central Poland: a monographic study. Part 1. W. Szafer Institute of Botany, Polish Academy of Sciences, Kraków, 340 pp.

Ram, M., Illing, M., 1995. Polar ice stratigraphy from laser-light scattering: scattering from meltwater. J. Glaciol. 40, 504–508.

Ramirez, E., Hoffman, G., Taupin, J.D., Francou, B., Ribstein, P., Caillon, N., Ferron, F.A., Landais, A., Petit, J.R., Pouyaud, B., Schotterer, U., Simões, J., Stievenard, M., 2003. A new deep Andean ice core from Nevado Illimani (6350m), Bolivia. Earth Planet. Sci. Lett. 212, 337–350.

Rampen, S.W., Abbas, B.A., Schouten, S., Sinninghe Damsté, J.S., 2010. A comprehensive study of sterols in marine diatoms (Bacillariophyta): implications for their use as tracers for diatom productivity. Limnol. Oceanogr. 55, 91–105.

Rampen, S.W., Willmott, V., Kim, J.-H., Uliana, E., Mollenhauer, G., Schefuß, E., Sinninghe Damsté, J.S., Schouten, S., 2012. Long chain 1,13- and 1,15-diols as a potential proxy for palaeotemperature reconstruction. Geochim. Cosmochim. Acta. 84, 204–216.

Rampino, M., Self, S., 1982. Historic eruptions of Tambora 1815), Krakatau 1883) and Agung 1963) their stratospheric aerosols and climatic impact. Quat. Res. 18, 127–143.

Rampino, M., Self, S., 1984. Sulfur-rich volcanic eruptions and stratospheric aerosols. Nature. 310, 677–679.

Ramsey, C.N., 1995. Radiocarbon calibration and analysis of stratigraphy: the Oxcal program. Radiocarbon. 37, 425–430.

Rasmussen, T.L., Thomsen, E., 2004. The role of the North Atlantic Drift in the millennial timescale glacial climate fluctuations. Palaeogeogr. Palaeoclimatol. Palaeoecol. 210, 101–116.

Rasmussen, T.L., Thomsen, E., 2008. Warm Atlantic surface water inflow to the Nordic seas 34–10 calibrated ka B.P. Paleoceanography. 23, PA1201. dx.doi.org/10.1029/2007PA001453.

Rasmussen, T.L., Thomsen, E., van Weering, T.C.E., Labeyrie, L., 1996. Rapid changes in surface and deepwater conditions at the Faeroe margin during the last 58,000 years. Paleoceanography. 11, 757–771.

Rasmussen, S.O., Andersen, K.K., Svensson, A.M., Steffensen, J.P., Vinther, B.M., Clausen, H.B., Siggard-Andersen, M.-L., Johnsen, S.J., Larsen, L.B., Dahl-Jensen, D., Bigler, M., Röthlisberger, R., Fischer, H., Goto-Azuma, K., Hansson, M.E., Ruth, U., 2006. A new Greenland ice core chronology for the last glacial termination. J. Geophys. Res. 111, D06102. dx.doi.org/10.1029/2005JD00607.

Rasmussen, S.O., Seierstad, I.K., Andersen, K.K., Bigler, M., Dahl-Jensen, D., Johnsen, S.J., 2008. Synchronization of the NGRIP, GRIP and GISP2 ice cores across MIS1 and paleoclimatic implications. Quat. Sci. Rev. 27, 18–28.

Ravelo, A.C., Hillaire-Marcel, C., 2007. The use of oxygen and carbon isotopes of foraminifera in paleoceanography. In: Hillaire-Marcel, C., de Vernal, A. (Eds.), Proxies in Late Cenozoic Paleoceanography. Elsevier, Amsterdam, pp. 735–764.

Ravelo, A.C., Andreasen, D.H., Lyle, M., Lyle, A.O., Wara, M.W., 2004. Regional climate shifts caused by gradual global cooling in the Pliocene epoch. Nature. 429, 263–267.

Raymo, M.E., 1992. Global climate change: a three million year perspective. In: Kukla, G.J., Went, E. (Eds.), Start of a Glacial. Springer-Verlag, Berlin, pp. 207–223.

Raymo, M.E., 1998. Glacial puzzles. Science. 281, 1467–1468.

Raymo, M.E., Huybers, P., 2008. Unlocking the mysteries of the ice ages. Nature. 451, 284–285.

Raymo, M.E., Nisancioglu, K., 2003. The 41 kyr world: Milankovitch's other unsolved mystery. Paleoceanography. 18. dx.doi.org/10.1029/2002PA000791.

Raymo, M., Ruddiman, W.F., Shackleton, N.J., Oppo, D., 1990. Evolution of global ice volume and Atlantic-Pacific $\delta^{13}C$ gradients over the last 2.5 m.y. Earth Planet. Sci. Lett. 97, 353–368.

Raymo, M.E., Lisiecki, L.E., Nisancioglu, K., 2006. Plio-Pleistocene ice volume, Antarctic climate and the global $\delta^{18}O$ record. Science. 313, 492–495.

Raynaud, D., 1992. The ice record of the atmospheric composition: a summary, chiefly of CO_2, CH_4 and O_2. In: Moore III, B., Shimel, D. (Eds.), Trace Gases and the Biosphere. University Corporation for Atmospheric Research, Boulder, pp. 165–176.

Raynaud, D., Barnola, J.-M., 1985. CO_2 and climate: information from Antarctica ice core studies. In: Ghazi, A., Fantechi, R. (Eds.), Current Issues in Climate Research. D. Reidel, Dordrecht, pp. 240–246.

Raynaud, D., Chappellaz, J., Barnola, J.-M., Korotkevich, Y.S., Lorius, C., 1988. Climatic and CH_4 cycle implications of glacial-interglacial CH_4 change in the Vostok ice core. Nature. 333, 655–657.

Raynaud, D., Jouzel, J., Barnola, J.M., Chappellaz, J., Delmas, R.J., Lorius, C., 1993. The ice record of greenhouse gases. Science. 259, 926–934.

Raynaud, D., Blunier, T., Ono, Y., Delmas, R.J., 2003. The Late Quaternary history of atmospheric trace gases and aerosols: interactions between climate and biogeochemical cycles. In: Alverson, K.D., Bradley, R.S., Pedersen, T.F. (Eds.), Paleoclimate, Global Change and the Future. Springer, Berlin, pp. 13–31.

Raynaud, D., Lipenkov, V., Lemieux-Dudon, B., Duval, P., Loutre, M.-F., Lhomme, N., 2007. The local insolation signature of air content in Antarctic ice. A new step toward an absolute dating of ice cores. Earth Planet. Sci. Lett. 261, 337–349.

Rea, D.K., 1994. The paleoclimatic record provided by eolian deposition in the deep sea: the geologic history of the wind. Rev. Geophys. 32, 159–195.

Rea, D.K., Snoeck, H., Joseph, L.H., 1998. Late Cenozoic aeolian deposition in the North Pacific: Asian drying, Tibetan uplift, and cooling of the Northern Hemisphere. Palaeoceanography. 13, 215–224.

Reeh, N., 1989. Dating by ice flow modeling: a useful tool or an exercise in applied mathematics? In: Oeschger, H., Langway Jr., C.C. (Eds.), The Environmental Record in Glaciers and Ice Sheets. Wiley, Chichester, pp. 141–159.

Reeh, N., 1991. The last interglacial as recorded in the Greenland Ice Sheet and Canadian Arctic Ice Caps. Quat. Int. 10–12, 123–142.

Reeh, N., Thomsen, H.H., Clausen, H.B., 1987. The Greenland ice sheet margin–a mine of ice for paleoenvironmental studies. Palaeogeogr. Palaeoclimatol. Palaeoecol. 58, 229–234.

Reeh, N., Oerter, H., Letreguilly, A., Miller, H., Hubberten, H.W., 1991. A new detailed ice-age oxygen-18 record from the ice-sheet margin in central West Greenland. Palaeogeogr. Palaeoclimatol. Palaeoecol. 90, 373–383.

Reeh, N., Oerter, H., Miller, H., 1993. Correlation of Greenland ice-core and ice-margin $\delta^{18}O$ records. In: Peltier, W. (Ed.), Ice in the Climate System. Springer-Verlag, Berlin, pp. 481–497.

Reeves, C.C., 1965. Pleistocene climate of the Llano Estacado. J. Geol. 73, 181–189.

Regnell, J., 1992. Preparing pollen concentrates for AMS dating—a methodological study from a hard-water lake in southern Sweden. Boreas. 21, 373–377.

Reimer, P.J., Hughen, K.A., 2008. Tree rings floating on ice cores. Nat. Geosci. 1, 218–219.

Reimer, P.J., Baillie, M.G.L., Bard, E., Bayliss, A., Beck, J.W., Blackwell, P.G., Bronk Ramsey, C., Buck, C.E., Burr, G.S., Edwards, R.L., Friedrich, M., Grootes, P.M., Guilderson, T.P., Hajdas, I., Heaton, T.J., Hogg, A.G., Hughen, K.A., Kaiser, K.F., Kromer, B., McCormac, G., Manning, S., Reimer, R.W., Richards, D.A., Southon, J.R., Talamo, S., Turney, C.S.M., van der Plicht, J., Weyhenmeyer, C.E., 2009. IntCal09 and Marine09 radiocarbon calibration curves, 0–50,000 years cal B.P. Radiocarbon. 51, 1111–1150.

Rein, B., Sirocko, F., 2002. In-situ reflectance spectroscopy—analysing techniques for high-resolution pigment logging in sediment cores. Int. J. Earth Sci. 91, 950–954.

Ren, L., Linsley, B.K., Wellington, G.M., Schrag, D.P., Hoegh-Guldberg, O., 2002. Deconvolving the $\delta^{18}O$ seawater component from subseasonal coral $\delta^{18}O$ and Sr/Ca at Rarotonga in the southwestern subtropical Pacific for the period 1726 to 1997. Geochim. Cosmochim. Acta. 67, 1609–1621.

Rendell, H.M., 1995. Luminescence dating of Quaternary sediments. In: Dunay, R.E., Hailwood, E.A. (Eds.), Non-biostratigraphical Methods of Dating and Correlation. Special Publication 89The Geological Society, London, pp. 223–235.

Renne, P.R., 2000. K-Ar and $^{40}Ar/^{39}Ar$ dating. In: Noller, J.S., Sowers, J.M., Lettis, W.R. (Eds.), Quaternary Geochronology: Methods and Applications. American Geophysical Union, Washington, DC, pp. 77–100.

Renne, P.R., Deino, A.L., Walter, R.C., Turrin, B.D., Swisher, C.C., Becker, T.A., Curtis, G.H., Sharp, W.D., Jaouni, A.R., 1994. Intercalibration of astronomical and radioisotopic time. Geology. 22, 783–786.

Reuter, J., Stott, L., Khider, D., Sinha, A., Cheng, H., Edwards, R.L., 2009. A new perspective on the hydroclimate variability in northern South America during the Little Ice Age. Geophys. Res. Lett. 36, L21706. dx.doi.org/10.1029/2009GL041051.

Revel, M., Sinko, J.A., Grousset, F.E., Biscaye, P.E., 1996. Sr and Nd isotopes as tracers of North Atlantic lithic particles: paleoclimatic implications. Paleoceanography. 11, 95–113.

Reynolds-Sautter, L., Thunell, R.C., 1989. Seasonal succession of planktonic foraminifera: results from a four year time-series sediment trap experiment in the Northeast Pacific. J. Foram. Res. 19, 253–267.
Richards, D.A., Dorale, J.A., 2003. Uranium-series chronology and environmental applications of speleothems. Rev. Mineral. Geochem. 52, 407–460.
Richards, D.A., Smart, P.L., 1991. Potassium-argon and argon-argon dating. In: Smart, P.L., Frances, P.F.D. (Eds.), Quaternary Dating Methods—a user's guide. Technical Guide 4, Quaternary Research Association, Cambridge, pp. 37–44.
Richards, D.A., Smart, P.L., Edwards, R.L., 1994. Maximum sea levels for the last glacial period from ages of submerged speleothems. Nature. 367, 357–360.
Richman, M.B., 1986. Rotation of principal components. J. Climatol. 6, 293–335.
Richmond, G.M., 1965. Glaciation of the rocky mountains. In: Wright, H.E., Frey, D.G. (Eds.), The Quaternary of the United States. Princeton University Press, Princeton, pp. 217–230.
Rind, D., 2002. The Sun's role in climate variations. Science. 296, 673–677.
Rind, D., Overpeck, J., 1993. Hypothesized causes of decadal-to-century climate variability: climate model results. Quat. Sci. Rev. 12, 357–374.
Rind, D., Peteet, D., 1985. Terrestrial conditions at the last glacial maximum and CLIMAP sea-surface temperature estimates: are they consistent? Quatern. Res. 24, 1–22.
Rind, D., Lean, J., Healy, R., 1999. Simulated time-dependent climate response to solar radiative forcing since 1600. J. Geophys. Res. 104D, 1973–1990.
Risebrobakken, B., Jansen, E., Andersson, C., Mjelde, E., Hevrøy, K., 2003. A high-resolution study of Holocene paleoclimatic and paleoceanographic changes in the Nordic Seas. Paleoceanography. 18, 1017. dx.doi.org/10.1029/2002PA000764.
Ritchie, J.C., 1976. The late-Quaternary vegetational history of the western interior of Canada. Can. J. Bot. 54, 1793–1818.
Ritchie, J.C., 1986. Climate change and vegetation response. Vegetatio. 67, 65–74.
Ritchie, J.C., 1987. Postglacial Vegetation of Canada. Cambridge University Press, Cambridge.
Ritchie, J.C., Hare, F.K., 1971. Late Quaternary vegetation and climate near the Arctic treeline of northwestern North America. Quat. Res. 1, 331–342.
Ritz, S.P., Stocker, T.F., Grimalt, J.O., Menviel, L., Timmermann, A., 2013. Estimated strength of the Atlantic Overturning Circulation during the last deglaciation. Nat. Geosci. 6, 208–212.
Roberts, A.P., 2008. Geomagnetic excursions: knowns and unknowns. Geophys. Res. Lett. 35, L17307. dx.doi.org/10.1029/2008GL034719.
Robertson, A., Overpeck, J.T., Rind, D., Mosley-Thompson, E., Zielinski, G., Lean, J., Koch, D., Penner, J., Tegen, I., Healy, R., 2001. Hypothesized climate forcing time series for the last 500 years. J. Geophys. Res. 106, 14783–14803.
Robin, G. de Q., 1977. Ice cores and climatic change. Philos. Trans. R. Soc. Lond. B. 280, 143–168.
Robinson, W.J., 1976. Tree-ring dating and archaeology in the American Southwest. Tree Ring Bull. 36, 9–20.
Robinson, L.F., van der Flierdt, T., 2008. Southern Ocean evidence for reduced export of North Atlantic deepwater during Heinrich event 1. Geol. Soc. Am. Bull. 37, 195–198.
Robinson, W.J., Cook, E., Pilcher, J.R., Eckstein, D., Kariukstis, L., Shiyatov, S., Norton, D.A., 1990. Some historical background on dendrochronology. In: Cook, E.R., Kariukstis, L.A. (Eds.), Methods of Dendrochronology. Applications on the Environmental Sciences. Kluwer, Dordrechy, pp. 1–21.
Robinson, L.F., Atkins, J.F., Keigwin, L.D., Southon, J., Fernandez, D.P., Wang, S.-L., Scheirer, D.S., 2005. Radiocarbon variability in the western North Atlantic during the last deglaciation. Science. 310, 1469–1473.
Robock, A., 1978. Internal and externally caused climate change. J. Atmos. Sci. 35, 1111–1122.
Robock, A., 2000. Volcanic eruptions and climate. Rev. Geophys. 38, 191–219.
Robock, A., Free, M.P., 1996. The volcanic record in ice cores for the past 2000 years. In: Jones, P.D., Bradley, R.S., Jouzel, J. (Eds.), Climatic Variations and Forcing Mechanisms of the Last 2000 Years. Springer, Berlin, pp. 533–546.
Robock, A., Mao, J.-P., 1995. The volcanic signal in surface temperature observations. J. Clim. 8, 1086–1103.
Rochefort, R.M., Little, R.L., Woodward, A., Peterson, D.L., 1994. Changes in subalpine tree distribution in western North America: a review of climatic and other causal factors. The Holocene. 4, 89–100.
Rockström, J., Steffen, W., Noone, K., Persson, Å., Chapin III, F.S., Lambin, E.F., Lenton, T.M., Scheffer, M., Folke, C., Schellnhuber, H.J., Nykvist, B., de Wit, C.A., Hughes, T., van der Leeuw, S., Rodhe, H., Sörlin, S., Snyder, P.K.,

Costanza, R., Svedin, U., Falkenmark, M., Karlberg, L., Corell, R.W., Fabry, V.J., Hansen, J., Walker, B., Liverman, D., Richardson, K., Crutzen, P., Foley, J.A., 2009. A safe operating space for humanity. Nature. 461, 472–475.
Rodbell, D.T., 1992. Lichenometric and radiocarbon dating of Holocene glaciation, Cordillera Blanca, Peru. The Holocene. 2, 19–29.
Rodbell, D.T., 1993. Subdivision of late Pleistocene moraines in the Cordillera Blanca, Peru based on rock-weathering features, soils and radiocarbon dates. Quat. Res. 39, 133–143.
Roden, J.S., Lin, G., Ehrlinger, J.R., 2000. A mechanistic model for interpreting hydrogen and oxygen isotope ratios in tree-ring cellulose. Geochim. Cosmochim. Acta. 64, 21–35.
Rognon, P., 1976. Essai d'interpretation des variations climatiques au Sahara depuis 40,000 ans. Rev. Géogr. Phys. Géol. Dyn. 18, 251–282.
Rognon, P., Williams, M.A.J., 1977. Late Quaternary climatic changes in Australia and NorthAfrica: a preliminary interpretation. Palaeogeogr. Palaeoclimatol. Palaeoecol. 21, 285–327.
Rohling, E.J., Bigg, G.R., 1998. Paleosalinity and δ18O: a critical assessment. J. Geophys. Res. 103, 1307–1318.
Rohling, E.J., Pälike, H., 2005. Centennial-scale climate cooling with a sudden cold event around 8,200 years ago. Nature. 343, 975–979.
Rohling, E.J., Grant, K., Bolshaw, M., Roberts, A.P., Siddall, M., Hemleben, Ch., Kucera, M., 2009. Antarctic temperature and global sea level closely coupled over the last five glacial cycles. Nat. Geosci. 2, 500–504.
Rohling, E.J., Medina-Elizalde, M., Shepherd, J.G., Siddall, M., Staford, J.D., 2012. Sea surface and high-latitude temperature sensitivity to radiative forcing of climate over several glacial cycles. J. Clim. 25, 1635–1656.
Rolph, T.C., Shaw, J., Derbyshire, E., Wang, J.T., 1989. A detailed geomagnetic record from Chinese loess. Phys. Earth Planet. Inter. 56, 151–164.
Rontani, J.-F., Volkman, J.K., Prahl, F.G., Wakeham, S.G., 2013. Biotic and abiotic degradation of alkenones and implications for $U^{K'}_{37}$ paleoproxy applications: a review. Org. Geochem. 59, 95–113.
Rood, D.H., Burbank, D.W., Finkel, R.C., 2011. Chronology of glaciations in the Sierra Nevada, California from ^{10}Be surface exposure dating. Quat. Sci. Rev. 30, 646–661.
Roof, S., Werner, A., 2011. Indirect growth curves remain the best choice for lichenometry: evidence from directly measured growth rates from Svalbard. Arctic Antarct Alpine Res. 43, 621–631.
Rosell-Melé, A., McClymont, E.L., 2007. Biomarkers as paleoceanographic proxies. In: Hillaire-Marcel, C., de Vernal, A. (Eds.), Proxies in Late Cenozoic Paleoceanography. Elsevier, Amsterdam, pp. 441–490.
Rosell-Melé, A., Eglinton, G., Pflaumann, U., Sarnthein, M., 1995. Atlantic core-top calibration of the U^{k}_{37} index as a sea-surface paleotemperature indicator. Geochim. Cosmochim. Acta. 59, 3099–3107.
Rosenthal, Y., 2007. Elemental proxies for reconstructing Cenozoic seawater paleotemperatures from calcareous fossils. In: Hillaire-Marcel, C., de Vernal, A. (Eds.), Proxies in Late Cenozoic Paleoceanography. Elsevier, Amsterdam, pp. 765–797.
Rosqvist, G., Jonsson, C., Yam, R., Karlén, W., Shemesh, A., 2004. Diatom oxygen isotopes in pro-glacial lake sediments from northern Sweden: a 5000 year record of atmospheric circulation. Quat. Sci. Rev. 23, 851–859.
Rostek, F., Ruhland, G., Bassinot, F.C., Muller, P.J., Labeyrie, L.D., Lancelot, Y., Bard, E., 1993. Reconstructing sea surface temperature and salinity using δ^{18}O and alkenone records. Nature. 364, 319–321.
Rotberg, R.I., Rabb, T.K. (Eds.), 1981. Climate and History: Studies in Interdisciplinary History. Princeton University Press, Princeton.
Rothlisberger, F., 1976. Gletscherund Klimaschwankungen im Raun Zermatt, Ferpecle und Arolla. Die Alpen. 52, 59–132.
Rothlisberger, F., 1986. 10,000 Jahre Gletschergeschichte der Erde. Verlag Sauerländer, Aarau.
Röthlisberger, R., Bigler, M., Hutterli, M., Sommer, S., Stauffer, B., Junghans, H., Wagenbach, D., 2000. Technique for continuous high-resolution analysis of trace substances in firn and ice cores. Environ. Sci. Technol. 34, 338–342.
Rothwell, R.G., Croudace, I. (Eds.), 2014. Micro-XRF Studies of Sediment Cores: A Non-destructive Tool for the Environmental Sciences. Springer, Berlin.
Rousseau, D.D., Wu, N.Q., 1997. A new molluscan record of the monsoon variability over the past 130,000 yr in the Luochuan loess sequence, China. Geology. 25, 275–278.
Rousseau, D.D., Wu, N.Q., 1999. Mollusk record of monsoon variability during the L2-S2 cycle in the Luochuan loess sequence, China. Quat. Res. 52, 286–292.

Rozanski, K., Araguas-Araguas, L., Gonfiantini, R., 1992. Relation between long-term trends of oxygen-18 isotope composition of precipitation and climate. Science. 258, 981–985.
Rozanski, K., Araguas-Araguas, L., Gonfiantini, R., 1993. Isotopic patterns in modern global precipitation. In: Swart, P.K., Lohmann, K.C., McKenzie, J., Savin, S. (Eds.), Climate Change in Continental Isotopic Records. American Geophysical Union, Washington, DC, pp. 1–36.
Ruddiman, W.F., 1971. Pleistocene sedimentation in the equatorial Atlantic: stratigraphy and faunal paleoclimatology. Geol. Soc. Am. Bull. 82, 283–302.
Ruddiman, W.F., 1977. Investigations of Quaternary climate based on planktonic foraminifera. In: Ramsay, A.T.S. (Ed.), Oceanic Micropaleontology. Academic Press, New York, pp. 101–161.
Ruddiman, W.F., 2003. The Anthropocene greenhouse era began thousands of years ago. Climate Change. 61, 261–293.
Ruddiman, W.F., 2006. Orbital changes and climate. Quat. Sci. Rev. 25, 3092–3112.
Ruddiman, W.F., 2007. The early anthropogenic hypothesis: challenges and responses. Rev. Geophys. 45, RG4001. dx.doi.org/10.1029/2006RG000207.
Ruddiman, W.F., Esmay, A., 1987. A streamlined foraminiferal transfer function for the subpolar North Atlantic. Initial Rep. Deep Sea Drill. Proj. 94, 1045–1057.
Ruddiman, W.F., Glover, L.K., 1972. Vertical mixing of ice-rafted volcanic ash in North Atlantic sediments. Geol. Soc. Am. Bull. 83, 2817–2836.
Ruddiman, W.F., Heezen, B.C., 1967. Differential solution of planktonic foraminifera. Deep-Sea Res. 14, 801–808.
Ruddiman, W.F., Kutzbach, J.E., 1989. Forcing of late Cenozoic northern hemisphere climate by plateau uplift in southern Asia and the American West. J. Geophys. Res. 94, 18409–18427.
Ruddiman, W.F., McIntyre, A., 1981. The mode and mechanism of the last deglaciation: oceanic evidence. Quat. Res. 16, 125–134.
Ruddiman, W.F., Raymo, M., Mcintyre, A., 1986. Matuyama 41,000-year cycles: north Atlantic Ocean and northern hemisphere ice sheets. Earth Planet. Sci. Lett. 80, 117–129.
Ruth, U., Bigler, M., Röthlisberger, R., Siggard-Andersen, M.-L., Kipfstuhl, S., Goto-Azuma, K., Hansson, M.E., Johnsen, S.J., Lu, H., Steffense, J.P., 2007. Ice core evidence for a very tight coupling between North Atlantic and east Asian glacial climate. Geophys. Res. Lett. 34. dx.doi.org/10.1029/2006GL027876.
Rutishauser, T., 2007. Historical phenology—plant phenological reconstructions and climate sensitivity in northern Switzerland. PhD thesis, Geographisches Institut, University of Bern, 167 pp.
Rutishauser, T., Luterbacher, J., Jeanneret, F., Pfister, C., Wanner, H., 2007. A phenology-based reconstruction of interannual changes in past spring seasons. J. Geophys. Res. Biogeosci. 112, G04016. dx.doi.org/10.1029/2006JG000382.
Rutter, N.W., Blackwell, B., 1995. Amino acid racemization dating. In: Rutter, N.W., Catto, N.R. (Eds.), Dating Methods for Quaternary Deposits. Geological Association of Canada, St. John's, pp. 125–166.
Rutter, N., Ding, Z., Evans, M.E., Wang, Y., 1990. Magnetostratigraphy of the Baoji loess-paleosol section in the north-central China loess plateau. Quat. Int. 718, 97–102.
Ruzmaikin, A.A., 1999. Can El Niño amplify the solar forcing of climate? Geophys. Res. Lett. 26, 2255–2258.
Rybnfckova, E., Rybnfcek, K., 1993. Late Quaternary forest line oscillations in the West Carpathians. In: Frenzel, B., Eronen, M., Vorren, K.D., Glaser, B. (Eds.), Oscillations of the Alpine and Polar Tree Limits in the Holocene. Gustav Fischer Verlag, Stuttgart, pp. 187–194.
Sabine, C.L., Feely, R.A., Gruber, N., Key, R.M., Lee, K., Bullister, J.L., Wanninkhof, R., Wong, C.S., Wallace, D.W.R., Tilbrook, B., Millero, F.J., Peng, T.-H., Kozyr, A., Ono, T., Rios, A.F., 2004. The oceanic sink for anthropogenic CO_2. Science. 305, 367–371.
Sachs, J.P., Lehman, S.J., 1999. Subtropical North Atlantic temperatures 60,000 to 30,000 years ago. Science. 286, 756–759.
Sachs, M.H., Webb, T., Clark, D.R., 1977. Paleoecological transfer functions. Annu. Rev. Earth Planet. Sci. 5, 159–178.
Sachs, J.P., Schneider, R.R., Eglinton, T.I., Freeman, K.H., Ganssen, G., McManus, J.F., Oppo, D.W., 2000. Alkenones as paleoceanographic proxies. Geochem. Geophys. Geosyst. 1. dx.doi.org/10.1029/2000GC000059.
Sachse, D., Radke, J., Gleixner, G., 2006. δD values of individual *n*-alkanes from terrestrial plants along a climatic gradient—implications for the sedimentary biomarker record. Org. Geochem. 37, 469–483.
Saenger, C., Cohen, A.L., Oppo, D.W., Halley, R.B., Carilli, J.E., 2009. Surface-temperature trends and variability in the low-latitude North Atlantic since 1552. Nat. Geosci. 2, 492–495.
Salgado-Labouriau, M.L., 1979. Modern pollen deposition in the Venezuelan Andes. Grana. 18, 53–68.

Salgado-Labouriau, M.L., Schubert, C., Valastro Jr., S., 1978. Paleoecologic analysis of a Late-Quaternary terrace from Mucubaji, Venezuelan Andes. J. Biogeogr. 4, 313–325.
Salvesen, H., 1992. The climate as a factor of historical causation. In: Frenzel, B., Pfister, C., Glaser, B. (Eds.), European Climate Reconstructed from Documentary Data: Methods and Results. Gustav Fischer Verlag, Stuttgart, pp. 219–233.
Salzer, M.W., Hughes, M.K., 2007. Bristlecone pine tree rings and volcanic eruptions over the last 5000 yr. Quat. Res. 67, 57–68.
Sancetta, C., 1979. Oceanography of the North Pacific during the last 18,000 years: evidence from fossil diatoms. Mar. Micropalaeontol. 4, 103–123.
Sancetta, C., 1995. Diatoms in the Gulf of California: seasonal flux patterns and the sediment record for the last 15,000 years. Paleoceanography. 10, 67–84.
Sancetta, C., Imbrie, J., Kipp, N.G., 1973a. Climatic record of the past 130,000 years in the North Atlantic deep-sea core V23-83: correlation with the terrestrial record. Quat. Res. 3, 110–116.
Sancetta, C., Imbrie, J., Kipp, N.G., 1973b. The climatic record of the past 14,000 years in North Atlantic deep-sea core V23-82: correlation with the terrestrial record. In: Mapping the Atmospheric and Oceanic Circulations and Other Climatic Parameters at the Time of the Last Glacial Maximum about 17,000 years ago. Publication No. 2, Climatic Research Unit, University of East Anglia, Norwich, pp. 62–65.
Santer, B.D., Wigley, T.M.L., Barnett, T.P., Anyamba, E., 1996. Detection of climate change and attribution of causes. In: Houghton, J.T., Meirho Filho, L.G., Callendar, B.A., Kattenberg, A., Maskell, K. (Eds.), Climate Change 1995: The Science of Climate Change. Cambridge University Press, Cambridge, pp. 407–443.
Sarnthein, M., 1978. Sand deserts during glacial maximum and climatic optimum. Nature. 272, 43–46.
Sarnthein, M., Tetzlaff, G., Koopman, B., Wolter, K., Pflaumann, U., 1981. Glacial and interglacial wind regimes over the eastern sub-tropical Atlantic and northwest Africa. Nature. 293, 193–196.
Sarnthein, M., Winn, K., Duplessy, J.-C., Fortugne, M.R., 1988. Global variations of surface ocean productivity in low and mid latitudes: influence on CO_2 reservoirs of the deep ocean and atmosphere during the last 21,000 years. Paleoceanography. 3, 361–379.
Sarnthein, M., Gersonde, R., Niebler, S., Pflaumann, U., Spielhagen, R., Thiede, J., Wefer, G., Weinelt, M., 2003. Overview of Glacial Atlantic Ocean Mapping (GLAMAP 2000). Paleoceanography. 18, 1065. dx.doi.org/10.1029/2002PA000769.
Savin, S.M., Stehli, F.G., 1974. Interpretation of oxygen isotope paleotemperature measurements: effect of the $^{18}O/^{16}O$ ratio of sea water depth stratification of foraminifera and selective solution. In: Les Methodes Quantitatives d'Etude des Variations du Climat au Cours du Pleistocene. Colloques lnternationaux du Centre National de Ia Recherche Scientifique No. 219, CNRS, Paris, pp. 183–191.
Schär, S., Vidale, P.L., Lüthi, D., Frei, C., Häberli, C., Linager, M.A., Appenzeller, C., 2004. The role of increasing temperature variability in European summer heatwaves. Nature. 427, 332–336.
Schaub, M., Kaiser, K.F., Frank, D.C., Buntgen, U., Kromer, B., Talamo, S., 2008a. Environmental change during the Allerød and Younger Dryas reconstructed from Swiss tree-ring data. Boreas. 37, 74–86.
Schaub, M., Buntgen, U., Kaiser, K.F., Kromer, B., Talamo, S., Andersen, K.K., Rasmussen, S.O., 2008b. Lateglacial environmental variability from Swiss tree rings. Quat. Sci. Rev. 27, 29–41.
Schiebel, R., 2002. Planktic foraminiferal sedimentation and the marine calcite budget. Glob. Biogeochem. Cycles. 16, 1065. dx.doi.org/10.1029/2001GB001459.
Schleip, C., Rutishauser, T., Menzel, A., Luterbacher, J., 2008. Time series modelling and central European temperature impact assessment of phenological records in the last 250 years. J. Geophys. Res. Biogeosci. 113. G04026.
Schleser, G.H., Helle, G., Lücke, A., Vos, H., 1999. Isotope signals as climate proxies: the role of transfer functions in the study of terrestrial archives. Quat. Sci. Rev. 18, 927–943.
Schmidt, G.A., 2010. Enhancing the relevance of palaeoclimate model/data comparisons for assessments of future climate change. J. Quat. Sci. 25, 79–87.
Schmidt, G.A., LeGrande, A.N., Hoffmann, G., 2007. Water isotope expressions of intrinsic and forced variability in a coupled ocean-atmosphere model. J. Geophys. Res. Atmos. 112, D10103. dx.doi.org/10.1029/2006JD007781.
Schmittner, A., Urban, N.M., Shakun, J.D., Mahowald, N.M., Clark, P.U., Bartrlein, P.J., Mix, A.C., Rosell-Melé, A., 2011. Climate sensitivity estimated from temperature reconstructions of the Last Glacial Maximum. Science. 334, 1385–1388.
Schmitz, W.J., 1992. On the interbasin-scale thermohaline circulation. Rev. Geophys. 33, 151–173.

Schneebeli, W., 1976. Untersuchungen von Gletscherschwankungen in Val de Bagnes. Die Alpen. 52, 5–58.
Schott, W., 1935. Die Foraminiferen in dem aequatorialen Teil des Atlantischen Ozeans. Deutsche Atlantische Expedition "Meteor" 1925-1927. Wissenschaftliche Ergebnisse. 3 (3), 43–134.
Schouten, S., Hopmans, E.C., Schefuß, E., Sinninghe Damsté, J.S., 2002. Distrubutional variations in marine crenarchaeotal membrane lipids: a new tool for reconstructing ancient sea water temperature? Earth Planet. Sci. Lett. 204, 265–274 (note: Corrigendum: EPSL 211, 205–206).
Schouten, S., Hopmans, E.C., Sinninghe Damsté, J.S., 2013. The organic geochemistry of glycerol dialkyl glycerol tetraethers: a review. Org. Geochem. 54, 19–61.
Schrag, D.P., DePaulo, D.J., 1993. Determination of $\delta^{18}O$ of sea water in the deep ocean during the last glacial maximum. Paleoceanography. 8, 1–6.
Schroeder, R.A., Bada, J.L., 1973. Glacial-postglacial temperature difference deduced from aspartic acid racemization in fossil bones. Science. 182, 479–482.
Schroeder, R.A., Bada, J.L., 1976. A review of the geochemical applications of the amino acid racemization reaction. Earth-Sci. Rev. 12, 347–391.
Schubert, C., 1992. The glaciers of the Sierra Nevada de Merida (Venezuela): a photographic comparison of recent deglaciation. Erdkunde. 46, 58–64.
Schüle, H., Pfister, C., 1992. Coding climate proxy information for the EURO-CLIMHIST data base. In: Frenzel, B., Pfister, C., Gläser, B. (Eds.), European Climate Reconstructed from Documentary Data: Methods and Results. Gustav Fischer Verlag, Stuttgart, pp. 235–262.
Schulte, S., Müller, P.J., 2001. Variations of sea surface temperature and primary productivity during Heinrich and Dansgaard-Oeschger events in the northeastern Arabian Sea. Geo-Mar. Lett. 21, 168–175.
Schulz, K.G., Zeebe, R.E., 2006. Pleistocene glacial terminations triggered by synchronous changes in Southern and Northern Hemisphere insolation: the insolation canon hypothesis. Earth Planet. Sci. Lett. 249, 326–336.
Schulz, H., von Rad, U., Erlenkeuser, H., 1998. Correlation between Arabian Sea and Greenland climate oscillations of the past 110,000 years. Nature. 393, 54–57.
Schwalb, A., 2003. Lacustrine ostracodes as stable isotope recorders of late-glacial and Holocene environmental dynamics and climate. J. Paleolimnol. 29, 265–351.
Schwander, J., Stauffer, B., 1984. Age difference between polar ice and the air trapped in its bubbles. Nature. 311, 45–47.
Schwarz-Zanetti, W., Pfister, C., Schwarz-Zanetti, G., Schüle, H., 1992. The EURO-CLIMHIST data base-a tool for reconstructing the climate of Europe in the pre-instrumental period from high resolution proxy data. In: Frenzel, B., Pfister, C., Glaser, B. (Eds.), European Climate Reconstructed from Documentary Data: Methods and Results. Gustav Fischer Verlag, Stuttgart, pp. 193–210.
Schweingruber, F.H., 1988. Tree Rings. Basics and Applications of Dendrochronology. Kluwer, Dordrecht.
Schweingruber, F.H., 1996. Tree Rings and Environment. Dendroecology. Paul Haupt, Berne.
Schweingruber, F.H., Briffa, K.R., 1996. Tree-ring density networks for climate reconstruction. In: Jones, P.D., Bradley, R.S., Jouzel, J. (Eds.), Climate Variations and Forcing Mechanisms of the Last 2000 Years. Springer-Verlag, Berlin, pp. 43–66.
Schweingruber, F.H., Fritts, H.C., Braker, O.U., Drew, L.G., Schar, E., 1978. The X-ray technique as applied to dendroclimatology. Tree Ring Bull. 38, 61–91.
Schweingruber, F.H., Braker, O.U., Schar, E., 1979. Dendroclimatic studies on conifers from central Europe and Great Britain. Boreas. 8, 427–452.
Schweingruber, F.H., Briffa, K.R., Jones, P.D., 1991. Yearly maps of summer temperatures in western Europe from A.D. 1750 to 1975 and western North America from 1600 to 1982: results of a radiodensitometrical study on tree rings. Vegetatio. 92, 5–71.
Schweingruber, F.H., Briffa, K.R., Nogler, P., 1993. A tree-ring densitometric transect from Alaska to Labrador. Int. J. Biometeorol. 37, 151–169.
Scott, L., Woodborne, S., 2007. Pollen analysis and dating of late Quaternary faecal deposits (hyraceum) in the Cederberg, Western Cape, South Africa. Rev. Palaeobot. Palynol. 144, 123–134.
Scott, E.M., Long, Q., Kra, R. (Eds.), 1990. Proceedings of International Workshop on Inter-comparison of Radiocarbon Laboratories. Radiocarbon. 32, 253–397.
Scourse, J.D., Hall, I.R., McCave, I.N., Young, J.R., Sugdon, C., 2000. The origin of Heinrich layers: evidence from H2 for European precursor events. Earth Planet. Sci. Lett. 182, 187–195.

Sear, C.B., Kelly, P.M., Jones, P.D., Godess, C.M., 1987. Global surface air temperature responses to major volcanic eruptions. Nature. 330, 365–367.
Sekiguti, T., 1969. The historical dates of Japanese cherry festivals since the 8th century and their climatic changes. Geogr. Rev. Jpn. 35, 67–76.
Self, S., Sparks, R.J.S. (Eds.), 1981. Tephra Studies. D. Reidel, Dordrecht.
Seltzer, G.O., 1990. Recent glacial history and paleoclimate of the Peruvian-Bolivian Andes. Quat. Sci. Rev. 9, 137–152.
Seltzer, G.O., 1994. Climatic interpretation of Alpine snowline variations on millennial ltime scales. Quat. Res. 41, 154–159.
Seltzer, G., Rodbell, D., Burns, S., 2000. Isotopic evidence for late Quaternary climatic change in tropical South America. Geology. 28, 35–38.
Seppä, H., Bennett, K.D., 2003. Quaternary pollen analysis: recent progress in palaeoecology and palaeoclimatology. Prog. Phys. Geogr. 27, 548–579.
Seret, G., Guiot, J., Wansard, G., de Beaulieu, J.L., Reille, M., 1992. Tentative paleoclimatic reconstruction linking pollen and sedimentology in La Grande Pile (Vosges, France). Quat. Sci. Rev. 11, 425–430.
Serre-Bacher, F., Guiot, J., Tessier, L., 1992. Dendrochmatic evidence from southwestern Europe and northwestern Africa. In: Bradley, R.S., Jones, P.D. (Eds.), Climate Since A.D. 1500. Routledge, London, pp. 349–365.
Severinghaus, J.P., Brook, E.J., 1999. Abrupt climate change at the end of the last glacial period inferred from trapped air in polar ice. Science. 286, 930–934.
Severinghaus, J.P., Sowers, T., Brook, E.J., Alley, R.B., Bender, M.L., 1998. Timing of abrupt climate change at the end of the Younger Dryas interval from thermally fractionated gases in polar ice. Nature. 391, 141–146.
Seurat, L.G., 1934. Etudes zoologiques sur le Sahara Central. Memoires de la Societe d'Histoire Naturelie de l'Afrique du Nord, No. 4, Mission du Hoggar Ill.
Shabalova, M.V., van Engelen, A.F.V., 2003. Evaluation of a reconstruction of winter and summer temperatures in the Low Countries, A.D. 764-1998. Clim. Chang. 58, 219–242.
Shackleton, N.J., 1967. Oxygen isotope analyses and Pleistocene temperatures re-assessed. Nature. 215, 15–17.
Shackleton, N.J., 1969. The last interglacial in the marine and terrestrial records. Proc. R. Soc. Lond. B174, 135–154.
Shackleton, N.J., 1974. Attainment of isotopic equilibrium between ocean water and the benthonic foraminifera Genus *Uvigerina*: isotopic changes in the ocean during the last glacial. In: Les Methodes Quantitatives d'Etude des Variations du Climat au Cours du Pleistocene. Colloques Internationaux du Centre National de la Recherche Scientifique No. 219CNRS, Paris, pp. 4–5.
Shackleton, N.J., 1977. The oxygen isotope stratigraphic record of the late Pleistocene. Philos. Trans. R. Soc. Lond. B280, 169–179.
Shackleton, N.J., 1987. Oxygen isotopes, ice volume and sea level. Quat. Sci. Rev. 6, 183–190.
Shackleton, N.J., 1993. Last interglacial in Devil's Hole, Nevada. Nature. 362, 596 (see also reply by Ludwig, K.R., et al., p. 596).
Shackleton, N.J., 2000. The 100,000-year ice-age cycle identified and found to lag temperature, carbon dioxide, and orbital eccentricity. Science. 289, 1897–1902.
Shackleton, N.J., Matthews, R.K., 1977. Oxygen isotope stratigraphy of late Pleistocene coral terraces in Barbados. Nature. 268, 618–620.
Shackleton, N.J., Opdyke, N.D., 1973. Oxygen isotope and paleomagnetic stratigraphy of equatorial Pacific core V28-238: oxygen isotope temperatures and ice volumes on a 10^5 year and 10^6 year scale. Quat. Res. 3, 39–55.
Shackleton, N.J., Opdyke, N.D., 1976. Oxygen-isotope and paleomagnetic stratigraphy of Pacific core V28-239. Late Pliocene to latest Pleistocene. In: Cline, R.M., Hays, J.D. (Eds.), Investigation of Late Quaternary Paleooceanography and Paleoclimatology. Memoir 145, Geological Society of America, Boulder, pp. 449–464.
Shackleton, N.J., Pisias, N.G., 1985. Atmospheric carbon dioxide, orbital forcing and climate. In: Sundquist, E.T., Broecker, W.S. (Eds.), The Carbon Cycle and Atmospheric CO_2: Natural Variations Archean to Present. American Geophysical Union, Washington, DC, pp. 303–317.
Shackleton, N.J., Wiseman, J.D.H., Buckley, H.A., 1973. Non-equilibrium isotopic fractionation between sea-water and planktonic foraminiferal tests. Nature. 242, 177–179.
Shackleton, N.J., Hall, M.A., Line, J., Cang, S., 1983. Carbon isotope data in core V19-30 confirm reduced carbon dioxide concentration of the ice age atmosphere. Nature. 306, 319–322.

Shackleton, N.J., Backman, J., Zimmerman, H., Kent, D.V., Hall, M.A., Roberts, D.G., Schnitker, D., Baldauf, J., 1984. Oxygen isotope calibration of the onset of ice rafting and history of glaciation in the North Atlantic region. Nature. 307, 620–623.

Shackleton, N.J., Duplessy, J.-C., Arnold, M., Maurice, P., Hall, M.A., Cartlidge, J., 1988. Radiocarbon age of Last Glacial Pacific deep water. Nature. 335, 708–711.

Shackleton, N.J., Berger, A., Peltier, W.R., 1990. An alternative astronomical calibration of the lower Pleistocene timescale based on ODP site 677. Trans. Roy. Soc. Edinb. Earth Sci. 81, 251–261.

Shackleton, N.J., Le, J., Mix, A., Hall, M.A., 1992. Carbon isotope records from Pacific surface waters and atmospheric carbon dioxide. Quat. Sci. Rev. 11, 387–400.

Shackleton, N.J., Hall, M.A., Vincent, E., 2000. Phase relationships between millennial-scale events 64,000-24,000 years ago. Paleoceanography. 15, 565–569.

Shaffer, G., Bendtsen, J., 1994. Role of the Bering Strait in controlling North Atlantic Ocean circulation and climate. Nature. 367, 354–357.

Shah, S.R., Mollenhauer, G., Ohkouchi, N., Eglinton, T.I., Pearson, A., 2008. Origins of archaeal tetraether lipids in sediments: Insights from radiocarbon analysis. Geochim. Cosmochim. Acta. 72, 4577–4594.

Shakun, J.D., Shaman, J., 2009. Tropical origins of North and South Pacific decadal variability. Geophys. Res. Lett. 36, L19711. dx.doi.org/10.1029.2009GL040313.

Shakun, J.D., Clark, P.U., He, F., Marcott, S.A., Mix, A.C., Liu, Z., Otto-Bliesner, B., Schmittner, A., Bard, E., 2012. Global warming preceded by increasing carbon dioxide concentrations during the last deglaciation. Nature. 484, 49–55.

Shanahan, T.M., Overpeck, J.T., Hubeny, J.B., King, J., Hu, F.S., Hughen, K., Miller, G.H., Black, J., 2008. Scanning micro-X-ray fluorescence elemental mapping: a new tool for the study of laminated sediment records. Geochem. Geophys. Geosyst. 9. dx.doi.org/10.1029/2007GC001800.

Shane, P.A.R., Froggatt, P.C., 1994. Discriminant function analysis of glass chemistry of New Zealand and North American tephra deposits. Quat. Res. 41, 70–81.

Sheets, P.D., Grayson, D.K. (Eds.), 1979. Volcanic Activity and Human Ecology. Academic Press, New York.

Shemesh, A., Peteet, D., 1998. Oxygen isotopes in fresh water biogenic opal—northeastern U.S. Allerød-Younger Dryas temperature shift. Geophys. Res. Lett. 25, 1935–1938.

Shemesh, A., Charles, C., Fairbanks, R.G., 1992. Oxygen isotopes in biogenic silica: global changes in ocean temperature and isotopic composition. Science. 256, 1434–1436.

Shemesh, A., Rosqvist, G., Rietti-Shati, M., Rubensdotter, L., Bigler, C., Yam, R., Karlén, W., 2001. Holocene climatic change in Swedish Lapland inferred from an oxygen-isotope record of lacustrine biogenic silica. The Holocene. 11, 447–454.

Shen, G.T., Sanford, C.L., 1990. Trace element indicators of climate variability in reef building corals. In: Glynn, P.W. (Ed.), Global Ecological Consequences of the 1981-83 El Niño-Southern Oscillation. Elsevier, New York, pp. 255–284.

Shen, G.T., Boyle, E.A., Lea, D.W., 1987. Cadmium in corals as a tracer of historical upwelling and industrial fallout. Nature. 328, 794–796.

Shen, G.T., Cole, J.E., Lea, D.W., McConnaughey, T.A., Fairbanks, R.G., 1992a. Surface ocean variability at Galapagos from 1936-1982: calibration of geochemical tracers in corals. Paleoceanography. 7, 563–583.

Shen, G.T., Lim, L.J., Campbell, T.M., Cole, J.E., Fairbanks, R.G., 1992b. A chemical indicator of trade wind reversal in corals from the eastern tropical Pacific. J. Geophys. Res. 97, 12689–12698.

Shen, C.C., Edwards, R.L., Cheng, H., Dorale, J.A., Thomas, R.B., Moran, S.B., Weinstein, S.E., Edmonds, H.N., 2002. Uranium and thorium isotopic concentration measurements by magnetic sector inductively coupled plasma mass spectrometry. Chem. Geol. 185, 165–178.

Shen, C., Wang, W.-C., Hao, Z., Gong, W., 2007. Exceptional drought events over eastern China during the last five centuries. Clim. Chang. 85, 453–471.

Shen, C.C., Li, K.S., Sieh, K., Natawidjaja, D., Cheng, H., Wang, X., Edwards, R.L., Lam, D.D., Hsieh, Y.-T., Fan, T.-Y., Meltzner, A.J., Taylor, F.W., Quinn, T.M., Chiang, H.-W., Kilbourne, K.H., 2008. Variation of initial $^{230}Th/^{232}Th$ and limits of high precision U–Th dating of shallow-water corals. Geochim. Cosmochim. Acta. 72, 4201–4223.

Shen, C.C., Wu, C.C., Cheng, H., Edwards, R.L., Hsieh, Y.T., Gallett, S., Chang, C.C., Li, T.Y., Lam, D.D., Kano, A., Hori, M., Spötl, C., 2012. High-precision and high-resolution carbonate ^{230}Th dating by MC-ICP-MS with SEM protocols. Geochim. Cosmochim. Acta. 99, 71–86.

Shindell, D.T., Rind, D., Balachandran, N., Lean, J., Lonergan, P., 1999. Solar cycle variability, ozone and climate. Nature. 284, 305–308.
Shindell, D.T., Schmidt, G.A., Mann, M.E., Rind, D., Waple, A., 2001. Solar forcing of regional climate change during the Maunder Minimum. Science. 294, 2149–2152.
Shiyatov, S.G., 1993. The upper timberline dynamics during the last 1100 years in the Polar-Ural mountains. In: Frenzel, B., Eronen, M., Vorren, K.D., Glaser, B. (Eds.), Oscillations of the Alpine and Polar Tree Limits in the Holocene. Gustav Fischer Verlag, Stuttgart, pp. 195–203.
Shiyatov, S.G., 1996. Tree growth decrease between 1800 and 1840 in subarctic and highland regions of Russia. In: Dean, J.S., Meko, D.M., Swetnam, T.W. (Eds.), Tree Rings, Environment and Humanity. Department of Geosciences, University of Arizona, Tucson, pp. 283–294.
Shopov, Y.Y., Ford, D.C., Schwarcz, H.P., 1994. Luminescent microbanding in speleothems: high resolution chronology and paleoclimate. Geology. 22, 407–410.
Shotton, F.W., 1972. An example of hard water error in radiocarbon dating of vegetable matter. Nature. 240, 460–461.
Shroder, J.F., 1980. Dendrogeomorphology: review and new techniques of tree-ring dating. Progr. Phys. Geogr. 4, 161–188.
Siddall, M., Rohling, E.J., Almogi-Labin, A., Hemleben, Ch., Meischner, D., Schmelzer, I., Smeed, D.A., 2003. Sea-level fluctuations during the last glacial cycle. Nature. 423, 853–858.
Siddall, M., Rohling, E.J., Thompson, W.G., Waelbroeck, C., 2008. Marine isotope stage 3 sea level fluctuations: data synthesis and new outlook. Rev. Geophys. 46, RG4003. dx.doi.org/10.1029/2007RG000226.
Siegenthaler, U., 1991. Glacial-Interglacial atmospheric CO_2 variations. In: Bradley, R.S. (Ed.), Global Changes of the Past. University Corporation for Atmospheric Research, Boulder, pp. 245–260.
Sigafoos, R.S., Hendricks, E.L., 1961. Botanical evidence of the modern history of Nisqually Glacier, Washington, US Geological Survey Professional Paper 387-A. US Geological Survey, Washington, DC.
Sigl, M., McConnell, J.R., Layman, L., Maselli, O., McGwire, K., Pasteris, D., Dahl-Jensen, D., Steffensen, J.P., Vinther, B., Edwards, R., Mulvaney, R., Kipfstuhl, S., 2013. A new bipolar ice core record of volcanism from WAIS Divide and NEEM and implications for climate forcing of the last 2000 years. J. Geophys. Res. Atmos. 118, 1151–1169.
Sigman, D.M., Hain, M.P., Haug, G.H., 2010. The polar ocean and glacial cycles in atmospheric CO_2 concentration. Nature. 466, 47–55.
Sikes, E.L., Keigwin, L.D., 1994. Equatorial Atlantic sea surface temperature for the last 30 kyrs: a comparison of U^K_{37}, $\delta^{18}O$ and foraminiferal assemblage temperature estimates. Paleoceanography. 9, 31–45.
Sikes, E.L., Keigwin, L.D., 1996. A re-examination of northeast Atlantic sea surface temperature and salinity over the last 16 kyr. Paleoceanography. 11, 327–342.
Sikes, E.L., Keigwin, L.D., Farrington, J.W., 1991. Use of the alkenone unsaturation ratio U^K_{37} to determine past sea surface temperatures: core-top SST calibration and methodology considerations. Earth Planet. Sci. Lett. 104, 36–47.
Sikes, E.L., Samson, C.R., Guilderson, T.P., Howard, W.R., 2000. Old radiocarbon ages in the southwest Pacific Ocean during the last glacial period and deglaciation. Nature. 405, 555–559.
Sime, L.C., Wolff, E.W., Oliver, K.I.C., Tindall, J.C., 2009. Evidence for warmer interglacials in East Antarctica. Nature. 462, 342–346.
Simpson, I.M., West, R.G., 1958. On the stratigraphy and palaeobotany of a late Pleistocene organic deposit at Cheflord, Cheshire. New Phytol. 57, 239–250.
Singhvi, A.K., Bluszcz, A., Bateman, M.D., Someshwar Rao, M., 2001. Luminescence dating of loess–palaeosol sequences and coversands: methodological aspects and palaeoclimatic implications. Earth-Sci. Rev. 54, 193–211.
Sinha, A., Cannariato, K.G., Stott, L.D., Cheng, H., Edwards, R.L., Yadava, M.G., Ramesh, R., Singh, I.B., 2007. A 900-year (600-1500A.D.) record of the Indian monsoon precipitation from the core monsoon zone of India. Geophys. Res. Lett. 34, L16707. dx.doi.org/10.1029/2007GL030431.
Sinha, A., Stott, L.D., Berkelhammer, M., Cheng, H., Edwards, R.L., Aldenderfer, M., Mudelsee, M., 2011a. A global context for megadroughts in monsoon Asia during the past millennium. Quaternary Sci. Rev. 30, 47–62.
Sinha, A., Berkelhammer, M., Stott, L.D., Mudelsee, M., Cheng, H., Biswas, J., 2011b. The leading mode of Indian summer monsoon variability during the last millennium. Geophys. Res. Lett. 38, L15703. http://dx.doi.org/10.1029/2011GL047713.
Sinninghe Damsté, J.S., Ossebaar, J., Abbas, B., Schouten, S., Verschuren, D., 2009. Fluxes and distribution of tetraether lipids in an equatorial African lake: constraints on the application of the TEX86 palaeothermometer and BIT index in lacustrine settings. Geochim. Cosmochim. Acta. 73, 4232–4249.

Sirocko, F., Sarnthein, M., 1989. Wind-borne deposits in the northwestern Indian Ocean: record of Holocene sediments versus modern satellite data. In: Leinen, M., Sarnthein, M. (Eds.), Paleoclimatology and Paleometeorology: Modern and Past Patterns of Global Atmospheric Transport. Kluwer Academic, Dordrecht, pp. 401–433.

Sirocko, F., Sarnthein, M., Lange, H., Erlenkeuser, H., 1991. Atmospheric summer circulation and coastal upwelling in the Arabian Sea during the Holocene and the last glaciation. Quat. Res. 36, 72–93.

Skinner, L.C., 2008. Revisiting the absolute calibration of the Greenland ice–core age-scales. Clim. Past. 4, 295–302.

Skinner, L.C., Shackleton, N.J., 2004. Rapid transient changes in northeast Atlantic deep water ventilation age across Termination I. Paleoceanography. 19, PA2005. dx.doi.org/10.1029/2003PA000983.

Skinner, L.C., Fallon, S., Waelbroeck, C., Michel, E., Barker, S., 2010. Ventilation of the deep Southern Ocean and deglacial CO_2 rise. Science. 328, 1147–1151.

Slowey, N.C., Henderson, G.M., Curry, W.B., 1996. Direct U-Th dating of marine sediments from the two most recent interglacial periods. Nature. 383, 242–244.

Sluijs, A., Schouten, S., Pagani, M., Woltering, M., Brinkhuis, H., Damsté, J.S., Dickens, G.R., Huber, M., Reichart, G.-J., Stein, R., Matthiessen, J., Lourens, L.J., Pedentchouk, N., Backman, J., Moran, K., the Expedition 302 scientists, 2006. Subtropical Arctic Ocean temperatures during the Palaeocene/Eocene thermal maximum. Nature. 44, 610–613.

Smalley, I., O'Hara-Dhand, K., Wint, J., Machalett, B., Jary, Z., Jefferson, I., 2009. Rivers and loess: the significance of long river transportation in the complex event-sequence approach to loess deposit formation. Quat. Int. 198, 7–18.

Smith, J.M., Quinn, T.M., Helmle, K.P., Halley, R.B., 2006. Reproducibility of geochemical and climatic signals in the Atlantic coral Montastraea faveolata. Paleoceanography. 21. dx.doi.org/10.1029/2005PA001187.

Smittenberg, R.H., Hopmans, E.C., Schouten, S., Hayes, J.M., Eglinton, T.I., Sinninghe Damsté, J.S., 2004. Compound-specific radiocarbon dating of the varved Holocene sedimentary record of Saanich Inlet, Canada. Paleoceanography. 19, PA2012. dx.doi.org/10.1029/2003PA000927.

Smol, J.P., 2008. Pollution of Lakes and Rivers: a paleoenvironmental perspective. Blackwell, Oxford 383 pp.

Smol, J.P., Stoermer, E.F., 2010. The Diatoms: Applications for the Environmental and Earth Sciences. Cambridge University Press, Cambridge, 667pp.

Smol, J.P., Birks, H.J.B., Last, W.M., 2001. Using biology to study long-term environmental change. In: Tracking Environmental Change Using Lake Sediments. Vol. 3. Terrestrial, Algal and Siliceous Indicators. Kluwer, Dordrecht, pp. 1–3.

Snowball, I., Muscheler, R., 2007. Palaeomagnetic intensity data: an Achilles heel of solar activity reconstructions. The Holocene. 17, 851–859.

Snowball, I., Zillén, L., Ojala, A., Saarinen, T., Sandgren, P., 2007. FENNOSTACK and FENNORPIS: Varve dated Holocene palaeomagnetic secular variation and relative palaeointensity stacks for Fennoscandia. Earth Planet. Sci. Lett. 255, 106–116.

Snyder, C.T., Langbein, W.B., 1962. The Pleistocene lake in Spring Valley, Nevada and its climatic implications. J. Geophys. Res. 67, 2385–2394.

Solomon, A., Webb III, T., 1985. Computer-aided reconstruction of Late Quaternary landscape dynamics. Annu. Rev. Ecol. Syst. 16, 63–84.

Sorenson, C.J., 1977. Holocene bioclimates. Ann. Assoc. Am. Geogr. 67, 214–222.

Sorenson, C.J., Knox, J.C., 1974. Paleosols and paleoclimate related to late Holocene forest-tundra border migrations: Mackenzie and Keewatin, NWT. In: Raymond, S., Schledermann, P. (Eds.), International Conference on Prehistory and Paleoecology of Western North American Arctic and Subarctic. Archaeological Association, University of Calgary, Calgary, pp. 187–203.

Sosef, M.S.M., 1991. New species of Begonia in Africa and their relevance to the study of glacial rain forest refugia. Wageningen Agr. Univ. Papers. 91, 120–151.

Sowers, T., Bender, M., Raynaud, D., Korotkevich, Y.S., Orchado, J., 1991. The ^{18}O of atmospheric O_2 from air inclusions in the Vostok ice core: timing of CO_2 and ice volume changes during the penultimate deglaciation. Paleoceanography. 6, 679–696.

Sowers, T., Bender, M., Raynaud, D., Korotkevich, Y.S., 1992. $\delta^{15}N$ of N in air trapped in polar ice: a tracer of gas transport in the firn and a possible constraint on ice age-gas-age difference. Geophys. Res. 97D, 15683–15697.

Sowers, T., Bender, M., Labeyrie, L., Martinson, D., Jouzel, J., Raynaud, D., Pichon, J.-J., Korotkevich, Y.S., 1993. A 135,000 year Vostok-SPECMAP common temporal framework. Paleoceanography. 8, 737–766.

Sowers, T., Alley, R.B., Jubenville, J., 2003. Ice core records of atmospheric N_2O covering the last 106,000 years. Science. 301, 945–948.

Sparks, T.H., Carey, P.D., 1995. The responses of species to climate over two centuries an analysis of the Marsham phenological record, 1736–1947. J. Ecol. 83, 321–329.

Spaulding, W.G., 1990. Vegetational and climatic development of the Mojave Desert: the Last Glacial Maximum to the Present. In: Betancourt, J.L., VanDevender, T.R., Martin, P.S. (Eds.), Packrat Middens: The Last 40,000 Years of Biotic Change. University of Arizona Press, Tucson, pp. 166–199.

Spaulding, W.G., 1991. A middle Holocene vegetation record from the Mojave Desert of North America and its paleoclimatic significance. Quat. Res. 35, 427–437.

Spaulding, W.G., Betancourt, J.L., Croft, L.K., Cole, K.L., 1990. Packrat middens: their composition and methods of analysis. In: Betancourt, J.L., VanDevender, T.R., Martin, P.S. (Eds.), Packrat Middens: The Last 40,000 Years of Biotic Change. University of Arizona Press, Tucson, pp. 59–84.

Speer, J.H., 2010. Fundamentals of Tree-Ring Research. The University of Arizona Press, Tucson, 333 pp.

Spell, T.L., McDougall, I., 1992. Revision to the age of the Brunhes-Matuyama boundary and the Pleistocene geomagnetic polarity time scale. Geophys. Res. Lett. 19, 1181–1184.

Spötl, C., Mangini, A., Frank, N., Eichstädter, R., Burns, S.J., 2002. Start of the last interglacial period at 135 ka: evidence from a high Alpine speleothem. Geology. 30, 815–818.

Staff, R.A., Schlolaut, G., Ramsey, C.B., Brock, F., Bryant, C.L., Kitagawa, H., van der Plicht, J., Marshall, M.H., Brauer, A., Lamb, H.F., Payne, R.L., Tarasov, P.E., Haraguchi, T., Gotanda, K., Yonenobu, H., Yokoyama, Y., Nakagawa, T., Suigetsu Project Members, 2013. Integration of the old and new Lake Suigetsu (Japan) terrestrial radiocarbon calibration data sets. Radiocarbon. 55, 1–10.

Staffelbach, T., Stauffer, B., Oeschger, H., 1988. A detailed analysis of the rapid changes in ice core parameters during the last ice age. Ann. Glaciol. 10, 167–170.

Stager, J.C., Mayewski, P.A., 1997. Abrupt early to mid-Holocene climatic transition registered at the Equator and the Poles. Science. 276, 1834–1836.

Stahle, D.W., 1996. The hydroclimatic application of tree-ring chronologies. In: Dean, J.S., Meko, D.M., Swetnam, T.W. (Eds.), Tree Rings, Environment and Humanity. Department of Geosciences, University of Arizona, Tucson, pp. 119–126.

Stahle, D.W., Cleaveland, M.K., 1992. Reconstruction and analysis of spring rainfall over the southeastern United States for the past 1000 years. Bull. Am. Meteorol. Soc. 73, 1947–1961.

Stahle, D.W., Cleaveland, M.K., 1993. Southern Oscillation extremes reconstructed from tree rings of the Sierra Madre Occidental and southern Great Plains. J. Clim. 6, 129–140.

Stahle, D.W., Dean, J.S., 2011. North American tree rings, climatic extremes and social disasters. In: Hughes, M.K., Swetnam, T.W., Diaz, H.F. (Eds.), Dendroclimatology: Progress and Prospects. Springer, Dordrecht, pp. 297–327.

Stahle, D.W., Cleaveland, M.K., Hehr, J.G., 1988. North Carolina climate changes reconstructed from tree-rings: A.D. 372-1985. Science. 240, 1517–1519.

Stahle, D.W., Cleaveland, M.K., Blanton, D.B., Therrell, M.D., Gay, D.A., 1998. The lost colony and Jamestown droughts. Science. 280, 564–567.

Stahle, D.W., Cook, E.R., Cleaveland, M.K., Therrell, D., Meko, D.M., Grissino-Mayer, H.D., Watson, E., Luckman, B.H., 2000. Tree-ring data document 16th century megadrought over North America. EOS. 81, 121 and 125.

Stahle, D.W., Fye, F.K., Cook, E.R., Griffin, R.D., 2007. Tree-ring reconstructed megadroughts over North America since A.D. 1300. Clim. Chang. 83, 133–149.

Stahle, D.W., Diaz, J.V., Burnette, D.J., Paredes, J.C., Heim Jr., R.R., Fye, F.K., Acuña-Soto, R., Therrell, M.D., Cleaveland, M.K., Stahle, D.K., 2011. Major Mesoamerican droughts of the past millennium. Geophys. Res. Lett. 38, L05703. dx.doi.org/10.1029/2010GL046472.

Stahle, D.W., Burnette, D.J., Villanueva, J., Cerano, J., Fye, F.F., Griffin, R.D., Cleaveland, M.K., Stahle, D.K., Edmondson, J.R., Wolff, K.P., 2012. Tree-ring analysis of ancient baldcypress trees and subfossil wood. Quat. Sci. Rev. 34, 1–15.

Standell, N.D., Polissar, P.J., Abbott, M.B., 2007. Last Glacial Maximum equilibrium-line altitude and paleotemperature reconstructions for the Cordillera de Mérida, Venezuelan Andes. Quat. Res. 67, 115–127.

State Meteorological Administration, 1981. Annals of 510 years of precipitation record in China. Cartographic Publishers, Beijing (in Chinese with English summary).

Stauffer, B.R., 1989. Dating of ice by radioactive isotopes. In: Oeschger, H., Langway Jr., C.C. (Eds.), The Environmental Record in Glaciers and Ice Sheets. Wiley, Chichester, pp. 123–129.
Stauffer, B.R., Neftel, A., 1988. What have we learned from the ice cores about atmospheric changes in the concentrations of nitrous oxide, hydrogen peroxide and other trace species? In: Rowland, E.S., Isaksen, I.S.A. (Eds.), The Changing Atmosphere. Wiley, Chichester, pp. 63–77.
Steffensen, J.P., 1985. Microparticles in snow from the South Greenland ice sheet. Tellus. 37B, 286–295.
Steffensen, J.P., 1988. Analysis of the seasonal variations in dust, Cl^-, NO_3 and SO_4 in two central Greenland fim cores. Ann. Glaciol. 10, 171–177.
Steffensen, J.P., Andersen, K.K., Bigler, M., Clausen, H.B., Dahl-Jensen, D., Fischer, H., Goto-Azuma, K., Hansson, M., Johnsen, S.J., Jouzel, J., Masson-Delmotte, V., Popp, T., Rasmussen, S.O., Röthlisberger, R., Ruth, U., Stauffer, B., Siggard-Andersen, M.-L., Sveinbjörnsdóttir, A.E., Svensson, A., White, J.W., 2008. High-resolution Greenland ice core data show abrupt climate change happens in few years. Science. 321, 680–684.
Steig, E.J., Grootes, P.M., Stuiver, M., 1994. Seasonal precipitation and ice core records. Science. 266, 1885–1886.
Stein, R., Hefter, J., Grützner, J., Voelker, A., Naafs, B.D.A., 2009. Variability of surface-water characteristics and Heinrich-like events in the Pleistocene midlatitude North Atlantic Ocean: biomarker and XRD records from IODP Site U1313 (MIS 16–9). Paleoceanography. 24, PA2203. dx.doi.org/10.1029/2008PA001639.
Steinhilber, F., Beer, J., Frohlich, C., 2009. Total solar irradiance during the Holocene. Geophys. Res. Lett. 36, L19704. dx.doi.org/10.1029/2009GL040142.
Steinhilber, F., Abreu, J.A., Beer, J., Brunner, I., Christl, M., Fischer, H., Heikkilä, U., Kubik, P.W., Mann, M., McCracken, K.G., Miller, H., Miyahara, H., Oerter, H., Wilhelms, F., 2012. 9,400 years of cosmic radiation and solar activity from ice cores and tree rings. Proc. Natl. Acad. Sci. U. S. A. 109, 5967–5971.
Stevens, T., Thomas, D.S.G., Armitage, S.J., Lunn, H.R., Lu, H.Y., 2007. Reinterpreting climate proxy records from late Quaternary Chinese loess: a detailed OSL investigation. Earth-Sci. Rev. 80, 111–136.
Stevens, T., Lu, H.Y., Thomas, D.S.G., Armitage, S.J., 2008. Optical dating of abrupt shifts in the late Pleistocene East Asian nonsoon. Geology. 36, 415–418.
Stevens, T., Carter, A., Watson, T.P., Vermeesch, P., Andò, S., Bird, A.F., Lu, H., Garzanti, E., Cottam, M.A., Sevastjanova, I., 2013. Genetic linkage between the Yellow River, the Mu Us desert and the Chinese Loess Plateau. Quat. Sci. Rev. 78, 355–368.
Stewart, J.R., Lister, A.M., 2001. Cryptic northern refugia and the origins of the modern biota. Trends Ecol. Evol. 16, 608–613.
Stidd, C.K., 1967. The use of eigenvectors for climatic estimates. J. Appl. Meteorol. 6, 255–264.
Stine, S., 1994. Extreme and persistent drought in California and Patagonia during Medieval time. Nature. 369, 546–549.
Stine, S., 1998. Medieval Climatic Anomaly in the Americas. In: Issar, A.S., Brown, N. (Eds.), Water, Environment and Society in Times of Climatic Change. Kluwer, Dordrecht, pp. 43–67.
Stirling, C.H., Anderson, M.B., 2009. Uranium-series dating of fossil coral reefs: extending the sea-level record beyond the last glacial cycle. Earth Planet. Sci. Lett. 284, 269–283.
Stirling, C.H., Esat, T.M., McCulloch, M.T., Lambeck, K., 1995. High-precision Useries dating of corals from western Australia and implications for the timing and duration of the Last Interglacial. Earth Planet. Sci. Lett. 135, 115–130.
Stocker, T.F., Johnsen, S.J., 2003. A minimum thermodynamic model for the bipolar seesaw. Paleoceanography. 18. dx.doi.org/10.1029/2003PA000920.
Stockmarr, J., 1971. Tablets with spores used in pollen analysis. Pollen Spores. 13, 615–621.
Stockton, C.W., 1975. Long term Streamflow Records Reconstructed from Tree Rings. Paper 5, Laboratory for Tree Ring Research. University of Arizona Press, Tucson.
Stockton, C.W., Boggess, W.R., 1980. Augmentation of hydrologic records using tree rings. In: Improved Hydrologic Forecasting. American Society of Civil Engineers, New York, pp. 239–265.
Stockton, C.W., Fritts, H.C., 1973. Long-term reconstruction of water level changes for Lake Athabasca by analysis of tree rings. Water Resour. Bull. 9, 1006–1027.
Stokes, M.A., Smiley, T.L., 1968. An Introduction to Tree-ring Dating. University of Chicago Press, Chicago.
Stone, J., 2000. Air pressure and cosmogenic isotope production. J. Geophys. Res. 105B, 23,753–23,759.
Stoner, J.S., St-Onge, G., 2007. Magnetic stratigraphy in paleoceanography: reversals, excursions, paleointensity and secular variation. In: Hillaire-Marcel, H., De Vernal, A. (Eds.), Proxies in Late Cenozoic Paleoceanography. Elsevier, Amsterdam, pp. 99–138.

Stothers, R.B., 1984. The great Tambora eruption in 1815 and its aftermath. Science. 224, 1191–1198.
Stothers, R.B., 1996. The great dry fog of 1783. Clim. Change. 32, 79–89.
Stothers, R.B., 2000. Climatic and demographic consequences of the massive volcanic eruption of 1258. Clim. Chang. 45, 361–374.
Stott, L., Southon, J., Timmermann, A., Koutavas, A., 2009. Radiocarbon age anomaly at intermediate water depth in the Pacific Ocean during the last deglaciation. Paleoceanography. 24, PA2223. dx.doi.org/10.1029/2008PA001690.
Stouffer, R.J., Yin, J., Gregory, J.M., Dixon, K.W., Spelman, M.J., Hurlin, W., Weaver, A.J., Eby, M., Flato, G.M., Hasumi, H., Hu, A., Jungclaus, J.H., Kamenkovich, I.V., Levermann, A., Montoya, M., Murakami, S., Nawrath, S., Oka, A., Peltier, W.R., Robitaille, D.Y., Sokolov, A., Vettoretti, G., Weber, S.L., 2006. Investigating the causes of the response of the thermohaline circulation to past and future climate changes. J. Clim. 19, 1365–1387.
Strack, M. (Ed.), 2008. Peatlands and Climate Change. International Peat Society, Jyvaskyla, 223 pp.
Street, E.A., Grove, A.T., 1976. Environmental and climatic implications of late Quaternary lake-level fluctuations in Africa. Nature. 261, 285–390.
Street, E.A., Grove, A.T., 1979. Global maps of lake-level fluctuations since 30,000 yr BP. Quat. Res. 12, 83–118.
Street-Perrott, E.A., 1994. Palaeo-perspectives: changes in terrestrial ecosystems. Ambio. 23, 37–43.
Street-Perrott, F.A., Harrison, S.P., 1985a. Lake levels and climate reconstruction. In: Hecht, A.D. (Ed.), Paleoclimate Analysis and Modeling. Wiley, Chichester, pp. 291–340.
Street-Perrott, F.A., Harrison, S.P., 1985b. Temporal variations in lake levels since 30,000 yr B.P.—an index of the global hydrological cycle. In: Hansen, J.E., Takahashi, T. (Eds.), Climate Processes and Sensitivity. American Geophysical Union, Washington D.C, pp. 118–129.
Street-Perrott, F.A., Perrott, R.A., 1993. Holocene vegetation, lake levels and climate of Africa. In: Wright, H.E., Kutzbach, J.E., Webb III, T., Ruddiman, W.F., Street-Perrott, F.A., Bartlein, P.J. (Eds.), Global Climates Since the Last Glacial Maximum. University of Minnesota Press, Minneapolis, pp. 318–356.
Street-Perrott, F.A., Marchand, D.S., Roberts, N., Harrison, S.P., 1983. Global Lake-level Variations from 18,000 to 0 years ago: a Paleoclimatic Analysis. Technical Report 046, Department of Energy, Washington, DC.
Street-Perrott, F.A., Huang, Y., Perrott, R.A., Eglinton, G., Barker, P., Khelifa, L.B., Harkness, D.D., Olago, D.O., 1997. Impact of lower atmospheric carbon dioxide on tropical mountain ecosystems. Science. 278, 1422–1426.
Street-Perrott, F.A., Huang, Y., Perrott, R.A., Eglinton, G., 1998. Carbon isotopes in lake sediments and peats of last glacial age: implications for the global carbon cycle. In: Griffith, H. (Ed.), Stable Isotopes. BIOS Scientific Publishers, Oxford, pp. 381–396.
Studhalter, R.A., 1955. Tree growth: I. Some historical chapters. Bot. Rev. 21, 1–72.
Stuiver, M., 1978a. Carbon-14 dating: a comparison of beta and ion counting. Science. 202, 881–883.
Stuiver, M., 1978b. Radiocarbon timescale tested against magnetic and other dating methods. Nature. 273, 271–274.
Stuiver, M., 1993. A note on single-year calibration of the radiocarbon time scale, A.D. 151-954. Radiocarbon. 35, 67–72.
Stuiver, M., Braziunas, T.F., 1991. Isotopic and solar records. In: Bradley, R.S. (Ed.), Global Changes of the Past. University Corporation for Atmospheric Research, Boulder, pp. 225–244.
Stuiver, M., Braziunas, T.F., 1992. Evidence of solar activity variations. In: Bradley, R.S., Jones, P.D. (Eds.), Climate Since A.D. 1500. Routledge, London, pp. 593–605.
Stuiver, M., Pearson, G.W., 1993. High-precision bidecadal calibration of the radiocarbon time scale, AD 1950-500 B.C. and 2500-6000 B.C. Radiocarbon. 35, 1–23.
Stuiver, M., Quay, P.D., 1980. Changes in atmospheric carbon-14 attributed to a variable sun. Science. 207, 11–19.
Stuiver, M., Reimer, P.J., 1993. Extended ^{14}C data base and revised Calib 3.0 ^{14}C age calibration program. Radiocarbon. 35, 215–230.
Stuiver, M., Pearson, G.W., Braziunas, T., 1986. Radiocarbon age calibration of marine samples back to 9000 cal. yr B.P. Radiocarbon. 28, 980–1021.
Stuiver, M., Braziunas, T.F., Becker, B., Kromer, B., 1991. Climatic, solar, oceanic and geomagnetic influences on Late-Glacial and Holocene atmospheric $^{14}C/^{12}C$ change. Quatern. Res. 35, 1–24.
Sturm, C., Zhang, Q., Noone, D., 2010. An introduction to stable water isotopes in climate models: benefits of forward modeling for paleoclimatology. Clim. Past. 6, 115–129.

Stute, M., Forster, M., Frischkorn, H., Serejo, A., Clark, J.F., Schlosser, P., Broecker, W.S., Bonani, G., 1995. Cooling of tropical Brazil (5°C) during the last glacial maximum. Science. 269, 379–383.

Suess, H.E., 1965. Secular variations of the cosmic-ray produced carbon-14 in the atmosphere and their interpretations. J. Geophys. Res. 70, 5937–5952.

Suess, H.E., 1980. The radiocarbon record in tree rings of the last 8000 years. Radiocarbon. 22, 200–209.

Sun, Y.B., An, Z.S., 2005. Late Pliocene-Pleistocene changes in mass accumulation rates of eolian deposits on the central Chinese Loess Plateau. J. Geophys. Res. 110, D23101. dx.doi.org/10.1029/2005JD006064.

Sun, D.H., Gagan, M.K., Cheng, H., Scott-Gagan, H., Dykoski, C.A., Edwards, R.L., Su, R.X., 2005. Seasonal and interannual variability of the mid-Holocene East Asia monsoon in coral $\delta^{18}O$ records from the South China Sea. Earth Planet. Sci. Lett. 237, 69–84.

Sun, Y.B., Clemens, S.C., An, Z.S., Yu, Z.W., 2006. Astronomical timescale and palaeoclimatic implication of stacked 3.6-Myr monsoon records from the Chinese Loess Plateau. Quat. Sci. Rev. 25, 33–48.

Sun, Y.B., An, Z.S., Clemens, S.C., Bloemendal, J., Vandenberghe, J., 2010. Seven million years of wind and precipitation variability on the Chinese Loess Plateau. Earth Planet. Sci. Lett. 297, 525–535.

Sun, Y.B., Clemens, S.C., Morrill, C., Lin, X.P., Wang, X.L., An, Z.S., 2012. Influence of Atlantic meridional overturning circulation on the East Asian winter monsoon. Nat. Geosci. 5, 46–49.

Sundquist, E.T., 1985. Geological perspectives on carbon dioxide and the carbon cycle. In: Sundquist, E.T., Broecker, W.S. (Eds.), *The Carbon Cycle and Atmospheric CO_2: Natural Variations Archean to Present*. American Geophysical Union, Washington D.C, pp. 5–59.

Sundquist, E.T., 1993. The global carbon dioxide budget. Science. 259, 934–941.

Suwa, M., Bender, M.L., 2008. Chronology of the Vostok ice core constrained by O_2/N_2 ratios of occluded air, and its implication for the Vostok climate records. Quat. Sci. Rev. 27, 1093–1106.

Suwa, M., von Fischer, J.C., Bender, M.L., Landais, A., Brook, E.J., 2006. Chronology reconstruction for the disturbed bottom section of the GISP2 and the GRIP ice cores: implications for Termination II in Greenland. J. Geophys. Res. 111, D02101. dx.doi.org/10.1029/2005JD006032.

Svensson, A., Andersen, K.K., Bigler, M., Clausen, H.B., Dahl-Jensen, D., Davies, S.W., Johnsen, S.J., Muscheler, R., Rasmussen, S.O., Röthlisberger, R., Steffensen, J.P., Vinther, B.M., 2006. The Greenland Ice Core Chronology 2005, 15–42 ka. Part 2: comparison to other records. Quat. Sci. Rev. 25, 3258–3267.

Svensson, A., Andersen, K.K., Bigler, M., Clausen, H.B., Dahl-Jensen, D., Davies, S.M., Johnsen, S.J., Muscheler, R., Parrenin, F., Rasmussen, S.O., Röthlisberger, R., Seierstad, I., Steffensen, J.P., Vinther, B.M., 2008. A 60000 year Greenland stratigraphic ice core chronology. Clim. Past. 4, 47–57.

Svensson, A., Bigler, M., Blunier, T., Clausen, H.B., Dahl-Jensen, D., Fischer, H., Fujita, S., Goto-Azuma, K., Johnsen, S.J., Kawamura, K., Kipfstuhl, S., Kohno, M., Parrenin, F., Popp, T., Rasmusssen, S.O., Schwander, J., Seierstad, I., Severi, M., Steffensen, J.P., Udisti, R., Uemura, R., Vallelonga, P., Vinther, B.M., Wegner, A., Wilhelms, F., Winstrup, M., 2012. Direct linking of Greenland and Antarctic ice cores at the Toba eruption (74 ka BP). Clim. Past. 9, 749–766.

Swain, A.M., 1978. Environmental changes during the last 2000 years in north-central Wisconsin: analysis of pollen, charcoal and seeds from varved lake sediments. Quat. Res. 10, 55–68.

Swart, P.K., Lohmann, K.C., McKenzie, J., Savin, S. (Eds.), 1993. Climate Change in Continental Isotopic Records. American Geophysical Union, Washington, DC.

Swart, P.K., Dodge, R.E., Hudson, H.J., 1996. A 240-year stable oxygen and carbon isotopic record in a coral from South Florida: implications for the prediction of precipitation in southern Florida. Palaios. 11, 362–375.

Swart, P.K., Greer, L., Rosenheim, B.E., Moses, C.S., Waite, A.J., Winter, A., Dodge, R.E., Helmle, K., 2010. The 13C Suess effect in scleractinian corals mirror changes in the anthropogenic CO2 inventory of the surface oceans. Geophys. Res. Lett. 37. dx.doi.org/10.1029/2009GL041397.

Swetnam, T.W., Betancourt, J.L., 1990. Fire-Southern Oscillation relations in the southwestern United States. Science. 249, 1017–1020.

Swetnam, T.W., Betancourt, J.L., 1992. Temporal patterns of El Niño/Southern Oscillation: wildfire patterns in the southwestern United States. In: Diaz, H.F., Markgraf, V.M. (Eds.), El Niño: Historical and Paleoclimatic Aspects of the Southern Oscillation. Cambridge University Press, Cambridge, pp. 259–270.

Swetnam, T.W., Brown, P.M., 2011. Climatic inferences from dendroecological reconstructions. In: Hughes, M.K., Swetnam, T.W., Diaz, H.F. (Eds.), Dendroclimatology: Progress and Prospects. Springer, Dordrecht, pp. 263–295.

Swetnam, T.W., Baisan, C.H., Caprio, A.C., Brown, P.M., Touchan, R., Anderson, R.S., Hallett, D.J., 2009. Multimillennial fire history of the giant forest, Sequoia National Park, California, USA. Fire Ecol. 5, 120–150.

Swingedouw, D., Terray, L., Cassou, C., Voldoire, A., Salas-Mélia, D., Servonnat, J., 2011. Natural forcing of climate during the last millennium: fingerprint of solar variability. Clim. Dyn. 36, 1349–1364.
Symonds, R.B., Rose, W.I., Reed, M.H., 1988. Contribution of Cl and F-bearing gases to the atmosphere by volcanoes. Nature. 334, 415–418.
Szabo, B.J., 1979a. Uranium-series age of coral reef growth on Rottnest Island, western Australia. Mar. Geol. 29, Mll-M15.
Szabo, B.J., 1979b. ^{230Th}, ^{231}Pa and open system dating of fossil corals and shells. J. Geophys. Res. 84, 4927–4930.
Szabo, B.J., Collins, D., 1975. Age of fossil bones from British interglacial sites. Nature. 254, 680–682.
Szabo, B.J., Rosholt, J.N., 1969. Uranium-series dating of Pleistocene molluscan shells from southern California-an open system model. J. Geophys. Res. 74, 3253–3260.
Szabo, B.J., Miller, G.H., Andrews, J.T., Stuiver, M., 1981. Comparison of uranium series, radiocarbon and amino acid data from marine molluscs, Baffin Island, Arctic Canada. Geology. 9, 451–457.
Szafer, W., 1935. The significance of isopollen lines for the investigation of geographical distribution of trees in the post-glacial period. Bulletin International de l'Academie Polonaise des Sciences et des Lettres, Bl, pp. 235–239.
Tagami, Y., Fukaishi, K., 1992. Winter and summer climatic variation in Japan during the Little Ice Age. In: Mikami, T. (Ed.), Proceedings of the International Symposium on the Little Ice Age Climate. Department of Geography, Tokyo Metropolitan University, Tokyo, pp. 188–193.
Takahara, H., Sugita, S., Harrison, S.P., Miyoshi, N., Morita, Y., Uchiyama, T., 2000. Pollen-based reconstructions of Japanese biomes at 0, 6000 and 18000 ^{14}C yr BP. J. Biogeogr. 27, 665–683.
Talbot, M.R., Delibrias, G., 1977. Holocene variations in the level of Lake Bosumptwi, Ghana. Nature. 268, 722–724.
Talbot, M.R., Johannessen, T., 1992. A high resolution palaeoclimate record for the last 27,500 years in tropical West Africa from the carbon and nitrogen isotopic composition of lacustrine organic matter. Earth Planet. Sci. Lett. 100, 23–37.
Talley, L.D., 1999. Some aspects of ocean heat transport by the shallow, intermediate and deep overturning circulations. In: Clark, P.U., Webb, R.S., Keigwin, L.D. (Eds.), Mechanisms of Global Climate Change at Millennial Time Scales. Monograph 112, American Geophysical Union, Washington, DC, pp. 1–22.
Tan, M., Liu, T.S., Hou, J.Z., Qin, X.G., Zhang, H.C., Li, T.Y., 2003. Cyclic rapid warming on centennial-scale revealed by a 2650-year stalagmite record of warm season temperature. Geophys. Res. Lett. 30, 1617. dx.doi.org/10.1029/2003GL017352.
Tapping, K.F., Boteler, D., Charbonneau, P., Crouch, A., Manson, A., Paquette, H., 2007. Solar magnetic activity and total irradiance since the Maunder Minimum. Sol. Phys. 246, 309–326.
Tarand, A., Kuiv, P., 1994. The beginning of the rye harvest – a proxy indicator of summer climate in the Baltic Area. In: Frenzel, B., Pfister, C., Glaser, B. (Eds.), Climatic Trends and Anomalies in Europe 1675–1715. Gustav Fischer, Stuttgart, pp. 61–72.
Tarling, D.H., 1975. Archeomagnetism: the dating of archaeological materials by their magnetic properties. World Archaeol. 7, 185–197.
Tarling, D.H., 1978. The geological-geophysical framework of ice ages. In: Gribbin, J. (Ed.), Climatic Change. Cambridge University Press, Cambridge, pp. 3–24.
Tarr, R.S., 1897. Difference in the climate of the Greenland and American side of Davis' and Baffin's Bay. Am. J. Sci. 3, 315–320.
Tarusov, L., Peltier, W.R., 2005. Freshwater forcing of the Younger Dryas cold reversal. Nature. 435, 662–665.
Tarusov, P.E., Pushenko, M.Ya., Harrison, S.P., Saarse, L., Andreev, A.A., Aleshinskaya, Z.V., Davydova, N.N., Dorofeyuk, N.L., Efremov, Yu.Y., Elina, G.A., Elovicheva, Ya.K., Filimonova, L.V., Gunova, V.S., Khomutova, V.I., Kvavadze, E.V., Nuestrueva, I.Yu., Pisareva, V.V., Sevastyanov, D.V., Shelekhova, T.S., Subetto, D.A., Uspenskaya, O.N., Zernitskaya, V.P., 1996. In: Lake Status Records from the Former Soviet Union and Mongolia: Documentation of the Second Version of the Database. Paleoclimatology Publication Series Report No.3, World Data Center-A for Paleoclimatology, Boulder.
Tarusov, P.E., Volkova, V.S., Webb, T., Guiot, J., Andreev, A.A., Bezusko, G., Bykova, T.V., Dorofeyuk, N.I., Kvavadze, E.V., Osipova, I.M., Panova, N.K., Sevastyanov, D.V., 2000. Last glacial maximum biomes reconstructed from pollen and plant macrofossil data from northern Europe. J. Biogeogr. 27, 609–620.
Tauber, H., 1965. Differential pollen dispersion and the interpretation of pollen diagrams. In: Danmarks Geologiske Undersogelse, Series II, p. 89.

Tauxe, L., Deino, A.D., Behrensmeyer, A.K., Potts, R., 1992. Pinning down the Brunhes-Matuyama and upper Jaramillo boundaries: a reconciliation of orbital and isotopic time scales. Earth Planet. Sci. Lett. 109, 561–572.
Tauxe, L., Herbert, T., Shackleton, N.J., Kok, Y.S., 1996. Astronomical calibration of the Matuyama-Brunhes boundary: consequences for magnetic remanence acquisition in marine carbonates and the Asian loess sequences. Earth Planet. Sci. Lett. 140, 113–146.
Taylor, K.C., Hammer, C.U., Alley, R.B., Clausen, H.B., Dahl-Jensen, D., Gow, A.J., Gundestrup, N.S., Kipfstuhl, J., Moore, J.C., Waddington, E.D., 1993a. Electrical conductivity measurements from the GISP2 and GRIP Greenland ice cores. Nature. 366, 549–552.
Taylor, K.C., Lamorey, G.W., Doyle, G.A., Alley, R.B., Grootes, P.M., Mayewski, P.A., White, J.W.C., Barlow, L.K., 1993b. The 'flickering switch' of late Pleistocene climate change. Nature. 361, 432–436.
Taylor, K.C., Alley, R.B., Lamorey, G.W., Mayewski, P.A., 1997. Electrical measurements on the Greenland Ice Sheet Project 2 core. J. Geophys. Res. 102, 26511–26517.
Ten Brink, N.W., 1973. Lichen growth rates in west Greenland. Arct. Alp. Res. 5, 323–331.
Tetzlaff, G., Adams, L.J., 1983. Present-day and early Holocene evaporation of Lake Chad. In: Street-Perrott, F.A., Beran, M., Ratcliffe, R. (Eds.), Variations in the Global Water Budget. D. Reidel, Dordrecht, pp. 347–360.
Thackray, G.D., 2008. Varied climatic and topographic influences on Late Pleistocene mountain glaciation in the western United States. J. Quat. Sci. 23, 671–681.
Thackray, G.D., Owen, L.A., Yi, C., 2008. Timing and nature of late Quaternary glaciation. J. Quat. Sci. 23, 503–508.
Therrell, M.D., Stahle, D.W., Acuña-Soto, R., 2004. Aztec drought and the "Curse of One Rabbit" Bull. Am. Meteorol. Soc. 85, 1263–1272.
Thierstein, H.R., Geitzenauer, K.R., Molfino, B., Shackleton, N.J., 1977. Global synchroneity of late Quaternary coccolith datum levels: validation by oxygen isotopes. Geology. 5, 400–404.
Thistlewood, L., Sun, J., 1991. A paleomagnetic and mineral magnetic study of the loess sequence at Liujiapo, Xian, China. J. Quat. Sci. 6, 13–26.
Thomas, E.R., Wolff, E.W., Mulvaney, R., Johnsen, S.J., Steffensen, J.P., Arrowsmith, C., 2009. Anatomy of a Dansgaard-Oeschger warming transition: high-resolution analysis of the North Greenland Ice Core Project ice core. J. Geophys. Res. 114. dx.doi.org/10.1029/2008JD011215.
Thompson, R.S., 1990. Late Quaternary vegetation and climate in the Great Basin. In: Betancourt, J.L., Van Devender, T.R., Martin, P.S. (Eds.), Packrot Middens: The Last 40,000 Years of Biotic Change. University of Arizona Press, Tucson, pp. 200–239.
Thompson, R.S., Anderson, K.H., 2000. Biomes of western North America at 18,000, 6,000 and 0 ^{14}C yr BP reconstructed from pollen and packrat midden data. J. Biogeogr. 27, 555–584.
Thompson, R., Oldfield, F., 1986. Environmental Magnetism,. Allen and Unwin, London.
Thompson, P.R., Saito, T., 1974. Pacific Pleistocene sediments: planktonic foraminifera dissolution cycles and geochronology. Geology. 2, 333–335.
Thompson, P., Schwarcz, H.P., Ford, D.C., 1976. Stable isotope geochemistry, geothermometry and geochronology of speleothems from West Virginia. Geol. Soc. Am. Bull. 87, 1730–1738.
Thompson, L.G., Mosley-Thompson, E., Grootes, P.M., Pourchet, M., Hastenrath, S., 1984a. Tropical glaciers: potential for ice core paleoclimatic reconstructions. J. Geophys. Res. 89D, 4638–4646.
Thompson, L.G., Mosley-Thompson, E., Arnao, B.M., 1984b. Major El Niño/Southern Oscillation events recorded in stratigraphy of the tropical Quelccaya Ice Cap. Science. 226, 50–52.
Thompson, L.G., Mosley-Thompson, E., Bolzan, J.F., Koci, B.R., 1985. A 1500 year record of tropical precipitation in ice cores from the Quelccaya Ice Cap, Peru. Science. 229, 971–973.
Thompson, L.G., Mosley-Thompson, E., Dansgaard, W., Grootes, P.M., 1986. The Little Ice Age as recorded in the stratigraphy of the tropical Quelccaya Ice Cap. Science. 234, 361–364.
Thompson, L.G., Davis, M., Mosley-Thompson, E., Liu, K., 1988. Pre-Incan agricultural activity recorded in dust layers in two tropical ice cores. Nature. 336, 763–765.
Thompson, L.G., Mosley-Thompson, E., Davis, M.E., Lin, N., Yao, T., Dyurgerov, M., Dai, J., 1993. "Recent warming": ice core evidence from tropical ice cores, with emphasis on central Asia. Glob. Planet. Chang. 7, 145–156.
Thompson, L.G., Mosley-Thompson, E., Davis, M.E., Lin, P.-N., Henderson, K.A., Cole-Dai, J., Bolzan, J.F., Liu, K.-B., 1995. Late Glacial Stage and Holocene tropical ice core records from Huascarán, Peru. Science. 269, 46–50.

Thompson, L.G., Yao, T., Davis, M.E., Henderson, K.A., Mosley-Thompson, E., Lin, P.-N., Beer, J., Synal, H.-A., Cole-Dai, J., Bolzan, J.F., 1997. Tropical climate instability: the last glacial cycle from a Qinghai-Tibetan ice core. Science. 276, 1821–1825.

Thompson, L.G., Mosley-Thompson, E., Davis, M.E., Henderson, K.A., Brecher, H.H., Zagorodnov, V.S., Mashiotta, T.A., Lin, P.-N., Mikhalenko, V.N., Hardy, D.R., Beer, J., 2002. Kilimanjaro ice core records: evidence of Holocene climate change in Tropical Africa. Science. 298, 589–593.

Thompson, W.G., Spiegelman, M.W., Goldstein, S.L., Speed, R.C., 2003. An open-system model for U-series age determinations of fossil corals. Earth Planet. Sci. Lett. 210, 365–381.

Thompson, L.G., Mosley-Thompson, E., Brecher, H., Davis, M., Leon, B., Les, D., Lin, P.-N., Mashiotta, T., Mountain, K., 2006. Abrupt tropical climate change: past and present. Proc. Natl. Acad. Sci. U. S. A. 103, 10536–10543.

Thompson, L.G., Mosley-Thompson, E., Davis, M.E., Zagorodnov, V.S., Howat, I.M., Mikhalenko, V.N., Lin, P.-N., 2013. Annually resolved ice core records of tropical climate variability over the past 1800 years. Science. 340, 945–950.

Thorarinsson, S., 1981. The application of tephrochronology in Iceland. In: Self, S., Sparks, R.J.S. (Eds.), Tephra Studies. D. Reidel, Dordrecht, pp. 109–134.

Tierney, J.E., Russell, J.M., Huang, Y.S., Sinninghe Damsté, J.S., Hopmans, E.C., Cohen, A.S., 2008. Northern hemisphere controls on tropical southeast African climate during the past 60,000 years. Science. 322, 252–255.

Tierney, J.E., Mayes, M.T., Meyer, N., Johnson, C., Swarzenski, P.W., Cohen, A.S., Russell, J.M., 2010a. Late-twentieth-century warming in Lake Tanganyika unprecedented since AD 500. Nat. Geosci. 3, 422–425.

Tierney, J.E., Russell, J.M., Huang, Y.S., 2010b. A molecular perspective on Late Quaternary climate and vegetation change in the Lake Tanganyika basin, East Africa. Quat. Sci. Rev. 29, 787–800.

Tikhomirov, B.A., 1961. The changes in biogeographical boundaries in the north of USSR as related with climatic fluctuations and activity of man. Botanisk Tidsskrift. 56, 285–292.

Tiljander, M., Saarnisto, M., Ojala, A.E.K., Saarinen, T., 2003. A 3000-year palaeoenvironmental record from annually laminated sediment of Lake Korttajärvi, central Finland. Boreas. 26, 566–577.

Tinner, W., Lotter, A.F., 2001. Central European vegetation response to abrupt climate change at 8.2ka. Geology. 29, 551–554.

Tinner, W., Ammann, B., Germann, P., 1996. Treeline fluctuations recorded for 12,500 years by soil profiles, pollen and plant macrofossils in the central Swiss Alps. Arct. Alp. Res. 28, 131–147.

Toney, J.L., Huang, Y.S., Fritz, S.C., Baker, P.A., Grimm, E., Nyren, P., 2010. Climatic and environmental controls on the occurrence and distributions of long chain alkenones in lakes of the interior United States. Geochim. Cosmochim. Acta. 74, 1563–1578.

Torres, V., Hooghiemstra, H., Lourens, L., Tzedakis, P.C., 2013. Astronomical tuning of long pollen records reveals the dynamic history of montane biomes and lake levels in the tropical high Andes during the Quaternary. Quat. Sci. Rev. 63, 59–72.

Toscano, M.A., Lundberg, J., 1999. Submerged Late Pleistocene reefs on the tectonically-stable SE Florida margin: high-precision geochronology, stratigraphy, resolution of Substage 5a sea-level elevation, and orbital forcing. Quat. Sci. Rev. 18, 753–767.

Tranquillini, A., 1993. Climate and physiology of trees in the Alpine timberline regions. In: Frenzel, B., Eronen, M., Vorren, K.D., Glaser, B. (Eds.), Oscillations of the Alpine and Polar Tree Limits in the Holocene. Gustav Fischer Verlag, Stuttgart, pp. 127–135.

Traverse, A. (Ed.), 1994. Sedimentation of Organic Particles. Cambridge University Press, Cambridge.

Treble, P.C., Chappell, J., Shelley, J.M.G., 2005a. Complex speleothem growth processes revealed by trace element mapping and scanning electron microscopy of annual layers. Geochim. Cosmochim. Acta. 69, 4855–4863.

Treble, P.C., Chappell, J., Gagan, M.K., McKeegan, K.D., Harrison, T.M., 2005b. In situ measurement of seasonal $\delta^{18}O$ variations and analysis of isotopic trends in a modern speleothem from southwest Australia. Earth Planet. Sci. Lett. 233, 17–32.

Trenberth, K.E., 1990. Recent observed interdecadal climate changes in the northern hemisphere. Bull. Am. Meteorol. Soc. 71, 988–993.

Trenberth, K.E., 1997. The use and abuse of climate models. Nature. 386, 131–133.

Trend-Staid, M., Prell, W.L., 2002. Sea surface temperature at the Last Glacial Maximum: a reconstruction using the modern analog technique. Paleoceanography. 17. dx.doi.org/10.1029/2000PA000536.

Treydte, K.S., Schleser, G.H., Helle, G., Frank, D.C., Winiger, M., Haug, G.H., Esper, J., 2006. The twentieth century was the wettest period in northern Pakistan over the past millennium. Nature. 440, 1179–1182.

Treydte, K., Frank, D., Esper, J., Andreu, L., Bednarz, Z., Berninger, F., Boettger, T., D'Alessandro, C.M., Etien, N., Filot, M., Grabner, M., Guillemin, M.T., Gutierrez, E., Haupt, M., Helle, G., Hilasvuori, E., Jungner, H., Kalela-Brundin, M., Krapiec, M., Leuenberger, M., Loader, N.J., Masson-Delmotte, V., Pazdur, A., Pawelczyk, S., Pierre, M., Planells, O., Pukiene, R., Reynolds-Henne, C.E., Rinne, K.T., Saracino, A., Saurer, M., Sonninen, E., Stievenard, M., Switsur, V.R., Szczepanek, M., Szychowska-Krapiec, E., Todaro, L., Waterhouse, J.S., Weigl, M., Schleser, G.H., 2007. Signal strength and climate calibration of a European tree-ring isotope network. Geophys. Res. Lett. 34, L24302. dx.doi.org/10.1029/2007GL03110.

Tricot, C., Berger, A., 1988. Sensitivity of present-day climate to astronomical forcing. In: Wanner, H., Siegenthaler, U. (Eds.), Long and Short-Term Variability of Climate. Springer-Verlag, New York, pp. 132–152.

Troll, C., 1973. The upper timberlines in different climatic zones. Arct. Alp. Res. 5, A3–A18.

Troughton, J.H., 1972. Carbon isotope fractionation by plants. In: Rafter, T.A., Grant-Taylor, T. (Eds.), Proceedings of the 8th International Conference on Radiocarbon Dating, vol. 2. Royal Society of New Zealand, Wellington, pp. 421–438.

Tudhope, A.W., Chilcott, C.P., McCulloch, M.T., Cook, E.R., Chappell, J., Ellam, R.M., Lea, D.W., Lough, J.M., Shimmield, G.B., 2001. Variability in the El Niño-Southern Oscillation through a glacial-interglacial cycle. Science. 291, 1511–1517.

Turich, C., Freeman, K.H., Bruns, M.A., Conte, M., Jones, A.D., Wakeham, S.G., 2007. Lipids of marine Archaea: patterns and provenance in the water-column and sediments. Geochim. Cosmochim. Acta. 71, 3272–3291.

Turney, C.S.M., Lowe, J.J., Davies, S.M., Hall, V., Lowe, D.J., Wastegard, S., Hoek, W.Z., Alloway, B., 2004. Tephrochronology of Last Termination sequences in Europe: a protocol for improved analytical precision and robust correlation procedures (a joint SCOTAV–INTIMATE proposal). J. Quat. Sci. 19, 111–120.

Turney, C.S.M., Van den Burg, K., Wastegård, S., Davies, S.M., Whitehouse, N.J., Pilcher, J.R., Callaghan, C., 2006. North European last glacial-interglacial transition (LGIT; 15–9 ka) tephrochronology: extended limits and new events. J. Quat. Sci. 21, 335–345.

Turney, C.S.M., Fifield, L.K., Hogg, A.G., Palmer, J.G., Hughen, K., Baillie, M.G.L., Galbraith, R., Ogden, J., Lorrey, A., Tims, S.G., Jones, R.T., 2010. The potential of New Zealand kauri (*Agathis australis*) for testing the synchronicity of abrupt climate change during the Last Glacial Interval (60,000-11,700 years ago). Quat. Sci. Rev. 29, 3677–3682.

Twining, A.C., 1833. On the growth of timber. Am. J. Sci. Arts. 24, 391–393.

Tzedakis, P.C., 1994. Hierarchical biostratigraphical classification of long pollen sequences. J. Quat. Sci. 9, 257–260.

Tzedakis, P.C., McManus, J.F., Hooghiemstra, H., Oppo, D.W., Wijmstra, T.J., 2003. Comparison of changes in vegetation in northeast Greece with records of climate variability on orbital and suborbital frequencies over the last 450,000 years. Earth Planet. Sci. Lett. 212, 197–212.

Tzedakis, P.C., Hooghiemstra, H., Pälike, H., 2006. The last 1.35million years at Tenaghi Philippon: revised chronostratigraphy and long-term vegetation trends. Quat. Sci. Rev. 25, 3416–3430.

Urey, H.C., 1947. The thermodynamic properties of isotopic substances. J. Chem. Soc. 152, 190–219.

Urey, H.C., 1948. Oxygen isotopes in nature and in the laboratory. Science. 108, 489–496.

Vacco, D.A., Clark, P.U., Mix, A.C., Cheng, H., Edwards, R.L., 2005. A speleothem record of Younger Dryas cooling, Klamath Mountains, Oregon, USA. Quat. Res. 64, 249–256.

Vaganov, E.A., Hughes, M.K., Shashkin, A.V., 2006. Growth Dynamics of Tree-rings: An Image of Past and Future Environments. Springer-Verlag, Berlin, 368 pp.

Vaganov, E.A., Anchukaitis, K.J., Evans, M.N., 2011. How well understood are the processes that create dendroclimatic records? A mechanistic model of the climatic control on conifer tree-ring growth dynamics. In: Hughes, M.K., Swetnam, T.W., Diaz, H.F. (Eds.), Dendroclimatology: Progress and Prospects. Springer, Dordrecht, pp. 37–75.

Vaks, A., Gutareva, O.S., Breitenbach, S.F.M., Avirmed, E., Mason, A.J., Thomas, A.L., Osinzev, A.V., Kononov, A.M., Henderson, G.M., 2013. Speleothems reveal 500,000-year history of Siberian permafrost. Science. 340, 183–186.

Valet, J.-P., Meynadier, L., Guyodo, Y., 2005. Geomagnetic diploe strength and reversal over the past 2 million years. Nature. 435, 802–805.

Van Breukelen, M.R., Vonhof, H.B., Hellstrom, J.C., Wester, W.C.G., Kroon, D., 2008. Fossil dripwater in stalagmites reveals Holocene temperature and rainfall variation in Amazonia. Earth Planet. Sci. Lett. 275, 54–60.
Van Calsteren, P., Thomas, L., 2006. Uranium-series dating applications in natural environmental science. Earth-Sci. Rev. 75, 155–175.
Van Campo, E., Guiot, J., Peng, C., 1993. A data-based re-appraisal of the terrestrial carbon budget at the last glacial maximum. Glob. Planet. Chang. 8, 189–201.
van de Flierdt, T., Robinson, L.F., Adkins, J.F., Hemming, S.R., Goldstein, S.L., 2006. Temporal stability of the neodymium isotope signature of the Holocene to glacial North Atlantic. Paleoceanography. 21. dx.doi.org/10.1029/2006PA001294.
Vandenberghe, J., Lu, H.Y., Sun, D.H., van Huissteden, J., Konert, M., 2004. The late Miocene and Pliocene climate in East Asia as recorded by grain size and magnetic susceptibility of the Red Clay deposits (Chinese Loess Plateau). Palaeogeogr. Palaeoclimatol. Palaeoecol. 204, 239–255.
van den Dool, H.M., Krijnen, H.J., Schuurmans, C.J.E., 1978. Average winter temperatures at De Bilt (The Netherlands), 1634-1977. Clim. Chang. 1, 319–330.
Vander Hammen, T., 1974. The Pleistocene changes of vegetation and climate in tropical South America. J. Biogeogr. 1, 3–26.
Vander Hammen, T., Absy, M.L., 1994. Amazonia during the last glacial. Palaeogeogr. Palaeoclimatol. Palaeoecol. 109, 247–261.
Vander Hammen, T., Maarleveld, G.C., Vogel, J.C., Zagwijn, W.H., 1967. Stratigraphy, climatic succession and radiocarbon dating of the last glacial in the Netherlands. Geol. Mijnbouw. 46, 79–95.
Van Devender, T.R., 1990a. Late Quaternary vegetation and climate of the Chihuahuan Desert, United States and Mexico. In: Betancourt, J.L., Van Devender, T.R., Martin, P.S. (Eds.), Packrat Middens: The Last 40,000 Years of Biotic Change. University of Arizona Press, Tucson, pp. 104–133.
Van Devender, T.R., 1990b. Late Quaternary vegetation and climate of the Sonoran Desert, United States and Mexico. In: Betancourt, J.L., Van Devender, T.R., Martin, P.S. (Eds.), Packrat Middens: The Last 40,000 Years of Biotic Change. University of Arizona Press, Tucson, pp. 134–165.
Van Devender, T.R., Spaulding, W.G., 1979. Development of vegetation and climate in the southwestern United States. Science. 204, 701–710.
Van Devender, T.R., Burgess, T.L., Piper, J.C., Turner, R.M., 1994. Paleoclimatic implications of Holocene plant remains from the Sierra Bacha, Sonora, Mexico. Quat. Res. 41, 99–108.
van Engelen, A.F.V., Buisman, J., IJnsen, F., 2001. A millennium of weather, winds and water in the Low Countries. In: Jones, P.D., Ogilvie, A.E.G., Davies, T.D., Briffa, K.R. (Eds.), History and Climate: Memories of the Future?. Kluwer, New York, pp. 101–124.
van Geel, B., Heusser, C.J., Schuurmans, J.E., 2000. Climatic change in Chile at around 2700 B.P. and global evidence for solar forcing: a hypothesis. The Holocene. 10, 659–664.
Van Loon, H., Taljaard, J.J., Sasamori, T., London, J., Hoyt, D.V., Labitze, K., Newton, C.W., 1972. Meteorology of the Southern Hemisphere. Meteorol. Monogr. 13. American Meteorological Society, Boston.
Vanzolini, P.E., 1973. Paleoclimates, relief and species multiplication in Equatorial forests. In: Meggers, B.J., Ayensu, E.S., Duckworth, W.D. (Eds.), Tropical Forest Ecosystems in Africa and South America: A Comparative Review. Smithsonian Institution, Washington, DC, pp. 255–258.
Vanzolini, P.E., Williams, E.E., 1970. South American anoles: the geographic differentiation and evolution of the *Anolis chrysolepsis* species group (Sauria, Iguanidae. Arquivos de Zoologia. 19, 1–298.
Vaquero, J.M., Trigo, R.M., 2012. A note on solar cycle length during the Medieval Climate Anomaly. Sol. Phys. 279, 289–294. dx.doi.org/10.1007/s11207-012-9964-1.
Vaquero, J.M., Vásquez, M., 2009. The Sun Recorded Through History. Springer, Dordrecht.
Vare, L.L., Massé, G., Gregory, T.R., Smart, C.W., Belt, S.T., 2009. Sea ice variations in the central Canadian Arctic Archipelago during the Holocene. Quat. Sci. Rev. 28, 1354–1366.
Varga, G., 2011. Similarities among the Plio–Pleistocene terrestrial aeolian dust deposits in the World and in Hungary. Quat. Int. 234, 98–108.
Vasquez-Bedoya, L.F., Cohen, A.L., Oppo, D., Blanchon, P., 2012. Corals record persistent multidecadal SST variability in the Atlantic Warm Pool since 1775 A.D. Paleoceanography. 27, PA3231. dx.doi.org/10.1029/2012PA002313.

Vaughan, T.A., 1990. Ecology of living *packrats*. In: Betancourt, J.L., VanDevender, T.R., Martin, P.S. (Eds.), Packrat Middens: The Last 40,000 Years of Biotic Change. University of Arizona Press, Tucson, pp. 14–27.
Veron, J.E.N., 1993. Corals of Australia and the Indo-Pacific. University of Hawaii Press, Honolulu.
Verosub, K.L., 1975. Paleomagnetic excursions as magnetostratigraphic horizons: a cautionary note. Science. 190, 48–50.
Verosub, K.L., 1977. Depositional and postdepositional processes in the magnetization of sediments. Rev. Geophys. Space Phys. 15, 129–143.
Verosub, K.L., 1988. Geomagnetic secular variations and the dating of Quaternary sediments. In: Easterbrook, D. (Ed.), Dating Quaternary Sediments. Special Paper 227Geological Society of America, Boulder, pp. 123–138.
Verosub, K.L., Banerjee, S.K., 1977. Geomagnetic excursions and their paleomagnetic record. Rev. Geophys. Space Phys. 15, 145–155.
Verosub, K.L., Fine, P., Singer, M.J., TenPas, J., 1993. Pedogenesis and paleoclimate: interpretation of the magnetic susceptibility record of Chinese loess-paleosol sequences. Geology. 21, 1011–1014.
Verschuren, D., Laird, K.R., Cumming, B.F., 2001. Rainfall and drought in equatorial east Africa during the past 1,100 years. Nature. 403, 410–414.
Vettoretti, G., Peltier, W.R., 2004. Sensitivity of glacial inception to orbital and greenhouse gas climate forcing. Quat. Sci. Rev. 23, 499–519.
Veum, T., Jansen, E., Arnold, M., Beyer, J.I., Duplessy, J.C., 1992. Water mass exchange between the North Atlantic and the Norwegian Sea during the past 28,000 years. Nature. 356, 783–785.
Viau, A.E., Gajewski, K., 2001. Holocene variations in the global hydrological cycle quantified by objective gridding of lake level databases. J. Geophys. Res. Atmos. 106, 31703–31716.
Vibe, C., 1967. Arctic animals in relation to climatic fluctuations. Meddelelser øm Gronland. 170 (5).
Vidal, L., Labeyrie, L., van Weering, T.C.E., 1998. Benthic $\delta^{18}O$ records in the North Atlantic over the last glacial period (60-10 kyr): evidence for brine formation. Paleoceanography. 13, 245–251.
Villalba, R., Luckman, B.H., Boninsegna, J., D'Arrigo, R.D., Lara, A., Villanueva-Diaz, J., Masiokas, M., Argollo, J., Soliz, C., LeQuesne, C., Stahle, D.W., Roig, F., Aravena, J.C., Hughes, M.K., Wiles, G., Jacoby, G., Hartsough, P., Wilson, R.J.S., Watson, E., Cook, E.R., Cerano-Paredes, C., Therrell, M., Cleaveland, M., Morales, M.S., Graham, N.E., Moya, J., Pacajes, J., Massacchesi, G., Biondi, F., Urrutia, R., Pastur, G.M., 2011. Dendroclimatology from regional to continental scales: understanding regional processes to reconstruct large-scale climatic variations across the western Americas. In: Hughes, M.K., Swetnam, T.W., Diaz, H.F. (Eds.), Dendroclimatology: Progress and Prospects. Springer, Dordrecht, pp. 175–227.
Villanueva, J., Grimalt, J.O., Cortijo, E., Vidal, L., Labeyrie, L., 1998. Assessment of sea surface temperature variations in the central North Atlantic using the alkenone unsaturation index ($U^{K'}_{37}$). Geochim. Cosmochim. Acta. 62, 2421–2427.
Villemant, B., Feuillet, N., 2003. Dating open systems by the ^{238}U–^{234}U–^{230}Th method: application to Quaternary reef terraces. Earth Planet. Sci. Lett. 210, 105–118.
Vimeux, F., 2009. Similarities and discrepancies between Andean ice cores over the last deglaciation: climate implications. In: Vimeux, F., Sylvestre, F., Khodri, M. (Eds.), Past Climate Variability in South America and Surrounding Regions. Springer, Berlin, pp. 239–255.
Vinot-Bertouille, A.C., Duplessy, J., 1973. Individual isotopic fractionation of carbon and oxygen in benthic foraminifera. Earth Planet. Sci. Lett. 18, 247–252.
Vinther, B.M., Clausen, H.B., Johnsen, S.J., Rasmussen, S.O., Andersen, K.K., Buchardt, S.L., Dahl-Jensen, D., Seierstad, I.K., Siggard-Andersen, M.-L., Steffensen, J.P., Svensson, A., 2006. A synchronized dating of three Greenland ice cores throughout the Holocene. J. Geophys. Res. Atmos. 111. dx.doi.org/10.1029/2005JD006921.
Vinther, B.M., Buchardt, S.L., Clausen, H.B., Dahl-Jensen, D., Johnsen, S.J., Fisher, D.A., Koerner, R.M., Raynaud, D., Lipenkov, V., Andersen, K.K., Blunier, T., Rasmussen, S.O., Steffensen, J.P., Svensson, A.M., 2009. Holocene thinning of the Greenland ice sheet. Nature. 461, 385–387.
Voelker, A.H.L., 2002. Global distribution of centennial-scale records for Marine Isotope Stage (MIS) 3: a database. Quat. Sci. Rev. 21, 1185–1212.
Voelker, A.H.L., Sarnthein, M., Grotes, P., Erlenkeuser, H., Laj, C., Mazaud, A., Nadeau, M.-J., Schleicher, M., 1998. Correlation of marine $\delta^{14}C$ ages from the Nordic Seas with the GISP2 isotope record: implications for radiocarbon calibration beyond 25 ka BP. Radiocarbon. 40, 517–534.

Volk, T., Hoffert, M.I., 1985. Ocean carbon pumps: analysis of relative strengths and efficiencies in ocean-driven atmospheric CO_2 strengths. In: Sundquist, E.T., Broecker, W.S. (Eds.), The Carbon Cycle and Atmospheric CO_2: Natural Variations Archean to Present. American Geophysical Union, Washington, DC, pp. 99–110.

von Grafenstein, U., Erlenkeuser, H., Kleinmann, A., Muller, J., Trimborn, P., 1994. High frequency climatic oscillations during the last deglaciation as revealed by oxygen-isotope records of benthic organisms (Ammersee, southern Germany). J. Paleolimnol. 11, 349–357.

von Grafenstein, U., Erlenkeuser, H., Kleinmann, A., Muller, J., Trimborn, P., Alefs, J., 1996. A 200 year mid-European air temperature record preserved in lake sediments: an extension of the $\delta^{18}O$-air temperature relation into the past. Geochim. Cosmochim. Acta. 60, 4025–4036.

von Grafenstein, U., Erlenkeuser, H., Brauer, A., Jouzel, J., Johnsen, S.J., 1999. A mid-European decadal isotope-climate record from 15,500 to 5,000 years B.P. Science. 284, 1654–1657.

von Gunten, L., Grosjean, M., Rein, B., Urrutia, R., Appleby, P.G., 2009. A quantitative high-resolution summer temperature reconstruction based on sedimentary pigments from Laguna Aculeo, Central Chile, back to AD 850. The Holocene. 19, 873–881.

von Gunten, L., D'Andrea, W.J., Bradley, R.S., Huang, Y., 2011. Proxy-to-proxy calibration: increasing the temporal resolution of quantitative climate reconstructions. Nat. Sci. Rep. 2, 609. dx.doi.org/10.1038/srep00609.

Vorren, K.-D., Jensen, C.E., Nilssen, E., 2012. Climate changes during the last c.7500 years as recorded by peat humification in the Lofoten region, Norway. Boreas. 41, 13–30.

Vuille, M., Bradley, R.S., Werner, M., Healy, R., Keimig, F., 2003. Modeling $\delta^{18}O$ in precipitation over the tropical Americas: 1. Interannual variability and climatic controls. J. Geophys. Res. 108. dx.doi.org/10.1029/2001JD002038.

Vuille, M., Francou, B., Wagnon, P., Juen, I., Kaser, G., Mark, B.G., Bradley, R.S., 2008. Climate change and tropical Andean glaciers: past, present and future. Earth-Sci. Rev. 89, 79–96.

Wagner, G., Beer, J., Laj, C., Kissel, C., Masarik, J., Muscheler, R., Synal, H.-A., 2000. Chlorine-36 evidence for the Mono Lake event in the summit GRIP ice core. Earth Planet. Sci. Lett. 181, 1–6.

Walker, I.R., 1987. Chironomidae (Diptera) in paleoecology. Quat. Sci. Rev. 6, 29–40.

Walker, M.J.C., 2005. Quaternary Dating Methods. J. Wiley, Chichester, 286 pp.

Walker, I.R., Cwynar, L.C., 2006. Midges and palaeotemperature reconstruction—the North American experience. Quat. Sci. Rev. 25, 1911–1925.

Walker, I.R., Smol, J.P., Engstrom, D.R., Birks, H.J.B., 1991a. An assessment of Chironomidae as quantitative indicators of past climate change. Can. J. Fish. Aquat. Sci. 48, 975–987.

Walker, I.R., Mott, R.J., Smol, J.P., 1991b. Allemd-Younger Dryas lake temperatures from midge fossils in Atlantic Canada. Science. 253, 1010–1012.

Walker, I.R., Wilson, S.E., Smol, J.P., 1995. Chironomidae (Diptera): quantitative palaeosalinity indicators for lakes of western Canada. Can. J. Fish. Aquat. Sci. 52, 950–960.

Walker, I.R., Levesque, A.J., Cwynar, L.C., Lotter, A.E., 1997. An expanded surface-water paleotemperature inference model for use with fossil midges from eastern Canada. J. Paleolimnol. 18, 165–178.

Walker, M.J.C., Björck, S., Lowe, J.J., Cwynar, L.C., Johnsen, S., Knudsen, K.-L., Wohlfarth, B., INTIMATE group, 1999. Isotopic 'events' in the GRIP ice core: a stratotype for the late Pleistocene. Quat. Sci. Rev. 18, 1143–1150.

Wallinga, J., 2002. Optically stimulated luminescence dating of fluvial deposits: a review. Boreas. 31, 303–322.

Wang, P.K., 1980. On the possible relationship between winter thunder and climatic changes in China over the past 2200 years. Clim. Chang. 3, 37–46.

Wang, S., 1991a. Reconstruction of temperature series of North China from 1380s to 1980s. Sci. China B. 34 (6), 751–759.

Wang, S., 1991b. Reconstruction of paleo-temperature series in China from the 1380s to the 1980s. Wurzburger Geographische Arbeiten. 80, 1–19.

Wang, R., Wang, S., 1989. Reconstruction of winter temperature in China for the last 500 year period. Acta Meteorol. Sin. 3 (3), 279–289.

Wang, S., Wang, R., 1990. Seasonal and annual temperature variations since 1470 A.D. in East China. Acta Meteorol. Sin. 4, 428–439.

Wang, S., Wang, R., 1991. Little Ice Age in China. Chin. Sci. Bull. 36 (3), 217–220.

Wang, P.K., Zhang, D., 1988. An introduction to some historical government weather records of China. Bull. Am. Meteorol. Soc. 69, 753–758.

Wang, P.K., Zhang, D., 1992. Reconstruction of 18th century summer precipitation of Nanjing, Suzhou and Hangzhou, China based on the Clear and Rain records. In: Bradley, R.S., Jones, P.D. (Eds.), Climate Since A.D. 1500. Routledge, London.
Wang, S., Zhao, Z.-C., 1981. Droughts and floods in China, 1470-1979. In: Wigley, T.M.L., Ingram, M.J., Farmer, G. (Eds.), Climate and History. Cambridge University Press, Cambridge, pp. 271–288.
Wang, R., Wang, S., Fraedrich, K., 1991. An approach to reconstruction of temperature on a seasonal basis using historical documents from China. Int. J. Climatol. 11, 381–392.
Wang, W.C., Portman, D., Gong, G., Zhang, P., Karl, T., 1992. Beijing summer tempera tures since 1724. In: Bradley, R.S., Jones, P.D. (Eds.), Climate Since A.D. 1500. Routledge, London, pp. 210–223.
Wang, Y.J., Cheng, H., Edwards, R.L., An, Z.S., Wu, J.Y., Shen, C.C., Dorale, J.A., 2001. A high-resolution absolute-dated Late Pleistocene monsoon record from Hulu Cave, China. Science. 294, 2345–2348.
Wang, X.F., Auler, A.S., Edwards, R.L., Cheng, H., Cristalli, P.S., Smart, P.L., Richards, D.A., Shen, C.C., 2004. Wet periods in northeastern Brazil over the past 210 ky linked to distant climate anomalies. Nature. 432, 740–743.
Wang, Y.-M., Lean, J.L., Sheeley, N.R., 2005a. Modeling the sun's magnetic field and irradiance since A.D. 1713. Astrophys. J. 625, 522–538.
Wang, Y.J., Cheng, H., Edwards, R.L., He, Y.Q., Kong, A.G., An, Z.S., Wu, J.Y., Kelly, M.J., Dykoski, C.A., Li, X.D., 2005b. The Holocene Asian monsoon: links to solar changes and North Atlantic climate. Science. 308, 854–857.
Wang, X.F., Auler, A.S., Edwards, R.L., Cheng, H., Ito, E., Solheid, M., 2006. Interhemispheric anti-phasing of rainfall during the last-glacial period. Quat. Sci. Rev. 25, 3391–3403.
Wang, Y.J., Chang, H., Edwards, R.L., Kong, X.G., Shao, X.H., Chen, S.T., Wu, J.Y., Jiang, X.J., Wang, X.F., An, Z.S., 2008. Millennial- and orbital-scale changes in the East Asian monsoon over the past 224,000 years. Nature. 451, 1090–1093.
Wang, Y.V., O'Brien, D.M., Jenson, J., Francis, D., Wooller, M.J., 2009. The influence of diet and water on the stable oxygen and hydrogen isotope composition of Chironomidae (Diptera) with paleoecological implications. Oecologia. 160, 225–233.
Wanner, H., Brazdil, R., Frich, P., Freyendahl, K., Jonsson, T., Kington, J., Pfister, C., Rosenorn, S., Wishman, E., 1994. Synoptic interpretation of monthly weather maps for the late Maunder Minimum 1675-1704. In: Frenzel, B., Pfister, C., Glaser, B. (Eds.), Climatic Trends and Anomalies in Europe 1675-1715. Gustav Fischer Verlag, Stuttgart, pp. 401–424.
Wanner, H., Brönnimann, S., Casty, C., Gyalistras, D., Luterbacher, J., Schmutz, C., Stephenson, D.B., Xoplaki, E., 2001. The North Atlantic Oscillation—concepts and status. Surv. Geophys. 22, 321–382.
Wanner, H., Beer, J., Bütikofer, J., Crowley, T., Cubasch, U., Flückiger, J., Goosse, H., Grosjean, M., Joos, F., Kaplan, J.O., Küttel, M., Müller, S.A., Prentice, I.C., Solomina, O., Stocker, T.F., Tarasov, P., Wagner, M., Widmann, M., 2008. Mid-to Late-Holocene climate change: a review. Quaternary Sci. Rev. 27, 1791–1828.
Waple, A.M., Mann, M.E., Bradley, R.S., 2001. Long-term patterns of solar irradiance forcing in model experiments and proxy-based surface temperature reconstructions. Clim. Dyn. 18, 563–578.
Warburton, J.A., Young, L.G., 1981. Estimating ratios of snow accumulation in Antarctica by chemical methods. J. Glaciol. 27, 347–358.
Wardle, P., 1974. Alpine timberlines. In: Ives, J.D., Barry, R.G. (Eds.), Arctic and Alpine Environments. Methuen, London, pp. 371–402.
Washburn, A.L., 1979a. Permafrost features as evidence of climatic change. Earth-Sci. Rev. 15, 327–402.
Washburn, A.L., 1979b. Geocryology. Arnold, London.
Wastegård, S., Rasmussen, T.L., Kuijpers, A., Nielsen, T., van Weering, T.C.E., 2006. Composition and origin of ash zones from Marine Isotope Stages 3 and 2 in the North Atlantic. Quat. Sci. Rev. 25, 2409–2419.
Watanabe, T., Winter, A., Oba, T., 2001. Seasonal changes in sea surface temperature and salinity during the Little Ice Age in the Caribbean Sea deduced from Mg/Ca and $^{18}O/^{16}O$ ratios in corals. Mar. Geol. 173, 21–35.
Watson, E., Morgan, A.V., 1977. The periglacial environment of great Britain during the devensian [and discussion]. Philos. Trans. R. Soc. Lond. B Biol. Sci. 280, 183–198.
Watson, E., Luckman, B.H., 2004. Tree-ring estimates of mass balance at Peyto Glacier for the last three centuries. Quat. Res. 62, 9–18.
Watts, W.A., Hansen, B.C.S., 1994. Pre-Holocene and Holocene pollen records of vegetation history from the Florida peninsula and their climatic implications. Palaeogeogr. Palaeoclimatol. Palaeoecol. 109, 163–176.
Weaver, A.J., Hughes, T.M.C., 1994. Rapid interglacial climate fluctuations driven by North Atlantic ocean circulation. Nature. 367, 447–450.

Weaver, A.J., Saenko, O.A., Clark, P.U., Mitrovica, J.X., 2003. Meltwater pulse 1A from Antarctica as a trigger of the Bølling-Allerød Warm interval. Science. 299, 1709–1713.
Webb III, T., 1974. Corresponding patterns of pollen and vegetation in lower Michigan: a comparison of quantitative data. Ecology. 55, 17–28.
Webb III, T., 1986. Is vegetation in equilibrium with climate? How to interpret late-Quaternary pollen data. Vegetatio. 67, 75–91.
Webb III, T., 1987. The appearance and disappearance of major vegetational assemblages: long-term vegetational dynamics in eastern North America. Vegetatio. 69, 177–187.
Webb III, T., 1988. Eastern North America. In: Huntley, B., Webb III, T. (Eds.), Vegetation History. Kluwer Academic, Dordrecht, pp. 385–414.
Webb III, T., 1991. The spectrum of temporal climate variability: current estimates and the need for global and regional time series. In: Bradley, R.S. (Ed.), Global Changes of the Past. University Corporation for Atmospheric Research, Boulder, pp. 61–82.
Webb, R.H., Betancourt, J.L., 1990. The spatial and temporal distribution of radiocarbon ages from packrat middens. In: Betancourt, J.L., VanDevender, T.R., Martin, P.S. (Eds.), Packrat Middens: The Last 40,000 Years of Biotic Change. University of Arizona Press, Tucson, pp. 85–102.
Webb III, T., McAndrews, J.H., 1976. Corresponding patterns of contemporary pollen and vegetation in central North America. In: Cline, R.M., Hays, J.D. (Eds.), Investigation of Late Quaternary Paleooceanography and Paleoclimatology. Memoir 145, Geological Society of America, Boulder, pp. 267–299.
Webb III, T., Yeracaris, G.Y., Richard, P., 1978. Mapped patterns in sediment samples of modern pollen from southeastern Canada and northeastern United States. Géog. Phys. Quatern. 32, 163–176.
Webb III, T., Howe, S.E., Bradshaw, R.H.W., Heide, K.M., 1981. Estimating plant abundances from pollen percentages: the use of regression analysis. Rev. Palaeobot. Palynol. 34, 269–300.
Webb III, T., Bartlein, P.J., Kutzbach, J.E., 1987. Climatic change in eastern North America during the past 18,000 years: comparison of pollen data with model results. In: Ruddiman, W.E., Wright, H.E. (Eds.), North America and Adjacent Oceans during the Last Deglaciation. The Geology of North America, vol. K-3. Geological Society of America, Boulder, pp. 447–462.
Webb III, T., Bartlein, P.J., Harrison, S.P., Anderson, K.H., 1993a. Vegetational, lake levels and climate in eastern North America for the past 18,000 years. In: Wright, H.E., Kutzbach, J.E., Webb III, T., Ruddiman, W.E., Street-Perrott, E.A., Bartlein, P.J. (Eds.), Global Climates Since the Last Glacial Maximum. University of Minnesota Press, Minneapolis, pp. 415–467.
Webb, R.S., Anderson, K.H., Webb III, T., 1993b. Pollen response-surface estimates of late Quaternary changes in the moisture balance of the northeastern United States. Quat. Res. 40, 213–227.
Weber, J.N., Woodhead, P.M.J., 1972. Temperature dependence of oxygen-18 concentration in reef coral carbonates. J. Geophys. Res. 77, 463–473.
Webster, P.J., Streten, N.A., 1978. Late Quaternary ice age climates of tropical Australasia: interpretations and reconstructions. Quat. Res. 10, 279–309.
Wehmiller, J.E., 1993. Applications of organic geochemistry for Quaternary research: aminostratigraphy and aminochronology. In: Engel, M.H., Macko, S.A. (Eds.), Organic Geochemistry. Plenum Press, New York, pp. 755–783.
Wei, K., Gasse, F., 1999. Oxygen isotopes in lacustrine carbonates of West China revisted: implications for post glacial changes in summer monsoon circulation. Quat. Sci. Rev. 18, 1315–1334.
Weijers, J.W.H., Schouten, S., van den Donker, J.C., Hopmans, E.C., Sinninghe Damsté, J.S., 2007. Environmental controls on bacterial tetraether membrane lipid distribution in soils. Geochim. Cosmochim. Acta. 71, 703–713.
Weiss, H., 2012. Quantifying collapse: the Late third millennium Khabur Plains. In: Weiss, H. (Ed.), Seven Generations Since the Fall of Akkad. Harrassowitz Verlag, Weisbaden, pp. 1–24.
Weiss, H., Bradley, R.S., 2001. What drives societal collapse? Science. 291, 609–610.
Weiss, H., Courty, M.-A., Wetterstrom, W., Meadow, R., Guichard, F., Senior, L., Curnow, A., 1993. The genesis and collapse of North Mesopotamian civilization. Science. 261, 995–1004.
Wells, P.V., 1976. Macrofossil analysis of wood rat (*Neotoma*) middens as a key to the Quaternary vegetational history of arid America. Quat. Res. 6, 223–248.
Wells, P.V., 1979. An equable glaciopluvial in the West: pleniglacial evidence of increased precipitation on a gradient from the Great Basin to the Sonoran and Chihuahuan Deserts. Quat. Res. 12, 311–325.

Wells, P.V., Berger, R., 1967. Late Pleistocene history of coniferous woodland in the Mohave Desert. Science. 155, 1640–1647.
Wells, P.V., Jorgensen, C.D., 1964. Pleistocene wood rat middens and climatic change in the Mohave desert: a record of Juniper woodlands. Science. 143, 1171–1173.
Wendland, W.M., Bryson, R.A., 1974. Dating climatic episodes of the Holocene. Quat. Res. 4, 9–24.
Wenk, T., Siegenthaler, U., 1985. The high-latitude ocean as a control of atmospheric CO_2. In: Sundquist, E.T., Broecker, W.S. (Eds.), The Carbon Cycle and Atmospheric CO_2: Natural Variations Archean to Present. American Geophysical Union, Washington, DC, pp. 185–194.
Westerling, A.L., Hidalgo, H.G., Cayan, D.R., Swetnam, T.W., 2006. Warming and earlier spring increase western US forest wildfire activity. Science. 313, 940–943.
Westgate, J.A., Gorton, M.P., 1981. Correlation techniques in tephra studies. In: Self, S., Sparks, R.J.S. (Eds.), Tephra Studies. D. Reidel, Dordrecht, pp. 73–94.
Westgate, J.A., Naeser, N.D., 1995. Tephrochronology and fission track dating. In: Rutter, N.W., Catto, N.R. (Eds.), Dating Methods for Quaternary Deposits. Geological Association of Canada, St. John's, pp. 15–28.
Wetter, O., Pfister, C., Weingartner, R., Luterbacher, J., Reist, T., Trösch, J., 2011. The largest floods in the High Rhine basin since 1268 assessed from documentary and instrumental evidence. Hydrol. Sci. J. 56, 733–758.
Weyl, P.K., 1968. The role of the oceans in climatic change: a theory of the ice ages. Meteorol. Monogr. 8, 37–62.
Wheeler, D., Suarez-Dominguez, J.M., 2005. Climatic reconstructions for the northeast Atlantic region 1685-1700: a new source of evidence from naval logbooks. The Holocene. 16, 39–49.
Wheeler, D., Garcia Herrera, R., Koek, F., Wilkinson, C., Können, G., Prieto, M.R., Jones, P.D., Casale, R., 2006. CLIWOC: Climatological Database for the World's Oceans: 1750-1850. European Communities, Luxembourg, 190 pp.
Whitlock, C., Bartlein, P.J., 1997. Vegetation and climate change in northwest North America during the past 125kyr. Nature. 388, 57–61.
Wigley, T.M.L., 1976. Spectral analysis and the astronomical theory of climatic change. Nature. 264, 629–631.
Wigley, T.M.L., 1978. Climatic change since 1000 AD. In: Evolution des Atmospheres Planetaires et Climatologie de la Terre. Centre National d'Etudes Spatiales, Toulouse, pp. 313–324.
Wigley, T.M.L., Kelly, P.M., 1990. Holocene climatic change, ^{14}C wiggles and variations in solar irradiance. Philos. Trans. R. Soc. Lond. A330, 547–560.
Wigley, T.M.L., Ingram, M.J., Farmer, G. (Eds.), 1981. Climate and History: Studies in Past Climates and their Impact on Man. Cambridge University Press, Cambridge.
Wijmstra, T.A., 1969. Palynology of the first 30 metres of a 120 m deep section in northern Greece. Acta Bot. Neerl. 18, 511–527.
Wild, M., Folini, D., Schär, C., Loeb, N., Dutton, E.G., König-Langlo, G., 2012. The global energy balance from a surface perspective. Clim. Dyn. 40, 3107–3134.
Wille, M., Hooghiemstra, H., Behling, H., Van der Borg, K., Negret, A.J., 2001. Environmental change in the Colombian subandean forest belt from 8 pollen records: the last 50 kyr. Veg. Hist. Archeobot. 10, 61–77.
Willerslev, E., Cappellini, E., Boomsma, W., Nielsen, R., Hebsgaard, M.B., Brand, T.B., Hofreiter, M., Bunce, M., Poinar, H.N., Dahl-Jensen, D., Johnsen, S., Steffensen, J.P., Bennike, O., Schwenninger, J.-L., Nathan, R., Armitage, S., de Hoog, C.-J., Alfimov, V., Christl, M., Beer, J., Muscheler, R., Barker, J., Sharp, M., Penkman, K.E.H., Haile, J., Taberlet, P., Gilbert, M.T.P., Casoli, A., Campani, E., Collins, M.J., 2007. Ancient biomolecules from deep ice cores reveal a forested southern Greenland. Science. 317, 111–114.
Williams, L.D., 1975a. The variation of come elevation and equilibrium line altitude with aspect in eastern Baffin Island, NWT, Canada. Arct. Alp. Res. 7, 169–181.
Williams, R.B.G., 1975b. The British climate during the last glaciation; an interpretation based on periglacial phenomena. In: Wright, A.E., Moseley, F. (Eds.), Ice ages: Ancient and Modern. Geological J. Special Issue No. 6, Liverpool University Press, Liverpool, pp. 95–120.
Williams, L.D., 1979. An energy balance model of potential glacierization of northern Canada. Arct. Alp. Res. 11, 443–456.
Williams, N.E., Eyles, N., 1995. Sedimentary and paleoclimatic controls on caddisfly (Insecta: Trichoptera) assemblages during the last interglacial-to-glacial transition in southern Ontario. Quat. Res. 43, 90–105.
Williams, J.W., Jackson, S.T., 2007. Novel climates, no-analog communities, and ecological surprises. Front. Ecol. Environ. 5, 475–482.

Williams, D.F., Johnson, W.C., 1975. Diversity of recent planktonic foraminifera in the southern Indian Ocean and late Pleistocene paleotemperatures. Quat. Res. 5, 237–250.
Williams, K.M., Smith, G.G., 1977. A critical evaluation of the application of amino acid racemization to geochronology and geothermometry. Orig. Life. 8, 91–144.
Williams, J., Barry, R.G., Washington, W.M., 1974. Simulation of the atmospheric circulation using the NCAR global circulation model with ice age boundary conditions. J. Appl. Meteorol. 13, 305–317.
Williams, L.D., Wigley, T.M.L., Kelly, P.M., 1981a. Climatic trends at high northern latitudes during the last 4000 years compared with ^{14}C fluctuations. In: Sun and Climate. Centre National d'Etudes Spatiales, Toulouse, pp. 11–20.
Williams, N.E., Westgate, J.A., Williams, D.D., Morgan, A., Morgan, A.V., 1981b. Invertebrate fossils (Insecta: Trichoptera, Diptera, Coloptera) from the Pleistocene Scarborough Formation at Toronto, Ontario and their paleoenvironmental significance. Quat. Res. 16, 146–166.
Williams, D.F., Peck, J., Karabanov, E.B., Prokopenko, A.A., Kravchinsky, V., King, J., Kuzmin, M.I., 1997. Lake Baikal record of continental climate response to orbital insolation during the past 5 million years. Science. 278, 1114–1117.
Williams, J.W., Shuman, B.N., Webb III, T., 1998. Applying plant functional types to construct biome maps from eastern North American pollen data: comparisons with model results. Quat. Sci. Rev. 17, 607–628.
Williams, J.W., Webb III, T., Richard, P.J.H., Newby, P., 2000. Late Quaternary biomes of Canada and the Eastern United States. J. Biogeogr. 27, 585–607.
Williams, J.W., Post, D.M., Cwynar, L.C., Lotter, A.F., Levesque, A.J., 2002. Rapid and widespread vegetation responses to past climate change in the North Atlantic region. Geology. 30, 971–974.
Williams, J.W., Shuman, B.N., Webb III, T., Bartlein, P.J., Leduc, P.L., 2004. Late-Quaternary vegetation dynamics in North America: scaling from taxa to biomes. Ecol. Monogr. 74, 309–334.
Wilson, A.T., Hendy, C.H., 1971. Past wind strength from isotope studies. Nature. 243, 344–346.
Wilson, A.T., Hendy, C.H., 1981. The chemical stratigraphy of polar ice sheets—a method of dating ice cores. J. Glaciol. 27, 3–9.
Wilson, C.J.N., Ambraseys, N.N., Bradley, J., Walker, G.P.L., 1980. A new date for the Taupo eruption, New Zealand. Nature. 288, 252–253.
Wilson, R., D'Arrigo, R., Buckley, B., Büntgen, U., Esper, J., Frank, D., Luckman, B., Payette, S., Vose, R., Youngblut, D., 2007. A matter of divergence—tracking recent warming at hemispheric scales using tree-ring data. J. Geophys. Res. Atmos. 112, D17103. dx.doi.org/10.1029/2006JD008318.
Wilson, R., Cook, E.R., D'Arrigo, R.D., Riedwyl, N., Evans, M.N., Tudhope, A., Allan, R., 2010. Reconstructing ENSO: the influence of method, proxy data, climate forcing and teleconnections. J. Quat. Sci. 25, 62–78.
Winckler, G., Anderson, R.F., Fleisher, M.Q., McGee, D., Mahowald, N., 2008. Covariant glacial-interglacial dust fluxes in the equatorial Pacific and Antarctica. Science. 320, 93–96.
Windom, H.L., 1975. Eolian contributions to marine sediments. J. Sediment. Petrol. 45, 520–529.
Winograd, I.J., Landwehr, J.M., 1993. A response to "Milankovitch theory viewed from Devil's Hole" In: Imbrie, J., Mix, A.C., Martinson, D.G. (Eds.), U.S.G.S. Open File Reportpp. 93–357.
Winograd, I.J., Szabo, B.J., Coplen, T.B., Riggs, A.C., 1988. A 250,000 year climatic record from Great Basin vein calcite: implications for Milankovitch theory. Science. 242, 1275–1280.
Winograd, I.J., Coplen, T.B., Landwehr, J.M., Riggs, A.C., Ludwig, K.R., Szabo, B., Kolesar, P.T., Revesz, K.M., 1992. Continuous 500,000 year climate record from vein calcite in Devil's Hole, Nevada. Science. 258, 255–260.
Winograd, I.J., Landwehr, J.M., Ludwig, K.R., Coplen, T.B., Rigg, A.C., 1997. Duration and structure of the past four interglaciations. Quat. Res. 48, 141–154.
Winter, A., Ishioroshi, H., Watanabe, T., Oba, T., Christy, J., 2000. Caribbean sea surface temperatures: two to three degrees cooler than present during the Little Ice Age. Geophys. Res. Lett. 27, 3365–3368.
Wintle, A.G., 1973. Anomalous fading of thermoluminescence in mineral samples. Nature. 244, 143–144.
Wintle, A.G., 1990. A review of current research on the TL dating of loess. Quat. Sci. Rev. 9, 385–397.
Wintle, A.G., 1993. Luminescence dating of aeolian sands: an overview. In: Pye, K. (Ed.), The Dynamics and Environmental Context of Aeolian Sedimentary Systems.Geological Society Special Publication No. 72, pp. 49–58.
Wintle, A.G., Aitken, M.J., 1977. Thermoluminescence dating of burnt flint: application to a lower palaeolithic site, Terra Amata. Archaeometry. 19, 111–130.
Wintle, A.G., Huntley, D.J., 1979. Thermoluminescence dating of a deep-sea ocean core. Nature. 279, 710–712.

Wintle, A.G., Li, S.H., Botha, G.A., 1993. Luminescence dating of colluvial deposits from Natal, South Africa. S. Afr. J. Sci. 89, 77–82.
Wintle, A.G., Lancaster, N., Edwards, S.R., 1994. Infra-red stimulated luminescence (IRSL) dating of the late-Holocene aeolian sands in the Mohave Desert, California, USA. The Holocene. 4, 74–78.
Wirrman, D., Mourguiart, P., 1995. Late Quaternary spatio-temporal limnological variations in the Altiplano of Bolivia and Peru. Quat. Res. 43, 344–354.
Wittfogel, M.A., 1940. Meteorological records from the divination inscriptions of Shang. Geogr. Rev. 30, 110–133.
Wohlfarth, B., Bjorck, S., Possnert, G., 1995. The Swedish time scale: a potential calibration tool for the radiocarbon time scale during the Late Weichselian. Radiocarbon. 37, 347–359.
Woillard, G.M., 1978. Grande Pile peat bog: a continuous pollen record for the past 140,000 years. Quat. Res. 9, 1–21.
Woillard, G.M., Mook, W.G., 1982. Carbon-14 dates at Grande Pile: correlation of land and sea chronologies. Science. 215, 159–161.
Wolfe, B.B., Edwards, T.W.D., Elgood, R.J., Beuning, K.R.M., 2001. Carbon and oxygen isotope analysis of lake sediment cellulose: methods and applications. In: Smol, J.P., Birks, H.J.B., Last, W.M. (Eds.), Tracking Environmental Change Using Lake sediments. Physical and Geochemical Methods, vol. 2. Kluwer Academic, Dordrecht, pp. 373–400.
Wolfe, A.P., Miller, G.H., Olsen, C.A., Forman, S.L., Doran, P.T., Holmgren, S.U., 2004. Geochronology of high latitude lake sediments. In: Pienitz, R., Douglas, M.S.V., Smol, J.P. (Eds.), Long-term Environmental Change in Arctic and Antarctic Lakes. Springer, Dordrecht, pp. 19–52.
Wolff, E., Spahni, R., 2007. Methane and nitrous oxide in the ice core record. Phil. Trans. R. Soc. A. 365, 1775–1792.
Wolff, E., Barbante, C., Becagli, S., Bigler, M., Boutron, C.F., Castellano, E., de Angelis, M., Federer, U., Fischer, H., Fundel, F., Hansson, M., Hutterli, M., Jonsell, U., Karlin, T., Kaufmann, P., Lambert, F., Littot, G.C., Mulvaney, R., Röthlisberger, R., Ruth, U., Severi, M., Siggard-Andersen, M.L., Sime, L.C., Steffensen, J.P., Stocker, T.F., Traversi, R., Twarloh, B., Udisti, R., Wagenbach, D., Wegner, A., 2010a. Changes in environment over the last 800,000 years from chemical analysis of the EPICA Dome C ice core. Quat. Sci. Rev. 1–2, 285–295.
Wolff, E., Chappellaz, J., Blunier, T., Rasmussen, S., Svensson, A., 2010b. Millennial-scale variability during the last glacial: the ice core record. Quat. Sci. Rev. 29, 2828–2838.
Woltering, M., Johnson, T.C., Werne, J.P., Schouten, S., Sinninghe Damsté, J.S., 2011. Late Pleistocene temperature history of Southeast Africa: a TEX86 temperature record from Lake Malawi. Palaeogeogr. Palaeoclimatol. Palaeoecol. 303, 93–102.
Wood, E.M., 1983. Reef Corals of the World: Biology and Field Guide. T.F.H Publications, Neptune City, New Jersey.
Woodhouse, C.A., Gray, S.T., Meko, D.M., 2006. Updated streamflow reconstructions for the Upper Colorado River Basin. Water Resour. Res. 42, W05415. dx.doi.org/10.1029/2005WR004455.
Woodhouse, C.A., Meko, D.M., MacDonald, G.M., Stahle, D.M., Cook, E.R., 2010. A 1,200-year perspective of 21st century drought in southwestern North America. Proc. Natl. Acad. Sci. U. S. A. 107, 21283–21288.
Woodwell, G.M., Whittaker, R.H., Reiners, W.A., Likens, G.E., Delwiche, C.C., Botkin, D.B., 1978. The biota and the world carbon budget. Science. 199, 141–146.
Wooller, M.J., Francis, D., Fogel, M.L., Miller, G.H., Walker, I.R., Wolfe, A.P., 2004. Quantitative paleotemperature estimates from $\delta^{18}O$ of chironomid head capsules preserved in arctic lake sediments. J. Paleolimnol. 31, 267–274.
Worbes, M., 2002. One hundred years of tree-ring research in the Tropics: a brief history and an outlook to future challenges. Dendrochronologia. 20, 217–231.
World Meteorological Organisation, 2007. The Role of Climatological Normals in a Changing Climate. WCDMP-No. 61, WMO-TD/No. 1377. World Meteorological Organization, Geneva.
Worthington, L.V., 1968. Genesis and evolution of water masses. Meteorol. Monogr. 8, 63–67.
Wright, H.E., Patten, H.L., 1963. The pollen sum. Pollen Spores. 5, 445–450.
Wright, H.E., Kutzbach, J.E., Webb III, T., Ruddiman, W.F., Street-Perrott, F.A., Bartlein, P.J. (Eds.), 1993. Global Climates Since the Last Glacial Maximum. University of Minnesota Press, Minneapolis.
Wu, G., Berger, W.H., 1989. Planktonic foraminifera: differential dissolution of the Quaternary stable isotope record in the west Equatorial Pacific. Paleoceanography. 4, 181–198.
Wu, G., Herguera, J.C., Berger, W.H., 1990. Differential dissolution: modification of Late Pleistocene oxygen isotope records in the western Equatorial Pacific. Paleoceanography. 5, 581–594.

Wu, H., Guiot, J., Brewer, S., Guo, Z., Peng, C., 2007a. Dominant factors controlling glacial and interglacial variations in the treeline elevation in tropical Africa. Proc. Natl. Acad. Sci. U. S. A. 104, 9720–9724.
Wu, N.Q., Chen, X.Y., Rousseau, D.D., Li, F.J., Pei, Y.P., Wu, B., 2007b. Climatic conditions recorded by terrestrial mollusk assemblages in the Chinese Loess Plateau during marine Oxygen Isotope Stages 12-10. Quat. Sci. Rev. 26, 1884–1896.
Wu, H.C., Linsley, B.K., Dassié, E.P., Schiraldi, B., deMenocal, P.B., 2013. Oceanographic variability in the South Pacific Convergence Zone region over the last 210 years from multi-site coral Sr/Ca records. Geochem. Geophys. Geosyst. 14, 1435–1453.
Wuchter, C., Schouten, S., Wakeham, S.G., Sinninghe Damsté, J.S., 2005. Temporal and spatial variation in tetraether membrane lipids of marine Crenarchaeota in particulate organic matter: implications for TEX86 paleothermometry. Paleoceanography. 20, PA3013. dx.doi.org/10.1029/2004PA001110.
Wuchter, C., Schouten, S., Wakeham, S.G., Sinninghe Damsté, J.S., 2006. Archaeal tetraether membrane lipid fluxes in the northeastern Pacific and Arabian Sea: implications for TEX86 paleothermometry. Paleoceanography. 21, PA4208. dx.doi.org/10.1029/2006PA001279.
Wunsch, C., 2002. What is the thermohaline circulation? Science. 298, 1179–1180.
Wunsch, C., 2003. The spectral description of climate change including the 100 ky energy. Clim. Dyn. 20, 353–363.
Wunsch, C., 2006. Abrupt climate change: an alternative view. Quat. Res. 65, 191–203.
Xiao, J., Porter, S.C., An, Z., Kumai, H., Yoshikawa, S., 1995. Grain size of quartz as an indicator of winter monsoon strength on the loess plateau of central China during the last 130,000 yr. Quat. Res. 43, 22–29.
Xoplaki, E., Luterbacher, J., Paeth, H., Dietrich, D., Steiner, N., Grosjean, M., Wanner, H., 2005. European spring and autumn temperature variability and change of extremes over the last half millennium. Geophys. Res. Lett. 32, L15713.
Xue, Y.K., 1997. Biosphere feedback on regional climate in tropical North Africa. Quart. J. Roy. Meteorol. Soc. 123, 1483–1515.
Yamamoto, T., 1971. On the nature of the climatic change in Japan since the "Little Ice Age" around 1800 AD. J. Meteorol. Soc. Jpn. 49 (special issue), 798–812.
Yancheva, G., Nowaczyk, N.R., Mingram, J., Dulski, P., Schettler, G., Negendank, J.F.W., Liu, J., Sigman, D.M., Peterson, L.C., Haug, G.H., 2007. Influence of the intertropical convergence zone on the East Asian monsoon. Nature. 445, 74–77.
Yao, S., 1942. The chronological and seasonal distribution of floods and droughts in Chinese history 206 BC-1911 AD. Harvard J. Asiat. Stud. 6, 273–312.
Yao, S., 1943. The geographical distribution of floods and droughts in Chinese history 206 BC-AD 1911. Far East Quart. 2, 357–378.
Yao, S., 1944. Flood and drought data in the *T'u Shu Chi Ch'eng* and the *Ch'ing Shi Kao*. Harvard J. Asiat. Stud. 8, 214–226.
Yao, T., Thompson, L.G., Jiao, K., Mosley-Thompson, E., Yang, Z., 1995. Recent warming as recorded in the Qinghai-Tibet cryosphere. Ann. Glaciol. 21, 196–200.
Yin, Q.Z., Berger, A., 2012. Individual contribution of insolation and CO_2 to the interglacial climates of the past 800,000 years. Clim. Dyn. 38, 709–724.
Yiou, F., Raisbeck, G.M., Bourles, D., Lorius, C., Barkov, N.I., 1985. ^{10}Be at Vostok Antarctica during the last climatic cycle. Nature. 316, 616–617.
Yoshimori, M., Hargreaves, J.C., Annan, J.D., Yokohata, T., Abe-Ouchi, A., 2011. Dependency of feedbacks on forcing and climate state in physics parameter ensembles. J. Clim. 24, 6440–6455.
Yoshimura, M., 1992. Historical weather data base system in Japan. In: Mikami, T. (Ed.), Proceedings of International Symposium on the Little Ice Age Climate. Department of Geography, Tokyo Metropolitan University, Tokyo, pp. 239–243.
Yoshimura, M., 1996. Climatic Condition in Latter Half of the Little lee Age. Department of Geography, Tamanashi University.
Yoshino, M.M., 1981. Orographically-induced atmospheric circulations. Prog. Phys. Geogr. 5, 76–98.
Yoshino, M., 2004. Development of phenological recognition and phenology in ancient China. Jpn. J. Biometeorol. 41, 141–154.
Young, M., Bradley, R.S., 1984. Insolation gradients and the paleoclimatic record. In: Berger, A.L., Imbrie, J., Hays, J., Kukla, G., Saltzman, B. (Eds.), Milankovitch and Climate, Part 2. D. Reidel, Dordrecht, pp. 707–713.

Yu, G., Harrison, S.P., 1995. Lake Status Records from Europe: Data Base Documentation. Paleoclimatology Publication Series Report No. 3, World Data Center-A for Paleoclimatology, Boulder.

Yu, Z., Ito, E., 1999. Possible solar forcing of century-scale drought frequency in the northern Great Plains. Geology. 27, 263–266.

Yu, G., Chen, X., Ni, J., Cheddadi, R., Guiot, J., Han, H., Harrison, S.P., Huang, C., Ke, M., Kong, Z., Li, S., Li, W., Liew, P., Liu, G., Liu, J., Liu, Q., Liu, K.-B., Prentice, I.C., Qui, W., Ren, G., Song, C., Sugita, S., Sun, X., Tang, L., Van Campo, E., Xia, Y., Xu, Q., Yan, S., Yang, X., Zhao, J., Zheng, Z., 2000. Paleovegetation of China: a pollen data-based synthesis for the mid-Holocene and last glacial maximum. J. Biogeogr. 27, 635–664.

Yu, J., Broecker, W.S., Elderfield, H., Jin, Z., McManus, J.F., Zhang, F., 2010. Loss of carbon from the deep sea since the Last Glacial Maximum. Science. 330, 1084–1087.

Yuan, D., Cheng, H., Edwards, R.L., Dykoski, C.A., Kelly, M.J., Zhang, M.L., Qing, J.M., Lin, Y.S., Wang, Y.J., Wu, J.Y., Dorale, J.A., An, Z.S., Cai, Y.J., 2004. Timing, duration and transitions of the Last Interglacial Asian monsoon. Science. 304, 575–578.

Zachos, J.C., Pagani, M., Sloan, L., Thomas, E., Billups, K., 2001. Trends, rhythms, and aberrations in global climate 65 Ma to present. Science. 292, 686–693.

Zachos, J.C., Dickens, G.R., Zeebe, R.E., 2008. An early Cenozoic perspective on greenhouse warming and carbon-cycle dynamics. Nature. 451, 279–283.

Zagwijn, W., Paepe, R., 1968. Die Stratigraphie der weichselzeitlichen Ablagerungen der Niederlande und Belgiens. Eiszeitalter Gegenwart. 19, 129–146.

Zahn, R., Winn, K., Sarnthein, M., 1986. Benthic foraminiferal and ^{13}C and accumulation rates of organic carbon: *Uvigerina peregrina* group and *Cibicidoides wuellerstorfi*. Paleoceanography. 1, 27–42.

Zaiki, M., Grossman, M.J., Mikami, T., 2012. Document-based reconstruction of past climate in Japan. PAGES News. 20, 82–83.

Zerefos, C.S., Gerogiannis, V.T., Balis, D., Zerefos, S.C., Kazantzidis, A., 2007. Atmospheric effects of volcanic eruptions as seen by famous artists and depicted in their paintings. Atmos. Chem. Phys. 7, 4027–4042.

Zhang, D., 1980. Winter temperature changes during the last 500 years in South China. Kexue Tongbao. 25 (6), 497–500.

Zhang, D., 1983. Analysis of dust rain in the historic times of China. Kexue Tongbao. 28 (3), 361–366.

Zhang, J. (Ed.), 1988. The Reconstruction of Climate in China for Historical Times. Science Press, Beijing.

Zhang, D. (Ed.), 2004. A Compendium of Chinese Meteorological Records of the Last 3000 Years. Jiangsu Education Press, Nanjing, 4 volumes: vol. 1, 23rd century BC to AD1367; vol 2, the Ming Dynasty, AD 1368–1643; vol. 3, the early Qing Dynasty, AD 1644–1795; vol. 4, the later Qing to the modern era, AD 1796–1911, 3666 pp. (in Chinese with English introduction).

Zhang, D., 2005. Severe drought events as revealed in the climate records of China over the past thousand years. Acta Meteorol. Sin. 19, 485–491.

Zhang, P., Gong, G., 1979. Some characteristics of climatic fluctuations in China since the 16th century. Acta Meteorol. Sin. 34, 238–247 (in Chinese with English summary: translation available from E.J. Bradley, c/o author).

Zhang, X.Y., Arimoto, R., An, Z.S., 1999. Glacial and interglacial patterns for Asian dust transport. Quat. Sci. Rev. 18, 811–819.

Zhang, M., Yuan, D., Lin, Y.S., Cheng, H., Qin, J.M., Zhang, H.L., 2004. The record of paleoclimatic change from stalagmites and the determination of Termination II in the south of Guizhou Province, China. Sci. China Ser. D Earth Sci. 47, 1–12.

Zhang, P.Z., Cheng, H., Edwards, R.L., Chen, F.H., Wang, Y.J., Yang, X.L., Liu, J., Tan, M., Wang, X.F., Liu, J.H., An, C.L., Dai, Z.B., Zhou, J., Zhang, D.Z., Jia, J.H., Jin, L.Y., Johnson, K.R., 2008. A test of climate, sun and culture relationships from an 1810-year Chinese cave record. Science. 322, 940–945.

Zhao, M., Beveridge, N.A.S., Shackleton, N.J., Sarnthein, M., Eglinton, G., 1995. Molecular stratigraphy of cores off northwest Africa: sea surface temperature history over the last 80 ka. Paleoceanography. 10, 661–675.

Zhao, J.X., Xia, Q.K., Collerson, K.D., 2001. Timing and duration of the Last Interglacial inferred from high resolution U-series chronology of stalagmite growth in Southern Hemisphere. Earth Planet. Sci. Lett. 184, 635–644.

Zhao, K., Wang, Y.J., Edwards, R.L., Cheng, H., Liu, D.B., 2010. High-resolution stalagmite $\delta^{18}O$ records of Asian monsoon changes in central and southern China spanning the MIS 3/2 transition. Earth Planet. Sci. Lett. 298, 191–198.

Zheng, S., Feng, L., 1986. Historical evidence on climatic instability above normal in cool periods in China. Sci. Sin. (B). 24, 441–448.
Zheng, J., Zheng, S., 1992. The reconstruction of climate and natural disaster in Shandong province during historical time. In: Collected Papers in Geography. publisher unknown.
Zheng, H.B., Powell, C. McA, Rea, D.K., Wang, J.L., Wang, P.X., 2004. Late Miocene and mid-Pliocene enhancement of the East Asian monsoon as viewed from the land and sea. Glob. Planet. Chang. 41, 147–155.
Zhou, L.P., Shackleton, N.J., 1999. Misleading positions of geomagnetic reversal boundaries in Eurasian loess and implications for correlation between continental and marine sedimentary sequences. Earth Planet. Sci. Lett. 168, 117–130.
Zhou, W.J., Priller, A., Beck, W.J., Wu, Z.K., Chen, M.B., An, Z.S., Kuschera, W., Feng, X., Yu, H.G., Liu, L., 2007. Disentangling geomagnetic and precipitation signals in an 80-kyr Chinese loess record of ^{10}Be. Radiocarbon. 49, 137–158.
Zhou, H.Y., Zhao, J.X., Feng, Y.X., Gagan, M.K., Zhou, G.Q., Yan, J., 2008. Distinct climate change synchronous with Heinrich event one, recorded by stable oxygen and carbon isotopic compositions in stalagmites from China. Quat. Res. 69, 306–315.
Ziegler, M., Diz, P., Hall, I.R., Zahn, R., 2013. Millennial-scale changes in atmospheric CO_2 levels linked to the Southern Ocean carbon isotope gradient and dust flux. Nat. Geosci. 6, 457–461.
Zielinski, G., 1995. Stratospheric loading and optical depth estimates of explosive volcanism over the last 2100 years as derived from the GISP2 Greenland ice core. J. Geophys. Res. 100D, 20937–20955.
Zielinski, G., Mayewski, P.A., Meeker, L.D., Whitlow, S., Twickler, M.S., Morrison, M., Meese, D.A., Gow, A.J., Alley, R.B., 1994. Record of explosive volcanism since 7000 B.C. from the GISP2 Greenland ice core and implications for the volcano-climate system. Science. 264, 948–952 (see also comments and discussion, 1995): Science 267, 256–258.
Zielinski, G., Mayewski, P.A., Meeker, L.D., Whitlow, S., Twickler, M.S., 1996. A 110,000-yr record of explosive volcanism from the GISP2 (Greenland) ice core. Quat. Res. 45, 109–118.
Zielinski, G., Mayewski, P.A., Meeker, L.D., Gronvold, K., Germani, M.S., Whitlow, S., Twickler, M.S., Taylor, K., 1997. Volcanic aerosol records and tephrochronology of the Summit, Greenland ice cores. J. Geophys. Res. 102C, 26625–26640.
Zink, K.-G., Leythaeuser, D., Melkonian, M., Schwark, L., 2001. Temperature dependency of long-chain alkenone distributions in recent to fossil limnic sediments and in lake waters. Geochim. Cosmochim. Acta. 65, 253–265.
Zinke, J., Dullo, W.C., Heiss, G.A., Eisenhauer, A., 2004. ENSO and Indian Ocean subtropical dipole variability is recorded in a coral record off southwest Madagascar for the period 1659 to 1995. Earth Planet. Sci. Lett. 228, 177–194.
Zinke, J., Pfeiffer, M., Timm, O., Dullo, W.-C., Davies, G.R., 2005. Atmosphere-ocean dynamics in the Western Indian Ocean recorded in corals. Philos. Trans. R. Soc. Lond. A. 363, 121–142.
Zolitschka, B., 1991. Absolute dating of late Quaternary lacustrine sediments by high resolution varve chronology. Hydrobiologia. 214, 59–61.
Zolitschka, B., 1998. A 14,000 year sediment yield record from western Germany based on annually laminated lake sediments. Geomorphology. 22, 1–17.
Zöller, L., Oches, E.A., McCoy, W.D., 1994. Towards a revised chronostratigraphy of loess in Austria, with respect to key sections in the Czech Republic and in Hungary. Quat. Sci. Rev. 13, 465–472.
Zreda, M.G., Phillips, F.M., 2000. Cosmogenic nuclide buildup in surficial materials. In: Noller, J.S., Sowers, J.M., Lettis, W.R. (Eds.), Quaternary Geochronology: Methods and Applications. American Geophysical Union, Washington, D.C., pp. 61–76.
Zumbühl, H.J., 1980. Die Schwankungen der Grindelwaldgletscher in den historischen Bildund Schriftquellen des 12. bis 19. Jahrunderts. Birkhäuser Verlag, Basel.

Index

Note: Page numbers followed by *f* indicate figures and *t* indicate tables.

A

Accelerator mass spectrometry (AMS), 62
Additive dose thermoluminescence dating method, 94–95, 94*f*
Adiabatic cooling, 145
Aeolian sediment, 410
Ahaggar Mountains, 448–449
Alkenones, 62–63
  lake sediments, 340–342, 341*f*, 342*f*, 343*f*
  paleotemperature reconstruction, 228–230, 229*f*, 231*f*, 232*f*
Allochthonous material, 319
Alpine glaciers, 360–362
Altithermal, 360–362
Ambrosia (ragweed) pollen, 413
Amino acid dating
  enantiomers and diastereomers, 113–115, 114*f*
  fragmentary hominid remains, 113
  numerical age estimates, 119–121, 119*f*, 120*f*
  paleotemperature estimate, 122–124
  racemization and epimerization rates, 113–118
  relative age estimates, 121–122, 123*f*
AMOC. *See* Atlantic meridional overturning circulation (AMOC)
AMS. *See* Accelerator mass spectrometry (AMS)
Anasazi culture, 487
Annealing, 100
Antarctic bottom water (AABW), 250, 250*f*
Antarctic ice cores
  accumulation record, 175–177, 176*f*
  atmospheric dust flux, 177–178, 177*f*, 179*f*
  locations of, 139*f*, 140*t*
  temperatures, 178–180, 180*f*
Antarctic Intermediate Water (AAIW), 250, 250*f*
Antarctic Isotope Maxima (AIM), 178, 180*f*, 304
Aphelion, 36, 38–39
Arboreal pollen (AP), 436–438
Archivo General de Indias, 539–540
Argentarola Cave, 318*f*
Argon-argon dating, 84–85, 85*f*
Aspartic acid, 115, 115*f*
Astronomical theory, 36
Atacama Desert, 398–399
Atlantic meridional overturning circulation (AMOC), 54, 251, 288, 304, 441–442
Atlantic multidecadal oscillation (AMO), 490
Autochthonous material, 319
Awatere Valley, 383*f*

B

Baffin Island, 354–356
Bahamas Cave, 319*f*
Big Lost excursion, 108–109
Biogenic ooze, 197–198
Biogenic sediments, 196
Biological dating methods
  dendrochronology, 135, 136*f*
  lichenometry (*see* Lichenometry)
Biological evidence
  insects (*see* Insects)
  plant macrofossils
    alpine tree line fluctuations, 392–395
    arctic tree line fluctuations, 389–392
    lower tree line fluctuations and rodent middens, 395–400
    topoclimatic factors, 388
Biomes, 421
Biosphere, 23–24, 24*t*
Black spruce *(Picea mariana)*, 391–392
Blake excursion, 108–109
Botuverá Cave, 308*f*, 316*f*
Bowen ratio, 27–29, 33
British Holocene deposits, 409*f*
Brunhes chron, 107
Brunhes dissolution cycle, 210
Byrd ice core, 71*f*, 178

C

Cadmium, 253
CAL. *See* Calvin photosynthetic cycle (CAL)
Calcareous marine fauna
  $\delta^{18}O$ and sea level changes, 222–225
  orbital forcing, 220–222
  orbital tuning, 215–220
  oxygen isotope stratigraphy, 211–214
  oxygen isotopic composition, 201–211
Calcite compensation depth (CCD), 206–209, 208*f*
Calvin photosynthetic cycle (CAL), 554–555
Camp Century ice core, 140*t*, 167, 168–170, 173
Canonical correlation analysis (CCA), 328

Carbon dioxide
atmospheric and oceans, 258–263
global energy balance, 30
positive feedbacks, 25
Carbon storage, 23, 24*t*
Carp Lake, 412*f*
Cascayunga Cave, 313
CCA. *See* Canonical correlation analysis (CCA)
^{14}C dating. *See* Radiocarbon dating
Chaac Cave, 296*f*
Chelford interstadial, 382
Chemical remanent magnetization (CRM), 106
Chihuahuan Desert, 398
China
drought/flood indices, 530*f*
loess distribution, 282*f*
spatial pattern and temporal evolution, 531*f*
Chironomids, 384
Chlorofluorocarbons, 184–186
Chron, 107–108
Climate and climatic variation, 15–16
atmosphere, 16
biosphere, 23–24, 24*t*
components, 16, 18*f*
cryosphere, 20–23, 21*t*, 22*f*
definition, 13–14
discontinuities, 15–16, 17*f*
of Earth's orbital parameters, 36–46
energy balance
annual net shortwave radiation, 30–33, 31*f*
atmospheric CO_2 and water vapor, 30
cloudiness, 29–30
for different surfaces, 33, 33*t*
land-based ice sheets, 30*t*
latent and sensible heat flux, 30–33, 32*f*
seasonal average surface albedo, 29–30, 29*f*
solar radiation, 27–29, 28*f*
examples of, 14, 15*f*
feedback mechanisms, 24–27, 26*f*
global warming, 13–14
land surface, 19–20, 19*f*, 20*f*
mean temperatures and temperature differences, 18*t*
nonlinear feedbacks, 14
oceanic thermohaline circulation, 14
oceans, 16–17, 18–19, 18*t*, 19*f*
radiocarbon variations, 82–83
solar forcing, 46–50
timescales of, 33–36, 34*f*, 35*f*
unexpected weather events, 14
volcanic forcing, 50–54
Climate: Long-range Investigation, Mapping, and Prediction (CLIMAP) project, 239–240
Climate system
atmosphere, 16
biosphere, 23–24, 24*t*
components of, 16, 18*f*
cryosphere, 20–23, 21*t*, 22*f*
land surface, 19–20, 19*f*, 20*f*
oceans, 16–17, 18–19, 18*t*, 19*f*
Climatological Database for the World's Oceans (CLIWOC), 539
Coleoptera, 378–379
Continental plate movements, 19
Continental scale vegetation patterns, 425
Continuous-flow analysis (CFA), 159
Corals
δ^{13}C, 510
Δ^{14}C, 510–511
δ^{18}O, 507–510
fossil coral records, 512–516
luminescence, 506
paleoclimate, coral growth rates, 506
past climate records, 503*t*
δ^{18}O records, 505*f*
environmental record, 501
hermatypic corals, 499–501
Montastraea faveolata colonies, 500*f*
Porites lutea, 502*f*
sclerosponges, 499–501
SSTs, 501
trace elements, 511–512
Cordilleran Mountains, 353–354
Cosmogenic isotope dating, 359–360
CRM. *See* Chemical remanent magnetization (CRM)
Cryosphere, 20–23, 21*t*, 22*f*

D

Dandak Cave, 314*f*
Dansgaard-Oeschger (D-O) events
Greenland ice cores, 168–170
marine sediments, 263–265, 264*f*, 266*f*, 267*f*
Data calibration, 5
Dating methods
amino acid (*see* Amino acid dating)
categories of, 56, 56*f*
dendrochronology, 135, 136*f*
fission-track, 100–101
lichenometry (*see* Lichenometry)
obsidian hydration, 111–113, 124–125
OSL and IRSL, 93*f*, 95–98
paleomagnetism (*see* Paleomagnetism)
potassium-argon, 83–85
radiocarbon (*see* Radiocarbon dating)
surface exposure, 98–100, 99*f*
tephrochronology, 125–128, 125*f*, 126*t*, 128*f*, 129*f*
thermoluminescence (*see* Thermoluminescence (TL) dating)
uranium-series, 85–91, 86*f*, 87*f*, 90*f*
Daughter deficiency dating method, 88
Daughter excess dating method, 88

$\delta^{13}C$
  C_3 and C_4 grasses, 556*f*
  lake sediments, 337–338
Deep-sea corals, 499–501
Deglacial preservation spike, 209–210
Dendrochronology, 135, 136*f*
Dendroclimatology
  cell structure drawing, 454*f*
  climatic reconstruction verification, 476–479
  cross dating, 458–462
  dendroclimatologists, 454–455
  density variations, 455
  divergence, 469–470
  isotopic variations, wood, 455–456
  meristematic tissues, 454–455
  ring-width data, standardization of, 463–469
  sample selection, 456–458
  tree-ring calibration, 470–476
  wood density, 455
Detrital remanent magnetization (DRM), 105, 106
Deuterium excess, 151–154
Devil's Hole, 301–304
Diastereomers, 113–115, 114*f*
Diatoms, 327–330, 329*f*, 330*f*
Dinoflagellates, 197–198, 241*f*
Diploastrea heliopora, 499–501
Diploria labyrinthiformis, 499–501
Diploria strigosa, 499–501
Dipole field, 104–105, 104*f*
Discontinuities, climatic, 15–16, 17*f*
Dishibao Cave, 307*f*
Dissolved inorganic carbon (DIC), 510
$\delta^{18}O$
  and deuterium excess, 153–154, 154*f*
  GRIP ice core and foram, 271, 272*f*
  lake water, 332–336, 333*f*, 334*f*, 335*f*, 337
  latitudinal influence on, 145
  mean January and July precipitation, 145, 146*f*
  NGRIP ice core, 168, 168*f*
  and salinity, 205, 206*f*
  and sea level changes, 222–225
  seasonal variations, 158–159
  and temperature, 145–151
Dongge Cave, 302*f*, 306, 309*f*
DRM. *See* Detrital remanent magnetization (DRM)
Dune systems, 371–373
Dust Bowl drought, 483*f*
Dust Veil Index (DVI), 545–547
Dye-3 ice core, 158*f*, 163, 165, 173

E

East Asia, historical records
  coded weather data, 543*f*
  Edo era, 543–544
  lower Yangtze River Basin, 540–543
  paleoclimate series, 541*t*
  phenological records, 540–543
  winter half-year temperature anomalies, 542*f*
  "winter-like" pressure pattern, 544*f*
Eccentricity, 36, 37*f*, 38, 39–41
Effective diagenetic temperature (EDT), 118
Eigenvectors
  drought and flood data, 529*f*
  precipitation anomalies, 528
ELA. *See* Equilibrium line altitude (ELA)
Electrical conductivity measurements (ECM), 160
El Niño-Southern Oscillation (ENSO), 501, 538–539
Empirical orthogonal functions (EOFs), 473
Enantiomers, 113–115, 114*f*
Eolian flux, 244, 245–246, 245*f*
EPICA Dronning Maud Land (EDML), 307*f*
Equilibrium line altitude (ELA), 351
Europe
  paleoclimatic reconstruction, 434–451
  PFT characteristics, 423*t*
European Flora Assessment, 422*t*
European paintings, 527*f*

F

Fagerlind effect, 412–413
Feedback mechanisms
  climate sensitivity, 26–27, 26*f*
  greenhouse effect, 25
  positive and negative, 24–25
Firn, 137–138
Fission-track dating, 100–101
Flowstones, 293–294
Foraminifera, 197–199, 197*f*, 198*f*, 199*f*, 200*f*
Fossil coral records, 514*t*
Fossil water, 141
Frost-free period, 525
Funza record, 438–440

G

Galápagos Islands, 509–510
Gastropods, 116*f*
General circulation models (GCMs), 10–11
Geomagnetic excursions, 108–109, 109*f*
Geomagnetic reversals, 108–109, 109*f*
GISP2 ice cores
  chemical components, 170, 171*f*
  electrical conductivity measurements, 160, 160*f*
  locations of, 140*t*
  volcanic sulfate and tephra, 163, 164*f*
Glacierization, 354–356
GLAMAP project, 239–240, 242*f*
Global meteoric water line (GMWL), 332–334
Global warming, 13–14
Glycerol dialkyl glycerol tetraethers (GDGTs), 338–340
GMWL. *See* Global meteoric water line (GMWL)

Greenhouse effect, 25, 27–29
Greenhouse gases, 2, 8, 10–11, 184–189
Greenland ice cores
  D-O events, 168–170
  $\delta^{18}O$ record, 168, 168*f*
  dust concentration, 172*f*
  event stratigraphy, 168–170, 169*f*
  glaciochemistry, components of, 170, 171*f*
  Holocene temperatures, 173, 174*f*
  ice-sheet margin, 175
  locations of, 139*f*, 140*t*
  NEEM site, 172–173
  temperature, 170–172, 171*f*
  thermohaline circulation, 172
Greenland Ice Sheet Project 2 (GISP2). *See* GISP2 ice cores
Grindelwald Glacier, 360–362
GRIP ice core
  annual layer counts, 155–156, 157*f*
  $\delta^{18}O$ and deuterium excess, 154*f*
  electrical conductivity measurements, 160, 160*f*
  ice age-gas age, 182–183, 183*f*
  locations of, 140*t*
  methane levels in, 186–187, 187*f*
  tephra horizons, 164*f*
Guliya ice core, 190–192

H

Haarlem-Leiden canal, 531–532
Hard-water effect, 65
Hatch-Slack (HS) cycle, 554–555
Heinrich events (HE), 304, 443
  age of, 269*t*
  GRIP ice core and foram, 271, 272*f*
  ice rafted detritus, 267–269, 268*f*
  North Atlantic sediments, 269–271, 270*f*
Hendy test, 297
Historical records
  climate forcing factors
    auroras, 548
    DVI, 545–547, 548*f*
    explosive volcanic eruptions, 545–547
    ice cores, 545–547
    long-term sunspot observations, 548
    postsunset sky colors, 545–547
    winter sea-level pressure (SLP) anomalies, 547*f*
  climate paradigms, last millennium
    hydroclimatic anomalies, 549*f*
    LIA, 548–550
    MWE, 548–550
    natural climate variability, 548–550
    Northern Hemisphere temperatures, 552*f*
    reconstructed temperature anomalies, 551*f*
  and interpretation
    diaries, 523
    Dutch canal freezing frequencies, 521
    Iceland, winter-spring thermal index, 520*f*
    long-term records, 519–520
    nonclimatic information, 519
    parameteorologic information, 520
    phenological and biological records, 534–538
    precipitation occurrence, 521
    reconstructed and observed July temperatures, 523*f*
    secondary sources, 521
    weather-dependent natural phenomena, 526–534
    weather observations, 524–526
  paleoclimatic data, 518
  regional studies
    East Asia, 540–544
    Europe, 544–545
Holocene paleoclimate, 356
Hoti Cave, 311*f*
Hudson's Bay Company, 532–534
Hudson Valley, 475*f*
Hulu Cave, 299*f*, 302*f*, 306, 307*f*, 308*f*

I

Ice cores
  accumulation, 137–138
  chronostratigraphic correlations, 167
  locations of, 138–141, 139*f*, 140*t*
  paleoclimatic information sources, 138–141, 138*t*
  paleoclimatic reconstruction
    Antarctica records, 175–180
    greenhouse gas records, 184–189
    Greenland records, 167–175
    low latitudes, 189–194
    polar ice cores, 180–184
  radioisotopic dating, 155
  seasonal variations and episodic events
    $\delta^{18}O$ values, 158–159
    electrical conductivity measurements, 160, 160*f*
    glaciochemistry, 159–160
    radioactive fallout, 161
    visual stratigraphy, 156–157
    volcanic sulfate and tephra, 161–165, 162*f*, 164*f*, 165*f*
  theoretical ice-flow model, 165–167, 166*f*
  water, stable isotopes in
    deuterium excess, 151–154
    $\delta^{18}O$ and temperature, 145–151
    fossil water, 141
    measurement and standardization, 143–144
    ^{18}O in atmospheric precipitation, 144–145
    $^{18}O/^{16}O$ ratio, 142*f*
Ice rafted detritus (IRD), 267–269, 268*f*

Infrared-stimulated luminescence (IRSL) dating, 93*f*, 95–98
Insects
  climatic indicator, 377–378
  Coleoptera, 378–379
  exoskeleton morphology, 378
  fossil assemblages, 377–378
  paleoclimatic reconstructions
    aquatic insects, 384–388
    fossil Coleoptera, 379–384
  palynology, 377–378
Intergovernmental Panel on Climate Change (IPCC), 10–11, 480–481
Internet resources, 557–558
Intertropical convergence zone (ITCZ), 75–78, 315–317, 441–442
IPCC. *See* Intergovernmental Panel on Climate Change (IPCC)
Ipswichian interglacial, 380–382
Isobaric effect, 145
Isochrones, 420*f*
Isopoll maps, 420–421
Isotopes
  lake sediments, 330–338
  in water
    deuterium excess, 151–154
    $\delta^{18}O$ and temperature, 145–151
    fossil water, 141
    measurement and standardization, 143–144
    ^{18}O in atmospheric precipitation, 144–145
    $^{18}O/^{16}O$ ratio, 142*f*
Isotopic dendroclimatology, 497
  $\delta^{13}C$, 495–497
  $\delta^{18}O$ and $\delta^{2}H$, 493–494
ITCZ. *See* Intertropical convergence zone (ITCZ)

J

Jaramillo subchron, 107–108

K

$^{40}K/^{40}Ar$ dating. *See* Potassium-argon dating
Karst landscapes, 293–294, 294*f*
Khumbu Glacier, 359
Kulishu Cave, 295*f*, 306, 308*f*
Kyoto record, 535

L

Lake Ammersee, 309–311
Lake Bosumtwi, 445–447, 446*f*
Lake Chad, 371–373
Lake Chad Basin, 448–449
Lake El'gygytgyn, 449–451
Lake Fúquene, 440*f*
Lake Lisan, 299–301
Lake Megachad Basin, 370
Lake Naivasha, 388
Lake Petén Itzá, 442–443
Lake sediments
  accumulation, 319, 320*f*
  allochthonous and autochthonous material, 319
  diatoms, 327–330, 329*f*, 330*f*
  inorganic geochemistry, 320–322, 322*f*
  macrofossils, 324
  organic biomarkers
    alkenones, 340–342, 341*f*, 342*f*, 343*f*
    TEX_{86}, GDGTs, 338–340, 339*f*
  ostracods, 327
  phytoliths, 326–327
  pollen, 324
  stable isotopes, 330–338
  varves, 323–324, 325*f*, 326*f*
Lake Suwa, 528–530
Lake Taihu, 528
Lake Windermere interstadial, 380–382
La Niña events, 506
Laschamp excursion, 108–109
Late glacial chironomid stratigraphy, 386*f*
Latent heat flux, 27–29, 32*f*
Laurentide ice sheet, 418–420
Libby half-lives, radioisotopic dating, 57–58, 59*f*
Lichenometry, 360
  glacial deposits, tundra environments, 129–130
  principles of, 130–131
  problems of
    biological factors, 132–133
    environmental factors, 133–134
    sampling factors, 134–135
Liquid scintillation techniques, 62
Little Ice Age (LIA), 360–362, 394, 548–550
Loess
  braided rivers, 279–280
  deposits, 280*f*
  desert conditions, 279–280
  distribution
    China, 282*f*
    Europe, 281*f*
  dust flux comparision, 284*f*
  dust storms, 280–283
  Eurasian temperatures, 280–283
  loess-paleosol sequences
    chronology, 284–286
    paleoclimatic significance, 287–290
  Miocene and Pliocene red clay units, 280–283
  outwash deposits, 279–280
  paleosol section, 283*f*
  pedogenic overprinting, 282*f*

Loess *(Continued)*
pedogenic processes, 280–283
Quaternary paleoclimatic conditions, 280–283
Loess-paleosol sequences
chronology
aminostratigraphic studies, 286
$\delta^{18}O$, stalagmites, 284–286
magnetic susceptibility, 284–286
orbital parameters, 284–286
OSL, 286
S5, 284–286
paleoclimatic significance
AMOC, 288
eolian and pedogenic hematite, 287
hygrophilous species, 288–289
pedogenic processes, 289
rainfall, 289–290
stacked magnetic susceptibility and MGSQ, 287*f*
Long-chain diol index (LDI), 234, 235*f*
Loss on ignition (LOI), 320–321
LowerMystic Lake (LML), 326*f*
Low-latitude ice cores, 139*f*, 189–194
Luminescence, 506
Luminescence dating
OSL and IRSL, 93*f*, 95–98
sample exposure age, 91
thermoluminescence (*see* Thermoluminescence (TL) dating)

M

Macrofossils, 324
Magnetic field of earth. *See also* Paleomagnetism
axis of rotation, 104–105, 104*f*
declination and inclination, 104–105, 104*f*
dipole field, 104–105, 104*f*
nondipole field, 105
reversals of, 103–104
secular variations of, 111, 112*f*
MARGO project, 239–240
Marine sediments
atmospheric carbon dioxide, 258–263
calcareous marine fauna
$\delta^{18}O$ and sea level changes, 222–225
orbital forcing, 220–222
orbital tuning, 215–220
oxygen isotope stratigraphy, 211–214
oxygen isotopic composition, 201–211
D-O events, 263–265, 264*f*, 266*f*, 267*f*
foraminifera, 197–199, 197*f*, 198*f*, 199*f*, 200*f*
Heinrich events, 267–277
inorganic material in, 244–248
last glacial maximum, 239–243
paleotemperature reconstruction
alkenones, 228–230, 229*f*, 231*f*, 232*f*
IP_{25} and related sea ice proxies, 234–238
Mg/Ca ratios, 238, 239*f*
TEX_{86} and long-chain diols, 231–234, 235*f*
pelagic sedimentation, 196, 196*f*
thermohaline circulation, 248–258
Matuyama chron, 107–108
MCA. *See* Medieval Climatic Anomaly (MCA)
Mean quartz grain size (MGSQ), 287*f*
Medieval Climatic Anomaly (MCA), 548–550
Medieval Warm Epoch (MWE), 526, 548–550
Mer deGlace, 360–362
Meteoric Water Line (MWL), 298
Milankovitch hypothesis, 301–304
Milankovitch theory, 36
Mojave Desert, 398
Mono Lake excursion, 108–109
Montastraea, 499–501
Multicollector inductively coupled plasma mass spectrometers (MC-ICP-MS), 295–296
Mutual climatic range
Awatere Valley, 383*f*
climatic conditions, 382–384
MWE. *See* Medieval Warm Epoch (MWE)

N

NADW. *See* North Atlantic Deep Water (NADW)
NAO. *See* North Atlantic Oscillation (NAO)
Negative feedback mechanisms, 24, 25
Neodymium (Nd), 253–254
Neoglaciations, 360–362
Neotoma middens, 396
Nonbiting midges, 384
Nondipole field, 105
Nonlinear feedbacks, 14
Nonmarine geologic evidence
lake-level fluctuations
closed lakes, 366
endoreic and areic drainage, 365*f*
Holocene glacier, 363*f*
hydrologic balance models, 366–369
hydrologic-energy balance models, 370–371
inland drainage, 362–366
lake sediments, 362–366
macrofossil and palynological evidence, 366
Mer de Glace, 364*f*
open-system lakes, 366
paleolake shoreline terraces, 365*f*
regional patterns of, 371–374
mountain glacier fluctuations
evidence of, 359–360
glacier front positions, 360–362
net ablation, 358

periglacial features
climatic threshold values, 348*t*
cracking and ice-wedge formation, 346–349
Europe, 350*f*
Netherlands, 349–351
paleoclimatic analysis, 349–351
paleotemperature reconstruction, 350*f*
paleotemperatures, 346–349
permafrost, 346
snowlines and glaciation thresholds
Alaska, modern andWisconsin snowlines, 352*f*
climatic and paleoclimatic interpretation, 352–356
ELA, 351
former snowlines, 356–357
paleoclimatic reconstructions, 351–352
paleosnowlines, 351
North Atlantic Deep Water (NADW), 250, 250*f*, 251
North Atlantic Oscillation (NAO), 490, 544–545

O

Obliquity, 36, 37*f*, 38, 38*f*, 39*f*, 40–41
Obsidian hydration dating, 111–113, 124–125
Oceans
and atmospheric carbon dioxide, 258–263
climate system, 16–17, 18–19, 18*t*, 19*f*
foraminifera, 197–199, 197*f*, 198*f*, 199*f*, 200*f*
last glacial maximum, 239–243
oxygen isotopic composition, 201–211
pelagic sedimentation in, 196, 196*f*
surface water reservoir age, 66–69, 68*f*
thermohaline circulation of, 248–258
Olduvai subchron, 107–108
Optically stimulated luminescence (OSL), 93*f*, 95–98, 286
Orbital forcing, 220–222
Orbital tuning, 215–220
Orogenies, 19
Ostracods, 327
Oxalic acid standard, 553–554

P

Pacific decadal oscillation (PDO), 489–490, 506
Pack rat (*Neotoma*), 396
Pacupahuain Cave, 304
Paleoclimatic reconstructions
Antarctic ice cores, 175–180
aquatic insects, 384–388
fossil Coleoptera, 379–384
greenhouse gas records, ice cores, 184–189
Greenland ice cores, 167–175
levels of analysis, 9–10
low-latitude ice cores, 189–194
model simulations, 10–11
Williams' model, 10–11
paleoclimatology, definition of, 1
paleosnowlines, 354–356
polar ice cores, 180–184
proxy data (*see* Proxy data)
Paleodose, 91
Paleomagnetic secular variations (PSV), 111, 112*f*
Paleomagnetism
chemical remanent magnetization, 106
detrital remanent magnetization, 105, 106
geomagnetic excursions, 108–109, 109*f*
magnetic field of earth, 104–105, 104*f*, 111, 112*f*
polarity timescale, 107–108, 107*f*
relative paleointensity variations, 110–111, 110*f*
thermoremanent magnetization, 105
Paleosnowlines, 356
Paleotemperature reconstruction
amino acid racemization and epimerization, 122–124
marine sediments
alkenones, 228–230, 229*f*, 231*f*, 232*f*
IP_{25} and related sea ice proxies, 234–238
Mg/Ca ratios, 238, 239*f*
TEX_{86} and long-chain diols, 231–234, 235*f*
Palmer Drought Severity Index (PDSI), 482
Palmyra Island, 508*f*, 512–514
Palynology, 407*t*
paleoclimatic information sources, 410
Plant Taxa, North America and Europe, 407*t*
Pavona clavus, 509–510
PDO. *See* Pacific decadal oscillation (PDO)
PDSI. *See* Palmer Drought Severity Index (PDSI)
Peatland mires, 401*f*
Peqiin Cave, 299–301, 300*f*
Phenological calendar, 534
Phytoliths, 326–327
Plant functional types (PFTs), 421
Plant macrofossils
alpine tree line fluctuations, 392–395
arctic tree line fluctuations, 389–392
lower tree line fluctuations and rodent middens, 395–400
topoclimatic factors, 388
Plant Taxa, 407*t*
Plate movements, 19
Pleistocene snowlines, 354
Podocarpus, 444–445
Polar ice cores, 180–184
Polarity chron, 107–108
Polarity events, 107–108
Polarity excursions, 108
Pollen
analysis
characteristics, 408–409
fossil pollen, sources of, 410–411

Pollen *(Continued)*
pollen diagram, 411–414
productivity and dispersal, 410
samples, preparation of, 411
lake sediments, 324
marine sediments and ice cores, 405–406
paleoclimatic reconstructions
Amazonia, 443–445
Central American Lowlands, 441–443
climate space, 428–431
dissimilarity coefficients, 428
Equatorial and Sub-Saharan Africa, 445–449
Europe, 434–438
fossil pollen spectra, 425–426
Holocene levels, 431–433
natural vegetation, 425–426
Northeastern Siberia, 449–451
paleobioclimate, 431–433
pollen-climate relationships, 426
precipitation changes, 431
reconstructed anomalies, 432*f*
response surfaces, 428–431
Sabana de Bogotá, Colombia, 438–441
scatter diagrams, 427*f*
soil moisture index, 428–431
spruce pollen, 428–431
temperature pattern, 431
transfer functions, 426–428
uniformitarian assumption, 426–428
spatial and temporal scales, 408*f*
vegetation composition and climate
climate changes, 422–425
isopolls and isochrones, 418–422
modern pollen rain, 416–417
paleoclimatic reconstruction, 414–415
pollen assemblages, 415
uniformitarian principle, 415
upslope pollen transport, 415–416
Pollen Taxa, 422*t*
Porites, 499–501
Positive feedback mechanisms, 24–25
Potassium-argon dating
$^{40}Ar/^{39}Ar$ dating, 84–85, 85*f*
lava flows and volcanic tuff, 83
problems of, 84
production, 83
seafloor basalts, 83
Precipitation anomalies patterns, 528
Pringle Falls excursion, 108–109
Proportional gas counters, 62
Proxy data
abrupt climate changes, 7–8
accurate dating, 8–9
calibration, 5
climate-tree growth relationships, 5
discontinuous/episodic information, 8
frequency dependence, 7
natural archives, characteristics of, 5–7, 7*t*
past climatic change, 8
sources of, 5–7, 6*t*
Pyramid Lake, 365*f*

Q

Qingtian Cave, 308*f*

R

Radiocarbon dating
accuracy of, 63–64
AMS dating, 62–63, 63*f*
atmospheric ^{14}C concentration, variations in, 72–81, 73*t*
climatic discontinuities, 15–16, 17*f*
deepwater ventilation rate, 69–71, 69*f*, 71*f*
fractionation effects, 71–72, 554–555
liquid scintillation techniques, 62
ocean surface water reservoir age, 66–69, 68*f*
principles of, 60–62
proportional gas counters, 62
sample contamination, 64–66, 66*f*, 67*f*
standardization procedure, 553–554
temporal variation causes, 81
variations and climate, 82–83
Radioisotopic dating
age ranges, 57*f*
^{14}C dating (*see* Radiocarbon dating)
fission-track dating, 100–101
groups, 58–59
half-lives of, 57–58, 58*t*
Libby and revised half-lives, 57–58, 59*f*
OSL and IRSL dating, 93*f*, 95–98
potassium-argon dating, 83–85
surface exposure dating, 98–100, 99*f*
TL dating (*see* Thermoluminescence (TL) dating)
uranium-series dating, 85–91, 86*f*, 87*f*, 89*f*, 90*f*
Reef-building corals, 499–501
Regional curve standardization (RCS), 466–468, 468*f*
Relative paleointensity (RPI), 110–111, 110*f*
Rhizocarpon geographicum, 130, 131*f*, 132*f*
Rock hyrax *(Procavia capensis)*, 399–400
Rocky Mountains, 353–354
Runaway greenhouse effect, 25
Rystad mire, 402*f*

S

Sacramento River basin, 484
Sample contamination, radiocarbon dating, 64–66, 66*f*, 67*f*
Sanbao Cave, 302*f*, 307*f*, 309*f*
Sea-surface salinity (SSS), 507–509
Sea-surface temperature (SST), 499–501
Sensible heat flux, 27–29, 32*f*

Siderastrea siderea, 499–501
Snow and ice
  permanent, 20–23, 21*t*
  seasonal changes, 20–23, 21*t*, 22*f*
Snowline depression, 367–369
Solar forcing, 46–50
Solar radiation, 40–41, 41*f*, 42, 43*f*, 44*f*
Sonoran Desert, 398
Soreq Cave, 298, 299–301, 300*f*
South American summer monsoon (SASM), 304
Spannagel Cave, 297
Spatial drought patterns, 486*f*
SPECMAP marine isotope record, 301–304
Spectral Mapping Project (SPECMAP), 239–240
Speleothems
  carbonate dissolution and deposition, 294*f*
  cave system, 294*f*
  glacial terminations, 301–304
  isotopic variations, 297–298
  late glacial and holocene records, 306–312
  millennial to centennial scales, 304–306
  paleoclimatic information, 313–317
  sea-level variations, 317–320
  stalactites, 293–294
  stalagmite records, 312–313
  stalagmites, 293–294
  tropical and subtropical paleoclimate variability, 298–301
  uranium-series disequilibrium methods, 296
Standard Mean Ocean Water (SMOW), 143–144
Subchrons, 107–108
Suess effect, 73
Surface exposure dating, 98–100, 99*f*

T

Tachinus caelatus, 378–379
Tassili n'Ajjer Mountains, 448–449
Tephrochronology
  GISP2 and GRIP ice-core records, 127, 129*f*
  glacial deposits, 125–126, 125*f*
  North America, 126, 126*t*
  North Atlantic region, 127, 128*f*
Thermal ionization mass spectrometers (TIMS), 295–296
Thermohaline circulation, 248–258
Thermoluminescence (TL) dating
  additive dose and regenerative methods, 94–95, 94*f*
  in archeology, 92
  definition, 91
  intensity *vs.* temperature, 93–94, 93*f*
  problems of, 95
Thermophilous beetle assemblage, 380–382
Thermoremanent magnetization (TRM), 105
Tilia, 410
Timescale
  of climatic variation, 33–36, 34*f*, 35*f*
  paleomagnetic polarity, 107–108, 107*f*
TIMS. *See* Thermal ionization mass spectrometers (TIMS)
Total solar irradiance (TSI), 480–481
Tree rings
  dendroclimatic reconstructions
    atmospheric circulation modes, 487–490
    drought reconstruction, 481–487
    Northern Hemisphere temperatures, 480–481
    wildfires and dendroclimatology, 490–492
  dendroclimatology
    cell structure drawing, 454*f*
    climatic reconstruction verification, 476–479
    cross dating, 458–462
    dendroclimatologists, 454–455
    density variations, 455
    divergence, 469–470
    isotopic variations, wood, 455–456
    meristematic tissues, 454–455
    ring-width data, standardization of, 463–469
    sample selection, 456–458
    tree-ring calibration, 470–476
    wood density, 455
  isotopic dendroclimatology
    $\delta^{13}C$, 495–497
    $\delta^{18}O$ and $\delta^{2}H$, 493–494

U

Unified ENSO proxy (UEP), 488*f*
Uniformitarianism, 5
Unsupported dating method, 88
Upton Warren interstadial, 380–382
Uranium-series dating, 85–91, 86*f*, 87*f*, 89*f*, 90*f*

V

Varves
  Lake Nuutajarvi, 325*f*
  thickness in Lower Mystic Lake, 326*f*
  types of, 323–324, 323*f*
Volcanic forcing, 50–54
Vostok ice core
  CO_2 concentrations, 184–186, 186*f*
  dust flux in, 177*f*
  locations of, 140*t*
  seasonal $\delta^{18}O$ variations, 159–160

W

Wanxiang Cave, 314*f*
Wiggle-matched tree-ring data, 463*f*

X

X-ray fluorescence (XRF) analysis, 321, 321*f*, 322*f*

Y

Yangtze River, 530
Yellow River, 528, 530